Halogen and Chalcogen Bonding Host Molecules for Anion Recognition and Sensing

Jason Y. C. Lim

St Cross College, University of Oxford



A thesis submitted for the degree of Doctor of Philosophy

Inorganic Chemistry Laboratory

University of Oxford

Trinity Term 2017

Halogen and Chalcogen Bonding Host Molecules for Anion Recognition and Sensing

Jason Yuan Chong Lim, St Cross College, University of Oxford

Abstract of thesis submitted for the degree of D.Phil., Trinity Term 2017

This thesis describes the preparation and study of acyclic, macrocyclic and mechanically-interlocked host molecules (MIMs) exploiting halogen and chalcogen bonding interactions for anion recognition and sensing.

Chapter 1 introduces the field of anion supramolecular chemistry and interlocked structures, with emphasis on halogen and chalcogen bonding receptors, as well as their applications in catalysis, molecular recognition and nanotechnology.

Chapter 2 explores the methodology development and synthesis of novel neutral and cationic macrocyclic and interlocked host molecules containing stable triazole-based halogen and chalcogen bonding motifs. The thermodynamic anion binding properties of these novel host molecules in wet and dry organic solvents are determined and compared.

Chapter 3 details the applications and influences of halogen and chalcogen bonding interactions for electrochemical anion sensing. The ability of ferrocene-based halogen bonding receptors to enhance the sensitivity of redox anion sensing compared with hydrogen bonding host analogues is demonstrated.

Chapter 4 investigates the unprecedented applications of halogen and chalcogen bonding interactions in enantioselective binding and sensing of chiral anions. The use of chiral [2]- and [3]rotaxanes for chiral anion discrimination is also demonstrated for the first time.

Chapter 5 describes the exploitation of hydrophilic polyether-based cationic halogen bonding receptors for anion binding and sensing in water. In particular, the halogen bonding-mediated recognition of oxoanions such as perrhenate and biologically-relevant phosphate species are discussed.

Chapter 6 summarises the main conclusions of this thesis.

Chapter 7 details the experimental procedures employed in this work, including synthetic protocols and characterisation data for novel compounds.

Additional information pertaining to crystallographic data, electrochemical measurements and computational modelling procedures are provided in the Appendices.

ACKNOWLEDGEMENTS

This thesis marks the end of an amazing four-year D.Phil journey in Oxford that has seen me grow in both spirit and mind. However, none of this would have been possible without the help, support and encouragement of the following people:

First and foremost, I am immensely grateful to Professor Paul Beer for being such a tremendous supervisor, and for allowing me to work on such a wide range of fascinating projects in his group. Although he always says that “you create your own luck”, his constant encouragement, guidance, and being always available for a chat to discuss any problems has undoubtedly been an invaluable source of motivation, especially during rough and tough days in the lab when the chemistry defies all expectations. His patience and support during my attempts to bring some of his ‘crazy ideas’ to life has been invaluable and I look forward to much future collaboration together.

From my first days in lab S7, the Beer Group has been a fantastic source of support and help. I have been fortunate enough to drink from the incredible fountain of chemical knowledge, Dr Asha Brown, whom I must also credit for introducing me to chemical crystallography. Her patient guidance, advice and our countless discussions, which have helped me overcome numerous seemingly impossible hurdles, will be something that I will be always grateful for. Special thanks also go to Drs Tim Barendt, Stuart Cornes, Robert Edkins and Matthew Langton for insightful discussions on various aspects of this thesis. In particular, I must also express my gratitude towards Xiaoxiong (George) Li, Hena Bagha and Jane Liew, especially for keeping me company and sane during the times when my urge to indulge in some chemistry overrides any need for other intellectual pursuits on weekends. Thanks are also due to current members of the Beer Group (S7 and S8), Robert Hein, Harry Klein, Valentine Bunchuay, Andrew Docker, Grace Turner, Tom Mole, Arseni Borissov, Luiza Bondila and Dr Lydia Gilday, who have made my days so entertaining. I am also thankful for an outstanding CDT student, David Ascough, whom I was lucky enough to look after and have contributed to some of the work in Chapter 2. In addition, credit is due to Dr Asha Brown, Dr

Tim Barendt, Valentine Bunchuay, Hena Bagha and Andrew Docker for the formidable task of diligently proof-reading this hefty tome.

A note of thanks needs to be made to the many Beer Group collaborators and CRL staff, for which none of the work presented here would be possible without. Firstly, I am very grateful to Dr. Igor Marques and Professor Vítor Félix at the University of Aveiro, Portugal, who performed all the modelling experiments described herein. The guidance of Dr. Matthew Cunningham (Jason Davis Group) must also be acknowledged in my fledging attempts at electrochemistry early in my degree. I am appreciative also to Dr Nick Rees, who has been instrumental in setting up various NMR experiments for my work, most notably ^{77}Se and ^{125}Te NMR and water-suppression sequences, as well as for providing quirky audio accompaniments to many NMR titration experiments in the CRL basement. Finally, I am extremely grateful to Drs Amber Thompson and Kirsten Christensen for organising and helping with many trips to the Diamond Light Source, for their company and chauffeuring on many a late night, and for help and advice with chemical crystallography as a whole.

Reaching deep back in time, I must credit my former teachers Ms Wong S. H., Mrs Phua P. L. and Mr Chok Y. K. for being so inspirational in my quest for knowledge. It may be said in fact that without this mighty trio, I would not have been doing this degree at all. Also, special thanks to Dr Alex Cowan, Professors Donald Craig and Nick Long at Imperial College London who truly opened my eyes to chemistry research. I am also lucky enough to be awarded the A*STAR scholarship, and am grateful for their financial support for my studies in UK the last seven years.

Last but definitely not least, my heartfelt appreciation to my loving parents, grandma, sister, wife and late grandpa for believing in me. Their unwavering and unconditional support and encouragement has been valuable beyond words.

This thesis is dedicated to my family.

J.Y.C.L, August 2017

千里之行，始于足下

“The journey of a thousand miles begins with a single step.”

Chinese proverb

PREVIOUSLY PUBLISHED WORK

Some of the work described in this thesis has been published:

Peer-reviewed journal articles

Chapter 2

"Chalcogen Bonding Macrocycles and [2]Rotaxanes for Anion Recognition"

J. Y. C. Lim, I. Marques, A. L. Thompson, K. E. Christensen, V. Félix and P. D. Beer, ***J. Am. Chem. Soc.***, 2017, *139*, 3122-3133.

"Strong and Selective Halide Anion Binding by Neutral Halogen Bonding [2]Rotaxanes in Wet Organic Solvents"

J. Y. C. Lim, T. Bunchuay and P. D. Beer, ***Chem. Eur. J.***, 2017, *23*, 4700-4707.

Chapter 3

"Neutral Redox-active Hydrogen and Halogen Bonding [2]Rotaxanes for the Electrochemical Sensing of Chloride"

J. Y. C. Lim, M. J. Cunningham, J. J. Davis and P. D. Beer, ***Dalton Trans.***, 2014, *43*, 17274-17282.

"Halogen bonding-enhanced Electrochemical Halide Anion Sensing by Redox-active Ferrocene Receptors"

J. Y. C. Lim, M. J. Cunningham, J. J. Davis and P. D. Beer, ***Chem. Commun.,*** 2015, *51*, 14640-14643.

"A Halogen Bonding 1,3-Disubstituted Ferrocene Receptor for Selective Recognition and Redox Sensing of Azide"

J. Y. C. Lim and P. D. Beer, ***Eur. J. Inorg. Chem.***, 2017, 220-224.

Chapter 4

"Enhancing the Enantioselective Recognition and Sensing of Chiral Anions by Halogen Bonding"

J. Y. C. Lim, I. Marques, V. Félix and P. D. Beer, ***Chem. Commun.***, 2016, *52*, 5527-5530.

"Enantioselective Anion Recognition by Chiral Halogen Bonding [2]Rotaxanes"

J. Y. C. Lim, I. Marques, V. Félix and P. D. Beer, ***J. Am. Chem. Soc.***, 2017, *139*, 12228-12239.

"Chiral Halogen Bonding [3]Rotaxanes for the Recognition and Sensing of Biologically-Relevant Dicarboxylate Anions"

J. Y. C. Lim, I. Marques, V. Félix and P. D. Beer, ***Angew. Chem. Int. Ed.***, 2017, DOI: 10.1002/anie.201711176.

"Halogen and Chalcogen Bonding Receptors for Discrimination of Stereo- and Geometric Dicarboxylate Isomers"

J. Y. C. Lim, I. Marques, V. Félix and P. D. Beer, ***Chem. Commun.***, *manuscript in preparation*.

Chapter 5

"Superior Perrhenate Anion Recognition in Water by a Halogen Bonding Acyclic Receptor"

J. Y. C. Lim and Paul D. Beer, ***Chem. Commun.***, 2015, *51*, 3686-3688.

Further work published during the course of this thesis:

"Neutral Iodotriazole Foldamers as Tetradentate Halogen Bonding Anion Receptors"

A. Borissov, J. Y. C. Lim, A. Brown, K. E. Christensen, A. L. Thompson, M. D. Smith and P. D. Beer, ***Chem. Commun.***, 2017, *53*, 2483-2486.

"Cationic All-Halogen Bonding Rotaxanes for Halide Anion Recognition"

X. Li, J. Y. C. Lim and P. D. Beer, ***Faraday Discuss.***, 2017, *203*, 245-255.

Review article: "*Sigma Hole Interactions in Anion Recognition"*

J. Y. C. Lim and P. D. Beer, ***Chem***, *manuscript in preparation.*

Poster Presentations

"Neutral Redox-active Hydrogen and Halogen Bonding [2]Rotaxanes for the Electrochemical Sensing of Chloride"

J. Y. C. Lim, M. J. Cunningham, J. J. Davis and P. D. Beer, 2014, Macrocyclic and Supramolecular Chemistry (MASC) Conference, Norwich, U.K., Dec 2014.

"Superior Perrhenate Anion Recognition in Water by a Halogen Bonding Acyclic Receptor"

J. Y. C. Lim and Paul D. Beer, 10th International Symposium on Macrocyclic and Supramolecular Chemistry (ISMSC), Strasbourg, France, Jul 2015.

"Enhancing the Enantioselective Recognition and Sensing of Chiral Anions by Halogen Bonding"

J. Y. C. Lim, I. Marques, V. Felíx and P. D. Beer, 11th International Symposium on Macrocyclic and Supramolecular Chemistry (ISMSC), Seoul, South Korea, Jul 2016.

"Chalcogen Bonding Macrocycles and [2]Rotaxanes for Anion Recognition"

J. Y. C. Lim, I. Marques, A. L. Thompson, K. E. Christensen, V. Felíx and P. D. Beer, 12th International Symposium on Macrocyclic and Supramolecular Chemistry (ISMSC), Cambridge, U.K., Jul 2017.

GLOSSARY OF ABBREVIATIONS

δ	chemical shift
λ	wavelength
μ	micro
ξ	magnitude of chiral selectivity ($\xi = K_S / K_R$)
+ve	positive
Δ	change in (a physical quantity)
Å	Ångstrom
A^-	anion
a.u.	arbitrary units
ADP	adenosine diphosphate
AeB	aerogen bonding
AMP	adenosine monophosphate
AMT	active metal template
aq.	aqueous
ATP	adenosine triphosphate
BINAM	1,1′-Binaphthyl-2,2′-diamine
BINOL	1,1'-Bi-2-naphthol
Bn	benzyl
Boc	tert-butyloxycarbonyl (protecting group)
BODIPY	boron-dipyrromethene
br.	broad
Bu	butyl
cat.	catalytic
CD	circular dichroism (spectroscopy)
ChB	chalcogen bonding
CI	chemical ionisation (mass spectrometry)
conc.	concentrated
COSY	homonuclear correlation spectroscopy
CuAAC	copper(I)-catalysed azide-alkyne cycloaddition
CV	cyclic voltammetry
DBU	1,8-diazabicycloundec-7-ene
DFT	density functional theory
DIBAL-H	diisobutylaluminium hydride
DIPEA	*N*,*N*-diisopropylethylamine
DMAP	4-Dimethylaminopyridine
DMF	*N*,*N*-dimethylformamide
DMSO	dimethyl sulfoxide
DNA	deoxyribonucleic acid
e.g.	*exempli gratia*
$E_{1/2}$	half-wave potential
EDTA	ethylenediaminetetraacetate
em	emission

eqv.	equivalents
ESI	electrospray ionisation (mass spectrometry)
ex	excitation
Fc	ferrocene
Fc^+	ferrocenium
FI	field ionisation (mass spectrometry)
g	gram
G	Gibbs free energy
Grubbs ‘ I/ II	Grubbs’ first/ second generation catalyst
h	hour
H	enthalpy
HB	hydrogen bonding
HEPES	4-(2-hydroxyethyl)-1-piperazineethanesulfonic acid
HOMO	highest-occupied molecular orbital
HRMS	high resolution mass spectrometry
Hz	Hertz
i.e.	*id est*
IDA	indicator displacement assay
J	coupling constant
J	Joule
k	kilo
K	Kelvin
K_a	association constant
L	litre
LUMO	lowest-unoccupied molecular orbital
m	metre
M	molar (moles per litre)
m/*z*	mass to charge ratio
MD	molecular dynamics
Me	methyl
MEP	molecular electrostatic potential
MIM	mechanically-interlocked molecule
MM	molecular mechanics
MOM	methoxymethyl acetal (protecting group)
MS	mass spectrometry
Ms	mesyl
MW	microwave
NDI	naphthalene diimide
NMR	nuclear magnetic resonance
oxone	potassium peroxymonosulfate
p	para
PnB	pnictogen bonding
ppm	parts per million
quart.	quartet

quint.	quintet
R.T.	room temperature
RCM	ring-closing metathesis
R_f	retention factor
RNA	ribonucleic acid
ROESY	rotating-frame nuclear Overhauser effect correlation spectroscopy
S	entropy
s	second
SAM	surface assembled monolayer
sat.	saturated
sep.	septet
SWV	square wave voltammetry
t	triplet
T	temperature
TBA	tetrabutylammonium
TBTA	tris[(1-benzyl-1,2,3-triazol-4-yl)methyl]amine
TEG	tetraethylene glycol
TFA	trifluoroacetic acid
THF	tetrahydrofuran
TLC	thin layer chromatography
TMS	trimethylsilyl (protecting group)
TrB	tetrel bonding
Ts	tosyl
TTF	tetrathiafulvene
UV	ultra-violet
v/*v*	volume/ volume percent
vdW	van der Waals
vis.	visible
V	volt
VT	variable temperature
WBI	Wiberg bond indices
XB	halogen bonding

TABLE OF CONTENTS

Chapter 1: Introduction 3

1.1 Fundamentals of Anion Supramolecular Chemistry 3

1.1.1 The Field of Supramolecular Chemistry 3

1.1.2 The Importance and Challenges of Anion Recognition 4

1.1.3 Biotic Anion Receptors 6

1.1.4 The Design of Synthetic Anion Receptors 7

1.2 Synthetic Receptors for Anion Recognition and Sensing 18

1.2.1 Hydrogen Bonding Receptors 18

1.2.2 Sigma Hole-donor Anion Receptors 21

1.2.3 Anion Sensing 27

1.2.4 Applications of Anion Binding and Sensing 33

1.3 Syntheses and Applications of Mechanically-Interlocked Molecules 38

1.3.1 The Mechanical Bond 38

1.3.2 Template-directed Syntheses of Interlocked Molecules 39

1.3.3 Applications of Interlocked Molecules 53

1.4 Project Aims 60

1.5 References 61

Chapter 2: Halogen and Chalcogen Bonding Macrocycles and [2]Rotaxanes for Anion Recognition 75

2.1 Introduction 75

2.1.1 CuAAC Active Metal-Templated Synthesis of Interlocked Structures 75

2.1.2 A Neutral All-Halogen Bonding [2]Rotaxane 78

2.1.3 Chapter Aims 79

2.2 Halogen and Chalcogen Bonding Macrocycles and [2]Rotaxanes for Anion Binding 80

2.2.1 Design and Syntheses of Halogen and Chalcogen Bonding Macrocycles 80

2.2.2 Copper(I) Binding Properties of Macrocycles 86

2.2.3 Synthesis and Characterisation of Halogen Bonding [2]Rotaxanes 92

2.2.4 Synthesis and Characterisation of Chalcogen Bonding [2]Rotaxanes 98

2.2.5 Anion Binding Studies with Neutral Halogen and Chalcogen Bonding Rotaxanes 104

2.2.6 Studies of Neutral Halogen Bonding Rotaxanes as Heteroditopic Axle-separated Ion-pair Receptors 112

2.2.7 Anion Binding Studies with Cationic Chalcogen Bonding Macrocycles and Rotaxanes 114

2.2.8 Probing Anion Binding with ChB Hosts using Heteronuclear ^{77}Se and ^{125}Te NMR 123

2.3 A Stable Cationic Tellurium-containing Chalcogen Bonding Motif 126

2.3.1 Design and Synthesis of Model Acyclic Receptor 126

2.3.2 Anion Binding Properties 127
2.3.3 Thermodynamics of Chalcogen Bonding with Anions 133
2.3.4 Towards an Anion-templated Cationic Tellurium-based ChB [2]Rotaxane 137
2.4 Towards Neutral Halogen and Chalcogen Bonding [2]Catenanes 140
2.4.1 Active Metal Template Synthesis of Neutral Halogen Bonding [2]Catenanes 140
2.4.2 Towards a Neutral ChB [2]Catenane by Passive Metal Templation 146
2.5 Conclusions and Future Work 149
2.5.1 Conclusions 149
2.5.2 Future Work 151
2.6 References 152

Chapter 3: Redox-active σ-Hole Donor Host Molecules for Anion Recognition and Sensing 157
3.1 Introduction 157
3.1.1 Theory of Electrochemical Anion Sensing 157
3.1.2 Redox-active Interlocked Host Molecules 158
3.1.3 σ-Hole-Mediated Redox Anion Sensing 161
3.1.4 Chapter Aims 162
3.2 Neutral Ferrocene-Appended Redox-active Rotaxanes 164
3.2.1 Design, Synthesis and Characterisation 164
3.2.2 Anion Recognition Studies 168
3.3 Redox-active σ-Hole Donor Model Host Systems 175
3.3.1 Design and Synthesis of Halogen Bonding Ferrocene Acyclic Receptors 175
3.3.2 Anion Binding and Recognition Studies of Halogen Bonding Receptors 183
3.3.3 A Redox-active Chalcogen Bonding Receptor 196
3.4 A Ferrocene-appended All-Halogen Bonding [2]Rotaxane for Anion Sensing 202
3.4.1 Design, Synthesis and Characterisation 202
3.4.2 ^{1}H NMR Titrations 211
3.4.3 Electrochemical Anion Sensing Studies 213
3.5 Conclusions and Future Work 217
3.5.1 Conclusions 217
3.5.2 Future Work 218
3.6 References 219

Chapter 4: Chiral σ-Hole Donor Host Molecules for Enantioselective Anion Recognition and Sensing 225

4.1 Introduction 225

4.1.1 Theory of Chiral Recognition 226

4.1.2 Enantiospecific Guest Binding in Nature 227

4.1.3 Abiotic Chiral Receptors for Enantioselective Anion Binding and Sensing 228

4.1.4 Chiral Interlocked Structures 229

4.1.5 Chapter Aims 232

4.2 Acyclic (*S*)-BINOL-based Chiral Halogen Bonding Receptors 233

4.2.1 Receptor Design and Syntheses 233

4.2.2 ^{1}H NMR Chiral Anion Recognition Studies 236

4.2.3 Redox Discrimination of Chiral Anions 242

4.2.4 Computational Modelling Studies 245

4.3 Chiral Macrocycles and [2]Rotaxanes for Enantioselective Anion Binding 250

4.3.1 Synthesis of Chiral Macrocycles 250

4.3.2 Chiral Anion Discrimination Studies with Chiral Macrocycles 252

4.3.3 Design and Synthesis of Chiral XB [2]Rotaxanes 260

4.3.4 Stereoselective Anion Binding using Chiral [2]Rotaxanes 269

4.3.5 Towards A Chiral Thiourea-containing [2]Rotaxane 285

4.4 Stereo- and Geometric Discrimination of Dicarboxylates 288

4.4.1 Introduction 288

4.4.2 Acyclic Halogen and Chalcogen Bonding Hosts for Dicarboxylate Recognition 290

4.4.3 A Chiral [3]Rotaxane for Dicarboxylate Binding 300

4.5 Conclusions and Future Work 314

4.5.1 Conclusions 314

4.5.2 Future Work 315

4.6 References 316

Chapter 5: Halogen Bonding Host Systems for Anion Recognition and Sensing in Water 323

5.1 Introduction 323

5.1.1 Recent Strategies for Binding Anions in Water 323

5.1.2 Water-soluble Interlocked Structures 326

5.1.3 Chapter Aims 327

5.2 Water-soluble Dicationic Halogen Bonding Acyclic Receptors 328

5.2.1 Design and Synthesis of Receptors 328

5.2.2 Anion Binding Studies 331

5.2.3 Binding and Sensing of Biologically-relevant Phosphates 336

5.2.4 Electrochemical Sensing of Redox-active Anions in Water 341

5.3 Towards a Polyether-stoppered Water-soluble [2]Rotaxane 343

5.4 Pyrrole-based Halogen Bonding Hosts for Anion Binding in Water 349

5.4.1 Introduction 349
5.4.2 Design and Synthesis of Pyrrole Hosts 350
5.4.3 Anion Binding Studies in Aqueous-Organic Mixtures 354
5.4.4 Binding of Phosphate Derivatives in Buffered Water 359
5.5 Conclusions and Future Work 361
5.6 References 363

Chapter 6: Conclusions 369

Chapter 7: Experimental 375
7.1 General Considerations 375
7.1.1 Instrumentation 375
7.1.2 ^{1}H NMR Titration Protocols 375
7.1.3 Optical Titration Protocols 376
7.1.4 Electrochemical Titration Protocols 377
7.3 Synthetic Procedures 378
7.3.1 Solvents and Reagents 378
7.3.2 Synthesis of Novel Compounds from Chapter 2 379
7.3.3 Synthesis of Novel Compounds from Chapter 3 413
7.3.4 Synthesis of Novel Compounds from Chapter 4 448
7.3.5 Synthesis of Novel Compounds from Chapter 5 488
7.4 References 507

Appendices 511
A. Crystallographic data 511
B. Electrochemical Reversibility Studies 514
C. Computational Simulations 534
References 567

Chapter 1

Introduction

CHAPTER 1: Introduction

1.1 Fundamentals of Anion Supramolecular Chemistry

1.1.1 The Field of Supramolecular Chemistry

> *"The 21st century will be the century of complexity. We have already discovered the basic laws that govern matter…there is no limit to the complexity that we can build using these basic laws."* – Stephen W. Hawking

Supramolecular chemistry, the study of non-covalent intermolecular interactions and their applications in the construction of complex multi-component molecular architectures and functional systems, embraces the concept of 'complexity' at its very core.[1,2] Arguably, the birth of the field was heralded by the seminal work of Pedersen,[3] Lehn[4,5] and Cram[6] in their study of cation binding using crown ethers, cryptands and spherands respectively (Figure 1.1A-C), earning them the 1987 Nobel Prize in Chemistry. Supramolecular chemistry broadly comprises of two main themes: (1) self-assembly, the spontaneous association of small molecules into larger and more complex structures, and (2) host-guest chemistry, the selective recognition and binding of one chemical entity to another. From its humble beginnings, the last two decades have witnessed dramatic advancements leading to the development of numerous interrelated sub-fields of specialisation, including molecular nanotechnology,[7–10] biomaterials,[11–13] chemical analytics and sensing[14,15] and systems chemistry.[16] In addition to the present possibility of constructing super-molecules in a rational manner from appropriately-functionalised molecular components due to these advancements (Figure 1.1D), a subtle paradigm shift is also ongoing where supramolecular chemists are now gradually moving away from traditional thermodynamically-driven assemblies to take advantage of diverse possibilities offered by non-equilibrium systems.[17] Indeed, the tremendous importance and potential in this highly interdisciplinary field has been very recently recognised by yet another Nobel Prize in Chemistry for "*the design and synthesis of molecular machines*" in 2016.[18]

Anion supramolecular chemistry, the subject of this thesis, has witnessed tremendous recent advances in fundamental understanding and applications such as anion-templated assembly, catalysis, molecular machinery and biology.[19,20] Accordingly, this chapter will focus

first on the fundamental aspects of anion recognition, followed by an introduction to template-directed assembly of mechanically-interlocked molecules (MIMs). Particular emphasis will be placed on the uses of sigma (σ)-hole interactions such as halogen and chalcogen bonding, as well as the applications of anion recognition and interlocked structures − the main leitmotifs occurring recurrently through the work presented in this thesis.

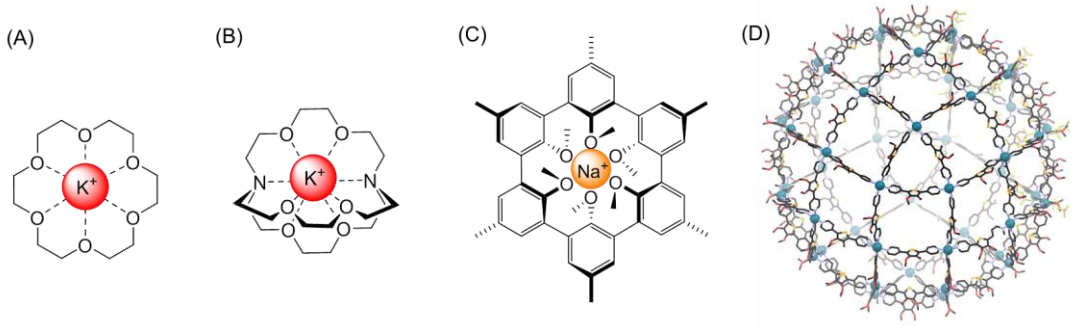


Figure 1.1. *Structures of (A) crown ether;[3] (B) cryptand[4] and (C) spherand;[6] (D) Fujita's Goldberg polyhedra formed from the rational self-assembly of 30 metal centres and 60 ligands.*[21]

1.1.2 The Importance and Challenges of Anion Recognition

Anions play crucial roles in nature, and consequently, are omnipresent in the biosphere. In biology, many key biomolecules are large polyanions. These include DNA and RNA, which govern transmission and translation of genetic information, enzymes in metabolic pathways (e.g. β-galactosidase),[22] as well as nucleoside triphosphates such as ATP, the 'energy currency' of cells.[23] In addition, smaller oxoanions such as glutamate and aspartate function as neurotransmitters, whilst lactate, pyruvate and oxaloacetate are important metabolic intermediates. Interestingly, the highly-reactive superoxide anion ($O_2^{\bullet-}$) is produced by phagocytes in the human immune system as part of an oxidative protective mechanism against invading pathogens.[24] Mineral anions such as chloride maintain physiological electrolyte balance, and hereditary mis-regulation of chloride transmembrane transport processes can cause cystic fibrosis.[25] Environmentally, anthropogenic activities have led to elevated concentrations of anionic pollutants.[26] For instance, excessive use of nitrate and phosphate fertilisers in agriculture has resulted in eutrophication in water bodies.[27] Improper regulations of human industrial activities have resulted in increased influx of highly-toxic azide, cyanide, perchlorate and transition metal-based oxoanions into the biosphere. The latter are

particularly harmful, including the radioactive pertechnetate ($^{99}TcO_4^-$) nuclear fuel-reprocessing by-product,[28] as well as perrhenate (ReO_4^-)[29] and chromate (CrO_4^{2-})[30] from manufacturing processes. As excessive quantities of these pollutants lead to environmental degradation and adversely affect human health, research into anion binding, sensing and sequestration remains highly pertinent and relevant in today's world.

Despite their importance, several intrinsic properties of anions pose formidable challenges for binding and recognition, especially in water. Firstly, anions can be pH-sensitive, and can be protonated under acidic conditions and lose their negative charge. Examples include oxoanions such as phosphate and their biological derivatives, hence potential receptors designed for them can only function effectively within a narrow pH window.[31] Highly basic anions such as fluoride and carboxylates can abstract acidic protons from receptor molecules to become protonated themselves. In addition, compared to their isoelectronic cations, anions are larger in size (radii of 1.81 Å for Cl^- versus 1.37 Å for K^+), resulting in lower charge densities and consequently, weaker electrostatic and ion-dipole interactions with receptor molecules. Anions also exhibit a diverse range of geometries (Figure 1.2), thus requiring host molecules with elaborate designs to achieve shape and size match for optimal binding selectivity. Finally, anions exhibit vastly varying free energies of solvation, which are highly dependent on the nature of the anion and the solvent. In protic solvents such as water, anions are hydrated to different extents, as reflected by the Hofmeister series of anion hydrophobicity (Figure 1.3).[32] From left to right of the series, the charge density of anions decrease, resulting in increasing lipophilicity and weaker hydration.[33] Thus, for anion recognition in water, the extent of anion hydration must be taken into consideration during the receptor design, since the host molecule will have to compete with and displace the water molecules in the anion hydration shell for effective anion binding. Contrastingly, in aprotic

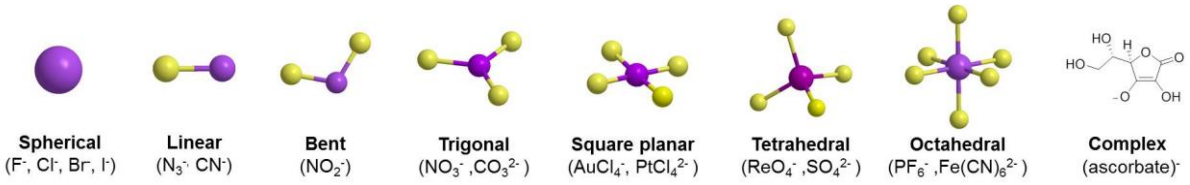


Figure 1.2. *Possible geometries adopted by anions.*

organic solvents with low dielectric constants such as chloroform, ion-pairing between the anion and its counter-cation becomes an important association which needs to be overcome for host-guest anion recognition to occur.[34]

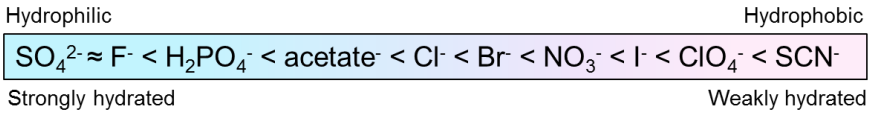


Figure 1.3. *The Hofmeister series.*

1.1.3 Biotic Anion Receptors

The abundance of various anions in the biosphere and their biological importance have led to the evolution of proteins capable of binding specific anions with exquisite selectivity over others in aqueous environments. Two important binding motifs present within natural anion binding cavities have been identified: the 'nest' and the $C^{\alpha}NN$ (Figure 1.4A). The former occurs with a minimum of two amino acid residues with alternating main-chain dihedral angles of -90 ^{o} and 70 ^{o},[35] and can be extended to include more residues in motifs such as the P-loop, abundant in ATP and GTP binding domains.[36] Structurally very similar, the $C^{\alpha}NN$ motif comprises of hydrogen bonds from two neighbouring main-chain amide linkages and an adjacent alpha-carbon, and has been found in phosphate recognition.[37] Moreover, the nature of the anion binding site complements the target anion's hydrophilicity. Strongly hydrated anions are often bound in sites containing metal cations such as Ca^{2+} [33] or in binding sites containing multiple convergent hydrogen bonding interactions such as that for SO_4^{2-} in the sulfate binding protein[38] of *Salmonella typhimurium* (K_d = 0.12 *μm*)[39]. Conversely, poorly-hydrated anions such as Br^- and I^- are often bound in sites containing weakly-hydrated residues such as lysine, proline and leucine.[40] Very recently, Whitesides and co-workers noted that perturbation of the water structure within carbonic anhydrase II by anions can also significantly influence the free energy of the binding process. [41]

Finally, impressive anion selectivity is achieved by binding site geometries designed to complement the target anion perfectly. This is best illustrated with the phosphate binding protein of the GFAJ-1 bacteria, which is able to discriminate phosphate with a 4500-fold selectivity over arsenate in water, an impressive feat considering that the two oxoanions share

identical charge, almost identical pK_a values and hydration enthalpies. Bound in their monoprotonated forms, the origin of selectivity arises from a subtle 4 % size difference between these two anions which results in a steric clash by $HAsO_4^{2-}$ with a leucine residue (Leu9) in the binding site, distorting a hydrogen bond from the –OH group of the anion to a proximal aspartate (Asp62) side chain. In contrast, all interactions are perfectly orientated for HPO_4^{2-} (Figure 1.4B).[42]

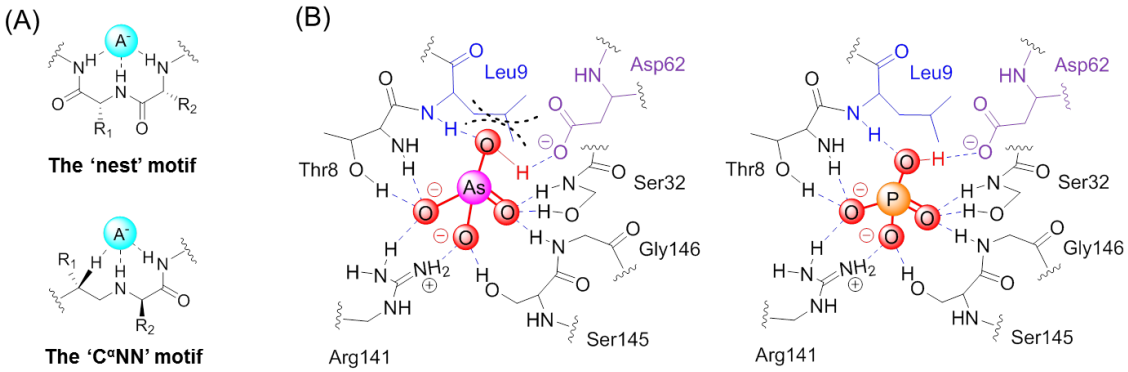


Figure 1.4. *(A) The 'nest' and 'CNN' anion binding motifs;*[35,37] *(B) The molecular basis of discrimination between* HPO_4^{2-} *and* $HAsO_4^{2-}$ *by the phosphate binding protein showing the different steric interactions within the protein binding site.*[42]

1.1.4 The Design of Synthetic Anion Receptors

1.1.4.1 General Considerations

The strategies adopted by natural biotic host structures for anion binding have served as valuable blueprints for the design of synthetic abiotic anion receptors. Common features of highly selective biotic anion receptors are their structurally-rigid and well-defined three dimensional binding cavities capable of completely encapsulating their guest anions, as well as judiciously-placed functional groups able to interact with their guests in a geometrically-optimal manner. Researchers have hence distilled the essentials of these features into the following concepts, which also underpin the entirety of supramolecular chemistry:

Complementarity: When interacting chemical entities are geometrically complementary to each other, the strengths of non-covalent interactions between them can be maximised. First proposed by Fischer in the late 19th century in the 'lock and key' hypothesis to

describe specific substrate recognition by enzymes, molecular hosts (lock) are frequently designed such that their binding cavities matches their guests (key) in shape and size.

Preorganisation and the macrocyclic effect: The concept of preorganisation was first introduced by Cram in the 1980s,[6] who recognised that the most stable host-guest complexes were formed with host molecules possessing the most favourable conformations before guest binding. This is manifested in the 'macrocyclic effect', where macrocyclic hosts possessing enclosed structural frameworks often bind guests more strongly than their acyclic counterparts due to their greater rigidity. Thus, the binding of a guest results in fewer degrees of freedom being lost upon complexation. In addition, by being structurally well-defined and rigid, macrocycles offer better shape and size complementarity to the guest than acyclic hosts, giving rise to more favourable binding enthalpies.

1.1.4.2 Non-covalent Interactions Employed for Anion Binding

Alongside structural preorganisation and complementarity, biological anion receptors employ a range of non-covalent interactions to enhance anion binding affinity and selectivity. While hydrogen bonding is the most prevalent, other interactions such as electrostatics, coordinate bonds with Lewis acidic metal centres and solvophobic interactions are often found. However, much less common in nature for anion recognition are anion-π and σ-hole interactions such as halogen bonding. The following sections survey the non-covalent interactions relevant for anion binding in greater detail.

***Electrostatic attractions*:** These include ion-ion and ion-dipole interactions (Figure 1.5). Ion-ion interactions occur via Coulombic attraction between oppositely-charged species, which are very strong but non-directional, with a small distance (r) dependence ($E \propto r^{-1}$). Ion-dipole

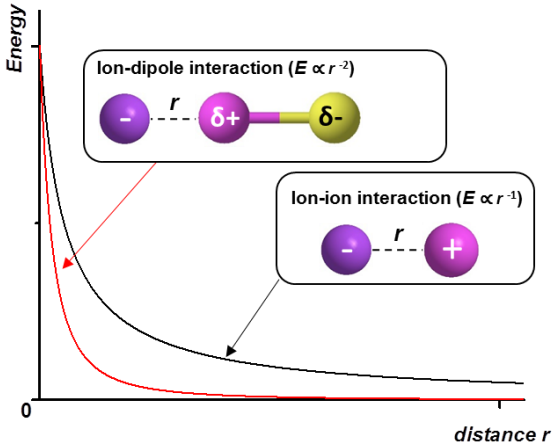


Figure 1.5. *Distance dependence of ion-ion and ion-dipole interactions.*

interactions, which include hydrogen bonding and sigma-hole interactions, are significantly weaker and are only effective at short-distances ($E \propto r^{-2}$). However, their more pronounced directionality has been exploited to achieve anion binding selectivity. To enhance the strength of ion-dipole interactions, anion receptors often bear positive charges as well.

***Hydrogen Bonding*:** When a hydrogen atom is covalently bonded to an atom more electronegative than itself (e.g. C, N, O, F), a permanent dipole is formed as electron density is drawn away from the hydrogen atom. The resulting electron-deficient hydrogen atom can then interact attractively with a Lewis base such as an anion. This interaction, termed hydrogen bonding (HB), can vary dramatically in strength depending on the interacting system (from 1 kJ mol^{-1} in $CH_4 \cdots F\text{-}CH_3$ [43] to 162 kJ mol^{-1} in HF_2^-)[44]. In addition, strong hydrogen bonds tend to exhibit a higher degree of linearity than weak ones, with a large range of possible A-H···:B bond angles for the latter.[45] Hydrogen bonding (HB) is thought to be a largely electrostatic interaction, with polarisation, dispersion and charge-transfer being small but significant contributions.[46] Owing to its strength, directionality and plethora of readily-accessible donor motifs, HB is the most ubiquitous non-covalent interaction in natural and artificial molecular recognition (Section 1.2.1), playing important roles in virtually every aspect of chemistry and biology.

***Solvophobic Interactions*:** In protic solvents such as water, non-polar molecules interact weakly with the solvent. Therefore, they tend to aggregate with each other to minimise the total energy of the system. Also termed the 'hydrophobic effect' in water, this phenomenon is currently still poorly understood, but is increasingly recognised to play important roles in biomolecular interactions[47] and host-guest recognition in water.[48] The 'classical' hydrophobic effect is mainly an entropically-driven process due to the release of water molecules in the hydration shells of the host and guest during their association.[49] Contrastingly, the 'non-classical' hydrophobic effect is characterised by a dominant enthalpic contribution, arising from the liberated water molecules forming hydrogen bonding networks with the bulk water.[50,51]

The exploitation of the hydrophobic effect for anion binding in water, while presently under-developed, has led to notable successes in recent years. Host molecules relying on this effect typically have deep hydrophobic cavities capable of shielding the bound anions from bulk water, with higher affinities for large, charge-diffuse and poorly-hydrated anions such as I^- and ClO_4^- (Figure 1.3). For example, γ-cyclodextrin was found to bind the dodecaborate cluster ($B_{12}Br_{12}^{2-}$) strongly in pure water (K_a = 960 M^{-1}) (Figure 1.6A),[52] Sindelar's bambusuril macrocycle binds I^- and ClO_4^- with affinities exceeding 10^7 M^{-1} in aqueous phosphate buffer (pH 7.1) (Figure 1.6B),[53] and Gibb's octa-acid cavitand (Figure 1.6C) shows significant affinity for the typically non-coordinating PF_6^- anion (K_a = 790 M^{-1}) in phosphate buffer at pH 11.3.[54] It is notable that the last two hosts display high anion affinities despite their polyanionic character. Interestingly, Gibb was able to increase the affinity of the poorly-hydrated ClO_4^- anion to the same cavitand by the presence of a hydrophilic co-salt (NaF or NaCl) in the aqueous medium. This was attributed to an increase in the ionic strength of the solution by the presence of the co-salts, enhancing the hydrophobic interactions driving ClO_4^- encapsulation.[55,56] Importantly, anion binding by these three systems are characterised by notable gains in enthalpy and losses of entropy, characteristics of the 'non-classical' hydrophobic effect and suggesting significant structure recovery in bulk water.

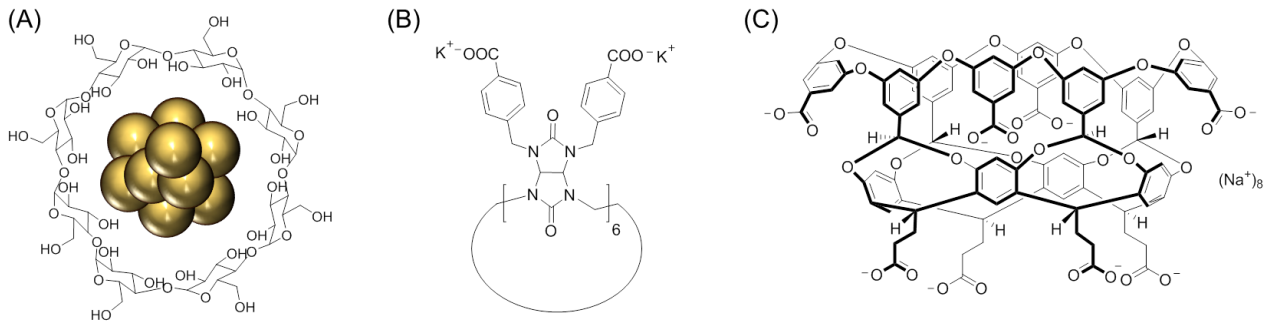


***Figure 1.6**. (A) γ-cyclodextrin encapsulation of a $B_{12}Br_{12}^{2-}$ cluster[52]; (B) Sindelar's bambusuril macrocycle[53] and (C) Gibb's octa-acid cavitand.[54]*

***Anion-π Interactions*:** This weak and presently poorly-exploited interaction occurs when an electron-deficient aromatic system interacts with an anion. Misleadingly, the π electrons of the aromatic system do not actually interact with the anion, as computational studies have shown

that the interaction arises largely from electrostatics and anion-induced polarisation effects.[57,58] These effects are maximised in non-polar aprotic solvents with small, charge-dense anions (e.g. F^-, Cl^-, OH^-), allowing close approach to the aromatic ring system. X-ray crystallographic studies have revealed the multiple hapticities of the interaction, where the anion can reside in various positions above the plane of a C_6 planar ring-system.[59,60] Indeed, the interaction energies show little variation when the position of the anion is changed within the *xy*-plane, but decrease significantly with increasing distance from the ring along the *z*-plane (Figure 1.7A).[61,62] Common electron-deficient aromatic systems for anion-π interactions include triazines, perfluoroarenes and the naphthalene diimide (NDI) motifs. Triazine and perfluoroarene groups were incorporated into a macrocycle by Wang which bound F^- and N_3^- exclusively in acetonitrile (K_a > 1000 M^{-1}) (Figure 1.7B),[63] while the NDI motif has been integrated into a molecular tweezer selective for F^- in DMSO (Figure 1.7C). Interestingly, the latter also exhibited a colorimetric response in the presence of F^- arising from charge-transfer interactions between the anion and NDI unit.[64]

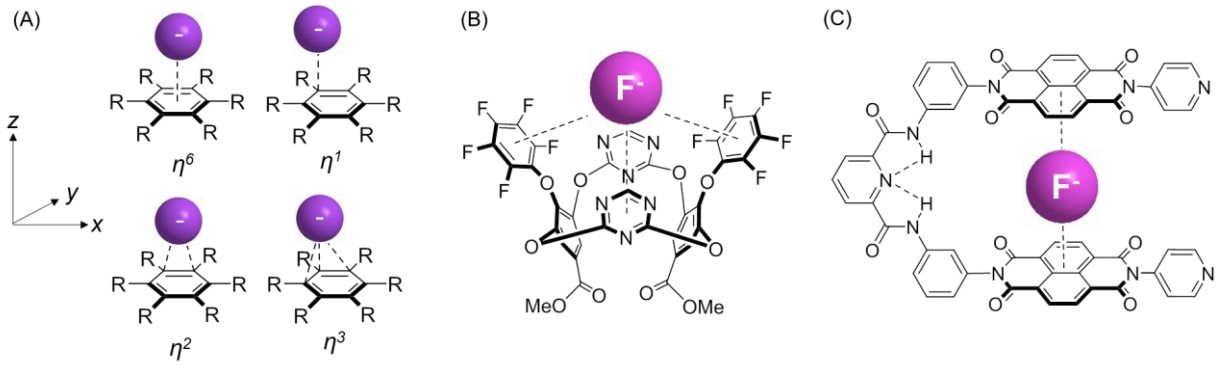


Figure 1.7. *(A) Hapticity of anion-π interactions; (B) Triazine- and perfluorobenzene-containing macrocycle by Wang*[63] *(C) Molecular tweezer incorporating the NDI motif for anion-π interactions.*[64]

***Coordinate Bond*:** This interaction between a Lewis acidic atom and a base such as an anion contains significant orbital overlap, and hence is not strictly non-covalent. Common neutral and cationic Lewis acid motifs include main group elements such as boron[65,66] and antimony,[67] transition metal cations such as Zn^{2+},[68] Ni^{2+} and Cu^{2+} [69] as well as lanthanide cations (Figure 1.8A).[70] Most effective with small and high charge-density anions (e.g. F^-) and strongly-

nucleophilic anions (e.g. N_3^-, CN^-), the directionality and strength of this interaction enables very strong and selective anion binding even in water. For instance, Gabbaï recently reported that a neutral bidentate antimony(V)-containing receptor[71] can bind F^- selectively over other anions in water between both Sb atoms, which is especially impressive given the anion's large hydration enthalpy (Figure 1.8B).[72] Interestingly, a recent computational study suggested that alkali earth metals such as beryllium, when integrated into small molecular structures, can also achieve very strong binding affinities with a variety of halides and oxoanions.[73]

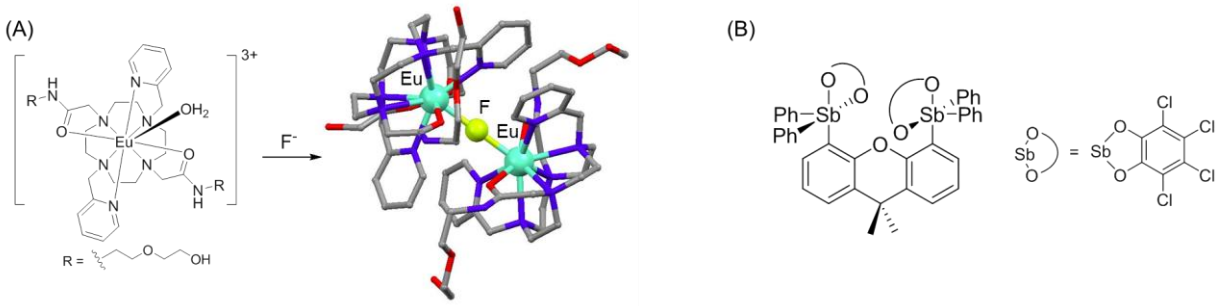


Figure 1.8. *(A) Parker's tricationic europium complex for F^- sensing[70]; (B) Gabbaï's bidentate antimony receptor for F^-.[71]*

1.1.4.3. Sigma (σ)-Hole Interactions

When a main group atom (donor atom A) is covalently bonded to a chemical functionality (Y) more electronegative than itself, electron density is drawn away from atom A such that a region of positive electrostatic potential, called a *σ*-hole, is formed collinear with the Y-A bond. This anisotropic distribution of electron density in the presence of electron-withdrawing groups has been observed empirically and computationally on many atoms belonging to Groups 14 (tetrel), 15 (pnictogen), 16 (chalcogen), 17 (halogen) and 18 (aerogen),[74] as shown in Figure 1.9. Consequently, the *σ*-hole formed can interact attractively with a Lewis base such as an anion, giving rise to what is termed as a '*σ*-hole interaction'. While the most familiar *σ*-hole interaction is halogen bonding (XB),[75–77] the other sister interactions have only very recently started to attract significant research attention, particularly with chalcogen bonding (ChB). From an orbital perspective, the *σ*-hole also corresponds to the location of the *σ**-antibonding orbital of the Y-A bond. Hence, when a *σ*-hole interacts non-covalently with a Lewis base such as an anion, concomitant lengthening of the Y-A covalent bond is observed.[78] While this

suggests a significant charge-transfer contribution to the σ-hole interaction,[79,80] electrostatic[81,82] and dispersion components also play significant roles,[83] and their relative contributions are likely to be highly dependent on the nature of the interacting σ-hole donor and acceptor atoms.[84] Importantly, the σ-hole interactions have shown comparable, or slightly greater binding strengths than hydrogen bonding.[85] Owing to the highly-localised σ-holes on the donor atoms, these interactions exhibit much greater Y-A···L linear directionality than hydrogen bonds, showing more drastic decreases in binding energies with increasing deviations from ideal binding geometries.[86] Furthermore, their binding strengths can be readily tuned by changing the nature of donor atom A and electron-withdrawing group Y, with more electropositive σ-holes formed when Y is more electronegative and atom A is more polarisable.[87,88] In addition to these properties, the greater hydrophobicity and contrasting solvation properties of the σ-hole donor atoms compared to hydrogen bond donors, as well as their pH independence and greater tolerance to basic conditions, also offer interesting opportunities for exploitation in supramolecular chemistry which complement the ubiquitous hydrogen bonding interactions.

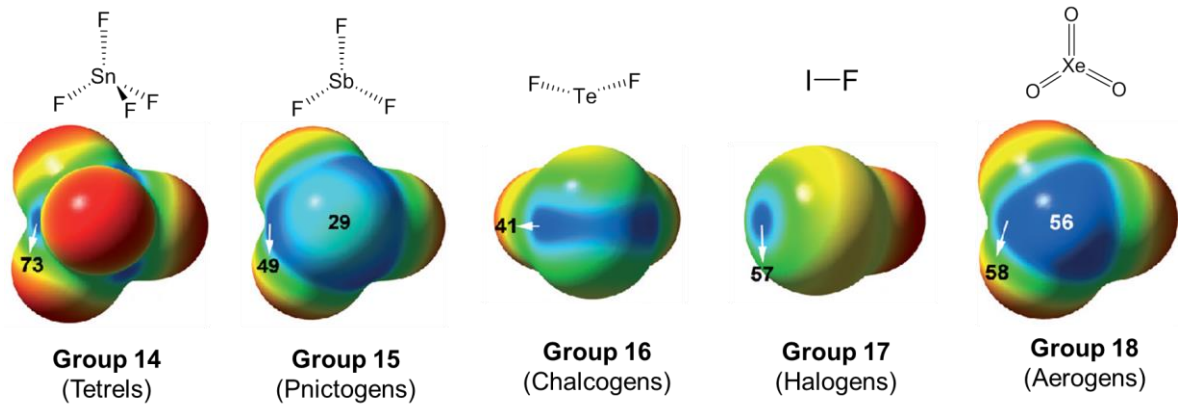


Figure 1.9. *Computed molecular electrostatic potential (MEP) surface (MP2/aug-cc-pVTZ level) showing the locations of σ-holes (in blue) on electron-deficient Group 14 - 18 elements. MEP values of σ-holes are indicated in kJ mol^{-1}. Reproduced from reference 89.*

Halogen bonding. Recently defined by IUPAC to occur when '*there is evidence of a net attractive interaction between an electrophilic region associated with a halogen atom in a molecular entity and a nucleophilic region in another, or the same, molecular entity*',[90] halogen bonding (XB) was first observed in the 19th century,[91] and demonstrated crystallographically in

1954 by Hassel.[92] However, the interaction has only been extensively studied within the last two decades, particularly in the solid state for crystal engineering due to ease of geometry control arising from strict linearity,[93,94] which has also led to numerous applications in solid-state functional materials.[75,95,96] Exhibiting a wide range of binding energies spanning 10-200 kJ mol^{-1},[84] subsequent solution-phase studies have also shown that XB interactions are more tolerant to solvent polarity than hydrogen bonds,[97] with more pronounced covalency.[98] As such, XB interactions have also been successfully applied in solution-phase applications such as self-assembly,[77,99,100] catalysis,[101] gelation,[102,103] medicinal chemistry[104] and molecular recognition.[84,105,106] Notable recent XB-related discoveries include their unprecedented use to switch the spin state of ground-state triplet diphenylcarbene to the singlet state by stabilising the latter, potentially altering its reactivity,[107] stabilizing explosive compounds,[108] and unexpected non-covalently interacting with a Pt(II) centre of a metal complex in the solid state.[109] For anion recognition applications, Resnati and Metrangolo's seminal report[110] of a neutral XB heteroditopic receptor for NaI in 2005 (Figure 1.10) marked the beginning of a decade of research seeing dramatic advances in the exploitation of XB in anion receptors, which will be covered in greater detail in Section 1.2.2.1.

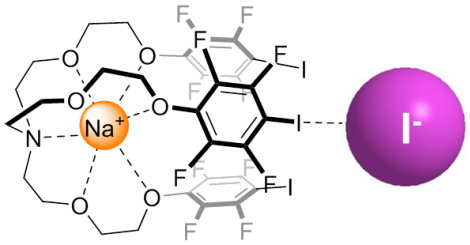


Figure 1.10. *Resnati and Metrangolo's heteroditopic XB receptor for NaI.*[110]

***Chalcogen bonding*.** This refers to the analogous attractive σ-hole interaction between an electron-deficient chalcogen atom and a Lewis base. In contrast with halogens, chalcogen atoms can be either sp^2 or sp^3 hybridised, resulting in the formation of either one or two σ-holes in the presence of electron-withdrawing substituents (Figure 1.11). Consequently, chalcogen bonding (ChB) interactions involving sp^3 chalcogen atoms have Y-A···L bond angles around 80° and 170°, while sp^2 chalcogens display more linear geometries.[111] Although ChB interactions are presently far less-studied than XB, they have been identified as important contributors to the biological activities of organo-sulfur[112,113] and organo-selenium

compounds,[114] implicated in stabilizing folded protein structures[115,116] and regulating enzymatic activities.[117,118] Owing to their unique geometric and steric properties which differ from XB, ChB interactions have been recently employed in crystal engineering,[119] conducting materials,[120,121] organocatalysis[122,123], self-assembly[124] and reactivity.[125] Inspired by numerous solid-state structures showing significant short contacts between chalcogen atoms and anions,[126–128] indicating the presence of substantial non-covalent interactions, the applications of ChB in solution-phase anion recognition is just beginning to be explored (see Section 1.2.2.2). Nevertheless, although the heavier chalcogen atoms, especially tellurium, are more effective ChB donors due to greater polarizability, their air and moisture sensitivity[129] arising from weak C-Te bonds (bond strength c.a. 200 kJ mol^{-1})[130] have severely limited their study to simple acyclic molecules. The search for heavy chalcogen-containing ChB-donor motifs stable enough to withstand chemical manipulation for incorporation into more complex structures is currently a major obstacle to the realisation of the full potential of ChB in supramolecular chemistry.

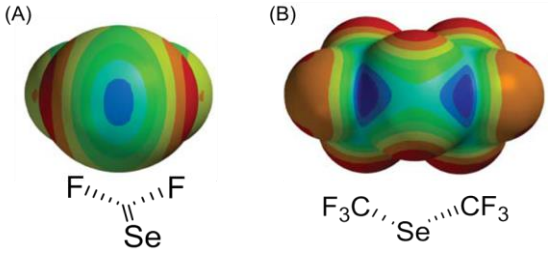


Figure 1.11. *Computed MEP surface showing the presence of (A) one σ-hole (in blue) on an sp^2-hybridised Se atom and (B) two σ-holes on an sp^3-hybridised Se atom. Diagram reproduced from reference 111.*

Pnictogen, tetrel and aerogen bonding currently represent virgin areas of research, and hence, very little is known about these poorly-studied *σ*-hole interactions. Their anion binding properties are presently studied only exclusively in the solid state and computationally[131,132]. With pnictogen (PnB) and tetrel bonding (TrB), several issues arise which increases the difficulty of their empirical study. Firstly, due to the increasing steric bulk of substituents around three- or four-ccordinate pnictogen and tetrel atoms respectively, the electropositive *σ*-holes may not be sufficiently exposed to enable significant interaction with Lewis bases. Secondly, the heaviest members of the pnictogen (Sb, Bi) and tetrel families (Sn, Pb), for which the strongest *σ*-hole interactions are expected, have significant metallic character, and hence participate in more traditional metallic coordination chemistry[133–135].

Examples of PnB interactions with anions in the solid state are scarce, with the complex shown in Figure 1.12A being a rare example that shows a short contact between Br^- and an electrophilic phosphorus PnB-donor atom.[136] However, computational studies have revealed that the PnB interaction strength is comparable to those of XB and ChB interactions using *σ*-hole-donor elements of the same Period with the same electron-withdrawing substituents.[137] More recently, a more detailed computational study of halide (F^-, Cl^-, Br^- and I^-)-PnB interactions using a bidentate model system (Figure 1.12B) also revealed strong binding affinities. The anion-PnB interactions were found to display classic characteristics of *σ*-hole interactions, i.e. *σ*-hole-dictated binding geometries, carbon-pnictogen bond of the receptor lengthening upon anion binding, and enhanced binding strength using larger pnictogen donor atoms for more charge dense halides. Interestingly, by changing donor atom from a chalcogen (sulfur) to pnictogen (phosphorus), an increase in anion binding energy of up to 10 kJ mol^{-1} was observed.[138] Notwithstanding the present dearth of viable PnB donor motifs, recent synthetic advances allowing access to electron-deficient aromatic triaza-phospholes[139–141] and triaza-arsoles[142] (Figure 1.12C) may offer new possibilities to study PnB-anion interactions in both solid and solution phases.

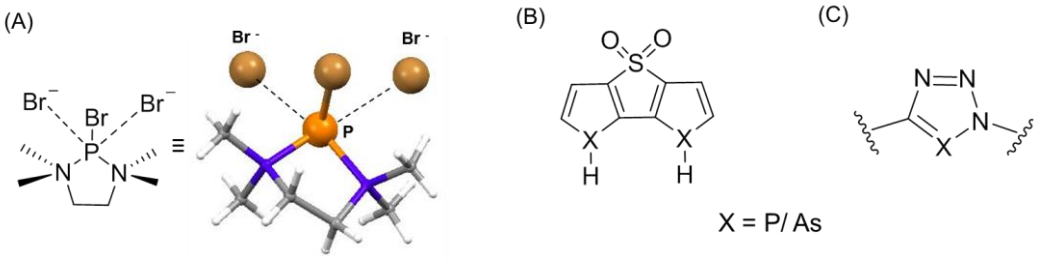


Figure 1.12. *(A) PnB interactions between an electrophilic P atom and bromide anions[136]; (B) Scheiner's bidentate model PnB receptor[138]; (C) Structure of potential PnB-donor motifs triaza-phospholes and triaza-arsoles.*

Tetrel bonding (TrB) with anions in the solid state has been observed with Lewis acidic silyl derivatives. In 2001, a dicationic disiloxane derivative was found to display bifurcated TrB interactions with a Cl^- anion (Figure 1.13A),[143] with Si···Cl^- distances considerably longer than that of an Si-Cl covalent bond,[144] but shorter than the sum of their van der Waals radii. Separately, Taylor and co-workers showed that the presence of F^- could improve the yields of spherosilicate synthesis, and isolated a complex where a F^- was trapped centrally within an

octasiloxane cage with eight symmetric Si···F^- TrB interactions (Figure 1.13B).[145] In another intriguing example, six simultaneous Si···halide (Cl^-, Br^- and I^-) TrB interactions with perhalogenated cyclohexasilane rings was found to planarise the original chair-conformation of the rings, increasing accessibility of the *σ*-holes on the Si atoms which interact with the halides to form 'inverse sandwich complexes' (Figure 1.13C).[146,147] Not just limited to silicon, the presence of *σ*-holes on carbon atoms capable of participating in TrB interactions with anions have also been suggested using cyclopropanes bearing electron-withdrawing substituents,[148,149] as well as on the trifluoro-substituted carbon atom of trifluorotoluene.[150]

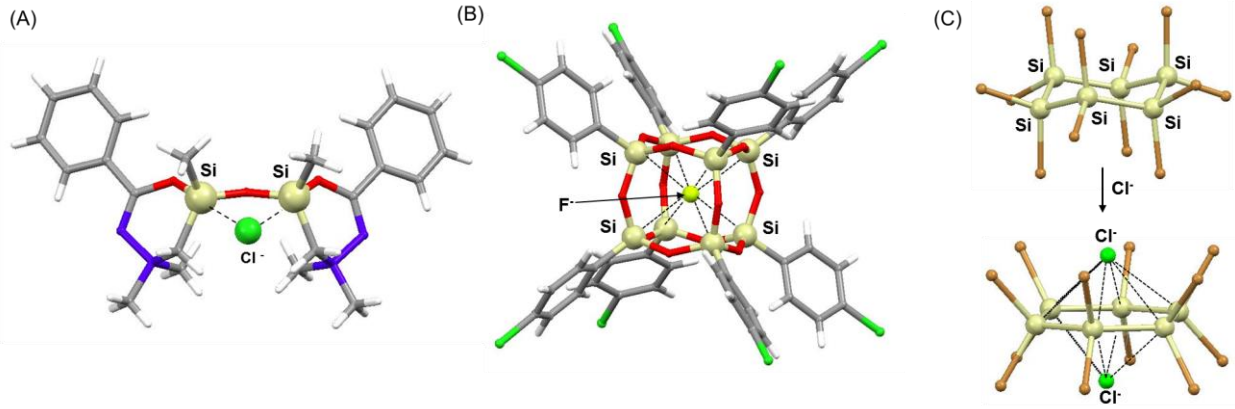


Figure 1.13. *(A) Kost's silicon complex showing two Si···Cl^- TrB interactions[143](B) Taylor's octasiloxane cage showing 8 Si···F^- TrB interactions[145]; (C) Chloride-induced planarity of Si_6Br_{12} cyclohexasilane.[147] All short contacts are shown by the dashed lines.*

Finally, aerogen bonding (AeB) represents the ultimate *σ*-hole interaction with noble gases as donors, first suggested by Frontera in 2015 based on crystallographic evidence of short contacts between XeO_3 molecules in the solid state,[151] interactions between XeF_2O and acetonitrile,[152] as well as that between $[C_6F_5XeF_2]^+$ and fluorine atoms of HF.[153] Although computational studies have indicated strong AeB interactions between XeO_3 and XeF_2O with Cl^- and Br^-,[89] and the possibility of AeB strengthening XB interactions very recently,[154] it is unlikely that AeB will see extensive applications in the near future due to the difficulty of incorporating nobel gases into host molecules and the inherent chemical instability of the resulting compounds.[155]

1.2 Synthetic Receptors for Anion Recognition and Sensing

Synthetic anion receptors, which can be either neutral or cationic, have been prepared containing a diverse range of chemical functionalities and structural complexities, ranging from simple acyclic molecules to elaborate multi-component interlocked systems. While neutral host molecules are employed to function largely in relatively non-polar aprotic organic solvents, the high dielectric constants and free energies of anion solvation in protic solvents such as water necessitates the use of Coulombic forces to effectively compete with the solvent for anion complexation. Due to advances in fundamental understanding over the last decades and with 'real-life' applications in mind, recent years have seen increasingly greater attention on receptors capable of strong and selective anion complexation in pure water or competitive aqueous-organic solvent mixtures,[19] which incorporate cationic motifs capable of strong, yet directional *charge-assisted* ion-dipole interactions with anions. Other than hydrogen bonding (Section 1.2.1), the most common ion-dipole interaction exploited in synthetic receptors, motifs for *σ*-hole interactions (especially XB) have also been increasingly incorporated into synthetic anions receptors (Section 1.2.2) to exploit their unique properties which complement those of HB interactions (Section 1.1.4.3). Occurring in parallel with these developments in fundamental anion recognition are anion sensors, which are receptor molecules capable of producing a detectable output signal (change in electrochemical, colorimetric, fluorescent or bulk viscosity properties) in the presence of anions (Section 1.2.3).

1.2.1 Hydrogen Bonding Receptors

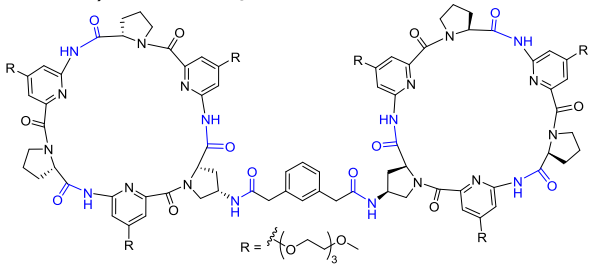
A multitude of HB-donors motifs have been incorporated into synthetic anion hosts. These functionalities can be either neutral or cationic, and include both C-H and N-H donors. Common HB-donor motifs and representative examples are collected in Table 1, with the relevant functional groups highlighted in blue.

Table 1.1. Common Hydrogen Bonding Anion Recognition Motifs and Examples.

Neutral hydrogen bonding motifs

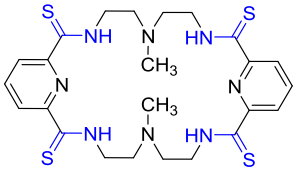
Amide

- Common anion binding motif found in nature and popular in synthetic receptors due to its easy accessibility.
- Kubik's cyclo-peptide 'molecular oyster' receptor sandwiches anions between both rings via convergent HB interactions, which shows high affinity for SO_4^{2-} (lgK_a = 3.70 ± 0.05) in H_2O/ CH_3OH 95:5 *v/v*:[156]



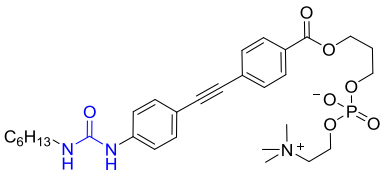
Thioamide

- Thioamides are stronger HB donors than amides but are more prone to deprotonation.
- Bowman-James' polythioamide macrocycle shown to bind $H_2PO_4^-$ and HSO_4^- strongly (lgK_a ≈ 5.0 for both) in DMSO:[157]



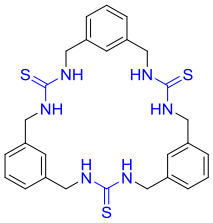
Urea

- Parallel HBs are optimal for binding Y-shaped anions (e.g. carboxylates).
- Urea-containing phospholipid analogue binds HCO_3^- selectively over NO_3^-, $H_2PO_4^-$ and Cl^- in CH_2Cl_2:[158]



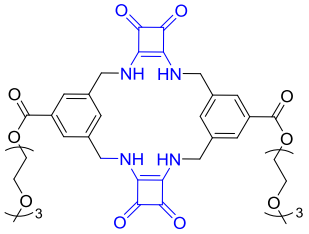
Thiourea

- More acidic and easier to deprotonate than ureas.[159]
- Tris-thiourea macrocycle binds acetate and $H_2PO_4^-$ preferentially over Cl^- and N_3^- in DMSO:[160]



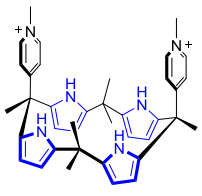
Squaramide

- More acidic and stronger HB donors than thioureas.
- Favourable for binding Y-shaped and tetrahedral oxoanions.[161]
- Jolliffe's squaramide macrocycle binds SO_4^{2-} selectively in water/ DMSO 1:2 *v/v*:[162]



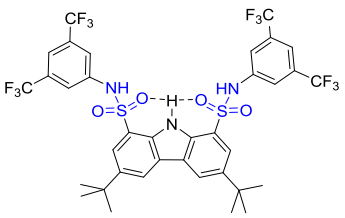
Pyrrole

- Often found in groups of pyrrole units, together with other functional groups such as amide,[163] or in larger aromatic systems such as carbazoles[164] and expanded porphyrins.[165]
- Sessler's calix[4]pyrrole derivative binds pyrophosphate ($HP_2O_7^{3-}$) strongly (K_a = 2.6 x 10^7 M^{-1}) in acetonitrile:[166]



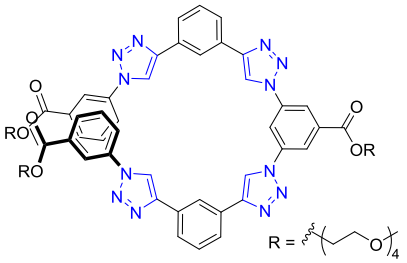
Sulfonamide

- Highly acidic HB donors.[167]
- Alcazar's sulfonamide receptor preorganised with intramolecular HB interactions binds Cl^- selectively (K_a = 7.9 x 10^6 M^{-1}) in $CHCl_3$:[168]



Triazole

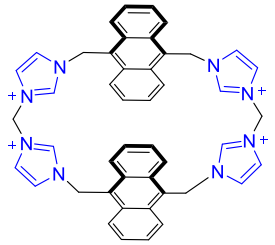
- As a C-H HB donor, it is less acidic than N-H motifs. However, its synthetic accessibility allows incorporation into many diverse anion receptor structures.
- Craig's tetra-triazole foldamer coordinates Cl^- (K_a = 1.7 x 10^4 M^{-1}) via convergent HBs from the triazoles in acetone:[169,170]



Cationic hydrogen bonding motifs

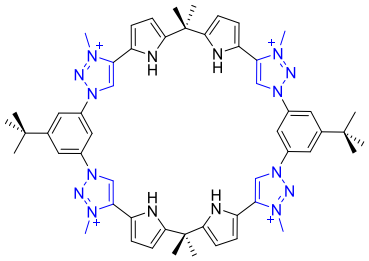
Imidazolium

- Allows strong electrostatic-mediated C-H···anion interactions which are insensitive to pH.[171]
- Kim's imidazolium cyclophane shown to bind I^- and guanosine triphosphate in buffered water at physiological pH:[172]



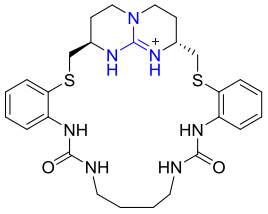
Triazolium

- Strong cationic C-H HB donor, and easily accessible by *N*-methylation of triazoles.[173,174]
- Sessler's triazolium-phane shows high affinities for oxoanions (HSO_4^-, $H_2PO_4^-$ and $HP_2O_7^{3-}$) in methanol:[175]



Guanidinium

- Weak acidity (pK_a 11-13) allows it to remain protonated over wider pH range than free amines.
- Often highly-complementary to oxoanions
- Mendoza's tris-guanidinium macrocycle binds nitrate strongly (K_a = 9.9 x 10^3) in acetonitrile:[176]



A recently-developed class of HB donor macrocyclic anion hosts are 'campestarenes', (from '*campester'* = flat in Latin and '*arene*'), which are planar, highly symmetric and shape-persistent macrocycles containing numerous conjugated arene subunits.[177,178] Flood and co-workers recently demonstrated a C_5-symmetric cyanostilbene *campestarene* (cyanostar) macrocycle (Figure 1.14A) capable of forming a host-guest 2:1 complex with large anions (BF_4^-, PF_6^- and ClO_4^-), where the anion is sandwiched between two stacked macrocycles and held in place by convergent HB interactions from both macrocycles.[179] Interestingly, the same stacked macrocycle arrangement was very recently found to encapsulate a bisulfate (HSO_4^-) anion-dimer (Figure 1.14B). While anion dimers have only been postulated theoretically,[180,181] this represents the first experimental evidence of anion dimer formation, where the stabilisation of the bisulfate-dimer by convergent HB interactions within the manifold was able to offset the electrostatic repulsion between them.[182]

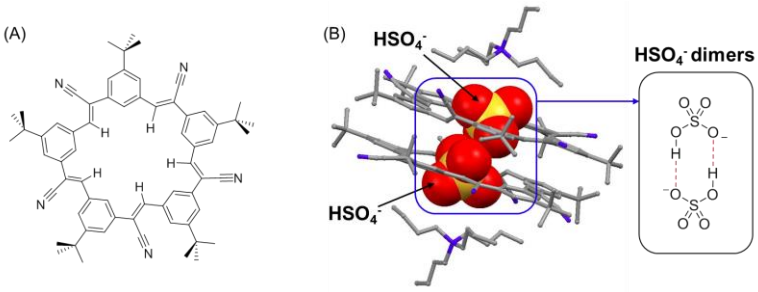


Figure 1.14 *(A) Flood's cyanostar macrocycle[179] and (B) crystal structure of a stacked cyanostar macrocycles encapsulating a bisulfate anion dimer between.[182]*

1.2.2 Sigma Hole-donor Anion Receptors

1.2.2.1 Halogen Bonding Receptors

While XB-donor anion hosts are presently still rare compared to their HB counterparts, they are rapidly growing in popularity. Amongst the halogens, the largest halogen atoms (Br and I) are most commonly employed in XB hosts due to their polarizability which allows them to form highly-electrophilic σ-holes for strong XB interactions.[76] Like HB receptors, neutral and cationic XB-donor motifs are known (Figure 1.15), of which the latter have found more widespread use in synthetic anion receptors due to their stronger charge-assisted XB properties. All solid-state structures of XB-anion interactions show very pronounced linearity, a consequence of direct interaction with the σ-holes on the XB-donor halogen atoms.

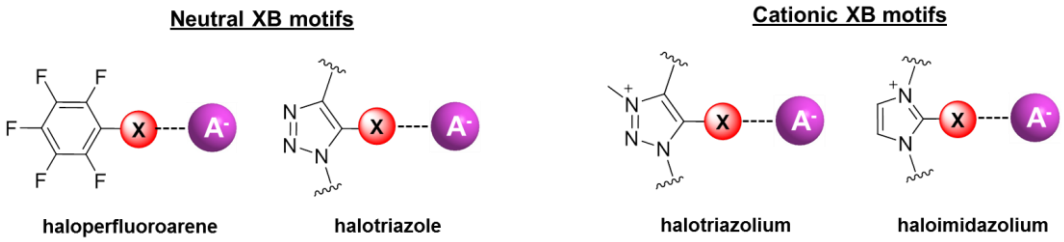


***Figure 1.15**. Common neutral and cationic XB-donor motifs for anion recognition (X = Br/ I).*

Neutral Halogen Bonding Receptors

A popular XB-donor motif in solid-state crystal engineering due to its electron-deficiency,[183,184] haloperfluoroarenes are also useful for solution-phase anion recognition due to the possibility of functionalising the perfluoroarene at any position with I or Br atoms to direct the geometry for anion coordination. While the divergent nature of the *para*-substituted XB-donor iodine atoms in Resnati's heteroditopic receptor for NaI (Figure 1.10) prevents all three iodines from cooperatively interacting with the bound iodide anion,[110] Taylor circumvented the problem with a neutral tripodal receptor incorporating *ortho*- substituted iodines which allow anions to be coordinated in a tridentate manner within the receptor cavity itself (Figure 1.16). In d_6-acetone, Taylor's receptor bound halides (Cl^- > Br^- > I^-) selectively over oxoanions (TsO^-, HSO_4^- and NO_3^-), which was postulated to arise from an intrinsic preference for XB to interact with 'softer' halides compared with 'harder' oxoanions.[185]

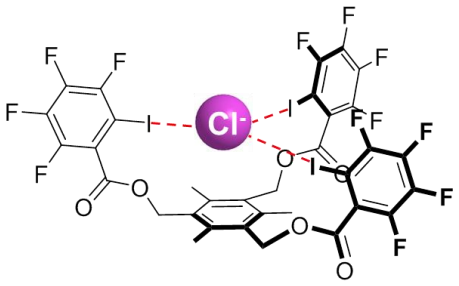


Figure 1.16. *Taylor's neutral tripodal iodoperfluoroarene receptor for Cl^-.*[185]

Halotriazoles are popular XB-donor motifs due to their synthetic accessibility from copper-catalysed azide-alkyne cycloaddition (CuAAC) reactions using terminal azides and haloalkynes,[186,187] or with proto-alkynes in the presence of an electrophilic halogen donor.[188,189] Iodotriazoles are more potent XB donors than bromotriazoles,[190] and hence are more commonly used. For instance, Schubert designed cleft-type receptors with varying spacers in between two iodotriazole units which allow bidentate coordination of halides (Figure 1.17A).[191] A reduction in binding affinity for Cl^- and Br^- in THF was found upon changing the central spacer from benzene to carbazole. However, enhanced anion binding was observed when the carbazole spacer was functionalised with phenol groups which allow receptor preorganisation with intramolecular HB interaction. Separately, Beer synthesised a picket fence-style Zn(II) metalloporphyrin complex decorated with four iodotriazole-containing pendant groups, which exhibited stronger halide binding affinities compared to its HB analogue in acetone, acetonitrile and chloroform (Figure 1.17B).[192]

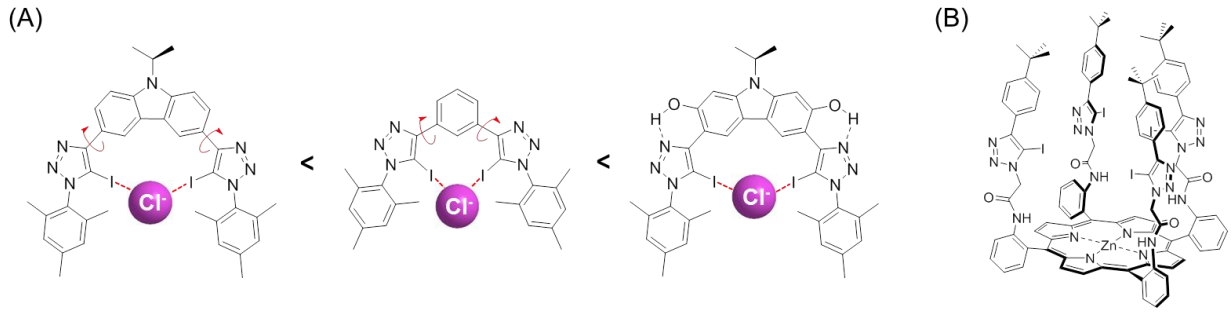


Figure 1.17. *(A) Schubert's bidentate XB receptors in increasing order of chloride binding affinities*[191]*; (B) Beer's neutral tetra-dentate XB Zn(II) metalloporphyrin receptor.*[192]

Cationic XB Receptors

When an iodotriazole is electronically conjugated to cationic groups such as pyridinium, the magnitude of the molecular electrostatic potential (MEP) of the σ-hole on the iodine atom can be enhanced by up to two times compared to an identical conjugation with neutral pyridine,[193] thus increasing its electrophilicity significantly. Beer and coworkers

exploited this magnified electrophilicity in an acyclic pyridinium bidentate XB anion receptor, which bound anions with association constants more than an order-of-magnitude larger than the HB analogue (Figure 1.18A).[98] Interestingly, the XB receptor also showed a preference for acetate over halides in d_6-DMSO. This motif has been incorporated into mechanically-interlocked host structures such as rotaxanes and catenanes, which showed impressive anion binding properties even in the presence of water (*vide infra*).[98,194–196] In addition, a halogen atom directly attached to a pyridinium motif can act as a potent XB donor as well, as exemplified by Berryman's XB receptor (Figure 1.18B) which showed strong XB-interactions with perrhenate (ReO_4^-) in both solid state and in a solution of $CDCl_3$/ d_6-acetone 3:2 *v/v* (K_a = 8990 M^{-1}).[197] More recently, the same group synthesized an acyclic tricationic receptor molecule containing three *p*-iodo-pyridinium groups. In the presence of iodide, a triple helix comprising of three intertwined monomers could be formed in the solid state which encapsulated two iodides via convergent XB interactions within the central channel of the helix (Figure 1.18C).[198]

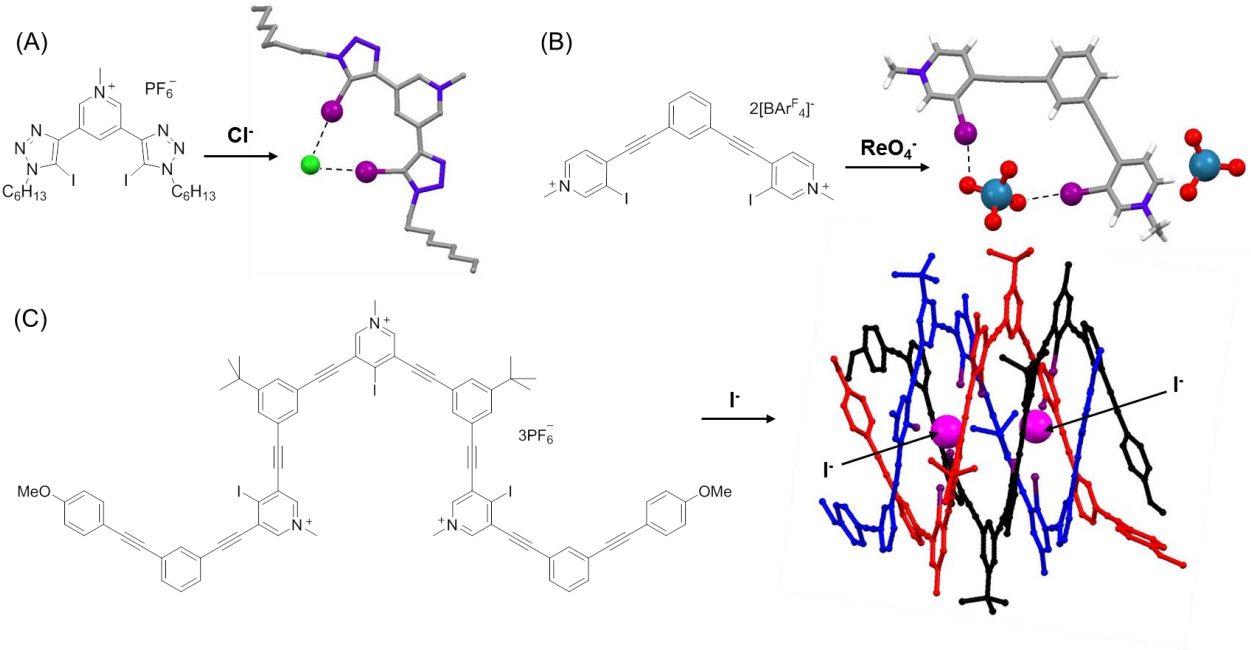


Figure 1.18. *(A) Beer's bidentate pyridinium iodotriazole XB receptor[98]; (B) Berryman's dicationic pyridinium XB host for perrhenate anion[197] (C) Triple helicate structure formed from the XB interactions of Berryman's host and iodide. Individual XB-donor monomer strands are shown in different colours for clarity.*[198]

To enhance the XB potency of halotriazoles, direct halotriazole *N*-methylation has been efficiently performed using strong methylating agents such as trimethyloxonium tetrafluoroborate (Meerwein's salt)[173] and methyl triflate.[174] Indeed, calculations of the MEPs on the resulting halogen atoms of halotriazoliums show further enhancement of their electrophilicity compared to halotriazole-pyridinium systems due to their more localised cationic character.[190,193] Capitalising on this, Schubert and co-workers synthesised a series of bidentate dicationic bromo-triazolium and iodotriazolium hosts using either phenyl or thiophene as a spacer between the XB-donor groups (Figure 1.19A). While the thiophene-centred receptors show weaker anion binding strength than the phenyl-centred analogues due to their wider XB-anion bite angles, it is noteworthy that the phenyl-iodotriazolium host bound oxoanions (acetate, $H_2PO_4^-$ and SO_4^{2-}) preferably over halides in d_6-DMSO,[199] which contrasted with Taylor's neutral iodotriazole hosts. A propensity for strong oxoanion binding was also observed with Molina's 1,1′-bi-2-naphthol (BINOL) bis-iodotriazolium receptors (Figure 1.19B), with association constant values for acetate, $H_2PO_4^-$ and $HP_2O_7^{3-}$ exceeding 1.0 x 10^3 M^{-1} in CD_3CN/ CD_3OD 9:1 *v/v* for all cases.[200]

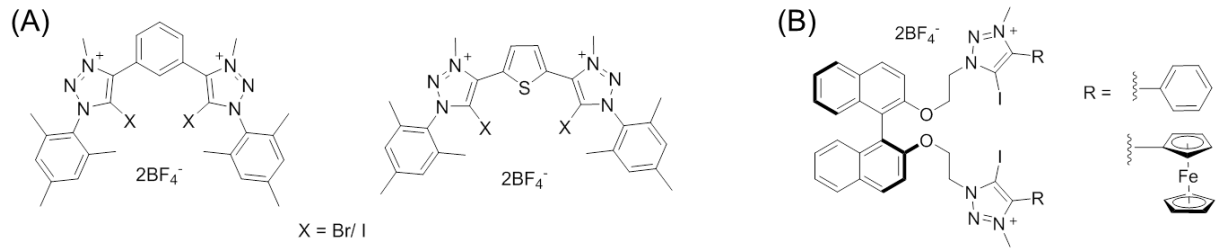


***Figure 1.19**. (A) Schubert's bidentate bromo- and iodotriazolium anion receptors[199]; (B) Molina's BINOL-based dicationic hosts for oxoanions.[200]*

As XB donors, haloimidazoliums have been shown to exhibit almost identical Lewis acidities as halotriazoliums.[201–203] Using simple acyclic bidentate haloimidazolium XB donors (Figure 1.20A), Huber and coworkers established that XB-mediated halide binding was driven both enthalpically ($\Delta H < 0$) and entropically ($\Delta S > 0$) via isothermal titration calorimetry experiments in acetonitrile.[204] By incorporating iodoimidazolium groups on the arms of a tripodal receptor, Ghosh demonstrated that even in the presence of chloride and iodide,

bromide could be selectively sequestered and crystallised out of solution (Figure 1.20B).[205] Strong binding of heavier halides was also observed with Beer's bis-haloimidazolium macrocycles (Figure 1.20C), of which bromide and iodide selectivity depended on the identity of the XB-donor atom and the spacer group between them.[206] Similarly, derivatives of haloimidazoliums are also known to be potent XB donors, such as Huber's iodo-benzimidazolium receptor (Figure 1.20D), which was able to bind chloride very strongly (K_a = 3.5 x 10^6 M^{-1}) in acetonitrile.[207]

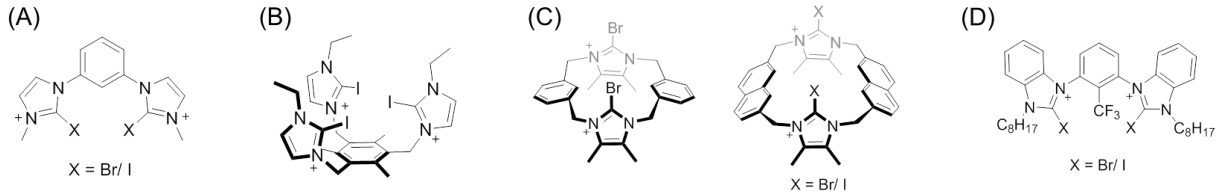


Figure 1.20. *(A) Huber's bidentate haloimidazolium XB receptors[204]; (B) Ghosh's tripodal iodoimidazolium receptor for bromide[205]; (C) Beer's haloimidazolium macrocycles[206]; (D) Huber's iodo-benzimidazolium receptor.[207]*

1.2.2.2 Chalcogen Bonding Receptors

The study of anion recognition involving ChB interactions is still very much in its infancy, and as such, available ChB hosts are much rarer compared to their XB counterparts and are largely limited to acyclic molecules. Like XB, stronger ChB···anion interactions occur with heavier chalcogen donors (Se, Te).[126] In 2010, Gabbaï synthesised a bidentate Lewis acidic anion host containing a rare sp^3-hybridised telluronium motif (Figure 1.21A), which coordinated fluoride strongly between the boron and tellurium atoms with a Te···F^- bond length just slightly longer than the sum of both elements' covalent radii in its solid-state structure.[208] Although computational studies have suggested that sp^3-hybridised chalcogen atoms are stronger ChB-donors than sp^2-hybridised ones,[209] the latter have been studied more extensively. To stabilise these sp^2-hybridised ChB-donor atoms from hydrolysis and decomposition, they are often integrated into electron-deficient aromatic rings. For instance, Taylor and coworkers very recently demonstrated that neutral benzo-tellurodiazoles are able to interact strongly with halides (Cl^-, Br^- and I^-) in THF via UV-Vis titration experiments. By incorporating electron-withdrawing substituents on the six-membered aromatic rings, the

magnitude of the halide binding affinities could be increased by two orders of magnitude (Figure 1.21B). Unfortunately, these benzo-tellurodiazoles were still found to be unstable to moisture and anions such as iodide, which hinders their incorporation into more elaborate host structures.[210] However, a related family of compounds, the 3,4-dicyano-tellurodiazoles, were stable enough for crystal structures of their complexes with all halides (F^-, Cl^-, Br^- and I^-) to be obtained. Interestingly, two polymorphs were found, each showing short Te···halide contacts indicative of ChB interactions (Figure 1.21C).[128,211] Similarly, short Se···iodine contacts in the solid state (c.a. 90 % of the sum of the Se and I van der Waals radii) which indicated strong ChB interactions, were also observed using cationic benzo-selenodiazoliums with iodide and triiodide (I_3^-) anions (Figure 1.21D).[127] Taylor has also recently shown that neutral tellurophenes (Figure 1.21E) can function as effective ChB host systems for solution-phase anion recognition, binding Cl^- selectively over the other halides and oxoanions (BzO^-, NO_3^- and TsO^-) in THF.[212]

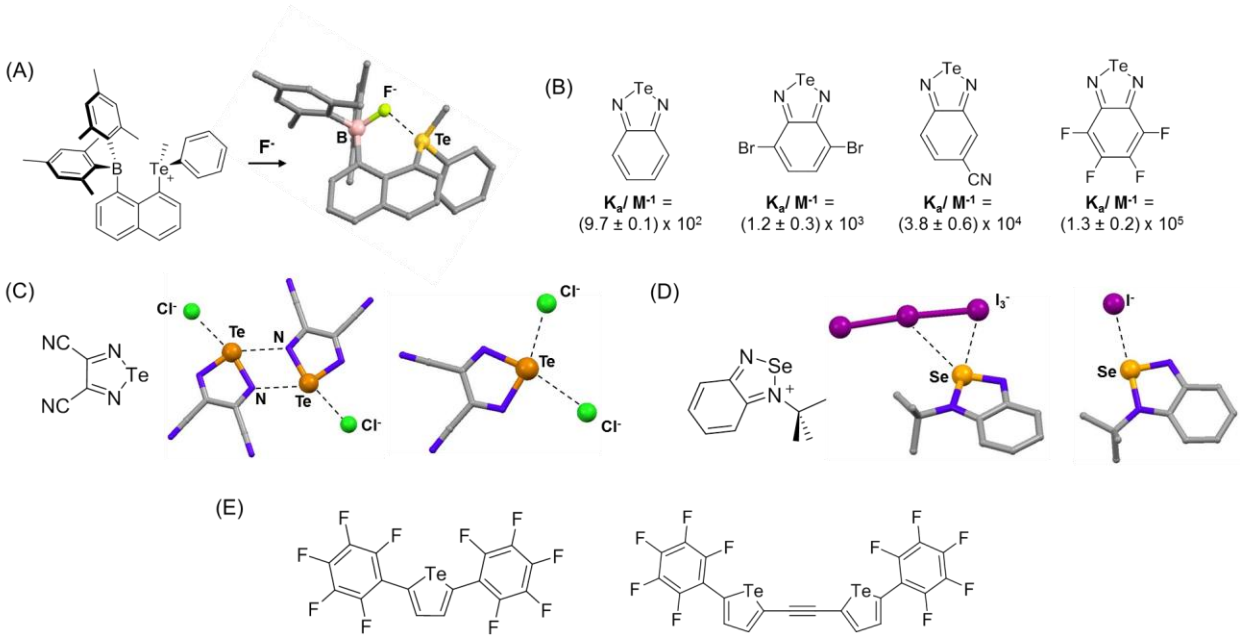


Figure 1.21. *(A) Gabbaï's telluronium ChB host for fluoride[208]; (B) Taylor's neutral benzo-tellurodiazoles, with their respective Cl^- association constants in THF indicated[210]; (C) Dicyano-tellurodiazoles and their solid-state anion structures[211]; (D) Benzo-selenodiazoliums and their iodide complexes[127]; (E) Taylor's neutral tellurophene ChB anion receptors.[212]*

1.2.3 Anion Sensing

Anion sensing occurs when the presence of an anion causes a detectable change in the macroscopic properties of a host molecule functionalised with suitable reporter groups. As shown in Figure 1.22, this can occur traditionally via electrochemical (e.g. perturbations in redox potential, conductivity, impedance) and optical (e.g. changes in visible colour and fluorescence/ luminescence intensity) means, and more recently, via changes in bulk sample viscosity (rheological sensing). Redox and optical anion sensors can be grouped into three categories depending on their mechanism of action. Firstly, in the receptor-reporter approach, anion binding through non-covalent interactions leads to changes in the redox and optical properties of the 'reporter' group. To ensure efficient electronic and spatial communication of the anion binding event, reporter groups are usually covalently linked in close proximity to the anion binding site. Secondly, using the indicator displacement assay (IDA) approach, anion binding displaces a dye originally weakly-bound to the receptor, leading to a 'turn on/ off' optical response. Finally, the chemodosimeter approach relies on covalent bond formation between the anion and receptor, hence changing its optical and electrochemical properties.

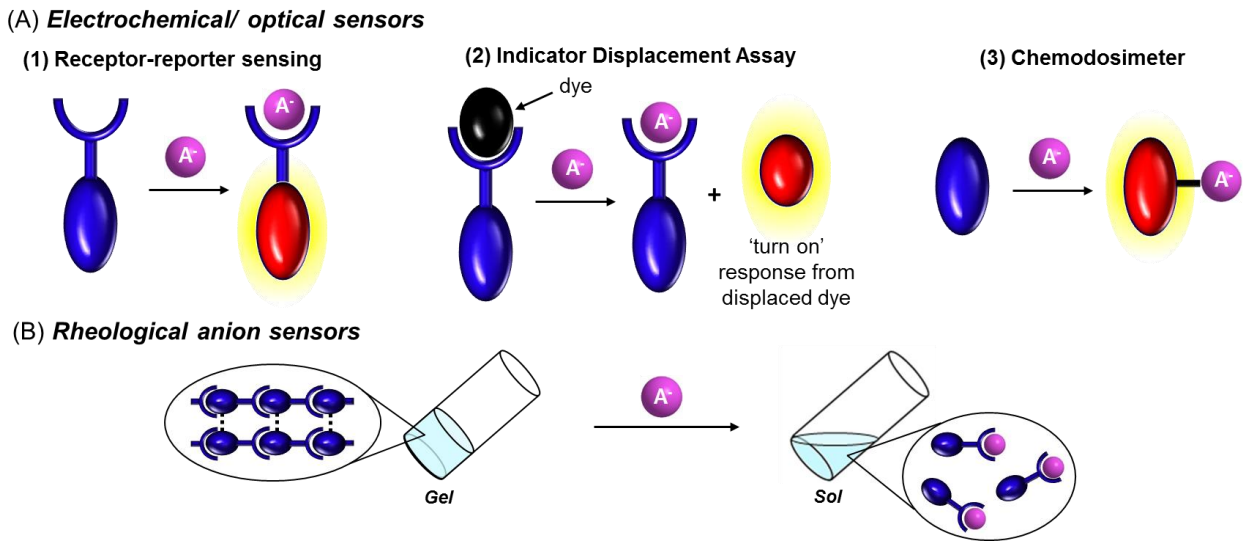


***Figure 1.22**. Anion sensing strategies: (A) Detectable electrochemical/ optical changes or (B) changes in bulk solvent viscosity in the presence of anions.*

Electrochemical Anion Sensing

Anion sensing via electrochemistry is highly desirable due to its high sensitivity, and has been demonstrated both in solution and on surfaces. In the presence of anions, stabilisation of the oxidised state of a redox-active motif results, giving rise to a detectable cathodic shift of its redox potential.[213] Direct coordination of the anion to the receptor, as well as through space and through-bond communication with the redox-active centre on the host, can give rise to distinct potential shifts. With direct anion coordination via anion-metal interactions or covalent bond formation (Figure 1.23A), significant changes to the host's electronic and redox properties can result, as exemplified by Aldridge's Lewis acidic ferrocenyl boronic acid receptor for F^- and CN^-.[214] Through-space interactions occur largely via electrostatics between the anion and the cationic oxidised ferrocenium redox group. For instance, this interaction resulted in a cathodic shift of -70 mV for Beer's ferrocene-appended guanidinium receptor with pyrophosphate ($P_2O_7^{4-}$) in 1:1 methanol/water (Figure 1.23B).[215] In contrast, through-bond sensing occurs when anion binding is communicated electronically across conjugated pathways to the redox centre, as in Sessler's tetrathiafulvalene (TTF)-integrated bis-indole receptor (Figure 1.23C), giving a cathodic shift of -112 mV for $H_2PO_4^-$ in dichloromethane.[216] Using these approaches, solution-phase redox anion sensing has been achieved using acyclic receptors,[217,218] tripods,[219,220] macrocycles,[221,222] cages,[223] dendrimers[224] and interlocked structures[225–227] (see Section 3.1).

Redox anion sensing on surface/solution interfaces, achieved by adsorption of redox-active anion receptors as highly-ordered self-assembled monolayers (SAMs) on surfaces (Si, Au and metal oxides) offer numerous advantages over solution-phase anion sensing, such as recyclability, solvent-intolerance and greater anion sensitivity. For instance, a ferrocenylurea-functionalised calixarene compound adsorbed onto a gold surface gave an enhanced cathodic shift of -115 mV for Cl^- as compared to -60 mV in 1:1 CH_3CN/ CH_2Cl_2 *v/v* solution (Figure 1.24A).[228] Measuring changes in film conductivity has also been demonstrated to be useful for redox anion sensing. When Anzenbacher's polythiophene conductive polymer deposited on an interdigitated indium tin oxide (ITO) electrode was connected to a positive potential

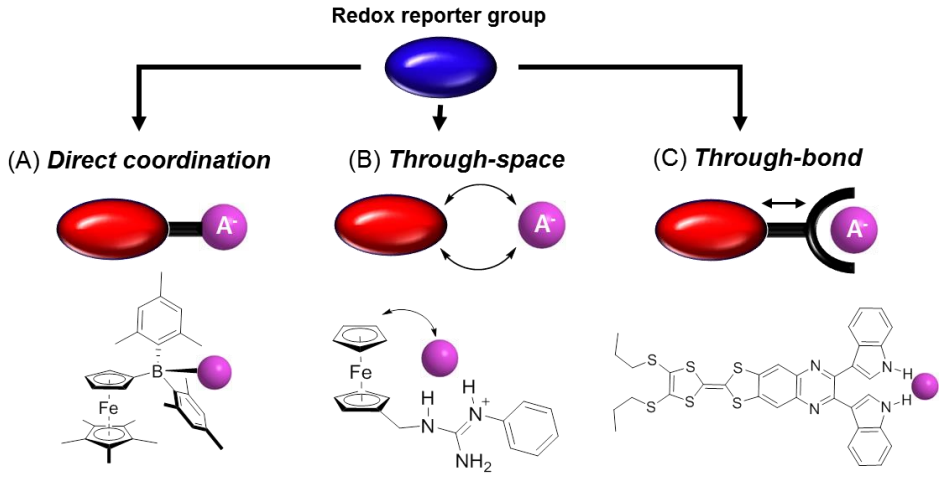


***Figure 1.23**. Redox anion sensing mechanisms and examples: (A) Aldridge's ferrocene-boronic acid for direct F^- coordination[214]; (B) Beer's ferrocene guanidinium through-space pyrophosphate anion sensor[215] and (C) Sessler's through-bond tetrathiafulvalene sensor for $H_2PO_4^-$.[216]*

(Figure 1.24B), an injection of positive charges into the polymer (*p*-doping) allowed anion-specific sensing by changing the polymer's conductivity in the presence of anions.[229] More recently, a phenylboronic acid (PBA) derivative incorporated into an organic field effect transistor (OFET) (Figure 1.24C) facilitated sensing of F^-, $H_2PO_4^-$ and acetate in buffered water by perturbing the OFET's threshold voltages.[230] Recent developments include sensing by electrochemical impedance spectroscopy (EIS), where accumulation of anions on a suitably-functionalised surface repels charged redox probes (e.g. $[Fe^{III}(CN)_6]^{3-}$/ $[Fe^{II}(CN)_6]^{4-}$] which lead to changes in the charge-transfer resistance of the monolayer. This powerful method does not require the anion receptor constituting the SAM to contain any redox-active groups, potentially allowing any existing receptor to be surface-mounted for EIS anion sensing.[231]

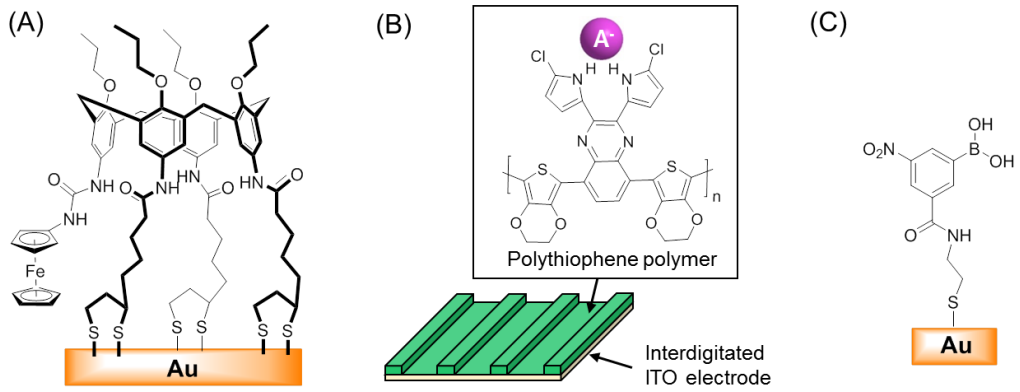


***Figure 1.24.** Examples of redox anion sensing on surfaces: (A) Beer's ferrocenylurea calixarene[228]; (B) Anzenbacher's pyrrolic polythiophene polymer[229] and (C) Minami's phenylboronic acid receptor incorporated into OFETs for anion sensing.[230]*

1.2.3.1 Optical Anion Sensing

Colorimetric Anion Sensors. This method of optical anion sensing is useful due to the possibility of anion-triggered colour changes detectable by the naked eye. Adopting the receptor-reporter approach, Dey designed a bis-indole receptor which gave a detectable colour change from colourless to bright pink (λ_{max} = 531 nm) due to formation of HB interactions with HSO_4^- anions in CH_3CN/ H_2O 1:1 *v/v* (Figure 1.25A).[232] Similarly, Gunnlaugsson's receptor underwent colour changes from yellow to shades of purple upon addition of one equivalent of F^-, $H_2PO_4^-$ and acetate in DMSO, attributed to HB interactions with the hydrazide moieties adjacent to the napthalimide unit. (Figure 1.25B).[233] By adopting the chemodosimeter approach and capitalising on the affinity of F^- for Lewis acidic-boron centres, Aldridge reported a ferrocene-indenyl receptor which underwent a colour change from green (λ_{max} = 596 nm) to pink (λ_{max} = 531 nm) upon fluoride chelation in THF (Figure 1.25C).[234] Combining the chemodosimeter approach with the distance-dependent colorimetric properties of chemically-functionalised colloidal gold nanoparticles (AuNPs), Mirkin utilised the Griess reaction specific for the nitrite (NO_2^-) anion to covalently couple aniline and naphthalene-functionalised AuNPs together in water (Figure 1.25D). This resulted in AuNP precipitation, changing the colour of the AuNP solution from red to colourless only in the presence of NO_2^-, but not with any other anion tested.[235]

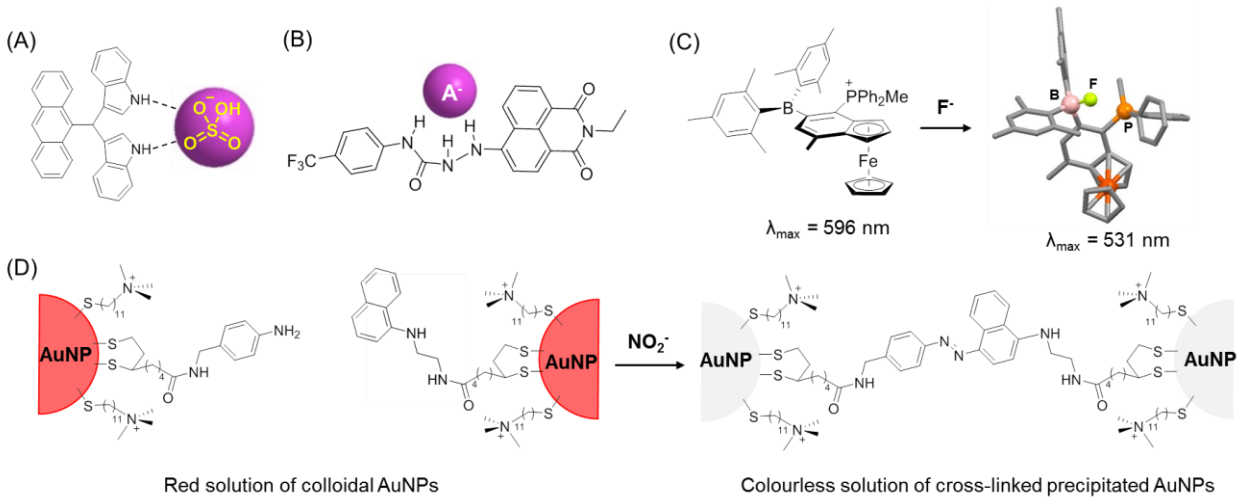


Figure 1.25. *Examples of colorimetric anion sensors: (A) Dey's bis-indole sensor[232]; (B) Gunnlaugsson's sensor for F^-, acetate and $H_2PO_4^-$ [233]; (C) Aldridge's ferrocene-indenyl chemidosimeter for F^-;[234] (D) Mirkin's colorimetric AuNP sensor for NO_2^- utilising the Griess reaction.[235]*

Fluorescent/ Luminescent Anion Sensors. Fluorescence/ luminescence offers a highly-sensitive means of anion sensing in solution, capable of anion detection at sub-micromolar concentrations. Very recently in 2016, Ghosh reported a rare example of a XB luminescent reporter-receptor anion sensor containing a heteroleptic Ru^{II} complex with an iodotriazole unit *N*-coordinated to the metal centre (Figure 1.26A). Other than polarising the XB-donor iodotriazoles and increasing its electrophilicity, iodotriazole *N*-ligation to Ru^{II} also ensured direct electronic communication of XB-anion binding, enabling highly sensitive and selective perturbations of the complex's luminescent intensity in the presence of $H_2PO_4^-$ and $HP_2O_7^{3-}$ in CH_3CN/ H_2O 4:1. Notably, the XB sensor proved superior to its HB analogue, which showed no luminescent response for the phosphates in the presence of water.[236]

IDAs and chemodosimeters for fluorescence anion sensing have also been developed. To demonstrate the former, binding of the inositol-1,4,5-trisphosphate (IP_3) anion to Anslyn's polyguanidinium tripodal receptor complex with 5-carboxyfluorescein dye led to dye displacement and a concomitant fluorescence quenching (Figure 1.26B).[237] Nevertheless, a major drawback of IDAs is the necessary use of excess dye, which can lower the sensitivity of anion detection. To circumvent this problem, Anzenbacher covalently integrated the dye into the receptor design, ensuring 1:1 receptor-dye stoichiometry which enhances sensitivity (Figure 1.26C). Exciplex formation between the naphthalene and napthalimide moieties in the absence of anions which lead to fluorescence quenching is turned off upon addition of phosphates (e.g. $HP_2O_7^{3-}$) in DMSO/water 95:5, with displacement of the naphthalene moiety from the binding cavity. Impressively, this intramolecular IDA also allowed highly-sensitive sensing of phosphate-based herbicide glyphosate with a detection limit of 0.2 parts-per-million in water.[238] Combining the chemodosimeter approach and the IDA, Gunnlaugsson's luminescent AuNPs functionalised with europium(III) complexes exhibited luminescence quenching when coordinating anions such as flavin monophosphate displaces the originally-complexed beta-ketone antennae ligand necessary for europium(III) luminescence (Figure 1.26D).[239]

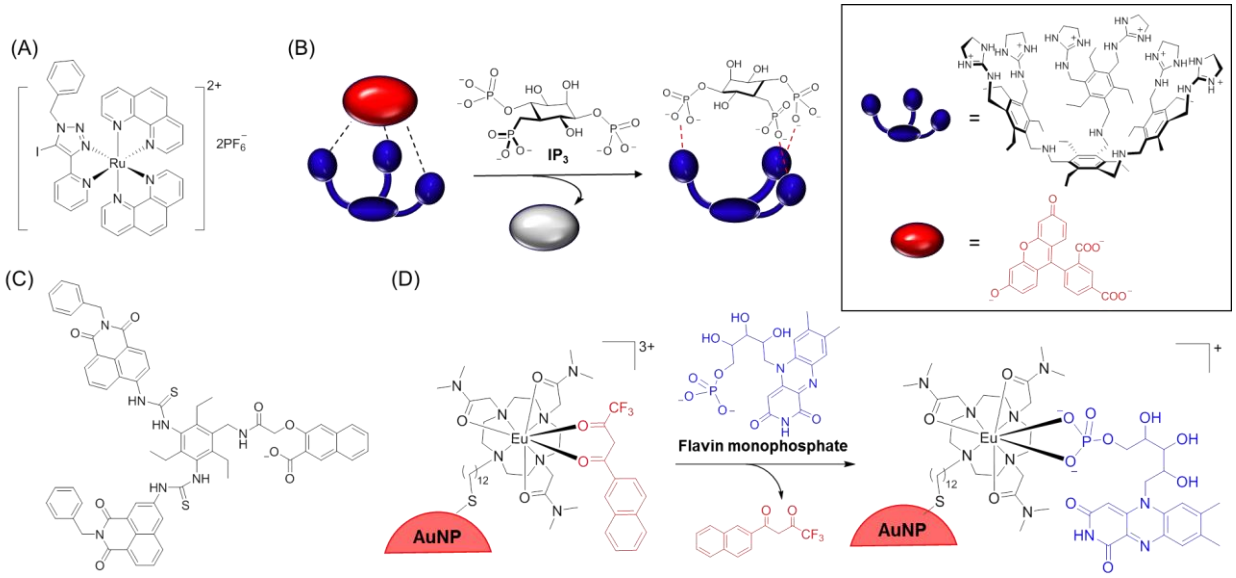


***Figure 1.26**. Examples of fluorescent/ luminescent anion sensors: (A) Ghosh's XB sensor for phosphates[236]; (B) Anslyn's tripodal IDA for $(IP_3)^{6-}$ [237]; (C) Anzenbacher's intramolecular IDA sensor for phosphates[238]; (D) Gunnlaugsson's lanthanide luminescent AuNPs functionalised with Eu(III) complexes.[239]*

1.2.3.3. Rheological Anion Sensors. Gels are solid-like matrices comprised of cross-linked molecular networks, which can form or break down in the presence of a molecular stimulus, that can range from polymers to small molecules and anions, resulting in a visible 'naked eye' change in the bulk viscosity properties of the sample.[240] These rheological 'soft matter' sensors have been applied for anion sensing only since the turn of the century.[241] For example, Zhu reported a bis-urea BINOL-based gel (Figure 1.27A) in DMSO which collapsed to form a solution (gel-to-sol transition) in the presence of F^- due to the anion disrupting the original intramolecular HB networks constituting the gel phase.[242] Similarly, F^- also caused a gel-to-sol transition of a glycine-glutamic acid-based organogelator in toluene (Figure 1.27B).[243] Very recently, the first XB-mediated rheological sensor selective for chloride was reported by Fan utilising iodoperfluoroaryl-functionalised dendritic organogelators (Figure 1.27C). In the absence of the anion, strong π-π stacking interactions between largely-planar monomers formed extensive fibrillar networks in acetone-hexane mixtures. Cl^- addition triggered gel collapse due to the formation of a non-planar XB-anion complex which disrupts the π-π stacking interactions. Notably, only Cl^- led to extensive gel-to-sol transition, whilst Br^-,

I^-, HSO_4^-, NO_3^- and CN^- resulted in negligible gel collapse, mirroring their solution-phase anion binding affinities.[244]

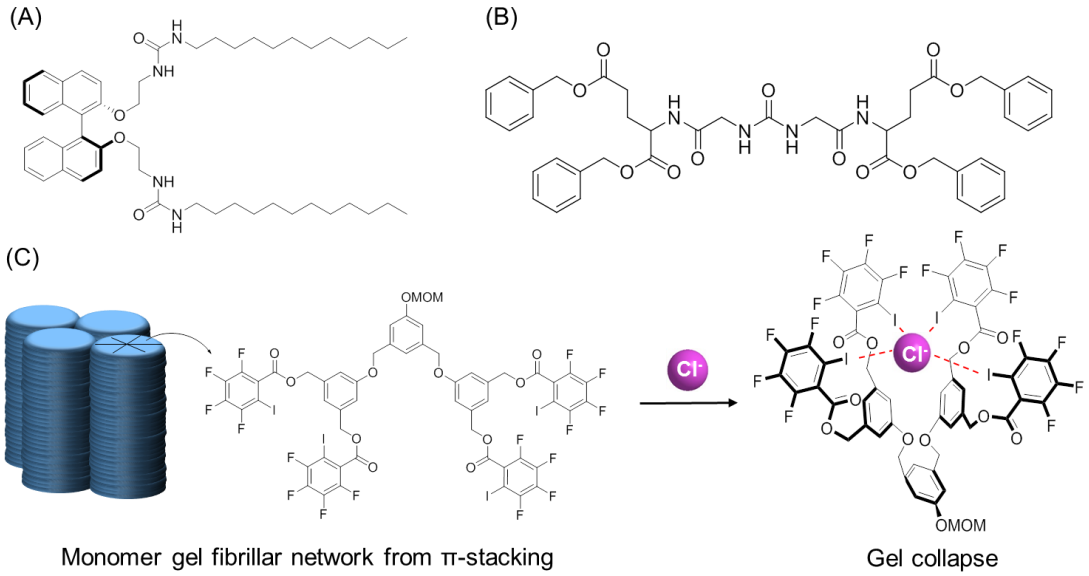


***Figure 1.27**. Examples of rheological anion sensing organogelators: (A) Zhu's bis-urea gel sensor for F^- [242]; (B) Wei's glycine-glutamic acid F^- sensor[243]; (C) Fan's iodoperfluoroarene XB dendrimer capable of Cl^- sensing due to formation of XB-Cl^- complexes leading to gel collapse.[244]*

1.2.4 Applications of Anion Binding and Sensing

Driven by the aforementioned fundamental advances in recognition and sensing, anion supramolecular chemistry has progressed beyond receptor chemistry to embrace functional applications in recent years. The following sections detail key advances in these areas.

1.2.4.1 Anion transport

Stimulated by the desire to combat diseases arising from anion misregulation (e.g. cystic fibrosis),[245] one of the most recently and intensely-studied applications is anion transport. Synthetic anion transport across bilayer membranes can occur either via (1) discrete 'anionophore' molecules which bind and convey the anion across the membrane or (2) membrane-spanning anion channels which provide a continuous path for anion movement. Inspired by natural anionophores such as prodigiosins, which possess antitumour and immunosuppressive biological activities,[246] synthetic examples are usually lipophilic to allow permeation across the hydrophobic membrane core. Notable recent examples include Davis' bis-squaramide anionophore (Figure 1.28A),[247] Gale's pH-switchable

phenylthiosemicarbazole-based receptor which shows a 640-fold enhancement in chloride transport efficacy when the pH is decreased from 7.2 to 4.0 (Figure 1.28B),[248] and Matile's unprecedented ChB dithienothiophene anionophores capable of transporting Cl^- and Br^- (Figure 1.28C).[249] Synthetic anion channels have been prepared by capitalising on the self-assembly of macrocycles into porous channels, such as Davis' tetrabutylamide calix[4]arenes (Figure 1.28D),[250–252] as well as by constructing covalently-linked oligomeric assemblies of recurring anion binding motifs. Examples of the latter include a halogen bonding cascade comprising multiple iodoperfluoroaryl monomers that transports Cl^- via a hopping mechanism (Figure 1.28E),[253] as well as π-slides incorporating naphthalenediimide[254] or perylenediimide[255] motifs that mediate transmembrane anion transport by anion-π interactions.

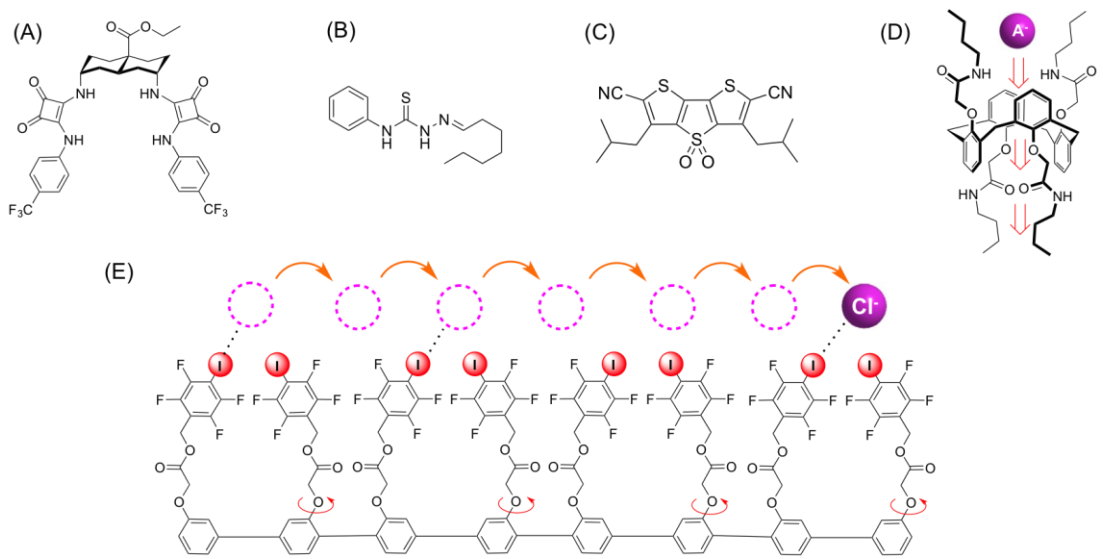


Figure 1.28. *(A) Davis' bis-squaramide anionophore[247]; (B) Gale's pH-switchable transporter[248]; (C) Matile's ChB dithienothiophene anionphore[249]; (D) Davis' 1,3-alternate tetrabutylamide calix[4]arene[250]; (E) Matile's XB oligomeric anion cascade.[253]*

1.2.4.2 Chiral Recognition

The ability to selectively bind one enantiomer of a guest molecule over the other is crucial for natural biochemical processes, as different guest enantiomers often elicit contrasting biological responses.[256] Partly driven by the fact that chiral anions play crucial biological roles, which include metabolism (e.g. lactate) and signal transduction (e.g. aspartate, glutamate),[257] and that many important medicinal compounds exist as chiral anions at physiological pH (e.g.

ibuprofen, hexobarbitals, naproxen), the field of chiral anion recognition has developed to better understand the fundamental processes driving the exquisite chiral selectivity seen in nature,[258] and for exploitation in analyte sensing[259,260], pharmaceutics[261] and chemical applications such as organocatalysis.[262] While amino acids[263] and sugars[264,265] constitute an important chiral pool from which many abiotic chiral anion receptors are derived (Figures 1.29A,B), axial-chiral motifs containing an axis of chirality but no stereogenic centre, e.g. 1,1'-Bi-2-naphthol (BINOL), are also frequently utilised (Figure 1.29C).[266] The incorporation of redox-active reporter groups such as ferrocene into chiral receptors has also allowed electrochemical distinguishing of chiral anion enantiomers, as exemplified by Tucker's ferrocenyl ureas (Figure 1.29D).[267,268] Motivated by the current poor understanding of chiral selectivity thwarting effective *a-priori* prediction of enantioselectivity, Jurczak and co-workers recently attempted a combinatorial approach to screen a library of acyclic chiral thiourea receptors to identify an effective chiral discriminator for the mandelate anion enantiomers.[269] With the most effective acyclic receptor showing only a modest selectivity of 1.2 ± 0.1 for (*R*)-mandelate (Figure 1.29E), this study highlights the necessity of using structurally more complex host molecules such as macrocycles and interlocked structures to achieve better chiral anion discrimination (see Section 4.1).

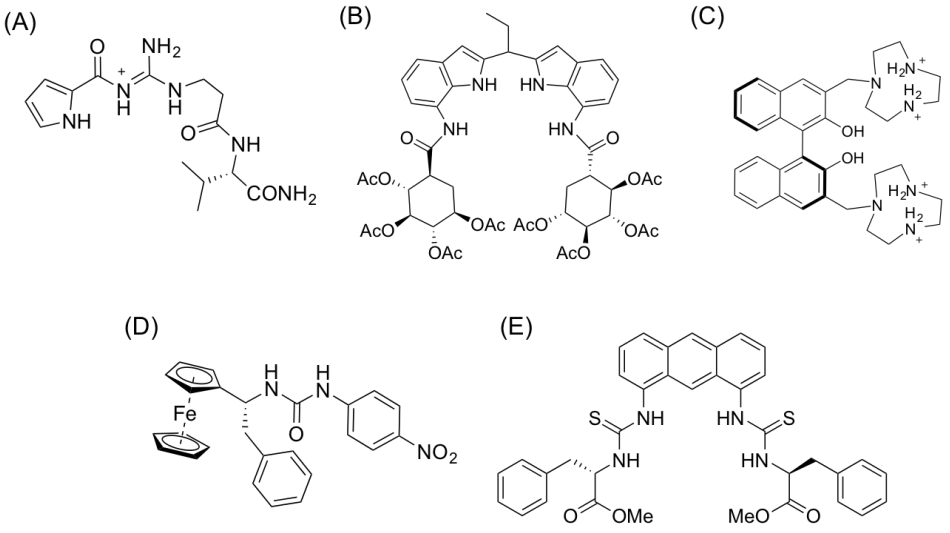


***Figure 1.29**. Examples of acyclic receptors for chiral anion discrimination: (A) Schmuck's receptor derived from (S)-valine[270]; (B) Jurczak's D-gluconic acid-derived receptor[265]; (C) Bencini's (S)-BINOL-based receptor[271]; (D) Tucker's chiral ferrocenyl-urea[267]; (E) Jurczak's thiourea receptor for (R)-mandelate from his combinatorial library.[269]*

1.2.4.3 Anion Binding Organocatalysis

Anions occur abundantly in chemical reactions as reagents, intermediates or counterions. As such, anion binding offers opportunities to (1) control the reaction outcome or (2) influence its rate. The former class of reactions is exemplified by Jacobson's use of a chiral thiourea catalyst in a Pictet-Spingler-type reaction, which forms a complex with $(OTMS)^-$ and associates with the cationic iminium intermediate, allowing cyclisations to occur with excellent stereoselectivity (up to 97 % ee) (Figure 1.30A).[272] The latter class of reactions include halide abstraction catalysis, where halide binding by anion host molecules shift the reaction equilibrium to favour product formation, enhancing reactivity and concomitantly increasing the rate of reaction. This concept has been demonstrated with both HB[273,274] and XB anion receptors.[101] Huber has demonstrated that XB-donor hosts can significantly accelerate the rate of the Ritter reaction compared to the background reaction rate and the presence of the HB-donor analogue (Figure 1.30B).[203] While this reaction required stoichiometric quantities of XB host, the reaction of ketene silyl acetals and 1-chloroisochroman[275] required only 0.5 mole percent catalyst loading for a optimised XB-donor organocatalyst (Figure 1.30C).[207]

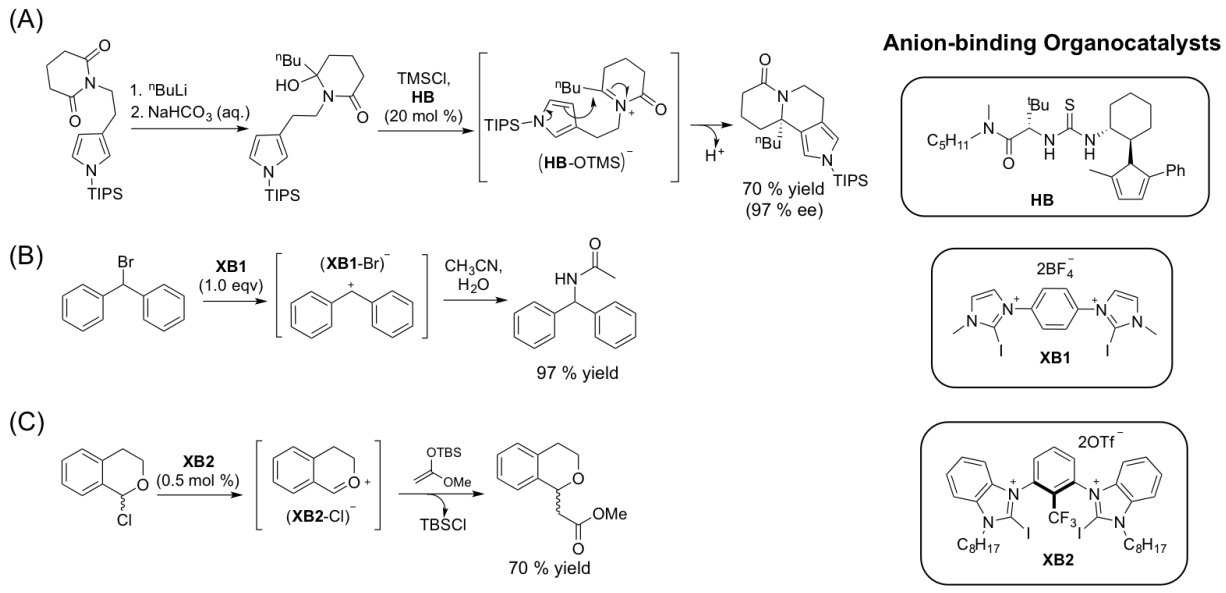
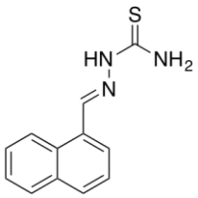


Figure 1.30. *Examples of anion-binding organocatalysis: (A) Jacobson's Pictet-Spengler-type enantioselective cyclisation[272]; (B) XB-catalysed Ritter reaction involving a reaction between a carbocation intermediate and CH_3CN[203]; (C) XB-catalysed reaction between 1-chloroisochroman and a ketene silyl acetal.[207]*

1.2.4.4 Nanotechnology

The ‘on’ and ‘off’ responses of colorimetric and fluorescent anion sensors to the presence of anions can be represented by the Boolean operations ‘1’ and ‘0’ respectively, and different combinations of anion-triggered responses can mimic the input and output signals of logic gates.[276] For example, the presence of F^- in DMSO changes the peak absorbance wavelength of Jiang’s thiosemicarbazide anion sensor from 348 nm to 421 nm. However, the absorbance at 348 nm can be restored by adding HSO_4^-. By defining F^- and HSO_4^- as input signals 1 and 2, the absorbances at 348 nm (Output 1) and 421 nm (Output 2) correspond to the IMP and INH logic gates respectively (Figure 1.31A)[277]. The IMP and INH logic responses brought about by combinations of F^- and HSO_4^- has also been demonstrated with a boron-dipyrromethene (BODIPY) receptor[278] (Figure 1.31B) and a thiosemicarbazone polymer (Figure 1.31C).[279] In addition, CN^- [280] and acetate-selective anion sensors[281] have been shown to exhibit IMP logic outputs as well.

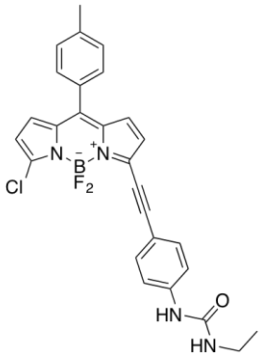
(A)



Truth table

Input signals		Output signals	
F^-	HSO_4^-	$A_{348\ nm}$	$A_{421\ nm}$
0	0	1	0
1	0	0	1
0	1	1	0
1	1	1	0

(B)



(C)

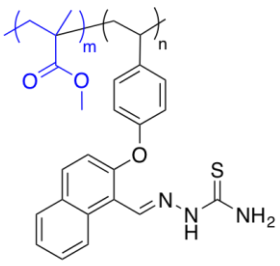


Figure 1.31*. Examples anion sensors giving IMP and INH logic outputs with F^-/HSO_4^- input combinations: (A) Jiang’s thiosemicarbazide and its associated truth table[277]; (B) Yin’s BODIPY receptor[278]; (C) Shen’s thiosemicarbazone polymer.[279]*

1.3 Syntheses and Applications of Mechanically-Interlocked Molecules

1.3.1 The Mechanical Bond

The mechanical bond, a term first coined by Frisch in 1953,[282] connects two or more molecular components mutually interlocked with each other, whereupon the components cannot be mutually separated without cleaving a covalent bond. Examples of such mechanostereochemical molecules include borromean rings,[283,284] [*n*]rotaxanes and [*n*]catenanes,[‡] where *n* represents the number of molecular components interlocked together (Figure 1.32).[291] Catenanes and borromean rings, comprising of inter-linked macrocycles, are topologically non-trivial, as distortion of the molecule by bending, stretching and bond rotation without allowing the bonds to pass through each other retains their three-dimensional interlocked nature. In contrast, rotaxanes can lose their interlocked nature by mechanical deformation (i.e. stretching of macrocycle or stopper shrinkage), and are hence considered topologically trivial in a mathematical sense, although this may not necessarily be chemically possible in practice.[290] Not just aesthetically-appealing compounds of purely theoretical curiosity, mechanically-interlocked molecules (MIMs) can also be found in nature: enzymes such as DNA polymerase[292] and λ-exonuclease[293,294] adopt rotaxane structures, while DNA forms intermediate catenane structures during replication and recombination.[295–297]

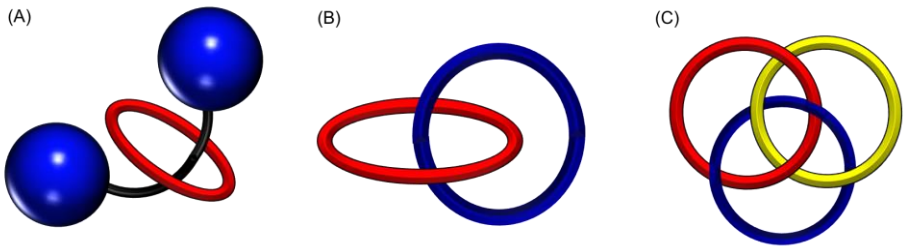


Figure 1.32. *Schematic structures of MIMs: (A) [2]Rotaxane; (B) [2]catenane and (C) Borromean ring.*

The presence of mechanical bonds has been shown to significantly alter the physical and chemical properties of their constituent components. For instance, the steric influence of the mechanical bond has been demonstrated to shield and confer kinetic stability to reactive

[‡] Although molecular knots[285–289] are often discussed in the same context, they strictly do not contain mechanical bonds that link separate molecular components together. Instead, they are considered to be mechanically-*entangled* from a mathematical perspective.[290]

functionalities[298] which is exploited in drug delivery applications (Section 1.3.3.2); as well as alter their reactive environments of these functionalities, with ramifications for the applications of MIMs as catalysts (Section 1.3.3.4). The close proximity of molecular components held by the mechanical bond which reduces their degrees of freedom also amplifies the strength of non-covalent interactions,[299] giving rise to the 'catenand effect' used to describe the enhanced stability of metal complexes ligated by MIMs.[300] Taking advantage of this, as well as the highly-preorganised and shielded space encapsulated by the mechanical bond, MIMs have also been applied in host-guest molecular recognition and sensing (Section 1.3.3.1). Uniquely, the non-covalent nature of the mechanical bond allows the various molecular components of the MIMs to move independently of each other, opening new avenues in catalysis[10] (Section 1.3.3.4) and nanotechnology (Section 1.3.3.3).[7,301,302] Not only does this controlled motion allow the development of novel rotaxane-based stimuli-responsive materials,[303] the mechanical bond has also been shown to bear and redistribute mechanical stress (Section 1.3.3.5).[304,305] Indeed, a recent sonochemical demonstration that mechanical bonds in a polycatenane are as strong as the covalent bonds constituting the polymer backbone[306] heralds the vast potential for development of this field in the coming decades.

1.3.2 Template-directed Synthesis of Interlocked Molecules

The challenges of synthesising interlocked molecules have captured the imaginations of synthetic chemists for decades. Wasserman reported the first-ever synthesis of a MIM in 1960 which relied on the statistical threading of a cycloalkane and a linear diester thread to form a [2]catenane without any attractive interactions between both components.[307] However, the resulting poor yield (< 1 %) of the target catenane stimulated the development of alternative template-directed synthetic methodologies capable of affording MIMs in higher yields.[308,309] A chemical template was defined by Busch as an entity which "*organises an assembly of atoms, with respect to one or more geometric loci, in order to achieve a particular linking of atoms*",[310] and can originate from the mutual interactions of all components in a system, or take the form of a separate chemical species (e.g. an additional ion).[311] The templating effect can be under

thermodynamic or kinetic control: the former requires an equilibrium established between individual chemical components which drives product formation, while the latter stabilises the transition states for product formation via irreversible reactions.[312] Chemical templates can also be classified as linear, cyclising or interweaving, of which the last two are most relevant to the construction of MIMs.[313]

Conceptually, templation offers numerous avenues for the synthesis of MIMs (Figure 1.33). Owing to their different topological properties (*vide supra*), more routes exist towards rotaxanes compared to catenanes. While catenanes have been only accessed via two main routes- a ring-closing reaction where both reactive ends of a thread interpenetrated into a macrocycle in a pseudorotaxane complex are clipped together, or double cyclisations of orthogonally-oriented macrocycle precursors held by an interweaving template,[314] numerous routes have afforded rotaxanes. Common methods include stoppering− the covalent addition of bulky stopper groups to a pseudorotaxane to prevent macrocycle dethreading;[315,316] clipping− the ring-closing of a macrocycle precursor around a stoppered axle component;[317,318] and snapping− where two half-axle components are joined through the macrocycle cavity.[319,320] Much rarer approaches to rotaxanes include chemical shrinkage of a large macrocycle around a stoppered axle,[321,322] swelling of small stopper groups in a pseudorotaxane complex to prevent macrocycle dethreading,[323] as well as slipping of a macrocycle over the stopper groups of an axle under elevated temperatures to form a kinetically-stable pseudorotaxane that remains stably interlocked under ambient conditions.[324,325]

By utilising specific properties of certain reactions, conceptually newer approaches towards MIMs have been demonstrated. For instance, capitalising on the reversibility of olefin metathesis, rotaxanes have also been produced from disjointing an olefin-containing ‘magic rod’ axle and snapping the resulting ‘broken’ axle together through a macrocycle cavity,[326] as well as ring-opening of an olefin-containing ‘magic ring’ macrocycle and subsequently clipping it around a stoppered axle.[327] Notably, the ‘magic ring’ approach has been employed for catenane synthesis as well.[328,329] Taking advantage of the more diverse synthetic routes

towards rotaxanes, catenanes have also been prepared by topological interconversion[309] of rotaxane and catenane structures using metal complexation[330] and photochemical cyclomerisation reactions.[331] Interestingly, the original rotaxane structures can be recovered from these catenanes by reversing these reactions, i.e. by ligand removal from a metal centre as well as using different wavelengths of light respectively.

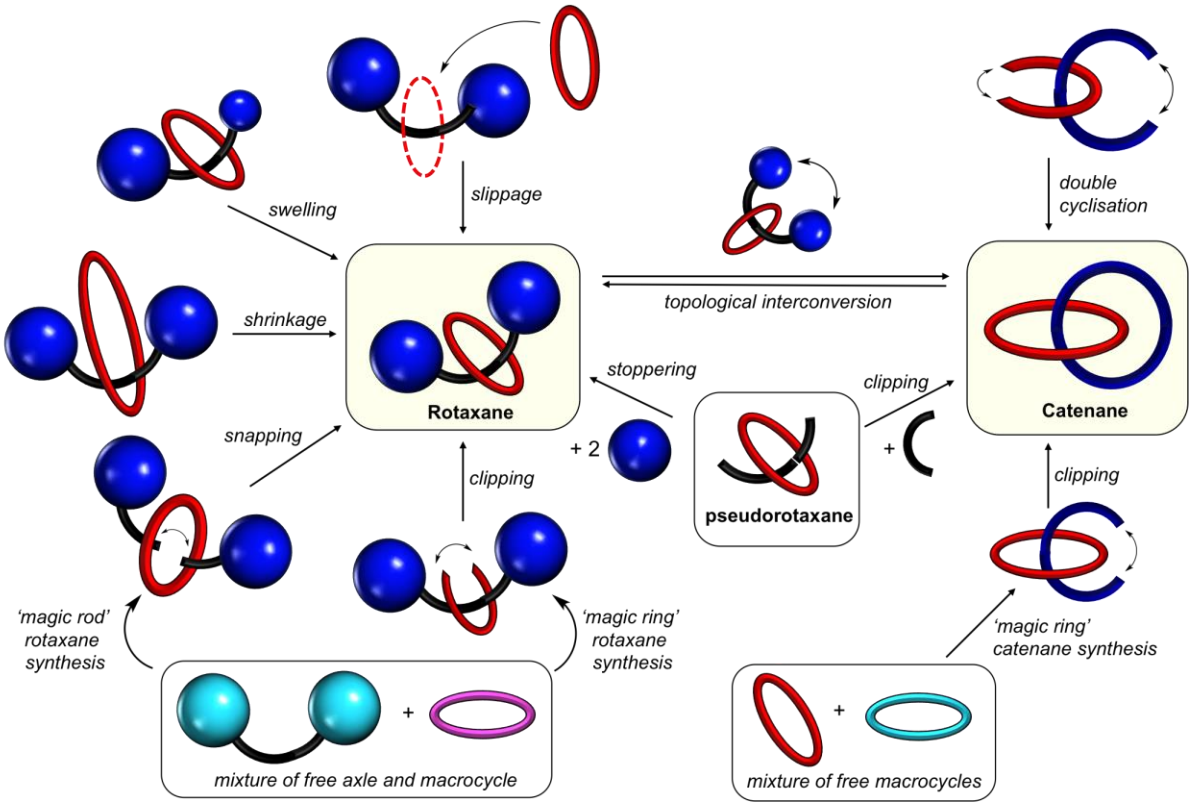


***Figure 1.33**. Schematic illustration of various routes for synthesising rotaxanes and catenanes.*

The following sections explore, in greater detail, the use of various templating strategies to synthesise MIMs.

1.3.2.1 Covalent Templates

During the synthesis of interlocked structures, the interpenetration of two or more molecular components to form a pseudorotaxane precursor is arguably the most challenging step. Early attempts to coax precursors to thread through each other made use of covalent templates to preorganise molecular components around it, which are subsequently cleaved to form the MIM. First utilised by Schill and Lüttringhaus to synthesise a [2]catenane in 1964,[332] a

number of MIMs were successfully prepared in significantly improved yields compared to statistical threading methods (*vide supra*), including [2]rotaxanes[333,334], [2]-[335–338] and [3]catenanes[339]. This principle was applied as recently as 2006 to synthesise rotaxanes (Figure 1.34), where the dynamic covalent chemistry of imine bonds allowed the formation of a bis-imine pseudorotaxane complex under thermodyamic control. Stoppering of the pseudorotaxane, followed by imine hydrolysis and 'switching off' the reactive aldehyde functionality by dithioacetylisation, formed the [2]rotaxane in impressive yields.[340] However, due to their inherent synthetic complexity, the use of covalent templates for MIM synthesis have been largely superseded by other methods of templation as discussed below, of which templation by cationic species are the most common.

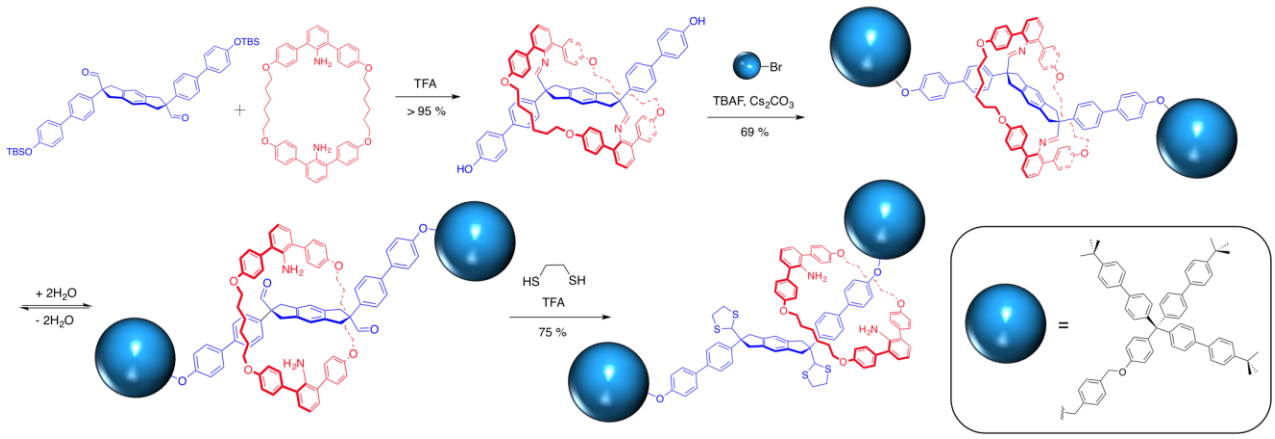


Figure 1.34. *Synthesis of Kawai's covalent-templated [2]rotaxane by reversible imine formation.*[340]

1.3.2.2 Cation Templates

The seminal 1983 report by Sauvage *et. al.* of a [2]catenane synthesised using a Cu(I) template revolutionised the field of MIMs (Figure 1.35). Capitalising on the preferred tetrahedral coordination of Cu(I), a phenanthroline ligand was threaded through a macrocycle bearing the same ligand motif to generate a 'crossing point', where both ligands were coordinated to Cu(I) orthogonally. Thereafter, a 'clipping' reaction involving the Williamson ether ring-closing reaction formed a metallo-catenane, with the free catenane subsequently obtained by Cu(I)-decomplexation using KCN.[341] In this process, the metal cation acts as a 'passive template' as it does not take part in the actual MIM-forming reaction, but merely

organises the ligands around it by strong and well-defined inner-sphere coordination bonds. Since Sauvage's pioneering work, linear (e.g. Au^{I}),[342] square-planar (e.g. Pd^{II}),[343,344] trigonal bipyrimidal (e.g. Cu^{II}, Zn^{II})[345] and octahedral (e.g. Cd^{II}, Ru^{II}, Ni^{II}, Co^{III}, Fe^{II})[346–349] coordination geometries have also been exploited for the metal template synthesis of MIMs (Figures 1.36A-C). The versatility of the passive metal template approach has since facilitated access to a range of higher-ordered interlocked structures, including an unsymmetrical [3]catenane,[350] [3]-,[351] [4]-[352] and [5]-rotaxanes,[353] as well as a Zn^{2+}-templated daisy-chain polyrotaxane which also function as a molecular muscle.[354] Particularly impressive are Leigh's 'Star of David' [2]catenane, which comprises two interlocked macrocycles which are triply-intertwined (Figure 1.36D) templated by six octahedral Fe^{2+} metal centres;[355] as well as Nitschke's Fe^{2+}-templated [3]catenane (Figure 1.36E).[356]

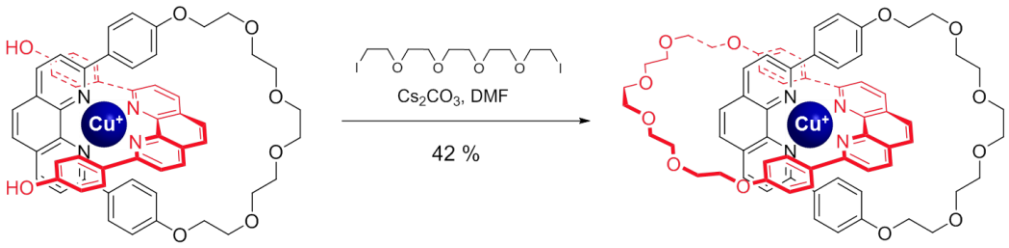


Figure 1.35. *Sauvage's Cu(I) passive metal templated [2]catenane.*[341]

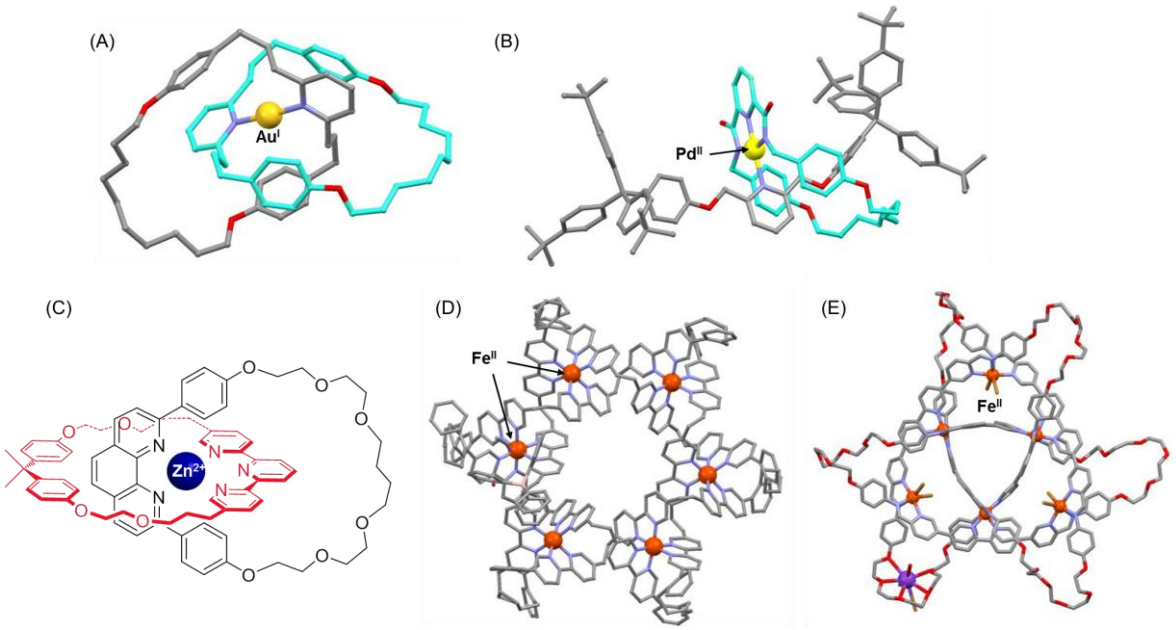


Figure 1.36. *Passive metal templated MIMs: (A) Leigh's linear Au(I)-templated [2]catenane*[342]*; (B) Leigh's square-planar Pd^{2+}-templated [2]rotaxane*[343]*; (C) Sauvage's trigonal bipyrimidal Zn^{2+}-templated catenane*[345] *(D) Leigh's octahedral Fe^{2+}-templated 'Star of David' [2]catenane*[355]*; (E) Nitschke's Fe^{2+}-templated [3]catenane.*[356]

In addition to transition metals, MIMs have been templated by discrete metal cations which include the alkali metals (e.g. Li^+, Na^+, K^+),[357–360] alkali earth metals (e.g. Ca^{2+}, Ba^{2+})[361,362] and lanthanides.[363] However, these metal cations generally have less well-defined coordination geometries than transition metals, and their applications in templation often relies on their 'hard-hard' interactions with atoms such as oxygen, which are often incorporated into macrocycles (e.g. crown ethers). For example, a combination of aromatic donor-acceptor interactions and Li^+-coordination with oxygen atoms on the polyether macrocycle and the pyromellitic diimide thread provides the driving force for the assembly of a [2]catenane by Sanders *et. al.* (Figure 1.37).[359]

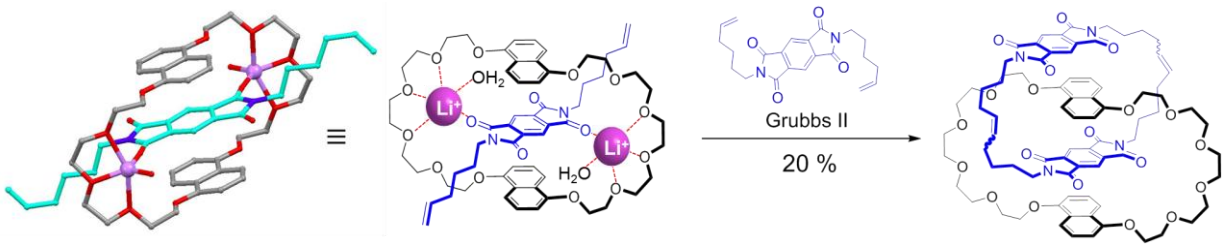


***Figure 1.37**. Sander's Li^+-templated [2]catenane.*[359]

In addition to their ability to preorganise molecular components, transition metal cations can also catalyse covalent bond formation. Taking advantage of this property, the 'active metal template' (AMT) strategy has been developed, where a catalytically-active metal cation coordinated endotopically within the cavity of a macrocycle catalyses covalent bond formation through the cavity itself between appropriately-functionalised precursors to form a MIM (Figure 1.38A).[364] Unlike the passive metal template approach, the precursor molecules need not have permanent recognition sites for metal cations, and catalytic quantities of metal cations can be used. While the copper(I)-catalysed azide-alkyne cycloaddition (CuAAC) reaction is arguably most commonly employed in AMT (see Section 2.1 for more details),[320,365,366] a range of transition-metal catalysed reactions have been employed for MIM synthesis. These include reactions catalysed by Cu^I (e.g. Ullmann,[367] Glaser,[368] Cadiot-Chodkiewicz[369] and Goldberg coupling[370]), Pd^{II} (e.g. Pd^{II}-mediated Michael addition,[371] alkyne-homocoupling,[372] Heck cross-coupling[373]), Ni^{II} (e.g. alkyne homocoupling,[374] C(sp^3)-C(sp^3)

homocoupling[375]) and Zn^{II} (e.g. Zn^{2+}-catalysed Diels-Alder reaction[376]). Using these reactions, an impressive diverse array of [2]rotaxanes,[367,369,373,375,377–380] [2]catenanes[368,381] and higher-order interlocked structures[320,365,382–384] (Figure 1.38B-D) have been prepared in synthetically useful yields, with 99 % [2]rotaxane formation observed in one remarkable case.[371]

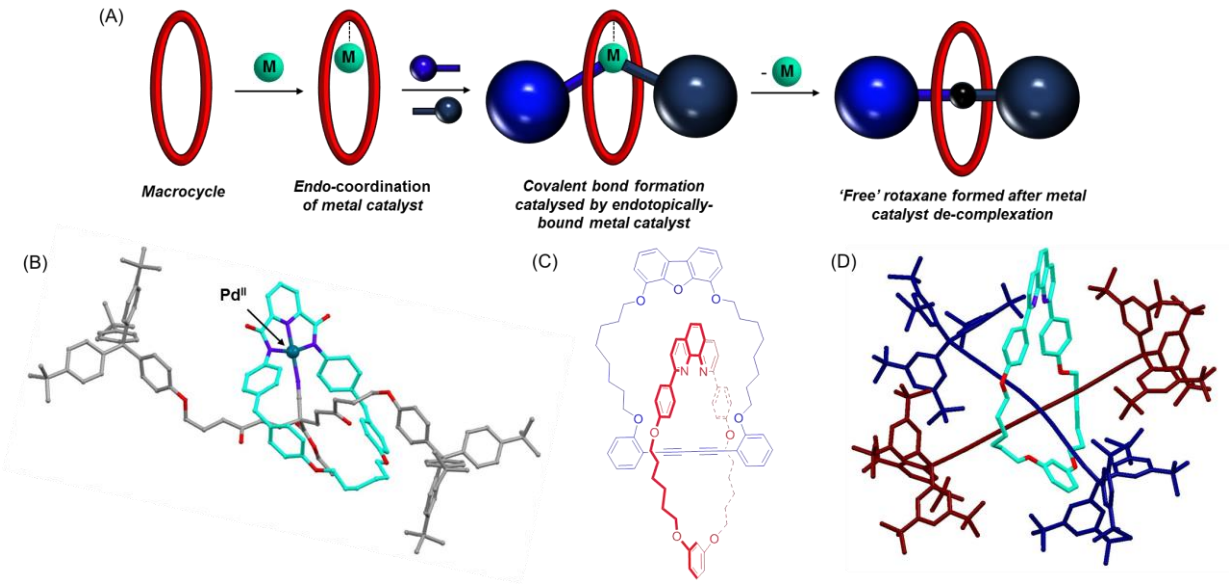
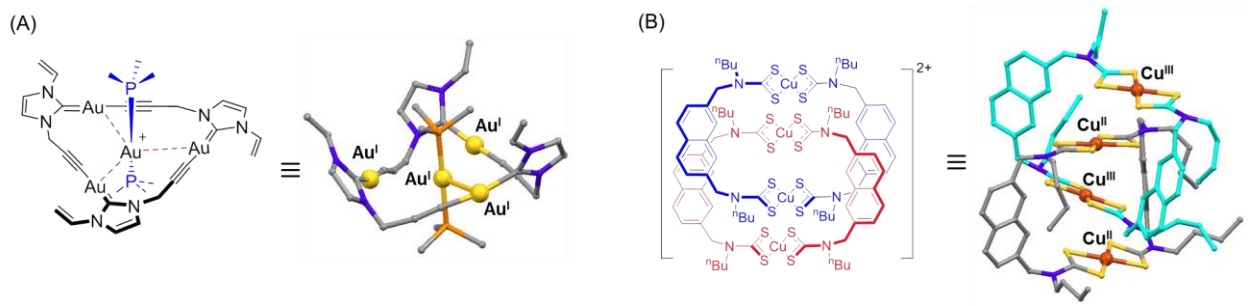


Figure 1.38. *Active metal template synthesis of MIMs: (A) Schematic illustration of the AMT strategy; (B) Leigh's [2]rotaxane from Pd^{II}-mediated Michael addition reactions[371]; (C) Saito's [2]catenane prepared using Cu(I)-catalysed Glaser alkyne-alkyne homocoupling[368]; (D) Anderson's double-threaded polyyne [3]rotaxane from Cu(I)-catalysed Cadiot-Chodkiewicz alkyne cross-coupling.[385]*

Attractive metal-metal interactions arising from charge transfer between transition metal cations have also been exploited in the synthesis of MIMs. For instance, aurophilic interactions between Au^{I} centres was shown to template the self-assembly of a [2]rotaxane, with short Au^{I}-Au^{I} contacts observed between the trinuclear Au^{I}-macrocycle and $Au(PMe_3)_2^+$ axle in the solid state (Figure 1.39A).[386] Similar strategies were employed to also assemble a series of [2]catenanes using aurophilic interactions,[387,388] as well as Cu^{II}-Cu^{III} [389](Figure 1.39B) and Cu^{II}-Au^{III} charge-transfer interactions.[329]


(A)
(B)
Au
Au
Au

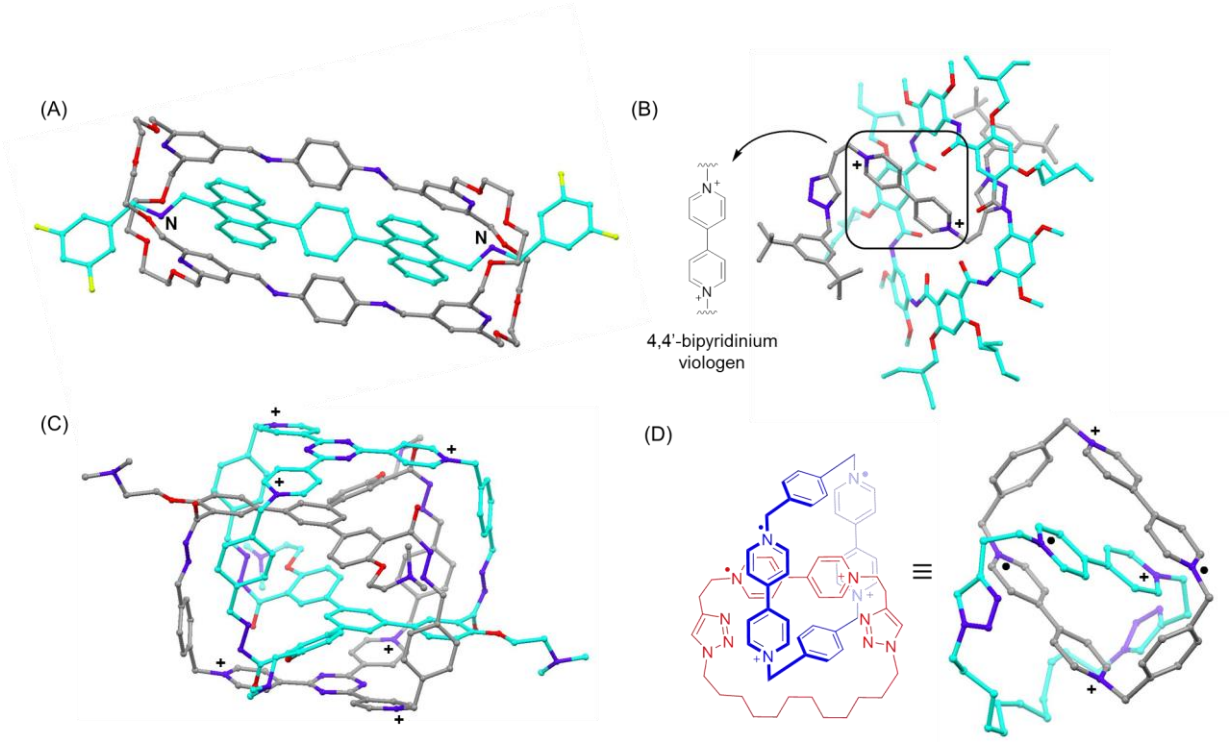


Figure 1.40. *Examples of cationic organic motifs templating MIM formation: (A) Stoddart's secondary ammonium-templated suit[2]ane[394]; (B) Yuan's viologen-cyclo[6]aramide [2]rotaxane[400]; (C) Sessler's hexa-pyridinium [2]catenane self-assembled in aqueous acid[405]; (D) Stoddart's tris-viologen cationic radical-pair templated [2]catenane.[408]*

1.3.2.3 Anion Templates

Compared to cations, syntheses of MIMs using anion templates are much rarer. Nevertheless, anionic functional groups incorporated into precursor molecules and discrete anions have been successfully shown to template the formation of rotaxanes and catenanes.

Organic anionic motifs were first used to template rotaxane synthesis *via* a 'snapping' strategy in 1999 by Vogtlë.[319] A bulky phenoxide 'half-axle' component held by HB interactions within a bis-isophthalamide macrocycle was used to perform an S_N2 reaction with another alkyl bromide 'half axle' to form a [2]rotaxane in 95 % yield (Figure 1.41A). Alternatively, forming a pseudorotaxane complex driven by interactions between a macrocycle and an axle precursor bearing anionic functionalities, followed by stoppering, offers another route towards rotaxanes. First pioneered by Schalley in 2002,[411] this approach has very recently been employed by Flood *et. al.* to form a [3]rotaxane by capitalising on the the ability of his oxoanion-binding 'cyanostar' macrocycles to form 2:1 'sandwich' complexes with dialkyl

phosphates. Subsequent CuAAC-stoppering reactions afforded the target [3]rotaxanes with yields of as high as 80 % (Figure 1.41B).[179,412]

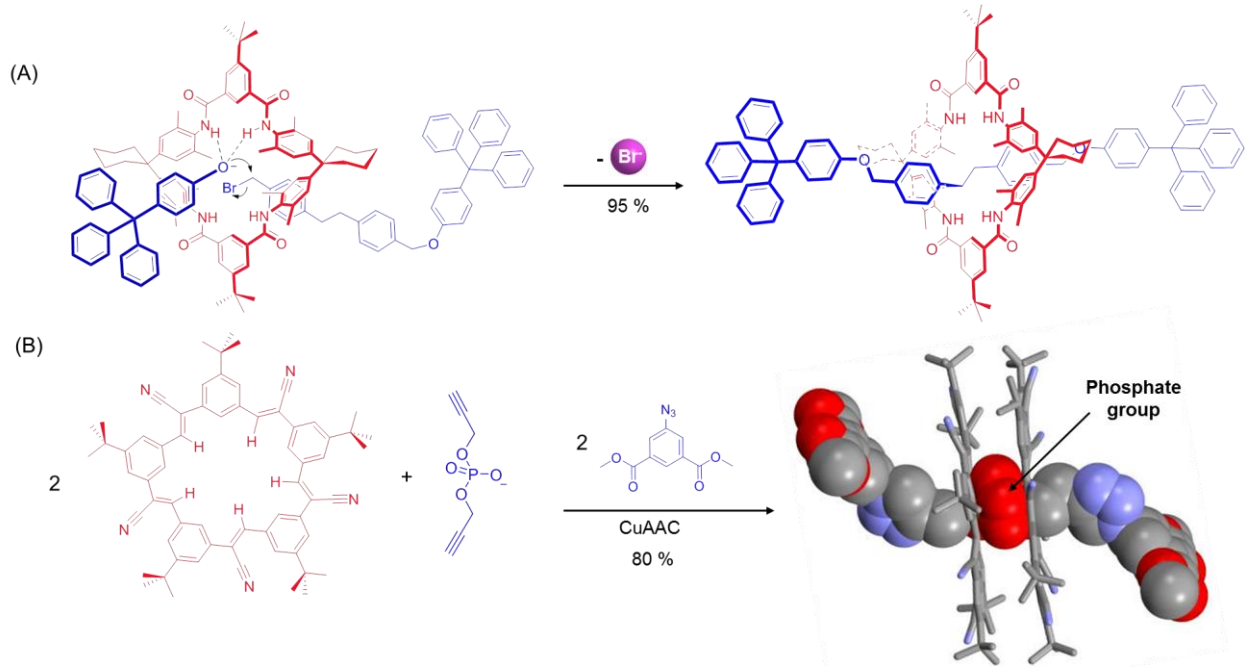


Figure 1.41. *Examples of rotaxane synthesis templated by organic anion motifs: (A) Vogtlë's phenoxide-templated rotaxane by 'snapping'* [319]*; (B) Flood's dialkyl-phosphate-templated [3]rotaxane.*[412]*.*

Although serendipitous discovery of MIM formation using anions have been reported as early as 1997,[413] a discrete anion templation strategy was not developed till the turn of the millennium by Beer and co-workers starting from the discovery that chloride was necessary to template the orthogonal self-assembly of a pair of isophthalamide-containing molecules, as well as pseudorotaxanes, in d_6-acetone (Figure 1.42A).[414] In this approach, the self-assembly of two or more MIM-precursors, usually forming a pseudorotaxane complex coordinated around the anion, is followed by clipping or stoppering reactions to produce the target rotaxanes or catenanes. Driven by chloride templation, the potent HB anion recognition isophthalamide motif incorporated into macrocycle and thread/axle designs has allowed successful syntheses of a series of MIMs including [2]-[415–417] and [3]rotaxanes,[226,418] [2]catenanes,[225,419–421] a 'Janus' rotaxane[422] and a handcuff catenane[423] (Figure 1.42B). Other than chloride, anions possessing other geometries such as bent (nitrite)[424] and trigonal planar (nitrate)[425,426] have been subsequently shown to also template MIM formation. In addition, the use of diverse anion binding motifs including indolocarbazole,[427] prototriazolium[428] and

imidazolium,[429] as well as XB functionalities such as bromo-imidazoliums,[430] pyridinium-iodotriazoles[98,194–196] and iodotriazoliums[431] have also been successfully demonstrated. Notably, XB-anion templating interactions capitalise on the linearity of XB interactions to maximise their strength, as exemplified by Beer's bis-bromoimidazolium containing [2]catenane[430] (Figure 1.42C) and all-XB [2]rotaxane (Figure 1.42D).[432]

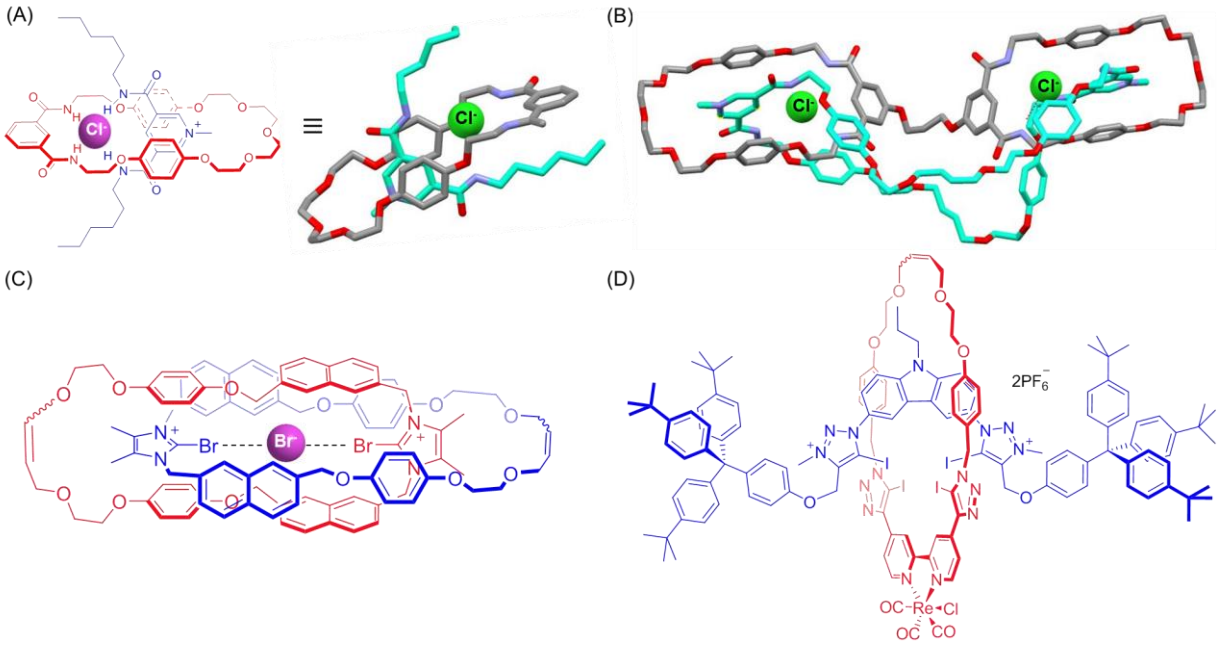


Figure 1.42. *(A) A chloride-templated pseudorotaxane and its crystal structure[414] ; (B) Solid state structure of Beer's Cl⁻-templated handcuff catenane[423]; (C) Beer's [2]catenane templated by XB-Br⁻ interactions [430]; (D) Beer's Cl⁻-templated all-XB rotaxane.[432]*

1.3.2.4 Neutral Templates

Neutral molecules can template the self-assembly of MIMs by forming intermolecular interactions between molecular precursors. Extending the early work of HB templation of neutral MIMs by Hunter,[433] Leigh[434] and Vogtlë,[435] Philp very recently demonstrated the synthesis of a self-replicating [2]rotaxane which relied crucially on the self-assembly of a pseudorotaxane from hydrogen bonds between an isophthalamide macrocycle and an amide motif on the axle precursor (Figure 1.43A).[436,437] A similar strategy has also been employed by Evans in 2015 to template the self-assembly of a [2]catenane (Figure 1.43B).[438] Other than HB interactions, solvophobic interactions can drive the self-assembly of MIMs under aqueous

conditions, such as the exploitation of aromatic donor-acceptor interactions by Sanders in the dynamic combinatorial synthesis of catenanes in water (Figure 1.43C).[439–441] Inclusion complexes of cyclodextrins with hydrophobic extended-π motifs such as anthracene[442] and bis-thiophene[443] have been shown to be another powerful avenue for assembling rotaxanes. Particularly impressive are Anderson's double-threaded hetero-[3]rotaxane formed using γ-cyclodextrin with stilbene and cyanine threads driven by the hydrophobic effect in water,[444] as well as Wang's [1]rotaxane formed from the inclusion complex of a pillar[5]arene and an aliphatic amine thread by C-H···π interactions in DMSO (Figure 1.43D).[445]

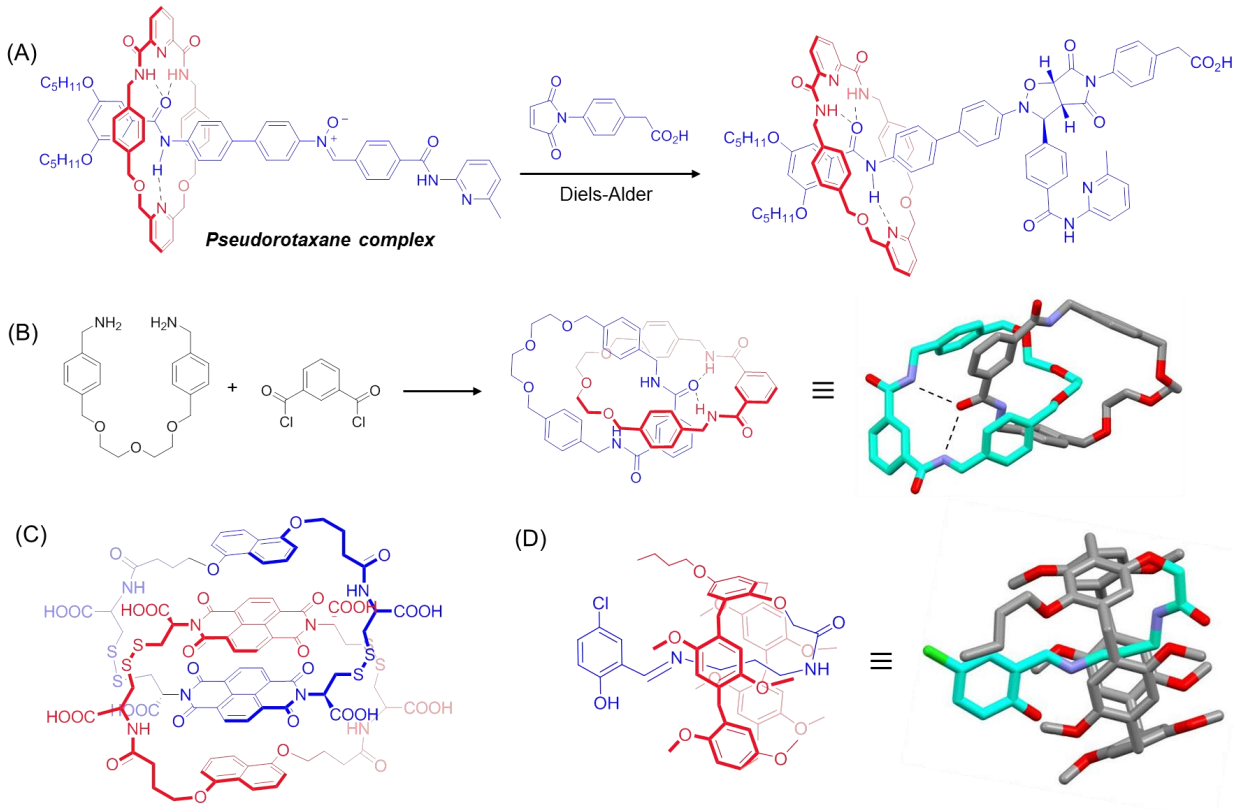


Figure 1.43. *(A) Philp's HB-templated self-replicating [2]rotaxane[436]; (B) Evan's HB-templated [2]catenane[438]; (C) Sanders' aromatic donor-acceptor interaction-driven [2]catenane[439]; (D) Wang's pillar[5]arene [1]rotaxane.[445]*

Ion pairs provide a powerful means of assembling MIMs. Alkali metal salts of organic phenoxides act as 'traceless ion pairs' which have been exploited by Smith *et. al.* to synthesise rotaxanes.[446,447] In this approach, the association of K^+ with the dibenzo-18-crown-6 moiety of a macrobicycle forms a contact ion pair with the phenoxide counteranion, which is

anchored within the macrobicycle by convergent HB interactions. Subsequent reaction of this complex with isophthaloyl chloride then produces a neutral rotaxane which does not retain the original potassium phenoxide templating ion pair (Figure 1.44A). Alternatively, contact ion pairing interactions between constituent components of MIMs can template their formation, which is exemplified by Leigh's [2]rotaxane containing an anionic PdCl-complexed macrocycle and a cationic pyridinium axle (Figure 1.44B),[448] as well as Yashima's amidinium-carboxylate salt bridge-containing [2]catenane (Figure 1.44C).[449] Finally, zwitterionic motifs such as squaraine has been used to template rotaxane formation due to its ability to form hydrogen bonds with isophthalamide motifs of a macrocycle (Figure 1.44D).[450,451]

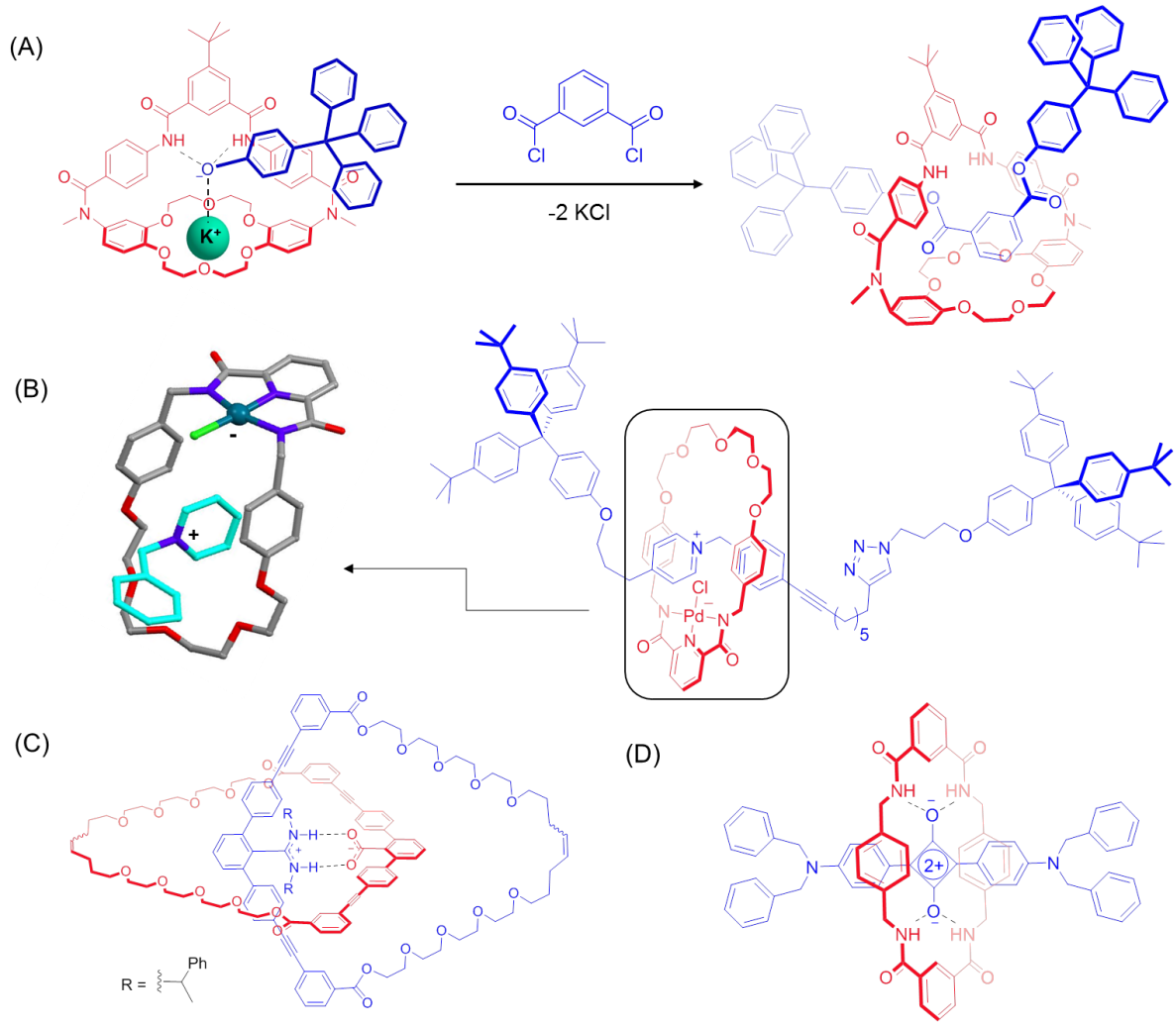


Figure 1.44. *(A) Synthesis of Smith's 'traceless ion pair' rotaxane[446]; (B) Leigh's ion pair-templated [2]rotaxane[448]; (C) Yashima's salt-bridge [2]catenane[449]; (D) Smith's zwitterionic squaraine-containing [2]rotaxane.[450]*

1.3.2.5 Biomolecular templates

The potential of structural biological nanotechnology has spurred developments in constructing MIMs from biological macromolecules (e.g. proteins and DNA) within the last decade.[452,453] Due to the size and structural complexity of these biological molecules, novel strategies of biological templation had to be devised to complement the existing strategies aforementioned, which capitalise on their intrinsic chemical properties such as the complementary base pairing of DNA.[454,455] In one strategy pioneered by Famulok and coworkers (Figure 1.45A), Watson-Crick base-pairing enabled spontaneous pseudorotaxane formation in quantitative yield from a double stranded DNA macrocycle and a linear thread, each containing a single-strand bearing sequences complementary to each other. Ligation of the bulky spherical stopper groups, and subsequent liberation of the axle and macrocycle using 'release oligonucleotides' ('RO's) which bind to each of the single stranded regions, afforded the free rotaxane.[456] Similar strategies have enabled DNA daisy chain rotaxanes,[457] [2]catenanes[458,459] and even a [7]catenane[460] to be produced, some of which can exhibit rotary motion[461] and catalytic activity.[462] In contrast, synthetic peptide-based MIMs are comparatively rare, and require different strategies for construction.[463,464] A very recent example utilised selective mutagenesis of naturally-occurring [1]rotaxane lasso peptides, where enzymatic cleavage of their loop region exposed reactive thiol groups which could be chemically reduced to form disulfide linkages. This enabled the self-assembly of a mixture [2]-, [3]- and [4]catenane structures, of which the [3]catenane was the dominant product (Figure 1.45B).[465]

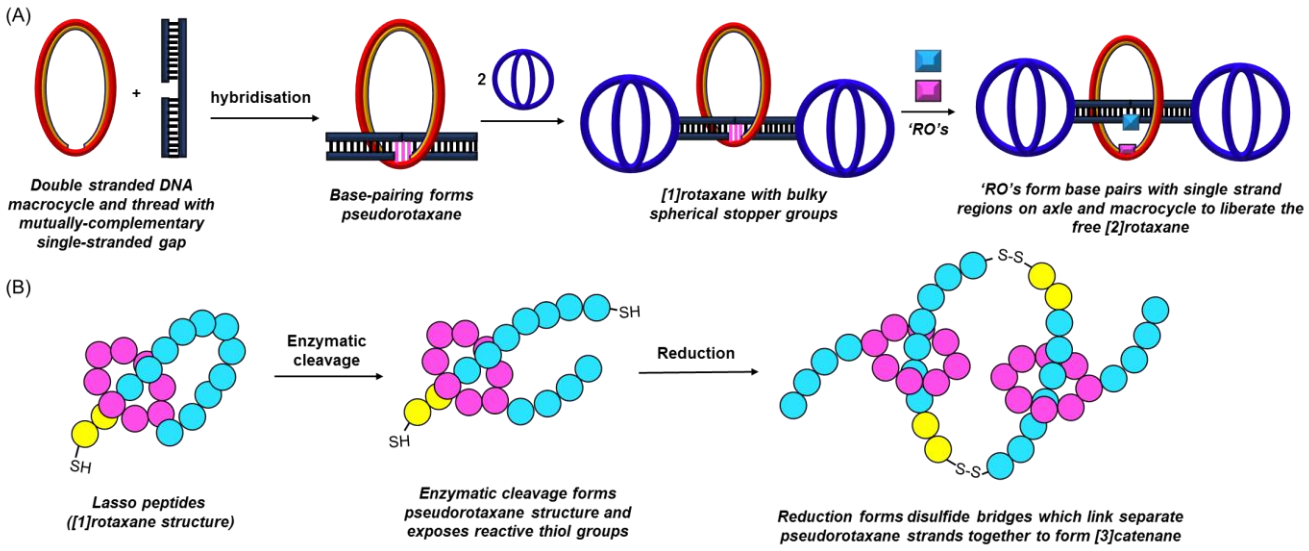


Figure 1.45. *Examples of biologically-templated MIMs: (A) Famulok's DNA rotaxane[456]; (B) Link's peptide [3]catenane formed from lasso peptides.[465]*

1.3.3 Applications of Interlocked Molecules

The aforementioned advances in synthetic methods and templating strategies have enabled MIMs to be accessed in synthetically useful yields, which have naturally led to a range of applications in interdisciplinary fields, each capitalising on the unique structural properties and mobility conferred by the mechanical bond (Section 1.3.1). The following sections offer a brief overview of recent developments.

1.3.3.1 Recognition and Sensing of Charged Species

The space between the interlocked components of MIMs can act as highly preorganised cavities for three-dimensional encapsulation of charged guest species.[466] Incorporating Lewis basic groups around the binding cavity has allowed rotaxanes and catenanes to act as hosts for alkali metal (Figure 1.46A),[467,468] alkali earth metal[469] and transition metal cations.[470,471] On the other hand, MIMs decorated with Lewis-acidic groups around the binding site can function as anion receptors. Using the discrete anion templation strategy (Section 1.3.2.3), Beer *et. al*. has synthesised numerous MIMs containing convergent electron-deficient HB and XB-donor groups which are capable of binding different halides[98,423,430–432,472–474] and oxoanions[196,425,426,475,476] in highly-competitive aqueous-organic solvent mixtures by modifying the space and geometry of the binding cavity. Recent work has

seen the preparation of β-cyclodextrin-stoppered XB water-soluble [2]rotaxanes capable of impressively strong and selective iodide association (K_a > 2000 M^{-1}) in pure water, where the anion is bound in the unique interlocked cavity between the axle and macrocycle subunits (Figure 1.46B).[194] In addition, higher-order MIMs can also be used for anion coordination, as seen by Beer's XB [3]rotaxane which binds nitrate (K_a = 1782 M^{-1} in 1:1 $CDCl_3$/ CD_3OD) preferentially over chloride, where the anion is bound in the space between both macrocycles in a sandwich-type structure (Figure 1.46C).[477] Furthermore, the appendage of suitable reporter groups on the MIM framework has enabled selective anion sensing via electrochemical[227,417,478,479] and optical[195,363,418,432,480] means as well. Not just limited to solution-phase studies, MIMs immobilised on solid surfaces, such as Beer's ferrocene-appended catenane, has also allowed sensitive electrochemical detection of chloride.[225] Finally, rotaxanes containing both anion recognition sites (e.g. isophthalamide) as well as cation binding motifs (e.g. calix[4]arenes) have been shown to bind ion pairs as exemplified by Beer's[481] (Figure 1.46D) and Ballester's[482] heteroditopic [2]rotaxanes selective for sodium chloride and tetrabutylammonium (TBA) cyanate respectively in chloroform-containing organic solvent media.

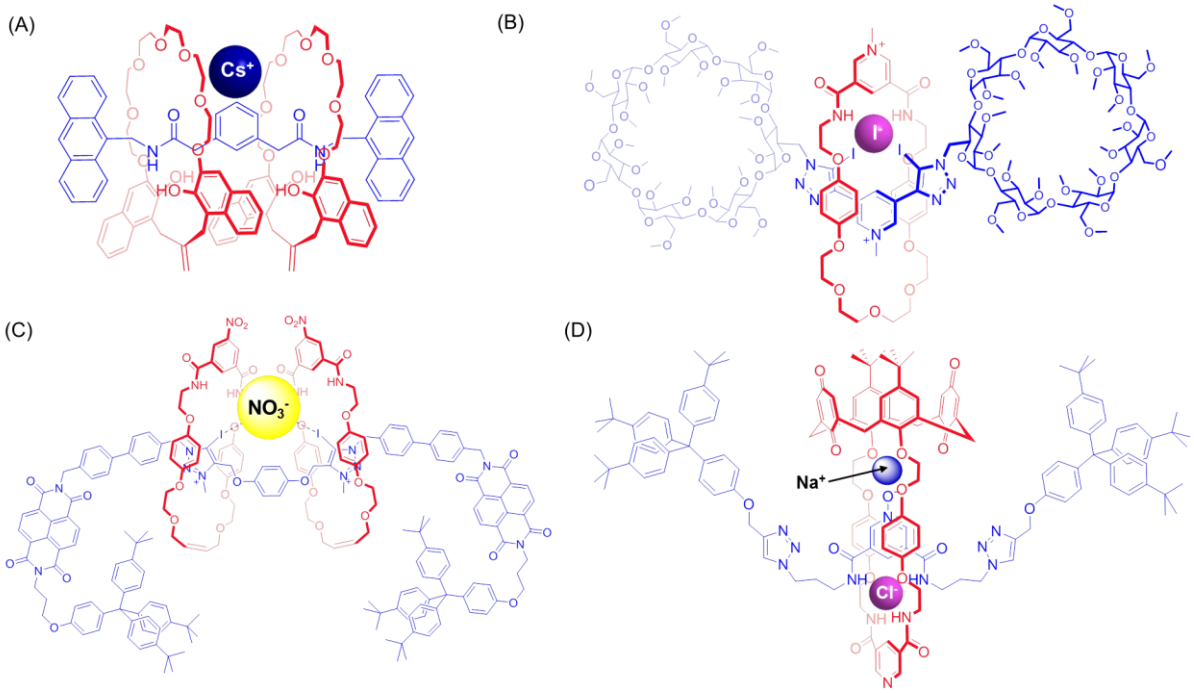


Figure 1.46. *Examples of MIM host molecules for binding of charged guests: (A) Kanesato's Cs^+-binding [3]rotaxane[468]; (B) Beer's water-soluble XB iodide-selective [2]rotaxane[194]; (C) Beer's nitrate-selective XB [3]rotaxane[477]; (D) Beer's NaCl-binding heteroditopic [2]rotaxane.*[481]

1.3.3.2 Nanomedicine

MIMs, in particular rotaxanes, have shown great promise as biological imaging and drug delivery systems. By incorporating the near-IR squaraine dye into rotaxane axles (structurally similar to that in Figure 1.44D),[483–485] kinetic stabilisation conferred by the macrocycle acting as a chemical shield protects the dye against biological degradation in cells[450] as well as reducing dye aggregation in aqueous media, thus allowing them to be used for *in-vivo* biological imaging studies. Their performance and stability for such studies has been compared to traditional dyes[486] and recent incorporation of an endoperoxide motif on the rotaxane macrocycle component has allowed dual-modality imaging with both chemiluminescent and fluorescent properties.[487]

Also using the enhanced kinetic stabilisation conferred by rotaxanes, the groups of Leigh and Papot have pioneered their use for delivery of drug molecules which are otherwise unstable *in vivo* as enzyme-responsive prodrugs.[488] In a recent example of this concept, the intracellular delivery of the anticancer drug paclitaxel, which is usually degraded in blood plasma, was successfully achieved by incorporation into a rotaxane axle, where the macrocycle component shields a crucial ester linkage from plasma esterase-mediated hydrolysis (Figure 1.47). Upon cellular uptake, intracellular β-galactosidase triggers macrocycle ring-opening to expose the paclitaxel-containing axle which can be degraded by esterases to release the drug within the cell.[489] In addition, the ready uptake of rotaxanes into cells, which has been shown to be an energy-independent process,[490] has enabled the transmembrane delivery of peptide-derivatives otherwise impermeable to cells for bioimaging,[491] as well as acting as therapeutic cytotoxic agents by delivering metal cations into cancer cell lines by acting as ionophores[492] or ligands (e.g. delivery of platinum).[493]

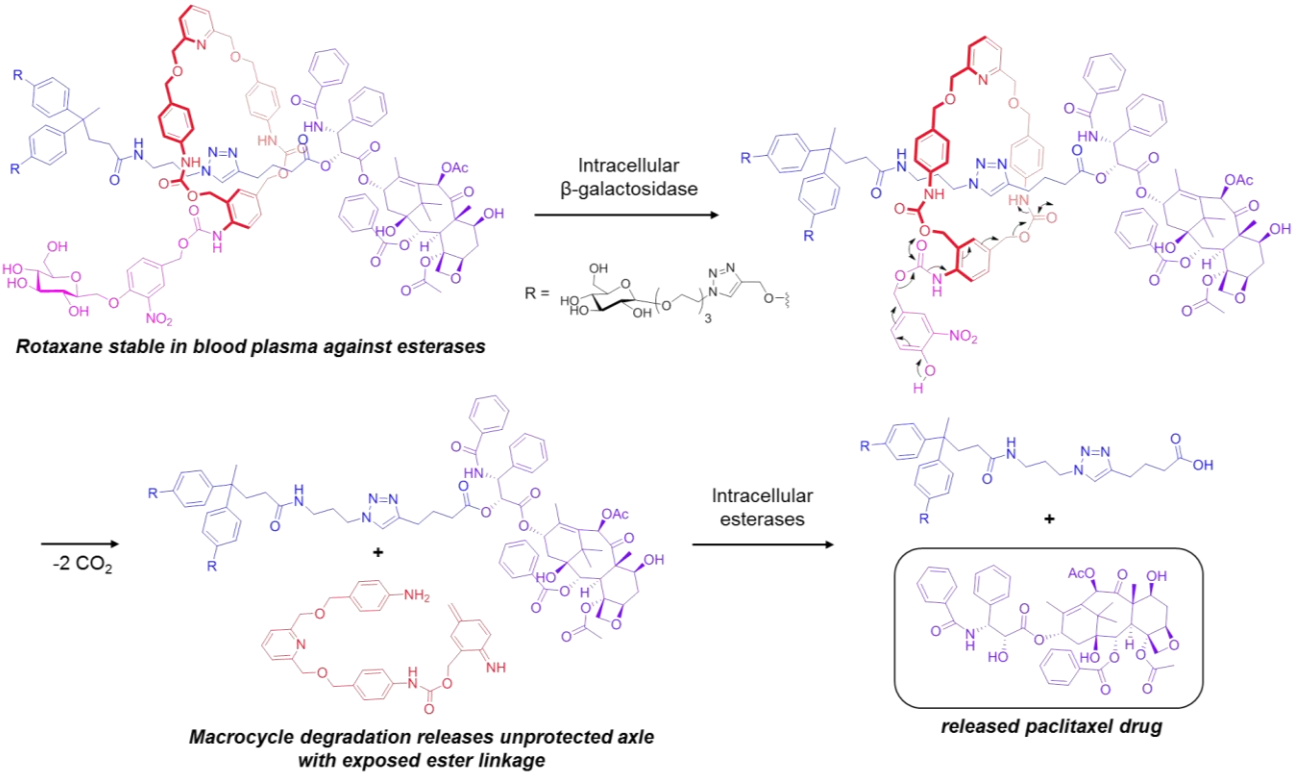


Figure 1.47. *Papot's enzyme-triggered rotaxane paclitaxel prodrug for intracellular delivery of paclitaxel.*[489]

1.3.3.3 Nanotechnology

The dynamic mobility of mechanically-bonded molecular components relative to each other has inspired the use of MIMs as nano-machines and switches by the engineering of stimuli-responsive conformational changes such as pH changes, metal complexation, anion coordination, and the presence of light.[7] For instance, the translational motion of a rotaxane's macrocycle along its linear axle to different stations, or rotation (pirouette) around it (Figure 1.48A), can be exploited to do useful work. Inspired by the seminal work of Stoddart in 1991, who demonstrated the first molecular shuttle,[494] numerous highly-imaginative systems have since been developed, which include molecular muscles that mimic the contraction and relaxation of muscle fibres,[410,495–497] nano-elevators,[498,499] a UV-light-driven rotaxane-based molecular machine which can move a liquid droplet against gravity,[500] as well as a ribosome-like [2]rotaxane which can synthesise sequence-specific oligopeptides (Figure 1.48B).[501] Methods to control the rate of movements were also elucidated, such as Leigh's discovery that

water can 'lubricate' and accelerate the translational motion of a rotaxane macrocycle,[502] Teixidor's finding that the pirouetting speed of a cationic macrocycle about an axle could be changed with the identity of the counteranion,[503] as well as XB-enhanced anion-triggered macrocycle translation in a [2]rotaxane compared to HB reported by Beer (Figure 1.48C).[504]

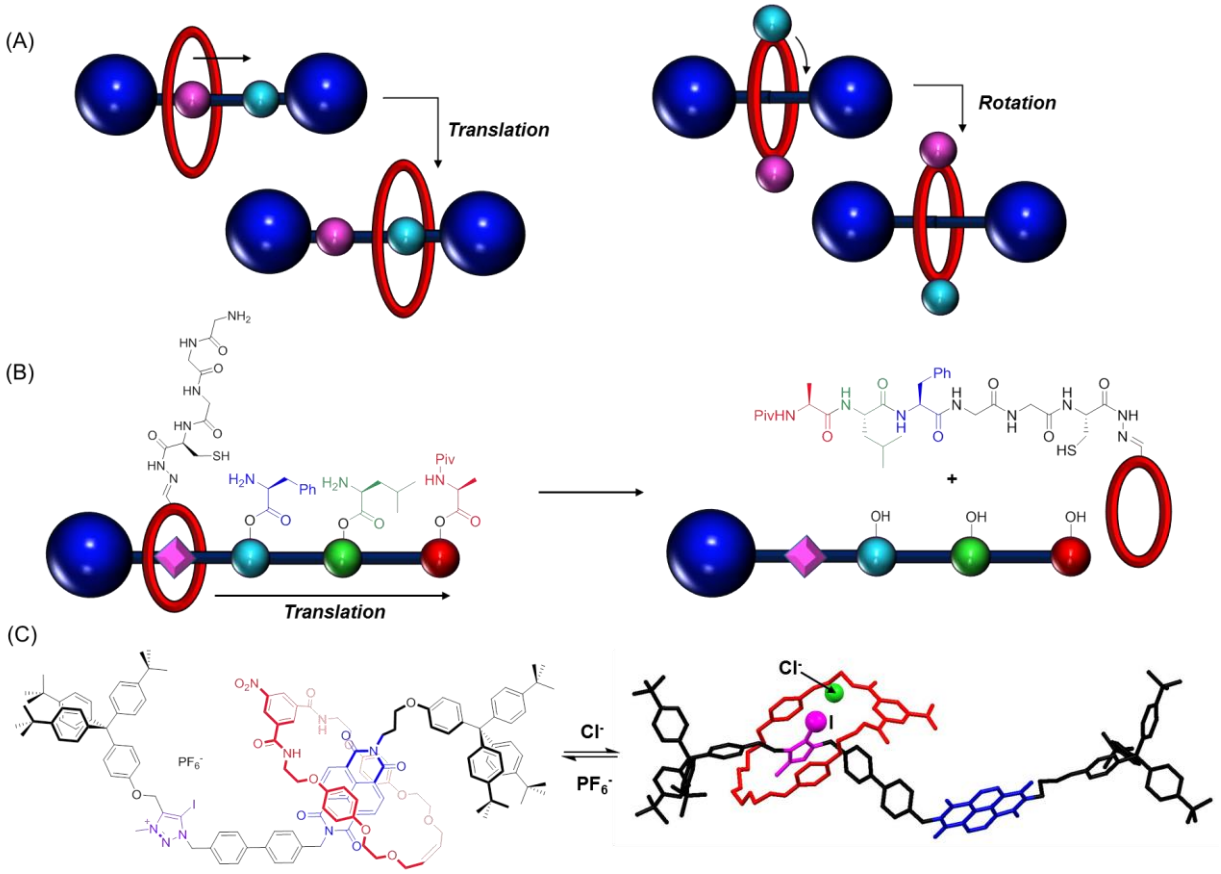


Figure 1.48. *(A) Schematic illustration of the possible stimuli-triggered motion that can be exhibited by a rotaxane; (B) Leigh's peptide-synthesising molecular machine[501]; (C) Beer's XB two-station [2]rotaxane which shows anion-triggered translational motion.[504]*

1.3.3.4 Catalysis

MIMs, in particular rotaxanes, have been used as catalysts by incorporating catalytically-active organic groups or transition metal complexes into their structure. Early forays into this field focused on the exploration of switchable catalysts by making use of the rotaxanes' stimuli-responsive conformational dynamism.[10] In a notable example, Leigh *et. al.* capitalised on the pH-triggered motion of a rotaxane axle to switch the chemoselectivity of a reaction containing a mixture of starting materials by exposing different catalytically-active

groups on an axle (Figure 1.49A).[505] More recently, the influence of the mechanical bond in altering the reaction field/ chiral environment has been studied. In a seminal early study, Takata demonstrated the importance of a 'rotaxane field' using a rotaxane organocatalyst bearing a catalytically-active thiazolium group on the axle, where the presence of a chiral macrocycle in close proximity could influence the stereochemical outcome of a benzoin condensation reaction by 'through-space chirality transfer' (Figure 1.49B).[506] This concept has since been extended to include Ni-catalysed conjugate addition reactions,[378] Rh-catalysed hydrogenation,[507] iminium-activated asymmetric Michael additions,[508] and a remarkable recent example from the Goldup group where a Cu(I) cofactor was found to be crucial for the catalytic activity of a Au(I) rotaxane towards the Ohe-Uemura cyclopropanation reaction by binding inside the rotaxane cavity itself (Figure 1.49C).[509] It is notable that the conformational changes in the rotaxane active site resulting from the Cu(I)-cofactor binding, which changes its catalytic activity, is akin to allosteric modulation seen in natural enzymes.

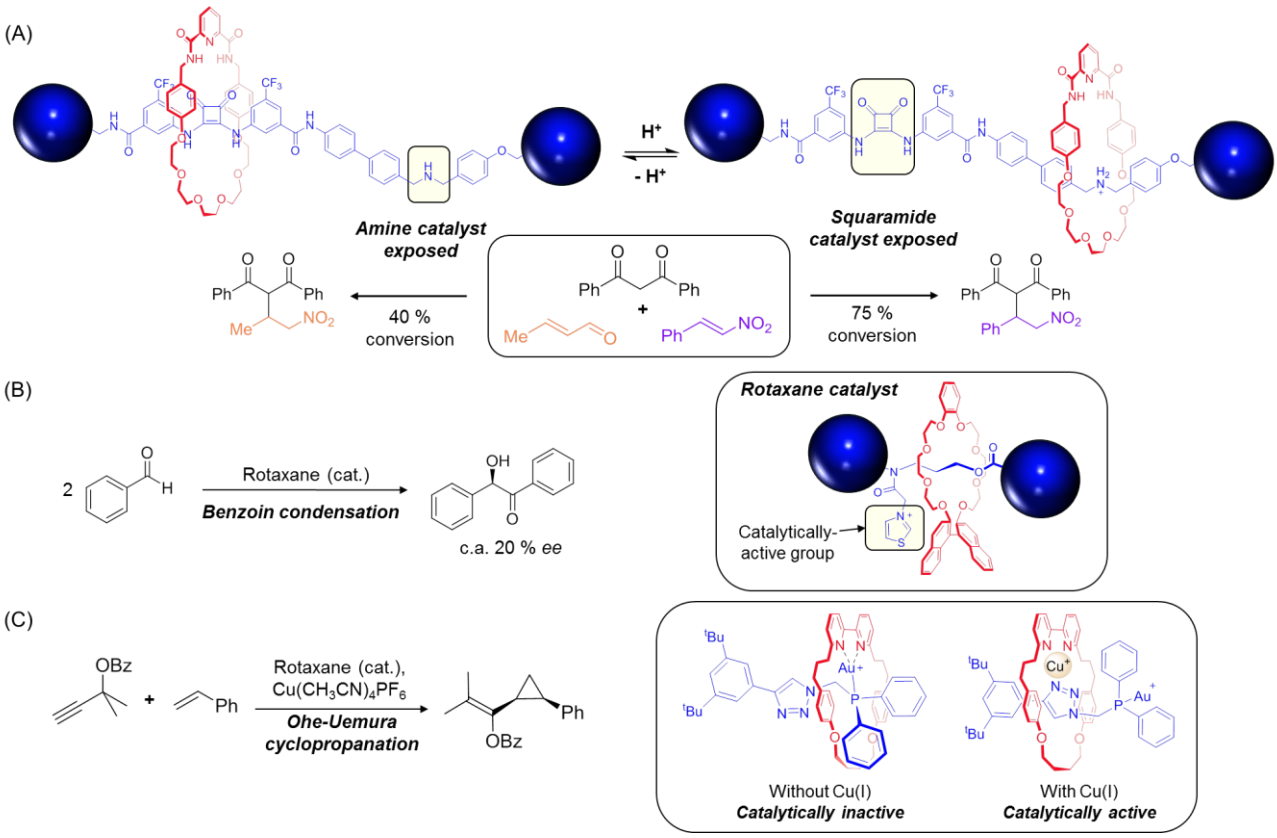


Figure 1.49. *(A) Leigh's pH-switchable [2]rotaxane catalyst[505]; (B) Takata's thiazolium [2]rotaxane for asymmetric benzoin condensation[506]; (C) Goldup's Cu(I)-switchable Au(I)-[2]rotaxane catalyst for Ohe-Uemura cyclopropanation.[509]*

1.3.3.5 Novel Materials

Polymeric materials containing mobile mechanically interlocked components combine the mechanical and physical properties of conventional polymers with the stimuli-responsiveness and conformational dynamism of discrete MIMs.[303,510,511] Owing to the structural complexity of polymers, the assembly of polyrotaxane polymers capitalise on specific host-guest interactions which enable self-sorting and assembly of monomers, such as the size-specific stable cucubit[8]uril-viologen[512] and crown-ether-secondary ammonium[513,514] inclusion complexes. For example, Harada produced a photo-responsive polyrotaxane polymer hydrogel by mixing an α-cyclodextrin-containing polymer with a *trans*-azobenzene-modified poly(acrylic acid) (Figure 1.50).[515] Photo-isomerism of azobenzene can give rise to reversible *gel-sol* transition, which can be exploited as a light-triggered molecular delivery platform.[516] Other than light, reversible redox-,[517–519] pH[520] and thermo-responsive[513,521] MIM-based supramolecular materials have also been reported. The incorporation of mechanical bonds in polymeric systems have also led to the recent development of slide-ring gels, a novel material which exhibits dramatically different visco-elastic properties from conventional physical gels.[304] In addition, their unique physical properties such as the ability to redistribute applied mechanical stress and large extensibility, promises a new generation of novel polymeric and gel-based materials.[522–524]

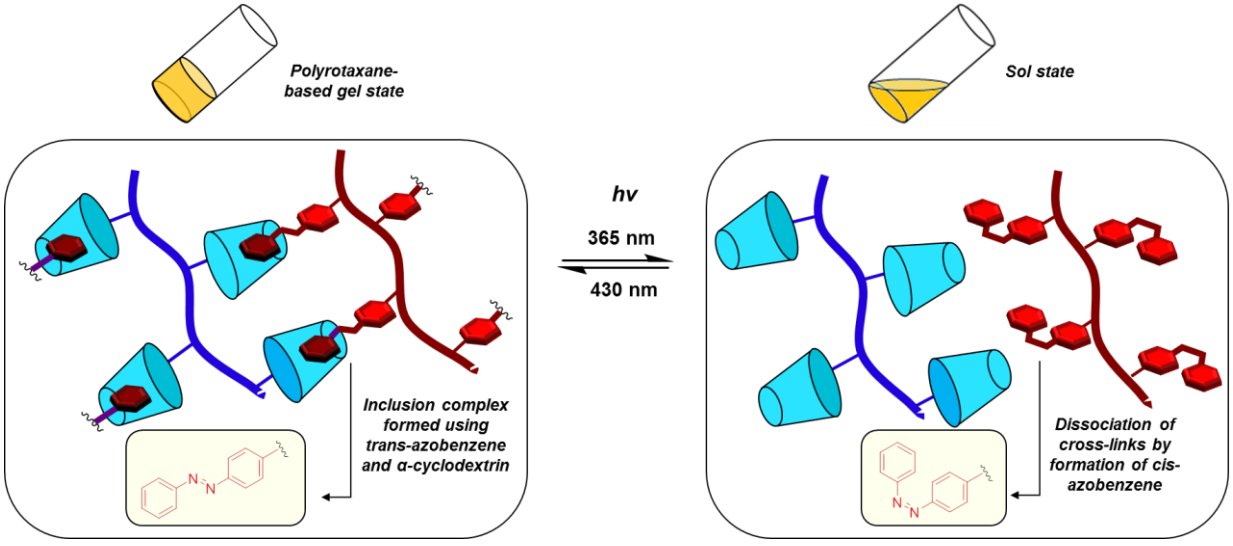


Figure 1.50. *Light-responsive behaviour of Harada's rotaxanebased polymeric azobenzene-α-cyclodextrin hydrogel.*[515]

1.4 Project Aims

Inspired by the diverse applications of anion binding and MIMs, as well as by the strength of XB···anion interactions demonstrated using the rare examples of acyclic and interlocked host molecules reported to date, this project aims to extend the scope of σ-hole mediated anion binding by exploring fundamental aspects of their binding properties in competitive solvent media, and developing further applications of rotaxanes containing σ-hole donor groups. In particular, the anion binding behaviour of ChB host molecules will be investigated and compared with those of XB host analogues in order to elucidate the solution-phase anion binding properties of the closely-related sister σ-hole interactions.

Chapter 2 initially describes the development of a general synthetic protocol for macrocycles containing XB or ChB-donor groups. After demonstrating the macrocycles' abilities to bind Cu(I), the syntheses of unprecedented neutral and cationic XB and ChB [2]rotaxane host molecules are presented using an active metal template strategy. Thereafter, a detailed study and comparison of the fundamental anion binding properties of these XB and ChB rotaxanes molecules with HB analogues is described. In addition, the syntheses of more diverse mechanically-interlocked structures (e.g. catenanes) bearing XB or ChB-donor groups is also explored using other metal and anion templation strategies.

Chapter 3 focuses on the application of σ-hole interactions in redox-active anion hosts for electrochemical anion sensing. The effects of σ-hole interactions on redox sensing are elucidated using a series of structurally-related bidentate XB/ ChB acyclic model receptors, and compared with their HB analogues. Furthermore, the syntheses of redox-active mixed-HB/XB and all-XB [2]rotaxanes, as well as their anion sensing properties in competitive aqueous-organic solvent mixtures is discussed.

Chapter 4 explores the unprecedented applications of XB interactions in the enantio-selective binding of chiral anions. After establishing the optimal bidentate XB geometry for chiral anion discrimination, a novel chiral XB macrocycle is prepared. Using these systems, the unique geometric advantages conferred by XB interactions to enhance chiral discrimination are established. These insights then lead to the design and syntheses of a family of chiral XB [2]rotaxanes, as well as a [3]rotaxane, allowing a detailed study and

comparison of their enantio-selective anion binding behaviour towards chiral mono-anions and dianions respectively. The influences of ChB interactions towards distinguishing stereo- and regioisomeric dicarboxylate anions are investigated as well.

Chapter 5 details the development of structurally-diverse water-soluble acyclic XB host molecules using polyether-based groups, as well as their anion binding properties in pure water. The preparation of water-soluble [2]rotaxanes using polyether-based water-solubilising stopper units is also investigated.

1.5 References

1 J. F. Stoddart, *Nat Chem*, 2009, **1**, 14-15.
2 J. F. Stoddart, *Angew. Chem. Int. Ed.*, 2012, **51**, 12902–12903.
3 C. J. Pedersen, *J. Am. Chem. Soc.*, 1967, **89**, 7017–7036.
4 J.-M. Lehn, *Angew. Chem. Int. Ed. Engl.*, 1988, **27**, 89–112.
5 J.-M. Lehn, *Chem Soc Rev*, 2007, **36**, 151–160.
6 D. J. Cram, *Angew. Chem. Int. Ed. Engl.*, 1988, **27**, 1009–1020.
7 E. R. Kay and D. A. Leigh, *Angew. Chem. Int. Ed.*, 2015, **54**, 10080–10088.
8 J. F. Stoddart, *Angew. Chem. Int. Ed.*, 2014, **53**, 11102–11104.
9 W. R. Browne and B. L. Feringa, *Nat Nano*, 2006, **1**, 25–35.
10 V. Blanco, D. A. Leigh and V. Marcos, *Chem Soc Rev*, 2015, **44**, 5341–5370.
11 R. Dong, Y. Zhou, X. Huang, X. Zhu, Y. Lu and J. Shen, *Adv. Mater.*, 2015, **27**, 498–526.
12 M. J. Webber, E. A. Appel, E. W. Meijer and R. Langer, *Nat Mater*, 2016, **15**, 13–26.
13 J. Boekhoven and S. I. Stupp, *Adv. Mater.*, 2014, **26**, 1642–1659.
14 E. V. Anslyn, *J. Org. Chem.*, 2007, **72**, 687–699.
15 L. You, D. Zha and E. V. Anslyn, *Chem. Rev.*, 2015, **115**, 7840–7892.
16 E. Mattia and S. Otto, *Nat Nano*, 2015, **10**, 111–119.
17 C. Cheng, P. R. McGonigal, J. F. Stoddart and R. D. Astumian, *ACS Nano*, 2015, **9**, 8672–8688.
18 R. D. Astumian, *Chem Sci*, 2017, **8**, 840-845.
19 N. Busschaert, C. Caltagirone, W. Van Rossom and P. A. Gale, *Chem. Rev.*, 2015, **115**, 8038–8155.
20 N. H. Evans and P. D. Beer, *Angew. Chem. Int. Ed.*, 2014, **53**, 11716–11754.
21 D. Fujita, Y. Ueda, S. Sato, N. Mizuno, T. Kumasaka and M. Fujita, *Nature*, 2016, **540**, 563–566.
22 D. Dalkara, G. Zuber and J.-P. Behr, *Mol Ther*, 2004, **9**, 964–969.
23 D. G. Nicholls and S. J. Ferguson, *Bioenergetics (3rd Edition)*, Academic Press, London, 2003.
24 M. Hayyan, M. A. Hashim and I. M. AlNashef, *Chem. Rev.*, 2016, **116**, 3029–3085.
25 M. Anderson, R. Gregory, S. Thompson, D. Souza, S. Paul, R. Mulligan, A. Smith and M. Welsh, *Science*, 1991, **253**, 202–205.
26 L. Keith and W. Telliard, *Environ. Sci. Technol.*, 1979, **13**, 416–423.
27 V. H. Smith and D. W. Schindler, *Trends Ecol. Evol.*, 2009, **24**, 201–207.
28 K. Yoshihara, in *Technetium and Rhenium Their Chemistry and Its Applications*, eds. K. Yoshihara and T. Omori, Springer Berlin Heidelberg, Berlin, Heidelberg, 1996, pp. 17–35.
29 W. A. Herrmann, A. M. J. Rost, J. K. M. Mitterpleininger, N. Szesni, S. Sturm, R. W. Fischer and F. E. Kühn, *Angew. Chem. Int. Ed.*, 2007, **46**, 7301–7303.
30 G. Anger, J. Halstenberg, K. Hochgeschwender, C. Scherhag, U. Korallus, H. Knopf, P. Schmidt and M. Ohlinger, in *Ullmann's Encyclopedia of Industrial Chemistry*, Wiley-VCH Verlag GmbH & Co. KGaA, 2000.
31 A. E. Hargrove, S. Nieto, T. Zhang, J. L. Sessler and E. V. Anslyn, *Chem. Rev.*, 2011, **111**, 6603–6782.
32 F. Hofmeister, *Arch. Für Exp. Pathol. Pharmakol.*, 1888, **24**, 247–260.
33 K. D. Collins, *Biophys. Chem.*, 2006, **119**, 271–281.
34 U. Mayer, *Coord. Chem. Rev.*, 1976, **21**, 159–179.
35 J. D. Watson and E. J. Milner-White, *J. Mol. Biol.*, 2002, **315**, 171–182.
36 M. Saraste, P. R. Sibbald and A. Wittinghofer, *Trends Biochem. Sci.*, 1990, **15**, 430–434.
37 K. A. Denessiouk, M. S. Johnson and A. I. Denesyuk, *J. Mol. Biol.*, 2005, **345**, 611–629.
38 J. He and F. Quiocho, *Science*, 1991, **251**, 1479.
39 B. L. Jacobson and F. A. Quiocho, *J. Mol. Biol.*, 1988, **204**, 783–787.
40 D. W. Christianson and C. A. Fierke, *Acc. Chem. Res.*, 1996, **29**, 331–339.

41 J. M. Fox, K. Kang, W. Sherman, A. Héroux, G. M. Sastry, M. Baghbanzadeh, M. R. Lockett and G. M. Whitesides, *J. Am. Chem. Soc.*, 2015, **137**, 3859–3866.
42 M. Elias, A. Wellner, K. Goldin-Azulay, E. Chabriere, J. A. Vorholt, T. J. Erb and D. S. Tawfik, *Nature*, 2012, **491**, 134–137.
43 J. A. K. Howard, V. J. Hoy, D. O'Hagan and G. T. Smith, *Tetrahedron*, 1996, **52**, 12613–12622.
44 J. Emsley, *Chem Soc Rev*, 1980, **9**, 91–124.
45 T. Steiner and G. R. Desiraju, *Chem Commun*, 1998, 891–892.
46 T. Steiner, *Angew. Chem. Int. Ed.*, 2002, **41**, 48–76.
47 P. W. Snyder, J. Mecinović, D. T. Moustakas, S. W. Thomas, M. Harder, E. T. Mack, M. R. Lockett, A. Héroux, W. Sherman and G. M. Whitesides, *Proc. Natl. Acad. Sci.*, 2011, **108**, 17889–17894.
48 M. B. Hillyer and B. C. Gibb, *Annu. Rev. Phys. Chem.*, 2016, **67**, 307–329.
49 M. S. Cubberley and B. L. Iverson, *J. Am. Chem. Soc.*, 2001, **123**, 7560–7563.
50 M. Fernández-Vidal, S. H. White and A. S. Ladokhin, *J. Membr. Biol.*, 2011, **239**, 5–14.
51 J. Seelig and P. Ganz, *Biochemistry (Mosc.)*, 1991, **30**, 9354–9359.
52 K. I. Assaf, M. S. Ural, F. Pan, T. Georgiev, S. Simova, K. Rissanen, D. Gabel and W. M. Nau, *Angew. Chem.*, 2015, **127**, 6956–6960.
53 M. A. Yawer, V. Havel and V. Sindelar, *Angew. Chem. Int. Ed.*, 2015, **54**, 276–279.
54 P. Sokkalingam, J. Shraberg, S. W. Rick and B. C. Gibb, *J. Am. Chem. Soc.*, 2016, **138**, 48–51.
55 R. S. Carnegie, C. L. D. Gibb and B. C. Gibb, *Angew. Chem.*, 2014, **126**, 11682–11684.
56 C. L. D. Gibb and B. C. Gibb, *J. Am. Chem. Soc.*, 2011, **133**, 7344–7347.
57 D. Quiñonero, C. Garau, A. Frontera, P. Ballester, A. Costa and P. M. Deyà, *Chem. Phys. Lett.*, 2002, **359**, 486–492.
58 C. Garau, A. Frontera, D. Quiñonero, P. Ballester, A. Costa and P. M. Deyà, *ChemPhysChem*, 2003, **4**, 1344–1348.
59 O. B. Berryman, V. S. Bryantsev, D. P. Stay, D. W. Johnson and B. P. Hay, *J. Am. Chem. Soc.*, 2007, **129**, 48–58.
60 M. Albrecht, C. Wessel, M. de Groot, K. Rissanen and A. Lüchow, *J. Am. Chem. Soc.*, 2008, **130**, 4600–4601.
61 A. Frontera, P. Gamez, M. Mascal, T. J. Mooibroek and J. Reedijk, *Angew. Chem. Int. Ed.*, 2011, **50**, 9564–9583.
62 C. Estarellas, A. Bauza, A. Frontera, D. Quinonero and P. M. Deya, *Phys Chem Chem Phys*, 2011, **13**, 5696–5702.
63 S. Li, S.-X. Fa, Q.-Q. Wang, D.-X. Wang and M.-X. Wang, *J. Org. Chem.*, 2012, **77**, 1860–1867.
64 S. Guha and S. Saha, *J. Am. Chem. Soc.*, 2010, **132**, 17674–17677.
65 H. Zhao, L. A. Leamer and F. P. Gabbai, *Dalton Trans*, 2013, **42**, 8164–8178.
66 M. J. Kelly, A. E. J. Broomsgrove, I. R. Morgan, I. Siewert, P. Fitzpatrick, J. Smart, D. Vidovic and S. Aldridge, *Organometallics*, 2013, **32**, 2674–2684.
67 J. S. Jones and F. P. Gabbaï, *Acc. Chem. Res.*, 2016, **49**, 857–867.
68 H. T. Ngo, X. Liu and K. A. Jolliffe, *Chem Soc Rev*, 2012, **41**, 4928–4965.
69 T. Zhang, N. Y. Edwards, M. Bonizzoni and E. V. Anslyn, *J. Am. Chem. Soc.*, 2009, **131**, 11976–11984.
70 S. J. Butler and D. Parker, *Chem Soc Rev*, 2013, **42**, 1652–1666.
71 M. Hirai and F. P. Gabbaï, *Angew. Chem. Int. Ed.*, 2015, **54**, 1205–1209.
72 Y. Marcus, *J Chem Soc Faraday Trans*, 1991, **87**, 2995–2999.
73 O. Brea, I. Corral, O. Mó, M. Yáñez, I. Alkorta and J. Elguero, *Chem. – Eur. J.*, 2016, **22**, 18322–18325.
74 J. S. Murray, P. Lane and P. Politzer, *J. Mol. Model.*, 2009, **15**, 723–729.
75 G. Cavallo, P. Metrangolo, R. Milani, T. Pilati, A. Priimagi, G. Resnati and G. Terraneo, *Chem. Rev.*, 2016, **116**, 2478–2601.
76 L. C. Gilday, S. W. Robinson, T. A. Barendt, M. J. Langton, B. R. Mullaney and P. D. Beer, *Chem. Rev.*, 2015, **115**, 7118–7195.
77 T. M. Beale, M. G. Chudzinski, M. G. Sarwar and M. S. Taylor, *Chem Soc Rev*, 2013, **42**, 1667–1680.
78 E. Cadoni, G. Ferino, P. Pitzanti, F. Secci, C. Fattuoni, F. Nicolò and G. Bruno, *ChemistryOpen*, 2015, **4**, 161–168.
79 J.-W. Zou, Y.-J. Jiang, M. Guo, G.-X. Hu, B. Zhang, H.-C. Liu and Q.-S. Yu, *Chem. – Eur. J.*, 2005, **11**, 740–751.
80 Y.-X. Lu, J.-W. Zou, Y.-H. Wang, Y.-J. Jiang and Q.-S. Yu, *J. Phys. Chem. A*, 2007, **111**, 10781–10788.
81 P. Politzer and J. S. Murray, *ChemPhysChem*, 2013, **14**, 278–294.
82 A. Bundhun, P. Ramasami, J. S. Murray and P. Politzer, *J. Mol. Model.*, 2013, **19**, 2739–2746.
83 M. D. Esrafili, M. Vakili and M. Solimannejad, *J. Mol. Model.*, 2014, **20**, 2102.
84 A. Brown and P. D. Beer, *Chem Commun*, 2016.
85 A. Bauzá, T. J. Mooibroek and A. Frontera, *ChemPhysChem*, 2015, **16**, 2496–2517.
86 U. Adhikari and S. Scheiner, *Chem. Phys. Lett.*, 2012, **532**, 31–35.
87 K. E. Riley, J. S. Murray, J. Fanfrlík, J. Řezáč, R. J. Solá, M. C. Concha, F. M. Ramos and P. Politzer, *J. Mol. Model.*, 2011, **17**, 3309–3318.
88 J. S. Murray, P. Lane, T. Clark, K. E. Riley and P. Politzer, *J. Mol. Model.*, 2012, **18**, 541–548.
89 A. Bauzá and A. Frontera, *Angew. Chem. Int. Ed.*, 2015, **54**, 7340–7343.
90 Desiraju Gautam R., Ho P. Shing, Kloo Lars, Legon Anthony C., Marquardt Roberto, Metrangolo Pierangelo, Politzer Peter, Resnati Giuseppe and Rissanen Kari, *Pure Appl. Chem.*, 2013, **85**, 1711.

91 F. Guthrie, *J Chem Soc*, 1863, **16**, 239–244.
92 O. Hassel and J. Hvoslef, *Acta Chem Scand*, 1954, **8**, 873–873.
93 P. Metrangolo, H. Neukirch, T. Pilati and G. Resnati, *Acc. Chem. Res.*, 2005, **38**, 386–395.
94 P. Metrangolo, F. Meyer, T. Pilati, G. Resnati and G. Terraneo, *Angew. Chem. Int. Ed.*, 2008, **47**, 6114–6127.
95 A. Priimagi, G. Cavallo, P. Metrangolo and G. Resnati, *Acc. Chem. Res.*, 2013, **46**, 2686–2695.
96 G. Berger, J. Soubhye and F. Meyer, *Polym Chem*, 2015, **6**, 3559–3580.
97 C. C. Robertson, R. N. Perutz, L. Brammer and C. A. Hunter, *Chem Sci*, 2014, **5**, 4179–4183.
98 S. W. Robinson, C. L. Mustoe, N. G. White, A. Brown, A. L. Thompson, P. Kennepohl and P. D. Beer, *J. Am. Chem. Soc.*, 2015, **137**, 499–507.
99 A. Priimagi, G. Cavallo, A. Forni, M. Gorynsztejn–Leben, M. Kaivola, P. Metrangolo, R. Milani, A. Shishido, T. Pilati, G. Resnati and G. Terraneo, *Adv. Funct. Mater.*, 2012, **22**, 2572–2579.
100 N. Houbenov, R. Milani, M. Poutanen, J. Haataja, V. Dichiarante, J. Sainio, J. Ruokolainen, G. Resnati, P. Metrangolo and O. Ikkala, *Nat. Commun.*, 2014, **5**, 4043.
101 D. Bulfield and S. M. Huber, *Chem. – Eur. J.*, 2016, **22**, 14434–14450.
102 L. Meazza, J. A. Foster, K. Fucke, P. Metrangolo, G. Resnati and J. W. Steed, *Nat Chem*, 2013, **5**, 42–47.
103 A. Bertolani, L. Pirrie, L. Stefan, N. Houbenov, J. S. Haataja, L. Catalano, G. Terraneo, G. Giancane, L. Valli, R. Milani, O. Ikkala, G. Resnati and P. Metrangolo, *Nat. Commun.*, 2015, **6**, 7574.
104 R. Wilcken, M. O. Zimmermann, A. Lange, A. C. Joerger and F. M. Boeckler, *J. Med. Chem.*, 2013, **56**, 1363–1388.
105 S. H. Jungbauer, D. Bulfield, F. Kniep, C. W. Lehmann, E. Herdtweck and S. M. Huber, *J. Am. Chem. Soc.*, 2014, **136**, 16740–16743.
106 O. Dumele, N. Trapp and F. Diederich, *Angew. Chem. Int. Ed.*, 2015, **54**, 12339–12344.
107 S. Henkel, P. Costa, L. Klute, P. Sokkar, M. Fernandez-Oliva, W. Thiel, E. Sanchez-Garcia and W. Sander, *J. Am. Chem. Soc.*, 2016, **138**, 1689–1697.
108 K. B. Landenberger, O. Bolton and A. J. Matzger, *J. Am. Chem. Soc.*, 2015, **137**, 5074–5079.
109 D. M. Ivanov, A. S. Novikov, I. V. Ananyev, Y. V. Kirina and V. Y. Kukushkin, *Chem Commun*, 2016, **52**, 5565–5568.
110 A. Mele, P. Metrangolo, H. Neukirch, T. Pilati and G. Resnati, *J. Am. Chem. Soc.*, 2005, **127**, 14972–14973.
111 A. Bauza, D. Quinonero, P. M. Deya and A. Frontera, *CrystEngComm*, 2013, **15**, 3137–3144.
112 Y. Nagao, T. Hirata, S. Goto, S. Sano, A. Kakehi, K. Iizuka and M. Shiro, *J. Am. Chem. Soc.*, 1998, **120**, 3104–3110.
113 S. Wu and A. Greer, *J. Org. Chem.*, 2000, **65**, 4883–4887.
114 S. P. Thomas, K. Satheeshkumar, G. Mugesh and T. N. Guru Row, *Chem. – Eur. J.*, 2015, **21**, 6793–6800.
115 M. Iwaoka, S. Takemoto, M. Okada and S. Tomoda, *Chem. Lett.*, 2001, **30**, 132–133.
116 M. Iwaoka, S. Takemoto and S. Tomoda, *J. Am. Chem. Soc.*, 2002, **124**, 10613–10620.
117 W. Brandt, A. Golbraikh, M. Täger and U. Lendeckel, *Eur. J. Biochem.*, 1999, **261**, 89–97.
118 J. C. Taylor and G. D. Markham, *J. Biol. Chem.*, 1999, **274**, 32909–32914.
119 E. S. Yandanova, D. M. Ivanov, M. L. Kuznetsov, A. G. Starikov, G. L. Starova and V. Y. Kukushkin, *Cryst. Growth Des.*, 2016, **16**, 2979–2987.
120 A. Kremer, A. Fermi, N. Biot, J. Wouters and D. Bonifazi, *Chem. – Eur. J.*, 2016, **22**, 5665–5675.
121 J. Roncali, P. Blanchard and P. Frere, *J Mater Chem*, 2005, **15**, 1589–1610.
122 V. B. Birman and X. Li, *Org. Lett.*, 2006, **8**, 1351–1354.
123 S. Benz, J. López-Andarias, J. Mareda, N. Sakai and S. Matile, *Angew. Chem. Int. Ed.*, 2016, n/a–n/a.
124 P. C. Ho, P. Szydlowski, J. Sinclair, P. J. W. Elder, J. Kübel, C. Gendy, L. M. Lee, H. Jenkins, J. F. Britten, D. R. Morim and I. Vargas-Baca, *Nat. Commun.*, 2016, **7**, 11299.
125 C. A. Leverett, V. C. Purohit and D. Romo, *Angew. Chem. Int. Ed.*, 2010, **49**, 9479–9483.
126 D. Quiñonero, *Molecules*, 2015, **20**, 11632.
127 L. M. Lee, V. B. Corless, M. Tran, H. Jenkins, J. F. Britten and I. Vargas-Baca, *Dalton Trans*, 2016, **45**, 3285–3293.
128 N. A. Semenov, A. V. Lonchakov, N. P. Gritsan and A. V. Zibarev, *Russ. Chem. Bull.*, 2015, **64**, 499–510.
129 H. Park, L. J. Edgar, M. A. Lumba, L. M. Willis and M. Nitz, *Org Biomol Chem*, 2015, **13**, 7027–7033.
130 T. Chivers and R. S. Laitinen, *Chem Soc Rev*, 2015, **44**, 1725–1739.
131 S. Scheiner, *Acc. Chem. Res.*, 2013, **46**, 280–288.
132 A. Bauzá, T. J. Mooibroek and A. Frontera, *Chem. Rec.*, 2016, **16**, 473–487.
133 N. C. Norman, *Phosphorus Sulfur Silicon Relat. Elem.*, 1994, **87**, 167–176.
134 J. Parr, *Polyhedron*, 1997, **16**, 551–566.
135 I. A. Mustafa and A. A. Taqa, *Synth. React. Inorg. Met.-Org. Chem.*, 2001, **31**, 517–526.
136 G. Müller, J. Brand and S. E. Jetter, *Naturforsch B*, 2001, **56**, 1163–1171.
137 A. Bauzá, I. Alkorta, A. Frontera and J. Elguero, *J. Chem. Theory Comput.*, 2013, **9**, 5201–5210.
138 S. Scheiner, *Chem. – Eur. J.*, 2016, **22**, 18850–18858.
139 J. A. W. Sklorz and C. Müller, *Eur. J. Inorg. Chem.*, 2016, **2016**, 595–606.
140 J. A. W. Sklorz, S. Hoof, N. Rades, N. De Rycke, L. Könczöl, D. Szieberth, M. Weber, J. Wiecko, L. Nyulászi, M. Hissler and C. Müller, *Chem. – Eur. J.*, 2015, **21**, 11096–11109.

141 J. A. W. Sklorz, S. Hoof, M. G. Sommer, F. Weißer, M. Weber, J. Wiecko, B. Sarkar and C. Müller, *Organometallics*, 2014, **33**, 511–516.
142 G. Pfeifer, M. Papke, D. Frost, J. A. W. Sklorz, M. Habicht and C. Müller, *Angew. Chem. Int. Ed.*, 2016, **55**, 11760–11764.
143 I. Kalikhman, O. Girshberg, L. Lameyer, D. Stalke and D. Kost, *J. Am. Chem. Soc.*, 2001, **123**, 4709–4716.
144 F. H. Allen, O. Kennard, D. G. Watson, L. Brammer, A. G. Orpen and R. Taylor, *J Chem Soc Perkin Trans 2*, 1987, S1–S19.
145 P. G. Taylor, A. R. Bassindale, Y. El Aziz, M. Pourny, R. Stevenson, M. B. Hursthouse and S. J. Coles, *Dalton Trans*, 2012, **41**, 2048–2059.
146 X. Dai, D. L. Schulz, C. W. Braun, A. Ugrinov and P. Boudjouk, *Organometallics*, 2010, **29**, 2203–2205.
147 X. Dai, S.-B. Choi, C. W. Braun, P. Vaidya, S. Kilina, A. Ugrinov, D. L. Schulz and P. Boudjouk, *Inorg. Chem.*, 2011, **50**, 4047–4053.
148 E. C. Escudero-Adán, A. Bauzá, A. Frontera and P. Ballester, *ChemPhysChem*, 2015, **16**, 2530–2533.
149 A. Bauzá, T. J. Mooibroek and A. Frontera, *Chem. – Eur. J.*, 2014, **20**, 10245–10248.
150 A. Bauza, T. J. Mooibroek and A. Frontera, *Chem Commun*, 2014, **50**, 12626–12629.
151 D. H. Templeton, A. Zalkin, J. D. Forrester and S. M. Williamson, *J. Am. Chem. Soc.*, 1963, **85**, 817–817.
152 D. S. Brock, V. Bilir, H. P. A. Mercier and G. J. Schrobilgen, *J. Am. Chem. Soc.*, 2007, **129**, 3598–3611.
153 K. Koppe, J. Haner, H. P. A. Mercier, H.-J. Frohn and G. J. Schrobilgen, *Inorg. Chem.*, 2014, **53**, 11640–11661.
154 M. D. Esrafili and S. Asadollahi, *Mol. Phys.*, 2016, **114**, 2177–2186.
155 J. Haner and G. J. Schrobilgen, *Chem. Rev.*, 2015, **115**, 1255–1295.
156 F. Sommer and S. Kubik, *Org Biomol Chem*, 2014, **12**, 8851–8860.
157 M. A. Hossain, S. O. Kang, J. M. Llinares, D. Powell and K. Bowman-James, *Inorg. Chem.*, 2003, **42**, 5043–5045.
158 D. M. Jessen, A. N. Wercholuk, B. Xiong, A. L. Sargent and W. E. Allen, *J. Org. Chem.*, 2012, **77**, 6615–6619.
159 D. E. Gomez, L. Fabbrizzi, M. Licchelli and E. Monzani, *Org Biomol Chem*, 2005, **3**, 1495–1500.
160 K. H. Lee and J.-I. Hong, *Tetrahedron Lett.*, 2000, **41**, 6083–6087.
161 J. Alemán, A. Parra, H. Jiang and K. A. Jørgensen, *Chem. – Eur. J.*, 2011, **17**, 6890–6899.
162 L. Qin, A. Hartley, P. Turner, R. B. P. Elmes and K. A. Jolliffe, *Chem Sci*, 2016, **7**, 4563–4572.
163 J. Jurczak, P. Dydio, P. Stepniak and T. Zielinski, *RSC Adv*, 2016, **6**, 41568–41571.
164 P. A. Gale, *Chem Commun*, 2008, 4525–4540.
165 F. Figueira, J. M. M. Rodrigues, A. A. S. Farinha, J. A. S. Cavaleiro and J. P. C. Tomé, *J. Porphyr. Phthalocyanines*, 2016, **20**, 950–965.
166 P. Sokkalingam, D. S. Kim, H. Hwang, J. L. Sessler and C.-H. Lee, *Chem Sci*, 2012, **3**, 1819–1824.
167 F. G. Bordwell, *Acc. Chem. Res.*, 1988, **21**, 456–463.
168 A. L. Fuentes de Arriba, M. G. Turiel, L. Simon, F. Sanz, J. F. Boyero, F. M. Muniz, J. R. Moran and V. Alcazar, *Org Biomol Chem*, 2011, **9**, 8321–8327.
169 H. Juwarker, J. M. Lenhardt, D. M. Pham and S. L. Craig, *Angew. Chem.*, 2008, **120**, 3800–3803.
170 H. Juwarker, J. M. Lenhardt, J. C. Castillo, E. Zhao, S. Krishnamurthy, R. M. Jamiolkowski, K.-H. Kim and S. L. Craig, *J. Org. Chem.*, 2009, **74**, 8924–8934.
171 J. Yoon, S. K. Kim, N. J. Singh and K. S. Kim, *Chem Soc Rev*, 2006, **35**, 355–360.
172 N. Ahmed, B. Shirinfar, I. Geronimo and K. S. Kim, *Org. Lett.*, 2011, **13**, 5476–5479.
173 B. Schulze, C. Friebe, M. D. Hager, W. Günther, U. Köhn, B. O. Jahn, H. Görls and U. S. Schubert, *Org. Lett.*, 2010, **12**, 2710–2713.
174 R. Lalrempuia, N. D. McDaniel, H. Müller-Bunz, S. Bernhard and M. Albrecht, *Angew. Chem. Int. Ed.*, 2010, **49**, 9765–9768.
175 J. Cai, B. P. Hay, N. J. Young, X. Yang and J. L. Sessler, *Chem Sci*, 2013, **4**, 1560–1567.
176 P. Blondeau, J. Benet-Buchholz and J. de Mendoza, *New J Chem*, 2007, **31**, 736–740.
177 S. Guieu, A. K. Crane and M. J. MacLachlan, *Chem Commun*, 2011, **47**, 1169–1171.
178 Y. Liu, A. Singharoy, C. G. Mayne, A. Sengupta, K. Raghavachari, K. Schulten and A. H. Flood, *J. Am. Chem. Soc.*, 2016, **138**, 4843–4851.
179 S. Lee, C.-H. Chen and A. H. Flood, *Nat Chem*, 2013, **5**, 704–710.
180 I. Mata, E. Molins, I. Alkorta and E. Espinosa, *J. Phys. Chem. A*, 2015, **119**, 183–194.
181 A. Knorr, P. Stange, K. Fumino, F. Weinhold and R. Ludwig, *ChemPhysChem*, 2016, **17**, 447–447.
182 E. M. Fatila, E. B. Twum, A. Sengupta, M. Pink, J. A. Karty, K. Raghavachari and A. H. Flood, *Angew. Chem.*, 2016, **128**, 14263–14268.
183 T. Caronna, R. Liantonio, T. A. Logothetis, P. Metrangolo, T. Pilati and G. Resnati, *J. Am. Chem. Soc.*, 2004, **126**, 4500–4501.
184 G. Marras, P. Metrangolo, F. Meyer, T. Pilati, G. Resnati and A. Vij, *New J Chem*, 2006, **30**, 1397–1402.
185 M. G. Sarwar, B. Dragisic, S. Sagoo and M. S. Taylor, *Angew. Chem. Int. Ed.*, 2010, **49**, 1674–1677.
186 J. E. Hein, J. C. Tripp, L. B. Krasnova, K. B. Sharpless and V. V. Fokin, *Angew. Chem. Int. Ed.*, 2009, **48**, 8018–8021.
187 B. H. M. Kuijpers, G. C. T. Dijkmans, S. Groothuys, P. J. L. M. Quaedflieg, R. H. Blaauw, F. L. van Delft and F. P. J. T. Rutjes, *Synlett*, 2005, **2005**, 3059–3062.
188 L. Li, G. Zhang, A. Zhu and L. Zhang, *J. Org. Chem.*, 2008, **73**, 3630–3633.

189 Y.-M. Wu, J. Deng, Y. Li and Q.-Y. Chen, *Synthesis*, 2005, **2005**, 1314–1318.
190 B. Nepal and S. Scheiner, *J. Phys. Chem. A*, 2015, **119**, 13064–13073.
191 R. Tepper, B. Schulze, H. Görls, P. Bellstedt, M. Jäger and U. S. Schubert, *Org. Lett.*, 2015, **17**, 5740–5743.
192 L. C. Gilday, N. G. White and P. D. Beer, *Dalton Trans*, 2013, **42**, 15766–15773.
193 B. Nepal and S. Scheiner, *Chem. – Eur. J.*, 2015, **21**, 13330–13335.
194 M. J. Langton, S. W. Robinson, I. Marques, V. Félix and P. D. Beer, *Nat Chem*, 2014, **6**, 1039–1043.
195 M. J. Langton, I. Marques, S. W. Robinson, V. Félix and P. D. Beer, *Chem. – Eur. J.*, 2016, **22**, 185–192.
196 S. W. Robinson and P. D. Beer, *Org Biomol Chem*, 2017, **15**, 153–159.
197 C. J. Massena, A. M. S. Riel, G. F. Neuhaus, D. A. Decato and O. B. Berryman, *Chem. Commun.*, 2015, **51**, 1417–1420.
198 C. J. Massena, N. B. Wageling, D. A. Decato, E. Martin Rodriguez, A. M. Rose and O. B. Berryman, *Angew. Chem. Int. Ed.*, 2016, **55**, 12398–12402.
199 R. Tepper, B. Schulze, M. Jäger, C. Friebe, D. H. Scharf, H. Görls and U. S. Schubert, *J. Org. Chem.*, 2015, **80**, 3139–3150.
200 L. González, F. Zapata, A. Caballero, P. Molina, C. Ramírez de Arellano, I. Alkorta and J. Elguero, *Chem. – Eur. J.*, 2016, **22**, 7533–7544.
201 B. Nepal and S. Scheiner, *ChemPhysChem*, 2016, **17**, 836–844.
202 S. M. Walter, S. H. Jungbauer, F. Kniep, S. Schindler, E. Herdtweck and S. M. Huber, *J. Fluor. Chem.*, 2013, **150**, 14–20.
203 S. M. Walter, F. Kniep, E. Herdtweck and S. M. Huber, *Angew. Chem. Int. Ed.*, 2011, **50**, 7187–7191.
204 S. M. Walter, F. Kniep, L. Rout, F. P. Schmidtchen, E. Herdtweck and S. M. Huber, *J. Am. Chem. Soc.*, 2012, **134**, 8507–8512.
205 S. Chakraborty, R. Dutta and P. Ghosh, *Chem Commun*, 2015, **51**, 14793–14796.
206 F. Zapata, A. Caballero, N. G. White, T. D. W. Claridge, P. J. Costa, V. Félix and P. D. Beer, *J. Am. Chem. Soc.*, 2012, **134**, 11533–11541.
207 S. H. Jungbauer and S. M. Huber, *J. Am. Chem. Soc.*, 2015, **137**, 12110–12120.
208 H. Zhao and F. P. Gabbaï, *Nat Chem*, 2010, **2**, 984–990.
209 A. Bauzá, I. Alkorta, A. Frontera and J. Elguero, *J. Chem. Theory Comput.*, 2013, **9**, 5201–5210.
210 G. E. Garrett, G. L. Gibson, R. N. Straus, D. S. Seferos and M. S. Taylor, *J. Am. Chem. Soc.*, 2015, **137**, 4126–4133.
211 N. A. Semenov, N. A. Pushkarevsky, J. Beckmann, P. Finke, E. Lork, R. Mews, I. Y. Bagryanskaya, Y. V. Gatilov, S. N. Konchenko, V. G. Vasiliev and A. V. Zibarev, *Eur. J. Inorg. Chem.*, 2012, **2012**, 3693–3703.
212 G. E. Garrett, E. I. Carrera, D. S. Seferos and M. S. Taylor, *Chem Commun*, 2016, **52**, 9881–9884.
213 P. D. Beer, P. A. Gale and G. Z. Chen, *J Chem Soc Dalton Trans*, 1999, 1897–1910.
214 A. E. J. Broomsgrove, D. A. Addy, C. Bresner, I. A. Fallis, A. L. Thompson and S. Aldridge, *Chem. – Eur. J.*, 2008, **14**, 7525–7529.
215 P. D. Beer, M. G. B. Drew and D. K. Smith, *J. Organomet. Chem.*, 1997, **543**, 259–261.
216 C. Bejger, J. S. Park, E. S. Silver and J. L. Sessler, *Chem Commun*, 2010, **46**, 7745–7747.
217 A. Singh, J. Singh, N. Singh and D. O. Jang, *Tetrahedron*, 2015, **71**, 6143–6147.
218 M. Alfonso, A. Tárraga and P. Molina, *Inorg. Chem.*, 2013, **52**, 7487–7496.
219 C. Jin, M. Zhang, L. Wu, Y. Guan, Y. Pan, J. Jiang, C. Lin and L. Wang, *Chem Commun*, 2013, **49**, 2025–2027.
220 M. del C. Gonzalez, F. Oton, A. Espinosa, A. Tarraga and P. Molina, *Org Biomol Chem*, 2015, **13**, 1429–1438.
221 B. Tomapatanaget, T. Tuntulani and O. Chailapakul, *Org. Lett.*, 2003, **5**, 1539–1542.
222 N. H. Evans, C. J. Serpell, K. E. Christensen and P. D. Beer, *Eur. J. Inorg. Chem.*, 2012, **2012**, 939–944.
223 V. Amendola, M. Boiocchi, B. Colasson, L. Fabbrizzi, E. Monzani, M. J. Douton-Rodriguez and C. Spadini, *Inorg. Chem.*, 2008, **47**, 4808–4816.
224 C. Villena, J. Losada, P. García-Armada, C. M. Casado and B. Alonso, *Organometallics*, 2012, **31**, 3284–3291.
225 N. H. Evans, H. Rahman, A. V. Leontiev, N. D. Greenham, G. A. Orlowski, Q. Zeng, R. M. J. Jacobs, C. J. Serpell, N. L. Kilah, J. J. Davis and P. D. Beer, *Chem Sci*, 2012, **3**, 1080–1089.
226 N. H. Evans, C. J. Serpell and P. D. Beer, *Chem Commun*, 2011, **47**, 8775–8777.
227 N. H. Evans and P. D. Beer, *Org Biomol Chem*, 2011, **9**, 92–100.
228 D. P. Cormode, A. J. Evans, J. J. Davis and P. D. Beer, *Dalton Trans*, 2010, **39**, 6532–6541.
229 D. Aldakov and P. Anzenbacher, *J. Am. Chem. Soc.*, 2004, **126**, 4752–4753.
230 T. Minami, T. Minamiki and S. Tokito, *Chem Commun*, 2015, **51**, 9491–9494.
231 S. Zhang and L. Echegoyen, *J. Am. Chem. Soc.*, 2005, **127**, 2006–2011.
232 D. Sain, C. Kumari, A. Kumar and S. Dey, *Supramol. Chem.*, 2016, **28**, 239–248.
233 H. D. P. Ali, P. E. Kruger and T. Gunnlaugsson, *New J Chem*, 2008, **32**, 1153–1161.
234 R. Tirfoin, J. A. B. Abdalla and S. Aldridge, *Chem. – Eur. J.*, 2015, **21**, 11813–11824.
235 W. L. Daniel, M. S. Han, J.-S. Lee and C. A. Mirkin, *J. Am. Chem. Soc.*, 2009, **131**, 6362–6363.
236 B. Chowdhury, S. Sinha and P. Ghosh, *Chem. – Eur. J.*, 2016, **22**, 18051–18059.
237 K. Niikura, A. Metzger and E. V. Anslyn, *J. Am. Chem. Soc.*, 1998, **120**, 8533–8534.
238 T. Minami, Y. Liu, A. Akdeniz, P. Koutnik, N. A. Esipenko, R. Nishiyabu, Y. Kubo and P. Anzenbacher, *J. Am. Chem. Soc.*, 2014, **136**, 11396–11401.

239 J. Massue, S. J. Quinn and T. Gunnlaugsson, *J. Am. Chem. Soc.*, 2008, **130**, 6900–6901.
240 T. Tu, W. Fang and Z. Sun, *Adv. Mater.*, 2013, **25**, 5304–5313.
241 H. Maeda, *Chem. – Eur. J.*, 2008, **14**, 11274–11282.
242 C. Wang, D. Zhang and D. Zhu, *Langmuir*, 2007, **23**, 1478–1482.
243 M. Teng, G. Kuang, X. Jia, M. Gao, Y. Li and Y. Wei, *J Mater Chem*, 2009, **19**, 5648–5654.
244 Z.-X. Liu, Y. Sun, Y. Feng, H. Chen, Y.-M. He and Q.-H. Fan, *Chem Commun*, 2016, **52**, 2269–2272.
245 J. T. Davis, O. Okunola and R. Quesada, *Chem Soc Rev*, 2010, **39**, 3843–3862.
246 A. Fürstner, *Angew. Chem. Int. Ed.*, 2003, **42**, 3582–3603.
247 H. Li, H. Valkenier, L. W. Judd, P. R. Brotherhood, S. Hussain, J. A. Cooper, O. Jurček, H. A. Sparkes, D. N. Sheppard and A. P. Davis, *Nat Chem*, 2016, **8**, 24–32.
248 E. N. W. Howe, N. Busschaert, X. Wu, S. N. Berry, J. Ho, M. E. Light, D. D. Czech, H. A. Klein, J. A. Kitchen and P. A. Gale, *J. Am. Chem. Soc.*, 2016, **138**, 8301–8308.
249 S. Benz, M. Macchione, Q. Verolet, J. Mareda, N. Sakai and S. Matile, *J. Am. Chem. Soc.*, 2016, **138**, 9093–9096.
250 V. Sidorov, F. W. Kotch, G. Abdrakhmanova, R. Mizani, J. C. Fettinger and J. T. Davis, *J. Am. Chem. Soc.*, 2002, **124**, 2267–2278.
251 J. L. Seganish, P. V. Santacroce, K. J. Salimian, J. C. Fettinger, P. Zavalij and J. T. Davis, *Angew. Chem. Int. Ed.*, 2006, **45**, 3334–3338.
252 O. A. Okunola, J. L. Seganish, K. J. Salimian, P. Y. Zavalij and J. T. Davis, *New Trends Calixarene Chem.*, 2007, **63**, 10743–10750.
253 A. Vargas Jentzsch and S. Matile, *J. Am. Chem. Soc.*, 2013, **135**, 5302–5303.
254 V. Gorteau, G. Bollot, J. Mareda, A. Perez-Velasco and S. Matile, *J. Am. Chem. Soc.*, 2006, **128**, 14788–14789.
255 A. Perez-Velasco, V. Gorteau and S. Matile, *Angew. Chem.*, 2008, **120**, 935–937.
256 J. McConathy and M. J. Owens, *Prim. Care Companion J. Clin. Psychiatry*, 2003, **5**, 70–73.
257 G. Wu, *Adv. Nutr. Int. Rev. J.*, 2010, **1**, 31–37.
258 A. Mezzetti, J. D. Schrag, C. S. Cheong and R. J. Kazlauskas, *Chem. Biol.*, 2005, **12**, 427–437.
259 M. G. Finn, *Chirality*, 2002, **14**, 534–540.
260 H. H. Jo, C.-Y. Lin and E. V. Anslyn, *Acc. Chem. Res.*, 2014, **47**, 2212–2221.
261 E. L. Izake, *J. Pharm. Sci.*, 2007, **96**, 1659–1676.
262 R. J. Phipps, G. L. Hamilton and F. D. Toste, *Nat Chem*, 2012, **4**, 603–614.
263 S. Kubik, *Chem. Soc. Rev.*, 2009, **38**, 585–605.
264 P. Hamankiewicz, J. M. Granda and J. Jurczak, *Tetrahedron Lett.*, 2013, **54**, 5608–5611.
265 J. M. Granda and J. Jurczak, *Chem. – Eur. J.*, 2015, **21**, 16585–16592.
266 L. Pu, *Acc. Chem. Res.*, 2012, **45**, 150–163.
267 Y. Willener, K. M. Joly, C. J. Moody and J. H. R. Tucker, *J. Org. Chem.*, 2008, **73**, 1225–1233.
268 A. Mulas, Y. Willener, J. Carr-Smith, K. M. Joly, L. Male, C. J. Moody, S. L. Horswell, H. V. Nguyen and J. H. R. Tucker, *Dalton Trans.*, 2015, **44**, 7268–7275.
269 F. Ulatowski and J. Jurczak, *J. Org. Chem.*, 2015, **80**, 4235–4243.
270 C. Schmuck and V. Bickert, *Org. Lett.*, 2003, **5**, 4579–4581.
271 A. Bencini, C. Coluccini, A. Garau, C. Giorgi, V. Lippolis, L. Messori, D. Pasini and S. Puccioni, *Chem Commun*, 2012, **48**, 10428–10430.
272 I. T. Raheem, P. S. Thiara and E. N. Jacobsen, *Org. Lett.*, 2008, **10**, 1577–1580.
273 M. Zurro, S. Asmus, S. Beckendorf, C. Mück-Lichtenfeld and O. G. Mancheño, *J. Am. Chem. Soc.*, 2014, **136**, 13999–14002.
274 O. García Mancheño, S. Asmus, M. Zurro and T. Fischer, *Angew. Chem. Int. Ed.*, 2015, **54**, 8823–8827.
275 F. Kniep, S. H. Jungbauer, Q. Zhang, S. M. Walter, S. Schindler, I. Schnapperelle, E. Herdtweck and S. M. Huber, *Angew. Chem. Int. Ed.*, 2013, **52**, 7028–7032.
276 Madhuprasad, M. P. Bhat, H.-Y. Jung, D. Losic and M. D. Kurkuri, *Chem. – Eur. J.*, 2016, **22**, 6148–6178.
277 W. Lu, M. Zhang, K. Liu, B. Fan, Z. Xia and L. Jiang, *Sens. Actuators B Chem.*, 2011, **160**, 1005–1010.
278 J. Liu, X. He, J. Zhang, T. He, L. Huang, J. Shen, D. Li, H. Qiu and S. Yin, *Sens. Actuators B Chem.*, 2015, **208**, 538–545.
279 W. Lu, D. Chen, H. Jiang, L. Jiang and Z. Shen, *J. Polym. Sci. Part Polym. Chem.*, 2012, **50**, 590–598.
280 H. Tavallali, G. Deilamy-Rad, A. Parhami and N. Hasanli, *J. Hazard. Mater.*, 2014, **266**, 189–197.
281 L. Wang, B. Li, L. Zhang, P. Li and H. Jiang, *Dyes Pigments*, 2013, **97**, 26–31.
282 H. Frisch, I. Martin and H. Mark, *Monatshefte Für Chem. Verwandte Teile Anderer Wiss.*, 1953, **84**, 250–256.
283 K. S. Chichak, S. J. Cantrill, A. R. Pease, S.-H. Chiu, G. W. V. Cave, J. L. Atwood and J. F. Stoddart, *Science*, 2004, **304**, 1308.
284 A. J. Peters, K. S. Chichak, S. J. Cantrill and J. F. Stoddart, *Chem Commun*, 2005, 3394–3396.
285 R. S. Forgan, J.-P. Sauvage and J. F. Stoddart, *Chem. Rev.*, 2011, **111**, 5434–5464.
286 J.-F. Ayme, J. E. Beves, D. A. Leigh, R. T. McBurney, K. Rissanen and D. Schultz, *Nat Chem*, 2012, **4**, 15–20.
287 J.-F. Ayme, J. E. Beves, C. J. Campbell and D. A. Leigh, *Chem Soc Rev*, 2013, **42**, 1700–1712.
288 P. E. Barran, H. L. Cole, S. M. Goldup, D. A. Leigh, P. R. McGonigal, M. D. Symes, J. Wu and M. Zengerle, *Angew. Chem. Int. Ed.*, 2011, **50**, 12280–12284.

289 J. J. Danon, A. Krüger, D. A. Leigh, J.-F. Lemonnier, A. J. Stephens, I. J. Vitorica-Yrezabal and S. L. Woltering, *Science*, 2017, **355**, 159.
290 C. J. Bruns and J. F. Stoddart, *The Nature of the Mechanical Bond: From Molecules to Machines*, John Wiley & Sons, Ltd, First Edition., 2017.
291 J. S. Siegel, *Science*, 2004, **304**, 1256.
292 M. A. Trakselis, S. C. Alley, E. Abel-Santos and S. J. Benkovic, *Proc. Natl. Acad. Sci.*, 2001, **98**, 8368–8375.
293 R. Kovall and B. W. Matthews, *Science*, 1997, **277**, 1824.
294 K. Subramanian, W. Rutvisuttinunt, W. Scott and R. S. Myers, *Nucleic Acids Res.*, 2003, **31**, 1585.
295 B. HUDSON and J. VINOGRAD, *Nature*, 1967, **216**, 647–652.
296 M. A. Krasnow, A. Stasiak, S. J. Spengler, F. Dean, T. Koller and N. R. Cozzarelli, *Nature*, 1983, **304**, 559–560.
297 K. N. Kreuzer and N. R. Cozzarelli, *Cell*, 1980, **20**, 245–254.
298 A. H. Parham, B. Windisch and F. Vögtle, *Eur. J. Org. Chem.*, 1999, **1999**, 1233–1238.
299 H. Lahlali, K. Jobe, M. Watkinson and S. M. Goldup, *Angew. Chem. Int. Ed.*, 2011, **50**, 4151–4155.
300 A. M. Albrecht-Gary, Z. Saad, C. O. Dietrich-Buchecker and J. P. Sauvage, *J. Am. Chem. Soc.*, 1985, **107**, 3205–3209.
301 S. Erbas-Cakmak, D. A. Leigh, C. T. McTernan and A. L. Nussbaumer, *Chem. Rev.*, 2015, **115**, 10081–10206.
302 A. Coskun, J. M. Spruell, G. Barin, W. R. Dichtel, A. H. Flood, Y. Y. Botros and J. F. Stoddart, *Chem Soc Rev*, 2012, **41**, 4827–4859.
303 X. Yan, F. Wang, B. Zheng and F. Huang, *Chem Soc Rev*, 2012, **41**, 6042–6065.
304 K. Ito, *Polym J*, 2007, **39**, 489–499.
305 M. Janke, Y. Rudzevich, O. Molokanova, T. Metzroth, I. Mey, G. Diezemann, P. E. Marszalek, J. Gauss, V. Bohmer and A. Janshoff, *Nat Nano*, 2009, **4**, 225–229.
306 B. Lee, Z. Niu and S. L. Craig, *Angew. Chem. Int. Ed.*, 2016, **55**, 13086–13089.
307 E. Wasserman, *J. Am. Chem. Soc.*, 1960, **82**, 4433–4434.
308 G. Agam, D. Graiver and A. Zilkha, *J. Am. Chem. Soc.*, 1976, **98**, 5206–5214.
309 G. Agam and A. Zilkha, *J. Am. Chem. Soc.*, 1976, **98**, 5214–5216.
310 D. H. Busch, *J. Incl. Phenom. Mol. Recognit. Chem.*, 1992, **12**, 389–395.
311 T. J. Hubin and D. H. Busch, *Coord. Chem. Rev.*, 2000, **200**–**202**, 5–52.
312 M. C. Thompson and D. H. Busch, *J. Am. Chem. Soc.*, 1964, **86**, 213–217.
313 S. Anderson, H. L. Anderson and J. K. M. Sanders, *Acc. Chem. Res.*, 1993, **26**, 469–475.
314 C. O. Dietrich-Buchecker and J. P. Sauvage, *Chem. Rev.*, 1987, **87**, 795–810.
315 P. R. Aston, P. T. Glink, J. F. Stoddart, P. A. Tasker, A. J. P. White and D. J. Williams, *Chem. – Eur. J.*, 1996, **2**, 729–736.
316 S. J. Cantrill, D. A. Fulton, M. C. . Fyfe, J. F. Stoddart, A. J. . White and D. J. Williams, *Tetrahedron Lett.*, 1999, **40**, 3669–3672.
317 J. Wu, K. C.-F. Leung and J. F. Stoddart, *Proc. Natl. Acad. Sci. U. S. A.*, 2007, **104**, 17266–17271.
318 J. Yin, S. Dasgupta and J. Wu, *Org. Lett.*, 2010, **12**, 1712–1715.
319 G. M. Hübner, J. Gläser, C. Seel and F. Vögtle, *Angew. Chem. Int. Ed.*, 1999, **38**, 383–386.
320 V. Aucagne, J. Berná, J. D. Crowley, S. M. Goldup, K. D. Hänni, D. A. Leigh, P. J. Lusby, V. E. Ronaldson, A. M. Z. Slawin, A. Viterisi and D. B. Walker, *J. Am. Chem. Soc.*, 2007, **129**, 11950–11963.
321 I. Yoon, M. Narita, T. Shimizu and M. Asakawa, *J. Am. Chem. Soc.*, 2004, **126**, 16740–16741.
322 S.-Y. Hsueh, J.-L. Ko, C.-C. Lai, Y.-H. Liu, S.-M. Peng and S.-H. Chiu, *Angew. Chem. Int. Ed.*, 2011, **50**, 6643–6646.
323 C.-W. Chiu, C.-C. Lai and S.-H. Chiu, *J. Am. Chem. Soc.*, 2007, **129**, 3500–3501.
324 P. R. Ashton, M. Belohradsky, D. Philp and J. F. Stoddart, *J. Chem. Soc. Chem. Commun.*, 1993, 1269–1274.
325 X. Huang, S. Huang, B. Zhai, Y. Zhang, Y. Xu and Q. Wang, *Tetrahedron Lett.*, 2012, **53**, 6414–6417.
326 J. S. Hannam, T. J. Kidd, D. A. Leigh and A. J. Wilson, *Org. Lett.*, 2003, **5**, 1907–1910.
327 A. F. M. Kilbinger, S. J. Cantrill, A. W. Waltman, M. W. Day and R. H. Grubbs, *Angew. Chem. Int. Ed.*, 2003, **42**, 3281–3285.
328 E. N. Guidry, S. J. Cantrill, J. F. Stoddart and R. H. Grubbs, *Org. Lett.*, 2005, **7**, 2129–2132.
329 W. W. H. Wong, J. Cookson, E. A. L. Evans, E. J. L. McInnes, J. Wolowska, J. P. Maher, P. Bishop and P. D. Beer, *Chem Commun*, 2005, 2214–2216.
330 D. I. Schuster, K. Li, D. M. Guldi and J. Ramey, *Org. Lett.*, 2004, **6**, 1919–1922.
331 A. Tron, H.-P. Jacquot de Rouville, A. Ducrot, J. H. R. Tucker, M. Baroncini, A. Credi and N. D. McClenaghan, *Chem Commun*, 2015, **51**, 2810–2813.
332 G. Schill and A. Lüttringhaus, *Angew. Chem. Int. Ed. Engl.*, 1964, **3**, 546–547.
333 G. Schill and R. Henschel, *Justus Liebigs Ann. Chem.*, 1970, **731**, 113–119.
334 G. Schill, C. Zürcher and W. Vetter, *Chem. Ber.*, 1973, **106**, 228–235.
335 G. Schill and H. Neubauer, *Justus Liebigs Ann. Chem.*, 1971, **750**, 76–90.
336 G. Schill and W. Vetter, *Chem. Ber.*, 1971, **104**, 3582–3586.
337 G. Schill, N. Schweickert, H. Fritz and W. Vetter, *Angew. Chem. Int. Ed. Engl.*, 1983, **22**, 889–891.
338 Ö. Ünsal and A. Godt, *Chem. – Eur. J.*, 1999, **5**, 1728–1733.
339 G. Schill and C. Zürcher, *Angew. Chem. Int. Ed. Engl.*, 1969, **8**, 988–988.

340 H. Kawai, T. Umehara, K. Fujiwara, T. Tsuji and T. Suzuki, *Angew. Chem.*, 2006, **118**, 4387–4392.
341 C. . Dietrich-Buchecker, J. . Sauvage and J. . Kintzinger, *Tetrahedron Lett.*, 1983, **24**, 5095–5098.
342 S. M. Goldup, D. A. Leigh, P. J. Lusby, R. T. McBurney and A. M. Z. Slawin, *Angew. Chem. Int. Ed.*, 2008, **47**, 6999–7003.
343 A.-M. Fuller, D. A. Leigh, P. J. Lusby, I. D. H. Oswald, S. Parsons and D. B. Walker, *Angew. Chem. Int. Ed.*, 2004, **43**, 3914–3918.
344 J. D. Crowley, D. A. Leigh, P. J. Lusby, R. T. McBurney, L.-E. Perret-Aebi, C. Petzold, A. M. Z. Slawin and M. D. Symes, *J. Am. Chem. Soc.*, 2007, **129**, 15085–15090.
345 C. Hamann, J.-M. Kern and J.-P. Sauvage, *Inorg. Chem.*, 2003, **42**, 1877–1883.
346 D. A. Leigh, P. J. Lusby, R. T. McBurney, A. Morelli, A. M. Z. Slawin, A. R. Thomson and D. B. Walker, *J. Am. Chem. Soc.*, 2009, **131**, 3762–3771.
347 L. Hogg, D. A. Leigh, P. J. Lusby, A. Morelli, S. Parsons and J. K. Y. Wong, *Angew. Chem. Int. Ed.*, 2004, **43**, 1218–1221.
348 A. I. Prikhod'ko and J.-P. Sauvage, *J. Am. Chem. Soc.*, 2009, **131**, 6794–6807.
349 D. Pomeranc, D. Jouvenot, J.-C. Chambron, J.-P. Collin, V. Heitz and J.-P. Sauvage, *Chem. – Eur. J.*, 2003, **9**, 4247–4254.
350 J. D. Megiatto and D. I. Schuster, *Chem. – Eur. J.*, 2009, **15**, 5444–5448.
351 J. C. Chambron, V. Heitz and J. P. Sauvage, *J. Am. Chem. Soc.*, 1993, **115**, 12378–12384.
352 J.-P. Collin, F. Durola, J. Frey, V. Heitz, F. Reviriego, J.-P. Sauvage, Y. Trolez and K. Rissanen, *J. Am. Chem. Soc.*, 2010, **132**, 6840–6850.
353 N. Solladié, J.-C. Chambron, C. O. Dietrich-Buchecker and J.-P. Sauvage, *Angew. Chem.*, 1996, **108**, 957–960.
354 J.-C. Chang, S.-H. Tseng, C.-C. Lai, Y.-H. Liu, S.-M. Peng and S.-H. Chiu, *Nat Chem*, 2017, **9**, 128–134.
355 D. A. Leigh, R. G. Pritchard and A. J. Stephens, *Nat Chem*, 2014, **6**, 978–982.
356 C. S. Wood, T. K. Ronson, A. M. Belenguer, J. J. Holstein and J. R. Nitschke, *Nat Chem*, 2015, **7**, 354–358.
357 S.-Y. Hsueh, C.-C. Lai and S.-H. Chiu, *Chem. – Eur. J.*, 2010, **16**, 2997–3000.
358 T.-H. Ho, C.-C. Lai, Y.-H. Liu, S.-M. Peng and S.-H. Chiu, *Chem. – Eur. J.*, 2014, **20**, 4563–4567.
359 G. Kaiser, T. Jarrosson, S. Otto, Y.-F. Ng, A. D. Bond and J. K. M. Sanders, *Angew. Chem. Int. Ed.*, 2004, **43**, 1959–1962.
360 T. Han and C.-F. Chen, *J. Org. Chem.*, 2008, **73**, 7735–7742.
361 R. Mitra, M. Thiele, F. Octa-Smolin, M. C. Letzel and J. Niemeyer, *Chem Commun*, 2016, **52**, 5977–5980.
362 L. M. Hancock and P. D. Beer, *Chem Commun*, 2011, **47**, 6012–6014.
363 F. Zapata, O. A. Blackburn, M. J. Langton, S. Faulkner and P. D. Beer, *Chem Commun*, 2013, **49**, 8157–8159.
364 J. D. Crowley, S. M. Goldup, A.-L. Lee, D. A. Leigh and R. T. McBurney, *Chem Soc Rev*, 2009, **38**, 1530–1541.
365 S. M. Goldup, D. A. Leigh, P. R. McGonigal, V. E. Ronaldson and A. M. Z. Slawin, *J. Am. Chem. Soc.*, 2010, **132**, 315–320.
366 J. Winn, A. Pinczewska and S. M. Goldup, *J. Am. Chem. Soc.*, 2013, **135**, 13318–13321.
367 S. Saito, E. Takahashi and K. Nakazono, *Org. Lett.*, 2006, **8**, 5133–5136.
368 Y. Sato, R. Yamasaki and S. Saito, *Angew. Chem. Int. Ed.*, 2009, **48**, 504–507.
369 M. Franz, J. A. Januszewski, D. Wendinger, C. Neiss, L. D. Movsisyan, F. Hampel, H. L. Anderson, A. Görling and R. R. Tykwinski, *Angew. Chem. Int. Ed.*, 2015, **54**, 6645–6649.
370 S. Hoekman, M. O. Kitching, D. A. Leigh, M. Papmeyer and D. Roke, *J. Am. Chem. Soc.*, 2015, **137**, 7656–7659.
371 S. M. Goldup, D. A. Leigh, P. J. Lusby, R. T. McBurney and A. M. Z. Slawin, *Angew. Chem. Int. Ed.*, 2008, **47**, 3381–3384.
372 J. Berná, J. D. Crowley, S. M. Goldup, K. D. Hänni, A.-L. Lee and D. A. Leigh, *Angew. Chem. Int. Ed.*, 2007, **46**, 5709–5713.
373 J. D. Crowley, K. D. Hänni, A.-L. Lee and D. A. Leigh, *J. Am. Chem. Soc.*, 2007, **129**, 12092–12093.
374 J. D. Crowley, S. M. Goldup, N. D. Gowans, D. A. Leigh, V. E. Ronaldson and A. M. Z. Slawin, *J. Am. Chem. Soc.*, 2010, **132**, 6243–6248.
375 S. M. Goldup, D. A. Leigh, R. T. McBurney, P. R. McGonigal and A. Plant, *Chem Sci*, 2010, **1**, 383–386.
376 J. D. Crowley, K. D. Hänni, D. A. Leigh and A. M. Z. Slawin, *J. Am. Chem. Soc.*, 2010, **132**, 5309–5314.
377 Z. Baranová, H. Amini, N. Bhuvanesh and J. A. Gladysz, *Organometallics*, 2014, **33**, 6746–6749.
378 S. Hoekman, M. O. Kitching, D. A. Leigh, M. Papmeyer and D. Roke, *J. Am. Chem. Soc.*, 2015, **137**, 7656–7659.
379 J. Berná, J. D. Crowley, S. M. Goldup, K. D. Hänni, A.-L. Lee and D. A. Leigh, *Angew. Chem. Int. Ed.*, 2007, **46**, 5709–5713.
380 M. J. Langton, Y. Xiong and P. D. Beer, *Chem. – Eur. J.*, 2015, **21**, 18910–18914.
381 S. M. Goldup, D. A. Leigh, T. Long, P. R. McGonigal, M. D. Symes and J. Wu, *J. Am. Chem. Soc.*, 2009, **131**, 15924–15929.
382 J. J. Danon, D. A. Leigh, P. R. McGonigal, J. W. Ward and J. Wu, *J. Am. Chem. Soc.*, 2016, **138**, 12643–12647.
383 J. E. M. Lewis, J. Winn, L. Cera and S. M. Goldup, *J. Am. Chem. Soc.*, 2016, **138**, 16329–16336.
384 E. A. Neal and S. M. Goldup, *Chem Sci*, 2015, **6**, 2398–2404.

385 L. D. Movsisyan, M. Franz, F. Hampel, A. L. Thompson, R. R. Tykwinski and H. L. Anderson, *J. Am. Chem. Soc.*, 2016, **138**, 1366–1376.
386 U. E. I. Horvath, J. M. McKenzie, S. Cronje, H. G. Raubenheimer and L. J. Barbour, *Chem Commun*, 2009, 6598–6600.
387 D. M. P. Mingos, J. Yau, S. Menzer and D. J. Williams, *Angew. Chem. Int. Ed. Engl.*, 1995, **34**, 1894–1895.
388 S. S.-Y. Chui, R. Chen and C.-M. Che, *Angew. Chem. Int. Ed.*, 2006, **45**, 1621–1624.
389 M. E. Padilla-Tosta, O. D. Fox, M. G. B. Drew and P. D. Beer, *Angew. Chem. Int. Ed.*, 2001, **40**, 4235–4239.
390 C. Zhang, S. Li, J. Zhang, K. Zhu, N. Li and F. Huang, *Org. Lett.*, 2007, **9**, 5553–5556.
391 S.-Y. Hsueh, K.-W. Cheng, C.-C. Lai and S.-H. Chiu, *Angew. Chem. Int. Ed.*, 2008, **47**, 4436–4439.
392 M. C. T. Fyfe and J. F. Stoddart, *Acc. Chem. Res.*, 1997, **30**, 393–401.
393 P. R. Ashton, P. J. Campbell, P. T. Glink, D. Philp, N. Spencer, J. F. Stoddart, E. J. T. Chrystal, S. Menzer, D. J. Williams and P. A. Tasker, *Angew. Chem. Int. Ed. Engl.*, 1995, **34**, 1865–1869.
394 A. R. Williams, B. H. Northrop, T. Chang, J. F. Stoddart, A. J. P. White and D. J. Williams, *Angew. Chem. Int. Ed.*, 2006, **45**, 6665–6669.
395 M. Xue, Y. Yang, X. Chi, Z. Zhang and F. Huang, *Acc. Chem. Res.*, 2012, **45**, 1294–1308.
396 M.-V. Martínez-Díaz, N. Spencer and J. F. Stoddart, *Angew. Chem. Int. Ed. Engl.*, 1997, **36**, 1904–1907.
397 S. J. Loeb and J. A. Wisner, *Chem. Commun.*, 2000, 845–846.
398 S. Li, M. Liu, J. Zhang, B. Zheng, C. Zhang, X. Wen, N. Li and F. Huang, *Org. Biomol. Chem.*, 2008, **6**, 2103–2107.
399 S. Li, M. Liu, J. Zhang, B. Zheng, X. Wen, N. Li and F. Huang, *Eur. J. Org. Chem.*, 2008, **2008**, 6128–6133.
400 X. Li, X. Yuan, P. Deng, L. Chen, Y. Ren, C. Wang, L. Wu, W. Feng, B. Gong and L. Yuan, *Chem Sci*, 2017.
401 S.-Z. Hu and C.-F. Chen, *Chem. – Eur. J.*, 2011, **17**, 5424–5431.
402 P. R. Ashton, T. T. Goodnow, A. E. Kaifer, M. V. Reddington, A. M. Z. Slawin, N. Spencer, J. F. Stoddart, C. Vicent and D. J. Williams, *Angew. Chem. Int. Ed. Engl.*, 1989, **28**, 1396–1399.
403 Z.-T. Li, P. C. Stein, J. Becher, D. Jensen, P. Mørk and N. Svenstrup, *Chem. – Eur. J.*, 1996, **2**, 624–633.
404 M. Asakawa, P. R. Ashton, V. Balzani, A. Credi, C. Hamers, G. Mattersteig, M. Montalti, A. N. Shipway, N. Spencer, J. F. Stoddart, M. S. Tolley, M. Venturi, A. J. P. White and D. J. Williams, *Angew. Chem. Int. Ed.*, 1998, **37**, 333–337.
405 H. Li, H. Zhang, A. D. Lammer, M. Wang, X. Li, V. M. Lynch and J. L. Sessler, *Nat Chem*, 2015, **7**, 1003–1008.
406 C. Cheng, T. Cheng, H. Xiao, M. D. Krzyaniak, Y. Wang, P. R. McGonigal, M. Frasconi, J. C. Barnes, A. C. Fahrenbach, M. R. Wasielewski, W. A. Goddard and J. F. Stoddart, *J. Am. Chem. Soc.*, 2016, **138**, 8288–8300.
407 I. C. Gibbs-Hall, N. A. Vermeulen, E. J. Dale, J. J. Henkelis, A. K. Blackburn, J. C. Barnes and J. F. Stoddart, *J. Am. Chem. Soc.*, 2015, **137**, 15640–15643.
408 Y. Wang, J. Sun, Z. Liu, M. S. Nassar, Y. Y. Botros and J. F. Stoddart, *Angew. Chem. Int. Ed.*, 2016, **55**, 12387–12392.
409 C. J. Bruns, M. Frasconi, J. Iehl, K. J. Hartlieb, S. T. Schneebeli, C. Cheng, S. I. Stupp and J. F. Stoddart, *J. Am. Chem. Soc.*, 2014, **136**, 4714–4723.
410 C. J. Bruns and J. F. Stoddart, *Acc. Chem. Res.*, 2014, **47**, 2186–2199.
411 P. Ghosh, O. Mermagen and C. A. Schalley, *Chem. Commun.*, 2002, 2628–2629.
412 B. Qiao, Y. Liu, S. Lee, M. Pink and A. H. Flood, *Chem Commun*, 2016, **52**, 13675–13678.
413 M. C. T. Fyfe, P. T. Glink, S. Menzer, J. F. Stoddart, A. J. P. White and D. J. Williams, *Angew. Chem. Int. Ed. Engl.*, 1997, **36**, 2068–2070.
414 J. A. Wisner, P. D. Beer and M. G. B. Drew, *Angew. Chem. Int. Ed.*, 2001, **40**, 3606–3609.
415 J. A. Wisner, P. D. Beer, M. G. B. Drew and M. R. Sambrook, *J. Am. Chem. Soc.*, 2002, **124**, 12469–12476.
416 J. M. Mercurio, F. Tyrrell, J. Cookson and P. D. Beer, *Chem Commun*, 2013, **49**, 10793–10795.
417 N. H. Evans, C. J. Serpell, N. G. White and P. D. Beer, *Chem. – Eur. J.*, 2011, **17**, 12347–12354.
418 M. J. Langton and P. D. Beer, *Chem. – Eur. J.*, 2012, **18**, 14406–14412.
419 M. D. Lankshear, N. H. Evans, S. R. Bayly and P. D. Beer, *Chem. – Eur. J.*, 2007, **13**, 3861–3870.
420 N. H. Evans, C. J. Serpell and P. D. Beer, *Chem. – Eur. J.*, 2011, **17**, 7734–7738.
421 M. R. Sambrook, P. D. Beer, J. A. Wisner, R. L. Paul and A. R. Cowley, *J. Am. Chem. Soc.*, 2004, **126**, 15364–15365.
422 N. H. Evans and P. D. Beer, *Chem. – Eur. J.*, 2011, **17**, 10542–10546.
423 N. H. Evans, C. J. Serpell and P. D. Beer, *Angew. Chem. Int. Ed.*, 2011, **50**, 2507–2510.
424 M. J. Langton, O. A. Blackburn, T. Lang, S. Faulkner and P. D. Beer, *Angew. Chem. Int. Ed.*, 2014, **53**, 11463–11466.
425 M. J. Langton, L. C. Duckworth and P. D. Beer, *Chem Commun*, 2013, **49**, 8608–8610.
426 M. J. Langton and P. D. Beer, *Chem Commun*, 2014, **50**, 8124–8127.
427 A. Brown, K. M. Mullen, J. Ryu, M. J. Chmielewski, S. M. Santos, V. Felix, A. L. Thompson, J. E. Warren, S. I. Pascu and P. D. Beer, *J. Am. Chem. Soc.*, 2009, **131**, 4937–4952.
428 N. G. White, H. G. Lovett and P. D. Beer, *RSC Adv*, 2014, **4**, 12133–12147.

429 G. T. Spence, N. G. White and P. D. Beer, *Org Biomol Chem*, 2012, **10**, 7282–7291.
430 A. Caballero, F. Zapata, N. G. White, P. J. Costa, V. Félix and P. D. Beer, *Angew. Chem.*, 2012, **124**, 1912–1916.
431 J. M. Mercurio, R. C. Knighton, J. Cookson and P. D. Beer, *Chem. – Eur. J.*, 2014, **20**, 11740–11749.
432 B. R. Mullaney, A. L. Thompson and P. D. Beer, *Angew. Chem. Int. Ed.*, 2014, **53**, 11458–11462.
433 C. A. Hunter, *J. Am. Chem. Soc.*, 1992, **114**, 5303–5311.
434 D. A. Leigh, A. Venturini, A. J. Wilson, J. K. Y. Wong and F. Zerbetto, *Chem. – Eur. J.*, 2004, **10**, 4960–4969.
435 F. Vögtle, S. Meier and R. Hoss, *Angew. Chem. Int. Ed. Engl.*, 1992, **31**, 1619–1622.
436 T. Kosikova, N. I. Hassan, D. B. Cordes, A. M. Z. Slawin and D. Philp, *J. Am. Chem. Soc.*, 2015, **137**, 16074–16083.
437 A. Vidonne, T. Kosikova and D. Philp, *Chem Sci*, 2016, **7**, 2592–2603.
438 C. N. Marrs and N. H. Evans, *Org Biomol Chem*, 2015, **13**, 11021–11025.
439 H. Y. Au-Yeung, G. D. Pantoş and J. K. M. Sanders, *Proc. Natl. Acad. Sci.*, 2009, **106**, 10466–10470.
440 H. Y. Au-Yeung, G. Dan Pantoş and J. K. M. Sanders, *J. Am. Chem. Soc.*, 2009, **131**, 16030–16032.
441 H. Y. Au-Yeung, G. D. Pantoş and J. K. M. Sanders, *J. Org. Chem.*, 2011, **76**, 1257–1268.
442 M. T. Stone and H. L. Anderson, *Chem Commun*, 2007, 2387–2389.
443 L. Zalewski, M. Wykes, S. Brovelli, M. Bonini, T. Breiner, M. Kastler, F. Dötz, D. Beljonne, H. L. Anderson, F. Cacialli and P. Samorì, *Chem. – Eur. J.*, 2010, **16**, 3933–3941.
444 E. J. F. Klotz, T. D. W. Claridge and H. L. Anderson, *J. Am. Chem. Soc.*, 2006, **128**, 15374–15375.
445 Y. Han, G.-F. Huo, J. Sun, J. Xie, C.-G. Yan, Y. Zhao, X. Wu, C. Lin and L. Wang, *Sci. Rep.*, 2016, **6**, 28748.
446 R. Shukla, M. J. Deetz and B. D. Smith, *Chem Commun*, 2000, 2397–2398.
447 M. J. Deetz, R. Shukla and B. D. Smith, *Tetrahedron*, 2002, **58**, 799–805.
448 M. J. Barrell, D. A. Leigh, P. J. Lusby and A. M. Z. Slawin, *Angew. Chem. Int. Ed.*, 2008, **47**, 8036–8039.
449 Y. Nakatani, Y. Furusho and E. Yashima, *Angew. Chem. Int. Ed.*, 2010, **49**, 5463–5467.
450 E. Arunkumar, C. C. Forbes, B. C. Noll and B. D. Smith, *J. Am. Chem. Soc.*, 2005, **127**, 3288–3289.
451 C. G. Collins, J. M. Lee, A. G. Oliver, O. Wiest and B. D. Smith, *J. Org. Chem.*, 2014, **79**, 1120–1130.
452 E. Stulz, G. Clever, M. Shionoya and C. Mao, *Chem Soc Rev*, 2011, **40**, 5633–5635.
453 N. C. Seeman, *Annu. Rev. Biochem.*, 2010, **79**, 65–87.
454 D. Ackermann, S.-S. Jester and M. Famulok, *Angew. Chem. Int. Ed.*, 2012, **51**, 6771–6775.
455 J. T. Powell, B. O. Akhuetie-Oni, Z. Zhang and C. Lin, *Angew. Chem. Int. Ed.*, 2016, **55**, 11412–11416.
456 D. Ackermann, T. L. Schmidt, J. S. Hannam, C. S. Purohit, A. Heckel and M. Famulok, *Nat Nano*, 2010, **5**, 436–442.
457 J. Weigandt, C.-L. Chung, S.-S. Jester and M. Famulok, *Angew. Chem. Int. Ed.*, 2016, **55**, 5512–5516.
458 T. L. Schmidt and A. Heckel, *Nano Lett.*, 2011, **11**, 1739–1742.
459 L. Hu, C.-H. Lu and I. Willner, *Nano Lett.*, 2015, **15**, 2099–2103.
460 C.-H. Lu, A. Cecconello, X.-J. Qi, N. Wu, S.-S. Jester, M. Famulok, M. Matthies, T.-L. Schmidt and I. Willner, *Nano Lett.*, 2015, **15**, 7133–7137.
461 C.-H. Lu, A. Cecconello, J. Elbaz, A. Credi and I. Willner, *Nano Lett.*, 2013, **13**, 2303–2308.
462 L. Hu, C.-H. Lu and I. Willner, *Nano Lett.*, 2015, **15**, 2099–2103.
463 L. Z. Yan and P. E. Dawson, *Angew. Chem. Int. Ed.*, 2001, **40**, 3625–3627.
464 X.-W. Wang and W.-B. Zhang, *Angew. Chem.*, 2016, **128**, 3503–3507.
465 C. D. Allen and A. J. Link, *J. Am. Chem. Soc.*, 2016, **138**, 14214–14217.
466 M. J. Langton and P. D. Beer, *Acc. Chem. Res.*, 2014, **47**, 1935–1949.
467 K. Hiratani, M. Kaneyama, Y. Nagawa, E. Koyama and M. Kanesato, *J. Am. Chem. Soc.*, 2004, **126**, 13568–13569.
468 Y. Nagawa, J. Suga, K. Hiratani, E. Koyama and M. Kanesato, *Chem Commun*, 2005, 749–751.
469 X. Wang, J. Zhu and D. B. Smithrud, *J. Org. Chem.*, 2010, **75**, 3358–3370.
470 S. S. Zhu, P. J. Carroll and T. M. Swager, *J. Am. Chem. Soc.*, 1996, **118**, 8713–8714.
471 S. S. Zhu and T. M. Swager, *J. Am. Chem. Soc.*, 1997, **119**, 12568–12577.
472 J. M. Mercurio, F. Tyrrell, J. Cookson and P. D. Beer, *Chem Commun*, 2013, **49**, 10793–10795.
473 L. C. Gilday and P. D. Beer, *Chem. – Eur. J.*, 2014, **20**, 8379–8385.
474 A. Brown, M. J. Langton, N. L. Kilah, A. L. Thompson and P. D. Beer, *Chem. – Eur. J.*, 2015, **21**, 17664–17675.
475 M. J. Langton and P. D. Beer, *Chem. – Eur. J.*, 2012, **18**, 14406–14412.
476 S. P. Cornes, C. H. Davies, D. Blyghton, M. R. Sambrook and P. D. Beer, *Org Biomol Chem*, 2015, **13**, 2582–2587.
477 T. A. Barendt, A. Docker, I. Marques, V. Félix and P. D. Beer, *Angew. Chem. Int. Ed.*, 2016, **55**, 11069-11076.
478 N. H. Evans, H. Rahman, A. V. Leontiev, N. D. Greenham, G. A. Orlowski, Q. Zeng, R. M. J. Jacobs, C. J. Serpell, N. L. Kilah, J. J. Davis and P. D. Beer, *Chem Sci*, 2012, **3**, 1080–1089.
479 N. H. Evans, C. J. Serpell and P. D. Beer, *Chem Commun*, 2011, **47**, 8775–8777.
480 C. Allain, P. D. Beer, S. Faulkner, M. W. Jones, A. M. Kenwright, N. L. Kilah, R. C. Knighton, T. J. Sorensen and M. Tropiano, *Chem Sci*, 2013, **4**, 489–493.
481 R. C. Knighton and P. D. Beer, *Chem Commun*, 2014, **50**, 1540–1542.
482 J. R. Romero, G. Aragay and P. Ballester, *Chem Sci*, 2017, **8**, 491-498.

483 S. Xiao, N. Fu, K. Peckham and B. D. Smith, *Org. Lett.*, 2010, **12**, 140–143.
484 J. J. Gassensmith, L. Barr, J. M. Baumes, A. Paek, A. Nguyen and B. D. Smith, *Org. Lett.*, 2008, **10**, 3343–3346.
485 J. J. Gassensmith, J. M. Baumes and B. D. Smith, *Chem Commun*, 2009, 6329–6338.
486 J. R. Johnson, N. Fu, E. Arunkumar, W. M. Leevy, S. T. Gammon, D. Piwnica-Worms and B. D. Smith, *Angew. Chem. Int. Ed.*, 2007, **46**, 5528–5531.
487 J. M. Baumes, J. J. Gassensmith, J. Giblin, J.-J. Lee, A. G. White, W. J. Culligan, W. M. Leevy, M. Kuno and B. D. Smith, *Nat Chem*, 2010, **2**, 1025–1030.
488 A. Fernandes, A. Viterisi, F. Coutrot, S. Potok, D. A. Leigh, V. Aucagne and S. Papot, *Angew. Chem. Int. Ed.*, 2009, **48**, 6443–6447.
489 R. Barat, T. Legigan, I. Tranoy-Opalinski, B. Renoux, E. Peraudeau, J. Clarhaut, P. Poinot, A. E. Fernandes, V. Aucagne, D. A. Leigh and S. Papot, *Chem Sci*, 2015, **6**, 2608–2613.
490 X. Wang, X. Bao, M. McFarland-Mancini, I. Isaacsohn, A. F. Drew and D. B. Smithrud, *J. Am. Chem. Soc.*, 2007, **129**, 7284–7293.
491 J. Zhu, B. E. House, E. Fleck, I. Isaacsohn, A. F. Drew and D. B. Smithrud, *Bioorg. Med. Chem. Lett.*, 2007, **17**, 5058–5062.
492 D. B. Smithrud, X. Wang, P. Tarapore and S. Ho, *ACS Med. Chem. Lett.*, 2013, **4**, 27–31.
493 X. Wang and D. B. Smithrud, *Bioorg. Med. Chem. Lett.*, 2011, **21**, 6880–6883.
494 P. L. Anelli, N. Spencer and J. F. Stoddart, *J. Am. Chem. Soc.*, 1991, **113**, 5131–5133.
495 M. C. Jiménez, C. Dietrich-Buchecker and J.-P. Sauvage, *Angew. Chem. Int. Ed.*, 2000, **39**, 3284–3287.
496 F. Niess, V. Duplan, C. S. Diercks and J.-P. Sauvage, *Chem. – Eur. J.*, 2015, **21**, 14393–14400.
497 K. Iwaso, Y. Takashima and A. Harada, *Nat Chem*, 2016, **8**, 625–632.
498 J. D. Badjić, V. Balzani, A. Credi, S. Silvi and J. F. Stoddart, *Science*, 2004, **303**, 1845.
499 J. D. Badjic, C. M. Ronconi, J. F. Stoddart, V. Balzani, S. Silvi and A. Credi, *J. Am. Chem. Soc.*, 2006, **128**, 1489–1499.
500 J. Berna, D. A. Leigh, M. Lubomska, S. M. Mendoza, E. M. Perez, P. Rudolf, G. Teobaldi and F. Zerbetto, *Nat Mater*, 2005, **4**, 704–710.
501 B. Lewandowski, G. De Bo, J. W. Ward, M. Papmeyer, S. Kuschel, M. J. Aldegunde, P. M. E. Gramlich, D. Heckmann, S. M. Goldup, D. M. D'Souza, A. E. Fernandes and D. A. Leigh, *Science*, 2013, **339**, 189.
502 M. R. Panman, B. H. Bakker, D. den Uyl, E. R. Kay, D. A. Leigh, W. J. Buma, A. M. Brouwer, J. A. J. Geenevasen and S. Woutersen, *Nat Chem*, 2013, **5**, 929–934.
503 P. Farràs, E. C. Escudero-Adán, C. Viñas and F. Teixidor, *Inorg. Chem.*, 2014, **53**, 8654–8661.
504 T. A. Barendt, S. W. Robinson and P. D. Beer, *Chem Sci*, 2016, **7**, 5171–5180.
505 J. Beswick, V. Blanco, G. De Bo, D. A. Leigh, U. Lewandowska, B. Lewandowski and K. Mishiro, *Chem Sci*, 2015, **6**, 140–143.
506 Y. Tachibana, N. Kihara and T. Takata, *J. Am. Chem. Soc.*, 2004, **126**, 3438–3439.
507 Y. Li, Y. Feng, Y.-M. He, F. Chen, J. Pan and Q.-H. Fan, *Tetrahedron Lett.*, 2008, **49**, 2878–2881.
508 Y. Cakmak, S. Erbas-Cakmak and D. A. Leigh, *J. Am. Chem. Soc.*, 2016, **138**, 1749–1751.
509 M. Galli, J. E. M. Lewis and S. M. Goldup, *Angew. Chem. Int. Ed.*, 2015, **54**, 13545–13549.
510 M. Xue, Y. Yang, X. Chi, X. Yan and F. Huang, *Chem. Rev.*, 2015, **115**, 7398–7501.
511 M. Wei, Y. Gao, X. Li and M. J. Serpe, *Polym Chem*, 2017, **8**, 127–143.
512 E. A. Appel, F. Biedermann, U. Rauwald, S. T. Jones, J. M. Zayed and O. A. Scherman, *J. Am. Chem. Soc.*, 2010, **132**, 14251–14260.
513 S. Dong, Y. Luo, X. Yan, B. Zheng, X. Ding, Y. Yu, Z. Ma, Q. Zhao and F. Huang, *Angew. Chem.*, 2011, **123**, 1945–1949.
514 X. Yan, D. Xu, X. Chi, J. Chen, S. Dong, X. Ding, Y. Yu and F. Huang, *Adv. Mater.*, 2012, **24**, 362–369.
515 S. Tamesue, Y. Takashima, H. Yamaguchi, S. Shinkai and A. Harada, *Angew. Chem. Int. Ed.*, 2010, **49**, 7461–7464.
516 K. Peng, I. Tomatsu and A. Kros, *Chem Commun*, 2010, **46**, 4094–4096.
517 M. A. Olson, A. B. Braunschweig, L. Fang, T. Ikeda, R. Klajn, A. Trabolsi, P. J. Wesson, D. Benítez, C. A. Mirkin, B. A. Grzybowski and J. F. Stoddart, *Angew. Chem. Int. Ed.*, 2009, **48**, 1792–1797.
518 X. Ma, R. Sun, W. Li and H. Tian, *Polym Chem*, 2011, **2**, 1068–1070.
519 M. Nakahata, Y. Takashima, H. Yamaguchi and A. Harada, *Nat. Commun.*, 2011, **2**, 511.
520 L. Fang, M. Hmadeh, J. Wu, M. A. Olson, J. M. Spruell, A. Trabolsi, Y.-W. Yang, M. Elhabiri, A.-M. Albrecht-Gary and J. F. Stoddart, *J. Am. Chem. Soc.*, 2009, **131**, 7126–7134.
521 Y.-S. Su, J.-W. Liu, Y. Jiang and C.-F. Chen, *Chem. – Eur. J.*, 2011, **17**, 2435–2441.
522 M. Nakahata, S. Mori, Y. Takashima, H. Yamaguchi and A. Harada, *Chem*, **1**, 766–775.
523 K. Kato, Y. Okabe, Y. Okazumi and K. Ito, *Chem Commun*, 2015, **51**, 16180–16183.
524 T. Karino, Y. Okumura, K. Ito and M. Shibayama, *Macromolecules*, 2004, **37**, 6177–6182.

Blank Page

Chapter 2

Halogen- and Chalcogen Bonding Macrocycles and [2]Rotaxanes for Anion Recognition

CHAPTER 2 : Halogen- and Chalcogen Bonding Macrocycles and [2]Rotaxanes for Anion Recognition

2.1 Introduction

This chapter focuses on the use of 1,2,3-triazole-/triazolium-based halogen and chalcogen bonding motifs for anion recognition, which are incorporated into acyclic, macrocyclic and rotaxane host structures. Aided by their facile synthesis using the copper(I)-catalysed azide-alkyne cycloaddition (CuAAC) reaction,[1–3] 1,2,3-triazoles are ideal motifs for anion binding due to their aromatic stability,[4] highly electron-deficient character,[5] as well as the possibility of functionalising them at the 5-position with various groups.[6] Furthermore, the *N*[3] atom on the triazole can be methylated and coordinated with metal cations to further augment their electron-deficiency (Figure 2.1).[7] As such, the triazole motif serves as a convenient framework to construct highly Lewis-acidic XB and ChB donor groups capable of potent anion binding. Nevertheless, their incorporation into macrocycles and MIMs necessitate the development of novel synthetic protocols, which are expounded in detail herein. In particular, we capitalised on the facile metal ligating properties of the triazole-containing macrocycles to explore the active metal template (AMT) strategy (Section 1.3.2.2) to prepare MIM hosts which contain combinations of XB/ ChB/ HB donor motifs within their anion binding cavity.

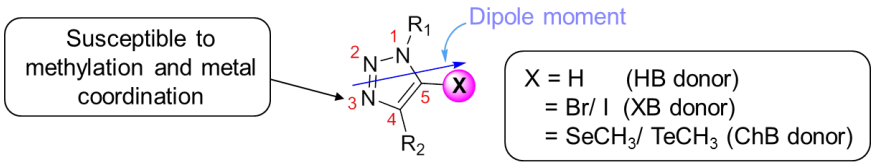


***Figure 2.1**. Chemical and physical properties of 1,2,3-triazoles.*[7]

2.1.1 CuAAC Active Metal-Templated Synthesis of Interlocked Structures

Of the many reactions amenable for AMT synthesis of MIMs (Section 1.3.2.2), the CuAAC reaction is the most frequently employed.[8] In a seminal study, Leigh and co-workers established the reaction conditions necessary for rotaxane formation using a pyridine-containing macrocycle (Figure 2.2). Briefly, it was discovered that a good ligating group

oriented into the macrocycle cavity is necessary for CuAAC-AMT rotaxane synthesis, and macrocycles can contain at most two coordination sites for Cu(I) binding, with tridentate macrocycles completely ineffective for AMT (Figure 2.2). Furthermore, the macrocycle: Cu(I) ratio was found to affect the rotaxane yield, with higher ratios favouring rotaxane formation over free axle production at the expense of time.[9] These findings led to the proposal of a mechanism shown in Figure 2.3A, where the endotopically-coordinated Cu(I) catalyst coordinates both azide and alkyne components through the macrocycle cavity and drives the formation of a Cu(I)-triazolide species, which has been demonstrated crystallographically in a separate later study (Figure 2.4).[10] De-complexation of the Cu(I) species then affords the free rotaxane in yields of up to 94 %. The reaction has been found to be surprisingly tolerant to the source of Cu(I), coordinating (e.g. DME, THF, NMP) and non-coordinating (e.g. toluene, dichloromethane, chloroform) solvents, and can also occur at elevated temperatures.[11] Other than rotaxanes, the use of CuAAC-AMT reactions to form catenanes has also been investigated.[12] Compared to rotaxanes, catenane formation is inherently more demanding as it necessitates *intramolecular* ring-closures (Figure 2.3B). However, this occurs simultaneously with non-productive precursor oligomerisation and free macrocycle formation, rendering preferential catenane formation inherently more sensitive to reaction conditions. Indeed, low reactant concentration, high temperatures, stoichiometric quantities of Cu(I) relative to macrocycle, and long reaction times were found to be necessary for good yields of [2]catenanes to be obtained.

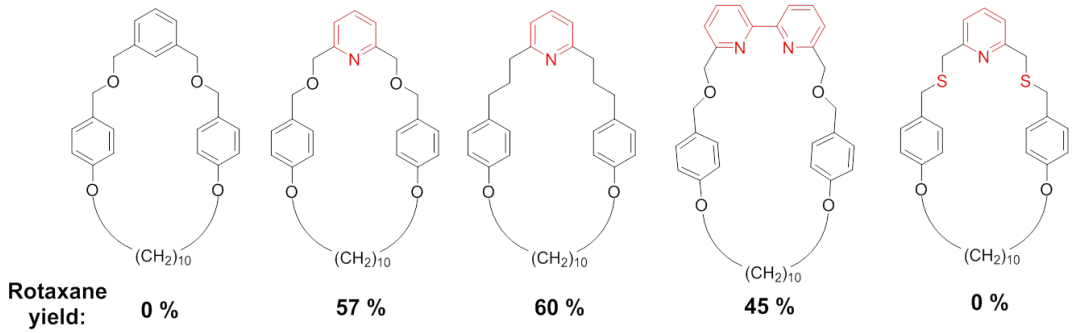


***Figure 2.2**. Selected examples of macrocycles screened for CuAAC-AMT [2]rotaxane formation, with isolated yields of rotaxane indicated with a 1:1:1:1 molar ratio of macrocycle:stopper-functionalised azide: alkyne: $[Cu(CH_3CN)_4]PF_6$. Cu(I)-ligating groups are highlighted in red.*[9]

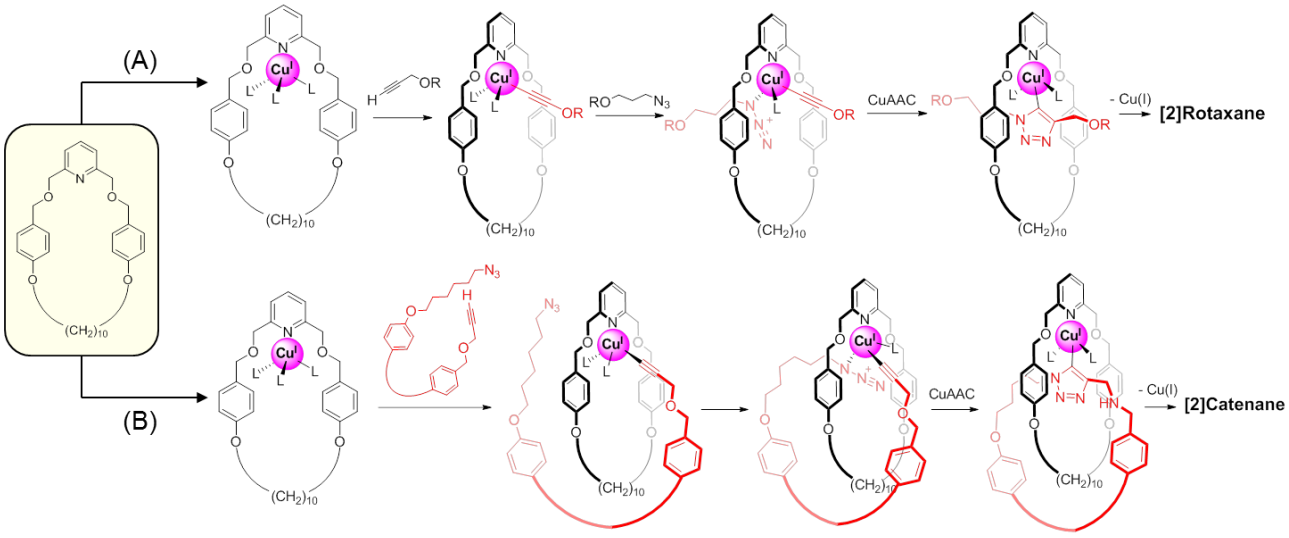


***Figure 2.3**. Proposed mechanisms for CuAAC-AMT formation of (A) [2]rotaxanes[9] and (B) [2]catenanes.[12]*

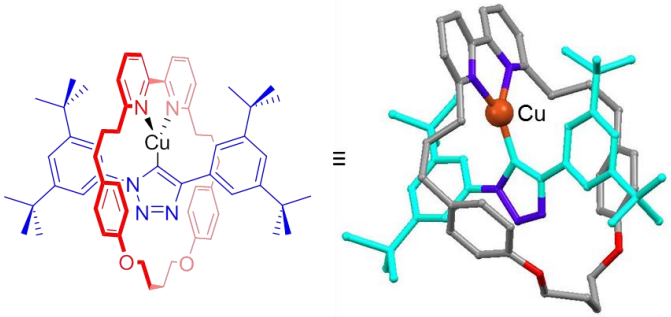


***Figure 2.4**. A Cu(I)-triazolide intermediate in CuAAC-AMT [2]rotaxane synthesis.[10]*

The CuAAC-AMT reaction has also afforded higher-ordered interlocked structures, in particular polyrotaxanes containing numerous macrocycles threaded through an axle. Early investigations by Leigh *et. al.* using a pyridine macrocycle revealed that conditions favouring [2]rotaxane formation, i.e high macrocycle: Cu(I) ratio, also resulted in the unexpected formation of a [3]rotaxane, albeit in a modest yield of 33 % (Figure 2.5A).[9] Contrastingly, a subsequent study by Goldup and coworkers found that using a bipyridine macrocycle, homocircuit [3]rotaxanes were favoured over [2]rotaxanes by higher Cu(I) loadings, larger macrocycles and elevated temperatures, suggesting that actual reaction conditions varies with the nature of the macrocycle used.[11] The AMT process could also be repeated iteratively to produce a linear [6]rotaxane in an impressive 67 % overall yield (Figure 2.5B),[13] as well as a trigonal-shaped [4]rotaxane (Figure 2.5C), albeit in a more modest yield of 16 % due to steric hindrance.[14] In addition, a structurally more complicated heterocircuit [3]rotaxane containing

macrocycles and stoppers of different sizes could be produced exclusively over other possible isomers by exploiting a size-dependent kinetic self-sorting process occurring during the AMT reaction.[15]

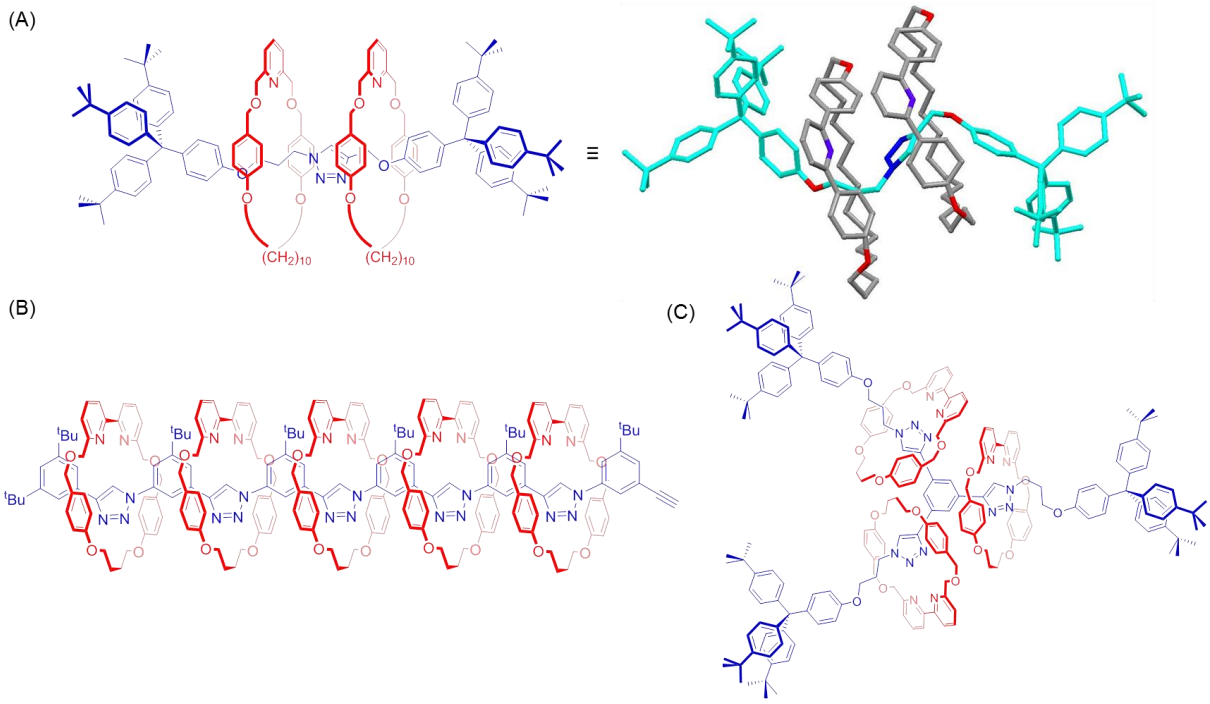


***Figure 2.5**. Examples of polyrotaxanes formed using CuAAC-AMT: (A) Leigh's [3]rotaxane[9]; (B) Goldup's AMT-[6]rotaxane[13] and (C) trigonal [4]rotaxane.[14]*

2.1.2 A Neutral All-Halogen Bonding [2]Rotaxane

Cognisant of the fact that iodotriazoles can act as both Lewis acids for anion recognition (via iodine atoms) or Lewis bases for cation coordination, Beer and co-workers recently designed a macrocycle containing two covalently-linked iodotriazole groups which act as a bidentate ligand for Cu(I). As shown in Figure 2.6, the flexibility of the macrocycle's alkyl linkers allow the Cu(I)-complex to be oriented into the macrocycle cavity for CuAAC-AMT synthesis of an all-XB rotaxane via an 'iodo-Click' reaction between an azide and terminal iodoalkyne stopper units. De-complexation of the Cu(I) catalyst, followed by coordination of a bulkier Re(I) complex, forced the metal to be oriented exotopically. This created a neutral binding cavity containing three XB-donor iodotriazoles, which was shown to bind halides in $CHCl_3$ (K_a of Cl^- = 560 M^{-1}) by UV-Vis titrations.[16]

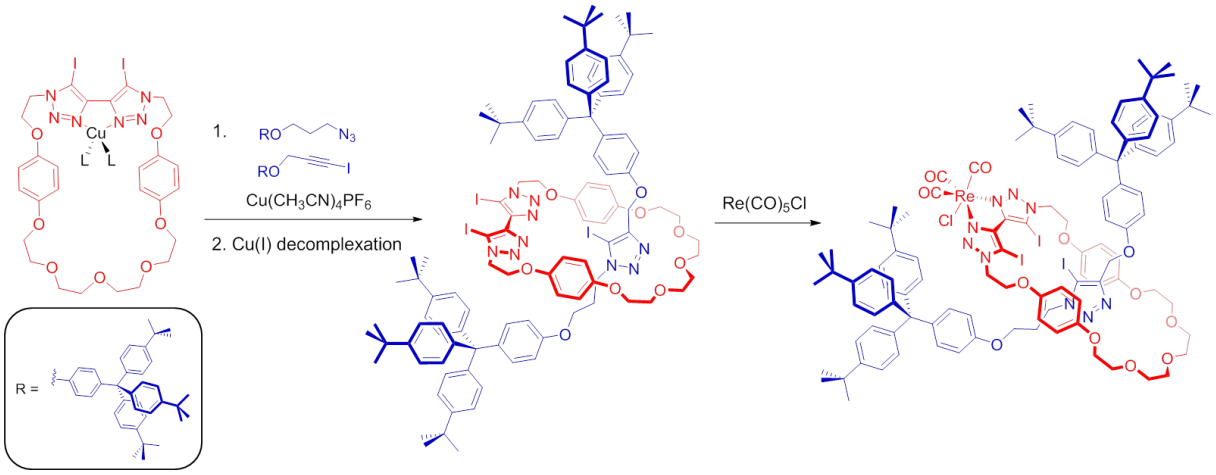


***Figure 2.6**. Beer's all-XB [2]rotaxane formed using the CuAAC-AMT reaction.*[16]

2.1.3 Chapter Aims

Building on these earlier findings, this chapter aims to fulfil the following goals:

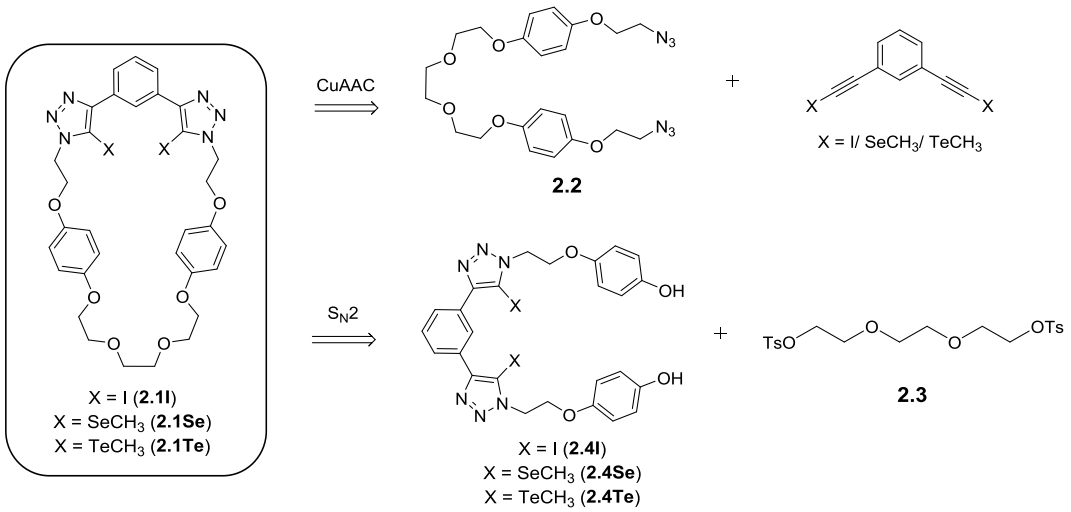
- Establish general synthetic routes towards macrocycle and rotaxane host systems containing triazole-based XB/ ChB/ HB -donor groups in their anion binding cavities.
- Investigate and compare the fundamental anion binding properties conferred by XB, ChB and HB-donor host molecules (i.e. binding affinities, trends and thermodynamic parameters) in organic solvents and water-containing media.

After establishing the CuAAC-AMT approach to synthesise a series of unprecedented neutral [2]rotaxanes bearing two, three or four iodotriazole units surrounding the binding cavity, the procedure is extended to prepare neutral ChB-donor rotaxanes bearing 5-methylchalcogeno-1,2,3-triazoles (chalcogen = Se/ Te) (Figure 2.1). The anion binding properties of these neutral σ-hole donor rotaxanes in dry and wet acetone are elucidated, followed by the effects of enhancing the strength of these σ-hole interactions by triazole N^3-methylation. Thereafter, a novel monocationic Te-containing acyclic model host molecule is used to determine the hitherto-unknown enthalpic and entropic contributions driving ChB-anion binding via van 't Hoff plots, and the results compared with HB and XB host analogues. Subsequently, the attempted preparation of other interlocked structures such as an all-ChB [2]catenane by passive metal templation, a mixed-ChB/ HB [2]rotaxane by anion templation, and neutral XB [2]catenanes by CuAAC-AMT are also investigated.

2.2 Halogen- and Chalcogen-Bonding Macrocycles and [2]Rotaxanes for Anion Binding‡

2.2.1 Design and Syntheses of Halogen- and Chalcogen-Bonding Macrocycles

Abiotic anion receptors bearing meta-substituted iodotriazole groups on a central benzene/ pyridine motif have been empirically and computationally shown to be highly effective in coordinating halide anions in a bidentate manner via highly linear XB interactions (see crystal structure in Figure 1.18A).[17–19] Thus, this anion binding motif was incorporated into macrocycle designs bearing XB iodotriazole (**2.1I**) or ChB methylchalcogeno-triazole groups (**2.1Se/ Te**). As shown in Scheme 2.1, the target macrocycles can be prepared either by CuAAC ring-closing between bis-azide **2.2** and a suitably-functionalised alkyne,[20–22] or double Williamson ether synthesis involving the S_N2 nucleophilic substitution of a bis-tosylate **2.3** with a bis-phenoxide macrocycle precursor **2.4**.[23]



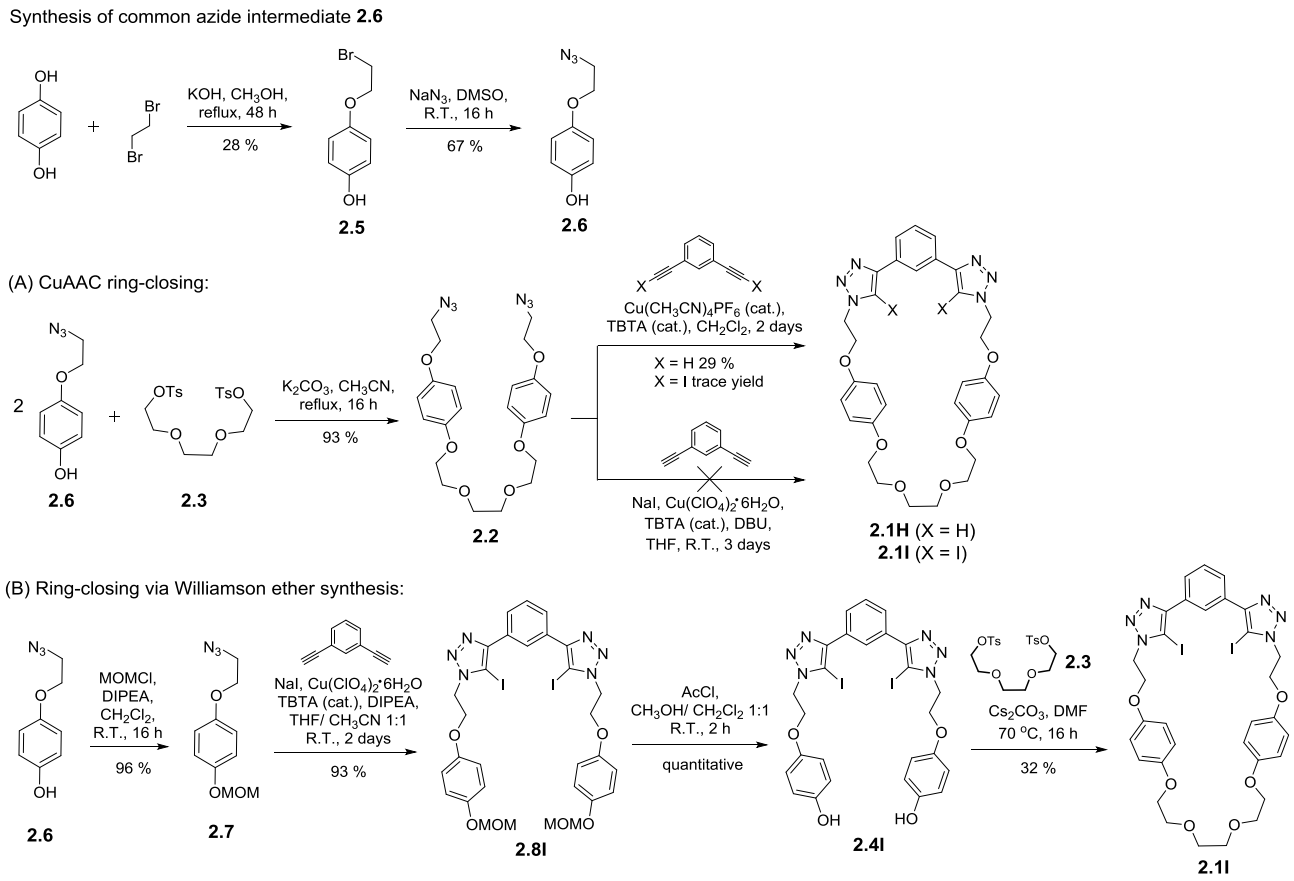
***Scheme 2.1**. Retrosynthesis of macrocycles bearing σ-hole-donor substituted triazoles.*

The multi-stepped attempted synthesis of macrocycle **2.1I** via both routes is shown in Scheme 2.2. The common azide precursor to both routes (**2.6**) was prepared from commercially-available hydroquinone in two successive steps, by first reacting with 1,2-

‡ The work in Section 2.2 has been published in Lim, J. Y. C., Marques, I., Thompson, A. L., Christensen, K. E., Felix, V., Beer, P. D., *Chalcogen Bonding Macrocycles and [2]Rotaxanes for Anion Recognition*, *J. Am. Chem. Soc.*, 2017, **139**, 3122-3133; and Lim, J. Y. C., Bunchuay, T., Beer, P. D., *Strong and Selective Halide Anion Binding by Neutral Halogen-bonding [2]Rotaxanes in Wet Organic Solvents*, *Chem. Eur. J.*, 2017, **23**, 4700-4707.

dibromoethane under reflux conditions to obtain intermediate **2.5** using a modified literature procedure,[24] followed by an S_N2 substitution with sodium azide in DMSO. To prepare the bis-azide macrocycle precursor **2.2** for the CuAAC ring-closing route, an acetonitrile solution of **2.6** was heated under reflux with bis-tosylate **2.3** in the presence of excess potassium carbonate base to afford **2.2** in 93 % yield. CuAAC ring-closing was then attempted with an equimolar mixture of **2.2** and 1,3-diethynylbenzene under high-dilution conditions (10 mM) with catalytic quantities of $[Cu(CH_3CN)_4]PF_6$ and rate-accelerating ligand TBTA,[22] to afford macrocycle **2.1H** in 29 % isolated yield. Following this success, an identical protocol was attempted towards XB macrocycle **2.1I** using 1,3-bis(iodoethynyl)benzene instead. Surprisingly, only trace quantities of macrocycle **2.1I** could be detected by mass spectrometry, and purification proved challenging. Unfortunately, neither reducing the concentration of the reactants to 2.0 mM, nor changing the reaction solvent (e.g. to THF) resulted in significant improvements in macrocycle yield. An attempted method to form **2.1I** directly from 1,3-diethynylbenzene and **2.2** using Zhu's 'one-pot iodo-Click' protocol using stoichiometric quantities of sodium iodide and copper(II) perchlorate hexahydrate[25] also failed to yield useful quantities of the macrocycle.

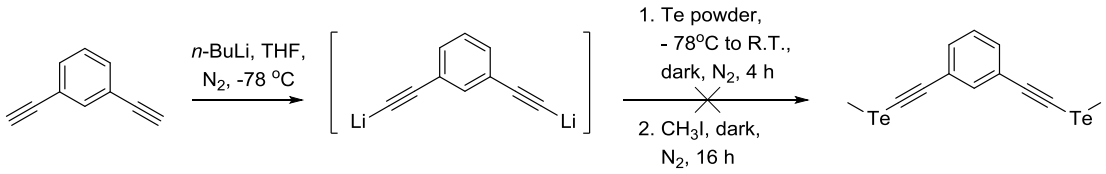
The S_N2 ring-closing method was attempted next (Scheme 2.2B). The phenol group of intermediate **2.6** was first protected with the acid-labile methoxymethyl acetal (MOM) group to form **2.7**,[26] and subjected to a 'one-pot iodo-Click' reaction with 1,3-diethynylbenzene to afford bis(iodotriazole)-bearing compound **2.8I** in an excellent yield of 93 %. Subsequently, quantitative removal of the MOM protecting group to afford **2.4I** was achieved using *in-situ* generated hydrochloric acid from the reaction of acetyl chloride and methanol solvent. Ring-closing via Williamson ether synthesis was then performed using a 1:1 molar ratio of bis-phenol **2.4I** with triethylene glycol bis-tosylate **2.3** in dry degassed DMF with excess cesium carbonate base, taking advantage of the so-called 'cesium effect' which supresses oligomerisation in favour of macrocycle formation.[27] Gratifyingly, thermal decomposition of **2.4I** was not observed, and macrocycle **2.1I** was isolated in 32 % yield following chromatographic purification.



***Scheme 2.2**. Attempted forward synthesis of macrocycle **2.1I** via (A) CuAAC ring-closing and (B) Williamson ether synthesis routes.*

Compared to iodotriazoles, the synthesis of chalcogeno-triazoles using azide-alkyne cycloaddition reactions are highly challenging. While phenylseleno-triazoles can be prepared by an 'interrupted' CuAAC reaction from terminal alkynes and azides, where the copper(I)-triazolide 'Click' intermediate is trapped with an electrophilic Se source ($PhSO_2SePh$)[28] or from an iridium-catalysed cycloaddition between azides and a selenium-substituted internal alkyne,[29] these reactions require highly-specialised reagents and typically give only modest conversions. Owing to the greater lability of the C-Te bond rendering it more prone to oxidative metal insertion,[30] organotelluro-triazoles prove to be even more challenging targets, with only one method reported to date in the literature involving CuAAC with organotellurium-substituted internal alkynes.[31] Nevertheless, to test the possibility of the CuAAC route towards ChB macrocycles **2.1Se/Te**, the synthesis of 1,3-bis(methyltelluro-ethynyl)benzene was attempted.[31] As shown in Scheme 2.3, 1,3-diethynylbenzene was first deprotonated with 2

equivalents of *n*-butyllithium in anhydrous THF at -78 °C for an hour to generate the bis-lithium acetylide complex. Subsequently, elemental Te powder was added and the reaction warmed up to ambient temperature and stirred in the dark to minimise any photo-dissociation reactions. After stirring for four hours and quenching the reaction with iodomethane, thin layer chromatography (TLC) and ^{1}H NMR spectroscopic analysis of the crude reaction mixture showed the formation of many side products with no evidence of the desired product seen. Thus, the CuAAC ring-closing route towards the target ChB macrocycles was not pursued further.

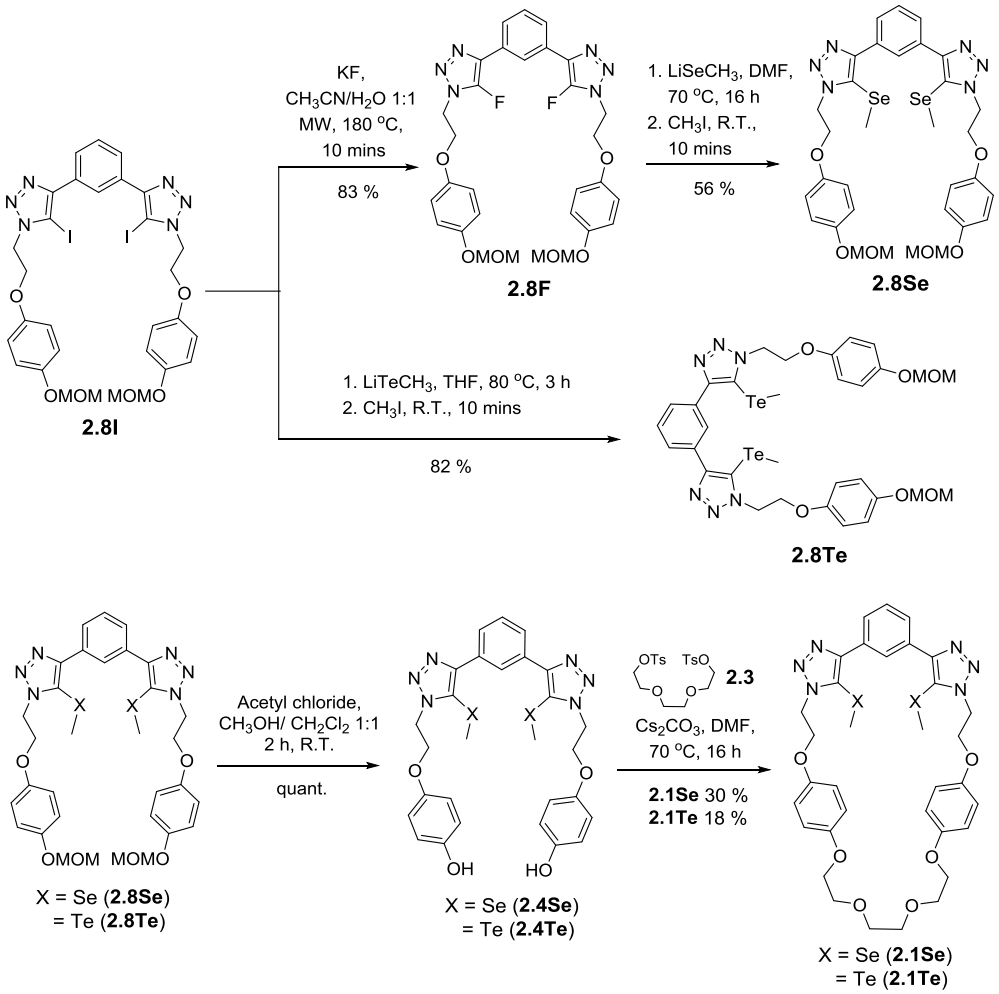


Scheme 2.3. *Attempted synthesis of 1,3-bis(methyltelluroethynyl)benzene.*

The target ChB macrocycles **2.1Se** and **2.1Te** were then assembled by the S_N2 ring-closing synthetic protocol analogous to **2.1I**. Firstly, to prepare the Se/Te analogues of **2.8I**, the possibility of performing aromatic nucleophilic substitution (S_NAr) on the electron-deficient iodotriazoles by nucleophiles[6] was investigated. **2.8Te** was prepared by reacting elemental Te powder and methyl lithium to generate the methyl telluride anion ($TeCH_3^-$) *in situ*, before **2.8I** was added to the reaction. After heating at 80 °C for three hours, **2.8Te** was obtained in 82 % yield after chromatographic purification (Scheme 2.4).[§] Interestingly, when the same procedure was used for the synthesis of **2.8Se** directly from **2.8I** with *in-situ*-generated[32] $SeCH_3^-$, **2.8Se** was obtained in very poor yields even after an overnight reaction, with numerous decomposition products formed instead. To circumvent the problem, the triazoles of **2.8I** were further activated for the S_NAr reaction by first substituting the iodine atoms with fluorine via Fokin's halide exchange protocol,[6] before the resulting bis-fluorotriazole (**2.8F**) was reacted overnight with

[§] The stability of **2.8Te** was investigated by daily monitoring of a 1.0 mM solution of the compound in d_6-DMSO using ^{1}H NMR spectroscopy for 7 days. No evidence of decomposition was seen despite the sample being left under ambient conditions between recording the spectra.

$SeCH_3^-$. Pleasingly, this method afforded the target **2.8Se** in an overall yield of 46 % after both steps. Following the generation of **2.4Se/Te** via quantitative acidic deprotection of the MOM group of **2.8Se/Te**, the target macrocycles were obtained by Williamson ether synthesis using bis-tosylate **2.3** under basic conditions.

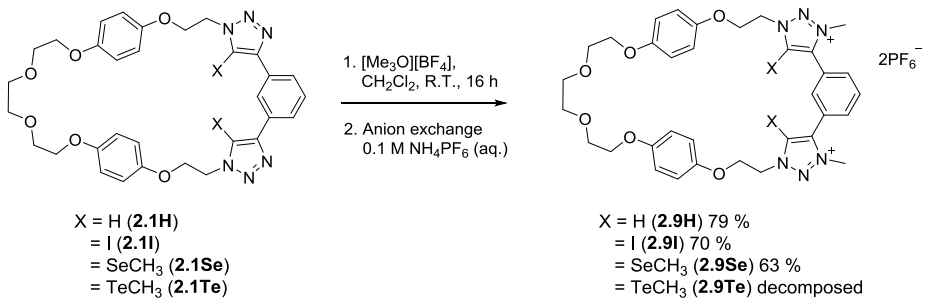


Scheme 2.4. *Forward synthesis of ChB macrocycles* ***2.1Se*** *and* ***2.1Te****.*

Macrocycle **2.1Te** was obtained in a significantly lower yield than **2.1Se** following this route, and macrocycle side products corresponding to the loss of one and two $TeCH_3$ groups were also obtained in 11 % and 6 % yields respectively, possibly due to the thermal lability of the C-Te bond.[30] It is noteworthy that no loss of the $SeCH_3$ groups was observed during the synthesis of **2.1Se**. Attempting to improve the yields of **2.1Te**, an analogous S_N2

macrocyclisation reaction was first performed at room temperature without heating. Although no macrocycle was formed after a 48 hour reaction, $TeCH_3$ lability from precursor **2.4Te** was not observed under these reaction conditions. The macrocyclisation reaction was then attempted by stirring **2.4Te** with sodium hydride, a stronger base, in dry degassed THF to first form the nucleophilic phenoxide intermediate before bis-tosylate **2.3** was added. Despite effervescence being observed upon the addition of excess sodium hydride, suggesting effective phenol deprotonation, it was surprising that no macrocycle could be detected by ESI-MS and TLC analysis even after an overnight reaction as well, although **2.4Te** was found to be stable to the presence of excess sodium hydride in the reaction mixture.

Following the successful syntheses of the **2.1** macrocycle family, the triazole groups were *N*-methylated using trimethyloxonium tetrafluoroborate to further enhance the electrophilicity of the donor atoms at the triazole 5-position for subsequent anion binding studies. While dicationic macrocycles **2.9H**, **2.9I** and **2.9Se** could be isolated in 79, 70 and 63 % yields respectively after chromatographic purification and anion exchange to the non-coordinating hexafluorophosphate (PF_6^-) salt (Scheme 2.5), complete decomposition of macrocycle **2.1Te** resulted from the reaction. Unfortunately, repeating the methylation of **2.1Te** under an inert atmosphere and in the absence of light still did not yield target macrocycle **2.9Te**, possibly due to the enhanced lability of the C-Te bond from lowering of the C-Te LUMO energy levels upon triazole methylation. Notably, methylation of the seleno-triazole groups of **2.1Se** resulted in a large downfield perturbation of the ^{77}Se NMR signal ($\Delta\delta$ = + 61.5 ppm) resulting from the enhanced electron-deficiency of the Se atoms in **2.9Se**.



Scheme 2.5. *Synthesis of dicationic macrocycles **2.9H**, **2.9I** and **2.9Se**.*

2.2.2 Copper(I) Binding Properties of Macrocycles

The ability of triazoles to act as *N*-donor ligands for the coordination of metal cations such as Cu(I) has been established in a number of solution-phase and solid-state studies.[33–39] Recognising the endo/exo-conformational flexibility of triazoles incorporated into macrocycles (see Section 2.1.2), it was envisaged that the neutral macrocycles (**2.1H/ I/ Se/ Te**) could act as ligands for catalytically-active Cu(I) species for active metal template rotaxane synthesis (see Section 2.1.1). Evidence for Cu(I) binding to the macrocycles was established via ^{1}H NMR and UV-Vis spectroscopy titrations, and by DFT simulations.

^{1}H NMR titrations were performed by adding increasing quantities of $[Cu(CH_3CN)_4]PF_6$ to separate solutions of the macrocycles in the non-coordinating solvents CD_2Cl_2 or d_6-acetone.[40] For all macrocycles, the addition of 0.25, 0.50 and 0.75 molar equivalents of Cu(I) increased the complexity of the macrocycles' ^{1}H NMR spectra, with noticeable peak broadening observed in all cases. This indicated that Cu(I)-binding to the macrocycles was slow on the ^{1}H NMR timescale, with multiple coordinated species formed in solution. In the presence of 1.0 equivalent of Cu(I) however, the ^{1}H NMR spectra showed significantly improved resolution and simplification for all macrocycles, indicating the formation of more well-defined 1:1 Cu(I)-macrocycle complexes. Indeed, electrospray ionisation mass spectrometry (ESI-MS) analyses of the mixtures showed distinct peaks at *m/z* = 661.2, 913.0, 849.0 and 945.0, corresponding to the 1:1 macrocycle-Cu(I) adducts $[M + Cu]^+$ of **2.1H**, **2.1I**, **2.1Se** and **2.1Te** respectively, with no other binding stoichiometries discernible. For macrocycle **2.1H**, 1.0 equivalent of Cu(I) resulted in desymmetrisation of the macrocycle's ^{1}H NMR spectrum (Figure 2.7A), with the aromatic region being the most diagnostic. The originally equivalent H_B and triazole aromatic proton environments were split into two sets of distinct signals, with one triazole proton resonance downfield shifted by +0.11 ppm and the other showing an upfield perturbation of -0.40 ppm. Presumably, the former results from direct *N*-coordination to Cu(I), increasing the electron deficiency of the triazole ring itself.[33] Importantly, this shows that only one triazole is coordinating to Cu(I) at any one time, implying that the two triazole units of **2.1H** may not be in a favourable conformation for bidentate Cu(I) coordination between their N^3 atoms simultaneously, which would have retained the spectral

symmetry of **2.1H**. Notably, macrocycle **2.1I** shows a similar coordination mode, with desymmetrisation of the aromatic region of its ^{1}H NMR spectrum consistent with asymmetric coordination in the presence of 1.0 equivalent of Cu(I) (Figure 2.7B).

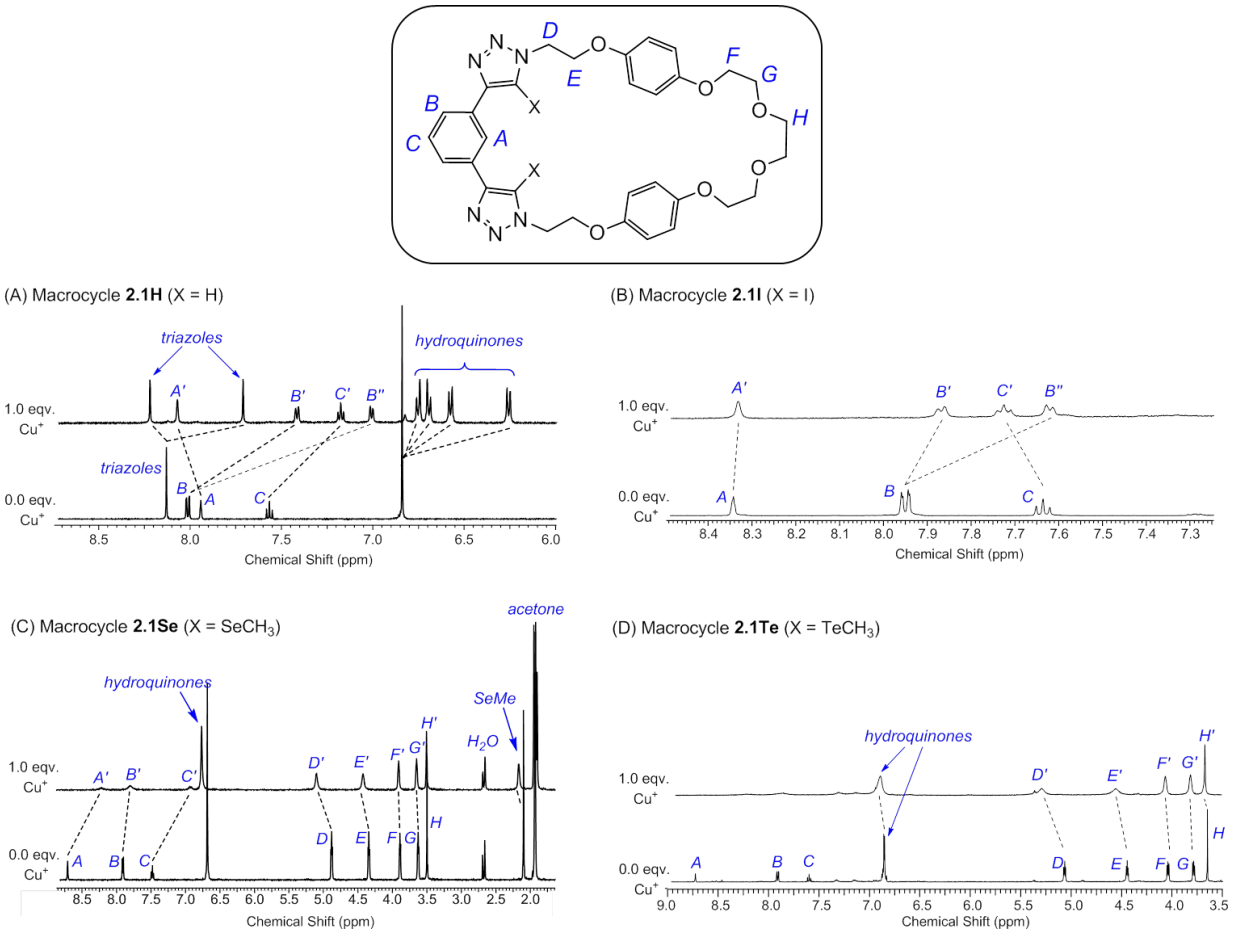


Figure 2.7. *Partial ^{1}H NMR spectra of macrocycles (A)* ***2.1H****, (B)* ***2.1I****, (C)* ***2.1Se*** *and (D)* ***2.1Te*** *in the presence of 0.0 and 1.0 equivalents of [Cu(CH$_3$CN)$_4$]PF$_6$. The spectra of (A) and (B) were recorded in CD$_2$Cl$_2$, while those for (C) and (D) were recorded in d$_6$-acetone for improved spectral resolution ([**2.1**] = 1.0 mM, T = 298 K).*

In stark contrast, ChB macrocycles **2.1Se** and **2.1Te** show a very different coordination mode with 1.0 equivalent of Cu(I), as retention of ^{1}H NMR spectral symmetry was observed (Figure 2.7C and D).** For **2.1Se**, increasing spatial distance from the methylseleno-triazole units gave smaller ^{1}H NMR signal shifts, with negligible perturbations of the polyether region of the macrocycle ($H_{F\text{-}H}$), clearly indicating that Cu(I) was coordinating with the methylchalcogeno-triazoles. In order to ascertain that these ^{1}H NMR spectroscopic changes in

** The **2.1Te**-Cu(I) adduct in d$_6$-acetone gave poorer ^{1}H NMR spectral resolution than that for **2.1Se**, such that the peaks in the aromatic region could not be clearly discerned despite an accumulation of 100 scans. However, the splitting of the hydroquinone peaks and $H_{D\text{-}H}$ gave clear indication that **2.1Te** bound Cu(I) symmetrically.

the presence of Cu(I) did not result from chalcogen lability due to Cu(I) insertion into the carbon-chalcogen bond during the timescale of the titrations, the solutions containing the macrocycle-Cu(I) complexes were washed with a basic solution of ethylenediaminetetraacetate (EDTA) to remove any Cu(I) present. ^{1}H NMR and ESI-MS analyses of the resulting solution showed only the presence of macrocycles **2.1Se** and **2.1Te**, with no evidence of any loss of chalcogen atoms seen.

Further differences in the triazole coordination modes of the various macrocycles were observed by UV-Vis titrations in CH_2Cl_2 (Figure 2.8). For macrocycle **2.1H**, an enhancement in the 290 nm absorption peak was observed with increasing quantities of Cu(I), with a distinct isosbestic point seen at 270 nm. This has been previously shown to arise from direct triazole *N*-coordination to Cu(I) which perturbed the energy levels of its frontier molecular orbitals.[33,41] While macrocycle **2.1I** also showed similar increases in intensity of the 290 nm peak with 0.0 - 0.5 equivalents of added Cu(I), its absorbance subsequently decreased with further addition of Cu(I) until 1.0 equivalents. From this evidence, it is likely that the iodotriazoles were also acting as *N*-ligands for Cu(I) coordination, with the difference in behaviour from **2.1H** possibly due to the steric bulk of the iodine atoms on the iodotriazoles of **2.1I** affecting the local coordination environment of Cu(I) and likely forming multiple complexed species in solution. However surprisingly, **2.1Se** and **2.1Te** gave only minute optical responses to Cu(I) binding (Figure 2.8C and D), suggesting that only small changes with the triazole energy levels accompanied the process. Considering the optical sensitivity of triazole absorbance to direct *N*-coordination with Cu(I), this implied that the methylchalcogeno-triazoles were not acting as *N*-ligands, but likely coordinating Cu(I) via the chalcogen atoms themselves.

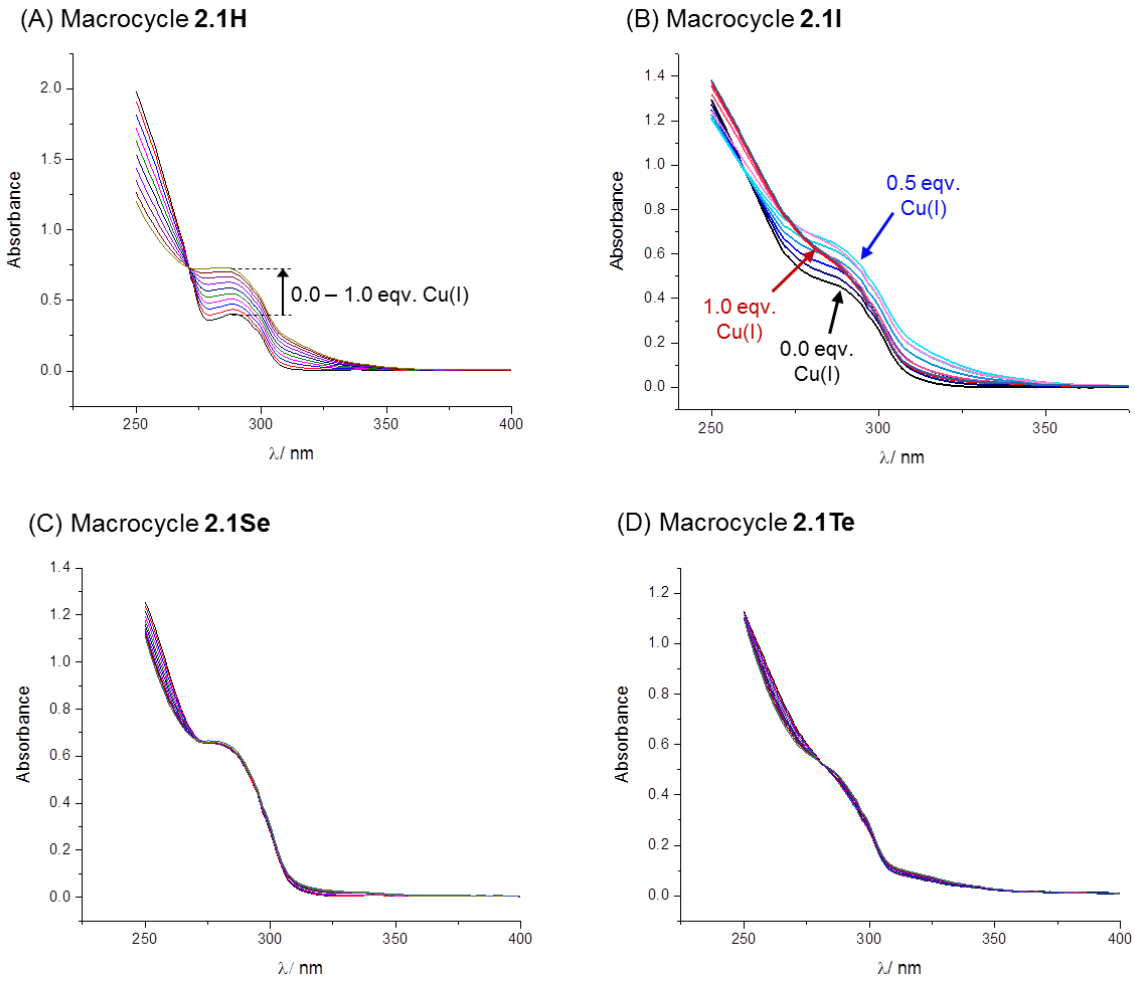


Figure 2.8. *UV-Vis spectra of macrocycles (A)* ***2.1H****, (B)* ***2.1I****, (C)* ***2.1Se*** *and (D)* ***2.1Te*** *upon addition of* $[Cu(CH_3CN)_4]PF_6$ *in 0.1 molar increments up to 1.0 equivalents of Cu(I) ([**2.1**] = 50 μM, CH_2Cl_2, T = 293 K).*

To test this deduction, heteronuclear ^{77}Se and ^{125}Te NMR spectra were recorded before and after the addition of 1.0 equivalent of $[Cu(CH_3CN)_4]PF_6$ to 3.0 mM solutions of macrocycles **2.1Se** and **2.1Te** in d_6-acetone respectively. Although both macrocycles initially showed distinct singlet resonances at δ_{Se} = 47 ppm and δ_{Te} = 146 ppm, the addition of Cu(I) led to complete loss of the signals. This was likely due to extensive signal broadening arising from direct ^1J coupling of the chalcogen atoms to the quadrupolar Cu(I) nuclei (I = 3/2 for ^{63}Cu and ^{65}Cu). Indeed, complexes of Cu(I) ligated by Se or Te atoms are known.[42–47] Taken together, all the evidence suggests that Cu(I) was coordinating simultaneously to both chalcogen atoms of **2.1Se** and **2.1Te**, which also accounts for the retention of ^{1}H NMR spectral symmetry of the ChB macrocycle-Cu(I) adducts (Figure 2.7C and D).

The bidentate Cu(I)-coordination mode by macrocycles **2.1Se** and **2.1Te** was explored by DFT calculations, performed by Dr. Igor Marques and Professor Vítor Felíx at the University of Aveiro, Portugal. Two conformational models for each of the macrocycles **2.1Se** and **2.1Te** were initially generated, with the chalcogen atoms facing either inside (model A) or outside (model B) the macrocycle cavity. A Cu(I) cation was then placed equidistant between the potential ligating atoms (Se/Te or N) on the triazoles of each model, and the coordination sphere of Cu(I) was completed with two acetonitrile molecules. Each model was then optimised by DFT using the Gaussian09 package,[48] using the B3LYP functional and the 6+31G** basis set for H, C, N and O atoms, and the aug-cc-pVDZ-PP basis set for Se, Te and Cu atoms.[49,50] The effects of the acetone solvent were also taken into account by using the integral equation formalism variant (IEFPCM) in the polarisable continuum model (PCM).[51]

As shown in Figure 2.9A, the *endo*-**2.1Se**/**Te**···Cu(I) complexes in model A maintained the initial tetrahedral coordination of Cu(I) throughout the simulations, with both chalcogen atoms of each macrocycle binding Cu(I) simultaneously. The calculated Cu-Se bond lengths of 2.561 and 2.594 Å are consistent with those of 33 solid-state structures containing the Cu(I)SeC_2 structural fragment in the Cambridge Structural Database (CSD), which range from 2.348 to 2.849 Å.[52] The analogous Cu-Te bond lengths of 2.669 and 2.693 Å are slightly longer, but comparable to the structures with a tetrahedral Cu(I)TeC_2 fragment from the CSD, corroborating the proposed bidentate coordination mode suggested from the solution-phase spectroscopic evidence.

Contrastingly, the initial tetrahedral triazole *N*-ligated Cu(I) metal centre of model B was converted to a trigonal planar geometry after DFT optimization (Figure 2.9B), where the metal centre was coordinated by a single triazole ligand (Cu-N bond lengths of 2.010 and 2.005 Å for **2.1Se** and **2.1Te** respectively) and two acetonitrile molecules. Clear decomplexation of the second triazole unit was observed from the large resulting computed distances between the Cu(I) metal centre and the triazole N^3 atom (4.573 Å for **2.1Se** and 4.638 Å for **2.1Te**). To further understand the preference for bidentate chalcogen coordination, the optimised distances between the Cu(I) ligating atoms in both models *A* (chalcogens) and *B* (N^3 triazole atom) were compared. For model *A*, the intramolecular distances between both chalcogen

atoms are 4.456 and 4.654 Å for **2.1Se** and **2.1Te** respectively. On the other hand, the corresponding distances between the Lewis basic N^3 atoms on both triazoles are considerably larger at 5.376 for **2.1Se** and 5.422 Å for **2.1Te**. Therefore, the bidentate endotopic chalcogen coordination of Cu(I) of model *A* would result in lower steric strain compared with the hypothetic scenario of model *B* involving ligation by both triazole N^3 atoms simultaneously, hence rendering the former to be more likely to occur in solution.

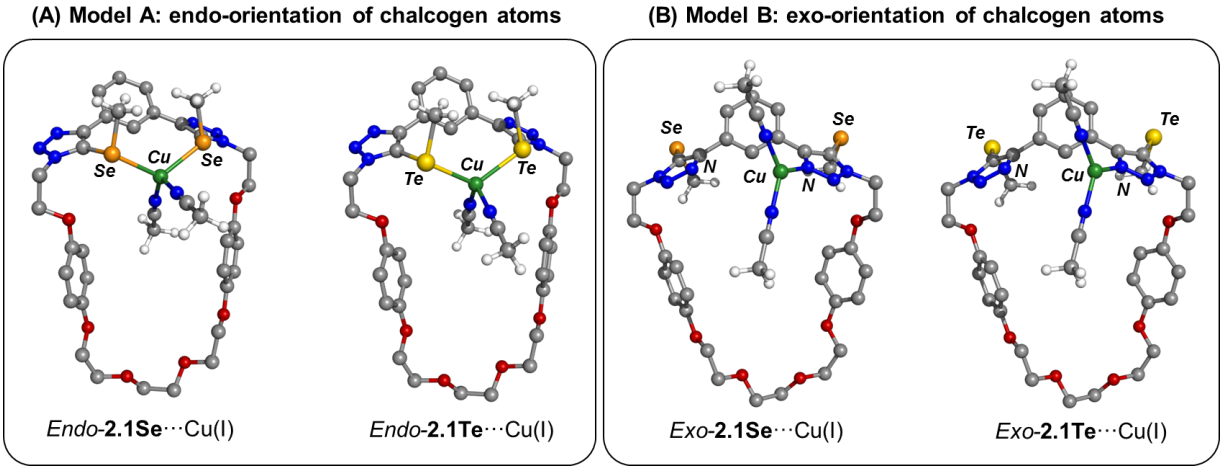
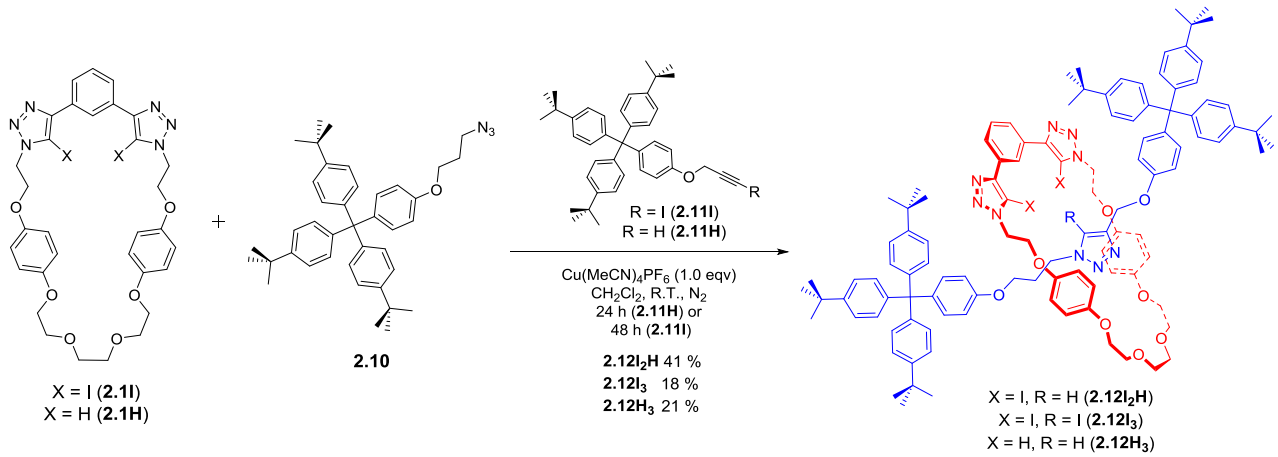


Figure 2.9. *DFT optimised structures of the two possible coordination modes of macrocycles **2.1Se** and **2.1Te** with Cu(I) using (A) model A and (B) model B. Atom colours: grey = C; blue = N; red = O; white = H; green = Cu; orange = Se; yellow = Te.*

Finally, the DFT studies provide support that regardless of the Cu(I) coordination mode, it is energetically possible for the macrocycle to adopt a conformation where the catalytically-active Cu(I) species is oriented within the macrocycle cavity. It is reasonable to assume that the asymmetric Cu(I) binding mode of **2.1H** and **2.1I** by their respective triazole N^3 atoms can resemble that of model *B* in Figure 2.9, where the Cu(I) is held slightly above the plane of the macrocycle cavity. Thus, although the spectroscopic and DFT modelling studies show that different substituents on the 5-position of the macrocycle triazoles exerts considerable influence on the geometry of Cu(I) coordination, it is possible that in all cases, the orientation of the Cu(I) catalyst allows CuAAC reaction through the macrocycle cavity for active metal template rotaxane synthesis. This is explored in the next section.

2.2.3 Synthesis and Characterisation of Halogen Bonding [2]Rotaxanes

Having determined the facile binding of all structurally-analogous bis-triazole macrocycles to Cu(I), the active metal template synthesis of neutral XB rotaxanes was first explored with XB macrocycle **2.1I**. Firstly, the terphenyl-stoppered terminal azide **2.10**[53] and proto/[53] iodo-alkyne[54] (**2.11H/I**) were synthesised according to literature procedures. Subsequently, an equimolar mixture macrocycle **2.1I** and $[Cu(CH_3CN)_4]PF_6$ was dissolved in thoroughly-degassed CH_2Cl_2 before 5.0 equivalents of azide **2.10** and (proto)alkyne **2.11H** were added (Scheme 2.6). After stirring the reaction under a N_2 atmosphere for 24 hours, complete consumption of **2.10** and **2.11H** was observed by TLC analysis. Pleasingly, ESI-MS analysis of the crude reaction mixture revealed the presence of target [2]rotaxane **2.12I$_2$H** (*m/z* = 1981 $[M + H]^+$) in the crude reaction mixture. Following demetallation with a solution of ethylenediamine-tetraacetate (EDTA) in dilute aqueous ammonia, neutral rotaxane **2.12I$_2$H** was isolated in 41 % yield after chromatographic purification. Following this success, the analogous rotaxanation reactions were performed using macrocycle **2.1I** with iodoalkyne **2.11I**. Despite using identical conditions, the 'iodo-Click' active metal template synthesis of neutral all-XB rotaxane **2.12I$_3$** was less facile than that for **2.12I$_2$H**, requiring a reaction of 48 hours under an inert N_2 atmosphere to reach completion. Using the same procedure also allowed access to the neutral all-HB rotaxane **2.12H$_3$** after a 24-hour reaction. Rotaxanes **2.12I$_3$** and **2.12H$_3$** were both isolated in yields of approximately 20 % by preparatory TLC.



***Scheme 2.6**. Synthesis of neutral [2]rotaxane family **2.12**.*

The ^{1}H NMR spectrum of isolated rotaxane **2.12I$_2$H** is consistent with the retention of their mechanically-interlocked nature after removal of the templating Cu(I) cation. As seen in Figure 2.10, diagnostic upfield perturbations and increased splitting of the macrocycle hydroquinine protons (H_f and H_g) and axle triazole proton (H_4) signals were observed compared with the free non-interlocked components, likely resulting from the aromatic donor-acceptor π-π stacking interactions between the electron-rich macrocycle hydroquinone groups and the relatively electron-deficient axle triazole unit. Notable upfield shifts were also seen for H_3 and H_5 on the axle immediately adjacent to the triazole unit, presumably due to the shielding effect of the aromatic ring currents on the macrocycle hydroquinone groups present in close spatial proximity. Further unequivocal evidence of the interlocked nature of all isolated [2]rotaxanes **2.12I$_2$H**, **2.12I$_3$** and **2.12H$_3$** were obtained by two-dimensional ^{1}H-^{1}H ROESY spectroscopy experiments (Figure 2.11), which showed numerous cross-peaks arising from through-space interactions between the interlocked axle and macrocycle components.

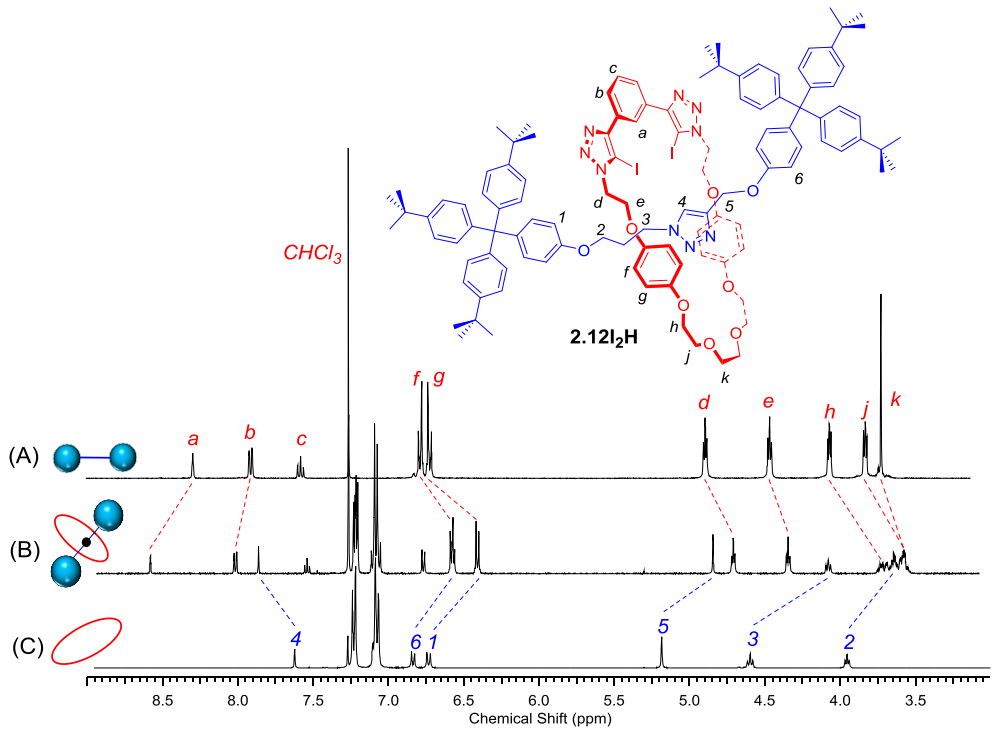


Figure 2.10. *Partial ^{1}H NMR spectra of (A) free prototriazole axle; (B) neutral [2]rotaxane **2.12I$_2$H** and (C) free XB macrocycle **2.1I** ($CDCl_3$, T = 298 K).*

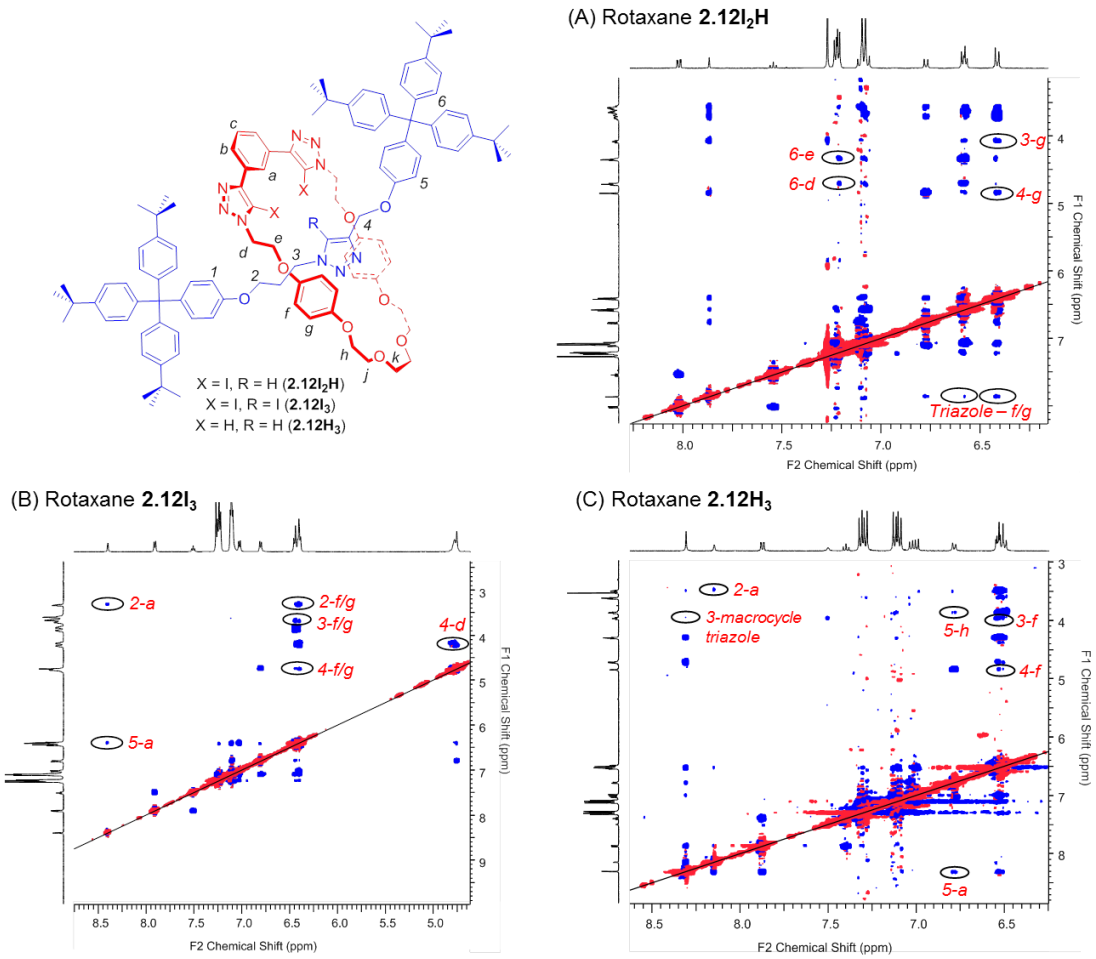
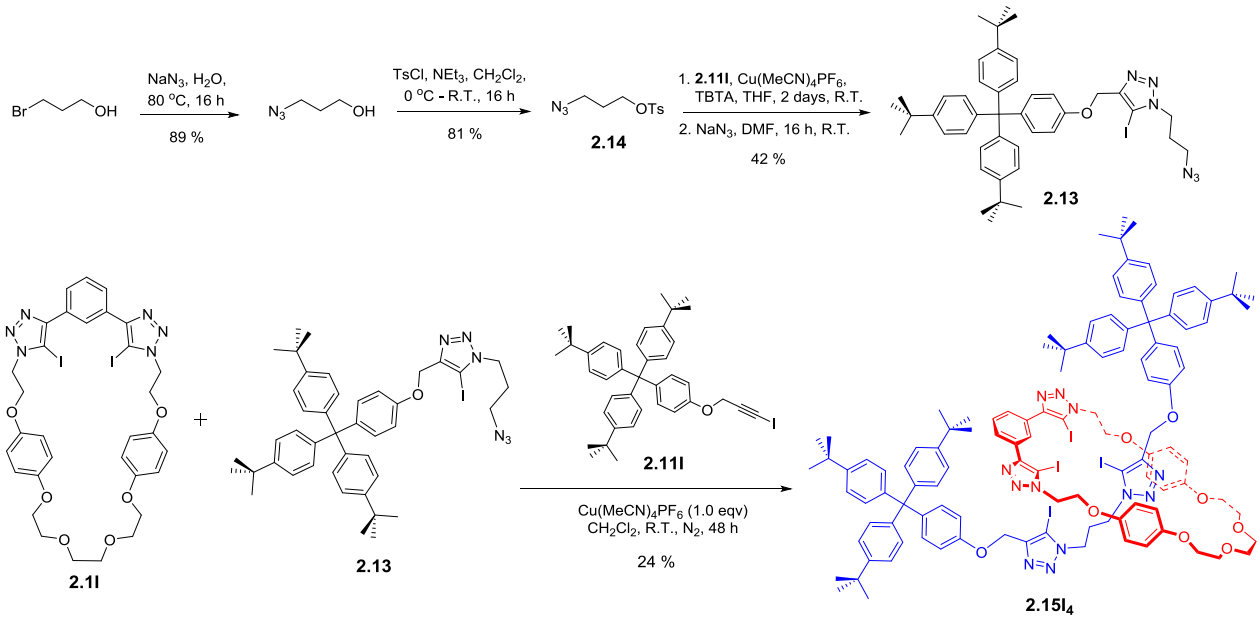


Figure 2.11. *Sections of the two-dimensional ^{1}H-^{1}H ROESY NMR spectra of rotaxanes (A)* ***2.12I$_2$H****, (B)* ***2.12I$_3$*** *and (C)* ***2.12H$_3$*** *in $CDCl_3$ (T = 298 K). Selected cross-peaks arising from through-space interactions of the interlocked macrocycle and axle components of each rotaxane are circled.*

Having demonstrated the success of macrocycle **2.1I** in the CuAAC-AMT synthesis of neutral XB rotaxanes, the scope of the reaction was further investigated using different axle precursors. Firstly, an additional Lewis basic group on the axle precursor that will may bind Cu(I) competitively with the macrocycle was prepared and used for rotaxane formation. A modified azide axle precursor **2.13** (Scheme 2.7), bearing an iodotriazole group, was synthesised from stoppered-iodoalkyne **2.11I** and azide **2.14**[53] via a CuAAC reaction, followed by S_N2 substitution using sodium azide. Rotaxane synthesis was performed in an analogous manner as for **2.12I$_3$** by adding a five-fold excess of azide **2.13** and iodoalkyne **2.11I** to a degassed CH_2Cl_2 solution of the **2.1I**-Cu(I) adduct. Pleasingly, this procedure afforded the all-XB neutral rotaxane **2.15I$_4$**, possessing four iodotriazole groups surrounding its cavity, with a

yield of 24 % after chromatographic purification. Characterisation by ^{1}H NMR, 2D ROESY spectroscopy and high-resolution ESI-MS confirmed the interlocked nature of **2.15I$_4$** (Figure 2.12). Clearly, this experiment demonstrated that despite the presence of the iodotriazole motif on **2.13**, the Cu(I) catalyst was still predominantly coordinated by macrocycle **2.1I** to facilitate AMT rotaxane formation.



***Scheme 2.7**. Synthesis of tetra-iodotriazole neutral all-XB rotaxane **2.15I$_4$**.*

Next, the synthesis of analogous neutral XB rotaxanes containing conformationally more restricted axle components was investigated. Instead of using axle precursor **2.10** which contained a propyl spacer between the stopper unit and the azide functionality, rotaxane synthesis was attempted using an aryl azide axle precursor **2.16** (Scheme 2.8). After synthesising stopper aryl azide **2.16** from the stopper amine precursor following a reported procedure,[55] rotaxane synthesis was attempted following the general procedure established earlier, using 1.0 equivalent of $[Cu(CH_3CN)_4]PF_6$ and 5.0 equivalents of azide **2.16** and iodoalkyne **2.11I** in degassed CH_2Cl_2. Curiously, only limited consumption of the axle precursors were observed even after 5 days. When the reaction was repeated using degassed THF, complete consumption of **2.16** and **2.11I** occurred after 5 days to form only the free iodotriazole axle, with no trace of the target rotaxane detectable by TLC, ^{1}H NMR and ESI-MS

analyses of the crude reaction mixture. Further attempts at rotaxane synthesis in THF, using a higher macrocycle: Cu(I) ratio of 4:1, which has been found to favour rotaxane formation by Leigh and co-workers,[9] as well as heating the reaction in a sealed vial to 80 °C, also did not yield any detectable trace of the target interlocked product.

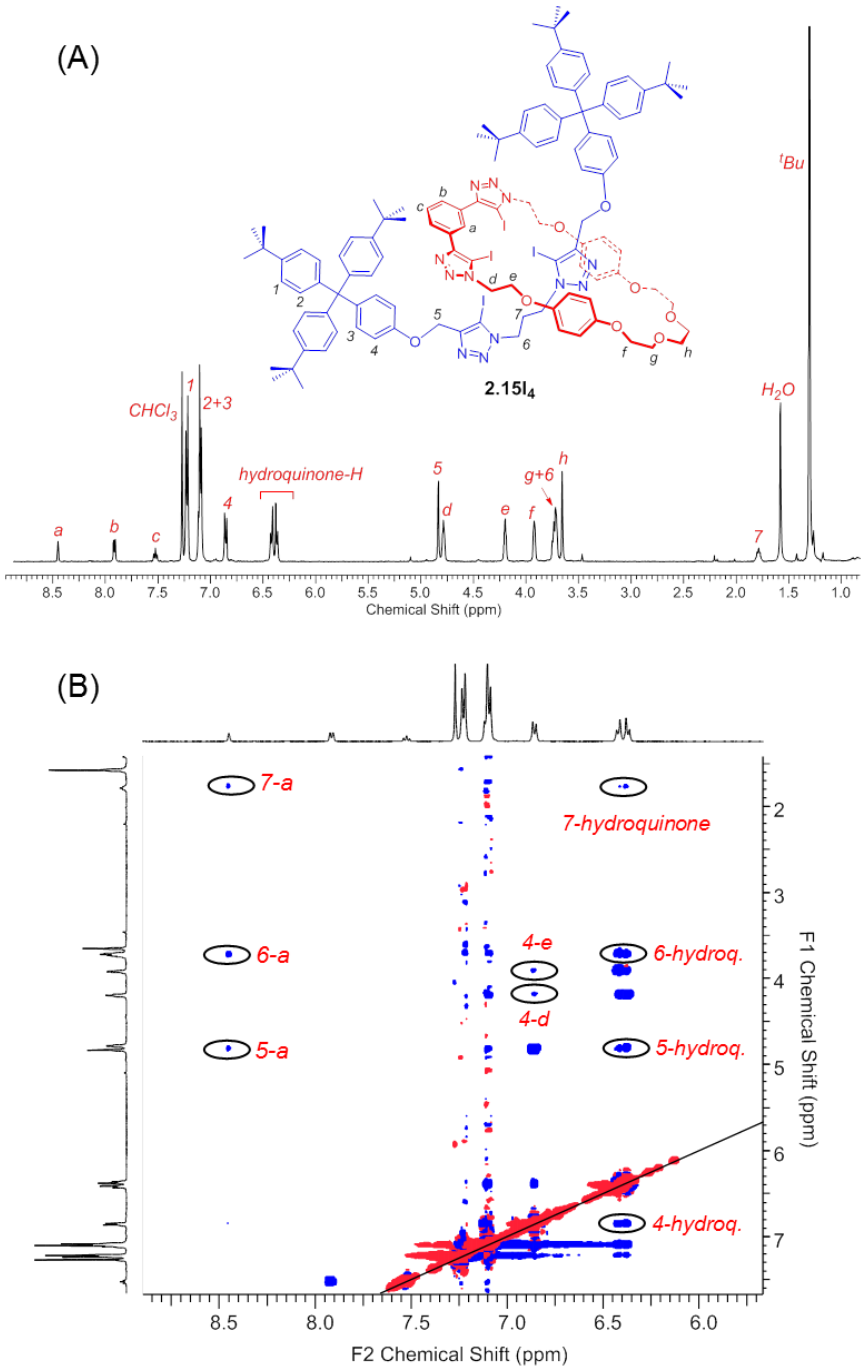
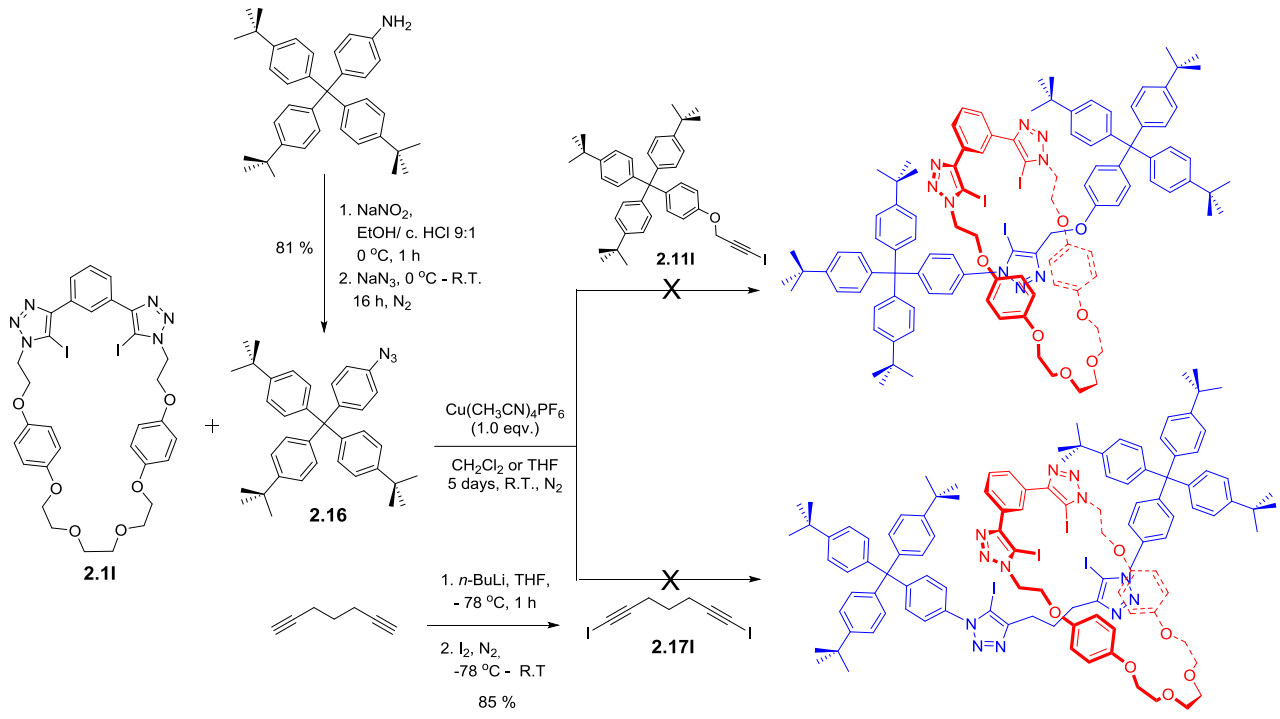


***Figure 2.12**. Characterisation of tetra-iodotriazole neutral XB rotaxane **2.15I$_4$** by (A) ^{1}H NMR and (B) 2D ROESY spectroscopy in $CDCl_3$ (T = 298 K). Cross peaks between the axle and macrocycle components of rotaxane **2.15I$_4$** are circled in (B).*

Hypothesising that this failure was due to unfavourable steric crowding, an AMT reaction was then attempted using bis-iodoalkyne **2.17I** (4.0 equivalents) and azide **2.16** (8.0 equivalents) relative to the macrocycle **2.1I** (10 mM concentration, 1.0 equivalent) and $[Cu(CH_3CN)_4]PF_6$ (1.0 equivalent) in degassed THF (Scheme 2.8), in the hope that the longer spacer between both bulky stopper units would favour rotaxane formation. Unfortunately, stirring the reaction for 5 days under an inert atmosphere failed to yield any rotaxane, although complete conversion to the bis-iodotriazole free axle was observed. Taken together, these results from both unsuccessful rotaxanation attempts suggest that in addition to its reduced propensity to participate in CuAAC reactions, aryl azide **2.16** is also likely to be too sterically bulky to thread through the macrocycle cavity to complex with the endotopically-bound Cu(I) catalyst for AMT rotaxane formation. As such, no further attempts were made using aryl azide **2.16** as an axle precursor.

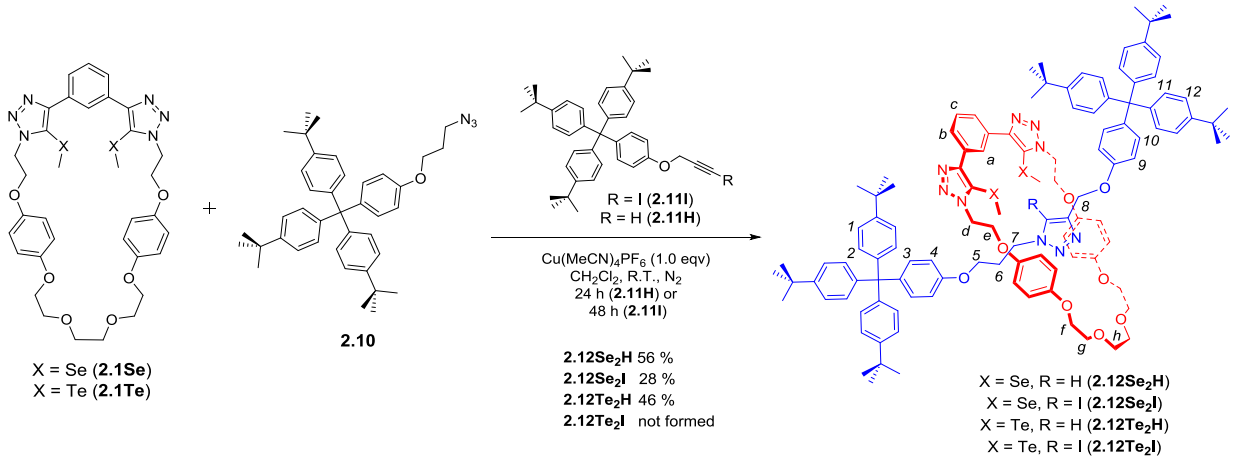


***Scheme 2.8**. Attempted synthesis of the more conformationally-rigid all XB-rotaxanes.*

2.2.4 Synthesis and Characterisation of Chalcogen Bonding [2]Rotaxanes

Given the success of preparing members of the **2.12** XB/HB neutral rotaxane family, the analogous CuAAC-AMT reactions were then performed using macrocycles **2.1Se** and **2.1Te** with stoppered alkyl azide **2.10** and alkynes (**2.11H/I**), as shown in Scheme 2.9. ChB rotaxanes **2.12Se$_2$H**, **2.12Se$_2$I** and **2.12Te$_2$H** were isolated in yields of 56, 28 and 46 % respectively after purification by preparatory thin layer chromatography (Figure 2.13). It is noteworthy that during the synthesis of **2.12Te$_2$H**, another [2]rotaxane product was isolated that had a very similar R_f as the desired product which showed an ESI-MS peak of *m/z* = 1873.9. ^{1}H NMR analysis of this unexpected product revealed that it was the analogue of **2.12Te$_2$H** but with the loss of one $TeCH_3$ group from the macrocycle. Possibly, this product (21 % yield) was formed from the oxidative insertion of Cu(I) into the weak $C_{triazole}$-Te bond of macrocycle **2.1Te**, which has been previously reported.[31] This propensity for Cu(I) insertion into the C-Te bond also resulted in the unsuccessful 'iodo-Click' AMT synthesis of rotaxane **2.12Te$_2$I** using macrocycle **2.1Te** and iodoalkyne **2.11I**. Surprisingly, the major product isolated in this reaction was **2.12I$_2$H** (c.a. 10 % yield), confirmed by ESI-MS (*m/z* = 1981.9 [M + H]$^+$) and ^{1}H NMR analyses, which suggested that exchange of the macrocycle $TeCH_3$ groups and iodine atoms on the iodoalkyne/ iodotriazoles occurred during the rotaxane synthesis reaction. Significantly, no loss of the $SeCH_3$ groups of macrocycle **2.1Se** were observed during the CuAAC-AMT rotaxanations, a testament to the stronger C-Se bond compared with C-Te (bond strengths of 234 and c.a. 200 kJ mol^{-1} respectively).[30] All neutral ChB rotaxanes (**2.12Se$_2$H**, **2.12Se$_2$I** and **2.12Te$_2$H**) isolated displayed the characteristic isotopic distribution in their high-resolution ESI spectra arising from the multiple stable isotopes of Se and Te, with 2D ROESY NMR characterisation providing clear evidence of their interlocked nature (Figure 2.14).

Notably, the yields of rotaxanes containing the HB prototriazole axles formed using the ChB macrocycles (56 % for **2.12Se$_2$H** and combined yield of 67 % for **2.12Te$_2$H** and the side product with loss of one $TeCH_3$ group) are consistently higher than those for **2.1I** and **2.1H** (41 % and 21 % respectively). This may be a result of the different Cu(I) coordination mode displayed by the macrocycles **2.1Se/Te** and **2.1I/H**, with the endotopic bidentate Cu(I) binding



***Scheme 2.9**. Synthesis of neutral ChB [2]rotaxanes bearing the structural skeleton of the **2.12** family.*

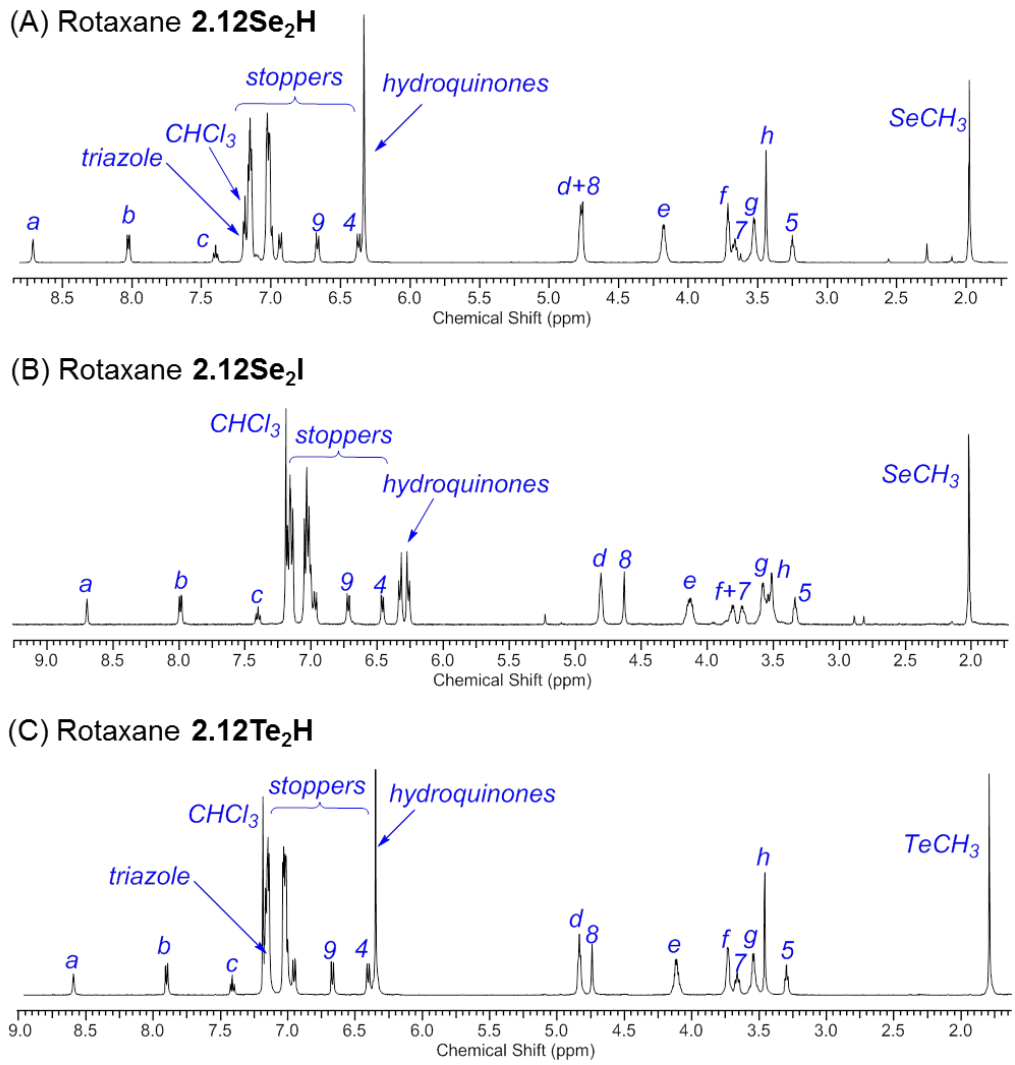


***Figure 2.13**. ^{1}H NMR spectra of ChB [2]rotaxanes (A) **2.12Se$_2$H**, (B) **2.12Se$_2$I** and (C) **2.12Te$_2$H** ($CDCl_3$, T = 298 K). Proton assignments follow those in Scheme 2.9.*

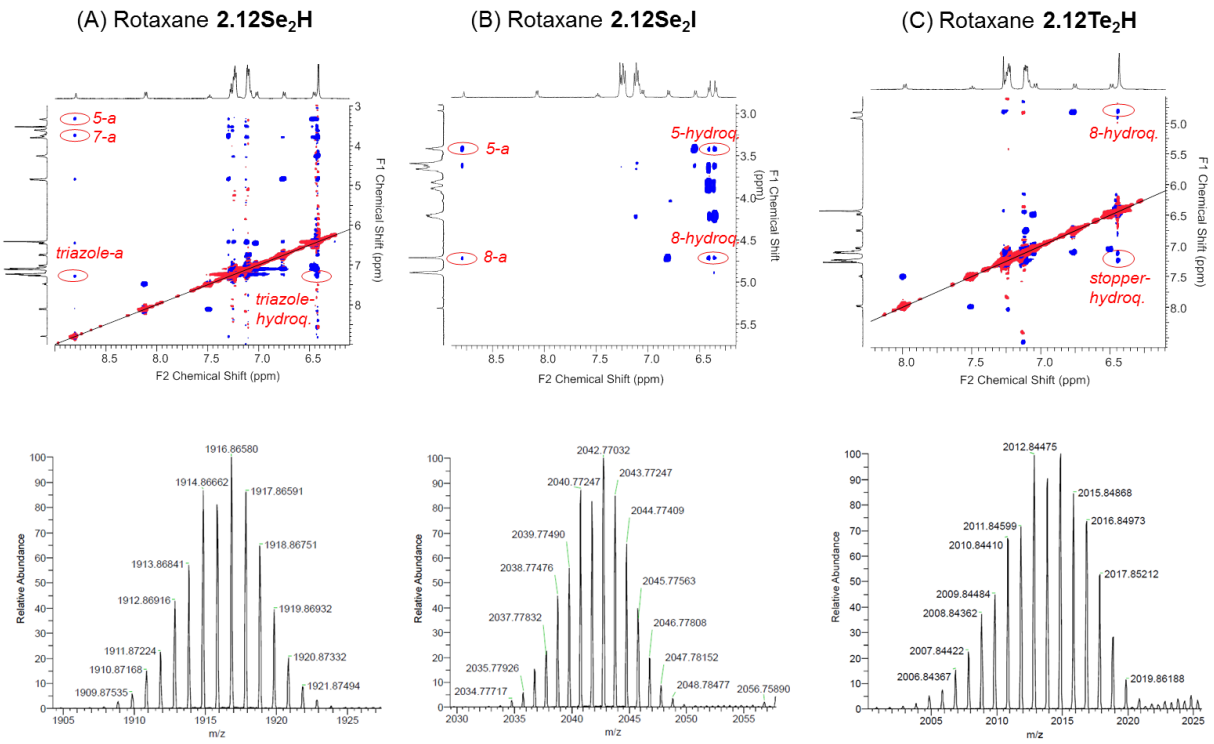
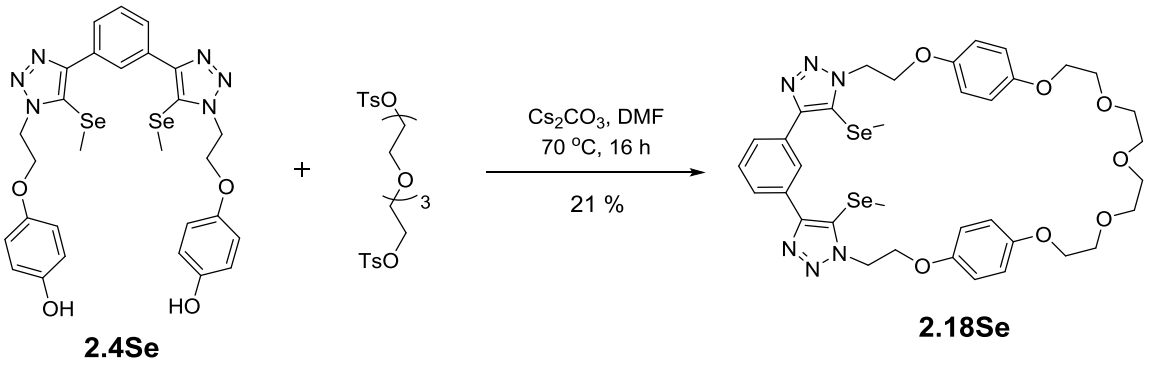


***Figure 2.14**. 2D ROESY NMR (top) and high-resolution ESI-MS (bottom) characterisation of ChB [2]rotaxanes (A) **2.12Se₂H**, (B) **2.12Se₂I** and (C) **2.12Te₂H**. All NMR spectra were obtained in $CDCl_3$ (T = 298 K). Assignments follow those of Scheme 2.9.*

by both chalcogen atoms of the former being more conducive for CuAAC-AMT reactions than the monodentate coordination by **2.1I/H**. Interestingly, the yields of rotaxanes bearing iodotriazole axles (28 % and 18 % for **2.12Se₂I** and **2.12I₃** respectively) are significantly lower than those with HB axles (56 % and 41 % for **2.12Se₂H** and **2.12I₂H** respectively). This is attributed to the greater steric bulk of the iodine atom which hinders the threading of iodoalkyne **2.11I** through the macrocycle cavity, as well as the greater steric repulsion between the macrocycle and the iodine-containing CuAAC intermediates, which may act in tandem to favour formation of the free iodotriazole-containing axle over rotaxane.

Recognising that the bulky $SeCH_3$ groups of rotaxane **2.12Se₂H** may sterically hinder anion binding in its cavity, the synthesis of a ChB rotaxane analogue with a larger macrocycle component was attempted. ChB macrocycle **2.18Se**, containing a longer tetra(ethylene glycol) chain instead of a tri(ethylene glycol) unit in **2.1Se**, was synthesised following the previously-developed procedure using bis-phenol **2.4Se** and tetra(ethylene glycol) bis-tosylate in 21 %

isolated yield (Scheme 2.10). Subsequently, CuAAC-AMT rotaxane synthesis was undertaken as previously described using 5.0 equivalents of azide **2.10** and (proto)alkyne **2.11H** relative to **2.18Se**. Interestingly, while the desired neutral rotaxane **2.19Se$_2$H** could be isolated in approximately 35 % by preparatory TLC following Cu(I)-decomplexation, it was found to be unstable with respect to dethreading. As shown in Figure 2.15, the ^{1}H NMR spectra of isolated rotaxane **2.19Se$_2$H** in $CDCl_3$ was found to become increasingly complicated with time. After 24 hours, approximately 35 % of the original rotaxane (peaks labelled in green) had decomposed to form free prototriazole axle (blue peaks) and macrocycle **2.18Se** (red peaks). Clearly, the macrocycle component of **2.19Se$_2$H** was too large for the rotaxane's stopper units and its conformational flexibility allowed gradual dethreading with time.



***Scheme 2.10**. Synthesis of a larger ChB macrocycle **2.18Se** containing a tetra(ethylene glycol)-derived polyether unit.*

Finally, to enhance the strength of the HB/ σ-hole interactions for anion binding via charge assistance, methylation of each triazole motif on the stable rotaxanes **2.12H$_3$**, **2.12I$_2$H** and **2.12Se$_2$H** was attempted using trimethyloxonium tetrafluoroborate in acetonitrile at 80 °C (Scheme 2.11). Following the progress of each reaction by TLC and ESI-MS showed that while double methylation occurred quickly after 2 days,[††] methylation of the final (third) triazole motif was very slow, likely due to electrostatic repulsion between the dicationic rotaxane intermediates and the positively-charged trimethyloxonium methylating agent. Monitoring the

[††] The positions of bis-methylation were found to be indiscriminate - any two of the three triazole motifs of the rotaxanes were methylated at any one time.

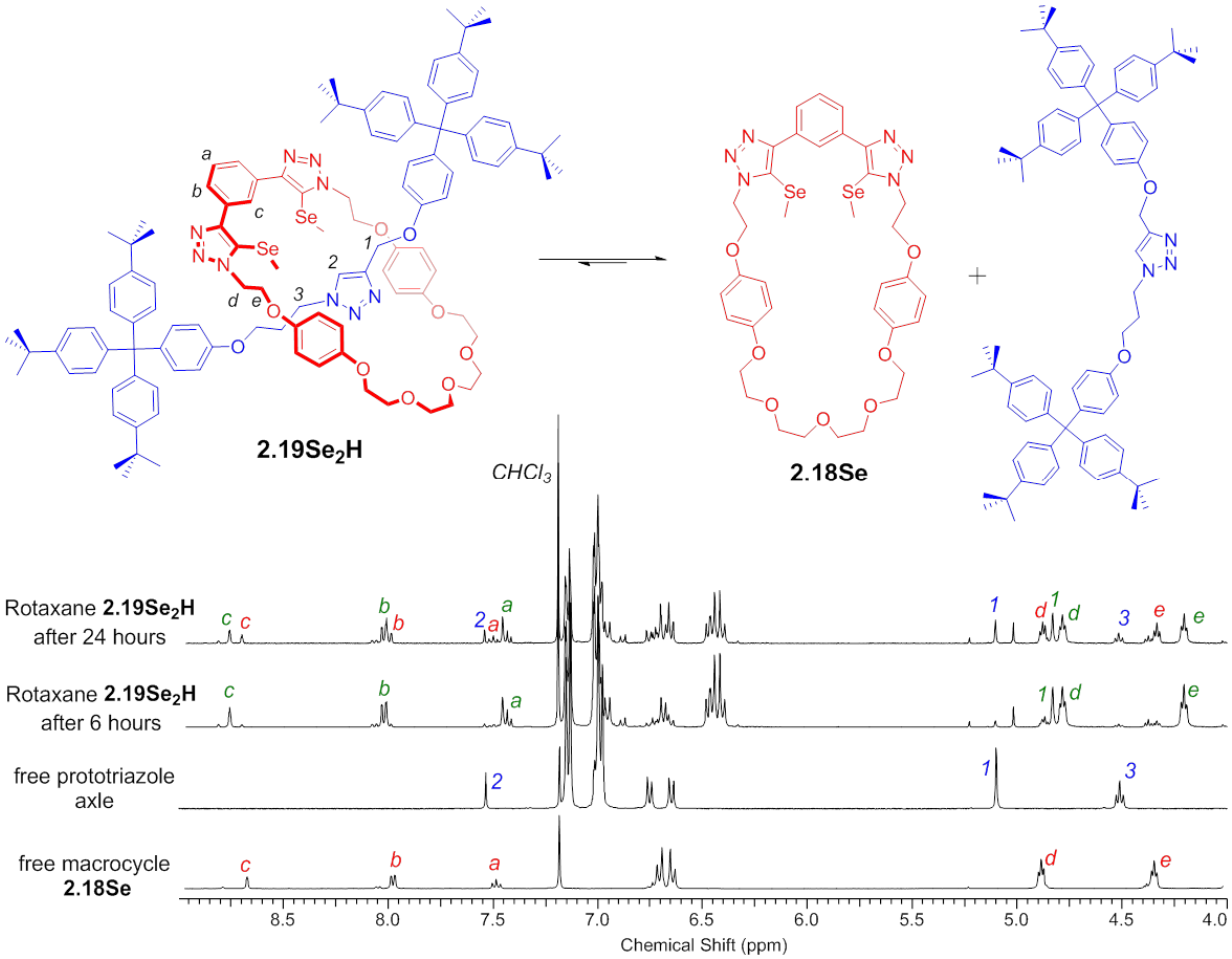
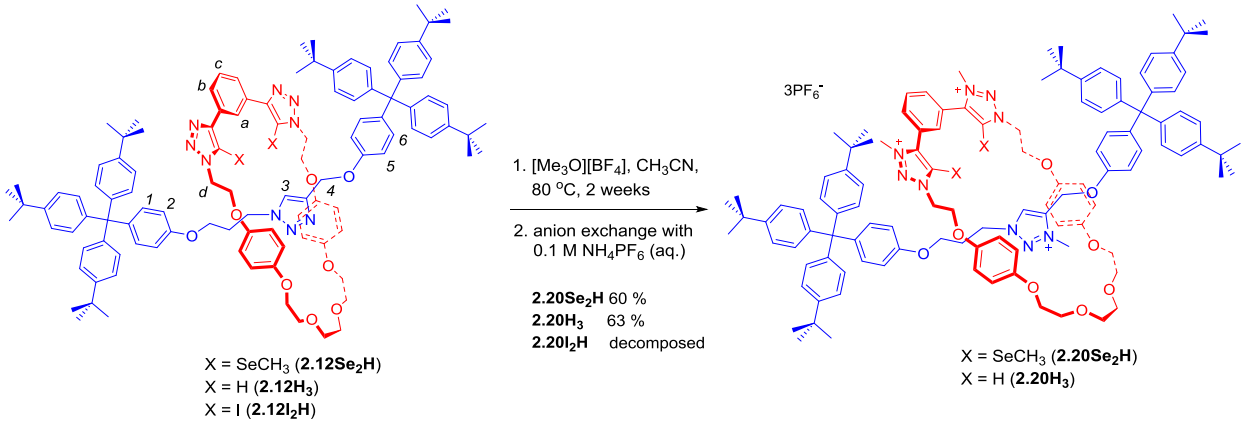


***Figure 2.15**. Partial ^{1}H NMR spectra of free prototriazole axle, free macrocycle **2.18Se** and rotaxane **2.19Se$_2$H** after 6 hours and 24 hours. Peaks corresponding to the free axle are labelled in blue, those for **2.18Se** in red, and those for the interlocked rotaxane in green.*

reactions daily and addition of more methylating agent when necessary afforded the target *tricationic* rotaxanes after 2 weeks. Purification by preparatory TLC and anion exchange gave the tris-PF_6^- salts of rotaxanes **2.20Se$_2$H** and **2.20H$_3$** in 60 % and 63 % yields respectively. Presumably due to the prolonged heating required to achieve tris-methylation, **2.12I$_2$H** decomposed during the reaction. Taking into account this observation, no further attempts were made to synthesise the tricationic analogues of iodotriazole-containing rotaxanes **2.12I$_3$**, **2.12Se$_2$I** and **2.15I$_4$**. Notably, tricationic rotaxanes **2.20Se$_2$H** and **2.20H$_3$** showed much larger splitting and desymmetrisation of their hydroquinone environments compared with their neutral congeners. This is likely due to rigidification of the rotaxane structure by HB interactions between the axle triazolium methyl protons and the macrocycle polyether chain,[23,56,57] as well

as enhanced aromatic donor-acceptor interactions between the macrocycle hydroquinones and the more electron-deficient triazolium motif of each axle.



Scheme 2.11. *Synthesis of tricationic rotaxanes* ***2.20Se$_2$H*** *and* ***2.20H$_3$****.*

2.2.5 Anion Binding Studies with Neutral Halogen and Chalcogen Bonding Rotaxanes

The binding energies of XB and ChB interactions towards Lewis bases have been shown via a number of computational studies to be comparable with each other in the gas phase.[58,59] However, a direct experimental comparison of their affinities for anions in solution is unprecedented thus far. The anion binding properties of rotaxanes **2.12H$_3$**, **2.12I$_2$H** and **2.12Te$_2$H** were probed and compared via ^{1}H NMR titration studies. In a typical titration procedure, increasing quantities of the anions, as their non-coordinating tetrabutylammonium (TBA) salts, were added to separate 1.0 mM solutions of each rotaxane host in d_6-acetone, and the chemical shifts of selected proton signals around the anion binding cavity of each rotaxane were monitored as a function of anion concentration.

The perturbations of the various proton environments of rotaxanes **2.12H$_3$**, **2.12I$_2$H** and **2.12Te$_2$H** observed in the presence of Cl^- (Figure 2.16) are representative of their interactions with the various anions investigated. For **2.12I$_2$H**, Cl^- gave the largest downfield shifts ($\Delta\delta$ > 0.2 ppm over 10 eqv.) for the signal arising from the axle triazole proton (H_3), indicating that it is directly participating in halide binding by HB interactions. Smaller downfield perturbations were seen for the H_4 axle environment immediately adjacent to the triazole, possibly due to

their proximity to the anion binding site. Significant changes were also observed for the macrocycle hydroquinone and axle stopper environments, indicative of conformational changes of the rotaxane structure on Cl^- binding.

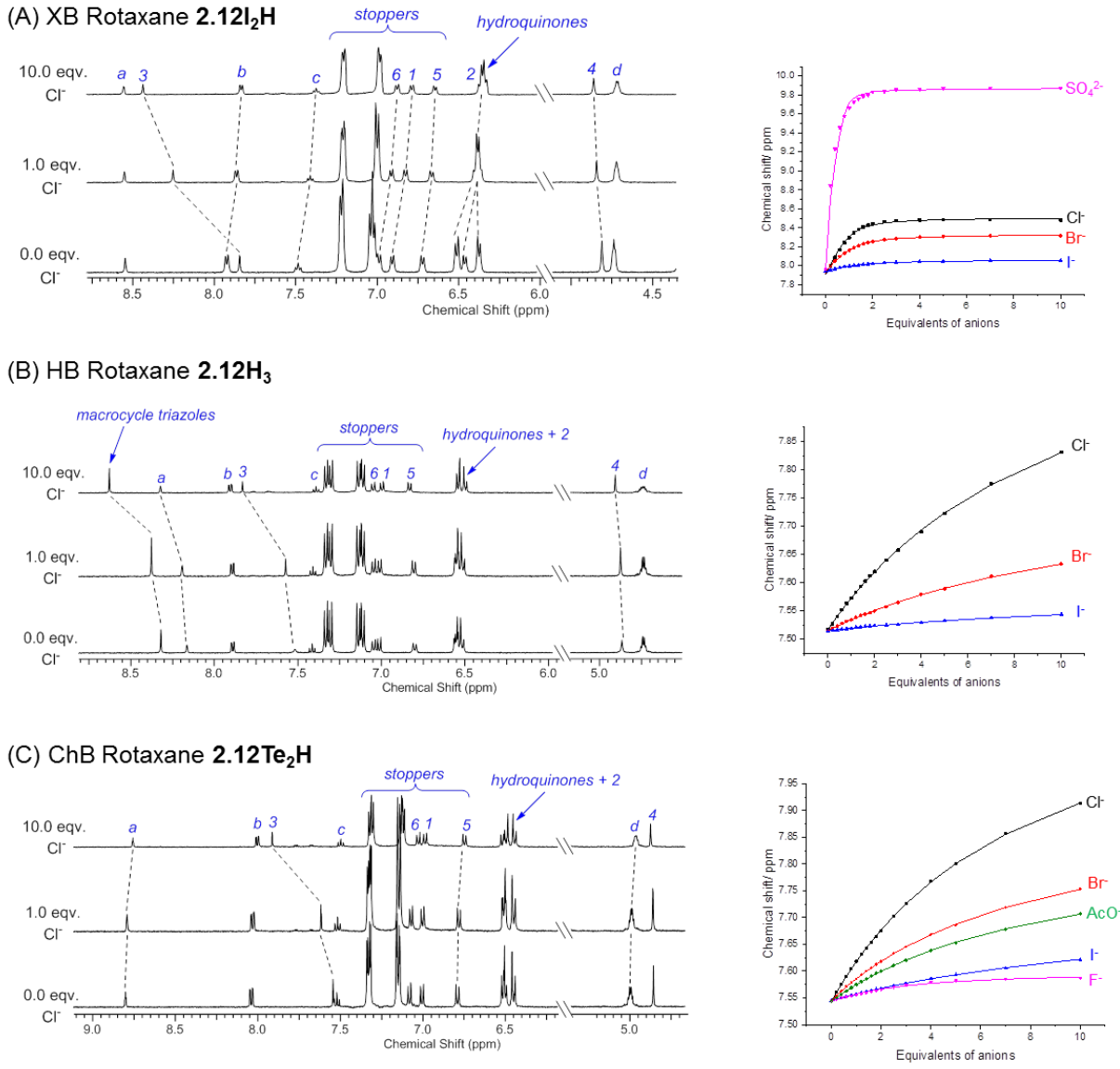


Figure 2.16. *(Left row) Partial ^{1}H NMR spectra of rotaxanes (A)* ***2.12I$_2$H****, (B)* ***2.12H$_3$*** *and (C)* ***2.12Te$_2$H*** *in the presence of 0.0, 1.0 and 10.0 equivalents of Cl^-. (Right row) Plots of the axle triazole proton's (H_3) chemical shifts of each rotaxane as a function of anion concentration ([rotaxane] = 1.0 mM, d_6-acetone, T = 298 K). All proton assignments follow those in Scheme 2.11.*

Replacing the iodotriazoles on the macrocycle components of **2.12I$_2$H** with prototriazole (**2.12H$_3$**) and methyltelluro-triazole (**2.12Te$_2$H**) resulted in notable differences in proton resonance perturbations around each rotaxane binding site upon anion coordination (Figure 2.16B and C). For **2.12H$_3$**, Cl^- binding gave large shifts of all proton environments surrounding the binding cavity (axle and macrocycle triazoles, as well as internal macrocycle aromatic proton H_a), with smaller shifts for other proton resonances, implying that anion binding is likely to be occurring within the rotaxane binding cavity between the macrocycle and axle components. However unlike **2.12I$_2$H**, the only significant downfield shift observed for rotaxane **2.12Te$_2$H** was that of the axle triazole (H_3), while that of H_a displayed an *upfield* perturbation, suggesting that the latter was not participating in direct HB interactions with Cl^-. Interestingly, H_a showed negligible shifts for **2.12I$_2$H** as well upon Cl^- addition, implying that the central benzene ring on the macrocycle component was possibly twisted out of plane relative to the triazoles, and that having bulky substituents on the macrocycle triazoles of rotaxanes **2.12I$_2$H** and **2.12Te$_2$H** were preventing the halide from fully penetrating their cavities. Thus, it is probable that Cl^- was binding above the plane of the macrocycle component in **2.12I$_2$H** and **2.12Te$_2$H**. WinEQNMR2[60] analyses of the titration data, monitoring the shifts of axle triazole H_3 as a function of anion concentration for all rotaxanes, determined 1:1 stoichiometric host-guest association constants summarised in Table 2.1.

For all three rotaxanes, anion binding affinities generally decreased in the order of $SO_4^{2-} > Cl^- > Br^- > I^-$, mirroring their decreasing charge density and basicity. While addition of F^- led to decomposition of rotaxanes **2.12I$_2$H** and **2.12H$_3$**, only slight degradation was seen for **2.12Te$_2$H** in the presence of a large excess (10 equivalents) of F^-. It is noteworthy that despite SO_4^{2-} being significantly larger than all the halides,[61] it was generally most strongly bound in the vicinity of the rotaxane binding site. This suggests that all the rotaxanes possibly bind anions though an induced-fit mode, where the macrocycle and axle components are able to adjust their relative positions to accommodate anions of various sizes.

Table 2.1. Anion association constants (K_a/ M^{-1}) of neutral rotaxanes **2.12H$_3$**, **2.12I$_2$H** and **2.12Te$_2$H** in dry d_6-acetone.[a]

	2.12H$_3$	**2.12I$_2$H**	**2.12Te$_2$H**
F^-	-[b]	-[b]	350 (35) [d]
Cl^-	81 (3)	4384 (322)	127 (2)
Br^-	65 (5)	2139 (68)	110 (2)
I^-	43 (1)	902 (57)	34 (3)
AcO^-	-[c]	-[c]	98 (2)
SO_4^{2-}	-[b]	> 10^4	1130 (63)

[a] Anions added as TBA salts, errors (±) given in parentheses. 1:1 association constants calculated using WinEQNMR2 software,[60] monitoring the perturbations of the axle triazole proton H_3 for all rotaxanes (d_6-acetone, T = 298 K). [b] extensive decomposition observed; [c] not performed; [d] Estimated value due to slight rotaxane decomposition seen in the presence of 10.0 equivalents of F^-.

Comparing the anion association constants for all three rotaxanes showed the anion binding affinities increased in the order **2.12H$_3$** < **2.12Te$_2$H** << **2.12I$_2$H**. While **2.12Te$_2$H** exhibited only a modest enhancement in K_a values relative to **2.12H$_3$**, **2.12I$_2$H** displayed more than an order-of-magnitude augmentation in magnitudes of K_a for all cases. This large discrepancy in anion affinities of **2.12Te$_2$H** and **2.12I$_2$H** is surprising, and may be attributed to a combination of factors, namely: (1) greater steric bulk of $TeCH_3$ groups compared to I which hinders anion access to the rotaxane binding cavity to a larger extent; (2) the presence of two σ-holes on the sp^3-hybridised Te atoms compared to only one for I atoms, rendering them individually less electrophilic as a result of the more diffuse electron-deficiency;[62] or (3) the electron-donating inductive effect of the methyl group bonded to Te which further reduces the electrophilicity of the Te σ-holes. While the enhanced anion binding strength of XB interactions over HB has been demonstrated in several prior studies,[63,64] the quantitative data reported in Table 2.1 importantly suggest that ChB interactions can also have comparable, or even slightly enhanced binding strengths compared with HB.

Encouraged by the notable binding affinities displayed by **2.12Te$_2$H** for anions, especially towards SO_4^{2-}, analogous titrations were also performed on rotaxane **2.12Se$_2$H** in d_6-acetone. While the axle triazole proton H_3 was the only one that showed appreciable downfield shifts during the titration, the binding was surprisingly too weak for reliable values of K_a to be determined. With Cl^-, negligible shifts of all proton environments were seen, including H_3 (Δδ = +0.01 ppm over 10.0 equivalents). Considering the structural similarity of rotaxanes

2.12Te$_2$H and **2.12Se$_2$H**, and coupled with the fact that the smaller Se atoms render the binding site of the latter to be slightly less sterically crowded, it is reasonable to assume that both SO_4^{2-} and Cl^- would be able to interact with the binding site of **2.12Se$_2$H** in a similar way as **2.12Te$_2$H**. Clearly, the significantly diminished anion binding affinities of **2.12Se$_2$H** can be attributed to the less polarisable nature and reduced electropositivity of Se compared to Te, resulting in much weaker ChB-anion interactions. Nevertheless, this also supports the dominance of ChB interactions for anion binding by the Te atoms in **2.12Te$_2$H**, confirming that the potential HB sites on the rotaxane framework contribute negligibly to its anion binding properties.

The anion binding properties of the neutral rotaxanes **2.12I$_3$** and **2.12Se$_2$I**, each bearing an iodotriazole axle, were also studied by ^{1}H NMR titrations in dry d_6-acetone. As shown in Figure 2.17, the addition of Cl^- to **2.12I$_3$** led to downfield shifts of the macrocycle internal benzene proton H_a, axle proton H_5 and stopper proton H_6. This suggests that Cl^- is bound above the plane of the macrocycle just below the proximal stopper group, likely due to the steric bulk of the three XB-donor iodine atoms around the rotaxane binding cavity preventing Cl^- from penetrating it. Very strong Cl^- binding was observed, with almost no further shifts of the various proton signals observed after the addition of more than 1.0 equivalent of Cl^-. Consequently, WinEQNMR2[60] analysis of the H_a shifts with increasing Cl^- concentration afforded a 1:1 stoichiometric association constant of > 10^4 M^{-1}, which is amongst the strongest anion binding observed by a neutral XB host molecule to date.[64] More importantly, the considerably enhanced Cl^- affinity compared with **2.12I$_2$H** reveal the important involvement of an additional XB interaction on anion binding, suggesting that Cl^- is held by convergent XB interactions from all three iodotriazole groups.

For rotaxane **2.12Se$_2$I**, although Cl^- addition in d_6-acetone led to significant downfield movement of only axle proton H_5 adjacent to the iodotriazole, binding was too weak to be reliably quantified. When the titrations were repeated with SO_4^{2-}, fitting the binding isotherm resulting from the modest downfield shifts of macrocycle proton H_a afforded a K_a value of (51 ± 4) M^{-1}. Thus in a similar way as **2.12I$_3$**, the presence of the additional iodotriazole group on the

axle enhanced the anion recognition properties, albeit only slightly, of **2.12Se$_2$I** compared to **2.12Se$_2$H**.

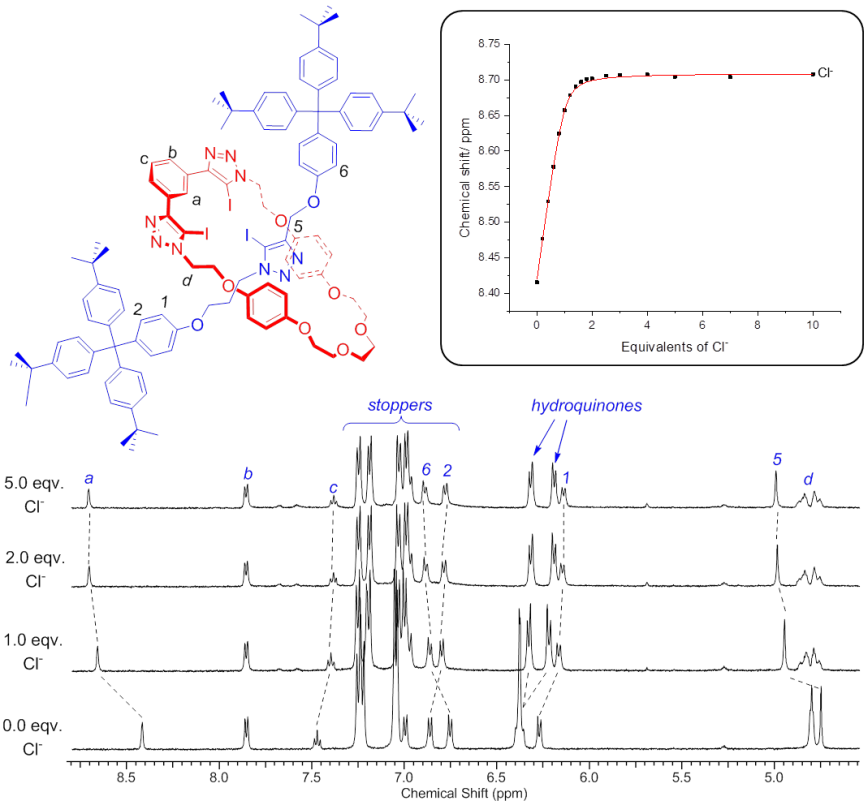


Figure 2.17. *Partial ^{1}H NMR spectra of neutral all-XB rotaxane **2.12I$_3$** in the presence of 0.0, 1.0, 2.0 and 5.0 equivalents of Cl$^-$ ([**2.12I$_3$**] = 1.0 mM, d$_6$-acetone, T = 298 K). Inset: Plot of chemical shift of H$_a$ as a function of Cl$^-$ concentration- filled dots represent empirical data points, while the smooth curve (in red) show fitted data.*

Encouraged by the favourable anion binding properties of the neutral rotaxanes in dry d$_6$-acetone, the ^{1}H NMR titrations were repeated in the presence of D$_2$O (2 % by volume) to study the effects of water on their anion binding properties. For rotaxanes **2.12I$_2$H** and **2.12I$_3$**, similar but smaller perturbations of their respective proton environments were observed as those seen in Figure 2.16A and Figure 2.17. The 1:1 stoichiometric association constants (K_a) were determined by WinEQNMR2[60] analysis (Table 2.2), and are compared with those of macrocycle **2.1I** and tetrakis(iodotriazole) neutral XB rotaxane **2.15I$_4$**. Owing to their modest binding affinities seen in dry d$_6$-acetone, anion binding of rotaxanes **2.12H$_3$** and **2.12Te$_2$H** were too weak to be quantified in d$_6$-acetone/ D$_2$O 98:2 *v/v*.

Table 2.2. Anion association constants (K_a/ M^{-1}) of neutral XB macrocycle **2.1I** and rotaxanes in acetone-water solvent mixtures. [a]

	2 % D_2O in d_6-acetone				5 % D_2O in d_6-acetone
	2.1I	**2.12I_2H**	**2.12I_3**	**2.15I_4**	**2.15I_4**
Cl^-	128 (3)	114 (6)	280 (6)	496 (2)	25 (2)
Br^-	296 (6)	371 (25)	461 (11)	1200 (4)	224 (8)
I^-	552 (31)	533 (7)	617 (27)	1101 (68)	562 (44)
SO_4^{2-}	66 (3)	38 (3)	19 (1)	-[b]	-[c]

[a] Anions added as TBA salts, errors (±) given in parentheses. 1:1 association constants calculated using WinEQNMR2 software[60], monitoring the perturbations of the axle triazole proton H_3 for **2.12I_2H** and the internal aromatic macrocycle proton H_a for the other receptors (d_6-acetone, 298 K). [b] No binding; [c] Not performed.

Comparing the anion binding behaviour of rotaxane **2.12I_2H** in dry d_6-acetone (Table 2.1) and in the presence of D_2O (Table 2.2) reveals the importance of water in governing anion binding behaviour. The presence of water led to a dramatic decrease in the anion binding affinities for all anions, with the largest decrease occurring with the most strongly hydrated anions (38- and 250-fold reduction in K_a values for Cl^- and SO_4^{2-} respectively) and the smallest difference for I^-. As a result, a complete reversal of anion binding trend was observed, with I^- being the most strongly bound anion in the wet solvent. Clearly, these results show that the stabilities of these XB-anion complexes are highly dependent on solvent polarity, which contrasted Hunter's earlier findings regarding the solvent-independence of XB interaction strengths.[65] In their study, the authors found that XB association constants between molecular iodine (I_2) and tetramethylthiourea decreased by a factor of 3 when the solvent was changed from *n*-octane to methanol, which corresponded to a very large increase in the solvent HB basicity.[66] While the differences in solvent dependency observed herein may be partly due to the inherently different XB-donor properties of I_2 and iodotriazoles, the much greater solvent sensitivity of anion binding is reflective of the greater solvation enthalpies of anions compared with neutral guests. In the case of anions, they are much more susceptible to changes in HB-donor ability of the solvent.[67] In fact, 'soft' and more poorly-hydrated anions such as I^- render the stabilities of the **2.12I_2H**-anion complexes less sensitive to solvent polarity, behaving more similarly to the neutral XB complexes in Hunter's study.

Table 2.2 shows that neutral rotaxane **2.12I$_2$H** did not exhibit enhanced anion affinities compared with the free macrocycle **2.1I** in wet acetone. This is surprising, considering that many prior examples of interlocked structures show significant enhancements in binding strength compared to their free components due to the rotaxanes' preorganised three dimensional binding cavity.[68,69] This may possibly be due to the comparatively weak HB donor ability of the prototriazole moiety on the axle of **2.12I$_2$H**, allowing XB interactions to completely dominate the binding interactions in wet acetone. Supporting this hypothesis are the observations that having increasing numbers of XB iodotriazole units on the rotaxane axle (**2.12I$_3$** and **2.15I$_4$**) led to larger halide binding affinities for all cases except SO_4^{2-}, highlighting the important additive effects of XB donor groups surrounding the rotaxane cavity in enhancing anion affinity.

Curiously, tetrakis(iodotriazole) rotaxane **2.15I$_4$** showed a modest selectivity for Br^- over I^- in d_6-acetone/ D_2O 98:2 *v/v* (Table 2.2). As seen from Figure 2.18, only the addition of halides (Cl^-, Br^- and I^-) led to noticeable changes in the ^{1}H NMR spectrum of **2.15I$_4$**, with anions of other geometries (tetrahedral: SO_4^{2-}, ReO_4^-; bent: AcO^-; linear: N_3^-) eliciting no changes at all. Considering the similarities in anion hydration energies of Cl^- and ReO_4^- (ΔG_{hyd} = - 330 and - 340 kJ mol^{-1} respectively)[70], as well as Br^- and N_3^- (ΔG_{hyd} = - 315 and - 295 kJ mol^{-1} respectively)[61], the selectivity for spherical halides in the presence of water, especially for Br^-, is impressive, and is likely a result of the binding cavity of **2.15I$_4$** being complementary in shape and size for the spherically-shaped anions. Further underscoring the importance of hydration in anion binding, increasing the percentage of D_2O in the solvent from 2 to 5 % resulted in a distinct Hofmeister bias binding trend with clear selectivity for I^- over Br^-, with the most hydrophilic anions showing the greatest reduction in binding affinities once again.

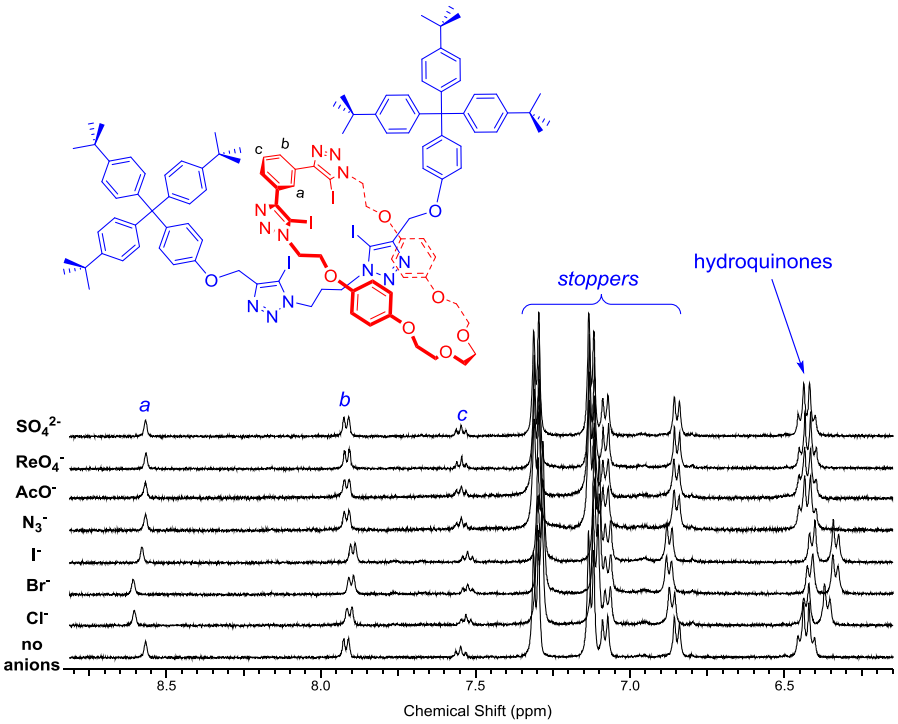


***Figure 2.18**. Partial ^{1}H NMR of all-XB rotaxane **2.15I$_4$** in the presence of 1.0 equivalent of various anions ([**2.15I$_4$**] = 1.0 mM, d_6-acetone/ D_2O 98:2 v/v, T = 298 K).*

2.2.6 Studies of Neutral Halogen Bonding Rotaxanes as Heteroditopic Axle-Separated Ion-pair Receptors

Heteroditopic receptors can bind cations and anions either in contact with each other, or as separated ion pairs. However, the binding of the latter is considerably more challenging, as the electrostatic attraction between the cation and anion needs to be overcome. Nevertheless, this has been achieved using [2]rotaxanes by Beer[71] and Ballester,[72] which contain separate anion and cation-recognition sites (see Section 1.3.3.2). Notably, in Beer's heteroditopic rotaxane which bound the cation and anion separated by the axle (see Figure 1.47D), the presence of Na^+ enhanced the magnitudes of the Cl^- and Br^- association constants by more than an order of magnitude compared to the absence of cation in $CDCl_3$/ CD_3OD 4:1 *v/v*. In a similar way, it was envisaged that the **2.12** rotaxane family could also act as heterotopic axle-separated ion pair receptors (see Figure 2.19), with the metal cation bound in the rotaxane region flanked by the Lewis basic atoms (macrocycle polyether O and the triazole *N* atoms),[73] and the anion bound at the other end of the axle flanked by the Lewis acidic XB triazole units on the macrocycle. It was hoped that metal cation binding would induce further

polarisation of the axle triazole group by interacting with its *N* atom to further enhance its electrophilicity for anion binding.

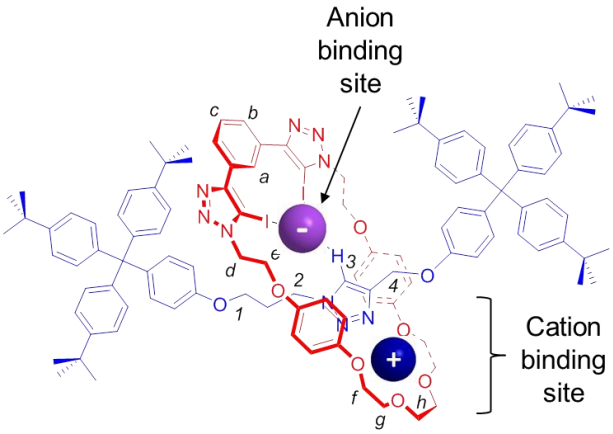


***Figure 2.19**. Schematic illustration of rotaxane **2.12I$_2$H** acting as a neutral heterotopic axle-separated ion-pair receptor.*

Titrations were performed using **2.12I$_2$H** in d_6-acetone/D_2O 98:2 *v/v* where 1.0 equivalent of Li^+ or Na^+ (as its PF_6^- or ClO_4^- salt respectively) was first added to a solution of the rotaxane, followed by TBAI. Iodide was chosen due to its low charge density, reducing the likelihood of forming NaI contact ion-pairs in solution that would prevent binding by the rotaxane. However, as shown in Figure 2.20, the addition of 1.0 equivalent of $LiPF_6$ resulted in no observed perturbations of the proton signals of **2.12I$_2$H**, even in the polyether regions ($H_{f\text{-}h}$), indicating that Li^+ was not binding with the rotaxane. Subsequent titration with TBAI afforded changes similar to those seen without $LiPF_6$, and yielded a 1:1 association constant of (413 ± 23) M^{-1}, which was determined by monitoring changes in shifts of axle triazole proton H_3. Postulating that Li^+ was too strongly hydrated to bind to the rotaxane in wet acetone, the titrations were repeated with $NaClO_4$. Unfortunately, no binding was observed as well with Na^+, and subsequent TBAI titration in the presence of 1.0 equivalents of Na^+ gave K_a = (469 ± 24) M^{-1}. Compared to the value of K_a (533 ± 7) M^{-1} obtained in the absence of cation (Table 2.2), the presence of Li^+ caused a greater reduction in I^- affinity compared to Na^+, indicating that ion-pairing between I^- and the alkali metal cations was occurring to some extent in solution that reduced the availability of free I^- in solution for binding to the rotaxane. Compared with crown

ethers, the lack of binding by Li^+ and Na^+ to the rotaxane may be a result of poorer preorganisation and size-complementarity of the polyether region of the rotaxane.

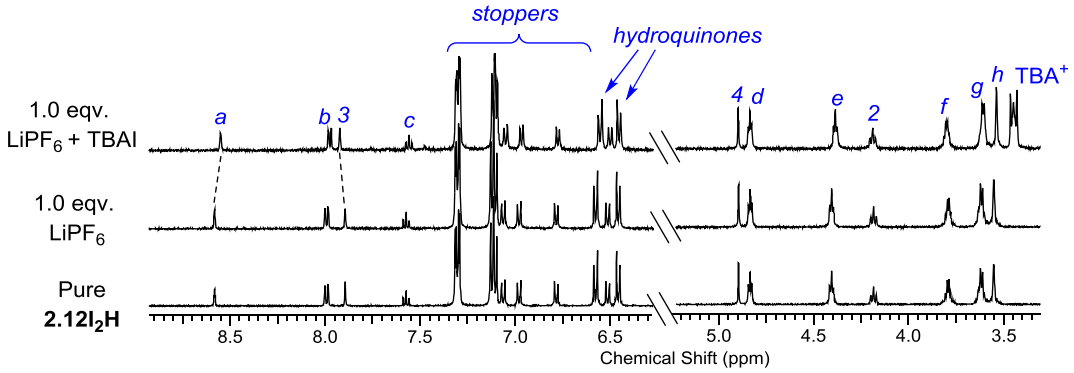


***Figure 2.20**. Partial ^{1}H NMR spectra of (A) pure rotaxane **2.12I$_2$H**, as well as in the presence of (B)1.0 equivalent of $LiPF_6$ and (C) 1.0 equivalent of $LiPF_6$ and TBAI each ([**2.12I$_2$H**] = 1.0 mM, d_6-acetone/D_2O 98:2 v/v, T = 298 K). Proton assignments follow those of Figure 2.19.*

2.2.7 Anion Binding Studies of Cationic Chalcogen Bonding Macrocycles and Rotaxanes

Having studied the anion binding properties of the neutral ChB rotaxanes in (dry) d_6-acetone, the effects of charge-assisted ChB interactions were investigated by ^{1}H NMR titrations in the presence of water using cationic macrocycle **2.9Se** and rotaxane **2.20Se$_2$H**. At the time of writing, the application of ChB interactions on anion recognition in water is unprecedented. The binding properties of the cationic ChB hosts were compared with those of the chalcogen-free HB analogues (**2.9H** and **2.20H$_3$**) to discern the influence of ChB interactions on anion recognition.

As shown in Figure 2.21, the presence of increasing quantities of halides in d_6-acetone/D_2O 98:2 *v/v* gave downfield shifts of the internal aromatic proton (H_a) of macrocycle **2.9Se**, with upfield shifts observed for H_b, H_c, H_d and H_e. Importantly, the triazolium methyl protons (H_f) did not show appreciable perturbations, suggesting that the halide anions were not bound by HB interactions from these electron-deficient proton environments. Monitoring the shifts of H_a during the titrations and fitting the data to a 1:1 host-guest binding model afforded association constants summarised in Table 2.3. Unfortunately, analogous titration experiments with SO_4^{2-} resulted in macrocycle precipitation, while complex binding equilibria

observed with acetate negated quantitative data from being obtained. When the titrations were repeated in the more competitive aqueous solvent mixture of d_6-acetone/D_2O 95:5 *v/v*, perturbations of H_a were too small for reliable determination of binding affinities.

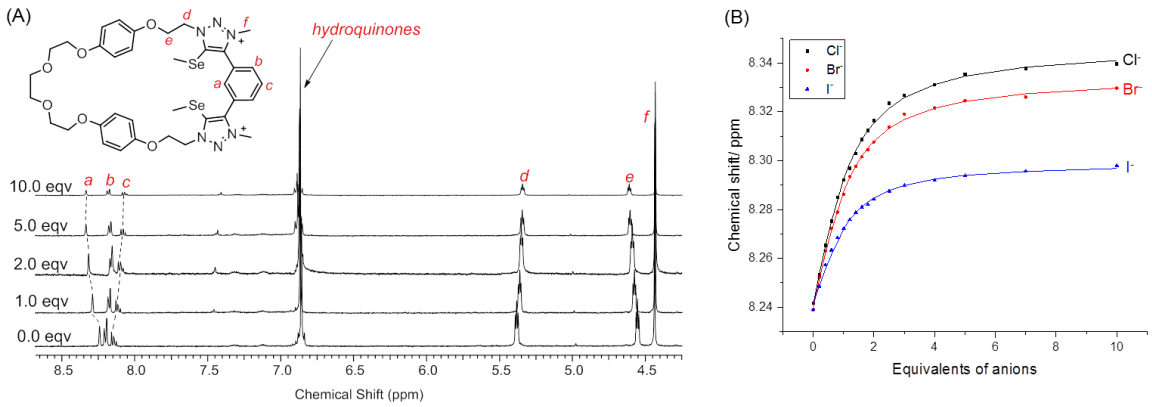


***Figure 2.21**. (A) Partial ^{1}H NMR of macrocycle **2.9Se** in the presence of increasing quantities of Cl^-. (B) Binding isotherms for macrocycle **2.9Se** showing the changes in the chemical shift of internal aromatic proton H_a with increasing equivalents of anions added ([**2.9Se**] = 1.0 mM, d_6-acetone/ D_2O 98:2; T = 298 K).*

The mode of I^- binding by macrocycle **2.9Se** in the solid state was determined from single crystal X-ray diffraction analysis (see Appendix A for details). Orange single crystals of the **2.9Se**-I^- complex were obtained by slow vapour diffusion of diethyl ether into a solution of **2.9Se** (as its PF_6^-) salt and excess TBAI in chloroform/ acetonitrile 1:1 *v/v*. Due to the small and weakly diffracting nature of the crystals, diffraction data was collected using synchrotron radiation with the I19-1 beamline at Diamond Light Source.[74] The complex of **2.9Se** and I^- crystallised in the $P2_1/c$ space group, with the macrocycle and I^- present in a 1:2 molar ratio (to maintain charge neutrality) in the absence of any PF_6^- counteranion present in the crystal structure (Figure 2.22). Despite significant thermal motion of the hydroquinone and polyether portions of the macrocycle, which could be modelled as positional disorder over two sites, the structure of **2.9Se** and the locations of I^- could be unambiguously determined.

From Figure 2.22A, it is evident that each $SeCH_3$ group is twisted out-of-plane relative to the central benzene spacer, with both $SeCH_3$ groups pointing in opposite directions, possibly to minimise steric repulsions in the solid state. Consequently, the I^- are not bound convergently by both Se atoms of the same macrocycle unit, but are interacting with the Se

atoms on *adjacent* macrocycles in the solid state. Three distinct short contacts between the Se atoms and I^- can be discerned (labelled a, b and c in Figure 2.22B), each being shorter than the sum of their respective van der Waals' (vdW) radii (91 - 97 %), indicative of charge-assisted ChB-I^- interactions. In each case, the C-Se···I^- angle approaches linearity, with two of the interactions nearly collinear with the triazolium ring (contacts a and b), and the last collinear with the methyl group on Se (contact c), highlighting the influence and participation of both σ-holes on each divalent Se atom in governing I^- binding geometry and crystal packing. It is notable that despite the presence of numerous electron-deficient regions such as the triazolium methyl groups, I^- is bound predominantly via ChB interactions from the Se atoms in the solid state.

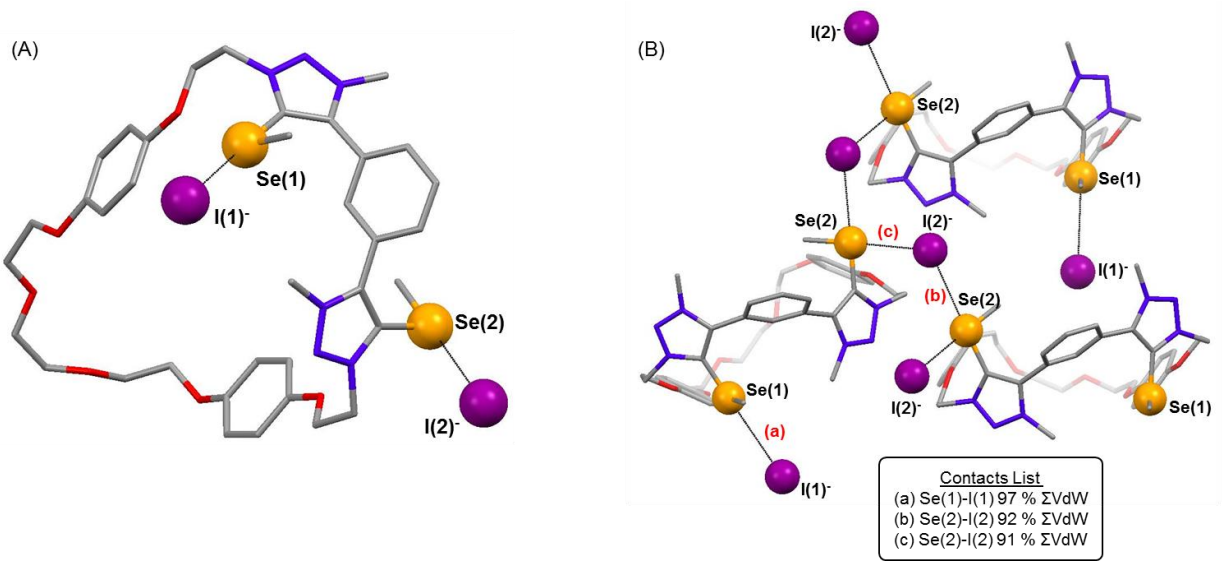


Figure 2.22. *Crystal structure of the* ***2.9Se****-I^- adduct, showing the short contacts (black lines) between the Se atoms (orange) and the major components of the iodide anions (purple), viewed from (A) the top and (B) showing the solid-state packing structure in the crystal lattice. H atoms, solvent molecules and all minor components of the disorder are omitted for clarity. Grey = C, blue = N and red = O.*

^{1}H NMR titrations were performed using *tricationic* rotaxane **2.20Se$_2$H** in d_6-acetone/ D_2O 4:1 *v/v.*[‡‡] With the halides (Cl^-, Br^- and I^-), the most prominent downfield shifts of the proton environments around the anion binding cavity were seen for axle triazolium proton H_3

[‡‡] Binding studies performed in less competitive wet acetone mixtures containing 5 % and 10 % D_2O *v/v* resulted in complex binding equilibria which could not be analysed using WinEQNMR2[60].

($\Delta\delta$ > + 0.5 ppm for 10.0 eqv. of I^-) and stopper proton H_4 ($\Delta\delta$ = +0.12 ppm for 10.0 eqv. of I^-) (Figure 2.23), together with increased splitting of the hydroquinone resonances. This suggests that the halides were bound slightly above the plane of the macrocycle component of rotaxane **2.20Se$_2$H** (as shown in Figure 2.22), held by the methylseleno-triazolium groups twisted slightly out of plane with the macrocycle and by HB interactions with the axle triazolium group (*vide infra*), allowing them to participate in weak HB interactions with the proximal stopper proton. Significantly, only small shifts of the proton signals arising from the macrocycle component's triazolium methyl protons were seen, consistent with the halides being mainly bound within the vicinity of the rotaxane's binding cavity.

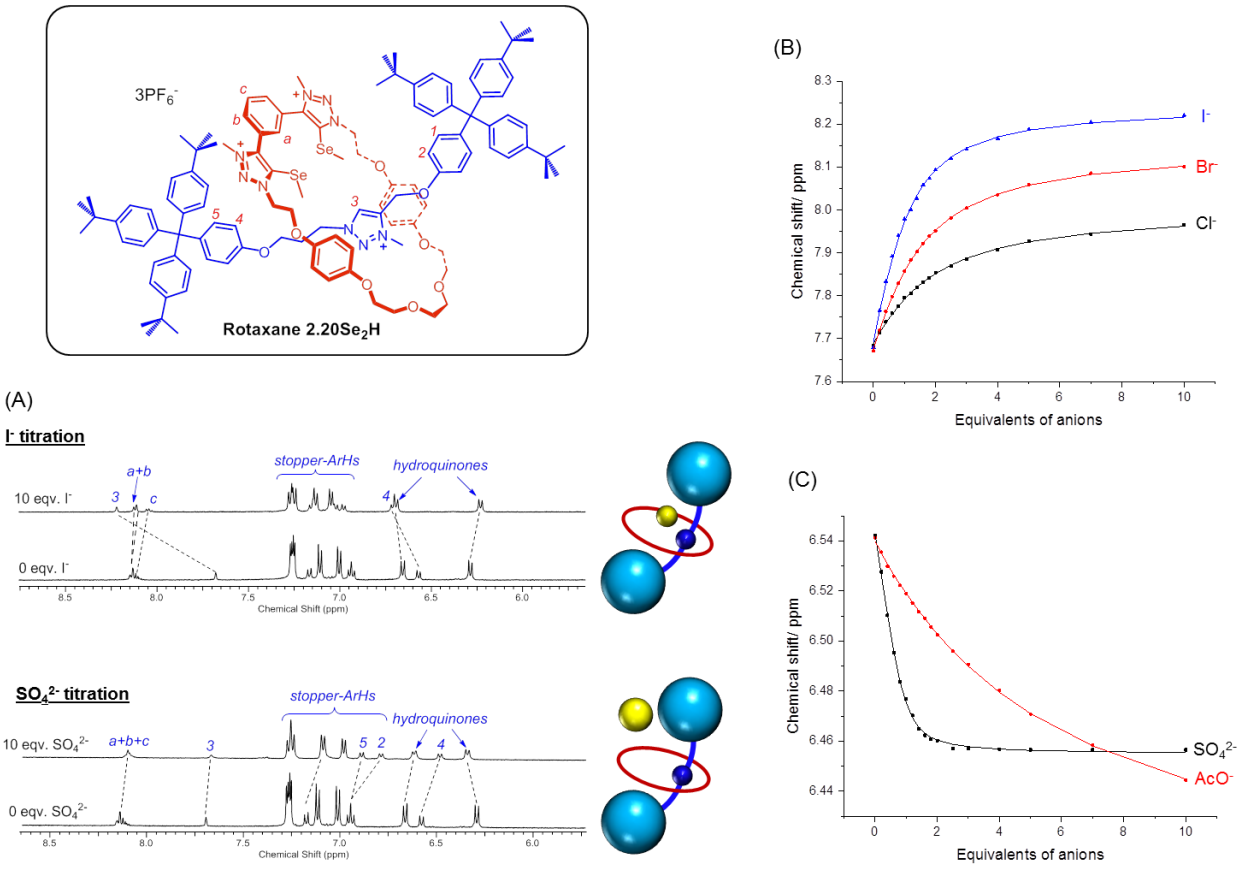


Figure 2.23. *(A) Partial ^{1}H NMR spectra of tricationic rotaxane **2.20Se$_2$H** in the presence of 0.0 and 10.0 equivalents of I^- (top) and SO_4^{2-} (bottom); Binding isotherms of (B) the halides monitoring the changes in chemical shifts of axle triazolium H_3; (C) oxoanions monitoring perturbations of stopper proton H_4 ([**2.20Se$_2$H**] = 1.0 mM; d_6-acetone/ D_2O 4:1; T = 298 K).*

Contrasting with halide binding, the presence of the oxoanions SO_4^{2-} and AcO^- gave small *upfield* shifts of the protons flanking the rotaxane cavity, in particularly axle triazolium H_3 (Figure 2.23A), clearly indicating that they were not binding in its vicinity. Instead, the most significant upfield shifts were seen for the stopper proton resonances (H_2 and H_4) (Figure 2.23C), suggesting an association at the periphery of the rotaxane. Comparatively, the tricationic HB rotaxane analogue **2.20H$_3$** showed large downfield shifts of its axle triazolium proton in the presence of these oxoanions, indicating of anion binding near the cavity. Evidently, the bulky $SeCH_3$ groups of **2.20Se$_2$H** were exerting considerable steric influence which prevented the larger anions from penetrating the more sterically-crowded binding site.

Analyses of the titration data using the WinEQNMR2[60] software revealed that despite the highly charged nature of the host molecules, all the anions were bound predominantly via a 1:1 host-guest stoichiometry, with no evidence of a second binding event discernible. From the calculated association constants shown in Table 2.3, the ChB hosts exhibited considerably different binding properties from their HB analogues. For both **2.9Se** and **2.20Se$_2$H**, a clear Hofmeister binding preference for the heavier halides can be discerned (I^- > Br^- > Cl^-), while **2.9H** and **2.20H$_3$** showed selectivity for Br^- over I^-. This ChB behaviour mirrors those of charged XB systems in the presence of water, favouring binding of the 'softer' and more lipophilic halide anions (I^-),[75,76] highlighting the intrinsic similarities between the closely-related σ-hole-based XB and ChB interactions. Notably, although the large oxoanions were associating only at the periphery of **2.20Se$_2$H**, analyses of the H_4 shifts during the titration revealed surprisingly strong association of SO_4^{2-} (Table 2.3). Given the hydrophilicity of SO_4^{2-} (ΔG_{hyd} = - 1080 kJ mol^{-1})[61] and the fact that the presence of water has a large detrimental effect on SO_4^{2-} by XB rotaxanes (shown in Table 2.2), it is likely that electrostatic attractions are playing a significant role in anion binding by tricationic **2.20Se$_2$H**. However, the biggest difference was seen for the binding of AcO^- by **2.20Se$_2$H** and **2.20H$_3$**, with K_a values for the latter larger than that of the former by more than an order of magnitude. Potentially arising partly from size-mismatch with the respective rotaxanes' binding cavity, the large difference also further highlights the fundamental differences between ChB and HB host systems to anion charge density and basicity.

Table 2.3. Anion association constants (K_a/ M^{-1}) for cationic macrocycles **2.9Se** and **2.9H**, as well as rotaxanes **2.20Se$_2$H** and **2.20H$_3$**.[a]

	acetone/ D_2O 98:2		acetone/ D_2O 4:1	
	2.9Se	**2.9H**	**2.20Se$_2$H**	**2.20H$_3$**
Cl^-	1180 (47)	-[c]	696 (28)	1319 (7)
Br^-	1298 (66)	2649 (153)	983 (18)	2365 (217)
I^-	1534 (115)	1248 (89)	2084 (109)	1068 (25)
SO_4^{2-}	-[b]	-[b]	3531 (232) [d]	-[c]
AcO^-	-[c]	-[c]	43 (1) [d]	1467 (123) [e]

[a] Calculated using the WinEQNMR2 software[60], monitoring the central internal aromatic proton H_a for **2.9Se** and **2.9H**, and axle triazolium proton H_3 for both rotaxanes unless otherwise stated; errors (±) in parentheses; [host] = 1.0 mM, T = 298 K. [b] Precipitation of host-anion adducts occurred. [c] Complex binding equilibria. [d] Values obtained by monitoring proton H_4 on stopper units. [e] Values obtained by monitoring internal aromatic proton H_a on the macrocycle component.

To obtain further insights into the conformational changes, geometries and solvation effects on anion binding to macrocycle **2.9Se** and **2.20Se$_2$H**, DFT and Molecular Dynamics simulations were performed by Dr. Igor Marques and Prof. Vítor Felíx at the University of Aveiro, Portugal. Using an acyclic model compound **2.9Se$_{model}$**, where the dicationic methylseleno-triazolium groups of **2.9Se** were capped with methyl groups, the gas-phase complexes of **2.9Se$_{model}$** with Cl^-, Br^- and I^- were DFT optimized with the M06-2X functional, using the aug-cc-pVDZ-PP basis set for Se, Br and I, the aug-cc-pVDZ basis set for Cl, and the 6-311++G** basis set for the remaining atoms (Figure 2.24).

The gas phase structures in Figure 2.24 show the bidentate coordination of each halide anion by **2.9Se$_{model}$** via two highly-linear ChB interactions from each Se atom, with the binding distances increasing with the size of the halide. In the unbound model receptor, two spatially separated regions of positive electrostatic potential (in red) surround the σ-hole (in black) at the termini of the $C_{triazolium}$-Se bond. However interestingly, the presence of halide induces a greater electron deficiency at the binding site, with a larger increase in $V_{S,max}$ on the Se atoms seen for smaller and more charge-dense halide. In addition, an estimation of the Wiberg Bond Indices (WBI) of each ChB interaction from these DFT-optimised structures revealed larger independent values for the heavier halides, increasing in the order Cl^- (0.189; 0.153) < Br^- (0.199; 0.167) < I^- (0.213; 0.167), with the values in parentheses representing the WBI for each ChB-halide interaction. This suggested a greater degree of covalency in the ChB

interactions for the heavier halides, which may partly account for the enhanced binding affinities for **2.9Se** and **2.20Se$_2$H** for the heavier halides (Table 2.2).

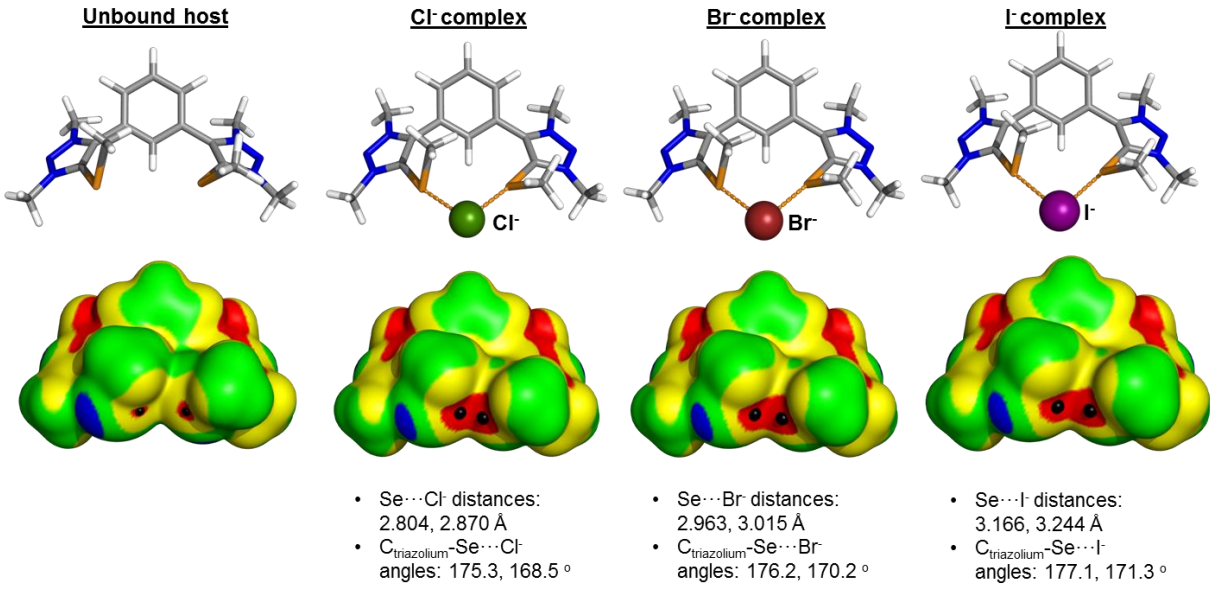


***Figure 2.24**.(Top) DFT-optimised structures and (bottom) electrostatic potential distribution mapped onto the electron density surface of **2.9Se$_{model}$** in the absence of anions and when bound to Cl⁻, Br⁻ and I⁻. The chalcogen bonds are drawn as orange dashed lines, with each $V_{S,max}$ is represented as a black dot corresponding to the σ-hole in front of each $SeCH_3$ binding unit. The color ranges, in kJ/mol, are as follows: blue – below 470.7; green – between 470.7 and 533.5; yellow – between 533.5 and 596.2; red – above 596.2.*

To model the halide associations with the cationic ChB hosts in their respective solvent media, classical Molecular Dynamics (MD) simulations were performed in a cubic box containing 84 water and 1005 acetone molecules (acetone/ water 98:2 *v/v*) for **2.9Se,** and 1802 and 1836 randomly-distributed acetone and water molecules (acetone/ water 4:1 *v/v*) for **2.20Se$_2$H**, in accordance with the ^{1}H NMR titration studies. The ChB interactions were simulated using an extra point charge to represent the σ-hole found in front of each C-Se bond, in a similar way as prior studies on XB systems,[75,77] using force field bonding parameters involving Se developed to be used together with the General Amber Force Field (GAFF)[78,79] (computational details in Appendix C). A suitable number of PF_6^- counter-anions was added to each halide complex to maintain charge neutrality, and the dynamical behavior of each halide complex was further ascertained through three independent MD runs of 10 ns and 50 ns for **2.9Se** and **2.20Se$_2$H** respectively carried out under periodic conditions using a

NPT ensemble and AMBER 16 (PMEMD),[80] with GPU acceleration,[81,82] as simulation engine. The distance between each halide (A) and the center of mass of the macrocycle component, taking into account only the non-hydrogen atoms (MAC_{cent}), was monitored along the simulation time of each MD run, together with individual ChB dimensions (Se···A distance and $C_{triazolium}$-Se···A angle) and the number of solvent molecules found within a 3.5 Å radius around the two Se centers and each halide anion when free and complexed. Representative snapshots of the halide complexes of macrocycle **2.9Se** and rotaxane **2.20Se$_2$H** are shown in Figure 2.25, while Table 2.4 lists the average values of the structural parameters of the halide complexes over 3 MD runs.

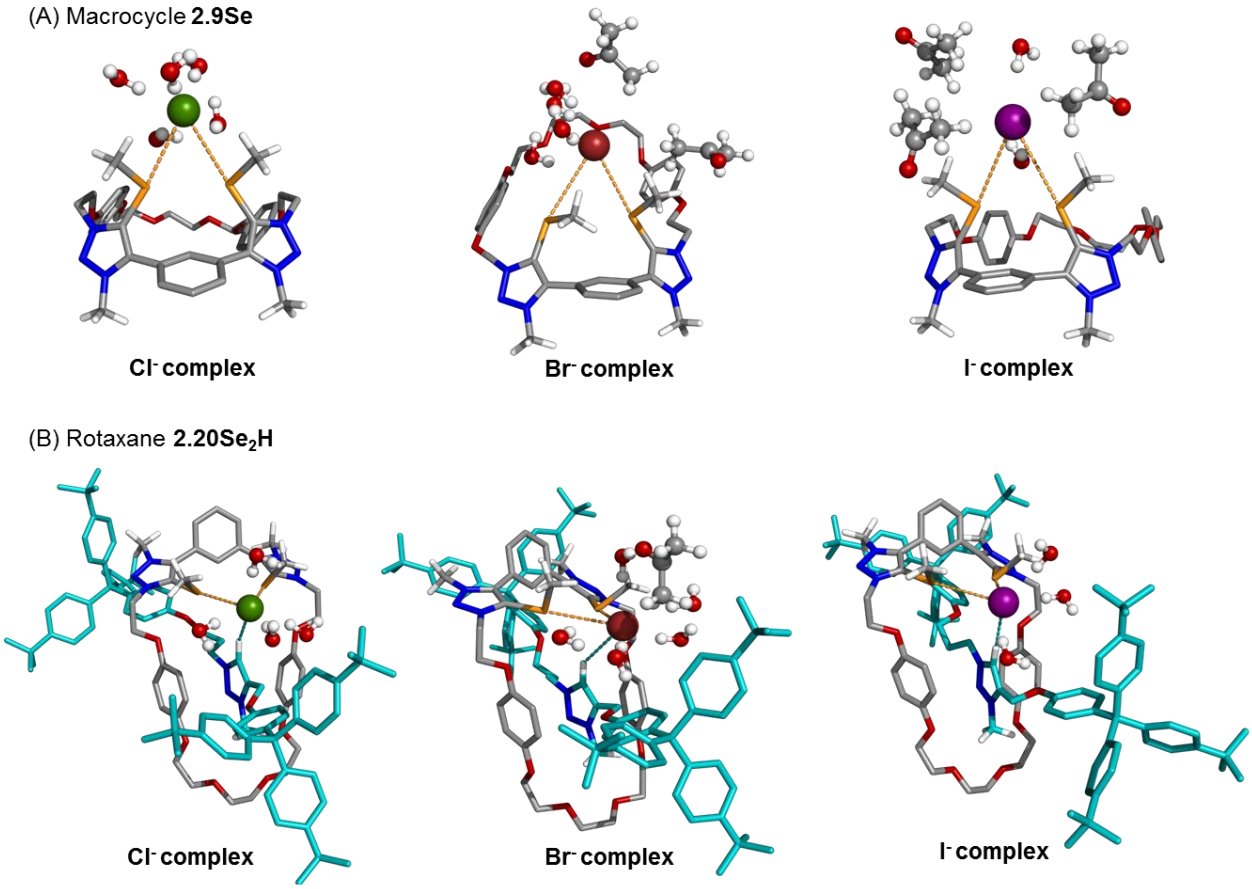


***Figure 2.25**. Illustrative snapshot of the MD simulations of halide complexes of (A) macrocycle **2.9Se** and (B) rotaxane **2.20Se$_2$H**, showing the bound anion surrounded by several acetone and water solvent molecules. In every case, each halide is bound by two convergent ChB (orange dashed lines). For rotaxane **2.20Se$_2$H**, the additional HB from the axle is shown by the teal dashed line. Each ChB-donor Se atom is coloured in orange.*

Table 2.4. Average ChB dimensions obtained from MD simulations of the halide complexes of **2.9Se** and **2.20Se$_2$H**, along with the distances between the halide guests and the center of mass of the macrocycle in either system.[a]

	Rotaxane **2.20Se$_2$H**			Macrocycle **2.9Se**		
	Se···A	∠C$_{triazolium}$-Se···A	A···MAC$_{cent}$	Se···A	∠C$_{triazolium}$-Se···A	A···MAC$_{cent}$[e]
Cl^-	3.712 ± 0.214; 3.700 ± 0.213	170.3 ± 4.0; 170.7 ± 3.9	4.462 ± 0.520	3.759 ± 0.240; 3.740 ± 0.232	169.0 ± 4.6; 169.3 ± 4.5	5.714 ± 0.582
Br^-	4.017 ± 0.261; 4.027 ± 0.268	170.3 ± 4.6; 170.2 ± 4.6	4.805 ± 0.536	4.070 ± 0.313; 4.088 ± 0.318	168.2 ± 5.6; 167.9 ± 5.7	6.040 ± 0.673
I^-	4.317 ± 0.274; 4.316 ± 0.280	169.6 ± 5.1; 169.8 ± 5.1	5.163 ± 0.644	4.422 ± 0.332; 4.403 ± 0.323	167.1 ± 6.3; 167.5 ± 6.1	6.380 ± 0.676

[a)] All distances and angles are given in Å and (°), respectively. *N* = 150000. Values quoted follow the format: average value ± standard deviation.

From the A···MAC$_{cent}$ distances shown in Table 2.4, the halides bind above the plane of the macrocycle for both **2.9Se** and **2.20Se$_2$H**, with Cl^- being bound closest and the larger Br^- and I^- being bound progressively further away. The small standard deviations of the Se···halide bond distances for **2.20Se$_2$H** also suggest that the halides are held by two convergent and highly-linear (average ∠C$_{triazolium}$-Se···A ≈ 170 ^{O}) ChB interactions maintained throughout the MD runs which are only occasionally broken. Comparatively, while the two convergent ChB interactions were also maintained for macrocycle **2.9Se**, the average Se···halide bond distances are longer, with larger standard deviations, suggesting that the ChB interactions of the **2.9Se**···halide complexes are more frequently broken.

The solvation of the Se atoms of **2.9Se** and **2.20Se$_2$H**, as well as their guest anions, were compared before and after complexation to further understand the binding selectivity trends. The free macrocycle and rotaxane were preferentially solvated by (2.4 ± 1.1) and (1.1 ± 0.9) acetone molecules, as well as (0.1 ± 0.2) and (0.3 ± 0.6) water molecules respectively, primarily reflecting the solvent content of the mixtures used in the binding studies. During halide complexation (represented by MD equilibration), the Se atoms of **2.9Se** and **2.20Se$_2$H** become more hydrated due to the hydration shell surrounding each halide, with the smaller halides increasing the water content around the Se atoms more significantly and displacing more acetone molecules simultaneously. Significantly, this increases the competition between the smaller and more hydrated halides and water molecules for interaction with Se, resulting in more frequent disruptions of the ChB-anion interactions. The more sustained ChB interactions

for the larger halides arising from diminished water-induced disruptions, together with the enhanced covalency suggested by the WBI calculations, account for the generally stronger binding affinities for the larger halides seen in Table 2.3.

Finally, these computational studies also offer insights on the observed superiority of rotaxane **2.20Se$_2$H** over macrocycle **2.9Se** for anion binding, where comparable binding affinities were obtained despite the much greater competitiveness of the solvent used for the former. From Table 2.4, the longer A···MAC$_{cent}$ distances of macrocycle **2.9Se** compared to rotaxane **2.20Se$_2$H** result in the halides bound to the former being more exposed and hydrated by the water molecules. Hence, the ChB-anion interactions of **2.9Se** are subjected to more extensive interruptions by the closely-associated water molecules, leading to lower binding affinities compared with **2.20Se$_2$H**. Although other factors also contribute to the superior halide binding properties of **2.20Se$_2$H**, including higher charge, HB from the axle prototriazolium motif and the preorganization of the rotaxane cavity, these computational results provide the first glimpse of the crucial roles played by the solvent, particularly water, in determining anion selectivity and binding affinities of ChB host systems.

2.2.8 Probing Anion Binding with ChB hosts using Heteronuclear ^{77}Se and ^{125}Te NMR

The direct involvement of Se and Te atoms in ChB interactions with anions suggested the possibility of using heteronuclear ^{77}Se and ^{125}Te NMR to probe anion binding, in an analogous way as that for ^{1}H NMR for HB systems. Like protons, both nuclei are highly sensitive to perturbations to their local electronic environments,[83,84] and have been applied as responsible probes for metal complexation,[85,86] non-covalent interactions,[87–89] as well as changes in chemical environment following conformational changes and encapsulation in biotic[90] and abiotic systems.[91] In an attempt to correlate the magnitudes of ^{77}Se and ^{125}Te signal perturbations (Δδ/ ppm) with the K_a values in Table 2.3, the heteronuclear spectra of neutral **2.12Te$_2$H**, cationic **2.9Se** and **2.20Se$_2$H** were recorded before and after addition of 10.0 equivalents of halides in the same solvent media as the ^{1}H NMR titrations.

Halide binding to neutral rotaxane **2.12Te$_2$H** in dry d_6-acetone resulted in large upfield perturbations of the ^{125}Te NMR signal by almost 8 ppm for Cl^-, which decreases in magnitude

for the heavier halides (Table 2.5). Interestingly, a plot of the magnitude of ^{125}Te shifts (Δδ) with r^{-2} (Figure 2.26A) with r being the anionic radius of the halide,[61] gave an excellent linear correlation (Pearson's R = -0.997). On the other hand, while larger Δδ values were obtained for the stronger binding halides (Table 2.1), poor linearity was obtained when Δδ was plotted as a function of K_a. This suggested that the charge density of the halide guest plays an important role in influencing the electronic properties of the Te atoms in dry solvents, with the larger upfield shifts observed for lighter halides possibly arising from greater donation of electron density from the halide into the C-Te σ* orbital, concomitantly increasing the local electron density on the Te atom.

Table 2.5. Shifts (Δδ/ ppm) of ^{125}Te and ^{77}Se NMR resonances of **2.12Te$_2$H**, **2.9Se** and **2.20Se$_2$H** in the presence of 10.0 equivalents of halides.[a]

	Δδ/ ppm		
	2.12Te$_2$H [b]	**2.9Se** [c]	**2.20Se$_2$H** [d]
Cl^-	-7.7	-5.1	-7.3
Br^-	-5.8	-4.6	-6.3
I^-	-2.8	-2.5	-2.0

[a] $\Delta\delta = \delta_{10\ eqv\ halide} - \delta_{0\ eqv\ halide}$; [host] = 4.0 mM, T = 298 K. [b] Solvent = pure d_6-acetone, $\delta_{Te,0\ eqv\ halide}$ = 116.5 ppm; [c] Solvent = d_6-acetone/ D_2O = 98:2, $\delta_{Se,0\ eqv\ halide}$ = 106.9 ppm; [d] Solvent = d_6-acetone/ D_2O = 4:1, $\delta_{Se,0\ eqv\ halide}$ = 105.2 ppm

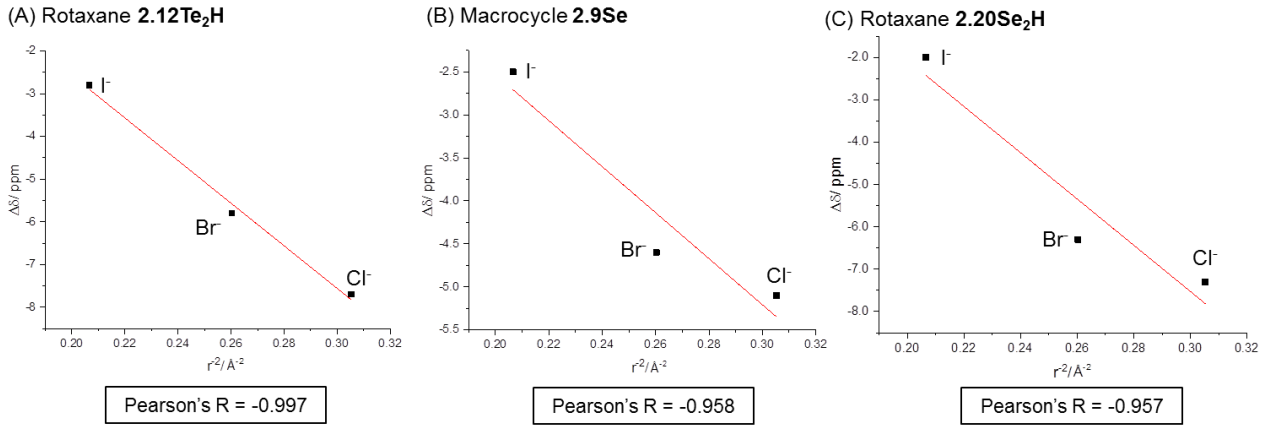


***Figure 2.26**. Plots of the changes in NMR chemical shift of the (A) ^{125}Te nuclei of rotaxane **2.12Te$_2$H**, (B) ^{77}Se nuclei of macrocycle **2.9Se** and (C) rotaxane **2.20Se$_2$H** as a function of r^{-2}/ Å^{-2}, where r is the ionic radii of the anion.[61]*

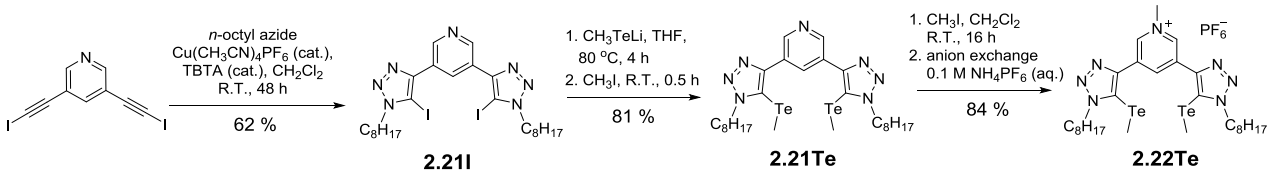
Contrastingly, analogous ^{77}Se NMR titration experiments with cationic ChB hosts **2.9Se** and **2.20Se$_2$H** in acetone/D_2O aqueous solvent mixtures show the reverse trend between $\Delta\delta$ and K_a values. Despite Cl^- being the most weakly bound halide to both receptors (Table 2.3), it was still able to elicit the largest ^{77}Se NMR signal shifts, with the converse observed for I^-. From the poor linear correlations of $\Delta\delta$ against halide r^{-2} in Figure 2.26B and C, it is likely that additional factors other than anion charge density contribute to the magnitude of $\Delta\delta$ seen. These may also include contributions from changes in hydration/ solvation of the ChB-donor Se atoms on halide binding, as well as spatial separation between the Se atoms and anions arising from different accessibilities of each binding cavity, which play a part in changing the local electronic environment of the Se atoms and the resulting ^{77}Se NMR resonances. While this study demonstrates the sensitivity of heteronuclear chalcogen NMR to anion binding, further studies involving a greater number of ChB host molecules are required before any trends can be conclusively discerned, especially in the presence of coordinating solvents bearing Lewis basic groups (e.g. water, ethers, alcohols and DMSO).

2.3 A Stable Cationic Tellurium-containing Chalcogen Bonding Motif

2.3.1 Design and Synthesis of Model Acyclic Receptor

As noted in Section 1.2.2.2, although divalent chalcogen atoms (R-Ch-R) are predicted to be more potent ChB donors than their monovalent counterparts (R=Ch), the only example in the literature is Gabbaï's Lewis acidic telluronium receptor for F^-.[87] We have shown that despite the thermal, photo- and moisture stability of the methyltelluro-triazole group, direct methylation on the triazole *N*[3] atom resulted in decomposition of the motif (Section 2.2.1). Thus, an alternative cationic bidentate Te-based ChB donor motif was designed by replacing the central benzene spacer of **2.1Te** with a pyridinium group (**2.22Te** in Scheme 2.12). Due to the electron-withdrawing resonance effect arising from electronic conjugation with the central cationic pyridinium spacer, the electrophilicity of the Te ChB-donor atoms can be enhanced for more potent ChB interactions with anions, in a similar manner as that previously reported for pyridinium-based XB donor molecules.[17,18]

The forward synthesis of cationic receptor **2.22Te** is shown in Scheme 2.12. A CuAAC reaction between 3,5-di(iodoethynyl)pyridine and *n*-octyl azide produced the neutral bis(iodotriazole) intermediate **2.21I** in 62 % isolated yield.[17] Nucleophilic substitution was performed in a similar manner to that used for **2.8Te**, with $[TeCH_3]^-$ generated *in situ* from methyllithium and Te powder, to produce the neutral ChB receptor precursor **2.21Te**. Pyridine *N*-methylation with iodomethane, followed by anion exchange to the non-coordinating hexafluorophosphate (PF_6^-) salt, afforded the desired cationic receptor **2.22Te** in 84 % yield. **2.22Te** was found to be surprisingly stable, with the presence of water in the solvent and heating to 65 ^oC showing no detrimental effects. As compared to the hypothetical methyltelluro-triazolium (shown to be unstable), the greater stability of the ChB motif of **2.22Te** may result from the smaller degree of $\sigma^*_{C\text{-}Te}$ energy stabilisation, rendering the C-Te bond less susceptible to cleavage by Lewis bases. Heteronuclear ^{13}C and ^{125}Te NMR spectroscopic characterisation of **2.22Te** in $CDCl_3$ showed diagnostic resonances at -11.6 ppm ($Te\underline{C}H_3$) and +91.6 ppm respectively, indicative of the electropositive nature of the sp^3 Te ChB donor atoms.



***Scheme 2.12**. Synthesis of monocationic sp^3-Te ChB model acyclic receptor **2.22Te**.*

2.3.2 Anion Binding Properties

Having synthesised cationic **2.22Te**, its anion binding properties were probed via ^{1}H NMR titration experiments in CD_3CN. Using Cl^- as an example, anion addition resulted in large downfield shifts ($\Delta\delta$ = +0.21 ppm over 10 eqv. Cl^-) of the resonance arising from the internal pyridinium proton H_a (Figure 2.27). While the $TeCH_3$ groups also show smaller but significant downfield perturbations ($\Delta\delta$ = +0.12 ppm), the external pyridinium proton (H_b) and *N*-methyl protons (H_d) showed negligible perturbations after 10 equivalents of Cl^-, clearly indicating that the halide was bound in the space flanked by both $TeCH_3$ groups, likely involving ChB interactions. Although analogous titration experiments using Br^-, I^-, N_3^- and AcO^- resulted in the same spectral changes (Figure 2.27B), the H_a signal curiously underwent a large *upfield* shift with $H_2PO_4^-$, while a downfield perturbation of the $TeCH_3$ resonance was still observed, suggesting that $H_2PO_4^-$ was probably binding via a different mode compared with the other anions. NO_3^- gave no discernible shifts, while F^- and $HP_2O_7^{3-}$ resulted in extensive receptor decomposition potentially due to their basicity. Anion association constants determined from the shifts of H_a or $TeCH_3$ during the titration using WinEQNMR2[60] are summarised in Table 2.6. For comparison, anion titrations were also performed using the HB analogue **2.22H**, synthesised according to previously-reported procedures,[17] and the K_a values were determined in an identical way (Table 2.6).

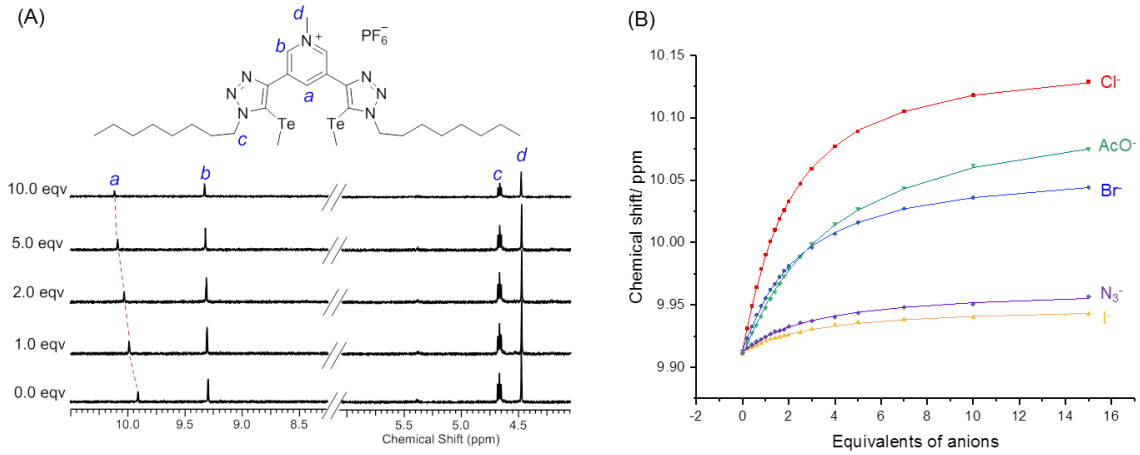


Figure 2.27. *(A) Partial ^{1}H NMR spectra of cationic ChB receptor **2.22Te** in the presence of increasing quantities of Cl^-; (B) Plots of chemical shift of the internal aromatic proton H_a as a function of anion concentration; ([**2.22Te**] = 1.5 mM, CD_3CN, T = 298 K).*

Table 2.6. Anion association constants (K_a/ M^{-1}) of **2.22Te** and **2.22H** with different anions in CD_3CN at 298K.[a]

	2.22Te	**2.22H**
Cl^-	652 (13)	263 (8)
Br^-	503 (16)	106 (3)[b]
I^-	305 (11)	59 (2)[b]
AcO^-	269 (9)	198 (6)
N_3^-	330 (22)	92 (3)
$H_2PO_4^-$	K_{21} = 411 (40)[c] K_{11} = 1530 (138)	-[b,d]

[a]Values of K_a determined using WinEQNMR2 software[60] by monitoring internal proton H_a **2.22Te** and triazole proton for **2.22H**; unless otherwise stated, a host-guest 1:1 stoichiometric binding model was used; errors (±) in parentheses; [host] = 1.0 mM, CD_3CN, T = 298 K). [b] Values previously reported in ref. 17. [c] $TeCH_3$ protons monitored instead of H_a. [d] precipitation of host during titration.

2.22Te and **2.22H** showed several notable differences in their anion binding behaviour in dry CD_3CN (Table 2.6), which suggested the dominance of ChB interactions in governing the anion binding properties of the former. Firstly, although **2.22Te** bound all anions consistently more strongly than **2.22H**, the greatest extents of enhancements in K_a values were seen for the heavier halides (Br^- and I^-), indicating that ChB interactions may have an intrinsic preference for binding softer and more lipophilic anions, a phenomenon that has been previously observed for XB interactions[92]. Nevertheless, halide binding affinity by **2.22Te** decreased in the order $Cl^- > Br^- > I^-$ in a similar way as **2.22H**, implying that anion binding was driven by charge density to some extent for both systems. Secondly, **2.22Te** bound acetate

more weakly than I^-, while **2.22H** bound AcO^- more favourably than both Br^- and I^-, which suggested that ChB interactions are less sensitive to anion basicity than HB. Finally, **2.22H** precipitated in the presence of $H_2PO_4^-$, but **2.22Te** bound $H_2PO_4^-$ surprisingly strongly via an initial 2:1 host-guest binding stoichiometry (K_{21}) that became 1:1 (K_{11}) at higher anion concentrations. Importantly, it is notable that acyclic **2.22Te** exhibits larger K_a values in the more competitive CD_3CN solvent than that for rotaxane **2.12Te$_2$H** in d_6-acetone,[92] which gives credence that charge assistance by the central pyridinium group enhanced the potency of ChB-mediated anion binding significantly.

Although **2.22Te** exhibited stronger anion binding compared with **2.22H**, it is a less potent anion receptor compared to the analogous XB pyridinium-3,5-bis(iodotriazole) receptor previously reported.[17] In d_6-DMSO,[§§] **2.22Te** bound Cl^- with a K_a value of (47 ± 3) M^{-1}, nearly an order-of-magnitude smaller than that for the XB analogue of (387 ± 20) M^{-1}. Notably, the reduced anion binding affinities of charge-assisted ChB interactions compared to XB, mediated by σ-hole donor atoms (Te and I respectively) belonging to the same period parallels the trend seen with neutral hosts previously demonstrated for rotaxanes **2.12Te$_2$H** and **2.12I$_2$H** in Section 2.2.4.

The presence of water in the solvent was previously found to significantly alter the binding affinities and trends seen with XB rotaxane **2.12I$_2$H** (Section 2.2.4). To study the effects of water on ChB anion binding, ^{1}H NMR titrations were repeated using **2.22Te/H** in CD_3CN/ D_2O 99:1 *v/v*. Just like the case seen for **2.12I$_2$H**, the presence of water gave similar but smaller magnitudes of shifts of their respective ^{1}H NMR signals, as well as significant reduction of all anion affinities (Table 2.7), with the most hydrophilic anions (Cl^- and $H_2PO_4^-$)[61] giving the largest decreases in K_a values for both receptors. It is notable, however, that larger percentage decreases in K_a values were observed for **2.22Te** compared with **2.22H** in the presence of water, implying the greater sensitivity of ChB-anion binding to solvent polarity than HB interactions. In addition, while **2.22Te** now showed a distinct binding preference for Br^- over the other halides, clear anti-Hofmeister selectivity was seen for **2.22H**. Hence, the

[§§] **2.22I** was reported to bind Cl^- very strongly in CD_3CN ($K_a > 10^4$ M^{-1}),[17] and hence reliable values of K_a could only be determined in d_6-DMSO. The titration of **2.22Te** with Cl^- was repeated in d_6-DMSO to enable a direct comparison of K_a values to be made.

observed solvent sensitivity of the ChB-anion binding strength, and the binding preference for heavier halides in the presence of water, mirrors the behaviour of XB interactions more so than HB.

Table 2.7. 1:1 stoichiometric association constants (K_a/ M^{-1}) of **2.22Te** and **2.22H** with different anions in CD_3CN/ D_2O 99:1 *v/v*.[a]

	2.22Te	**2.22H**
Cl^-	122 (1)	79 (3)
Br^-	183 (4)	62 (2)
I^-	139 (1)	44 (1)
$H_2PO_4^-$	100 (2)	-[c]

[a] Values of K_a determined using WinEQNMR2 software[60] by monitoring internal proton H_a for **2.22Te** and triazole proton for **2.22H** in all cases; errors (±) in parentheses; [host] = 1.0 mM, CD_3CN/ D_2O 99:1 *v/v*, *T* = 298 K). [b] Values not previously reported; [c] precipitation of host during titration.

Interestingly, CN^- was found to interact in a different way to **2.22Te** than the rest of the anions studied. As shown in Figure 2.28A, when ^1H NMR titrations were performed using **2.22Te** with TBACN in dry CD_3CN, a new set of peaks appeared upon CN^- addition (marked in red). Dramatic *upfield* shifts of the aromatic proton resonances of **2.22Te** were observed, with the largest change seen for the internal aromatic proton H_a. With 1.0 equivalent of CN^-, complete consumption of **2.22Te** was seen. When the titrations were repeated in CD_3CN/ D_2O mixtures containing increasing percentages of water, a similar behaviour was seen, although progressively greater excesses of CN^- were required to achieve complete consumption of **2.22Te** - a result of more extensive CN^- hydration. To determine if these observations were due to the presence of the electron-deficient Te atoms, which were susceptible to attack by the highly nucleophilic CN^- anion, TBACN was added to a dry-CD_3CN solution of **2.22H** as well. A similar change was observed (Figure 2.28B), clearly indicating that CN^- was interacting with **2.22H** in the same way independently of the Te atoms. Considering the chemical shifts of the resulting **2.22Te/H**-CN^- adduct, it is very likely that CN^- was causing the dearomatisation of the pyridinium group of both receptors by nucleophilic addition to the pyridinium group. Due to the retention of ^1H NMR symmetry after CN^- addition, substitution probably occurred at the *para*-position on the pyridinium ring (Scheme 2.13). Furthermore, the significant upfield shift of the

pyridinium *N*-methyl proton resonance from δ = 4.47 ppm to 3.30 ppm is consistent with a loss of the cationic nature of the pyridinium motif as well.

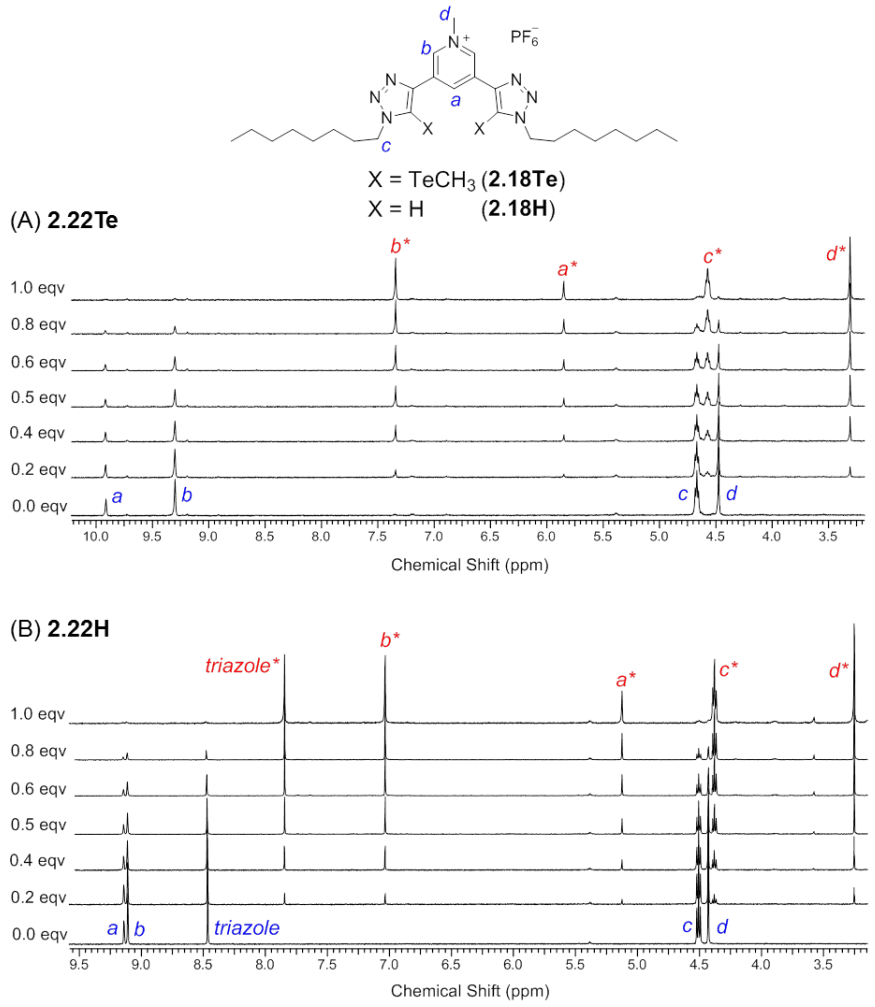
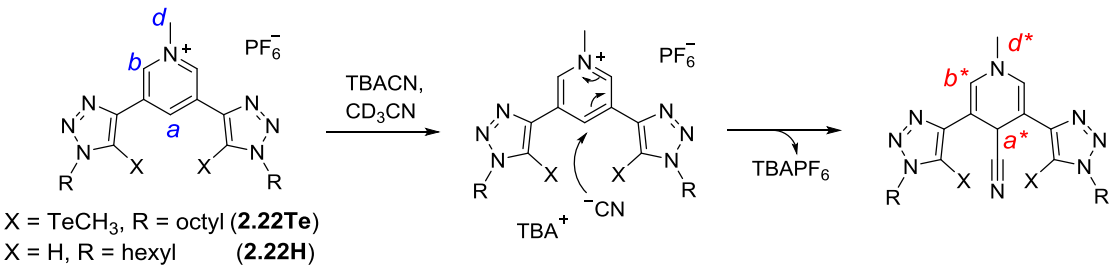


***Figure 2.28**. Partial ^{1}H NMR spectra of (A) **2.22Te** and (B) **2.22H** in the presence of increasing quantities of CN^-, showing the appearance of a new set of signals for the CN adducts ([**2.22**] = 1.5 mM, CD_3CN, T = 298 K). Proton labels of the native host are shown in blue, while those of the adduct are shown in red.*



***Scheme 2.13**. Proposed mechanism of reaction between receptors **2.22Te** and **2.22H** and CN^-. Labels (in blue and red) correspond to the peaks indicated in Figure 2.28.*

The proposed nucleophilic pyridine dearomatisation by CN^- is expected to bring about dramatic changes to the optical properties of **2.22Te**/**H**. UV-Vis spectra of **2.22Te**/**H** were recorded in the presence of increasing quantities of CN^- in acetonitrile (Figure 2.29A, C) and Cl^- (Figure 2.29B, D) for comparison. For both receptors, the addition of incremental quantities of CN^- led to dramatic reduction in the initial absorbance peak at λ = 263 nm, with the simultaneous appearance of a new lower energy absorption peak between 360-380 nm and an isosbestic point at c.a. 330 nm, clearly indicating that CN^- addition directly led to the formation of a new distinct chemical species. As a control, anion binding by Cl^- did not lead to appreciable spectral changes for both **2.22Te** and **2.22H**, suggesting only small perturbations to the frontier molecular orbital energy levels of both receptors upon non-covalent anion binding by ChB and HB interactions respectively. Indeed, these changes to the absorption

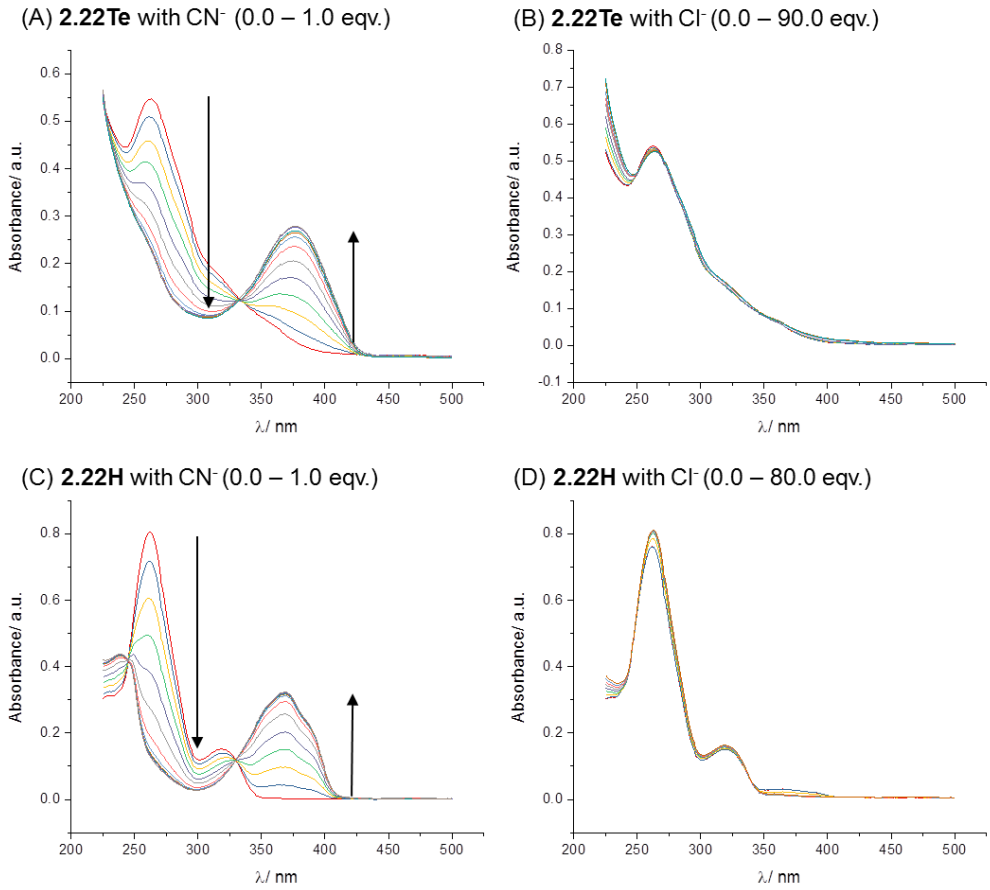


***Figure 2.29**. UV-Vis spectra of **2.22Te** with incremental quantities of (A) CN^- and (B) Cl^-; as well as those of **2.22H** with (C) CN^- and (D) Cl^- for comparison ([**2.22Te/H**] = 50 μM, CD_3CN, T = 293 K).*

spectra of **2.22Te/H** are consistent with those observed during nucleophilic addition of anionic nucleophiles (CN^- and OH^-) to the *para*-position of pyridinium salts in the literature, leading to formation of neutral 1,4-dihydropyridines**.**[93,94] In further support of the hypothesis, Gauthier *et. al.* found that this reaction could occur only in the presence of electron-withdrawing groups at the *meta*-positions of pyridinium salts,[95] once again consistent with the structures of **2.22Te/H**. It is noteworthy that despite the nucleophilicity of N_3^-, no evidence of a similar addition reaction was observed with **2.22Te/H** during titration experiments.

2.3.3 Thermodynamics of Chalcogen Bonding with Anions

Having determined the binding trends and solvent sensitivity of ChB-mediated anion binding, the thermodynamic (enthalpic and entropic) contributions of ChB···halide binding was determined by van 't Hoff analysis using variable temperature (VT) ^{1}H NMR titration experiments performed at 298, 313, 323 and 338 K with **2.22Te** in wet and dry CD_3CN. It is significant that **2.22Te** did not show any evidence of thermal decomposition even at 338 K in the presence of water, a testament to its thermal and chemical stability. From the values of 1:1 stoichiometric anion association constants (K_a) (Table 2.8), the enthalpic (ΔH/ kJ mol^{-1}) and entropic contributions ($T\Delta S$/ kJ mol^{-1}) to halide binding could be determined from the gradients and ordinates respectively of the resulting best-fit lines by plotting ln(K_a / M^{-1}) against T^{-1}/ K^{-1} according to Equation 1. As seen from Figure 2.30, all van 't Hoff plots gave excellent linearity (Pearson's R > 0.990), showing the invariance of the enthalpic contributions of anion complexation and heat capacity of the system in the temperature range studied. For comparison, analogous van 't Hoff analyses were also performed using **2.22H.** The calculated thermodynamic parameters (ΔG, ΔH, $T\Delta S$/ kJ mol^{-1}) for halide binding by **2.22Te/H** in wet and dry CD_3CN are summarised in Table 2.9.

$$\ln K_a = -\frac{\Delta H}{RT} + \frac{\Delta S}{R} \qquad \text{(Equation 1)}$$

Table 2.8. 1:1 stoichiometric association constants (K_a/ M^{-1}) of receptors **2.22Te** and **2.22H** at various temperatures in dry and wet CD_3CN.[a]

T/ K	Receptor 2.22Te				Receptor 2.22H	
	Dry CD_3CN			CD_3CN/ D_2O 99:1	Dry CD_3CN	CD_3CN/ D_2O 99:1
	Cl^-	Br	I^-	Br^-	Cl^-	Br^-
298	652 (13)	501 (16)	305 (11)	183 (4)	263 (8)	62 (2)
313	484 (3)	348 (9)	216 (5)	141 (3)	252 (7)	59 (2)
323	410 (18)	295 (8)	175 (3)	117 (3)	242 (7)	58 (2)
338	356 (3)	242 (2)	139 (2)	102 (3)	229 (8)	56 (2)

[a] Values of K_a determined using WinEQNMR2 software[60] by monitoring internal proton H_a in all cases; unless otherwise stated, a host-guest 1:1 stoichiometric binding model was used; errors (±) in parentheses.

Table 2.9. Thermodynamic parameters (ΔG/ ΔH/ TΔS) for anion binding by **2.22Te** and **2.22H** in dry and wet acetonitrile.[a]

	Solvent	Anion	Δ*G*/ kJ mol^{-1}	Δ*H*/ kJ mol^{-1}	*T*Δ*S*/ kJ mol^{-1}	Pearson's R [b]
2.22Te	CD_3CN	Cl^-	- 16.1	- 12.8	+ 3.2	0.991
	CD_3CN	Br^-	- 15.4	- 15.2	+ 0.1	0.993
	CD_3CN	I^-	- 14.2	- 16.6	- 2.4	0.998
	CD_3CN/ D_2O 99:1	Br^-	- 12.9	- 12.5	+ 0.4	0.993
2.22H	CD_3CN	Cl^-	- 13.8	- 2.9	+ 10.9	0.994
	CD_3CN/ D_2O 99:1	Br^-	- 10.2	- 2.1	+ 8.1	0.995

[a] Thermodynamic parameters were determined by van 't Hoff analysis by plotting ln(K_a/ M^{-1}) against T^{-1}/ K^{-1}, with the host-guest 1:1 association constants (*K*) determined by ^{1}H NMR titrations at 298, 313, 323, 338 K; Errors for individual titrations < 10 %; [host] = 1.0 mM. [b] Pearson's R reflects the quality of linear fit used to extract the thermodynamic data.

From Table 2.9, the ChB-mediated binding of all halides to **2.22Te** in dry CD_3CN is enthalpically dominated in all cases. Halide binding becomes progressively more exothermic, with the magnitude of Δ*H* increasing from 12.8 kJ mol^{-1} for Cl^- to 16.6 kJ mol^{-1} for I^-. At the same time, the increased exothermicity is offset by more unfavourable binding entropies for the heavier halides: the favourable binding entropy of Cl^- decreases to an almost negligible contribution for Br^-, and becomes disfavoured for I^-. Significantly, a larger loss of entropy was observed down the halide group than a gain in enthalpy, which resulted in an overall less exergonic free energy of binding from Cl^- to I^-. Possibly, these observations can be accounted

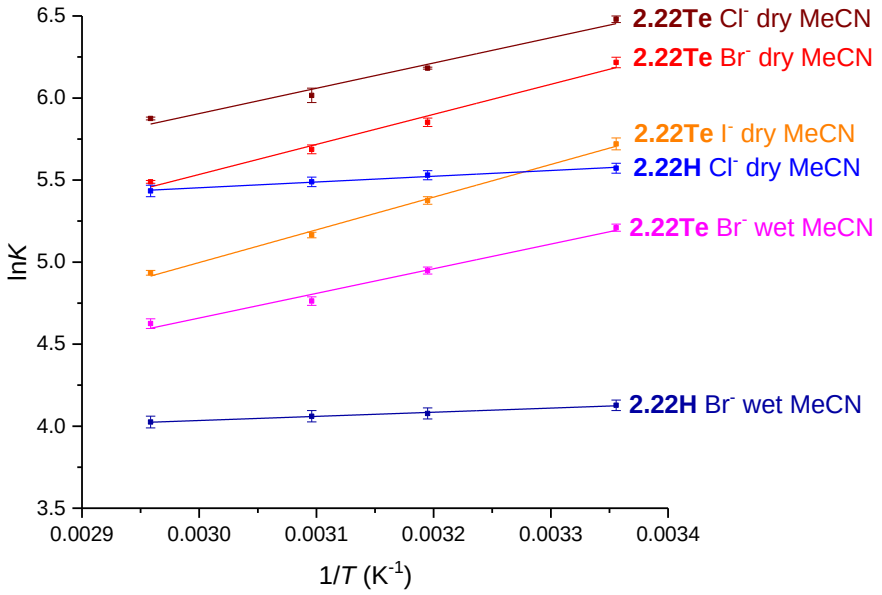


***Figure 2.30**. van 't Hoff plots showing the changes of association constant (K_a/ M^{-1}) of **2.22Te** and **2.22H** with different halides at different temperatures (T/ K), determined using VT ^{1}H NMR titration experiments. Errors (±) are indicated as error bars ([host] = 1.0 mM, T = 298, 313, 323, 338 K).*

for by a tighter association between **2.22Te** and the heavier halides (reflected by the more negative ΔH values), while at the same time giving an overall greater loss of degrees of freedom in the system, resulting in a larger decrease in entropy. It is noteworthy that a similar trend was observed by Huber and co-workers using isothermal titration calorimetry (ITC) to probe the binding of Cl^-, Br^- and I^- to a dicationic iodoimidazolium XB host in dry CH_3CN: down the halide series, binding became increasingly exothermic accompanied by gradually decreasing entropy contribution (ΔS was positive in all cases).[96] This suggested that XB and ChB interactions were inherently similar in favouring association with the heavier halides, as well as the importance of considering both enthalpic and entropic terms in thermodynamic analyses of anion binding.

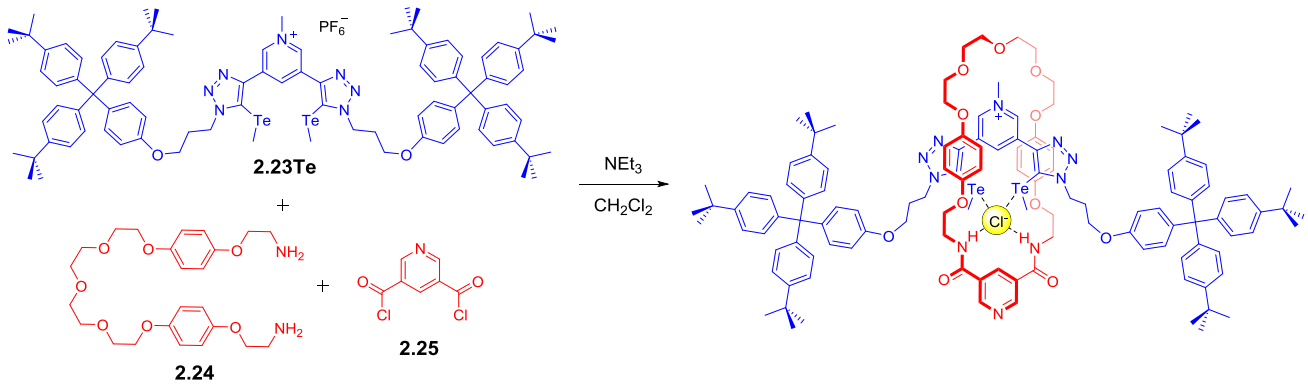
Although **2.22Te** and **2.22H** both bind Cl^- by favourable enthalpic and entropic contributions, Cl^- binding to **2.22H** in dry CD_3CN is driven mainly by entropy, with the $T\Delta S$ term accounting for nearly 80 % of the magnitude of ΔG. The binding of anions to HB host molecules in polar solvents with strong HB basicity[66] such as acetonitrile has been shown to be entropically-driven in a number of independent studies,[97–100] and has been attributed to

desolvation of the Lewis acidic host binding site during anion complexation. As such, this contrast seen between **2.22Te** and **2.22H** suggests a smaller degree of desolvation for the former during anion binding. Furthermore, the much more favourable ΔH of binding by **2.22Te** observed implied stronger halide association by ChB interactions compared to HB, possibly arising from a greater degree of covalency and charge-transfer, as determined by WBI estimation aforementioned in Section 2.2.6.

Although ^{1}H NMR binding studies have shown that the presence of water is detrimental to ChB-anion binding (Table 2.7), van 't Hoff analysis was insightful in elucidating the origins of this reduced affinity and the influences of water in the solvent. From Table 2.9, although 1 % D_2O *v/v* retained the enthalpic dominance in binding, the loss in resulting Br^- affinity was mainly due to a significant decrease in the magnitude of the enthalpic term ($\Delta\Delta H$ = - 2.7 kJ mol^{-1}), as only a small increase in binding entropy ($\Delta[T\Delta S]$ = + 0.3 kJ mol^{-1}) was observed. While the increase in the $T\Delta$S term could be accounted for by Br^- dehydration with the release of more free solvent (water) molecules during binding, the enthalpic loss is consistent with observations from the computational binding studies performed using rotaxane **2.20Se$_2$H** in the presence of water. Possibly, the binding of Br^- brings water molecules in its hydration shell into close proximity to the ChB-donor Te atoms of **2.22Te**, which disrupts the ChB···Br^- interactions more frequently, leading to the diminished exothermicity of Br^- binding. Contrastingly, Br^- binding to **2.22H** is still entropically-dominated in the presence of water, underscoring the importance of host/guest desolvation in the HB-mediated anion binding process.

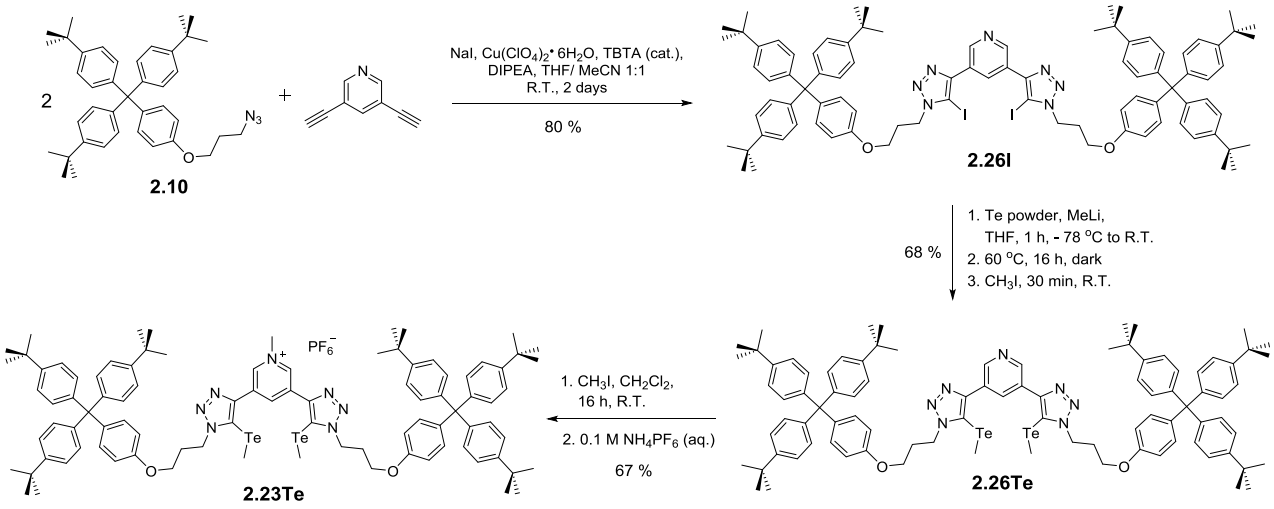
2.3.4 Towards an Anion-templated Cationic Tellurium-based ChB [2]Rotaxane

Building on the chemical stability and potency of the pyridinium-3,5-bis(methyltelluro-triazole) motif of **2.22Te** in anion binding, it was hoped that by incorporating this ChB anion recognition motif in an axle structure (**2.23Te**), [2]rotaxane synthesis by macrocycle clipping around the axle could be achieved by anion templation using Cl^- released in the condensation reactions between bis-amine **2.24** and bis-acid **2.25** (Scheme 2.14). Indeed, the incorporation of the analogous XB pyridinium-3,5-bis(iodotriazole) motif into the structures of macrocycles and axle components has enabled the successful Cl^- anion-templated synthesis of a [2]catenane[17] and a range of [2]rotaxanes[75,76,101] for anion recognition.



***Scheme 2.14**. Proposed synthesis of a cationic ChB [2]rotaxane by Cl^- templation.*

The synthesis of axle **2.23Te** is summarised in Scheme 2.15. Following the procedure developed earlier for macrocycle **2.1Te**, a CuAAC reaction between 3,5-di(ethynyl)pyridine and two equivalents of stopper azide **2.10** under 'one-pot iodo-Click' conditions[25] afforded the neutral bis(iodotriazole) precursor **2.26I** in 80 % yield. Curiously, when nucleophilic aromatic substitution was performed on **2.26I** using the *in-situ* generated $[TeCH_3]^-$ anion, a 3 hour reaction at 80 ^oC afforded poor product conversion. However, when the reaction was left to proceed overnight (16 h) at a reduced temperature of 60 ^oC to minimise $TeCH_3$ lability, complete consumption of **2.26I** occurred to form the target product **2.26Te**. Subsequent pyridine *N*-methylation and anion exchange afforded the cationic axle **2.23Te** in 67 % isolated yield.



***Scheme 2.15**. Synthesis of cationic ChB axle **2.23Te**.*

Using isolated axle **2.23Te**, rotaxane synthesis was attempted using bis-amine **2.24** and bis-acid chloride **2.25**, prepared using previously-reported procedures,[102] as shown in Scheme 2.14. To a vigorously-stirred anhydrous CH_2Cl_2 solution of **2.23Te** (5 mM) and excess trimethylamine base was added **2.24** and **2.25** in a 1:1 molar ratio and the reaction was left overnight under an inert N_2 atmosphere at ambient temperature. Interestingly, analysis of the crude reaction mixture by ESI mass spectrometry (Figure 2.31) revealed that although formation of macrocycle (*m/z* = 597.3 $[M + H]^+$) occurred from the 1:1 condensation reaction between **2.24** and **2.25**, only trace [2]rotaxane was formed (*m/z* = 2197.7 $[M]^+$). Unfortunately, the yield of the rotaxane was too low for it to be isolated by preparatory TLC and characterised. More worryingly, the mass spectrum of the crude reaction mixture (Figure 2.31) showed evidence of some $TeCH_3$ loss from axle **2.23Te** during the reaction itself (peak at *m/z* = 1460.7), which may be a result of interaction with the amine base or free Cl^- in the reaction solution for a prolonged duration (16 h). When the reaction was attempted again with a lower starting axle concentration of 2 mM to favour macrocycle ring-closing around the axle, the same results were obtained with only trace formation of the target rotaxane. While it is tempting to attribute the lack of success to the weaker Cl^- affinity of the ChB anion recognition motif compared to the iodine-containing XB analogue, it should also be noted that the HB pyridinium-bis(prototriazole) motif, which forms even weaker anion complexes than the ChB

analogue, has been successfully demonstrated to allow preparation of a [2]catenane[103] and [2]rotaxane[55] with Cl^- templation, as well as pseudorotaxane complexes with a range of anions.[104] Therefore, it may be more likely that Cl^- binding by the $TeCH_3$ groups, occurring out-of-plane with the pyridinium-3,5-bis(triazole) motif as demonstrated for macrocycles **2.9Se** and rotaxane **2.20Se$_2$H**, may be occurring in a geometry unsuitable for the macrocycle to ring-close around the axle. Alternatively, the steric bulk of the $TeCH_3$ groups may be disfavouring rotaxane formation over that of free macrocycle.

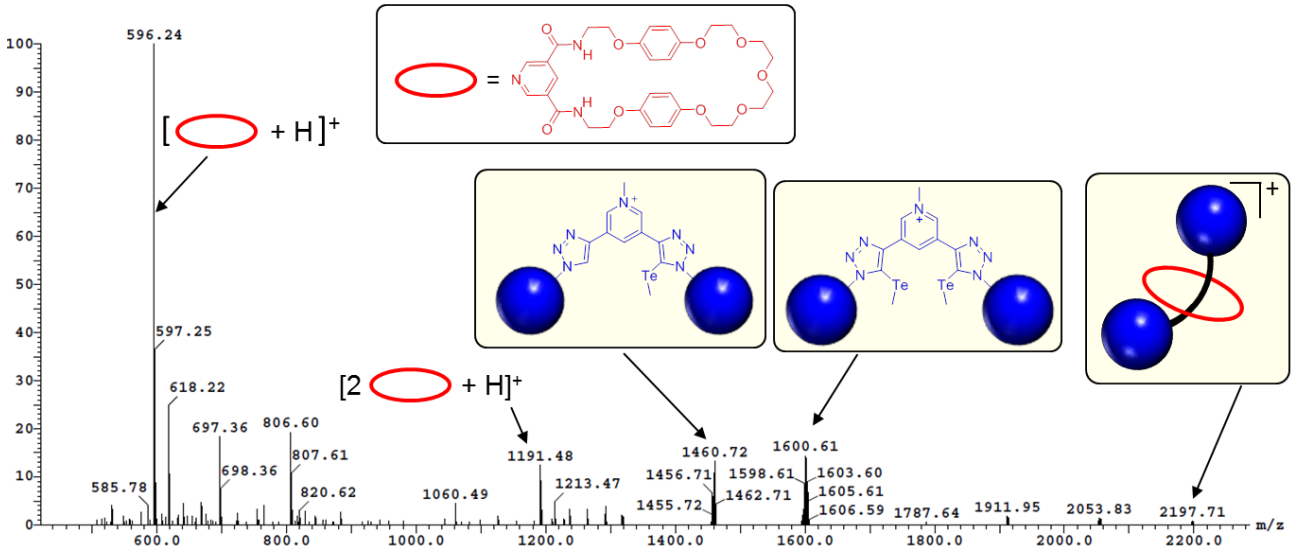
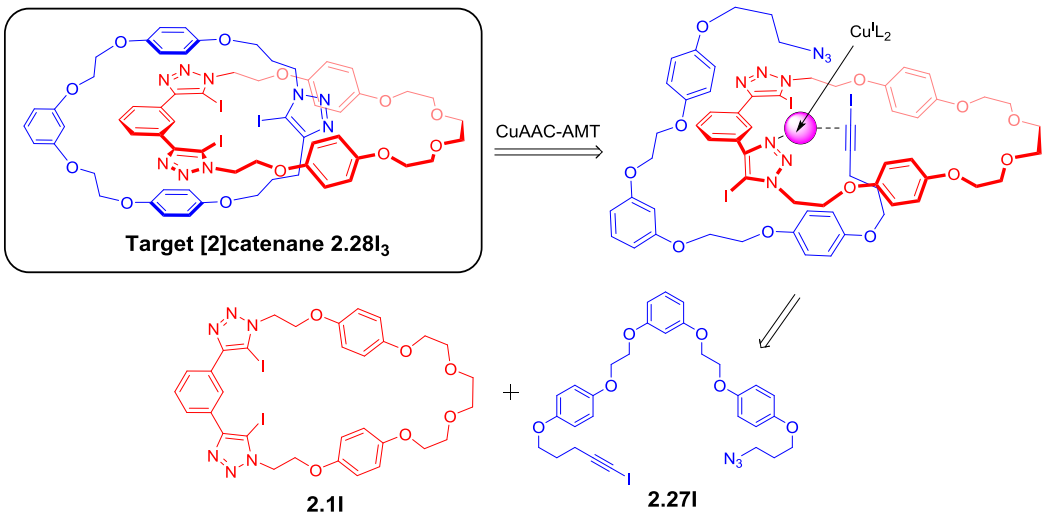


***Figure 2.31**. ESI mass spectrum analysis of the Cl^--templated rotaxane synthesis crude reaction mixture. Relevant peaks are labelled.*

2.4 Towards Neutral Halogen and Chalcogen Bonding [2]Catenanes

2.4.1 Active Metal Template Synthesis of Neutral Halogen Bonding [2]Catenanes

The success of the CuAAC-AMT reaction to synthesise neutral all-XB rotaxanes (**2.12I$_3$** and **2.15I$_4$)**, which showed strong anion binding behaviour in wet and dry acetone dominated by XB interactions, stimulated the design of an all-XB catenane for a similar purpose. Following the procedure developed by Leigh and co-workers for the CuAAC-AMT synthesis of [2]catenanes (detailed in Section 2.1.2 and Figure 2.3),[12] the endotopically-coordinated Cu(I) in macrocycle **2.1I** was envisaged to perform an 'iodo-Click' CuAAC ring-closing reaction through its cavity using catenane precursor thread **2.27I**, which contained a terminal iodoalkyne and azide (Scheme 2.16).*** With the three iodotriazole units surrounding the anion binding cavity of the target neutral [2]catenane **2.28I$_3$**, it was hoped that **2.28I$_3$** could exhibit similar anion binding behaviour as rotaxane **2.12I$_3$.**

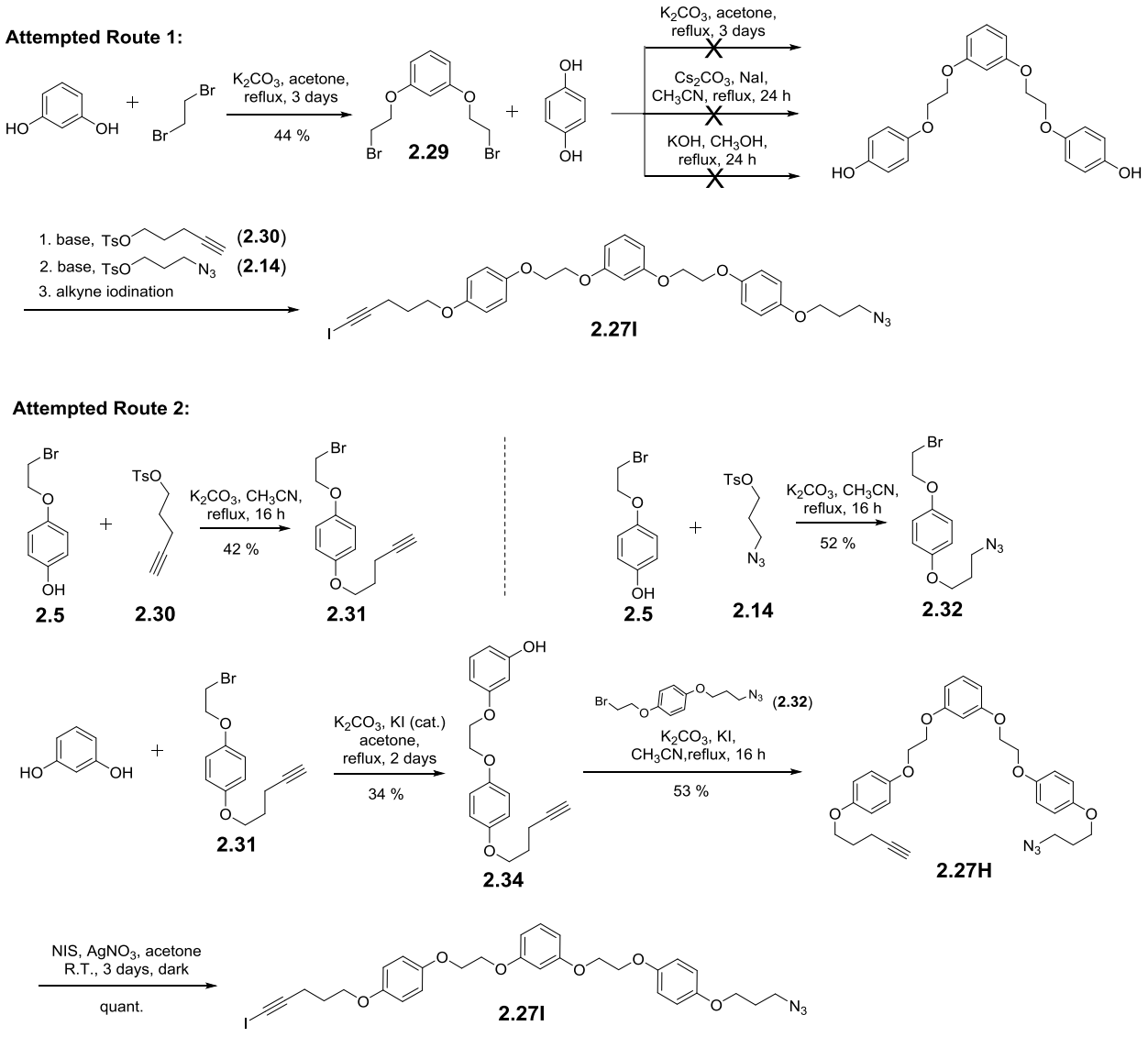


***Scheme 2.16**. Retrosynthetic strategy for the synthesis of the tris(iodotriazole) all-XB [2]catenane **2.28I$_3$**.*

The synthesis of macrocycle precursor **2.27I** was initially pursued. As shown in Scheme 2.17 (Attempted route 1), Williamson ether synthesis was first performed using commercially-available resorcinol and an excess of 1,2-dibromoethane under basic conditions

*** The work towards synthesising the all-XB neutral [2]catenanes was performed together with David Ascough, a Centre for Doctoral Training (CDT) student on rotation in the Beer Group.

to afford the dibromo intermediate **2.29** in 44 % yield. This synthon presented the possibility of further nucleophilic substitution with an excess of hydroquinone to form a bis-phenol, which could then be subjected to sequential reactions with alkyne **2.30**[105] and azide **2.14**[53], prepared from reported procedures. Late-stage alkyne iodination was expected to form the target **2.27I**. However, it was surprising that despite performing the hydroquinone substitution reaction under vigorously-degassed conditions using a five-fold excess of hydroquinone under various basic conditions, no trace of the expected bis-phenol compound could be detected.



***Scheme 2.17**. Attempted forward synthesis of catenane precursor **2.27I**.*

An alternative strategy was then adopted (Scheme 2.17B). Starting from intermediate **2.5** (synthesis described in Scheme 2.2), S_N2 ether formation was achieved using **2.30** and **2.14** under basic conditions to access the individual terminal (proto)alkyne (**2.31**) and azide (**2.32**) 'arms' of precursor **2.27I** in 42 % and 52 % yields respectively. These 'arms' were sequentially installed onto resorcinol: in the presence of excess K_2CO_3 base and catalytic quantities of KI, monoalkylation of resorcinol with **2.31** was achieved in refluxing acetone to give **2.33** in 34 % yield. Appending the second 'arm' to afford **2.27H** however, necessitated using more forcing conditions, with stoichiometric quantities of KI at higher temperatures in refluxing acetonitrile. It is notable that the modest yields of **2.33** and **2.34** were a result of poor solubility of these compounds, which hampered chromatographic purification. Pleasingly, terminal alkyne iodination was successfully performed using established conditions with *N*-iodosuccinimide (NIS) and $AgNO_3$,[106] to afford the target compound **2.27I** quantitatively. Encouragingly, the solubility of **2.27I** in common organic solvents was significantly better than that of **2.27H**, possibly as a consequence of the appended lipophilic iodine atom.

The synthesis of target catenane **2.28I** was attempted as summarised in Table 2.10. Initial conditions were those reported by Leigh and co-workers in their successful CuAAC 'proto-Click' AMT synthesis of catenanes at 80 ^oC in 1,2-dichloroethane (Entry 1).[12] Although this attempt led to complete consumption of **2.27I**, only trace quantities of CuAAC ring-closed macrocycle was detected by ESI-MS[†††] and TLC, and no catenane was observed after 14 days. Large quantities of unidentifiable side products were observed at the base of the TLC plate, possibly resulting from the thermal decomposition of **2.27I** or unproductive non-cyclic oligomerisation. The reaction was repeated at ambient temperature to reduce possible thermal decomposition (Entry 2). Instead, only partial consumption of **2.27I** resulted, and similar unidentifiable side products were observed at the expense of ring-closed macrocycle and catenane. To maximise the chances of CuAAC ring-closing, the reaction was attempted at 80 ^oC with a lower concentration of reactants (Entry 3) to afford similar observations as Entry 1.

[†††] Although the ring-closed macrocycle has the same mass as acyclic thread **2.27I**, the latter does not seem to be detectable via ESI-MS. Evidence of the presence of the iodotriazole-containing macrocycle was obtained by TLC, with a spot having a different R_f as **2.27I** but having an identical mass by ESI-MS analysis. Presumably, the iodotriazole unit formed on ring-closing of **2.27I** allowed protonation using this technique and was thus detectable.

Finally, in order to increase the probability of catenane formation, the quantity of thread **2.27I** added to the reaction was doubled. Disappointingly, no trace of target catenane could be detected by ESI-MS, TLC or ^{1}H NMR analysis of the crude reaction mixture.

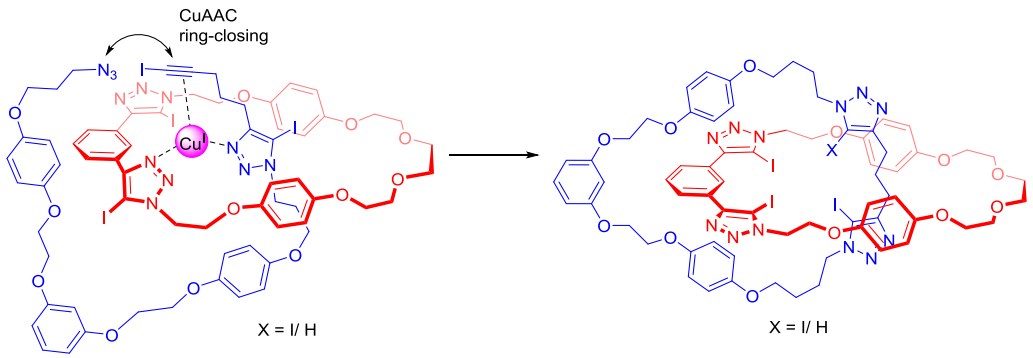
Table 2.10. Attempted reaction conditions towards the synthesis of catenane **2.28I$_3$**.[a]

Entry	Conc. of **2.1I**]/ mM	Equivalents of **2.27I**	Equivalents of $Cu(CH_3CN)_4PF_6$	Solvent	Reaction time/ days	*T*/ °C	Result
1	6.5	5.0	1.0	$(CH_2Cl)_2$	14	80	Complete consumption of **2.27I** but no catenane detected
2	6.5	5.0	1.0	CH_2Cl_2	14	R.T.	Partial consumption of **2.27I**, no catenane detected
3	1.0	5.0	1.0	$(CH_2Cl)_2$	14	80	Complete consumption of **2.27I** but no catenane detected
4	1.0	10.0	1.0	$(CH_2Cl)_2$	14	80	Complete consumption of **2.27I** but no catenane detected

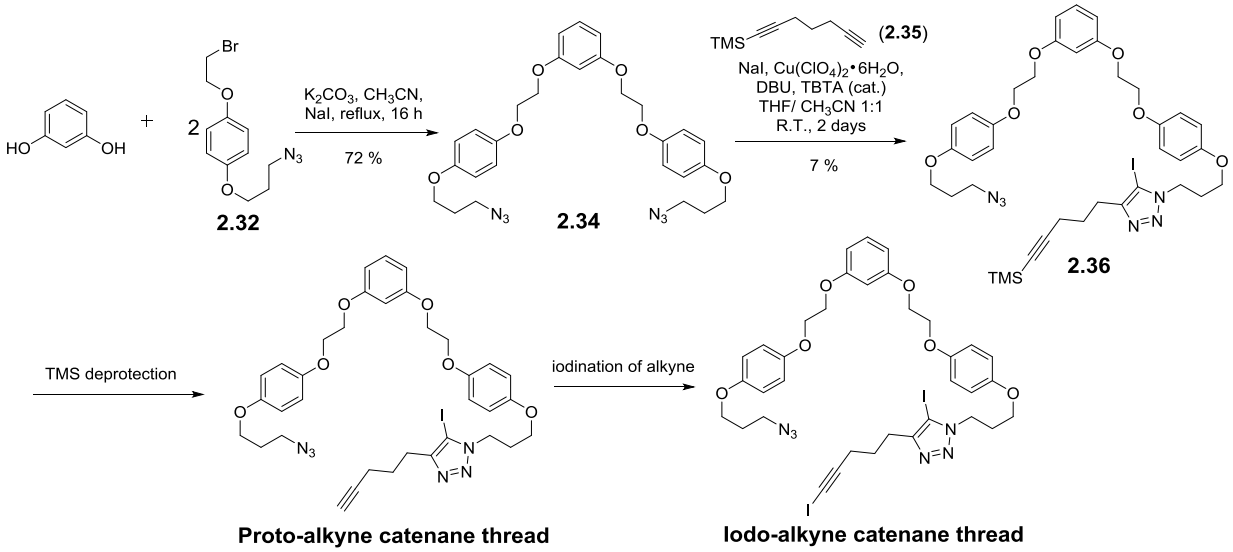
[a]All reactions were performed using vigorously degassed solvents and were performed under an inert atmosphere of N_2.

A second strategy at synthesising neutral XB catenanes for anion recognition was undertaken (Scheme 2.18), where a catenane precursor thread containing an iodotriazole group terminated with iodo/proto-alkyne and azide functionalities was designed. The Lewis-basicity of the iodotriazole *N*[3] atoms on both macrocycle **2.1I** and the catenane thread may allow Cu(I) to be coordinated between them, potentially facilitating the penetration of the thread through the macrocycle, as well as bringing the reactive Cu(I) catalytic centre into close proximity with the terminal alkyne and azide functionalities to promote CuAAC ring-closing.

The attempted synthesis of the catenane precursor thread followed the route shown in Scheme 2.19. Williamson ether synthesis involving resorcinol and azide **2.32** performed under basic conditions in the presence of stoichiometric quantities of NaI afforded the bis-azide **2.34** in a decent yield of 72 %. Using the mono-TMS-protected 1,6-heptadiyne **2.35**, prepared according to a literature procedure,[107] direct iodotriazole formation under 'one-pot' conditions[25] gave the thread precursor **2.36** in a poor yield of only 7 %. Further analysis of the crude reaction mixture indicated the poor product yield was likely due to dimerisation of alkyne **2.35** during the reaction, possibly by Cu(I)-catalysed alkyne-alkyne coupling. Given the poor isolated yield of **2.36**, this route was abandoned.

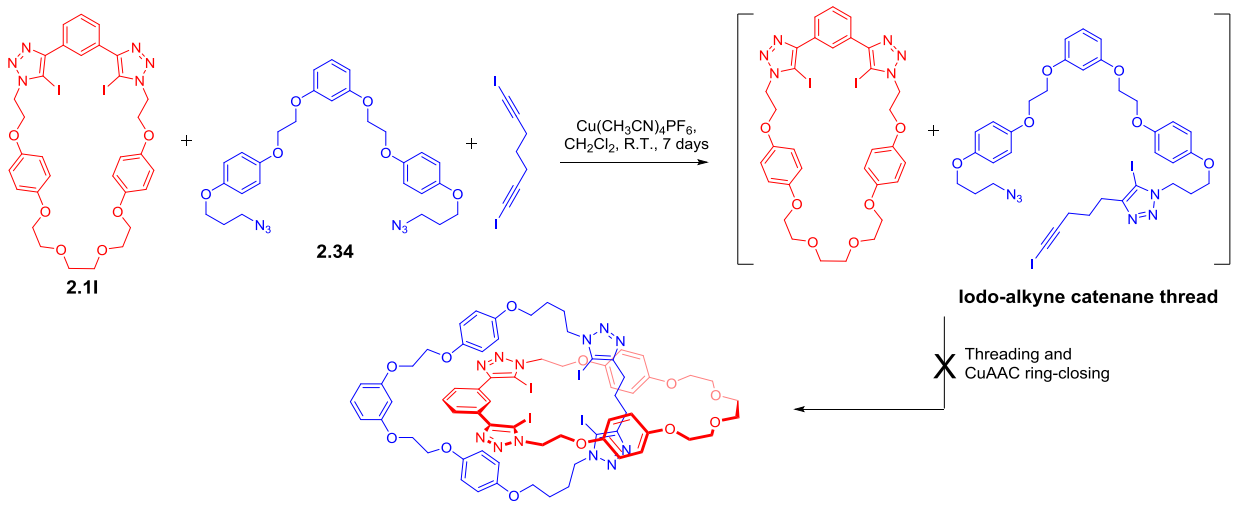


***Scheme 2.18**. The second proposed strategy for the CuAAC-AMT synthesis of a neutral XB [2]catenane.*



***Scheme 2.19**. Attempted synthesis of catenane thread precursor.*

A final attempt towards the neutral XB catenane was carried out where the iodo-alkyne thread generated *in-situ* participates in the same CuAAC-AMT catenane synthesis within the same reaction (Scheme 2.20). To a 5.0 mM solution of macrocycle **2.1I** in THF, 5.0-fold excess of bis-axle **2.34** and bis-iodo-heptadiyne were added, together with 1.0 equivalent of $[Cu(CH_3CN)_4]PF_6$. Although ESI-MS reaction monitoring revealed the presence of a peak at *m/z* = 893.1 $[M + H]^+$, corresponding to either ring-closed macrocycle formed from the double CuAAC reaction of **2.34** and bis-iodo-heptadiyne, or more likely, the acyclic iodo-alkyne thread, no evidence of the target catenane was observed after 7 days. Repeating the reaction using two equivalents of $[Cu(CH_3CN)_4]PF_6$ in 1,2-dichloroethane at 80 ^oC also failed to produce any trace of the target catenane after the same duration.

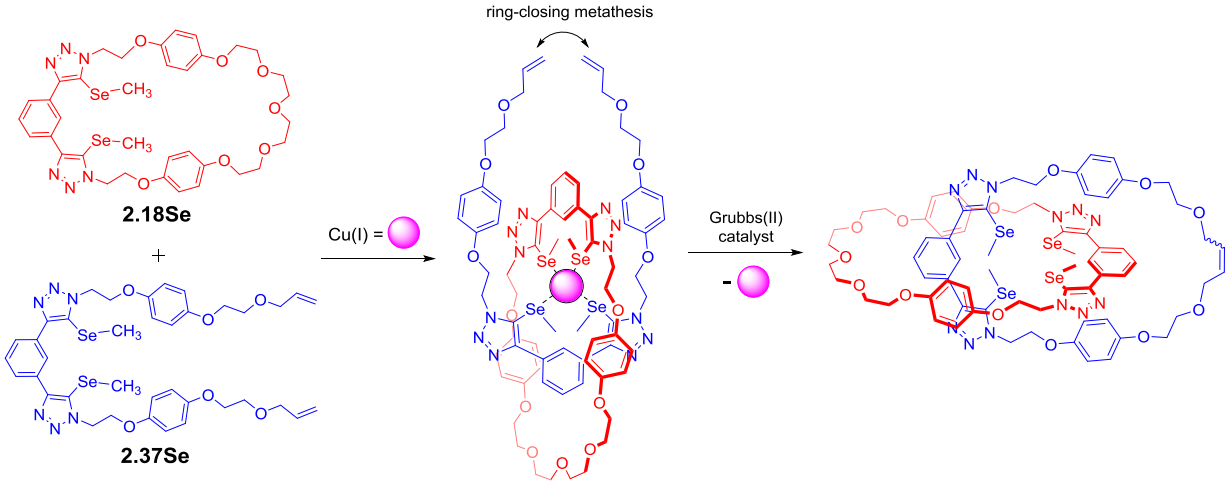


***Scheme 2.20**. Attempted direct synthesis of a neutral XB catenane via a double iodo-Click strategy.*

Given the numerous unsuccessful attempts towards the preparation of a neutral XB catenane using the CuAAC-AMT strategy, it may be reasonable to surmise that the conformations of the complex formed between Cu(I), macrocycle **2.1I** and the alkyne-azide functionalised threads are unsuitable for catenane formation by Click ring-closing. Indeed, successful catenane syntheses by the AMT protocol using the CuAAC or Glaser/ Cadiot-Chodkiewicz alkyne-alkyne coupling conditions all involved the use of a templating macrocycle component which possessed at least one endotopically-oriented Lewis-basic nitrogen atom on a pyridine, bipyridine or phenanthroline motif.[12,108]

2.4.2 Towards A Neutral Chalcogen Bonding [2]Catenane by Passive Metal Templation

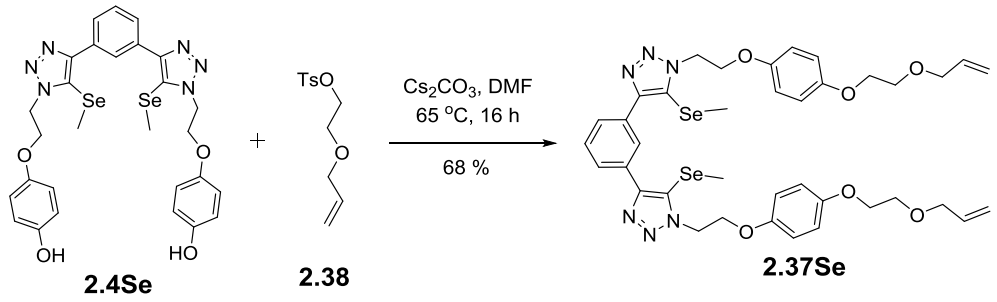
Recognising the ability of the methylchalcogeno-triazoles to coordinate Cu(I) via the chalcogen atoms (Section 2.2.2), the synthesis of a [2]catenane containing a binding cavity surrounded by four ChB donor groups via a passive metal template approach was attempted.[109,110] As shown in Scheme 2.21, the ChB thread **2.37Se** could penetrate the macrocycle cavity of **2.18Se** by coordination with Cu(I), with the metal centre ligated by the four Se atoms in a tetrahedral arrangement. For this purpose, the larger macrocycle **2.18Se** was chosen to spatially accommodate the bulky tetrahedral coordination sphere around the Cu(I) template in the resulting pseudorotaxane complex. With the catenane precursors organised in this manner, alkene ring-closing metathesis (RCM) may then produce the interlocked product.



***Scheme 2.21**. Passive metal template strategy for the synthesis of a [2]catenane bearing an all-ChB binding cavity.*

ChB thread **2.37Se** was prepared in a yield of 68 % by heating a mixture of bis-phenol **2.4Se** and allyloxyethyl tosylate **2.38** (prepared according to a literature protocol[111]) in the presence of excess Cs_2CO_3 base (Scheme 2.22). Catenane synthesis was then attempted via the reaction conditions of an equimolar mixture of macrocycle **2.18Se** (10 mM) $[Cu(CH_3CN)_4]PF_6$ and **2.37Se** in CH_2Cl_2, to which Grubbs' 2nd generation catalyst (0.1 molar equivalents) was added. After an overnight reaction in the dark under N_2, TLC and ESI-MS

analysis of the crude mixture revealed that surprising, no RCM reaction of **2.37Se** had occurred, even when an additional 0.1 molar equivalents of the Grubbs' catalysts was added. Possibly, the susceptibility of the Grubbs' catalyst to coordination by Lewis basic sites (e.g. the Se atoms) on **2.18Se** and **2.37Se**, may compromise its reactivity towards the RCM reaction.



***Scheme 2.22**. Synthesis of ChB bis-vinyl catenane thread **2.37Se**.*

The reaction was repeated using the 2nd-generation Hoveyda-Grubbs' catalyst (0.1 molar equivalents), which has greater tolerance and stability towards Lewis basic functionalities.[112] Pleasingly, after stirring the equimolar mixture overnight under N_2, complete consumption of **2.37Se** was observed by TLC and ESI-MS analyses, with evidence of the ring-closed macrocycle product of **2.37Se** seen at *m/z* = 813.2 $[M + H]^+$. However, only trace quantities of the target catenane was seen by ESI-MS (*m/z* = 1641.4 $[M + H]^+$), which proved challenging to isolate even by preparatory TLC. A repeat of the reaction using half ([**2.18Se**] = 5 mM) the original concentration of reactants with the Hoveyda Grubbs catalyst (0.2 molar equivalents) also failed to yield satisfactory quantities of the target catenane, although complete consumption of thread **2.37Se** was consistently observed.

The unsuccessful passive metal template synthesis of the target ChB catenane prompted a more detailed investigation into the Cu(I) binding properties of thread **2.37Se**. A titration experiment was performed where increasing quantities of $[Cu(CH_3CN)_4]PF_6$ was added to a solution of thread **2.37Se** in d_6-acetone. From Figure 2.32A, the presence of 1.0 equivalent of Cu(I) resulted in significant broadening of the spectrum in the aromatic region such that the resonances of H_a, H_b and H_c cannot be unambiguously discerned. However, the

once coincidental hydroquinone signals were split into four distinct doublets, with a pair perturbed downfield relative to the original signal and the other upfield, which could be assigned using 2D COSY spectroscopy. Further splitting and broadening of signals arising from H_d and H_e could be seen as well. Together, these observations suggested that **2.37Se** was binding Cu(I) asymmetrically, likely via only one Se atom, unlike the symmetric bidentate coordination mode of macrocycle **2.1Se** (Section 2.2.2). Considering the identical Cu(I)-ligating benzene-1,3-(methylseleno-triazole) functionality in both **2.1Se** and **2.37Se**, the contrasting Cu(I) coordination mode observed further implied that the bidentate Cu(I) binding by macrocycle **2.1Se** could be a result of its more preorganised macrocyclic nature, which restricts the possibility of both triazole-bearing 'arms' twisting out of plane to minimise the steric clash between the bulky $SeCH_3$ units. The inability of **2.37Se** to bind Cu(I) between its Se atoms may account for the failure of the passive metal templation of the ChB catenane. Indeed, when 1.0 equivalent of $[Cu(CH_3CN)_4]PF_6$ was added to an equimolar mixture of **2.18Se** and **2.37Se** in d_6-acetone, extensive broadening and loss of spectral resolution of the ^{1}H NMR spectrum resulted (Figure 2.32B), notably differing from the individual Cu(I) adducts of **2.18Se** and **2.37Se**. This indicated the formation of numerous Cu(I) coordination complexes between both ChB donor molecules in solution, and not the well-defined pseudorotaxane complex with tetrahedral Cu(I) coordination necessary for passive metal templated catenane formation to occur.

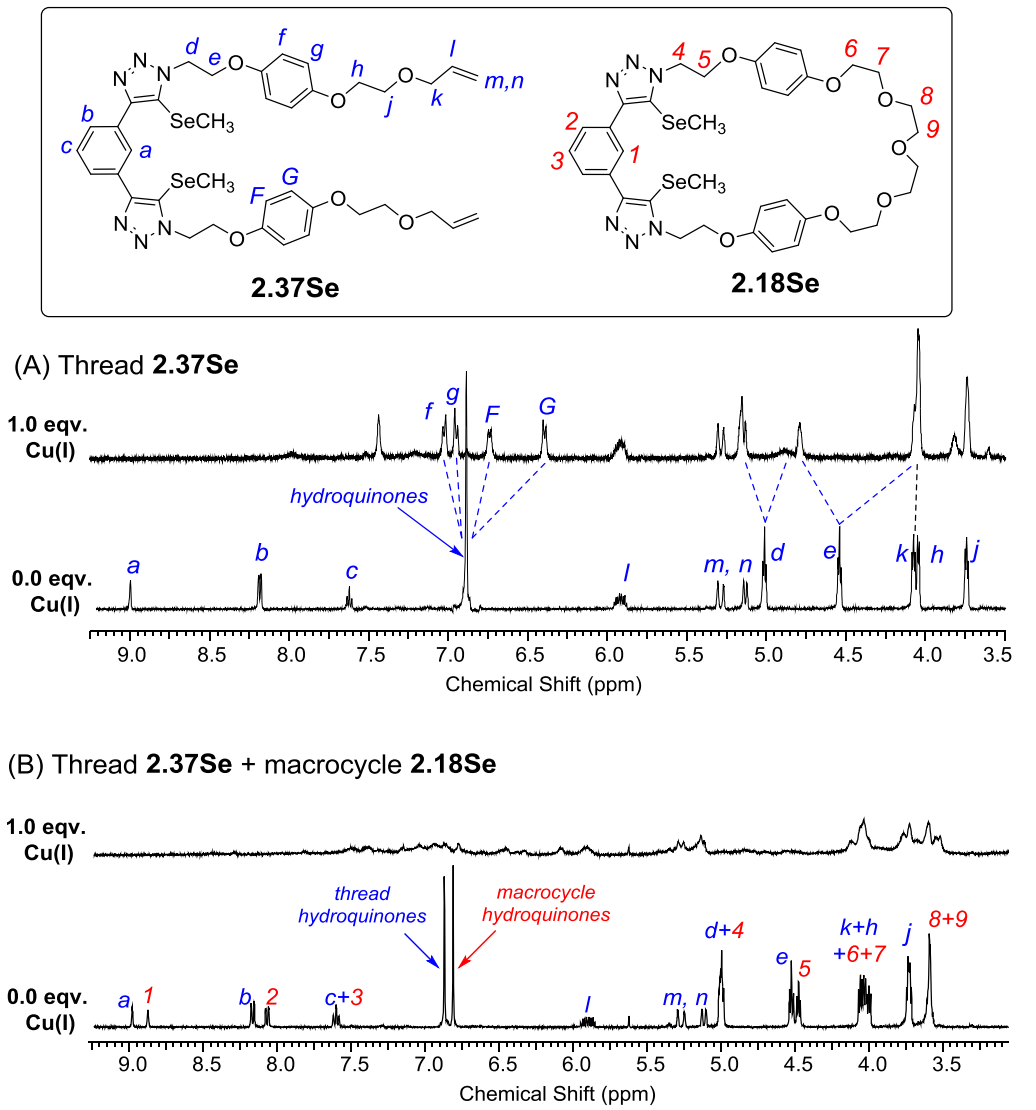


***Figure 2.32**. Partial ^{1}H NMR spectra of (A) ChB catenane thread **2.**37Se and (B) an equimolar mixture of **2.37Se** and macrocycle **2.18Se** in the presence of 0.0 and 1.0 equivalent of Cu(I) ([**2.37Se**] = [**2.18Se**] = 1.5 mM, d_6-acetone, T = 298 K).*

2.5 Conclusions and Future Work

2.5.1 Conclusions

In conclusion, it has been demonstrated in this chapter that substitution of the 5-position on a triazole unit with iodine and chalcogen (Se/Te) atoms can afford stable, robust and potent XB- and ChB-donor groups for anion recognition in solution. Notably, the Lewis-amphoteric nature of the chalcogen atoms on the ChB methylchalcogeno-triazoles allows coordination of both metal cations and anions. By capitalising on the exo/endo-conformational flexibility of HB/ ChB/ XB-donor triazole-containing macrocycles, a range of rotaxanes can be

accessed in reasonable yields by CuAAC-AMT protocols. These include the first ever examples of neutral and cationic interlocked anion host structures containing ChB-donor groups, whose anion binding properties were demonstrated to be dominated by ChB interactions. Using heteronuclear ^{77}Se and ^{125}Te NMR, the ChB donor atoms were demonstrated to be highly sensitive to changes in their electronic environments on anion binding, although the magnitudes of their signal perturbations may not necessarily be reflective of binding affinities.

Solution-phase anion binding studies performed on the neutral acyclic and interlocked σ-hole donor host molecules offer numerous empirical insights on the similarities and differences between XB, ChB and HB interactions, which has thus far only been predicted computationally. Considering only the σ-hole-donor atoms of the same period (i.e. Te, I), the anion binding affinities decrease in the order XB > ChB > HB - a trend which is consistent for both neutral and cationic host molecules. The enhanced anion binding potency of XB interactions over ChB may arise from a combination of differences in steric accessibility of the binding site as well as electrophilicity of the donor atom. Consequently, only neutral XB interactions are potent enough for anion recognition and binding in the presence of water, even when incorporated into highly preorganised host systems such as rotaxanes.

Despite these differences, ChB and XB, as sister σ-hole interactions, share numerous similarities. Although anion charge density appears to play a dominant role in determining the binding preference of ChB, XB and HB hosts in dry organic solvents, anion binding by ChB interactions, like XB demonstrated in a prior study by Huber *et. al.*,[96] have a pronounced enthalpic contribution to the overall free energy of binding, which contrasts with the overwhelming entropic dominance by HB hosts. In addition, anion binding by neutral and cationic ChB and XB host molecules are invariably highly sensitive to solvent HB-donor ability, with the presence of water being highly detrimental to the stability of anion complexes in all cases. In wet solvent mixtures, XB and ChB hosts show predominant Hofmeister bias, with preference for binding of heavier halides, driven by an inherent preference for ‘soft-soft’ interactions and greater ease of halide dehydration. Contrastingly, less well-defined trends were observed for the analogous HB host molecules.

2.5.2 Future Work

The work presented in this chapter has set the groundwork for further exploitation of the CuAAC-AMT protocol for preparing novel interlocked host architectures for various applications of anion recognition. For instance, this strategy could form the basis for preparing novel all-XB redox-active rotaxanes for anion sensing as well as chiral rotaxanes for enantioselective anion recognition, topics which will be further explored in Chapters 3 and 4 of this thesis respectively. In addition, capitalising on the unprecedented stability of the sp^3-hybridised ChB-donor methylchalcogeno-triazoles, numerous avenues can be pursued to further exploit the unique steric and electronic properties of ChB-donor hosts for selective anion recognition. These may include, but are not necessarily limited to:

- the replacement of the CH_3 group on the methylchalcogeno-triazoles with electron-withdrawing CF_3-groups to further enhance the electrophilicity of the donor chalcogen atoms (Figure 2.33A). Indeed, the preparation of the $TeCF_3$ group has been reported and has shown decent air and moisture stability.[113]
- a new design for the passive metal templated synthesis of a catenane with a binding cavity surrounded by ChB donor groups. To reduce the possibility of forming multiple coordination species, the use of a catenane thread containing a single methylseleno-triazole may be investigated (Figure 2.33B). Triazole N^3-methylation can then allow charge-assisted ChB interactions to enhance the potency of the catenane for anion binding.
- synthesis of a water-soluble cationic Te-based host molecule, possibly terminated by permethylated β-cyclodextrin groups,[75] to investigate the fundamental properties and thermodynamics of halide anion binding in pure water for comparison to those of known XB systems (Figure 2.33C).

In addition, with the use of X-ray absorption spectroscopy, experimental quantification of the covalency of ChB-anion interactions may be determined,[114–116] and compared between neutral and cationic Se and Te-based ChB hosts. The findings can also be compared with those of previously-reported XB host systems[17] to shed insights on the weaker anion binding properties of ChB hosts compared to their XB analogues observed empirically in this chapter.

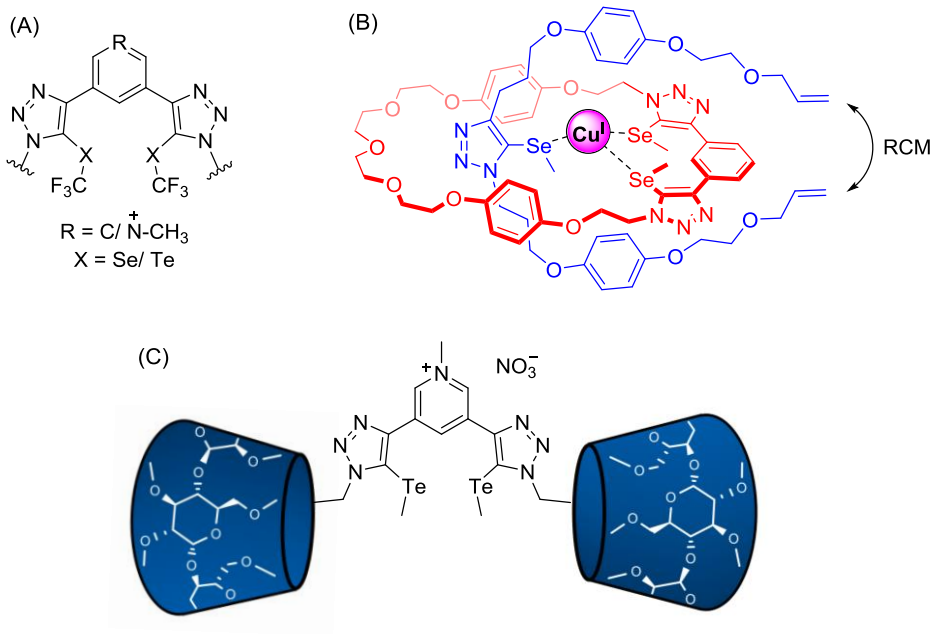


***Figure 2.33**. Suggested areas for further exploration of ChB-mediated anion recognition: (A) CF_3-based ChB-donor motifs; (B) alternative design for passive metal template synthesis of an all-ChB [2]catenane; (C) possible permethylated β-cyclodextrin-terminated ChB host for anion binding in pure water.*

2.6 References

1 V. V. Rostovtsev, L. G. Green, V. V. Fokin and K. B. Sharpless, *Angew. Chem. Int. Ed.*, 2002, **41**, 2596–2599.
2 C. W. Tornøe, C. Christensen and M. Meldal, *J. Org. Chem.*, 2002, **67**, 3057–3064.
3 J. E. Hein and V. V. Fokin, *Chem Soc Rev*, 2010, **39**, 1302–1315.
4 C. A. Ramsden, *Tetrahedron*, 2010, **66**, 2695–2699.
5 K. Jug, S. Chiodo, P. Calaminici, A. Avramopoulos and M. G. Papadopoulos, *J. Phys. Chem. A*, 2003, **107**, 4172–4183.
6 B. T. Worrell, J. E. Hein and V. V. Fokin, *Angew. Chem. Int. Ed.*, 2012, **51**, 11791–11794.
7 B. Schulze and U. S. Schubert, *Chem Soc Rev*, 2014, **43**, 2522–2571.
8 J. D. Crowley, S. M. Goldup, A.-L. Lee, D. A. Leigh and R. T. McBurney, *Chem Soc Rev*, 2009, **38**, 1530–1541.
9 V. Aucagne, J. Berná, J. D. Crowley, S. M. Goldup, K. D. Hänni, D. A. Leigh, P. J. Lusby, V. E. Ronaldson, A. M. Z. Slawin, A. Viterisi and D. B. Walker, *J. Am. Chem. Soc.*, 2007, **129**, 11950–11963.
10 J. Winn, A. Pinczewska and S. M. Goldup, *J. Am. Chem. Soc.*, 2013, **135**, 13318–13321.
11 E. A. Neal and S. M. Goldup, *Chem Sci*, 2015, **6**, 2398–2404.
12 S. M. Goldup, D. A. Leigh, T. Long, P. R. McGonigal, M. D. Symes and J. Wu, *J. Am. Chem. Soc.*, 2009, **131**, 15924–15929.
13 J. E. M. Lewis, J. Winn, L. Cera and S. M. Goldup, *J. Am. Chem. Soc.*, 2016, **138**, 16329–16336.
14 E. J. Lewis, J. Winn and M. S. Goldup, *Molecules*, 2017, **22**, 89-100.
15 E. A. Neal and S. M. Goldup, *Angew. Chem. Int. Ed.*, 2016, **55**, 12488–12493.
16 M. J. Langton, Y. Xiong and P. D. Beer, *Chem. – Eur. J.*, 2015, **21**, 18910–18914.
17 S. W. Robinson, C. L. Mustoe, N. G. White, A. Brown, A. L. Thompson, P. Kennepohl and P. D. Beer, *J. Am. Chem. Soc.*, 2015, **137**, 499–507.
18 B. Nepal and S. Scheiner, *Chem. – Eur. J.*, 2015, **21**, 13330–13335.
19 B. Nepal and S. Scheiner, *ChemPhysChem*, 2016, **17**, 836–844.
20 A. H. Flood, *Beilstein J. Org. Chem.*, 2016, **12**, 611–627.
21 Y. Li and A. H. Flood, *Angew. Chem. Int. Ed.*, 2008, **47**, 2649–2652.
22 N. G. White, H. G. Lovett and P. D. Beer, *RSC Adv*, 2014, **4**, 12133–12147.
23 J. A. Wisner, P. D. Beer and M. G. B. Drew, *Angew. Chem. Int. Ed.*, 2001, **40**, 3606–3609.
24 T. R. Bell-Horwath, A. K. Vadukoot, F. S. Thowfeik, G. Li, M. Wunderlich, J. C. Mulloy and E. J. Merino, *Bioorg. Med. Chem. Lett.*, 2013, **23**, 2951–2954.
25 W. S. Brotherton, R. J. Clark and L. Zhu, *J. Org. Chem.*, 2012, **77**, 6443–6455.
26 D. Enders, G. Geibel and S. Osborne, *Chem. – Eur. J.*, 2000, **6**, 1302–1309.
27 G. Dijkstra, W. H. Kruizinga and R. M. Kellogg, *J. Org. Chem.*, 1987, **52**, 4230–4234.

28 W. Wang, X. Peng, F. Wei, C.-H. Tung and Z. Xu, *Angew. Chem. Int. Ed.*, 2016, **55**, 649–653.
29 S. Ding, G. Jia and J. Sun, *Angew. Chem. Int. Ed.*, 2014, **53**, 1877–1880.
30 T. Chivers and R. S. Laitinen, *Chem Soc Rev*, 2015, **44**, 1725–1739.
31 H. A. Stefani, S. N. S. Vasconcelos, F. Manarin, D. M. Leal, F. B. Souza, L. S. Madureira, J. Zukerman-Schpector, M. N. Eberlin, M. N. Godoi and R. de Souza Galaverna, *Eur. J. Org. Chem.*, 2013, **2013**, 3780–3785.
32 M. Tiecco, L. Testaferri, M. Tingoli, D. Chianelli, D. Bartoli and R. Balducci, *Tetrahedron*, 1988, **44**, 4883–4894.
33 O. Fleischel, N. Wu and A. Petitjean, *Chem Commun*, 2010, **46**, 8454–8456.
34 L. Jiang, Z. Wang, S.-Q. Bai and T. S. A. Hor, *Dalton Trans*, 2013, **42**, 9437–9443.
35 C. M. Alvarez, L. A. Garcia-Escudero, R. Garcia-Rodriguez and D. Miguel, *Chem Commun*, 2012, **48**, 7209–7211.
36 R. Qiu and H. Luo, *RSC Adv*, 2015, **5**, 96213–96221.
37 S. Özçubukçu, E. Ozkal, C. Jimeno and M. A. Pericàs, *Org. Lett.*, 2009, **11**, 4680–4683.
38 P. S. Donnelly, S. D. Zanatta, S. C. Zammit, J. M. White and S. J. Williams, *Chem Commun*, 2008, 2459–2461.
39 H. Struthers, T. L. Mindt and R. Schibli, *Dalton Trans*, 2010, **39**, 675–696.
40 R. Diaz-Torres and S. Alvarez, *Dalton Trans*, 2011, **40**, 10742–10750.
41 U. Monkowius, S. Ritter, B. König, M. Zabel and H. Yersin, *Eur. J. Inorg. Chem.*, 2007, **2007**, 4597–4606.
42 S. Mishra, E. Jeanneau and S. Daniele, *2009 Young Investig. Spec. Issue*, 2010, **29**, 500–506.
43 J. S. Ritch and T. Chivers, *Inorg. Chem.*, 2009, **48**, 3857–3865.
44 M. M. Kimani, H. C. Wang and J. L. Brumaghim, *Dalton Trans*, 2012, **41**, 5248–5259.
45 J. R. Black, N. R. Champness, W. Levason and G. Reid, *Inorg. Chem.*, 1996, **35**, 4432–4438.
46 M. M. Kimani, C. A. Bayse and J. L. Brumaghim, *Dalton Trans*, 2011, **40**, 3711–3723.
47 M. J. Poropudas, L. Vigo, R. Oilunkaniemi and R. S. Laitinen, *Dalton Trans*, 2013, **42**, 16868–16877.
48 M. J. Frisch, G. W. Trucks, H. B. Schlegel, G. E. Scuseria, M. A. Robb, J. R. Cheeseman, G. Scalmani, V. Barone, G. A. Petersson, H. Nakatsuji, X. Li, M. Caricato, A. V. Marenich, J. Bloino, B. G. Janesko, R. Gomperts, B. Mennucci, H. P. Hratchian, J. V. Ortiz, A. F. Izmaylov, J. L. Sonnenberg, Williams, F. Ding, F. Lipparini, F. Egidi, J. Goings, B. Peng, A. Petrone, T. Henderson, D. Ranasinghe, V. G. Zakrzewski, J. Gao, N. Rega, G. Zheng, W. Liang, M. Hada, M. Ehara, K. Toyota, R. Fukuda, J. Hasegawa, M. Ishida, T. Nakajima, Y. Honda, O. Kitao, H. Nakai, T. Vreven, K. Throssell, J. A. Montgomery Jr., J. E. Peralta, F. Ogliaro, M. J. Bearpark, J. J. Heyd, E. N. Brothers, K. N. Kudin, V. N. Staroverov, T. A. Keith, R. Kobayashi, J. Normand, K. Raghavachari, A. P. Rendell, J. C. Burant, S. S. Iyengar, J. Tomasi, M. Cossi, J. M. Millam, M. Klene, C. Adamo, R. Cammi, J. W. Ochterski, R. L. Martin, K. Morokuma, O. Farkas, J. B. Foresman and D. J. Fox, *Gaussian 09, revision A.01*, Gaussian Inc., Wallingford, CT, 2009.
49 K. L. Schuchardt, B. T. Didier, T. Elsethagen, L. Sun, V. Gurumoorthi, J. Chase, J. Li and T. L. Windus, *J. Chem. Inf. Model.*, 2007, **47**, 1045–1052.
50 D. Feller, *J. Comput. Chem.*, 1996, **17**, 1571–1586.
51 S. Miertuš, E. Scrocco and J. Tomasi, *Chem. Phys.*, 1981, **55**, 117–129.
52 C. R. Groom, I. J. Bruno, M. P. Lightfoot and S. C. Ward, *Acta Crystallogr. Sect. B*, 2016, **72**, 171–179.
53 V. Aucagne, K. D. Hänni, D. A. Leigh, P. J. Lusby and D. B. Walker, *J. Am. Chem. Soc.*, 2006, **128**, 2186–2187.
54 N. L. Kilah, M. D. Wise, C. J. Serpell, A. L. Thompson, N. G. White, K. E. Christensen and P. D. Beer, *J. Am. Chem. Soc.*, 2010, **132**, 11893–11895.
55 N. G. White and P. D. Beer, *Org Biomol Chem*, 2013, **11**, 1326–1333.
56 J. A. Wisner, P. D. Beer, M. G. B. Drew and M. R. Sambrook, *J. Am. Chem. Soc.*, 2002, **124**, 12469–12476.
57 J. M. Mercurio, R. C. Knighton, J. Cookson and P. D. Beer, *Chem. – Eur. J.*, 2014, **20**, 11740–11749.
58 Y. Fang, A. Y. Li and F. Y. Ma, *J. Mol. Model.*, 2015, **21**, 61.
59 A. Bauza, D. Quinonero, P. M. Deya and A. Frontera, *CrystEngComm*, 2013, **15**, 3137–3144.
60 M. J. Hynes, *J. Chem. Soc. Dalton Trans.*, 1993, 311–312.
61 Y. Marcus, *J Chem Soc Faraday Trans*, 1991, **87**, 2995–2999.
62 A. Bauzá, T. J. Mooibroek and A. Frontera, *ChemPhysChem*, 2015, **16**, 2496–2517.
63 L. C. Gilday, S. W. Robinson, T. A. Barendt, M. J. Langton, B. R. Mullaney and P. D. Beer, *Chem. Rev.*, 2015, **115**, 7118–7195.
64 A. Brown and P. D. Beer, *Chem Commun*, 2016, **52**, 8645–8658.
65 C. C. Robertson, R. N. Perutz, L. Brammer and C. A. Hunter, *Chem Sci*, 2014, **5**, 4179–4183.
66 M. H. Abraham, *Chem Soc Rev*, 1993, **22**, 73–83.
67 M. G. Sarwar, B. Dragisic, L. J. Salsberg, C. Gouliaras and M. S. Taylor, *J. Am. Chem. Soc.*, 2010, **132**, 1646–1653.
68 A. Caballero, F. Zapata and P. D. Beer, *Coord. Chem. Rev.*, 2013, **257**, 2434–2455.
69 M. J. Langton and P. D. Beer, *Acc. Chem. Res.*, 2014, **47**, 1935–1949.
70 E. A. Katayev, G. V. Kolesnikov and J. L. Sessler, *Chem Soc Rev*, 2009, **38**, 1572–1586.
71 R. C. Knighton and P. D. Beer, *Chem Commun*, 2014, **50**, 1540–1542.
72 J. R. Romero, G. Aragay and P. Ballester, *Chem Sci*, 2017, **8**, 491–498.
73 Y.-J. Lee, T.-H. Ho, C.-C. Lai and S.-H. Chiu, *Org Biomol Chem*, 2016, **14**, 1153–1160.

74 H. Nowell, S. A. Barnett, K. E. Christensen, S. J. Teat and D. R. Allan, *J. Synchrotron Radiat.*, 2012, **19**, 435–441.
75 M. J. Langton, S. W. Robinson, I. Marques, V. Félix and P. D. Beer, *Nat Chem*, 2014, **6**, 1039–1043.
76 M. J. Langton, I. Marques, S. W. Robinson, V. Félix and P. D. Beer, *Chem. – Eur. J.*, 2016, **22**, 185–192.
77 T. A. Barendt, A. Docker, I. Marques, V. Félix and P. D. Beer, *Angew. Chem. Int. Ed.*, 2016, n/a–n/a.
78 J. Wang, R. M. Wolf, J. W. Caldwell, P. A. Kollman and D. A. Case, *J. Comput. Chem.*, 2004, **25**, 1157–1174.
79 J. Wang, R. M. Wolf, J. W. Caldwell, P. A. Kollman and D. A. Case, *J. Comput. Chem.*, 2005, **26**, 114–114.
80 D. A. Case, R. M. Betz, W. Botello-Smith, D. S. Cerutti, T. E. Cheatham III, T. A. Darden, R. E. Duke, T. J. Giese, H. Gohlke, A. W. Goetz, N. Homeyer, S. Izadi, P. Janowski, J. Kaus, A. Kovalenko, T. S. Lee, S. LeGrand, P. Li, C. Lin, T. Luchko, R. Luo, B. Madej, D. Mermelstein, K. M. Merz, G. Monard, H. Nguyen, H. T. Nguyen, I. Omelyan, A. Onufriev, D. R. Roe, A. Roitberg, C. Sagui, C. L. Simmerling, J. Swails, R. C. Walker, J. Wang, R. M. Wolf, X. Wu, L. Xiao, D. M. York and P. A. Kollman, *Amber 2016*, University of California: San Francisco, 2016.
81 A. W. Götz, M. J. Williamson, D. Xu, D. Poole, S. Le Grand and R. C. Walker, *J. Chem. Theory Comput.*, 2012, **8**, 1542–1555.
82 R. Salomon-Ferrer, A. W. Götz, D. Poole, S. Le Grand and R. C. Walker, *J. Chem. Theory Comput.*, 2013, **9**, 3878–3888.
83 L. Ronconi and P. J. Sadler, *Appl. NMR Inorg. Organomet. Chem.*, 2008, **252**, 2239–2277.
84 H. Duddeck, in *Annual Reports on NMR Spectroscopy*, Academic Press, 2004, vol. Volume 52, pp. 105–166.
85 A. K. Singh and S. Sharma, *Coord. Chem. Rev.*, 2000, **209**, 49–98.
86 D. E. Smiles, G. Wu, P. Hrobárik and T. W. Hayton, *J. Am. Chem. Soc.*, 2016, **138**, 814–825.
87 H. Zhao and F. P. Gabbaï, *Nat Chem*, 2010, **2**, 984–990.
88 P. C. Ho, P. Szydlowski, J. Sinclair, P. J. W. Elder, J. Kübel, C. Gendy, L. M. Lee, H. Jenkins, J. F. Britten, D. R. Morim and I. Vargas-Baca, *Nat. Commun.*, 2016, **7**, 11299.
89 J. Viger-Gravel, J. E. Meyer, I. Korobkov and D. L. Bryce, *CrystEngComm*, 2014, **16**, 7285–7297.
90 S. A. Schaefer, M. Dong, R. P. Rubenstein, W. A. Wilkie, B. J. Bahnson, C. Thorpe and S. Rozovsky, *J. Mol. Biol.*, 2013, **425**, 222–231.
91 R. Custelcean, P. V. Bonnesen, N. C. Duncan, X. Zhang, L. A. Watson, G. Van Berkel, W. B. Parson and B. P. Hay, *J. Am. Chem. Soc.*, 2012, **134**, 8525–8534.
92 L. C. Gilday, N. G. White and P. D. Beer, *Dalton Trans*, 2013, **42**, 15766–15773.
93 K. Wallenfels and W. Hanstein, *Justus Liebigs Ann. Chem.*, 1967, **709**, 151–169.
94 K. Wallenfels, H. Schüly and D. Hofmann, *Justus Liebigs Ann. Chem.*, 1959, **621**, 106–136.
95 R. E. Lyle and G. J. Gauthier, *Tetrahedron Lett.*, 1965, **6**, 4615–4621.
96 S. M. Walter, F. Kniep, L. Rout, F. P. Schmidtchen, E. Herdtweck and S. M. Huber, *J. Am. Chem. Soc.*, 2012, **134**, 8507–8512.
97 J. L. Sessler, L. R. Eller, W.-S. Cho, S. Nicolaou, A. Aguilar, J. T. Lee, V. M. Lynch and D. J. Magda, *Angew. Chem. Int. Ed.*, 2005, **44**, 5989–5992.
98 P. Plitt, D. E. Gross, V. M. Lynch and J. L. Sessler, *Chem. – Eur. J.*, 2007, **13**, 1374–1381.
99 M. Berger and F. P. Schmidtchen, *J. Am. Chem. Soc.*, 1999, **121**, 9986–9993.
100 V. D. Jadhav, E. Herdtweck and F. P. Schmidtchen, *Chem. – Eur. J.*, 2008, **14**, 6098–6107.
101 S. W. Robinson and P. D. Beer, *Org Biomol Chem*, 2017, **15**, 153–159.
102 K.-Y. Ng, V. Felix, S. M. Santos, N. H. Rees and P. D. Beer, *Chem Commun*, 2008, 1281–1283.
103 N. G. White and P. D. Beer, *Chem Commun*, 2012, **48**, 8499–8501.
104 N. G. White, C. J. Serpell and P. D. Beer, *Cryst. Growth Des.*, 2014, **14**, 3472–3479.
105 A. Hoshi, T. Sakamoto, J. Takayama, M. Xuan, M. Okazaki, T. L. Hartman, R. W. Buckheit Jr., C. Pannecouque and M. Cushman, *Bioorg. Med. Chem.*, 2016, **24**, 3006–3022.
106 A.-C. Bédard and S. K. Collins, *Org. Lett.*, 2014, **16**, 5286–5289.
107 C. D. Campbell, R. L. Greenaway, O. T. Holton, H. A. Chapman and E. A. Anderson, *Chem Commun*, 2014, **50**, 5187–5189.
108 Y. Sato, R. Yamasaki and S. Saito, *Angew. Chem. Int. Ed.*, 2009, **48**, 504–507.
109 C. . Dietrich-Buchecker, J. . Sauvage and J. . Kintzinger, *Tetrahedron Lett.*, 1983, **24**, 5095–5098.
110 J. E. Beves, B. A. Blight, C. J. Campbell, D. A. Leigh and R. T. McBurney, *Angew. Chem. Int. Ed.*, 2011, **50**, 9260–9327.
111 E. Ascic, R. G. Ohm, R. Petersen, M. R. Hansen, C. L. Hansen, D. Madsen, D. Tanner and T. E. Nielsen, *Chem. – Eur. J.*, 2014, **20**, 3297–3300.
112 G. C. Vougioukalakis and R. H. Grubbs, *Chem. Rev.*, 2010, **110**, 1746–1787.
113 H. Park, L. J. Edgar, M. A. Lumba, L. M. Willis and M. Nitz, *Org Biomol Chem*, 2015, **13**, 7027–7033.
114 M. U. Delgado-Jaime, J. C. Conrad, D. E. Fogg and P. Kennepohl, *Protag. Chem. Brian James*, 2006, **359**, 3042–3047.
115 M. U. Delgado-Jaime, C. P. Mewis and P. Kennepohl, *J. Synchrotron Radiat.*, 2010, **17**, 132–137.
116 M. U. Delgado-Jaime and P. Kennepohl, *J. Synchrotron Radiat.*, 2010, **17**, 119–128.

Blank Page

Chapter 3

Redox-active σ-Hole Donor Host Molecules for Anion Recognition and Sensing

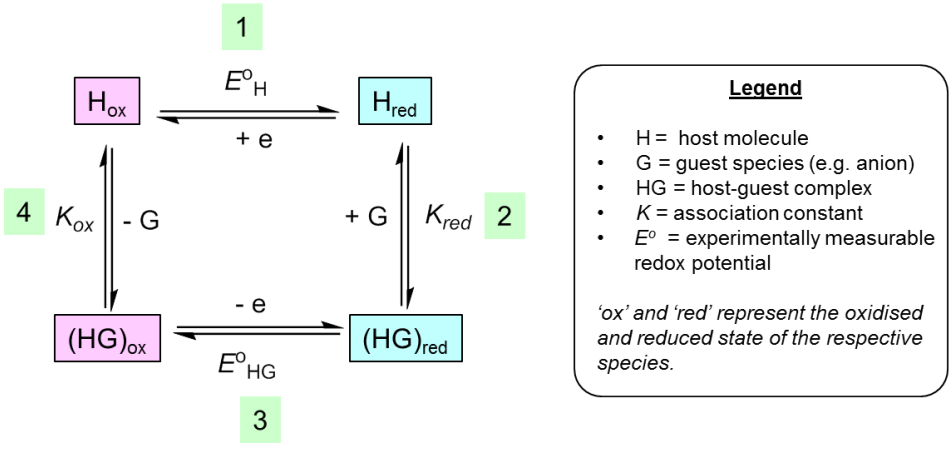
CHAPTER 3 : Redox-active σ-Hole Donor Host Molecules for Anion Recognition and Sensing

3.1 Introduction

As demonstrated in the previous chapter, the incorporation of XB and ChB-donor groups into anion binding host molecules confers contrasting, yet generally augmented anion recognition properties compared to their HB host counterparts. This chapter aims to investigate the effects of incorporating σ-hole donor groups into acyclic and interlocked ferrocene-based redox-active host molecules for electrochemical anion sensing. Compared with redox active HB receptors, the contrasting steric, geometric and electronic properties of σ-hole interactions are expected to significantly alter the anion electrochemical sensory responses of XB and ChB host molecules. Furthermore, the enhanced covalent character of the σ-hole interactions, in particular with XB,[1] is also expected to facilitate electronic communication between the bound anion and the redox-active reporter group, potentially enhancing the sensitivity of electrochemical anion sensing.

3.1.1 Theory of Electrochemical Anion Sensing

Electrochemical anion sensing occurs by a detectable change in the redox potential (ΔE) of a reporter group (e.g. ferrocene) in the presence of an added anion, which can be measured using cyclic voltammetry (CV) or square-wave voltammetry (SWV). Generally, the sensing process can be represented by the square scheme shown in Scheme 3.1:[2]



***Scheme 3.1**. Scheme of one square showing the electron transfer processes and anion binding.*

The overall change in free energy of the four numbered processes shown in Scheme 3.1 is zero, as they form a thermodynamically closed loop. Therefore,

$$\Sigma G = \Delta G_1 + \Delta G_2 + \Delta G_3 + \Delta G_4 = 0$$

$$-nF(E^o_H - E) - RT\ln K_{red} + nF(E^o_{HG} - E) + RT\ln K_{ox} = 0$$

$$nF(E^o_{HG} - E^o_H) = RT\ln(K_{red}/K_{ox}) \qquad \text{(Equation 1)}$$

From Equation 1, the measurable perturbation of the host's redox potential ($\Delta E = E^o_{HG} - E^o_H$) in the presence of the guest is related to the ratio K_{red}/K_{ox}, which has been termed the binding enhancement factor[3] or the reaction coupling efficiency.[4] For the case of ferrocene-based receptors, the oxidation process leads to the formation of the cationic ferrocenium species, which has an enhanced binding affinity towards anionic guests (K_{ox}) compared to the original (reduced) ferrocene host (K_{red}). Accordingly, this gives a detectable cathodic (negative) potential shift, the magnitude of which depends on the degree of enhancement in values of K_{ox} over K_{red}, and does not necessarily require strong host-guest binding. The redox-active reporter group is often covalently linked in close proximity to the anion binding site (noted in Section 1.2.3) to facilitate efficient communication via through-space or through-bond pathways.[2]

3.1.2 Redox-active Interlocked Host Molecules

The appendage and incorporation of redox-active motifs into interlocked structures has enabled numerous functional systems to be created. For example, the tetrathiafulvene (TTF) motif incorporated into MIMs allowed Stoddart and co-workers to electrochemically control reversible large-scale translational motion of macrocycles in rotaxanes and catenanes, driven by electrostatic repulsion between a bis-paraquat containing cationic macrocycle component and the resulting oxidised TTF^{2+} (Figure 3.1).[6] Similarly, translational motion with Willner's surface-assembled rotaxanes containing redox-active paraquat-based macrocycles enabled electrochemical modulation of surface hydrophobicity[7] as well as creation of a glucose-oxidising biocatalyst.[8]

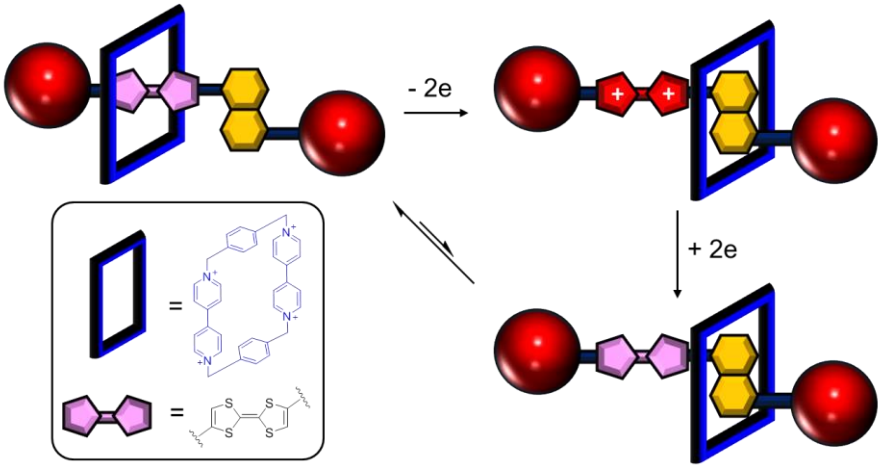


***Figure 3.1**. Schematic illustration of the electrochemically-controlled molecular motion driven by TTF oxidation in Stoddart's redox-active [2]rotaxane.*[9]

Ferrocene is a commonly utilised electrochemical reporter group due to its favourable voltammetric properties and vast chemical repertoire, facilitating the redox centre's incorporation into diverse molecular architectures.[10–16] The earliest attempt at incorporating ferrocene into rotaxane structures by Parker *et. al.* made use of neutral templation driven by the stable inclusion complexes formed between ferrocene and β-cyclodextrin.[17] Since then, the development of ferrocene as a distance-dependent fluorescence quencher in rotaxanes,[18] and as a reporter group for redox anion sensing in MIMs has been realised.[19] Notably, the latter application capitalises on the well-defined and preorganised three dimensional binding cavity of MIMs for anion binding, allowing greater selectivity in the redox sensing of anions capable of penetrating the interlocked host cavity.[20] Ferrocene and its derivatives have been *appended* onto the macrocycle component of a [2]rotaxane (Figure 3.2A),[21] a [2]catenane (Figure 3.2B),[22] as well as incorporated into rotaxane stoppers units[23] (Figure 3.2C) and the axle component of a [3]rotaxane (Figure 3.2D).[24] Interestingly, while the appendage of ferrocene onto macrocycles or as stoppers give comparable magnitudes of cathodic shifts of the respective ferrocene/ ferrocenium (Fc/ Fc^+) redox couple (ΔE = -20 mV) in the presence of 10.0 equivalents of Cl^- in anhydrous CH_3CN solvent mixtures, incorporation of ferrocene into the axle component of the [3]rotaxane gave much larger shifts of -55 mV and -265 mV in the

presence of Cl^- and SO_4^{2-} respectively. Towards the fabrication of sensory devices, ferrocene-appended MIMs have also been assembled onto gold surfaces. [20,22,25]

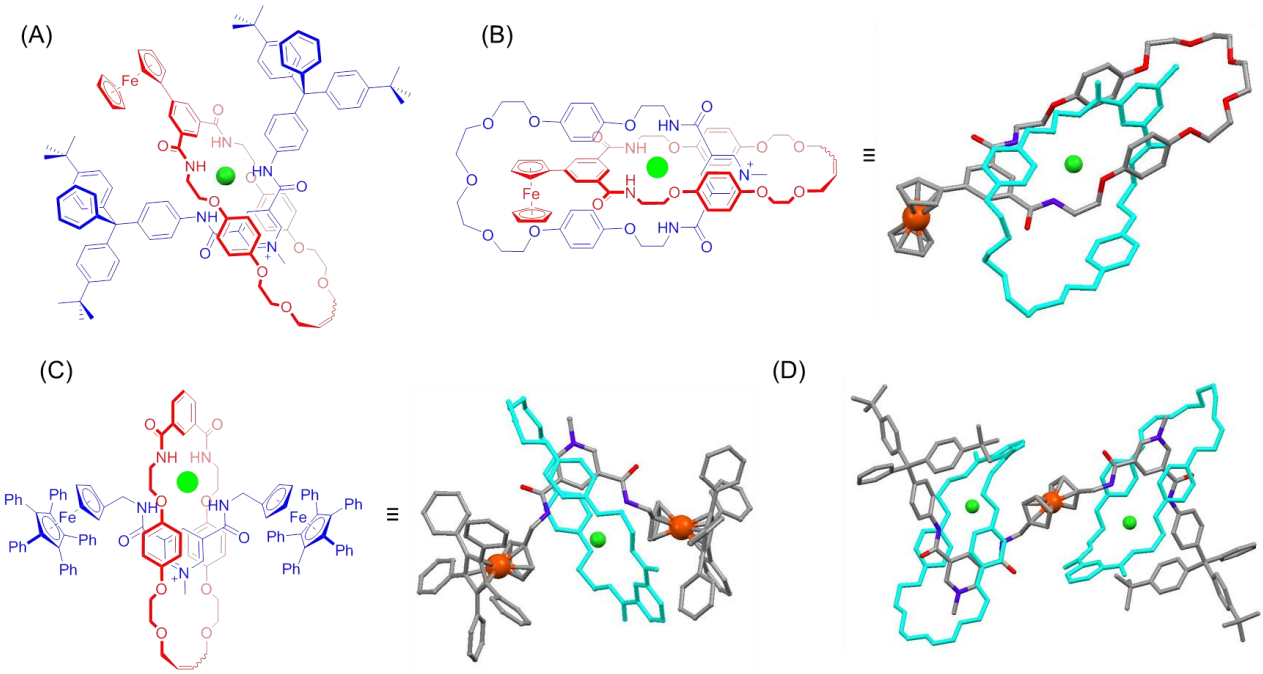


***Figure 3.2**. Examples of ferrocene-containing interlocked structures for anion sensing in solution by Beer: (A) a [2]Rotaxane with ferrocene-appended macrocycle;[21] (B) a ferrocene-appended [2]-catenane;[22] (C) a [2]rotaxane with pentaphenylferrocene stoppers[23] and (D) crystal structure of a [3]rotaxane with a ferrocene-containing axle.[24] The anion (green) shown in each interlocked cavity is Cl^-.*

Other redox-active motifs have been incorporated into rotaxane structures for electrochemical anion sensing. For instance, the osmium(II) bipyridyl motif (Figure 3.3A) has been incorporated into the macrocycle units of a series of [2]rotaxanes by Beer *et. al*.[26] Although the free Os(II)-containing macrocycle gave modest cathodic shifts of the Os(III)/ Os(II) and bipy/ $bipy^-$ redox couples of -25 mV and -40 mV respectively with Cl^- in CH_3CN, incorporation into rotaxane structures resulted in irreversible redox behaviour. The functionalisation of rotaxanes with free-base porphyrin (P) (Figure 3.3B) as stoppers or on the macrocycle has also been shown to produce detectable cathodic shifts of the P/P^+ redox couple with Cl^-.[27] Contrary to the earlier ferrocene examples, the rotaxanes with porphyrins as stoppers gave an enhanced redox response to Cl^- compared to macrocycle functionalisation,

which has been attributed to conformational distortions of the oxidised P^+ radical leading to better electronic communication with the rotaxane anion binding site.[28]

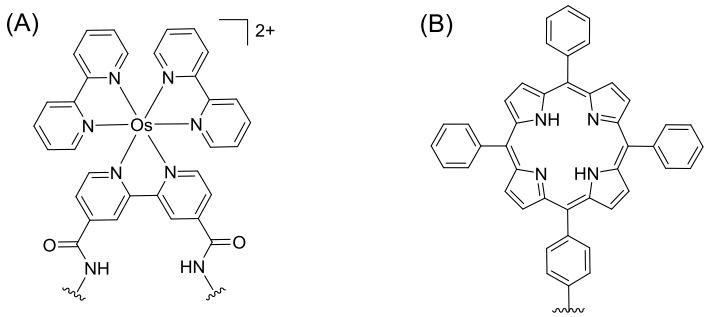


***Figure 3.3**. Structures of other redox-active motifs incorporated into rotaxanes: (A) osmium(II) bipyridyl[26] and (B) free-base porphyrin.[27]*

3.1.3 Sigma Hole-mediated Redox Anion Sensing

Amongst the acyclic and interlocked hosts capable of redox anion sensing, σ-hole donors are by far under-represented. After some of the work described in this chapter was published,[29,30] the incorporation of XB donor groups into redox-active functionalities were also reported by the groups of Schöllhorn and Molina. Schöllhorn and co-workers reported the use of iodo-tetrathiafulvene (I-TTF) (Figure 3.4A) as an electrochemical sensor for Cl^- and Br^-, capable of giving larger magnitudes of cathodic shifts of the I-TTF/ $(I\text{-}TTF)^+$ redox potential in DMF than the halogen-free analogue.[31] Significantly, the presence of Cl^- elicited larger shifts of the second oxidation wave of I-TTF (1+/2+) than the first (0/1+), which was attributed to stronger Cl^- stabilisation of dicationic $(I\text{-}TTF)^{2+}$ than $(I\text{-}TTF)^+$ due to enhanced charge-assisted XB interactions. More recently, Molina *et. al.* reported the use of a tris-ferrocene-bis-iodotriazole XB receptor (Figure 3.4B) for the redox sensing of oxoanions (AcO^-, $H_2PO_4^-$ and $HP_2O_7^{3-}$) via cathodic shifts of the Fc/ Fc^+ redox couples of both ferrocene environments in CH_2Cl_2/ CH_3CN 1:1 *v/v*.[32] Interestingly, similar magnitudes of potential shift were observed for the XB receptor and its HB analogue in this case. Very recently, Beer *et. al.* have also studied the use of iodotriazole-substituted diquat derivatives in XB-mediated anion sensing (Figure 3.4C).[33] At the time of writing, the applications of ChB in electrochemical anion sensing are unprecedented.

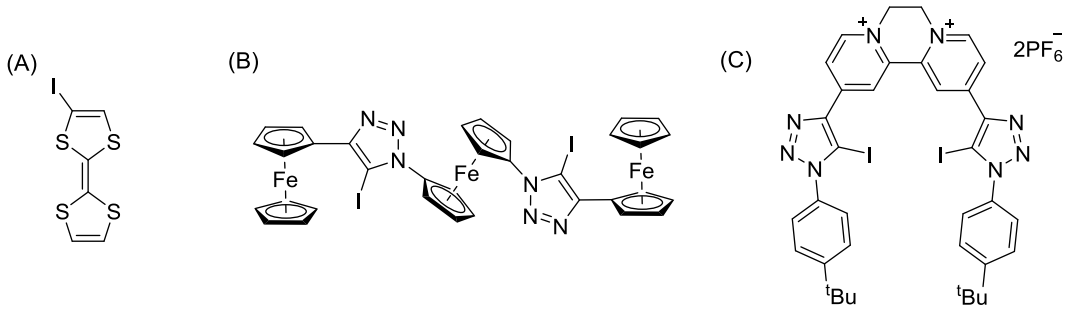


***Figure 3.4**. XB-donor redox-active host molecules for anion sensing: (A) Schöllhorn's I-TTF receptor;[31] (B) Molina's tri-ferrocene host for redox sensing of oxoanions[32] and (C) Beer's diquat XB redox anion sensor.[33]*

3.1.4 Chapter Aims

The overall goals of this chapter include investigating the effects of incorporating σ-hole donor groups into ferrocene-based acyclic, macrocyclic and interlocked host structures and elucidating their influences on the redox anion sensory behaviour. To complement the cationic redox-active interlocked systems aforementioned, the synthesis of *neutral* ferrocene-appended rotaxanes were first investigated. Although primarily binding anions via HB interactions, the effects of changing the geometric and steric properties of the interlocked cavity on electrochemical sensing behaviour was investigated by introducing XB-donor iodotriazoles at their periphery (Section 3.2, Figure 3.5A). At the time of work commencement on this chapter, redox-active motifs containing σ-hole donor groups were unknown. Hence, the construction and anion sensory properties of a series of unprecedented bidentate ferrocene-based σ-hole (XB and ChB) model host systems were pursued, with the effects of varying the anion coordination bite angles studied by changing the triazole substitution positions on ferrocene (Section 3.3, Figure 3.5B). These preliminary findings culminated in the active metal template synthesis and anion binding sensory properties of a novel redox-active [2]rotaxane bearing an all-XB interlocked anion binding site flanked by four iodotriazole units (Section 3.4, Figure 3.5C).

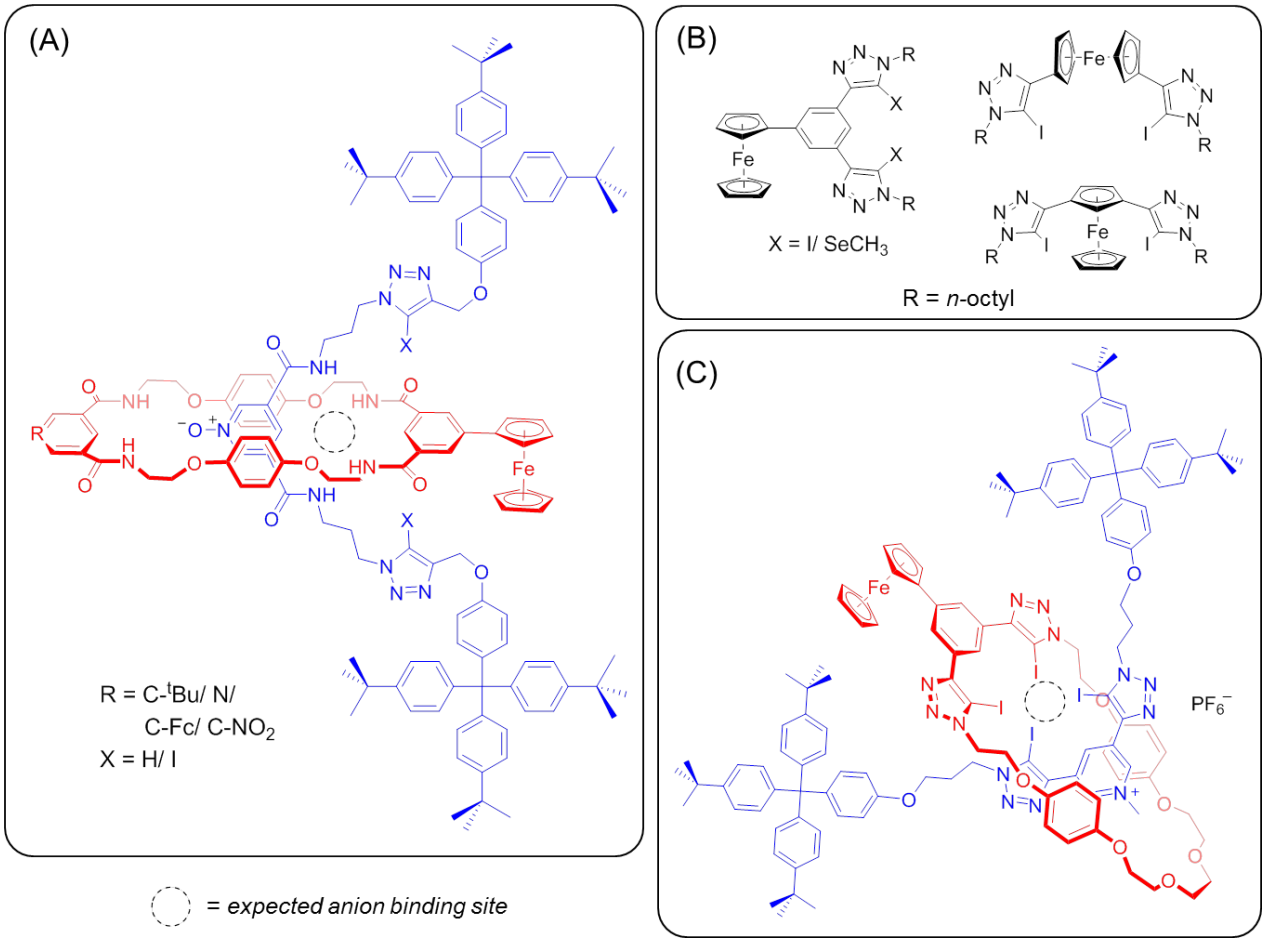


***Figure 3.5**. The various influences of σ-hole donor groups on redox anion sensing studied in this chapter: (A) binding site modulation on neutral HB [2]rotaxanes by peripheral XB donor groups; (B) direct σ-hole-mediated redox anion sensing; (C) XB-mediated redox anion sensing by an all-XB rotaxane.*

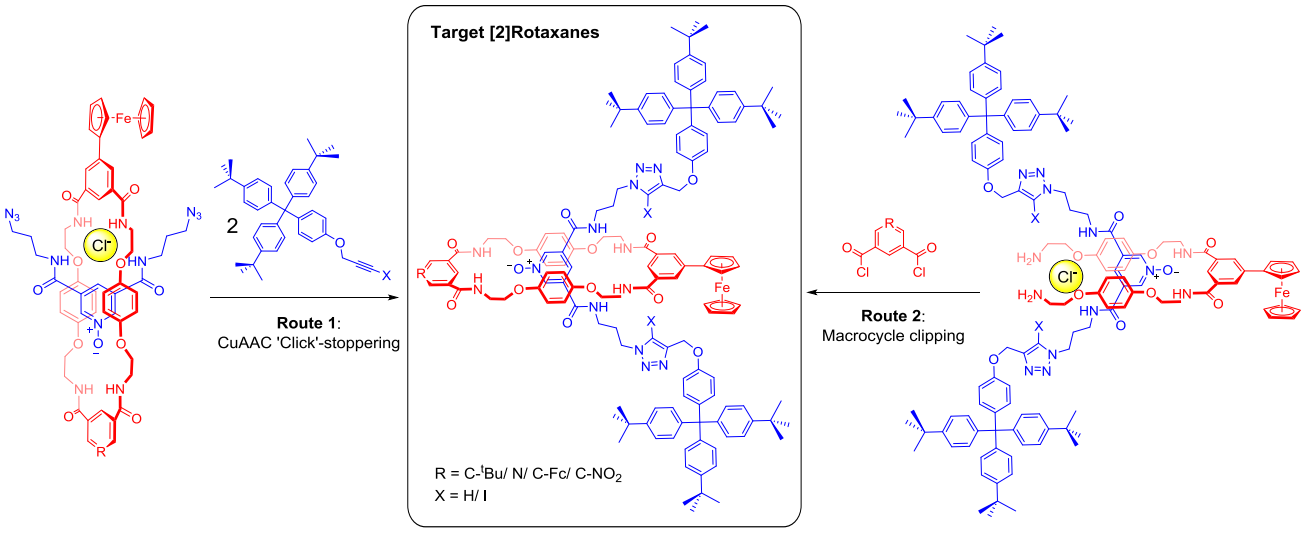
3.2 Neutral Ferrocene-Appended Redox-active Rotaxanes‡

3.2.1 Design, Synthesis and Characterisation

As shown in Figure 3.5A, the target neutral [2]rotaxanes comprise of a pyridine *N*-oxide axle component threaded through a ferrocene-appended macrocycle containing two spatially-separated isophthalamide HB anion binding sites. The ferrocene redox reporter group was appended onto an isophthalamide motif on the macrocycle component to allow direct electronic communication with the interlocked anion binding site. The anion redox sensing properties of these neutral rotaxanes will be compared with those of the cationic rotaxanes previously reported (Section 3.1.2), to determine if the presence of charge on the rotaxane was essential for the rotaxanes' redox sensory behaviour. In addition, the different electron-donating/ withdrawing substituents on the other isophthalamide motif of the macrocycle components would determine the effects of varying the electron deficiency of the rotaxanes' anion binding and sensing properties. Crucially, replacing the prototriazole units positioned at the periphery of the axle component with iodotriazoles would modulate the geometry and size of the binding cavity, likely changing the anion selectivity and redox response.

As shown in Scheme 3.2, the target neutral [2]rotaxanes can be constructed with Cl^- anion-templation, either by (1) double CuAAC 'click'-stoppering of a pre-formed Cl^- templated pseudorotaxane complex between the macrocycle and a bis-azide-terminated pyridine *N*-oxide thread; or (2) clipping of the macrocycle precursor around the free axle by a double acid-chloride condensation ring-closing reaction. As the formation of Cl^--templated pseudorotaxane complexes using a bis-isophthalamide macrocycle and an identical pyridine *N*-oxide thread had previously been demonstrated,[34] Route 1 was attempted first.

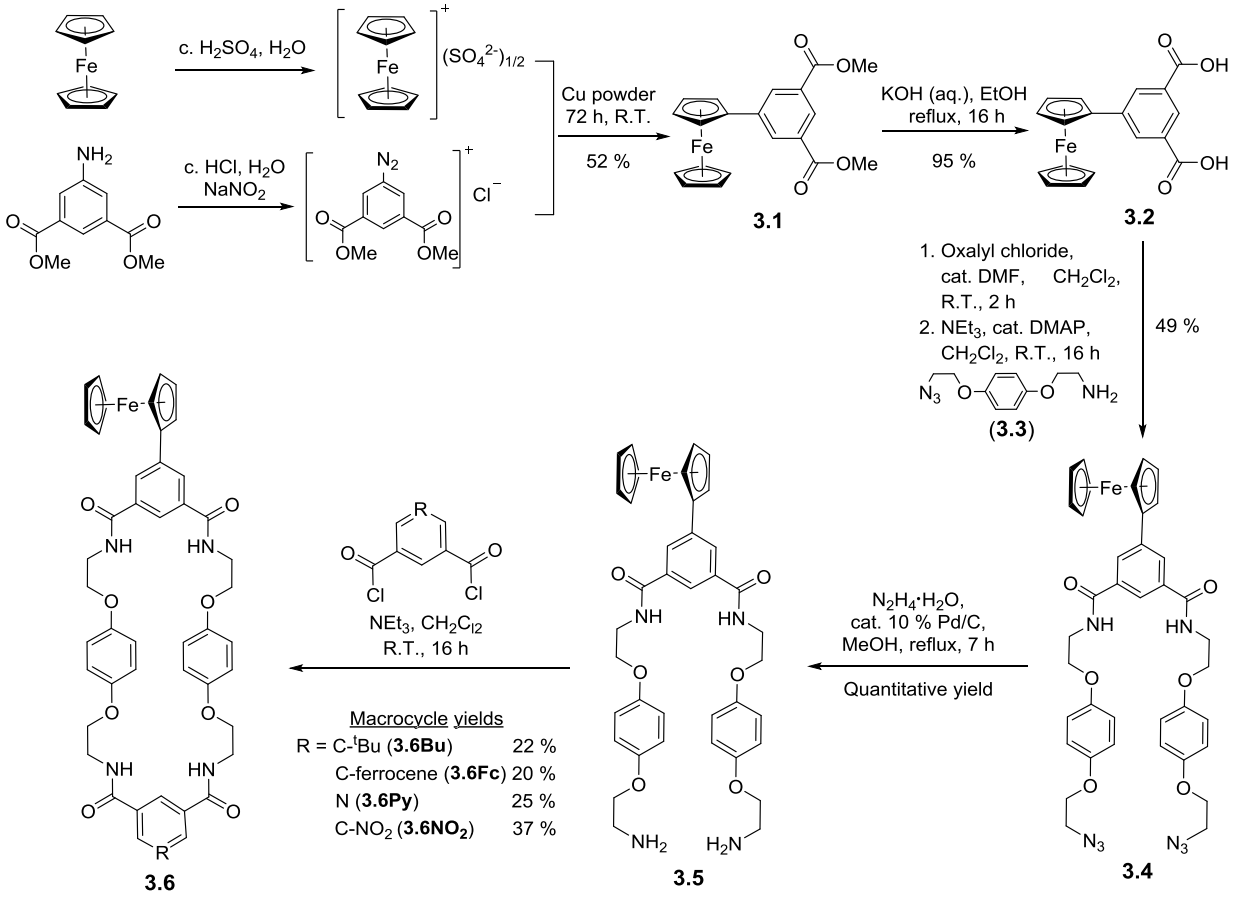
‡ The work in Section 3.2 has been published: Lim, J. Y. C., Cunningham M. J., Davis, J. J., Beer, P. D., *Neutral Redox-active Hydrogen- and halogen-bonding [2]Rotaxanes for the Electrochemical Sensing of Chloride*, *Dalton Trans.*, 2014, **43**, 17274-17282.



***Scheme 3.2**. Anion-templation strategies towards the target neutral [2]rotaxanes.*

The syntheses of the ferrocene-appended bis-isophthalamide macrocycles are summarised in Scheme 3.3. Ferrocene was first appended to an isophthalate ester motif by Sandmeyer-type coupling between ferrocenium and 5-diazonium isophthalate methyl ester[22] produced from commercially-available ferrocene and the corresponding aniline precursor respectively. Base hydrolysis of the ester groups of **3.1** then afforded the key ferrocene-isophthalic acid synthon **3.2** in a good yield of 95 %. Subsequently, a condensation reaction between the bis-acid chloride of **3.2** and two equivalents of primary amine **3.3**[34] produced the bis-azide macrocycle precursor **3.4** in 49 % yield. Initial attempts at reducing the azide functionality of **3.4** to the corresponding amine **3.5** using heterogeneous catalysis with 10 % Pd/C under 3 atmospheres of hydrogen gas[34] afforded a series of unidentifiable and inseparable mixture of products. However pleasingly, when the Pd/C catalysed azide reduction was carried out using hydrazine monohydrate instead of hydrogen gas in refluxing methanol,[35] quantitative formation of **3.5** was obtained after 7 hours. Macrocycle formation was then performed under high dilution conditions in anhydrous CH_2Cl_2 by the amide condensation reactions of bis-amine **3.5** and the relevant acid chloride. Although the target ferrocene-appended macrocycles were obtained in yields ranging from 20 - 37 % following chromatographic purification, all macrocycles other than ^{t}Bu-functionalised **3.6Bu** were

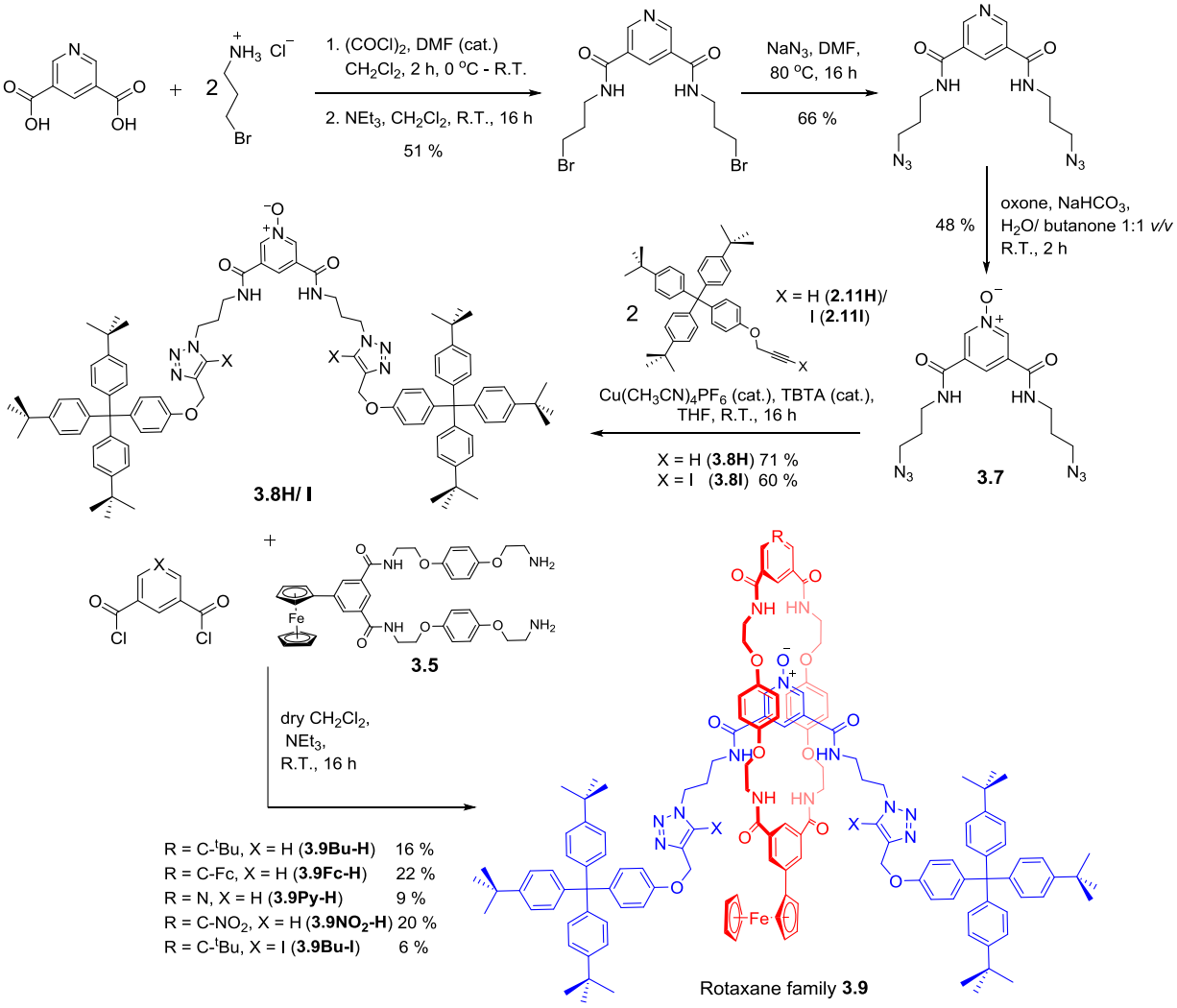
sparingly soluble in halogenated solvents such as CH_2Cl_2 and $CHCl_3$ commonly used for anion-templated rotaxane synthesis. As a result, rotaxane synthesis via CuAAC stoppering in Route 1 could not be performed.



***Scheme 3.3**. Synthesis of the ferrocene-appended bis(isophthalamide) macrocycle family **3.6**.*

Hence, Route 2 (Scheme 3.2) was attempted, which necessitated preparation of the pyridine *N*-oxide axle shown in Scheme 3.4. This was achieved by performing CuAAC reactions with the bis-azide precursor **3.7**, which was synthesised according to a reported procedure,[34] and two equivalents of stopper proto (**2.11H**) or iodo-alkyne (**2.11I**) in degassed THF with catalytic quantities of $[Cu(CH_3CN)_4]PF_6$. [2]Rotaxane formation was achieved by a Cl^--templated clipping synthetic procedure which involved condensation of bis-amine **3.5** with the relevant bis-acid chloride around the axle component. Following removal of the templating

chloride anion by repeated washings with water, the series of [2]rotaxanes **3.9** were purified by preparatory thin layer chromatography in yields ranging from 6 to 22 %, and fully characterised via ^{1}H and ^{13}C-NMR spectroscopy and high resolution ESI mass spectrometry.



***Scheme 3.4**. Synthesis of neutral rotaxane family **3.9** by the macrocycle clipping strategy.*

Using rotaxane **3.9Bu-H** as an example, comparing the ^{1}H-NMR spectrum of the [2]rotaxane with those of the free macrocycle and axle components (Figure 3.6) showed significant upfield shifts for the macrocycle's hydroquinone protons and the pyridine *N*-oxide of the axle (H_1 and H_2), arising from aromatic donor-acceptor interactions. In addition, the macrocycle internal isophthalamide protons H_a and H_c also underwent significant downfield

shifts on rotaxane formation, possibly due to HB interactions with the oxygen atom of the pyridine *N*-oxide axle. Interestingly, both H_a and H_c showed almost equal perturbations despite only one of them being able to interact by HB with the pyridine *N*-oxide oxygen atom at any one time, suggesting that pirouetting of the macrocycle around the axle occurs fast relative to the NMR timescale.[34] Perhaps, this may also account for the lack of desymmetrisation of both hydroquinone environments in the spectrum of rotaxane **3.9Bu-H**, commonly seen in rotaxanes.[24,36–38] Conclusive evidence of the interlocked nature of all members of the **3.9** rotaxane family is seen in their 2D ROESY NMR spectra (Figure 3.7) from the numerous cross-peaks arising from the through-space interactions between axle and macrocycle components.

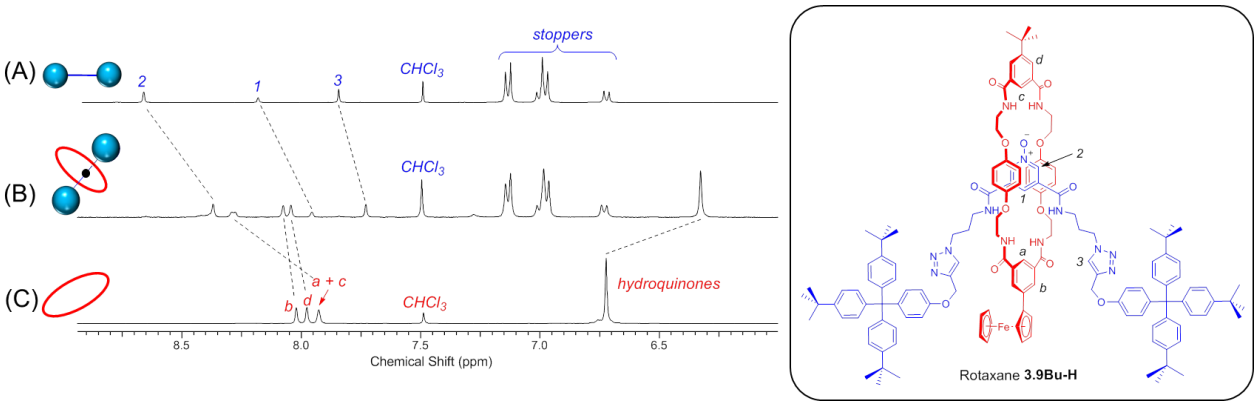


***Figure 3.6**. Partial ^{1}H NMR spectra of (A) free axle **3.8H**; (B) rotaxane **3.9Bu-H** and (C) macrocycle **3.6Bu** ($CDCl_3$/ CD_3OD 1:1 v/v, T = 298 K).*

3.2.2 Anion Recognition Studies

3.2.2.1 ^{1}H NMR Binding Studies

^{1}H NMR titration experiments were performed in $CDCl_3$/ CD_3OD/ D_2O 45:45:10 *v/v* to study the anion binding behaviour of the rotaxanes. As shown in Figure 3.8A, the addition of Cl^- resulted in significant downfield perturbations of the resonances arising from macrocycle isophthalamide protons H_a and H_c, as well as the internal pyridine *N*-oxide proton H_1 flanking the anion binding cavity, due to HB interactions with the Cl^- guest bound in the rotaxane cavity.

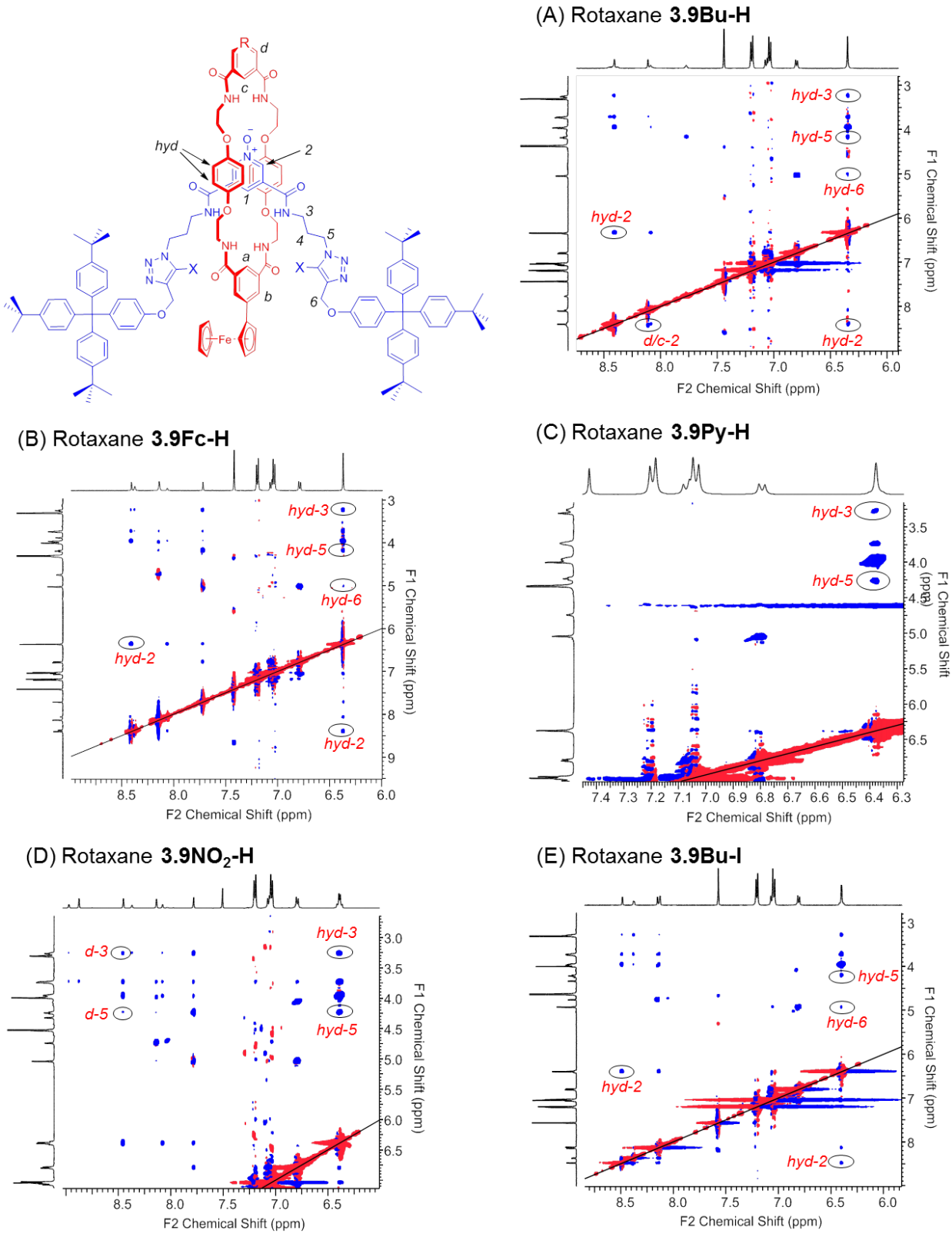


***Figure 3.7**. 2D ROESY NMR spectra of members of the rotaxane family **3.9**, with selected cross peaks indicated ($CDCl_3$/ CD_3OD 1:1 v/v, T = 298 K).*

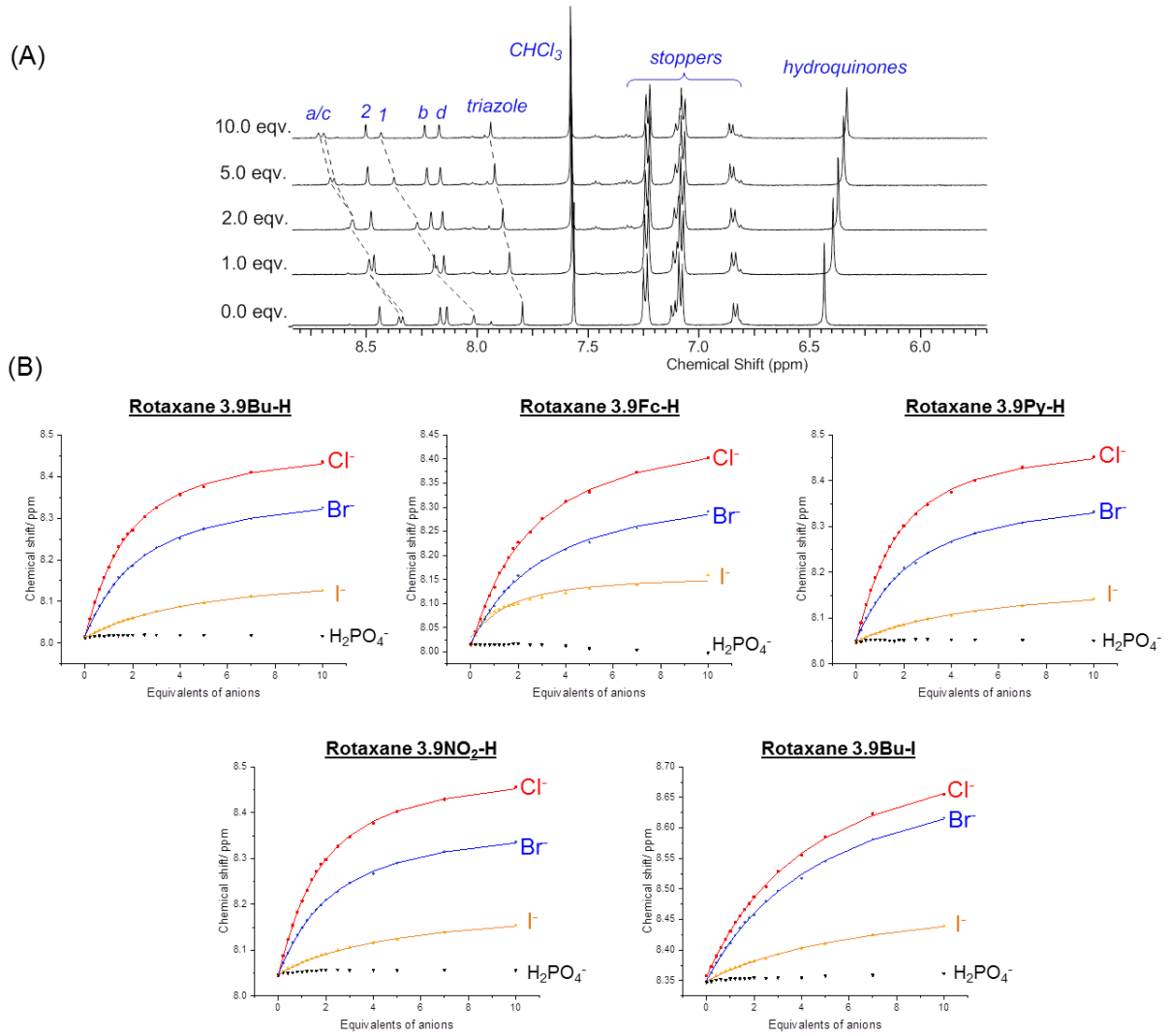


***Figure 3.8**. (A) Partial ^{1}H NMR of rotaxane **3.9Bu-H** in the presence of increasing quantities of Cl^-; (B) Anion binding isotherms obtained from ^{1}H NMR titrations on the **3.9** rotaxane family. Internal axle pyridinium proton H_1 monitored for all cases except **3.9Bu-I** where the Fc-isophthalamide internal proton H_a was monitored- proton assignments follow those in Figure 3.7. In all cases, empirical data are represented by filled dots, while the calculated best-fit isotherms are shown as solid lines ([**3.9**] = 1.5 mM, $CDCl_3$/ CD_3OD/ D_2O 45:45:10 v/v; T = 298 K).*

Table 3.1. Anion association constants (K_a/ M^{-1}) of the rotaxane family **3.9** with halide anions.[a]

	3.9Bu-H	**3.9Fc-H**	**3.9Py-H**	**3.9NO_2-H**	**3.9Bu-I**
Cl^-	546 (10)	423 (13)	569 (12)	542 (16)	152 (5)
Br^-	373 (15)	259 (20)	346 (16)	376 (13)	133 (5)
I^-	138 (5)	120 (16)	124 (3)	149 (9)	81 (8)

[a] Values obtained by fitting the titration data to a 1:1 host-guest binding model using the WinEQNMR2 software;[39] Anions added as their TBA salts; errors (±) in parentheses; No binding of $H_2PO_4^-$ was observed in all cases. [**3.9**] = 1.5 mM, $CDCl_3$/ CD_3OD/ D_2O 45:45:10 *v/v*; *T* = 298 K.

It is noteworthy that macrocycle protons H_a and H_c showed almost identical magnitudes of downfield shifts, indicative that the added Cl^- was binding at both sites in fast exchange on the NMR timescale with a lack of preference for binding at either site. The axle prototriazole proton signals shifted downfield as well, indicating that the axle wraps around the Cl^- anion bound in the interlocked cavity. With Br^- and I^-, similar but smaller signal perturbations are observed (Figure 3.8B), while oxoanions such as $H_2PO_4^-$ did not give any significant shifts of the proton environments surrounding the binding cavity, presumably due to their strongly-hydrated nature. WinEQNMR2 analysis[39] of the halide titration data, monitoring axle pyridine *N*-oxide proton H_1 for all rotaxanes except **3.9Bu-I** (macrocycle proton H_a was monitored instead due to coalescence of H_1 signals with H_b during the titrations) determined 1:1 stoichiometric association constants summarised in Table 3.1.

From Table 3.1, all rotaxanes show a distinct anti-Hofmeister binding selectivity of $Cl^- > Br^- > I^-$. Interestingly, the most strongly hydrated halide (Cl^-)[40] was the strongest bound, presumably arising from complementary shape and size of the rotaxanes' binding site. Despite having substituents of different electron-withdrawing character on the macrocycle, the prototriazole rotaxanes show no appreciable difference in their halide binding affinities, possibly attributed to the dynamic pirouetting nature of the macrocycle component which allow the halide to bind in either isophthalamide binding site. With the introduction of the XB iodotriazole motifs at the periphery of the binding site on the axle in **3.9Bu-I**, a significant reduction in the magnitudes of halide association constants were seen compared to the all-HB analogue **3.9Bu-H**, with the largest decrease noted for Cl^-. As a result, Cl^- and Br^- exhibit comparable binding affinities with **3.9Bu-I**. It is likely that introducing bulky iodine atoms at those axle positions substantially alters the steric accessibility of the rotaxane binding site, thereby reducing the halide binding affinities.

3.2.2.2 Electrochemical Anion Sensing Studies

Having investigated the anion binding behaviour of the rotaxanes by ^{1}H NMR titrations, their redox anion sensing properties were probed by cyclic voltammetry (CV) in the electrolyte

solution of 0.1M $TBAPF_6$ in CH_2Cl_2/ CH_3CN 1:1 *v/v*. A standard three electrode electrochemical cell was used, with a glassy carbon working electrode, a Pt wire auxiliary electrode and a Ag/ $AgNO_3$ non-aqueous reference electrode.[41] By recording CVs in the presence of increasing quantities of anions, the magnitudes of anion-induced cathodic shifts (ΔE) were determined for each rotaxane. For comparison, the redox anion sensing properties of free macrocycle **3.6Bu** was determined under identical conditions.

Macrocycle **3.6Bu** and all rotaxanes exhibit quasi-reversibility of their respective ferrocene/ ferrocenium (Fc/ Fc^+) redox couples (Figure 3.9)[§]. Due to their uncharged nature, no significant difference was observed for the $E_{1/2}$ values of the rotaxanes ($E_{1/2}$ values between +207 and +219 mV) and that of free macrocycle **3.6Bu** ($E_{1/2}$ = +204 mV) relative to the Ag/ $AgNO_3$ reference electrode, in contrast with the cationic rotaxanes previously reported.[21,24]

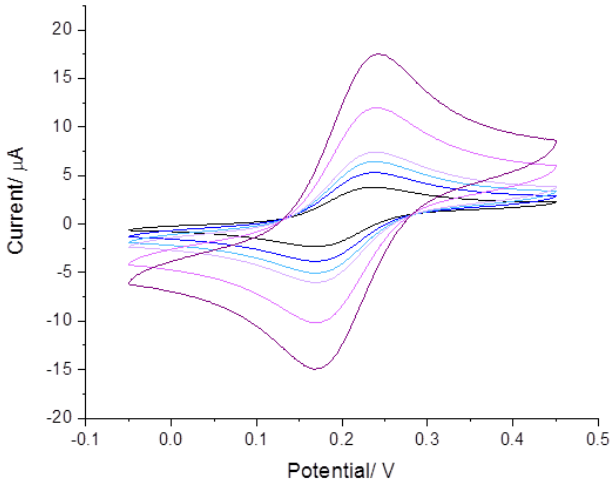


***Figure 3.9**. Reversibility studies performed on rotaxane **3.9Bu-H**, with CVs obtained at increasing scan rates of 25, 50, 75, 100, 250 and 500 mV s^{-1}. Potentials taken in reference to the Ag/$AgNO_3$ reference electrode ([**3.9Bu-H**] = 0.5 mM, 0.1 M $TBAPF_6$ in CH_2Cl_2/ CH_3CN 1:1 v/v, T = 293 K).*

Figure 3.10 shows the resulting cathodic shifts and changes in electrochemical reversibility of the Fc/ Fc^+ redox couple of rotaxane **3.9Bu-H** in the presence of halides (Cl^- and Br^-)[**] and oxoanions (AcO^- and $H_2PO_4^-$). From Table 3.2, macrocycle **3.6Bu** and rotaxane

[§] Details of the reversibility studies performed on all the redox-active host systems studied in this thesis are provided in Appendix B.

[**] The redox sensing properties of the host molecules towards I^- could not be determined as the oxidation of I^- is more favourable than that of the ferrocene moieties, i.e. at a lower redox potential.

3.9Bu-H exhibit larger magnitudes of cathodic shifts with Cl^- than Br^-, arising from the greater degree of stabilisation of the ferrocenium moiety conferred by Cl^- than the more charge diffuse Br^-. With the oxoanions, loss of electrochemical reversibility was observed in the presence of greater than 1.0 equivalent of anion for rotaxane **3.9Bu-H** and macrocycle **3.6Bu**, presumably due to an electron transfer-chemical (EC) mechanism where the ferrocenium moiety of the oxidised host molecules reacts chemically and irreversibly with the anions.[42]

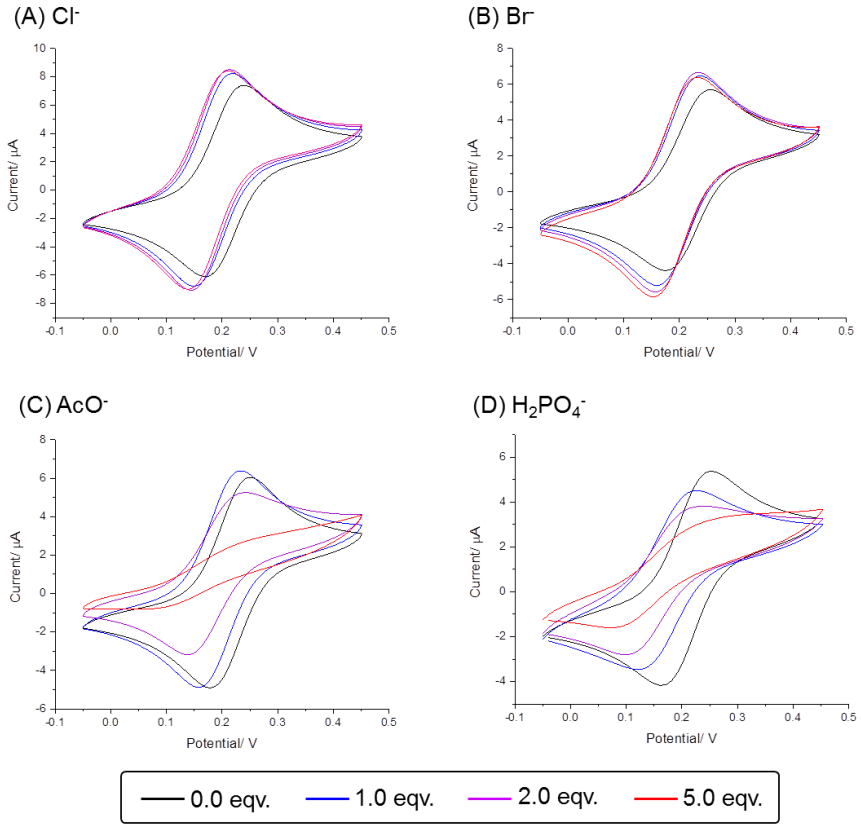


***Figure 3.10**. CVs of rotaxane **3.9Bu-H** in the presence of 0.0, 1.0, 2.0 and 5.0 equivalents of added (A) Cl^-; (B) Br^-; (C) AcO^- and (D) $H_2PO_4^-$. Electrolyte: 0.1 M $TBAPF_6$ in CH_2Cl_2/ CH_3CN 1:1 v/v; potentials compared to the Ag/ $AgNO_3$ reference electrode ([**3.9Bu-H**] = 0.5 mM, T = 293 K).*

Table 3.2. Shifts of the ferrocene/ ferrocenium redox couples of free macrocycle **3.6Bu** and members of the rotaxane family **3.9** in the presence of 5.0 equivalents of different anions.[a]

	3.6Bu	**3.9Bu-H**	**3.9Fc-H**	**3.9Py-H**	**3.9NO_2-H**	**3.9Bu-I**
Cl^-	-31	-37	-34	-24	-33	-31
Br^-	-21	-25				
AcO^-	-[b]	-[b]			-[c]	
$H_2PO_4^-$	-[b]	-[b]				

[a] Anions added as their TBA salts, error estimated to be ± 5 mV. Electrolyte: 0.1M $TBAPF_6$ in CH_2Cl_2/ CH_3CN 1:1 *v/v*; glassy carbon working electrode, Pt wire auxiliary electrode and Ag/ $AgNO_3$ reference electrode; [host] = 0.5 mM, *T* = 293 K. [b] Loss of redox reversibility. [c] not determined.

A comparison of the anion redox sensing behaviour of the rotaxane family **3.9** show comparable magnitudes of Cl^--induced cathodic perturbations in all cases (Table 3.2), with similar retention of redox reversibility even in the presence of excess Cl^- (Figure 3.11). Interestingly, despite the significantly diminished halide binding affinities of XB rotaxane **3.9Bu-I** compared with **3.9Bu-H**, comparable cathodic perturbations were seen. It is also notable that the neutral rotaxanes also display similar Fc/ Fc^+ cathodic shift magnitudes as the *cationic* rotaxane analogues containing the same ferrocenyl-isophthalamide redox-active motif.[21,24] This indicates that these neutral host molecules show similar extents of binding enhancement upon electrochemical ferrocene oxidation, which is likely to be dictated by the through-bond communicative distance between the ferrocene reporter group and the anion binding site.[21] Although the presence of the axle XB iodotriazole groups were able to exert an important steric influence on the anion binding affinities of the rotaxanes, it is ultimately the through-bond communication between the anion binding cavity and the redox reporter group which determines the electrochemical sensory response and sensitivity to the anion recognition process.

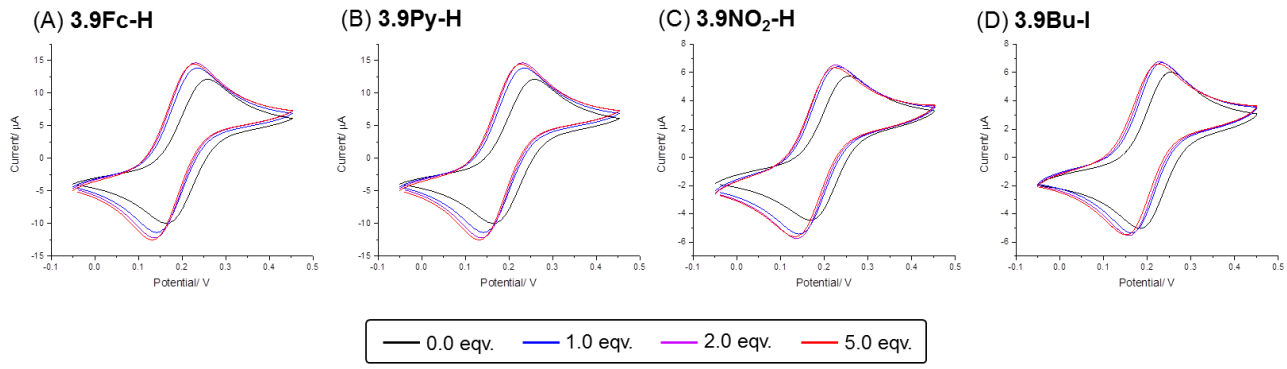
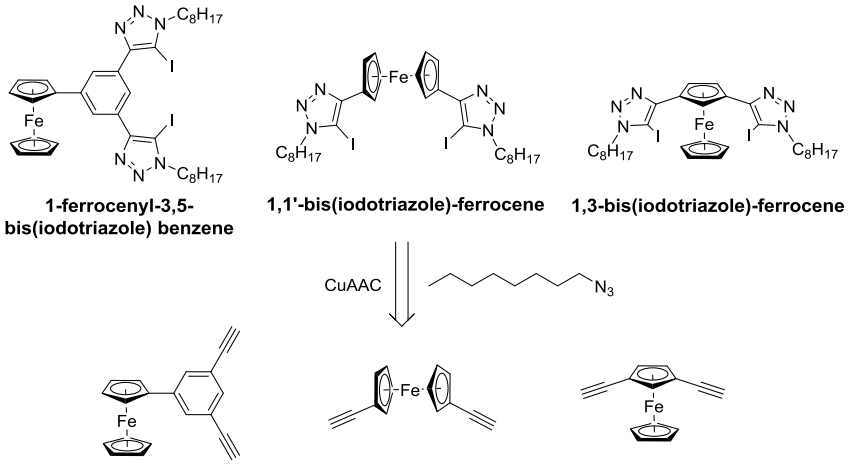


***Figure 3.11**. CVs of rotaxanes (A) **3.9Fc-H**; (B) **3.9Py-H**; (C) **3.9NO$_2$-H** and (D) **3.9Bu-I** in the presence of 0.0, 1.0, 2.0 and 5.0 equivalents of Cl^-. Electrolyte: 0.1 M $TBAPF_6$ in CH_2Cl_2/ CH_3CN 1:1 v/v; potentials compared to the Ag/ $AgNO_3$ reference electrode ([**3.9Bu-H**] = 0.5 mM, T = 293 K).*

3.3 Redox-active σ-Hole Donor Model Host Systems††

3.3.1 Design and Synthesis of Halogen Bonding Ferrocene Acyclic Receptors

Following on from work in the previous section, it was envisaged that by replacing the HB isophthalamide motif with XB-donor iodotriazole groups, the through-bond communicative pathway between the anion binding site and redox reporter group may be enhanced due to the more pronounced covalent character of the XB···anion interaction compared to HB. Three unique ferrocene-containing bidentate XB motifs were investigated: the appendage of ferrocene to a central benzene unit meta-substituted with two iodotriazole groups, as well as incorporation of ferrocene into the anion binding motif itself with bis-iodotriazole substitution at either the 1,1'- or 1,3-positions (Scheme 3.5). Not only does this confer different anion binding geometries and bite angles, the varying electronic conjugation pathways and spatial separation between the binding site and ferrocene are expected to modulate the host binding and redox sensing properties. In all cases, the analogous HB receptors were synthesised to determine the roles played by the XB donor groups in the redox anion sensing process. As shown in Scheme 3.5, all target redox-active hosts were prepared by CuAAC reactions of *n*-octyl azide with their respective ferrocene-containing bis-alkyne precursors, whose syntheses are detailed in the following sections.

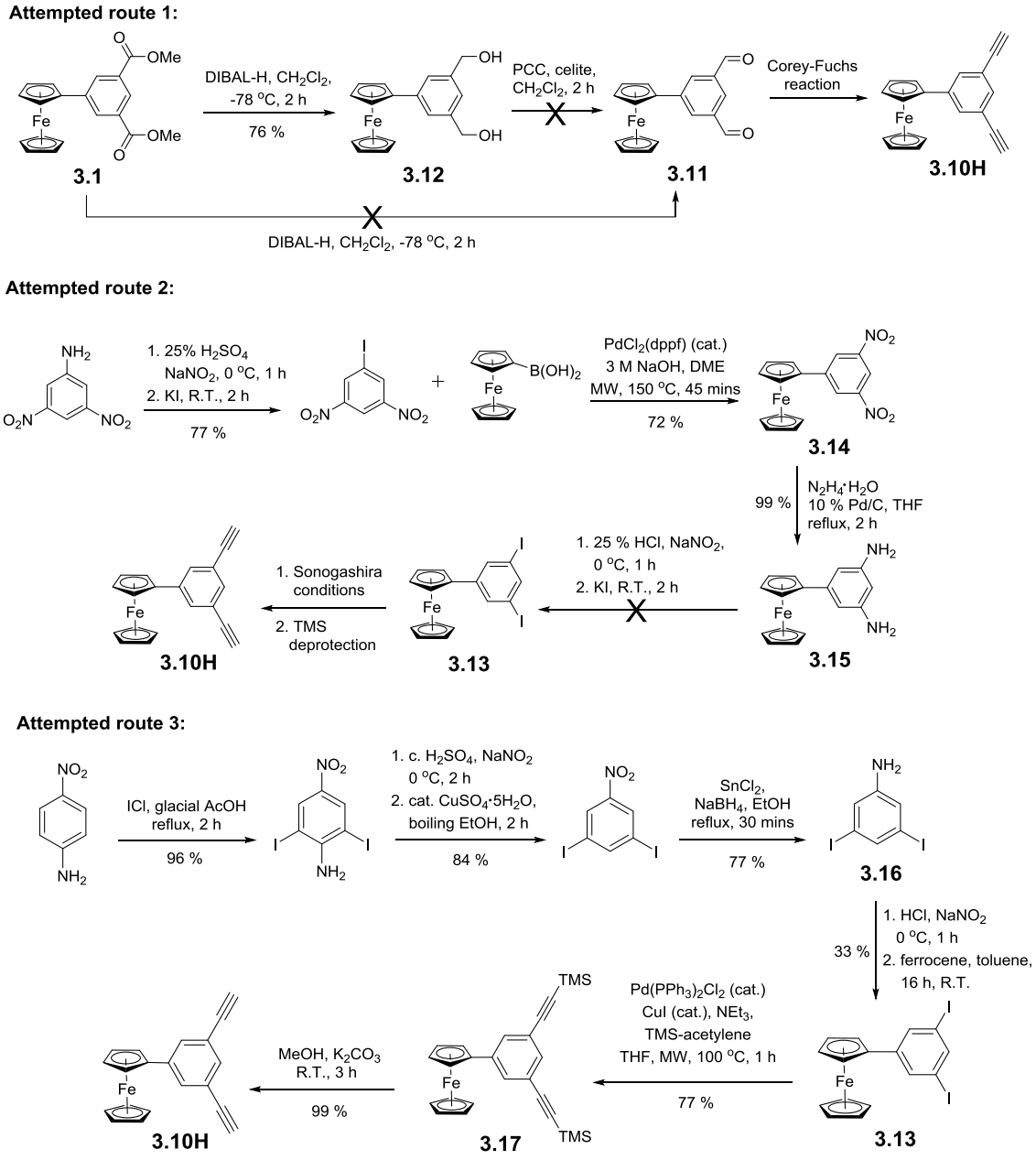


***Scheme 3.5**. Retrosynthesis of redox-active XB model acyclic receptors.*

†† Some of the work described in this section has been published: Lim, J. Y. C., Cunningham, M. J., Davis, J. J., Beer, P. D., *Halogen Bonding-enhanced Electrochemical Halide Anion Sensing by Redox-active Ferrocene Receptors*, *Chem. Commun.*, 2015, **51**, 14640; Lim, J. Y. C., Beer, P. D., *A Halogen Bonding 1,3-Disubstituted Ferrocene Receptor for Recognition and Sensing of Azide*, *Eur. J. Inorg. Chem.*, **2017**, 220-224.

3.3.1.1 The 1-Ferrocenyl-3,5-bis(iodotriazole) Benzene Motif

The multi-stepped synthesis of the bis-alkyne synthon **3.10H** was pursued via a number of routes (Scheme 3.6). Initially, it was envisaged that the ferrocene bis-isophthalate methyl ester **3.1** could be reduced using diisobutyl-aluminium hydride (DIBAL-H) to the corresponding bis-aldehyde **3.11**, and converted to the target bis-alkyne **3.10H** in one step via a Corey- Fuchs reaction.[43] However, DIBAL-H reduction of the ester **3.1** was problematic, as



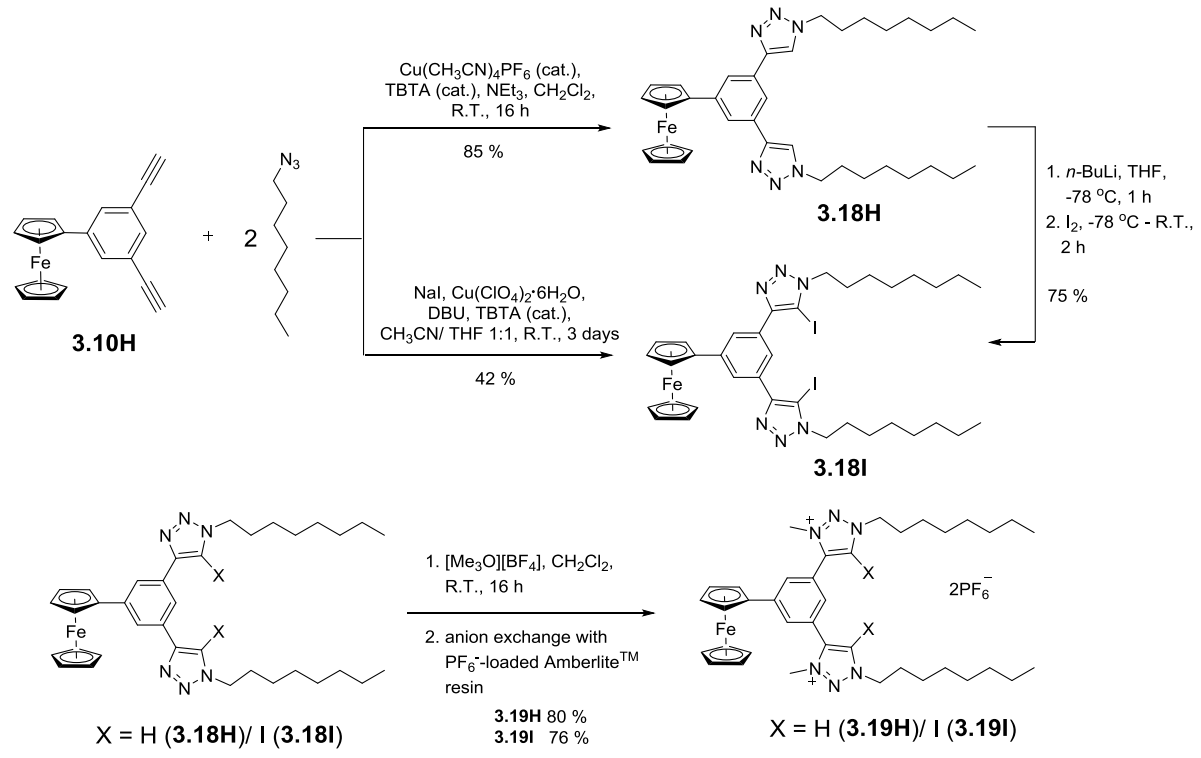
***Scheme 3.6**. Attempted synthetic routes towards ferrocene-appended benzene bis-alkyne **3.10H**.*

two equivalents of DIBAL-H failed to bring about any noticeable reaction after 6 hours, and an excess of DIBAL resulted in complete reduction to the bis-alcohol **3.12** even at -78 ^{o}C. Due to the sensitivity of the ferrocenium moiety towards oxidation, gentle oxidation of **3.12** to **3.11** was then attempted using pyridinium chlorochromate (PCC). Unfortunately, this reaction afforded a mixture of unidentifiable products with no evidence of **3.11** seen by ESI-MS and ^{1}H NMR analyses. Although not attempted at the time, other mild oxidation conditions such as the Swern[44] could perhaps have been performed.

An alternative route for the preparation of **3.10H** was pursued, where the bis-alkyne was installed using Sonogashira procedures from bis-iodobenzene precursor **3.13**. To construct **3.13**, Route 2 (Scheme 3.6) was attempted where commercially-available 3,5-dinitroaniline was first converted to 3,5-dinitro-iodobenzene via a diazonium intermediate in a good yield of 77 %. Suzuki coupling of the iodobenzene with ferrocene boronic acid[21] afforded the dark red ferrocene-substituted dinitrobenzene **3.14**, which could be reduced to the diaminobenzene **3.15** in near-quantitative yields using hydrazine monohydrate. Unfortunately, attempts to convert **3.15** to **3.13** via formation of the bis-diazonium intermediate using either 25 % HCl (aq.) or H_2SO_4 (aq.) with sodium nitrite were unsuccessful. This was likely due to instability of the bis-diazonium intermediate, resulting in the consistent formation of a dark brown tar upon addition of sodium nitrite to the reaction even under an inert atmosphere in the dark.

In light of the difficulty encountered in forming **3.13** via Route 2, another strategy was attempted where 3,5-diiodoaniline **3.16** was used as a key intermediate. As shown in Route 3 in Scheme 3.6, commercially-available *para*-nitroaniline was first regioselectively bis-iodinated at the *ortho*-positions using iodine monochloride, followed by removal of the central aniline group and then reduction of the nitro functionality using tin dichloride to afford **3.16**.[45] After diazotisation of **3.16** and coupling to ferrocene, key intermediate **3.13** was obtained in a modest yield of 33 %. Microwave-assisted Sonogashira coupling reaction with ethynyltrimethylsilane, followed by TMS-deprotection using potassium carbonate finally afforded the bis-alkyne synthon **3.10H** which was found to be air-, light- and moisture-stable, with no evidence of decomposition observed after two weeks under ambient conditions.

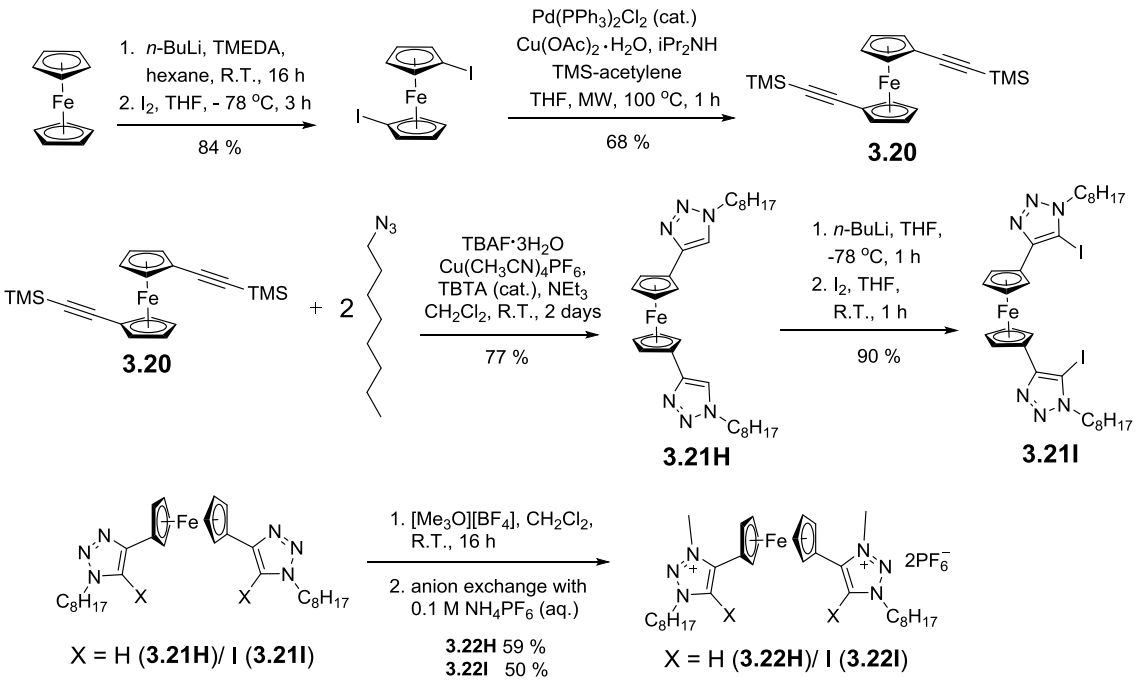
Using **3.10H**, the synthesis of the target bidentate receptors **3.18H/I** is summarised in Scheme 3.7 using standard CuAAC conditions with two equivalents of *n*-octyl azide. To prepare the bis-iodotriazole receptor **3.18I**, one-pot iodo-'Click' conditions were first attempted[46] to afford the target compound in a modest isolated yield of 42 %. In an attempt to improve the yield, the HB analogue **3.18H** was reacted with *n*-butyllithum, which regioselectively deprotonated the triazoles. Subsequent quenching of the lithium triazolides with molecular iodide furnished bis-iodotriazole **3.18I** in 75 % yield. To enhance the strength of the XB interactions, N^3-methylation of each triazole on **3.18H/I** was performed using two equivalents of trimethyloxonium tetrefluoroborate. Following purification using preparatory TLC, anion exchange with a PF_6^--loaded Amberlite™ column gave the target receptors **3.19H** and **3.19I** in 80 % and 76 % yields respectively, which were characterised by ^{1}H, ^{13}C, ^{19}F and ^{31}P NMR spectroscopy and high resolution ESI-MS.



***Scheme 3.7**. Forward synthesis of neutral receptors **3.17I/H** and dicationic receptors **3.18I/H**.*

3.3.1.2 The 1,1'-bis(Iodotriazole)-Ferrocene Motif

The target host compounds were prepared from the 1,1'-disubstituted bis(trimethylsilylethyne) synthon **3.20** which was synthesised from ferrocene following the procedure reported by Pudelski[47] (Scheme 3.8). Cognisant of the reported observation that the TMS-deprotected 1,1'-di(ethynyl)ferrocene was susceptible to intramolecular cyclisation and oligomerisation reactions,[47] **3.20** was subjected to *in-situ* TMS-deprotection using TBAF before immediate CuAAC reaction was performed with two equivalents of *n*-octyl azide and stoichiometric quantities of $[Cu(CH_3CN)_4]PF_6$, which afforded **3.21H** in 77 % yield. Notably, a much poorer yield of **3.21H** (< 10 %) was obtained using catalytic quantities of the Cu(I) catalyst. To synthesise the XB iodotriazole analogue **3.21I**, an initial attempt of reacting the *in-situ* deprotected bis-alkyne with octyl azide under one-pot iodo-'Click' conditions[46] failed to yield any products. Therefore, **3.21I** was prepared by deprotonating the acidic (proto)triazoles of **3.21H** using *n*-butyllithium and quenching the lithium triazolide intermediate with molecular I_2 in 90 % isolated yield. Subsequent bis-methylation of **3.21H/I** with trimethyloxonium tetrafluoroborate afforded the dicationic products **3.22H/I**, which were found to be slightly unstable to light when subjected to chromatographic purification. As a consequence,



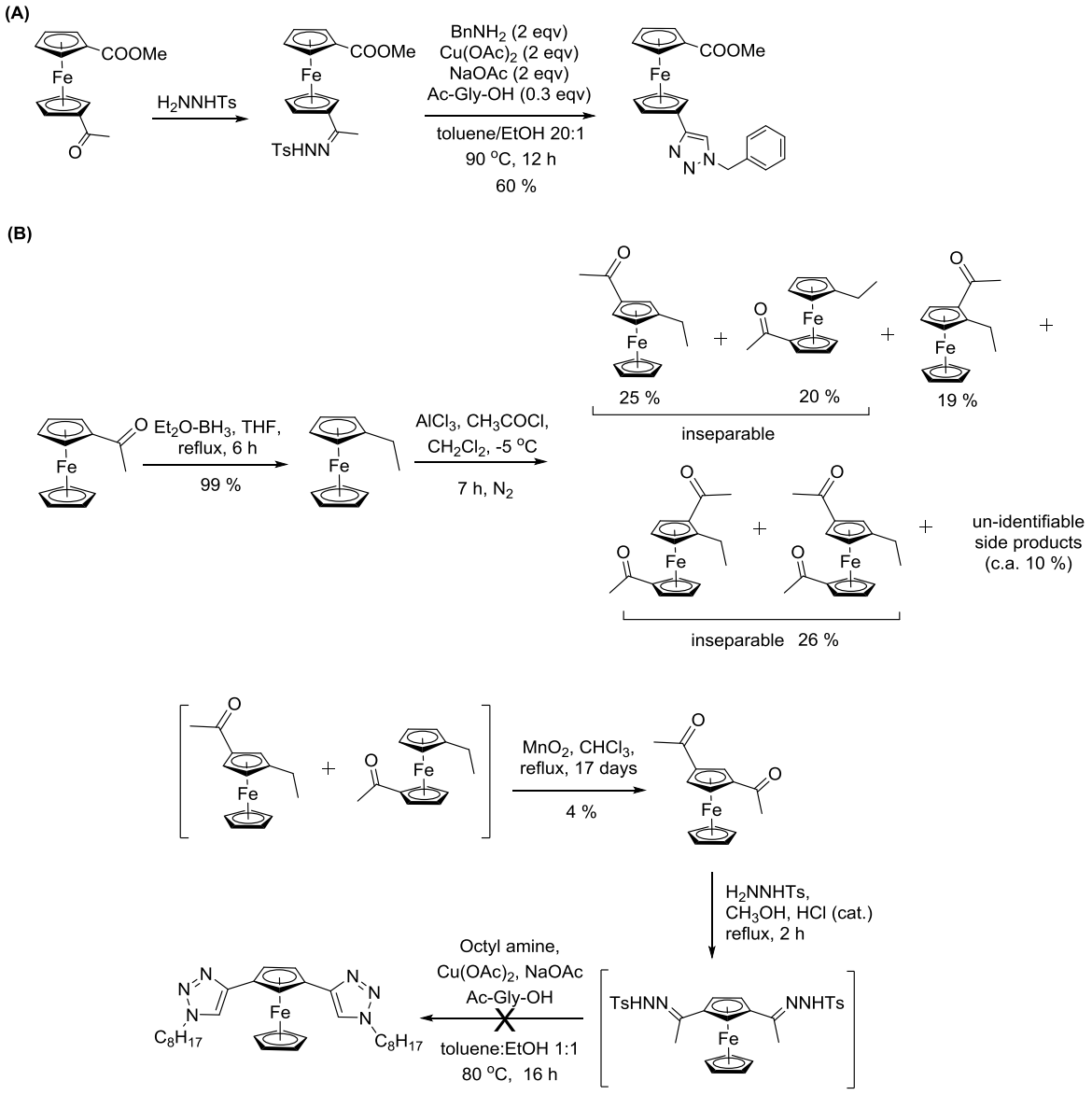
***Scheme 3.8**. Synthesis of the neutral and dicationic 1,1'-disubstituted ferrocene receptors.*

preparatory TLC purification was performed in the dark to reduce the extent of photo-decomposition, and anion exchange to the PF_6^- salt was achieved by repeated washing of chloroform solutions of the receptors with 0.1 M NH_4PF_6 (aq.).

3.3.1.3 The 1,3-Bis(iodotriazole)-Ferrocene Motif

Although 1,3-substituted ferrocene compounds have been reported in applications such as liquid crystals[48] and as pincer ligands for metal complexation,[49,50] their applications have been limited by the synthetic difficulties of selectively functionalising ferrocene on the same cyclopentadienyl ring. Indeed, very few methods have been reported since the 1970s, with an overwhelming majority of 1,3-substituted ferrocene systems reported based on functionalising 1,3-diacetylferrocene, whose preparation commonly followed the statistical functionalisation protocol reported by Makarovskaya and co-workers in 1975 (*vide infra*).[51] While another method of synthesising 1,3-diacetylferrocene has since been reported,[52,53] this method requires highly reactive intermediates, necessitating the use of Schlenk line techniques. With these synthetic precedents in mind, initial attempts to prepare the target 1,3-bis(triazole) ferrocene receptor focused on converting the acetyl groups of Makarovskaya's 1,3-diacetylferrocene directly to triazoles.[54–57] Towards this goal, a recent novel method reported by Zhang *et. al.* was pursued, where an *N*-tosylhydrazone derived from a methyl ketone was converted to the triazole with an aliphatic or aromatic primary amine in the presence of stoichiometric quantities of copper(II),[58] allowing the authors to successfully synthesise a ferrocene-substituted triazole from an acetylferrocene starting material (Scheme 3.9A).

The synthesis of 1,3-bis(triazole)-ferrocene was attempted using this route (Scheme 3.9B). As reported by Makarovskaya, acetylferrocene was first reduced to ethylferrocene using borane under reflux conditions in near quantitative yields. Although statistical Friedel Crafts acetylation of ethyl ferrocene using $AlCl_3$ and acetyl chloride gave a mixture of 1,1'-, 1,2-, 1,3-, 1,2,1'- and 1,3,1'-substituted ferrocenes, the 1,3-substituted ferrocene intermediate was the major product (25 % yield by ^{1}H NMR) due to the presence of the ethyl group activating the



***Scheme 3.9**. (A) Reported synthesis of a ferrocene-triazole from an N-tosylhydrazone by Zhang;[58] (B) Attempted forward synthesis of target 1,3-bis(triazole)-ferrocene receptors via 1,3-diacetylferrocene.*

substituted cyclopentadienyl ring towards electrophilic attack. Unfortunately, as the 1,1'- and 1,3-substituted ferrocene products had exactly the same R_f values in all attempted solvent mixtures, it was not possible to separate these products by column chromatography. The ethyl group of the resulting intermediate was then oxidised with a 20-fold excess of manganese(IV) oxide under reflux conditions for 17 days. However despite many attempts (see Table 3.3 for list of conditions attempted), only trace ethyl oxidation was achieved, with the best isolated yield of 1,3-diacetylferrocene obtained being only 4 %. Subsequently as a test reaction, 1,3-diacetylferrocene was reacted with *N*-tosylhydrazine under acid catalysis to form the bis-

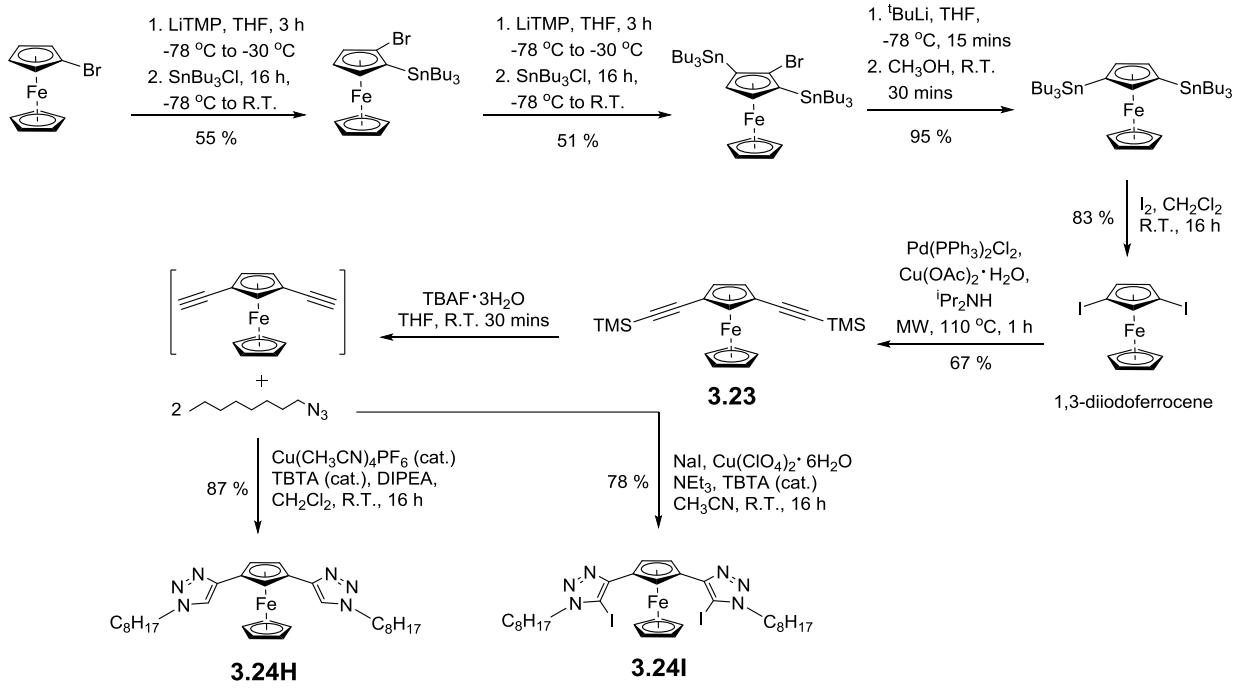
(tosylhydrazone), which was shown to be formed by ESI-MS analysis (*m/z* = 607.2 $[M+H]^+$). After work-up, the resulting crude mixture was reacted onwards without further purification using Zhang's reported conditions, Unfortunately, no trace of any triazole formation could be detected in the multitude of products formed in the reaction. Due to the inherent difficulties encountered and the very low yields obtained, this method was eventually abandoned.

Table 3.3. Attempted conditions for synthesis of 1,3-diacetylferrocene from 1-ethyl-3-acetylferrocene.

S/N	Reaction conditions	Yield
1	MnO_2, $CHCl_3$, 17 days, reflux	0
2	MnO_2 activated according to literature procedure of azeotropic dehydration,[59] $CHCl_3$, 17 days, 70 ^oC	trace
3	MnO_2 activated, $CHCl_3$, 4 hours, MW, 140 ^oC [a]	trace
4	Freshly-prepared MnO_2,[b] $CHCl_3$, 17 days, 70 ^oC	4 %
5	Freshly-prepared MnO_2, [b] CH_3CN,[c] 3 days, reflux	trace

[a] MW conditions were attempted in order to reduce MnO_2 deactivation during long reaction times. [b] MnO_2 was freshly-prepared with $MnCl_2$ and $KMnO_4$ according to the method by Fatiadi.[60] [c] CH_3CN is another solvent sometimes used for oxidations using MnO_2.[61]

An alternative strategy for ferrocene 1,3-substitution relies on the selective removal of the central functionality of a 1,2,3-trisubstituted precursor,[62–65] which has allowed Weissensteiner *et. al.* to prepare 1,3-diiodoferrocene starting from bromoferrocene.[66] As shown in Scheme 3.10, successive *ortho*-lithiations of bromoferrocene facilitated the construction of the 2-bromo-1,3-bis(tributylstannyl)ferrocene intermediate by taking advantage of the enhanced acidity of the cyclopentadienyl protons *ortho*- to the bromo-substituent. Thereafter, the central bromine group was removed by lithium-bromine exchange using *t*-BuLi and quenching the resulting lithiated species with methanol, without affecting the tributylstannyl groups. Substitution of the tributylstannyl groups with iodine afforded the 1,3-diiodoferrocene synthon, which was then subjected to microwave-assisted Sonogashira conditions to produce the corresponding bis-TMS acetylene **3.23** in 67 % yield. *In-situ* TMS deprotection of **3.23**, followed by standard 'proto'- and one-pot 'iodo-Click' conditions produced the target neutral 1,3-substituted ferrocene receptors **3.24H** and **3.24I** in 87 % and 78 % isolated yields respectively, which were then characterised by ^1H and ^{13}C NMR and high-resolution ESI-MS.



***Scheme 3.10**. Synthesis of 1,3-bis(triazole)-ferrocene receptors via 1,3-diiodoferrocene.*

Attempts to methylate each triazole on **3.24H/I** with trimethyloxonium tetrafluoroborate were unsuccessful due to decomposition of the cationic derivatives observed even when the reactions were performed in the absence of light and under an inert atmosphere.

3.3.2 Anion Binding and Recognition Studies of Halogen Bonding Receptors

3.3.2.1 ^{1}H NMR Titrations

<u>The Effects of XB Bite Angle on Anion Affinity</u>

To study the effects of XB bite angle on binding anions with different geometries, ^{1}H NMR titrations were performed on neutral receptors **3.18I**, **3.21I** and **3.24I** in d_6-acetone‡‡ with spherical Cl^- and linear N_3^-. From Figure 3.12, addition of Cl^- elicited notable downfield shifts of internal aromatic proton resonances H_a for receptor **3.18I**, as well as ferrocene protons H_A for **3.21I** and H_1 for **3.24I**, indicating HB interactions with the anions bound in close proximity by

‡‡ A polar aprotic solvent (acetone) was chosen for the titrations to reduce the effects of anion solvation, commonly seen with protic solvents, to render the effects of complementary host-guest shape, size and geometry more apparent.[67]

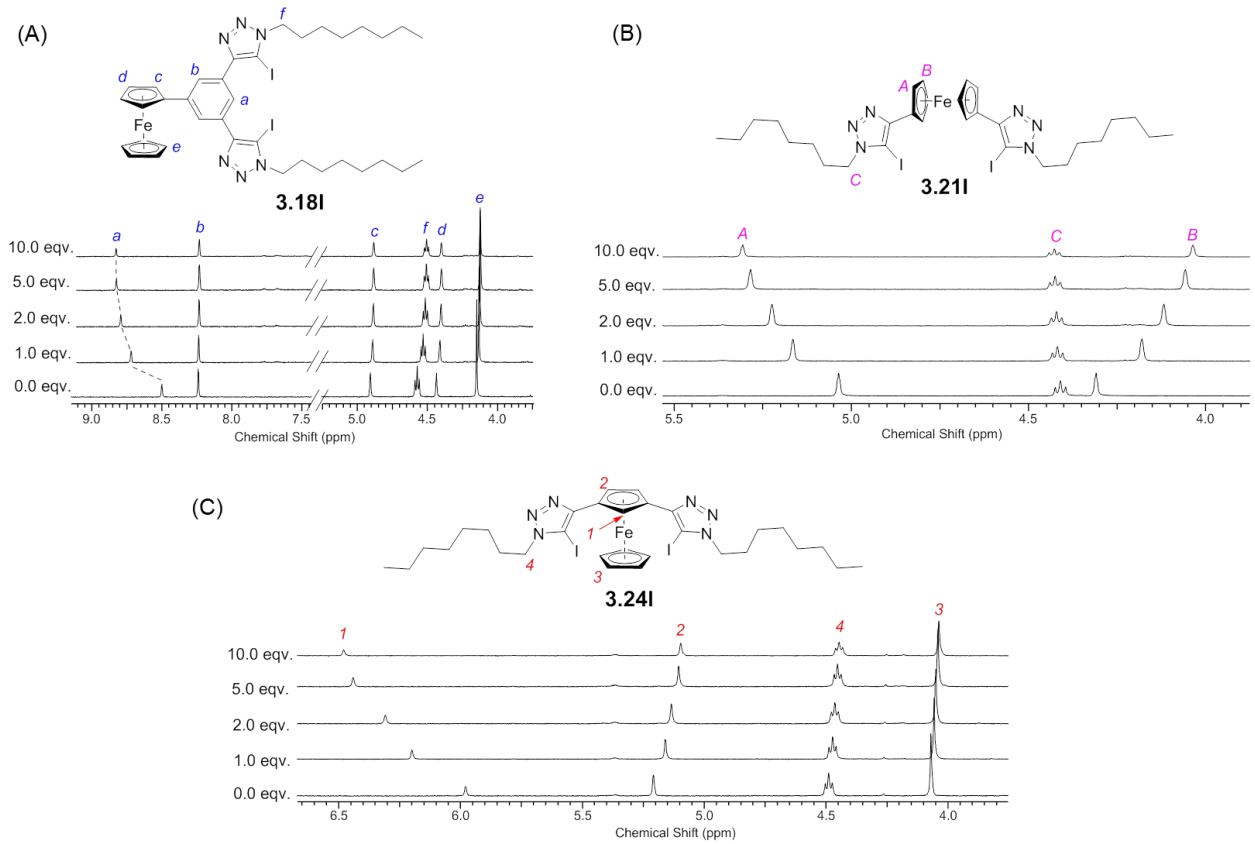


***Figure 3.12**. Partial ^{1}H NMR spectra of neutral ferrocene-containing XB hosts (A) **3.18I**; (B) **3.21I** and (C) **3.24I** in the presence of increasing quantities of TBACl ([host] = 1.5 mM, d_6-acetone, T = 298 K).*

Table 3.4. Anion association constants (K_a/ M^{-1}) for neutral XB receptors **3.18I**, **3.21I** and **3.24I**.[a]

	3.18I	**3.21I**	**3.24I**
Cl^-	3750 (129)	903 (20)	649 (21)
N_3^-	413 (21)	225 (4)	669 (16)

[a] Values of K_a determined using WinEQNMR2 software,[39] monitoring internal proton H_a for **3.18I**, H_A for **3.21I** and H_1 for **3.24I** (see Figure 3.12 for assignments). Anions added as their TBA salts; errors (±) in parentheses ([host] = 1.5 mM; d_6-acetone, T = 298 K).

the XB donor iodotriazoles. Similar notable downfield shifts of these proton environments were also observed during the titrations performed with N_3^-. Non-linear regression analyses of these signal changes as a function of anion concentration, using the WinEQNMR2 software,[39] determined the 1:1 stoichiometric anion association constants (K_a) for Cl^- and N_3^- (Table 3.4). In addition, smaller but significant upfield shifts were seen for all ferrocene proton environments not involved in direct HB with the bound anion ($H_{c\text{-}e}$ for **3.18I**; H_B for **3.21I**; H_2 and H_3 for **3.24I**). These shifts suggested a degree of electronic communication between

ferrocene and the binding site, likely resulting from donation of electron density into the conjugated framework of the receptor molecules.

The quantitative binding data shown in Table 3.4 highlights the clear influences of XB bite angle on binding anions of different geometries in the absence of charge assistance. Amongst the three receptor designs, **3.18I** bound the spherical Cl^- most strongly, while wider XB bite angles in **3.21I** and **3.24I** resulted in a diminution of Cl^- binding affinities. Contrastingly, **3.24I** was found to possess the most optimal XB geometry for bidentate N_3^- coordination, such that its binding affinity for N_3^- was slightly larger than that for Cl^-. Attempts to study the **3.24I**-N_3^- complex in the solid state were unsuccessful as crystals of sufficient quality for X-ray diffraction analysis could not be obtained, however it was postulated that the spatial separation between both iodotriazoles was optimal for interacting with the Lewis basic terminal N atoms of N_3^-. Although it is reasonable to expect that the wide XB bite angle of **3.21I** may also favour coordination of the linear N_3^- anion over Cl^-, the latter anion was surprisingly bound more strongly. This may be due to the less preorganised nature of **3.21I** arising from the rotary flexibility of the 1,1'-substituted ferrocene unit,[24] which may prevent convergent bidentate coordination of N_3^- by both iodotriazoles. Indeed, the smaller K_a values for N_3^- obtained for **3.18I** and **3.21I** emphasises the importance of host-guest size complementarity for anion complexation.

<u>The Influences of Charge and Increasing Solvent Polarity</u>

To understand how solvent polarity affected the binding affinities of the XB hosts, ^{1}H NMR titration experiments were performed with neutral receptor **3.21I** in the more competitive polar aprotic solvent CD_3CN. In this solvent, a significant decrease in anion binding affinity was observed compared to d_6-acetone, with the K_a values for Cl^- and Br^- determined to be only (72 ± 2) and (53 ± 1) M^{-1} respectively, showing that halide charge density played a role in governing anion affinities in CD_3CN. For comparison, the HB host analogue **3.21H** bound Cl^- and Br^- with K_a values of (4.0 ± 0.3) and (3.0 ± 0.3) M^{-1} respectively, showing the superiority of XB hosts for anion binding compared to HB.

Analogous anion binding investigations with dicationic host molecules **3.19I** and **3.22I** revealed charge assistance enhances the XB interactions greatly, giving very strong binding of Cl^- to dicationic **3.19I** ($K_a > 10^4$ M^{-1}) in CD_3CN. Hence, the ^1H NMR titrations were repeated in the highly-competitive aqueous media of CD_3CN/ D_2O 9:1 *v/v*. Crucially in the presence of water, the addition of Cl^- still resulted in significant perturbations of the proton environments of **3.19I**, most notably that of H_a (Figure 3.13A), which suggested that Cl^- was still coordinated predominantly in the binding cleft flanked by both iodotriazolium groups. With the dicationic 1,1'-disubstituted ferrocene receptor **3.22I**, substantial downfield shifts of the H_A resonance were also seen following Cl^- addition (Figure 3.13B) in a similar way to that of its neutral congener **3.21I**. Despite the possibility of the electron-deficient triazolium methyl groups (H_g and H_D for **3.19I** and **3.22I** respectively) hydrogen bonding with the halide guest in both receptors, negligible shifts of these signals were seen during the titrations, clearly indicating that Cl^- was interacting mainly with the XB-donor iodine atoms on the iodotriazolium groups. When the titrations were performed with Br^-, slightly larger downfield perturbations were seen

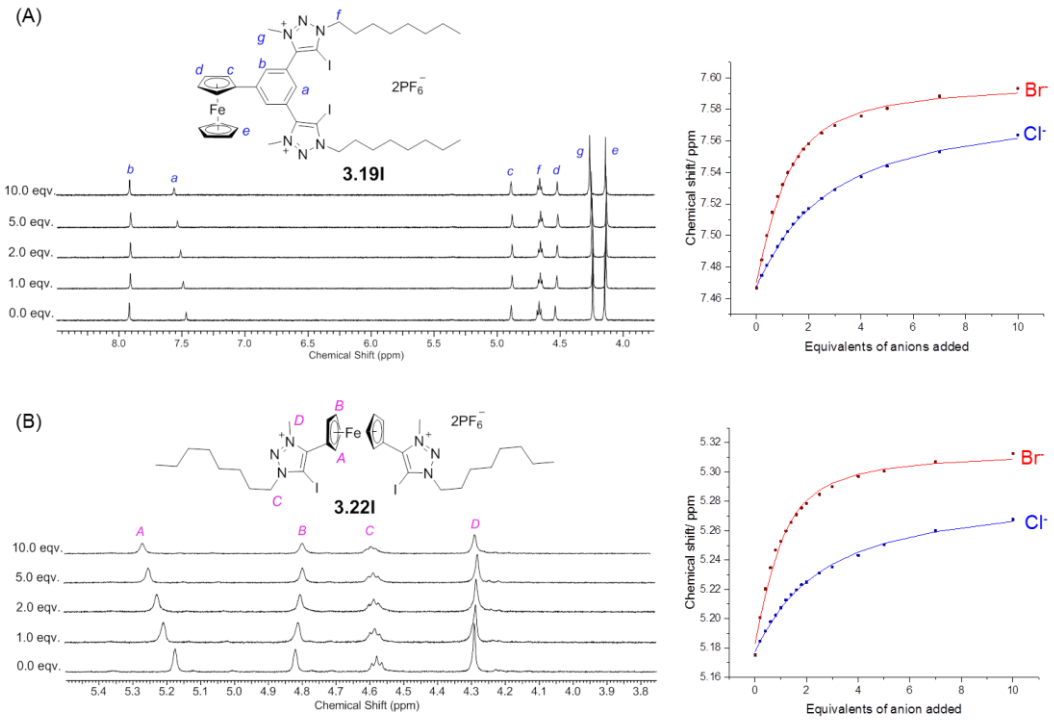


***Figure 3.13**. (Left) Partial ^1H NMR spectra of dicationic XB receptors (A) **3.19I** and (B) **3.22I** in the presence of increasing quantities of TBACl in CD_3CN/ D_2O 9:1 v/v. (Right) Plot of the corresponding changes in the chemical shifts of (A) proton H_a for **3.19I** and (B) proton H_A for **3.22I** in the presence of increasing quantities of halides ([host] = 1.5 mM, T = 298 K). Dots represent empirical data points; solid lines represent the calculated binding isotherms.*

for H_a and H_A for **3.19I** and **3.22I** compared to the Cl^- titrations (Figure 3.13, right), suggesting enhanced interactions with Br^-. The 1:1 stoichiometric anion association constants determined by monitoring these proton signals are collected in Table 3.5, together with those with their HB host analogues for comparison.

Table 3.5. Anion association constants for redox-active dicationic receptors in wet acetonitrile.[a]

	Cl^-	Br^-
3.19I	286 (13)	1139 (87)
3.19H	77 (2)	86 (3)
3.22I	312 (21)	1024 (15)
3.22H	94 (3)	100 (3)

[a]1:1 association constants calculated using WinEQNMR2,[39] following internal aromatic proton H_a for **3.19H/I**, ferrocene proton H_A for **3.22I** and the triazolium aromatic proton for **3.22H**; anions added as their TBA salts; errors (±) in parentheses ([host] = 1.5 mM, CD_3CN/ D_2O 9:1 *v/v*, *T* = 298 K).

All dicationic XB hosts bound the halides more strongly than their HB analogues, with the K_a values for Br^- magnified by more than an order of magnitude for both **3.19I** and **3.22I** (Table 3.5). Compared to binding in dry solvents, a reversal of binding selectivity resulted, which is likely due to the greater ease of Br^- desolvation than Cl^-. Br^- was bound significantly more strongly than Cl^- for both XB hosts, while only a slight preference for Br^- was seen for the HB counterparts. Notably, the significant differences in binding characteristics of the XB and HB hosts suggest the dominant roles of XB interactions in governing the binding behaviour of the former. Interestingly however, dicationic hosts **3.19I** and **3.22I** now bound Cl^- with comparable affinities, unlike their neutral congeners, where **3.18I** formed distinctly more stable Cl^- complexes than **3.21I** (Table 3.4). Furthermore, a slightly larger, whilst still modest enhancement of Br^- binding affinity was seen for **3.19I** compared to **3.22I**. This suggests that the electrostatic interactions between the dicationic host molecules and the anion guests may play a significant role in binding, reducing the effects of the strict directionality and geometry that characterised the highly-discriminatory binding of the neutral hosts.

A Halogen Bonding Receptor Selective for Azide

The unexpected binding preference of 1,3-bis(iodotriazole)-ferrocene receptor **3.24I** for N_3^- over Cl^- prompted a more detailed investigation of its anion binding properties. ^1H NMR titration experiments were performed in d_6-acetone with a range of anions that reflect contrasting geometries, basicities and charge densities. In all cases, shifts of the signal arising from the central ferrocene proton H_1 (Figure 3.12C) between both iodotriazole units was monitored as a function of anion concentration (Figure 3.14), with 1:1 stoichiometric anion association constants determined using the WinEQNMR2 software (Table 3.6).[39]

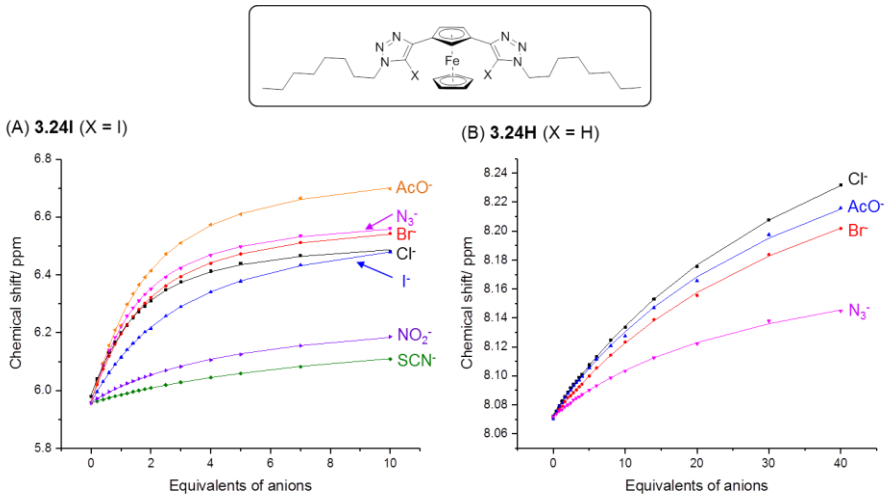


***Figure 3.14**. Plots of the chemical shifts of (A) internal ferrocene proton H_1 for **3.24I** and (B) triazole proton for **3.24H** with changes in concentrations of different anions ([**3.24**] = 1.5 mM, d_6-acetone, T = 298 K).*

Table 3.6. Association constants (K_a/ M^{-1}) of various anions with receptors **3.24I** and **3.24H** in d_6-acetone. [a]

	3.24I	**3.24H**
Cl^-	649 (21)	8.3 (0.4)
Br^-	557 (11)	7.1 (0.6)
I^-	250 (4)	-[b]
N_3^-	669 (16)	15.3 (0.7)
SCN^-	59 (1)	-[b]
NO_2^-	138 (7)	-[b]
AcO^-	553 (25)	11.0 (0.9)
NO_3^-	-[b]	-[b]
ReO_4^-	-[b]	-[b]

[a] Anions added as TBA salts; proton H_1 monitored for receptor **3.24I** and triazole proton monitored for **3.24H**, K_a determined using the WinEQNMR2 software.[39] Errors (±) shown in parentheses; ([receptors] = 1.5 mM, T = 298 K).
[b] Binding too weak for reliable values of K_a to be determined.

The XB receptor **3.24I** bound all anions much more strongly compared with its HB analogue, with an enhancement in K_a values of more than 40-fold in all cases. This large difference clearly demonstrates the dominant roles played by XB in anion binding. Amongst the halides, stronger binding was seen for the smaller and more charge dense anions in the absence of water. Highly charge-diffuse anions such as NO_3^- and ReO_4^- did not show any appreciable binding, while receptor decomposition was seen during the SO_4^{2-} and CN^- titrations. It is impressive that amongst all the linear (SCN^-) and bent anions (AcO^-, NO_2^-) studied, N_3^- was still bound the strongest, highlighting the importance of host-guest size complementarity in the binding process. Indeed, from the reported solid-state anion dimensions determined by X-ray crystallography (Figure 3.15),[68–71] anions which differed more greatly in size from N_3^- were bound more weakly. Nevertheless, it is impressive that **3.24I** gave detectable binding with the highly charge-diffuse SCN^- in the absence of charge[72] or solvophobic assistance.[73]

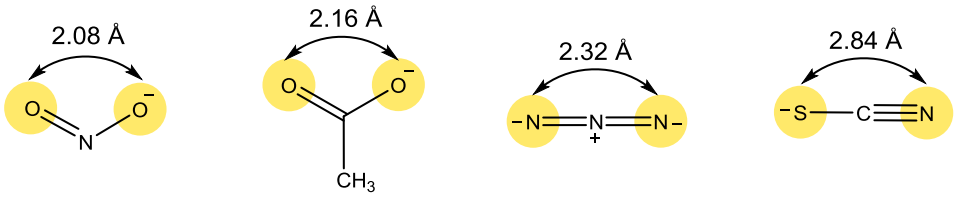


***Figure 3.15**. Linear distances between the termini of nitrite,[68] acetate,[69] azide[71] and thiocyanate[70] anions obtained from crystallographic data. The atoms of the anions possessing the most negative potentials, which are the sites mainly involved in anion binding, are highlighted in yellow.*

An attempt to improve the selectivity for N_3^- over the other anions by exploiting the differences in their free energies of hydration[40] by repeating the ^{1}H NMR titrations in the presence of water was undertaken. Table 3.7 shows that the addition of just 1 % water by volume in acetone resulted in diminution of all anion binding affinities with **3.24I**, with the most hydrated anions showing the largest decrease (extent of decrease: $AcO^- > Cl^- > Br^- > N_3^-$), thus giving a distinct selectivity for N_3^-. No binding was observed for the HB receptor analogue **3.24H** due to the strength of anion hydration. Given the acute toxicity of N_3^- [74–77] and its increased usage in vehicular airbags, agriculture and laboratory research, its selective binding,

sensing and sequestration has received much scientific attention in recent years.[78] Although N_3^- selective receptors have been reported containing Lewis acidic transition metals[79–83] and main group elements,[84–86] as well as capitalising on the anion's reacitivity,[87–89] receptors capable of binding N_3^- purely via non-covalent interactions (e.g. HB) are exceedingly rare.[90,91] At the time of writing, **3.24I** is the first and only example of a XB receptor selective for N_3^- known.

Table 3.7. Association constants (K_a/ M^{-1}) of various anions with receptor **3.24I** in d_6-acetone/ D_2O 99:1 *v/v*, as well as their free energies of hydration (ΔG_{hyd}/ kJ mol^{-1}).[a]

	K_a for 3.24I/ M^{-1}	ΔG_{hyd}/ kJ mol^{-1} [b]
Cl^-	82 (2)	-340
Br^-	103 (2)	-315
AcO^-	31 (1)	-365
N_3^-	168 (3)	-295

[a] Proton H_1 monitored for receptor **3.24I**. Errors (±) are in parentheses; ([**3.24I**] = 1.5 mM, T = 298 K). [b] Values reported by Marcus.[40]

3.3.2.2 UV-Vis Binding Studies

Changes in the optical properties of neutral **3.24I** and the dicationic receptors **3.19I** and **3.22I** were probed by UV-Vis spectroscopy titration experiments in CH_3CN. Compared with ferrocene (λ_{max} ≈ 440 nm in CH_3CN),[92,93] all receptors show an increase in the λ_{max} values of their ferrocene chromophores (λ_{max} of **3.22I** < **3.19I** < **3.24I**), consistent with smaller d-d energy gaps arising from increased electronic conjugation with the various aromatic functionalities of each receptor (Figure 3.16). Indeed, the slightly different λ_{max} values seen in each case reflects the different extents of electronic conjugation in each receptor, confirming that the varying iodotriazole substitution patterns could influence and communicate differently with the ferrocene unit. When up to 50 equivalents of anions (Cl^- for **3.19I** and **3.22I**; N_3^- for **3.24I**) were added to the individual receptor solutions in CH_3CN, only very small spectral changes were seen. This suggests that anion binding resulted in small perturbations to the ferrocene d-d energy levels, possibly due to a lack of receptor conformational change upon binding due to their structural rigidity.

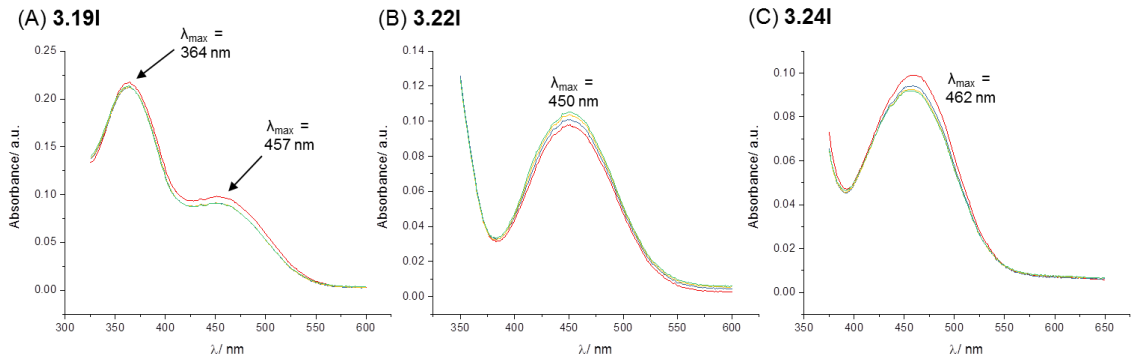


***Figure 3.16**. UV-vis spectra of dicationic receptors (A) **3.19I** and (B) **3.21I** with Cl^-; and (C) neutral receptor **3.24I** with N_3^-. Spectra were recorded in the presence of 0, 10, 20 and 50 equivalents of anion added ([host] = 0.25 mM, CH_3CN, T = 293 K).*

3.3.2.3 Electrochemical Anion Sensory Studies

The redox anion sensing behaviour of the ferrocene-appended receptor pairs **3.19H/I**, **3.21H/I**, **3.22H/I** and **3.24H/I** was initially probed by CV or square wave voltammetry (SWV) in an electrolyte solution of 0.1 M $TBAPF_6$ in CH_3CN. A standard three-electrode cell comprising of a glassy carbon working electrode, Pt wire auxiliary electrode and Ag/ $AgNO_3$ reference electrode[41] was used in all cases.

Electrochemical reversibility studies on each receptor were first performed by recording CVs at different scan rates (Figure 3.17). Whilst receptors **3.19H/I**, **3.21I** and **3.24I** exhibited redox quasi-reversibility (see Appendix B), no evidence of electrochemical oxidation could be detected for **3.22H/I** in the accessible solvent window of the electrolyte solution. This may be due to the direct conjugation of the highly electron-withdrawing (iodo)triazolium groups to the receptors' ferrocene units, rendering their oxidations to be highly disfavoured thermodynamically. Comparing the Fc/ Fc^+ redox potentials of receptors **3.19H/I**, **3.21I** and **3.24I** (Table 3.8) revealed generally larger $E_{1/2}$ values for the XB hosts than their HB analogues, which is consistent with their enhanced electron deficiency from the presence of the electron-withdrawing iodine atoms. Unsurprisingly, dicationic receptors **3.19H/I** display more anodic $E_{1/2}$ values than their neutral counterparts.

Table 3.8. Redox potentials ($E_{1/2}$/ V) of redox-active hosts.[a]

	3.19X	3.21X	3.24X
X = I	+ 0.260	+ 0.250	+ 0.250
X = H	+ 0.220	+ 0.160	+ 0.170

[a] Values reported relative to the Ag/ $AgNO_3$ reference electrode; glassy carbon working electrode, Pt wire auxiliary electrode, electrolyte: 0.1 M $TBAPF_6$ in CH_3CN, T = 293 K.

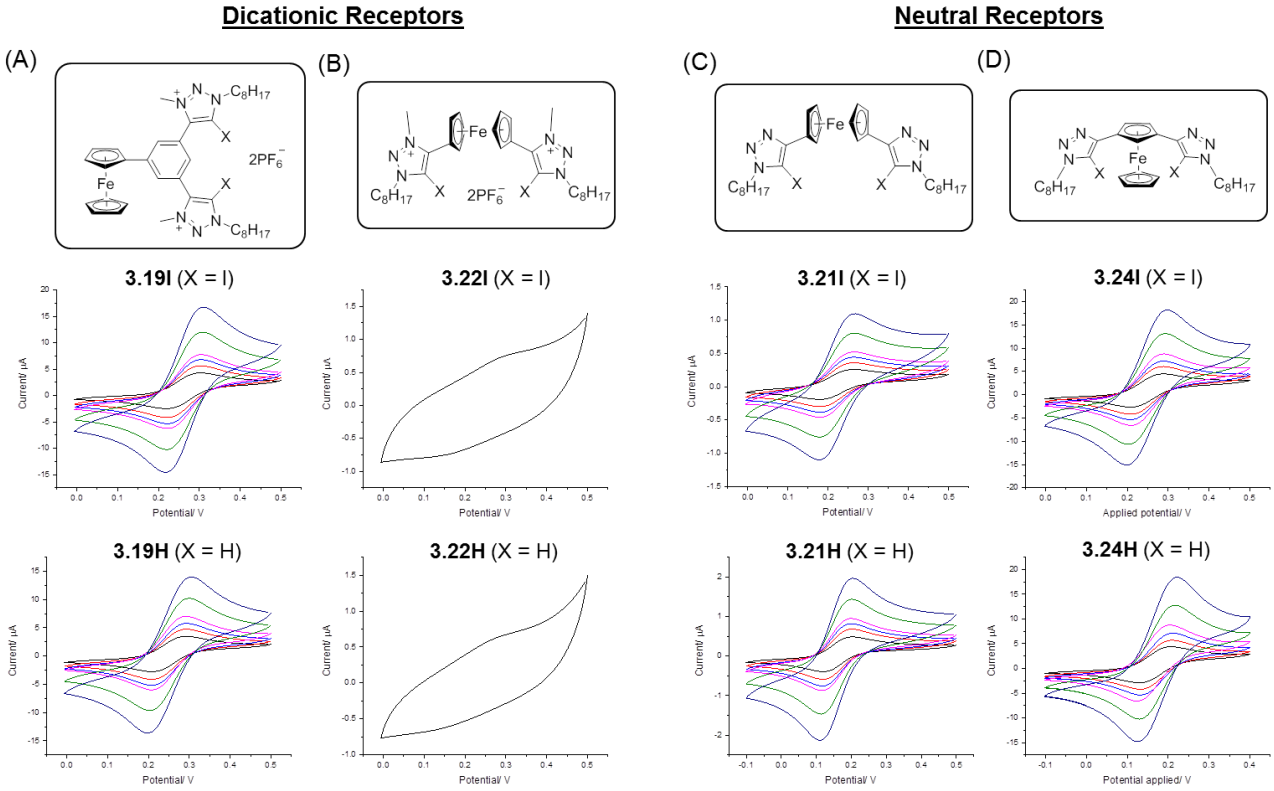


***Figure 3.17**. Electrochemical reversibility studies: CVs of dicationic receptors (A) **3.19I/H** and (B) **3.22I/H**, as well as neutral receptors (C) **3.21I/H** and (D) **3.24I/H**, recorded at scan rates of 25, 50, 75, 100, 250 and 500 mV s^{-1} ([receptor] = 0.5 mM, electrolyte: 0.1 M $TBAPF_6$ in CD_3CN, T = 293 K).*

In the presence of Cl^- in dry electrolyte solution, cathodic perturbations of the Fc/ Fc^+ redox couples of **3.19I/H** and **3.21I/H** were seen with retention of redox reversibility (Figure 3.18A, B), arising from the bound halide stabilising the oxidised ferrocenium state. Notably, larger magnitudes of cathodic shift were seen for the XB receptors compared with their HB analogues (Figure 3.18C, D), demonstrating a greater sensitivity for anion sensing. For instance, the addition of 2.0 equivalents of Cl^- elicited the same magnitude of cathodic shift for **3.19I** as 10.0 equivalents for **3.19H**. For neutral receptors **3.21I/H**, a more pronounced

enhancement is observed between the XB and HB receptors: the cathodic shift arising with 10.0 equivalents of added Cl^- for **3.21H** was seen with 0.5 Cl^- equivalents for **3.21I**. As seen from Table 3.9, which summarises the magnitudes of cathodic shifts observed for each receptor in the presence of 10.0 equivalents of anion, Br^- induced smaller shifts than Cl^- in all cases due to its more charge-diffuse nature. It is likely that communication between the anion binding site of each receptor with the ferrocene redox reporter group occurs via a through-bond mechanism due to the highly-conjugated nature of each receptor. Possibly, the greater covalent character of the XB···halide interaction compared to HB may facilitate the through-bond communication, leading to an enhanced redox response to anion binding. With F^- and oxoanions such as SO_4^{2-} and $H_2PO_4^-$ however, significant loss of redox reversibility was seen for **3.19H/I** and **3.21 H/I** (Figure 3.19), possibly due to EC processes with the oxidised ferrocenium species.

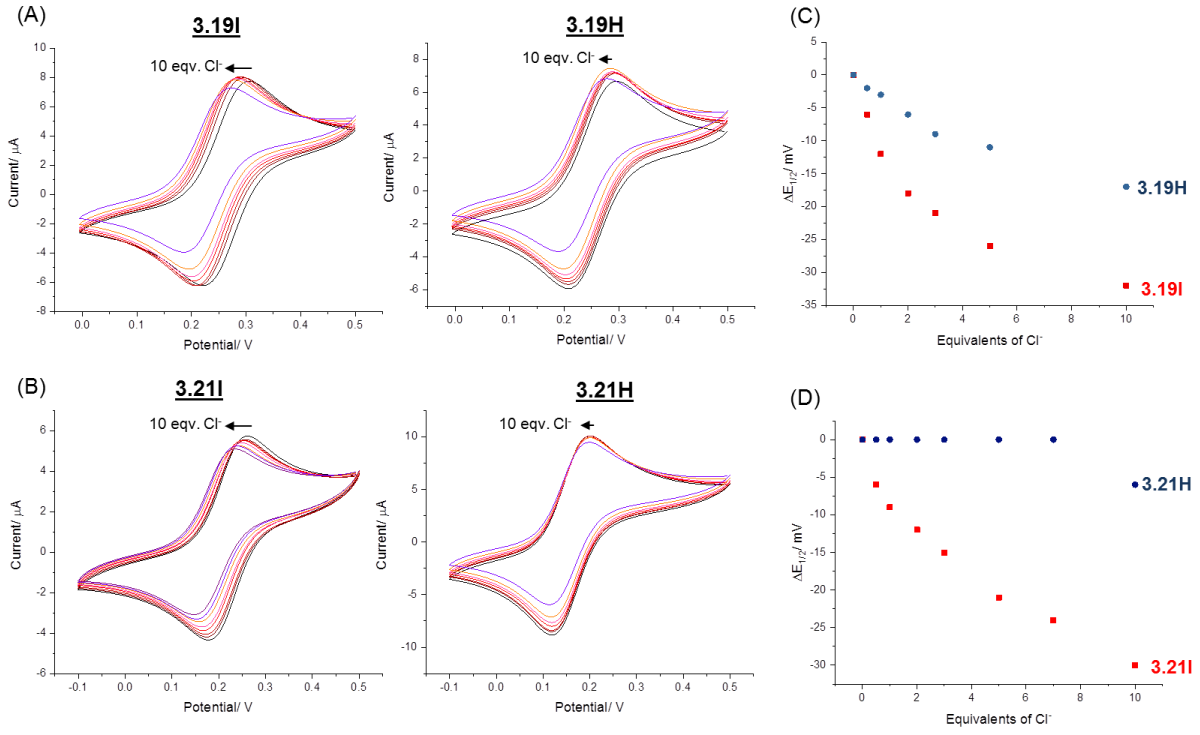


***Figure 3.18**. CVs of receptors (A) **3.19I/H** and (B) **3.21I/H** in the presence of 0.0, 0.5, 1.0, 2.0, 3.0, 5.0 and 10.0 equivalents of Cl^-; Plot of cathodic shift of the redox couples of (C) **3.19I/H** and (D) **3.21I/H** with increasing equivalents of Cl^-; all potentials taken relative to the Ag/ $AgNO_3$ reference electrode ([receptor] = 0.5 mM, electrolyte: 0.1 M $TBAPF_6$ in CH_3CN, T = 293 K).*

Table 3.9. Cathodic shifts ($\Delta E_{1/2}$/ V) of the ferrocene/ ferrocenium redox couples of **3.19I/H** and **3.21I/H** upon addition of 10 equivalents of Cl^- and Br^- in dry and wet CH_3CN.[a]

	Dry CH_3CN		CH_3CN/ H_2O 9:1 *v/v*	
	Cl^-	Br^-	Cl^-	Br^-
3.19I	- 32	- 19	- 12	- 15
3.19H	- 17	- 11	- 6	- 6
3.21I	- 30	- 18	0	0
3.21H	- 6	0	0	0

[a] Anions added as TBA salts, electrolyte: 0.1 M $TBAPF_6$ in the respective solvents; errors estimated at ± 5 mV ([receptor] = 0.5 mM, *T* = 293 K).

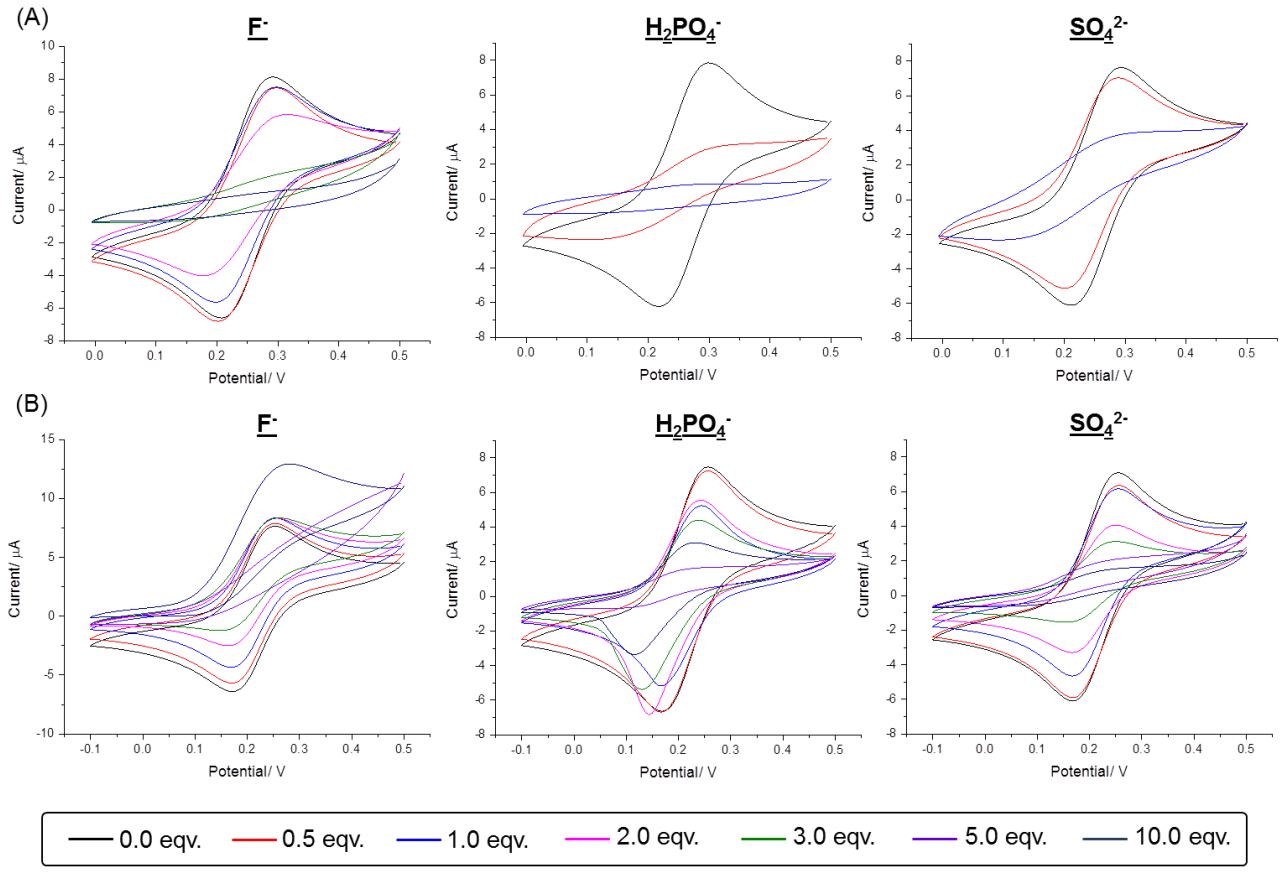


***Figure 3.19**. CVs of receptors (A) **3.19I** and (B) **3.21I** with incremental quantities of F^-, $H_2PO_4^-$ and SO_4^{2-}; potentials taken relative to the Ag/ $AgNO_3$ reference electrode ([receptor] = 0.5 mM, electrolyte: 0.1 M $TBAPF_6$ in CH_3CN, T = 293 K).*

The enhanced voltammetric response of XB hosts to anions prompted a study of the effects of water on redox anion sensing: the CV studies were undertaken in an electrolyte solution containing 10 % water by volume (Table 3.9). While no redox response was seen for neutral receptors **3.21H/I**, reflective of the diminished anion binding affinities due to anion hydration, dicationic receptor **3.19I** showed a significantly more pronounced redox response

compared to **3.19H** for both Cl^- and Br^-, with Br^- now giving comparable Fc/ Fc^+ cathodic shifts compared to Cl^-.

Electrochemical sensing studies were also performed on neutral 1,3-bis(triazole)-ferrocene receptors **3.24H/I** with N_3^-, Cl^-, Br^- and AcO^- in an electrolyte solution comprising CH_3CN/ H_2O 99:1 *v/v* (Figure 3.20). Amongst all the anions studied, N_3^- gave the largest magnitude of cathodic shift for **3.24I**, approximately double the magnitude seen for the other anions (Table 3.10), suggesting that N_3^- stabilises the ferrocenium oxidation to the greatest extent upon complexation. Cl^-, Br^- and AcO^- gave comparable cathodic shift responses, reflective of their hydration in the wet CH_3CN electrolyte solution. It is especially noteworthy that the presence of water considerably attenuated the loss of redox reversibility commonly

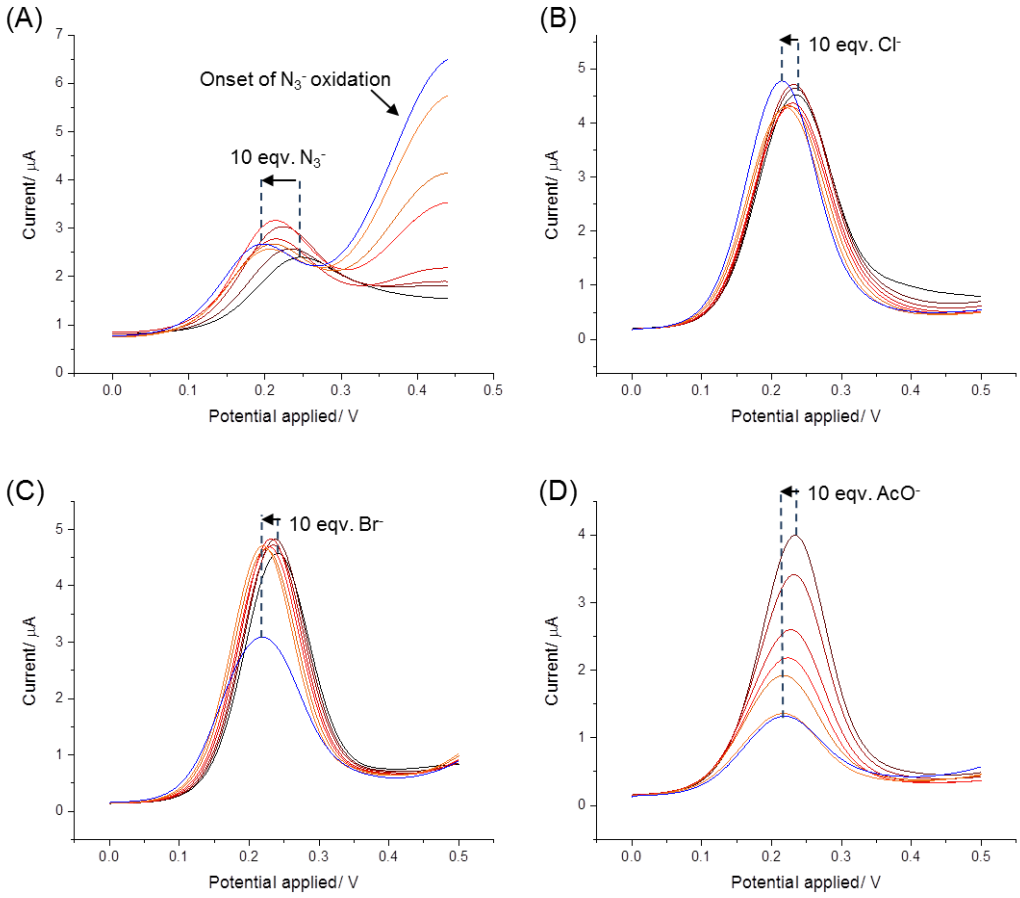


***Figure 3.20**. SWVs of receptor **3.24I** in the presence of 0.0, 0.5, 1.0, 2.0, 3.0, 5.0, 7.0 and 10.0 equivalents of (A) N_3^-; (B) Cl^-; (C) Br^- and (D) AcO^-. Potentials taken relative to the Ag/ $AgNO_3$ reference electrode ([receptor] = 0.5 mM, electrolyte: 0.1 M $TBAPF_6$ in CH_3CN, T = 293 K).*

Table 3.10. Cathodic shifts ($\Delta E_{1/2}$/ V) of the ferrocene/ ferrocenium redox couples of **3.24I/H** upon addition of 10 equivalents of anion in CH_3CN/ H_2O 99:1 *v/v*.[a]

	3.24I	**3.24H**
Cl^-	-21	0
Br^-	-22	0
AcO^-	-19	-15
N_3^-	-40	-18

[a] Electrolyte 0.1 M $TBAPF_6$ in CH_3CN/ H_2O 99:1 *v/v*; errors estimated to be ± 5 mV ([receptor] = 0.5 mM, *T* = 293 K).

observed for AcO^-,[24] likely due to its hydration and resulting weak binding reducing its propensity to participate in EC reactions with the oxidised ferrocenium state. Comparatively, **3.24H** gave much smaller cathodic shifts for all anions, highlighting the dominant roles played by the XB donor groups for redox sensing of anions, in particular N_3^-.

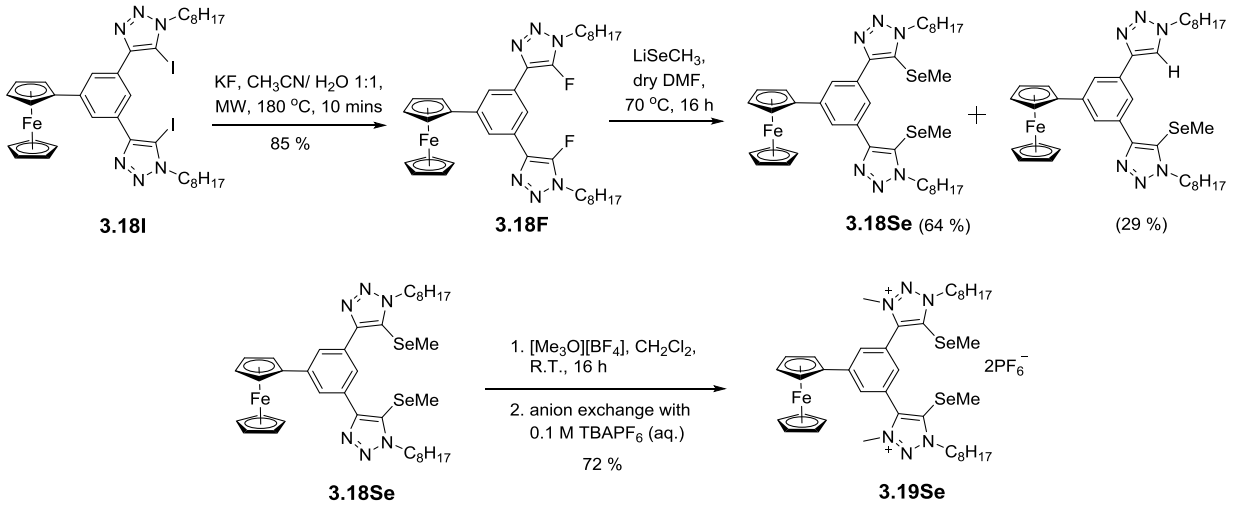
3.3.3 A Redox-active Chalcogen Bonding Model Receptor

3.3.3.1 Receptor Design and Synthesis

Recognising the similarities between XB and ChB interactions established in Chapter 2 and the optimal halide binding geometry provided by **3.19I**, its dicationic ChB analogue **3.19Se** was synthesised with methylseleno-triazolium donor motifs and its anion redox sensing properties probed.

As summarised in Scheme 3.11, the neutral Se-containing precursor **3.18Se** was prepared from **3.18I** in a manner akin to the ChB macrocycles described in Chapter 2. Initial attempts were undertaken to prepare **3.18Se** directly from the iodotriazoles of **3.18I** using *in-situ* generated $LiSeCH_3$ in DMF.[94] Despite multiple attempts and an excess of the $SeCH_3^-$ nucleophile, yields were consistently poor (< 25 %). Thus, Fokin's halide exchange protocol was performed where the bis-fluorotriazole intermediate **3.18F** was first synthesised in excellent yields using excess KF in CH_3CN/ H_2O 1:1 *v/v* under microwave assistance at 180 ^oC for 10 minutes. With longer reaction times, poorer yields of **3.18F** were obtained due to decomposition, and changing the solvent to DMSO resulted in only formation of the bis-prototriazole analogue **3.18H**. S_NAr substitution carried out on **3.18F** using $LiSeCH_3$ at 70 ^oC afforded the target **3.18Se** in a significantly improved yield of 64 %, concomitant with some

prototriazole-containing side products formed (29 %). Double methylation of **3.18Se** with trimethyloxonium tetrafluoroborate and anion exchange afforded the PF_6^- salt of dicationic **3.19Se** in 72 % yield as an orange solid, characterised by ^{1}H, ^{13}C, ^{19}F, ^{31}P and ^{77}Se NMR spectroscopy. In addition, high-resolution ESI-MS of **3.19Se** showed an isotopic distribution conforming perfectly to a predicted theoretical model of the compound (Figure 3.21).



***Scheme 3.11**. Synthesis of dicationic redox-active ChB receptor **3.19Se**.*

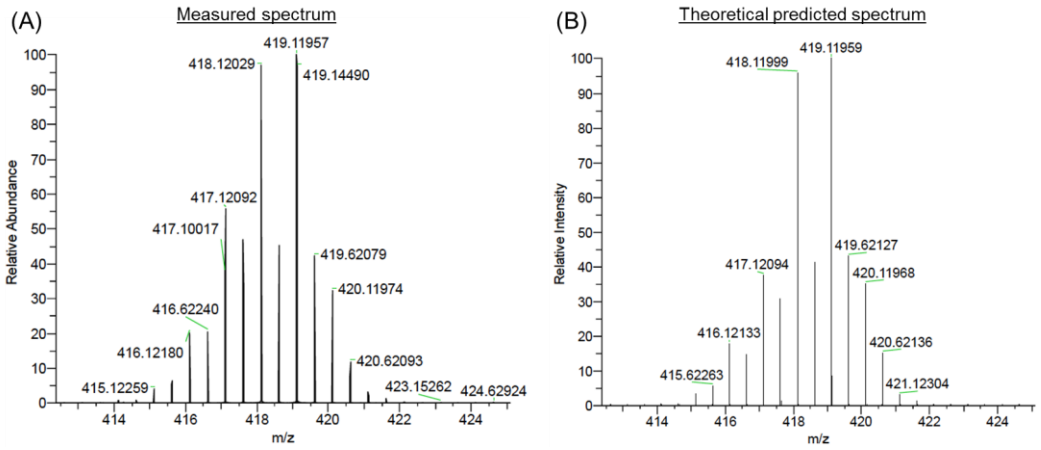


***Figure 3.21**. (A) Measured and (B) theoretical high-resolution ESI mass spectra of ChB receptor **3.19Se** (m/z = **[3.19Se]**$^{2+}$).*

3.3.3.2 Anion Binding Studies

The ^{1}H NMR chemical shift perturbations of the resonances of **3.19Se** in the presence of increasing quantities of various anions (Cl^-, Br^-, I^-, $H_2PO_4^-$, AcO^-, NO_3^- and SO_4^{2-}) are shown in Figure 3.22. Downfield shifts were seen for aromatic protons H_a and H_b, ferrocene H_c, triazolium methyl proton H_f and those of the $SeCH_3$ moiety (Figure 3.22A). However, the largest downfield perturbations were observed for H_a for all anions investigated, while those of H_c, $SeCH_3$ and H_f were typically < 25 % the magnitude of H_a (Table 3.11), suggesting that the anions were binding in the cavity flanked by the Se-triazolium units and not along the periphery of the receptor adjacent to the cationic triazolium groups. The small perturbations of the $SeCH_3$ units showed that HB interactions from the methyl groups on the Se atoms were also unlikely to be the main anion binding interaction. WinEQNMR2[45] analysis of the titration data, monitoring proton H_a for all anions, determined 1:1 stoichiometric association constants summarised in Table 3.11.

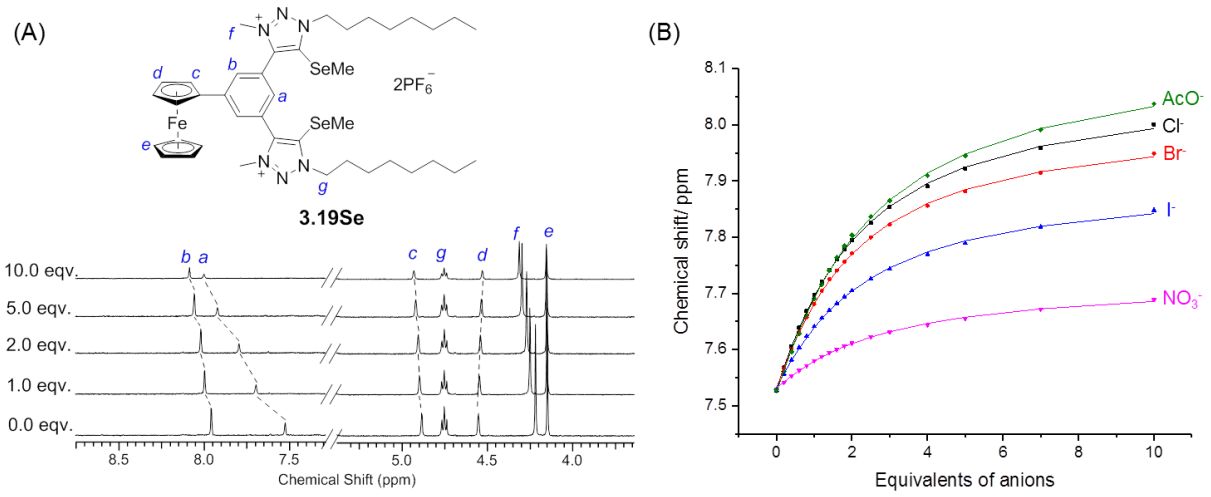


***Figure 3.22**. (A) Partial ^{1}H NMR spectra of ChB receptor **3.19Se** with incremental quantities of Cl^-; (B) Plots of changes in chemical shift of internal aromatic proton H_a of **3.19Se** with increasing quantities of different anions ([**3.19Se**] = 1.5 mM, CD_3CN, T = 298 K). For the binding isotherms, filled dots represent empirical points while the solid lines represents the best-fit binding curves obtained from WinEQNMR2 analysis.[39]*

Table 3.11. Anion binding studies on receptors **3.19Se** and **3.19H** in CD_3CN.

Anion		Receptor 3.19Se			Receptor 3.19H	
		$\Delta\delta_H$/ ppm [a]	K_a/ M^{-1} [b]	$\Delta\delta_{Se}$/ ppm [a]	$\Delta\delta_H$/ ppm [a]	K_a/ M^{-1} [b]
Cl^-	H_a	+ 0.474	391 (9)	- 1.54	+ 0.621	909 (14)
	H_f	+ 0.097			+ 0.159	
	$SeCH_3$	+ 0.054			NA	
Br^-	H_a	+ 0.421	419 (12)	- 1.89	+ 0.468	404 (4)
	H_f	+ 0.078			+ 0.057	
	$SeCH_3$	+ 0.058			NA	
I^-	H_a	+ 0.321	358 (16)	- 1.46	+ 0.327	319 (4)
	H_f	+ 0.057			+ 0.076	
	$SeCH_3$	+ 0.061			NA	
NO_3^-	H_a	+ 0.159	273 (3)	- 1.30	+ 0.192	368 (14)
	H_f	+ 0.035			+ 0.054	
	$SeCH_3$	+ 0.018			NA	
AcO^-	H_a	+ 0.509	323 (11)	- 1.72	+ 0.746	2765 (73)
	H_f	+ 0.091			+ 0.161	
	$SeCH_3$	+ 0.031			NA	
$H_2PO_4^-$	H_a	+ 0.957	decomposition	multiple peaks	- [c]	- [c]
	H_f	+ 0.181			- [c]	
	$SeCH_3$	+ 0.094			NA	
SO_4^{2-}	H_a	NA	decomposition	NA	- [c]	- [c]
	H_f	NA			- [c]	
	$SeCH_3$	NA			NA	

[a] Δδ values reported in the presence of 10 equivalents of anions. [b] 1:1 stoichiometric association constants were calculated from ^1H NMR titrations at 298 K using the WinEQNMR2 software[39] by monitoring the internal aromatic proton H_a. Analysis of the titration data using H_f and $SeCH_3$ protons gave similar values of K_a. Anions were added as their TBA salts. Errors (±) are given in parentheses and are < 10 %. [c] Titrations not performed.

The quantitative anion binding data (Table 3.11) revealed contrasting anion binding behaviour between **3.19Se** and its HB analogue, indicative of the dominant influence of ChB interactions in governing anion coordination. Unlike **3.19H** which bound AcO^- selectively, no distinct anion binding preferences were seen for **3.19Se**. Also, while anion charge density and basicity govern the binding trends of **3.19H** (Cl^- > Br^- > I^-), these factors appear not to significantly influence the selectivity of **3.19Se**, where all three halides were bound with approximately the same affinity in dry CH_3CN. The observation that **3.19Se** binds the more

basic AcO^- slightly more weakly than Cl^-, which is in stark contrast to **3.19H**, further reinforces the insensitivity of ChB interactions to anion basicity. This is consistent with the observations with rotaxane **2.16Se$_2$H** described in Chapter 2. For **3.19Se**, addition of $H_2PO_4^-$ and SO_4^{2-} resulted in receptor decomposition.

Monitoring the changes of the ^{77}Se NMR resonances of **3.19Se** in the presence of anions (Table 3.11) showed surprisingly much smaller upfield shifts than those for macrocycle **2.9Se** and rotaxane **2.16Se$_2$H** (Section 2.2.8), implying that smaller changes in the local electronic environment of the ChB Se atoms resulted upon anion binding. Amongst the anions, a larger magnitude of ^{77}Se NMR signal shift was seen with increasing binding affinity with the exception of AcO^-, though a plot of $\Delta\delta_{77Se}$/ ppm as a function of K_a/ M^{-1} gave very poor linear correlation (Pearson's R = -0.70). No distinct correlations were also seen between $\Delta\delta_{77Se}$ and anionic radii[40]. Akin to the ChB host systems studied in Chapter 2, these non-linear trends suggest that the perturbations of the electronic environments of the Se atoms were due to a complex interplay of many competing interactions in solution.

Electrochemical anion titrations were performed with **3.19Se** using the electrolyte solution of 0.1 M $TBAPF_6$ in dry CH_3CN, in a similar manner as **3.19I/H**. Like its XB and HB analogues, **3.19Se** show electrochemical quasi-reversibility in solution, with a redox potential of + 0.250 mV relative to the Ag/ $AgNO_3$ reference electrode. This value lies midway between that of **3.19H** and **3.19I** (Table 3.8), indicating that the $SeCH_3$ groups on **3.19Se** were less electron-withdrawing than the iodine atoms of **3.19I**. Despite the rich redox chemistry of organoselenium compounds,[95,96] the only redox couple seen in the potential window studied resulted from the Fc/ Fc^+ redox couple.

The addition of 10.0 equivalents of Cl^- or Br^- both resulted in a modest -12 mV cathodic shift of the Fc/ Fc^+ redox couple of **3.19Se**, with retention of redox reversibility (Figure 3.23). It is probable that the reduced propensity of Br^- to stabilise the oxidised ferrocenium state was compensated by its larger binding affinity (Table 3.11). This contrasted with **3.19H**, where Cl^- elicited a larger cathodic shift than Br^- (Table 3.9). Similarly as with **3.19H/I**, loss of redox reversibility was seen upon addition of F^-, SO_4^{2-}, $H_2PO_4^-$ and AcO^- (Figure 3.23). Importantly,

3.19Se showed comparable magnitudes of voltammetric response to the halides as **3.19H**, which are significantly smaller than those observed for **3.19I**, indicating that the ChB-donor Se atoms were less effective through-bond conduits for electronic communication with ferrocene. Nevertheless at the time of writing, these results provide the first evidence of ChB-mediated redox anion sensing.

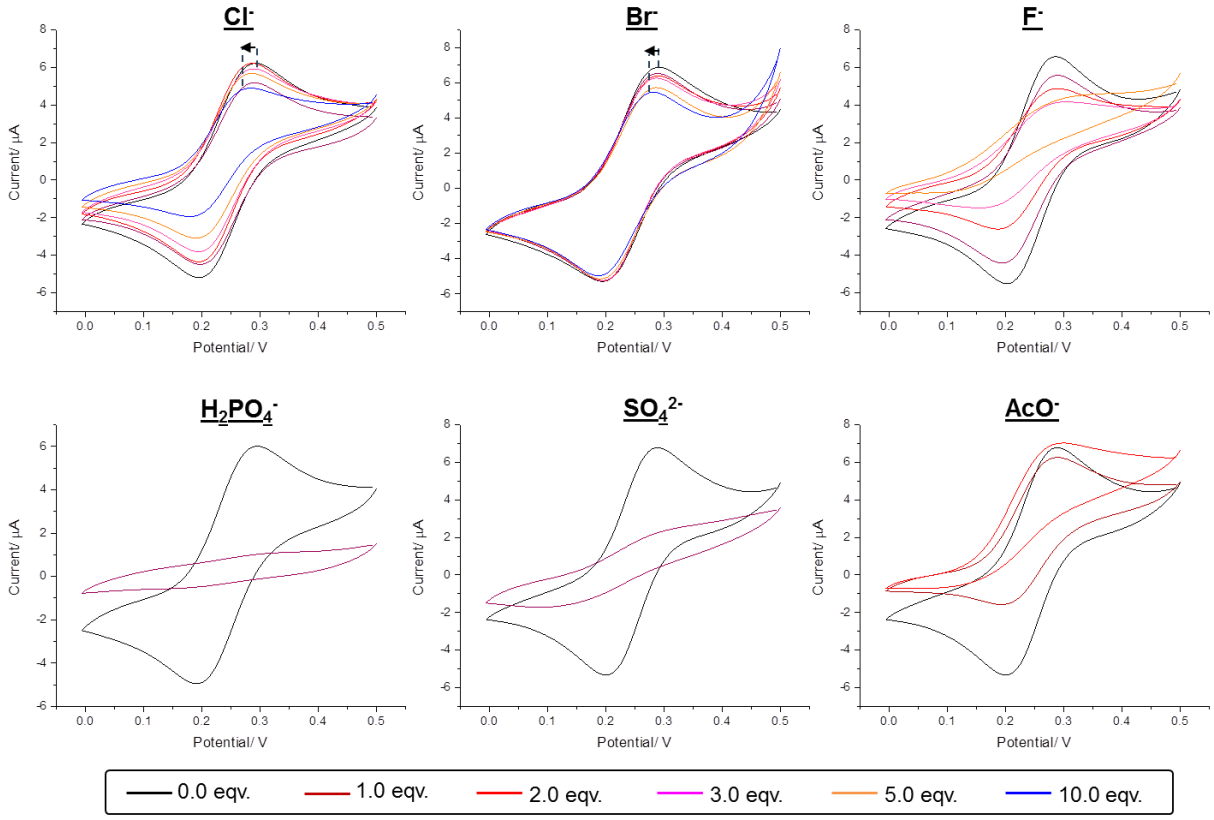


***Figure 3.23**. CVs of dicationic ChB receptor **3.19Se** with incremental quantities of Cl^-, Br^-, F^-, $H_2PO_4^-$, SO_4^{2-} and AcO^- ([**3.19Se**] = 0.5 mM, electrolyte: 0.1 M $TBAPF_6$ in CH_3CN, T = 293 K).*

3.4 A Ferrocene-appended All-Halogen Bonding [2]Rotaxane for Anion Sensing

3.4.1 Design, Synthesis and Characterisation

With the ability of XB donor groups to enhance redox anion sensing established, novel [2]rotaxanes containing the 1-ferrocenyl-3,5-bis(iodotriazole) and 1,3-bis(iodotriazole)-ferrocene motifs were designed (Figure 3.24). In both cases, the redox-active functionality was incorporated into the macrocycle component in close proximity to the all-XB anion binding cavity to facilitate redox communication, with the different resulting XB bite angles anticipated to provide contrasting anion selectivities. To enhance the strength of anion complexation, charge-assisted XB interactions were provided by the cationic pyridinium-3,5-bis(iodotriazole) motif on the axle component, which also enhances rotaxane preorganisation by HB interactions between the pyridinium methyl group and the macrocycle polyether unit. The target rotaxanes are to be prepared by the CuAAC-AMT approach expounded in Chapter 2 using pyridine-3,5-bis(iodoalkyne) and stopper azide precursors with the appropriate ferrocene-containing XB macrocycle.

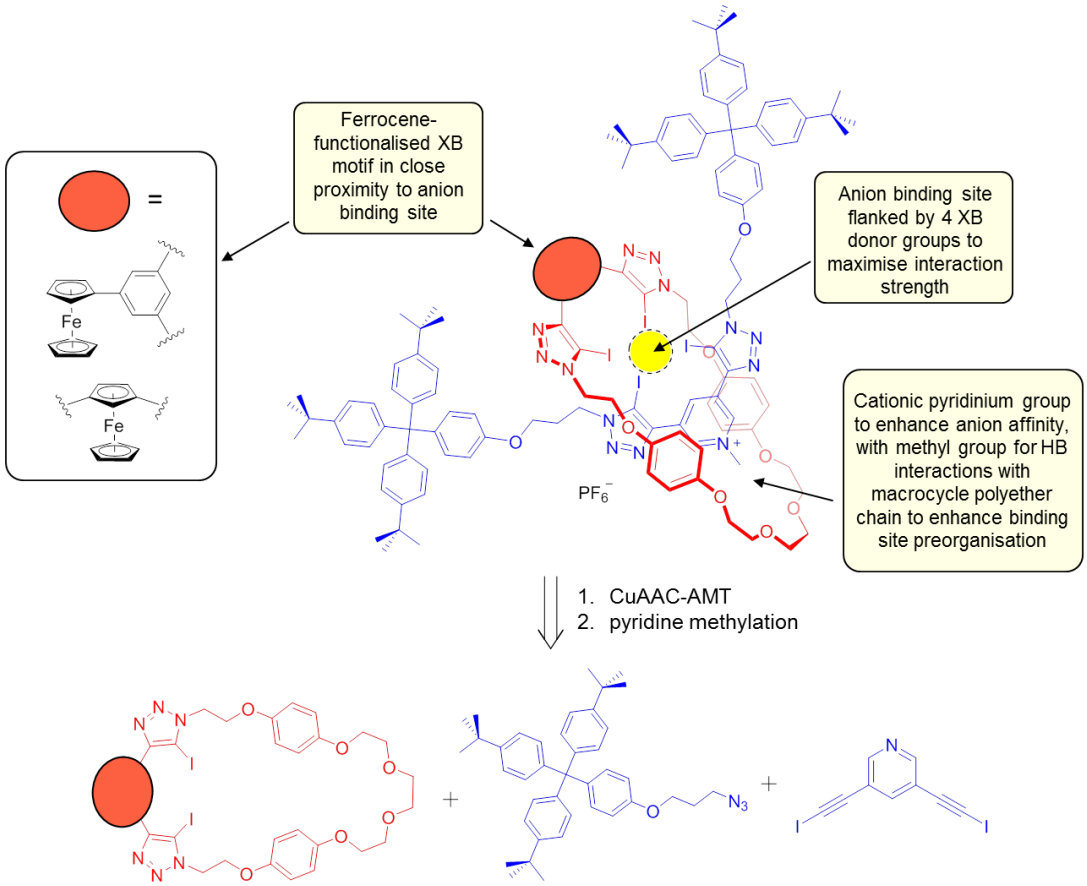
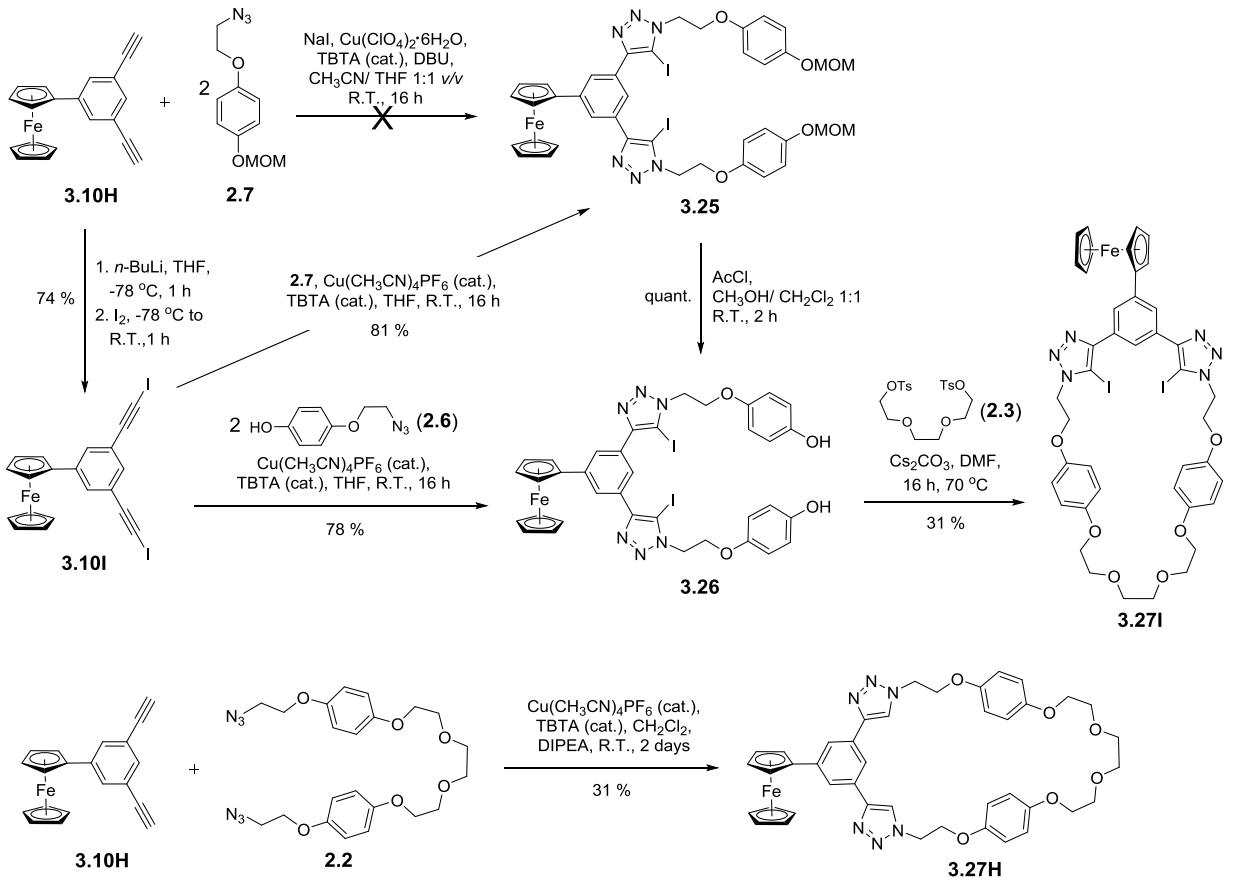


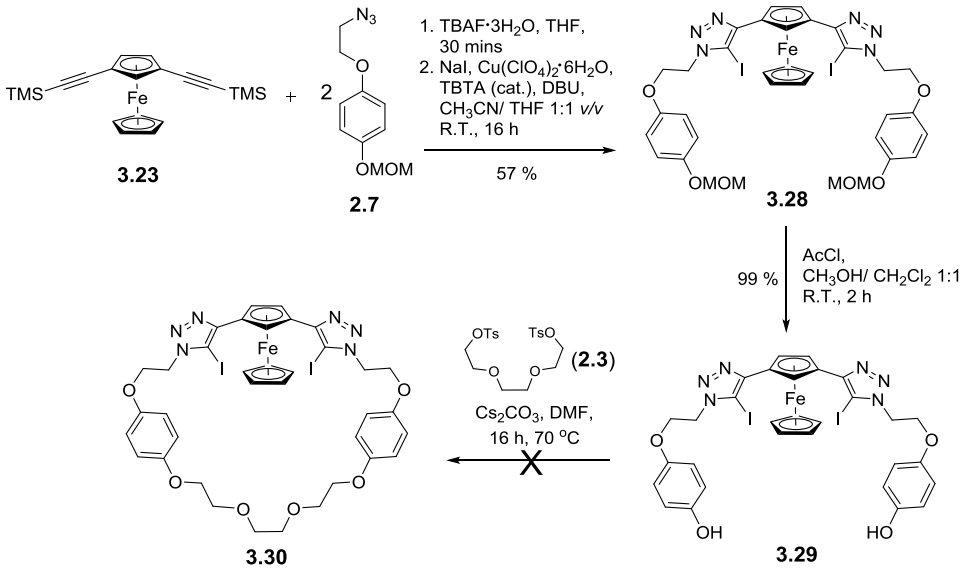
***Figure 3.24**. Design of cationic redox-active [2]rotaxanes with an all-XB binding cavity for electrochemical anion sensing and strategy for synthesis.*

The macrocycles were prepared following the general S_N2 ring-closing approach (described in Section 2.2.1) by Williamson ether synthesis between the bis-tosylate and appropriate bis-phenol precursors. As shown in Scheme 3.12, the 1-ferrocenyl-3,5-bis(ethynyl)benzene starting material **3.10H** was first reacted with two equivalents of MOM-protected azide **2.7** using Zhu's one-pot 'iodo-Click' conditions.[46] Surprisingly, ESI-MS analysis of the crude reaction mixture after an overnight reaction showed no evidence of the bis-iodotriazole product **3.25**, with multiple side products observed on the TLC. Therefore, **3.10H** was first converted to its bis-iodoalkyne analogue **3.10I** using *n*-BuLi and quenching the lithium-bis(acetylide) intermediate with I_2. The bis-phenol XB macrocycle precursor **3.26** could be accessed via two routes in comparable overall yields: by CuAAC reaction with **2.7** then acid-deprotection of the MOM group, or by direct CuAAC reaction with the free phenol azide **2.6**. Thereafter, S_N2 ring-closing with triethylene glycol-bis(tosylate) **2.3** afforded the XB ferrocene-appended macrocycle **3.27I** in 31 % isolated yield. For a comparison of the anion binding and sensing properties, the corresponding HB analogue **3.27H** was synthesised via CuAAC ring-closing using bis-azide **2.2** and alkyne **3.10H**.

The synthesis of analogous 1,3-bis(iodotriazole)-ferrocene macrocycle **3.30** followed a similar approach (Scheme 3.13). *In-situ* TMS-deprotection of the 1,3-disubstituted ferrocene bis-alkyne synthon **3.23** using TBAF and one-pot 'iodo-Click' conditions with azide **2.7** afforded precursor **3.28** in a modest yield of 57 %. Acid-deprotection of the MOM group afforded the corresponding bis-phenol **3.29** which was used without further purification in the subsequent S_N2 ring-closing reaction using Cs_2CO_3 in DMF at 70 ^oC. Unfortunately, these conditions resulted in significant decomposition of **3.29**, and only a trace of the target macrocycle **3.30** could be observed from ESI-MS analysis. Reducing the reaction temperature to 50 ^oC did not show any improvements. Therefore, no further work was performed with this motif.



***Scheme 3.12**. Synthesis of macrocycles **3.27H/I** containing the 1-ferrocenyl-3,5-bis(triazole) motif.*



***Scheme 3.13**. Attempted synthesis of 1,3-bis(iodotriazole)-ferrocene macrocycle **3.30I**.*

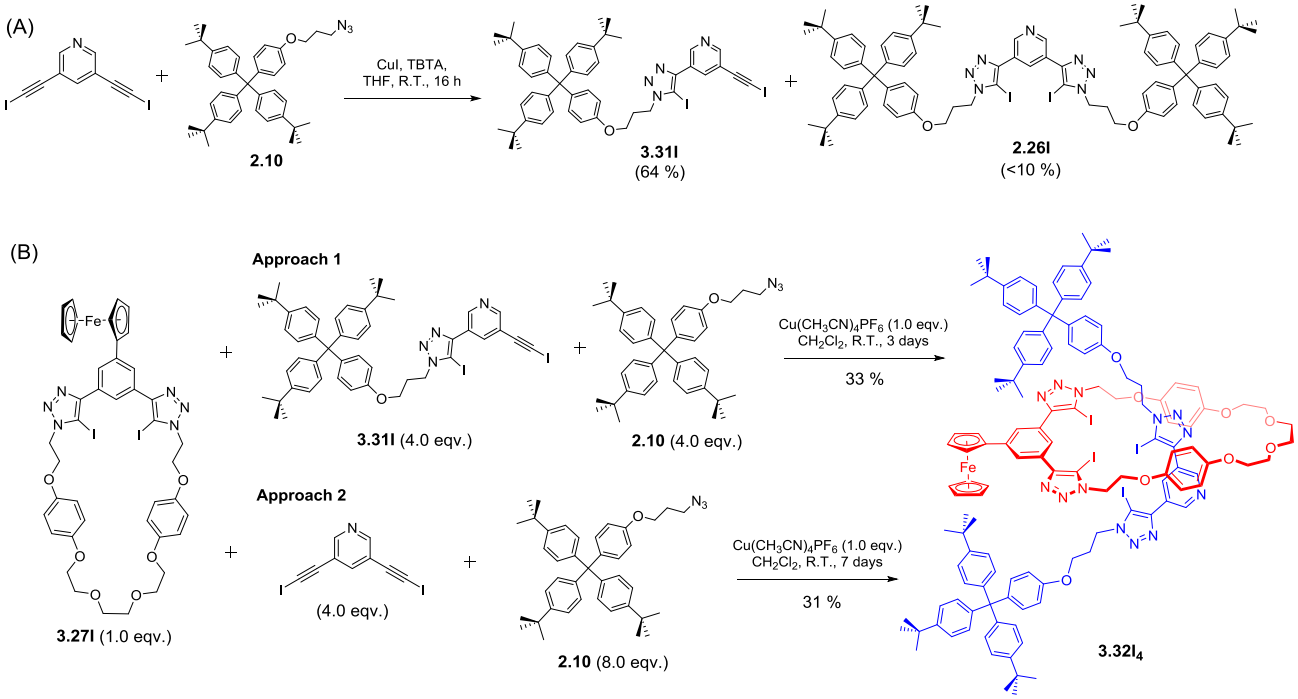
With macrocycle **3.27I** in hand, synthesis of the all-XB rotaxane was attempted via the CuAAC-AMT approach using pyridine-3,5-bis(iodoalkyne) and stopper azide **2.10**. Initial investigations centred on using a single CuAAC reaction between the terminal iodoalkyne **3.31I** and azide **2.10** to form the target neutral rotaxane **3.32I$_4$** (Approach 1 in Scheme 3.14B). When the synthesis of the **3.31I** axle precursor was first attempted using equimolar quantities of pyridine-3,5-bis(iodoalkyne) and azide **2.10**, only modest yields of the target single-'Clicked' product (33 %) was obtained, which is consistent with previously-reported observations.[38] Interestingly, more double-stoppered product (49 %) was isolated, implying that the formation of the first iodotriazole on **3.31I** increased the susceptibility of the second iodoalkyne functionality towards CuAAC reaction. Hence, the reaction was repeated, where the azide **2.10** was slowly added over 3 hours to a mixture comprising of a 2.5-fold excess of the bis-alkyne with stoichiometric quantities of CuI. Pleasingly under such conditions, **3.31I** could be isolated in the much-improved yield of 64 %, with the bis-'Clicked' side product formed in < 10 % yield.[§§] Thereafter, when 1.0 equivalent of $[Cu(CH_3CN)_4]PF_6$ was added to a solution containing an equimolar quantity of macrocycle **3.27I** and four-fold excess of **3.31I** and **2.10** in thoroughly-degassed CH_2Cl_2,[***] complete consumption of the axle precursors were only observed after 3 days. Under such conditions, the target neutral [2]rotaxane **3.32I$_4$** could be detected by ESI-MS analysis of the crude reaction mixture (*m/z* = 2588.7 $[M+H]^+$), and subsequently isolated by preparatory TLC in 33 % yield (Approach 1 in Scheme 3.14B).

Encouraged by this result, the direct formation of the all-XB rotaxane was attempted using pyridine-3,5-bis(iodoalkyne) (4.0 equivalents) and azide **2.10** (8.0 equivalents) under identical conditions (Approach 2 in Scheme 3.14B). Monitoring the reaction daily by TLC and ESI-MS showed that **3.31I** was formed as an intermediate in rotaxane synthesis, and complete consumption of the axle precursors was seen only after 7 days. Pleasingly, this approach also afforded rotaxane **3.32I$_4$** in an almost identical yield, suggesting that AMT rotaxane formation in this reaction occurred by first formation of **3.31I**, which then threaded through the

[§§] The unreacted bis-iodoalkyne could be recovered and recycled for other reactions.

[***] Performing the reaction under a strictly inert atmosphere and thorough degassing of the solvent with N_2 was necessary to ensure effective reaction. Interestingly, very facile oxidation of Cu(I) to Cu(II) was observed if not properly degassed, possibly due to the formation of Cu(I)-pyridine complexes which could be thermodynamically disposed towards oxidation.

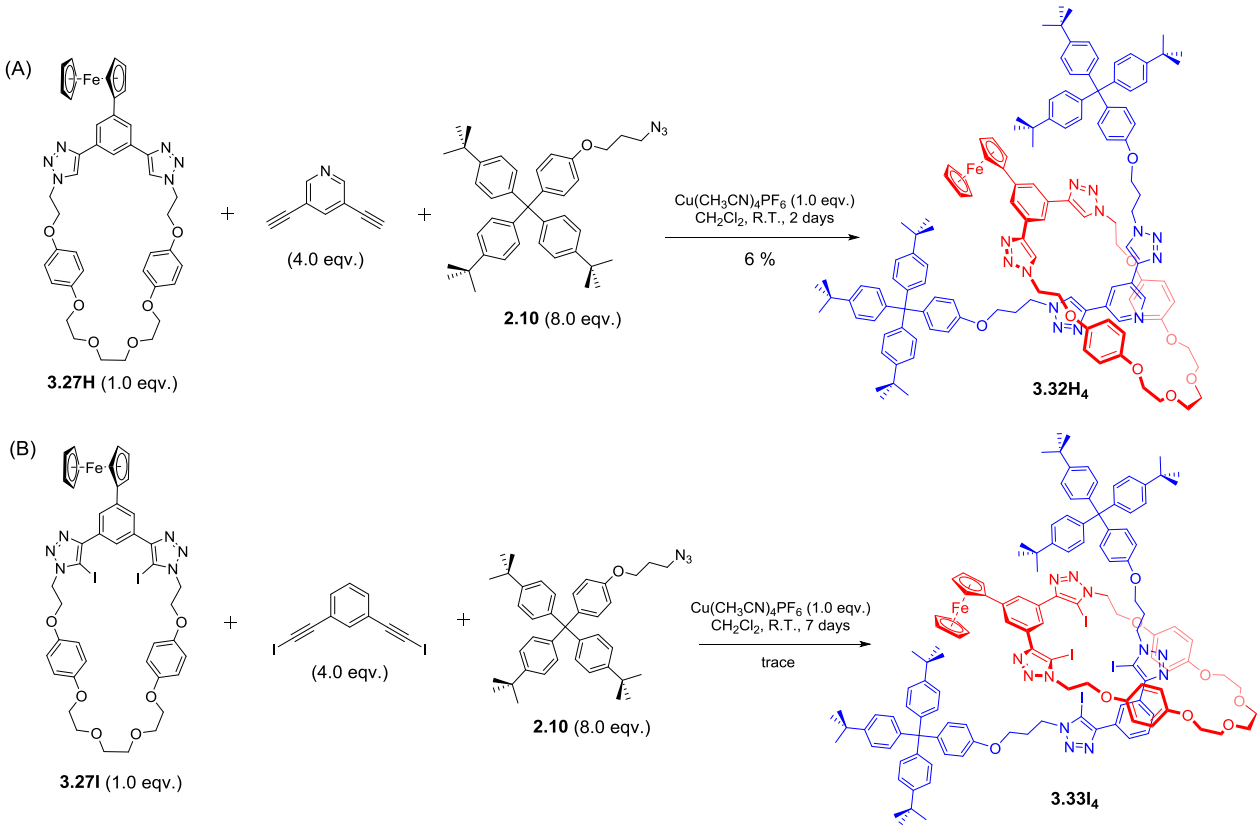
macrocycle cavity and underwent CuAAC rotaxane formation with the endotopically-coordinated Cu(I) catalyst.



***Scheme 3.14**. Synthesis of (A) terminal iodoalkyne axle precursor **3.31I** and (B) neutral rotaxane **3.32I$_4$** using the CuAAC-AMT strategy.*

The synthesis of the all-HB rotaxane analogue **3.32H$_4$** was attempted following the same procedure as **3.32I$_4$** in degassed CH_2Cl_2 using equimolar quantities of $[Cu(CH_3CN)_4]PF_6$ and macrocycle **3.27H** with four and eight equivalents of 3,5-diethynylpyridine and azide **2.10** respectively (Scheme 3.15A). Although all axle precursors were consumed only after 2 days, a significantly-reduced yield of the all-HB target rotaxane was obtained (c.a. 10 % from the crude reaction mixture but only 6 % after chromatographic purification). A repeat of the reaction under identical conditions afforded similar results. Hypothesising that potential XB interactions between the iodotriazole groups of macrocycle **3.27I** and the Lewis basic pyridine *N* atom of the axle precursor **3.31I** may aid in rotaxane formation, an analogous rotaxane synthesis reaction as **3.32I$_4$** was attempted using 1,3-di(iodoethynyl)benzene instead of 3,5-di(iodoethynyl)pyridine (Scheme 3.15B). In the 7 days necessary for complete consumption of

all axle precursors in the two repeats performed, the target all-XB rotaxane **3.33I$_4$** was consistently formed in very small quantities detectable only by ESI-MS analysis. Considering that rotaxanes **3.32I$_4$** and **3.33I$_4$** differed only by the presence of a pyridine *N* atom, the difference in reaction outcome highlights the important roles played by XB-pyridine interactions between the macrocycle and axle precursor **3.31I**. Further evidence for these interactions is provided by a qualitative pseudorotaxane titration of **3.31I** into macrocycle **3.27I** in CD_2Cl_2.



***Scheme 3.15**. Attempted synthesis of rotaxane variants (A) **3.32H$_4$** and (B) **3.33I$_4$**.*

From Figure 3.25, the addition of 1.0 equivalent of **3.31I** into a solution of macrocycle **3.27I** in CD_2Cl_2 afforded a number of changes. Firstly, the macrocycle aromatic protons H_a and H_b underwent significant downfield shift, with the latter perturbed to a larger extent than the former, suggesting the presence of XB interactions between both species. Furthermore, significant sharpening of the spectrum for **3.27I** was observed, indicating that complex formation improved the solubility of the macrocycle by breaking up some of the aggregation

initially present in the non-polar CD_2Cl_2 solvent. Curiously, no upfield perturbations of the hydroquinone proton resonances of **3.27I** was seen, which would have been expected from donor-acceptor aromatic-stacking interactions with the relatively electron-deficient iodotriazole-containing pyridine fragment of **3.31I** if it was threaded through the macrocycle cavity. Taken together, this evidence suggests the likelihood of **3.31I** being assembled by XB interactions above the plane of the macrocycle **3.27I** by the out-of-plane oriented iodotriazole units (Figure 3.25 left) such that the pyridine and/or iodotriazole *N* atoms of **3.31I** are positioned more closely to macrocycle aromatic proton H_b than H_a, allowing more extensive HB interactions and downfield perturbation. Addition of a second equivalent of **3.31I** gave negligible changes, suggesting strong XB association between **3.31I** and **3.27I**. Indeed, XB interactions with the pyridine *N* atom have been known to be strong enough to control long-range ordering in the solid state[97–99] and in soft materials.[100–103]

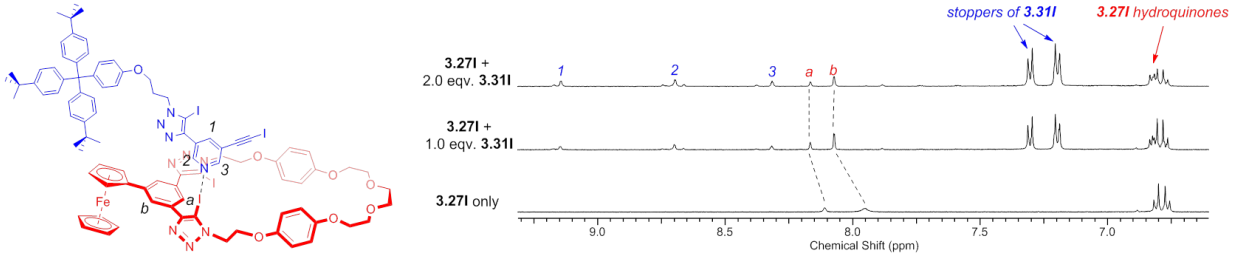
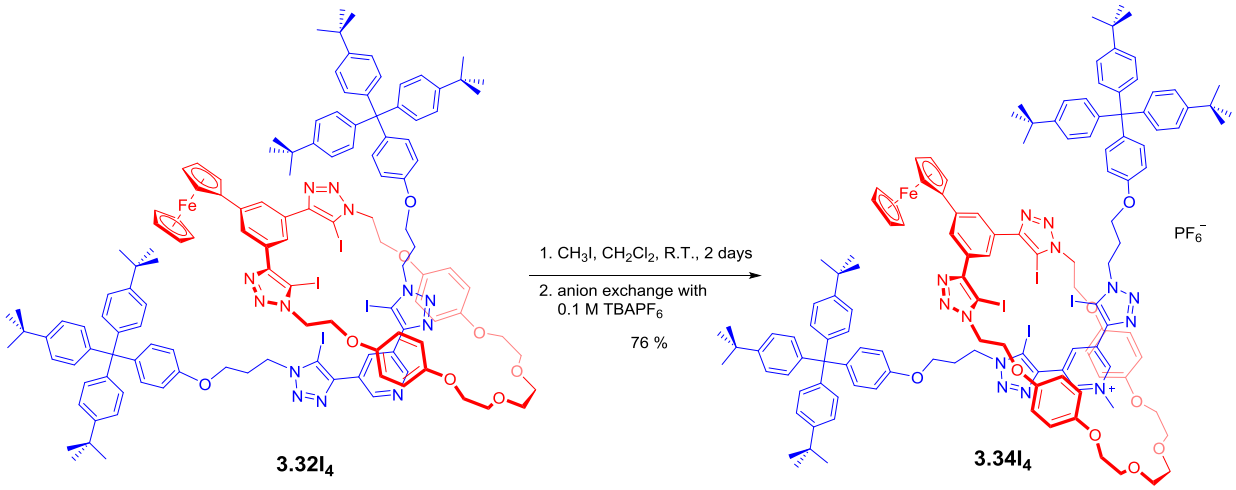


***Figure 3.25**. Aromatic region of the ^{1}H NMR spectra of macrocycle **3.27I** in the presence of 0.0, 1.0 and 2.0 equivalents of pyridine axle precursor **3.31I**, and the possible orientation of the XB between them ([**3.27I**] = 1.0 mM, CD_2Cl_2, T = 298 K).*

Nevertheless, despite the importance of XB interactions in governing the formation of these rotaxanes, the roles played by subsequent addition of Cu(I) in orienting the macrocycle-axle precursor complexes cannot be excluded. However, these Cu(I) complexes formed in the presence of 1.0 equivalent of $[Cu(CH_3CN)_4]PF_6$ are difficult to characterise, with the peaks in the resulting ^{1}H NMR spectra being too complex, broad and indistinct for proper assignment, suggesting that the binding of **3.27I** and **3.31I** to Cu(I) was slow on the ^{1}H NMR timescale and multiple species were formed in solution. Thus, it is likely that a combination of intermolecular XB interactions and AMT processes allowed the preferential formation of **3.32I$_4$** over **3.32H$_4$**

and **3.33I$_4$**, where the initial XB adduct formed between **3.27I** and **3.31I** helps to initially orientate the axle precursor to facilitate endotopic coordination with Cu(I) and the subsequent CuAAC reaction with azide **2.10** through the macrocycle cavity to form the rotaxane.

Having formed the target all-XB neutral rotaxane **3.32I$_4$**, methylation of the axle pyridine moiety was performed by initially reacting the rotaxane with a large excess of iodomethane (CH_3I/ CH_2Cl_2 1:1 *v/v*).[38,104] While the monocationic pyridinium rotaxane was the main product formed after an overnight reaction, ESI-MS showed significant quantities of a dicationic rotaxane formed from a second methylation, possibly of an iodotriazole motif on the macrocycle. Hence, the reaction was repeated using a small quantity of iodomethane (CH_3I/ CH_2Cl_2 10:1 *v/v*), which afforded clean formation of the monocationic rotaxane product. Anion exchange to the PF_6^- salt was achieved by repeatedly washing a chloroform solution of the rotaxane with 0.1 M NH_4PF_6 to afford **3.34I$_4$** in 76 % overall yield (Scheme 3.16). Rotaxane **3.34I$_4$** was characterised by high-resolution ESI-MS, ^{1}H, ^{13}C, ^{19}F and ^{31}P NMR spectroscopy, with the interlocked nature of the rotaxane confirmed by the numerous cross-peaks between the macrocycle and axle components in the 2D ROESY NMR spectrum (Figure 3.26).



***Scheme 3.16**. Synthesis of target cationic ferrocene-appended all-XB rotaxane **3.34I$_4$**.*

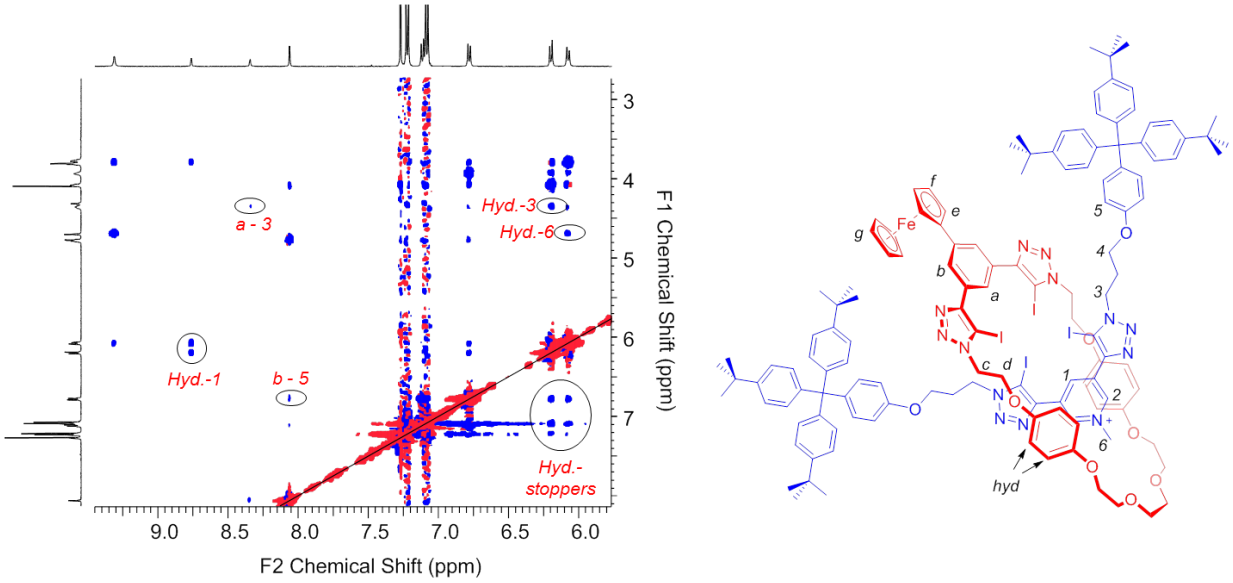


***Figure 3.26**. 2D ROESY NMR spectrum of cationic rotaxane **3.34I$_4$** ($CDCl_3$, T = 298 K).*

As shown in its ^{1}H NMR spectrum (Figure 3.27), the hydroquinone protons of neutral rotaxane **3.32I$_4$** are significantly upfield shifted relative to those of the free macrocycle **3.27I**, resulting from donor-acceptor aromatic π-π stacking interactions with the electron-deficient pyridine-3,5-bis(iodotriazole) functionality on the axle. Upon axle pyridinium methylation, further upfield shifts of these protons are seen, likely due to enhanced aromatic stacking, together with increased splitting of the resonances suggesting a greater degree of rotaxane rigidification due to possible HB interactions of the axle pyridinium methyl group with the macrocycle polyether segment- the latter supported by downfield shifts of the macrocycle component's polyether region. At the same time, downfield perturbations of macrocycle proton H_a and axle pyridinium proton H_2 result from the increased electron deficiency of the cationic rotaxane binding cavity. Slight changes to the rotaxane conformation also likely results from methylation, with notable upfield shift of H_d on the macrocycle component and downfield movement of axle H_3 seen as well.

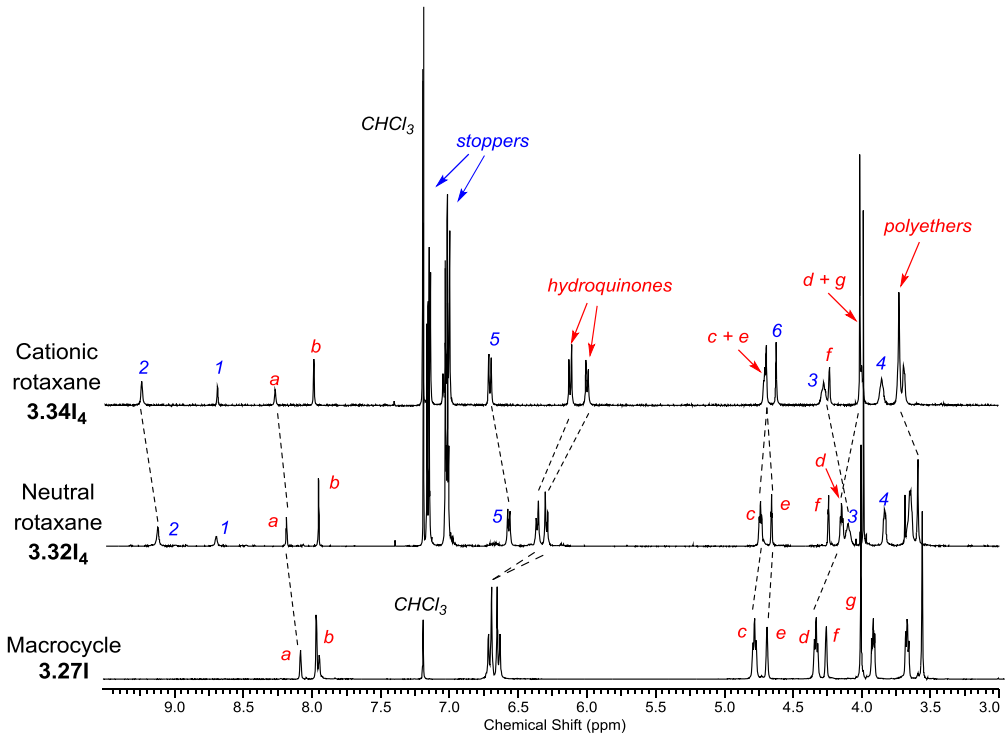


Figure 3.27. *Partial ^{1}H NMR spectrum of macrocycle **3.27I**, neutral rotaxane **3.32I$_4$** and cationic rotaxane **3.34I$_4$** ($CDCl_3$, T = 298 K). Proton assignments follow those in Figure 3.26.*

3.4.2 ^{1}H NMR Titrations

Anion binding studies were performed by ^{1}H NMR titration experiments in the competitive aqueous solvent mixture of CD_3CN/ d_6-acetone/ D_2O 45:45:10 *v/v.*[†††] Addition of TBAI to the rotaxane solution gave downfield shifts of the proton resonances surrounding the rotaxane cavity (H_1 and H_a) (Figure 3.28A), which implied that I^- was binding in its vicinity likely due to XB interactions from the iodotriazoles. Due to the steric bulk of the XB-donor iodine atoms surrounding the anion binding cavity, it is likely that I^- is bound above the plane of the macrocycle. Significant shifts were also observed for H_2, H_3, H_4 and H_5 on the axle component, as well as H_d and H_e on the macrocycle, suggesting that halide anion binding was accompanied by notable rotaxane conformational changes. This probably occurs as the axle and macrocycle components adjust their relative positions to accommodate the bulky I^- and to maximise the number of convergent linear XB interactions with the bound anion. Compared to

[†††] ^{1}H NMR titrations were performed in the same solvent mixture as the subsequent electrochemical sensory studies (*vide infra*). CD_3CN ensured compatibility with the non-aqueous Ag/ $AgNO_3$ reference electrode, while d_6-acetone was necessary to maintain solubility of the rotaxane in the presence of anions thoughout the titration.

I^-, smaller chemical shift perturbations were seen for all proton resonances upon the addition of Cl^-, Br^- and SCN^- (Figure 3.28B). The large SO_4^{2-} anion gave very small shifts of all proton signals (Figure 3.28C), with the internal pyridinium proton H_1 only moving downfield by +0.03 ppm after addition of 10.0 equivalents. Furthermore, the lack of any notable perturbations to the proton signals, unlike those seen for I^-, suggests very weak interaction of the rotaxane with SO_4^{2-}, which is probably a consequence of the anion's strong hydration, large size preventing access to the binding cavity, and the intrinsic unfavourable interactions of XB towards 'hard' oxoanions. Monitoring the shifts of internal pyridinium proton H_1 during the course of the titration and fitting the data to a 1:1 stoichiometric host-guest binding model using WinEQNMR2[39] enabled determination of the anion association constants (Table 3.12).

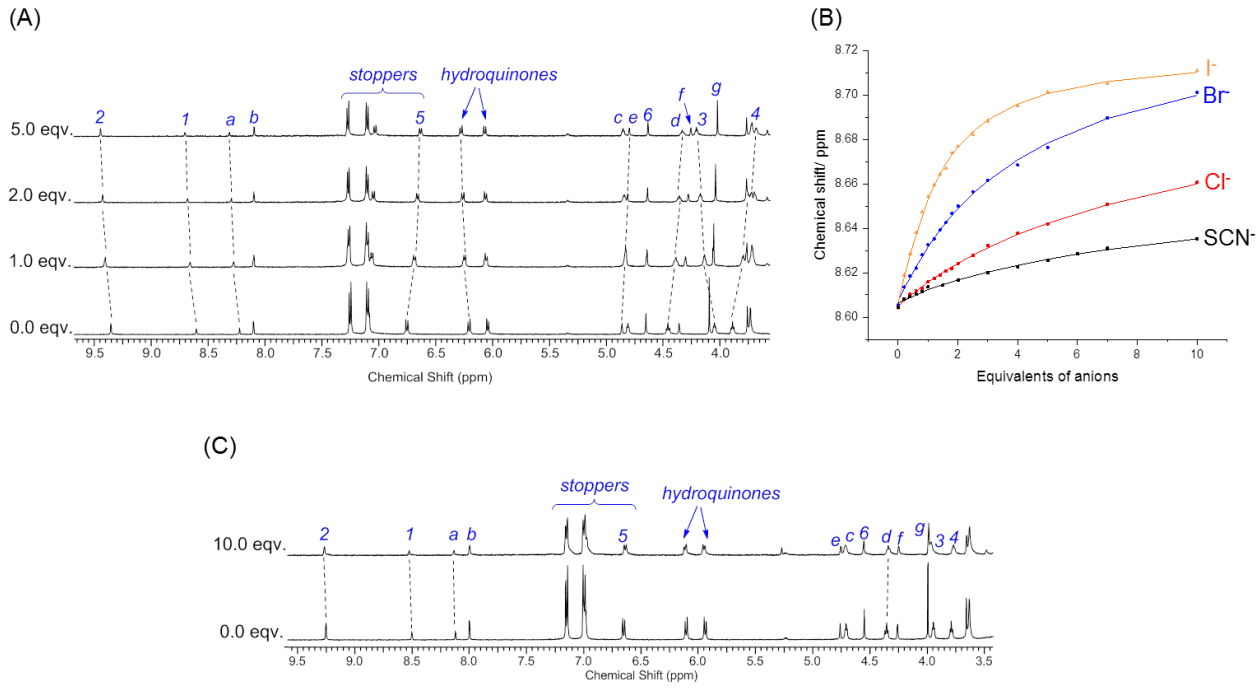


***Figure 3.28**. (A) Partial ^{1}H NMR spectra of cationic rotaxane **3.34I$_4$** in the presence of 0.0, 1.0, 2.0 and 5.0 equivalents of I^-; (B) Plots of the chemical shifts of the internal pyridinium proton H_1 with increasing concentration of anions; (C) Partial ^{1}H NMR spectra of **3.34I$_4$** with 0.0 and 10.0 equivalents of SO_4^{2-} present ([**3.34I$_4$**] = 1.0 mM; CD_3CN/ d_6-acetone/ D_2O 45:45:10 v/v, T = 298 K). Proton assignments follow those in Figure 3.26.*

Table 3.12. Anion association constants (K_a/ M^{-1}) of rotaxane **3.34I$_4$**.[a]

	K_a/ M^{-1}
Cl^-	101 (4)
Br^-	340 (15)
I^-	1125 (5)
SCN^-	102 (8)

[a] K_a values determined by WinEQNMR2 software[39] by monitoring axle pyridinium proton H_1; errors (±) in parentheses ([**3.34I$_4$**] = 1.0 mM; CD_3CN/ d_6-acetone/ D_2O 45:45:10 *v/v*, *T* = 298 K).

Amongst the halide anions, a clear Hofmeister binding preference for I^- can be seen, with the K_a value for I^- more than an order of magnitude larger than that for Cl^-. This trend is consistent with those of other all-XB rotaxanes described in Chapter 2 in the presence of water. Despite the dominant role played by anion hydration in governing binding affinity, SCN^-, which is even more poorly hydrated than I^-,[40] was found to bind much more weakly. This indicated that host-guest shape and size complementarity also played important roles in the anion binding, with the spherical halides bound preferentially over other anion geometries. Nevertheless, it is probable that favourable electrostatic interactions between the cationic rotaxane host and anion guests are also contributing to the binding to some extent.

3.4.3 Electrochemical Anion Sensing Studies

Redox anion sensory studies were performed on neutral macrocycles **3.27I/H** and cationic rotaxane **3.34I$_4$** with Cl^-, Br^- and SCN^- ‡‡‡ in wet and dry acetone/ CH_3CN mixtures. At the time of writing, the use of redox-active interlocked molecules for electrochemical anion sensing in the presence of water is unprecedented.

Receptors **3.27I/H** and **3.34I$_4$** display redox quasi-reversibility in dry acetone/ CH_3CN 1:1 *v/v* (Figure 3.29), as well as in acetone/ CH_3CN/ H_2O 45:45:10 *v/v*, with the redox potentials of each receptor's Fc/ Fc^+ couple reported in Table 3.13. While the more anodic $E_{1/2}$ value of macrocycle **3.27I** compared to **3.27H** due to the presence of electron-withdrawing iodine atoms has been noted previously, it is surprising that *cationic* rotaxane **3.34I$_4$** shows

‡‡‡ SCN^- was studied to investigate the effects of hydrophobicity on redox anion sensing behaviour, especially in the presence of water. SO_4^{2-} was not studied due to the ^{1}H NMR titration results which established that it does not bind within the rotaxane cavity.

comparable and only a very slightly more positive $E_{1/2}$ value compared to *neutral* macrocycle **3.27I**. In the presence of 10 % water by volume, a consistent cathodic shift of the $E_{1/2}$ values were seen for all receptors, with the smallest change seen for **3.34I$_4$**. The cathodic shift may arise from the presence of water solvating and hence thermodynamically stabilising the charged ferrocenium species following oxidation. Thus, a greater change in hydration-induced oxidised receptor stabilisation can be expected from that of a neutral species (0 to +1 charge) compared to rotaxane **3.34I$_4$** which is already cationic (+1 to +2 charge). This gives rise to more pronounced differences in $E_{1/2}$ values between the receptors in the presence of water, which becomes distinctly more anodic with the increased electron-deficiency of the host (i.e. **3.27H** < **3.27I** < **3.34I$_4$**).

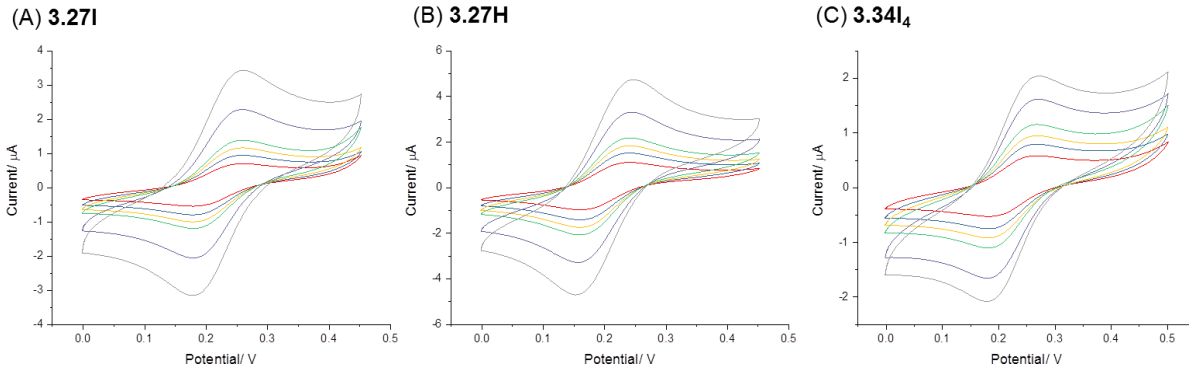


***Figure 3.29**. Reversibility studies: CVs recorded at the scan rates of 25, 50, 75, 100, 250 and 500 mV s^{-1} for macrocycles (A) **3.27I** and (B) **3.27H**; and (C) 25, 50, 75, 100, 250 and 400 mV s^{-1} for rotaxane **3.34I$_4$** ([host] = 0.1 mM, electrolyte: 0.1 M $TBAPF_6$ in acetone/ CH_3CN 1:1 v/v; T = 293 K). All potentials taken with reference to the Ag/ $AgNO_3$ reference electrode.*

Table 3.13. Redox potentials ($E_{1/2}$/ V) of the Fc/ Fc^+ couples of macrocycles **3.27I/H** and rotaxane **3.34I$_4$** in wet and dry solvents.[a]

	Acetone/ CH_3CN 1:1	Acetone/ CH_3CN/ H_2O 45:45:10	$\Delta E_{1/2}$ [b]
3.27I	0.218	0.184	-34
3.27H	0.200	0.161	-39
3.34I$_4$	0.224	0.212	-12

[a] Values reported relative to the Ag/ $AgNO_3$ reference electrode; glassy carbon working electrode, Pt wire auxiliary electrode, electrolyte: 0.1 M $TBAPF_6$ in the appropriate solvent, T = 293 K. [b] $\Delta E_{1/2} = E_{1/2\ (wet)} - E_{1/2\ (dry)}$.

In dry acetone/ CH_3CN 1:1, all host systems display modest cathodic shifts upon addition of anions, as shown in Figure 3.30 and Table 3.14, which decreases in magnitude following the order $Cl^- > Br^- > SCN^-$ for all receptors in order of their charge density and ability to stabilise the oxidised ferrocenium state. Just like the model systems described in Section 3.3, the XB macrocycle **3.27I** showed considerably augmented voltammetric responses for Cl^- and Br^- relative to its HB analogue **3.27H**. Interestingly, despite the cationic nature of rotaxane **3.34I$_4$** which facilitates anion binding, comparable cathodic shift magnitudes were seen with

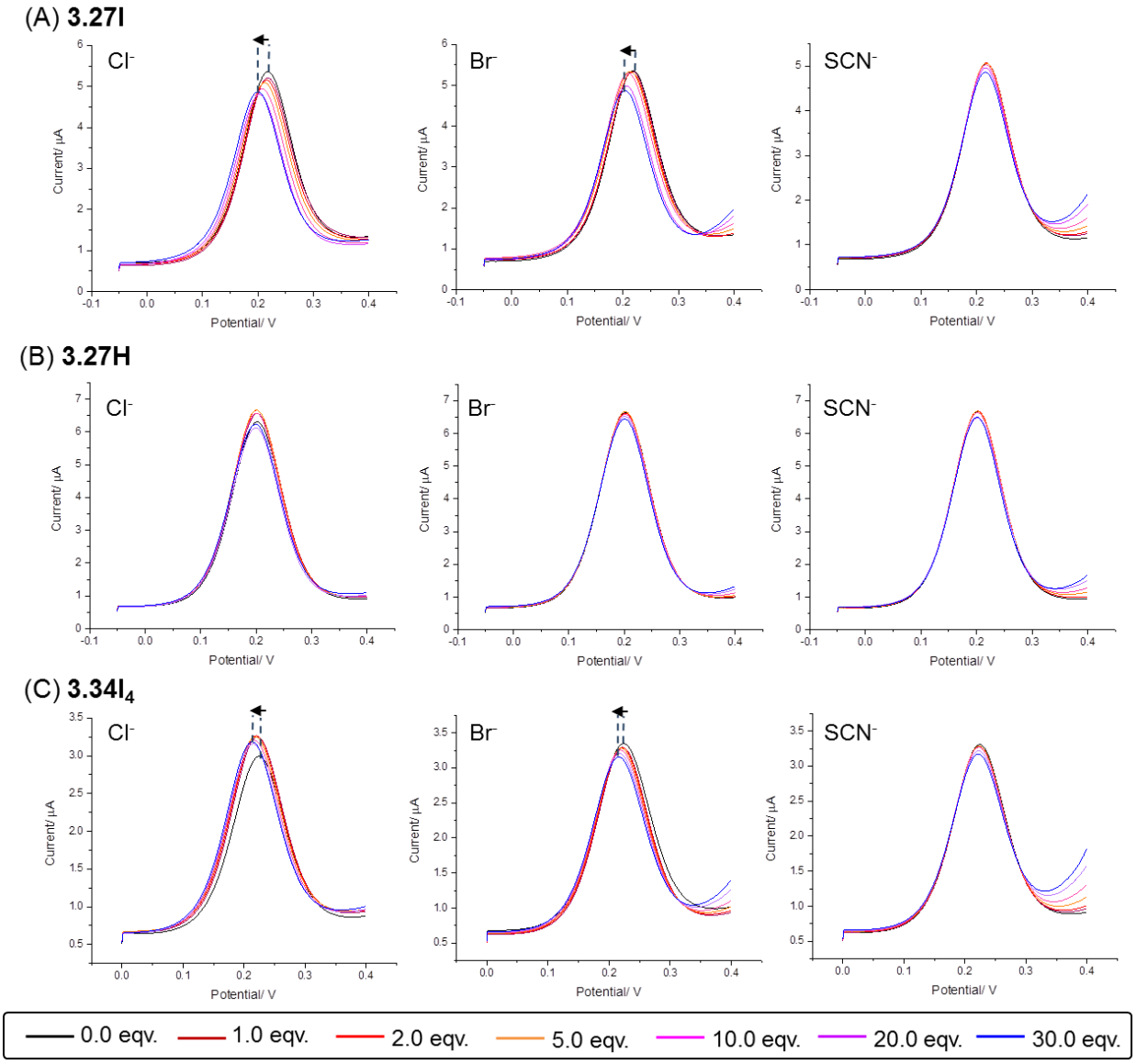


***Figure 3.30**. SWVs of macrocycles (A) **3.27I** and (B) **3.27H** as well as (C) rotaxane **3.34I$_4$** in the presence of 0, 1, 2, 5, 10, 20 and 30 equivalents of Cl^-, Br^- and SCN^- ([host] = 0.1 mM, electrolyte: 0.1 M $TBAPF_6$ in acetone/ CH_3CN 1:1 v/v; T = 293 K).*

Table 3.14. Magnitudes of cathodic shifts ($\Delta E_{1/2}$/ mV) of the Fc/ Fc^+ redox couple of each receptor in dry and wet solvents.

Receptor	Solvent	Equiv. of anions	$\Delta E_{1/2}$/ mV		
			Cl^-	Br^-	SCN^-
3.27I	Acetone/ CH_3CN 1:1	20	-16	-13	-2
3.27H	Acetone/ CH_3CN 1:1	20	-3	-2	-1
3.34I$_4$	Acetone/ CH_3CN 1:1	20	-11	-8	-2
	Acetone/ CH_3CN/ H_2O 45:45:10	20	-2	-10	-1
	Acetone/ CH_3CN/ H_2O 45:45:10	150	-11	-21	-4

[a] Anions added as TBA salts, electrolyte: 0.1 M $TBAPF_6$ in the respective solvents; errors estimated at ± 5 mV; ([receptor] = 0.1 mM, T = 293 K).

neutral macrocycle **3.27I**. It is noteworthy that these host systems show greatly diminished redox responses compared to the dicationic acyclic model receptor **3.19I/H** in dry electrolyte, likely a consequence of the uncharged 1-ferrocenyl-3,5-bis(triazole)benzene anion binding/sensing motif. Specifically, the charge-assisted XB interactions with the bis(iodotriazolium) of **3.19I** is likely to possess more pronounced covalent character in anion binding compared to the neutral bis(iodotriazole) motif in **3.27I** and **3.34I$_4$**,[§§§] facilitating electronic communication with the ferrocene reporter group to give larger cathodic shift responses to anions.

In the competitive electrolyte solution of acetone/ CH_3CN/ H_2O 45:45:10 *v/v*, rotaxane **3.34I$_4$** showed considerably improved redox anion sensory properties than macrocycle **3.27I**. With 20-fold excess of anions relative to **3.34I$_4$**, a considerably diminished and negligible response was seen for Cl^- in wet solvent but surprisingly, Br^- gave similar cathodic shifts compared to analogous titrations in dry solvent (Figure 3.31 and Table 3.14). Contrastingly, macrocycles **3.27H/I** showed no cathodic shifts even in the presence of 50 equivalents of Cl^- in wet electrolyte. In the presence of a large excess of anions (150 equivalents) with **3.34I$_4$**, Br^- showed a notably enhanced cathodic shift magnitude compared to Cl^- due to its stronger association with the rotaxane. Significantly, while SCN^- and Cl^- showed comparable values of

[§§§] Although **3.34I$_4$** is overall cationic, the binding motif conjugated to and directly responsible for communication with ferrocene is neutral as the positive charge lies on the rotaxane's axle component.

K_a in the same solvent mixture (Table 3.12), Cl^- elicited greatly enhanced voltammetric response due to its greater charge density. Nevertheless, it is noteworthy that **3.34I$_4$** is the first example of a rotaxane which demonstrates preferential sensing behaviour for Br^- in highly-competitive aqueous solvent milieu.

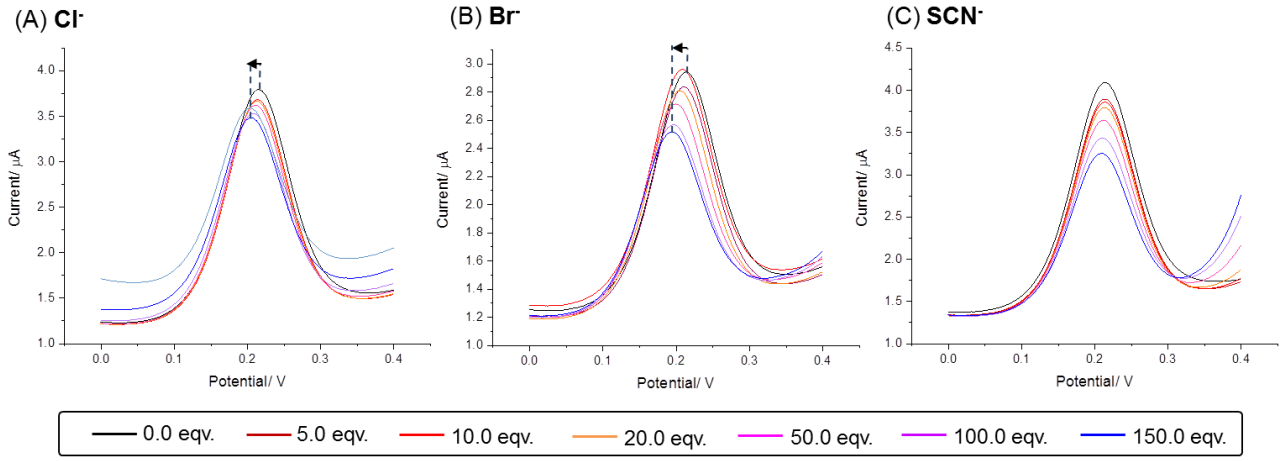


***Figure 3.31**. SWVs of rotaxane **3.34I$_4$** in the presence of 0, 5, 10, 20, 50, 100 and 150 equivalents of Cl^-, Br^- and SCN^- ([host] = 0.1 mM, electrolyte: 0.1 M $TBAPF_6$ in acetone/ CH_3CN/ H_2O 45:45:10 v/v; T = 293 K).*

3.5 Conclusions and Future Work

3.5.1 Conclusions

This chapter aimed to demonstrate the important influences of σ-hole donor groups on electrochemical anion sensing. For the neutral rotaxane family **3.9**, while appendage of XB-donor iodotriazoles on the axle at the periphery of the binding site reduced the resulting affinities of all anions, the magnitudes of cathodic perturbations to the Fc/ Fc^+ redox couples were unaffected, highlighting the importance of the through-bond communication between the anion binding site and the ferrocene redox reporter group. Thus, in an attempt to enhance the voltammetric response, a series of model acyclic XB host receptors, containing XB iodotriazoles electronically conjugated with ferrocene, were designed and synthesised. Compared to their HB analogues, these XB receptors generally showed magnified anion binding affinities and redox sensing behaviour, which is attributed to the enhanced degree of covalency of XB···anion interactions which facilitated through-bond communicative pathways,

and was observed for both neutral and cationic receptors. By varying the iodotriazole substitution positions around ferrocene, concomitantly changing the bidentate XB bite angle for anion coordination, the anion binding preference could be modulated. For instance, the unique geometric requirements of the 1,3-bis(iodotriazole) ferrocene receptor allowed selective binding and redox sensing of N_3^-, showing the importance of host-guest size complementarity for anion selectivity and redox sensing. Notably, the enhanced redox response of XB receptors faciltated anion sensing in the presence of water as well. Comparatively, the presence of ChB-donor methylseleno-triazolium groups gave smaller anion-induced redox responses, being of comparable magnitude to those of HB systems.

The CuAAC-AMT protocol allowed the synthesis of an unprecedented all-XB redox-active rotaxane from a ferrocene-containing XB macrocycle. The cationic methylated all-XB rotaxane host bound anions following a Hofmeister bias selectivity, and displayed preferential redox anion sensing behaviour for Br^- over Cl^- in a highly-competitive aqueous-organic solvent media. Contrastingly, the free XB macrocycle did not show any redox sensory behaviour in the same solvent mixture. In all, this chapter has demonstrated that σ-hole interactions, particularly XB, can enhance the sensory behaviour of ferrocene-functionalised redox-active acyclic and interlocked host molecules, by both modulating the stability of the host-anion complexes as well as improving the through-bond communication with the redox-active ferrocene reporter group.

3.5.2 Future Work

Work in this chapter has set the precedents for further exploitation of σ-hole interactions, particularly XB, in redox anion sensing. Other than incorporating XB-donor groups into novel host systems, such as the use of a redox-active chiral XB host for enantioselective anion sensing described in the next chapter, assembling receptors onto conductive surfaces could allow the fabrication of novel anion sensory devices. In particular, the 1,3-bis(iodotriazole)-ferrocene N_3^--sensing motif could be incorporated into thiol-terminated receptors for assembly as SAMs on gold surfaces to allow sensitive N_3^- detection in aqueous

media. The same could be performed using the halide selective 1-ferrocenyl-3,5-bis(iodotriazole) and 1,1'-bis(iodotriazole)-ferrocene motifs (Figure 3.32A). In addition, more in-depth studies on ChB-mediated redox anion sensing could be performed, using the more electropositive methyltelluro-triazole ChB-donor motif to enhance redox communication (Figure 3.32B).

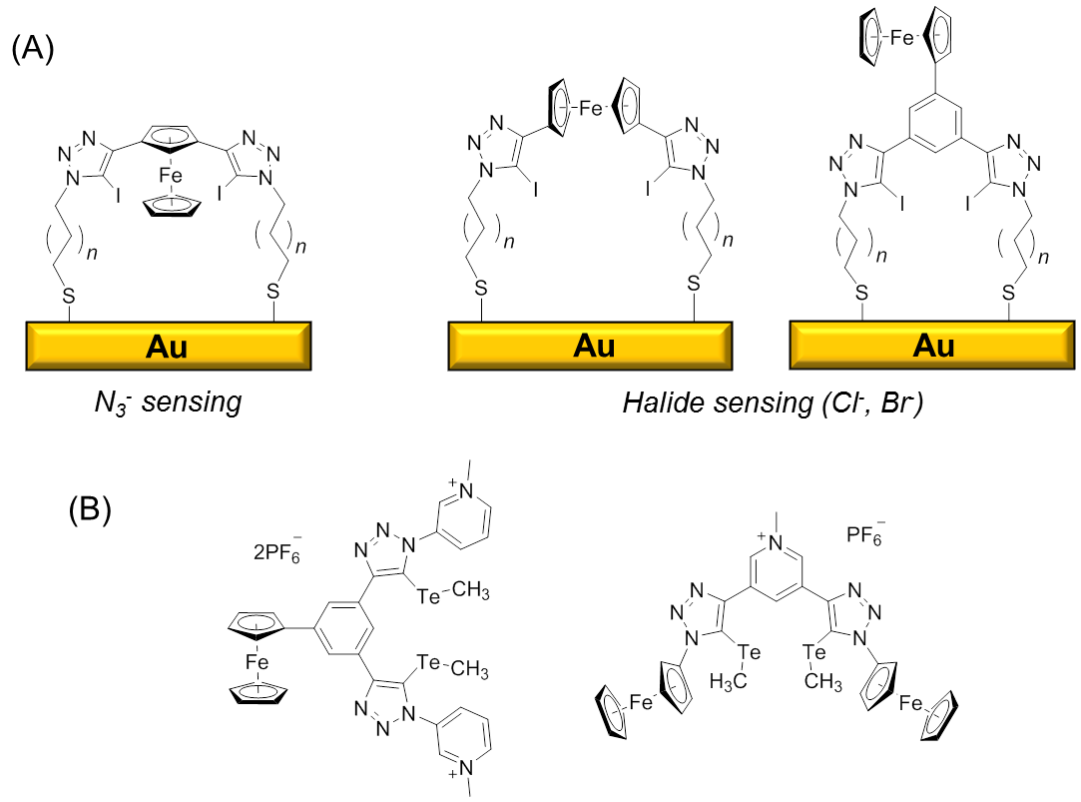


***Figure 3.32**. Suggested receptor designs for future exploration: (A) thiolated XB redox-active hosts for anion sensing device fabrication by immobilisation onto solid Au surfaces; (B) Te-based redox-active host molecules for ChB-mediated electrochemical anion sensing.*

3.6 References

1 S. W. Robinson, C. L. Mustoe, N. G. White, A. Brown, A. L. Thompson, P. Kennepohl and P. D. Beer, *J. Am. Chem. Soc.*, 2015, **137**, 499–507.
2 P. D. Beer, P. A. Gale and G. Z. Chen, *J Chem Soc Dalton Trans*, 1999, 1897–1910.
3 J. C. Medina, T. T. Goodnow, M. T. Rojas, J. L. Atwood, B. C. Lynn, A. E. Kaifer and G. W. Gokel, *J. Am. Chem. Soc.*, 1992, **114**, 10583–10595.
4 P. D. Beer, P. A. Gale and Z. Chen, *Adv. Phys. Org. Chem.*, 1999, **31**, 1–90.
5 Z. Chen, A. R. Graydon and P. D. Beer, *J Chem Soc Faraday Trans*, 1996, **92**, 97–102.
6 A. C. Fahrenbach, C. J. Bruns, H. Li, A. Trabolsi, A. Coskun and J. F. Stoddart, *Acc. Chem. Res.*, 2014, **47**, 482–493.
7 E. Katz, O. Lioubashevsky and I. Willner, *J. Am. Chem. Soc.*, 2004, **126**, 15520–15532.
8 E. Katz, L. Sheeney-Haj-Ichia and I. Willner, *Angew. Chem. Int. Ed.*, 2004, **43**, 3292–3300.
9 A. H. Flood, J. F. Stoddart, D. W. Steuerman and J. R. Heath, *Science*, 2004, **306**, 2055.

10 M. Alfonso, A. Tárraga and P. Molina, *Inorg. Chem.*, 2013, **52**, 7487–7496.
11 M. del C. González, F. Otón, R. A. Orenes, A. Espinosa, A. Tárraga and P. Molina, *Organometallics*, 2014, **33**, 2837–2852.
12 O. Karagollu, M. Gorur, F. Gode, B. Sennik and F. Yilmaz, *Sens. Actuators B Chem.*, 2014, **193**, 788–798.
13 A. Mulas, Y. Willener, J. Carr-Smith, K. M. Joly, L. Male, C. J. Moody, S. L. Horswell, H. V. Nguyen and J. H. R. Tucker, *Dalton Trans.*, 2015, **44**, 7268–7275.
14 T. Romero, R. A. Orenes, A. Tárraga and P. Molina, *Organometallics*, 2013, **32**, 5740–5753.
15 Y. Willener, K. M. Joly, C. J. Moody and J. H. R. Tucker, *J. Org. Chem.*, 2008, **73**, 1225–1233.
16 Q.-Y. Cao, T. Pradhan, S. Kim and J. S. Kim, *Org. Lett.*, 2011, **13**, 4386–4389.
17 P. J. Skinner, S. Blair, R. Kataky and D. Parker, *New J Chem*, 2000, **24**, 265–268.
18 Y. Suzaki, E. Chihara, A. Takagi and K. Osakada, *Dalton Trans*, 2009, 9881–9891.
19 M. J. Langton and P. D. Beer, *Acc. Chem. Res.*, 2014, **47**, 1935–1949.
20 S. R. Bayly, T. M. Gray, M. J. Chmielewski, J. J. Davis and P. D. Beer, *Chem Commun*, 2007, 2234–2236.
21 N. H. Evans and P. D. Beer, *Org Biomol Chem*, 2011, **9**, 92–100.
22 N. H. Evans, H. Rahman, A. V. Leontiev, N. D. Greenham, G. A. Orlowski, Q. Zeng, R. M. J. Jacobs, C. J. Serpell, N. L. Kilah, J. J. Davis and P. D. Beer, *Chem Sci*, 2012, **3**, 1080–1089.
23 N. H. Evans, C. J. Serpell, N. G. White and P. D. Beer, *Chem. – Eur. J.*, 2011, **17**, 12347–12354.
24 N. H. Evans, C. J. Serpell and P. D. Beer, *Chem Commun*, 2011, **47**, 8775–8777.
25 J. J. Davis, G. A. Orlowski, H. Rahman and P. D. Beer, *Chem Commun*, 2010, **46**, 54–63.
26 J. Lehr, T. Lang, O. A. Blackburn, T. A. Barendt, S. Faulkner, J. J. Davis and P. D. Beer, *Chem. – Eur. J.*, 2013, **19**, 15898–15906.
27 A. Brown and P. D. Beer, *Dalton Trans*, 2012, **41**, 118–129.
28 M. W. Renner, K. M. Barkigia, Y. Zhang, C. J. Medforth, K. M. Smith and J. Fajer, *J. Am. Chem. Soc.*, 1994, **116**, 8582–8592.
29 J. Y. C. Lim, M. J. Cunningham, J. J. Davis and P. D. Beer, *Chem Commun*, **51**, 14640–14643.
30 J. Y. C. Lim and P. D. Beer, *Eur. J. Inorg. Chem.*, 2017, **2017**, 220–224.
31 R. Oliveira, S. Groni, C. Fave, M. Branca, F. Mavre, D. Lorcy, M. Fourmigue and B. Schollhorn, *Phys Chem Chem Phys*, 2016, **18**, 15867–15873.
32 F. Zapata, A. Caballero and P. Molina, *Eur. J. Inorg. Chem.*, 2017, **2017**, 237–241.
33 B. R. Mullaney, M. J. Cunningham, J. J. Davis and P. D. Beer, *Polyhedron*, 2016, **116**, 20–25.
34 J. M. Mercurio, F. Tyrrell, J. Cookson and P. D. Beer, *Chem Commun*, 2013, **49**, 10793–10795.
35 A. A. Malik, S. B. Preston, T. G. Archibald, M. P. Cohen and K. Baum, *Synthesis*, 2002, **21**, 450–451.
36 J. A. Wisner, P. D. Beer, M. G. B. Drew and M. R. Sambrook, *J. Am. Chem. Soc.*, 2002, **124**, 12469–12476.
37 M. J. Langton, I. Marques, S. W. Robinson, V. Félix and P. D. Beer, *Chem. – Eur. J.*, 2016, **22**, 185–192.
38 S. W. Robinson and P. D. Beer, *Org Biomol Chem*, 2017, **15**, 153–159.
39 M. J. Hynes, *J. Chem. Soc. Dalton Trans.*, 1993, 311–312.
40 Y. Marcus, *J Chem Soc Faraday Trans*, 1991, **87**, 2995–2999.
41 B. Kratochvil, E. Lorah and C. Garber, *Anal. Chem.*, 1969, **41**, 1793–1796.
42 A. J. Bard and L. R. Faulkner, *Electrochemical Methods: Fundamentals an Applications*, Wiley, New York, 7th ed., 2001.
43 E. J. Corey and P. L. Fuchs, *Tetrahedron Lett.*, 1972, **13**, 3769–3772.
44 K. Omura and D. Swern, *Tetrahedron*, 1978, **34**, 1651–1660.
45 M. Bérubé and D. Poirier, *Org. Lett.*, 2004, **6**, 3127–3130.
46 W. S. Brotherton, R. J. Clark and L. Zhu, *J. Org. Chem.*, 2012, **77**, 6443–6455.
47 J. K. Pudelski and M. R. Callstrom, *Organometallics*, 1994, **13**, 3095–3109.
48 R. Deschenaux, J. Santiago, D. Guillon and B. Heinrich, *J Mater Chem*, 1994, **4**, 679–682.
49 A. A. Koridze, A. M. Sheloumov, S. A. Kuklin, V. Y. Lagunova, I. I. Petukhova, F. M. Dolgushin, M. G. Ezernitskaya, P. V. Petrovskii, A. A. Macharashvili and R. V. Chedia, *Russ. Chem. Bull.*, 2002, **51**, 1077–1078.
50 A. A. Koridze, S. A. Kuklin, A. M. Sheloumov, F. M. Dolgushin, V. Y. Lagunova, I. I. Petukhova, M. G. Ezernitskaya, A. S. Peregudov, P. V. Petrovskii, E. V. Vorontsov, M. Baya and R. Poli, *Organometallics*, 2004, **23**, 4585–4593.
51 A. N. Nesmeyanov, E. V. Leonova, N. S. Kochetkova, A. I. Malkova and A. G. Makarovskaya, *J. Organomet. Chem.*, 1975, **96**, 275–278.
52 P. Bickert, B. Hildebrandt and K. Hafner, *Organometallics*, 1984, **3**, 653–657.
53 B. F. Bonini, E. Capitò, M. Comes-Franchini, M. Fochi and A. Ricci, *ARKIVOC*, 2006, **2006**, 85–96.
54 D. B. Ramachary, K. Ramakumar and V. V. Narayana, *Chem. – Eur. J.*, 2008, **14**, 9143–9147.
55 L. J. T. Danence, Y. Gao, M. Li, Y. Huang and J. Wang, *Chem. – Eur. J.*, 2011, **17**, 3584–3587.
56 M. Belkheira, D. El Abed, J.-M. Pons and C. Bressy, *Chem. – Eur. J.*, 2011, **17**, 12917–12921.
57 S. S. van Berkel, S. Brauch, L. Gabriel, M. Henze, S. Stark, D. Vasilev, L. A. Wessjohann, M. Abbas and B. Westermann, *Angew. Chem. Int. Ed.*, 2012, **51**, 5343–5346.
58 Z. Chen, Q. Yan, H. Yi, Z. Liu, A. Lei and Y. Zhang, *Chem. – Eur. J.*, 2014, **20**, 13692–13697.
59 I. M. Goldman, *J. Org. Chem.*, 1969, **34**, 1979–1981.
60 A. J. Fatiadi, *Synthesis*, 2002, **1976**, 65–104.
61 G. Cahiez, M. Alami, R. J. K. Taylor, M. Reid, J. S. Foot and L. Fader, in *Encyclopedia of Reagents for Organic Synthesis*, John Wiley & Sons, Ltd, 2001.

62 M. Steurer, K. Tiedl, Y. Wang and W. Weissensteiner, *Chem Commun*, 2005, 4929–4931.
63 M. Steurer, Y. Wang, K. Mereiter and W. Weissensteiner, *Organometallics*, 2007, **26**, 3850–3859.
64 M. J. Kelly, A. E. J. Broomsgrove, I. R. Morgan, I. Siewert, P. Fitzpatrick, J. Smart, D. Vidovic and S. Aldridge, *Organometallics*, 2013, **32**, 2674–2684.
65 T. Sasamori, Y. Suzuki and N. Tokitoh, *Organometallics*, 2014, **33**, 6696–6699.
66 A. Zirakzadeh, A. Herlein, M. A. Groß, K. Mereiter, Y. Wang and W. Weissensteiner, *Organometallics*, 2015, **34**, 3820–3832.
67 B. Qiao, J. R. Anderson, M. Pink and A. H. Flood, *Chem Commun*, 2016, **52**, 8683–8686.
68 G. B. Carpenter, *Acta Crystallogr.*, 1952, **5**, 132–135.
69 T. S. Cameron, K. M. Mannan and M. O. Rahman, *Acta Crystallogr. Sect. B*, 1976, **32**, 87–90.
70 C. Akers, S. W. Peterson and R. D. Willett, *Acta Crystallogr. Sect. B*, 1968, **24**, 1125–1126.
71 E. D. Stevens and H. Hope, *Acta Crystallogr. Sect. A*, 1977, **33**, 723–729.
72 I. Dilovic and K. Uzarevic, *CrystEngComm*, 2015, **17**, 3153–3161.
73 P. Sokkalingam, J. Shraberg, S. W. Rick and B. C. Gibb, *J. Am. Chem. Soc.*, 2016, **138**, 48–51.
74 S. Chang and S. H. Lamm, *Int. J. Toxicol.*, 2003, **22**, 175–186.
75 R. P. Smith and D. E. Wilcox, *Crit. Rev. Toxicol.*, 1994, **24**, 355–377.
76 A. Dalmia, R. F. Savinell and C. C. Liu, *J. Electrochem. Soc.*, 1996, **143**, 1827–1833.
77 J. M. Stellman, *Encyclopedia of Occupational Health and Safety*, International Labour Organisation, Geneva, Switzerland, 4th edn., 1998.
78 E. A. Betterton, *Crit. Rev. Environ. Sci. Technol.*, 2003, **33**, 423–458.
79 L. Fabbrizzi and I. Faravelli, *Chem Commun*, 1998, 971–972.
80 K. Dhara, U. C. Saha, A. Dan, S. Sarkar, M. Manassero and P. Chattopadhyay, *Chem Commun*, 2010, **46**, 1754–1756.
81 J. Zhang, Y. Li, W. Yang, S.-W. Lai, C. Zhou, H. Liu, C.-M. Che and Y. Li, *Chem Commun*, 2012, **48**, 3602–3604.
82 A. K. Singh, U. P. Singh, V. Aggarwal and S. Mehtab, *Anal. Bioanal. Chem.*, 2008, **391**, 2299–2308.
83 C. J. Harding, F. E. Mabbs, E. J. L. MacInnes, V. McKee and J. Nelson, *J Chem Soc Dalton Trans*, 1996, 3227–3230.
84 C. R. Wade and F. P. Gabbaï, *Z. Naturforsch.*, 2014, **69b**, 1199–1205.
85 Y. Kim, T. W. Hudnall, G. Bouhadir, D. Bourissou and F. P. Gabbai, *Chem Commun*, 2009, 3729–3731.
86 A. Rai, N. Kumari, A. K. Srivastava, S. K. Singh, S. Srikrishna and L. Mishra, *J. Photochem. Photobiol. Chem.*, 2016, **319**–**320**, 78–86.
87 Y. A. Jeong, I. J. Chang and S.-K. Chang, *Sens. Actuators B Chem.*, 2016, **224**, 73–80.
88 J. W. Lee, H. W. Kim, H. G. Im, H. Y. Kim and S.-K. Chang, *Sens. Actuators B Chem.*, 2014, **192**, 9–14.
89 Y. Zhou, Y.-W. Yao, Q. Qi, Y. Fang, J.-Y. Li and C. Yao, *Chem Commun*, 2013, **49**, 5924–5926.
90 J. M. Lehn, E. Sonveaux and A. K. Willard, *J. Am. Chem. Soc.*, 1978, **100**, 4914–4916.
91 A. Sahana, A. Banerjee, S. Guha, S. Lohar, A. Chattopadhyay, S. K. Mukhopadhyay and D. Das, *Analyst*, 2012, **137**, 1544–1546.
92 K. M. Roberts, M. A. Flahive and J. E. House, *Polyhedron*, 2013, **53**, 240–242.
93 M. S. Inkpen, S. Du, M. Hildebrand, A. J. P. White, N. M. Harrison, T. Albrecht and N. J. Long, *Organometallics*, 2015, **34**, 5461–5469.
94 M. Tiecco, L. Testaferri, M. Tingoli, D. Chianelli, D. Bartoli and R. Balducci, *Tetrahedron*, 1988, **44**, 4883–4894.
95 M. R. Detty and M. E. Logan, in *Advances in Physical Organic Chemistry*, Academic Press, 2004, vol. Volume 39, pp. 79–145.
96 H. J. Reich and C. P. Jasperse, *J. Am. Chem. Soc.*, 1987, **109**, 5549–5551.
97 C. B. Aakeroy, S. Panikkattu, P. D. Chopade and J. Desper, *CrystEngComm*, 2013, **15**, 3125–3136.
98 C. B. Aakeröy, P. D. Chopade and J. Desper, *Cryst. Growth Des.*, 2013, **13**, 4145–4150.
99 E. Corradi, S. V. Meille, M. T. Messina, P. Metrangolo and G. Resnati, *Angew. Chem.*, 2000, **112**, 1852–1856.
100 J. A. Foster, PiepenbrockMarc-Oliver M., G. O. Lloyd, N. Clarke, HowardJudith A. K. and J. W. Steed, *Nat Chem*, 2010, **2**, 1037–1043.
101 L. Meazza, J. A. Foster, K. Fucke, P. Metrangolo, G. Resnati and J. W. Steed, *Nat Chem*, 2013, **5**, 42–47.
102 A. R. Hirst, B. Escuder, J. F. Miravet and D. K. Smith, *Angew. Chem. Int. Ed.*, 2008, **47**, 8002–8018.
103 J. Xu, X. Liu, T. Lin, J. Huang and C. He, *Macromolecules*, 2005, **38**, 3554–3557.
104 M. J. Langton, S. W. Robinson, I. Marques, V. Félix and P. D. Beer, *Nat Chem*, 2014, **6**, 1039–1043.

Blank Page

Chapter 4

Chiral σ-Hole Donor Host Molecules for Enantioselective Anion Recognition and Sensing

CHAPTER 4 : Chiral σ-Hole Donor Host Molecules for Enantioselective Anion Recognition and Sensing

4.1 Introduction

Chiral compounds are non-superimposable molecules containing spatially asymmetric arrangements of atoms around one or more chiral centres, and are found extensively in nature (e.g. DNA, sugars and proteins) and artificial systems.[1] The process of chiral recognition, where an asymmetric molecule selectively discriminates and interacts with one guest enantiomer over the other, is of fundamental importance in biology, materials science, crystallisation, asymmetric synthetic chemistry and catalysis.[2] However, the subtlety and complexity of the process has thus precluded a complete understanding of the underlying mechanisms.[3] Although some theoretical frameworks have been developed (Section 4.1.1), man-made chiral receptors have yet to achieve the exceptional levels of enantioselectivity found in natural enzymes (Section 4.1.2).[4] Part of the difficulty lies in the fact that chiral compounds have completely identical physicochemical properties in an isotropic achiral environment, rendering them completely indistinguishable from each other. To further complicate the process, molecules can exhibit different types of chirality, being asymmetric about an atom, axis or plane (Figure 4.1), thus necessitating different stereochemical requirements for discrimination. While elucidating the mechanisms guiding enantiospecificity in biological systems has proven challenging due to their structural complexity, some progress has been made in recent years with simpler abiotic acyclic and macrocyclic chiral receptor systems (Section 4.1.3).

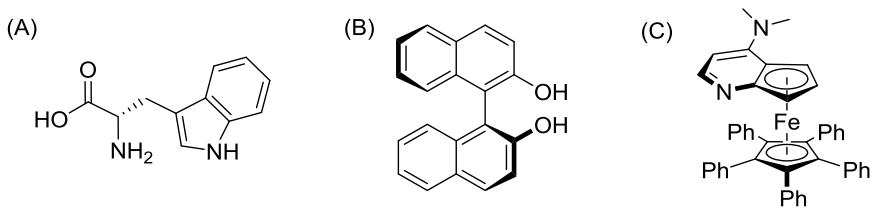


***Figure 4.1**. Examples of different types of molecular chirality: (A) point: amino acid tryptophan; (B) axial: 1,1'-bi-2-naphthol (BINOL)[5] and (C) planar chirality: a derivative of ferrocene used in asymmetric catalysis.[6]*

4.1.1 Theory of Chiral Recognition

At a fundamental level, the chiral substrate selectively bound by a chiral host is the one capable of forming the energetically most stable diastereomeric host-guest complex, mediated by a complex interplay of non-covalent interactions. The first attempt to rationalise discrimination between enantiomers is the 'three-point attachment (TPA) model', proposed independently by Ogston[7] as well as Easson and Stedman[8] to explain enzyme-guest enantio-specificity, which states that the preferentially-bound guest enantiomer (labelled X in Figure 4.2A) can be attached to a host at three sites, while the opposite guest enantiomer (Y) cannot. Since then, it has been recognised that in addition to attractive supramolecular interactions (e.g. HB, π-π stacking), repulsive forces (e.g. electrostatics, steric hindrance) also play equally important roles in chiral recognition, resulting in a revision of the TPA model to that of 'three-point *interaction* (TPI)'.[9–11] However, Wilcox realised that these models inherently assume that the substrate is oriented in the same way,[12] as a rotation of the less preferentially-bound enantiomer Y in Figure 4.2A can potentially restore all the three interactions seen for X (illustrated in Figure 4.2B). This led to the proposal of the 'four location (FL)' model which contends that a fourth constraint is necessary[13,14]- in this case conformational rigidity holding both substrate enantiomers in the 'upright' orientation of Figure 4.2A for the TPI model to work. Nevertheless, both TPI and FL models only apply to tetrahedral substrates containing *one* point-chiral centre, and fails with those with multiple stereocentres. To address this, a 'stereocentre-recognition (SR)' model has been proposed recently, which states that a minimum of $N + 2$ interactions is necessary to achieve chiral selectivity for a linear substrate containing N stereocentres, with the interactions distributed across all chiral centres[‡].[15] This principle is illustrated in Figure 4.2C using an example containing two stereocentres,[16] and has been demonstrated to rationalise the selectivity of proteins such as adrenergic receptors,[17] inhibition of carboxypeptidase A[18] and phenylalanine ammonia-lyase[19,20] by substrates containing two chiral centres. Satisfactory models for rationalising selectivity for axial or planar chiral substrates have yet to be developed due to their structural diversity.

[‡] The TPI model (for substrates containing one chiral centre, i.e. $N = 1$) is a special case of the SR model, where a minimum of 3 interactions ($N + 2$) establishes chiral selectivity.

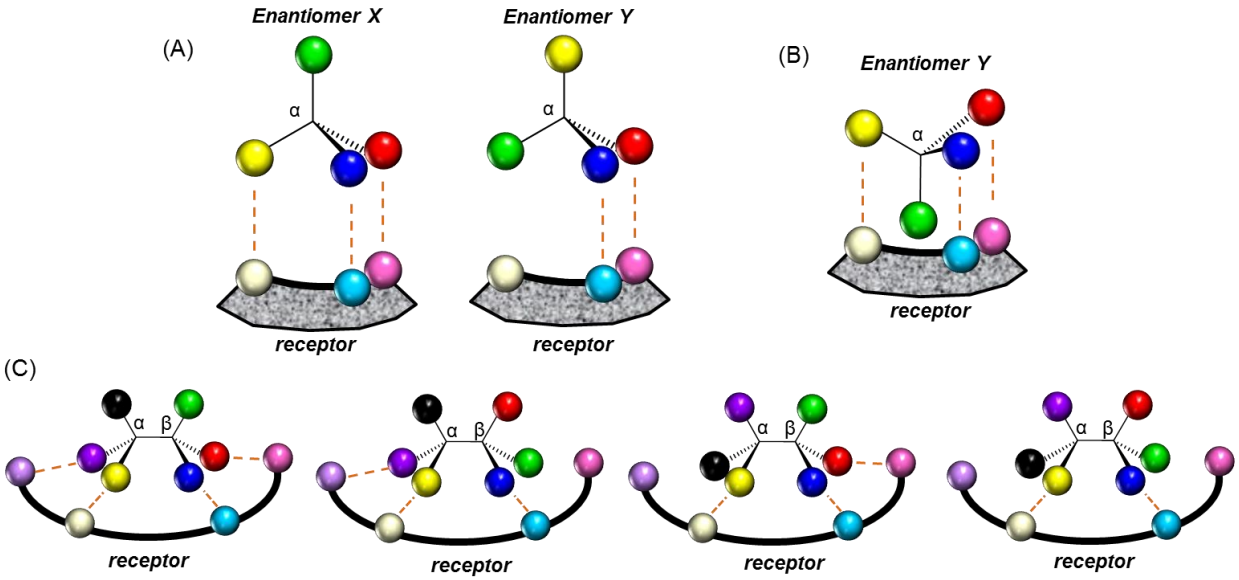


***Figure 4.2**. (A) Illustration of the TPA/ TPI model with two substrate enantiomers X and Y; (B) Re-establishment of the three interactions by re-orienting enantiomer Y in (A); (C) Illustration of the SR model using a linear substrate with N = 2 chiral centres, showing that a minimum of four (N + 2) interactions are necessary to achieve chiral selectivity amongst the four possible diastereomers.[16] Stereocentres on guest substrates are labelled with α and β.*

4.1.2 Enantiospecific Guest Binding in Nature

The ability to enantio-specificially bind to a chiral substrate is a cornerstone of natural biological processes ranging from metabolism to signal transduction, with different stereoisomers often eliciting contrasting biological responses.[21] To achieve enantio-specificity, substrates are encapsulated within a three dimensional highly-preorganised binding site with exquisite complementarity, with chirality imposed by the enantiopure amino acid residues present. This process can be illustrated with the enzyme isocitrate dehydrogenase (IDH), which selectively catalyses oxidative decarboxylation of trianionic (1*R*, 2*S*)-isocitrate to α-ketoglutarate in the presence of Mg^{2+}.[22,23] As seen from the crystal structure of the IDH complex with (1*R*, 2*S*)-isocitrate (Figure 4.3A), the substrate is held within an active site,[24] whose complementarity and rigidity is maintained by the protein's entire globular structure. At least seven HB interactions and Mg^{2+} coordination from the active site anchors two locations on each chiral centre of (1*R*, 2*S*)-isocitrate in place. On the other hand, the substrate diastereoisomer (1*S*, 2*S*)-isocitrate can only be held through three locations distributed in a (1,2) arrangement across both chiral centres (Figure 4.3B), which is energetically-significant enough for it to be discriminated against according to the SR model.[16] Similar principles

govern the chiral selectivity observed for other enzyme-substrate systems, often allowing selectivities in excess of 100-fold for specific substrate stereoisomers.[4,25–27]

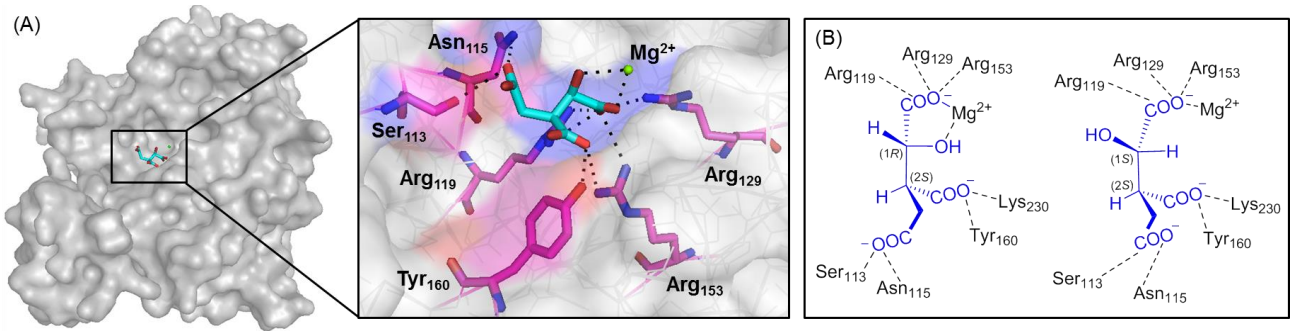


***Figure 4.3**. (A) Crystal structure of isocitrate dehydrogenase (IDH) with (1R, 2S)-isocitrate bound within its cavity and an expanded view showing the crucial HB interactions with the active site amino acid residues. Diagrams were generated from a crystal structure (PDB ID: 1CW7)[24]; (B) Schematic illustration of the interactions giving rise to preferential (1R, 2S)-isocitrate binding over (1S, 2S)-isocitrate.[16]*

4.1.3 Abiotic Chiral Receptors for Enantioselective Anion Binding and Sensing

Natural chiral biomolecules such as sugars and amino acids,[28] together with common axial-chiral motifs such as 1,1'-bi-2-naphthol (BINOL)[5] constitute an important and convenient class of starting materials from which abiotic chiral molecules are constructed. As seen in Section 1.2.4.2, acyclic receptors often elicit only modest enantio-selectivities. Thus, inspired by the need for constrained three dimensional chiral binding cavities for effective enantio-discrimination of chiral anions seen in natural enzymes, tripodal receptors, macrocycles and their strapped counterparts have been studied for their chiral discriminatory abilities. Using a tripodal receptor derived from cholic acid, Davis has demonstrated a 7-10 fold selective extraction of *N*-acetyl (*S*)-amino acids from aqueous buffer into chloroform compared to the (*R*)-enantiomers (Figure 4.4A).[29] Excellent selectivity for *N*Boc-(*S*)-glutamate was also seen for Kilburn's chiral bis-guanidinium macrocycles in DMSO/ H_2O 1:1 *v/v*, with K_S/K_D = 13 comparing only the first binding event (Figure 4.4B).[30] Other recently-reported macrocyclic chiral hosts include Anzenbacher's (*R*)-BINOL example used to determine enantiomeric excesses of chiral carboxylates,[31] and Zheng's tetraphenylethylene macrocycle capable of enantioselectively sensing chiral carboxylic acids by aggregation-induced emission.[32] To provide even more restricted cavities for enantiodiscrimination, Sessler *et. al.* constructed a

receptor comprising of a pair of sapphyrin dimers bridged by chiral 1,2-diamino cyclohexane linkers capable of showing a selectivity of K_R/ K_S = 4.3 for *N*-Cbz-glutamate in CH_2Cl_2/ CH_3OH 95:5 *v/v* (Figure 4.4C).[33] In another example, Lee and Sessler's calix[4]pyrrole receptor containing a strapped (*S*)-BINOL bridge displays selectivity (K_S/ K_R = 10) for 2-phenylbutyrate in CH_3CN, with chiral discrimination arising from the favourable π-stacking between the (*S*)-substrate enantiomer with the (*S*)-BINOL group (Figure 4.4D).[34]

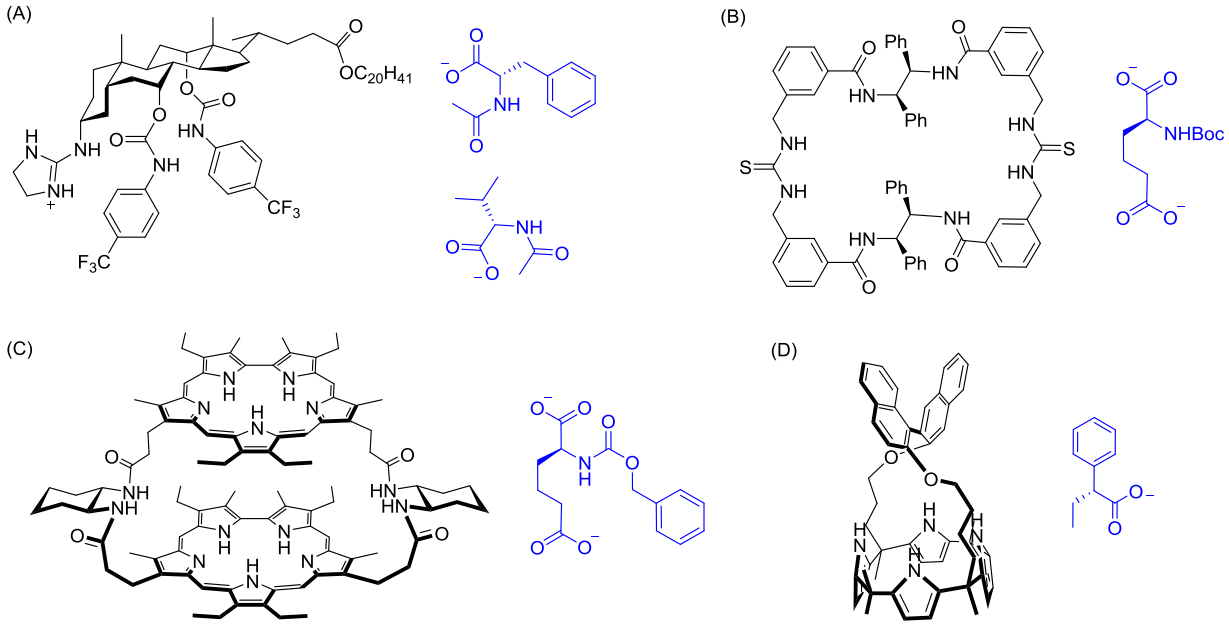


***Figure 4.4**. Examples of chiral receptors capable of three dimensional guest encapsulation: (A) Davis' tripodal receptor derived from cholic acid;[29] (B) Kilburn's bis-guanidinium macrocycle;[30] (C) Sessler's sapphyrin-dimer chiral receptor;[33] (D) Lee and Sessler's BINOL-strapped calix[4]arene receptor.[34] Substrates enantiomers which are preferentially bound are shown in blue beside the host molecules.*

4.1.4 Chiral Interlocked Structures

The most obvious form of chirality encountered for MIMs is covalent chirality, where point- or axial-chiral motifs are incorporated into the MIM framework[35–39] or stopper groups[40–42] (Figure 4.5A). However, due to the presence of their mechanical bond(s), MIMs offer new dimensions of chirality not accessible to their non-interlocked counterparts simply due to the spatial arrangement of their constituent components, even though these may not possess innate chiral units. For instance, rotaxanes comprising rotationally-asymmetric macrocycles and translationally-asymmetric axles exist as stereoisomers (Figure 4.5B).[43–46] Mechanically-

chiral catenanes, which possess rotationally-asymmetric macrocycles (Figure 4.5C), can also exhibit topological stereoisomerism, which is defined mathematically by a chiral molecular graph[47,48] and exist only if the enantiomers cannot be interconverted by structural deformation.[49] Since the first synthesis of a topologically-chiral singly-interlocked [2]catenane by Sauvage,[50] a range of other examples have been reported,[51–53] including a handcuff catenane[54] alongside doubly-interlocked [2]catenanes, otherwise known as Solomon rings.[55,56] Nevertheless, the study of these mechanically-chiral MIMs has been thwarted largely by formidable synthetic difficulties, which has only recently been partially overcome with HB templation,[57] aurophilic interactions[58] as well as active[46,59] and passive metal templation protocols- the latter being especially valuable due to the possibility of precise geometric control.[60,61] Although most examples are synthesised in racemic form and then subjected to enantio-resolution, recent advances by Goldup have allowed highly enantioselective synthesis of mechanically-chiral rotaxanes without the need for chiral separation by HPLC.[59]

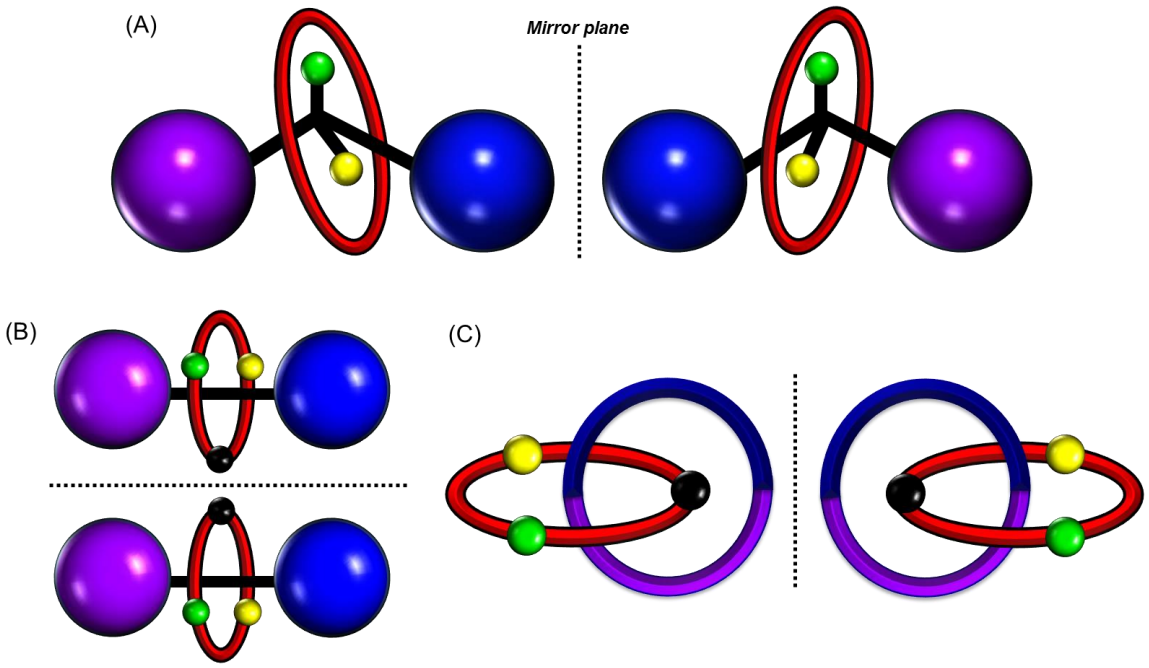


***Figure 4.5**. Different types of chirality possible with MIMs: (A) covalent-chirality and (B) mechanical-chirality of [2]rotaxanes and (C) [2]catenanes. Mechanical chirality can be achieved without any of the individual interlocked components bearing point, axial or planar chiral units. Dashed lines represent mirror planes.*[62]

The advances in synthetic methodologies are accompanied by an exploration of chiral MIMs for various applications. In nanotechnology, Leigh's peptide-synthesising ribosome-mimic polyrotaxane contains various (*S*)-amino acids incorporated into the structure (Section 1.3.3.3, Figure 1.48B).[39] In medicine, chiral rotaxanes have been used as carriers for intracellular drug delivery, such as Papot's paclitaxel-releasing example[63] and Leigh's rotaxane for met-enkephalin delivery (Section 1.3.3.2, Figure 1.47).[64] As detailed in Section 1.3.3.4, chiral rotaxanes can act as chiral ligands for transition metal-catalysed reactions,[65,66] or affect the stereochemical outcome of a reaction via rotaxane organocatalysis by 'through-space chirality transfer'.[67–69] In an interesting recent example, Leigh *et. al.* synthesised a point-chiral rotaxane containing an achiral macrocycle on one side of an achiral axle component, which was used as an organocatalyst to enhance the stereoselectivity of a Michael addition reaction (Figure 4.6).[70,71] Nevertheless, despite the rich chiral properties of catenanes, they have yet to find significant applications in these areas.

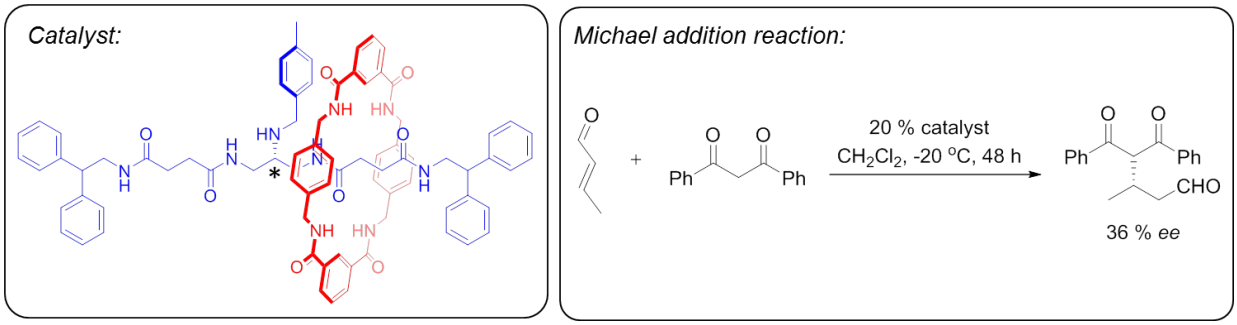


***Figure 4.6**. Leigh's point-chiral [2]rotaxane for asymmetric Michael addition organocatalysis.[70] The point-chiral centre in the rotaxane structure is marked with an asterisk (*).*

The applications of MIMs, particularly rotaxanes in asymmetric catalysis, suggests their potential for enantio-selective guest binding as well. However despite their highly-preorganised cavities capable of three dimensional guest encapsulation, chiral MIMs have scarcely been exploited for enantio-discrimination, with only two examples known at the time of writing. In an early preliminary study, Hiratani's mechanically-chiral [2]rotaxane (studied as a racemate) was found to distinguish between (*S*)- and (*R*)-phenylalaninol by fluorescence in $CDCl_3$, although the value of K_S/ K_R was not reported (Figure 4.7A).[72] Very recently, Niemeyer *et. al.* prepared a

chiral dianionic [2]catenane by Ca^{2+}-templation and studied the enantio-selective binding of cationic diamines by ^{1}H NMR titration experiments (Figure 4.7B).[73] Despite having two bulky (*S*)-BINOL motifs flanking the catenane binding cavity, only modest chiral selectivities were seen with K_S/ K_R = 1.4 - 1.6 in d_6-DMSO. Evidently, the study of MIMs as chiral receptors is still in its infancy, with much remaining to be understood.

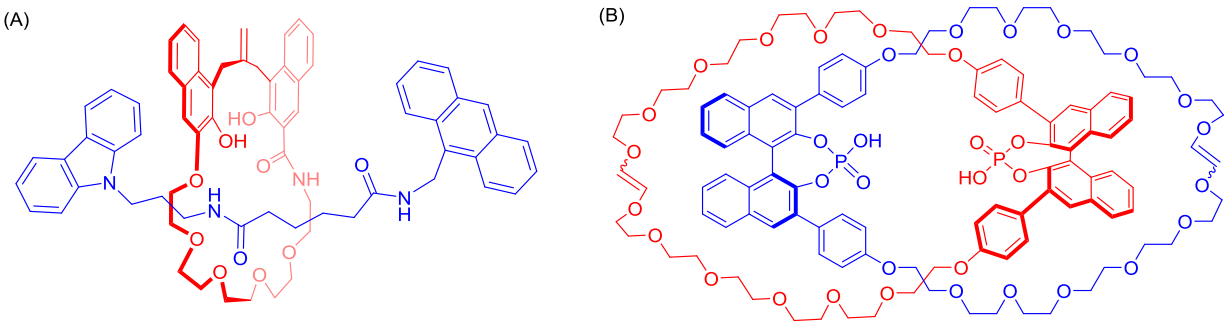


***Figure 4.7**. Examples of chiral MIMs used for enantio-selective guest binding: (A) Hiratani's [2]rotaxane for amino alcohols[72] and (B) Niemeyer's anionic [2]catenane for cationic chiral diamines.[73]*

4.1.5 Chapter Aims

This chapter investigates the unprecedented applications of σ-hole interactions such as XB and ChB, as tools for enantio-selective chiral anion recognition, envisaging that their stringent linear geometric requirements, steric bulk of the σ-hole-donor groups decorating the receptors' binding cavities, and their often enhanced anion affinities compared to ubiquitous HB chiral receptors can lead to augmentated chiral discrimination. Initial studies with a series of model acyclic (*S*)-BINOL-based XB chiral host molecules first identify the XB motif providing the optimal geometry for discrimination of chiral anions possessing one chiral centre/ axis. This XB motif is then incorporated into a macrocycle and subsequently, a family of novel cationic chiral XB [2]rotaxanes to study in detail the unique attributes of interlocked [2]rotaxane cavities for chiral selectivity. Recognising the natural and anthropogenic diversity of dicarboxylate anions, which include a range of stereoisomers and geometric isomers, the influence of XB, ChB and HB interactions on discriminating between them were then studied with model acyclic chiral receptors. Finally, a novel chiral XB [3]rotaxane was prepared and

investigated for its unprecedented ability to distinguish between dicarboxylate stereo- and geometric isomers. Figure 4.8 lists the range of chiral oxoanion guest species that are investigated in this chapter.[§]

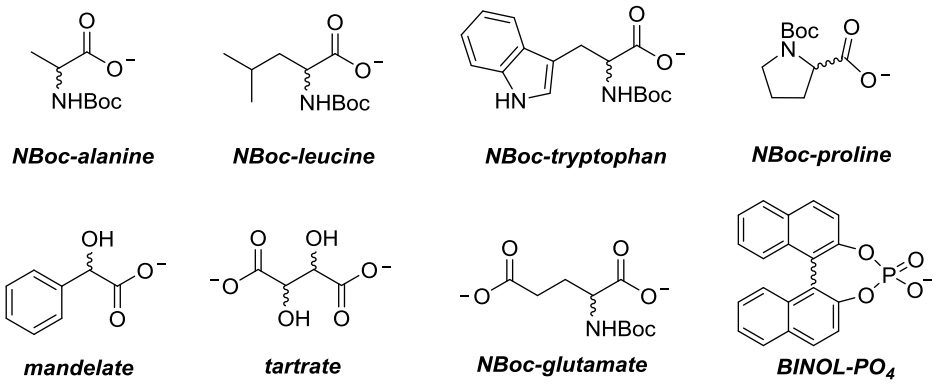


***Figure 4.8**. Structures of all chiral anions studied in this chapter. Structures are shown here as racemates.*

4.2 Acyclic (*S*)-BINOL-based Chiral Halogen Bonding Receptors[**]

4.2.1 Receptor Design and Syntheses

BINOL is an important member of the 1,1'-binaphthyl family of anthropogenic atropisomers, existing as axial-chiral stereoisomers due to hindered rotation about the bridging C-C bond between both naphthalene rings. Owing to their stable chiral configuration with good chemical tolerance,[75,76] commercial-availability of its enantiopure forms, established synthetic repertoire allowing functionalisation at various ring positions and favourable fluorescence properties, BINOL has found important applications in organic synthesis,[77,78] asymmetric catalysis,[79–81] molecular recognition and sensing[5,82–84] and materials science.[85,86] Three chiral XB motifs were designed containing the (*S*)-BINOL core and incorporated into acyclic model receptors **4.1I**, **4.2I** and **4.3I** (Figure 4.9) for XB-mediated chiral discrimination studies. To

[§] The TBA salts of the chiral anions are prepared according to a general literature procedure using TBAOH from their commercially-available neutral acids.[74]

[**] Some of the work described herein has been published: Lim, J. Y. C., Marques, I., Ferreira, L., Felix, V., Beer, P.D., *Enhancing the Enantioselective Recognition and Sensing of Chiral Anions by Halogen Bonding*, *Chem. Commun.*, 2016, **52**, 5527-5530.

identify the unique contributions of XB towards enantio-discrimination, the analogous HB receptor **4.1H** was also prepared for comparison.

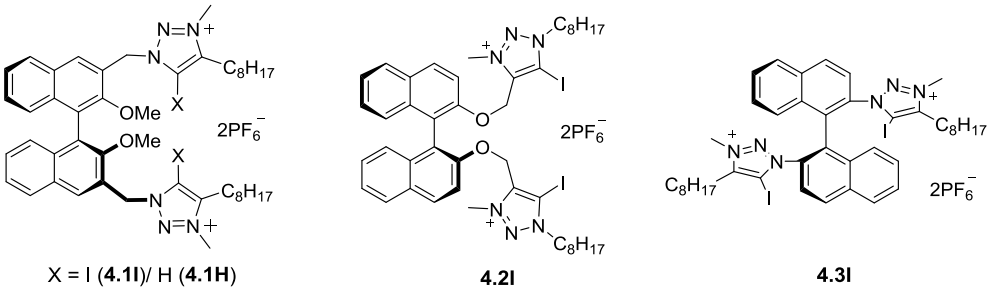


***Figure 4.9**. Structures of target (S)-BINOL receptors with different XB bite angles and anion binding geometries.*

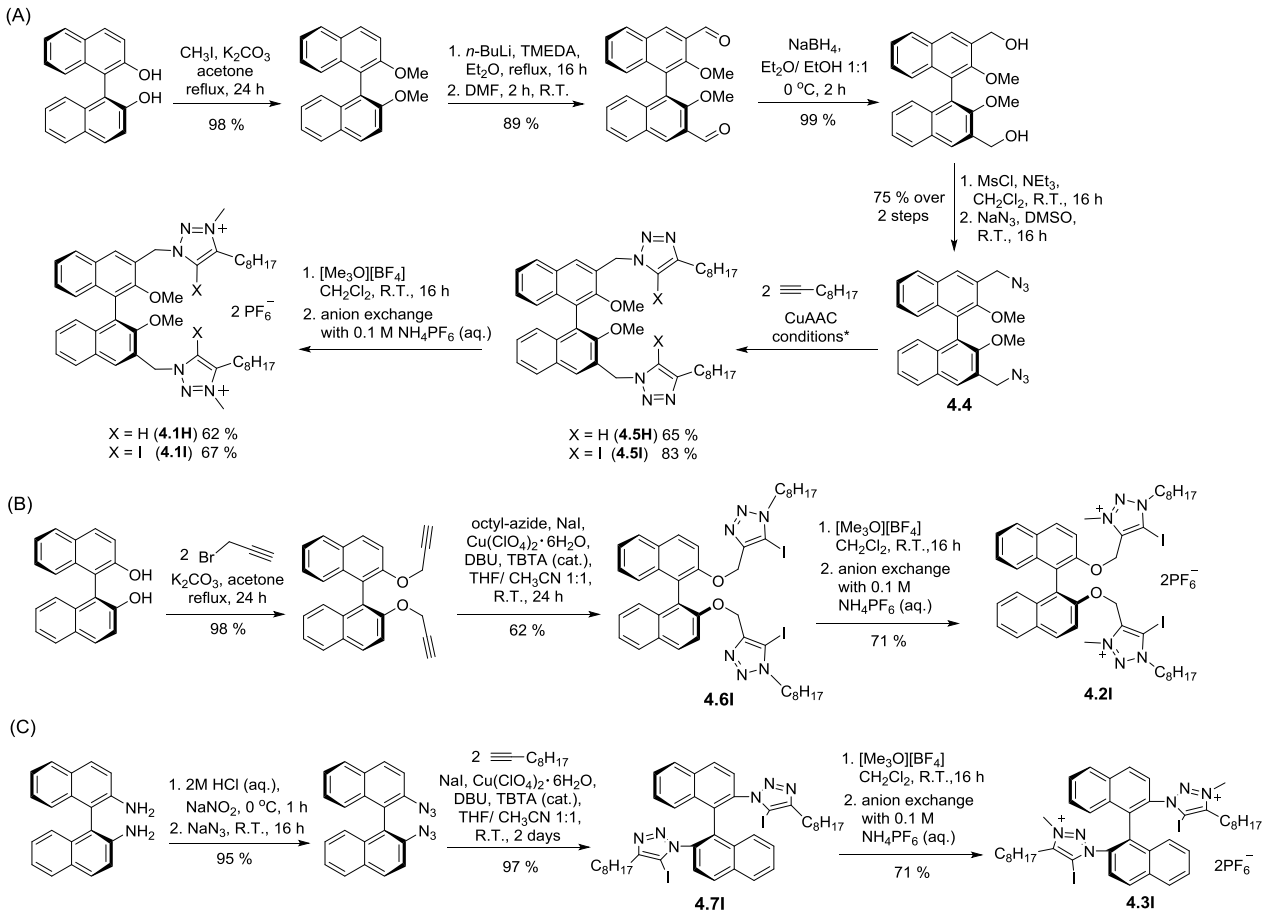
*Synthesis of (S)-BINOL 3,3'-substituted Receptors **4.1I/H***

Receptors **4.1I/H** were designed to contain a methylene spacer between the chiral (*S*)-BINOL core and the XB/HB-donor (iodo)triazolium groups, to permit some degree of conformational flexibility and allow bidentate coordination of chiral oxoanions in the space between them. Furthermore, 3,3'-functionalisation of BINOL also leaves the phenol groups at the 2,2'-positions available for either additional HB interactions with the chiral guests, or modification with other binding functionalities to provide more multi-point contacts for chiral discrimination.[73,87–91] For receptors **4.1I/H**, in order to only study the effects of XB on chiral discrimination without the additional HB binding influence, the 2,2'-phenol positions were methylated.[††]

To synthesise the target receptors, the 3,3'-substituted (*S*)-BINOL bis-azide synthon **4.4** was first prepared. As shown in Scheme 4.1A, commercially-available enantiopure (*S*)-BINOL was initially methoxy-protected using iodomethane, before selective 3,3'-functionalisation with formaldehyde groups was achieved by ortho-lithiation using *n*-BuLi and TMEDA, followed by quenching with DMF. The aldehyde units were reduced to the primary alcohols in near-quantitative yield,[92] then converted to the corresponding bis-azide **4.4** by mesylation and S_N2 substitution with NaN_3. Thereafter, CuAAC reactions between **4.4** and two

[††] Preliminary studies using ^{1}H NMR and fluorescence spectroscopic titrations demonstrated that in wet organic solvents, the highly basic chiral oxoanions could also deprotonate the acidic (unprotected) phenol units.

equivalents of 1-decyne afforded the neutral receptor precursors **4.5H/I**, which were doubly-methylated using trimethyloxonium tetrafluoroborate. Anion exchange of the resulting dicationic compounds using a PF_6-loaded Amberlite™ column afforded the receptors **4.1H/I** as their PF_6^- salts.



***Scheme 4.1**. Syntheses of dicationic receptors (A) **4.1I/H**, (B) **4.2I** and (C) **4.3I**. *Conditions for synthesis of **4.5H**: [Cu(CH3CN)4]PF6 (cat.), TBTA (cat.), DIPEA, CH2Cl2, R.T., 16 h; **4.5I**: NaI, Cu(ClO4)2·6H2O, DBU, TBTA (cat.), THF/ CH3CN 1:1 v/v, R.T., 16 h.*

*Synthesis of (S)-BINOL 2,2'-substituted Receptors **4.2I** and **4.3I***

Two variants of XB chiral receptors based on functionalisation of (*S*)-BINOL at the 2,2'-positions were prepared, possessing either flexible linkers between the iodotriazolium groups and the (*S*)-BINOL core (receptor **4.2I**) or having the iodotriazoliums directly attached to the naphthalene groups (receptor **4.3I**).

Scheme 4.1B describes the synthesis of receptor **4.2I**. Williamson ether synthesis between (*S*)-BINOL and two equivalents of propargyl bromide afforded the bis-alkyne synthon in excellent yields,[93] which was then converted directly to the bis-iodotriazole intermediate **4.6I** using octyl azide.[94] Bis-methylation of **4.6I** followed by anion exchange afforded receptor **4.2I** as its PF_6^- salt. To prepare receptor **4.3I** (Scheme 4.1C), commercially-available (*S*)-1,1′-binaphthyl-2,2′-diamine (BINAM) was first converted to its corresponding bis-azide by Sandmeyer-type substitution following reported procedures.[95] Iodo-CuAAC with 1-decyne using Zhu's procedure,[94] followed by bis-methylation and anion exchange similarly afforded the bis-PF_6^- salt of **4.3I**.

4.2.2 ^{1}H NMR Chiral Anion Recognition Studies

Identifying the Optimal XB Geometry for Chiral Selectivity

The chiral discriminatory abilities of receptors **4.1I**, **4.2I** and **4.3I** were determined via ^{1}H NMR titrations, where increasing quantities of TBA[*N*Boc-(*S*/*R*)-leucine carboxylate] were added to individual receptor solutions in CH_3CN/ H_2O 99:1 *v/v*. For comparing the enantioselectivities of each XB receptor, *N*Boc-leucine was chosen as the model guest species as its bulky isobutyl R group lacks any other functionalities capable of forming additional HB/ aromatic π-stacking interactions with the receptors, thus rendering XB-carboxylate interactions as the dominant factor governing enantioselectivity. The chiral selectivity (ξ) of each receptor was then determined by taking the ratio of the association constants arising from each individual anion enantiomer (i.e. K_S/ K_R), which is the definition used throughout the chapter.

Figure 4.10 shows the changes in the ^{1}H NMR spectra of each receptor in the presence of increasing quantities of *N*Boc-(*S*)-leucine carboxylate. For receptor **4.1I** (Figure 4.10A left), anion addition led to downfield shifts of its (*S*)-BINOL aromatic proton signal H_f, concomitant with only very small shifts of external proton resonances arising from H_b and H_c accompanied by a small *upfield* shift of the iodotriazolium methyl proton, suggesting that the oxoanion is held predominantly between the XB-donor iodotriazole groups and is not being bound on the receptor's periphery. Notably, the BINOL-OCH_3 protons (not shown) show a

slight upfield shift as well, suggesting that they were not participating in any significant HB interactions with the bound anion in close proximity. The initially slightly split diastereotopic protons H_a signals, initially appearing as a roofed doublet, also coalesce during the titration, suggesting that oxoanion binding likely leads to receptor conformational changes which rendered the diastereotopic environments more equivalent. Monitoring the shifts of H_f during the titrations show clear differences in the shape of the resulting binding isotherms for both anion enantiomers (Figure 4.10A right), clearly indicating that the chiral cavity of **4.1l** is able to distinguish between them.

For receptor **4.2l**, *N*Boc-leucine carboxylate binding results in distinct downfield shifts seen for H_f, while either small or negligible perturbations for the rest of the (*S*)-BINOL aromatic protons are observed (Figure 4.10B left). Unlike **4.1l**, the diastereotopic protons H_g of **4.2l** show downfield movement and increased splitting during the titration, suggesting further desymmetrisation of both proton environments. With receptor **4.3l** (Figure 4.10C left), chiral oxoanion binding resulted in dramatic *upfield* shifts of H_f, implying significant conformational changes of the receptor. Interestingly however, despite the XB binding site of **4.3l** being located closer to the (*S*)-BINOL group than **4.2l**, anion binding did not elicit notably greater perturbations of its aromatic protons. Curiously, the binding isotherms of H_f for both **4.2l** and **4.3l** show only marginal differences in the presence of both anion enantiomers (Figure 4.10B and C, right), suggesting poor enantio-discrimination. Anion association constants were determined by non-linear regression analyses of the titration data using the WinEQNMR2 software[96] for all receptor-anion enantiomer combinations by monitoring the shifts of H_f, and are collected in Table 4.1.

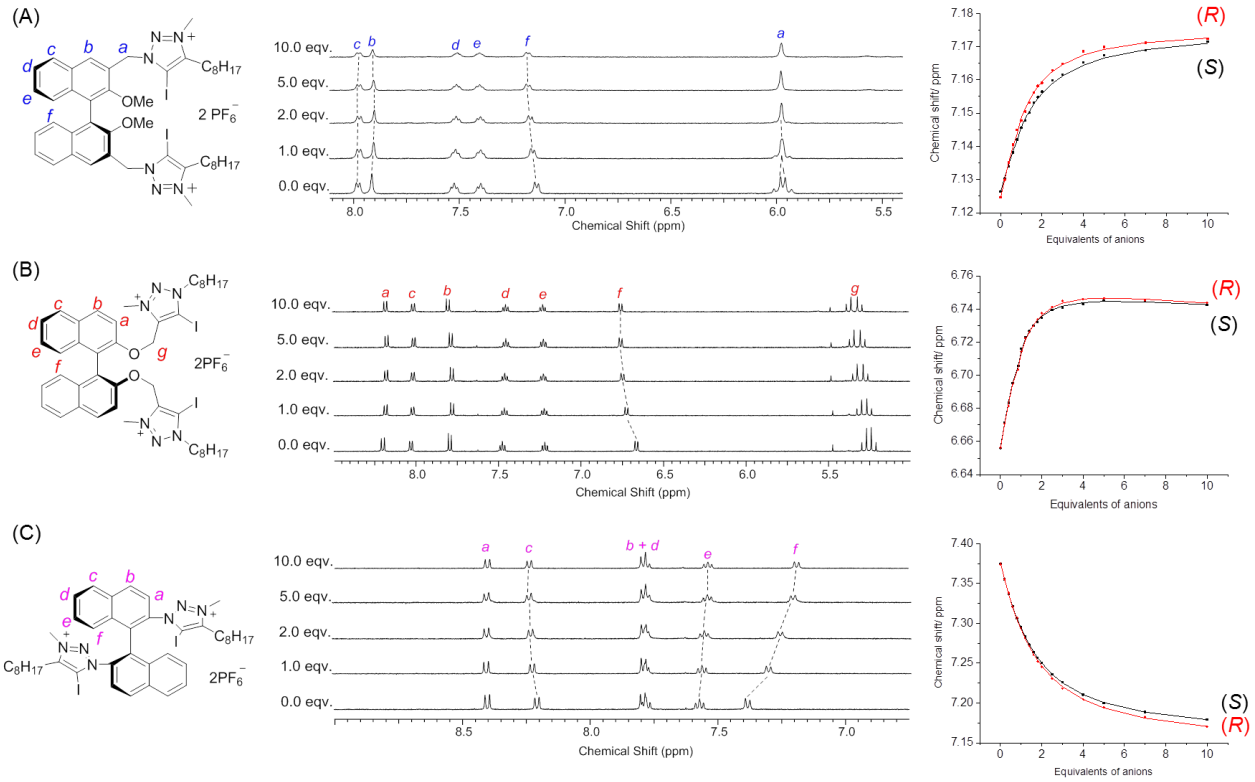


Figure 4.10. *Partial ^{1}H NMR spectra of receptors (A)* ***4.1l****, (B)* ***4.2l*** *and (C)* ***4.3l*** *in the presence of 0.0, 1.0, 2.0, 5.0 and 10.0 equivalents of NBoc-(S)-leucine carboxylate, as well as plots of chemical shifts of H_f as a function of increasing amounts of both (S) and (R)-NBoc-leucine carboxylate enantiomers ([host] = 1.5 mM, CD_3CN/ D_2O 99:1 v/v, T = 298 K).*

Table 4.1. Anion association constants (*K*/ M^{-1}) of acyclic XB receptors for both enantiomers of *N*Boc-leucine carboxylate and their enantioselectivities (ξ).[a]

	K_S	K_R	ξ
4.1l	680 (3)	1040 (60)	0.65 (0.04)
4.2l	K_{11} = 2308 (102) K_{12} = 18 (2)	K_{11} = 1964 (120) K_{12} = 25 (2)	1.18 (0.09) [b]
4.3l	613 (8)	585 (21)	1.05 (0.04)

[a] ξ = K_S/K_R; association constants calculated using WinEQNMR2[96] following a 1:1 host-guest binding stoichiometries for all cases except for receptor **4.2l**, in which a 1:2 model was used. Receptor (*S*)-BINOL aromatic proton H_f was monitored in all cases; all anions added as their TBA salts; errors (±) in parentheses ([host] = 1.5 mM, CD_3CN/ D_2O 99:1 *v/v*, *T* = 298 K). [b] K_S / K_R determined only for the first binding event (K_{11}).

From Table 4.1, receptors **4.1l** and **4.3l** were found to bind the chiral oxoanions with a predominantly 1:1 host-guest stoichiometry, while **4.2l** showed a detectable second binding event. However, only the first association constants for **4.2l** (K_{11}) were considered for chiral selectivity determination, as only the first anion was tightly bound by the receptor and hence influenced by its chiral binding domain. Amongst the three XB chiral motifs, that of receptor

4.1I exhibited the best anion enantio-discriminatory behaviour, giving an approximately 1.5-fold preference for *N*Boc-(*R*)-leucine carboxylate compared to its (*S*)-enantiomer. Surprisingly, receptor **4.3I**, despite the XB binding site being closest in proximity to the (*S*)-BINOL motif, barely showed any selectivity with only a small preference seen for *N*Boc-(*S*)-leucine carboxylate. It is curious nonetheless that the receptors did not show a consistent preference for a particular guest enantiomer, with **4.2I** and **4.3I** showing opposite stereo-preferences compared with **4.1I**. While the reason for this trend cannot be definitively ascertained, the different iodotriazolium substitution positions of **4.1I** compared to **4.2I** and **4.3I** may potentially play a role.

Comparing the anion affinities of all three receptors reveal that their association constants decrease in the order **4.2I** > **4.1I** > **4.3I** (Table 4.1), correlating to the increased spatial distance between the XB anion binding site and the bulky (*S*)-BINOL receptor motif. This suggests that steric interactions were exerting a large influence in determining the interactions of the chiral oxoanions and the host. For receptor **4.2I**, although strong receptor-anion interactions were observed minimally-encumbered by sterics, the large spatial separation between the bound anions from the receptor's (*S*)-BINOL unit reduce the influence of its chiral field for enantio-discrimination. On the other hand, the considerable steric constraints of the receptor **4.3I** binding site, coupled with the bulky XB-donor iodine atoms, may prevent the chiral oxoanions from approaching close enough or properly oriented for appreciable chiral discrimination to take place. It appears that receptor **4.1I**, having the XB binding site positioned some distance away from the (*S*)-BINOL chiral unit, yet conformationally-flexible enough for bidentate anion coordination by both iodotriazolium units, offers the most optimal combination for stereo-discrimination of the chiral anions (see Section 4.2.4).

Comparison between XB and HB Interactions for Enantio-discrimination

Having determined that the XB binding motif in receptor **4.1I** allows appreciable chiral anion discrimination, analogous ^{1}H NMR titration studies were performed on its HB receptor analogue **4.1H** in the same solvent mixture. A wider range of chiral anion pairs were

investigated, including amino acid-derivatives *N*Boc-alanine and *N*Boc-tryptophan carboxylates as well as axial-chiral BINOL-PO_4^-, to also study the influences of guest steric bulk on XB-mediated chiral discrimination.

A comparison of the ^{1}H NMR proton resonance perturbations of receptors **4.1I** and **4.1H** in the presence of *N*Boc-(*S*)-leucine carboxylate shows that the replacement of XB-donor iodines with hydrogen atoms in the latter gave different host-guest receptor interactions. As shown in Figure 4.11A, oxoanion addition to receptor **4.1H** led to large downfield shifts of its triazolium aromatic protons, accompanied by smaller shifts of aromatic proton H_b in the same direction. Contrastingly, H_b showed small *upfield* shifts for receptor **4.1I**. Furthermore, the H_f resonances showed negligible perturbations for **4.1H**, while a modest downfield shift was observed for **4.1I**. The same differences were also observed for the spectra of **4.1H** and **4.1I** with the other chiral oxoanion pairs, confirming that the XB interactions of **4.1I** were able to influence the host-guest interactions geometrically and electronically. Notably, comparing the binding isotherms arising from H_f for **4.1I** and triazolium aromatic protons for **4.1H** with the various chiral oxoanion pairs show much larger variations between each set of guest enantiomers for **4.1I** compared to **4.1H**, suggesting an enhanced ability of the former to discriminate between them. A quantitative comparison of the host-guest 1:1 stoichiometric anion association constants for each chiral oxoanion and the magnitudes of stereo-selectivity are collected in Table 4.2.

Receptors **4.1I** and **4.1H** show numerous differences which highlight the influences of XB on chiral discrimination (Table 4.2). Firstly, **4.1I** exhibited greatly enhanced anion affinities compared with **4.1H**, with more than an order of magnitude increase in association constant values observed in all cases. More importantly, compared with **4.1H**, the presence of the XB donor groups on **4.1I** led to significantly improved enantioselectivity of all chiral anions with the exception of *N*Boc-alanine carboxylate. For the amino acid-derivatives, bulkier R groups result in better stereoselectivity with **4.1I**, improving in the order *N*Boc-alanine < *N*Boc-leucine < *N*Boc-tryptophan. Interestingly, a reversal of the enantiomer preference was seen for *N*Boc-tryptophan (*S*-selectivity) compared with the other two amino acids (*R*-selectivity). Slightly reduced chiral discrimination was seen for BINOL-PO_4^-, with the *S*-enantiomer preferentially

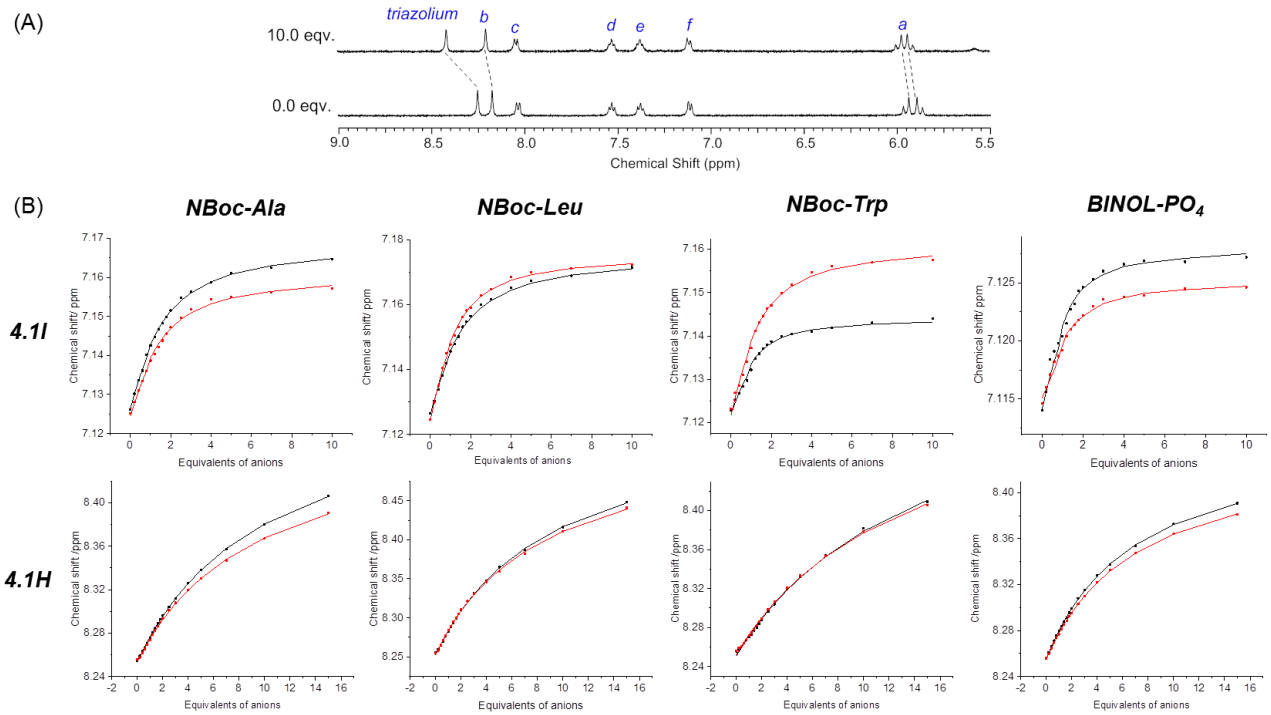


***Figure 4.11**. (A) Partial ^{1}H NMR spectra of receptor **4.1H** in the presence of 0.0 and 10.0 equivalents of NBoc-(S)-leucine carboxylate. Proton assignments follow those in Figure 4.10A.; (B) Binding isotherms obtained from monitoring the shifts of H_f for **4.1I** and triazolium proton for **4.1H** as a function of increasing quantities of chiral anions ([host] = 1.5 mM, CD_3CN/ D_2O 99:1 v/v, T = 298 K). Binding isotherms for the (S)-enantiomers are shown in black while those for the (R)-enantiomers are shown in red.*

Table 4.2. Anion association constants (K/ M^{-1}) of receptors **4.1I** and **4.1H** towards both (S)- and (R)-oxoanion enantiomers and their enantioselectivities (ξ).[a]

	*Receptor **4.1I***			*Receptor **4.1H***		
	K_S	K_R	ξ	K_S	K_R	ξ
*N*Boc-Ala	620 (25)	727 (56)	0.85 (0.07)	58 (1)	63 (2)	0.92 (0.03)
*N*Boc-Leu	680 (3)	1040 (60)	0.65 (0.04)	68 (3)	74 (4)	0.92 (0.06)
*N*Boc-Trp	1661 (72)	990 (82)	1.7 (0.2)	34 (3)	37 (3)	0.9 (0.1)
BINOL-PO_4	1394 (115)	924 (67)	1.5 (0.2)	92 (2)	89 (2)	1.03 (0.03)

[a] ξ = K_S/K_R; 1:1 association constants calculated using WinEQNMR2[96], monitoring H_f for **4.1I** and the triazolium aromatic proton for **4.1H**; all anions added as their TBA salts; errors (±) in parentheses ([host] = 1.5 mM, CD_3CN/ D_2O 99:1 *v/v*, *T* = 298 K).

bound (see Section 4.2.4 for computational modelling experiments to rationalise these trends). In stark contrast, the HB analogue **4.1H** showed minimal discrimination of the chiral anion pairs investigated, with the magnitude of selectivity (ξ) surprisingly independent of the guest anion's steric bulk. This may be a consequence of their weak association, preventing the chiral oxoanions from interacting strongly enough with **4.1H** for effective chiral discrimination.

4.2.3 Redox Discrimination of Chiral Anions

The ability to stereo-selectively sense chiral guest species electrochemically is highly sought-after for its sensitivity and the possibility of device fabrication by immobilising receptors on surfaces.[97] Numerous redox-active chiral receptors have been prepared for this purpose, including Canary's Cu(II)-tripodal receptor[98] and Kim's azophenolic crown ethers for chiral amines,[99] as well as Tucker's ferrocene boronic acid receptor for sensing enantiomeric excess of BINOL.[100] Redox chiral anion sensing has thus far been mainly limited to the efforts of Tucker and co-workers with a family of chiral ferrocene-appended urea receptors bearing either point- or planar-chirality (Figure 4.12).[101,102] However, while notable cathodic shifts ($\Delta E_{1/2}$) of their redox potentials were seen in the presence of amino acid derivatives, different anion enantiomers only elicited very small differences in $\Delta E_{1/2}$ for all acyclic ferrocene chiral hosts studied.

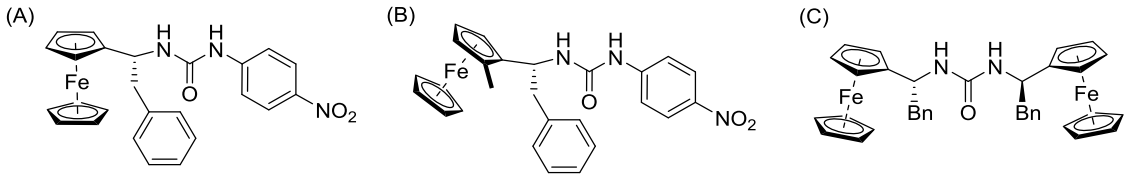
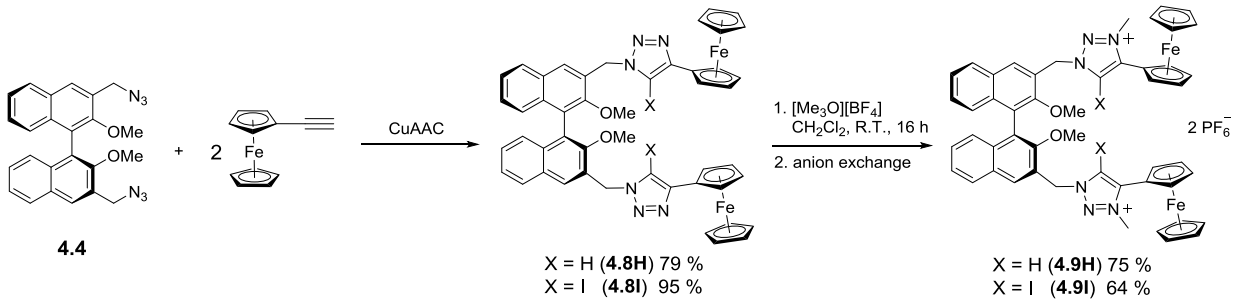


***Figure 4.12**. Examples of redox-active chiral receptors by Tucker possessing (A) one point-chiral centre[101]; (B) one point-chiral centre and planar chirality, as well as (C) two point-chiral centres.[102]*

Encouraged by the XB-mediated enhancement in enantio-selectivity exhibited by **4.1I** compared with **4.1H**, it was envisaged that XB groups incorporated into a chiral ferrocene-appended receptor could enhance the redox discrimination of chiral anion enantiomers. Thus, chiral receptors **4.9I/H** were prepared where the octyl termini of **4.1I/H** were replaced with ferrocene units and synthesised in an analogous fashion. As shown in Scheme 4.2, 'proto'- and 'iodo'-CuAAC reactions between bis-azide synthon **4.4** and two equivalents of ethynylferrocene gave the neutral host precursors, which upon methylation and anion exchange using a PF_6^--loaded Amberlite column afforded the $2PF_6^-$ salts of **4.9H/I**.



***Scheme 4.2**. Synthesis of ferrocene-appended chiral receptors **4.9I/H**. CuAAC conditions are identical to those shown in Scheme 4.1.*

The enantio-discriminatory behaviour of **4.9I** was first determined using ^{1}H NMR titration experiments with *N*Boc-(*S*/*R*)-leucine carboxylate using identical conditions as that for **4.1I**. From the partial ^{1}H NMR spectra of **4.9I** (Figure 4.13A), the addition of *N*Boc-(*S*)-leucine elicited largely similar changes in the proton signals as **4.1I**. Furthermore, downfield perturbation of the ferrocene aromatic resonance H_h was also seen, likely due to direct electronic conjugation with the adjacent iodotriazoliums and indicating electronic communication between the binding site and redox reporter group. Similarly, the H_f binding isotherms for both anion enantiomers supports the enantio-discriminatory ability of the **4.9I** chiral binding site (Figure 4.13B). WinEQNMR2[96] determination of host-guest 1:1 stoichiometric association constants, monitoring H_f, revealed the *S* and *R* anion enantiomers bound with K_a values of (803 ± 3) and (1141 ± 64) M^{-1} respectively, giving identical enantioselectivity (K_S/ K_R = 0.70 ± 0.04) as **4.1I**. This also shows that the termini groups of the receptor, regardless of their rigidity (ferrocene for **4.9I**) or conformational flexibility (octyl chains for **4.1I**), influenced the receptors' enantioselectivity negligibly.

The ability of receptors **4.9I** and **4.9H** to distinguish anion enantiomers electrochemically was then studied using square wave voltammetry (SWV) in a standard three-electrode cell with 0.1 M $TBAPF_6$ electrolyte solution in acetonitrile using a Ag/ $AgNO_3$ reference electrode,[103] glassy carbon working electrode and Pt wire auxiliary electrode. Surprisingly, while receptor **4.9I** showed redox quasi-reversibility of its ferrocene/ferrocenium redox couple ($E_{1/2}$ = +0.425 mV), poor reversibility was found for **4.9H** which prevented anion

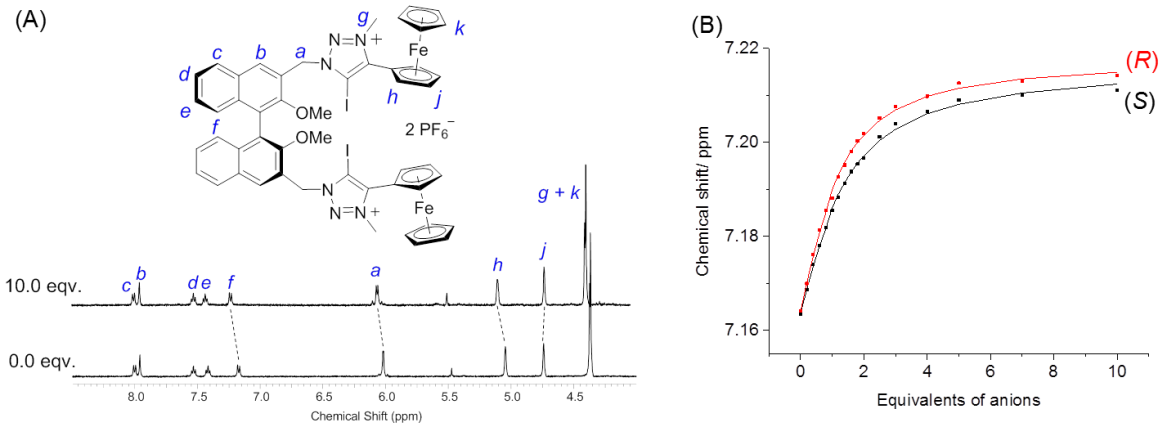


***Figure 4.13**. (A) Partial ^{1}H NMR spectra of receptor **4.9I** in the presence of 0.0 and 10.0 equivalents of NBoc-(S)-leucine carboxylate; (B) Changes in the chemical shifts of H_f as a function of increasing quantities of both enantiomers of NBoc-leucine ([**4.9I**] = 1.5 mM, CD_3CN/ D_2O 99:1 v/v, T = 298 K).*

sensing experiments from being performed (Figure 4.14 and Appendix B)[‡‡]. In the presence of various anion enantiomers (Table 4.3), significant $E_{1/2}$ cathodic perturbations were seen for **4.9I**, which also showed some loss of redox reversibility (Figure 4.15).[§§] Nevertheless, it is noteworthy that the stronger binding enantiomer (Table 4.2) elicited the larger magnitude of cathodic shift due to its greater ability to stabilise the ferrocenium oxidation state. The values of ΔE_S/ ΔE_R obtained were also found to be in good agreement with K_S/ K_R within experimental error.

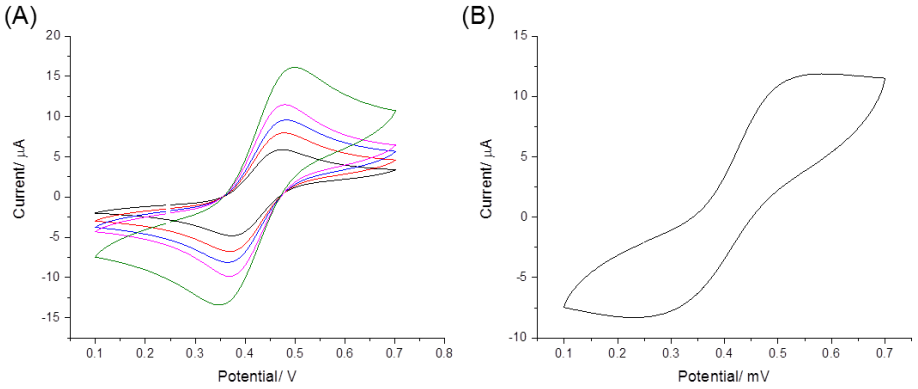


***Figure 4.14**. Electrochemical reversibility studies: CVs recorded at scan rates of (A) 25, 50, 75, 100 and 250 mV s^{-1} for receptor **4.9I** and (B) 250 mV s^{-1} for **4.9H** ([**4.9I**/ **H**] = 0.5 mM, electrolyte: 0.1 M $TBAPF_6$ in CH_3CN, T = 293 K).*

[‡‡] Other than the poorly-defined CV shown in Figure 4.14, the $E_{1/2}$ values of **4.1H**'s ferrocene-ferrocenium redox couple were found to fluctuate significantly with repeated CV scans at different scan rates.

[§§] Due to the possibility of electrochemical oxidation of the indole unit of the *N*Boc-tryptophan carboxylates, no reliable electrochemical data could be obtained for these anion enantiomers.

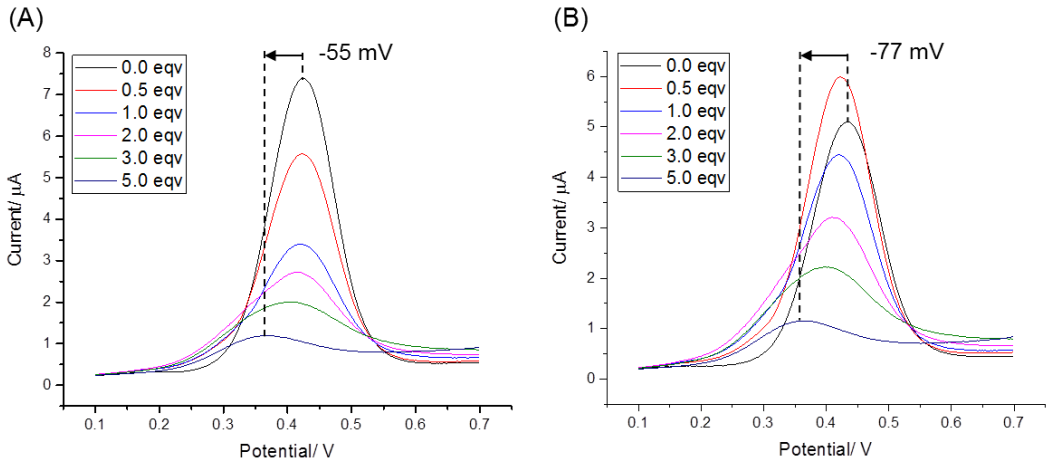


***Figure 4.15**. SWVs of receptor **4.9l** in the presence of 0.0, 0.5, 1.0, 2.0, 3.0 and 5.0 equivalents of (A) NBoc-(S)-leucine and (B) NBoc-(R)-leucine ([**4.9l**] = 0.5 mM, electrolyte: 0.1 M $TBAPF_6$ in CH_3CN, T = 293 K). Cathodic shifts with 5.0 equivalents of added anion are indicated.*

Table 4.3. Cathodic shifts of the ferrocene/ ferrocenium redox couples (ΔE/ mV) of **4.9l** in the presence of 5.0 equivalents of chiral anions.[a]

	ΔE_S	ΔE_R	ΔE_S / ΔE_R [b]
*N*Boc-Ala	-57	-63	0.9 (0.1)
*N*Boc-Leu	-55	-77	0.71 (0.08)
BINOL-PO_4	-55	-38	1.5 (0.2)

[a] Anions added as TBA salts; glassy carbon electrode, Pt wire auxiliary electrode and Ag/ $AgNO_3$ reference electrode, electrolyte: 0.1 M $TBAPF_6$ in acetonitrile ([**4.9l**] = 0.5 mM, T = 293 K). [b] Errors of ΔE_S /ΔE_R calculated based on estimated measurement errors of ± 5 mV for ΔE values.

4.2.4 Computational Modelling Studies

To obtain further insights on the enhanced chiral discrimination conferred by XB interactions, DFT calculations and molecular mechanics (MD) simulations were performed by Dr Igor Marques and Professor Vítor Felíx at the University of Aveiro, Portugal. Optimisation of the diastereomeric host-guest complexes with receptors **4.1l/H** and the chiral anions listed in Table 4.2 were performed by DFT calculations using the B3LYP functional, with the σ-holes on each iodine described by a positively-charged extra point.[104] Solvent effects were taken into account through the Polarizable Continuum Model (PCM), using the integral equation formalism variant (IEFPCM),[105] allowing determination of the XB parameters (bond lengths and angles) in gas phase or acetonitrile/ water mixtures (computational details in Appendix C).

The distribution of the electrostatic potentials (V_S) of the free uncomplexed chiral receptors were calculated using the M06-2X functional and mapped onto their electron density surfaces. As shown in Figure 4.16, the most positive $V_{S,max}$ values of 612 and 606 kJ mol^{-1} were found in front of each C-I unit for **4.1I** (in black), corresponding to the location of the σ-holes, while the electropositive regions (in red) are highly localised in their vicinity. Contrastingly, although the $V_{S,max}$ values computed for **4.1H** (638 and 616 kJ mol^{-1}) were also close to the HB-donor prototriazolium protons, the regions of positive V_S were more broadly distributed across the receptor's binding cleft. Furthermore, the C-I···O$_{anion}$ XB bond angles from **4.1I** were found to deviate only slightly from linearity while those of HB show a larger spread (Figure 4.17). Taken together, the combination of more localised electrophilic anion binding sites and the more stringent directionality of XB interactions compared with HB places tighter geometric and spatial restrictions on the number of possible anion binding modes with **4.1I**.

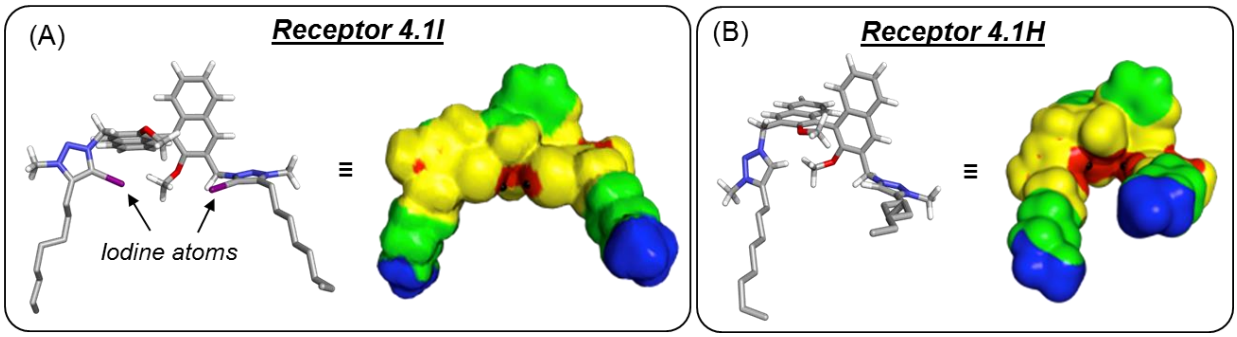


***Figure 4.16**. Distribution of the electrostatic potential onto the electron density surface (0.001 electrons per Bohr^3) of (A) **4.1I** and (B) **4.1H**. More electropositive potentials are shown in warmer colours, with red representing V_S > 526 kJ mol^{-1}. The most positive values of each binding unit, $V_{S,max}$, are identified by black dots in front of the iodine atoms for **4.1I** and hydrogen atoms for **4.1H**.*

The degree of covalency of the interactions between the anions and **4.1I/H** were assessed using Wiberg Bond Indices[106] determined from the DFT-optimised host-guest complexes. Those for the XB interactions range between 0.074 and 0.173, while much lower values were found for the HB interactions between 0.014 and 0.042. This enhanced XB-anion covalent character may partially account for the greatly augmented anion affinities seen for **4.1I** compared to **4.1H** (Table 4.2), thus corroborating earlier findings.[107]

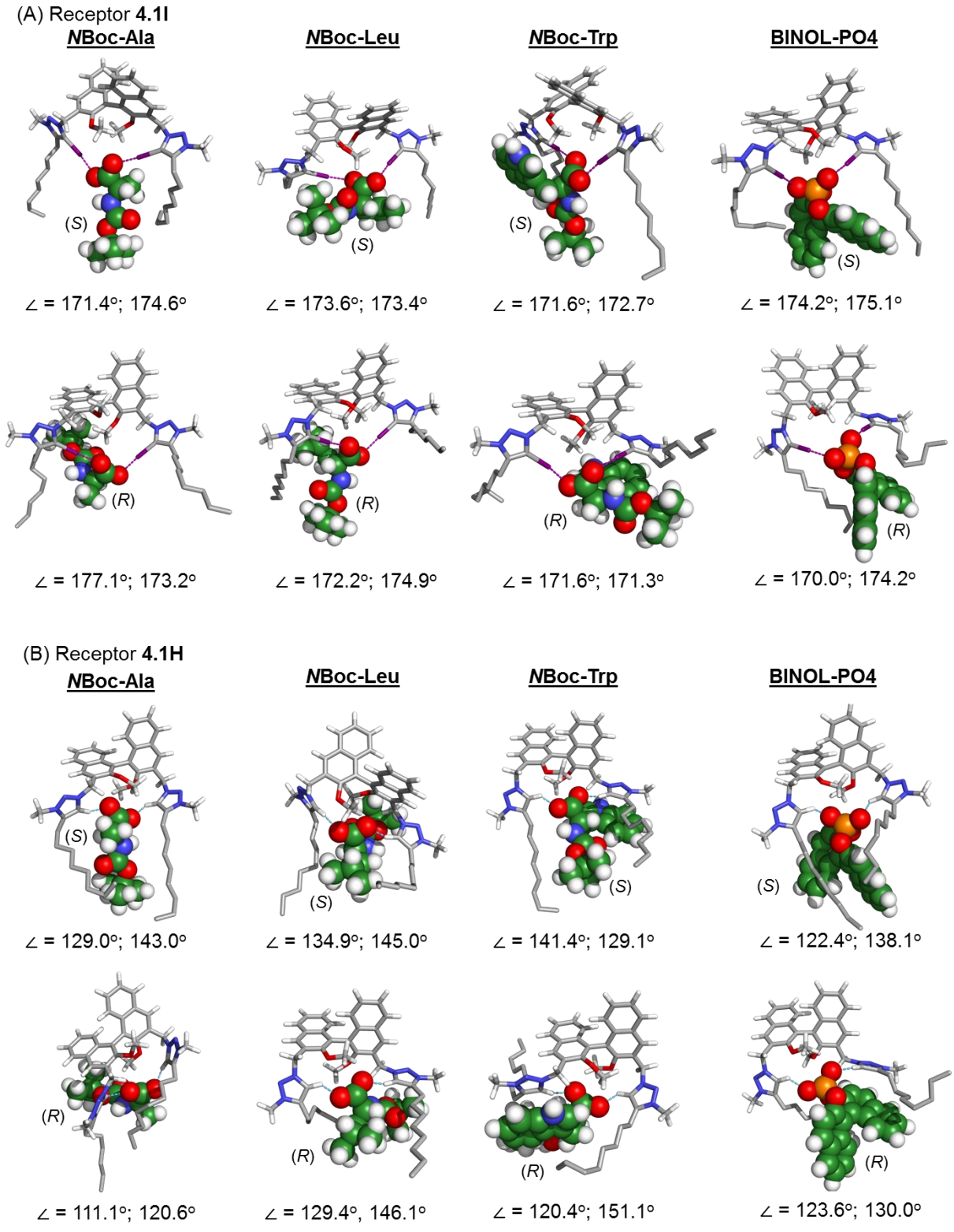


***Figure 4.17**. Optimised DFT structures of the diastereomeric host-guest complexes between the chiral anions and (A) **4.1I** or (B) **4.1H**. XB and HB interactions are shown as purple and blue dashed lines respectively. For each receptor, the complexes formed with the (S) and (R)-anion enantiomers are shown in the top and bottom rows respectively. The C-X···O_{anion} bond angles (X = I/H) are indicated below each structure.*

The stereo-discriminatory behaviour of each receptor towards the anion enantiomers were then studied computationally using Molecular Dynamics (MD) simulations with the AMBER14 suite[108] using the General Amber Force Field (GAFF) parameters[109,110] for **4.1I/H** and all enantiopure chiral anions. The optimised host-guest complexes were immersed in periodic cubic boxes composed of 1426 CH_3CN and 42 H_2O molecules (CH_3CN/ H_2O 99:1 *v/v*) with two PF_6^- and one TBA counter-ions, and their dynamic behaviour were determined from three independent MD runs of 100 ns each (details in Appendix C). Throughout these simulations, **4.1I** was able to maintain two convergent and highly-directional XB interactions with the chiral anions. However, these were subjected to sporadic interruptions from aqueous solvation of **4.1I**'s binding site and the chiral anions, arising from water molecules establishing HB (HO–H···I) and XB interactions (C-I···OH_2) with the iodine atoms of the former and hydration of the anions' oxygen atoms (*via* HO–H···O_{anion} hydrogen bonds). Contrastingly, the MD simulations with **4.1H** resulted in water-assisted host-guest decomplexation, consistent with the weak anion affinities observed in Table 4.2, and likely accounting for the lack of significant enantio-selectivity seen. Notably, along several simulation durations of the complexes between the *N*Boc-tryptophan enantiomers and **4.1I**, sporadic donor-acceptor π–π stacking interactions were observed when the triazolium ring of **4.1I** adopts parallel dispositions with the guest anion's indole ring. This additional geometry-restraining supramolecular interaction may account for the slightly superior enantio-discrimination seen for *N*Boc-tryptophan compared with the other anion pairs studied.

The degree of enantioselectivity of **4.1I** towards the chiral anion enantiomers may be estimated using the parameter ($\Delta\Delta E_{bind(S,R)}$), defined according to the following equation:

$$\Delta\Delta E_{bind(S,R)} = \langle E \rangle_{complex,S} - \langle E \rangle_{complex,R}$$

where $\langle E \rangle_{complex,X}$ represents the average molecular mechanics (MM) energy of the solvated diastereoisomeric complexes, directly obtained from the MD simulations undertaken with equal number of molecules using the isothermal-isobaric (NPT) ensemble. This energy difference corresponds to the binding enthalpy of the anion enantiomers to **4.1I** and also takes into account the interactions of the host-guest complexes with solvent molecules. When the calculated $\Delta\Delta E_{bind(S,R)}$ energy differences were plotted as a function of the empirical K_S/K_R

ratios in Table 4.2, excellent linear correlation (R^2 = 0.99) was obtained (Figure 4.18). Moreover, $\Delta\Delta E_{bind(S,R)}$ is also consistent with the difference in enantiomer preference seen for *N*Boc-tryptophan carboxylate and BINOL-PO_4^- over the other two chiral anion pairs studied.

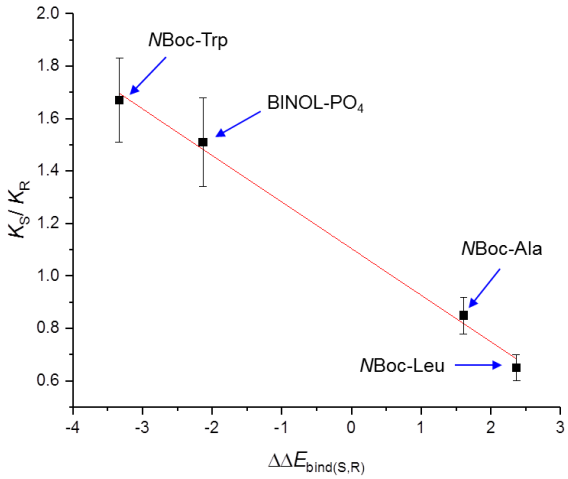


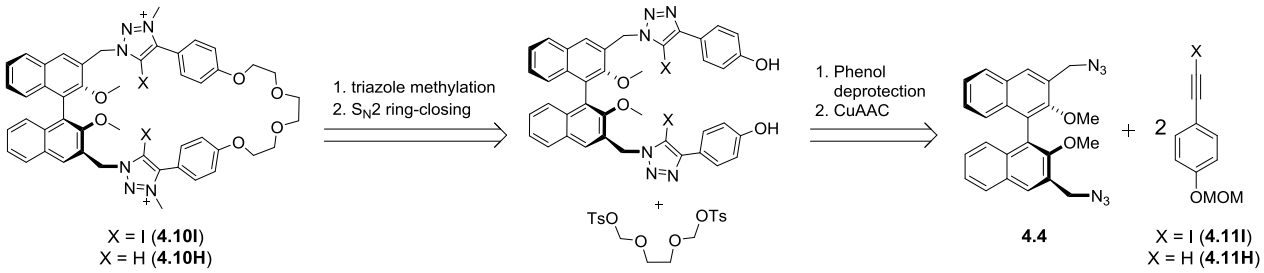
***Figure 4.18**. Plot of the empirical K_S/K_R of each chiral anion pair with XB receptor **4.1l** against the computed values of $\Delta\Delta E_{bind(S, R)}$.*

In summary, the computational modelling results suggested that the enhanced chiral selectivity seen for **4.1l** over its HB analogue likely arises from the geometry-restricting combination of more localised electrophilic sites in the binding cleft of **4.1l** and greater XB-anion linearity. This prevents the chiral guest anions from freely adopting binding conformations which may compromise enantioselectivity but minimise steric repulsions. The findings also support the SR/ TPI binding models of chiral discrimination (Section 4.1.1), where at least three interactions (one from each XB donor, stereochemically-dependent steric interactions with the receptor (*S*)-BINOL unit and additional non-covalent interactions such as π–π stacking) govern chiral selectivity of the anion enantiomers by **4.1l**. The subtle energetic contributions arising from these factors, together with host-guest hydration also account for the enantiomer binding preferences.

4.3 Chiral Macrocycles and [2]Rotaxanes for Enantioselective Anion Binding

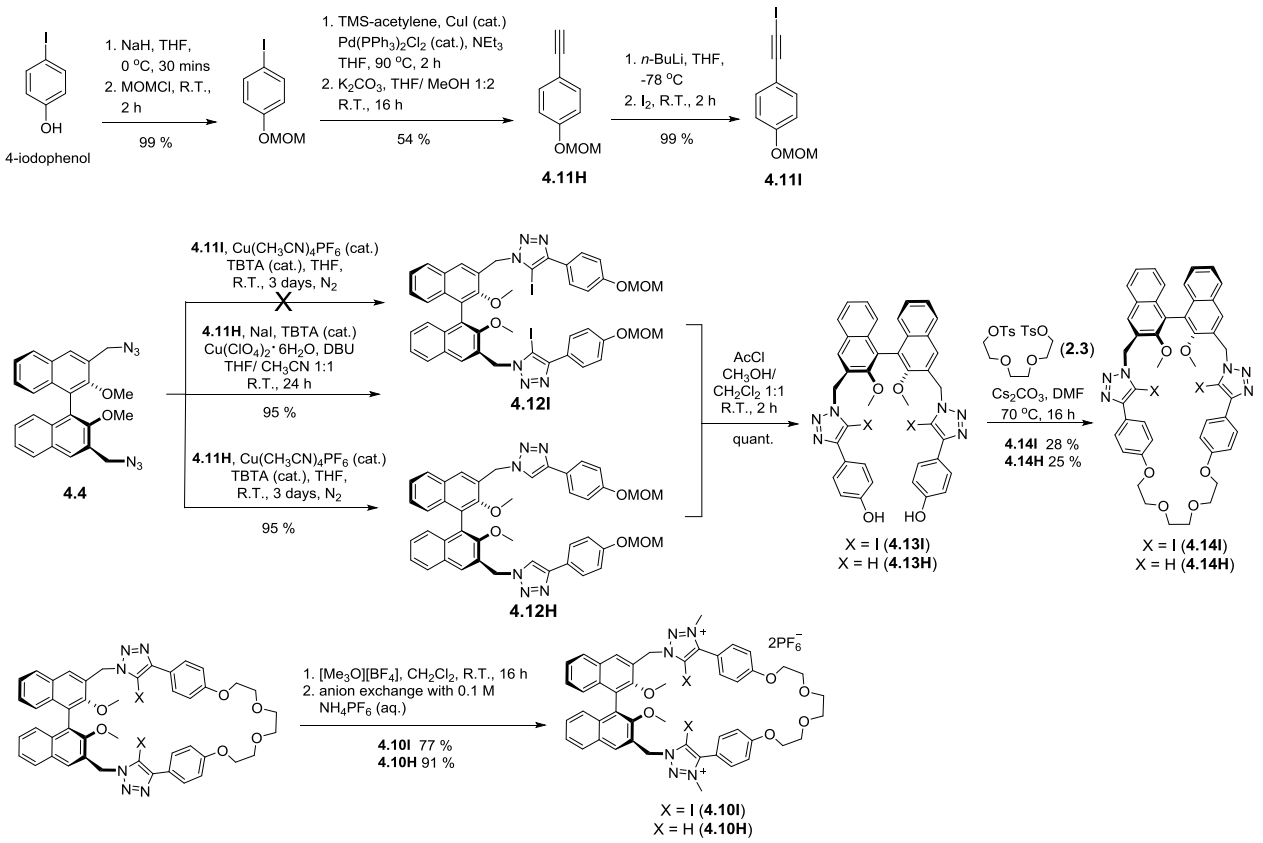
4.3.1 Syntheses of Chiral Macrocycles

Encouraged by the notable chiral selectivity of acyclic receptor **4.1I**, the (*S*)-BINOL 3,3'-substituted bis-iodotriazolium chiral recognition motif was incorporated into a macrocycle in an effort to augment enantio-discrimination via conformational preorganisation. To confirm if the beneficial geometric and steric effects of XB extend to macrocyclic host systems for chiral selectivity, the HB macrocycle analogue was prepared as well. The retrosynthetic strategy towards target chiral macrocycles **4.10I/H** are shown in Scheme 4.3, starting from the key synthons of (*S*)-BINOL bis-azide **4.4** and MOM-protected aryl (iodo)alkyne **4.11I/H**.



***Scheme 4.3**. Retrosynthesis of chiral dicationic macrocycles **4.10I/H**.*

The forward syntheses of macrocycles **4.10I/H** are detailed in Scheme 4.4. To prepare the aryl (iodo)alkyne synthons **4.11H/I**, 4-iodophenol was first subjected to MOM-protection before Sonogashira coupling to TMS-acetylene was performed.[111] Following alkyne TMS-deprotection, **4.11H** was obtained in 54 % yield over 2 steps. Conversion of **4.11H** to the iodoalkyne analogue **4.11I** was achieved in excellent yields and purity by *n*-BuLi alkyne lithiation and quenching with molecular iodine.



***Scheme 4.4**. Forward syntheses of dicationic chiral macrocycles **4.10I/H**.*

Thereafter, a standard 'iodo'-CuAAC reaction[112] was performed using bis-azide **4.4** and iodoalkyne **4.11I** with catalytic $[Cu(CH_3CN)_4]PF_6$. Surprisingly, these reaction conditions failed to produce any evidence of iodotriazole formation after 3 days even in the presence of the rate-accelerating ligand TBTA. Another attempt using similar conditions also failed to yield any **4.12I** product despite heating the reaction at 60 °C for 2 days. However, a product with similar R_f as iodoalkyne **4.11I** was isolated from the resulting crude reaction mixtures. While this product showed very similar ^{1}H NMR peak distribution as **4.11I**, ^{13}C NMR analysis revealed the loss of the characteristic iodoalkyne ^{13}C-I peak of **4.11I** at δ = 4.1 ppm, suggesting that possible Cu(I)-catalysed homo-coupling of the iodoalkynes to form a diyne occurred preferentially under the reaction conditions.

Therefore, the synthesis of **4.12I** was re-attempted using Zhu's conditions[94] directly from protoalkyne **4.11H**. Although this method allowed access to **4.12I**, using two equivalents of **4.11H** gave only a modest product yield of 42 %, with a large quantity of the same homo-

coupled diyne isolated as well, which is unsurprising as the 'one-pot' CuAAC protocol required a stoichiometric quantity of copper catalyst as well as involving the *in-situ* formation of **4.11I**.[113] However, using a four-fold excess of **4.11H** resulted in complete consumption of azide **4.4** within 16 hours, to give target **4.12I** in an excellent yield of 95 %. MOM-deprotection under acidic conditions, followed by S_N2 macrocycle ring-closing with triethylene glycol bis-tosylate **2.3** using Cs_2CO_3 as base afforded the neutral XB macrocycle **4.14I** in 28 % yield after chromatographic purification. The target dicationic macrocycle **4.10I**, as its $2PF_6^-$ salt, was obtained after bis-iodotriazole methylation of **4.14I** with trimethyloxonium tetrafluoroborate, followed by anion exchange by repeated washing with 0.1 M aqueous NH_4PF_6. The preparation of the dicationic HB macrocycle host **4.10H** was achieved following an analogous route shown in Scheme 4.4 with comparable yields.

4.3.2 Chiral Anion Discrimination Studies with Chiral Macrocycles

The chiral discrimination properties of dicationic macrocycles **4.10I** and **4.10H** were studied using ^{1}H NMR titration experiments in d_6-acetone/ D_2O 98:2 *v/v* in a similar manner to those described in Section 4.2.2. The same chiral substrates possessing single point or axis of chirality were studied, with the exception of *N*Boc-alanine due to its poor enantio-selectivity. Instead, *N*Boc-proline carboxylate, containing a conformationally-rigid pyrrolidine ring, was investigated.

A comparison of the ^{1}H NMR signal perturbations of macrocycles **4.10I** and **4.10H** during the titrations reveal several notable differences which highlight the important roles played by XB interactions in chiral discrimination. Using *N*Boc-(*S*)-proline carboxylate as an example (Figure 4.19), the presence of the anion resulted in shifts of signals H_g and H_h on the aromatic ring conjugated to the triazoliums for both macrocycles, likely arising from electronic communication of anion binding by the cationic triazolium moieties. For macrocycle **4.10H**, one of the diastereotopic alkyl proton environments (H_{f1}) and H_g proximal to the prototriazolium unit displayed significant downfield shifts, likely due to hydrogen bonding interactions with the anion present in close proximity. Notably, the contrasting directions of perturbations of both

diastereotopic proton environments (H_{f1} and H_{f2}) imply that anion binding occurs predominantly on one face above the plane of the macrocycle, allowing HB interactions with only one of these diastereotopic proton environments. This also suggests that the chiral anions are likely to be too bulky to fit into the restricted and rigid binding cavity of the macrocycle. Contrastingly for XB macrocycle **4.10I**, H_g is shifted downfield by a much smaller extent, and the diastereotopic proton environments (H_{f1} and H_{f2}) show unidirectional movement. These observations convey a lack of significant HB interactions with the bound anion, and suggest that the anion is bound more distant from H_g, likely further above the plane of the macrocycle by the bulky iodine atoms of the XB-donor iodotriazolium units (*vide infra*). As a result of this XB-directed geometric arrangement, the chiral anion was found to interact with the (*S*)-BINOL motif of macrocycle **4.10I** to a greater extent compared with **4.10H**. This is also evident from Figure 4.19, where distinct upfield shifts of the BINOL proton environments H_a, H_b, H_c and H_d could be discerned for **4.10I** in the presence of 1.0 equivalent of *N*Boc-(*S*)-proline carboxylate, while negligible shifts were seen for these environments of **4.10H**. Confirmation of the chiral discriminatory ability of both macrocycles can be seen from the H_{f1} binding isotherms shown in Figure 4.20, where different guest enantiomers elicit varying magnitudes and steepness of signal shifts.

Using both enantiomers of *N*Boc-(*S*)-proline carboxylate as model guests, molecular dynamics (MD) simulations were performed by Dr Igor Marques and Prof. Vitor Felix (University of Aveiro, Portugal) to study their binding with macrocycles **4.10I/H**. Gas-phase DFT geometry-optimisation was first performed to generate the initial host-guest binding scenarios (see Appendix C) with the CAM-B3LYP functional using TeraChem,[114–119] before the MD simulations were performed using the AMBER16 suite.[120] Both quantum mechanics and classical force field calculations were performed with GPU acceleration. For the MD simulations, the DFT-optimised host-guest complexes were immersed in periodic cubic boxes composed of 111 water and 1337 acetone molecules in accordance with the solvent mixture

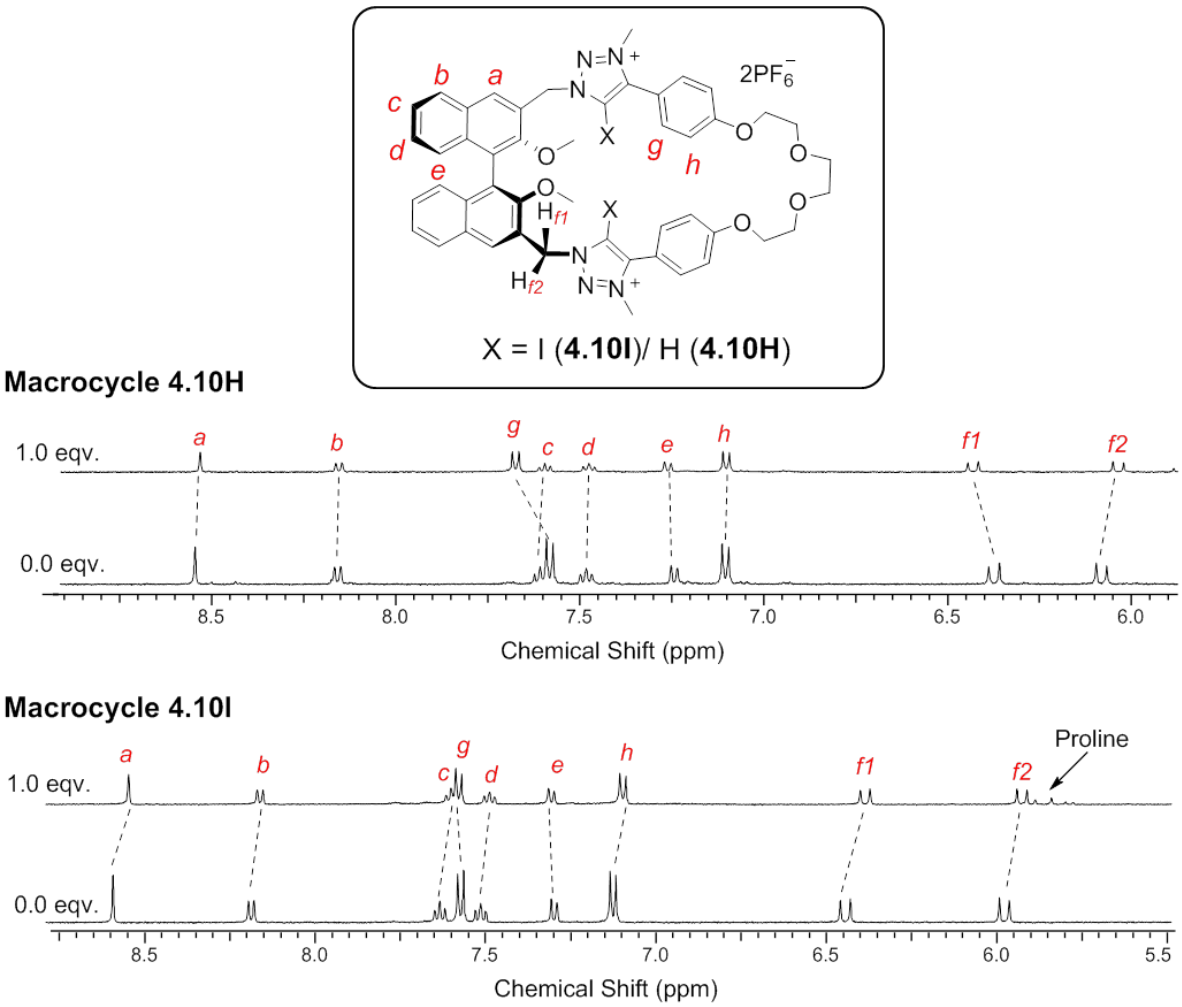


***Figure 4.19**. Partial ^{1}H NMR spectra of dicationic macrocycles **4.10H** and **4.10I** in the presence of 0.0 and 1.0 equivalents of NBoc-(S)-proline carboxylate ([**4.10I/H**] = 1.0 mM, d_6-acetone/ D_2O 98:2 v/v, T = 298 K).*

used for the ^{1}H NMR titrations (acetone/ water 98:2 *v/v*), and five independent 20 ns MD runs were performed for each system. To simulate the HB complexes, two distance restraints between **4.10H**'s prototriazoliums and the anions' carboxylate groups were used to maintain the host-guest complexes' integrity, while for XB complexes, the extra-point-of-charge approach was used.[104] Throughout the general MD simulations, the same host-guest binding arrangements were obtained for each enantiomer regardless of their initial DFT optimised binding scenario (further computational details are provided in Appendix C) - the most common arrangements of which form the basis of the following discussions.

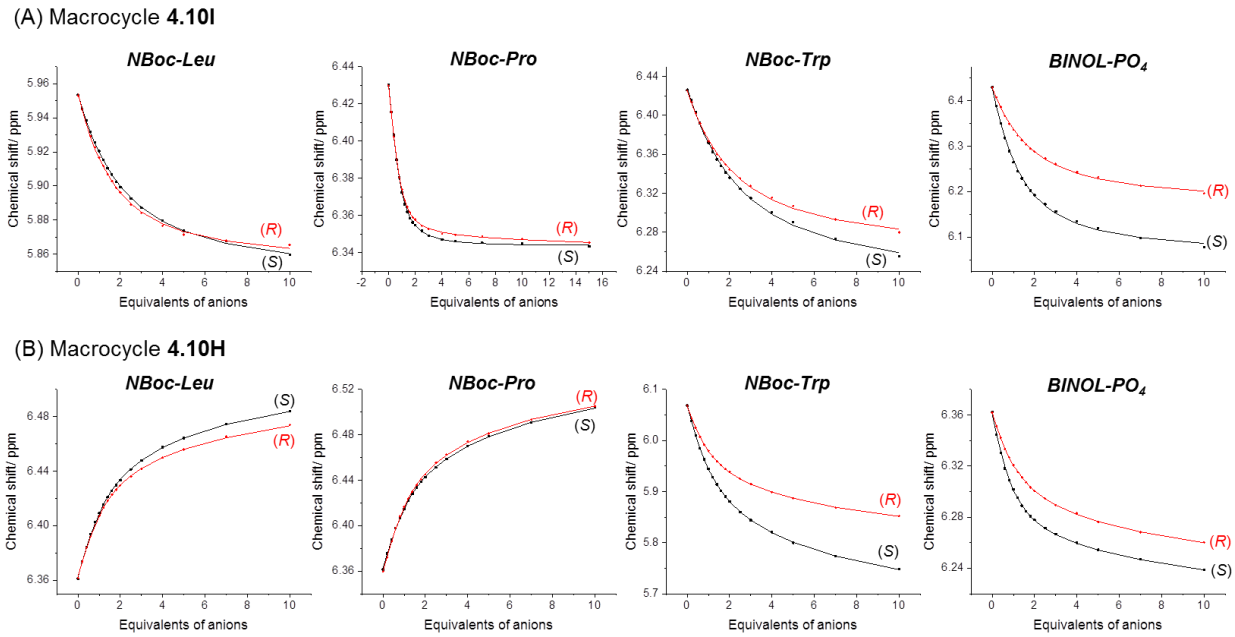


***Figure 4.20**. Binding isotherms obtained from monitoring the shifts of H_{f1} for both **4.10I** and **4.10H** as a function of increasing quantities of chiral anions ([host] = 1.5 mM, d_6-acetone/ D_2O 98:2 v/v, T = 298 K). Binding isotherms for the (S)-enantiomers are shown in black while those for the (R)-enantiomers are shown in red.*

For macrocycle **4.10H**, anion binding was found to occur with considerable distortion of the flexible macrocycle structure, with the carboxylate group of both guest enantiomers bound by two HB interactions from the triazolium groups which show significant deviation from linearity in some cases. As shown in Figure 4.21A, the solvent water molecules play important roles in the binding process, often forming $(C_{triazolium}\text{-}H)_{host}\cdots OH_2\cdots(O{=}C)_{anion}$ bridges between the triazolium groups and the anions' carboxylate groups. Notably for all MD binding scenarios obtained, the anion is held close to, but slightly above the plane of the macrocycle regardless of the anion enantiomer studied. This proximity allows the anion to participate in weak interactions with proton environments H_{f1} and H_g of the bridging methylene unit and aromatic ring immediately adjacent to the triazolium units, accounting for their downfield signal perturbations observed during the ^{1}H NMR titrations shown in Figure 4.19.

On the other hand, both *N*Boc-proline carboxylate enantiomers were bound further above the plane of macrocycle **4.10I** than **4.10H** due to the linearity of XB interactions and steric bulk of the XB-donor iodotriazolium units. In all cases, the carboxylate anions are held mainly by only one oxygen atom to the iodotriazoliums via a direct XB interaction and a

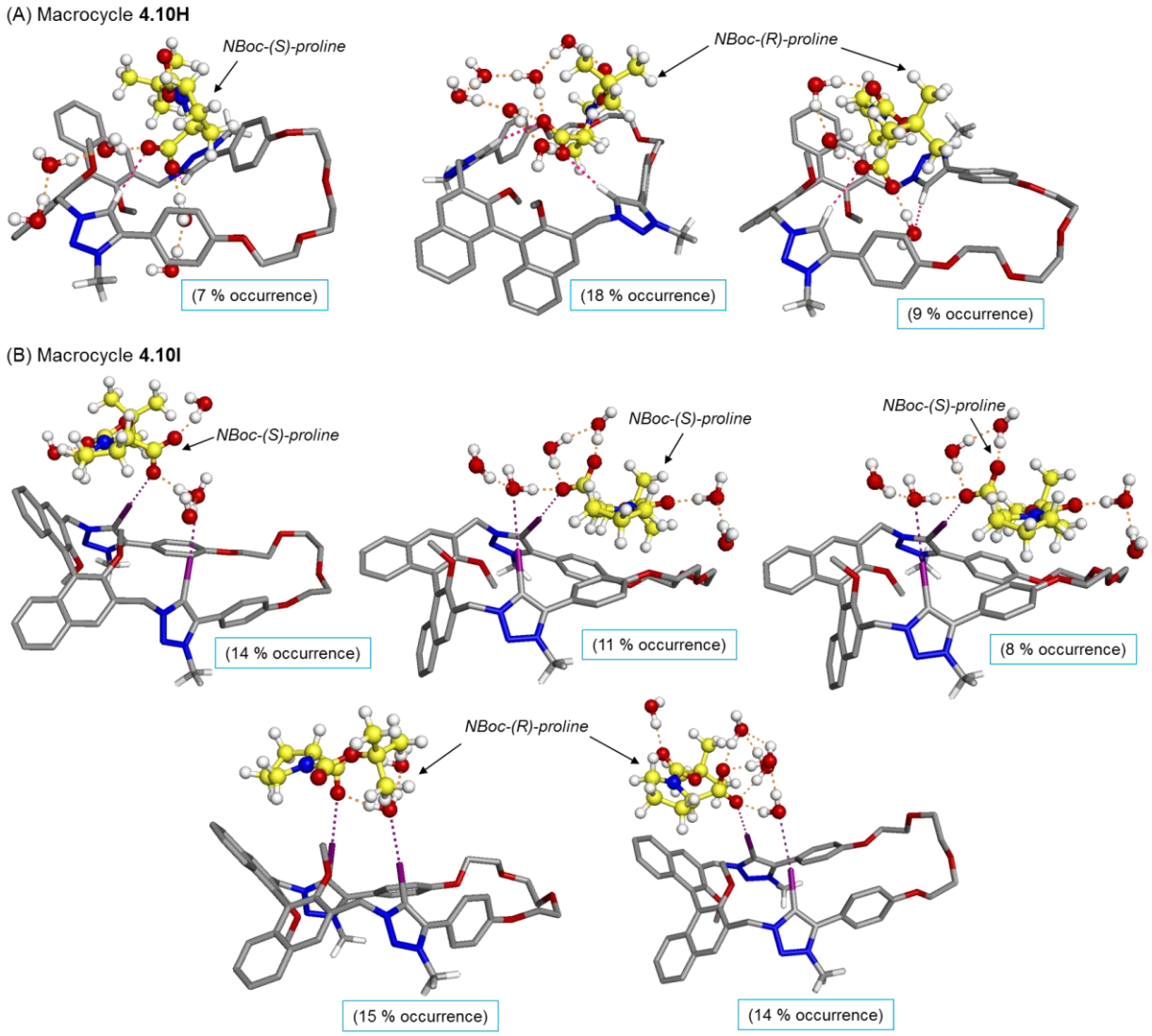


***Figure 4.21**. Most common host-guest binding scenarios of macrocycles (A) **4.10H** and (B) **4.10I** with both enantiomers of NBoc-proline carboxylate, with percentage occurrences indicated below each host-guest complex. Direct HB interactions between **4.10H** and the anion are shown as pink dashed lines, while those to water molecules are shown in orange. XB interactions between **4.10I** and anions are represented as purple dashes.*

bridged water molecule [$(C\text{-}I)_{host}\cdots OH_2\cdots(O{=}C)_{anion}$]. In contrast to **4.10H**, where both guest anion enantiomers are bound with similar binding arrangements, more distinct variation was found for **4.10I** (Figure 4.21B). For the most common binding arrangement of *N*Boc-(*S*)-proline carboxylate, the anion's pyrrolidine ring is oriented close to the macrocycle's (*S*)-BINOL unit. However, the entire anion is oriented away from the same host unit in the next two most common binding scenarios. For *N*Boc-(*R*)-proline carboxylate, the two most common binding arrangements show close interaction between the anion's pyrrolidine ring and the macrocycle's (*S*)-BINOL group. Once again, the modelling results corroborate the deductions

obtained from ^{1}H NMR titrations, as the large spatial separation between the anion and the plane of the macrocycle prevents significant HB interactions with proton environments H_{f1} and H_g (Figure 4.19). Nevertheless compared to the MD-simulated anion complexes with **4.10H**, the *N*Boc-proline carboxylate comes into closer contact with the (*S*)-BINOL group of macrocycle **4.10I**, resulting in the more prominent BINOL proton shifts seen in Figure 4.19.

The anion association constants for each guest enantiomer with macrocycles **4.10I** and **4.10H** were obtained by non-linear regression analysis of the perturbations of diastereotopic alkyl protons H_{f1} during the titrations using WinEQNMR2.[96] These values, as well as the corresponding magnitudes of chiral selectivity ($\xi = K_S/ K_R$) for each chiral anion pair are shown in Table 4.4. Although both macrocycles were found to bind the anions in a 1:2 host-guest stoichiometry, the magnitudes of the second binding constant (K_2) were much smaller than the first (K_1) in all cases. This suggests that the second anion is likely to be simply associating with the bound complex at its periphery, possibly driven by electrostatic attractions. As only the first anion is most likely binding within the macrocycle cavity, and hence properly influenced by its chiral environment as depicted in our MD simulations, the values of K_1 were solely used to determine chiral selectivity (ξ). From Table 4.4, both macrocycles show a general selectivity

Table 4.4. Anion association constants (K/ M^{-1}) of chiral anion pairs and the magnitudes of chiral selectivity (ξ) by macrocycles **4.10I** and **4.10H** in d_6-acetone/ D_2O 98:2.[a]

	Macrocycle **4.10I** [b]			Macrocycle **4.10H**		
	K_S	K_R	ξ [c]	K_S	K_R	ξ [c]
(*N*Boc-Leu)$^-$	423 ± 3	635 ± 31	0.67 ± 0.03	K_1 = 1516 ± 74 K_2 = 78 ± 4	K_1 = 2057 ± 87 K_2 = 66 ± 3	ξ_1 = 0.74 ± 0.05
(*N*Boc-Trp)$^-$	324 ± 6	488 ± 21	0.66 ± 0.03	K_1 =1289 ± 41 K_2 = 55 ± 2	K_1 = 1667 ± 49 K_2 = 52 ± 2	ξ_1 = 0.77 ± 0.03
(*N*Boc-Pro)$^-$	3495 ± 64	4961 ± 47	0.70 ± 0.01	K_1 = 1641 ± 53 K_2 = 64 ± 2	K_1 = 1776 ± 81 K_2 = 67 ± 3	ξ_1 = 0.92 ± 0.05
(BINOL-PO_4)$^-$	854 ± 43	540 ± 24	1.58 ± 0.11	K_1 = 2595 ± 206 K_2 = 40 ± 5	K_1 = 3243 ± 177 K_2 = 56 ± 5	ξ_1 = 0.80 ± 0.08

[a] Values of K calculated using the WinEQNMR2 software[96] using a host-guest 1:2 binding model, monitoring one of the diastereotopic protons H_f for both macrocycles during the titrations; anions added as TBA salts; [macrocycle] = 1.0 mM, T = 298 K. [b] Although **4.10I** bound anions with host-guest 1:2 binding stoichiometry, $K_{1:2}$ < 10 M^{-1} for all cases and hence not shown. [c] $\xi = K_S/ K_R$

for the (*R*)-enantiomer of the chiral guest anions, with the XB macrocycle **4.10I** exhibiting enhanced chiral selectivity over **4.10H** in all cases, likely resulting from the more prominent interactions of the guest anions with the BINOL motif of the macrocycle as noted above.

The chiral oxoanion binding behavior of macrocycles **4.10I/H** also show several notable differences with those of acyclic receptors **4.1I/H**. Firstly, while **4.1I** displays much stronger anion affinities than **4.1H** (Table 4.2), the anions are bound to macrocycle **4.10H** more strongly than **4.10I** in most cases (Table 4.3). This may be a consequence of the more preorganised nature of **4.10H**'s macrocyclic structure, as well as the less polar d_6-acetone/D_2O solvent mixture used in the latter case compared to the CD_3CN/D_2O media of **4.1I/H**. The same factors are likely to account for the significantly enhanced enantio-selectivity observed for macrocycle **4.10H** compared to acyclic receptor **4.1H**. Interestingly, XB macrocycle **4.10I** did not show augmented chiral selectivity over acyclic receptor **4.1I**, with *N*Boc-leucine carboxylate and BINOL-PO_4^- showing comparable selectivity and *N*Boc-tryptophan carboxylate surprisingly better discriminated by the latter. In addition, while acyclic **4.1I** showed different enantiomer preferences for the amino acid-derived anions, macrocycle **4.10I** favoured the (*R*)-guest enantiomers in all cases. These may be a consequence of the different anion binding geometries displayed by receptors **4.1I** and **4.10I**. For the latter, anion coordination significantly above the plane of the macrocycle, enforced by the macrocycle size, linearity of XB interactions and steric bulk of the XB-donor iodotriazoles, increases the spatial separation between the anions and the macrocycle's chiral (*S*)-BINOL group (Figure 4.21B). This is likely to reduce the overlap of their respective chiral fields and negatively impact enantio-selectivity. On the other hand, the predominantly in-plane anion binding to acyclic receptor **4.1I** (Figure 4.17A) is expected to favour chiral recognition.

Moreover, while **4.1I** showed greater variation in selectivity amongst the different chiral anion pairs than **4.1H**, the opposite was seen for the macrocyclic receptors, with **4.10I** showing surprisingly uniform magnitudes of selectivity (discounting enantiomer preference). This may be attributed to the more stringent linear directionality of XB-anion interactions compared to HB, which restricts the binding geometry of the anions invariably far above the plane of the macrocycle (Figure 4.21B). The HB interactions of **4.10H**, on the other hand, may allow a

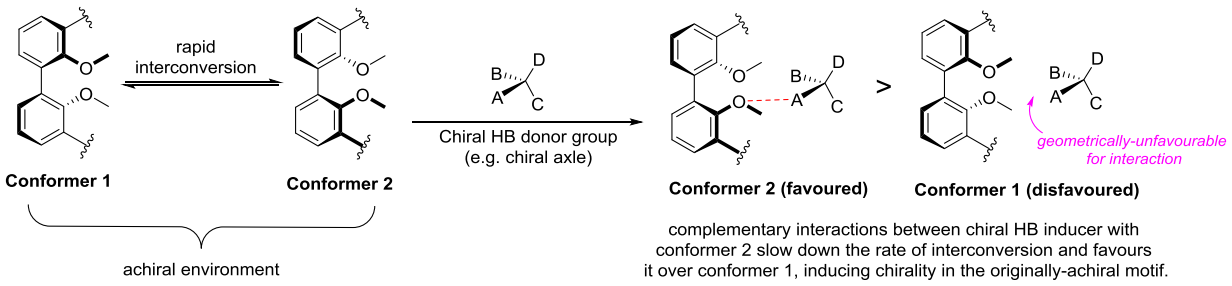
greater degree of flexibility in adopting binding conformations that minimizes the host-guest steric repulsions, which can compromise on enantioselectivity in the process.

In summary, while having a constrained macrocyclic host structure improves the selectivity of HB-mediated chiral recognition, XB showed no significant enhancements. This is largely due to the restricted XB geometric requirements, which proved beneficial for chiral discrimination by acyclic receptors but less so for macrocyclic hosts as they limit the loci of anion binding to a considerable distance above the plane of the macrocycle. Despite this, the anions are still free to adopt a range of binding conformations which includes arrangements where the anion is oriented away from the macrocycle's chiral units, evident from the MD simulations. Furthermore, these modelling studies also reveal that different anion enantiomers can adopt remarkably conformationally-similar binding arrangements (most common binding scenarios for both enantiomers of *N*Boc-proline to **4.10I** shown in Figure 4.21B), reducing the effectiveness of chiral discrimination by the largely two-dimensional macrocycle plane. In light of these findings, it was expected that further constraining the anion binding geometry and location in a more preorganised binding cavity of a rotaxane, which also provides a well-defined three dimensional surface for chiral recognition, can potentially enhance the effectiveness of stereo-selective anion binding.

4.3.3 Design and Syntheses of Chiral XB [2]Rotaxanes

The target chiral [2]rotaxanes, shown in Figure 4.22, comprise an axle containing a XB-donor 3,5-bis-iodotriazole pyridinium component that threads through the macrocycle cavity. HB interactions between the axle's pyridinium methyl group and the macrocycle component's polyether region are expected to lock both components together,[121] preorganising the chiral rotaxane binding pocket by limiting the macrocycle's rotational flexibility. The rotaxanes contain four centrally-located XB-donor iodotriazoles, facilitating binding to the carboxylate/ phosphate motifs of chiral oxoanion guest species and therefore sandwiching the anions in the restricted binding space between the axle and macrocycle components (depicted by the yellow shaded region in Figure 4.22, left). This binding arrangement also orientates the anions' bulky chiral substituents towards the asymmetric motifs of the rotaxane binding site to achieve optimal enantioselectivity. Three structurally-related [2]rotaxanes were designed to study and compare the roles played by individual axle and macrocycle components for chiral discrimination. These include one with both chiral axle and macrocycle components (rotaxane **4.15**), another with a chiral macrocycle but an achiral axle (rotaxane **4.16**) and the last containing just a chiral axle component, with an achiral biphenyl spacer replacing the (*S*)-BINOL group on the macrocycle unit*** (rotaxane **4.17**). Importantly, all rotaxanes contain

*** For the achiral macrocycle unit, a biphenyl spacer was used without the presence of methoxy (OCH_3) groups at their 2,2'-positions to avoid the possibility of chiral induction by non-covalent interactions (e.g. HB) from the chiral axle unit.[122] Had the 2,2'-methoxy biphenyl spacer been used, constraining them in a macrocyclic structure will force both phenyl rings to be twisted out of plane relative to each other. Although both resulting axial-chiral enantiomers can invert rapidly at room temperature in an achiral setting, the presence of the chiral axle in close proximity can cause one enantiomer to be favoured over the other, setting up another chiral axis on the macrocycle (see diagram below). This would necessarily prevent rotaxane **4.17** from having a truly achiral macrocycle component.



macrocycle and axle units which are identical on both sides of a mirror plane passing through the centre of each component to avoid the occurrence of additional mechanically-bonded chirality (Section 4.1.4).

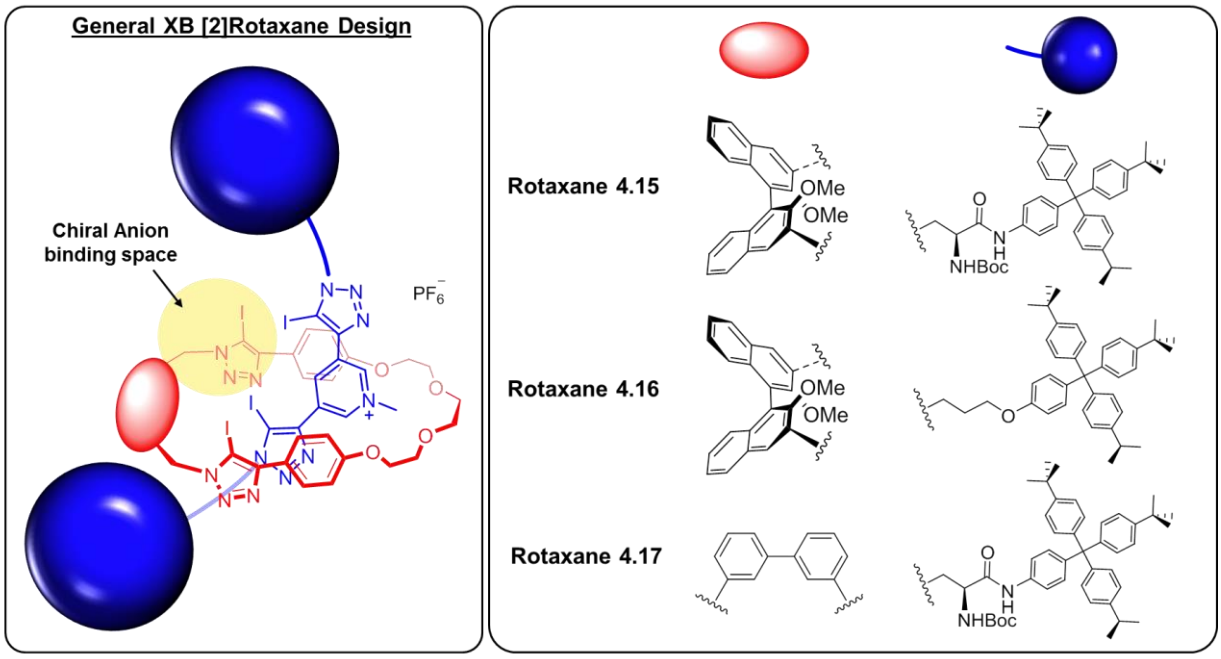


***Figure 4.22**. Design and structure of target chiral XB [2]rotaxanes **4.15**-**4.17**.*

Given the success of the active metal template (AMT) CuAAC approach in synthesising rotaxane **3.34I$_4$** containing an all-XB anion binding cavity (see Section 3.4), the same approach was adopted to synthesise the target chiral XB [2]rotaxanes from the appropriate neutral XB macrocycle, stoppered azide and pyridine-3,5-bis(iodoalkyne) precursors. To better understand the Cu(I)-complexation properties of macrocycle **4.14I** for AMT-CuAAC, a qualitative ^{1}H NMR titration was first performed by adding increasing quantities of $[Cu(CH_3CN)_4]PF_6$ to a solution of neutral macrocycle **4.14I** in the non-coordinating solvent, d_6-acetone.[123] As shown in Figure 4.23, Cu(I) addition resulted in notable perturbations of the aromatic proton resonances of **4.14I**, as well as the diastereotopic methylene spacer protons H_{f1} and H_{f2}. For instance, H_{f1} showed a downfield shift of ca. +0.3 ppm up until 1.0 equivalent of Cu(I), followed by a small upfield shift of ca -0.05 ppm between 1.0 and 4.0 equivalents. It is noteworthy that unlike bis-iodotriazole XB macrocycle **2.1I**

discussed in Section 2.2.2 of this thesis, no desymmetrisation of any of the proton resonances were observed with less than 1.0 equivalent of added Cu(I), suggesting that Cu(I) binding by **4.14I** was occurring faster than the ^{1}H NMR timescale. From the signal shifts obtained, it is evident that **4.14I** was predominantly binding Cu(I) with a 1:1 stoichiometry, with a weak second cation coordination in the presence of excess Cu(I). This can be seen from the continued but small movements of the proton signal H_{f1} in the opposite direction beyond 2.0 equivalents of added Cu(I), probably due to electrostatic repulsion between the initially-formed cationic [**4.14I**-Cu]$^{+}$ complex and a second equivalent of $[Cu(CH_3CN)_4]^{+}$. Therefore to maximise the possibility of any Cu(I) added being coordinated to the macrocycle and hence able to direct rotaxane synthesis through its cavity, 1.0 equivalent of $[Cu(CH_3CN)_4]PF_6$ with respect to **4.14I** was used for the AMT-CuAAC reaction.

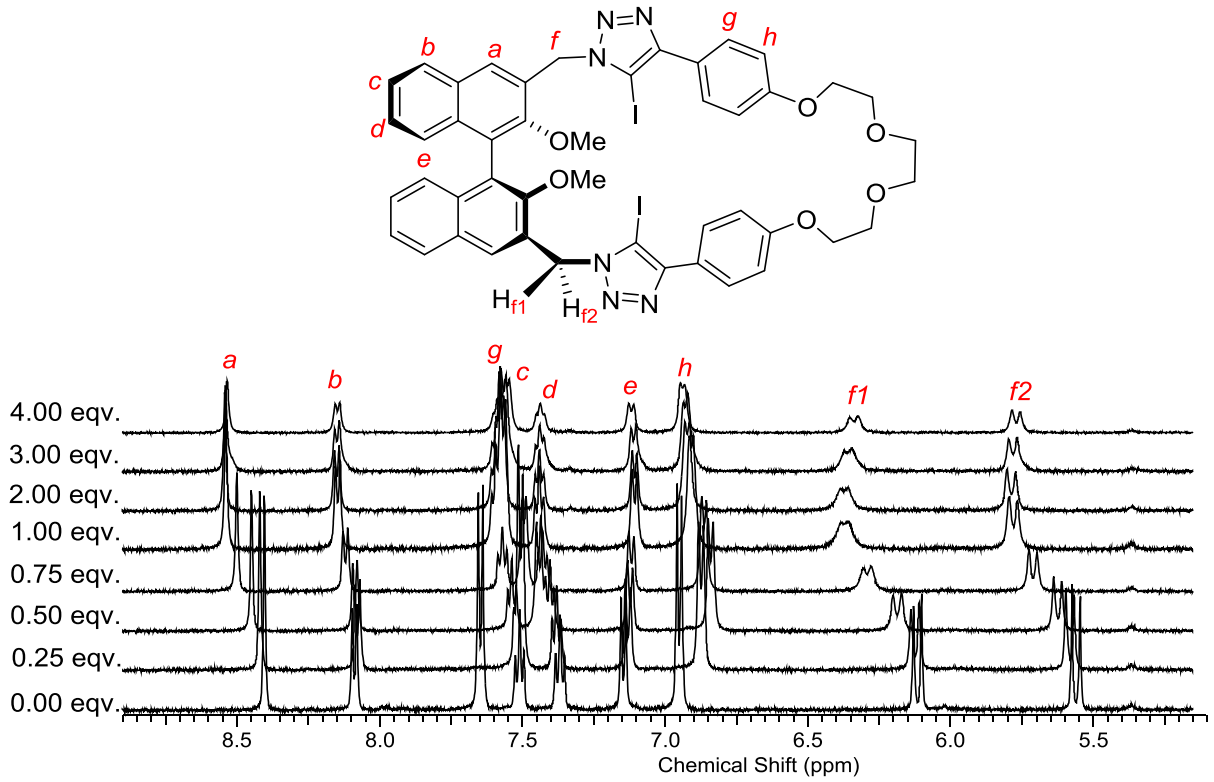
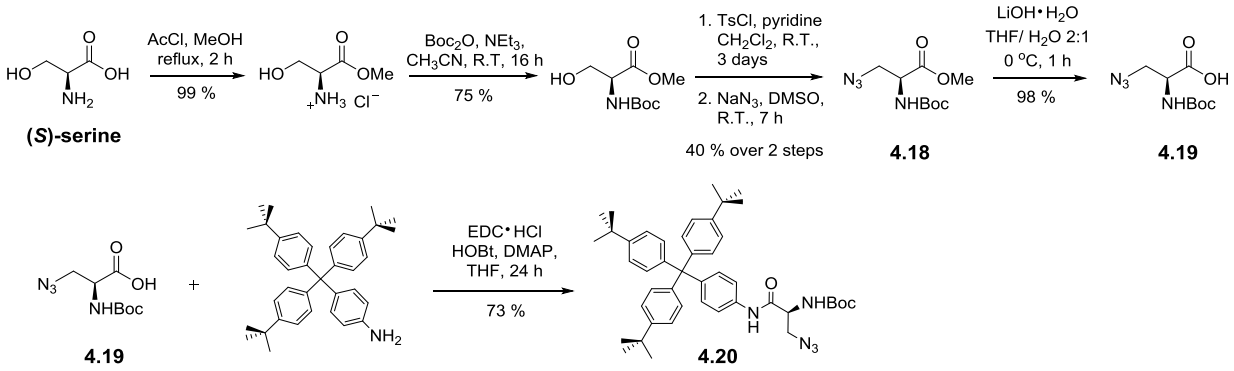


***Figure 4.23**. Partial ^{1}H NMR spectra of macrocycle **4.14I** in the presence of increasing quantities of $[Cu(CH_3CN)_4]PF_6$ ([**4.14I**] = 1.5 mM, d_6-acetone, T = 298 K).*

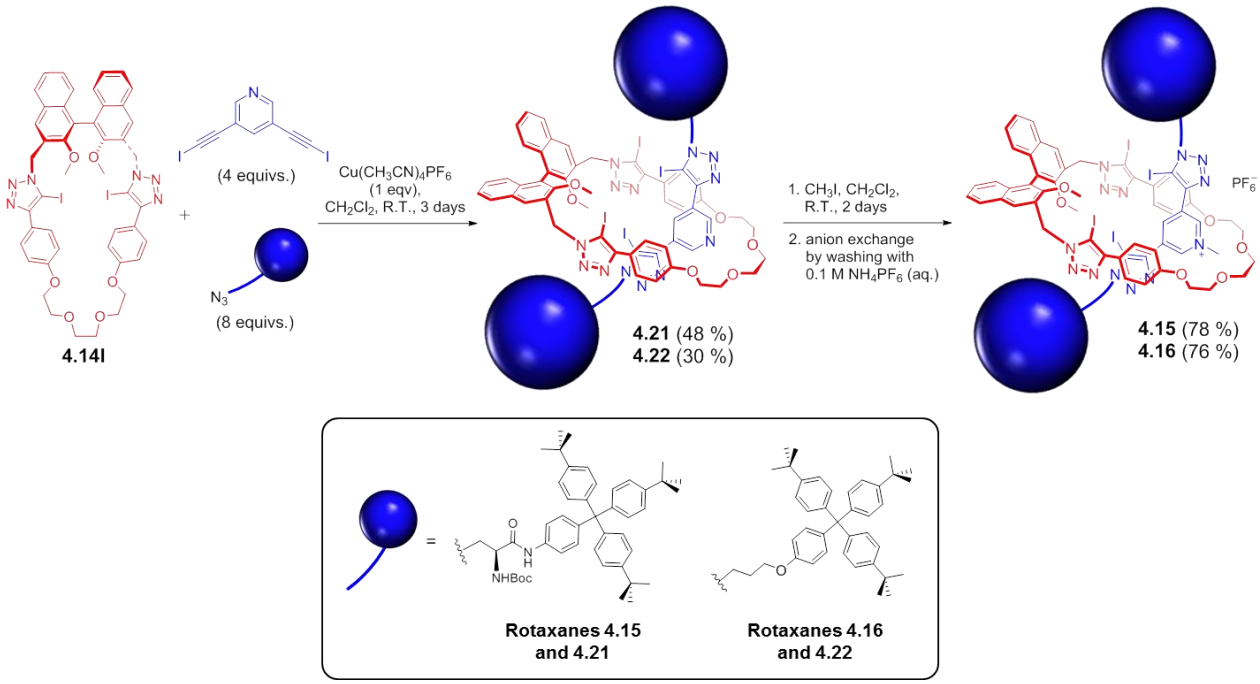
To synthesise the chiral axle unit, commercially-available (*S*)-serine was chosen as a convenient source of enantiopure starting material as its three parent functional groups (amine, carboxylic acid and alcohol) allow convenient orthogonal chemical manipulation. As shown in Scheme 4.5, the synthesis of azide precursor **4.18** was performed as reported. [124] Consecutive methyl ester and *N*HBoc-protection of the free carboxylic acid and amine groups of (*S*)-serine respectively was followed by tosylation of the hydroxyl group, where S_N2 substitution with NaN_3 then afforded **4.18**. Thereafter, near-quantitative deprotection of the methyl ester of **4.18** was achieved using $LiOH{\cdot}H_2O$ at 0 ^oC to minimise base-induced racemisation of the chiral centre.[125] The resulting free acid **4.19** was then reacted with the stopper aniline under enantio-retentive conditions involving activated ester formation using EDC·HCl and HOBt[126] to yield the chiral stopper azide **4.20**.



Scheme 4.5. Synthesis of point-chiral azide synthon **4.20**.

CuAAC-AMT rotaxane synthesis was then attempted using equimolar quantities of neutral chiral macrocycle **4.14I** and $[Cu(CH_3CN)_4PF_6]$ in degassed CH_2Cl_2, with 4.0 and 8.0 equivalents of pyridine-3,5-bis(iodoalkyne) and chiral stopper azide **4.20** respectively (Scheme 4.6). To monitor the progress of rotaxanation, a sample of the reaction mixture was extracted after 24 hours and quenched with basic EDTA solution. TLC separation and ESI-MS analysis of each isolated individual component of the reaction mixture revealed the unequivocal presence of free macrocycle **4.14I**, unreacted azide **4.20**, singly- and doubly-'Clicked' products

of azide **4.20** and pyridine-3,5-bis(iodoalkyne) and neutral rotaxane **4.21** (Figure 4.24A). This suggested that similar to rotaxane **3.34I$_4$** (Section 3.4), rotaxane formation likely occurred via the reaction of the singly-'Clicked' terminal iodoalkyne intermediate with another equivalent of azide **4.20** though the cavity of macrocycle **4.14I**, catalysed by Cu(I) bound endotopically by the macrocycle iodotriazole groups (Figure 4.24B). Complete consumption of the azide and iodoalkyne starting materials was observed after 3 days. After decomplexation of the Cu(I) catalyst, neutral chiral rotaxane **4.21** was isolated via preparatory TLC in a yield of 48 %. When the analogous CuAAC-AMT reaction was performed using the achiral stopper azide synthon **2.10** bearing a propylene linker, ESI-MS similarly showed the presence of the corresponding rotaxane **4.22** at m/z = 2581 $[M+H]^+$, which was isolated in 30 % yield. Thereafter, exclusive single methylation of the rotaxane on the axle component's central pyridine group was achieved using iodomethane to afford the target rotaxanes **4.15** and **4.16** in 78 % and 76 % yields respectively, after which anion exchange was performed to obtain their PF_6^- salts.



***Scheme 4.6**. Synthesis of cationic [2]rotaxanes **4.15** and **4.16** containing chiral macrocycle components.*

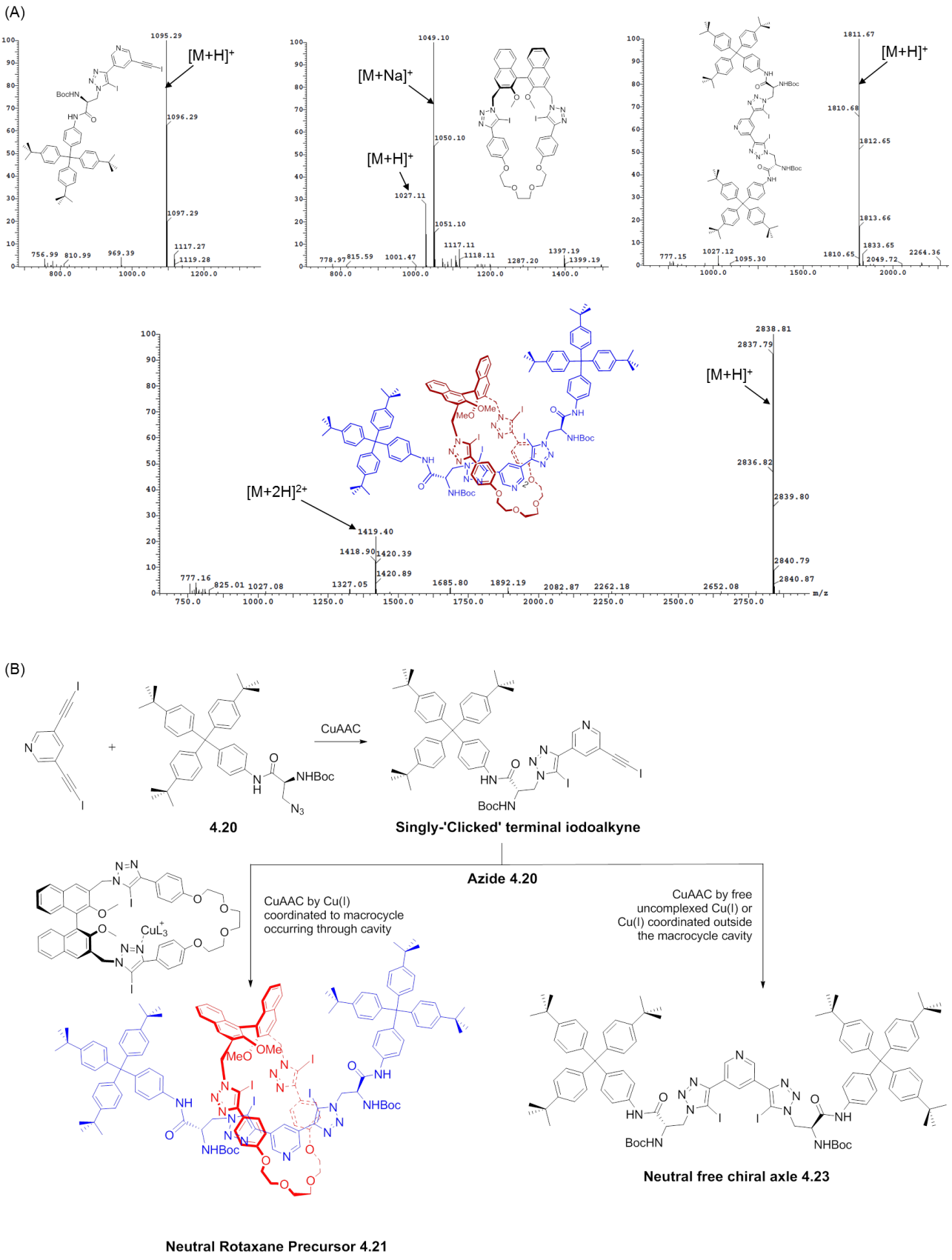
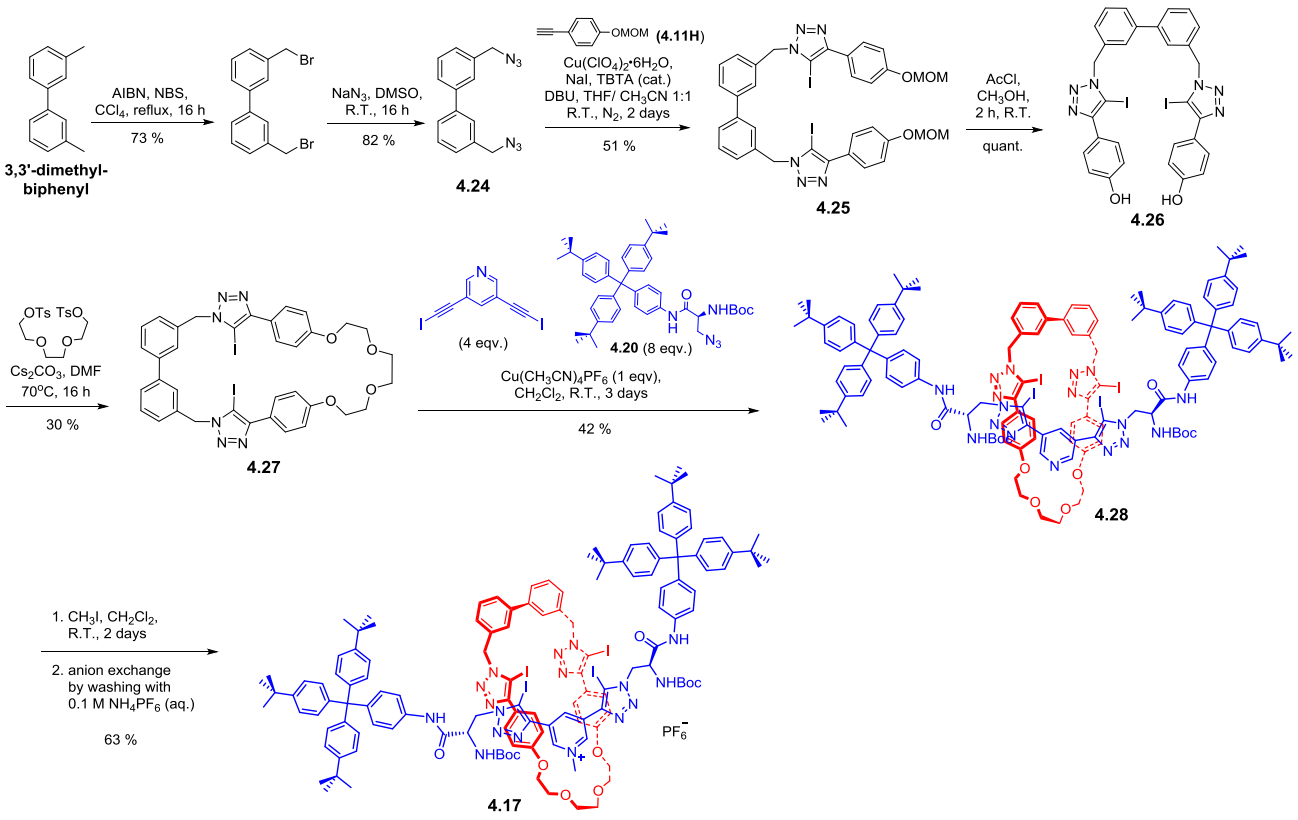


***Figure 4.24**. (A) ESI mass spectra of intermediates isolated from the CuAAC-AMT reaction for synthesis of neutral rotaxane **4.21**; and (B) proposed mechanism of rotaxane formation.*

The synthesis of rotaxane **4.17** containing the achiral macrocycle component was then performed (Scheme 4.7). Starting from commercially-available 3,3'-dimethyl-biphenyl, free radical substitution with *N*-bromosuccinimide (NBS) and the radical initiator azobisisobutyronitrile (AIBN) afforded the dibromo-intermediate,[127] which was then converted to the bis-azide synthon **4.24** with sodium azide. Following a successful 'one-pot' CuAAC reaction directly from aryl (proto)alkyne **4.11H**, the resulting bis-iodotriazole intermediate **4.25** was subjected to quantitative MOM-deprotection under acidic conditions to afford the biphenol macrocycle precursor **4.26**. Macrocycle **4.27** was subsequently obtained by S_N2 ring-closing with triethylene glycol bis(tosylate) in the presence of cesium carbonate using an identical procedure as that for macrocycle **4.14l** (Section 4.3.1). Thereafter, CuAAC-AMT rotaxane synthesis was performed as previously described for neutral rotaxanes **4.21** and **4.22**, to obtain the target rotaxane **4.28**, bearing only a chiral axle in 42 % yield after isolation



Scheme 4.7. Synthesis of achiral neutral macrocycle **4.27** and target chiral rotaxane **4.17**.

by preparatory TLC. Axle pyridine *N*-methylation with iodomethane, followed by anion exchange to the PF_6^- salt then afforded the target cationic rotaxane **4.17**.

Comparing the respective CuAAC-AMT rotaxane-forming reactions revealed that higher yields were obtained for **4.21** and **4.28** (48 % and 42 % respectively), both formed using the (*S*)-serine-derived chiral stopper azide **4.20**, compared to rotaxane **4.22** (30 %) using the achiral stopper azide possessing an unfunctionalised propylene chain. This may be a consequence of additional secondary non-covalent interactions (e.g. HB) between the macrocycle units and the chiral azide axle precursor which aids in the threading process through the macrocycle cavity required for rotaxane formation. Indeed, these interactions persist even after formation of the neutral rotaxanes, allowing the macrocycle components of **4.21** and **4.28** to adopt a range of conformations around the axles in slow exchange on the NMR timescale, resulting in the complex resonance patterns in their respective ^{1}H NMR spectra (Figure 4.25A and C). Contrastingly, neutral rotaxane **4.22** shows well-defined peaks in its ^{1}H NMR spectrum (Figure 4.25B) arising from the lack of these secondary interactions, suggesting a smaller degree of conformational dynamism. Nevertheless, all three rotaxanes show increased structural rigidification upon pyridine *N*-methylation of their axle components, evident from the dramatic simplication of the ^{1}H NMR spectra of monocationic rotaxanes **4.15** and **4.17** compared to their neutral congeners (Figure 4.25A and C), suggesting that the macrocycle components are now conformationally locked predominantly around their axles' central pyridinium units.[121] This can also be clearly seen with rotaxane **4.16** (Figure 4.25B), where increased upfield shifts of the macrocycle aromatic proton signals adjacent to the iodotriazole units and those of the axle component's pyridine group suggest enhanced donor-acceptor π-stacking interactions between them. Unequivocal evidence of the interlocked nature of each cationic rotaxane **4.15**-**4.17** can be seen from their two-dimensional ^{1}H-^{1}H ROESY spectra (Figure 4.26), which show numerous cross-peaks between their axle and macrocycle components.

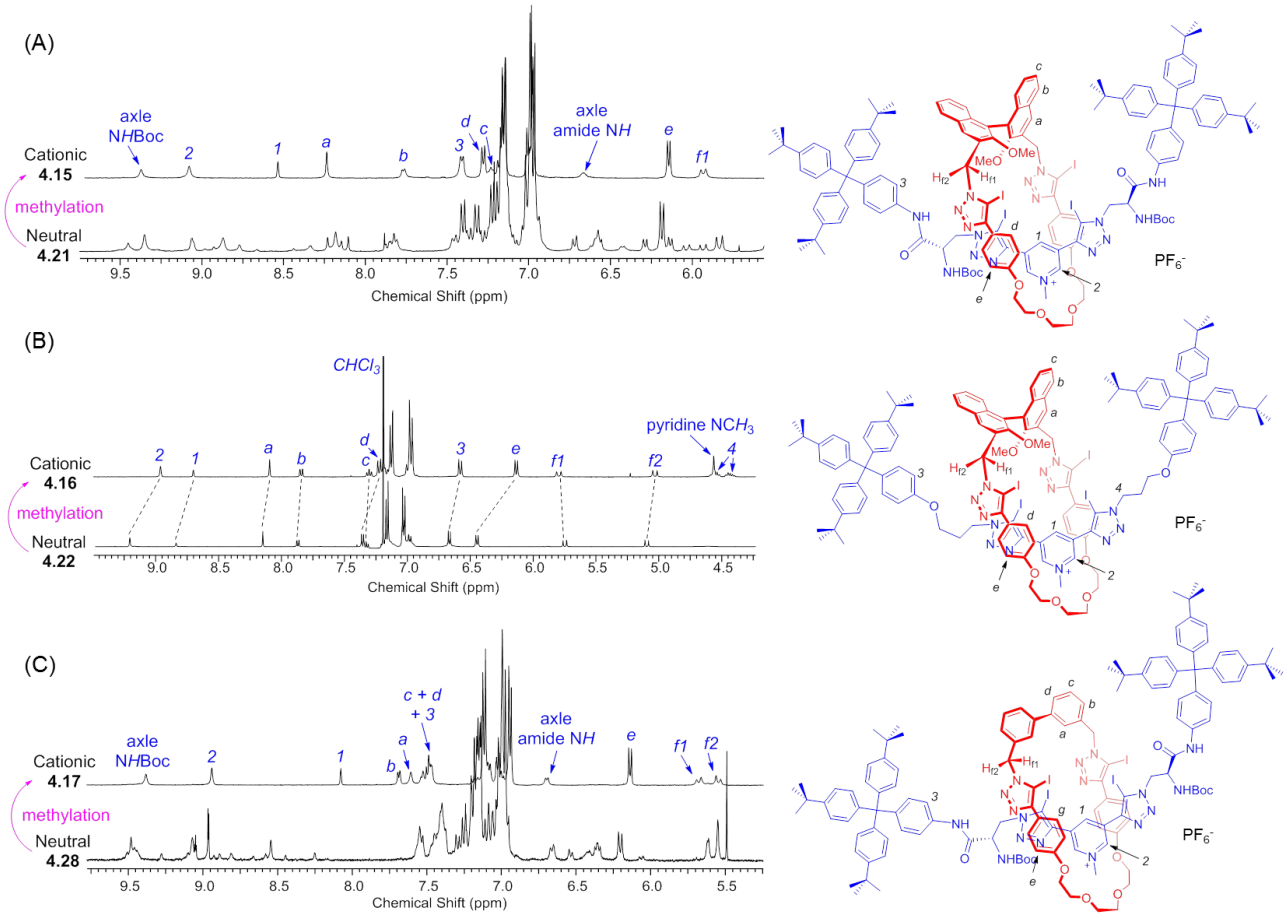


Figure 4.25. *^{1}H NMR spectra (T = 298 K) of each neutral and cationic rotaxanes: (A)* ***4.21*** *and* ***4.15*** *(d_6-acetone), bearing both chiral axle and macrocycle components; (B)* ***4.22*** *and* ***4.16*** *($CDCl_3$), containing only a chiral macrocycle component; (C)* ***4.28*** *and* ***4.17*** *(d_6-acetone), possessing only a chiral axle component.*

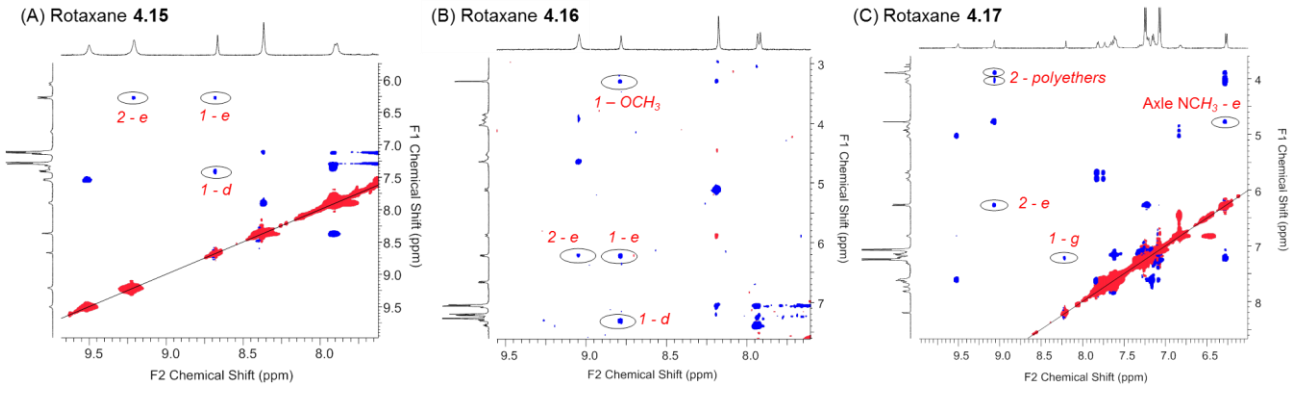


Figure 4.26. *2D ROESY NMR spectra of chiral rotaxanes (A)* ***4.15****; (B)* ***4.16*** *and (C)* ***4.17*** *in d_6-acetone. Proton assignments follow those of Figure 4.25.*

4.3.4 Stereoselective Anion Binding using Chiral [2]Rotaxanes

4.3.4.1 ^{1}H NMR Chiral Recognition Studies

The stereo-selective binding properties of cationic rotaxane **4.15** towards chiral anion pairs were studied in d_6-acetone/ D_2O 98:2 *v/v* by ^{1}H NMR titration experiments. *N*Boc-protected amino acid carboxylates containing bulky or rigid R-groups (leucine, proline and tryptophan) were studied, in addition to BINOL-PO_4^-. Further inspired by the recent finding that the presence of a strong HB donor located alpha to a carboxylate group resulted in good chiral selectivity by a series of acyclic sugar-based chiral receptors,[128] both enantiomers of mandelate were investigated as well (anion structures shown in Figure 4.8).

The titration of rotaxane **4.15** with *N*Boc-(*S*)-proline carboxylate is shown as a representative example in Figure 4.27. In the presence of the added carboxylate, numerous perturbations of the ^{1}H NMR signals arising from various proton environments flanking the rotaxane cavity were observed. For instance, significant downfield shifts of the aromatic H_3 signal on the stopper were seen, together with more modest upfield shifts of the (*S*)-BINOL resonances on the macrocycle component. In addition, the internal pyridinium aromatic proton on the axle component (H_1) showed very small shifts in the presence of 5.0 equivalents of anion, suggesting that true to our design, the anion is likely predominantly perching in the binding space flanked by the axle and macrocycle components (as shown in Figure 4.22), allowing their respective chiral units to contribute synergistically for chiral recognition. Amongst all the various signals, those arising from the diastereotopic proton H_{f1} on the macrocycle component were most sensitive to variations in the conformation and electronic environment of the binding cavity in the presence of different anion enantiomers. Indeed, monitoring the H_{f1} signals gave distinctly different binding isotherm shapes and steepness in the presence of both enantiomers of the various chiral anion pairs (Figure 4.27B). The most dramatic difference was seen for BINOL-PO_4^- (Figure 4.27B, bottom middle), where the (*S*)-enantiomer elicited a significant *upfield* shift of -0.13 ppm of H_{f1}, while the opposite (*R*)-guest gave a small *downfield* shift of the same proton signal by +0.012 ppm, clearly demonstrating that the rotaxane's chiral binding pocket is able to effectively distinguish between different guest stereoisomers. WinEQNMR2[96] analysis of the ^{1}H NMR titration data using a host-guest 1:2

stoichiometric binding model, determined association constants collected in Table 4.5. It is noteworthy that the second association constants (K_2) are consistently much smaller in magnitude than K_1, implying that only one chiral anion guest is associating within the rotaxane chiral binding cavity, while the second is presumably associating weakly with the bound rotaxane-anion complex at its periphery. Therefore, only the values of K_1 were used for determination of chiral selectivity (ξ).

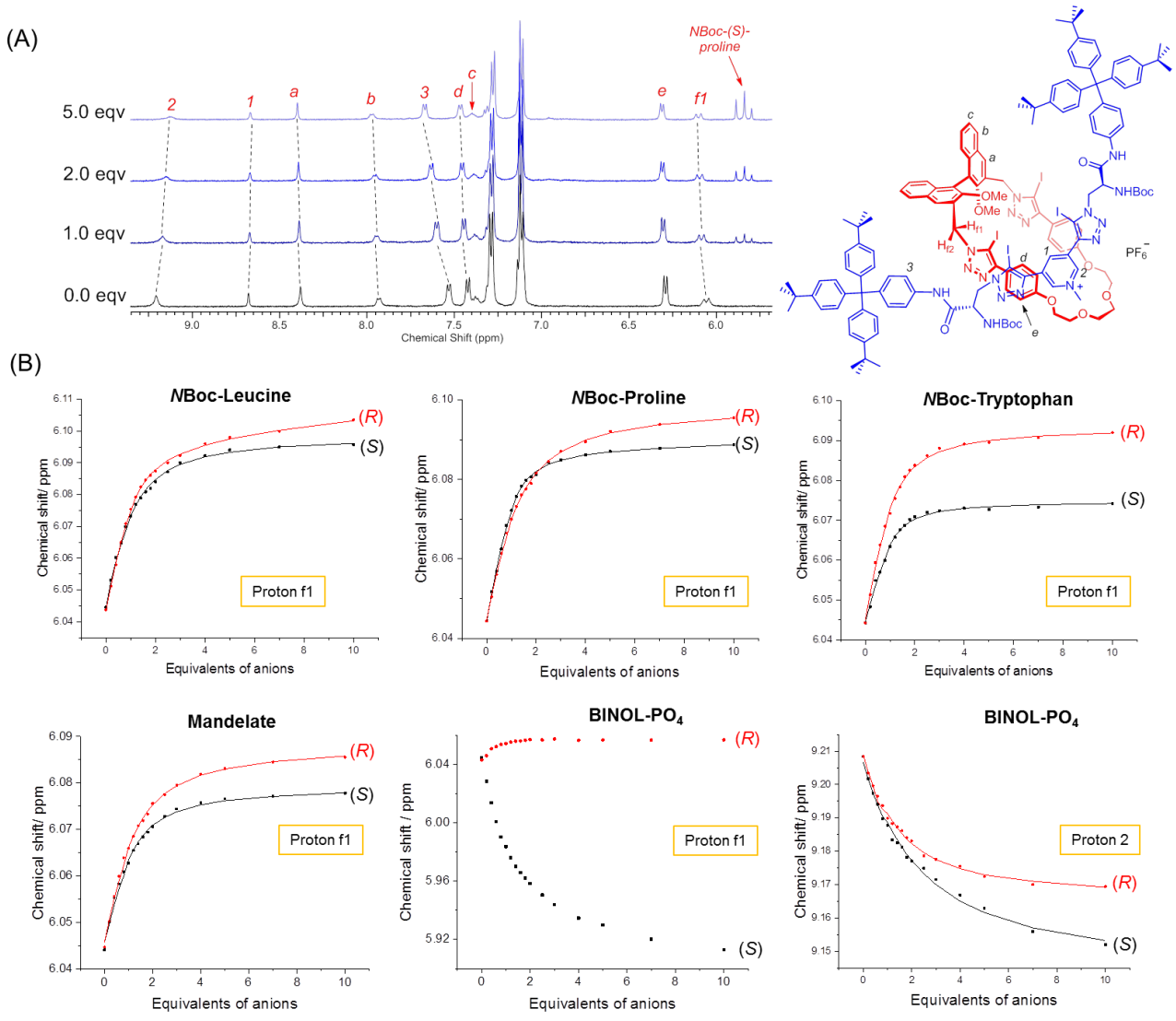


Figure 4.27. *(A) Partial ^{1}H NMR spectra of rotaxane **4.15** in the presence of increasing quantities of NBoc-(S)-proline carboxylate; (B) Changes in chemical shifts of proton environments H_{f1} or H_2 as a function of guest anion enantiomer concentration- filled dots represent empirical data points while smooth curves represent the best-fit binding isotherms obtained ([**4.15**] = 1.0 mM, d_6-acetone/ D_2O 98:2, T = 298 K).*

Amongst the five chiral anion pairs investigated, the best stereo-discrimination was observed for *N*Boc-proline carboxylate and BINOL-PO_4^- (Table 4.5), which possess the most conformationally rigid chiral units. For the remaining anion stereoisomers, the magnitudes of ξ increase in the order mandelate < *N*Boc-leucine < *N*Boc-tryptophan, mirroring the increase in steric bulk of the substitutents around each anion's chiral centre. Notably, the influence of sterics in governing the effectiveness of chiral selectivity by rotaxane **4.15** appear to override the beneficial contributions of the HB donor α-OH group of mandelate previously reported by Jurczak *et. al.*,[128] as its enantiomers were found to be most poorly discriminated.

To appreciate the roles of the rotaxane **4.15**'s interlocked cavity for chiral discrimination, the enantio-selectivities of the free macrocycle **4.10I** and acyclic axle components were compared. Comparing the values of ξ for rotaxane **4.15** and macrocycle **4.10I** in Tables 4.5 and 4.4 respectively revealed notably augmented chiral discrimination by the rotaxane, with the greatest improvements seen for the conformationally highly-rigid *N*Boc-proline carboxylate and BINOL-PO_4^- anion enantiomers. Undoubtedly, this is a consequence of the more complete three-dimensional anion guest encapsulation possible within the rotaxane's chiral binding pocket compared to the predominantly two-dimensional planar macrocycle chiral surface of **4.10I** (Figure 4.21), allowing more stereoselective interactions to take place for more effective enantio-discrimination.

The free cationic chiral axle **4.29** was prepared by *N*-methylating the pyridine unit of the neutral chiral axle side product (**4.23**), obtained during the CuAAC-AMT synthesis of **4.15**, by iodomethane followed by anion exchange to its PF_6^- salt (Figure 4.28A). When ^{1}H NMR titrations were performed using **4.29** with *N*Boc-(*S*)-proline carboxylate in the same solvent mixture as that for rotaxane **4.15**, the most prominent signal shifts observed where those of the internal pyridinium proton H_1 (Figure 4.28B), which moved downfield by +0.25 ppm in the presence of 5.0 equivalents of added anion. Unlike rotaxane **4.15**, anion addition led to negligible shifts of the proximal stopper proton H_3, despite the presence of the adjacent amide units capable of HB interactions with the anion. Clearly, the carboxylate is binding to axle **4.29** via a drastically different arrangement compared with rotaxane **4.15**, where the absence of the macrocycle component in the former host allows direct anion interaction with the axle's central

pyridinium-3,5-bis(iodotriazole) motif (*vide infra*). This binding conformation appears to limit the stereo-specific interactions with the axle's asymmetric units responsible for chiral discrimination, as seen from the small perturbations of the H_4 and H_5 resonances around the free axle's point-chiral centre. Unsurprisingly, this resulted in poorer enantioselectivity than rotaxane **4.15** as evident from the binding isotherms of the guest enantiomers (Figure 4.28C) and magnitudes of ξ shown in Table 4.5.

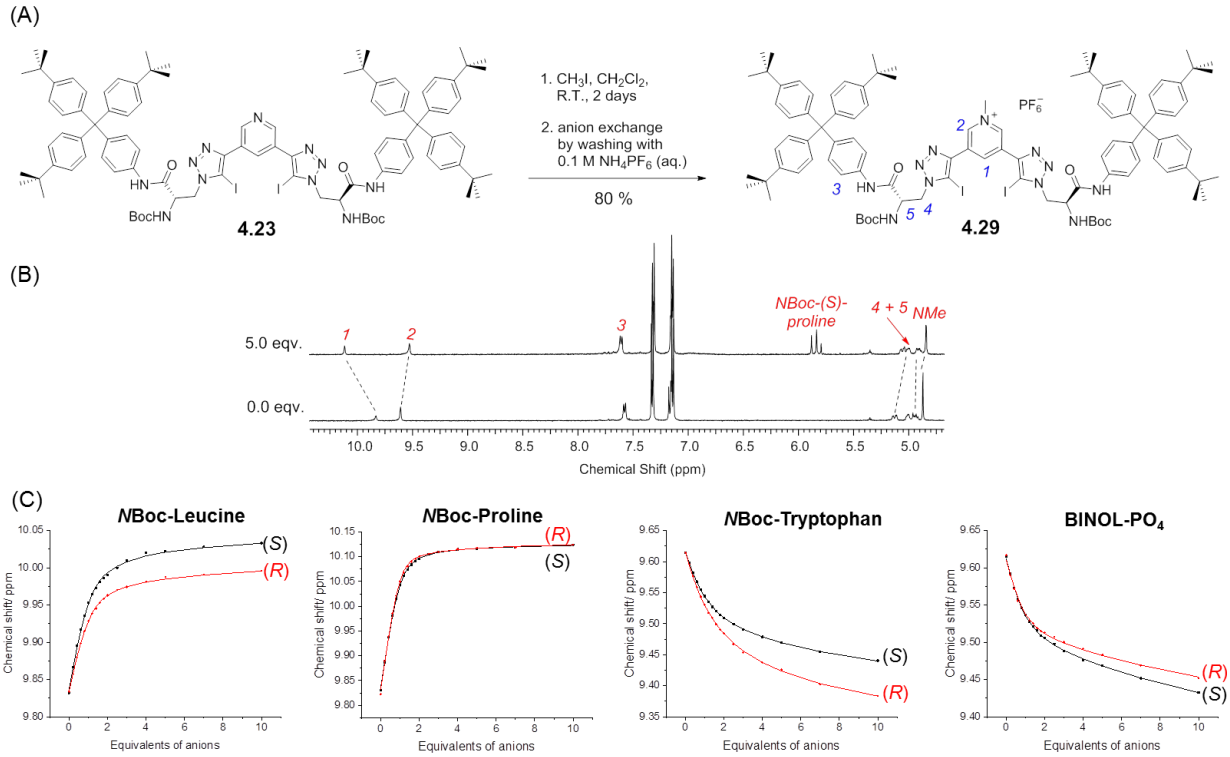


***Figure 4.28**. (A) Synthesis of free cationic axle **4.29**; (B) Partial ^{1}H NMR spectrum of **4.29** in the presence of 0.0 and 5.0 equivalents of NBoc-(S)-proline carboxylate; (C) Binding isotherms obtained by monitoring the shifts of H_1 with increasing quantities of both (S) and (R)-guest anion enantiomers ([**4.29**] = 1.0 mM, d_6-acetone/ D_2O 98:2, T = 298 K).*

The importance of each individual chiral interlocked component in determining the overall enantio-selectivity of the rotaxane was determined by comparing the binding results of rotaxane analogues **4.16** and **4.17**, possessing one chiral and one achiral component each. Using *N*Boc-(*S*)-proline carboxylate as a representative example, the presence of oxoanions perturbed the proton resonances of rotaxane **4.16** arising from the macrocycle component's (*S*)-BINOL group, as well as those on the axle (H_1 and H_6 especially in Figure 4.29A).

Similarly, notable shifts of protons H_a, H_b, H_c and H_e on the macrocycle component, and H_1 and H_5 on the axle were seen for rotaxane **4.17** (Figure 4.29B). These observations suggested that for both rotaxanes, the anions were binding in the chiral interlocked binding space between the axle and macrocycle components as envisaged in Figure 4.22. Given that only one interlocked component surrounding the binding site is chiral, fewer enantio-specific host-guest interactions can be expected compared to rotaxane **4.15** when the chiral anion is bound, resulting in the expected poorer enantioselectivity in general as shown in the binding isotherms of Figure 4.29 and Table 4.5. Figure 4.30 summarizes the guest enantiomer preference and magnitudes of enantioselectivity of chiral discrimination by all chiral XB host molecules collected in Table 4.5 visually.

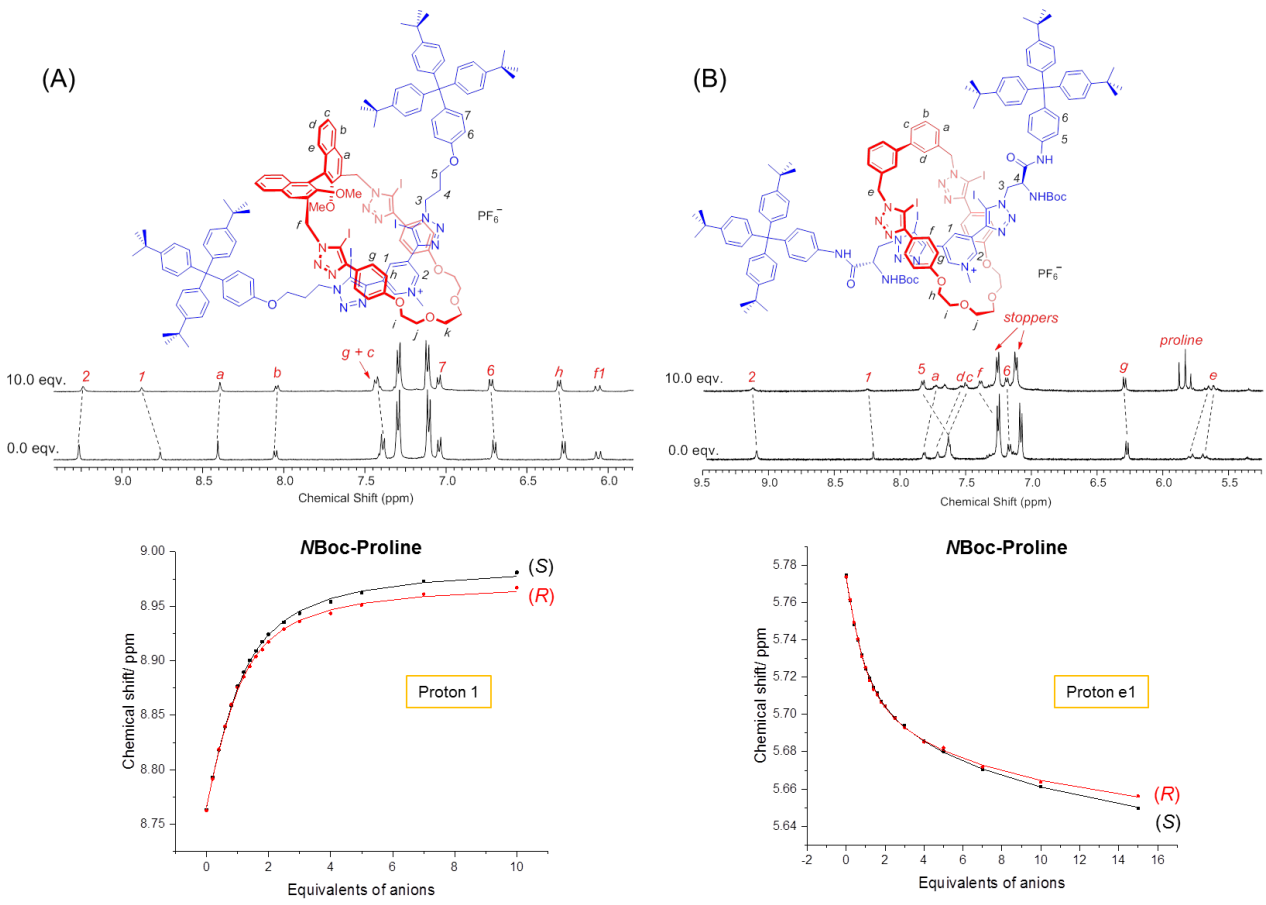


***Figure 4.29**. (Top) Partial ^{1}H NMR spectra of rotaxanes (A) **4.16** (d_6-acetone/ D_2O 99:1) and (B) **4.17** (d_6-acetone/ D_2O 98:2) in the presence of 0.0 and 10.0 equivalents of NBoc-(S)-proline carboxylate; (Bottom) Binding isotherms obtained by monitoring the shifts of H_1 and H_{e1} for **4.16** and **4.17** respectively with increasing quantities of both (S) and (R)-guest enantiomers ([host] = 1.0 mM, T = 298 K).*

Table 4.5. Anion association constants (K/ M^{-1}) for chiral anion pairs and the magnitudes of chiral selectivity ($\xi = K_S/K_R$) by rotaxanes **4.15**, **4.16**, **4.17** and free axle **4.29**.[a]

	K_S	K_R	ξ	K_S	K_R	ξ
	Rotaxane **4.15** [b]			Rotaxane **4.16** [c]		
(*N*Boc-Leu)$^-$	2450 ± 154	1511 ± 131	1.62 ± 0.17	138 ± 11	471 ± 38	0.29 ± 0.03
(*N*Boc-Trp)$^-$	4990 ± 196	2886 ± 203	1.73 ± 0.14	471 ± 37	760 ± 45	0.62 ± 0.06
(*N*Boc-Pro)$^-$	4298 ± 125	1465 ± 52	2.93 ± 0.13	1719 ± 59	2586 ± 110	0.66 ± 0.04
(BINOL-PO_4)$^-$	547 ± 16	1170 ± 99	0.47 ± 0.04	354 ± 22	631 ± 48	0.56 ± 0.06
(Mandelate)$^-$	2372 ± 182	1569 ± 37	1.51 ± 0.12	350 ± 2	498 ± 31	0.70 ± 0.04
	Rotaxane **4.17** [d]			Axle **4.29** [e]		
(*N*Boc-Leu)$^-$	K_1 = 2100 ± 147 K_2 = 62 ± 5	K_1 = 2244 ± 99 K_2 = 49 ± 3	ξ_1 = 0.94 ± 0.08	K_1 = 6027 ± 321 K_2 = 166 ± 9	K_1 = 4630 ± 86 K_2 = 142 ± 11	ξ_1 = 1.30 ± 0.07
(*N*Boc-Trp)$^-$	K_1 = 1905 ± 107 K_2 = 34 ± 2	K_1 = 2253 ± 138 K_2 = 32 ± 3	ξ_1 = 0.85 ± 0.07	K_1 = 2581 ± 91 K_2 = 56 ± 2	K_1 = 1836 ± 117 K_2 = 95 ± 6	ξ_1 = 1.41 ± 0.10
(*N*Boc-Pro)$^-$	K_1 = 4031 ± 100 K_2 = 55 ± 2	K_1 = 4468 ± 131 K_2 = 55 ± 2	ξ_1 = 0.90 ± 0.03	K_1 = 6193 ± 89 K_2 = 33 ± 1	K_1 = 5057 ± 128 K_2 = 39 ± 1	ξ_1 = 1.22 ± 0.04
(BINOL-PO_4)$^-$	K_1 = 4159 ± 100 K_2 = 86 ± 3	K_1 = 3491 ± 148 K_2 = 93 ± 4	ξ_1 = 1.19 ± 0.06	K_1 = 4861 ± 122 K_2 = 24 ± 1	K_1 = 5942 ± 270 K_2 = 17 ± 1	ξ_1 = 0.82 ± 0.04

[a] Values of K calculated using the WinEQNMR2 software[96] using a host-guest 1:2 binding model in d_6-acetone/ D_2O 98:2 monitoring the perturbation of proton H_{f1} for all hosts unless otherwise stated; $\xi = K_S/K_R$ only for the first binding event; anions added as TBA salts; [host] = 1.0 mM, T = 298 K. [b] Although rotaxane **4.15** bound chiral anions with host-guest 1:2 binding stoichiometry, K_2 < 10 M^{-1} for all cases. [c] Titrations were performed in d_6-acetone/ D_2O 99:1 due to weak binding, with the exception of (BINOL-PO_4)$^-$ for which H_{f1} gave substantial shifts, axle pyridinium proton H_1 was monitored instead; values of K fit using a host-guest 1:1 binding model, with no evidence of a second binding event occurring. [d] Macrocycle proton H_{e1} monitored; [e] Internal pyridinium proton H_1 monitored.

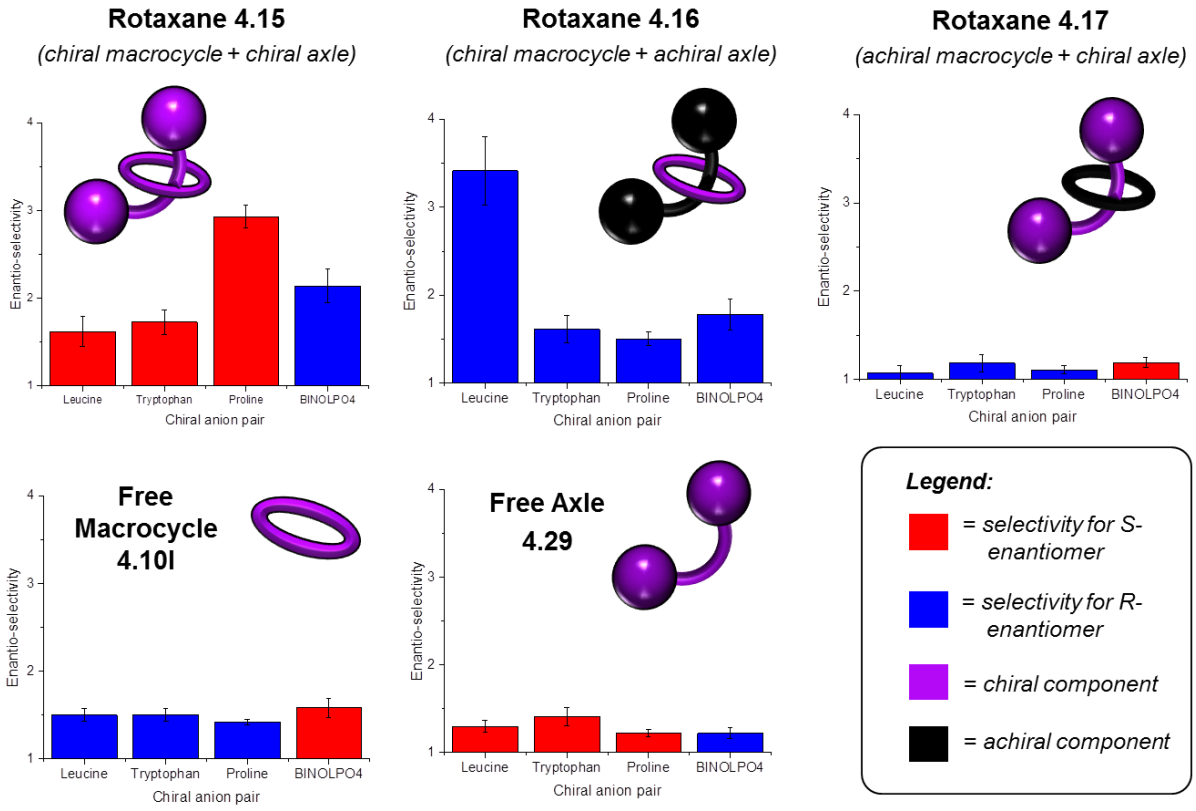


***Figure 4.30**. Bar chart summarising the magnitudes of chiral selectivity and enantiomer binding preference by rotaxanes **4.15**-**4.17** as well as free macrocycle **4.10l** and axle **4.29**.*

Comparing the anion affinities of the XB chiral hosts in Table 4.5 revealed a general decrease of the anion binding strengths in the order of axle **4.29** > rotaxane **4.15** ≈ rotaxane **4.17** > rotaxane **4.16**. Despite having four convergent XB donor groups in their central regions, the rotaxanes bound the chiral oxoanions surprisingly more weakly than free chiral axle **4.29** possessing just two iodotriazole units presumably due to their topologically and sterically constrained binding cavities (*vide infra*). Interestingly, monocationic **4.15**, **4.17** and **4.29** bound the oxoanions more strongly than dicationic free macrocycle **4.10I** (Table 4.4), which implied that host-guest electrostatic attractions were not dominating the binding affinities, and that other secondary non-covalent interactions such as HB and even donor-acceptor π-π stacking interactions play significant roles (*vide infra*). Indeed, the importance of these interactions can be clearly seen from the significantly diminished binding affinities seen for rotaxane **4.16**, which contains the unfunctionalised propylene achiral axle component, compared with rotaxanes **4.15** and **4.17**. In fact, anion affinity reduction was so significant that the binding studies of rotaxane **4.16** had to be performed in a less-competitive solvent mixture of d_6-acetone/D_2O 99:1 (*v/v*) to achieve appreciable proton shifts for reliable values of association constants to be obtained. However, although all three rotaxanes investigated possess the same structural skeleton, their respective anion binding cavities are very different from one another due to the various combinations of chiral and achiral components. This results in each XB rotaxane host possessing unique chiral anion guest preference. For instance, *N*Boc-(*S*)-tryptophan carboxylate is bound most strongly by rotaxane **4.15**, while *N*Boc-(*R*)-proline carboxylate is bound by **4.16** and **4.17** with the highest affinity. Significantly, the *N*Boc-proline carboxylate enantiomers exhibit consistently strong anion binding for all chiral XB hosts, with smaller variations in binding affinity compared to the other chiral anion pairs. Likely due to their smaller size compared to all the other anion pairs investigated, they are expected to encounter less steric repulsions with the bulky chiral groups decorating the hosts' binding cavities, allowing deeper penetration and hence stronger binding.

Important insights regarding the chiral discrimination behaviour of the rotaxanes can be gleaned from Figure 4.30. Regarding magnitudes of chiral selectivity, replacing the chiral axle of rotaxane **4.15** with an achiral axle in **4.16** generally afforded only small reductions in

selectivity. A notable exception, however, is *N*Boc-leucine carboxylate, which displays greatly enhanced selectivity, attributed to optimal host-guest stereo-complementarity for the (*S*)-enantiomer. Contrastingly, substituting rotaxane **4.15**'s chiral macrocyclic component for an achiral counterpart in rotaxane **4.17** resulted in an unexpectedly large loss of stereo-selectivity for all chiral anion pairs investigated to the extent that better discrimination was seen for free axle **4.29**. While **4.17** effectively showed no selectivity for the amino-acid derived chiral anions, slightly better discrimination was seen for the sterically bulky and rigid BINOL-PO_4^- enantiomers with a modest preference of only 1.19 ± 0.06 for the (*S*)-enantiomer. This suggests that in the design of this series of rotaxanes, the macrocycle component played more important roles than the axle in influencing enantioselectivity (see Section 4.3.4.2 for a rationalisation).

Despite this, the influences of each interlocked component on the rotaxanes' overall enantiomer binding preference are more subtle. For instance, while the macrocycle component of rotaxane **4.16**, being its only chiral component, appears to be driving a generally similar preference for binding the (*R*)-anion enantiomers as the free macrocycle **4.10l**, the selectivity patterns observed are not entirely identical, as exemplified with BINOL-PO_4^-. Rotaxane **4.17**, bearing only the chiral axle, surprisingly exhibits the opposite enantiomer binding preference to that of the chiral axle **4.29**. Although these two examples seem to suggest that the influence of the macrocycle also outweighs that of the axle in enantiomer binding preference, rotaxane **4.15** displays the same preference as the free chiral axle, contrary to the expected macrocycle-dominated behaviour. As previously noted, each chiral rotaxane's structurally-unique interlocked cavity results in different contributions of attractive and repulsive interactions responsible for anion binding. The complex interplay of these multiple interactions result in subtle energy differences between the various rotaxane-anion diastereomeric complexes, which govern enantiomer preference in each case, making it difficult to predict their behavior *a priori* by extrapolation from the free chiral axle and macrocycle host molecules alone. Nevertheless, all point-chiral amino acid derivatives were found to exhibit the same chiral selectivity pattern with each host molecule (e.g. all (*S*)-selective for rotaxane **4.15** and all (*R*) for macrocycle **4.10l**). It is interesting that the chiral

BINOL-PO_4^- enantiomers generally gave opposite selectivities in comparison to the amino acid derivatives.

4.3.4.2 Computational Modelling Studies

To shed light on the chiral discrimination behaviour of the chiral rotaxanes, MD simulations were performed in solution by Professor Vítor Felíx and Dr. Igor Marques at the University of Aveiro, Portugal. *N*Boc-proline carboxylate anion enantiomers were used as the model guest species for these studies as they were largely representative of the amino acid derivatives' binding behaviour (Figure 4.30). The initial host-guest binding scenarios were generated in the gas-phase via DFT geometry optimisations with the CAM-B3LYP functional using TeraChem,[114–119] differing in the orientations of each guest enantiomer within each host binding cavity (labelled S_A, S_B, R_A and R_B- details in Appendix C). Thereafter, each initial host-guest complex was immersed in periodic cubic boxes composed of suitable numbers of acetone and water molecules for the MD simulations, in accordance with the ^{1}H NMR titrations. The MD simulations were performed using the AMBER16 software[120] taking advantage of GPU acceleration, with the rotaxanes' components being described with the General AMBER Force Field (GAFF)[109,110] and XB interactions modelled using the extra point of charge approach.[104] Five independent 20 ns MD runs were performed for each DFT optimized complex, yielding sets of binding arrangements generally independent of the initial conformations, with the most frequent of these forming the basis of the following discussions. The modelling experiments are described in more detail in the Appendices.

Owing to the spatially and geometrically-restricted interlocked cavity of rotaxane **4.15**, each *N*Boc-proline carboxylate enantiomer showed distinct binding arrangements. Nevertheless in all cases, the (*S*)-anion enantiomer is held within the chiral binding pocket of rotaxane **4.15** in the space between the axle and macrocycle components throughout all simulation runs, bound by XB and HB interactions from both interlocked components. Notably, several water molecules bound to the host by XB and HB interactions were found to actively participate in anion binding by forming bridging HB interactions with the carboxylate anion held in the rotaxane's binding cavity. For instance, the most frequent binding arrangement shows a

direct XB interaction between the axle's central pyridinium-3,5-bis(iodotriazole) unit with one oxygen atom of the anion's carboxylate group (Figure 4.31A). The other carboxylate oxygen atom forms a HB network with water molecules held by a XB interaction with the macrocycle iodotriazole unit (C-I···OH_2) and the *N*Boc and amide units in close proximity on the axle. In the second most common binding arrangement (Figure 4.31B), each carboxylate oxygen atom is held by a direct XB interaction, one from an iodotriazole from the macrocycle and the other from the axle. Simultaneously, one of these oxygen atoms is indirectly bound to the axle's *N*HBoc and amide unit bridged by a single water molecule. It is noteworthy that due to the anion's binding geometry, largely dictated by the iodotriazole-carboxylate XB interactions, the rigid proline pyrrolidine ring is brought into close proximity with the chiral units flanking the binding site, especially the (*S*)-BINOL unit on the macrocycle, which also accounts for the ^{1}H NMR signal perturbations seen on both components during the titration experiments (Figure 4.27A).

In stark contrast, the *N*Boc-(*R*)-proline carboxylate enantiomer was found to bind significantly less favourably by MD simulations. Systematic decomplexation of the (*R*)-guest was found for one of the initial DFT-generated binding scenarios, while the other showed slightly more preferable association. Even so, the anion's carboxylate group was held by one weak and sporadically-broken direct halogen bond from the rotaxane's macrocycle component, which is assisted by a $(N–H)_{host}\cdots OH_2\cdots(O=C)_{guest}$ bridge from the rotaxane axle's *N*Boc unit. However, for a significant simulation period, the anion was also found outside the rotaxane binding pocket, interacting peripherally only with the axle's amide NH group. This dynamical behavior suggests a significantly weaker interaction between rotaxane **4.15** and the *N*Boc-(*R*)-proline carboxylate than with the (*S*)-enantiomer, accounting for its (S)-selectivity shown in Table 4.5.

As seen from Figure 4.31, the *N*Boc-proline carboxylate anions are encapsulated within rotaxane **4.15**'s conformationally-rigid and spatially-restricted binding site, surrounded and held by stereo-dependent interactions in a three dimensional manner, unlike that for free macrocycle **4.10I** described in Section 4.3.2 and shown in Figure 4.21. Unsurprisingly, this accounted for the notably improved enantio-selectivity seen with the rotaxane. For axle **4.29**,

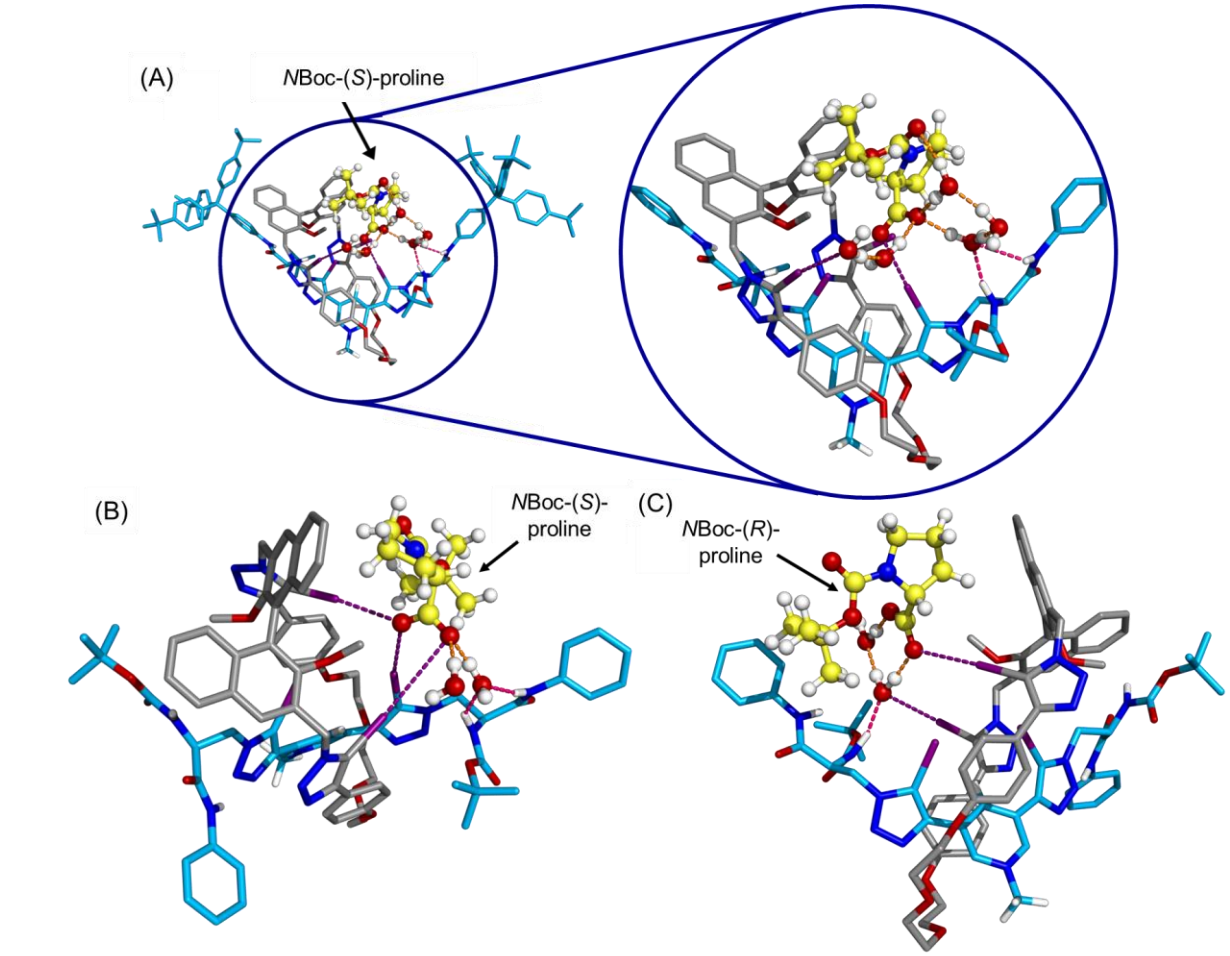


***Figure 4.31**. (A) The most common binding arrangement of rotaxane **4.15** with NBoc-(S)-proline carboxylate, with an expanded view of the binding cavity showing the contributions of the various non-covalent interactions and the water bridges; (B) view of the second most common binding arrangement of NBoc-(S)-proline carboxylate within **4.15**'s binding cavity; (C) the most common binding arrangement of **4.15** with NBoc-(R)-proline carboxylate. XB interactions are depicted by purple dashes, HB interactions between the axle units and water molecules are shown in pink, while those between water molecules are in orange. Rotaxane stoppers omitted from (B) and (C) for clarity.*

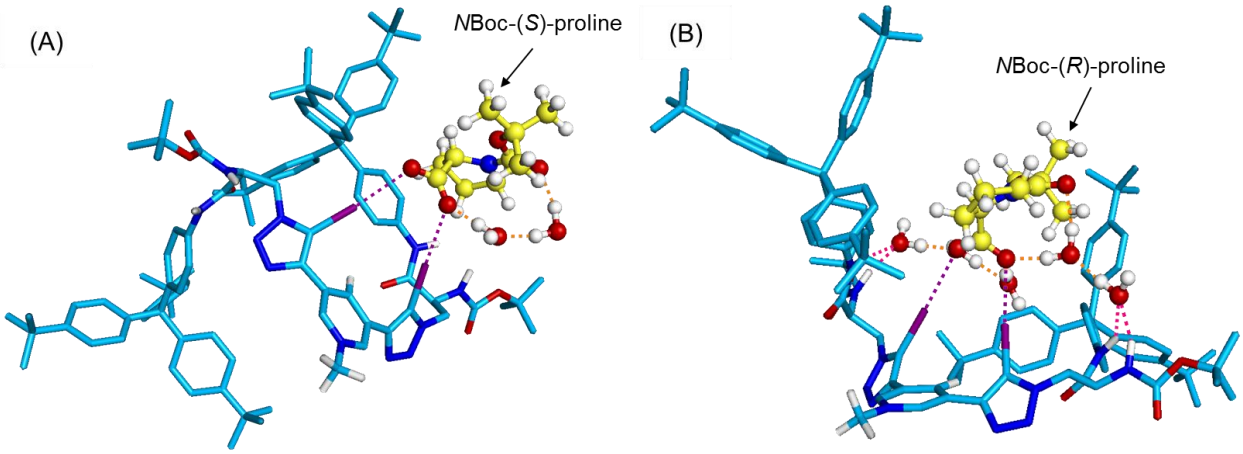


***Figure 4.32**. The most common binding arrangement of free axle **4.29** with (A) NBoc-(S)-proline and (B) NBoc-(R)-proline carboxylate anions. XB and HB interactions are depicted as that shown for Figure 4.31.*

MD simulations corroborated the binding geometry deduced from ^{1}H NMR titrations, showing both *N*Boc-proline carboxylate guest enantiomers to be tightly bound to the axle's central pyridinium-3,5-bis(iodotriazole) motif *via* direct XB interactions (Figure 4.32), which also accounted for the strong anion associations observed in Table 4.5. Due to this binding arrangement, both anion enantiomers can interact only indirectly with the axle's point-chiral amide binding units through water bridges, which is in particular evident with *N*Boc-(*R*)-proline carboxylate. It should be noted that these water bridges are highly non-directional due to the poor linearity of the HB interactions involved, facilitating anion binding even for anion guests which are less stereo-complementary to the point-chiral groups on the free axle, justifying the axle's general poor enantioselectivity. Furthermore, the XB interactions to *N*Boc-(*S*)-proline carboxylate are maintained throughout the sampling time, while those to the (*R*)-guest enantiomer are sporadically interrupted, with one halogen bond being occasionally established with water molecules, possibly accounting for the observed modest chiral selectivity for *N*Boc-(*S*)-proline carboxylate.

Analogous MD simulations on the binding of *N*Boc-(*S*/*R*)-proline carboxylate enantiomers to rotaxanes **4.16** and **4.17** also revealed insights on their chiral discrimination behaviour, as well as the observed dominance of the rotaxane macrocycle component in determining stereo-selectivity. With rotaxane **4.16**, bearing only a chiral macrocycle subunit, MD runs revealed that the (*R*)-carboxylate is more strongly bonded to the rotaxane binding cavity compared to the (*S*)-enantiomer, accounting for the rotaxane's observed (*R*)-selectivity. In the most common binding scenario with the (*R*)-enantiomer anion guest (Figure 4.33A), both oxygen atoms on the carboxylate unit are held by three direct XB interactions, with two arising from the macrocycle iodotriazoles and the other from the axle component. Despite a lower water content in the solvent mixture (acetone/ water 99:1 *v*/*v*), these XB interactions are still susceptible to bridging by water molecules which insert into the iodotriazole-carboxylate XB interactions to form $(C\text{-}I)_{host}\cdots(OH_2)_2\cdots(O{=}C)_{anion}$ networks, as depicted in Figure 4.33B. Contrastingly, the simulations show systematic decomplexation of the fully-hydrated (*S*)-anion enantiomer from rotaxane **4.16**'s binding pocket during the MD runs. Importantly, the unfunctionalised propylene arms of its axle component do not allow the formation of (N–

H)$_{host}$···OH$_2$···(O=C)$_{anion}$ bridges seen between the bound anion and rotaxane **4.15**, which aid in anchoring the anion within the rotaxane's cavity. The fact that anion binding is now driven solely by the sporadically-broken XB interactions from the iodotriazole units results in the dramatically reduced anion binding strength shown in Table 4.5.

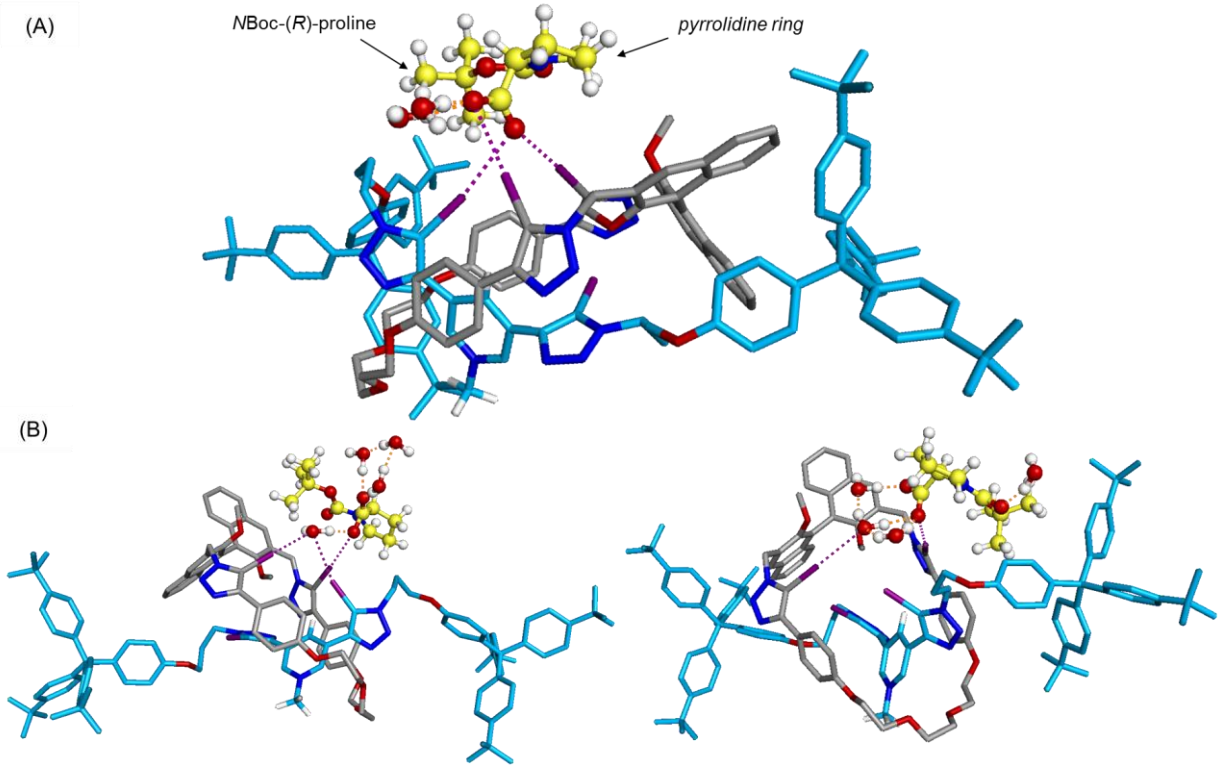


***Figure 4.33**. (A) Illustrative binding scenario of rotaxane **4.16** via direct XB formation with the carboxylate group of the NBoc-(R)-proline anion; (B) Binding arrangements of the same rotaxane-anion complex with indirect XB interactions bridged by water molecules. XB and HB interactions are depicted as described in Figure 4.31.*

Substituting the bulky chiral (*S*)-BINOL group on rotaxane **4.15**'s macrocycle component with the less sterically-encumbering achiral biphenyl spacer in rotaxane **4.17** considerably enlarges the set of possible anion binding arrangements possible within the rotaxane cavity, such that the final MD binding scenarios for both anion enantiomers are highly-dependent on the initial DFT optimized binding arrangements (Figure 4.34). Typically, the *N*Boc-(*S*)-proline carboxylate is bound by two XB interactions, either directly from the iodotriazoles or indirectly via water bridges, with some HB assistance between the axle component and the *N*Boc group of the anion (Figure 4.34A). However, more frequent XB

interactions are seen for the (*R*)-guest enantiomer, which is generally held by three halogen bonds across the different binding arrangements (Figure 4.34B), possibly accounting for the slightly enhanced (*R*)-selectivity seen for the amino acid anion derivatives. These XB interactions are often assisted by water-bridged HB interactions similar to rotaxane **4.15**, resulting in the comparable anion affinities observed (Table 4.5).

Carboxylate anion binding by all three rotaxanes **4.15**-**4.17** occurs preferentially via XB interactions with the iodotriazoles in the central region of each interlocked binding cavity, dictating the orientation of anion coordination in each case. Due to the reduced steric constraints and geometric flexibility of anion binding in rotaxane **4.17**'s cavity, the proline's asymmetric pyrrolidine rings can be either oriented towards the achiral biphenyl spacer on the macrocycle component, or held by poorly-directional HB interactions and water bridges above the axle's chiral centre (Figure 4.34). Together with the conformational flexibility of the substituents around the axle's point-chiral centre, these factors allow opposite anion enantiomers to adopt remarkably similar binding arrangements (e.g. the complexes shown in the bottom left and top right of Figure 4.34), resulting in the poor enantioselectivity seen. On the other hand, the XB-directed anion binding geometries for rotaxanes **4.15** and **4.16** forces the proline's asymmetric units into close proximity with the macrocycle components' rigid and sterically-bulky chiral (*S*)-BINOL groups (Figure 4.31 and Figure 4.33A). This manifests in the observed dominant influence of the chiral macrocycle component over the axle for effective chiral discrimination to occur in our rotaxane design.

The MD modelling experiments also offered insights on the general opposite enantiomer preference observed for BINOL-PO_4^- compared to the amino acid anion derivatives. Using the optimal binding arrangements of (*S*/*R*)-BINOL-PO_4^- in the binding cavity of rotaxane **4.15** obtained from DFT optimisations, five independent 20 ns MD runs were performed, which confirmed the stability of the host-guest diastereomeric complexes. As shown in Figure 4.35, each BINOL-PO_4^- enantiomer was bound to the rotaxane via a single phosphate oxygen atom by two convergent XB interactions of comparable dimensions exclusively from the rotaxane axle component's iodotriazoles. Importantly, the spatial arrangement of the bound anions permitted the (*R*)-BINOL-PO_4^- guest to be further stabilised

by additional π···π stacking interactions with the macrocycle component's (*S*)-BINOL unit (Figure 4.35B), whilst no evidence of such interactions could be discerned for the opposite anion enantiomer (Figure 4.35A), resulting in a binding preference for the former.

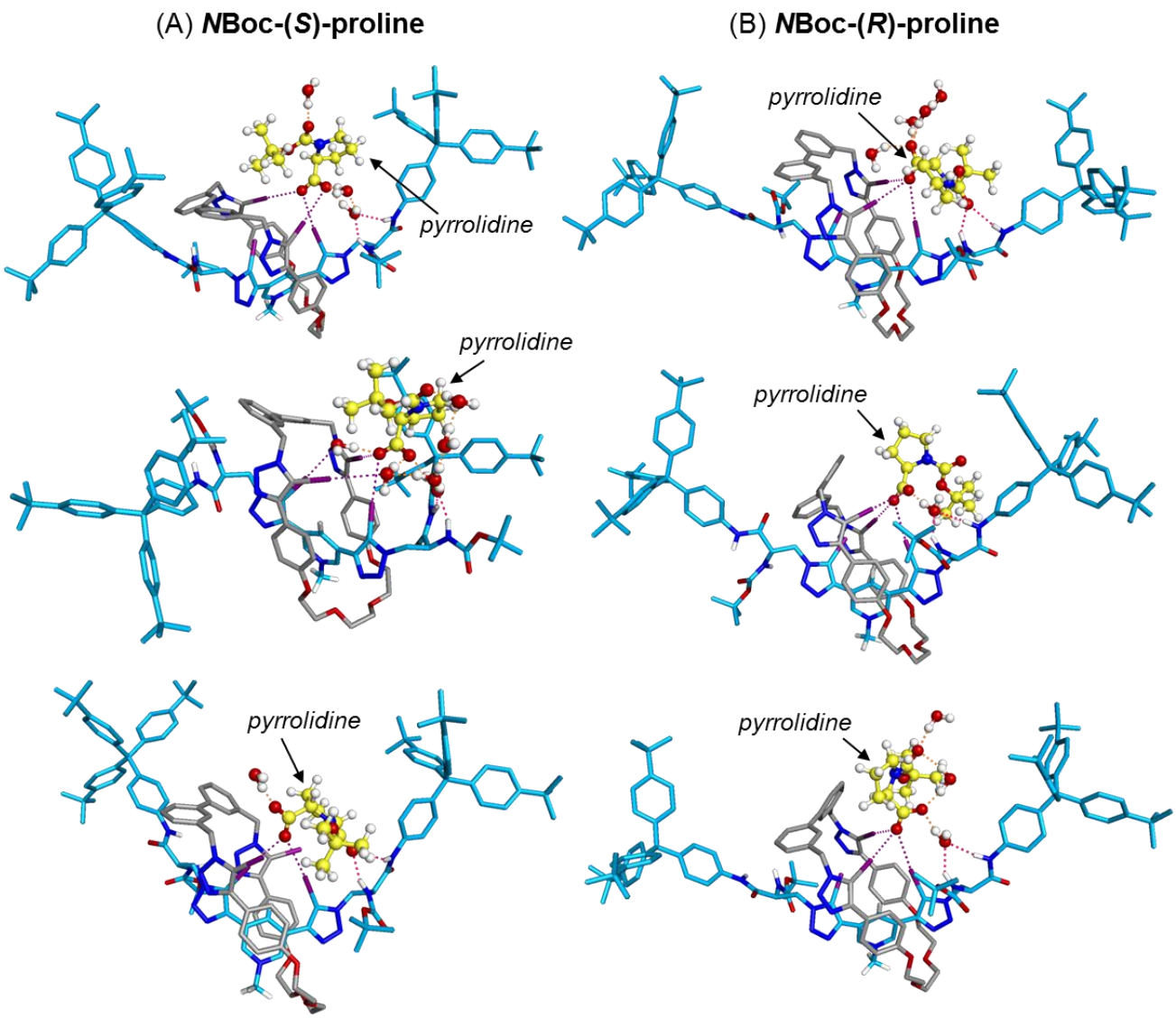


***Figure 4.34**. Illustrations of the most common binding scenarios of rotaxane **4.17** with (A- left column) (S)- and (B- right column) (R)-NBoc-proline carboxylate, from initial binding scenarios S_A (top left and middle left), S_B (bottom left), R_A (top right) and R_B (middle right and bottom right). XB interactions are shown in purple, while the axle's HB interactions with the water molecules or to the anions are shown as pink dashed lines.*

To sum up, this present family of chiral XB [2]rotaxanes were found to exhibit generally augmented stereo-selective anion binding compared to their free non-interlocked components

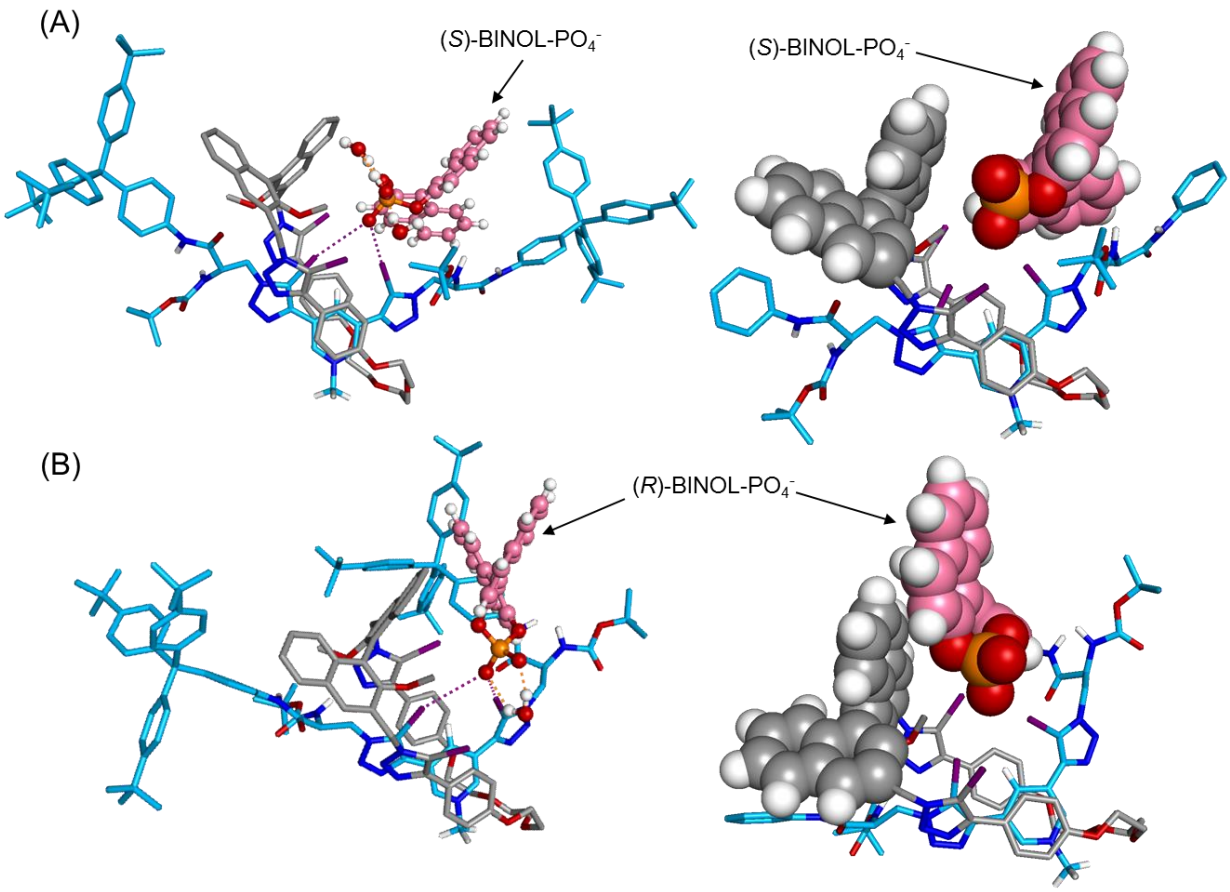


Figure 4.35. *Illustrative binding scenarios of rotaxane* ***4.15*** *with (A) (S)-BINOL-PO_4^- and (B) (R)-BINOL-PO_4^-. The space filling models (right column) of the BINOL groups on both the rotaxane and the anion guests clearly show the existence of aromatic π-π stacking interactions for the (R)-BINOL-PO_4^- guest, and not for the (S)-enantiomer. XB and HB interactions are depicted as described in Figure 4.31.*

only if they possess a chiral macrocycle component. This is an important consequence of the generally more favourable XB-oxoanion interactions with the iodotriazole units in the centre of the rotaxanes' interlocked cavity compared with HB from the axle components. Thus arguably, chiral discrimination of each point-chiral enantiomeric anion pair may be said to obey the TPI/SR model, where each anion is anchored by at least two attractive interactions (XB, HB or via water bridges) from at least two distinct sites on the rotaxane framework, which orientates the anion towards the macrocycle component's (*S*)-BINOL group for the crucial stereochemically-dependent interaction necessary for enantio-selectivity. Although the rotaxanes' axle component exerted relatively minor influence on the overall chiral selectivity, it was found to be crucial for strong oxoanion binding by the rotaxane via facilitating the formation of water bridges necessary to anchor the anion within the binding cavity. Nevertheless, it proved

difficult to predict the enantiomer preference for each chiral rotaxane host from the behaviour of their individual non-interlocked components *a priori*, largely due to the extremely subtle interplay of attractive and repulsive non-covalent host-guest interactions in three dimensions, often greatly and unpredictably influenced by the hydration shell of each oxoanion. Despite the similarities to chiral discrimination by natural enzymes seen in Section 4.1.2, these natural receptors still greatly outperform abiotic rotaxanes **4.15**-**4.17**. The following sections explore the further usage of chiral rotaxanes containing different structures and functionalities to better understand the behaviour of this unique class of chiral hosts in enantio-discrimination.

4.3.5 Towards A Chiral Thiourea-containing [2]Rotaxane

Thioureas are versatile and strong HB donors which have been shown to favour binding of oxoanions over halides.[129] Inspired by their proven effectiveness and diverse applications in asymmetric organocatalysis,[130–132] including examples involving anion binding as key intermediate processes,[133,134] synthetic attempts were made to incorporate thioureas into the macrocycle component of rotaxanes **4.30** and **4.31** immediately adjacent to the (*S*)-BINOL motif, as shown in Figure 4.36. Compared to rotaxanes **4.15** - **4.17**, where the anionic motif of the guest species are primarily coordinated by the iodotriazoles in centre of the binding cavity, this structural modification in **4.30**/ **4.31** will either bind the anion closer to the macrocycle (*S*)-BINOL motif, or enhance coordination of other Lewis basic portions of the anions (e.g. *N*Boc oxygen atoms). In either scenario, the asymmetric portions of the chiral anion guests will be brought into closer proximity for interaction with the (*S*)-BINOL motif for enhanced stereo-selectivity.

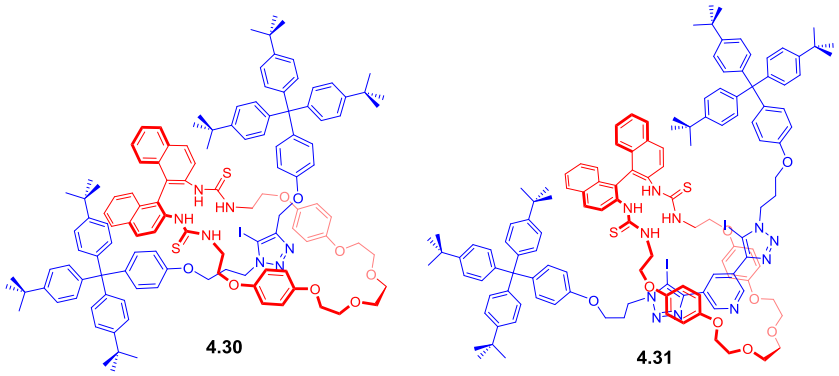


***Figure 4.36**. Design of chiral thiourea-XB [2]rotaxanes for stereo-selective anion binding.*

To synthesise the target [2]rotaxanes, the CuAAC-AMT strategy was adopted with macrocycle **4.32** (the macrocycle components of rotaxanes **4.30** and **4.31**), motivated by a recent thiourea-Cu(I) complex characterised by Nembenna and co-workers which was shown to be highly active and recyclable for the CuAAC reaction.[135] As shown in Figure 4.37A, the Cu(I) metal centre of Nembenna's complex adopts a trigonal planar ligand coordination environment, bound by two thiourea sulphur atoms. This suggested that it may be possible for the (*S*)-BINOL thiourea macrocycle **4.32** to bind Cu(I) in a similar manner (Figure 4.37B), with the metal catalyst favourably oriented above the macrocycle cavity for CuAAC-AMT rotaxane synthesis to occur.

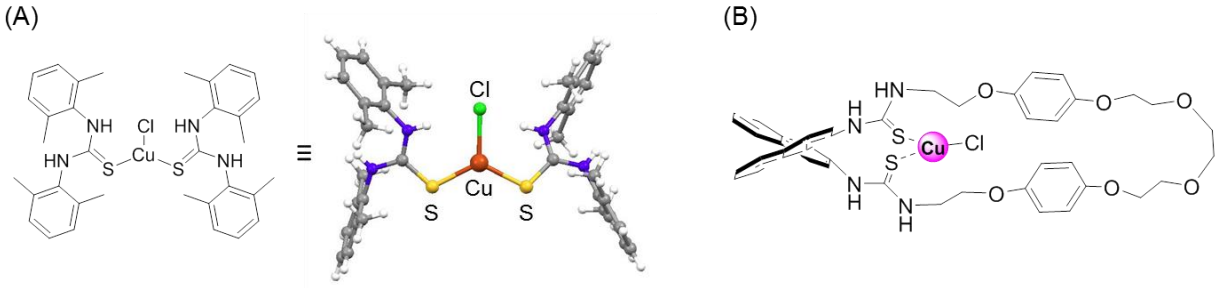
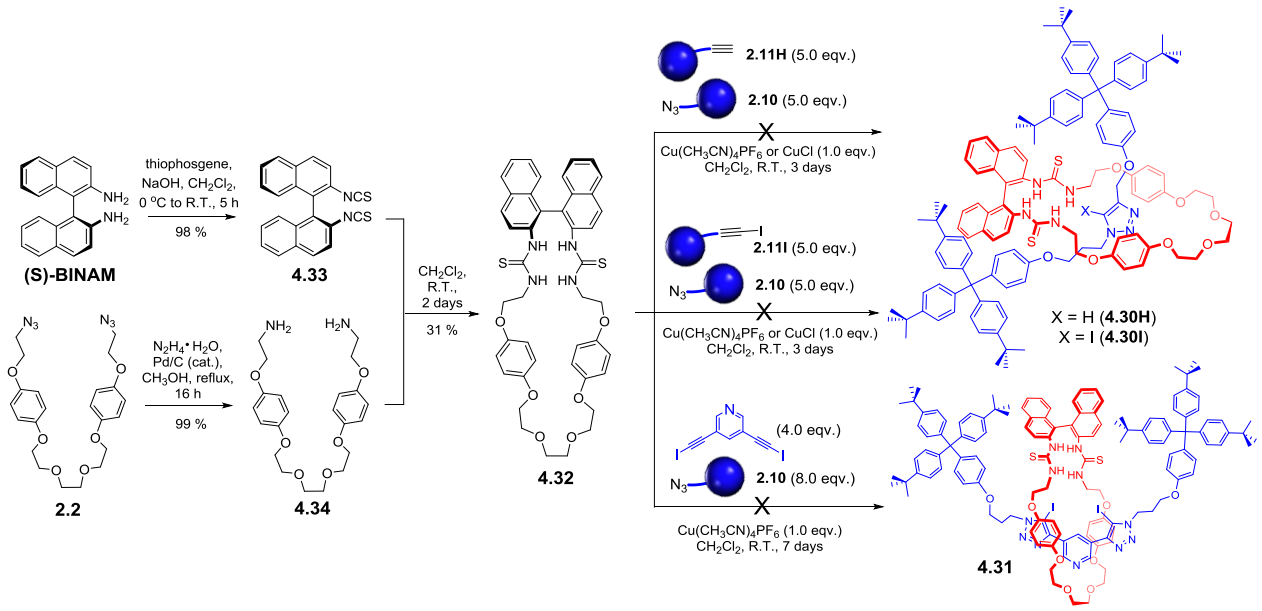


***Figure 4.37**. (A) Nembenna's CuAAC-active bis-thiourea complex of Cu(I) and its solid-state structure[135]; (B) expected Cu(I) coordination mode by bis-thiourea macrocycle **4.32**, viewed from the top of the macrocycle plane.*

Macrocycle **4.32** was prepared as shown in Scheme 4.8. The (*S*)-BINOL bis-isothiocyanate synthon **4.33** was prepared using thiophosgene under basic conditions from commercially-available enantiopure (*S*)-BINAM, while the bis-amine synthon **4.34** was prepared by Pd/C-catalysed hydrazine reduction from bis-azide **2.2** (synthesis described in Chapter 2). Thereafter, reactions between equimolar quantities of **4.33** and **4.34**, performed under high dilution conditions, afforded the target macrocycle **4.32** in 31 % yield after chromatographic purification. To synthesise target rotaxane **4.30**, equimolar quantities of **4.32** and $[Cu(CH_3CN)]_4PF_6$ were stirred with five-fold excess of stoppered proto/iodoalkyne **2.11H/I** and stoppered azide **2.10** in degassed CH_2Cl_2 for 3 days. Despite the facile coordination of macrocycle **4.32** and Cu(I) observed in TLC, in which the macrocycle-Cu(I) complex displayed a dramatically lower R_f value than the uncomplexed **4.32**, no evidence of the target rotaxanes

could be observed by ESI-MS analysis of the respective crude reaction mixtures, whilst complete consumption of both axle precursors were observed. Changing the Cu(I) source to CuCl, according to Nembenna's procedure to synthesise this thiourea-Cu(I) complex, also failed to produce any rotaxane. Postulating that HB interactions between the strongly Lewis-acidic macrocycle thiourea motifs and 3,5-di(iodoethynyl)pyridine may encourage the formation of an adduct predisposed towards CuAAC-AMT rotaxane formation (as described for XB rotaxane **3.34I$_4$** in Chapter 3), the synthesis of target rotaxane **4.31** was then attempted by first stirring macrocycle **4.32** with the 3,5-di(iodoethynyl)pyridine synthon for 15 minutes before addition of $[Cu(CH_3CN)]_4PF_6$ and stoppered azide **2.10**. Unfortunately, no evidence of rotaxane could be detected after 7 days by ESI-MS or TLC analyses. The failure of the macrocycle-Cu(I) adduct to template rotaxane formation is perplexing, and may be possibly due to the close spatial separation between the ligating sulphur atoms of the macrocycle's thiourea groups, which may render the macrocycle cavity too sterically hindered for effective threading of the axle precursors to occur for rotaxane formation. Therefore, no further attempts at rotaxane synthesis were attempted using macrocycle **4.32**.



***Scheme 4.8**. Synthesis of chiral thiourea macrocycle **4.32** and attempts at CuAAC-AMT rotaxane synthesis.*

4.4 Stereo- and Geometric Discrimination of Dicarboxylates

4.4.1 Introduction

Dicarboxylates constitute a structurally highly-diverse class of anions which are extremely important in biology and industry. In biology, they play key roles in cellular metabolism and biosynthetic processes (e.g. succinate, fumarate, glutarate),[136,137] as well as in signal transduction as neurotransmitters (e.g. aspartate and glutamate).[138,139] Furthermore, dicarboxylates constitute key ingredients in important industries including plastics and manufacturing (e.g. furan-dicarboxylates, phthalates),[140,141] pharmaceutics (e.g. adipate, maleate, tartrate)[142,143] and food (e.g. glutamate, tartrate),[144,145] and unsurprisingly have also been implicated as environmental pollutants (e.g. phthalates, oxalate).[146] Other than their hydrophilicity[147] and propensity for acid-base protonation, the design of abiotic receptors capable of selectively binding and sensing one dicarboxylate species over others is further complicated by the structural diversity of the guests' spacer units between their anionic termini. For instance, this can take the form of structural homologues (e.g. aspartate and glutamate differing in structure by only one CH_2 methylene unit), which result in very similar physicochemical properties between members of a series, or exist as different regioisomers (e.g. *E*/*Z*-isomerism or varying positions of substitution on phthalates), possess different functional groups (e.g. amine, hydroxyl or keto) or exhibit stereo-isomerism (e.g. glutamate, aspartate) (Figure 4.38). These subtle structural variations can often lead to huge differences in biological activities, as exemplified by fumarate (*E*-alkene) and maleate (*Z*-alkene), where the former is an important Krebs cycle intermediate but the latter is a known inhibitor of the process and has been implicated in kidney diseases.[148–150] Therefore, the ability of abiotic receptors to selectively recognise and bind dicarboxylates is highly sought after and remains an area of active research.[151]

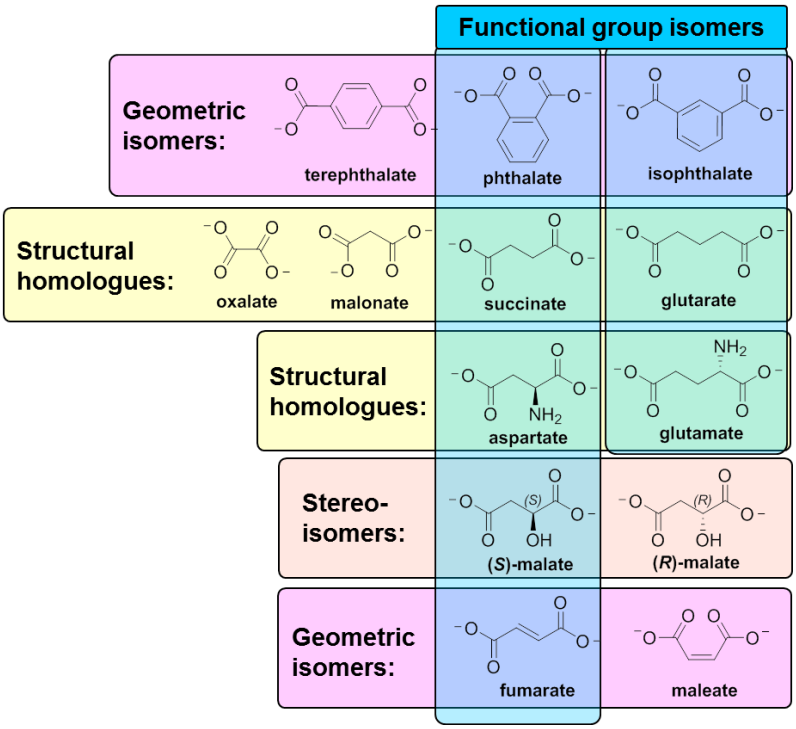


***Figure 4.38**. Structures of common dicarboxylate anions of biological and industrial importance and their structural relationships with each other.*

The ditopic nature of dicarboxylates necessitate that receptors designed for them are invariably structurally complementary, possessing two spatially separated Lewis acidic sites bridged by a spacer motif designed for geometric /stereo-selectivity or to elicit a sensory response to binding (Figure 4.29A). Receptors utilising HB-donor motifs are highly popular due to their ease of construction, often incorporating moieties such as ureas,[152–154] thioureas[155–158] or guanidiniums[159–161] due to their preferential association with Y-shaped carboxylate groups. These include Kilburn's glutamate-binding bis-thiourea macrocycle[30] (Figure 4.4B) and Costero's 1,2-disubstituted cyclohexane receptor (Figure 4.39B) which recognises maleate selectively over fumarate in DMSO owing to the spatial arrangement of the thiourea groups.[162] Anion coordinate-bond formation with Lewis acidic elements have also been investigated, such as Houston's tartrate-selective boronic-acid receptor (Figure 4.39C).[163] Finally, metal cations have been incorporated into host structures, which have enabled selective dicarboxylate sensing in competitive aqueous mixtures. For instance, Kim and co-workers reported a ditopic Cu^{2+} complex capable of binding oxalate over its longer-chain homologues malonate, succinate and glutarate in water at pH 7 due to optimal host-guest size

complementarity (Figure 4.39D).[164] Other metal complexes containing transition metals (e.g. Zn^{2+}, Co^{2+}),[165–167] lanthanides (e.g. Tb^{3+}, Eu^{3+})[168,169] and actinides (e.g. uranyl species)[170] have also been recently studied for selective dicarboxylate sensing. At the time of writing, the applications of σ-hole interactions in recognising and sensing of dicarboxylates has yet to be explored.

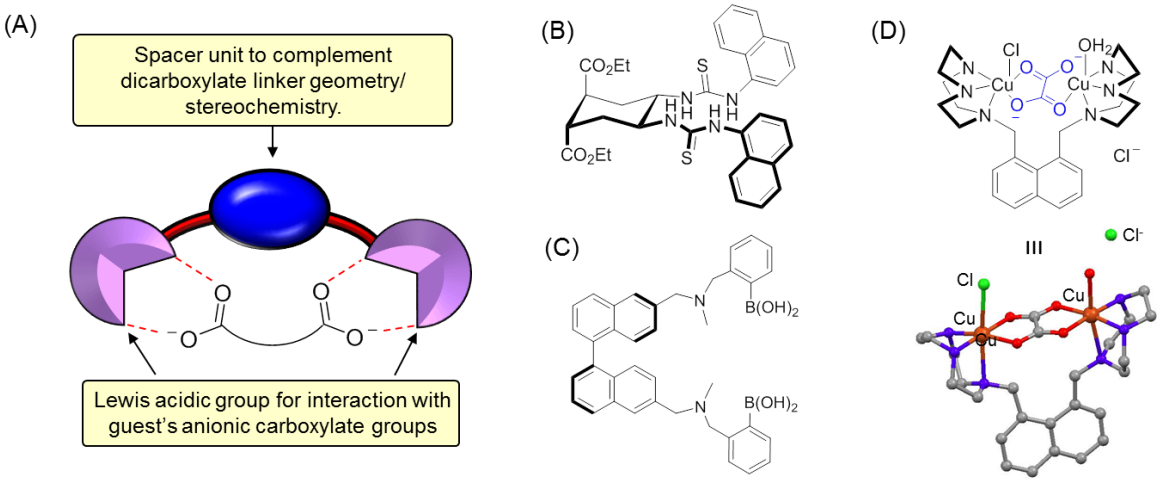


***Figure 4.39**. Structures of abiotic dicarboxylate anion receptors: (A) General design; (B) Costero's substituted cyclohexane HB receptor for maleate binding over fumarate[162]; (C) Houston's tartrate-selective boronic acid receptor[163]; (D) Kim's Cu^{2+}-based receptor selective for oxalate.[164]*

4.4.2 Acyclic Halogen and Chalcogen Bonding Hosts for Dicarboxylate Recognition

4.4.2.1 Receptor Design and Synthesis

Like chiral discrimination, the selective recognition and sensing of dicarboxylates has been shown to be a geometry-dependent process. Consequently, it was envisaged that employing σ-hole interactions such as XB and ChB could enforce more stringent geometric restrictions on binding that lead to better selectivity between dicarboxylate geometric and stereo-isomers. To test this hypothesis, XB, ChB and HB analogues of the conformationally highly-rigid 2,2'-triazolium substituted (*S*)-BINOL receptors **4.3** were studied to maximise the geometric influences of each interaction on dicarboxylate recognition. It was expected that the two spatially-separated Lewis-acidic triazolium binding sites would coordinate each anionic termini of the dicarboxylate guests separately, bringing the spacer unit of each guest into close proximity with the rigid aromatic chiral receptor framework for stereo- and geometric-selective recognition (Figure 4.40).

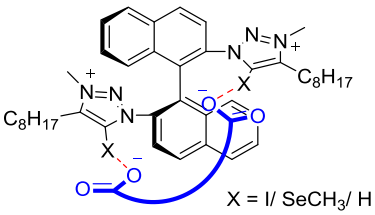
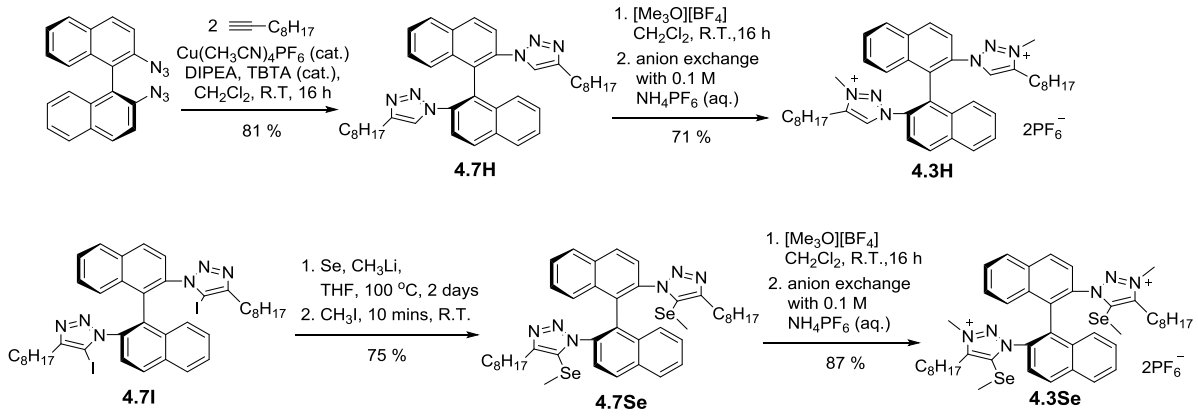


***Figure 4.40**. Proposed dicarboxylate coordination mode of receptor analogues **4.3I/Se/H**.*

While the synthesis of the XB analogue **4.3I** has been shown in Scheme 4.1, the analogous preparation of **4.3Se** and **4.3H**, together with their neutral receptor precursors **4.7Se/H** is summarised in Scheme 4.9. **4.7H** was synthesised under standard CuAAC conditions from (*S*)-BINOL 2,2'-bis-azide and 1-decyne. While conversion of an iodotriazole to a methylseleno-triazole unit was previously achieved in Chapter 2 via a fluorotriazole intermediate, the procedure could not be applied for **4.7Se** due to the high temperatures required for fluorotriazole formation (180 ^{o}C), which would result in significant thermal racemisation of the (*S*)-BINOL motif.[75] Therefore, a modification of the original S_NAr reaction conditions was adopted, involving a prolonged reaction time of 2 days in THF at 100 ^{o}C, which afforded **4.7Se** in a good yield of 75 % after chromatographic isolation. Both precursors **4.7Se** and **4.7H** were subjected to triazole N^3-methylation with trimethyloxonium tetrafluoroborate, followed by anion exchange to their $2PF_6^-$ salts, to afford dicationic receptors **4.3Se** and **4.3H** in 87 % and 71 % yields respectively.



***Scheme 4.9**. Synthesis of 2,2-triazolium substituted (S)-BINOL receptors **4.3Se** and **4.3H**.*

4.4.2.2 Anion Recognition Studies

The discriminatory properties of receptors **4.3Se/I/H** towards stereo- and geometric dicarboxylate isomer guest species were probed by ^{1}H NMR titrations in d_6-acetone/ D_2O 85:15 *v/v* using (*S*,*S*)/ (*R*,*R*)-tartrate, as well as maleate/ fumarate and phthalate/ isophthalate/ terephthalate, as their TBA salts. Using the titrations of (*S*,*S*)-tartrate as an example (Figure 4.41), the addition of dicarboxylate anion to each receptor led to generally similar signal perturbation patterns for the ^{1}H NMR aromatic region of each receptor. In each case, a notable downfield shift of H_b closely-located to the triazolium Lewis acidic group was seen, likely arising from weak HB with the carboxylate group of the anions held close by. More distant aromatic environments H_d, H_e and H_f showed an upfield perturbation instead, possibly resulting from alterations to their electronic environments brought about by receptor conformation change (e.g. dihedral angle between the naphthalene groups). Compared to receptors **4.3Se** and **4.3I**, an additional slight upfield perturbation of aromatic H_c was seen for **4.3H**, possibly a consequence of the less sterically-bulky prototriazolium groups allowing dicarboxylate binding to occur closer to the (*S*)-BINOL aromatic core of the receptor. For each receptor, opposite tartrate enantiomers elicited slightly different binding behaviours with the host, evident from the binding isotherms shown on the left of Figure 4.42.

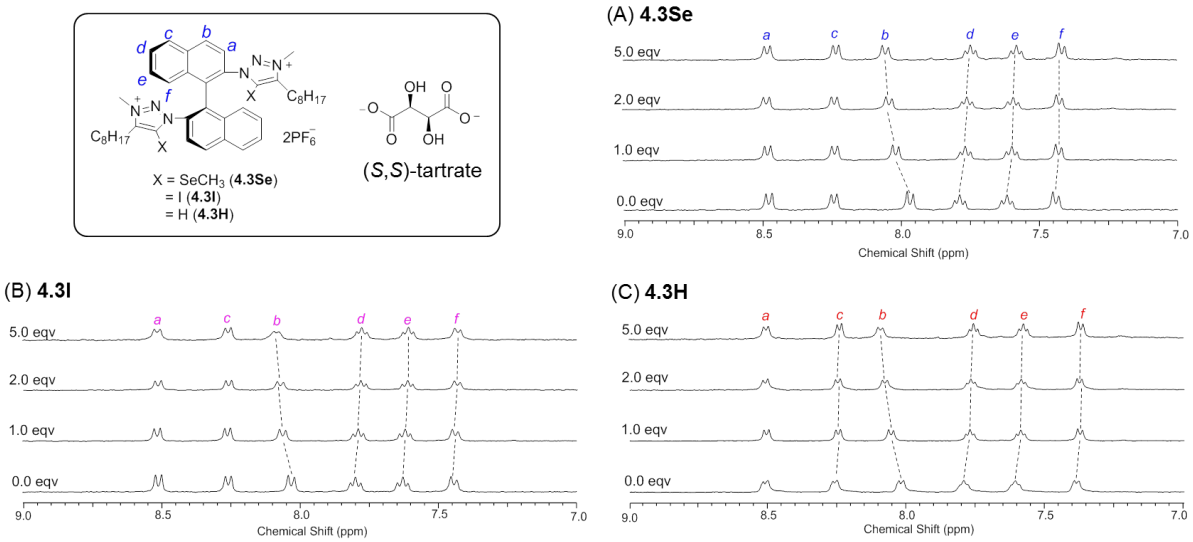


Figure 4.41. *Partial ^{1}H NMR spectra of dicationic receptors (A)* ***4.3Se****, (B)* ***4.3I*** *and (C)* ***4.3H*** *in the presence of increasing quantities of (TBA)$_2$(S,S-tartrate) ([**4.3**] = 1.0 mM; d_6-acetone/ D_2O 85:15; T = 298 K).*

Receptors **4.3Se/I/H** showed notable differences in their behaviours towards the dicarboxylate geometric isomers (Figure 4.42 middle and right columns). With **4.3Se**, maleate binding showed clear 1:1 host-guest association, while a second anion binding event could be readily discerned for fumarate. More dramatically, maleate addition resulted in rapid decomposition of **4.3I** even in the presence of water, while receptor integrity was retained even in the presence of 20-fold excess of fumarate during its titration. Notable differences could be seen as well during the titrations of phthalate, isophthalate and terephthalate with each receptor. For instance, phthalate gave notable downfield perturbations of **4.3Se**'s H_b resonance, accompanied by small shifts of H_f ($\Delta\delta$ = -0.03 ppm over 10 equivalents). Contrastingly, the main signal perturbations seen with isophthalate and terephthalate were

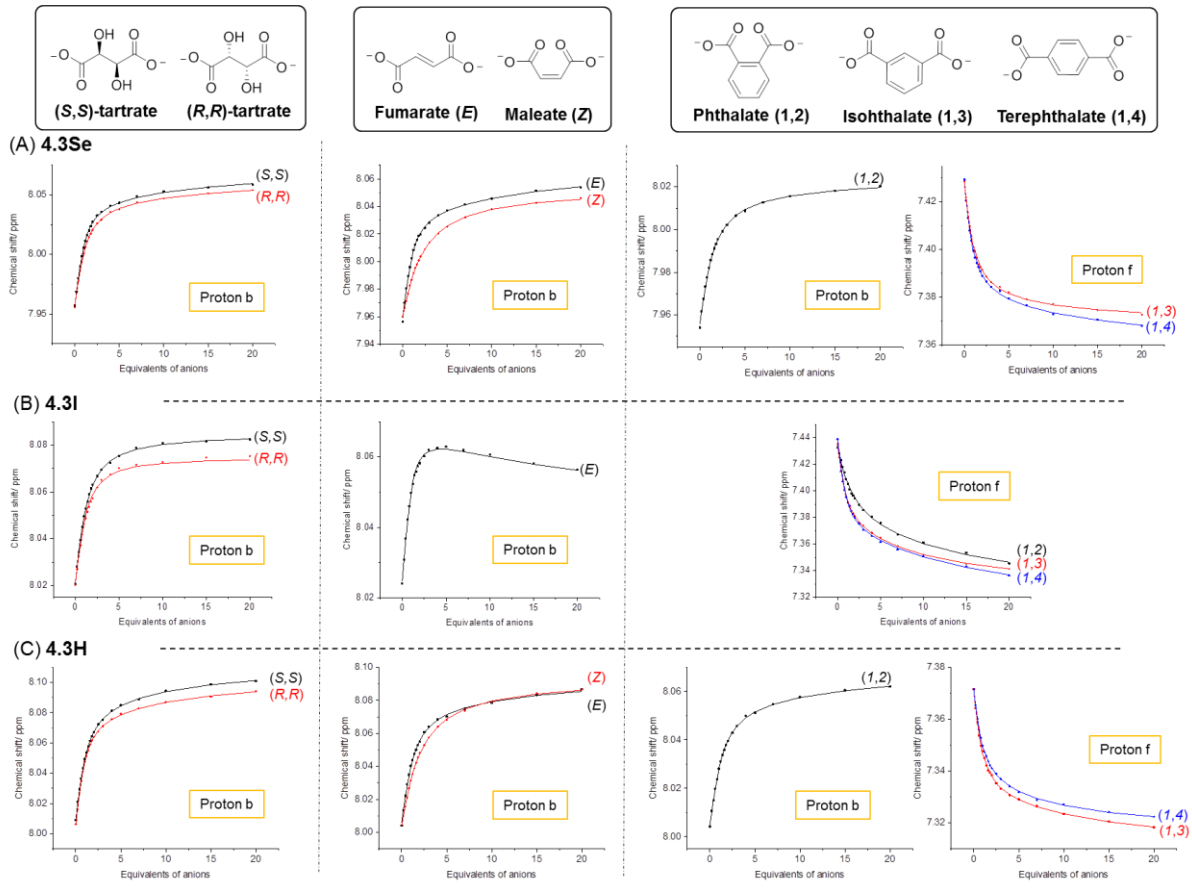


***Figure 4.42**. Binding isotherms obtained by monitoring the resonances shifts of either proton H_b or H_f on receptor (A) **4.3Se**, (B) **4.3I** or (C) **4.3H** in the presence of increasing quantities of anion stereo- or regio-isomers ([**4.3**] = 1.0 mM; d_6-acetone/ D_2O 85:15 v/v; T = 298 K). No binding isotherms could be obtained for the titration of receptor **4.3I** with maleate due to anion-induced receptor decomposition.*

those of H_f, while H_b showed insignificant *upfield* movements, which suggested that all three regioisomers were binding and interacting with receptor **4.3Se** in different ways. Although phthalate, isophthalate and terephthalate showed similar patterns of receptor aromatic signal shifts for **4.3H** and **4.3Se**, those of the XB receptor analogue **4.3I** differed: all three benzene dicarboxylate geometric isomers were found to cause the largest upfield shifts for **4.3I**'s aromatic H_f signal, with small changes for H_b consistently. Taken together, these titrations showed that the different Lewis acid-donor interactions of **4.3Se/I/H**, even between closely-related XB and ChB interactions, could elicit dramatically different dicarboxylate binding arrangements between different stereo- and regioisomers. BindFit[171] analysis of the ^{1}H NMR titration data afforded in general 1:2 stoichiometric host-guest association constants (K/ M^{-1}) summarised in Table 4.6, together with the selectivities (ξ) observed between different geometric and stereo-isomers calculated from the respective first association constant values (K_{11}). The values of K_{11} are also depicted pictorially in Figure 4.43 for greater ease of comparison.

Table 4.6. Anion association constants (K/ M^{-1}) and selectivities (ξ) of receptors **4.3Se**, **4.3I** and **4.3H** with various anion stereo- and regio-isomers.[a]

Anion	Receptor **4.3Se**		Receptor **4.3I**		Receptor **4.3H**	
	K	ξ [b]	*K*	ξ [b]	*K*	ξ [b]
S,*S*-tartrate	K_{11} = 2631 (66) K_{12} = 70 (5)	$\frac{K_{S,S}}{K_{R,R}}$ = 1.09 (0.04)	K_{11} = 3565 (89) K_{12} = 223 (6)	$\frac{K_{S,S}}{K_{R,R}}$ = 2.0 (0.1)	K_{11} = 2348 (96) K_{12} = 55 (4)	$\frac{K_{S,S}}{K_{R,R}}$ = 0.69 (0.04)
R,*R*-tartrate	K_{11} = 2411 (55) K_{12} = 65 (4)		K_{11} = 1815 (92) K_{12} = 81 (5)		K_{11} = 3412 (147) K_{12} = 59 (3)	
Maleate	K_{11} = 532 (10) [c]	$\frac{K_{fum}}{K_{mal}}$ = 5.5 (0.2)	- e	- e	K_{11} = 596 (13) [c]	$\frac{K_{fum}}{K_{mal}}$ = 2.0 (0.1)
Fumarate	K_{11} = 2926 (93) K_{12} = 39 (1)		K_{11} = 3183 (53) K_{12} = 32 (1)		K_{11} = 1216 (78) [c]	
Phthalate	K_{11} = 1858 (48) K_{12} = 80 (4) [d]	$\frac{K_{iso}}{K_{phth}}$ = 3.5 (0.4)	K_{11} = 1336 (139) K_{12} = 49 (6) [f]	$\frac{K_{iso}}{K_{phth}}$ = 5.8 (0.8)	K_{11} = 1343 (32) K_{12} = 15.2 (1.5)[d]	$\frac{K_{iso}}{K_{phth}}$ = 3.1 (0.3)
Isophthalate	K_{11} = 6502 (640) K_{12} = 78 (8)	$\frac{K_{tereph}}{K_{phth}}$ = 2.3 (0.1)	K_{11} = 7774 (769) K_{12} = 93 (4)	$\frac{K_{tereph}}{K_{phth}}$ = 3.2 (0.5)	K_{11} = 4161 (395) K_{12} = 50 (5)	$\frac{K_{tereph}}{K_{phth}}$ = 3.6 (0.5)
Terephthalate	K_{11} = 4346 (230) K_{12} = 98 (7)		K_{11} = 4235 (538) K_{12} = 17 (1)		K_{11} = 4802 (465) K_{12} = 111 (9)	

[a] Proton H_b monitored and data fit to a host-guest 1:2 stoichiometric binding model with BindFit[171] unless otherwise stated; errors (±) in parentheses; [**4.3**] = 1.0 mM, d_6-acetone/ D_2O 85:15 *v/v*, *T* = 298 K. [b] Selectivity ratios (ξ) calculated using only the first association constants (K_{11}); [c] No evidence of second binding event occurring, hence data fit only to a host-guest 1:1 model; [d] Proton H_e monitored instead of H_b due to the small perturbations of the latter signal; [e] receptor decomposition observed on anion addition; [f] slight receptor decomposition seen at 10 eqv. of phthalate, hence values reported are only estimates.

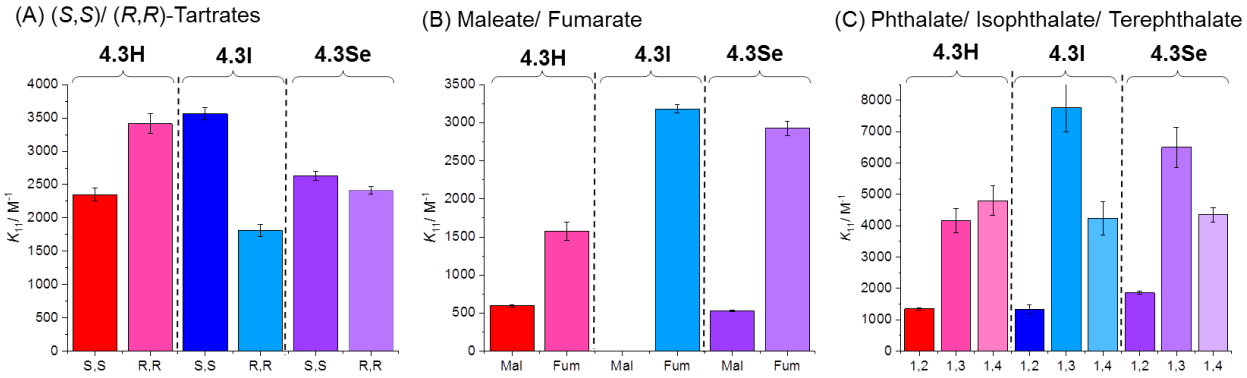


***Figure 4.43**. Bar chart showing the variations in K_{11}/ M^{-1} values pictorially between the different anion (A) stereo- and (B and C) geometric isomers for receptors **4.3H**, **4.3I** and **4.3Se**.*

Amongst the three receptors, the extent of chiral discrimination towards the tartrate dicarboxylate enantiomers decreased in the order **4.3I** > **4.3H** > **4.3Se**. Despite the poor enantioselectivity towards the monoanionic *N*Boc-leucine carboxylate enantiomers by **4.3I** previously described (Section 4.2.2), significantly improved chiral discrimination was seen for tartrate, which may be a result of the postulated ditopic dicarboxylate binding arrangement shown in Figure 4.40 forcing both stereocentres of the anion into close proximity with the asymmetric binaphthyl receptor motif. While the enantioselectivity enhancement for **4.3I** over **4.3H** may be expected based on earlier findings, the poor chiral discrimination of **4.3Se** is surprising, given the comparable linearity and sterics of ChB and XB interactions. Although it has been previously shown that ChB interactions are often weaker than XB due to the more diffuse and consequently less electrophilic σ-holes on the donor atoms (Chapter 2), comparable anion affinities were observed in this case for receptors **4.3Se** and **4.3I** in Table 4.6, suggesting that host-guest Coulombic attractions were playing important roles in binding of the highly-hydrated dicarboxylate anions in this highly-competitive aqueous solvent mixture. Thus, the poor enantioselectivity for **4.3Se** may be due to the geometry of anion association governed more by isotropic electrostatic interactions than the more directional ChB interactions. Nevertheless despite its limited influence in **4.3Se**, the σ-hole-directed binding geometry allowed both **4.3Se** and **4.3I** to show identical enantiomer preference for (*S*,*S*)-tartrate, contrasting with the opposite selectivity for **4.3H**.

For the dicarboxyate geometric isomers, all three receptors bound fumarate preferentially over maleate. Although maleate resulted in decomposition of **4.3I** and hence precluded a quantitative comparison with fumarate, a notably enhanced binding preference for fumarate was observed for **4.3Se** ($\xi = 5.5 \pm 0.2$) compared with **4.3H** ($\xi = 2.0 \pm 0.1$). Between the benzene dicarboxylate geometric isomers, phthalate was bound least preferentially by all receptors, which is unsurprising considering its geometric similarity with maleate. Despite this, phthalate elicited stronger binding affinities than maleate, possibly a result of additional aromatic host-guest donor-acceptor interactions (observed from shifts of the anions' aromatic proton signals during the titrations). Notably, the influence of σ-hole interactions were found to change the receptors' geometric isomer binding preference (Figure 4.43C). While both isophthalate and terephthalate were bound with comparable affinities by **4.3H**, with a slight preference for the latter, **4.3Se** and **4.3I** both displayed distinct biases towards isophthalate. Clearly, this well-defined geometric binding preference is due to the more stringent linear directionality imposed by the XB and ChB interactions of **4.3I** and **4.3Se** respectively. However, the more limited influence of the ChB interactions compared to XB noted earlier manifests in the reduced extent of selectivity for **4.3Se**.

Having demonstrated the differences in binding preferences amongst the three receptors for the dianionic geometric isomers, fluorescence titrations were performed in acetone/ H_2O 85:15 *v/v* with fumarate/ maleate and the benzene dicarboxylates. Despite sharing the same binaphthyl core, receptors **4.3Se/I/H** exhibit slightly different peak fluorescence emission wavelengths (λ_{em}) (Figure 4.44), suggesting some variations in their electronic levels and hydration status due to their different anion binding motifs. In the presence of the dicarboxylate geometric isomers however, all three receptors exhibit unique fluorescence behaviours.

For receptor **4.3Se** (Figure 4.44A), addition of benzene dicarboxylates led to different extents of fluorescence enhancement. Both terephthalate and phthalate elicited modest intensity increases, accompanied by larger bathochromic shifts of λ_{em} for the latter. In contrast isophthalate, which was found to be most strongly bound via ^{1}H NMR titrations (Table 4.6), gave the largest fluorescence enhancement of **4.3Se** with a notable λ_{em} hypsochromic shift of

nearly 20 nm. This may be a consequence of the wider distance between the carboxylate groups of isophthalate (4.98 Å) compared with phthalate (3.16 Å),[172] forcing an increase of the binaphthyl dihedral angle when each $SeCH_3$ unit binds with a carboxylate group of isophthalate. The resulting increased relative twist reduces the extent of electronic conjugation between both naphthalene rings, leading to increased energy separation between the S_1 and S_0 states, causing a fluorescence blue-shift. The converse may account for the bathochromic shifts seen for phthalate, caused by a decrease in the binaphthyl dihedral angle upon host interaction with both *ortho*-substituted carboxylate groups on the anion. The much smaller λ_{em} shift seen for terephthalate may be due to the anion not being able to bridge between both selenotriazolium groups due to its rigidity, thus inducing only small structural changes to the receptor's binaphthyl core during binding. Interestingly, while maleate and fumarate addition brought about similar changes to λ_{em} as phthalate and terephthalate respectively due to their similar geometries, quenching of **4.3Se**'s fluorescence occurred upon anion binding, with the weaker bound maleate anion giving rise to a larger degree of quenching than fumarate.

With receptor **4.3I**, addition of terephthalate, isophthalate and fumarate brought about large increases in the fluorescence intensity (Figure 4.44B). No reliable fluorescence binding data could be obtained for phthalate and maleate due to receptor decomposition in the presence of excess anion. Bathochromic shifts of **4.3I**'s λ_{em} were seen in all cases, consistent with a reduction in the binaphthyl dihedral angle during the binding of all dicarboxylates. However, fumarate and terephthalate showed larger shifts than isophthalate, suggesting that larger receptor conformational changes resulted during the binding of the former anions. This contrasting behaviour with **4.3Se** may be due to the different geometric requirements of XB and ChB interactions, with the former requiring greater linearity due to the influence of only one σ-hole compared to the latter's two. Although isophthalate was found to bind more strongly than fumarate and terephthalate (Table 4.6), it did not give the largest fluorescence enhancement, unlike that for **4.3Se**.

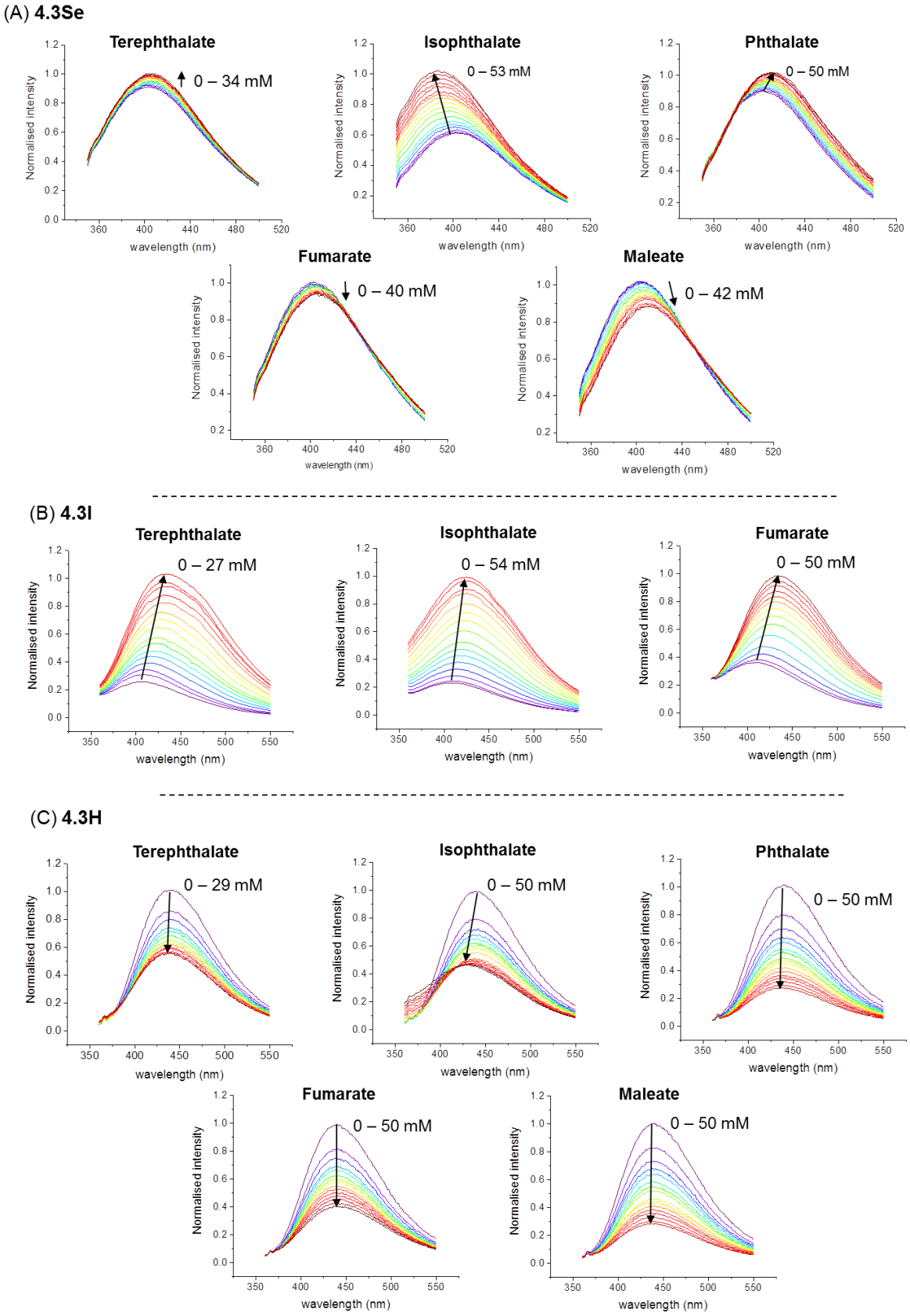


***Figure 4.44**. Changes in fluorescence intensities of receptors (A) **4.3Se** (λ_{ex} = 320 nm), (B) **4.3I** (λ_{ex} = 325 nm) and (C) **4.3H** (λ_{ex} = 330 nm) in the presence of increasing quantities of dicarboxylate geometric isomers ([**4.3**] = 50 μM; acetone/ H_2O 85:15 v/v; T = 293 K). Concentrations indicated represent the changes in anion concentrations during the titrations.*

On the other hand, large fluorescence quenching was observed for all anion titrations with **4.3H**. Like **4.3I**, the extent of quenching did not correlate with the observed association constants (Table 4.6), as exemplified with the stronger-binding fumarate anion giving smaller intensity decreases than the weaker-binding maleate (Figure 4.44C). Also notable is the lack of significant λ_{em} shifts distinctly seen for **4.3Se** and **4.3I**, with only isophthalate bringing about a hypsochromic shift after a large excess (> 250 equivalents) was added. This may imply that the first binding event of all dicarboxylates with **4.3H** elicited only small changes to the inter-naphthalene dihedral angle due to the less stringent linearity constraints imposed by HB interactions of the prototriazolium groups compared with the σ-hole-donor analogues.

In summary, by just changing the Lewis acidic group on the same chiral binaphthyl receptor framework, dramatic differences in selectivities between dicarboxylate stereo- and geometric isomers resulted. Owing to the different geometric restrictions conferred by XB, ChB and HB interactions, binding of the same series of isomers (e.g. benzene dicarboxylates) result in different equilibrium host-guest arrangements, evident from the contrasting behaviour seen during the ^{1}H NMR and fluorescence titrations. Nevertheless, dicarboxylate recognition by **4.3Se** and **4.3I** show numerous similarities, seen from the geometric isomer preferences in Table 4.6, as well as more pronounced host conformational changes giving rise to shifts of fluorescence λ_{em} enforced by the greater directionality of XB and ChB. However between **4.3Se** and **4.3I**, more prominent differences from **4.3H** was seen for the latter, possibly due to the stronger XB interactions than ChB arising from the greater polarizability and more electropositive σ-hole on the iodine atoms compared with the seleniums.

4.4.3 A Chiral [3]Rotaxane for Dicarboxylate Binding

4.4.3.1 Chiral [3]Rotaxane Design Considerations and Synthesis

The use of higher-ordered interlocked structures such as [3]rotaxanes for molecular sensing applications is less common than [2]rotaxanes, with rare examples reported for cesium[173] and oxoanions such as nitrate and sulfate.[174,175] For dicarboxylate recognition and sensing, [3]rotaxanes offer unique advantages over [2]rotaxanes as the guests are often too large to fit into the latter's binding pocket. By incorporating Lewis acidic groups (e.g. XB and HB) around each interlocked cavity capable of anchoring the anionic termini of a dicarboxylate guest, a 1:1 stoichiometric host-guest 'sandwich' complex can be formed (Figure 4.45A). A lengthy spacer unit between both interlocked cavities containing a chiral (*S*)-BINOL unit was integrated into the axle component to complement the shape, geometry and stereochemistry of the potential guest species' dicarboxylate linker (labelled R in Figure 4.45A), allowing geometric and stereo-discrimination. Furthermore, the (*S*)-BINOL fluorophore may be capable of displaying selective fluorescent responses for dicarboxylate guests long enough to bridge the gap between each interlocked Lewis acidic binding site, as the resulting ditopic coordination is likely to affect the local electronic environment of the fluorophore by the presence of guest in close proximity, or by conformational changes to the [3]rotaxane framework brought about during 'sandwich' complex formation. This fluorescence response is also particularly valuable, as shorter oxoanions (e.g. oxalate) and spherical halides are expected to bind predominantly at each individual interlocked cavity (*vide infra*), thus interacting with the centrally-located (*S*)-BINOL fluorophore to a smaller extent to give diminished fluorescence changes. This additional level of optical discrimination is often difficult to achieve using acyclic receptors or [2]rotaxanes and has only been rarely demonstrated,[176,177] as their binding cavities often bind smaller guests, especially halides, indiscriminately. To prepare these higher-order interlocked hosts, a Cl^- anion-templated macrocycle clipping strategy around potent XB halide recognition motifs (e.g. iodotriazolium) on the axle component was undertaken, ensuring separate macrocycle ring-closing around each XB-donor site to form the target [3]rotaxane (Figure 4.45B).

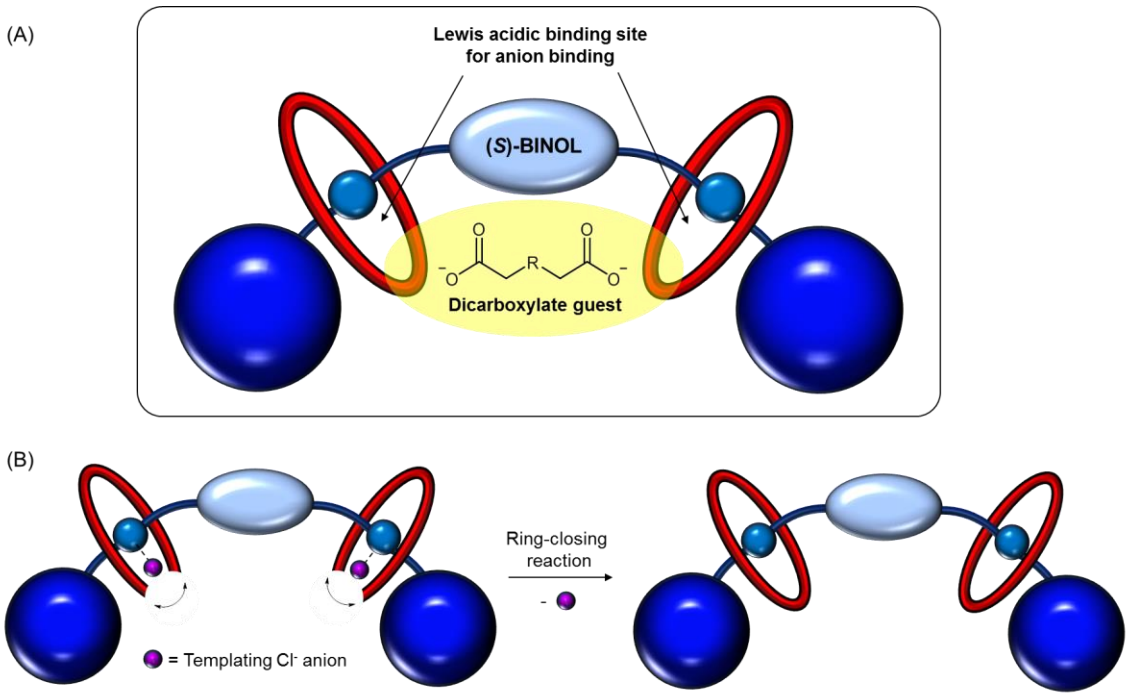
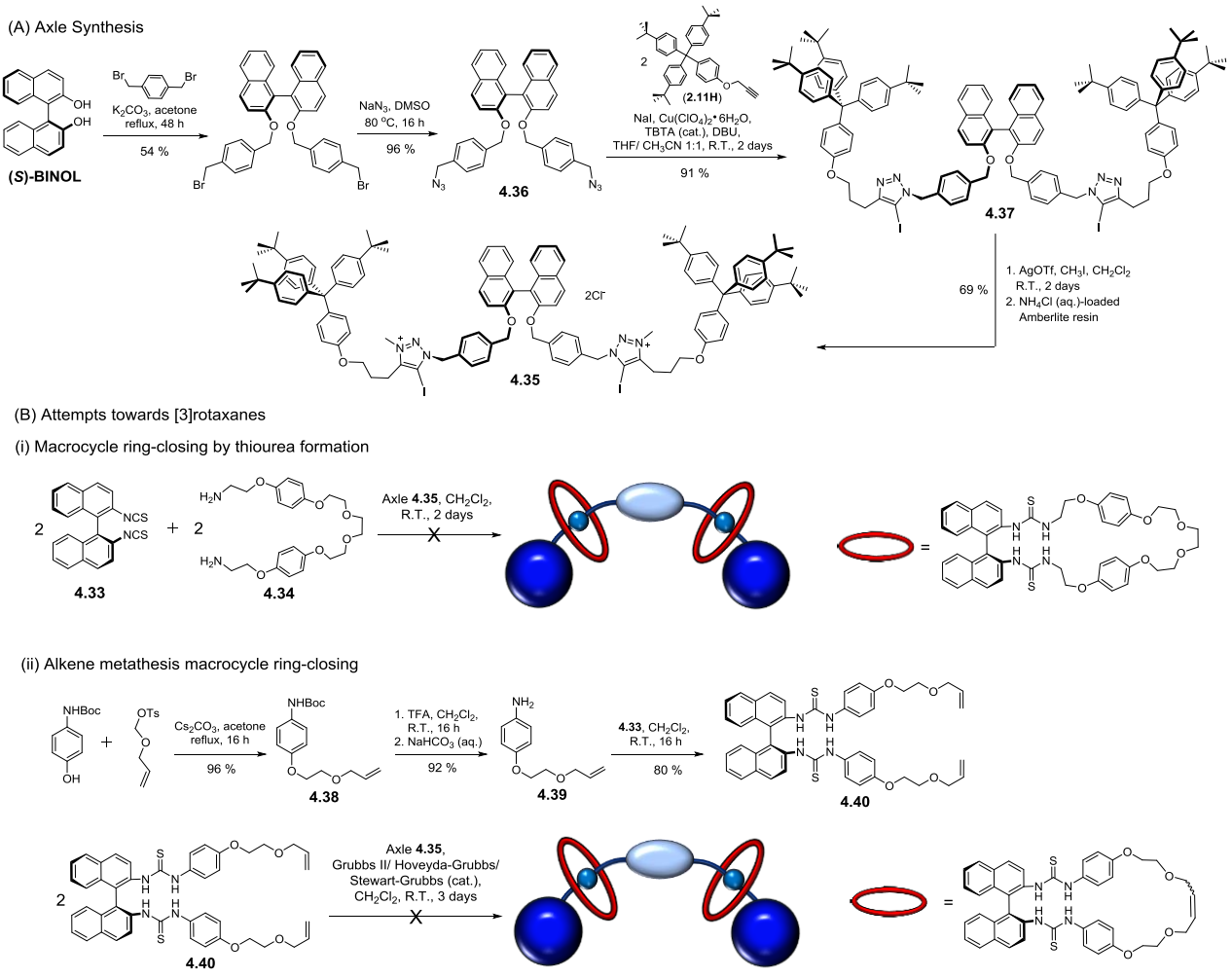


***Figure 4.45**. (A) General design of chiral [3]rotaxane host systems for dicarboxylate recognition; (B) Chloride-templated [3]rotaxane synthesis strategy.*

The synthesis of the bis-iodotriazolium dicationic axle **4.35** is summarised in Scheme 4.10A. Starting from (*S*)-BINOL, Williamson ether synthesis under basic conditions with an excess of dibromo-*p*-xylene afforded the dibromo intermediate, which was converted to the bis-azide synthon **4.36** by nucleophilic substitution with NaN_3. Following which, CuAAC reaction with stopper (proto)alkyne **2.11H** afforded the bis-iodotriazole neutral axle precursor **4.37** in an excellent yield of 91 % using Zhu's protocol.[94] Iodotriazole N^3-methylation with trimethyloxonium tetrafluoroborate, followed by anion exchange to the Cl^- salt afforded target dicationic axle **4.35**.

[3]Rotaxane synthesis was first attempted using Cl^--templated macrocycle clipping by thiourea formation using bis-isothiocyanate **4.33** and bis-amine **4.34** [Scheme 4.10B(i)]. However, ESI mass spectrometry analysis of the crude reaction mixture after 2 hours (Figure 4.46A) showed the loss of an iodine atom from axle **4.35** (m/z = 908 $[M]^{2+}$, peak 2) together with evidence of the ring-closed macrocycle or its mono-thiourea acyclic intermediate (m/z = 789 $[M+H]^+$, peak 4). After 24 hours [Figure 4.46B(i)], complete loss of axle **4.35** resulted to form the bis-prototriazolium axle analogue (m/z = 846 $[M]^{2+}$, peak 3) was observed. Curiously,

no evidence of the bis-thiourea macrocycle could be detected after 24 hours (m/z = 789 $[M+H]^+$), with the formation of an unknown side product at m/z = 755. Unfortunately, no trace of the target [3]rotaxane nor its bis-prototriazolium analogue was also observed after 2 days. Nevertheless, to find out the reason for the instability of the iodotriazolium groups of **4.35**, the free axle was mixed with equimolar quantities of **4.34**, which also led to the loss of iodine atoms after 24 hours. Repeating this experiment with anhydrous triethylamine produced the same results, clearly indicating that the iodotriazolium groups were unstable to amine bases, possibly due to extensive donation of the amine lone pairs into the highly-polarised C-I σ* orbital. This instability thus precluded the use of any amine macrocycle precursors for [3]rotaxane formation.



***Scheme 4.10**. (A) Synthesis of bis-iodotriazolium axle **4.35** and (B) attempts at synthesis of a target [3]rotaxane host using axle **4.35** via chloride anion templation.*

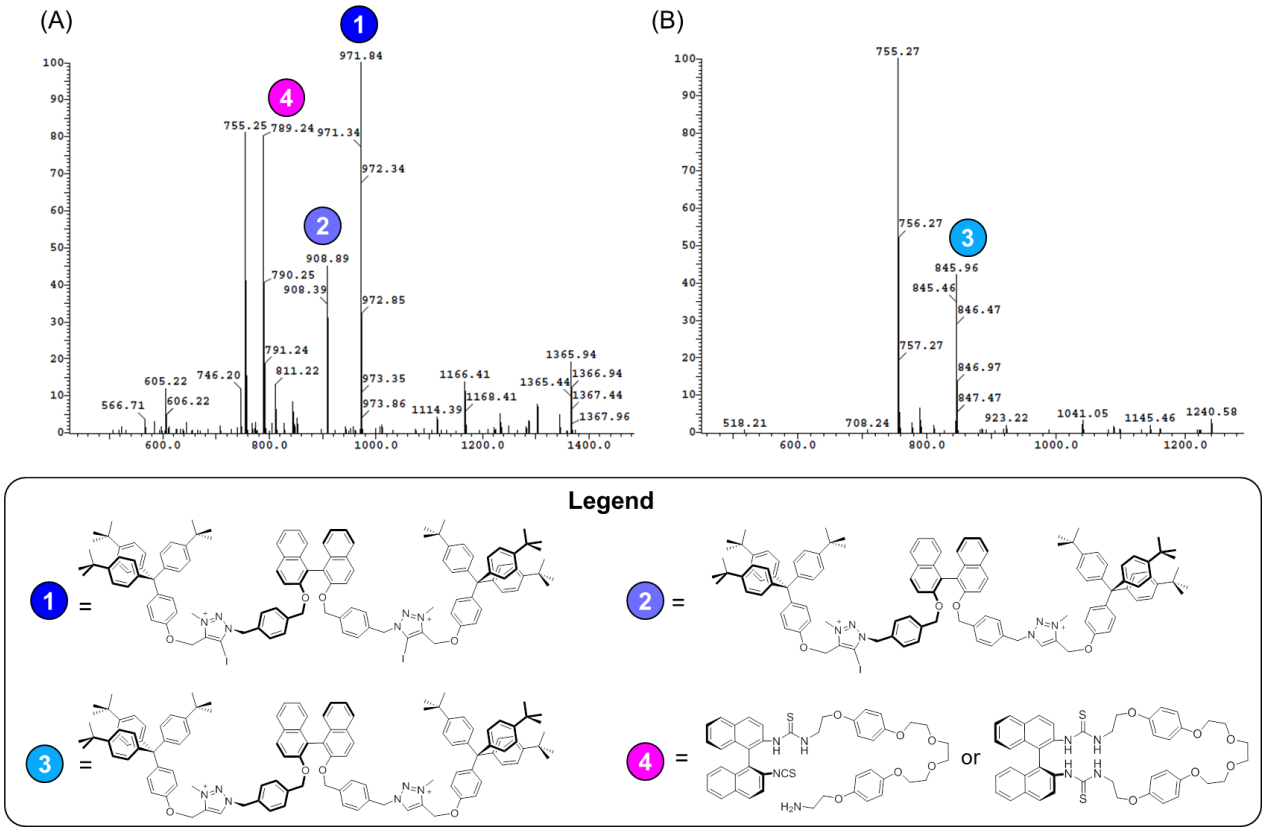
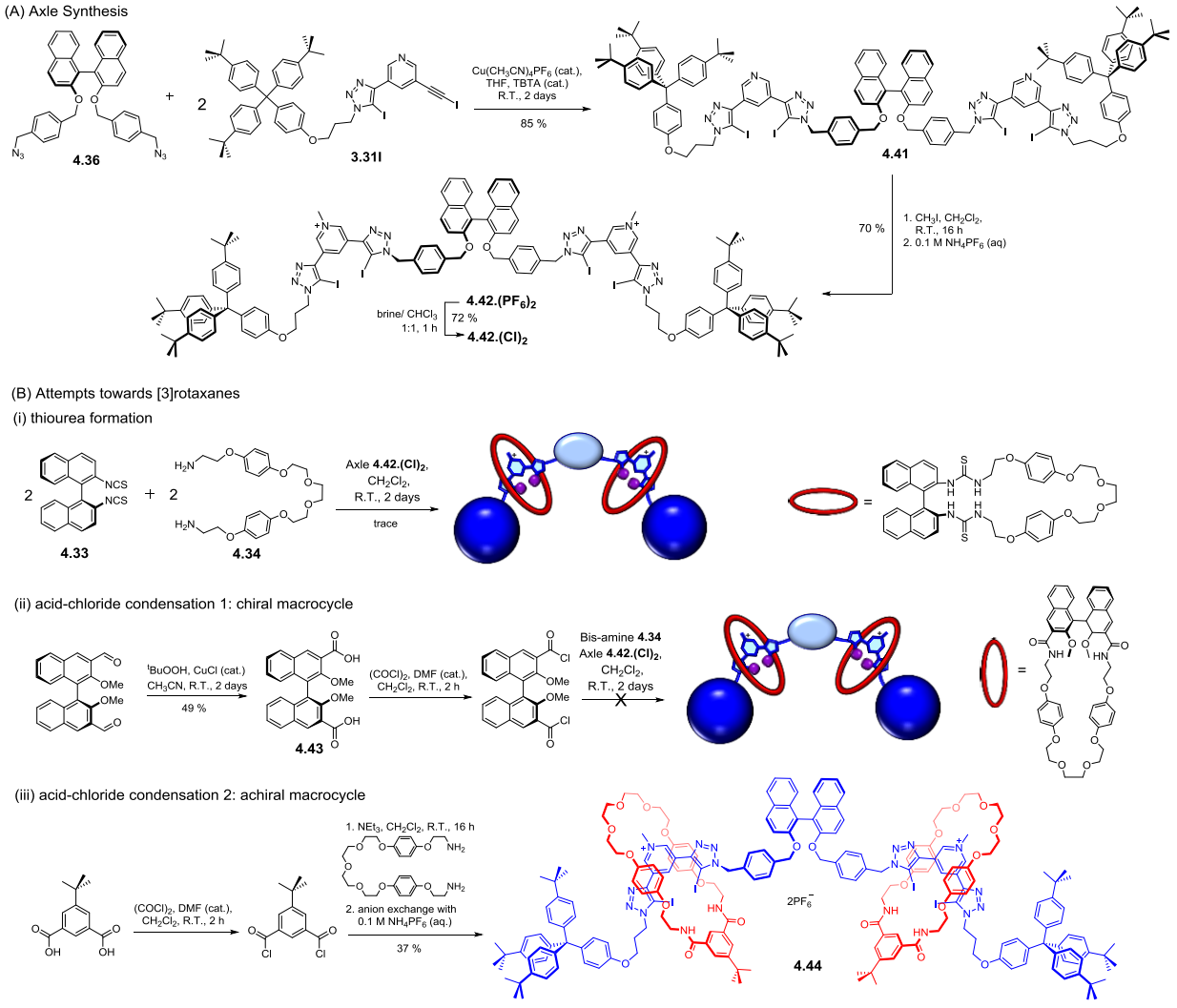


***Figure 4.46**. ESI mass spectra monitoring the progress of the attempted [3]rotaxane synthesis by Cl^--templated thiourea macrocycle ring-closing at (A) 2 hours and (B) 24 hours after the progress of reaction.*

[3]Rotaxane formation was then attempted using ring-closing metathesis (RCM) of a bis-vinyl macrocycle precursor **4.40**, constructed by addition of two equivalents of amine **4.39** to bis-isothiocyanate **4.33** [Scheme 4.10B(ii)]. Interestingly, neither the presence of Grubbs II, Hoveyda-Grubbs nor Stewart-Grubbs RCM catalysts gave noticeable ring-closing of **4.40** even after 3 days to form either free macrocycle or rotaxane, despite employing analogous conditions of previously-successful RCM rotaxane synthesis reactions.[175,178] In light of this failure, together with the inherent instability of iodotriazolium groups towards bases, the use of axle **4.35** for rotaxane synthesis was abandoned.

An alternative axle was then designed, containing the cationic pyridinium-3,5-iodotriazole anion binding motif which has been shown to be stable towards free amines.[179–181] As shown in Scheme 4.11A, neutral axle precursor **4.41** was prepared by CuAAC from bis-azide synthon **4.36** and two equivalents of terminal iodoalkyne **3.31I**. Although pyridine *N*-methylation gave clean conversion of **4.41** to the desired dicationic axle, the product was

much less readily soluble in common organic solvents compared to its neutral congener, rendering direct anion exchange to its Cl^- salt challenging. To circumvent this, anion exchange was first performed using 0.1 M NH_4PF_6 (aq.) to the significantly more soluble **4.42.$(PF_6)_2$**, followed by anion exchange to form **4.42.$(Cl)_2$** by vigorous stirring of a chloroform solution of **4.42.$(PF_6)_2$** with brine. ^{31}P and ^{19}F NMR analysis of **4.42.$(Cl)_2$** showed complete loss of any resonances arising from these nuclei, confirming that successful anion exchange had occurred.



***Scheme 4.11**. (A) Synthesis of alternative dicationic XB axle **4.42** and (B) attempts towards preparating a [3]rotaxane.*

Thiourea macrocycle ring-closing was first performed using **4.33** and **4.34** [Scheme 4.11B(i)]. Pleasingly, the presence of **4.34** did not result in any de-iodination of axle **4.42**. Despite this, no [3]rotaxane and only trace evidence of [2]rotaxane (m/z = 1664 $[M]^{2+}$) was found after an overnight reaction using ESI-MS analysis which could not be isolated chromatographically. This suggests that the geometry of the thiourea macrocycle intermediate was unconducive for interlocking around the axle, even in the presence of templating Cl^- anions. In a bid to retain the chiral (*S*)-BINOL motif on the macrocycle component, rotaxane synthesis was then attempted using the 3,3'-functionalised dicarboxylic acid of methoxy-(*S*)-BINOL **4.43**, which was prepared by oxidation of the di-aldehyde congener [Scheme 4.11B(ii)]. Unfortunately, conversion of **4.43** to its corresponding acid chloride, followed by condensation with bis-amine **4.34** gave neither ring-closed macrocycle nor interlocked structure. Therefore in a final attempt, rotaxane synthesis was performed using 5-tertbutyl-isophthalic acid [Scheme 4.11B(iii)]. Gratifyingly, the target [3]rotaxane was clearly observed in ESI-MS analysis of the crude reaction (*m/z* = 1920 $[M]^{2+}$) with small quantities of [2]rotaxane seen. Purification by preparatory TLC followed by anion exchange to the PF_6^- salt afforded target chiral [3]rotaxane **4.44** in 37 % yield as a pale beige solid.

Comparison of the ^{1}H NMR spectrum of **4.44** with its non-interlocked axle and macrocycle components showed numerous changes diagnostic of rotaxane formation (Figure 4.47A). Most prominently, the dramatic upfield perturbations and increased splitting of the macrocycle hydroquinone proton signals, together with large upfield shifts of axle internal pyridinium proton H_l, are consistent with strong donor-acceptor π-π stacking interactions between axle and macrocycle components. Upfield shifts of axle proton H_K immediately adjacent to the iodotriazoles were also seen, likely resulting from increased shielding of the macrocycle hydroquinone protons present in close proximity. Furthermore, the originally separate double-doublet splitting pattern of diastereotopic protons H_g in the free axle coalesced in the rotaxane, which suggested significant conformational changes to the central portion of the axle component upon rotaxane formation, and is further supported by upfield shifts of the (*S*)-BINOL aromatic protons $H_{a\text{-}c}$. Interestingly also, the sharp singlet peak of the macrocycle isophthalamide external aromatic protons H_2 desymmetrised in the rotaxane to

form two distinct singlets (labelled 2' and 2'') . Other than implying that the macrocycles were not oriented perfectly orthogonal to the plane of the axle (which would have resulted in both H_2 environments being chemically and magnetically indistinguishable), this was also strong evidence that the macrocycle components were conformationally locked around the axle, likely due to a combination of aromatic stacking interactions and HB between the pyridinium methyl group with the polyether chain to form well-defined Lewis acidic interlocked cavities. Further evidence of **4.44**'s interlocked nature was obtained through 2D ROESY NMR spectroscopy (Figure 4.47 inset).

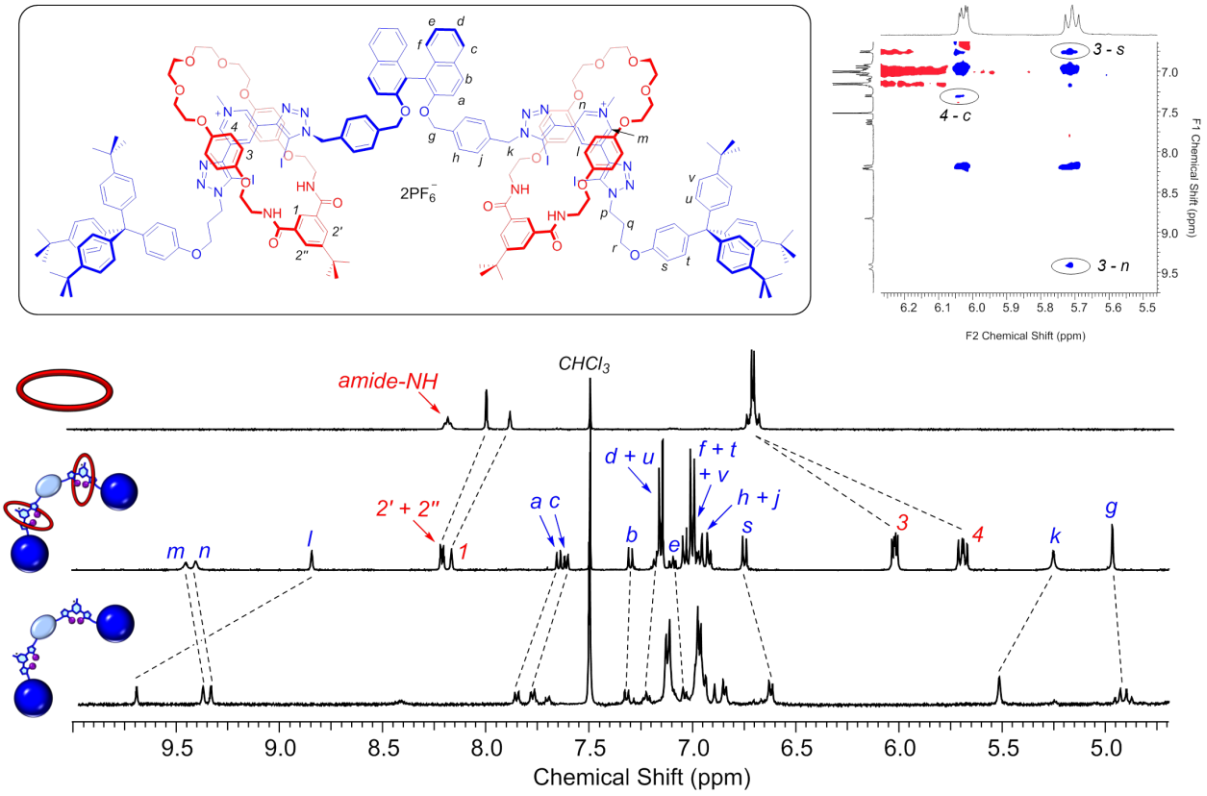


***Figure 4.47**. Partial ^{1}H-NMR spectra of the free macrocycle, [3]rotaxane **4.44** and free axle **4.42**; (Inset) Two-dimensional ROESY spectra of [3]rotaxane **4.44**, with cross-peaks between axle and macrocycle components circled ($CDCl_3$/ CD_3OD 1:1 v/v).*

4.4.3.2 Dicarboxylate Anion Binding Studies

The dicarboxylate binding behaviour of [3]rotaxane **4.44** was first studied by ^{1}H NMR titrations using TBA salts of stereoisomers *N*Boc-*S*/*R*-glutamate and geometric isomers fumarate/ maleate in $CDCl_3$/ CD_3OD/ D_2O 60:39:1 *v/v*.[†††] For comparison, analogous titrations were also performed using Cl^- and SO_4^{2-}.

Dicarboxylates elicited notably different changes in the rotaxane ^{1}H NMR spectra compared to Cl^- and SO_4^{2-} during the titrations. As shown in Figure 4.48, *N*Boc-(*S*)-glutamate dicarboxylate addition led to modest perturbations of the H_1 and H_l resonances arising from the internal aromatic protons flanking each interlocked binding cavity, while significantly augmented shifts were seen for Cl^-, suggesting that unlike the dicarboxylate, Cl^- could be bound within each binding cavity. Interestingly, the external pyridinium proton H_n showed larger downfield shift than H_m, giving signal coalescence between 1.0 and 2.0 equivalents of added anion, clearly indicating that H_n was interacting with *N*Boc-(*S*)-glutamate to a greater extent and that the carboxylate anion was binding closer to it. Contrastingly for Cl^-, both proton signals moved downfield by similar extents without the diagnostic signal 'crossover' seen for the dicarboxylate. Furthermore, while the centrally-located axle protons H_g adjacent to the chiral (*S*)-BINOL motif showed modest upfield movements during *N*Boc-(*S*)-glutamate dicarboxylate binding, no changes were seen for the Cl^- titrations. Taken together, this evidence implied that the dicarboxylate was binding in the space sandwiched between both macrocycle components, while Cl^- was likely binding in each individual interlocked cavity (cartoon representations in Figure 4.48, right). Similar shifts were seen with the other dicarboxylates (*N*Boc-(*R*)-glutamate, maleate and fumarate), showing that they were all binding predominantly via formation of the host-guest 1:1 stoichiometric sandwich complex.

Despite this, varying extents of ^{1}H NMR signal perturbations were observed for the different dicarboxylates studied (Figure 4.49), showing clearly that the rotaxane was able to distinguish between them. For instance, slower H_n/ H_m signal coalescence was seen for maleate than fumarate or the glutamates. In addition, monitoring the shifts of internal

[†††] An excess of $CDCl_3$ was necessary to maintain the solubility of rotaxane during the titration, while wet CD_3OD was essential for good ^{1}H NMR spectral resolution and fitting of the titration data to reasonable binding models.

pyridinium proton H_l gave a sigmoidal-shaped binding isotherm for maleate at ^{1}H NMR titration concentrations, whilst giving a well-defined hyperbolic curve for fumarate. This is likely to be a consequence of the very different anion geometries of both dicarboxylates, where the longer fumarate anion was presumably able to more effectively bridge the space between the macrocycles on the rotaxane. With the *N*Boc-glutamates, binding of the (*S*)-enantiomer elicited a larger magnitude of H_l shift than the opposite stereoisomer, clearly showing that chiral discrimination could result from the host-guest sandwich complex bringing the asymmetric groups of the anion into close contact with the central (*S*)-BINOL motif. Due to the small magnitudes of signal perturbations seen during the titrations, reliable non-linear regression analyses could not be performed for the dicarboxylates. However, WinEQNMR2[96] analysis for the Cl^- titration revealed a strong first association (K_{11} = 2609 ± 201 M^{-1}) and a significant second binding component (K_{12} = 123 ± 10 M^{-1}), suggesting that Cl^- is bound to both spatially-

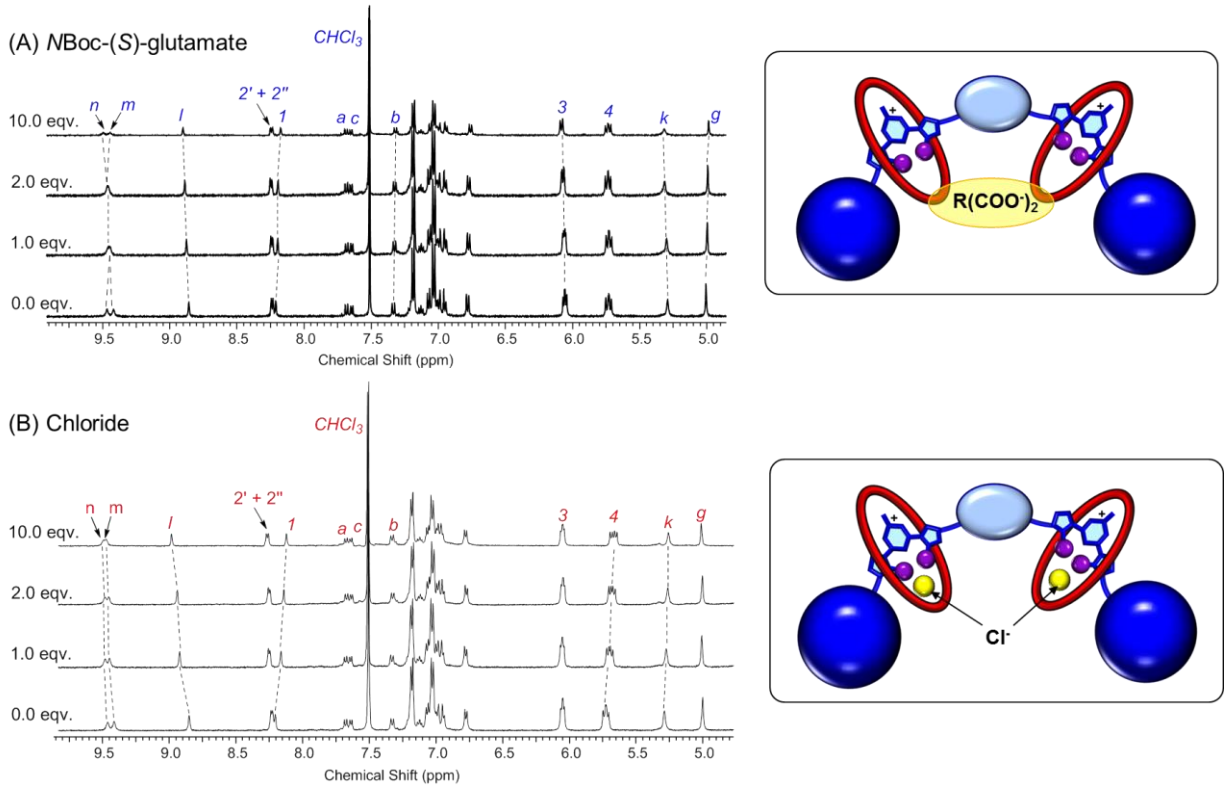


***Figure 4.48**. Partial ^{1}H NMR spectra of rotaxane **4.44** in the presence of increasing quantities of (A) NBoc-glutamate dicarboxylate and (B) chloride ([**4.44**] = 1.0 mM; $CDCl_3$/ CD_3OD/ D_2O 60:39:1 v/v, T = 298 K). Proton assignments follow those of Figure 4.47.*

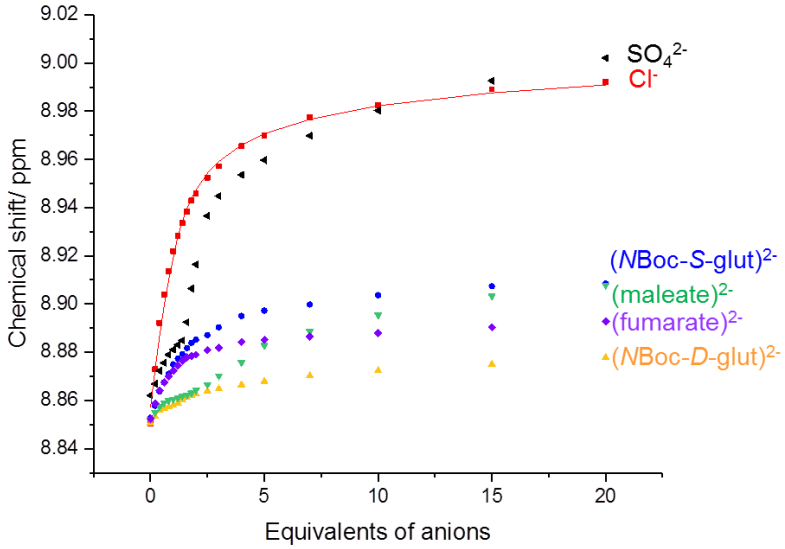


***Figure 4.49**. Binding isotherms of **4.44** with various anions by monitoring changes of axle internal pyridinium proton H_I as a function of anion concentration ([**4.44**] = 1.0 mM; $CDCl_3$/ CD_3OD/ D_2O 60:39:1 v/v, T = 298 K).*

separate macrocycle binding sites with appreciable affinities. Although titrations with SO_4^{2-} resulted in large H_I perturbations (Figure 4.49), which implied binding in the vicinity of each interlocked cavity, complex binding equilibria was evident from the sigmoidal-shaped binding isotherm. This was possibly a result of poor SO_4^{2-} size-match with either each individual rotaxane interlocked cavity.

Further evidence of the different anion binding modes of the dicarboxylates and Cl^- were were obtained using qualitative circular dichroism (CD) spectroscopy titrations (Figure 4.50). In $CHCl_3$/ CH_3OH/ H_2O 60:39:1, rotaxane **4.44** shows a trisignate CD spectrum (red traces), with bands centred at 360 nm, 305 nm and 280 nm showing alternating positive, negative and positive Cotton effects respectively. In the presence of non CD-active fumarate and maleate, all bands showed enhancements in intensity, with the 280 nm-centred band likely arising from the characteristic absorbance of the rotaxane's chiral (S)-BINOL group[182] showing the largest increase. At the same time, a slight bathochromic shift of the band showing the negative Cotton effect was seen. These changes were consistent with dicarboxylate binding between both macrocycle components enforcing a change in rotaxane conformation/ BINOL twist. Slightly larger spectral changes were seen for fumarate compared to maleate, which is consistent with the prior ^1H NMR titrations suggesting that maleate was

less able to bridge the space between the Lewis acidic interlocked binding sites, thus affecting the rotaxane geometry to a smaller extent. In stark contrast, the presence of a large excess of Cl^- (c.a. 570 eqv.) relative to rotaxane resulted in negligible changes in its CD spectrum, once again corroborating the earlier deduction that the halide was binding predominantly in each interlocked cavity and thus not inducing any changes to the helicity of the rotaxane as a whole.

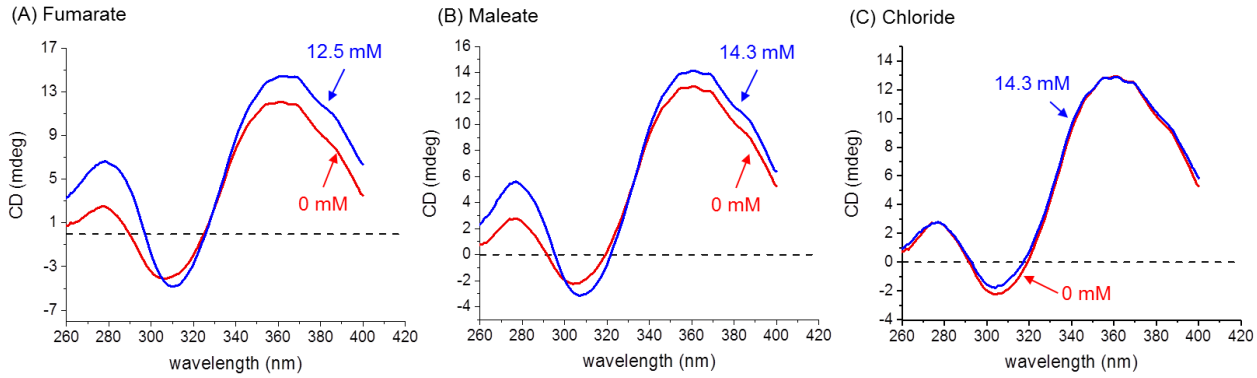


***Figure 4.50**. Circular dichroism spectral traces of [3]rotaxane **4.44** before and after the addition of (A) 12.5 mM fumarate; (B) 14.3 mM maleate and (C) 14.3 mM of Cl^- ([**4.44**] = 25 μM; $CDCl_3$/ CD_3OD/ D_2O 60:39:1 v/v, T = 293 K).*

The contrasting dicarboxylate and Cl^- coordination mode of rotaxane **4.44** suggested that fluorescence spectroscopy could distinguish both classes of anions, as only the lengthier dicarboxylates are expected to interact significantly with the central (S)-BINOL fluorophore to elicit an optical response. Indeed, fluorescence titrations performed with **4.44** in $CHCl_3$/ CH_3OH/ H_2O 60:39:1 *v/v* showed general quenching of the (*S*)-BINOL fluorescence ($\lambda_{em.}$= 360 nm) upon addition of complex dicarboxylates (Figure 4.51), resulting from the formation of a sandwich binding complex. It is noteworthy that both Cl^- and oxalate (the simplest dicarboxylate), which are likely to be binding around the vicinity of each interlocked cavity and thus held away from the fluorophore, led to significantly smaller extents of quenching. Compared to the free dicationic axle **4.42**, rotaxane **4.44** gave more pronounced discriminatory responses for the more complex dicarboxylate. As shown in Figure 4.51B, although Cl^- also elicited a diminished response compared with the complex dicarboxylates,

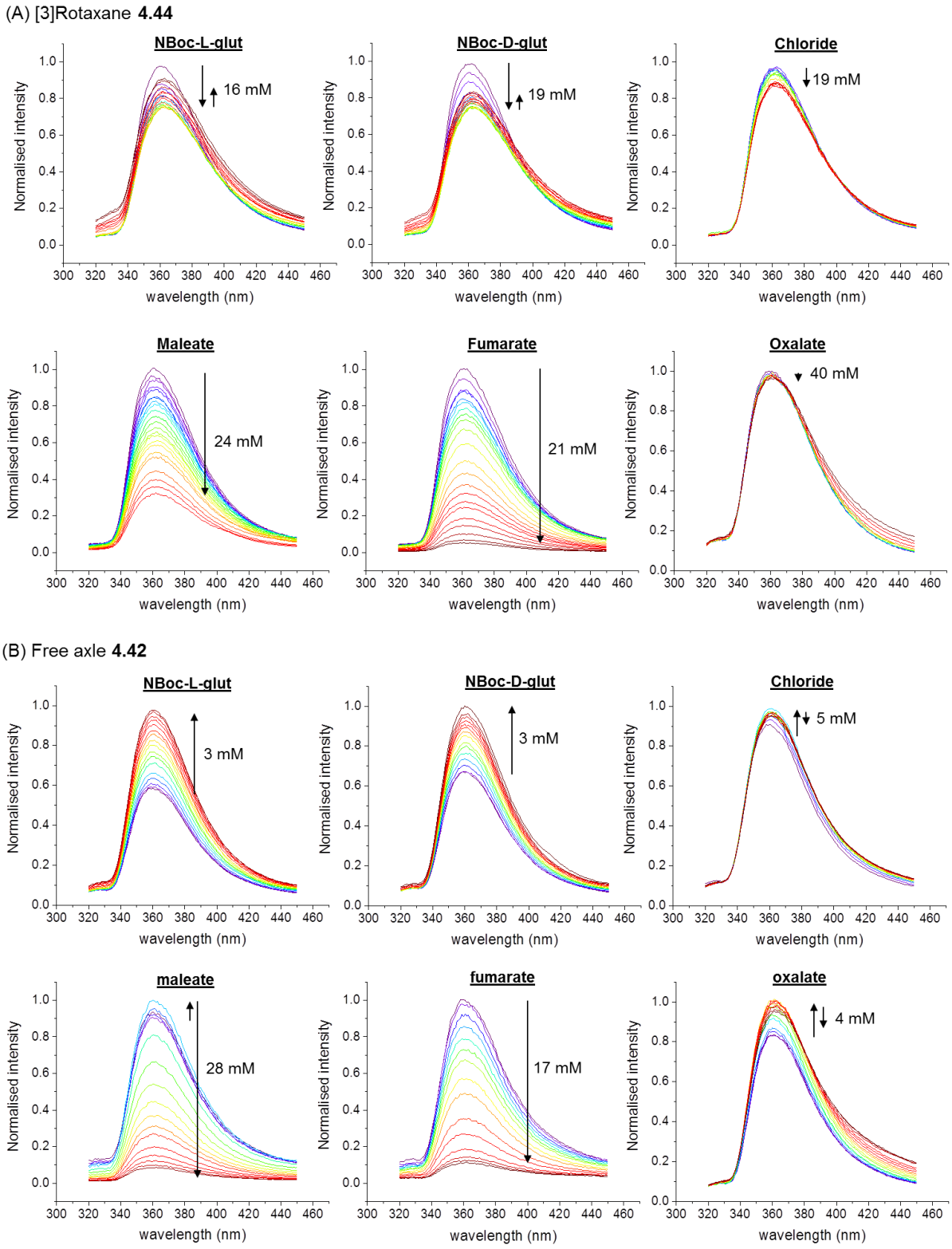


***Figure 4.51**. Fluorescence spectra of (A) [3]rotaxane **4.44** and (B) free axle **4.42** in the presence of increasing quantities of anions ([host] = 50 μM; λ_{ex} = 280 nm; $CHCl_3$/ CH_3OH/ H_2O 60:39:1 v/v; T = 293 K).*

oxalate binding to **4.42** resulted in notable fluorescence enhancement. Unlike **4.44**, binding of the *N*Boc-glutamates and oxalate with axle **4.42** resulted in fluorescence enhancement, suggesting that they were binding in a different way to rotaxane **4.44**. While MD simulation experiments are required to shed light on this, free axle **4.42** may be binding the dicarboxylates via formation of a pincer complex (Figure 4.52), which is not possible with the [3]rotaxane due to the steric bulk of the macrocycle components and the different orientation of the Lewis acidic interlocked binding sites. Interestingly, both maleate and fumarate caused consistently large fluorescence quenching of **4.42** and **4.44**, possibly due to anion binding bringing the (*S*)-BINOL fluorophore and the anions' olefin group into close contact and facilitating exciplex formation.[183,184] Quantitative comparison of the dicarboxylate selectivity of **4.42** and **4.44** could be performed by modelling the fluorescence titration data using BindFit[171] to determine host-guest 1:1 and 1:2 stoichiometric association constants summarised in Table 4.7.

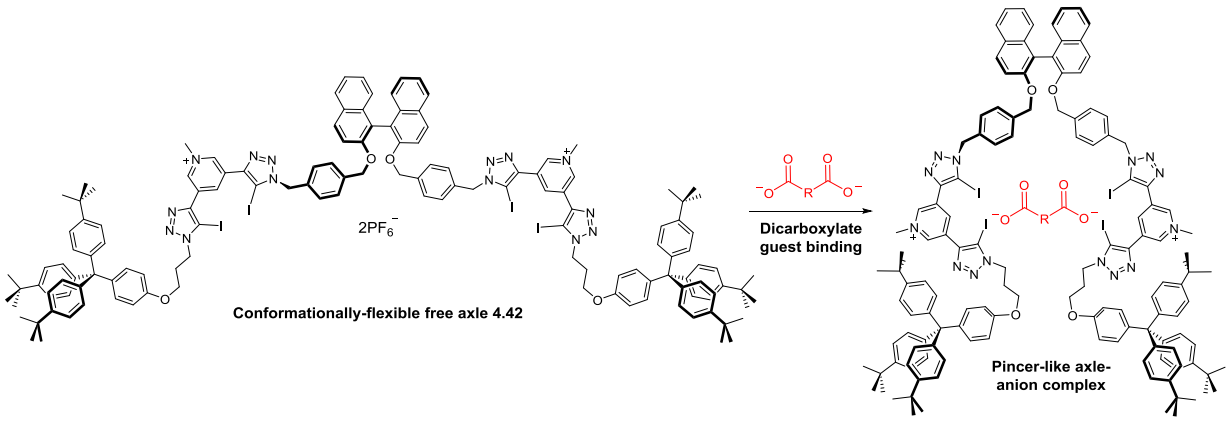


***Figure 4.52**. Proposed mode of dicarboxylate binding to free axle **4.42** via formation of a host-guest 1:1 pincer complex.*

Table 4.7. Association constants (*K*) of rotaxane **4.44** and free axle **4.42** with different anions from fluorescence binding studies. [a]

Anion	Rotaxane **4.44**	Free axle **4.42**
(*N*Boc-(*S*)-Glu)$^{2-}$	K_{11} = 35227 ± 2114 K_{12} = 13 ± 1	K_{11} = 1598 ± 18
(*N*Boc-(*R*)-Glu)$^{2-}$	K_{11} = 6226 ± 68 K_{12} = 111 ± 1	K_{11} = 1660 ± 25
Fumarate^{2-}	K_{11} = 18365 ± 1164 K_{12} = 139 ± 1	K_{11} = 106 ± 2 K_{12} = 589 ± 9
Maleate^{2-}	K_{11} = 4179 ± 81 K_{12} = 12.6 ± 0.4	-[c]
Oxalate^{2-}	-[b]	K_{11} = 1427 ± 26 K_{12} = 357 ± 6

[a] *K* values determined by global spectral fitting using BindFit[171] to a host-guest 1:2 binding model; *T* = 293 K, [host] = 50 μM, $\lambda_{ex.}$= 280 nm, $CHCl_3$/ CH_3OH/ H_2O 60:39:1 *v/v*; [b] Fluorescence changes too small to accurately determine *K* values; [c] Complex binding equilibria preventing accurate determination of *K* values.

From Table 4.7, rotaxane **4.44** showed strong first association (K_{11}) with all complex dicarboxylates, with K_{12} at least an order of magnitude smaller in all cases, once again consistent with the anions being bound predominantly via host-guest 1:1 sandwich complex formation. Notable stereo-discrimination was also observed, where *N*Boc-(*S*)-glutamate dicarboxylate preferentially bound over the opposite enantiomer with selectivity of K_S/ K_R = 5.7 ± 0.3. Rotaxane **4.44** was also able to distinguish between geometric isomers by showing a large preference for fumarate over maleate (K_{fum}/ K_{mal} = 4.4 ± 0.3), likely due to better host-guest size-complementarity for the former. At the time of writing, rotaxane **4.44** is the first known example of an interlocked structure capable of simultaneously discriminating between stereo- and geometric isomers.

On the other hand, while free axle **4.42** showed similar anion-induced fluorescence responses as rotaxane **4.44**, it exhibited significantly reduced dicarboxylate binding affinities, as exemplified by the *N*Boc-glutamates which did not show any evidence of second anion binding. In addition, barely any enantioselectivity was seen with the *N*Boc-glutamates (K_R/ K_S = 1.04 ± 0.02), possibly a consequence of the pincer complex formation holding the dicarboxylates away from the central (*S*)-BINOL unit of **4.42** for effective chiral discrimination (Figure 4.52). Compared with the rotaxane, axle **4.42** also showed less well-defined binding of

maleate and fumarate, where the former showed complex binding equilibria and the latter exhibited a surprising cooperative binding mode ($K_{12} > 4K_{11}$) which is difficult to rationalise without computational modelling. Axle **4.42** also bound oxalate surprisingly strongly with significant magnitudes of both K_{11} and K_{12}. This possibly indicated that oxalate may be too small to effectively bridge the separation between the XB-donor binding sites on **4.42** in the pincer complex, allowing binding to occur at both sites.

4.5 Conclusions and Future Work

4.5.1 Conclusions

This chapter has demonstrated that the stringent directionality constraints of σ-hole interactions can influence the stereoselective recognition properties of chiral host molecules. 3,3'-Substitution on a chiral (*S*)-BINOL motif permits effective stereo-discrimination of chiral anions, where the presence of XB-donor iodotriazolium groups were found to enhance its effectiveness relative to the HB host analogue largely due to the more restricted directional anion binding geometries and arrangements conferred by XB. However, incorporating this XB motif into a macrocycle resulted in smaller improvements in enantioselectivity than expected, which was rationalised by MD simulations to be due to the steric bulk of the XB-donor iodotriazolium groups holding the chiral anion far above the plane of the macrocycle, reducing the influence of the macrocycle (*S*)-BINOL motif's chiral environment on binding. Constraining the chiral anion cavity even further in a XB [2]rotaxane containing both chiral axle and macrocycle components led to significant augmentation of enantioselectivity due to three dimensional encapsulation of the chiral guest in the interlocked space. MD simulations demonstrated that the XB donor groups in the centre of the interlocked cavity were predominantly anchoring the anionic portions of the guests, which 'forced' the asymmetric components of the guest into close proximity with the [2]rotaxanes' macrocycle components, and accounted for the greater influence of the macrocycle component over the axle towards the overall chiral selectivity of the chiral [2]rotaxane host design.

For binding of structurally-diverse dicarboxylate anions, σ-hole (XB/ ChB) donors incorporated into an acyclic receptor molecule gave dramatically different discrimination properties towards stereo- and geometric isomers. Other than enhancing chiral selectivity over the HB analogue, the iodotriazolium-containing XB receptor also led to different dicarboxylate enantiomer and geometric isomer preferences, likely attributable to their contrasting geometric and steric constraints with HB for dicarboxylate binding. While the methylseleno-triazolium ChB host gave similar dicarboxylate binding trends as the XB analogue, highlighting the influences of σ-hole in both cases, the effects were noticeably less pronounced due to weaker ChB interactions arising from the less polarisable ChB-donor Se atoms. Adopting the ditopic host design in an unprecedented XB [3]rotaxane allowed dicarboxylate binding to occur primarily via formation of a 1:1 stoichiometric host-guest sandwich complex in the space between the rotaxane's two macrocycle components, whereas the smaller Cl^- was bound in each interlocked site. Other than providing a valuable means of distinguishing dicarboxylates from smaller anions via fluorescence spectroscopy, the [3]rotaxane design also led to the best stereo-discrimination yet seen amongst existing chiral XB-donor hosts, as well as a notable selectivity observed for the more size-complementary dicarboxylate geometric isomer. Contrastingly, significantly diminished selectivity was discerned for the non-interlocked free axle component, highlighting the importance of the [3]rotaxane host design for these purposes.

4.5.2 Future Work

All instances of chiral discrimination examined in this chapter obey the SR binding model expounded in Section 4.1.1, where a minimum of two interactions (e.g. XB, ChB, HB and water bridges) are responsible for guest coordination, leaving at least one stereochemically-dependent interaction for enantioselectivity. Despite the success of this model for *rationalising* chiral selectivity, it does not provide guidelines to achieve the impressive enantioselectivities of natural enzymes. Future work may thus involve first screening a larger library of chiral XB or ChB host systems with a greater diversity of chiral substrates to better identify optimal host design criteria specific to these σ-hole interactions. The following may also be considered as extension of the present work:

- Studying the effects of mechanical chirality in interlocked host systems for chiral guest discrimination, and comparing their behaviour with covalently chiral counterparts (i.e the systems studied herein).
- Chiral anion discrimination using a [2]catenane or more diverse interlocked structures such as an unusual handcuff [2]rotaxane such as that illustrated schematically in Figure 4.53- the latter offers greater structural preorganisation than [3]rotaxane **4.44** and thus may enhance chiral and geometric selectivity.

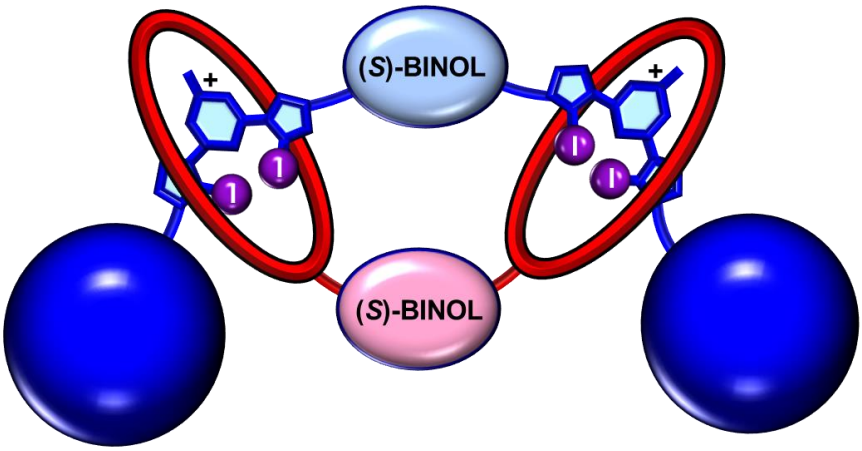


***Figure 4.53**. Cartoon representation of a chiral handcuff [2]rotaxane for enantio-discrimination.*

4.6 References

1 F. R. Keene, Ed., *Chirality in Supramolecular Assemblies: Causes and Consequences*, John Wiley & Sons, Ltd, 2016.
2 G. A. Hembury, V. V. Borovkov and Y. Inoue, *Chem. Rev.*, 2008, **108**, 1–73.
3 A. Berthod, *Anal. Chem.*, 2006, **78**, 2093–2099.
4 A. Mezzetti, J. D. Schrag, C. S. Cheong and R. J. Kazlauskas, *Chem. Biol.*, 2005, **12**, 427–437.
5 L. Pu, *Acc. Chem. Res.*, 2012, **45**, 150–163.
6 J. C. Ruble, H. A. Latham and G. C. Fu, *J. Am. Chem. Soc.*, 1997, **119**, 1492–1493.
7 A. G. Ogston, *Nature*, 1948, **162**, 963–963.
8 L. H. Easson and E. Stedman, *Biochem. J.*, 1933, **27**, 1257–1266.
9 V. A. Davankov, *Chirality*, 1997, **9**, 99–102.
10 W. H. Pirkle, *Chirality*, 1997, **9**, 103–103.
11 W. H. Pirkle and T. C. Pochapsky, *Chem. Rev.*, 1989, **89**, 347–362.
12 P. E. Wilcox, C. Heidelberger and V. R. Potter, *J. Am. Chem. Soc.*, 1950, **72**, 5019–5024.
13 A. D. Mesecar and D. E. Koshland, *IUBMB Life*, 2000, **49**, 457–466.
14 R. Bentley, *Arch. Biochem. Biophys.*, 2003, **414**, 1–12.
15 V. Sundaresan and R. Abrol, *Protein Sci.*, 2002, **11**, 1330–1339.
16 V. Sundaresan and R. Abrol, *Chirality*, 2005, **17**, S30–S39.
17 Ruffolo Jr R.R., in *Stereochemistry and biological activity of drugs*, Blackwell Scientific, Oxford, U.K., 1983, pp. 103–125.
18 S.-E. Ryu, H.-J. Choi and D. H. Kim, *J. Am. Chem. Soc.*, 1997, **119**, 38–41.
19 K. R. Hanson, *Arch. Biochem. Biophys.*, 1981, **211**, 575–588.

20 C. J. Easton and C. A. Hutton, *J Chem Soc Perkin Trans 1*, 1994, 3545–3548.
21 J. McConathy and M. J. Owens, *Prim. Care Companion J. Clin. Psychiatry*, 2003, **5**, 70–73.
22 D. A. Matteo, A. J. Grunseth, E. R. Gonzalez, S. L. Anselmo, M. A. Kennedy, P. Moman, D. A. Scott, A. Hoang and C. D. Sohl, *J. Biol. Chem.*, 2017, **292**, 7971-7983.
23 R. P. P. Neves, P. A. Fernandes and M. J. Ramos, *ACS Catal.*, 2016, **6**, 357–368.
24 D. B. Cherbavaz, M. E. Lee, R. M. Stroud and D. E. Koshland Jr, *J. Mol. Biol.*, 2000, **295**, 377–385.
25 D. A. Lang, M. L. M. Mannesse, G. H. De Haas, H. M. Verheij and B. W. Dijkstra, *Eur. J. Biochem.*, 1998, **254**, 333–340.
26 A. N. Morozov, C. D'Cunha, C. A. Alvarez and D. C. Chatfield, *Biophys. J.*, **100**, 1066–1075.
27 T. A. Müller, M. I. Zavodszky, M. Feig, L. A. Kuhn and R. P. Hausinger, *Protein Sci.*, 2006, **15**, 1356–1368.
28 N. H. Evans and P. D. Beer, in *Chirality in Supramolecular Assemblies*, John Wiley & Sons, Ltd, 2016, pp. 142–158.
29 B. Baragaña, A. G. Blackburn, P. Breccia, A. P. Davis, J. de Mendoza, J. M. Padrón-Carrillo, P. Prados, J. Riedner and J. G. de Vries, *Chem. – Eur. J.*, 2002, **8**, 2931–2936.
30 S. Bartoli, T. Mahmood, A. Malik, S. Dixon and J. D. Kilburn, *Org Biomol Chem*, 2008, **6**, 2340–2345.
31 A. Akdeniz, T. Minami, S. Watanabe, M. Yokoyama, T. Ema and P. Anzenbacher, *Chem Sci*, 2016, **7**, 2016–2022.
32 H.-T. Feng, X. Zhang and Y.-S. Zheng, *J. Org. Chem.*, 2015, **80**, 8096–8101.
33 J. L. Sessler, A. Andrievsky, V. Král and V. Lynch, *J. Am. Chem. Soc.*, 1997, **119**, 9385–9392.
34 H. Miyaji, S.-J. Hong, S.-D. Jeong, D.-W. Yoon, H.-K. Na, J. Hong, S. Ham, J. L. Sessler and C.-H. Lee, *Angew. Chem. Int. Ed.*, 2007, **46**, 2508–2511.
35 S. J. Cantrill, M. C. T. Fyfe, A. M. Heiss, J. Fraser Stoddart, A. J. P. White and D. J. Williams, *Chem Commun*, 1999, 1251–1252.
36 S. Anderson and H. L. Anderson, *Angew. Chem. Int. Ed. Engl.*, 1996, **35**, 1956–1959.
37 Y. Li, Y. Feng, Y.-M. He, F. Chen, J. Pan and Q.-H. Fan, *Tetrahedron Lett.*, 2008, **49**, 2878–2881.
38 W. Yang, Y. Li, J. Zhang, N. Chen, S. Chen, H. Liu and Y. Li, *Small*, 2012, **8**, 2602–2607.
39 B. Lewandowski, G. De Bo, J. W. Ward, M. Papmeyer, S. Kuschel, M. J. Aldegunde, P. M. E. Gramlich, D. Heckmann, S. M. Goldup, D. M. D'Souza, A. E. Fernandes and D. A. Leigh, *Science*, 2013, **339**, 189.
40 T. Schmidt, R. Schmieder, W. M. Müller, B. Kiupel and F. Vögtle, *Eur. J. Org. Chem.*, 1998, **1998**, 2003–2007.
41 S. Shinoda, T. Maeda, H. Miyake and H. Tsukube, *Supramol. Chem.*, 2011, **23**, 244–248.
42 C. Kauffmann, W. M. Müller, F. Vögtle, S. Weinman, S. Abramson and B. Fuchs, *Synthesis*, 2000, **1999**, 849–853.
43 C. Reuter, C. Seel, M. Nieger and F. Vögtle, *Helv. Chim. Acta*, 2000, **83**, 630–640.
44 C. Reuter, A. Mohry, A. Sobanski and F. Vögtle, *Chem. – Eur. J.*, 2000, **6**, 1674–1682.
45 P. E. Glen, J. A. T. O'Neill and A.-L. Lee, *Tetrahedron*, 2013, **69**, 57–68.
46 E. A. Neal and S. M. Goldup, *Angew. Chem. Int. Ed.*, 2016, **55**, 12488–12493.
47 D. M. Walba, *Tetrahedron*, 1985, **41**, 3161–3212.
48 G. A. Breault, C. A. Hunter and P. C. Mayers, *Tetrahedron*, 1999, **55**, 5265–5293.
49 L. E. Orgel, *Acc. Chem. Res.*, 1995, **28**, 109–118.
50 D. K. Mitchell and J.-P. Sauvage, *Angew. Chem. Int. Ed. Engl.*, 1988, **27**, 930–931.
51 A. Mohry, F. Vögtle, M. Nieger and H. Hupfer, *Chirality*, 2000, **12**, 76–83.
52 F. Vögtle, T. Dünnwald and T. Schmidt, *Acc. Chem. Res.*, 1996, **29**, 451–460.
53 S.-H. Li, H.-Y. Zhang, X. Xu and Y. Liu, *Nat. Commun.*, 2015, **6**, 7590.
54 K. J. Hartlieb, A. K. Blackburn, S. T. Schneebeli, R. S. Forgan, A. A. Sarjeant, C. L. Stern, D. Cao and J. F. Stoddart, *Chem Sci*, 2014, **5**, 90–100.
55 C. Dietrich-Buchecker and J.-P. Sauvage, *Chem Commun*, 1999, 615–616.
56 J. F. Nierengarten, C. O. Dietrich-Buchecker and J. P. Sauvage, *J. Am. Chem. Soc.*, 1994, **116**, 375–376.
57 S. Ottens-Hildebrandt, T. Schmidt, J. Harren and F. Vögtle, *Liebigs Ann.*, 1995, **1995**, 1855–1860.
58 C. P. McArdle, S. Van, M. C. Jennings and R. J. Puddephatt, *J. Am. Chem. Soc.*, 2002, **124**, 3959–3965.
59 R. J. Bordoli and S. M. Goldup, *J. Am. Chem. Soc.*, 2014, **136**, 4817–4820.
60 J.-C. Chambron and J.-P. Sauvage, *New J Chem*, 2013, **37**, 49–57.
61 G. Gil-Ramírez, D. A. Leigh and A. J. Stephens, *Angew. Chem. Int. Ed.*, 2015, **54**, 6110–6150.
62 E. A. Neal and S. M. Goldup, *Chem Commun*, 2014, **50**, 5128–5142.
63 R. Barat, T. Legigan, I. Tranoy-Opalinski, B. Renoux, E. Peraudeau, J. Clarhaut, P. Poinot, A. E. Fernandes, V. Aucagne, D. A. Leigh and S. Papot, *Chem Sci*, 2015, **6**, 2608–2613.
64 A. Fernandes, A. Viterisi, F. Coutrot, S. Potok, D. A. Leigh, V. Aucagne and S. Papot, *Angew. Chem. Int. Ed.*, 2009, **48**, 6443–6447.
65 G. Hattori, T. Hori, Y. Miyake and Y. Nishibayashi, *J. Am. Chem. Soc.*, 2007, **129**, 12930–12931.
66 M. Galli, J. E. M. Lewis and S. M. Goldup, *Angew. Chem. Int. Ed.*, 2015, **54**, 13545–13549.
67 V. Blanco, D. A. Leigh, V. Marcos, J. A. Morales-Serna and A. L. Nussbaumer, *J. Am. Chem. Soc.*, 2014, **136**, 4905–4908.
68 Y. Tachibana, N. Kihara and T. Takata, *J. Am. Chem. Soc.*, 2004, **126**, 3438–3439.
69 Y. Tachibana, N. Kihara, K. Nakazono and T. Takata, *Phosphorus Sulfur Silicon Relat. Elem.*, 2010, **185**, 1182–1205.
70 Y. Cakmak, S. Erbas-Cakmak and D. A. Leigh, *J. Am. Chem. Soc.*, 2016, **138**, 1749–1751.
71 S. M. Goldup, *Nat Chem*, 2016, **8**, 404–406.

72 N. Kameta, Y. Nagawa, M. Karikomi and K. Hiratani, *Chem Commun*, 2006, 3714–3716.
73 R. Mitra, M. Thiele, F. Octa-Smolin, M. C. Letzel and J. Niemeyer, *Chem Commun*, 2016, **52**, 5977–5980.
74 E. Zhou, J. Zhang and C. Dong, *ARKIVOC*, 2014, **v**, 351–364.
75 L. Meca, D. Řeha and Z. Havlas, *J. Org. Chem.*, 2003, **68**, 5677–5680.
76 E. P. Kyba, G. W. Gokel, F. De Jong, K. Koga, L. R. Sousa, M. G. Siegel, L. Kaplan, G. D. Y. Sogah and D. J. Cram, *J. Org. Chem.*, 1977, **42**, 4173–4184.
77 J. M. Brunel, *Chem. Rev.*, 2005, **105**, 857–898.
78 C. Rosini, L. Franzini, A. Raffaelli and P. Salvadori, *Synthesis*, 2002, **1992**, 503–517.
79 Y. Chen, S. Yekta and A. K. Yudin, *Chem. Rev.*, 2003, **103**, 3155–3212.
80 P. Kočovský, Š. Vyskočil and M. Smrčina, *Chem. Rev.*, 2003, **103**, 3213–3246.
81 R. Noyori and H. Takaya, *Acc. Chem. Res.*, 1990, **23**, 345–350.
82 L. Pu, *Chem. Rev.*, 1998, **98**, 2405–2494.
83 D. J. Cram, *Nature*, 1992, **356**, 29–36.
84 B. Dietrich, J.-M. Lehn and J. Simon, *Angew. Chem. Int. Ed. Engl.*, 1974, **13**, 406–407.
85 V. J. Pugh, Q.-S. Hu, X. Zuo, F. D. Lewis and L. Pu, *J. Org. Chem.*, 2001, **66**, 6136–6140.
86 P. Lin, in *1,1'-Binaphthyl-Based Chiral Materials*, Imperial College Press, London, U. K., 2009, pp. 13–86.
87 G. Wei, Y. Jiang, F. Li, Y. Quan, Y. Cheng and C. Zhu, *Polym Chem*, 2014, **5**, 5218–5222.
88 Q.-S. Lu, L. Dong, J. Zhang, J. Li, L. Jiang, Y. Huang, S. Qin, C.-W. Hu and X.-Q. Yu, *Org. Lett.*, 2009, **11**, 669–672.
89 F. Wang, R. Nandhakumar, Y. Hu, D. Kim, K. M. Kim and J. Yoon, *J. Org. Chem.*, 2013, **78**, 11571–11576.
90 H. Zhou, Y. Zhao, G. Gao, S. Li, J. Lan and J. You, *J. Am. Chem. Soc.*, 2013, **135**, 14908–14911.
91 A. Bencini, C. Coluccini, A. Garau, C. Giorgi, V. Lippolis, L. Messori, D. Pasini and S. Puccioni, *Chem Commun*, 2012, **48**, 10428–10430.
92 L. Yang, S. Qin, X. Su, F. Yang, J. You, C. Hu, R. Xie and J. Lan, *Org Biomol Chem*, 2010, **8**, 339–348.
93 T. J. Burchell, M. C. Jennings and R. J. Puddephatt, *Inorg Chim Acta*, 2006, **359**, 2812–2818.
94 W. S. Brotherton, R. J. Clark and L. Zhu, *J. Org. Chem.*, 2012, **77**, 6443–6455.
95 Y. Takeda, M. Okazaki and S. Minakata, *Chem Commun*, 2014, **50**, 10291–10294.
96 M. J. Hynes, *J. Chem. Soc. Dalton Trans.*, 1993, 311–312.
97 S. Zhang, C. M. Cardona and L. Echegoyen, *Chem Commun*, 2006, 4461–4473.
98 Z. Dai, X. Xu and J. W. Canary, *Chirality*, 2005, **17**, S227–S233.
99 K. Chun, T. H. Kim, O.-S. Lee, K. Hirose, T. D. Chung, D. S. Chung and H. Kim, *Anal. Chem.*, 2006, **78**, 7597–7600.
100 G. Mirri, S. D. Bull, P. N. Horton, T. D. James, L. Male and J. H. R. Tucker, *J. Am. Chem. Soc.*, 2010, **132**, 8903–8905.
101 Y. Willener, K. M. Joly, C. J. Moody and J. H. R. Tucker, *J. Org. Chem.*, 2008, **73**, 1225–1233.
102 A. Mulas, Y. Willener, J. Carr-Smith, K. M. Joly, L. Male, C. J. Moody, S. L. Horswell, H. V. Nguyen and J. H. R. Tucker, *Dalton Trans.*, 2015, **44**, 7268–7275.
103 B. Kratochvil, E. Lorah and C. Garber, *Anal. Chem.*, 1969, **41**, 1793–1796.
104 M. A. A. Ibrahim, *J. Comput. Chem.*, 2011, **32**, 2564–2574.
105 S. Miertuš, E. Scrocco and J. Tomasi, *Chem. Phys.*, 1981, **55**, 117–129.
106 K. B. Wiberg, *Tetrahedron*, 1968, **24**, 1083–1096.
107 S. W. Robinson, C. L. Mustoe, N. G. White, A. Brown, A. L. Thompson, P. Kennepohl and P. D. Beer, *J. Am. Chem. Soc.*, 2015, **137**, 499–507.
108 D. A. Case, R. M. Betz, W. Botello-Smith, D. S. Cerutti, T. E. Cheatham III, T. A. Darden, R. E. Duke, T. J. Giese, H. Gohlke, A. W. Goetz, N. Homeyer, S. Izadi, P. Janowski, J. Kaus, A. Kovalenko, T. S. Lee, S. LeGrand, P. Li, C. Lin, T. Luchko, R. Luo, B. Madej, D. Mermelstein, K. M. Merz, G. Monard, H. Nguyen, H. T. Nguyen, I. Omelyan, A. Onufriev, D. R. Roe, A. Roitberg, C. Sagui, C. L. Simmerling, J. Swails, R. C. Walker, J. Wang, R. M. Wolf, X. Wu, L. Xiao, D. M. York and P. A. Kollman, *AMBER 14*, University of California: San Francisco, 2014.
109 J. Wang, R. M. Wolf, J. W. Caldwell, P. A. Kollman and D. A. Case, *J. Comput. Chem.*, 2004, **25**, 1157–1174.
110 J. Wang, R. M. Wolf, J. W. Caldwell, P. A. Kollman and D. A. Case, *J. Comput. Chem.*, 2005, **26**, 114–114.
111 K. Gebauer and A. Fürstner, *Angew. Chem. Int. Ed.*, 2014, **53**, 6393–6396.
112 J. E. Hein, J. C. Tripp, L. B. Krasnova, K. B. Sharpless and V. V. Fokin, *Angew. Chem. Int. Ed.*, 2009, **48**, 8018–8021.
113 D. N. Barsoum, N. Okashah, X. Zhang and L. Zhu, *J. Org. Chem.*, 2015, **80**, 9542–9551.
114 I. S. Ufimtsev and T. J. Martinez, *J. Chem. Theory Comput.*, 2009, **5**, 2619–2628.
115 A. V. Titov, I. S. Ufimtsev, N. Luehr and T. J. Martinez, *J. Chem. Theory Comput.*, 2013, **9**, 213–221.
116 C. Song, L.-P. Wang and T. J. Martínez, *J. Chem. Theory Comput.*, 2016, **12**, 92–106.
117 J. Kästner, J. M. Carr, T. W. Keal, W. Thiel, A. Wander and P. Sherwood, *J. Phys. Chem. A*, 2009, **113**, 11856–11865.
118 T. P. M. Goumans, C. R. A. Catlow, W. A. Brown, J. Kastner and P. Sherwood, *Phys Chem Chem Phys*, 2009, **11**, 5431–5436.
119 S. Tomov, J. Dongarra and M. Baboulin, *Parallel Matrix Algorithms Appl.*, 2010, **36**, 232–240.
120 D. A. Case, R. M. Betz, W. Botello-Smith, D. S. Cerutti, T. E. Cheatham III, T. A. Darden, R. E. Duke, T. J. Giese, H. Gohlke, A. W. Goetz, N. Homeyer, S. Izadi, P. Janowski, J. Kaus, A. Kovalenko, T. S. Lee, S. LeGrand, P. Li, C. Lin, T. Luchko, R. Luo, B. Madej, D. Mermelstein, K. M. Merz, G. Monard, H. Nguyen,

H. T. Nguyen, I. Omelyan, A. Onufriev, D. R. Roe, A. Roitberg, C. Sagui, C. L. Simmerling, J. Swails, R. C. Walker, J. Wang, R. M. Wolf, X. Wu, L. Xiao, D. M. York and P. A. Kollman, *AMBER 2016*, University of California: San Francisco, 2016.
121 J. A. Wisner, P. D. Beer and M. G. B. Drew, *Angew. Chem. Int. Ed.*, 2001, **40**, 3606–3609.
122 T. Mizutani, H. Takagi, O. Hara, T. Horiguchi and H. Ogoshi, *Tetrahedron Lett.*, 1997, **38**, 1991–1994.
123 R. Diaz-Torres and S. Alvarez, *Dalton Trans*, 2011, **40**, 10742–10750.
124 D. Shetty, J. M. Jeong, C. H. Ju, Y. J. Kim, J.-Y. Lee, Y.-S. Lee, D. S. Lee, J.-K. Chung and M. C. Lee, *Bioorg. Med. Chem.*, 2010, **18**, 7338–7347.
125 R. Colombo, M. Mingozzi, L. Belvisi, D. Arosio, U. Piarulli, N. Carenini, P. Perego, N. Zaffaroni, M. De Cesare, V. Castiglioni, E. Scanziani and C. Gennari, *J. Med. Chem.*, 2012, **55**, 10460–10474.
126 E. Valeur and M. Bradley, *Chem Soc Rev*, 2009, **38**, 606–631.
127 G. Haberhauer, C. Tepper, C. Wölper and D. Bläser, *Eur. J. Org. Chem.*, 2013, **2013**, 2325–2333.
128 J. M. Granda and J. Jurczak, *Chem. – Eur. J.*, 2015, **21**, 16585–16592.
129 K. H. Lee and J.-I. Hong, *Tetrahedron Lett.*, 2000, **41**, 6083–6087.
130 X. Fang and C.-J. Wang, *Chem Commun*, 2015, **51**, 1185–1197.
131 O. V. Serdyuk, C. M. Heckel and S. B. Tsogoeva, *Org Biomol Chem*, 2013, **11**, 7051–7071.
132 S. Narayanaperumal, D. G. Rivera, R. C. Silva and M. W. Paixão, *ChemCatChem*, 2013, **5**, 2756–2773.
133 Z. Zhang and P. R. Schreiner, *Chem Soc Rev*, 2009, **38**, 1187–1198.
134 I. T. Raheem, P. S. Thiara and E. N. Jacobsen, *Org. Lett.*, 2008, **10**, 1577–1580.
135 M. K. Barman, A. K. Sinha and S. Nembenna, *Green Chem*, 2016, **18**, 2534–2541.
136 D. Voet and J. G. Voet, *Biochemistry*, Wiley, New York, 2nd edn., 1995.
137 J. G. Zeikus, M. K. Jain and P. Elankovan, *Appl. Microbiol. Biotechnol.*, 1999, **51**, 545–552.
138 S. R. Platt, *Vet. J.*, 2007, **173**, 278–286.
139 A. Cavallero, A. Marte and E. Fedele, *J. Neurochem.*, 2009, **110**, 924–934.
140 R. D. Sanderson, D. F. Schneider and I. Schreuder, *J. Appl. Polym. Sci.*, 1994, **53**, 1785–1793.
141 B. F. Ward, C. G. Force, A. M. Bills and F. E. Woodward, *J. Am. Oil Chem. Soc.*, 1975, **52**, 219–224.
142 A. T. M. Serajuddin, *Adv. Drug Deliv. Rev.*, 2007, **59**, 603-616,
143 A. O. Surov, A. N. Manin, A. P. Voronin, K. V. Drozd, A. A. Simagina, A. V. Churakov and G. L. Perlovich, *Eur. J. Pharm. Sci.*, 2015, **77**, 112–121.
144 H.-D. Belitz, W. Grosch and P. Schieberle, *Food Chemistry, 4th Ed.*, SpringerVerlag, Berlin, Heidelberg, 4th Edition., 2009.
145 T. A. M. Msagati, in *Chemistry of Food Additives and Preservatives*, Blackwell Publishing Ltd., 2012, pp. 125–130.
146 H. Kwon, W. Jiang and E. T. Kool, *Chem Sci*, 2015, **6**, 2575–2583.
147 S. E. McLain, A. K. Soper and A. Watts, *J. Phys. Chem. B*, 2006, **110**, 21251–21258.
148 S. Angielski and J. Rogulski, *Acta Biochim. Pol.*, 1962, **9**, 357–365.
149 A. Munnich, *Nat Genet*, 2008, **40**, 1148–1149.
150 S. Eiam-ong, M. Spohn, N. A. Kurtzman and S. Sabatini, *Kidney Int.*, 1995, **48**, 1542–1548.
151 D. Curiel, M. Más-Montoya and G. Sánchez, *Coord. Chem. Rev.*, 2015, **284**, 19–66.
152 Z.-Y. Dong, D.-W. Zhang, X.-Z. Jiang, H. Li and G.-H. Gao, *Chin. Chem. Lett.*, 2013, **24**, 688–690.
153 M. Mei and S. Wu, *New J Chem*, 2001, **25**, 471–475.
154 T. Gunnlaugsson, A. P. Davis, J. E. O'Brien and M. Glynn, *Org Biomol Chem*, 2005, **3**, 48–56.
155 T. Gunnlaugsson, A. P. Davis, J. E. O'Brien and M. Glynn, *Org. Lett.*, 2002, **4**, 2449–2452.
156 Y.-P. Yen and K.-W. Ho, *Tetrahedron Lett.*, 2006, **47**, 1193–1196.
157 G.-Y. Qing, Y.-B. He, Y. Zhao, C.-G. Hu, S.-Y. Liu and X. Yang, *Eur. J. Org. Chem.*, 2006, **2006**, 1574–1580.
158 A. J. Lowe, B. M. Long and F. M. Pfeffer, *J. Org. Chem.*, 2012, **77**, 8507–8517.
159 V. D. Jadhav and F. P. Schmidtchen, *Org. Lett.*, 2006, **8**, 2329–2332.
160 C. Schmuck and V. Bickert, *J. Org. Chem.*, 2007, **72**, 6832–6839.
161 J. Raker and T. E. Glass, *J. Org. Chem.*, 2002, **67**, 6113–6116.
162 A. M. Costero, M. Colera, P. Gavina and S. Gil, *Chem Commun*, 2006, 761–763.
163 C. W. Gray and T. A. Houston, *J. Org. Chem.*, 2002, **67**, 5426–5428.
164 L. Tang, J. Park, H.-J. Kim, Y. Kim, S. J. Kim, J. Chin and K. M. Kim, *J. Am. Chem. Soc.*, 2008, **130**, 12606–12607.
165 C. He, X. Qian, Y. Xu, C. Yang, L. Yin and W. Zhu, *Dalton Trans*, 2011, **40**, 1034–1037.
166 T. Noguchi, B. Roy, D. Yoshihara, Y. Tsuchiya, T. Yamamoto and S. Shinkai, *Chem. – Eur. J.*, 2014, **20**, 381–384.
167 R. J. Motekaitis and A. E. Martell, *Inorg. Chem.*, 1992, **31**, 5534–5542.
168 A. J. Harte, P. Jensen, S. E. Plush, P. E. Kruger and T. Gunnlaugsson, *Inorg. Chem.*, 2006, **45**, 9465–9474.
169 S. E. Plush and T. Gunnlaugsson, *Org. Lett.*, 2007, **9**, 1919–1922.
170 S. M. Lacy, D. M. Rudkevich, W. Verboom and D. N. Reinhoudt, *J Chem Soc Perkin Trans 2*, 1995, 135–139.
171 *www.supramolecular.org*, .
172 L. Fabbrizzi and A. Poggi, *Chem Soc Rev*, 2013, **42**, 1681–1699.
173 Y. Nagawa, J. Suga, K. Hiratani, E. Koyama and M. Kanesato, *Chem Commun*, 2005, 749–751.
174 M. J. Langton and P. D. Beer, *Chem. – Eur. J.*, 2012, **18**, 14406–14412.

175 T. A. Barendt, A. Docker, I. Marques, V. Félix and P. D. Beer, *Angew. Chem. Int. Ed.*, 2016, **55**, 11069-11076
176 M.-P. Teulade-Fichou, J.-P. Vigneron and J.-M. Lehn, *J Chem Soc Perkin Trans 2*, 1996, 2169–2175.
177 A. Mishra, V. Vajpayee, H. Kim, M. H. Lee, H. Jung, M. Wang, P. J. Stang and K.-W. Chi, *Dalton Trans*, 2012, **41**, 1195–1201.
178 T. A. Barendt, S. W. Robinson and P. D. Beer, *Chem Sci*, 2016, **7**, 5171–5180.
179 M. J. Langton, S. W. Robinson, I. Marques, V. Félix and P. D. Beer, *Nat Chem*, 2014, **6**, 1039–1043.
180 M. J. Langton, I. Marques, S. W. Robinson, V. Félix and P. D. Beer, *Chem. – Eur. J.*, 2016, **22**, 185–192.
181 S. W. Robinson and P. D. Beer, *Org Biomol Chem*, 2017, **15**, 153–159.
182 Y. Wang, Y. Li, S. Liu, F. Li, C. Zhu, S. Li and Y. Cheng, *Macromolecules*, 2016, **49**, 5444–5451.
183 M. V. Encinas, E. Guzman and E. A. Lissi, *J. Phys. Chem.*, 1983, **87**, 4770–4772.
184 D. A. Labianca, G. N. Taylor and G. S. Hammond, *J. Am. Chem. Soc.*, 1972, **94**, 3679–3683.

Chapter 5

Halogen Bonding Host Systems for Anion Recognition and Sensing in Water

CHAPTER 5 : Halogen Bonding Host Systems for Anion Recognition and Sensing in Water

5.1 Introduction

Inspired by extensive 'real-world' applications of anion recognition in medicine, industry, biology and environmental monitoring,[1] the development of receptors capable of recognising and binding anions selectively in aqueous media is receiving increasing scientific attention.[2,3] However, the vast majority of anion receptors developed to date operate only in organic solvents, and examples capable of potent and selective anion binding in 100 % water are rare. Possibly, this reflects the formidable challenges that need to be overcome for anion binding in pure water, most notably the strong hydration and pH dependence of anions, as well as their generally large size and low charge densities, resulting in weaker Coulombic attractions with cationic host molecules that is further screened by the high dielectric constant of water (Section 1.1.2). Furthermore, organic-based abiotic receptors generally have low water solubilities, which limit their usage to aqueous-organic solvent media. While early examples of cryptands by Lehn have partially overcome these problems by possessing multiple cationic ammonium groups, enabling them to bind anions with impressive affinities in acidic aqueous media via a combination of size/shape complementarity, multiple HB interactions and electrostatic attractions, their applicability is limited by their narrow functional pH range.[4–6]

The last decade has seen notable advances in anion recognition and sensing in water using both abiotic acyclic and mechanically-interlocked host molecules, with recent strategies and examples discussed in the following sections.

5.1.1 Recent Strategies for Binding Anions in Water

The presence of convergent HB interactions and electrostatics has always been a popular combination in designing abiotic receptors for anion binding in water, as exemplified by recent examples containing cationic HB motifs such as ammonium,[7,8] guanidinium[9,10] and imidazolium groups.[11,12] However, alternative strategies such as coordinate bond formation

with metal complexes, the hydrophobic effect and the applications of XB are gaining increasing traction.

The strength of anion ligation to coordinatively-unsaturated metal complexes has enabled the binding and sensing of highly-hydrated anions in water which is difficult to achieve using non-covalent interactions such as HB. For instance, the Zn^{II}-dipicolylamine motif has been effectively demonstrated for binding and sensing of phosphates in buffered water at physiological pH (Figure 5.1A).[13] As discussed in Section 1.1.4.2, lanthanide complexes have been employed for the selective luminescent sensing of F^-, driven mainly by electrostatic 'hard-hard' interactions with the Ln^{III} metal centre.[14–16] Taking a slightly different approach, Faulkner and co-workers very recently reported phenacyl DO3A Eu^{III} complexes which respond to CN^- in water by capitalising on its propensity for nucleophilic addition to a carbonyl unit on the ligand scaffold to form cyanohydrins, resulting in luminescence quenching (Figure 5.1B).[17] In addition, water-soluble actinide complexes such as Schiaffino's uranyl-salophen host have been used for binding ATP and ADP in buffered water with impressive affinities of $\lg K_a > 4$ (Figure 5.1C).[18] More recently, the same group demonstrated that when lipophilic uranyl-salophen complexes are incorporated into cationic cetyltrimethylammonium bromide (CTABr) micelles in water, aqueous F^- sensing can still be achieved.[19–21]

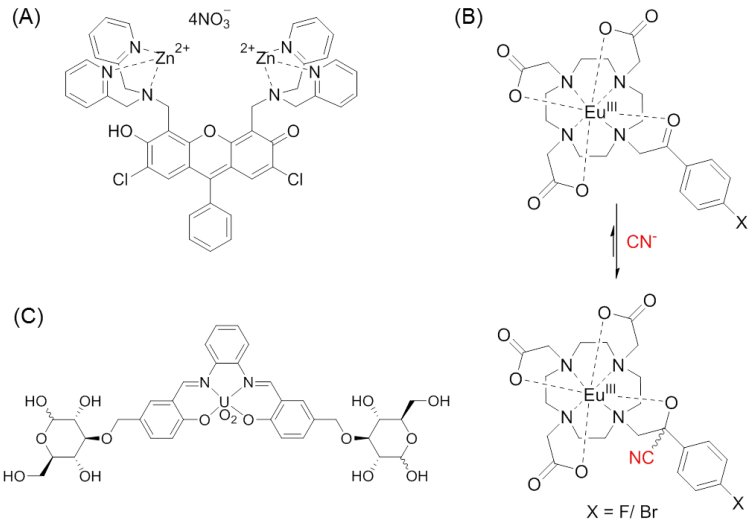


***Figure 5.1**. Examples of anion sensing in water using metal complexes: (A) Yoon's Zn^{II}-dipicolylamine receptor for pyrophosphate in water[22]; (B) Faulkner's Eu^{III} DO3A receptor for CN^- [17]; (C) Schiaffino's water-soluble uranyl-salophen host for binding ATP and ADP.[18]*

The exploitation of the hydrophobic effect has achieved spectacular success for anion binding in water with a series of recently-reported host molecules possessing deep hydrophobic binding pockets solubilised by multiple carboxylate groups along their outer rims, which include Sindelar's bambusuril macrocycle,[23,24] Pittelkow's biotin[6]uril,[25] and Gibb's cavitands.[26,27] The affinity of these receptors for hydrophobic and poorly-solvated anions (e.g. ClO_4^-, PF_6^-, I^-) can be modulated by changing the ionic strength and pH of the solution,[28] and the substituents on the outer rim of the macrocycles.[29] Remarkably, the combination of metal complexation and hydrophobic effect enabled Reinaud to bind partially-hydrated F^- within a calix[6]arene cavity containing a Cu^{II} metal centre with affinities as high as log*K* = 4.9 in acidic water (Figure 5.2A).[30]

Halogen bonding interactions have only very recently been demonstrated as an effective interaction for anion binding in 100 % water. Beer *et. al.* reported a novel receptor with diametrically-opposite pendant XB-donor arms functionalised on a central perbenzylated α-cyclodextrin core (Figure 5.2B).[31] In unbuffered D_2O, the XB receptor exhibited high selectivity for ReO_4^- (K_a = 950 M^{-1}) over other much more hydrophobic anions such as I^- and ClO_4^-. Compared with the HB analogue and native (unfunctionalised) α-cyclodextrin, the XB receptor showed greatly enhanced binding of ReO_4^-. Furthermore, binding was driven strongly by enthalpy (ΔH = -54.0 kJ mol^{-1}) and disfavoured entropically ($-T\Delta S$ = + 37.9 kJ mol^{-1}), suggesting the dominant role of XB and its strong interactions with ReO_4^- in water.

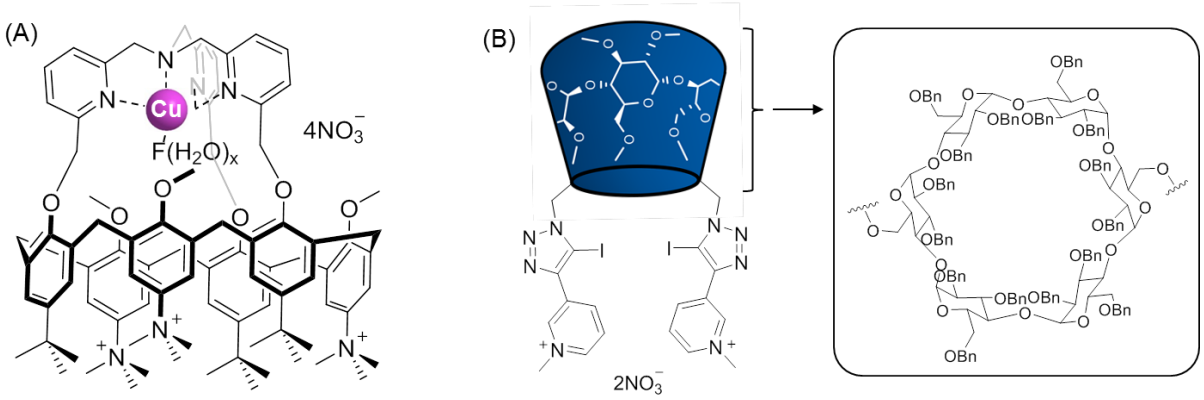


***Figure 5.2**. (A) Reinaud's Cu^{II}-calix[6]arene host for F^- binding in acidic water (pH 5.9)[30] ; (B) Beer's XB-decorated perbenzylated α-CD receptor for ReO_4^- in water[31]*

5.1.2 Water-soluble Interlocked Structures

The appendage of water-solubilising groups on mechanically-interlocked structures presents a significant advancement in their practical applicability, and can be achieved by the presence of metal cations,[32] or hydrophilic units such as sugars,[33] cyclodextrins[34] or peptides.[35] Water-soluble rotaxane structures containing dye subunits[36] have enabled them to be used in biological imaging studies.[37] Furthermore, their conformational dynamism have suggested the possibility of nanotechnological applications, such as molecular machines, also in water.[38–40] By enclosing axle components with extensive π-conjugation within macrocycles, 'encapsulated molecular wires' can be produced, potentially enabling applications of single-molecule electronics in aqueous media. [41–43]

The three dimensional binding pocket of an interlocked structure provides a shielded hydrophobic microenvironment distinct from the bulk aqueous media for guest encapsulation. For example, Sanders and Stoddart have prepared water-soluble [2]-[44] and [3]-catenanes[45] capable of binding aromatic guest molecules, driven by enhanced donor-acceptor π-π stacking interactions in water (Figure 5.3A). By incorporating XB donor groups within the binding cavity of a dicationic [2]rotaxane solubilised by bulky β-cyclodextrin stopper groups, Beer *et. al.* achieved impressive and selective binding of I^- (K_a = 2200 M^{-1}) over other halides in water, which was shown to be enthalpically-driven and entropically-disfavoured.[46] Notably, the HB analogue displayed negligible I^- association, suggesting the important roles played by XB interactions for I^- binding. More recent work with a tricationic Ru^{II}-containing rotaxane showed further augmentation of I^- binding in water (K_a = 6300 M^{-1}), capable of concomitant luminescent sensing of the halide guest.[47]

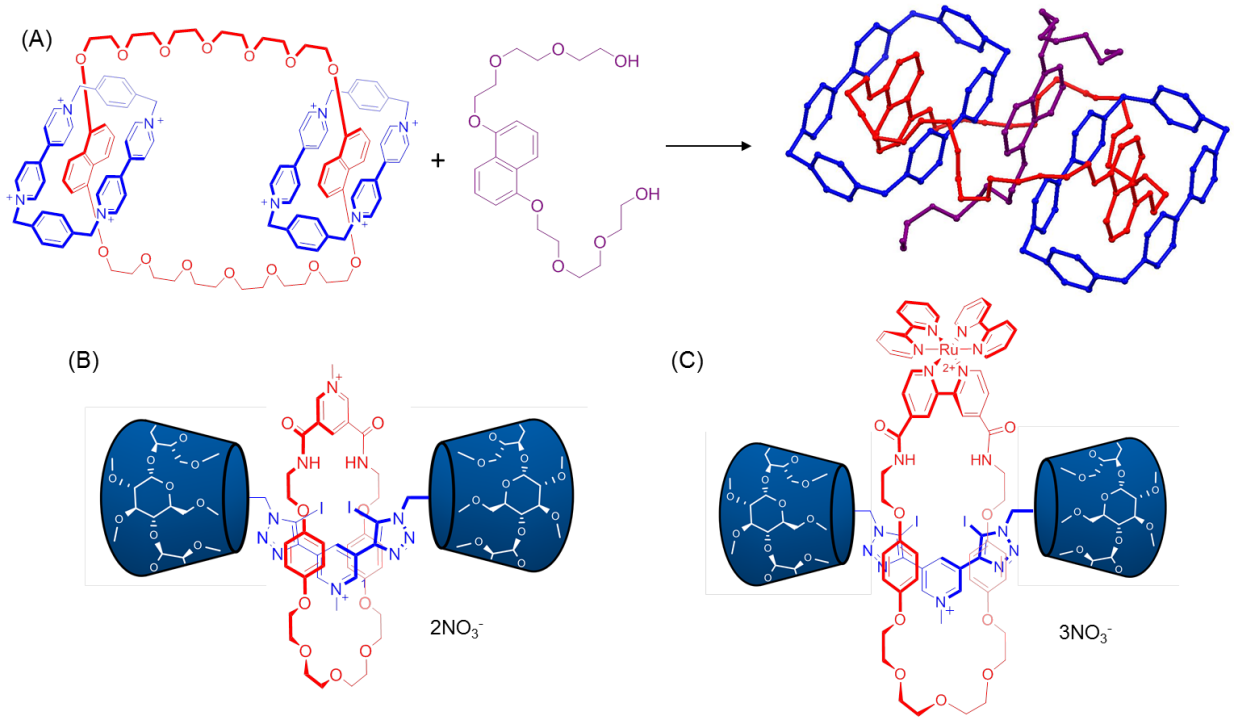


***Figure 5.3**. Examples of water-soluble interlocked molecules capable of molecular recognition: (A) 1:1 complex formed by Stoddart's [3]catenane and a naphthalene guest in water[45]; (B) Water-soluble dicationic[46] and (C) tricationic XB [2]rotaxanes by Beer for I^- recognition and sensing in water.[47]*

5.1.3 Chapter Aims

Inspired by the applications of hydrophilic poly(ethylene glycol) groups in areas such as drug delivery,[48–52] hydrophilic polymer coatings[53,54] and in biology and medicine,[55–58] together with their low cost, biocompatibility[59] and established synthetic repertoire, this chapter investigates their use as water-solubilising groups in a series of acyclic and interlocked XB and HB host systems. Initial efforts focus on the anion binding and sensing properties of a series of dicationic acyclic XB host systems containing tetra(ethylene glycol) (TEG) units at their termini to confer water solubility (Figure 5.4A). The unprecedented influences of XB on the binding properties of biological phosphate species such as HPO_4^{2-}, ATP^{4-}, ADP^{3-} and AMP^{2-} are also investigated. Following which, the synthesis of a water soluble [2]rotaxane stoppered by a novel TEG-containing unit is pursued (Figure 5.4B), as an alternative to the β-cyclodextrin-stoppered [2]rotaxanes previously reported in the group.[46,47,60] Finally, a new dicationic pyrrole-based XB anion binding motif (Figure 5.4C) is prepared and its anion recognition properties probed initially in aqueous-organic solvents, followed by pure water.

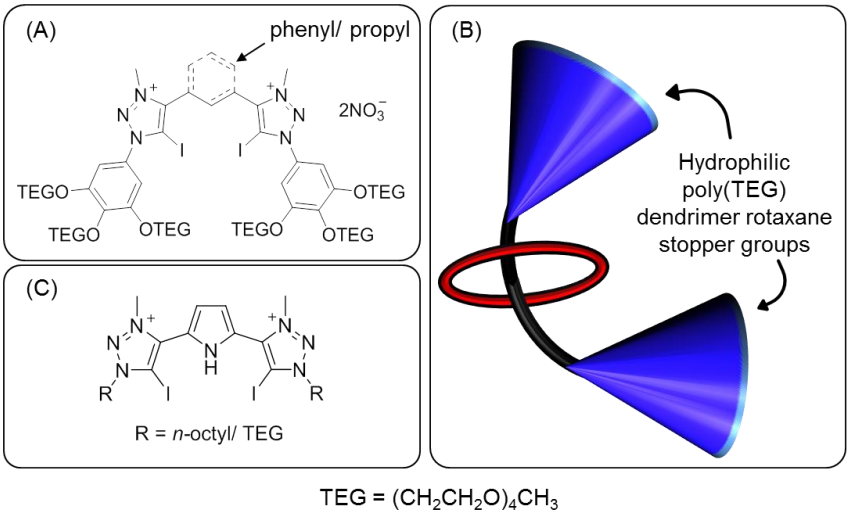


***Figure 5.4**. Tetra(ethylene glycol) (TEG)-based water-soluble host systems investigated in this chapter: (A) dicationic acyclic XB hosts; (B) a water-soluble [2]rotaxane stoppered by pseudo-dendritic stoppers; (C) pyrrole-based XB receptors.*

5.2 Water-soluble Dicationic XB Acyclic Receptors[‡]

5.2.1 Design and Syntheses of Receptors

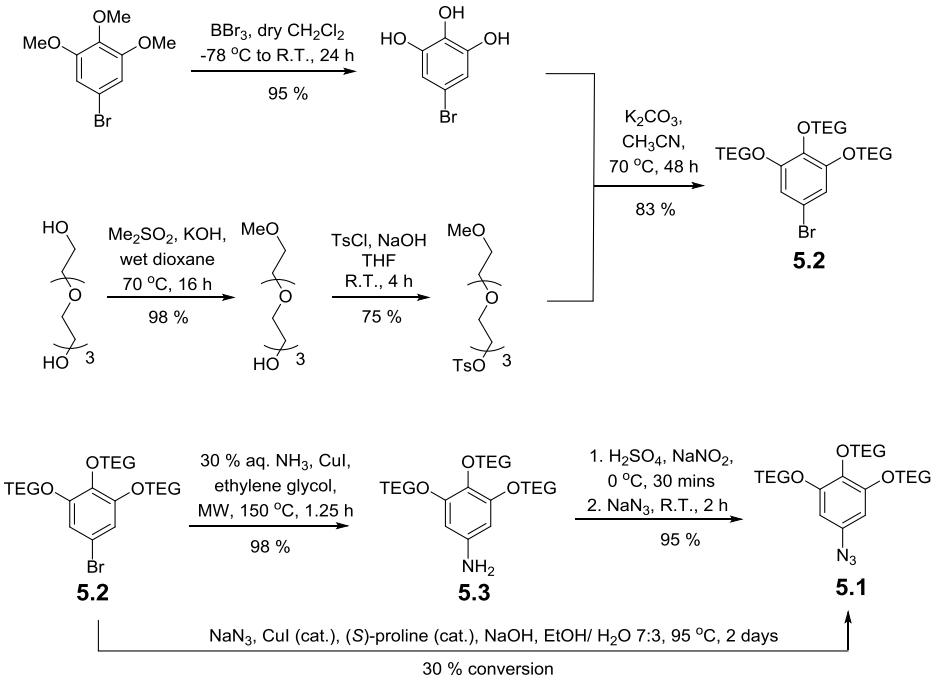
The target receptors shown in Figure 5.4A contain highly electron-deficient iodotriazolium groups to enhance the anion affinity of the binding cleft in water. Two different spacer units, namely phenyl and propyl, allowing different degrees of host rigidity, were investigated as well. Furthermore, the conjugated nature of the receptors may facilitate anion sensing in water via optical techniques. In order to identify the unique attributes of anion binding mediated by XB, the HB host analogues were also prepared and studied for comparison.

The target XB and HB host molecules were synthesised from the appropriate bis-iodo/ proto-alkyne and the tris(TEG)-functionalised aryl azide **5.1** via CuAAC reactions. Synthon **5.1** was first synthesised following a multi-stepped procedure shown in Scheme 5.1. Commercially-available 5-bromo-1,2,3-trimethoxybenzene was deprotected with BBr_3 to afford 5-bromo-1,2,3-trihydroxybenzene[61] in 95 % yield, and subsequent Williamson ether synthesis with 3 equivalents of tosyl-functionalised TEG[62] afforded aryl bromide **5.2** in 83 % yield following a reported procedure.[63] Thereafter, an attempt to convert **5.2** directly to aryl azide **5.1**

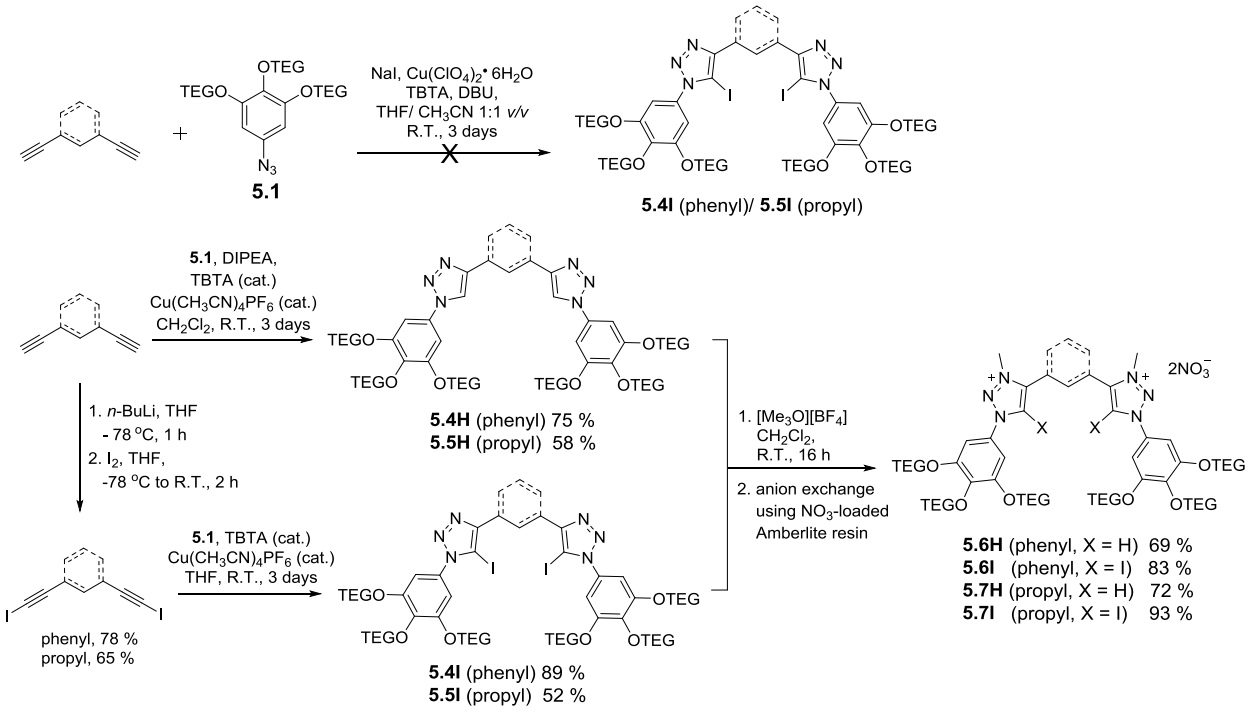
[‡] Some of the work in this section has been published: Lim, J. Y. C. and Beer, P. D., *Superior Perrhenate Anion Recognition in Water by a Halogen Bonding Acyclic Receptor*, *Chem. Commun.*, 2015, **51**, 3686-3688.

under Ullmann-type coupling conditions with NaN_3, catalysed by a CuI/ (*S*)-proline complex,[64] afforded the desired compound in approximately 30 % by ^{1}H NMR analysis. Unfortunately, the purification of **5.1** proved challenging, as its polarity was dominated by the tris(TEG) substituents and hence produced poor separation on the TLC plate from the starting material **5.2** due to similar R_f values. Therefore an alternative route was pursued, where aryl bromide **5.2** was first converted to the corresponding aniline intermediate **5.3** by a microwave-assisted copper(I)-catalysed Ullmann amination at 150 ^{o}C, followed by a Sandmeyer-type substitution to form the aryl azide **5.1** in excellent overall yields. Notably, a very clean two-step conversion of the aryl bromide **5.2** to the azide **5.1** was achieved, with no chromatographic purification necessary.

Synthesis of the XB neutral receptor precursors **5.4I** and **5.5I**, shown in Scheme 5.2, was attempted utilising Zhu's one-pot methodology directly from the appropriate terminal (proto)alkynes and aryl azide **5.1**.[65] Disappointingly, no iodotriazoles were formed regardless of performing the reaction under ambient conditions or under microwave assistance. Hence, a two-pot methodology, where the terminal alkynes were first converted to the bis-iodoalkynes followed by the CuAAC reaction, was undertaken. Bis-iodination was successfully carried out on 1,3-diethynylbenzene and 1,6-heptadiyne using *n*-butyllithium and I_2 to afford the corresponding bis-iodoalkynes in good yields. Following which, CuAAC reaction with azide **5.1** afforded the neutral receptor precursors **5.4I** and **5.5I**, which were bis-methylated with trimethyloxonium tetrafluoroborate. Following purification with either an alumina column or preparatory TLC, anion exchange using a nitrate-loaded Amberlite anion exchange resin gave the nitrate salts of receptors **5.6I** and **5.7I.** The analogous HB neutral receptor precursors and dicationic target receptors were produced in good yields following a similar protocol with the terminal (proto)alkyne starting materials (Scheme 5.2). Notably, the nitrate salts of all four dicationic receptors showed good solubility in water even at concentrations of 2.5 mM.



Scheme 5.1. *Synthesis of tris(TEG)-aryl azide synthon* ***5.1***.



Scheme 5.2. *Synthesis of water-soluble acyclic XB receptors and their HB analogues.*

5.2.2 Anion Binding Studies

Despite the water solubility of the dicationic acyclic receptors conferred by the terminal tris-TEG units, their central binding cavities containing the phenyl/propyl spacers are relatively hydrophobic. To confirm that no self-association driven by the hydrophobic effect is occurring in water, a series of dilution experiments were first performed with ^{1}H NMR spectroscopy[§] where a 1.5 mM D_2O solution of receptor **5.6I** was gradually diluted to 1.0, 0.5, 0.15, 0.10 and 0.01 mM. No signal perturbations arising from any proton environments of **5.6**I were observed during the dilutions, showing that no receptor self-aggregation or micellar formation is occurring.

^{1}H NMR binding studies were then performed by adding increasing quantities of anions (Cl^-, Br^-, I^-, ClO_4^-, ReO_4^- and SO_4^{2-}), as their sodium salts, to individual solutions of each dicationic receptor in unbuffered D_2O. Due to the modest anion binding affinities observed for all receptors in the highly-competitive all-aqueous environment, up to 120 equivalents of anions were added for reliable binding isotherms to be obtained (Figure 5.5).

As shown in Figure 5.5A, the addition of NaI to receptor **5.6I** in D_2O led to notable downfield perturbations of the signals arising from protons flanking the binding cleft (H_a and H_d). Contrastingly, the resonances from the external proton environments H_b, H_c and H_e showed *upfield* shifts upon anion addition, showing clearly that I^- was bound in the space flanked by the iodotriazolium units. With XB receptor **5.7I** containing a central propyl spacer, NaI addition only gave significant shifts of aromatic proton H_d (Figure 5.5B), accompanied by negligible shifts of any of the central alkyl proton resonances. In all cases, slight changes to the signals from the polyether solubilising groups were seen during the titrations, possibly due to changes in the ionic strengths of the aqueous environment following salt addition. As all receptors showed consistent downfield shifts of aromatic proton H_d in close proximity to the (iodo)triazolium units during the anion titrations, this signal was monitored for all receptors to obtain 1:1 stoichiometric host-guest association constants using the WinEQNMR2 software[66] (Table 5.1). Despite the large excess of anions added, no evidence of second anion

[§] The water suppression ^{1}H NMR pulse sequence *NOESYGPPR1d*, set up by Dr. Nick Rees, was used to perform the binding studies to improve the signal-to-noise ratio of the resulting spectra in D_2O.

association was observed, predominantly due to the strength of anion hydration and competitive nature of the aqueous solvent media used.

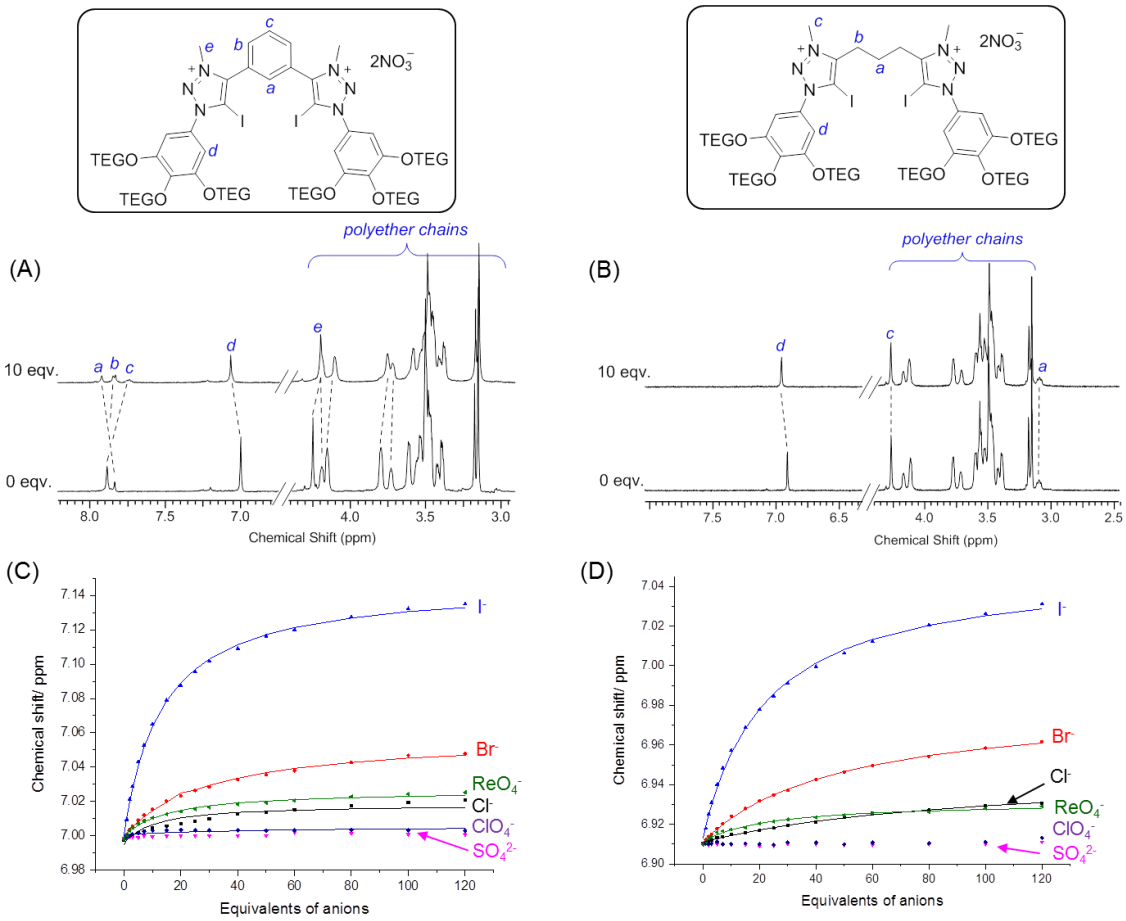


***Figure 5.5**. Partial ^{1}H NMR spectra of dicationic XB receptor (A) **5.6I** and (B) **5.7I** in the presence of 0 and 10 equivalents of NaI. Plots of changes in chemical shift of aromatic proton H_d with increasing concentrations of anions for (C) **5.6I** and (D) **5.7I** ([receptor] = 1.5 mM, D_2O, T = 298 K).*

Table 5.1. Anion association constants (K_a/ M^{-1}) of dicationic receptors in D_2O.[a]

	ΔG_{hyd}/ kJ mol^{-1} [b]	Phenyl spacer		Propyl spacer	
		5.6I	5.6H	5.7I	5.7H
Cl^-	-340	10.0 (0.1)	11.4 (0.6)	5.7 (0.4)	10.3 (0.9)
Br^-	-315	22 (2)	14.0 (0.7)	12.4 (0.5)	20 (2)
I^-	-275	51 (3)	29 (1)	30 (2)	39 (3)
ClO_4^-	-245	12 (2)	13.7 (0.5)	- [c]	24 (1)
ReO_4^-	-330	44 (2)	- [c]	29 (3)	30 (3)

[a] K_a values obtained by fitting the binding isotherms (from monitoring proton H_d) to a host-guest 1:1 stoichiometric binding model using WinEQNMR2;[66] errors (±) in parentheses; anions added as sodium salts. [b] Values obtained from Marcus[67]; [c] No binding.

In general, all receptors exhibit modest anion binding strengths due to their acyclic nature and the highly-competitive aqueous solvent environment. All receptors show Hofmeister bias for halide binding in general (affinities decreasing in the order $I^- > Br^- > Cl^-$), regardless of the nature of the central spacer unit (phenyl or propyl). Despite the dianionic nature of SO_4^{2-}, no evidence of binding was observed, likely due to the oxoanion's very strong aqueous hydration (ΔG_{hyd} = -1080 kJ mol^{-1}).[67] Although ClO_4^- is less strongly hydrated than I^-, it surprisingly binds much more weakly to the receptors, probably due to its larger anionic radius (240 nm, compared to 210 nm for I^-)[67] and resulting lower charge density. Notably, all XB receptors did not show a pronounced enhancement in ClO_4^- binding over their HB analogues, demonstrating that anion binding by XB is not driven mainly by the hydrophobic effect. The binding properties of ReO_4^- are more varied amongst the receptors (*vide infra*), where with the exception of **5.6H**, stronger association of ReO_4^- compared to Cl^- is observed, despite the fact that both anions have very similar free energies of hydration (Table 5.1).

Comparing the association constants of HB receptors **5.6H** and **5.7H** with various anions revealed that the latter, with the propyl spacer, exhibited slightly stronger anion binding than the former in general. The largest contrast was found with ReO_4^-, where **5.7H** showed modest binding (K_a = 30 M^{-1}) while **5.6H** did not show any evidence for binding. This is contrary to one's expectations that the more rigid binding site of **5.6H** would be more preorganised for anion binding than the more conformationally-flexible analogue (**5.7H**). On the other hand, these observations support the fact that the propyl spacer of **5.7H** breaks up the contiguous π-network between the cationic triazolium units of receptor **5.6H**, thereby resulting in more localised positive charges for interaction with anions.[68] In light of the very highly competitive nature of the aqueous solvent used, the effects of increased charge localisation seem to dominate the effects of preorganisation for anion binding for the HB receptors in general, accounting for the slightly enhanced binding observed. Interestingly, the binding affinities of the XB receptors show the opposite trend, with **5.6I**, bearing the more rigid phenyl spacer, showing generally augmented K_a values compared to propyl-containing **5.7I**. This may be a consequence of the greater directionality of XB interactions compared with HB, where the more rigid and preorganised cavity of **5.6I** allow the anions to be coordinated by

linear convergent XB interactions in the manner shown by X-ray diffraction studies[69] and computational modelling.[70,71] Contrastingly, the less preorganised nature of **5.7I** results in a greater degree of conformational flexibility, where the stringent linear directionality of XB may impose entropically-disfavoured geometric constraints on the binding conformations available for the receptor to adopt.

The difference in directionality of interaction between XB and HB may also account for the observation that **5.6I** generally shows improved binding affinities over its HB analogue **5.6H**, while **5.7I** and **5.7H** display less pronounced differences (Table 5.1). For example, **5.6I** bound Br^- and I^- more strongly than **5.6H**, and most interestingly, a modest binding affinity for ReO_4^- compared with no binding at all by **5.6H**. On the other hand, both **5.7I** and **5.7H** display comparable binding affinities for most anions, with the XB receptor even showing diminished K_a values. Presumably, when the binding site is poorly preorganised, such as that for **5.7H/I**, the less stringent directionality constraints of HB allow a wider range of anion binding geometries by **5.7H**, enabling the receptor to adopt many energetically and entropically more accessible binding conformations than **5.7I** which favour anion coordination.

The remarkable difference in the ReO_4^- binding properties of the rigid receptors **5.6I** and **5.6H** prompted an investigation into the thermodynamic origins of XB-mediated ReO_4^- binding in water. Hence, variable temperature (VT) ^{1}H NMR titrations of **5.6I** with $NaReO_4$ were performed in D_2O at 298, 308, 318 and 338 K. An increase in temperature resulted in weaker association between ReO_4^- and **5.6I**. A van 't Hoff analysis was then performed by plotting $R\ln(K_a/\ M^{-1})$ against T^{-1} (K^{-1}), and the binding enthalpy (ΔH) and entropy (ΔS) were obtained from the gradient and the ordinate intercept of the best-fit line (Figure 5.6) as described in Section 2.3.

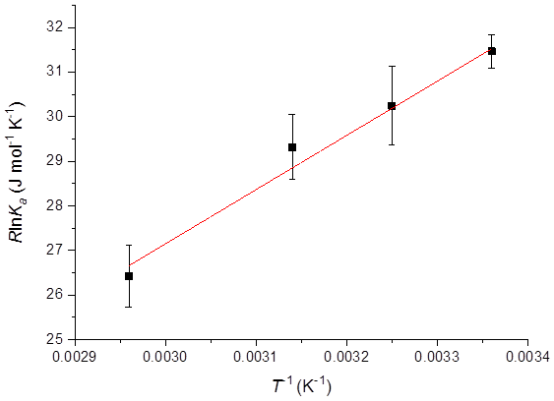


***Figure 5.6**. van 't Hoff analysis of ReO_4^- binding by XB receptor **5.6I** in D_2O, with values of K_a determined at 298, 308, 318 and 338 K ([**5.6I**] = 1.5 mM, D_2O). Pearson's R = 0.993.*

The van 't Hoff analysis revealed that ReO_4^- binding is driven by a favourable enthalpic contribution (ΔH = -12 kJ mol^{-1}) and is disfavoured entropically (ΔS = -9 J K^{-1} mol^{-1}). This is a clear indication that the classical hydrophobic effect, well-known to be driven largely by an entropic increase arising from desolvation,[3] may not be the dominant factor accounting for binding in this case. The enthalpic gain may arise from the iodotriazolium moieties of **5.6I** forming strong XB interactions with the perrhenate anion, a consequence of the significant covalency arising from XB. Indeed, the dominant enthalpic contribution to XB-mediated ReO_4^- binding is also observed in a subsequent study by Beer using an α-cyclodextrin-containing XB receptor for ReO_4^- binding,[31] as well as I^- binding by a XB rotaxane host system in water.[46] When VT-NMR titrations were performed using the HB analogue **5.6H** with ReO_4^- at 338 K, no evidence of binding was found.

In light of the observed superior ReO_4^- binding seen with receptor **5.6I** compared to **5.6H**, fluorescence titrations were performed as well in buffered water (10 mM HEPES, pH 7.4). Increasing quantities of an aqueous solution of $NaReO_4$ (up to 500 molar equivalents with respect to the receptors) were added to individual 10 μM solutions of **5.6I** and **5.6H**, and the changes in fluorescence intensity were monitored. As shown in Figure 5.7 below, ReO_4^- binding resulted in a fluorescence 'turn on' response (c.a. 80 % intensity increase) for **5.6I**, while **5.6H** showed no change in fluorescence intensity even in the presence of 500 equivalents of ReO_4^-, corroborating the augmented XB-mediated ReO_4^- affinities seen from the

^{1}H NMR titration studies. The fluorescence enhancement of **5.6I** may arise from increased receptor rigidity resulting from ReO_4^- binding in the XB binding cavity, decreasing the probability of non-radiative decay pathways. Although ReO_4^- binding and sequestration has been achieved by receptors functioning mainly in organic solvents,[72–75] examples capable of binding this anion in water have been slow to emerge.[31,76–78] At the time of writing, **5.6I** is the first XB anion receptor reported to sense the ReO_4^- anion in water via a fluorescence response, which is especially useful given the anion's inherent toxicity,[79] wide applications in medicine[80] and industry,[81] and common use as a surrogate for study of the radioactive pertechnetate ($^{99}TcO_4^-$) anion present in low levels in nuclear waste material.[75]

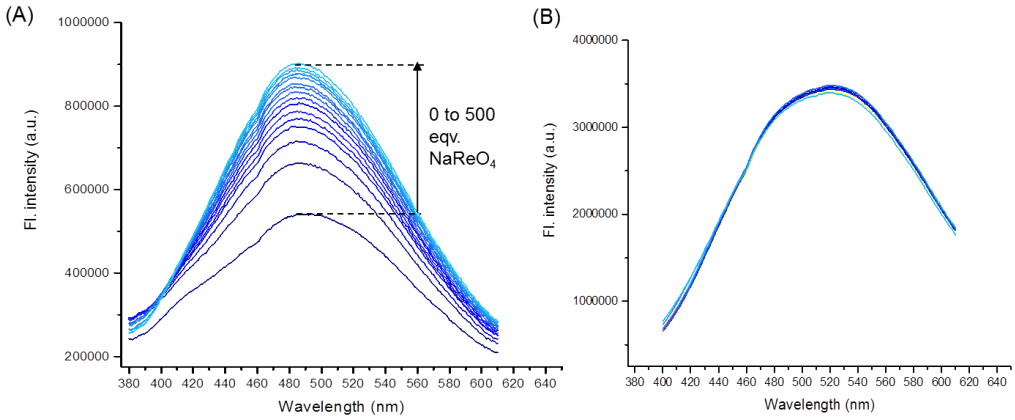


***Figure 5.7**. Fluorescence emission spectra of (A) receptor **5.6I** and (B) receptor **5.6H** upon titration of increasing quantities of NaReO4 up to 500 equivalents ([host] = 10 μM, 10 mM HEPES buffer pH 7.4, λ_{ex} = 320 nm, T = 293 K).*

5.2.3 Binding and Sensing of Biologically-relevant Phosphates

Phosphates are anions of supreme importance in nature. Inorganic phosphates (PO_4^{3-}, HPO_4^{2-} and $H_2PO_4^-$) are continuously cycled between the environment and the biosphere through the natural phosphorus cycle,[82] which is essential for maintenance of life on Earth. In biology, phosphates are incorporated into the sugar-phosphate backbone of DNA and RNA, allowing replication and control of virtually every biochemical process in the body. Their presence as a component in nucleotides such as ATP enables the molecule to function as the cellular energy currency. Despite their importance, the levels of phosphates in the human body

need to be maintained within narrow limits. For instance, excess phosphates can cause tissue calcification and heart conditions,[83] and a surplus in the environment results in eutrophication. Hence, there is much interest in the scientific community for developing phosphate sensors that can function in aqueous media. Despite the huge repertoire of artificial receptors capable of binding and sensing phosphates and their derivatives in buffered water reported in recent years,[13,84,85] XB-mediated phosphate binding remains extremely rare[86] and to the best of our knowledge, none have been reported to function in water at the time of writing.

The design of abiotic receptors capable of binding biologically-relevant nucleotide phosphates (e.g. ATP^{4-}) in water presents an even greater challenge. Archetypical examples contain a Lewis acidic (poly)cationic binding site for interacting with the anionic phosphate tail, and an aromatic region for donor-acceptor π-π stacking with the nitrogeneous base component (Figure 5.8A), as exemplified by Lehn's early examples of receptors designed to bind nucleotide phosphates in acidic aqueous media (pH 6)[87–90] (Figure 5.8B). Due to the reliance on electrostatic interactions governing the binding, the strongest association is usually observed for the phosphate species bearing the greatest charge (i.e. ATP^{4-} > ADP^{3-} > AMP^{2-}). Furthermore, selectivity for the triphosphate bearing a specific nitrogeneous base can be achieved by judicious design of the aromatic receptor component. For example, the large π surface of the pyrene component in Inouye's receptor favoured the binding of purine phosphates (ATP^{4-}, GTP^{4-}) over their pyrimidine counterparts (CTP^{4-}, TTP^{4-}) in water (Figure 5.8C).[91] More recently, Pradeep *et. al.* reported a 'spider-like' receptor capable of giving a selective fluorescence response to ATP^{4-} over ADP^{3-}, AMP^{2-} and CTP^{4-} (50 mM TRIS buffer, pH 7.2) with binding achieved via a combination of HB and π-π stacking interactions with the central aromatic core of the receptor (Figure 5.8D).[92]

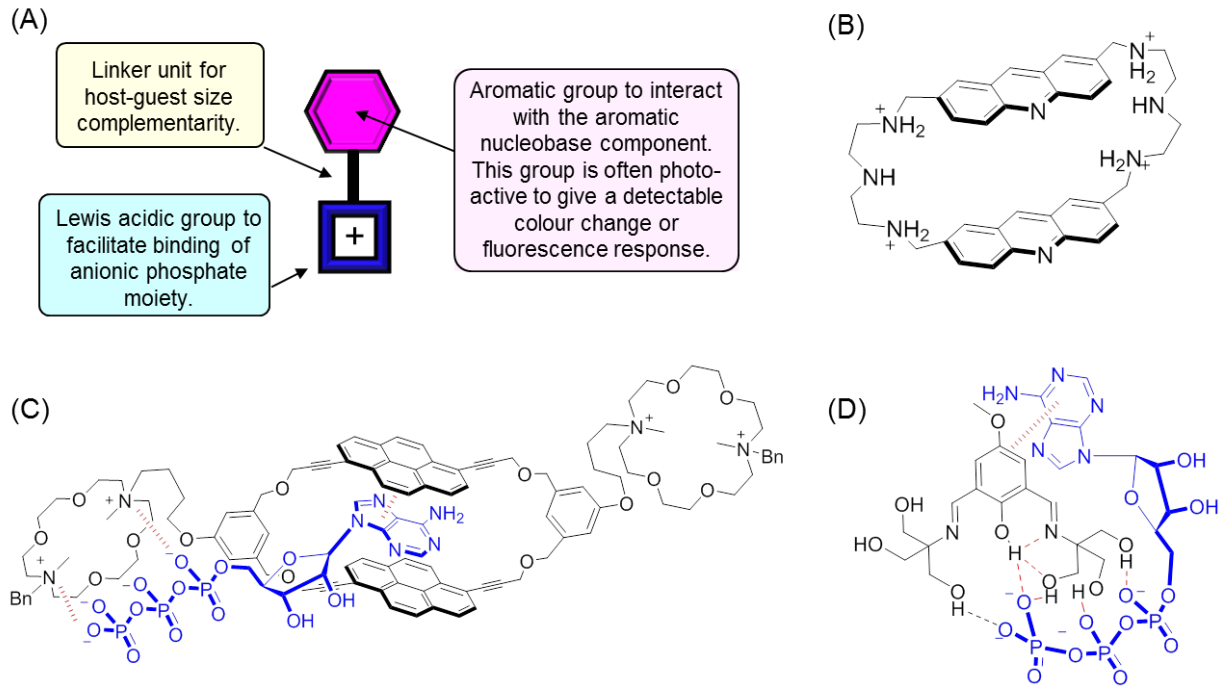


***Figure 5.8**. (A) General receptor design for binding nucleotide phosphates in water; (B) Lehn's aza-acridine macrocycle for ATP binding, showing its major protonated form at pH 6 [90]; (C) Inouye's pyrene receptor [91] and (D) Pradeep's receptor and their proposed binding mode with ATP^{4-}.[92] Non-covalent interactions are shown by red dashed lines.*

The unique ability of receptor **5.6l** to bind and sense ReO_4^- in water suggested the possibility of sensing phosphates as well, as both anions share the same tetrahedral geometry. Furthermore, electrostatic interactions between dicationic **5.6l** and polyanionic phosphate nucleotide derivatives such as ATP^{4-}, ADP^{3-} and AMP^{2-} would favour binding. Due to the complex protonation equilibria of these phosphate derivatives (Figure 5.9A), all binding studies were performed in buffered water at physiological pH (10 mM HEPES, pH 7.4). From the known pK_a values of the protonation equilibria,[93,94] a simulation of the relative distributions of each nucleotide phosphate and their protonated forms using the Hyperquad Simulation and Speciation (HySS) software[95] shows that the dominant anionic species in solution at pH 7.4 are ATP^{4-}, ADP^{3-} and AMP^{2-} (Figure 5.9B and Table 5.2).**

** Hyperquad software[95] simulations using known pK_a values show that at pH 7.4, HPO_4^{2-} exist as the dominant phosphate species in solution, present in a 62:38 mole ratio with its protonated counterpart $H_2PO_4^-$. As such, the K_a values reported actually represent the apparent binding affinities for the total phosphate species (ATP, ADP etc.) present in solution, which is inevitable given their well-established acid-base equilibria.[96,97]

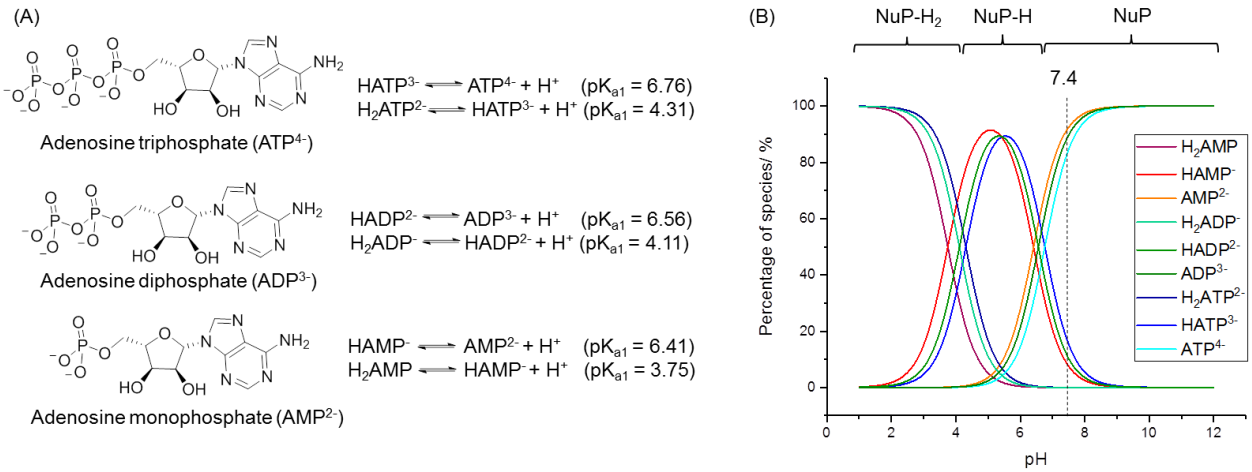


***Figure 5.9**. (A) Structures of ATP^{4-}, ADP^{3-}, AMP^{2-} and their associated acid-base equilibria;[94] (B) Percentage abundances of ATP^{4-}, ADP^{3-}, AMP^{2-} at different pH (NuP = nucleotide phosphate), species distribution determined using the Hyperquad simulation and speciation (HySS) software.[95]*

Table 5.2. Relative distribution of each nucleotide phosphate species (NuP) and their monoprotonated forms (NuP-H) at pH 7.4.[a]

NuP	Mole percent/ %	NuP-H	Mole percent/ %
ATP^{4-}	81.3	$HATP^{3-}$	18.7
ADP^{3-}	87.4	$HADP^{2-}$	12.6
AMP^{2-}	90.7	$HAMP^{-}$	9.3

[a] Species distribution determined using the Hyperquad simulation and speciation (HySS) software[95] using pK_a values reported by Handel.[94]

Fluorescence titrations were performed by addition of increasing quantities of Na_4ATP, Na_3ADP, Na_2AMP and Na_2HPO_4 salts to separate 10 μM solutions of receptors **5.6I/H** in 10 mM HEPES buffer at physiological pH (pH = 7.4). In the presence of increasing quantities of all anions, a marked enhancement in fluorescence intensity of **5.6I/H** was observed in almost all cases (Figure 5.10 shows the fluorescence increase at the peak λ_{em}), which is likely to be due to increased rigidification of the host molecule on anion binding. Generally, ATP^{4-} and ADP^{3-} elicited notable fluorescence enhancements for both HB and XB receptor analogues, while a more pronounced optical response was observed for AMP^{2-} and HPO_4^{2-} with the XB receptor **5.6I**. Global fitting of the fluorescence titration data by the SpecFit™ software[98] showed that the phosphate anions were associating with the host with a 1:1 stoichiometry, likely due to the extensive host guest hydration in the aqueous media. The association constants are summarised in Table 5.3.

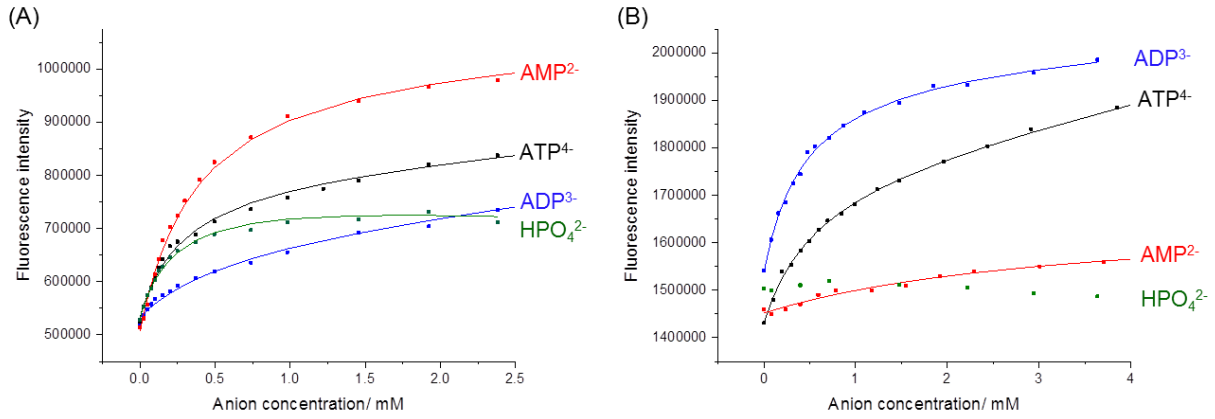


Figure 5.10. *Plot of peak fluorescence intensity of (A) receptor* ***5.6I*** *(λ_{em} = 489 nm) and (B) receptor* ***5.6H*** *(λ_{em} = 505 nm) against equivalents of anions added ([host] = 10 μM, 10 mM HEPES buffer pH 7.4, λ_{ex} = 320 nm, T = 293 K).*

Table 5.3. Anion association constants $\log_{10}(K_a/\ M^{-1})$ of receptors **5.6I** and **5.6H**.[a]

	5.6I	**5.6H**
ATP^{4-}	3.55 (0.06)	3.25 (0.05)
ADP^{3-}	3.20 (0.06)	3.22 (0.04)
AMP^{2-}	3.43 (0.03)	2.37 (0.08)
HPO_4^{2-}	3.62 (0.04)	-[b]

[a] 1:1 stoichiometric association constants were calculated from global fitting of fluorescence titration spectra using SpecFit™ .[98] Anions were added as their sodium salts ([host] = 10 μM, 10 mM HEPES buffer pH 7.4, λ_{ex} = 320 nm, T = 293 K). [b] No evidence of binding by fluorescence titrations.

Receptors **5.6I** and **5.6H** exhibit notable differences in their binding behaviours with the phosphates. Firstly, the binding affinities of the phosphates decrease in the order of $ATP^{4-} \approx ADP^{3-} > AMP^{2-} > HPO_4^{2-}$ for **5.6H**, whilst following the trend of $HPO_4^{2-} > ATP^{4-} > AMP^{3-} > ADP^{3-}$ for **5.6I**. This suggests that electrostatics were dominating the interactions of the nucleotide phosphates with **5.6H**. In stark contrast, the smaller differences in binding affinities observed for **5.6I** may be a consequence of contributions from electrostatics, anion hydration, and XB interactions. The dominance of electrostatics in governing binding of the highly-charged ATP^{4-} and ADP^{3-} can be seen where both **5.6I** and **5.6H** show comparable association constants, rendering any effects of XB insignificant. At the same time, the extensive anion hydration of the most highly charged species may overwhelm the influence of XB interactions, as demonstrated in Chapters 2 and 3 where the presence of water in the solvent media proved

highly detrimental to XB-mediated binding. Less charged and more weakly-hydrated species (AMP^{2-} and HPO_4^{2-}) render the beneficial effects of XB towards anion binding more apparent. For instance, the association constant of the dianionic AMP^{2-} to **5.6I** was found to be larger than that for **5.6H** by more than an order of magnitude. Even more impressively, HPO_4^{2-} showed surprisingly strong binding to **5.6I**, while not interacting and eliciting any fluorescence response with **5.6H** under identical conditions. While it is expected that electrostatic and aromatic π-stacking interactions play significant roles towards AMP^{2-} binding in water, the enhanced strength of XB-anion interactions may account for the enhanced binding for AMP^{2-} and HPO_4^{2-} observed for **5.6I**.

5.2.4 Electrochemical Sensing of Redox-active Anions in Water

Detection of anion binding by monitoring the shifts of a redox-active anion's $E_{1/2}$ value in the presence of increasing quantities of receptor is an unusual method for probing host-guest association.[99] Nonetheless, this method offers a unique means to probe the binding of the octahedral $[Fe^{III}(CN)_6]^{3-}$ anion by dicationic receptors **5.6I/H** and **5.7I/H**. The low-spin iron(III) centre[100] of $[Fe^{III}(CN)_6]^{3-}$ can be electrochemically reduced to iron(II) to form the *ferrocyanide* anion $[Fe^{II}(CN)_6]^{4-}$, and hence the anion is commonly used as an electrochemical standard[101] and found in a plethora of chemical, industrial and biological applications.[102–105] Upon reduction, the tetra-anionic $[Fe^{II}(CN)_6]^{4-}$ is expected to bind more strongly with a suitable Lewis acidic host molecule than its oxidised congener $[Fe^{III}(CN)_6]^{3-}$ by electrostatics, thus thermodynamically favouring reduction and resulting in a cathodic shift of the Fe^{II}/ Fe^{III} redox couple. Although the paramagnetic nature of $[Fe^{III}(CN)_6]^{3-}$ precludes studying its binding by ^{1}H NMR titrations, such binding studies have been performed with its diamagnetic $[Fe^{II}(CN)_6]^{4-}$ form in water.[99,106] However, it has been shown in Section 5.2.3 that stronger electrostatic dominance of the host-guest association result in less apparent XB contributions towards anion binding. Therefore, electrochemical sensing of the Fe^{II}/ Fe^{III} redox couple shifts of $[Fe^{III}(CN)_6]^{3-}$ would provide an ideal method of probing the influence of XB on the binding of this scarcely-studied target anion.

Electrochemical experiments in water were performed using a glassy carbon working electrode, a platinum wire counter electrode and a mercury sulphate ($HgSO_4$) reference electrode in a 100 mM $NaNO_3$ supporting electrolyte solution. Control experiments with the aqueous solutions of receptors **5.6I/H** and **5.7I/H** demonstrated their lack of redox activity in the accessible solvent window, confirming that any CVs subsequently recorded during titrations will be arising from $[Fe(CN)_6]^{3-}$ alone. $[Fe(CN)_6]^{3-}$ was found to show good electrochemical reversibility in water, with an $E_{1/2}$ value of -0.200 V with respect to the $HgSO_4$ reference electrode.

Electrochemical titrations were performed with increasing quantities of each receptor added to a 50 μM aqueous electrolyte solution of $K_3[Fe(CN)_6]$. As shown in Figure 5.11, no detectable perturbations of the $E_{1/2}$ value of $[Fe(CN)_6]^{3-}$ could be detected even in the presence of 30-fold excess of receptor **5.6I**. Disappointingly, no shifts were also seen with receptors **5.6H**, **5.7I** and **5.7H**, indicating that the anion was likely to be interacting very weakly with the receptors in the aqueous solution. Presumably, this was due to the extensive $[Fe(CN)_6]^{3-}$ hydration in water, supported by infra-red photodissociation (IRPD) spectroscopy results reported by Williams *et. al.* which suggested that the anion could influence the hydrogen bonding structure of water well beyond its third hydration shell.[107]

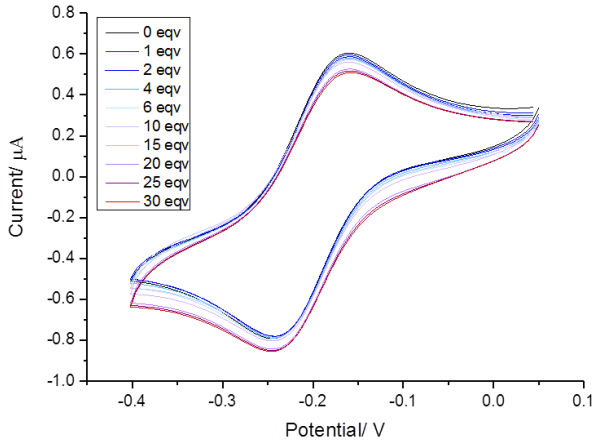


***Figure 5.11**. CVs of $[Fe(CN)_6]^{3-}$ recorded in the presence of increasing quantities of receptor **5.6I** ([**5.6I**] = 50 μM, electrolyte: 0.1 M $NaNO_3$ in water; $HgSO_4$ reference electrode; scan rate = 100 mV s^{-1}; T = 293 K).*

5.3 Towards a Polyether-stoppered Water-soluble [2]Rotaxane

Encouraged by the appreciable water-solubility conferred by the tris(TEG) groups on the acyclic receptors **5.6** and **5.7**, we envisaged that rotaxanes could be rendered water soluble by incorporating these motifs into their stopper units. Indeed, a stopper comprising of successive appendages of these repeating motifs could constitute a dendritic unit, where the number of successive dendrimer generations could be used to tune the solubility of the resulting rotaxane in a variety of solvents, including water. Dendrimer rotaxanes were formally classified by Lee and Kim in 2003, with rotaxanes bearing dendritic units only at the stopper groups being termed 'Type 1a dendrimer rotaxanes'.[108] Since then, synthetic advances have led to numerous applications of the various classes of dendrimer rotaxanes,[109,110] which include examples of Type 1a rotaxanes bearing dendritic poly(ethylene glycol) stopper units shown to possess liquid crystalline properties.[111,112] As a proof-of-concept study to investigate the possibility of using this rotaxane family for anion recognition in water, the basic design of neutral ferrocene-appended pyridine *N*-oxide rotaxane family **3.9** (described in Section 3.2) was modified by replacing the stopper groups with dendritic poly(TEG) motifs shown in Figure 5.12. Both stopper designs contained rigid inflexible linker units (tetraphenyl in A and amide bonds in B) in an effort to minimise the possibility of macrocycle dethreading following rotaxane formation. To synthesise the target Type 1a dendrimer rotaxanes, Cl^--templated macrocycle clipping around a pre-formed poly(TEG) dendrimer-terminated axle component will be pursued.

As the rotaxane axle component consists of a more extensive hydrophobic central region between the hydrophilic termini than the acyclic receptors described in the previous section, preliminary investigations centred on elucidating whether the TEG groups conferred water solubility on the axle unit. Aryl alkyne **5.9** was first synthesised by Sonogashira coupling of aryl bromide **5.2** with TMS-acetylene, and subsequent TMS-deprotection of intermediate **5.8** (Scheme 5.3). Pyridine *N*-oxide axle precursor **3.7** (preparation detailed in Section 3.2) was reacted with two equivalents of **5.9** under standard CuAAC conditions to afford model axle **5.10** in a modest yield of 40 % owing to challenging purification. Gratifyingly, **5.10** showed

appreciable water solubility at concentrations of approximately 1.5 mM in D_2O, which is noteworthy considering its charge neutrality.

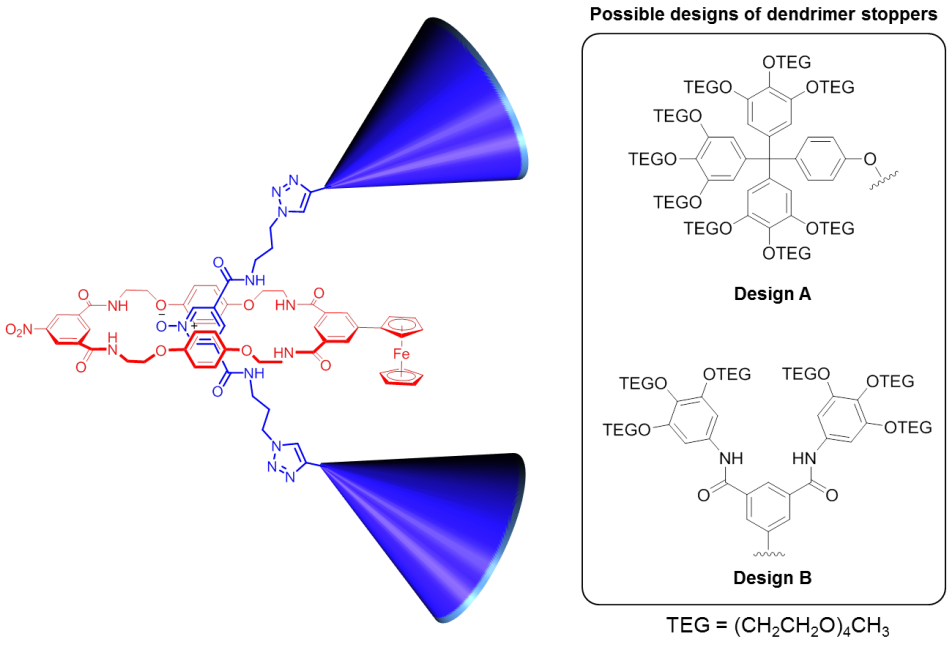
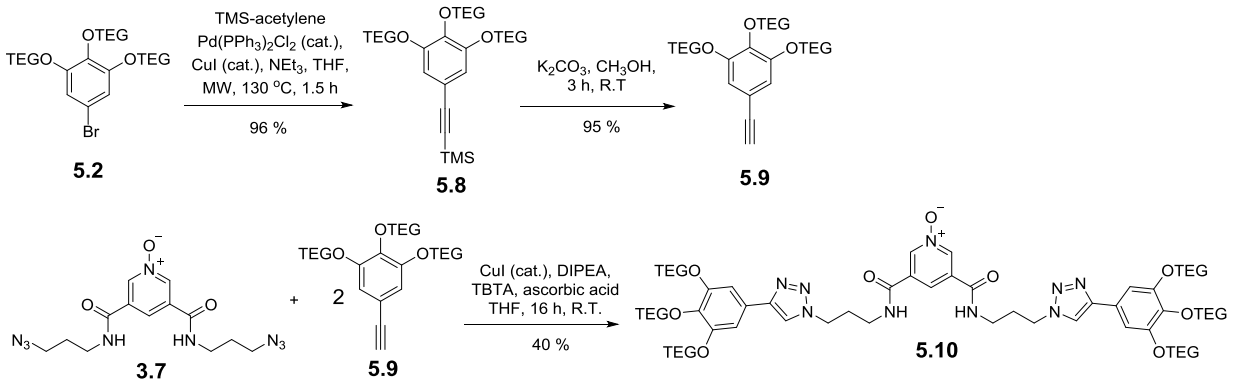


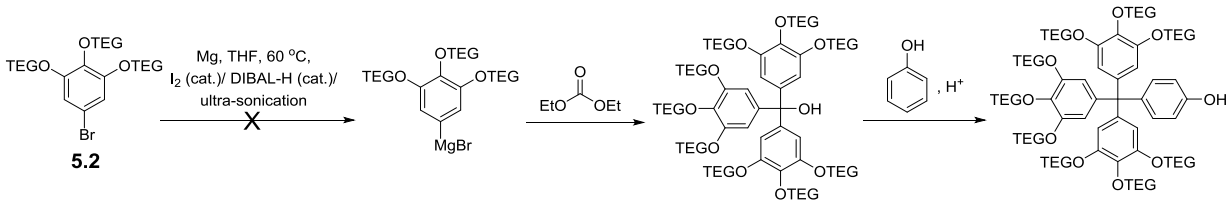
***Figure 5.12**. Proposed design of water-soluble Type 1a dendrimer design with two possible poly(TEG) dendritic stopper groups.*



***Scheme 5.3**. Synthesis of model rotaxane axle **5.10**.*

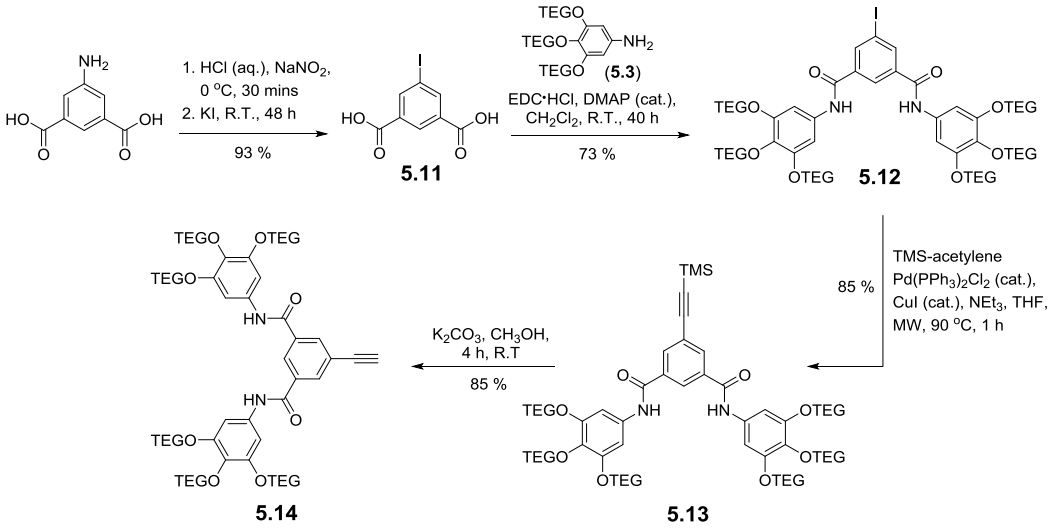
Encouraged by the water solubility of **5.10**, attempts to prepare the bulkier dendritic stopper units following designs A and B (Figure 5.12) were undertaken. As summarised in Scheme 5.4, tetraphenyl stopper design A may be prepared following the same route as that for the regular hydrophobic organic-soluble rotaxane stoppers employed throughout this thesis, beginning with nucleophilic addition of a Grignard reagent to diethyl carbonate.[113]

However, when this route was attempted using aryl bromide **5.2**, formation of the Grignard reagent could not be achieved despite exhausting all common methods of reaction initiation, including the use of I_2, ultrasonication[114,115] and DIBAL-H.[116] It was hypothesised that the Lewis basic oxygen atoms on the multiple TEG units could coordinate to any de-passivated reactive Mg surface, preventing any Mg atoms from oxidatively inserting into the C-Br bond of **5.2** to form the desired Grignard reagent. In light of the synthetic difficulties encountered, the synthesis of stopper design B was pursued instead (Scheme 5.5).



***Scheme 5.4**. Attempted preparation of tetraphenyl stopper design A.*

Commercially-available 5-amino-isophthalic acid was first converted to 5-iodo-isophthalic acid **5.11** by aniline diazotisation and reaction with KI (Scheme 5.5), followed by amide formation with two equivalents of aniline **5.3** mediated by 1-ethyl-3-(3-dimethylaminopropyl)carbodiimide hydrochloride (EDC·HCl). Thereafter, Pd-catalysed Sonogashira coupling of aryl iodide **5.12** with TMS-acetylene afforded precursor **5.13** in a good yield of 85 % following chromatographic purification. The target dendrimer aryl alkyne **5.14** was then obtained by TMS deprotection of **5.13** using K_2CO_3 in methanol.

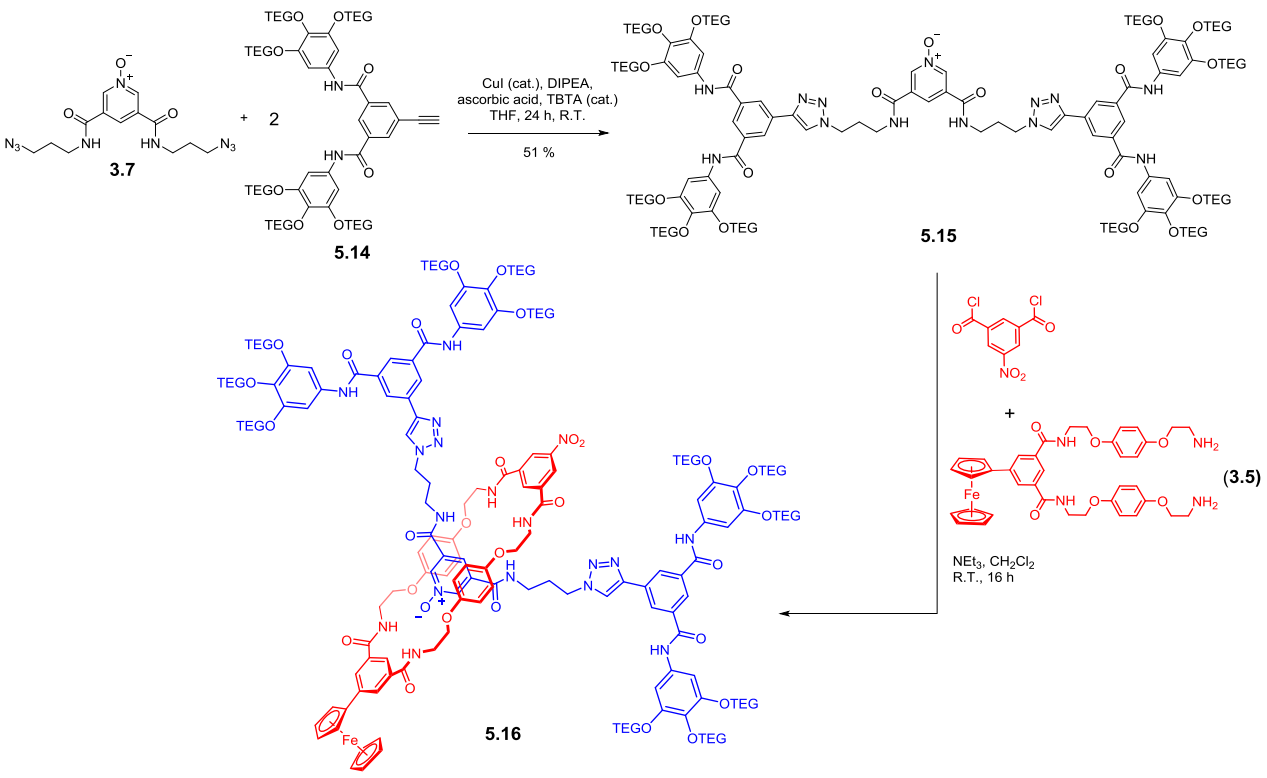


***Scheme 5.5**. Synthesis of dendrimer stopper units of design B.*

With alkyne **5.14** in hand, standard CuAAC conditions with bis-azide **3.7** afforded neutral axle **5.15** (Scheme 5.6). Owing to the presence of twelve TEG chains on the compound, purification of **5.15** proved especially challenging, and could be achieved only using Brockmann Grade 1 basic alumina as the stationary phase during column chromatography. Axle **5.15** showed significant water solubility, capable of giving a homogeneous solution in water at concentrations of approximately 5 mM. Encouraged by this finding, rotaxane synthesis (Scheme 5.6) was performed using 5-nitro-bis(isophthaloyl chloride) and bis-amine macrocycle precursor **3.5** in the presence of NEt_3, templated by Cl^- generated *in-situ* from the acid chloride condensation reactions to form the macrocycle component. Pleasingly, crude ESI-MS analysis of the reaction mixture showed the presence of the target rotaxane, and hence its purification was attempted.

On the preparatory silica TLC plate, appreciable separation of rotaxane **5.16** (as an orange band) from free axle **5.15** (colourless band) could be obtained using a highly polar eluent system (CH_3OH/ CH_2Cl_2 7:93 *v/v*). After extracting the rotaxane product from the silica gel, ESI-MS analysis was performed to confirm its identity. The mass spectrum (Figure 5.13) shows evidence of rotaxane appearing in a range of charged states with different quantities of Na^+ and H^+. More worryingly, a distinct peak for axle **5.15** was observed (*m/z* = 1772.6 $[M + 2Na]^{2+}$), which is unlikely to be an artefact of purification due to the good separation from the

rotaxane band, suggesting that the rotaxane may be unstable with respect to dethreading. This was subsequently confirmed by ^{1}H NMR monitoring the rotaxane in CD_3OD over time following initial isolation (Figure 5.14). Although the aromatic region of the spectrum after 6 hours could not be unambiguously assigned due to the presence of multiple species resulting from dethreading, the signals arising from proton H_3 on the stopper was diagnostic of the presence of free axle together with the rotaxane in an approximate 3:4 molar ratio. After 2 days, almost complete dethreading of the macrocycle was observed, which was confirmed by ESI-MS analysis. Clearly, these observations demonstrated that despite the presence of the rigid amide linkages, the rotaxane stoppers were still conformationally flexible enough for macrocycle dethreading to occur and hence no further work was performed using this rotaxane design. Nevertheless, the initially isolated rotaxane product showed good water solubility at typical ^{1}H NMR titration concentrations of ca. 1.5 mM. Hence future attempts at rotaxane synthesis using this stopper design should utilise a smaller macrocycle component or perhaps a higher dendritic generation of the stopper to increase its steric bulk.



***Scheme 5.6**. Synthesis of water-soluble neutral axle **5.15** and attempted synthesis of rotaxane **5.16**.*

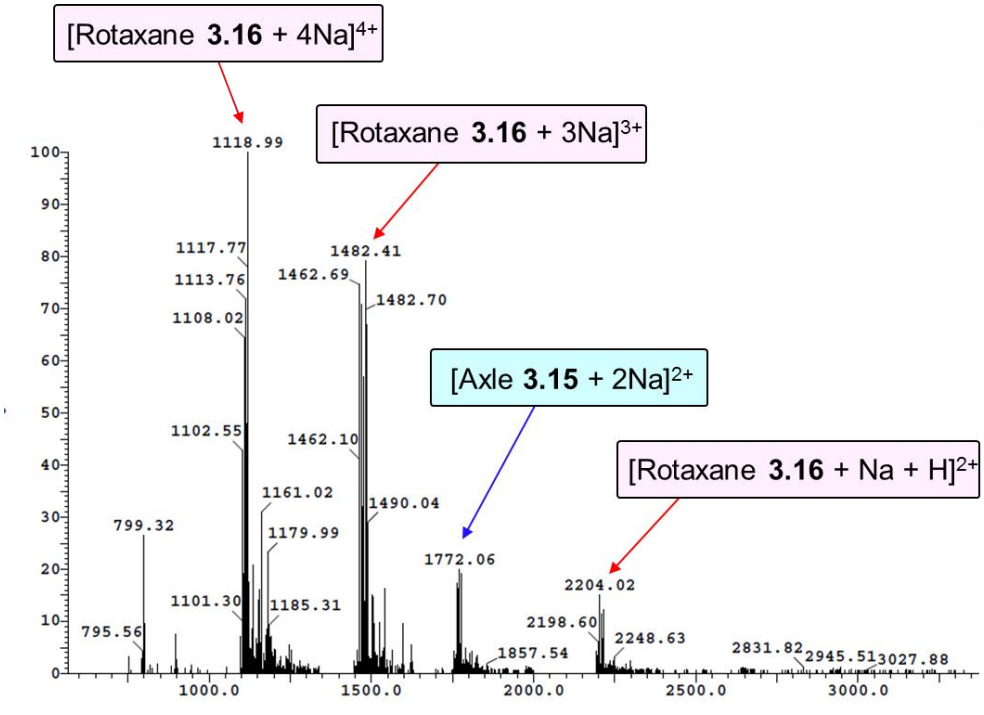


***Figure 5.13**. ESI-MS of rotaxane **5.16** obtained approximately 3 hours after isolation.*

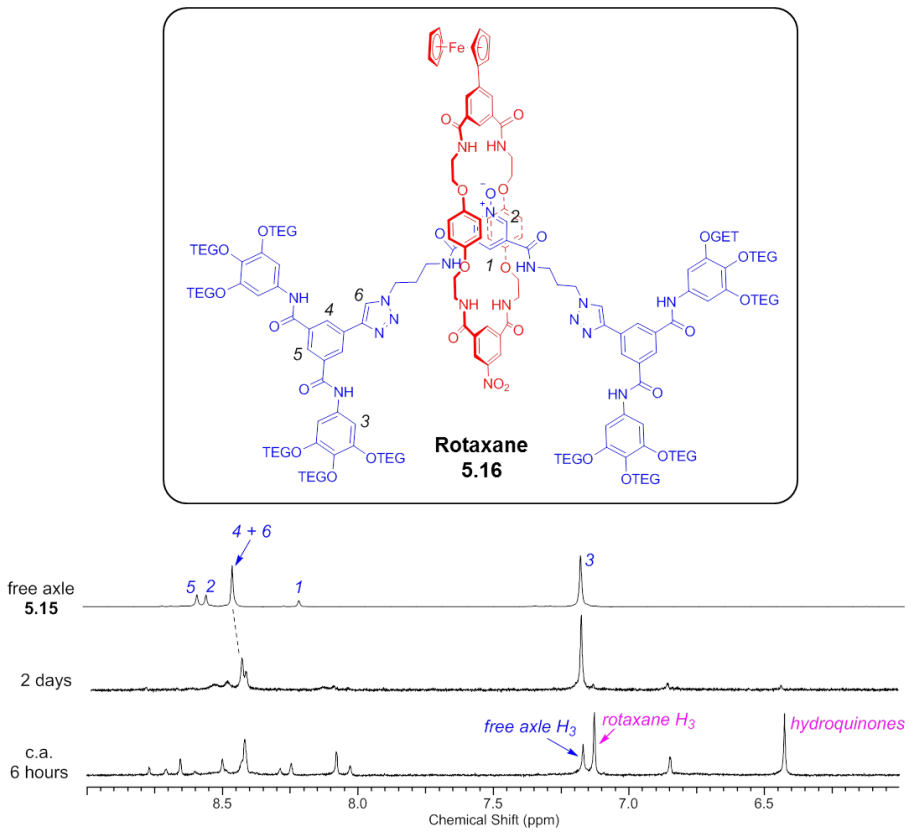


***Figure 5.14**. Partial ^{1}H NMR spectra of isolated rotaxane **5.16** after c.a. 6 hours and 2 days following isolation, with the spectra of free axle **5.15** provided for comparison. The multiple species present in the rotaxane sample at 6 hours prevented an unambiguous assignment of the aromatic region (CD_3OD, T = 298 K).*

5.4 Pyrrole-based Halogen Bonding Hosts for Anion Binding in Water

5.4.1 Introduction

Anion receptors containing the pyrrole motif constitute a highly successful class of host molecules owing to the highly-polarised pyrrolic NH group which is capable of forming strong hydrogen bonding interactions with a range of anions running the gamut from CN^- to F^-.[117,118] In nature for instance, tripyrrolic anion receptor prodigiosin (Figure 5.15A), produced by many strains of bacteria plays crucial roles in H^+ and Cl^- transport across cell membranes, and has recently been shown to possess anti-malarial, anti-fungal and anti-cancer properties.[119] Artificial acyclic anion receptors containing pyrroles include Gale's family of pyrrole-based anion membrane transporters,[120,121] Sessler's pyrrole-based pyridine 2,6-dicarboxyamide receptors,[122] and Anzenbacher's ruthenium(II)-complexed dipyrrolyl quinoxalines (DPQs) for CN^- sensing (Figure 5.15B).[123] Macrocycles incorporating pyrrole units include porphyrins[124,125] and their expanded counterparts[126,127] such as smaragdyrins (Figure 5.15C),[128] sapphyrins (Figure 5.15D),[129–133] calixpyrroles and their strapped analogues (Figure 5.15E).[134–140] In addition, they are often combined with other anion binding motifs such as ureas and amides[141] for effective anion binding even in highly competitive water-containing solvent media.[142,143]

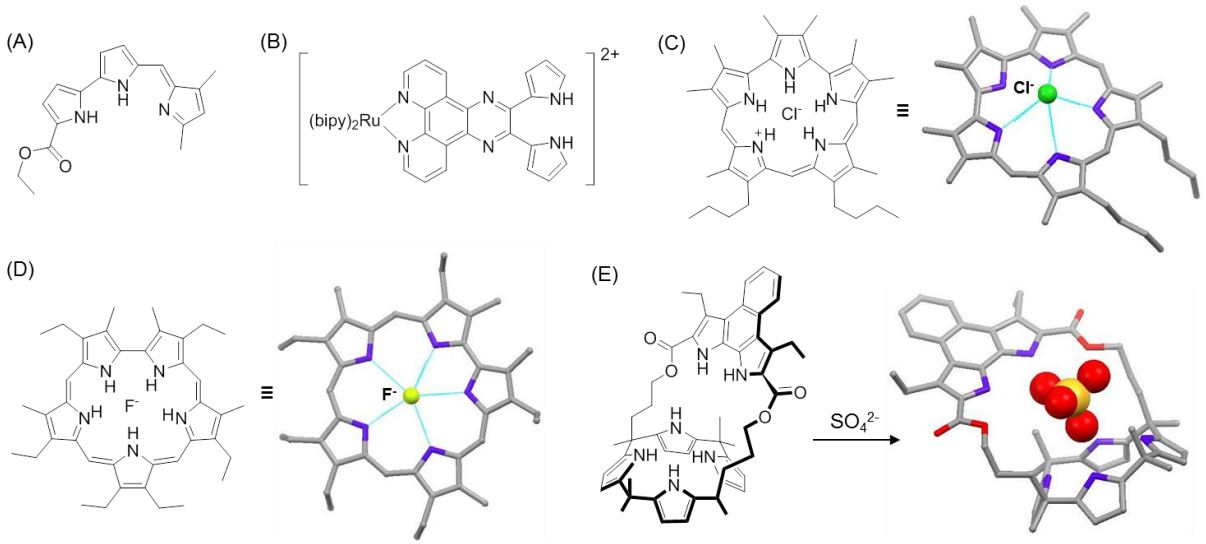


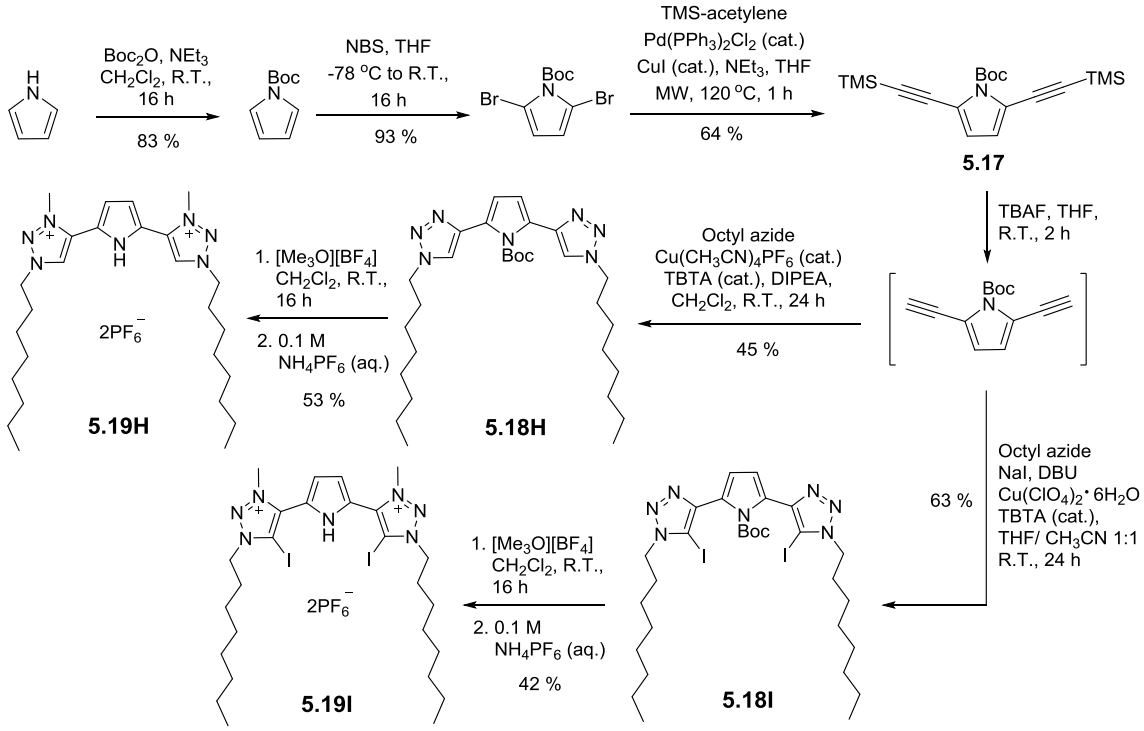
Figure 5.15. *Pyrrole-based natural and abiotic anion receptors: (A) naturally-occurring bacterial prodigiosin; (B) Anzenbacher's CN^- binding ruthenium(II)-complexed dipyrrolyl quinoxaline receptor;[123] (C) Sessler's smaragdyrin and its Cl^- binding mode;[144] (D) Sessler's F^- binding sapphyrin;[145] (E) SO_4^{2-}-adduct of Moyer and Sessler's bipyrrole-strapped calix[4]pyrrole.*[140]

5.4.2 Design and Synthesis of Pyrrole Hosts

To further enhance the anion binding properties of the dicationic XB receptors investigated thus far, a pyrrole motif was incorporated as a 2,5-substituted spacer between iodotriazolium groups (Figure 5.4C and Scheme 5.7). Indeed, this unique combination also results in a wide XB bite angle resulting from a central 5-membered heterocycle, favouring coordination of larger and more basic oxoanions in aqueous solvent media, aided by the potent HB acidity of the central pyrrole NH functionality. Initial studies centred on establishing the binding properties of this XB receptor motif in organic solvents, which are compared with the HB receptor analogue. Subsequently, the binding studies are performed in water using water-soluble TEG-appended receptor analogues (Figure 5.4C).

The key step in the preparation of the target pyrrole receptors involves the double CuAAC reactions between 2,5-bis(ethynyl)pyrrole and the appropriate azide. As detailed in Scheme 5.7, the multi-stepped synthesis of the 2,5-bis(ethynyl)pyrrole synthon began with the initial *N*Boc-protection of the pyrrole nitrogen atom to prevent the acidic NH group from interfering with later stages of receptor synthesis (e.g. 'one-pot' iodo-Click reaction). In addition, this step promotes selective pyrrole functionalisation at the 2,5-positions with electrophiles, mitigating the possibility of indiscriminate substitution at all four possible positions on the electron-rich pyrrole ring.[146] Indeed, bis-bromination of the *N*Boc-protected pyrrole using *N*-bromosuccinimide in THF showed exclusive 2,5-substitution, with no evidence of reactions occurring at the 3 or 4-position. It is notable that these first two steps could be performed on multi-gram scales in good yields (see Chapter 7). Microwave-assisted Sonogashira coupling converted 2,5-dibromo-*N*Boc-pyrrole to the corresponding bis(TMS-protected) alkyne **5.17** in a reasonable yield of 64 % after chromatographic purification. While **5.17** was stable as a brown oil under ambient conditions, TMS-deprotection was found to result in significant darkening of the bis-ethyne product, possibly due to the propensity of the electron-rich pyrrole aromatic system towards oxidation. Hence, all CuAAC reactions with synthon **5.17** were performed by *in-situ* deprotecting the TMS group with TBAF, and immediately reacting the bis-ethyne intermediate with the appropriate azide. Using this procedure, 'Click' reactions with *n*-octyl azide afforded **5.18H** and **5.18I** in yields of 45 % and

63 % respectively. Finally, when compounds **5.18H/I** were reacted with 3 equivalents of trimethyloxonium tetrafluoroborate, bis-methylation of the triazole units occurred with simultaneous deprotection of the *N*Boc units in one step to afford the organic-soluble octyl-substituted dicationic pyrrole receptors **5.19H** and **5.19I**, which were then anion exchanged to their respective PF_6^- salts.

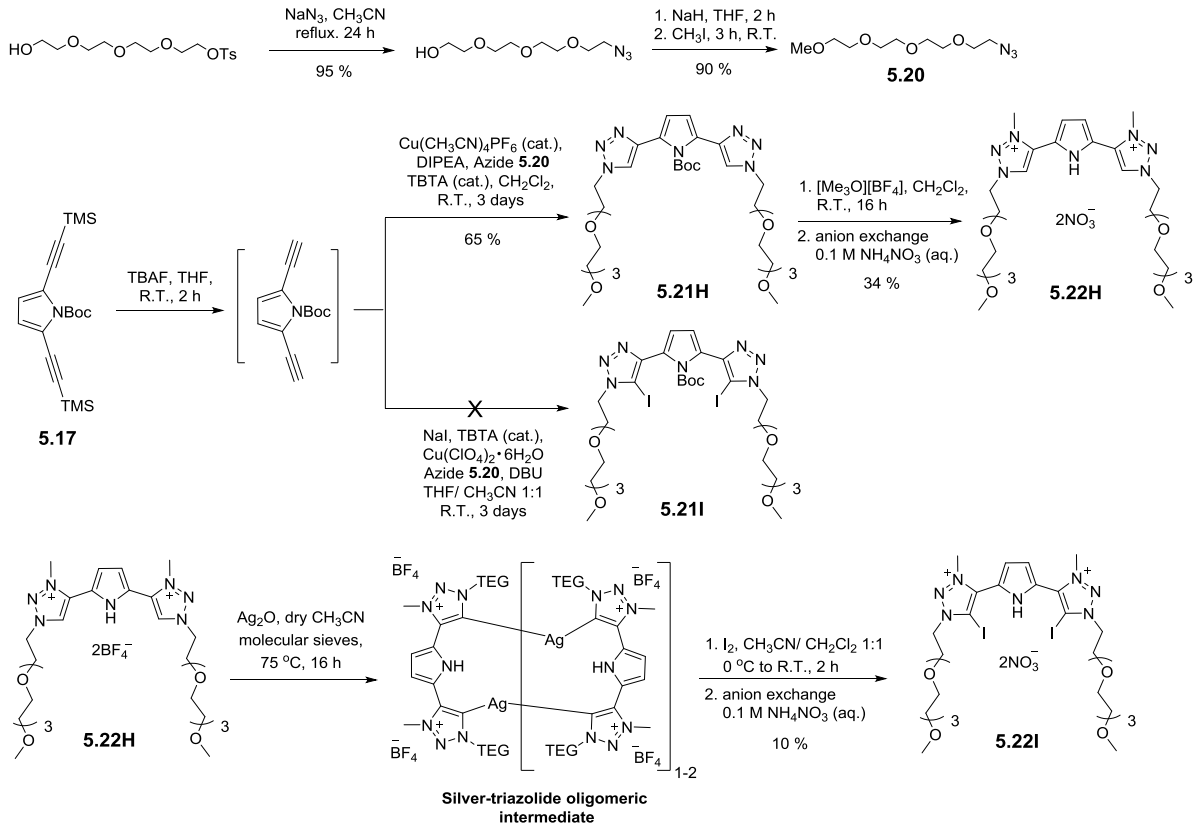


***Scheme 5.7**. Synthesis of dicationic pyrrole-based receptors **5.19I/H**.*

The analogous TEG-appended receptors were assembled as detailed in Scheme 5.8. TEG-azide synthon **5.20** was first prepared by S_N2 substitution of mono-tosyl TEG with NaN_3, followed by methylation of the other free hydroxyl group. Thereafter, *in-situ* TMS-deprotection of **5.17** with TBAF, followed by a standard proto-'Click' CuAAC reaction with azide **5.20**, afforded **5.21H** in 65 % yield. Bis-triazole methylation with $[Me_3O][BF_4]$ resulted in simultaneous *N*Boc-deprotection, and subsequent anion exchange using a nitrate-loaded Amberlite™ column afforded **5.22H** as a sticky white solid in modest yields. Surprisingly, the one-pot iodo-'Click' reaction, which had allowed access to **2.18I**, failed to yield the target XB

TEG-appended **5.21I** after 3 days. Instead, a host of unidentifiable side products were obtained. Another attempt to form the iodotriazoles by electrophilic trapping of the Cu(I)-triazolide intermediate formed in the CuAAC reaction using iodine monochloride also failed to yield **5.21I**.[147]

Due to the sensitivity of the pyrrole functionality, post-synthetic methods to convert the (proto)triazole of **5.21H** to iodotriazole using *n*-butyllithium and molecular iodine are unsuitable. Therefore, to deprotonate the 5-position on the triazolium groups, dicationic **5.22H** (as its $2BF_4^-$ salt prior to anion exchange) was reacted with dry Ag_2O. Following overnight heating in dry acetonitrile at 75 ^oC, ^1H NMR analysis of the resultant crude solution showed complete disappearance of the triazolium proton of **5.22H**, indicating that successful formation of oligomeric silver(I)-triazolide complexes had occurred (confirmed with ESI-MS).[148] The addition of two equivalents of I_2 to the resulting silver-triazolide complexes afforded the target XB dicationic receptor analogue **5.22I** in a poor yield of 10 % following Amberlite^{TM}-mediated anion exchange to the NO_3^- salt. The reason for the unfavourable conversion was revealed by ESI-MS and ^1H NMR analysis of the various side products isolated from the reaction (Figure 5.16), which showed that multiple iodine substitutions had occurred on the triazolium and the central pyrrole core. Surprisingly, all three major products, containing two, three and four iodine atoms, were isolated in near equimolar quantities, indicating that the central pyrrole core was more prone to iodine substitution than the flanking silver-triazolides.



Scheme 5.8. *Synthesis of water-soluble dicationic pyrrole-based receptors* ***5.22I/H***.

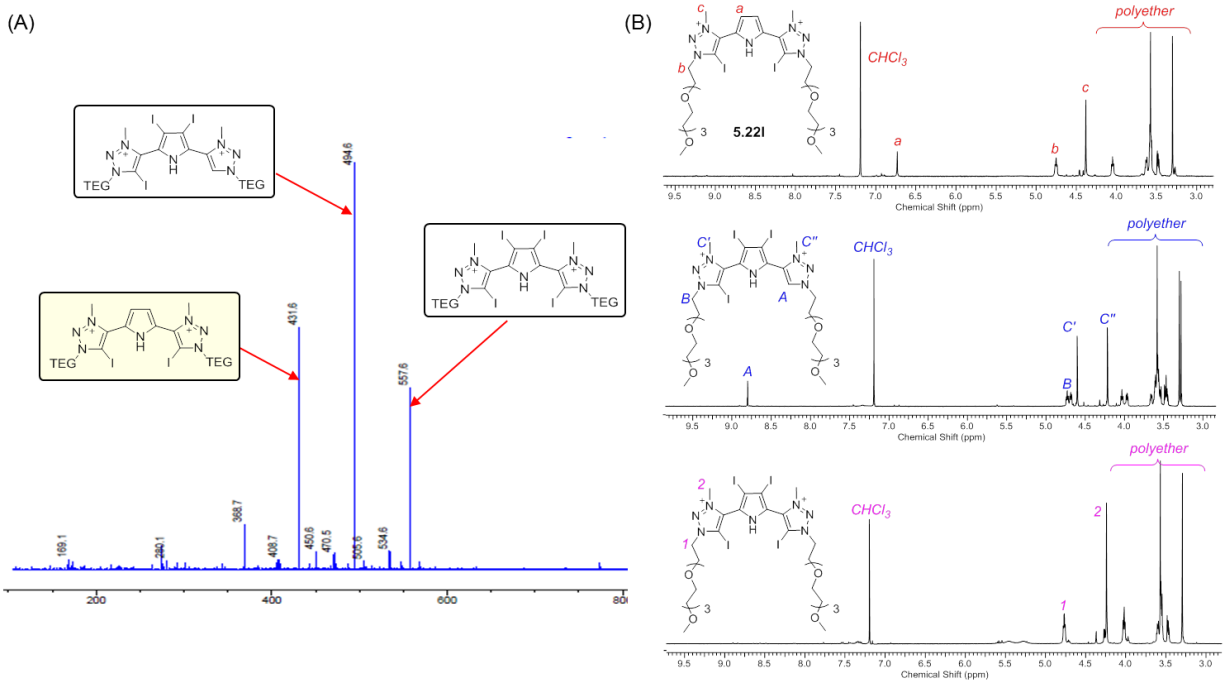


Figure 5.16. *(A) Partial ESI mass spectrum of the crude reaction mixture of* ***5.22I*** *after reacting the silver(I)-triazolide oligomers with* I_2. *The positions of iodine substitution on each product indicated were obtained after* ^1H *NMR characterisation of each chromatographically-isolated product in* $CDCl_3$, *shown in (B).*

5.4.3 Anion Binding Studies in Aqueous-Organic Mixtures

Preliminary ^{1}H NMR titrations were initially performed on dicationic receptor **5.19H** in $CDCl_3$/ CD_3OD/ D_2O 45:45:10 *v/v* with TBACl. As shown in Figure 5.17, the presence of 10.0 equivalents of Cl^- led to significant downfield perturbations of the triazolium protons signal H_a ($\Delta\delta$ = + 0.20 ppm) and small upfield shifts for those of H_b from the central pyrrole unit and triazolium methyl groups ($\Delta\delta$ c.a. - 0.02 ppm in both cases). This provides strong evidence of Cl^- binding in the receptor cleft containing the acidic pyrrole NH proton flanked by the triazolium units, and not at the receptor's external periphery. An analogous titration performed on **5.19I** also resulted in very small perturbations of the pyrrole protons. Due to these small signal shifts, and the lack of proton environments surrounding the anion binding cleft that could be monitored during the titrations, reliable association constant values could not be determined using ^{1}H NMR titrations, and hence the anion binding properties were probed using UV-Vis spectroscopy instead.

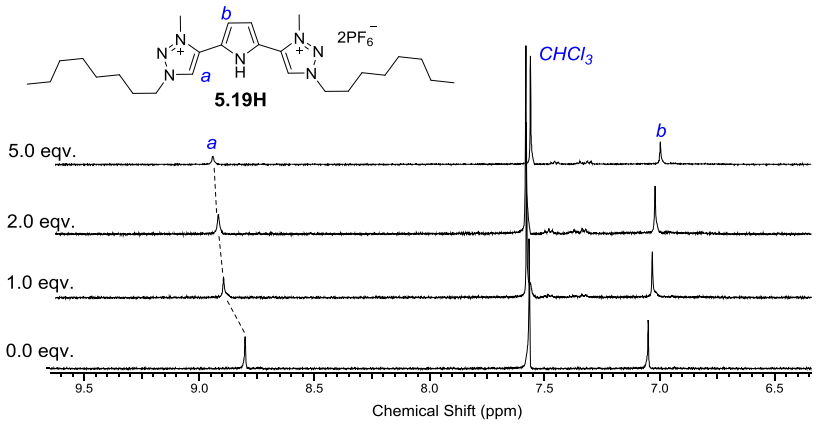


***Figure 5.17**. Partial ^{1}H NMR spectra of receptor **5.19H** in the presence of 0.0, 1.0, 2.0 and 5.0 equivalents of TBACl ([**5.19H**] = 1.5 mM, $CDCl_3$/ CD_3OD/ D_2O 45:45:10 v/v, T = 298 K).*

UV-Vis titration experiments were performed by adding increasing quantities of anions, as their TBA salts, to receptors **5.19I** and **5.19H** in CH_3CN/ H_2O 9:1 *v/v*. Due to the electronic conjugation between the (iodo)triazolium unit and the central pyrrole core, absorbance peaks were observed at approximately 300 and 360 nm for both receptors, possibly arising from $\pi \rightarrow \pi^*$ and $n \rightarrow \pi^*$ electronic transitions respectively.[149] The absorbance wavelengths and molar

extinction coefficients of the XB and HB receptors are almost identical, showing that the presence of the XB-donor iodine atoms on **5.19I** had negligible influence on the electronic energy levels of the receptor framework.

The binding of a range of anions possessing various geometries and basicities was investigated. Significantly different optical responses were observed during the titrations of different anions, as shown in Figure 5.18 and Figure 5.19. In the presence of Cl^- and Br^-, distinct bathochromic shifts of the absorbance peak at 300 nm was observed for **5.19I**, which was more pronounced for the heavier halides (Figure 5.18). This was attributed to the possible increased receptor planarity enforced by bidentate halide coordination between the XB-donor iodine atoms, which decreased the receptor's HOMO-LUMO energy gap, hence causing an absorption red-shift. While addition of Cl^- showed spectroscopic evidence for binding to **5.19H**, no spectral changes were observed for Br^- even when the anions were present in 200-fold excess. Interestingly, the addition of F^- led to dramatic changes in the UV-Vis spectra of both receptors. For **5.19I**, monotonous increases in the absorbances of the 300 and 360 nm bands were seen, with the former band also showing a slight bathochromic peak shift. In contrast with **5.19H**, F^- elicited a decrease in the 300 nm absorbance band and an increase in the 360 nm peak accompanied by a distinct isosbestic point at 320 nm. The contrasting optical behaviour with F^- with the other halides suggests an alternative mode of interaction with both pyrrole-based receptors.

The absorbance changes during the titration of oxoanions with both receptors are shown in Figure 5.19, which reveal differences to those seen in the presence of halides, most notably in the behaviour of the lower energy 360 nm band. With receptor **5.19I**, initial addition of $H_2PO_4^-$ and SO_4^{2-} resulted in a slight increase of the 360 nm absorbance, which then decreased at higher concentrations. On the other hand, this peak showed a unidirectional intensity decrease with NO_3^-. In all cases, these oxoanions elicited small but detectable enhancements in the 300 nm peak of **5.19I** accompanied by slight bathochromic shifts. Interestingly, with the HB receptor analogue **5.19H**, only intensity increases and decreases were seen for the 300 nm and 360 nm peak maxima with all three oxoanions, with distinct isosbestic points observed in all cases around 340 nm. AcO^- elicited similar drastic changes as

F^- even when only 1.0 equivalent of anion was added to solutions of both receptors. Considering their basicity (pK_a of HF and HOAc = 4.8 and 3.2 in water respectively),[150] it is likely that these changes arose from deprotonation of the central pyrrole NH proton. Negligible spectral changes were seen during the titrations of ClO_4^-, indicating that the anion was not interacting appreciably to either receptor. Global spectral fitting of the UV-Vis spectroscopy titration data was performed using the BindFit software, and the calculated association constants are summarised in Table 5.4. All other anions were found to bind via 1:1 stoichiometry with the exception of receptor **5.22I** with $H_2PO_4^-$ and SO_4^{2-}, which only showed good agreements with host-guest 1:2 and 2:1 binding models respectively.

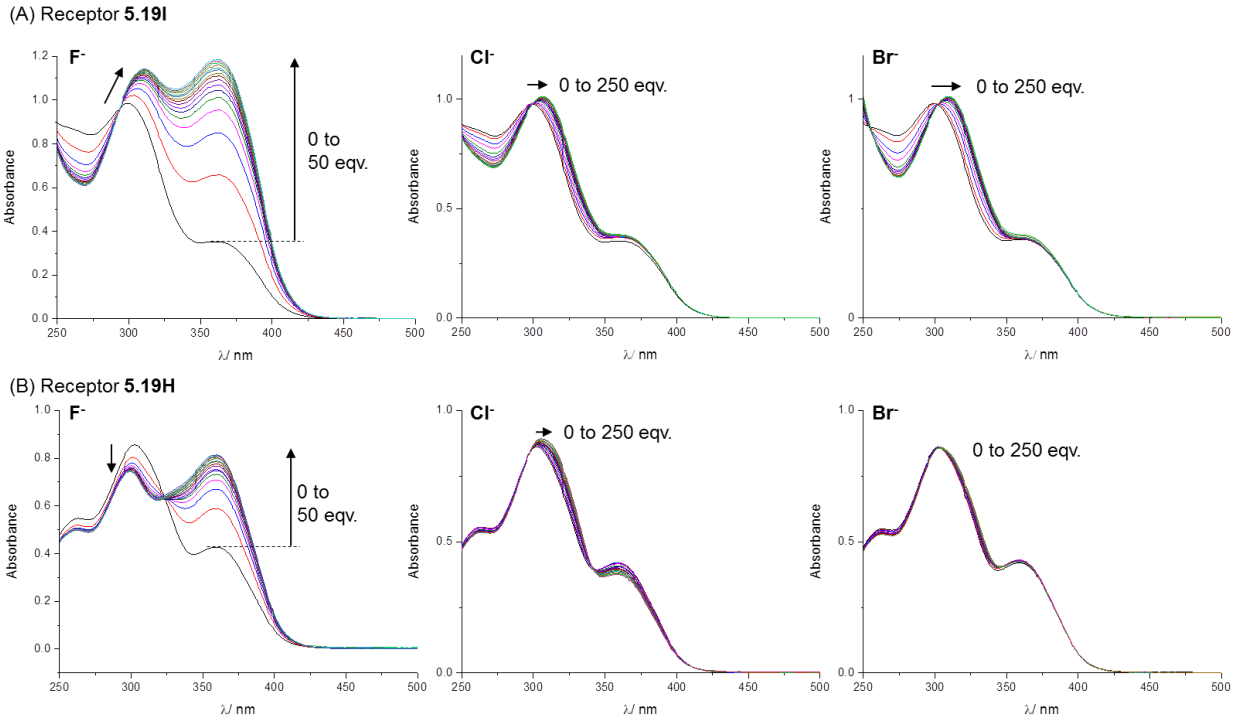


***Figure 5.18**. UV-Vis spectra of dicationic pyrrole receptors (A) **5.19I** and (B) **5.19H** in the presence of increasing quantities of the halides F^-, Cl^- and Br^- ([**5.19H/I**] = 50 μM; CH_3CN/ H_2O 9:1 v/v, T = 293 K).*

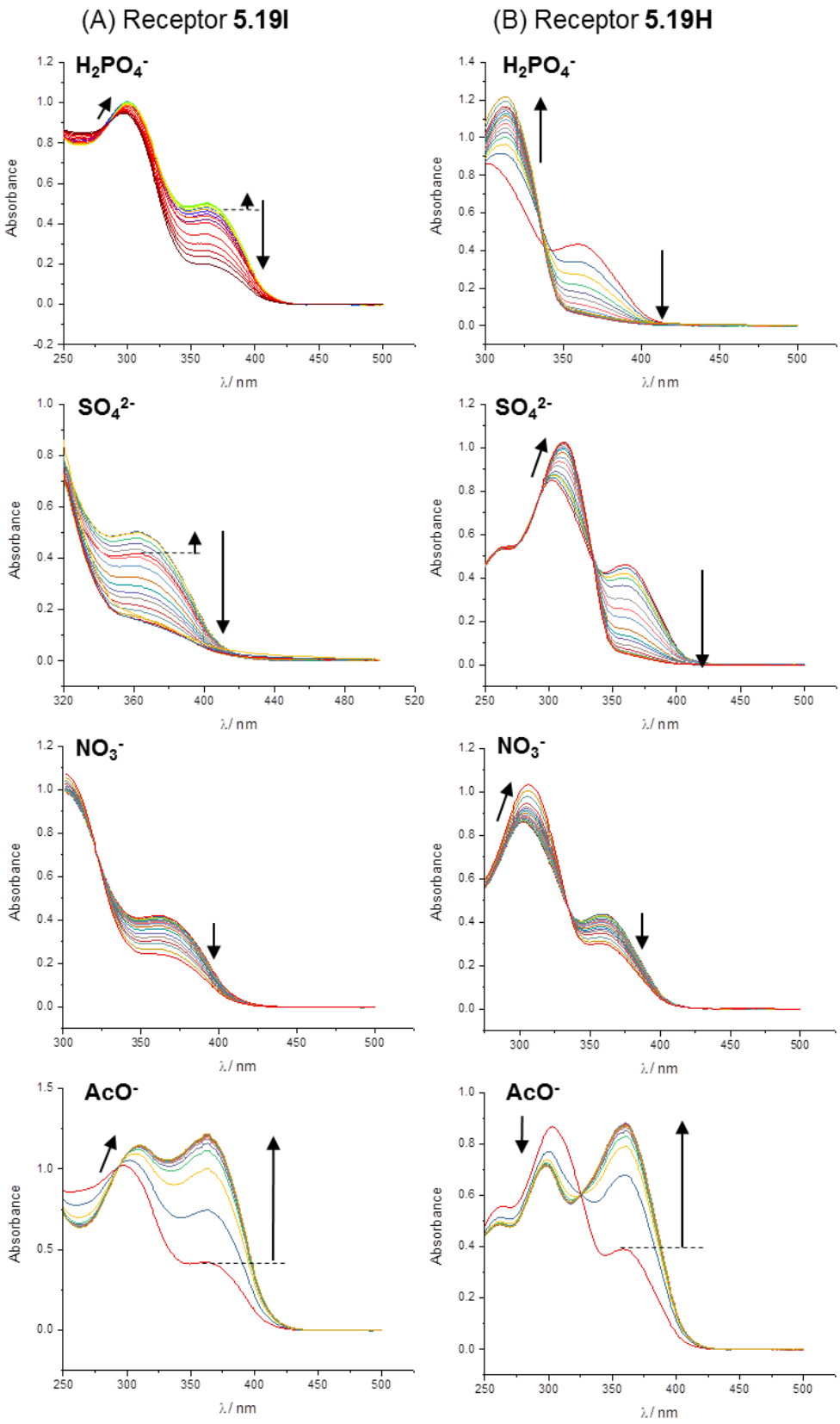


***Figure 5.19**. UV-Vis oxoanion titrations showing the spectra of (A) **5.19I** and (B) **5.19H** in the presence of increasing quantities of the AcO^-, NO_3^-, $H_2PO_4^-$ and SO_4^{2-} ([**5.19H/I**] = 50 μM; CH_3CN/ H_2O 9:1 v/v, T = 293 K).*

Table 5.4. Anion association constants K_a/ M^{-1} of receptors **5.19I** and **5.19H**.[a]

Anion	pK_a[b]	K_a/ M^{-1}	
		5.19I	**5.19H**
F^-	3.2	-[c]	-[c]
Cl^-	-7.0	1390 (30)	630 (10)
Br^-	-9.0	2660 (40)	-[d]
I^-	-10.0	-[e]	-[d]
$H_2PO_4^-$	2.1	$K_{1:1}$ = 3460 (60) $K_{1:2}$ = 70.4 (0.2)	1210 (9)
SO_4^{2-}	2.0	$K_{1:1}$ = 7700 (200) $K_{2:1}$ = 9900 (200)	$K_{1:1}$ = 5450 (40) $K_{1:2}$ = 4710 (70)
ClO_4^-	-10.0	-[d]	-[d]
NO_3^-	-1.3	44.7 (0.2)	96.5 (0.7)
AcO^-	4.8	-[c]	-[c]

[a] A 1:1 host-guest binding model, unless otherwise stated, was used to determine association constants from global fitting of fluorescence titration spectra using BindFit. Anions were added as their TBA salts ([host] = 50 μM, CH_3CN/H_2O 9:1, T = 293 K). Errors (±) are shown in parentheses. [b] pK_a values are for the conjugate acids reported in water by Smith and March.[150] [c] No reliable association constants could be obtained as deprotonation of the receptor had occurred. [d] No evidence of binding. [e] Complex equilibria

Comparing the anion binding affinities in Table 5.4 revealed that with the exception of NO_3^-, the XB receptor **5.19I** exhibited generally superior binding strength compared to its HB analogue. Binding of the halides (Cl^- and Br^-) to receptor **5.19I** displayed Hofmeister bias, with association constant magnitudes decreasing in the order $Br^- > Cl^-$, in accordance with the preference for 'softer' and less strongly hydrated halides seen in the earlier chapters. Contrastingly, receptor **5.19H** showed only detectable binding for the most charge-dense and Lewis basic halide Cl^-. Amongst the oxoanions ($H_2PO_4^-$, SO_4^{2-}, NO_3^- and ClO_4^-), binding affinities generally decreased in the order of their charge densities, with the dianionic SO_4^{2-} being the most strongly bound. The greater charge density of SO_4^{2-} compared to $H_2PO_4^-$ may also account for their different anion coordination modes seen with **5.19I** and **5.19H**. Together, these results suggest that although the acidic pyrrole NH proton was contributing to anion association in the receptors' binding clefts, the binding behaviour of **5.19I** was still dominated by the charge assisted XB interactions. A significant contribution from host-guest electrostatic interactions also likely accounted for the observed anion association.

5.4.4 Binding of Phosphate Derivatives in Buffered Water

The successful demonstration of anion binding by organic-soluble receptors **5.19H/I** by UV-Vis spectroscopy titrations prompted further investigations into the ability of the analogous water-soluble pyrrole receptors **5.22I/H** to bind biological phosphates (ATP^{4-}, ADP^{3-}, AMP^{2-} and HPO_4^{2-}) in 10 mM aqueous HEPES buffer at physiological pH of 7.4.

In general, very small changes in the UV-Vis spectra of both receptors **5.22I** and **5.22H** were observed in the presence of increasing concentrations of phosphates. Owing to the intrinsic absorbances of the adenosine moieties,[151,152] UV-Vis spectra gave only meaningful changes at wavelengths longer than 320 nm. Nevertheless, as shown by the representative spectra of ATP^{4-} titrations in Figure 5.20, anion addition led to only small decreases in the intensity of an absorbance shoulder peak centred around 360 nm. While receptor **5.22H** showed similar peak decreases for all phosphate species investigated, miniscule spectral changes were surprisingly seen during the titrations of AMP^{2-} and HPO_4^{2-} with **5.22I**. SpecFit™ analysis of the titration data determined stoichiometric association constants collected in Table 5.5.

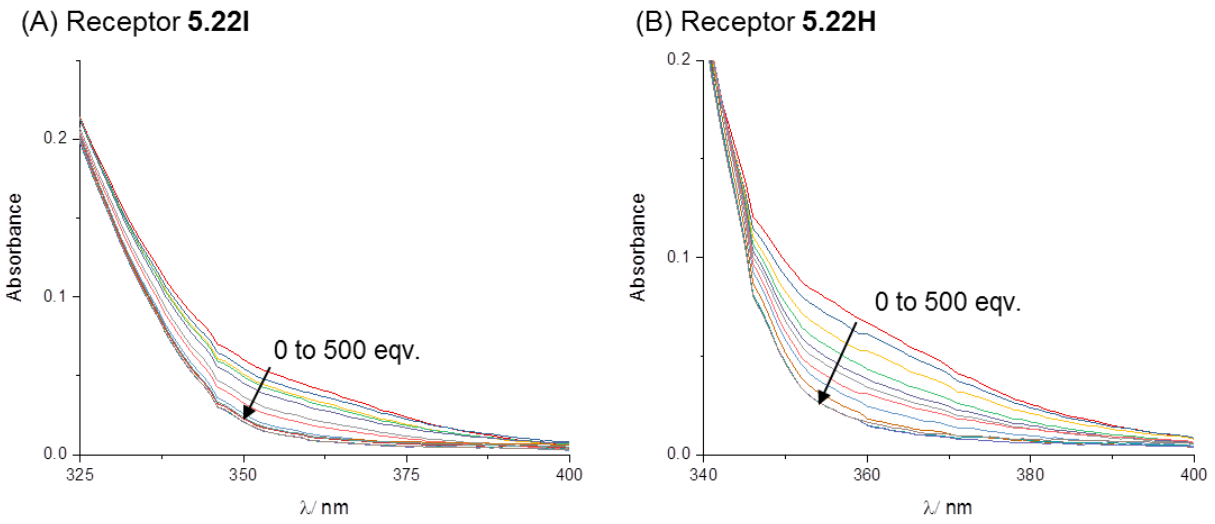


***Figure 5.20**. Partial UV-vis spectra showing the changes in absorbances of receptors (A) **5.22I** and (B) **5.22H** in the presence of increasing quantities of ATP^{4-} ([host] = 50 μM, 10 mM HEPES buffer pH 7.4, T = 293 K).*

Table 5.5. Estimated anion association constants [$\log_{10}(K_a/ M^{-1})$ of receptors **5.22I** and **5.22H** in pH 7.4 aqueous HEPES buffer.[a]

Anion	**5.22H**	**5.22I**
ATP^{4-}	3.26 (0.05)	2.92 (0.07)
ADP^{3-}	2.81 (0.05)	2.68 (0.05)
AMP^{2-}	1.79 (0.07)	-[b]
HPO_4^{2-}	1.81 (0.04)	-[b]

[a] 1:1 stoichiometric association constants were calculated from global fitting of UV-Vis titration spectra using SpecFit™. Errors (±) are given in parentheses. Anions were added as their sodium salts ([host] = 50 μM, 10 mM HEPES buffer pH 7.4, T = 293 K). [b] Spectral changes during UV-Vis titrations were too small for lgK_a values to be determined.

Generally, the affinities of the phosphate anions to **5.22H** correlated with their charged state, indicating that electrostatic interactions were primarily governing anion binding in water. Compared with **5.22H**, no augmentation of ATP^{4-} and ADP^{3-} binding by **5.22I** was seen. This may be expected based on the dominant influence of Coulombic host-guest attractions between multiply-charged host and guest species, seen during the binding studies performed with water-soluble receptors **5.6I** (Section 5.2) which overrides any perturbation consequential of XB interactions.

To gain more insights into the nature of ATP^{4-} binding with **5.22H/I**, their association were probed by qualitative NMR titration experiments in HEPES-buffered D_2O (pD = 7.4). In the presence of 1.0 equivalent of ATP^{4-}, minute upfield shifts of c.a. 0.02 ppm were observed for the ^{1}H NMR signals corresponding to the protons at the 3,4-position of the pyrrole unit of **5.22I** and **5.22H**, possibly suggesting that a small extent of π-stacking was taking place between the electron-deficient conjugated aromatic systems of these receptors with the relatively electron-rich adenosine moiety of ATP^{4-}. When the binding was probed using ^{31}P NMR,[153,154] no perturbations to any of the phosphorus resonances could be detected, which may be a consequence of the extensive hydration of the polyanion triphosphate tail of ATP^{4-} in water[155].

5.5 Conclusions and Future Work

In summary, highly-hydrophilic polyether groups are effective in conferring water-solubility to organic-based acyclic and interlocked host molecules to facilitate anion recognition and sensing investigations in 100 % water. As illustrated with acyclic receptors **5.6I/H** and **5.7I/H**, charge assisted-XB interactions can prove superior to HB for the binding and sensing of anions such as I^- and ReO_4^-, only if the receptor possesses a well-defined rigid and preorganised binding cleft capable of forming optimal linear XB-anion interactions with the anions bound. Van 't Hoff analysis of ReO_4^- binding by **5.6I** revealed that anion recognition was enthalpically-driven and disfavoured entropically, suggesting that the classical hydrophobic effect was not the main contributing factor towards binding. With polyanionic and extensively-hydrated anions such as ATP^{4-}, interactions with the cationic receptors was dominated by Coulombic attraction, which overwhelms any effects of XB. Indeed, although a pyrrole-containing XB motif showed effective anion binding and sensing behaviour in aqueous-organic solvent mixtures, the binding of polyanionic nucleotide phosphates in water was similarly dominated by electrostatic interactions. Attempts to incorporate polyether units into the stopper of a Type 1a water-soluble dendrimer [2]rotaxane met with qualified success: while water solubility was achieved, the rotaxane formed was found to be unstable with respect to dethreading, indicating that the dendritic stoppers were not of sufficient size to kinetically stabilise the interlocked structure.

Future work could involve the construction of water soluble XB-substituted acyclic foldameric structures, similar to HB foldamer systems reported by Flood.[156] In water, conformational changes of the foldamer structure would expose the hydrophilic polyether units to the aqueous environment, concomitantly creating a hydrophobic central region containing Lewis acidic XB-donor groups for anion coordination (Figure 5.21). To achieve water solubility in interlocked structures, higher-generation polyether-bearing dendritic stoppers need to be considered.

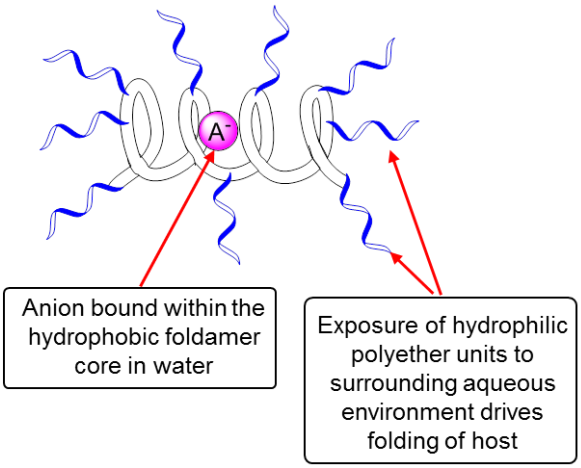


***Figure 5.21**. Schematic illustration of a polyether appended foldamer host capable of aqueous anion binding within the hydrophobic Lewis acidic foldamer core.*

5.6 References

1 J. L. Sessler, P. Gale and W.-S. Cho, *Anion Receptor Chemistry*, The Royal Society of Chemistry, 2006.
2 M. J. Langton, C. J. Serpell and P. D. Beer, *Angew. Chem. Int. Ed.*, 2016, **55**, 1974–1987.
3 S. Kubik, *Chem Soc Rev*, 2010, **39**, 3648–3663.
4 B. Dietrich, J. Guilhem, J.-M. Lehn, C. Pascard and E. Sonveaux, *Helv. Chim. Acta*, 1984, **67**, 91–104.
5 B. Dietrich, B. Dilworth, J.-M. Lehn, J.-P. Souchez, M. Cesario, J. Guilhem and C. Pascard, *Helv. Chim. Acta*, 1996, **79**, 569–587.
6 J. M. Lehn, E. Sonveaux and A. K. Willard, *J. Am. Chem. Soc.*, 1978, **100**, 4914–4916.
7 A. Bencini, C. Coluccini, A. Garau, C. Giorgi, V. Lippolis, L. Messori, D. Pasini and S. Puccioni, *Chem Commun*, 2012, **48**, 10428–10430.
8 C. Bazzicalupi, A. Bencini, C. Giorgi, B. Valtancoli, V. Lippolis and A. Perra, *Inorg. Chem.*, 2011, **50**, 7202–7216.
9 H. Y. Kuchelmeister and C. Schmuck, *Chem. – Eur. J.*, 2011, **17**, 5311–5318.
10 C. Schmuck and V. Bickert, *Org. Lett.*, 2003, **5**, 4579–4581.
11 H. Zhou, Y. Zhao, G. Gao, S. Li, J. Lan and J. You, *J. Am. Chem. Soc.*, 2013, **135**, 14908–14911.
12 N. Ahmed, B. Shirinfar, I. Geronimo and K. S. Kim, *Org. Lett.*, 2011, **13**, 5476–5479.
13 H. T. Ngo, X. Liu and K. A. Jolliffe, *Chem Soc Rev*, 2012, **41**, 4928–4965.
14 S. J. Butler and D. Parker, *Chem Soc Rev*, 2013, **42**, 1652–1666.
15 L. M. P. Lima, A. Lecointre, J.-F. Morfin, A. de Blas, D. Visvikis, L. J. Charbonnière, C. Platas-Iglesias and R. Tripier, *Inorg. Chem.*, 2011, **50**, 12508–12521.
16 T. Liu, A. Nonat, M. Beyler, M. Regueiro-Figueroa, K. Nchimi Nono, O. Jeannin, F. Camerel, F. Debaene, S. Cianférani-Sanglier, R. Tripier, C. Platas-Iglesias and L. J. Charbonnière, *Angew. Chem. Int. Ed.*, 2014, **53**, 7259–7263.
17 S. Faulkner, J. Routledge, X. Zhang, M. Connolly, M. Tropiano, O. Blackburn, A. Kenwright, P. Beer and S. Aldridge, *Angew. Chem. Int. Ed.*, 2017, **129**, 7891-7894.
18 A. Dalla Cort, G. Forte and L. Schiaffino, *J. Org. Chem.*, 2011, **76**, 7569–7572.
19 M. Cametti, A. Dalla Cort and K. Bartik, *ChemPhysChem*, 2008, **9**, 2168–2171.
20 F. Keymeulen, P. De Bernardin, A. Dalla Cort and K. Bartik, *J. Phys. Chem. B*, 2013, **117**, 11654–11659.
21 F. Keymeulen, P. De Bernardin, I. Giannicchi, L. Galantini, K. Bartik and A. Dalla Cort, *Org Biomol Chem*, 2015, **13**, 2437–2443.
22 Y. J. Jang, E. J. Jun, Y. J. Lee, Y. S. Kim, J. S. Kim and J. Yoon, *J. Org. Chem.*, 2005, **70**, 9603–9606.
23 V. Havel, V. Sindelar, M. Necas and A. E. Kaifer, *Chem Commun*, 2014, **50**, 1372–1374.
24 M. A. Yawer, V. Havel and V. Sindelar, *Angew. Chem. Int. Ed.*, 2015, **54**, 276–279.
25 M. Lisbjerg, B. E. Nielsen, B. O. Milhoj, S. P. A. Sauer and M. Pittelkow, *Org Biomol Chem*, 2015, **13**, 369–373.
26 P. Sokkalingam, J. Shraberg, S. W. Rick and B. C. Gibb, *J. Am. Chem. Soc.*, 2016, **138**, 48–51.
27 C. L. D. Gibb and B. C. Gibb, *J. Am. Chem. Soc.*, 2011, **133**, 7344–7347.
28 R. S. Carnegie, C. L. D. Gibb and B. C. Gibb, *Angew. Chem.*, 2014, **126**, 11682–11684.
29 V. Havel, M. Babiak and V. Sindelar, *Chem. – Eur. J.*, 2017, **23**, 8963-8968.
30 A. Brugnara, F. Topic, K. Rissanen, A. de la Lande, B. Colasson and O. Reinaud, *Chem Sci*, 2014, **5**, 3897–3904.
31 S. P. Cornes, M. R. Sambrook and P. D. Beer, *Chem Commun*, 2017, **53**, 3866–3869.

32 M. Fujita, F. Ibukuro, H. Hagihara and K. Ogura, *Nature*, 1994, **367**, 720–723.
33 P. R. Ashton, S. R. L. Everitt, M. Gómez-López, N. Jayaraman and J. F. Stoddart, *Tetrahedron Lett.*, 1997, **38**, 5691–5694.
34 G. Wenz, B.-H. Han and A. Müller, *Chem. Rev.*, 2006, **106**, 782–817.
35 C. J. Bruns, H. Liu and M. B. Francis, *J. Am. Chem. Soc.*, 2016, **138**, 15307–15310.
36 S. Anderson, T. D. W. Claridge and H. L. Anderson, *Angew. Chem. Int. Ed. Engl.*, 1997, **36**, 1310–1313.
37 E. L. Cole, E. Arunkumar, S. Xiao, B. A. Smith and B. D. Smith, *Org Biomol Chem*, 2012, **10**, 5769–5773.
38 H. Y. Au-Yeung, G. D. Pantoş and J. K. M. Sanders, *Angew. Chem. Int. Ed.*, 2010, **49**, 5331–5334.
39 F. B. L. Cougnon, N. Ponnuswamy, G. D. Pantos and J. K. M. Sanders, *Org Biomol Chem*, 2015, **13**, 2927–2930.
40 L. Fang, C. Wang, A. C. Fahrenbach, A. Trabolsi, Y. Y. Botros and J. F. Stoddart, *Angew. Chem. Int. Ed.*, 2011, **50**, 1805–1809.
41 S. Anderson and H. L. Anderson, *Angew. Chem. Int. Ed. Engl.*, 1996, **35**, 1956–1959.
42 S. Anderson, R. T. Aplin, T. D. W. Claridge, T. Goodson III, A. C. Maciel, G. Rumbles, J. F. Ryan and H. L. Anderson, *J Chem Soc Perkin Trans 1*, 1998, 2383–2398.
43 P. N. Taylor, A. J. Hagan and H. L. Anderson, *Org Biomol Chem*, 2003, **1**, 3851–3856.
44 H. Y. Au-Yeung, G. D. Pantoş and J. K. M. Sanders, *Proc. Natl. Acad. Sci.*, 2009, **106**, 10466–10470.
45 R. S. Forgan, J. J. Gassensmith, D. B. Cordes, M. M. Boyle, K. J. Hartlieb, D. C. Friedman, A. M. Z. Slawin and J. F. Stoddart, *J. Am. Chem. Soc.*, 2012, **134**, 17007–17010.
46 M. J. Langton, S. W. Robinson, I. Marques, V. Félix and P. D. Beer, *Nat Chem*, 2014, **6**, 1039–1043.
47 M. J. Langton, I. Marques, S. W. Robinson, V. Félix and P. D. Beer, *Chem. – Eur. J.*, 2016, **22**, 185–192.
48 M. Liu, K. Kono and J. M. J. Fréchet, *J. Polym. Sci. Part Polym. Chem.*, 1999, **37**, 3492–3503.
49 R. S. Dhanikula, A. Argaw, J.-F. Bouchard and P. Hildgen, *Mol. Pharm.*, 2008, **5**, 105–116.
50 R. Barat, T. Legigan, I. Tranoy-Opalinski, B. Renoux, E. Peraudeau, J. Clarhaut, P. Poinot, A. E. Fernandes, V. Aucagne, D. A. Leigh and S. Papot, *Chem Sci*, 2015, **6**, 2608–2613.
51 M. Jayaraman and J. M. J. Fréchet, *J. Am. Chem. Soc.*, 1998, **120**, 12996–12997.
52 L.-A. Tziveleka, C. Kontoyianni, Z. Sideratou, D. Tsiourvas and C. M. Paleos, *Macromol. Biosci.*, 2006, **6**, 161–169.
53 C. Ungureanu, C. Pirvu, M. Mindroiu and I. Demetrescu, *Prog. Org. Coat.*, 2012, **75**, 349–355.
54 N. A. Alcantar, E. S. Aydil and J. N. Israelachvili, *J. Biomed. Mater. Res.*, 2000, **51**, 343–351.
55 M. Fanucchi, J. Glaspy, J. Crawford, J. Garst, R. Figlin, W. Sheridan, D. Menchaca, D. Tomita, H. Ozer and L. Harker, *N. Engl. J. Med.*, 1997, **336**, 404–409.
56 A. Abuchowski, T. van Es, N. C. Palczuk and F. F. Davis, *J. Biol. Chem.*, 1977, **252**, 3578–3581.
57 M. S. Hershfield, R. H. Buckley, M. L. Greenberg, A. L. Melton, R. Schiff, C. Hatem, J. Kurtzberg, M. L. Markert, R. H. Kobayashi, A. L. Kobayashi and A. Abuchowski, *N. Engl. J. Med.*, 1987, **316**, 589–596.
58 J. A. DiPalma, P. H. DeRidder, R. C. Orlando, B. E. Kolts and M. vB Cleveland, *Am J Gastroenterol*, 2000, **95**, 446–450.
59 V. O. Sheftel, *Indirect Food Additives and Polymers: Migration and Toxicology*, Lewis Publishers, Boca Raton, Fl., 2000.
60 S. W. Robinson and P. D. Beer, *Org Biomol Chem*, 2017, **15**, 153–159.
61 C. Nagamani, J. Guo and S. Thayumanavan, *J. Polym. Sci. Part Polym. Chem.*, 2012, **50**, 1187–1196.
62 M. R. J. Vallée, P. Majkut, I. Wilkening, C. Weise, G. Müller and C. P. R. Hackenberger, *Org. Lett.*, 2011, **13**, 5440–5443.
63 J. Wu, J. Li, U. Kolb and K. Mullen, *Chem Commun*, 2006, 48–50.
64 W. Zhu and D. Ma, *Chem Commun*, 2004, 888–889.
65 W. S. Brotherton, R. J. Clark and L. Zhu, *J. Org. Chem.*, 2012, **77**, 6443–6455.
66 M. J. Hynes, *J. Chem. Soc. Dalton Trans.*, 1993, 311–312.
67 Y. Marcus, *J Chem Soc Faraday Trans*, 1991, **87**, 2995–2999.
68 N. G. White, H. G. Lovett and P. D. Beer, *RSC Adv*, 2014, **4**, 12133–12147.
69 S. W. Robinson, C. L. Mustoe, N. G. White, A. Brown, A. L. Thompson, P. Kennepohl and P. D. Beer, *J. Am. Chem. Soc.*, 2015, **137**, 499–507.
70 B. Nepal and S. Scheiner, *J. Phys. Chem. A*, 2015, **119**, 13064–13073.
71 B. Nepal and S. Scheiner, *Chem. – Eur. J.*, 2015, **21**, 13330–13335.
72 R. Cao, B. D. McCarthy and S. J. Lippard, *Inorg. Chem.*, 2011, **50**, 9499–9507.
73 M. Saeki, Y. Sasaki, A. Nakai, A. Ohashi, D. Banerjee, A. C. Scheinost and H. Foerstendorf, *Inorg. Chem.*, 2012, **51**, 5814–5821.
74 C. J. Massena, A. M. S. Riel, G. F. Neuhaus, D. A. Decato and O. B. Berryman, *Chem. Commun.*, 2015, **51**, 1417–1420.
75 E. A. Katayev, G. V. Kolesnikov and J. L. Sessler, *Chem Soc Rev*, 2009, **38**, 1572–1586.
76 R. Alberto, G. Bergamaschi, H. Braband, T. Fox and V. Amendola, *Angew. Chem. Int. Ed.*, 2012, **51**, 9772–9776.
77 V. Amendola, G. Bergamaschi, M. Boiocchi, R. Alberto and H. Braband, *Chem Sci*, 2014, **5**, 1820–1826.
78 V. Amendola, G. Alberti, G. Bergamaschi, R. Biesuz, M. Boiocchi, S. Ferrito and F.-P. Schmidtchen, *Eur. J. Inorg. Chem.*, 2012, **2012**, 3410–3417.
79 L. Keith and W. Telliard, *Environ. Sci. Technol.*, 1979, **13**, 416–423.
80 F. Jaubert, *Appl. Radiat. Isot.*, 2008, **66**, 960–964.

81 W. A. Herrmann, A. M. J. Rost, J. K. M. Mitterpleininger, N. Szesni, S. Sturm, R. W. Fischer and F. E. Kühn, *Angew. Chem. Int. Ed.*, 2007, **46**, 7301–7303.
82 G. M. Filippelli, *Rev. Mineral. Geochem.*, 2002, **48**, 391.
83 J. A. Delmez and E. Slatopolsky, *Am. J. Kidney Dis.*, 1992, **19**, 303–317.
84 A. E. Hargrove, S. Nieto, T. Zhang, J. L. Sessler and E. V. Anslyn, *Chem. Rev.*, 2011, **111**, 6603–6782.
85 S. Lee, K. K. Y. Yuen, K. A. Jolliffe and J. Yoon, *Chem Soc Rev*, 2015, **44**, 1749–1762.
86 M. Cametti, K. Raatikainen, P. Metrangolo, T. Pilati, G. Terraneo and G. Resnati, *Org Biomol Chem*, 2012, **10**, 1329–1333.
87 O. Baudoin, F. Gonnet, M.-P. Teulade-Fichou, J.-P. Vigneron, J.-C. Tabet and J.-M. Lehn, *Chem. – Eur. J.*, 1999, **5**, 2762–2771.
88 M. Dhaenens, J.-M. Lehn and J.-P. Vigneron, *J Chem Soc Perkin Trans 2*, 1993, 1379–1381.
89 M.-P. Teulade-Fichou, J.-P. Vigneron and J.-M. Lehn, *J Chem Soc Perkin Trans 2*, 1996, 2169–2175.
90 M.-P. Teulade-fichou, J.-P. Vigneron and J.-M. Lehn, *Supramol. Chem.*, 1995, **5**, 139–147.
91 H. Abe, Y. Mawatari, H. Teraoka, K. Fujimoto and M. Inouye, *J. Org. Chem.*, 2004, **69**, 495–504.
92 A. K. Gupta, A. Dhir and C. P. Pradeep, *Eur. J. Org. Chem.*, 2015, **2015**, 122–129.
93 D. G. Nicholls and S. J. Ferguson, *Bioenergetics (3rd Edition)*, Academic Press, London, 2003.
94 A.-S. Delepine, R. Tripier and H. Handel, *Org Biomol Chem*, 2008, **6**, 1743–1750.
95 L. Alderighi, P. Gans, A. Ienco, D. Peters, A. Sabatini and A. Vacca, *Coord. Chem. Rev.*, 1999, **184**, 311–318.
96 C. D. Moffat, D. J. Weiss, A. Shivalingam, A. J. P. White, P. Salaün and R. Vilar, *Chem. – Eur. J.*, 2014, **20**, 17168–17177.
97 S. L. Tobey and E. V. Anslyn, *J. Am. Chem. Soc.*, 2003, **125**, 14807–14815.
98 *SpecFit v. 2.02 ed.*, Spectrum Software Associates, Chapel Hill, NC, USA, 1997.
99 F. Peter, M. Gross, M. W. Hosseini, J. M. Lehn and R. B. Sessions, *J Chem Soc Chem Commun*, 1981, 1067–1069.
100 P. B. Merrithew and A. J. Modestino, *J. Am. Chem. Soc.*, 1972, **94**, 3361–3363.
101 A. J. Bard and L. R. Faulkner, *Electrochemical Methods: Fundamentals an Applications*, Wiley, New York, 7th ed., 2001.
102 E. Gail, S. Gos, R. Kulzer, J. Lorösch, A. Rubo, M. Sauer, R. Kellens, J. Reddy, N. Steier and W. Hasenpusch, in *Ullmann's Encyclopedia of Industrial Chemistry*, Wiley-VCH Verlag GmbH & Co. KGaA, 2000.
103 A. A. Shul'ga, M. Koudelka-Hep, N. F. de Rooij and L. I. Netchiporouk, *Anal. Chem.*, 1994, **66**, 205–210.
104 O. Mergel, A. P. H. Gelissen, P. Wünnemann, A. Böker, U. Simon and F. A. Plamper, *J. Phys. Chem. C*, 2014, **118**, 26199–26211.
105 D. Grieshaber, J. Vörös, T. Zambelli, V. Ball, P. Schaaf, J.-C. Voegel and F. Boulmedais, *Langmuir*, 2008, **24**, 13668–13676.
106 M. Savastano, P. Arranz-Mascaros, C. Bazzicalupi, A. Bianchi, C. Giorgi, M. L. Godino-Salido, M. D. Gutierrez-Valero and R. Lopez-Garzon, *RSC Adv*, 2014, **4**, 58505–58513.
107 M. J. DiTucci, S. Heiles and E. R. Williams, *J. Am. Chem. Soc.*, 2015, **137**, 1650–1657.
108 J. W. Lee and K. Kim, in *Dendrimers V: Functional and Hyperbranched Building Blocks, Photophysical Properties, Applications in Materials and Life Sciences*, eds. C. A. Schalley and F. Vögtle, Springer Berlin Heidelberg, Berlin, Heidelberg, 2003, pp. 111–140.
109 K. C.-F. Leung and K.-N. Lau, *Polym Chem*, 2010, **1**, 988–1000.
110 W. Wang, L.-J. Chen, X.-Q. Wang, B. Sun, X. Li, Y. Zhang, J. Shi, Y. Yu, L. Zhang, M. Liu and H.-B. Yang, *Proc. Natl. Acad. Sci.*, 2015, **112**, 5597–5601.
111 I. Aprahamian, T. Yasuda, T. Ikeda, S. Saha, W. R. Dichtel, K. Isoda, T. Kato and J. F. Stoddart, *Angew. Chem. Int. Ed.*, 2007, **46**, 4675–4679.
112 T. Yasuda, K. Tanabe, T. Tsuji, K. K. Coti, I. Aprahamian, J. F. Stoddart and T. Kato, *Chem Commun*, 2010, **46**, 1224–1226.
113 V. Aucagne, K. D. Hänni, D. A. Leigh, P. J. Lusby and D. B. Walker, *J. Am. Chem. Soc.*, 2006, **128**, 2186–2187.
114 J. P. Lorimer and T. J. Mason, *Chem Soc Rev*, 1987, **16**, 239–274.
115 J. Lindley and T. J. Mason, *Chem Soc Rev*, 1987, **16**, 275–311.
116 U. Tilstam and H. Weinmann, *Org. Process Res. Dev.*, 2002, **6**, 906–910.
117 W.-S. Cho and J. L. Sessler, in *Functional Synthetic Receptors*, Wiley-VCH Verlag GmbH & Co. KGaA, 2005, pp. 165–256.
118 P. A. Gale and C. J. E. Haynes, in *Supramolecular Chemistry*, John Wiley & Sons, Ltd, 2012.
119 J. L. Sessler, L. R. Eller, W.-S. Cho, S. Nicolaou, A. Aguilar, J. T. Lee, V. M. Lynch and D. J. Magda, *Angew. Chem. Int. Ed.*, 2005, **44**, 5989–5992.
120 P. A. Gale, *Acc. Chem. Res.*, 2011, **44**, 216–226.
121 P. A. Gale, *Chem Commun*, 2005, 3761–3772.
122 J. L. Sessler, N. M. Barkey, G. D. Pantos and V. M. Lynch, *New J Chem*, 2007, **31**, 646–654.
123 Anzenbacher Pavel, D. S. Tyson, K. Jursíková and F. N. Castellano, *J. Am. Chem. Soc.*, 2002, **124**, 6232–6233.
124 J. L. Sessler, S. Camiolo and P. A. Gale, *35 Years Synth. Anion Recept. Chem. 1968-2003*, 2003, **240**, 17–55.
125 M. Biesaga, K. Pyrzyńska and M. Trojanowicz, *Talanta*, 2000, **51**, 209–224.

126 J. L. Sessler and D. Seidel, *Angew. Chem. Int. Ed.*, 2003, **42**, 5134–5175.
127 R. Misra and T. K. Chandrashekar, *Acc. Chem. Res.*, 2008, **41**, 265–279.
128 Y. Pareek, M. Ravikanth and T. K. Chandrashekar, *Acc. Chem. Res.*, 2012, **45**, 1801–1816.
129 J. L. Sessler, A. Andrievsky, V. Král and V. Lynch, *J. Am. Chem. Soc.*, 1997, **119**, 9385–9392.
130 J. L. Sessler and J. M. Davis, *Acc. Chem. Res.*, 2001, **34**, 989–997.
131 P. K. Panda, Y.-J. Kang and C.-H. Lee, *Angew. Chem. Int. Ed.*, 2005, **44**, 4053–4055.
132 T. Chatterjee, A. Srinivasan, M. Ravikanth and T. K. Chandrashekar, *Chem. Rev.*, 2017, **117**, 3329–3376.
133 K.-C. Chang, T. Minami, P. Koutnik, P. Y. Savechenkov, Y. Liu and P. Anzenbacher, *J. Am. Chem. Soc.*, 2014, **136**, 1520–1525.
134 D. S. Kim and J. L. Sessler, *Chem Soc Rev*, 2015, **44**, 532–546.
135 J. R. Blas, M. Márquez, J. L. Sessler, F. J. Luque and M. Orozco, *J. Am. Chem. Soc.*, 2002, **124**, 12796–12805.
136 H. Miyaji, S.-J. Hong, S.-D. Jeong, D.-W. Yoon, H.-K. Na, J. Hong, S. Ham, J. L. Sessler and C.-H. Lee, *Angew. Chem. Int. Ed.*, 2007, **46**, 2508–2511.
137 C.-H. Lee, H. Miyaji, D.-W. Yoon and J. L. Sessler, *Chem Commun*, 2008, 24–34.
138 I. Saha, J. T. Lee and C.-H. Lee, *Eur. J. Org. Chem.*, 2015, **2015**, 3859–3885.
139 P. Ballester, *Isr. J. Chem.*, 2011, **51**, 710–724.
140 S. K. Kim, J. Lee, N. J. Williams, V. M. Lynch, B. P. Hay, B. A. Moyer and J. L. Sessler, *J. Am. Chem. Soc.*, 2014, **136**, 15079–15085.
141 P. Dydio, D. Lichosyt and J. Jurczak, *Chem Soc Rev*, 2011, **40**, 2971–2985.
142 D. Hernandez-Alonso, S. Zankowski, L. Adriaenssens and P. Ballester, *Org Biomol Chem*, 2015, **13**, 1022–1029.
143 J. Cai, B. P. Hay, N. J. Young, X. Yang and J. L. Sessler, *Chem Sci*, 2013, **4**, 1560–1567.
144 J. L. Sessler, J. M. Davis and V. Lynch, *J. Org. Chem.*, 1998, **63**, 7062–7065.
145 J. L. Sessler, M. J. Cyr, V. Lynch, E. McGhee and J. A. Ibers, *J. Am. Chem. Soc.*, 1990, **112**, 2810–2813.
146 J. A. Joule and K. Mills, *Heterocyclic Chemistry, 5th Edition*, Wiley-Blackwell, Chichester, UK, 2010.
147 Y.-M. Wu, J. Deng, Y. Li and Q.-Y. Chen, *Synthesis*, 2005, **2005**, 1314–1318.
148 R. Tepper, B. Schulze, M. Jäger, C. Friebe, D. H. Scharf, H. Görls and U. S. Schubert, *J. Org. Chem.*, 2015, **80**, 3139–3150.
149 J. Wan, J. Meller, M. Hada, M. Ehara and H. Nakatsuji, *J. Chem. Phys.*, 2000, **113**, 7853–7866.
150 M. B. Smith and J. March, *March's Advanced Organic Chemistry: Reactions, Mechanism, and Structure, 5th Ed.*, John Wiley & Sons, Ltd, New York, 2001.
151 R. M. Bock, N.-S. Ling, S. A. Morell and S. H. Lipton, *Arch. Biochem. Biophys.*, 1956, **62**, 253–264.
152 Y. YAMAZAKI and H. SUZUKI, *Eur. J. Biochem.*, 1978, **92**, 197–207.
153 S. G. Brown, R. M. Hawk and R. A. Komoroski, *J. Inorg. Biochem.*, 1993, **49**, 1–8.
154 E. K. Jaffe and M. Cohn, *Biochemistry (Mosc.)*, 1978, **17**, 652–657.
155 D. Faizullin, N. Zakharchenko, Y. Zuev, A. Puzenko, E. Levy and Y. Feldman, *Int. J. Mol. Sci.*, 2013, **14**, 22876–22890.
156 Y. Hua, Y. Liu, C.-H. Chen and A. H. Flood, *J. Am. Chem. Soc.*, 2013, **135**, 14401–14412.

Blank Page

Chapter 6

Conclusions

CHAPTER 6: Conclusions

The work in this thesis was organised around two main themes, namely the fundamental study of σ-hole interactions such as XB and ChB towards anion binding, as well as their utility in various facets of anion recognition and sensing. In many cases, XB and ChB hosts emerged superior to HB for various anion binding applications, underscoring their importance as complementary and promising non-covalent interactions for host-guest recognition and self-assembly processes in solution.

Chapter 2 explored and established the basic synthetic methodologies for constructing neutral and cationic macrocycles, as well as [2]rotaxane host structures containing triazole-based XB and ChB donor groups- the latter being especially notable for their unprecedented stability and chemical robustness. Extensive ^{1}H NMR binding studies across the range of XB, ChB and HB systems revealed that generally, anion binding strength decreased in the order of XB > ChB > HB in dry and wet organic solvents. Importantly, anion binding using XB and ChB-donor hosts share numerous similarities, which contrasted significantly with their HB host analogues. These include their general Hofmeister preference for binding softer and less-strongly solvated anions in the presence of water, dramatic sensitivity of anion binding strength towards solvent polarity, as well as a much more pronounced enthalpic contribution to the overall free energy of anion binding compared with HB interactions.

Building on these findings, Chapter 3 demonstrated the beneficial influences of σ-hole interactions, in particular XB, towards redox sensing of anions. While the presence of XB-donor motifs at the periphery of redox-active HB [2]rotaxane anion binding sites resulted in no significant enhancement in the hosts' redox sensitivity towards anions, their appendage onto neutral and cationic motifs with direct electronic conjugation with ferrocene resulted in dramatic enhancements of the hosts' electrochemical response relative to analogous HB ferrocene receptors. This may be a consequence of the greater covalent character of the XB-anion interaction compared with HB. Contrastingly, a Se-based ChB redox-active host was found to show similar redox responses as the HB analogue. By varying the bidentate bite

angle of XB-donor motifs and changing the solvent polarity, selective redox sensing of azide and different halides was achieved. Finally, a ferrocene-appended [2]rotaxane with an all-XB anion binding site showed unprecedented selectivity for redox sensing of bromide over chloride in the presence of water.

Chapter 4 extended the applications of XB and ChB interactions towards the discrimination of oxoanion enantiomers and geometric isomers. XB interactions were found to enhance the enantioselectivity of acyclic (*S*)-BINOL-derived chiral host molecules towards chiral oxoanions over their HB analogues, by virtue of the augmented anion affinities and more stringent control of host-guest binding geometries. Although incorporation of these XB motifs into macrocycles led to surprisingly no significant improvements in chiral anion discrimination, notable enhancements were seen using XB chiral [2]rotaxanes. With this chiral [2]rotaxane host design, the presence of a chiral macrocycle component was found to be overwhelmingly important over a chiral axle for effective enantioselective anion recognition, which was rationalised by MD simulations to arise from the anion binding geometries dictated by the position of the XB donor groups within the rotaxane structural framework. Similarly, the stringent directionality of charge-assisted XB and ChB interactions elicited notably distinct binding preferences for chiral and geometric dicarboxylate isomers over HB interactions. Finally, a chiral ditopic XB [3]rotaxane was designed and found to bind dicarboxylates via formation of 1:1 stoichiometric host-guest sandwich complexes. Other than giving a selective fluorescence response for dicarboxylate anions over halides and smaller oxoanions, the [3]rotaxane host was capable of effectively discriminating between chiral and geometric dicarboxylate isomers.

In Chapter 5, the integration of hydrophilic polyether motifs into XB acyclic host design facilitated XB-mediated anion recognition in 100 % water. A rigid dicationic XB acyclic receptor solubilised by these polyether groups was found to be superior to its HB analogue for perrhenate anion binding and fluorescent sensing in water, driven not by the classical hydrophobic effect but largely by favourable enthalpic contributions. When incorporated into stopper units for rotaxane synthesis, the polyether motifs were found to be too

conformationally-flexible, resulting in the synthesised [2]rotaxane being unstable with respect to macrocycle dethreading.

In summary, the results of this thesis highlight the ability of XB and ChB interactions to complement the ubiquitous HB interactions in many solution-phase applications of anion binding, capable of often remarkable augmentation of their effects. Moreover, the kinship of the XB and ChB sister σ-hole interactions are also amply demonstrated, which show more similarities than differences in the various applications studied. It should be noted, nonetheless, that the applications of XB and especially, ChB interactions, are only in their infancy at the time of writing, and will undoubtedly be exploited more extensively in the very near future.

Blank Page

Chapter 7

Experimental

CHAPTER 7: Experimental

7.1 General Considerations

7.1.1 Instrumentation

NMR spectra for the nuclei ^{1}H, ^{13}C (^{1}H), ^{19}F (^{1}H) and ^{31}P (^{1}H) were recorded using Bruker Avance III 400 HD nanobay NMR spectrometers (Hg400 or Venus400) each equipped with a 9.4T magnet, or Bruker Avance 500 machines (AVD500 or AVC500) equipped with 11.75T magnets, with the latter also containing a ^{13}C cryoprobe. ^{77}Se and ^{125}Te NMR spectra were recorded using the Bruker Avance 500 spectrometer (AVD500). All chemical shifts are noted in parts per million (ppm) with signal splittings denoted as singlet (s), doublet (d), triplet (t), quartet (quart.), quintet (quint.), septet (sep.) and multiplet (m). Coupling constants are reported as 3-bond (^{3}J) unless otherwise stated and are recorded to the nearest 0.1 ppm. Spectra are recorded relative to the residual solvent peak (for ^{1}H and ^{13}C), or the solvent with greatest number of deuterium atoms if mixed solvent systems are used, and are assigned with aid from 2D techniques such as COSY and ROESY. Low and high resolution ESI mass spectra were recorded on a Waters LCT premier spectrometer and a Bruker microTOF spectrometer respectively. Fluorescence, UV-Vis and circular dichroism spectra were recorded on a Horiba Fluorolog 3, T60U (PG Instruments Ltd) spectrophotometer and Applied Photophysics Chirascan instrument respectively using a quartz cuvette with path length of 1 cm. Optical rotation data were measured on a Perkin-Elmer 241 polarimeter with a path length of 1 dm (using the 589 nm sodium D), with concentrations (c) reported in g/100 mL and temperatures reported in °C.

7.1.2 ^{1}H NMR Titration Protocols

All deuterated solvents used were purchased from chemical suppliers. Where available, all tetrabutylammonium (TBA) or sodium salts were used as purchased, with the former stored in vacuum dessicators at room temperature with P_2O_5 dessicant. TBA salts of amino acid derivatives, BINOLPO$_4$ and dicarboxylates (Chapter 4) were prepared as described from the

commercially-available acid(s) and 1.0 M solution of TBAOH in methanol[1] and stored in vacuum dessicators with P_2O_5 at -20 ^oC to minimise racemisation.

^1H NMR titrations were performed on the Bruker Avance 400 and 500 spectrometers (Venus400 and AVD500 respectively) at 298 K unless otherwise stated. In a typical titration experiment, a solution of the salt of interest was added to a 0.5 mL solution of the host (1.0 mM or 1.5 mM), and the chemical shift of the appropriate proton environments were monitored for at least 17 data points, or till saturation of the binding curve was seen. For titrations performed in organic solvents, the spectra were referenced to the residual solvent peak, while for those in D_2O, a trace quantity of acetone (<0.05 % of the total volume) was added as an internal reference for all spectra to be referenced to its resonance at 2.10 ppm.

The observed chemical shift values at each guest concentration were entered into the WinEQNMR2 software[2] for every titration point, together with initial estimates of association constants and limiting chemical shifts. Nonlinear least squares analyses were then performed to refine the parameters using either a host-guest 1:1 or 1:2 stoichiometric binding model to obtain the best-fit between the empirical and calculated chemical shifts during convergence of the best-fit binding constant values and their errors. For van't Hoff analyses, variable temperature (VT) ^1H NMR titrations were performed using the same protocol with a suitable range of temperatures. Prior to each titration, the temperature of the host NMR solution was allowed to equilibrate for 20 minutes, and for a further 2-5 minutes after each anion titration, before each ^1H NMR spectra was recorded.

7.1.3 Optical Titration Protocols

UV-vis spectroscopy titrations were performed on a T60U (PG Instruments Ltd) spectrophotometer, while fluorescence titrations were performed using HORIBA Fluorolog, and the data were processed using FluorEssence and OriginPro software. In each case, titrations were performed at 293 K using standard 1 or 3 mL quartz cuvettes with sample volumes of either 0.75 mL or 2.5 mL respectively. The anion of interest was dissolved in the same receptor solution as that being studied to maintain the same receptor concentration during titrations, with the concentration of anion depending on the expected binding affinities.

In a typical experiment, an aliquot of the anion solution was added to the receptor solution in the cuvette and the sample was thoroughly mixed by shaking before the UV-Vis/ fluorescence spectra were recorded. After each aliquot addition, the spectra were recorded at least twice till consistent spectra were obtained. Association constants were calculated from the optical titration data by non-linear global fitting analysis using either the Specfit[3] or Bindfit softwares.[4]

For the qualitative CD spectroscopy titrations, the receptor (rotaxane **4.44**, Chapter 4) and anion solutions were prepared as described for UV-Vis and fluorescence spectroscopy. Spectral acquisitions were obtained using a 25 uM solution of rotaxane in a 1 mL quartz cuvette at 1 mm intervals from 260 nm to 400 nm with an Applied Photophysics Chirascan instrument at 293 K. The CD spectra of chiral rotaxane **4.44** were recorded in the absence and presence of the guest anion (after thorough mixing) by taking the average of triplicate repeats, and subtracted from a triplicate-averaged background scan of the solvent mixture (e.g. $CHCl_3$/ CH_3OH/ H_2O 60:39:1 *v/v*). The averaged spectra was then smoothed using OriginPro 2017 using the Savitzky-Golay protocol[5] with polynomial order 2 and smoothing window of 10 points.

7.1.4 Electrochemical Titration Protocols

Cyclic voltammetry (CV) and square wave voltammetry (SWV) spectra were recorded using an Autolab Potentiostat/Galvanostat model PG-STAT 12 (Metrohm Autolab, Netherlands), using a standard single compartment three-electrode electrochemical cell placed inside a Faraday cage. A glassy carbon solid disc working electrode, platinum wire counter (auxiliary) electrode and a non-aqueous Ag/ $AgNO_3$ reference electrode (prepared as described[6]) was used for electrolyte solutions containing 0.1 M $TBAPF_6$ in organic solvent mixtures. CV experiments were typically performed with 1 s equilibration time, a step potential of 1 mV and a scan rate of 100 mV s^{-1}, while SWVs were recorded with 1 s equilibration time, a step potential of 3 mV and a frequency of 30 Hz. Prior to performing redox titration experiments, the redox reversibility of the receptor was first studied by recording successive CV scans at typical scan rates of 25, 50, 75, 100, 250 and 500 mV s^{-1} (see Appendix B for more details). After establishing receptor redox quasi-reversibility and reproducibility of each

receptor's Fc/Fc^+ $E_{1/2}$ value, a typical redox titration experiment involved recording the CVs/ SWVs of the host (0.1 mM for macrocycles **3.27H/I** and rotaxane **3.34I$_4$** and 0.5 mM otherwise) solution (2.5 mL) in the presence of increasing quantities of anion solution (typically 5 uL = 1.0 equivalent), with the solutions thoroughly mixed by mechanical agitation after each anion addition.

For redox titrations performed in 100 % water, the same three-electrode cell was used with the same working and counter electrodes, but using a mercury sulphate (HgSO4) reference electrode instead in a 100 mM $NaNO_3$ supporting electrolyte solution.

7.2 Synthetic Procedures

7.2.1 Solvents and Reagents

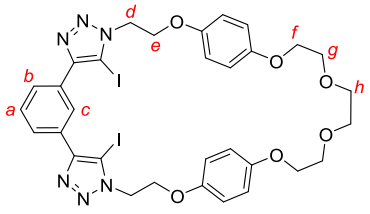
All solvents and reagents were purchased from commercial suppliers and used as received unless otherwise stated. Dry organic solvents were degassed with nitrogen and then dehydrated by passing through an MBraun MPSP-800 column, and water was de-ionised and micro filtered using a Milli-Qr Millipore machine. Triethylamine was distilled from potassium hydroxide and stored over the same base prior to usage. TBTA was synthesised as described[7] and stored under ambient conditions. The various Grubbs catalysts (Grubbs II, Hoveyda-Grubbs, Stewart-Grubbs) and $[Cu(CH_3CN)_4]PF_6$ were stored in vacuum desiccators containing P_2O_5 powder in between usage. Ratios of solvent mixtures are reported by volume. Brine refers to a saturated aqueous solution of NaCl, aqueous ammonia refers to an approximately 10 % solution of NH_3 in water, basic EDTA refers to a 0.02 M aqueous solution of EDTA in a 1 % NH_3 solution, bleach refers to general purpose aqueous sodium hypochlorite solution typically containing c.a. 10 % NaClO by weight, and petroleum ether refers to the fraction of petrol boiling between 40 - 60 ^oC. Thin layer chromatography (TLC) analysis was performed using Merck silica Kieselgel 60 F_{254} 0.25 mm or Fluka 60 Å aluminium oxide matrix on precoated aluminium plates, with spots visualised under UV light (254 nm) and/ or staining with $KMnO_4$ solution (only for silica TLC). Column chromatography was performed using silica gel (particle size 40-63 uM) or neutral/ basic Brockmann grade I alumina gel (50-200 uM particle size) under a positive N_2 head pressure, and preparatory TLC on 20 x 20 cm glass

plates with 1 cm silica thickness. Amberlite® anion exchange columns were packed using IRA-400 resin beads containing styrene/divinylbenzene gel with quarternary ammonium matrix active groups (Cl^- salt), and prepared/ preloaded by washing the beads sequentially with water and 1 M NaOH (aq) till the eluent becomes colourless, water, 10 % aqueous NH_4X (X = anion of interest), water and finally the organic solvent mixture (containing water) used for anion exchange. Microwave-assisted reactions were performed in a Biotage® Initiator 2.0 reactor using sealed standard Biotage pyrex-glass microwave vials with caps containing rubber septa.

Safety note: Organic azides, NaN_3, 1,2,3-triazole/triazoliums and the amide coupling agent HOBt used throughout this thesis are potentially explosive and should be handled with care and in small quantities. In particular, direct heating under reduced pressure should be avoided, and especially for reactions with NaN_3, chlorinated solvents (i.e. CH_2Cl_2, $CHCl_3$ and CCl_4) should be strictly avoided even for reaction work-ups due to their potential for forming highly-explosive poly-azidomethanes.[8,9] In addition, NaN_3 should not be used in the presence of acids due to formation of highly toxic HN_3 (g).[10] If this is unavoidable, the reaction should be performed strictly in the fume hood.

7.2.2 Synthesis of Novel Compounds from Chapter 2

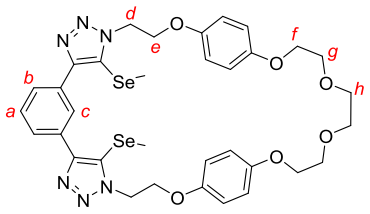
Macrocycle 2.1l



Triethylene glycol bis-tosylate **2.3** (188 mg, 0.410 mmol), synthesised according to reported procedures,[11] and bis-phenol macrocycle precursor **2.4l** (300 mg, 0.410 mmol) were dissolved in anhydrous degassed DMF (75 mL). Cesium carbonate (534 mg, 1.64 mmol) was added and the vigorously-stirred suspension was allowed to stir for 16 hours at 70 ^oC under N_2. After which, the DMF was removed on the rotary and the resulting solid stirred in a mixture of

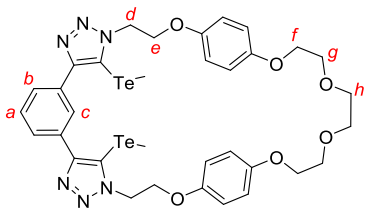
chloroform (50 mL) and water (50 mL). The aqueous and organic layers were separated and the aqueous layer extracted thoroughly with chloroform (4 x 30 mL). The combined organics were then dried with brine (3 x 20 mL) followed by $MgSO_4$. After solvent removal, the crude reaction mixture was purified by preparatory TLC (2.5 % methanol in dichloromethane) to afford the target macrocycle **2.1I** as a white solid (112 mg, 32 %). ^{1}H-NMR (400 MHz, $CDCl_3$) δ 8.24 (1H, s, H_c), 7.85 (2H, m, H_b), 7.51 (1H, t, ^{3}J = 8.0 Hz, H_a), 6.63-6.72 (8H, m, hydroquinone-Ar*H*), 4.79 (4H, t, ^{3}J = 6.0 Hz, H_d), 4.35 (4H, t, ^{3}J = 6.0 Hz, H_e), 3.95 (4H, t, ^{3}J = 6.0 Hz, H_f), 3.71 (4H, t, ^{3}J = 6.0 Hz, H_g), 3.60 (6H, s, H_h); ^{13}C-NMR (100 MHz, $CDCl_3$) δ 153.6, 152.2, 150.0, 130.6, 129.1, 128.1, 127.1, 115.8, 115.6, 78.6, 70.8, 69.7, 68.2, 67.5, 50.1; MS (ESI +ve) *m/z* 851.0545 ($[M + H]^+$, $C_{32}H_{33}O_6N_6{}^{127}I_2$, calc. 851.0546).

Macrocycle 2.1Se



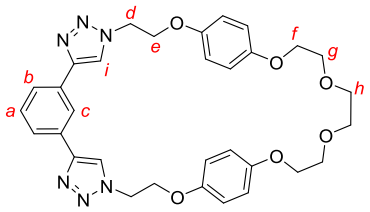
An identical procedure was adopted as that for macrocycle **2.1I**, but using macrocycle precursor **2.4Se** (92.0 mg, 0.137 mmol), triethylene glycol bis-tosylate **2.3** (62.8 mg, 0.137 mmol) and cesium carbonate (179 mg, 0.548 mmol) in anhydrous degassed DMF (20 mL). Purification was performed by preparatory TLC (2.5 % methanol in dichloromethane), affording macrocycle **1.Se** as a white solid (112 mg, 32 %). **^{1}H-NMR** (400 MHz, $CDCl_3$) δ 8.72 (1H, s, H_c), 8.04 (2H, d, ^{3}J = 7.8 Hz, H_b), 7.59 (1H, t, ^{3}J = 7.8 Hz, H_a), 6.79 (4H, m, hydroquinone-Ar*H*), 6.72 (4H, m, hydroquinone-Ar*H*), 4.96 (4H, t, ^{3}J = 6.0 Hz, H_d), 4.40 (4H, t, ^{3}J = 6.0 Hz, H_e), 4.03 (4H, t, ^{3}J = 6.0 Hz, H_f), 3.81 (4H, t, ^{3}J = 6.0 Hz, H_g), 3.70 (6H, s, H_h), 2.14 (6H, s, SeC*H*$_3$); **^{13}C-NMR** (100 MHz, $CDCl_3$) δ 153.6, 152.2, 149.3, 131.4, 129.1, 127.6, 126.0, 121.7, 115.8, 115.5, 70.9, 69.7, 68.3, 67.8, 43.6, 10.1; **^{77}Se-NMR** (95 MHz, d_6-acetone) δ 47.2; **MS** (ESI +ve) *m/z* 787.1256 ($[M + H]^+$, $^{80}Se_2C_{34}H_{39}O_6N_6$, calc. 787.1256).

Macrocycle 2.1Te



Identical procedure as that for macrocycle **2.1I**, using macrocycle precursor **2.4Te** (110 mg, 0.143 mmol), triethylene glycol bis-tosylate **2.3** (66.0 mg, 0.143 mmol), cesium carbonate (373 mg, 1.14 mmol) in anhydrous DMF (30 mL). Purification using preparatory TLC (ethyl acetate/ dichloromethane 3:2) afforded the target macrocycle as a white solid (23 mg, 18 %). **^{1}H-NMR** (400 MHz, CD_2Cl_2) δ 8.58 (1H, s, H_c), 7.88 (2H, d, ^{3}J = 7.8 Hz, H_b), 7.56 (1H, t, ^{3}J = 7.8 Hz, H_a), 6.66-6.71 (8H, m, hydroquinone-Ar*H*), 4.99 (4H, t, ^{3}J = 4.6 Hz, H_d), 4.36 (4H, t, ^{3}J = 4.6 Hz, H_e), 4.01 (4H, t, ^{3}J = 4.0 Hz, H_f), 3.81 (4H, t, ^{3}J = 4.0 Hz, H_g), 3.70 (6H, s, H_h), 1.89 (6H, s, TeCH_3); **^{13}C-NMR** (100 MHz, CD_2Cl_2) δ 153.6, 152.7, 152.2, 132.2, 128.8, 128.2, 127.2, 115.5, 102.1, 70.7, 69.6, 68.1, 67.9, 50.3, -12.9; **^{125}Te-NMR** (157 MHz, d_6-acetone) δ 146.0; **MS** (ESI +ve) *m/z* 887.1055 ($[M + H]^+$, $^{130}Te_2C_{34}H_{39}O_6N_6$, calc. 887.1050).

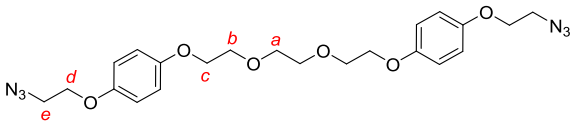
Macrocycle 2.1H



Bis-azide intermediate **2.2** (178 mg, 0.377 mmol), TBTA (20 mg, 0.038 mmol) and $[Cu(CH_3CN)_4]PF_6$ (56 mg, 0.15 mmol) were dissolved in thoroughly-degassed dichloromethane (150 mL). To the vigorously stirred solution was added DIPEA (0.26 mL, 1.50 mmol) and 1,3-diethynylbenzene (0.05 mL, 0.377 mmol), and the yellow solution was left to stir under N_2 for 2 days. After which, the solvent was evaporated on a rotary evaporator till c.a. 20 mL remained, and was washed with basic EDTA solution (2 x 10 mL). The aqueous layer was extracted with chloroform (2 x 10 mL) and the combined organics were dried with $MgSO_4$. Solvent removal then afforded a yellow sticky solid. The pure product was obtained after

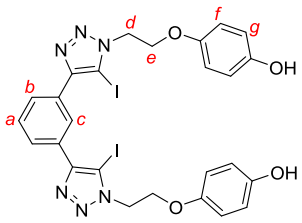
purification by preparatory TLC (3 % methanol in dichloromethane) as a white solid (66 mg, 29 %). **^{1}H-NMR** (400 MHz, $CDCl_3$) δ 8.04 (2H, s, H_i), 7.98 (2H, d, ^{3}J = 8.0 Hz, H_b), 7.89 (1H, s, H_c), 7.51 (1H, t, ^{3}J = 8.0 Hz, H_a), 6.74-6.82 (8H, m, hydroquinone-Ar*H*), 4.78 (4H, t, ^{3}J = 6.4 Hz, H_d), 4.31 ((4H, t, ^{3}J = 6.4 Hz, H_e), 4.04 (4H, t, ^{3}J = 6.2 Hz, H_d), 3.81 (4H, t, ^{3}J = 6.4 Hz, H_d), 3.69 (4H, s, H_h); **^{13}C-NMR** (100 MHz, $CDCl_3$) δ 153.8, 152.2, 147.6, 131.2, 129.8, 125.5, 123.1, 121.2, 115.9, 115.6, 70.9, 69.7, 68.2, 67.4, 50.0 ; **MS** (ESI +ve) *m/z* 599.2612 ($[M + H]^+$, $C_{32}H_{35}O_6N_6$, calc. 599.2613).

Bis-azide 2.2



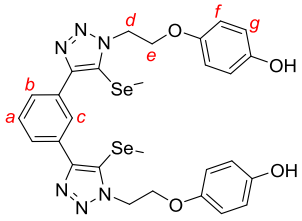
2-azidoethoxyphenol **2.6** (520 mg, 2.90 mmol) and triethylene glycol bis-tosylate **2.3** (651 mg, 1.42 mmol) were dissolved in dry degassed acetonitrile (10 mL), and anhydrous potassium carbonate (785 mg, 5.68 mmol) was added portionwise. The vigorously-stirred suspension was heated at reflux under N_2 for 16 h. Subsequently, the reaction was cooled back to room temperature, and stirred in a mixture of chloroform (10 mL) and water (10 mL) till a clear biphasic mixture was obtained. The chloroform layer was separated from the aqueous layer, and the latter was back-extracted with chloroform (3 x 10 mL). The combined organics were dried with brine and $MgSO_4$. A beige solid was obtained after solvent evaporation, which was purified by passing the crude product through a short plug of silica (2 % methanol in dichloromethane) to obtain the the product as an off-white crystalline solid (619 mg, 93 %) after solvent removal *in vacuo*. **^{1}H-NMR** (400 MHz, $CDCl_3$) δ 6.86 (8H, m, hydroquinone-Ar*H*), 4.08-4.12 (8H, m, H_c + H_d), 3.85 (4H, t, ^{3}J = 6.2 Hz, H_b), 3.76 (4H, s, H_a), 3.57 (4H, t, ^{3}J = 6.2 Hz, H_e); **^{13}C-NMR** (100 MHz, $CDCl_3$) δ 153.5, 152.5, 115.7, 115.6, 70.9, 69.9, 68.1, 67.9, 50.3; **MS** (ESI +ve) *m/z* 495.19611 ($[M + Na]^+$, $C_{22}H_{28}O_6N_6Na$, calc. 495.19735).

Bis-phenol macrocycle precursor 2.4I



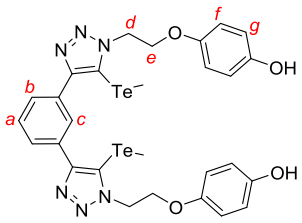
Acetyl chloride (1.22 mL, 17.1 mmol) was added to methanol (5 mL) at 0 ^{o}C and stirred for 5 minutes, before being warmed to ambient temperature and stirred for a further 15 minutes. Compound **2.8I** (470 mg, 0.57 mmol) was dissolved in dichloromethane (5 mL) and added portionwise to the vigorous acidic methanol solution and stirred for 2 hours. After the reaction was complete (checked using TLC with 5 % methanol in dichloromethane), the solvent was evaporated and the product dried on the high vacuum for a day to yield the product as an off-white solid in excellent purity (414 mg, quantitative). The product was used without further purification. **^{1}H-NMR** (400 MHz, d_6-acetone) δ 8.66 (1H, s, H_c), 8.04 (2H, m, H_b), 7.64 (1H, t, ^{3}J = 8.0 Hz, H_a), 6.73-6.82 (8H, m, $H_f + H_g$), 4.91 (4H, t, ^{3}J = 6.0 Hz, H_d), 4.50 (4H, d, ^{3}J = 6.0 Hz, H_e); **^{13}C-NMR** (100 MHz, d_6-acetone) δ 151.8, 151.5, 148.8, 131.4, 128.9, 127.2, 125.9, 115.8, 115.7, 79.1, 67.0, 50.1 **MS** (ESI +ve) *m/z* 736.9871 ($[M + H]^+$, $C_{26}H_{23}O_4N_6{}^{127}I_2$, calc. 736.9865).

Bis-phenol macrocycle precursor 2.4Se



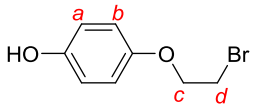
Identical procedure as that for **2.4I**. Reagents: acetyl chloride (0.20 mL, 2.8 mmol) and compound **2.8Se** (80 mg, 0.11 mmol) in methanol/ dichloromethane 1:1 (4 mL). Target compound **2.4Se** was obtained as a pale beige solid in excellent purity (70 mg, 99 %) and was used without further purification. **^{1}H-NMR** (400 MHz, CD_3OD) δ 8.73 (1H, s, H_c), 8.04 (2H, d, ^{3}J = 7.8 Hz, H_b), 7.61 (1H, t, ^{3}J = 7.8 Hz, H_a), 6.73 (4H, m, H_f), 6.67 (4H, m, H_g), 4.97 (4H, t, ^{3}J = 3.9 Hz, H_d), 4.45 (4H, d, ^{3}J = 3.9 Hz, H_e), 2.18 (6H, s, SeCH_3); **MS** (ESI +ve) *m/z* 673.0580 ($[M + H]^+$, $^{80}Se_2C_{28}H_{29}O_4N_6$, calc. 673.0581).

Bis-phenol macrocycle precursor 2.4Te



Similar procedure used as that for **2.4I**. Reagents: acetyl chloride (0.25 mL, 3.51 mmol) and compound **2.8Te** (100 mg, 0.117 mmol); solvent: methanol/ dichloromethane 1:1 (4 mL). Product **2.4Te** was obtained as light brown solid (90 mg, quantitative) in decent purity and used without further purification. **^{1}H-NMR** (400 MHz, CD_3OD) δ 8.49 (1H, s, H_c), 7.97 (2H, d, ^{3}J = 7.8 Hz, H_b), 7.64 (1H, t, ^{3}J = 7.8 Hz, H_a), 6.75 (4H, m, H_f), 6.67 (4H, m, H_g), 5.05 (4H, t, ^{3}J = 4.9 Hz, H_d), 4.42 (4H, d, ^{3}J = 4.9 Hz, H_e), 1.90 (6H, s, TeCH_3); **MS** (ESI +ve) *m/z* 773.0372 ([M + H]$^{+}$, $^{130}Te_2C_{28}H_{29}O_4N_6$, calc. 773.0369).

2-bromoethoxyphenol 2.5

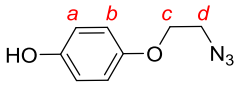


Although not a novel compound, a modified synthetic protocol was used from that reported.[12]

Hydroquinone (20.0 g, 182 mmol) was dissolved in methanol (250 mL) that was thoroughly degassed by vigorous N_2 bubbling for 30 minutes. Freshly-ground potassium hydroxide (10.2 g, 182 mmol) was added to the solution and allowed to stir under N_2 for a further 30 minutes to yield an orange solution. 1,2-dibromoethane (18.8 mL, 218 mmol) was then added dropwise using a syringe over 10 minutes, and the reaction mixture was heated at reflux for 48 hours. After cooling to ambient temperature, the methanol was evaporated to obtain a beige solid, which was then taken up in a mixture of ethyl acetate (200 mL) and water (100 mL) to form a biphasic mixture. The organic layer was separated from the aqueous layer, and the aqueous layer was extracted with ethyl acetate (3 x 50 mL). The combined organics were then dried with brine (100 mL) and $MgSO_4$, and the solvent removed to obtain a beige solid which was mainly hydroquinone. To this solid was then added chloroform (100 mL) and the suspension

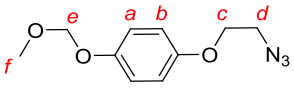
stirred for 15 minutes at room temperature. After filtration, the residue was washed with chloroform (50 mL) and the filtrate was evaporated to obtain the desired product in decent purity as an off-white solid (11.0 g, 28 %). The product was used without any further purification. **^{1}H-NMR** (400 MHz, $CDCl_3$) δ 6.76-6.84 (4H, m, H_a + H_b), 4.48 (1H, s, OH), 4.24 (2H, t, ^{3}J = 6.0 Hz, H_c), 3.62 (2H, t, ^{3}J = 6.0 Hz, H_d); **^{13}C-NMR** (100 MHz, $CDCl_3$) δ 152.3, 150.1, 116.3, 116.1, 68.9, 29.3; **MS (ESI)** *m/z* calc. for $[M + H]^+$ = 217.0, found 217.1.

2-azidoethoxyphenol 2.6



2-bromoethoxyphenol **2.5** (11.0 g, 50.7 mmol) was dissolved in DMSO (100 mL) and sodium azide (6.6 g, 101 mmol) was added portionwise to the solution. After stirring at room temperature for 16 h, water (200 mL) was added, followed by diethyl ether (100 mL). The organic layer was separated from the aqueous layer, and the latter was extracted with diethyl ether (4 x 100 mL). The combined organics was dried with brine and $MgSO_4$ and the solvent was removed to obtain a sticky beige solid. Purification by column chromatography (dichloromethane) gave the product **2.6** as an pale beige solid (6.1 g, 67 %). **^{1}H-NMR** (400 MHz, $CDCl_3$) δ 6.77-6.84 (4H, m, H_a + H_b), 4.84 (1H, br. s, OH), 4.11 (2H, t, ^{3}J = 6.0 Hz, H_c), 3.57 (2H, t, ^{3}J = 6.0 Hz, H_d); **^{13}C-NMR** (100 MHz, $CDCl_3$) δ 152.4, 150.1, 116.1, 115.9, 67.8, 50.3; **MS (ESI)** *m/z* calc. for $[M + H]^+$ = 180.1, found 180.1.

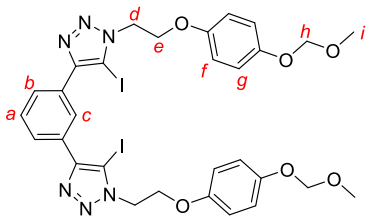
MOM-protected 2-azidoethoxyphenol 2.7



2-azidoethoxyphenol **2.6** (4.00 g, 22.3 mmol) was dissolved in dry dichloromethane (20 mL) and the solution chilled to 0 ^{o}C in an ice bath. DIPEA (4.6 mL, 27 mmol) was added dropwise over 5 minutes and the reaction was stirred at 0 ^{o}C for a further 10 minutes. To the resulting light brown solution was added chloromethyl methyl ether (2.0 mL, 27 mmol) dropwise over 5

minutes. The reaction was then warmed up to ambient temperature and left to stir for 16 h under N_2. Water (10 mL) was then added to quench the reaction, and the organic and aqueous layers separated. The organic layer was washed successively with water (10 mL) and saturated aqueous $NaHCO_3$ (10 mL), and dried with brine (10 mL) and $MgSO_4$. Removal of solvent gave a reddish-brown liquid which was purified using a silica plug (eluent: dichloromethane) to give the product as a colourless oil (4.7 g, 96 %). **^{1}H-NMR** (400 MHz, $CDCl_3$) δ 7.00 (2H, d, ^3J = 8.0 Hz, H_a), 6.87 (2H, d, ^3J = 8.0 Hz, H_b), 5.12 (2H, s, H_e), 4.12 (2H, t, ^3J = 4.0 Hz, H_c), 3.58 (2H, t, ^3J = 4.0 Hz, H_d), 3.49 (3H, s, H_f); **^{13}C-NMR** (100 MHz, $CDCl_3$) δ 153.3, 151.8, 117.6, 115.6, 95.2, 67.6, 55.9, 50.2; **MS (ESI)** *m/z* calc. for $[M + H]^+$ = 246.1, found 246.1.

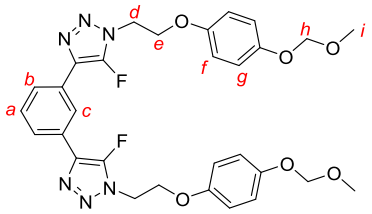
MOM-protected macrocycle precursor 2.8l



To a vigorously-stirred suspension of sodium iodide (3.78 g, 25.2 mmol) in dry THF (20 mL) was added copper(II) perchlorate hexahydrate (4.67 g, 12.6 mmol) and the resulting dark brown suspension was stirred for 5 minutes under N_2. Following which, azide **2.7** (1.4 g, 6.3 mmol), TBTA (80 mg, 0.15 mmol), DBU (0.90 mL, 6.0 mmol) and 1,3-diethynylbenzene (0.4 mL, 3.0 mmol) were successively added before being diluted with acetonitrile (20 mL). The reaction was vigorously stirred under N_2 in the dark at room temperature for 2 days, after which the reaction mixture was found to turn light brown. Chloroform (100 mL) was then added and the reaction was washed with 10 % aqueous ammonia solution (2 x 30 mL). The aqueous layer was back-extracted with chloroform (2 x 20 mL) and the combined organics were dried with brine (50 mL) and $MgSO_4$. Solvent removal *in vacuo* gave a brown solid, which was purified by column chromatography (3 % methanol in dichloromethane) to afford the pure product as a white solid (2.32 g, 93 %). **^{1}H-NMR** (400 MHz, $CDCl_3$) δ 8.56 (1H, s, H_c), 7.61

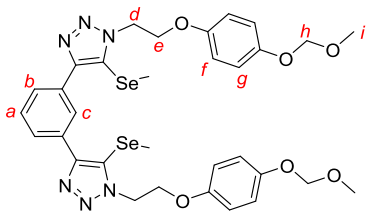
(2H, m, H_b), 7.61 (1H, t, ^3J = 8.0 Hz, H_a), 6.98 (4H, d, ^3J = 8.0 Hz, H_f), 6.85 (4H, d, ^3J = 8.0 Hz, H_g), 5.11 (4H, s, H_h), 4.87 (4H, t, ^3J = 5.2 Hz, H_d), 4.47 (4H, d, ^3J = 5.2 Hz, H_e), 3.48 (6H, s, H_i); **^{13}C-NMR** (100 MHz, $CDCl_3$) δ 148.0, 147.0, 145.2, 132.8, 132.6, 130.0, 128.0, 126.2, 77.6, 76.7, 66.6, 47.3, 29.1, 21.7 **MS** (ESI +ve) *m/z* 825.0387 ($[M + H]^+$, $C_{30}H_{31}O_6N_6{}^{127}I_2$, calc. 825.0389).

MOM-protected macrocycle precursor 2.8F



Compound **2.8I** (183 mg, 0.220 mmol) was dissolved in acetonitrile (6 mL) with heating and transferred to a microwave vial. Separately, potassium fluoride (128 mg, 2.20 mmol) was dissolved in water (6.0 mL) and transferred to the same microwave vial, whereupon a uniform white suspension formed. The vial was sealed and heated in the microwave reactor at 180 °C for 10 minutes to obtain a slightly cloudy solution. Subsequently, the reaction was diluted with chloroform (20 mL) and water (10 mL) was added. The aqueous and organic layers were separated, and the aqueous layer extracted with chloroform (3 x 10 mL). The combined organics were dried with brine and $MgSO_4$. Purification using silica gel column chromatography (3 % methanol in dichloromethane) gave the product as a white solid (122 mg, 90 %). **^{1}H-NMR** (400 MHz, $CDCl_3$) δ 8.31 (1H, s, H_c), 7.87 (2H, d, ^3J = 7.7 Hz, H_b), 7.55 (1H, t, ^3J = 7.7 Hz, H_a), 6.96 (4H, d, ^3J = 8.0 Hz, H_f), 6.81 (4H, d, ^3J = 8.0 Hz, H_g), 5.09 (4H, s, H_h), 4.67 (4H, t, ^3J = 5.2 Hz, H_d), 4.41 (4H, d, ^3J = 5.2 Hz, H_e), 3.45 (6H, s, H_i); **^{19}F-NMR** (376 MHz, $CDCl_3$) δ 150.9; **^{13}C-NMR** (100 MHz, $CDCl_3$) δ 152.9, 152.1, 151.8, 148.9, 129.5, 127.9 (d, $^1J_{C\text{-}F}$ = 282 Hz), 125.0, 122.0, 117.6, 115.7, 95.1, 66.3, 55.9, 46.8; **MS** (ESI +ve) *m/z* 609.2267 ($[M + H]^+$, $C_{30}H_{31}O_6N_6F_2$, calc. 609.2268).

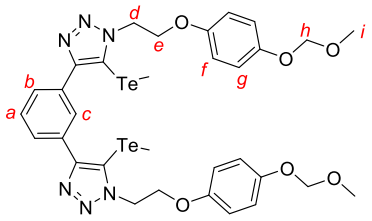
MOM-protected macrocycle precursor 2.8Se



Warning: handle with care in fume cupboard due to malodourous nature of Se-containing volatiles formed in this reaction. All glassware in contact with the reaction was deodorized by soaking in bleach for at least 6 hours.

To a microwave vial containing powdered elemental selenium (96.0 mg, 1.21 mmol) was added a minimum amount of anhydrous THF to fully submerge the selenium. After sealing the vial under N_2, a 1.6 M solution of methyl lithium in hexane (0.76 mL, 1.2 mmol) was added with vigorous stirring at room temperature, whereupon a light brown slurry forms (sonicate if necessary to ensure homogeniety). The slurry was stirred for 15 minutes, before a solution of compound **2.8F** (122 mg, 0.20 mmol) in anhydrous DMF (1.5 mL) was added portionwise to afford a light brown solution, which was stirred at 70 ^{o}C in the dark for 16 h. After which, the resulting brown solution was cooled back to ambient temperature, and iodomethane (0.13 mL, 2.0 mmol) was added. The solution was stirred vigorously at room temperature for a further 30 minutes, forming a uniform light brown solution. Subsequently, the solution was poured into water to form a light brown suspension, which was extracted with chloroform (4 x 10 mL). The combined organics were dried with brine (20 mL) and $MgSO_4$ and solvents thoroughly removed. Purification of the sticky brown crude product using column chromatography (eluent: ethyl acetate/ petroleum ether 3:2) afforded the desired product as an off-white solid (86 mg, 56 %). **^{1}H-NMR** (400 MHz, $CDCl_3$) δ 8.89 (1H, s, H_c), 8.15 (2H, d, ^{3}J = 7.8 Hz, H_b), 7.57 (1H, t, ^{3}J = 7.8 Hz, H_a), 6.96 (4H, m, H_f), 6.80 (4H, m, H_g), 5.10 (4H, s, H_h), 4.95 (4H, t, ^{3}J = 5.4 Hz, H_d), 4.45 (4H, d, ^{3}J = 5.4 Hz, H_e), 3.46 (6H, s, H_i), 2.21 (6H, s, SeCH_3); **^{13}C-NMR** (100 MHz, $CDCl_3$) δ 153.1, 151.9, 149.2, 131.3, 128.9, 127.3, 125.9, 120.3, 117.6, 115.6, 95.2, 67.8, 55.9, 48.4, 10.1 ; **MS** (ESI +ve) *m/z* 761.1102 ($[M + H]^+$, $^{80}Se_2C_{32}H_{36}O_6N_6$, calc. 761.1100).

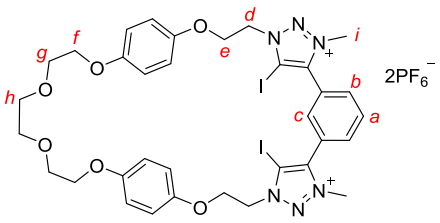
MOM-protected macrocycle precursor 2.8Te



Warning: handle with care in fume cupboard due to malodourous nature of Te-containing volatiles formed in this reaction. All glassware in contact with the reaction was deodorized by soaking in bleach for at least 6 hours.

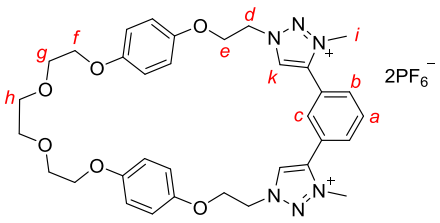
Elemental tellurium powder (232 mg, 1.82 mmol) was suspended in a minimum amount of dry degassed THF in a sealed microwave vial and chilled to -78 ^{o}C. A 1.6 M solution of methyl lithium in hexane (1.13 mL, 1.82 mmol) was added dropwise and the reaction was stirred at -78 ^{o}C for 5 minutes before being warmed up to ambient temperature and stirred for a further 1 hour in the dark. A solution of compound **2.8I** (300 mg, 0.363 mmol) in dry THF (4 mL) was added portionwise via a syringe to the resulting red-brown suspension in the microwave vial to afford a bright red solution. The reaction was then heated at 80 ^{o}C in the dark for 3 hours, cooled back down to ambient temperature before iodomethane (0.6 mL) was added and the reaction vigorously stirred for another 30 minutes. The suspension was poured into water (20 mL) and the organics extracted using chloroform (3 x 20 mL). The combined organics were dried with brine (20 mL) and anhydrous $MgSO_4$ and the solvent removed *in vacuo*. Silica gel chromatography (ethyl acetate/ dichloromethane 3:7) afforded the pure product as a pale yellow sticky solid (255 mg, 82 %). **^{1}H-NMR** (400 MHz, $CDCl_3$) δ 8.69 (1H, s, H_c), 8.05 (2H, d, ^{3}J = 7.8 Hz, H_b), 7.56 (1H, t, ^{3}J = 7.8 Hz, H_a), 6.96 (4H, m, H_f), 6.81 (4H, m, H_g), 5.10 (4H, s, H_h), 5.01 (4H, t, ^{3}J = 5.2 Hz, H_d), 4.40 (4H, d, ^{3}J = 5.2 Hz, H_e), 3.46 (6H, s, H_i), 1.96 (6H, s, TeCH_3); **^{13}C-NMR** (100 MHz, $CDCl_3$) δ 153.1, 152.7, 151.9, 131.8, 128.7, 127.8, 127.5, 117.6, 115.6, 101.4, 95.2, 67.7, 55.9, 50.3, -13.0 ; **MS** (ESI +ve) *m/z* 883.0717 ([M + Na]$^{+}$, $^{130}Te_2C_{32}H_{36}O_6N_6Na$, calc. 883.0713).

Dicationic XB Macrocycle 2.9I



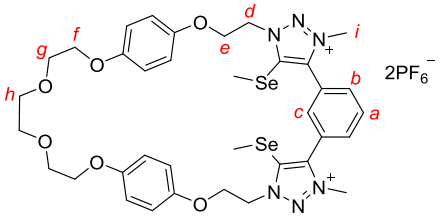
To a solution of macrocycle **2.1I** (25 mg, 0.029 mmol) in dry dichloromethane (1.0 mL) was added trimethyloxonium tetrafluoroborate (9.4 mg, 0.064 mmol) portionwise, and the reaction was left to stir overnight at room temperature. Following which, a drop of methanol was added to the reaction mixture and stirred for 15 minutes to quench any unreacted trimethyloxonium tetrafluoroborate, and the solvent was removed *in vacuo*. The solid was then taken up in dichloromethane (2 mL) and filtered to obtain the desired product as the residue in good purity. Anion exchange was performed by passing a solution of the macrocycle in acetonitrile/water 99:1 three times through an Amberlite™ column pre-loaded with 0.1 M NH_4PF_6 (aq.). Removal of solvent afforded the PF_6^- salt of the macrocycle as a white solid (24 mg, 70 %). **^{1}H-NMR** (400 MHz, CD_3CN) δ 7.99 (1H, t, ^3J = 7.7 Hz, H_a), 7.83 (2H, d, ^3J = 7.9 Hz, H_b), 7.64 (1H, s, H_c), 6.79 (8H, m, hydroquinone-Ar*H*), 5.03 (4H, t, ^3J = 4.7 Hz, H_d), 4.40 (4H, t, ^3J = 4.6 Hz, H_e), 4.16 (6H, s, H_i), 3.97 (4H, t, ^3J = 4.3 Hz, H_f), 3.71 (4H, t, ^3J = 4.3 Hz, H_g), 3.59 (4H, s, H_h); **^{13}C-NMR** (100 MHz, CD_3CN) δ 154.9, 153.1, 147.0, 134.9, 133.6, 132.6, 125.6, 116.7, 116.5, 92.6, 71.5, 70.5, 69.3, 67.5, 55.6, 40.7; **^{19}F-NMR** (376 MHz, CD_3CN) δ -72.9 (d, $^1J_{F-P}$ = 707 Hz); **^{31}P-NMR** (162 MHz, CD_3CN) δ -144.7 (sep., $^1J_{P-F}$ = 707 Hz); **MS** (ESI +ve) *m/z* 440.0464 ($[M]^{2+}$, $C_{34}H_{38}O_6N_6\,^{127}I_2$, calc. 440.0466).

Dicationic HB Macrocycle 2.9H



Identical synthetic procedure as that for macrocycle **2.9I**. Reagents: neutral macrocycle **2.1H** (28 mg, 0.047 mmol), trimethyloxonium tetrafluoroborate (15.3 mg, 0.103 mmol) in dry dichloromethane (1.5 mL). Purification by preparatory TLC (eluent: 4 % methanol in dichloromethane), followed by anion exchange through a PF_6^-- loaded Amberlite column afforded **2.9H** as a white solid (34 mg, 79 %). **^{1}H-NMR** (400 MHz, CD_3CN) δ 8.58 (2H, s, H_k), 7.85-7.89 (3H, m, H_a + H_b), 7.68 (1H, s, H_c), 6.77-6.83 (8H, m, hydroquinone-Ar*H*), 4.97 (4H, t, ^3J = 4.6 Hz, H_d), 4.37 (4H, t, ^3J = 4.6 Hz, H_e), 4.19 (6H, s, H_i), 3.98 (4H, t, ^3J = 4.3 Hz, H_f), 3.71 (4H, t, ^3J = 4.3 Hz, H_g), 3.59 (4H, s, H_h); **^{13}C-NMR** (100 MHz, CD_3CN) δ 154.3, 152.4, 142.4, 133.1, 131.6, 131.4, 130.3, 124.3, 116.3, 116.0, 70.8, 69.8, 68.6, 66.3, 54.4, 39.2; **^{19}F-NMR** (376 MHz, CD_3CN) δ -73.0 (d, $^1J_{F\text{-}P}$ = 707 Hz); **^{31}P-NMR** (162 MHz, CD_3CN) δ -144.7 (sep., $^1J_{P\text{-}F}$ = 707 Hz); **MS** (ESI +ve) *m/z* 314.1499 ($[M]^{2+}$, $C_{34}H_{40}O_6N_6$, calc. 314.1499).

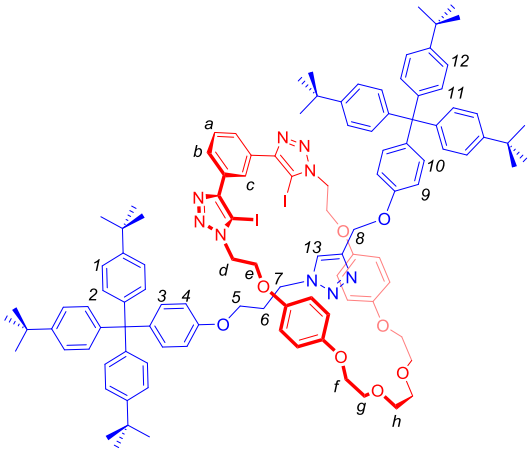
Dicationic ChB Macrocycle 2.9Se



Identical procedure adopted as that for macrocycle **2.9I**, using neutral macrocycle **2.1Se** (25 mg, 0.032 mmol) and trimethyloxonium tetrafluoroborate (10.4 mg, 0.070 mmol) in dry dichloromethane (1.0 mL). Purification by preparatory TLC (eluent: 8 % methanol in dichloromethane) followed by anion exchange through a PF_6^--loaded Amberlite column afforded **2.9Se** as a white solid (34 mg, 79 %). **^{1}H-NMR** (400 MHz, d_6-acetone) δ 8.12-9.19 (4H, m, H_a + H_b + H_c), 6.85 (8H, m, hydroquinone-Ar*H*), 5.34 (4H, t, ^3J = 4.7 Hz, H_d), 4.54 ((4H, t, ^3J = 4.7 Hz, H_e), 4.39 (6H, s, H_i), 4.05 (4H, t, ^3J = 4.6 Hz, H_f), 3.81 (4H, t, ^3J = 4.6 Hz, H_g),

3.67 (4H, s, H_h), 2.31 (6H, s, SeCH_3); **^{13}C-NMR** (100 MHz, d_6-acetone) δ 154.7, 152.6, 145.5, 134.3, 132.8, 132.7, 131.9, 125.5, 116.2, 116.1, 71.3, 70.1, 68.8, 67.2, 53.3, 39.3, 10.5; **^{19}F-NMR** (376 MHz, d_6-acetone) δ -72.8 (d, $^1J_{F\text{-}P}$ = 707 Hz); **^{31}P-NMR** (162 MHz, d_6-acetone) δ -144.4 (sep., $^1J_{P\text{-}F}$ = 707 Hz); **^{77}Se-NMR** (95 MHz, d_6-acetone) δ 107.1; **MS** (ESI +ve) *m/z* 961.1289 ([M + PF_6]$^+$, $C_{36}H_{44}O_6N_6F_6P^{80}Se_2$, calc. 961.1289).

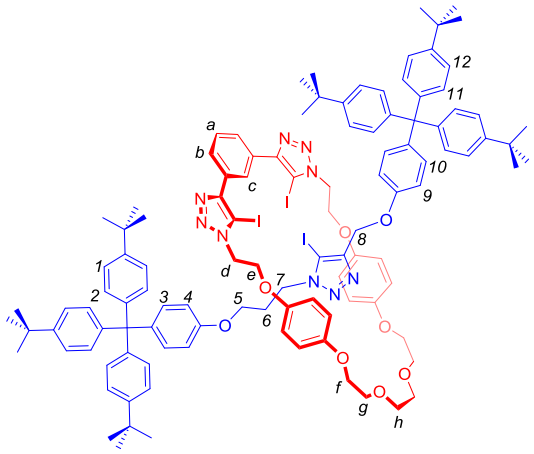
Neutral Bis-iodotriazole [2]Rotaxane 2.12I$_2$H



Macrocycle **2.1I** (38 mg, 0.045 mmol) was mixed with [Cu(CH$_3$CN)$_4$]PF$_6$ (16.8 mg, 0.045 mmol) in dry degassed dichloromethane (4 mL) and stirred for 15 minutes under N_2. To the colourless solution was added stopper proto-alkyne **2.11H**[13] (122 mg, 0.225 mmol) and stopper azide **2.10**[14] (132 mg, 0.225 mmol) portionwise successively, and the reaction stirred under N_2 for 24 hours. After which, the reaction was diluted with chloroform (20 mL) and washed with basic EDTA (2 x 20 mL), followed by water (3 x 20 mL). The organic layer was dried with $MgSO_4$ (no brine!) and the solvent removed to give a white solid. Purification by preparatory TLC (2.5 % methanol in dichloromethane) afforded the rotaxane as a white solid (37 mg, 41 %). **^{1}H-NMR** (400 MHz, $CDCl_3$) δ 8.59 (1H, s, H_c), 8.02 (2H, d, ^3J = 6.4 Hz, H_b), 7.87 (1H, s, H_{13}), 7.54 (1H, t, ^3J = 6.4 Hz, H_a), 7.22 (12H, m, H_2 + H_{11}), 7.10 (16H, m, H_1 + H_3 + H_{10} + H_{12}), 6.77 (2H, d, ^3J = 7.2 Hz, H_9), 6.58 (6H, m, hydroquinone-ArH + H_4), 6.41 (4H, d, ^3J = 7.2 Hz, hydroquinone-ArH), 4.85 (2H, s, H_8), 4.72 (4H, t, ^3J = 4.4 Hz, H_d), 4.35 (4H, t, ^3J = 4.4 Hz, H_e), 4.09 (2H, t, ^3J = 6.0 Hz, H_7), 3.48-3.68 (14H, m, H_f + H_g + H_h + H_5), 2.07 (2H, quint., ^3J = 6.0 Hz, H_6), 1.30 (27H, s, stopper-^{t}Bu), 1.29 (27H, s, stopper-^{t}Bu); **^{13}C-NMR** (100 MHz,

$CDCl_3$) δ 156.2, 153.0, 151.8, 149.3, 148.4, 144.2, 144.1, 142.9, 140.0, 139.8, 132.3, 130.7, 130.6, 129.2, 127.7, 125.2, 124.1, 116.2, 115.0, 113.3, 112.9, 80.5, 70.8, 69.9, 67.4, 67.1, 64.1, 63.1, 61.4, 49.1, 47.0, 34.3, 31.4; **MS** (ESI +ve) *m/z* 1981.7950 ($[M + H]^+$, $C_{112}H_{128}O_8N_9{}^{127}I_2$, calc. 1981.8003).

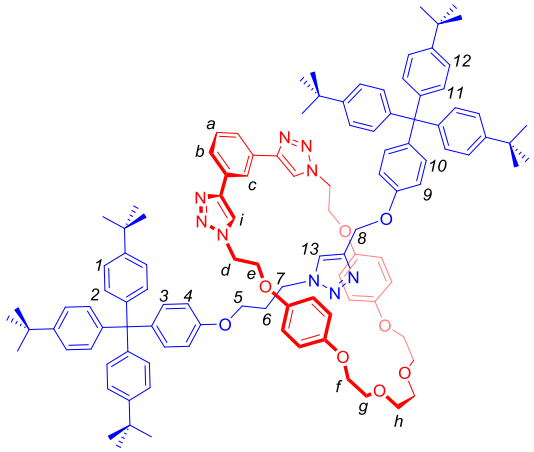
Neutral Tris-iodotriazole [2]Rotaxane 2.12I$_3$



Macrocycle **2.1I** (29 mg, 0.034 mmol) was mixed with $[Cu(CH_3CN)_4]PF_6$ (13 mg, 0.034 mmol) in dry degassed dichloromethane (3 mL) and stirred for 15 minutes under N_2. To the colourless solution was added iodoalkyne **2.11I** (114 mg, 0.17 mmol) and azide **2.10** (100 mg, 0.17 mmol) portionwise successively, and the reaction stirred under N_2 for 48 hours. After which, the reaction was diluted with chloroform (20 mL) and washed with basic EDTA (2 x 20 mL), followed by water (3 x 20 mL). The organic layer was dried with $MgSO_4$ (no brine!) and the solvent removed to give a white solid. Purification by preparatory TLC (2.5 % methanol in dichloromethane) afforded the rotaxane as a white solid (13 mg, 18 %). **^{1}H-NMR** (400 MHz, $CDCl_3$) δ 8.32 (1H, s, H_c), 7.83 (2H, d, ^3J = 6.4 Hz, H_b), 7.43 (1H, t, ^3J = 6.4 Hz, H_a), 7.22 (12H, m, H_2 + H_{11}), 7.03 (14H, m, H_1 + H_{10} + H_{12}), 6.94 (2H, d, ^3J = 7.2 Hz, H_3), 6.72 (6H, d, ^3J = 7.2 Hz, H_9), 6.30-6.38 (10H, m, hydroquinone-Ar*H* + H_4), 4.70 (4H, t, ^3J = 4.4 Hz, H_d), 4.67 (2H, s, H_8), 4.08-4.17 (4H, m, H_e), 3.74-3.82 (4H, m, H_f), 3.63 (2H, t, ^3J = 6.0 Hz, H_7), 3.52-3.60 (8H, m, H_g + H_h), 3.26 (2H, t, ^3J = 6.0 Hz, H_5), 1.53 (2H, quint., ^3J = 6.0 Hz, H_6), 1.30 (27H, s, stopper-^{t}Bu), 1.29 (27H, s, stopper-^{t}Bu); **^{13}C-NMR** (100 MHz, $CDCl_3$) δ 160.6, 156.2, 156.1, 153.1, 151.8, 149.6, 148.2, 146.7, 144.3, 144.1, 139.9, 139.5, 132.1, 130.7, 130.6, 128.9,

127.8, 126.9, 124.1, 115.2, 113.4, 113.0, 81.7, 78.6, 75.2, 70.8, 69.7, 67.6, 66.9, 63.9, 63.1, 61.2, 50.0, 47.4, 34.3, 31.4; **MS** (ESI +ve) *m/z* 2107.6936 ($[M + H]^+$, $C_{112}H_{127}O_8N_9{}^{127}I_3$, calc. 2107.6970).

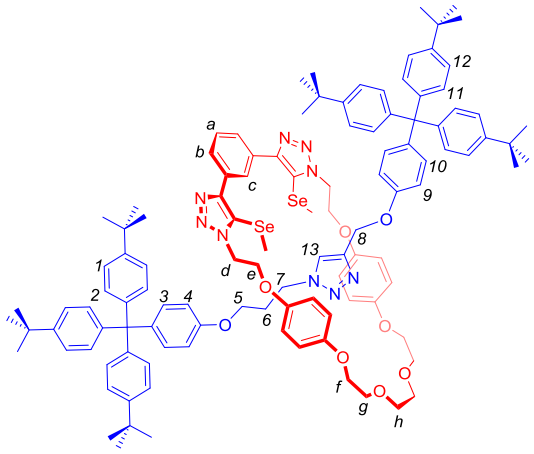
Neutral Tris-prototriazole [2]Rotaxane 2.12H$_3$



Identical synthetic procedure used as for rotaxane **2.12I$_2$H**.

Reagents and conditions: Macrocycle **2.1H** (40 mg, 0.067 mmol), $[Cu(CH_3CN)_4]PF_6$ (25 mg, 0.067 mmol), stopper alkyne **2.11H** (182 mg, 0.335 mmol), stopper azide **2.10** (197 mg, 0.335 mmol) in degassed dichloromethane (6.7 mL) for 24 hours. The target rotaxane was obtained as a white solid (24 mg, 21 %) after purification by preparatory TLC (2.5 % methanol in dichloromethane). **^{1}H-NMR** (400 MHz, $CDCl_3$) δ 7.93 (5H, m, H_b + H_c + H_i), 7.41 (1H, t, ^3J = 9.0 Hz, H_a), 7.21 (13H, m, H_2 + H_{11} + H_{13}), 7.03-7.09 (16H, m, H_1 + H_3 + H_{10} + H_{12}), 6.70 (2H, d, ^3J = 7.2 Hz, H_9), 6.41-6.50 (10H, m, hydroquinone-Ar*H* + H_4), 4.73 (2H, s, H_8), 4.53-4.65 (4H, m, H_d), 4.15 (4H, t, ^3J = 6.2 Hz , H_e), 3.84-3.88 (4H, m, H_f), 3.67 (2H, t, ^3J = 6.0 Hz, H_7), 3.67 (4H, t, ^3J = 6.2 Hz , H_g), 3.58 (4H, s, H_h), 3.39 (2H, t, ^3J = 6.2 Hz, H_5), 1.66 (2H, quint., ^3J = 6.2 Hz, H_6), 1.30 (27H, s, stopper-^{t}Bu), 1.29 (27H, s, stopper-^{t}Bu); **^{13}C-NMR** (100 MHz, $CDCl_3$) δ 156.1, 156.0, 153.3, 151.8, 148.4, 148.3, 147.5, 144.2, 144.1, 140.2, 139.9, 132.3, 132.2, 131.1, 130.9, 130.7, 129.6, 125.5, 124.1, 123.7, 123.1, 121.1, 115.9, 115.8, 115.7, 115.3, 113.1, 112.9, 70.9, 70.7, 69.6, 67.9, 67.0, 63.9, 63.1, 61.2, 49.7, 46.7, 34.3, 31.5, 31.4, 31.3, 29.2; **MS** (ESI +ve) *m/z* 1729.0007 ($[M + H]^+$, $C_{112}H_{130}O_8N_9$, calc. 1729.0037).

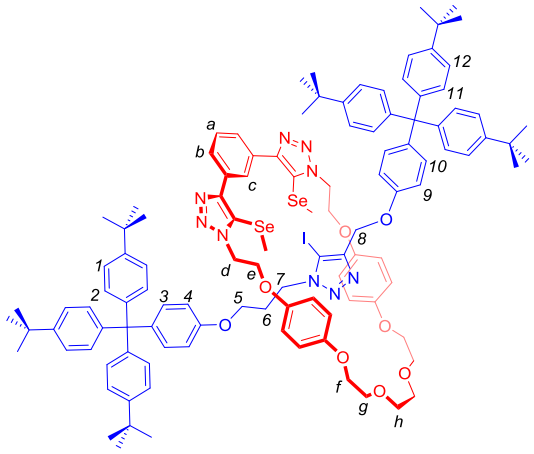
Neutral Bis(methylseleno-triazole)-[2]Rotaxane 2.12Se$_2$H



Identical synthetic procedure used as for rotaxane **2.12I$_2$H**.

Reagents and conditions: Macrocycle **2.1Se** (30 mg, 0.038 mmol), [Cu(CH$_3$CN)$_4$]PF$_6$ (14.2 mg, 0.038 mmol), stopper alkyne **2.11H** (103 mg, 0.190 mmol), stopper azide **2.10** (112 mg, 0.190 mmol) in degassed dichloromethane (3.8 mL) for 24 hours. The target rotaxane was obtained as a white solid (41 mg, 56 %) after purification by preparatory TLC (2.5 % methanol in dichloromethane). **^{1}H-NMR** (500 MHz, CDCl$_3$) δ 8.80 (1H, s, H$_c$), 8.11 (2H, d, ^3J = 8.6 Hz, H$_b$), 7.48 (1H, t, ^3J = 8.6 Hz, H$_a$), 7.28 (1H, s, H$_{13}$), 7.14-7.16 (12H, m, H$_2$ + H$_{11}$), 6.99-7.03 (14H, m, H$_1$ + H$_{12}$ + H$_{10}$), 7.02 (2H, d, ^3J = 8.8 Hz, H$_3$), 6.75 (2H, d, ^3J = 8.8 Hz, H$_9$), 6.45 (2H, d, ^3J = 7.0 Hz, H$_4$), 6.41 (8H, m, hydroquinone-Ar*H*), 4.84-4.87 (6H, m, H$_d$ + H$_8$), 4.27 (4H, m, H$_e$), 3.80 (4H, d, ^3J = 5.0 Hz, H$_f$), 3.75 (2H, t, ^3J = 7.5 Hz, H$_7$), 3.59-3.63 (4H, m, H$_g$), 3.53 (4H, s, H$_h$), 3.34 (2H, t, ^3J = 7.2 Hz, H$_5$), 2.06 (6H, s, SeC*H*$_3$), 1.60 (2H, m, H$_6$), 1.31 (54H, s, stopper-^{t}Bu); **^{13}C-NMR** (125 MHz, CDCl$_3$) δ 155.3, 155.2, 152.1, 151.0, 147.7, 147.2, 147.1, 143.2, 143.1, 142.2, 138.7, 138.5, 131.1, 130.9, 130.2, 129.7, 129.6, 127.9, 125.9, 124.6, 123.1, 122.6, 120.3, 114.3, 112.2, 111.9, 69.6, 68.5, 66.7, 66.6, 62.9. 62.0, 61.9, 60.4, 47.5, 45.8, 33.3, 30.4, 28.7, 9.1; **^{77}Se-NMR** (95 MHz, CDCl$_3$) δ 45.6; **MS** (ESI +ve) *m/z* 1915.8671 ([M + H]$^+$, ^{80}Se$_2$C$_{114}$H$_{133}$O$_8$N$_9$, calc. 1915.8602).

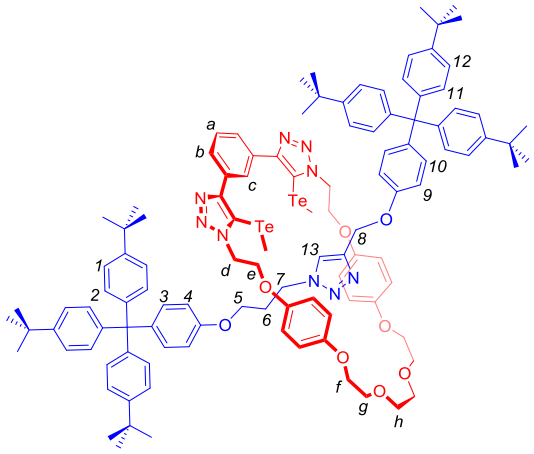
Neutral Iodotriazole-bis(methylseleno-triazole) [2]Rotaxane 2.12Se$_2$I



Identical synthetic procedure used as for rotaxane **2.12I$_3$**.

Reagents and conditions: Macrocycle **2.1Se** (35 mg, 0.045 mmol), [Cu(CH$_3$CN)$_4$]PF$_6$ (16.8 mg, 0.045 mmol), stopper iodoalkyne **2.11I** (150 mg, 0.225 mmol), stopper azide **2.10** (132 mg, 0.225 mmol) in degassed dichloromethane (4.1 mL) for 2 days. The target rotaxane was obtained as a white solid (25 mg, 28 %) after purification by preparatory TLC (2.5 % methanol in dichloromethane). **^{1}H-NMR** (500 MHz, CDCl$_3$) δ 8.77 (1H, s, H$_c$), 8.07 (2H, d, ^3J = 7.8 Hz, H$_b$), 7.48 (1H, t, ^3J = 7.8 Hz, H$_a$), 7.21-7.26 (12H, m, H$_2$ + H$_{11}$), 7.08-7.13 (14H, m, H$_1$ + H$_{12}$ + H$_{10}$), 7.05 (2H, d, ^3J = 8.8 Hz, H$_3$), 6.80 (2H, d, ^3J = 8.8 Hz, H$_9$), 6.54 (2H, d, ^3J = 8.7 Hz, H$_4$), 6.41 (4H, d, ^3J = 9.2 Hz, hydroquinone-Ar*H*), 6.34 (4H, d, ^3J = 9.2 Hz, hydroquinone-Ar*H*), 4.88 (4H, m, H$_d$), 4.71 (2H, s, H$_8$), 4.21 (4H, m, H$_e$), 3.80-3.89 (4H, m, H$_f$), 3.59-3.66 (10H, m, H$_g$ + H$_h$ + H$_7$), 3.41 (2H, m, H$_5$), 2.10 (6H, s, SeC*H*$_3$), 1.51 (2H, m, H$_6$), 1.31 (54H, s, stopper-^{t}Bu); **^{13}C-NMR** (125 MHz, CDCl$_3$) δ 156.4, 156.2, 153.1, 151.8, 149.0, 148.3, 148.2, 146.6, 144.3, 144.2, 139.5, 132.1, 132.0, 131.4, 130.7, 128.9, 127.1, 126.3, 124.1, 121.5, 115.3, 115.0, 113.4, 113.1, 81.6, 70.7, 69.6, 67.5, 67.4, 65.7, 64.1, 63.1, 61.2, 48.7, 34.3, 31.4, 29.7, 10.1 ; **^{77}Se-NMR** (95 MHz, CDCl$_3$) δ 44.7; **MS** (ESI +ve) *m/z* 2042.7703 ([M + H]$^+$, ^{80}Se$_2$C$_{114}$H$_{132}$O$_8$N$_9$^{127}I, calc. 2042.7647).

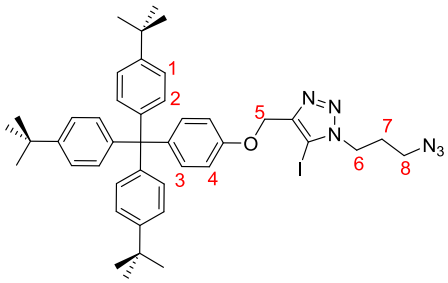
Neutral Bis(methyltelluro-triazole) [2]Rotaxane 2.12Te$_2$H



Identical synthetic procedure used as for rotaxane **2.12I$_2$H**.

Reagents used: Macrocycle **2.1Te** (20 mg, 0.023 mmol), [Cu(CH$_3$CN)$_4$]PF$_6$ (8.6 mg, 0.023 mmol), stopper alkyne **2.11H** (62.4 mg, 0.115 mmol), stopper azide **2.10** (67.6 mg, 0.115 mmol) in degassed dichloromethane (2.3 mL). The target rotaxane was obtained as a white solid (21 mg, 46 %) after purification by preparatory TLC (2.5 % methanol in dichloromethane). **^{1}H-NMR** (500 MHz, CDCl$_3$) δ 8.68 (1H, s, H$_c$), 7.98 (2H, d, ^3J = 9.0 Hz, H$_b$), 7.48 (1H, t, ^3J = 9.0 Hz, H$_a$), 7.22-7.26 (13H, m, H$_2$ + H$_{11}$ + H$_{13}$), 7.08-7.12 (14H, m, H$_1$ + H$_{12}$ + H$_{10}$), 7.03 (2H, d, ^3J = 8.8 Hz, H$_3$), 6.75 (2H, d, ^3J = 8.8 Hz, H$_9$), 6.48 (2H, d, ^3J = 7.0 Hz, H$_4$), 6.43 (8H, m, hydroquinone-Ar*H*), 4.92 (4H, t, ^3J = 7.0 Hz, H$_d$), 4.82 (2H, s, H$_8$), 4.20 (4H, m, H$_e$), 3.81 (4H, m, H$_f$), 3.75 (2H, t, ^3J = 7.2 Hz, H$_7$), 3.60-3.63 (4H, m, H$_g$), 3.54 (4H, s, H$_h$), 3.38 (2H, t, ^3J = 7.2 Hz, H$_5$), 1.87 (6H, s, TeC*H*$_3$), 1.63 (2H, quint., ^3J = 7.2 Hz, H$_6$), 1.31 (54H, s, stopper-^{t}Bu); **^{13}C-NMR** (125 MHz, CDCl$_3$) δ 156.3, 156.2, 153.1, 152.3, 151.9, 148.3, 148.2, 144.3, 144.2, 143.2, 139.7, 139.5, 132.1, 132.0, 131.8, 130.7, 130.6, 128.7, 127.8, 126.9, 124.1, 123.6, 115.4, 115.3, 113.3, 113.0, 101.9, 70.7, 69.5, 67.8, 64.1, 63.0, 61.4, 50.4, 46.8, 34.3, 31.4, 29.4, -12.7; **^{125}Te-NMR** (157 MHz, d_6-acetone) δ 116.5; **MS** (ESI +ve) *m/z* 2016.8497 ([M + H]$^+$, ^{130}Te$_2$C$_{114}$H$_{133}$O$_8$N$_9$, calc. 2016.8474).

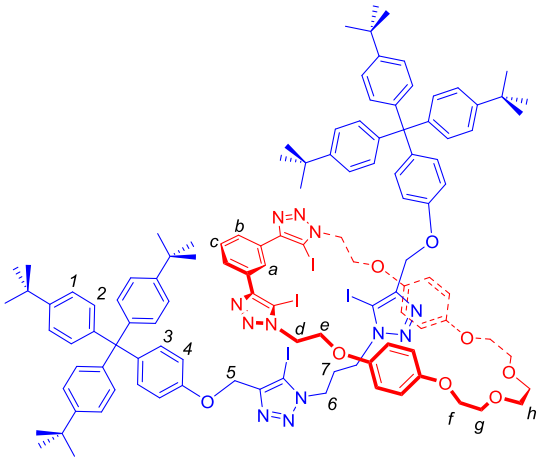
Stoppered iodotriazole azide axle precursor 2.13



Stopper-iodoalkyne **2.11I** (160 mg, 0.24 mmol) was dissolved in degassed THF (2 mL), and 1-tosyl-3-azidopropane[14] (67 mg, 0.264 mmol), TBTA (13 mg, 0.024 mmol), $[Cu(CH_3CN)_4]PF_6$ (27 mg, 0.072 mmol) were added successively. The reaction was stirred overnight for 2 days under N_2 at room temperature. After the reaction was complete, chloroform (10 mL) was added and the organic layer washed with 10 % aqueous ammonia (10 mL) and water (10 mL). Following brine wash (10 mL) and drying with $MgSO_4$, solvent removal afforded the crude product as an off-white solid which was reacted on without further purification. The identity of product was confirmed with mass spectrometry: **MS** (ESI +ve) *m/z* 924.3264 ($[M + H]^+$, $C_{50}H_{59}O_4N_3{}^{127}I$, calc. 924.3271).

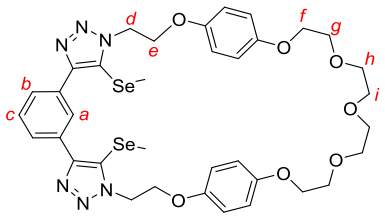
The crude reaction product was dissolved in DMF (3 mL) and sodium azide (23 mg, 0.35 mmol) added before the reaction was left to stir overnight. Following which, the reaction was poured into water (20 mL) and the aqueous suspension extracted with chloroform (3 x 20 mL). The combined organics were dried with brine (20 mL) and $MgSO_4$ and the solvent was removed. Purification by silica gel chromatography (dichloromethane/ hexane 1:1) yielded the target molecule as a white solid (93 mg, 42 % over 2 steps). **^{1}H-NMR** (400 MHz, $CDCl_3$) δ 7.24 (6H, d, ^3J = 8.0 Hz, H_2), 7.08-7.12 (8H, m, H_1 + H_3), 6.91 (2H, d, ^3J = 8.0 Hz, H_4), 5.11 (2H, s, H_5), 4.49 (2H, t, ^3J = 6.4 Hz, H_6), 3.42 (2H, t, ^3J = 6.4 Hz, H_8), 2.20 (2H, quint., ^3J = 6.4 Hz, H_7); **^{13}C-NMR** (100 MHz, $CDCl_3$) δ 156.2, 148.4, 147.6, 144.1, 140.4, 132.3, 130.7. 124.1, 113.5, 63.1, 61.7, 48.1, 47.8, 34.3, 31.4, 29.1; **MS** (ESI +ve) *m/z* 795.3243 ($[M + H]^+$, $C_{43}H_{52}ON_6{}^{127}I$, calc. 795.3242).

Neutral Tetrakis(iodotriazole)-[2]Rotaxane 2.15I$_4$



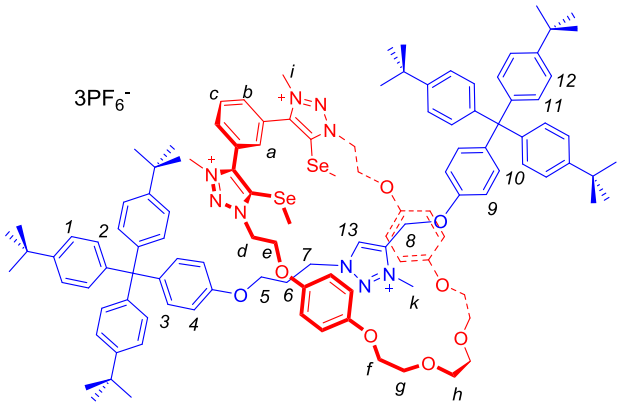
Macrocycle **2.1I** (13.3 mg, 0.016 mmol) was mixed with [Cu(CH$_3$CN)$_4$]PF$_6$ (6.0 mg, 0.016 mmol) in dry degassed dichloromethane (1.6 mL) and stirred for 15 minutes under N$_2$. To the colourless solution was added azide **2.13** (63.7 mg, 0.080 mmol) and stopper iodoalkyne **2.11I** (53.5 mg, 0.080 mmol) portionwise successively, and the reaction stirred under N$_2$ for 48 hours. After which, the reaction was diluted with chloroform (20 mL) and washed with 0.02 M EDTA in 1 M aqueous ammonia (2 x 20 mL), followed by water (3 x 20 mL). The organic layer was dried with MgSO$_4$ (no brine!) and the solvent removed to give a white solid. Purification by preparatory TLC (2.5 % methanol in dichloromethane) afforded the rotaxane as a white solid (9 mg, 24 %). **^{1}H-NMR** (500 MHz, CDCl$_3$) δ 8.45 (1H, s, H$_a$), 7.92 (2H, d, ^3J = 6.0 Hz, *H*$_b$), 7.53 (1H, t, ^3J = 6.0 Hz, H$_c$), 7.22 (12H, m, H$_2$), 7.10 (16H, m, H$_1$ + H$_3$), 6.86 (4H, d, ^3J = 7.2 Hz, *H*$_4$), 6.36-6.43 (8H, m, hydroquinone-Ar*H*), 4.83 (2H, s, H$_5$), 4.79 (4H, t, ^3J = 4.4 Hz, H$_d$), 4.20 (4H, t, ^3J = 4.4 Hz, H$_e$), 3.92 (2H, t, ^3J = 6.0 Hz, H$_f$), 3.72-3.75 (8H, m, H$_g$ + H$_6$), 1.79 (2H, quint., ^3J = 6.0 Hz, H$_6$), 1.30 (27H, s, stopper-^{t}Bu); **^{13}C-NMR** (125 MHz, CDCl$_3$) δ 171.46, 165.2, 156.2, 153.0, 151.7, 149.8, 148.3, 144.1, 140.1, 132.2, 130.7, 129.1, 127.9, 127.1, 124.1, 115.1, 113.5, 81.6, 78.8, 70.8, 69.7, 67.5, 66.8, 63.1, 61.2, 50.2, 47.2, 34.3, 31.4 ; **MS** (ESI +ve) *m/z* 2335.6047 ([M + Na]$^+$, C$_{115}$H$_{128}$O$_8$N$_{12}$^{127}I$_4$Na, calc. 2335.6049).

Neutral Penta-oxo ChB macrocycle 2.18Se



Tetraethylene glycol bis-tosylate (29 mg, 0.057 mmol), synthesised according to reported procedures,[15] and bis-phenol macrocycle precursor **2.4l** (38 mg, 0.057 mmol) were dissolved in anhydrous degassed DMF (7 mL). Cesium carbonate (74 mg, 0.228 mmol) was added and the vigorously-stirred suspension was allowed to stir for 16 hours at 70 ^{o}C under N_2. After which, the DMF was removed *in vacuo* and the resulting solid stirred in a mixture of chloroform (50 mL) and water (50 mL). The aqueous and organic layers were separated and the aqueous layer extracted thoroughly with chloroform (4 x 30 mL). The combined organics were then dried with brine (3 x 20 mL) followed by $MgSO_4$. After solvent removal, the crude reaction mixture was purified by preparatory TLC (2.5 % methanol in dichloromethane) to afford the target macrocycle as a white solid (10 mg, 21 %). **^{1}H-NMR** (400 MHz, $CDCl_3$) δ 8.77 (1H, s, H_a), 8.07 (2H, d, ^{3}J = 7.8 Hz, H_b), 7.57 (1H, t, ^{3}J = 7.8 Hz, H_c), 6.71-6.82 (8H, m, hydroquinone-Ar*H*), 4.95 (4H, t, ^{3}J = 4.9 Hz, H_d), 4.41 (4H, t, ^{3}J = 4.8 Hz, H_e), 4.02 (4H, t, ^{3}J = 4.7 Hz, H_f), 3.79 (4H, t, ^{3}J = 4.7 Hz, H_g), 3.60 (8H, m, H_h + H_i), 2.16 (6H, s, SeCH_3); **^{13}C-NMR** (100 MHz, $CDCl_3$) δ 153.5, 152.3, 149.2, 131.3, 129.1, 127.5, 125.8, 121.5, 115.7, 115.6, 70.9, 70.7, 69.7, 68.1, 67.7, 48.6, 10.1; **MS** (ESI +ve) *m/z* 831.1520 ([M + H]$^{+}$, $^{80}Se_2C_{36}H_{43}O_7N_6$, calc. 831.1518).

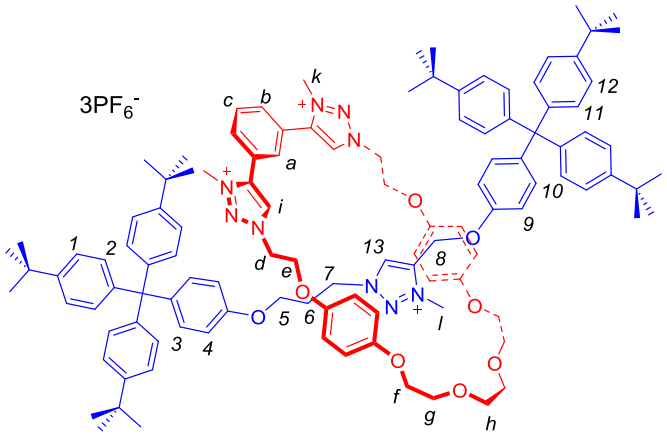
Tricationic Bis(methylseleno-triazolium)-[2]Rotaxane 2.20Se$_2$H



To a solution of neutral rotaxane **2.12Se$_2$H** (28 mg, 0.015 mmol) in dry acetonitrile in was added trimethyloxonium tetrafluoroborate (7.6 mg, 0.051 mmol), and the reaction was heated at 80 ^{o}C in a sealed tube for 2 days. Thereafter, the reaction was monitored daily by TLC (15 % methanol in dichloromethane) and ESI-MS, and 1.0 equivalent of trimethyloxonium tetrafluoroborate (2.2 mg, 0.015 mmol) was added each time till the tricationic rotaxane was the dominant product (after c.a. 14 days). Thereafter, the solvent was removed *in vacuo* and purification by preparatory TLC (10 % methanol in dichloromethane) afforded the clean tricationic rotaxane product. Anion exchange was performed by dissolving the clean rotaxane in chloroform (30 mL), and washing the organic layer successively with 0.1 M NH_4PF_6 (8 x 10 mL) and water (3 x 10 mL). After drying the organic layer with $MgSO_4$, solvent removal afforded the target $3PF_6^-$ -salt of the rotaxane (21 mg, 60 %) as a white solid. **^{1}H-NMR** (400 MHz, CD_3CN) δ 8.67 (1H, s, H_a), 8.02 (1H, t, ^3J = 8.0 Hz, H_c), 7.91 (2H, d, ^3J = 8.0 Hz, H_b), 7.46 (1H, s, H_{13}), 7.30 (12H, m, H_2 + H_{11}), 7.24 (2H, d, ^3J = 8.8 Hz, H_{10}), 7.17 (6H, d, ^3J = 8.5 Hz, H_{12}), 7.03-7.09 (8H, m, H_1 + H_3), 6.87 (2H, d ^3J = 8.8 Hz, H_9), 6.57-6.61 (6H, m, H_4 + hydroquinone-Ar*H*), 6.26 (4H, d, ^3J = 9.2 Hz, hydroquinone-Ar*H*), 5.10 (4H, t, ^3J = 4.5 Hz, H_d), 4.84 (2H, s, H_8), 4.43 (2H, t, ^3J = 7.6 Hz, H_7), 4.32 (4H, t, ^3J = 4.5 Hz, H_e), 4.10 (6H, s, H_i), 3.93 (2H, t, ^3J = 7.6 Hz, H_5), 3.54-3.69 (15H, m, H_f + H_g + H_h + H_k), 2.21 (2H, quint., ^3J = 7.6 Hz, H_6), 2.07 (6H, s, SeCH_3), 1.29 (27H, s, stopper-^{t}Bu), 1.28 (27H, s, stopper-^{t}Bu); **^{13}C-NMR** (100 MHz, CD_3CN) δ 156.6, 155.4, 153.3, 152.2, 149.2, 145.2, 144.9, 142.2, 140.7, 139.3, 134.3, 132.5, 132.3, 132.0, 131.9, 131.6, 130.8, 130.7, 125.2, 125.1, 124.8, 116.2, 114.8, 114.4, 113.9, 71.0, 70.3, 67.8, 67.2, 64.5, 63.7, 63.6, 58.3, 53.5, 51.4, 39.5, 38.4, 34.6, 31.2, 28.5,

10.4; **^{19}F-NMR** (376 Hz, CD_3CN) δ -72.9 (d, $^1J_{F\text{-}P}$ = 707 Hz); **^{31}P-NMR** (142 MHz, CD_3CN) δ -144.7 (sep., $^1J_{P\text{-}F}$ = 707 Hz); **^{77}Se-NMR** (95 MHz, d_6-acetone/D_2O 4:1) δ 105.2; **MS** (ESI +ve) *m/z* 653.6440 ($[M]^{3+}$, $^{80}Se_2C_{117}H_{142}O_8N_9$, calc. 653.6432).

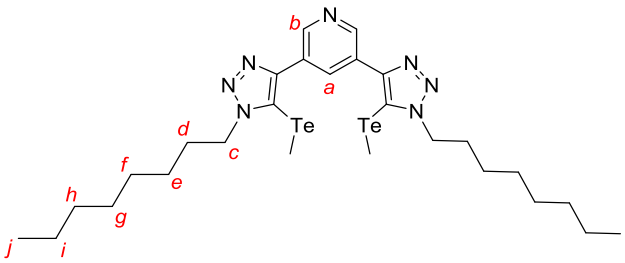
Tricationic Tris(prototriazolium)-[2]Rotaxane 2.20H$_3$



Identical procedure as that for tricationic rotaxane **2.20Se$_2$H**, using neutral rotaxane **2.12H$_3$** (21 mg, 0.012 mmol) in dry acetonitrile (1 mL), with trimethyloxonium tetrafluoroborate (7.2 mg, 0.048 mmol initially, continuous addition till tricationic product was the dominant product). Purification by preparatory TLC (10 % methanol in dichloromethane), and anion exchange by washing with 0.1 M NH_4PF_6 (aq.) afforded **2.20H$_3$** as a white solid (17 mg, 63 %). **^{1}H-NMR** (500 MHz, CD_3CN) δ 8.62 (1H, s, H_a), 8.59 (2H, s, macrocycle triazolium-Ar*H*), 7.81-7.84 (3H, m, H_b + H_c), 7.60 (1H, s, H_{13}), 7.29-7.32 (12H, m, H_2 + H_{11}), 7.24 (2H, d, ^3J = 8.8 Hz, H_{10}), 7.12-7.19 (14H, m, H_1 + H_{12} + H_3), 6.84 (2H, d ^3J = 8.8 Hz, H_9), 6.66 (2H, d, ^3J = 8.4 Hz, H_4), 6.58 (4H, m, ^3J = 9.0 Hz, hydroquinone-Ar*H*), 6.23 (4H, d, ^3J = 9.0 Hz, hydroquinone-Ar*H*), 4.98 (4H, m, H_d), 4.69 (2H, s, H_8), 4.67 (2H, t, ^3J = 7.7 Hz, H_7), 4.30 (4H, t, ^3J = 4.7 Hz, H_e), 4.18 (6H, s, H_k), 3.85 (2H, t, ^3J = 4.7 Hz, H_5), 3.54-3.70 (12H, m, H_f + H_g + H_h), 3.50 (3H, s, H_l), 2.09 (2H, m, H_6), 1.28 (27H, s, stopper-^{t}Bu), 1.27 (27H, s, stopper-^{t}Bu); **^{13}C-NMR** (125 MHz, CD_3CN) δ 156.6, 155.4, 153.2, 152.1, 149.1, 145.1, 144.9, 142.4, 142.2, 140.8, 139.2, 133.5, 132.5, 132.3, 131.6, 131.5, 130.8, 130.7, 129.9, 125.2, 125.1, 124.2, 115.8, 114.7, 113.9, 70.9, 70.2, 67.9, 65.9, 64.4, 63.7, 63.6, 58.3, 54.4, 51.3, 39.2, 38.1, 34.6, 31.1, 28.5; **^{19}F-NMR**

(376 Hz, CD_3CN) δ -72.8 (d, $^1J_{F-P}$ = 707 Hz); **^{31}P-NMR** (142 MHz, CD_3CN) δ -144.7 (sep., $^1J_{P-F}$ = 707 Hz); **MS** (ESI +ve) *m/z* 591.0216 ($[M]^{3+}$, $C_{115}H_{138}O_8N_9$, calc. 591.0217).

Pyridine-3,5-bis(methyltelluro-triazole) 2.21Te

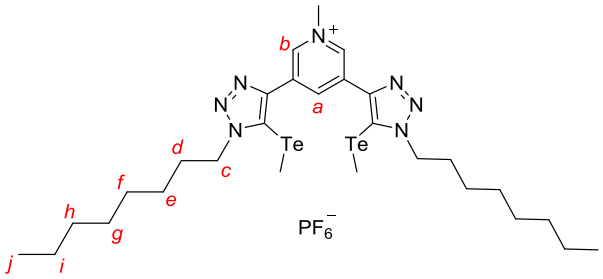


Note: malodorous side products necessitate performing the reaction in the fume cupboard and deodorising all glassware used with bleach.

Powdered Te (130 mg, 1.02 mmol) was suspended in dry degassed THF (just sufficient to submerge the Te) and chilled in an ice bath to 0 ^oC. To the chilled vigorously-stirred suspension was added 1.6 M methyllium solution in diethyl ether (0.64 mL, 1.02 mmol), and the reaction was sonicated and warmed up to ambient temperature before being left to stir at 1 hour in the dark to yield a brown suspension. Separately, the bis-iodotriazole precursor (70.0 mg, 0.102 mmol), synthesised as reported,[16] was suspended in dry THF (1.5 mL) and added portionwise to the brown resulting suspension at ambient temperature, and the reaction vessel was then sealed. The vigorously-stirred reaction was then heated at 80 ^oC in the dark for 4 hours to afford a dark brown suspension. After cooling back to room temperature, iodomethane (0.051 mL, 0.82 mmol) was added to the suspension which was stirred for a further 30 minutes. Subsequently, the reaction was poured into water (20 mL) and the organics were extracted into chloroform (3 x 10 mL). The combined organics were dried with $MgSO_4$ and the solvent was removed *in vacuo* to afford the crude product as a brown malodourous solid. Purification by silica gel column chromatography (ethyl acetate/ hexane 3:2 *v/v*) afforded the target compound as a yellow solid (59 mg, 81 %). **^{1}H-NMR** (500 MHz, $CDCl_3$) δ 9.27 (2H, d, ^4J = 2.2 Hz, H_b), 8.94 (1H, t, ^4J = 2.1 Hz, H_a), 4.61 (4H, t, ^3J = 7.5 Hz, H_c), 2.04 (6H, s, TeCH_3), 1.97 (4H, quint., ^3J = 7.0 Hz, H_d), 1.25 - 1.45 (20H, m, H_{e-i}), 0.89 (6H, t, ^3J =

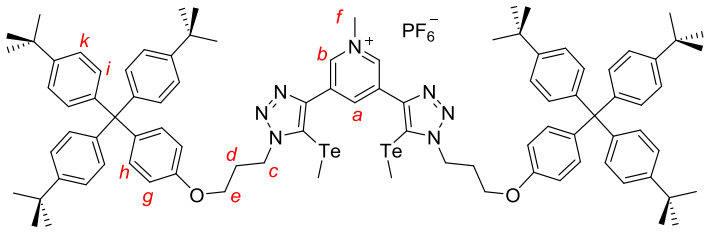
6.8 Hz, H_j); **^{13}C-NMR** (125 MHz, $CDCl_3$) δ 150.7, 148.3, 134.4, 127.4, 99.6, 51.5, 31.7, 31.0, 29.1, 26.6, 22.6, 14.1, -12.9; **^{125}Te-NMR** (158 MHz, $CDCl_3$) δ 88.0 Hz; **MS** (ESI +ve) *m/z* 724.17590 ($[M + H]^+$, $C_{28}H_{44}N_7{}^{130}Te_2$, calc. 724.17464).

Monocationic pyridinium-3,5-bis(methyltelluro-triazole) receptor 2.22Te



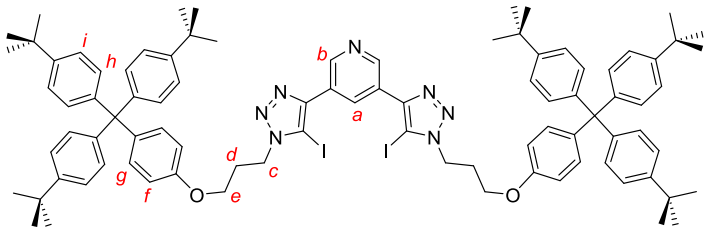
To a solution of compound **2.21Te** (37 mg, 0.051 mmol) in dry dichloromethane (1.0 mL) was added iodomethane (0.032 mL, 0.51 mmol) portionwise and the reaction was stirred overnight at ambient temperature. Removal of solvent *in vacuo* afforded the iodide salt of the product as a yellow solid in excellent purity, and hence no further purification was required. Anion exchange was performed by dissolving the product in chloroform (30 mL), and washing successively with saturated aqueous sodium thiosulfate (5 mL), 0.1 M aqueous NH_4PF_6 (8 x 10 mL) and water (2 x 10 mL). Drying the organic layer with $MgSO_4$ and removal of the solvent afforded the desired product, as its PF_6^- salt, as a pale beige solid (38 mg, 84 %). **^{1}H-NMR** (500 MHz, $CDCl_3$) δ 9.93 (1H, s, H_a), 9.36 (2H, s, H_b), 4.63 (4H, t, ^3J = 7.5 Hz, H_c), 4.59 (3H, s, pyN-CH_3), 2.14 (6H, s, TeCH_3), 1.98 (4H, quint., ^3J = 7.1 Hz, H_d), 1.26 - 1.40 (20H, m, $H_{e\text{-}i}$), 0.89 (6H, t, ^3J = 6.9 Hz, H_j); **^{13}C-NMR** (125 MHz, $CDCl_3$) δ 145.8, 141.2, 139.3, 133.1, 101.7, 51.7, 49.7, 31.7, 30.9, 29.1, 26.5, 22.6, 14.1, -11.6; **^{19}F-NMR** (376 MHz, $CDCl_3$) δ -73.1 (d, $^1J_{F\text{-}P}$ = 714 Hz); **^{31}P-NMR** (162 MHz, $CDCl_3$) δ -144.9 (sep., $^1J_{P\text{-}F}$ = 714 Hz); **^{125}Te-NMR** (158 MHz, $CDCl_3$) δ 91.6 Hz; **MS** (ESI +ve) *m/z* 738.19153 ($[M]^+$, $C_{28}H_{46}N_7{}^{128}Te^{130}Te$, calc. 738.19160).

Cationic Pyridinium-3,5-bis(methyltelluro-triazole) Axle 2.23Te



Neutral axle precursor **2.26Te** (15 mg, 0.0095 mmol) was dissolved in anhydrous dichloromethane (1 mL) and iodomethane (0.1 mL) was added portionwise. The reaction was left to stir overnight under ambient conditions to give clean conversion to the pyridine *N*-methylated product. Removal of solvent was followed by anion exchange by dissolving the product in chloroform (20 mL) and successively washing with 0.1 M NH_4PF_6 (8 x 10 mL) then water (10 mL). The organic layer was dried with $MgSO_4$ and solvent removed to give **2.23Te** (11 mg, 67 %) as a pale beige solid in good purity. **^{1}H-NMR** (400 MHz, $CDCl_3$) δ 9.95 (1H, s, H_a), 9.33 (2H, s, H_b), 7.24 (12H, d, ^3J = 8.6 Hz, H_i), 7.11 (4H, d, ^3J = 9.0 Hz, H_h), 7.08 (12H, d, ^3J = 8.6 Hz, H_k), 6.78 (4H, d, ^3J = 9.0 Hz, H_g), 4.87 (4H, t, ^3J = 7.0 Hz, H_c), 4.57 (3H, s, H_f), 4.06 (4H, t, ^3J = 6.8 Hz, H_e), 2.49 (4H, quint. ^3J = 6.8 Hz, H_d), 2.11 (6H, s, TeCH_3), 1.30 (54H, s, stopper-^{t}Bu); **^{13}C-NMR** (100 MHz, $CDCl_3$) δ 156.1, 148.4, 145.8, 144.0, 141.2, 140.2, 133.3, 132.4, 130.7, 124.1, 113.0, 102.3, 64.0, 63.1, 49.7, 48.8, 34.3, 31.4, 29.7, -11.5; **^{19}F-NMR** (376 MHz, $CDCl_3$) δ -73.1 ($^1J_{F\text{-}P}$ = 716 Hz); **^{31}P-NMR** (162 MHz, $CDCl_3$) δ -144.8 ($^1J_{P\text{-}F}$ = 716 Hz); **MS** (ESI +ve) *m/z* 1604.6803 ([M]$^+$, $C_{92}H_{110}O_2N_7{}^{130}Te_2$, calc. 1604.6840).

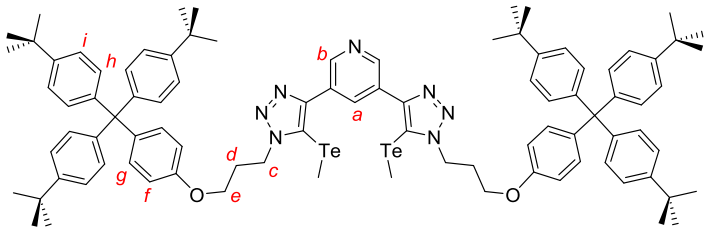
Neutral Pyridine-3,5-bis(iodotriazole) Axle Precursor 2.26I



To a acetonitrile/THF 1:1 mixture (2 mL) was added sodium iodide (99.0 mg, 0.660 mmol) followed by copper(II) perchlorate hexahydrate (122 mg, 0.330 mmol). After stirring for 5 minutes, stopper azide **2.10** (97.0 mg, 0.165 mmol), DBU (24 mg, 0.16 mmol), TBTA (4.2 mg, 0.0079 mmol) and 3,5-di(ethynyl)pyridine[17] (10 mg, 0.079 mmol) were added portionwise. The

reaction was left to stir under N_2 for 2 days, whereupon a yellow slurry was observed. The solvent was removed and the crude mixture suspended in chloroform (50 mL). The organic layer was washed sequentially with basic EDTA solution (3 x 20 mL), water (20 mL) and brine (20 mL), then dried with $MgSO_4$. Purification with column chromatography (2 % methanol in dichloromethane) afforded the target compound as a white solid (97 mg, 80 %). **^{1}H-NMR** (400 MHz, $CDCl_3$) δ 9.25 (2H, s, H_b), 8.85 (1H, s, H_a), 7.24 (12H, d, ^3J = 8.4 Hz, H_h), 7.07-7.12 (16H, m, H_i + H_g), 6.79 (4H, d, ^3J = 8.8 Hz, H_f), 4.70 (4H, t, ^3J = 6.8 Hz, H_c), 4.07 (4H, t, ^3J = 5.6 Hz, H_e), 2.48 (4H, quint. ^3J = 6.0 Hz, H_d), 1.30 (54H, s, stopper-^{t}Bu); **^{13}C-NMR** (100 MHz, $CDCl_3$) δ 156.3, 148.3, 148.1, 147.1, 144.2, 140.2, 132.4, 130.8, 126.4, 124.2, 113.2,64.0, 63.2, 48.4, 34.3, 31.4, 29.8; **MS** (ESI +ve) *m/z* 1554.6198 ($[M + H]^+$, $C_{89}H_{102}O_2N_7{}^{127}I_2$, calc. 1554.6184).

Neutral Pyridine-3,5-bis(methyltelluro-triazole) Axle Precursor 2.26Te

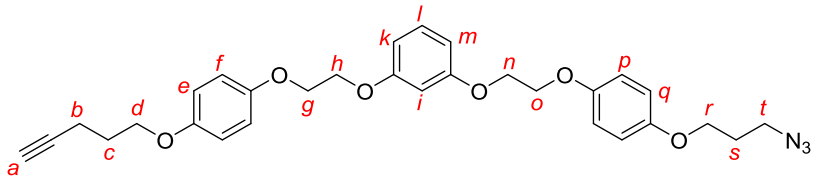


Note: malodorous side products necessitate performing the reaction in the fume cupboard and deodorising all glassware used with bleach.

Powdered Te (34 mg, 0.26 mmol) was suspended in dry degassed THF (just sufficient to submerge the Te) in a sealed microwave vial and chilled in an ice bath to 0 ^{o}C. To the chilled vigorously-stirred suspension was added 1.6 M methyllium solution in diethyl ether (0.17 mL, 0.26 mmol), and the reaction was sonicated and warmed up to ambient temperature before being left to stir at 1 hour in the dark to yield a brown suspension. Separately, compound **2.26I** (69 mg, 0.044 mmol) was dissolved in dry THF (1 mL) and added to the vigorously-stirred reaction, which was then heated at 60 ^{o}C for 16 hours. After cooling down to ambient temperature, iodomethane (11 µL, 0.18 mmol) was added and the reaction left to stir for 30 minutes before being poured into water (20 mL). Chloroform (20 mL) was added and the

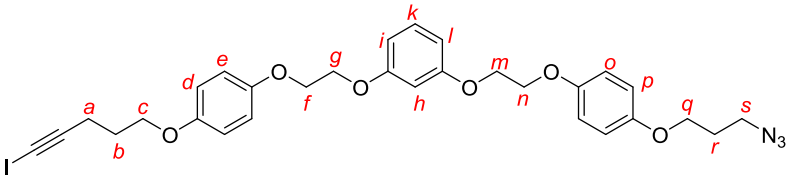
organic layer was separated from the aqueous layer. After back-extracting the aqueous layer with chloroform (2 x 10 mL), the combined organics were dried with brine and $MgSO_4$. Solvent removal, followed by column chromatography (4 % methanol in dichloromethane) afforded the target compound as a yellow solid (48 mg, 68 %). **^{1}H-NMR** (400 MHz, $CDCl_3$) δ 9.27 (2H, s, H_b), 8.94 (1H, s, H_a), 7.24 (12H, d, ^3J = 8.7 Hz, H_h), 7.07-7.11 (16H, m, H_i + H_g), 6.78 (4H, d, ^3J = 8.9 Hz, H_f), 4.84 (4H, t, ^3J = 7.0 Hz, H_c), 4.05 (4H, t, ^3J = 5.7 Hz, H_e), 2.49 (4H, quint. ^3J = 6.0 Hz, H_d), 1.96 (6H, s, TeCH_3), 1.30 (54H, s, stopper-^{t}Bu); **MS** (ESI +ve) *m/z* 1590.6709 ([M + H]$^+$, $C_{91}H_{108}O_2N_7{}^{130}Te_2$, calc. 1590.6684).

Protoalkyne-Azide Catenane Thread Precursor 2.27H



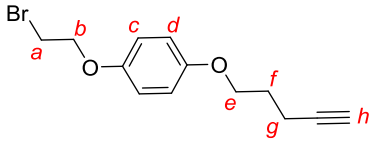
Compound **2.33** (92 mg, 0.29 mmol) was added to thoroughly-degassed acetonitrile (10 ml) under N_2, followed sequentially by potassium carbonate (122 mg, 0.88 mmol), potassium iodide (48 mg, 0.29 mmol) and compound **2.32** (88 mg, 0.29 mmol) before heating under reflux for 16 hours under N_2. The solvent was removed *in vacuo* and the residue partitioned between chloroform and water. After separating the layers, the aqueous phase was extracted with chloroform (3 x 30 mL). The organic layers were then combined, washed with water (20 mL) and brine (20 mL), dried with $MgSO_4$ and the solvent removed *in vacuo*. The crude mixture was suspended in chloroform and filtered through a silica plug. Removal of the solvent *in vacuo* yielded the product as a white solid (81 mg, 53 %). **^{1}H-NMR** (400 MHz, $CDCl_3$) δ 7.19 (1H, t, ^3J = 8.7 Hz, H_l), 6.95 – 6.79 (8H, m, 8H, H_e + H_f + H_p + H_q), 6.57 (3H, m, H_K + H_i + H_m), 4.27 (8H, m, H_g + H_h + H_n + H_o), 4.01 (4H, quart, ^3J = 6.4 Hz, H_d + H_r), 3.51 (2H, t, ^3J = 6.7 Hz, H_t), 2.40 (2H, m, H_b), 2.09 – 1.91 (5H, m, H_a + H_c + H_s); **^{13}C-NMR** (100 MHz, d_6-acetone) δ 161.3, 154.5, 154.2, 131.0, 116.6, 116.4, 108.1, 102.5, 70.4, 68.2, 67.8, 67.6, 66.2, 49.1, 34.2, 15.7; **MS** (ESI/ EI/ FI +ve) *not observed*.

Iodoalkyne-Azide XB Catenane Thread 2.27I



To a solution of **2.27H** (73 mg, 0.14 mmol) in acetone (5 ml) was added *N*-iodosuccinimide (33.9 mg, 0.15 mmol) and silver nitrate (2.32 mg, 0.014 mmol). The reaction was stirred in the dark for 3 days, before removal of the solvent *in vacuo*. The crude was then stirred in a mixture of chloroform (30 mL) and water (10 mL), before separation of the layers and extraction of the aqueous with further chloroform (3 x 10 mL). The combined organics were washed with water (10 mL) and brine (10 mL), then dried with Na_2SO_4 and the solvent removed *in vacuo*. The resulting solid (92 mg, quantitative) was used without further purification. **^{1}H-NMR** (400 MHz, $CDCl_3$) δ 7.63 (1H, d, ^3J = 8.5 Hz, H_h), 6.96 – 6.80 (9H, m, 9H, $H_d + H_e + H_i/H_l + H_o + H_p$), 6.56 (1H, s, H_k), 6.39 (1H, d, ^3J = 8.5 Hz, H_i/H_l), 4.37 – 4.24 (8H, m, $H_f + H_g + H_m + H_n$), 4.01 (4H, m, $H_c + H_q$), 3.51 (2H, t, ^3J = 6.5 Hz, H_s), 2.40 (2H, d, ^3J = 7.0, H_a), 2.09 – 1.92 (4H, m, $H_b + H_r$); **^{13}C-NMR** (100 MHz, d_6-acetone) δ 160.4, 158.3, 153.6, 153.4, 153.1, 153.0, 152.9, 152.8, 139.4, 116.3, 116.2, 116.0, 115.9, 115.6, 115.6, 108.6, 107.5, 101.7, 83.7, 83.7, 76.2, 69.0, 68.2, 67.4, 67.3, 67.1, 66.9, 65.3, 48.4, 29.0, 28.4, 15.3; **MS** (ESI/ EI/ FI +ve) *not observed*.

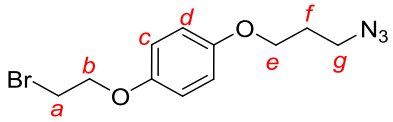
1-(2-bromoethoxy)-4-(pent-4-yn-1-yloxy)benzene 2.31



Compound **2.5** (651 mg, 3.0 mmol) was dissolved in dry degassed acetonitrile (20 ml) under N_2, followed by the addition of pent-4-yn-1-yl tosylate **2.30** (786 mg, 3.3 mmol) and potassium carbonate (1.66 g, 12.0 mmol) before heating under reflux for 16 hours under N_2. After solvent removal *in vacuo*, the crude mixture was suspended in chloroform (30 mL) and washed sequentially with water (2 x 20 mL) and brine (10 mL) then dried with $MgSO_4$. Solvent removal was followed by silica gel column chromatography (5 % ethyl acetate in hexane) to afford the

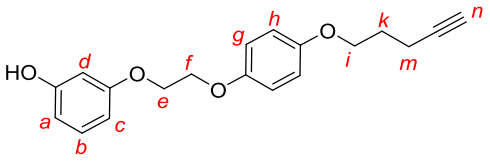
product as a white solid (359 mg, 42 %). **^{1}H-NMR** (400 MHz, $CDCl_3$) δ 6.91 – 6.80 (4H, m, H_c + H_d), 4.24 (2H, t, ^{3}J = 6.5 Hz, H_b), 4.02 (2H, t, ^{3}J = 6.0 Hz, H_e), 3.61 (2H, t, ^{3}J = 6.5 Hz, H_a), 2.40 (2H, t, ^{3}J = 7.0, H_f), 2.04 – 1.92 (3H, m, H_f + H_h); **^{13}C-NMR** (100 MHz, d_6-acetone) δ 153.8, 152.4, 116.2, 115.7, 83.7, 69.0, 68.9, 66.9, 29.5, 28.4, 15.3; **MS** (Ammonia CI +ve) *m/z* 300.0598 ($[M + NH_4]^+$, $C_{13}H_{19}O_2N^{79}Br$, calc. 300.0594).

1-(3-azidopropoxy)-4-(2-bromoethoxy)benzene 2.32



Compound **2.5** (435 mg, 2.0 mmol) was dissolved in dry degassed acetonitrile (13 ml) under N_2, followed by the addition of 3-azidoproyl-tosylate **2.14** (563 mg, 2.2 mmol) and potassium carbonate (1.11 g, 8.0 mmol) before heating under reflux for 16 hours under N_2. After solvent removal *in vacuo*, the crude mixture was suspended in chloroform (30 mL) and washed sequentially with water (2 x 20 mL) and brine (10 mL) then dried with $MgSO_4$. Solvent removal was followed by silica gel column chromatography (5 % ethyl acetate in hexane) to afford the product as a white solid (313 mg, 52 %). **^{1}H-NMR** (400 MHz, $CDCl_3$) δ 6.90 – 6.79 (4H, m, H_c + H_d), 4.24 (2H, t, ^{3}J = 6.5 Hz, H_b), 4.00 (2H, t, ^{3}J = 6.0 Hz, H_e), 3.61 (2H, t, ^{3}J = 6.5 Hz, H_a), 3.51 (2H, t, ^{3}J = 6.5 Hz, H_g), 2.03 (2H, t, ^{3}J = 6.5 Hz, H_f). **^{13}C-NMR** (100 MHz, $CDCl_3$) δ 153.6, 152.5, 116.2, 115.6, 68.9, 65.3, 48.4, 29.5, 29.0. **MS** (Ammonia CI +ve) *m/z* 317.0608 ($[M + NH_4]^+$, $C_{11}H_{18}O_2N_4{}^{79}Br$, calc. 317.0608).

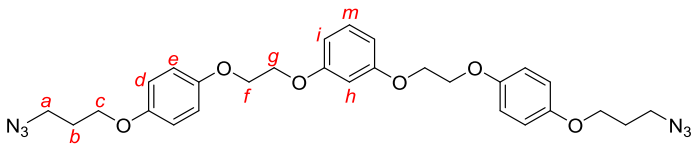
3-(2-(4-(pent-4-yn-1-yloxy)phenoxy)ethoxy)phenol 2.33



To a round bottomed flask containing degassed acetone (35 ml) under N_2 was added sequentially resorcinol (123 mg, 1.12 mmol), potassium carbonate (465 mg, 3.36 mmol) and

potassium iodide (9.3 mg, 0.060 mmol). To the resulting suspension was added compound **2.31** (350 mg, 1.24 mmol) before heating under reflux for 2 days under N_2. The solvent was removed *in vacuo* and the crude product partitioned between dichloromethane and saturated aqueous NH_4Cl. The layers were separated, and the aqueous extracted with dichloromethane (3 x 20 mL), before the combined organics were washed with water (20 mL) and brine (20 mL). The organic layer was then dried with MgSO4 and the solvent removed *in vacuo*. The crude was purified by silica gel column chromatography (20 % ethyl acetate in hexane) yielding a white solid (118 mg, 34 %). **^{1}H-NMR** (400 MHz, $CDCl_3$) δ 7.13 (1H, t, ^3J = 8.0 Hz, Hb), 6.87 (4H, m, H_g + H_h), 6.61 – 6.40 (3H, m, H_a + H_c + H_d), 4.86 (1H, br. s, O*H*), 4.27 (4H, m, H_e + H_f), 4.02 (2H, t, ^3J = 6.0 Hz, Hi), 2.40 (2H, t, ^3J = 7.0 Hz, Hm), 2.04 – 1.92 (3H, m, H_k + H_n); **^{13}C-NMR** (100 MHz, $CDCl_3$) δ 160.2, 156.8, 153.6, 153.0, 130.3, 116.0, 115.6, 108.3, 107.2, 102.5, 83.7, 69.0, 67.4, 67.0, 66.8, 28.4, 15.3; **MS** (ESI +ve) *m/z* 313.1431 ($[M + H]^+$, $C_{19}H_{21}O_4$, calc. 313.1434).

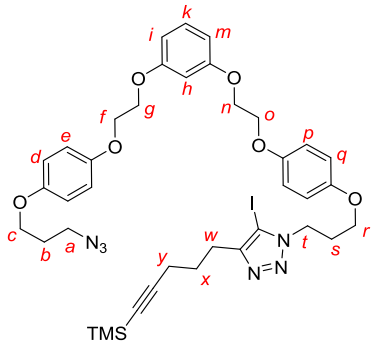
Bis-azide Catenane Precursor 2.34



Resorcinol (61 mg, 0.56 mmol), compound **2.32** (350 mg, 1.17 mmol), sodium iodide (175 mg, 1.17 mmol) and potassium carbonate (384 mg, 2.78 mmol) were mixed together and thoroughly degassed, before dry degassed acetonitrile (6 mL) was added and the mixture heated under reflux for 2 days. The solvent was then removed *in vacuo* and the resulting solids partitioned between chloroform (30 mL) and water (20 mL). The organic layer was separated and washed successively with saturated aqueous sodium bicarbonate (20 mL), water (20 mL), before drying with brine (20 mL) and $MgSO_4$. Following solvent removal, silica gel column chromatography (4 % ethyl acetate in dichloromethane) yielded the product as a white solid (219 mg, 72 %). **^{1}H-NMR** (400 MHz, $CDCl_3$) δ 7.21 (1H, t, ^3J = 8.5 Hz, H_m), 6.83-6.92 (8H, m, H_d + H_e), 6.58-6.60 (3H, m, H_i + H_h), 4.28 (8H, br. s, H_f + H_g), 4.01 (4H, t, ^3J = 6.0

Hz, H_c), 3.52 (4H, t, ^3J = 6.7 Hz, H_a), 2.04 (4H, quint., ^3J = 6.2 Hz); **^{13}C-NMR** (100 MHz, $CDCl_3$) δ 160.0, 156.7, 153.2, 130.2, 115.8, 115.5, 108.1, 102.3, 67.2, 66.6, 65.1, 48.3, 28.9. **MS** (ESI/ EI/ FI +ve) *not observed*.

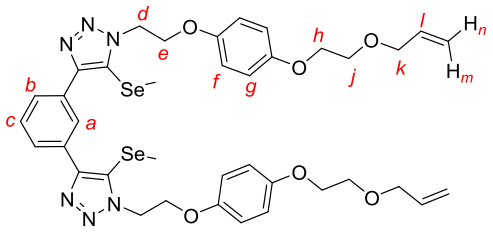
TMS-protected Catenane Thread 2.36



Sodium iodide (291 mg, 1.94 mmol) was stirred in a THF/ acetonitrile 1:1 mixture (3 mL) before copper(II) perchlorate hexahydrate (360 mg, 0.972 mmol) was added portionwise. After stirring for 5 minutes, compound **2.34** (147 mg, 0.267 mmol) was added, followed by DBU (37 mg, 0.24 mmol), TBTA (6.4 mg, 0.012 mmol) and mono-TMS protected 1,6-heptadiyne **2.35**[18] (40 mg, 0.243 mmol) sequentially. The reaction was stirred overnight before being quenched with basic EDTA (10 mL). Chloroform (20 mL) was added to the mixture and the aqueous and organic layers separated. The organic layer was washed further with basic EDTA (10 mL), water (20 mL) and brine (20 mL), then dried with $MgSO_4$ before the solvent was removed on the rotary. Purification of the dried crude product by column chromatography (2 % methanol in dichloromethane, followed by a second column using 5 % ethyl acetate in dichloromethane) afforded the product as a white solid (15 mg, 7 %). **^{1}H-NMR** (400 MHz, $CDCl_3$) δ 7.20 (1H, t, ^3J = 8.5 Hz, H_k), 6.83-6.91 (8H, m, H_d + H_e), 6.57-6.59 (3H, m, H_h + H_i + H_m), 4.57 (2H, t, ^3J = 6.9 Hz, H_t), 4.28 (8H, br. s, H_f + H_g), 4.01 (2H, t, ^3J = 5.9 Hz, H_c), 3.96 (2H, t, ^3J = 5.8 Hz, H_r), 3.52 (2H, t, ^3J = 6.7 Hz, H_a), 2.77 (2H, t, ^3J = 7.6 Hz, H_w), 2.39 (2H, quint., ^3J = 6.2 Hz, H_s), 2.31 (2H, t, ^3J = 7.0 Hz, H_y), 2.04 (2H, quint., ^3J = 6.2 Hz, H_b), 1.93 (2H, quint., ^3J = 7.5 Hz, H_x), 0.17 (9H, s, TMS); **^{13}C-NMR** (100 MHz, $CDCl_3$) δ 159.9, 153.2, 153.0, 152.9, 151.0, 129.9, 115.8,

115.4, 107.3, 106.6, 102.0, 85.2, 78.6, 67.2, 66.6, 65.1, 64.7, 48.3, 47.6, 29.7, 28.9, 27.8, 25.1, 19.4, 0.2; **MS** (ESI +ve) *m/z* 839.2440 ($[M + H]^+$, $C_{38}H_{48}O_6N_6{}^{127}I^{28}Si$, calc. 839.2444).

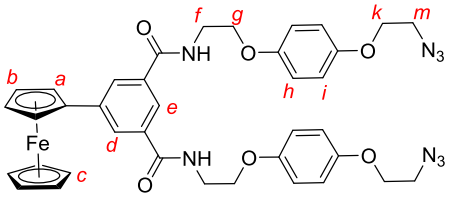
Bis-vinyl ChB catenane precursor 2.37Se



Compound **2.4Se** (40 mg, 0.060 mmol) was mixed with cesium carbonate (78 mg, 0.24 mmol) and allylethoxy tosylate **2.38**[19] (38 mg, 0.15 mmol) and suspended in dry degassed DMF (3 mL). The reaction was heated to 65 ^oC and left to react overnight under N_2. After azeotropic removal of DMF on a rotary with toluene, the crude product was partitioned between water (10 mL) and chloroform (20 mL). The separated organic layer was washed with water (10 mL) then brine (10 mL) and dried with $MgSO_4$. Silica gel column chromatography (4 % methanol in dichloromethane) isolated the product as a pale beige solid (34 mg, 68 %). **^{1}H-NMR** (400 MHz, $CDCl_3$) δ 8.89 (1H, s, H_a), 8.14 (2H, d, ^3J = 7.7 Hz, H_b), 7.57 (1H, t, ^3J = 7.8 Hz, H_c), 6.77-6.85 (8H, m, H_f + H_g), 5.90-5.97 (2H, m, H_l), 5.30 (2H, d, ^3J = 17.2 Hz, H_m), 5.20 (2H, d, ^3J = 10.2 Hz, H_n), 4.93 (4H, t, ^3J = 5.5 Hz, H_d), 4.44 (4H, t, ^3J = 5.55 Hz, H_e), 4.06-4.09 (8H, m, H_h + H_k), 3.77 (4H, t, ^3J = 4.8 Hz, H_j), 2.20 (6H, s, SeCH_3); **^{13}C-NMR** (100 MHz, $CDCl_3$) δ 153.6, 152.3, 149.2, 134.5, 131.3, 128.9, 127.2, 125.9, 120.8, 117.3, 115.7, 115.6, 72.3, 68.6, 68.0, 67.4, 48.4, 10.1; **MS** (ESI +ve) *m/z* 841.1731 ($[M + H]^+$, $C_{38}H_{45}O_6N_6{}^{80}Se_2$, calc. 841.1726).

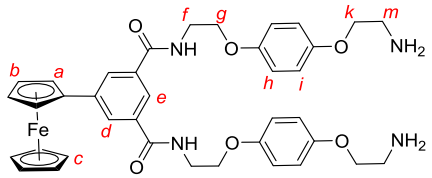
7.2.3 Synthesis of Novel Compounds from Chapter 3

Ferrocene-appended bis-azide macrocycle precursor 3.4



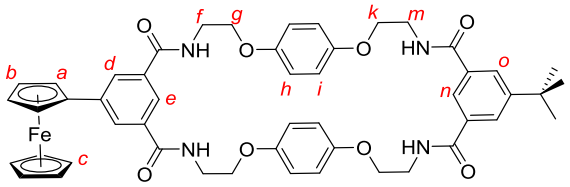
To a vigorously stirred suspension of 5-ferrocenyl isophthalic acid **3.2** (630 mg, 1.80 mmol), synthesised as reported,[20] in dry dichloromethane (5 mL) containing catalytic quantities of DMF was added oxalyl chloride dropwise (0.46 mL, 5.40 mmol) under N_2. The reaction was stirred for 2 hours to obtain a clear red solution, which was evaporated to dryness *in vacuo* to yield the acid chloride as a dark red solid, which was then re-dissolved in dry dichloromethane (2 mL). This solution was added dropwise to a colourless solution of amine **3.3**[21] (0.800 g, 3.60 mmol) in dry dichloromethane (50 mL) containing anhydrous triethylamine (1.50 mL, 10.8 mmol) and catalytic quantities of DMAP at 0 ^{o}C. The reaction was allowed to warm up to room temperature and stirred overnight. After which, the reaction mixture was washed successively with 10 % HCl (20 mL) and water (2 x 20 mL). The combined organics were dried with $MgSO_4$ and the solvent removed *in vacuo* to form a sticky red-orange liquid. Silica gel column chromatography (ethyl acetate/ petroleum ether 3:2) gave compound **3.4** as an orange solid (602 mg, 45 %). **^{1}H NMR** (400 MHz, $CDCl_3$) δ 8.09 (2H, d, ^{4}J =1.6 Hz, H_d), 7.91 (1H, t, ^{4}J =1.6 Hz, H_e), 6.88 (8H, m, H_h + H_i), 6.70 (2H, br. t, ^{3}J = 5.2 Hz, CON*H*), 4.73 (2H, t, ^{3}J = 1.6 Hz, H_a), 4.40 (2H, t, ^{3}J = 1.6 Hz, H_b), 4.16 (4H, t, ^{3}J = 4.8 Hz, H_k), 4.11 (4H, t, ^{3}J = 5.2 Hz, H_g), 4.05 (5H, s, H_c), 3.90 (4H, quart., ^{3}J = 5.2 Hz, H_f), 3.57 (4H, t, ^{3}J = 4.8 Hz, H_m); **^{13}C NMR** (100 MHz, $CDCl_3$) δ 167.0, 153.1, 152.8, 141.5, 134.9, 127.5, 122.2, 115.8, 115.6, 83.3, 69.9, 69.9, 67.7, 67.3, 66.9, 50.2, 39.8 ; **MS** (ESI +ve) *m/z* 781.2137 ($[M + Na]^+$, $C_{38}H_{38}{}^{56}FeNaN_8O_6$, calc. 781.2157).

Ferrocene-appended bis-amine macrocycle precursor 3.5



Compound **3.4** (610 mg, 0.804 mmol) was dissolved in a minimum amount of methanol (c.a. 30 ml), and 10 % by weight Pd/C (150 mg) was added portionwise to the orange solution. To the vigorously stirred suspension was added hydrazine monohydrate (0.13 mL, 4.02 mmol) and the reaction heated under reflux for 7 hours. After cooling to ambient temperature, the reaction was filtered through celite, and the resulting orange solution was dried *in vacuo* to obtain **6** as an orange solid in quantitative yield. **^{1}H NMR** (400 MHz, $CDCl_3$) δ 8.01 (2H, s, H_d), 7.91 (1H, s, H_e), 6.86 (8H, m, H_h + H_i), 6.77 (2H, t, ^{3}J = 5.6 Hz, CON*H*), 4.73 (2H, s, H_a), 4.39 (2H, s, H_b), 4.15 (4H, t, ^{3}J = 4.8 Hz, H_g), 4.04 (5H, s, H_c), 3.94 (4H, t, ^{3}J = 4.8 Hz, H_k), 3.89 (4H, quart., ^{3}J = 4.8 Hz, H_f), 3.06 (4H, t, ^{3}J = 4.8 Hz, H_m); **^{13}C NMR** (100 MHz, $CDCl_3$) δ 167.0, 153.5, 152.7, 141.4, 134.9, 127.4, 122.2, 115.5, 115.4, 83.0, 70.7, 69.7, 69.6, 67.3, 66.7, 41.6, 39.8; **MS** (ESI +ve) *m/z* 707.2528 ($[M + H]^+$, $C_{38}H_{43}{}^{56}FeN_4O_6$, calc. 707.2527).

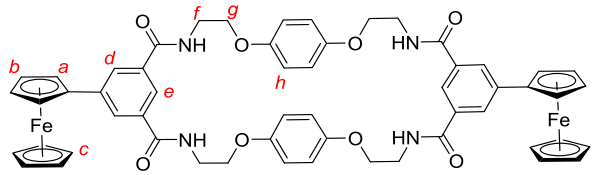
Ferrocene-appended 5-^{t}Bu-isophthalamide macrocycle 3.6Bu



To a suspension of commercially-available 5-*tert*-butyl isophthalic acid (65.2 mg, 0.293 mmol) in dry dichloromethane (5 mL) was added oxalyl chloride (0.075 mL, 0.88 mmol) and catalytic quantities of DMF and the mixture was stirred under N_2 for 3 hours to obtain a clear solution. Removal of solvent *in vacuo* gave the corresponding bis-acid chloride as a yellow solid, which was then re-dissolved in dry dichloromethane (8 mL) and taken up in a syringe. Separately, bis-amine **3.5** was dissolved in dry dichloromethane (8mL) and taken up in another syringe. The contents of both syringes were added to a vigorously stirred solution of dry triethylamine (0.25 mL, 1.8 mmol) in dry dichloromethane (400 mL) over 4 hours using a syringe pump, and

the resulting solution was stirred overnight under N_2. The clear orange reaction mixture was concentrated till a volume of c.a. 50 mL before being washed with 1M HCl (20 mL), followed by water (2 x 20 mL). After drying with $MgSO_4$, the solvent was removed to yield a red-brown solid which was purified with silica gel chromatography (gradient from pure dichloromethane to 2 % methanol in dichloromethane) to give macrocycle **3.6Bu** as an orange solid (53 mg, 20 %).**^{1}H-NMR** (400 MHz, $CDCl_3$/ CD_3OD 1:1) δ 8.08 (2H, s, H_d), 8.04 (2H, s, H_o), 8.00 (2H, m, H_e + H_n), 6.79 (8H, s, H_h + H_i), 4.73 (2H, s, H_a), 4.34 (2H, s, H_b), 4.05 - 4.10 (8H, m, H_g + H_k), 3.98 (5H, s, H_c), 3.76 – 3.80 (8H, m, H_f + H_m), 1.33 (9H, s, ^{t}Bu-*H*); **^{13}C-NMR** (100 MHz, 1:1 $CDCl_3$/ CD_3OD) δ 168.4, 168.1, 153.0, 152.5, 141.4, 134.3, 133.9, 127.9, 127.8, 122.2, 122.1, 155.4, 83.0, 69.5, 67.1, 66.5, 39.7, 39.6, 34.9, 30.7 ; **MS** (ESI +ve) *m/z* 915.3034 ([M + Na]$^+$, $C_{50}H_{52}{}^{56}FeN_4O_8Na$, calc. 915.3028).

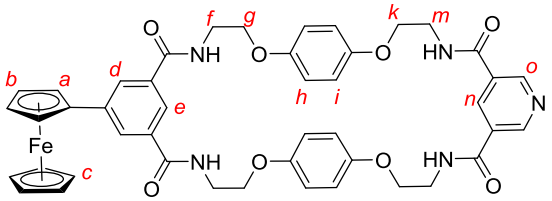
Bis-ferrocene-appended bis-isophthalamide macrocycle 3.6Fc



5-ferrocene isophthalic acid **3.2** (99.1 mg, 0.283 mmol) was suspended in dry dichloromethane (5 mL) containing catalytic quantities of DMF and cooled to 0 ^{o}C. Oxalyl chloride (0.073 mL, 0.85 mmol) was added dropwise and the reaction was stirred for 2 h under N_2 till a clear red solution was obtained. The solvent was then removed *in vacuo* to yield the bis-acid chloride as a red-brown solid, which was then redissolved in dry dichloromethane (6 mL) and loaded into a syringe. Bis-amine **3.5** (200 mg, 0.283 mmol) was dissolved in dry dichloromethane (6 mL) containing triethylamine (0.24 mL, 1.70 mmol) and loaded into another syringe. The contents of both syringes were added to vigorously-stirred dry dichloromethane (450 mL) dropwise using a syringe pump over 3 h, and stirred overnight under N_2. The reaction mixture was then concentrated to approximately 50 mL, and washed with 10 % HCl (20 mL), followed by water (3 x 20 mL). The combined organics were dried with $MgSO_4$ and dried *in vacuo* to give an orange-brown solid. Purification via silica gel column chromatography (gradient from 1 % to 3

% methanol in dichloromethane) yielded macrocycle **3.6Fc** as an orange solid (64 mg, 22 %). **^{1}H-NMR** (400 MHz, 1:1 $CDCl_3$/ CD_3OD) δ 8.10 (4H, s, H_d), 7.98 (2H, s, H_e), 6.83 (8H, s, H_h), 4.77 (4H, s, H_a), 4.36 (4H, s, H_b), 4.09 (8H, t, ^{3}J = 4.7 Hz, H_g), 4.00 (10H, s, H_c), 3.80 (8H, t, ^{3}J = 5.0 Hz, H_f); **^{13}C-NMR** (100 MHz, 1:1 $CDCl_3$/ CD_3OD) δ 167.6, 152.7, 141.2, 134.1, 127.7, 121.5, 115.2, 82.7, 69.4, 66.9, 66.4, 49.0, 39.5; **MS** (ESI +ve) *m/z* 1043.2380 ($[M + Na]^+$, $C_{56}H_{52}{}^{56}Fe_2N_4NaO_8$, calc. 1043.2379).

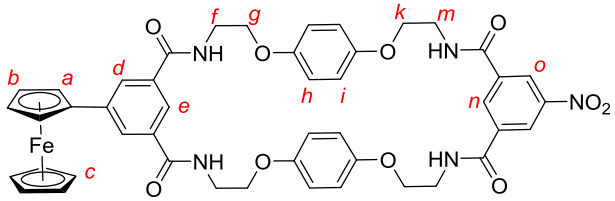
Ferrocene-appended pyridine isophthalamide macrocycle 3.6Py



Commercially-available 3,5-pyridine dicarboxylic acid (28.0 mg, 0.167 mmol) was suspended in dry dichloromethane (2 mL) at 0 °C . To this white suspension was added a drop of dry DMF followed by oxalyl chloride dropwise (0.043 mL, 0.50 mmol), and the reaction was allowed to stir for 2 hours under N_2 until a clear pale yellow solution was obtained. After removing the solvent *in vacuo*, the resulting off-white solid was redissolved in 6.0 mL of dry dichloromethane and taken up in a syringe. Separately, the ferrocene-functionalised bisamine macrocycle precursor **3.5** (117 mg, 0.164 mmol) and anhydrous triethylamine (0.14 mL, 1.0 mmol) was dissolved in 6 mL of dry dichloromethane, and the resulting red solution was taken up in another syringe. The contents of both syringes were added dropwise over 4 hours to vigorously-stirred dry dichloromethane (300 mL) and the reaction was left overnight under N_2. After removal of solvent on a rotary till approximately 50 mL, the crude reaction was washed with 10 % citric acid (2 x 30 mL) then water (2 x 30 mL). The organic layer was dried with $MgSO_4$ and dried *in vacuo* to obtain an orange solid. Silica gel column chromatography (gradient from 2 % to 5 % methanol in dichloromethane) yielded the macrocycle **3.6Py** as an orange powder (34 mg, 25 %). **^{1}H-NMR** (400 MHz, d_6-DMSO) δ 9.09 (2H, s, H_o), 8.98 (2H, t, ^{3}J = 4.0 Hz, PyArCON*H*), 8.79 (2H, t, ^{3}J = 4.0 Hz, FcArCON*H*), 8.58 (1H, s, Ar*H* H_n), 8.11 (1H, s,

H_e), 8.09 (2H, s, H_d), 6.88 (8H, m, H_h + H_i), 4.91 (2H, s, H_a), 4.44 (2H, s, H_b), 4.06 (8H, t, ^3J = 6.4 Hz, H_g + H_k), 4.04 (5H, s, H_c), 3.63 (8H, m, H_f + H_m) ; **^{13}C-NMR** (125 MHz, d_6-DMSO) δ 166.7, 165.2, 153.1, 153.0, 152.8, 151.0, 140.3, 135.2, 134.3, 130.0, 127.2, 124.2, 115.9, 83.8, 70.0, 69.9, 67.7, 67.1, 67.0, 50.1; **MS** (ESI +ve) 860.2339 *m/z* ([M + Na]$^+$, $C_{45}H_{43}{}^{56}FeN_5NaO_8$, calc. 860.2354).

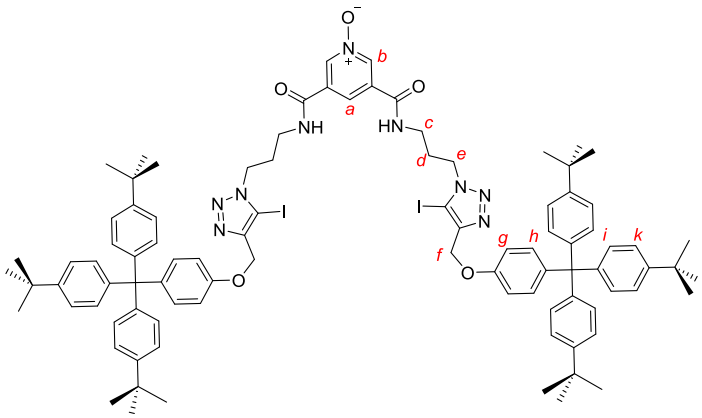
Ferrocene-appended 5-nitro-isophthalamide macrocycle 3.6NO$_2$



5-nitroisophthalic acid (35.0 mg, 0.167 mmol) and a drop of dry DMF was mixed with dry dichloromethane (2 mL) to give a white suspension which was then cooled to 0 ^{o}C, before oxalyl chloride (0.043 mL, 0.50 mmol) was added dropwise. After stirring for 2 hours, the clear yellow solution was dried *in vacuo* to afford the bis-acid chloride as a pale yellow solid. This was dissolved in dry dichloromethane (6 mL) and taken up in a syringe, and was added to vigorously-stirred dry dichloromethane (400 mL) together with the contents of another syringe containing bis-amine **3.5** (116 mg, 0.164 mmol) and anhydrous triethylamine (0.14 mL, 1.0 mmol) dissolved in dry dichloromethane (6.0 mL) over 3 hours using a syringe pump. The reaction was stirred overnight under N_2, before being concentrated on a rotary to c.a. 50 mL. After washing with 10 % citric acid (2 x 30 mL) and water (2 x 30 mL), the organic layer was dried over $MgSO_4$ and solvent removed to afford an orange solid. Silica gel column chromatography (2 % methanol in dichloromethane) gave the macrocycle **3.6NO$_2$** as an orange powder (54 mg, 37 %). **^{1}H-NMR** (400 MHz, d_6-DMSO) δ 9.17 (2H, t, ^3J = 5.0 Hz, NO_2ArCON*H*), 8.79 (2H, t, ^3J = 5.0 Hz, FcArCON*H*), 8.77 (2H, s, H_o), 8.74 (1H, s, H_n), 8.10 (1H, s, H_e), 8.08 (2H, s, H_d), 6.87 (8H, m, H_h + H_i), 4.90 (2H, s, H_a), 4.43 (2H, s, H_b), 4.07 (8H, m, H_g + H_k), 4.03 (5H, s, H_c), 3.64 (8H, m, H_f + H_m); **^{13}C-NMR** (125 MHz, d_6-DMSO) δ 166.6, 164.6, 153.2, 153.0, 148.4, 140.3, 136.5, 135.2, 132.6, 127.2, 124.8, 124.2, 116.0, 115.9,

83.8, 69.9, 69.8, 67.1, 67.0, 66.8; **MS** (ESI +ve) *m/z* 904.2221 ([M + Na]$^+$, $C_{46}H_{43}{}^{56}FeN_5NaO_{10}$, calc. 904.2253).

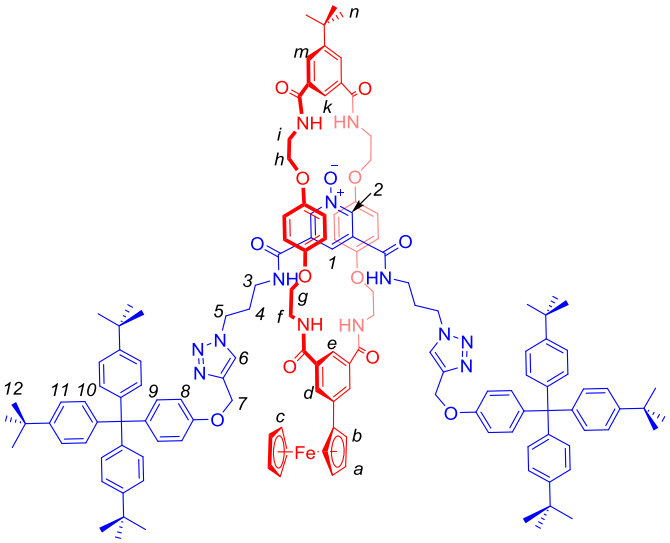
Pyridine N-oxide Bis-iodotriazole XB Axle 3.8I



*The synthesis of the analogous HB axle **3.8H** has been previously reported.*[21]

Pyridine *N*-oxide bis-azide **3.7** (21 mg, 0.061 mmol), synthesised as reported,[21] and iodoalkyne stopper **2.11I** (81 mg, 0.121 mmol) were dissolved in THF (3 mL) at elevated temperatures, and allowed to cool to ambient temperature before copper(I) iodide (1.2 mg, 0.0061 mmol) and TBTA (3.2 mg, 0.0061 mmol) were added portionwise. After an overnight reaction at room temperature under N_2, the reaction mixture was washed with 10 % aqueous ammonia (2 x 5 mL) and the aqueous layer back-extracted with chloroform (2 x 10 mL). The combined organic layer was dried with $MgSO_4$ and solvent removed to give a pale green solid. Silica gel chromatographic purification (5 % methanol in dichloromethane) gave the product as a white solid (61 mg, 60 %). **^{1}H NMR** (400 MHz, $CDCl_3$) δ 9.10 (2H, s, H_b), 8.39 (2H, t, ^3J = 5.6 Hz, CON*H*), 8.35 (1H, s, H_a), 7.22 (12H, d, ^3J = 8.4 Hz, H_i), 7.10-7.06 (16H, m, H_h + H_k), 6.82 (4H, d, ^3J = 9.2 Hz, H_g), 4.99 (4H, s, H_f), 4.49 (4H, t, ^3J = 6.6 Hz, H_e), 3.55 (4H, quart., ^3J = 5.6 Hz, H_c), 2.30 (4H, quint., ^3J = 6.0 Hz, H_d), 1.29 (54H, s, stopper-^{t}Bu); **^{13}C NMR** (100 MHz, $CDCl_3$) δ 162.5, 156.1, 148.3, 147.7, 144.0, 140.5, 140.3, 133.7, 132.4, 130.7, 124.1, 113.3, 81.3, 63.1, 61.5, 48.8, 37.6, 34.3, 31.4, 28.7 ; **MS** (ESI +ve) *m/z* 1706.6375 ([M + Na]$^+$, $C_{93}H_{107}{}^{127}I_2N_9NaO_5$, calc. 1706.6377).

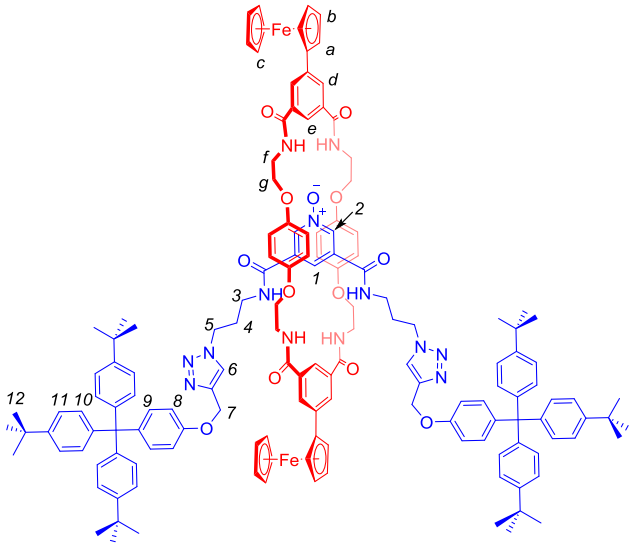
^{t}Bu-isophthalamide Hydrogen Bonding Rotaxane 3.9Bu-H



To a suspension of 5-*tert*-butyl isophthalic acid (18.8 mg, 0.085 mmol) in dry dichloromethane (2 mL) containing a drop of DMF was added oxalyl chloride (0.022 mL, 0.26 mmol) and the reaction was stirred for 4 hours till a clear solution was obtained. The solvent was removed and the yellow bis-acid chloride was thoroughly dried under vacuum before being redissolved in dry dichloromethane (5 mL) and taken up in a syringe. In a separate round bottom flask, axle **3.8H** (124 mg, 0.085 mmol), triethylamine (0.047 mL, 0.34 mmol) and bis-amine **3.5** (60 mg, 0.085 mmol) were dissolved in dry dichloromethane (30 mL) and the bis-acid chloride solution was added portionwise. The resulting clear orange reaction mixture was stirred under N_2 overnight. Following which, the organic layer was washed successively with 1 M citric acid (20 mL), saturated aqueous $NaHCO_3$ (20 mL) and water (10 x 20 mL), before being dried with $MgSO_4$. The solvent was removed *in vacuo* to give an orange solid, which was purified using preparatory TLC (3 % methanol in dichloromethane) to give the desired [2]rotaxane as an orange solid (32 mg, 16 %). **^{1}H NMR** (500 MHz, $CDCl_3$/ CD_3OD 1:1) δ 8.44 (2H, s, H_2), 8.42 (1H, s, H_e), 8.39 (1H, s, H_k), 8.11 (2H, s, H_d), 8.10 (1H, s, H_1), 8.10 (2H, s, H_m), 7.82 (2H, s, H_6), 7.20 (12H, d, ^{3}J = 8.3 Hz, H_{10}), 7.05 (16H, m, H_9 + H_{11}), 6.80 (4H, d, ^{3}J = 8.8 Hz, H_8), 6.37 (8H, s, hydroquinone Ar*H*), 5.06 (4H, s, H_7), 4.84 (2H, br. s, H_b), 4.41 (2H, br. s, H_a), 4.21 (4H, t, ^{3}J = 6.5 Hz, H_5), 4.10 (5H, s, H_c), 3.97 (8H, m, H_h + H_g), 3.73 (8H, m, H_f + H_i), 3.26 (4H, t, ^{3}J = 6.5 Hz, H_3), 2.04 (4H, t, ^{3}J = 6.5 Hz, H_4), 1.34 (9H, s, H_n), 1.27 (54H, s, H_{12}); **^{13}C NMR** (125 MHz, $CDCl_3$/ CD_3OD 1:1) δ 169.1, 168.7, 162.7, 156.6, 153.2, 148.9, 144.7, 142.0, 140.9,

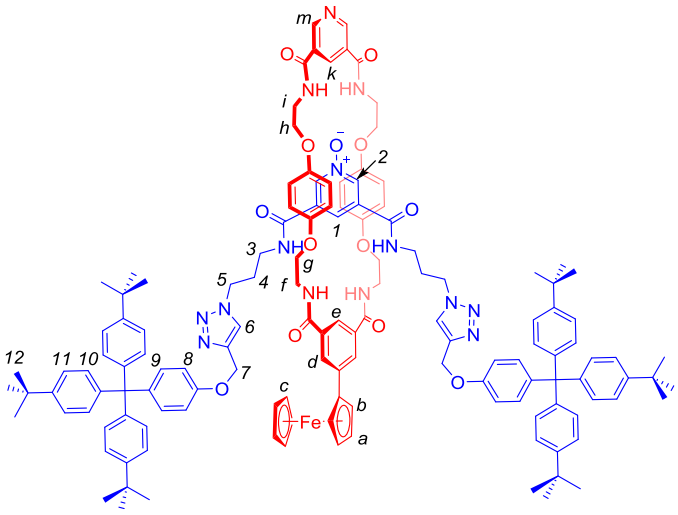
140.0, 134.7, 134.4, 133.1, 132.9, 131.2, 128.9, 128.7, 124.6, 123.1, 115.5, 113.7, 67.1, 63.6, 62.0, 40.8, 37.7, 35.6, 34.8, 31.7, 31.5, 30.4, 30.2; **MS** (ESI +ve) *m/z* 2348.1594 ($[M + Na]^+$, $C_{143}H_{161}{}^{56}FeN_{13}NaO_{13}$, calc. 2348.1613).

Bis-ferrocene-isophthalamide Hydrogen Bonding Rotaxane 3.9Fc-H



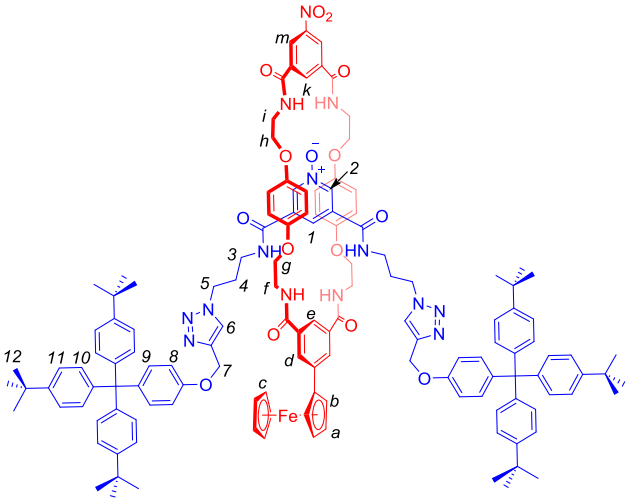
Same procedure as rotaxane **3.9Bu-H**. Reagents: 5-ferrocene isophthalic acid (20 mg, 0.057 mmol), oxalyl chloride (0.015 mL, 0.171 mmol), axle **3.8H** (81 mg, 0.057 mmol), bis-amine **3.5** (40 mg, 0.057 mmol) and triethylamine (0.032 mL, 0.23 mmol) gave the target rotaxane as an orange solid (30 mg, 22 %) after purification by preparatory TLC (3 % methanol in dichloromethane). **^{1}H NMR** (500 MHz, $CDCl_3$/ CD_3OD 1:1) δ 8.41 (2H, s, H_2), 8.37 (2H, s, H_e), 8.14 (4H, s, H_d), 8.06 (1H, s, H_1), 7.72 (2H, s, H_6), 7.19 (12H, d, ^3J = 8.5 Hz, H_{10}), 7.05 (16H, m, H_9 + H_{11}), 6.79 (4H, d, ^3J = 8.8 Hz, H_8), 6.37 (8H, s, hydroquinone Ar*H*), 5.03 (4H, s, H_7), 4.75 (4H, s, H_a), 4.33 (4H, s, H_b), 4.20 (4H, t, ^3J = 6.5 Hz, H_5), 4.01 (10H, s, H_c), 3.97 (8H, m, H_g), 3.74 (8H, m, H_f), 3.25 (4H, t, ^3J = 6.5 Hz, H_3), 2.04 (4H, t, ^3J = 6.5 Hz, H_4), 1.26 (54H, s, H_{12}); **^{13}C NMR** (125 MHz, $CDCl_3$/ CD_3OD 1:1) δ 168.7, 162.7, 156.6, 153.2, 148.9, 144.7, 142.0, 141.0, 140.0, 134.9, 133.1, 132.9, 131.3, 128.8, 124.6, 124.2, 123.0, 115.6, 113.7, 83.6, 70.3, 67.3, 63.6, 62.0, 48.5, 40.8, 37.8, 34.8, 31.8, 30.4; **MS** (ESI +ve) *m/z* 2475.0965 ($[M + Na]^+$, $C_{149}H_{161}{}^{56}Fe_2N_{13}NaO_{13}$, calc. 2475.0928).

Pyridine-isophthalamide Hydrogen Bonding Rotaxane 3.9Py-H



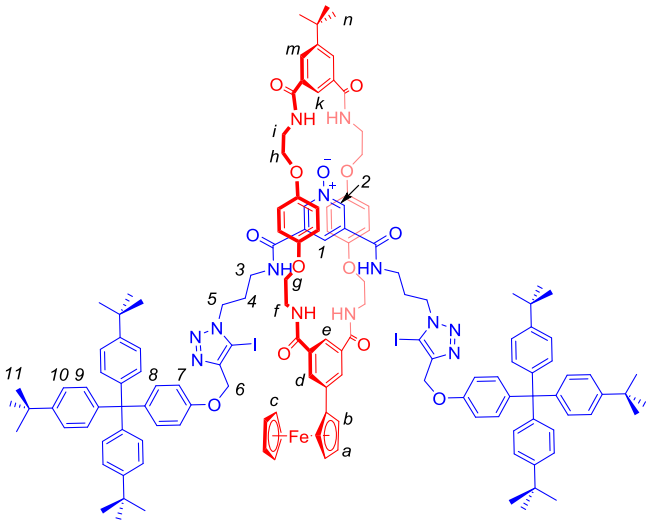
Same procedure as rotaxane **3.9Bu-H**. Reagents: 3,5-pyridine dicarboxylic acid (12 mg, 0.070 mmol), oxalyl chloride (0.018 mL, 0.21 mmol), axle **3.8H** (100 mg, 0.070 mmol), bis-amine **3.5** (49 mg, 0.070 mmol) and triethylamine (0.040 mL, 0.28 mmol) gave rotaxane **3.9Py-H** (14 mg, 9 %) as an orange powder after preparatory TLC purification (5 % methanol in dichloromethane). **^{1}H-NMR** (500 MHz, $CDCl_3$/ CD_3OD 1:1) δ 9.15 (2H, s, H_m), 8.96 (1H, s, H_k), 8.45 (2H, s, H_2), 8.36 (1H, s, H_e), 8.13 (2H, s, H_d), 8.07 (1H, s, H_1), 7.80 (2H, s, H_6), 7.19 (12H, d, ^{3}J = 8.5 Hz, H_{10}), 7.05 (16H, m, H_9 + H_{11}), 6.79 (4H, d, ^{3}J = 8.8 Hz, H_8), 6.39 (8H, m, hydroquinone Ar*H*), 5.05 (4H, s, H_7), 4.75 (2H, s, H_b), 4.33 (2H, s, H_a), 4.25 (4H, t, ^{3}J = 6.7 Hz, H_5), 4.00 (5H, s, H_c), 3.95-3.98 (8H, m, H_h + H_g), 3.72-3.74 (8H, m, H_f + H_i), 3.26 (4H, t, ^{3}J = 6.7 Hz, H_3), 2.06 (4H, t, ^{3}J = 6.8 Hz, H_4), 1.27 (54H, s, H_{12}); **^{13}C-NMR** (125 MHz, $CDCl_3$/ CD_3OD 1:1) δ 169.1, 166.9, 163.1, 157.0, 153.7, 153.5, 152.1, 149.2, 145.0, 145.0 (repeat), 124.4, 141.3, 140.4, 135.3, 134.7, 133.6, 133.2, 131.6, 130.5, 128.9, 126.6, 124.9, 124.7, 123.6, 116.0, 114.1, 83.9, 70.6, 70.6 (repeat), 67.6, 67.5, 64.0, 62.3, 50.0, 40.9, 38.1, 35.0, 32.1, 32.0, 30.6, 29.6; **MS** (ESI +ve) *m/z* 2292.0956 ([M + Na]$^{+}$, $C_{138}H_{152}{}^{56}FeN_{14}NaO_{13}$, calc. 2292.0905).

5-nitro-isophthalamide Hydrogen Bonding Rotaxane 3.9NO$_2$-H



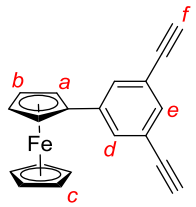
Same procedure as rotaxane **3.9Bu-H**. Reagents: 5-nitro isophthalic acid (15 mg, 0.070 mmol), oxalyl chloride (0.018 mL, 0.21 mmol), axle **3.8H** (100 mg, 0.070 mmol), bis-amine **3.5** (49 mg, 0.070 mmol) and triethylamine (0.040 mL, 0.28 mmol) gave rotaxane **3.9NO$_2$-H** (32 mg, 20 %) as an orange powder after preparatory TLC (4 % methanol in dichloromethane). **^{1}H-NMR** (500 MHz, $CDCl_3$/ CD_3OD 1:1) δ 8.97 (1H, s, H_k), 8.88 (2H, s, H_m), 8.45 (2H, s, H_2), 8.37 (1H, s, H_e), 8.14 (2H, s, H_d), 8.08 (1H, s, H_1), 7.78 (2H, s, H_6), 7.19 (12H, d, ^3J = 8.5 Hz, H_{10}), 7.05 (16H, m, H_9 + H_{11}), 6.79 (4H, d, ^3J = 8.8 Hz, H_8), 6.41-6.37 (8H, m, hydroquinone Ar*H*), 5.04 (4H, s, H_7), 4.74 (2H, s, H_b), 4.33 (2H, s, H_a), 4.25 (4H, t, ^3J = 6.5 Hz, H_5), 4.00 (5H, s, H_c), 3.99 (8H, m, H_g + H_h), 3.74 (8H, m, H_f + H_i), 3.26 (4H, t, ^3J = 6.5 Hz, H_3), 2.06 (4H, t, ^3J = 6.5 Hz, H_4), 1.26 (54H, s, H_{12}); **^{13}C-NMR** (125 MHz, $CDCl_3$/ CD_3OD 1:1) δ 168.9, 166.5, 162.9, 156.7, 153.5, 153.3, 149.4, 149.0, 144.8, 144.8 (repeated), 142.4, 141.1, 140.2, 136.8, 135.1, 133.4, 133.0, 131.9, 131.4, 128.7, 126.4, 126.2, 124.7, 124.5, 123.3, 116.2, 115.8, 115.7, 113.8, 83.7, 70.4, 70.3, 67.3, 63.7, 62.0, 40.9, 40.8, 37.9, 34.8, 31.8, 30.4, 29.4; **MS** (ESI +ve) *m/z* 2336.0797 ([M + Na]$^+$, $C_{139}H_{152}{}^{56}FeN_{14}NaO_{15}$, calc. 2336.0803).

^{t}Bu-isophthalamide Halogen Bonding Rotaxane 3.9Bu-I



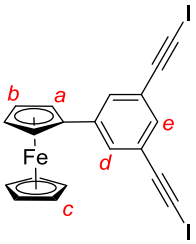
Same procedure as rotaxane **3.9Bu-H**. Reagents: 5-*tert*-butyl isophthalic acid (19 mg, 0.085 mmol), oxalyl chloride (0.022 mL, 0.26 mmol), axle **3.8I** (143 mg, 0.085 mmol), bis-amine **3.5** (60 mg, 0.085 mmol) and triethylamine (0.047 mL, 0.34 mmol) gave rotaxane **3.9Bu-I** (13 mg, 6.0 %) as an orange powder after preparatory TLC (6 % methanol in dichloromethane). **^{1}H-NMR** (500 MHz, $CDCl_3$/ CD_3OD 1:1) δ 8.48 (2H, s, H_2), 8.38 (1H, s, H_e), 8.37 (1H, s, H_k), 8.15 (2H, s, H_d), 8.14 (1H, s, H_1), 8.13 (2H, s, H_m), 7.20 (12H, d, ^{3}J = 8.6 Hz, H_9), 7.07-7.04 (16H, m, H_8 + H_{10}), 6.81 (4H, d, ^{3}J = 8.9 Hz, H_7), 6.40 (8H, m, hydroquinone Ar*H*), 4.92 (4H, s, H_6), 4.76 (2H, s, H_b), 4.37 (2H, s, H_a), 4.21 (4H, t, ^{3}J = 7.0 Hz, H_5), 4.00 (5H, s, H_c), 3.97 (8H, m, H_g + H_h), 3.73 (8H, m, H_f + H_i), 3.29 (4H, t, ^{3}J = 6.9 Hz, H_3), 2.04 (4H, t, ^{3}J = 6.9 Hz, H_4), 1.35 (9H, s, H_n), 1.27 (54H, s, H_{11}); **^{13}C-NMR** (125 MHz, $CDCl_3$/ CD_3OD 1:1) δ 169.3, 168.9, 163.0, 156.9, 153.4, 153.3, 149.1, 148.2, 144.9, 142.2, 141.2, 140.3, 135.1, 134.7, 133.5, 133.0, 131.4, 129.0, 128.8, 126.8, 124.8, 123.6, 123.5, 115.8, 114.1, 83.7, 83.0, 70.5, 70.4, 67.5, 67.5 (repeat), 67.4, 63.8, 62.1, 40.8, 38.0, 35.7, 34.9, 31.8, 31.6, 29.9; **MS** (ESI +ve) *m/z* 2598.9513 ($[M + Na]^+$, $C_{143}H_{159}{}^{56}Fe^{127}I_2N_{13}NaO_{13}$, calc. 2598.9511).

1-ferrocene-3,5-bis(ethynyl)benzene 3.10H



To a solution of compound **3.17** (272 mg, 0.598 mmol) in dichloromethane/ methanol 1:1 (10 mL) was added anhydrous potassium carbonate (540 mg, 3.91 mmol) portionwise and the reaction stirred under N_2 for 5 hours. Following which, water (10 mL) was added, the organic layer was separated and the aqueous layer was extracted with chloroform (3 x 15 mL). The combined organics were dried with $MgSO_4$ and solvent was removed *in vacuo* to afford the desired product **3.10H** (184 mg, 99 %) as an orange solid in good purity and hence was used without further purification. **^{1}H-NMR** (400 MHz, $CDCl_3$) δ 7.57 (2H, s, H_d), 7.45 (1H, s, H_e), 4.65 (2H, m, H_a), 4.36 (2H, m, H_b), 4.07 (5H, s, H_c), 3.11 (2H, s, H_f); **^{13}C-NMR** (100 MHz, $CDCl_3$) δ 140.5, 132.9, 129.8, 122.5, 83.0, 82.8, 69.8, 69.5, 68.6, 66.5; **MS** (EI +ve) *m/z* 310.0436 ($[M]^+$, $C_{20}H_{14}{}^{56}Fe$, calc. 310.0440).

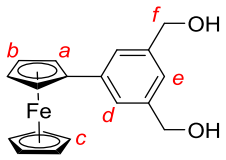
1-ferrocene-3,5-bis(iodoethynyl)benzene 3.10I



Compound **3.10H** (210 mg, 0.68 mmol) was dissolved in dry THF (4 mL) and chilled to -78 ^{o}C in a dry ice/acetone bath. A 2.5 M solution of *n*-butyllithium (0.82 mL, 2.0 mmol) was added dropwise under N_2 over 5 minutes and the reaction left to stir at -78 ^{o}C for 1 hour. In a separate vessel, molecular iodine (518 mg, 2.04 mmol) was dissolved in dry THF (2 mL) and added dropwise to the vigorously-stirred reaction, whereupon the reaction was left to gradually warm up to ambient temperature, and stirred for a further 2 hours. Following which, saturated aqueous sodium thiosulfate (10 mL) and chloroform (20 mL) was added to the reaction. The

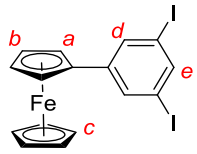
separated organic layer was washed successively with aqueous sodium thiosulfate (10 mL), water (2 x 10 mL) and brine (10 mL) then dried with $MgSO_4$. Purification by silica gel column chromatography (10 % ethyl acetate in hexane) afforded the target compound as an orange solid (281 mg, 74 %). **^{1}H-NMR** (400 MHz, $CDCl_3$) δ 7.47 (2H, s, H_d), 7.32 (1H, s, H_e), 4.64 (2H, m, H_a), 4.36 (2H, m, H_b), 4.08 (5H, s, H_c); **^{13}C-NMR** (100 MHz, $CDCl_3$) δ 140.3, 133.2, 129.8, 123.6, 93.3, 82.9, 69.8, 69.6, 66.5, 7.3; **MS** (ESI/ EI/ FI +ve) *not observed*.

1-ferrocene-3,5-bis(hydroxymethyl)benzene 3.12



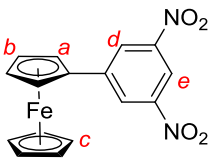
5-ferrocenyl-methyl-isophthalate (100 mg, 0.264 mmol), prepared according to reported procedures,[20] was dissolved in dry dichloromethane and chilled to -78 °C in a dry ice/ acetone bath. A toluene solution of diisobutylaluminium hydride (25 % *w/w*) (0.35 mL, 0.53 mmol) was added dropwise and the reaction stirred for 2 hours. Subsequently, the reaction was quenched by slow addition of 1 M aqueous ammonium chloride (1 mL) dropwise at -78 °C and then allowed to warm up to ambient temperature whereupon more 1 M aqueous ammonium chloride (5 mL) was added, followed by water (10 mL) to give a thick slurry. Chloroform (20 mL) was then added and the mixture stirred to break up all aggregates before the organic layer was separated. The aqueous layer was back-extracted with chloroform (2 x 10 mL) and the combined organics dried with $MgSO_4$. Solvent removal gave a dark orange crystalline crude product which was purified by column chromatography (4 % methanol in dichloromethane), affording the product as an orange solid (64 mg, 76 %). **^{1}H-NMR** (400 MHz, $CDCl_3$) δ 7.41 (2H, s, H_d), 7.21 (1H, s, H_e), 4.73 (4H, s, H_f), 4.67 (2H, t, ^3J = 1.8 Hz, H_a), 4.34 (2H, t, ^3J = 1.8 Hz, H_b), 4.05 (5H, s, H_c), 1.76 (2H, br. s, O*H*); **^{13}C-NMR** (100 MHz, $CDCl_3$) δ 141.3, 140.2, 124.0, 123.2, 84.9, 69.6, 69.1, 66.6, 65.3; **MS** (ESI +ve) *m/z* 323.0729 ($[M + H]^+$, $C_{18}H_{19}{}^{56}FeO_2$, calc. 323.0729).

1-ferrocene-3,5-diiodobenzene 3.13



To a slurry of 3,5-diiodoaniline (400 mg, 1.16 mmol) in 5 M HCl (3 mL) chilled to 0 ^{o}C in an ice bath was added an aqueous solution of sodium nitrite (176 mg, 2.55 mmol in 2 mL of water) dropwise over 5 minutes. The reaction was stirred for 1 hour at 0 ^{o}C till no further gas evolution occurred to form an orange-brown suspension of the diazonium salt. In a separate round bottom flask, ferrocene (259 mg, 1.39 mmol) was dissolved in toluene (5 mL) and chilled to 0 ^{o}C, before the suspension of diazonium salt was added dropwise over 5 minutes. After stirring for 15 minutes at 0 ^{o}C, the reaction was warmed up to ambient temperature and stirred under N_2 for 16 hours. The reaction was then cooled to 0 ^{o}C again and aqueous saturated sodium bicarbonate was added dropwise to the reaction till a neutral pH was attained. Chloroform (10 mL) was then added and the organic and aqueous layers separated. The aqueous layer was extracted with chloroform (4 x 15 mL), and the combined organics were dried with brine, then $MgSO_4$. After removal of solvent, silica gel column chromatography (5 % ethyl acetate in hexane) yielded an orange solid, which was then further purified by recrystallisation (c.a. 10 mL of hexane with a minimal quantity of dichloromethane) to give the product as orange crystals (194 mg, 33 %). **^{1}H-NMR** (400 MHz, $CDCl_3$) δ 7.85 (1H, s, H_e), 7.74 (2H, s, H_d), 4.59 (2H, m, H_a), 4.36 (2H, m, H_b), 4.08 (5H, s, H_c); **^{13}C-NMR** (100 MHz, $CDCl_3$) δ 144.3, 142.1, 134.1, 94.9, 81.9, 69.8, 69.7, 66.6; **MS** (EI +ve) *m/z* 513.8372 ($[M]^+$, $C_{16}H_{12}{}^{56}Fe^{127}I_2$, calc. 513.8372).

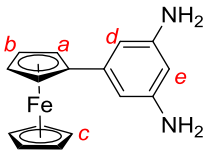
1-ferrocene-3,5-dinitrobenzene 3.14



Ferrocene boronic acid (100 mg, 0.440 mmol) and 3,5-dinitro-iodobenzene[22] (129 mg, 0.440 mmol) were dissolved in DME (3 mL) in a microwave vial. To the red solution was added 3 M

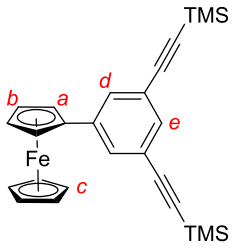
aqueous sodium hydroxide (0.44 mL, 1.32 mmol), and the resulting suspension was vigorously degassed with N_2 for 15 minutes before $PdCl_2$(dppf) (16 mg, 0.022 mmol) was added. The vial was then sealed and heated in the microwave reactor at 150 ^oC for 45 minutes to give a brown slurry which was then partitioned between chloroform (20 mL) and water (10 mL). The organic layer was washed with water (2 x 10 mL), and the combined organic layer back-extracted with chloroform (2 x 10 mL), whereby the combined organics were dried with $MgSO_4$ and evaporated to dryness. Purification with a silica plug (20 % ethyl acetate in hexane) gave the product as fine dark red-brown crystals (112 mg, 72 %). **^{1}H-NMR** (400 MHz, $CDCl_3$) δ 8.82 (1H, t, ^4J = 2.1 Hz, H_e), 8.54 (2H, d, ^4J = 2.1 Hz, H_d), 4.82 (2H, t, ^3J = 1.8 Hz, H_a), 4.55 (2H, t, ^3J = 1.8 Hz, H_b), 4.12 (5H, s, H_c); **^{13}C-NMR** (100 MHz, $CDCl_3$) δ 148.8, 145.6, 125.0, 115.2, 80.0, 71.0, 70.1, 67.2; **MS** (EI +ve) *m/z* 352.0146 ($[M]^+$, $C_{16}H_{12}{}^{56}FeN_2O_4$, calc. 352.0135).

1-ferrocene-3,5-diaminobenzene 3.15



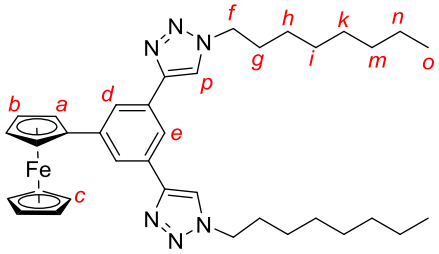
Compound **3.14** (98 mg, 0.28 mmol) was dissolved in a methanol/ THF 1:1 mixture (10 mL). To the resulting red solution was added 10 % by weight Pd/C (20 mg) followed by hydrazine monohydrate (0.14 mL, 2.78 mmol) and the reaction heated at reflux for 2 hours. After cooling the reaction to ambient temperature, the crude reaction was filtered through celite, which was washed with THF to give an orange solution. Removal of solvent gave the product as an orange solid (81 mg, 99 %) in decent purity, which was used without further purification. **^{1}H-NMR** (400 MHz, $CDCl_3$) δ 6.30 (2H, d, ^4J = 2.1 Hz, H_d), 5.92 (1H, t, ^4J = 2.1 Hz, H_e), 4.85 (2H, t, ^3J = 1.8 Hz, H_a), 4.25 (2H, t, ^3J = 1.8 Hz, H_b), 4.06 (5H, s, H_c); **^{13}C-NMR** (100 MHz, $CDCl_3$) δ 147.2, 141.2, 104.4, 100.3, 69.5, 68.5, 66.5, 62.3; **MS** (ESI +ve) *m/z* 293.0734 ($[M + H]^+$, $C_{16}H_{17}{}^{56}FeN_2$, calc. 293.0736).

1-ferrocene-3,5-bis(trimethylsilylethynyl)benzene 3.17



Copper(I) iodide (14.8 mg, 0.078 mmol), $Pd(PPh_3)_2Cl_2$ (27 mg, 0.038 mmol) and compound **3.13** (400 mg, 0.778 mmol) were dissolved in dry degassed THF (2 mL) in a microwave vial. Dry triethylamine (1.09 mL, 7.78 mmol) and ethynyltrimethylsilane (0.33 mL, 2.3 mmol) were then added portionwise and the mixture briefly degassed with N_2 for 1 minute. The microwave vial was then sealed and the reaction reacted in the microwave for 1 hour at 100 ^oC. Upon cooling to ambient temperature, the crude reaction mixture was filtered through celite, which was washed with dichloromethane till the filtrate turned colourless, and solvent removed to give an orange solid. Silica gel chromatography (hexane) isolated **3.17** as orange crystals (272 mg, 77 %). **^{1}H-NMR** (400 MHz, $CDCl_3$) δ 7.49 (2H, s, H_d), 7.43 (1H, s, H_e), 4.65 (2H, m, H_a), 4.34 (2H, m, H_b), 4.06 (5H, s, H_c), 0.28 (18H, s, SiCH_3); **^{13}C-NMR** (100 MHz, $CDCl_3$) δ 140.1, 133.0, 129.0, 123.4, 104.4, 94.6, 83.2, 69.7, 69.4, 66.5, 0.00; **MS** (EI +ve) *m/z* 454.1215 ($[M]^+$, $C_{26}H_{30}{}^{56}Fe^{28}Si_2$, calc. 454.1230).

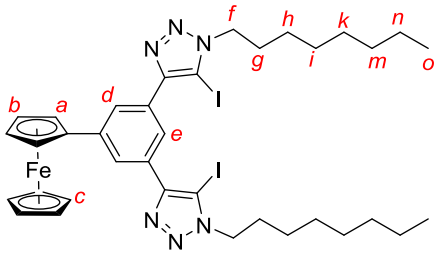
Neutral 1-ferrocene-3,5-bis(prototriazole)benzene receptor 3.18H



Octyl azide (40.1 mg, 0.258 mmol) and bis-alkyne **3.10H** (40 mg, 0.13 mmol) were dissolved in degassed dichloromethane (1.5 mL), followed by TBTA (13.7 mg , 0.026 mmol), $[Cu(MeCN)_4]PF_6$ (24 mg, 0.065 mmol) and triethylamine (0.09 mL, 0.52 mmol). The reaction was stirred under N_2 for 16 h before 10 % aqueous ammonia (10 mL), then chloroform (10 mL) were added. The organic layer was separated from the aqueous layer, which was extracted

with chloroform (2 x 20 mL). The combined organics was washed with 1 M HCl, and dried with brine and $MgSO_4$. Purification by silica gel column chromatography (2 % methanol in dichloromethane) to afford the product as an orange sticky solid (68 mg, 85 %). **^{1}H-NMR** (400 MHz, $CDCl_3$) δ 8.06 (1H, s, H_e), 7.98 (2H, s, H_d), 7.89 (2H, s, H_p), 4.80 (2H, m, H_a), 4.43 (4H, t, ^3J = 7.2 Hz, H_f), 4.36 (2H, m, H_b), 4.08 (5H, s, H_c), 1.98 (4H, quint., ^3J = 6.8 Hz, H_g), 1.28-1.37 (20H, m, $H_{h\text{-}n}$), 0.88 (6H, t, ^3J = 6.8 Hz, H_o); **^{13}C-NMR** (100 MHz, $CDCl_3$) δ 147.5, 140.9, 131.3, 122.8, 120.5, 119.8, 84.5, 69.7, 69.2, 66.7, 50.5, 31.7, 30.2, 29.1, 29.0, 26.5, 22.6, 14.1; **MS** (ESI +ve) *m/z* 621.3360 ($[M + H]^+$, $C_{36}H_{49}{}^{56}FeN_6$, calc. 621.3363).

Neutral 1-ferrocene-3,5-bis(iodotriazole)benzene receptor 3.18I



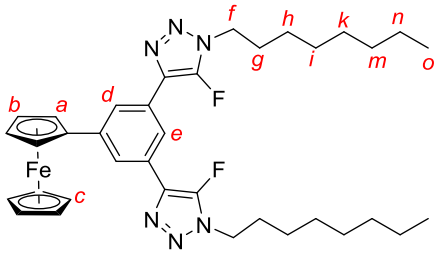
*Method 1: Direct CuAAC from **3.10H** using one-pot 'iodo-CuAAC' conditions*: To a round bottom flask charged with acetonitrile/ THF 1:1 (1 mL) was added sodium iodide (155 mg, 1.03 mmol) and copper(II) perchlorate hexahydrate (191 mg, 0.516 mmol). After stirring for 5 minutes, octyl azide (40 mg, 0.26 mmol), TBTA (1.4 mg, 0.0065 mmol) and DBU (39 mg, 0.26 mmol) were added successively, followed by a solution of **3.10H** (40 mg, 0.13 mmol) in the same solvent mixture (1 mL), and the reaction was left to stir overnight at room temperature. Following which, chloroform (20 mL) was added to the reaction which was washed sequentially with basic EDTA (2 x 10 mL), water (10 mL) and dried with brine (10 mL) and $MgSO_4$. Purification by silica gel column chromatography (20 % ethyl acetate in hexane) afforded the target compound as an orange solid (47 mg, 42 %).

*Method 2: Post-synthetic triazole iodination of **3.18H**:* To a solution of compound **3.18H** (33 mg, 0.053 mmol) in dry THF chilled to -78 ^oC in a dry ice/acetone bath was added a 2.5 M solution of *n*-butyllithium in hexane (0.080 mL, 0.21 mmol) under N_2. After stirring the reaction

at -78 ^{o}C for 1 hour, a solution of iodine (54 mg, 0.21 mmol) in dry THF (1 mL) was added dropwise and the reaction was allowed to gradually warm up to ambient temperature and stirred for a further 2 hours. The solvent was then removed *in vacuo* and the resulting orange paste was taken up in chloroform (20 mL), which was washed successively with saturated aqueous sodium thiosulfate (10 mL) and water (20 mL), then dried with brine (10 mL) and $MgSO_4$. Purification of the crude product by silica gel chromatography (20 % ethyl acetate in hexane) afforded the target compound as an orange solid (35 mg, 75 %).

^{1}H-NMR (400 MHz, $CDCl_3$) δ 8.38 (1H, s, H_e), 8.12 (2H, s, H_d), 4.80 (2H, m, H_a), 4.48 (4H, t, ^{3}J = 7.2 Hz, H_f), 4.37 (2H, m, H_b), 4.12 (5H, s, H_c), 1.99 (4H, quint., ^{3}J = 6.8 Hz, H_g), 1.26-1.41 (20H, m, $H_{h\text{-}n}$), 0.87 (6H, t, ^{3}J = 6.8 Hz, H_o); **^{13}C-NMR** (100 MHz, $CDCl_3$) δ 149.4, 140.4, 130.7, 125.2, 123.8, 84.5, 76.5, 69.7, 69.2, 66.8, 51.1, 31.8, 30.0, 29.1, 29.0, 26.5, 22.6, 14.1; **MS** (ESI +ve) *m/z* 873.1267 ($[M + H]^+$, $C_{36}H_{47}{}^{56}FeN_6{}^{127}I_2$, calc. 873.1296).

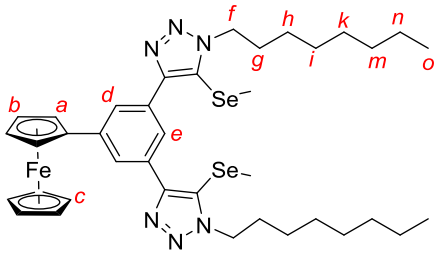
Neutral 1-ferrocene-3,5-bis(fluorotriazole)benzene receptor 3.18F



To a suspension of compound **3.18I** (53 mg, 0.061 mmol) in acetonitrile (2.5 mL) in a microwave vial was added 2.5 mL of an aqueous solution of potassium fluoride (53 mg, 0.92 mmol). The vial was sealed and heated in a microwave reactor at 180 ^{o}C for 10 minutes. After cooling to ambient temperature, ethyl acetate (10 mL) was added to the reaction and the aqueous layer was separated. This aqueous layer was back-extracted with ethyl acetate (2 x 20 mL) and the combined organics were dried with brine (20 mL) and $MgSO_4$. Purification by silica gel column chromatography (ethyl acetate/ hexane 1:3) gave the target compound as a sticky orange liquid (32 mg, 80 %). **^{1}H-NMR** (400 MHz, $CDCl_3$) δ 8.04 (1H, s, H_e), 7.97 (2H, s, H_d), 4.84 (2H, s, H_a), 4.41 (2H, s, H_b), 4.32 (4H, t, ^{3}J = 7.0 Hz, H_f), 4.12 (5H, s, H_c), 1.97 (4H,

quint., ^{3}J = 6.8 Hz, H_g), 1.24-1.38 (20H, m, H_h-$_n$), 0.89 (6H, t, ^{3}J = 6.7 Hz, H_o); **^{13}C-NMR** (100 MHz, $CDCl_3$) δ 151.2, 148.4, 141.1, 127.9 ($^{1}J_{C\text{-}F}$ = 290 Hz), 122.4, 119.4, 84.7, 70.0, 69.6, 67.0, 47.4, 31.7, 29.2, 29.0, 28.9, 26.4, 22.5, 14.0; **^{19}F-NMR** (376 MHz, $CDCl_3$) δ -151.7; **MS** (ESI +ve) *m/z* 657.3167 ($[M + H]^+$, $C_{36}H_{47}{}^{56}FeN_6{}^{19}F_2$, calc. 657.3174).

Neutral 1-ferrocene-3,5-bis(methylseleno-triazole)benzene receptor 3.18Se

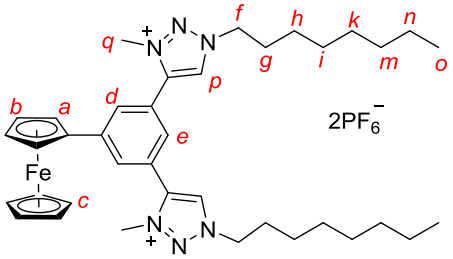


Warning: handle with care in fume cupboard due to malodourous nature of Se-containing volatiles formed in this reaction. All glassware in contact with the reaction was deodorized by soaking in bleach for at least 6 hours.

Elemental Se (24 mg, 0.31 mmol) was suspended in a minimum quantity of dry THF in a microwave vial and a 1.6 M solution of methyl lithium in diethyl ether (0.27 mL, 0.43 mmol) was added portionwise. The reaction was sonicated and left to stir at room temperature for 15 minutes to form a light brown slurry. Compound **3.18F** (32 mg, 0.049 mmol) was dissolved in dry DMF (1 mL) and added to the suspension of $LiSeCH_3$, upon which the slurry turned into a brown solution and was heated at 70 ^{o}C overnight in the dark. After cooling to ambient temperature, iodomethane (0.1 mL) was added portionwise and the reaction was vigorously stirred for 30 minutes to yield an orange suspension. Subsequently, the reaction was poured into water (15 mL) and extracted with diethyl ether (3 x 20 mL). The combined organics were dried with brine (20 mL) and $MgSO_4$, and column chromatography purification of the dried crude mixture (ethyl acetate/ hexane 1:3) gave the product as an orange sticky solid (25 mg, 64 %). **^{1}H-NMR** (400 MHz, $CDCl_3$) δ 8.61 (1H, s, H_e), 8.10 (2H, s, H_d), 5.10 (2H, br. s, H_a), 4.63 (2H, br. s, H_b), 4.54 (4H, t, ^{3}J = 7.0 Hz, H_f), 4.34 (5H, br. s, H_c), 2.20 (6H, s, SeCH_3), 1.97 (4H, m, H_g), 1.28-1.40 (20H, m, H_h-$_n$), 0.89 (6H, t, ^{3}J = 6.7 Hz, H_o); **^{13}C-NMR** (100 MHz, $CDCl_3$) δ

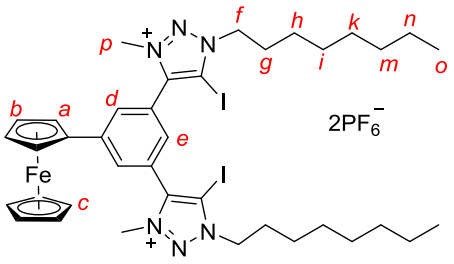
149.2, 140.0, 131.1, 124.6, 123.8, 119.1, 89.4, 73.0, 72.2, 68.4, 49.4, 31.7, 30.7, 29.1, 29.0, 26.5, 22.6, 14.0, 10.1; **MS** (ESI +ve) *m/z* 809.2006 ($[M + H]^+$, $C_{38}H_{53}{}^{56}FeN_6{}^{80}Se_2$, calc. 809.2006).

Dicationic 1-ferrocene-3,5-bis(prototriazolium)benzene receptor 3.19H



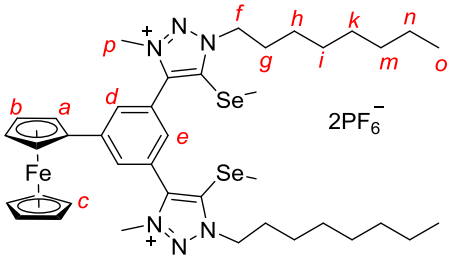
Precursor compound **3.18H** (46 mg, 0.074 mmol) was dissolved in dry dichloromethane (1 mL) and trimethyloxonium tetrafluoroborate (24 mg, 0.16 mmol) was added portionwise. The reaction was stirred under N_2 overnight before methanol (1 mL) was added. The solvent was removed *in vacuo* to yield an orange solid which was purified by preparatory TLC (5 % methanol in dichloromethane). Anion exchange of the purified product to the $2PF_6^-$ salt was achieved by washing a chlorofom solution (30 mL) of the product with 0.1 M NH_4PF_6 (10 x 20 mL), then water (2 x 20 mL) and drying with $MgSO_4$. Solvent removal then afforded the receptor **3.19H** as an orange solid (56 mg, 80 %). **^{1}H-NMR** (400 MHz, $CDCl_3$) δ 8.37 (2H, s, H_p), 7.74 (2H, s, H_d), 7.51 (1H, s, H_e), 4.74 (2H, m, H_a), 4.49 (4H, t, ^3J = 7.2 Hz, H_f), 4.33 (2H, m, H_b), 4.18 (6H, s, H_q), 3.99 (5H, s, H_c), 2.05 (4H, quint., ^3J = 6.8 Hz, H_g), 1.26-1.35 (20H, m, $H_{h\text{-}n}$), 0.90 (6H, t, ^3J = 6.8 Hz, H_o); **^{13}C-NMR** (100 MHz, $CDCl_3$) δ 144.3, 141.9, 128.8, 128.7, 126.5, 123.7, 80.8, 70.5, 70.1, 66.8, 54.4, 38.6, 31.7, 29.0, 28.9, 28.8, 26.2, 22.6, 14.1; **^{19}F-NMR** (376 MHz, $CDCl_3$) δ -72.6 (d, $^1J_{F\text{-}P}$ = 696 Hz); **^{31}P-NMR** (162 MHz, $CDCl_3$) δ -144.7 (sep., $^1J_{P\text{-}F}$ = 716 Hz); **MS** (ESI +ve) *m/z* 325.1870 ($[M]^{2+}$, $C_{38}H_{54}{}^{56}FeN_6$, calc. 325.1874).

Dicationic 1-ferrocene-3,5-bis(iodotriazolium)benzene receptor 3.19I



Identical procedure adopted as **3.19H**. Reagents: **3.18I** (31 mg, 0.036 mmol) and trimethyloxonium tetrafluoroborate (12 mg, 0.079 mmol) in dry dichloromethane (1 mL). Purification by preparatory TLC (2 % methanol in dichloromethane) followed by anion exchange to the $2PF_6^-$ salt by washing with 0.1 M NH_4PF_6 afforded **3.19I** (32 mg, 76 %) as an orange powder. **^{1}H-NMR** (400 MHz, CD_3OD) δ 8.08 (2H, s, H_d), 7.64 (1H, s, H_e), 4.96 (2H, m, H_a), 4.71 (4H, t, ^3J = 7.2 Hz, H_f), 4.51 (2H, m, H_b), 4.31 (6H, s, H_p), 4.16 (5H, s, H_c), 2.09 (4H, quint., ^3J = 6.8 Hz, H_g), 1.296-1.55 (20H, m, $H_{h\text{-}n}$), 0.92 (6H, t, ^3J = 6.8 Hz, H_o); **^{13}C-NMR** (100 MHz, CD_3OD) δ 145.7, 144.4, 130.0, 127.8, 124.8, 90.7, 81.0, 70.3, 69.7, 66.7, 54.7, 38.4, 31.5, 28.8, 28.7, 28.6, 26.0, 22.3, 13.0; **^{19}F-NMR** (376 MHz, CD_3OD) δ -74.4 (d, $^1J_{F\text{-}P}$ = 726 Hz); **^{31}P-NMR** (162 MHz, CD_3OD) δ -144.8 (sep., $^1J_{P\text{-}F}$ = 709 Hz); **MS** (ESI +ve) *m/z* 451.0841 ($[M]^{2+}$, $C_{38}H_{52}{}^{56}FeN_6{}^{127}I_2$, calc. 451.0841).

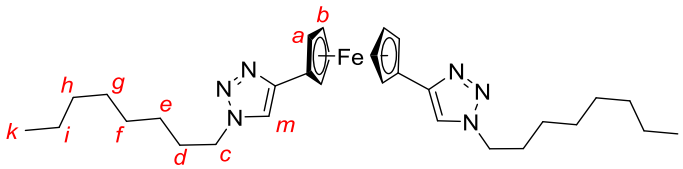
Dicationic 1-ferrocene-3,5-bis(methylseleno-triazolium)benzene receptor 3.19Se



Identical procedure as that for **3.19H** above. Reagents: compound **3.18Se** (17 mg, 0.021 mmol), trimethyloxonium tetrafluoroborate (6.8 mg, 0.046 mmol) in dry dichloromethane (1 mL). Purification with preparatory TLC (7 % methanol in dichloromethane) and anion exchange by washing with 0.1 M NH_4 PF_6 afforded product (17 mg, 72 %) as an orange solid. **^{1}H-NMR** (500 MHz, CD_3CN) δ 7.93 (2H, s, H_d), 7.50 (1H, s, H_e), 4.86 (2H, t, ^3J = 1.9 Hz, H_a),

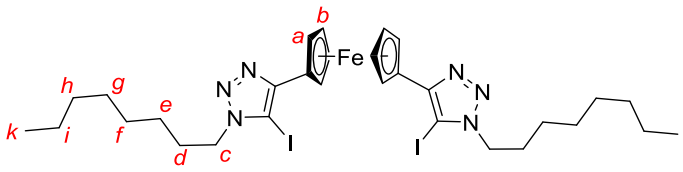
4.72 (4H, t, ^3J = 7.3 Hz, H_f), 4.52 (2H, t, ^3J = 1.9 Hz, H_b), 4.19 (6H, s, H_p), 4.12 (5H, s, H_c), 2.20 (6H, s, SeCH_3), 2.04 (4H, quint., ^3J = 7.2 Hz, H_g), 1.31-1.49 (20H, m, $H_{h\text{-}n}$), 0.91 (6H, t, ^3J = 6.9 Hz, H_o); **^{13}C-NMR** (125 MHz, CD_3CN) δ 146.1, 144.6, 130.9, 130.8, 128.7, 125.4, 81.9, 71.5, 70.8, 67.8, 54.0, 39.8, 32.4, 30.2, 29.7, 29.5, 26.7, 23.3, 14.3, 10.7; **^{19}F-NMR** (376 MHz, CD_3CN) δ -73.0 (d, $^1J_{F\text{-}P}$ = 726 Hz); **^{31}P-NMR** (162 MHz, CD_3CN) δ -144.7 (sep., $^1J_{P\text{-}F}$ = 709 Hz); **^{77}Se-NMR** (95 MHz, CD_3CN) δ 92.0; **MS** (ESI +ve) *m/z* 419.1196 ($[M]^{2+}$, $C_{40}H_{58}N_6{}^{56}Fe^{80}Se_2$, calc. 419.1196).

Neutral 1,1'-bis(prototriazole) ferrocene receptor 3.21H



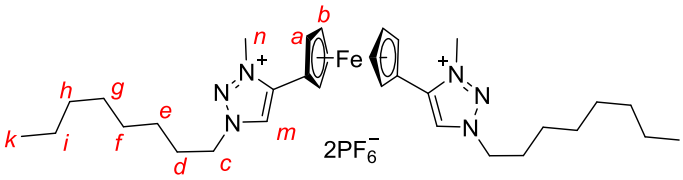
1,1'-bis(trimethylsilylethynyl)ferrocene **3.20** (100 mg, 0.264 mmol), which was prepared as reported,[23] $[Cu(MeCN)_4]PF_6$ (197 mg, 0.528 mmol), TBTA (28 mg, 0.053 mmol) and octyl azide (86 mg, 0.55 mmol) were dissolved in dry degassed THF. To this mixture was added tetrabutylammonium fluoride trihydrate (207 mg, 0.792 mmol) and dry triethylamine (0.15 mL, 1.1 mmol) portionwise. The reaction was then left to stir in the dark under N_2 for 2 days. Thereafter, chloroform (10 mL) was added to the reaction, which was washed successively with 10 % aqueous ammonia (2 x 10 mL) and water (10 mL). After drying the organic phase with brine and $MgSO_4$, column chromatography (2 % methanol in dichloromethane) yielded receptor **3.21H** as an orange solid (111 mg, 77 %). **^{1}H-NMR** (400 MHz, $CDCl_3$) δ 7.28 (2H, s, H_m), 4.64 (4H, m, H_a), 4.27 (4H, t, ^3J = 7.2 Hz, H_c), 4.25 (4H, m, H_b), 1.87 (4H, quint., ^3J = 6.8 Hz, H_d), 1.27-1.32 (20H, m, $H_{e\text{-}i}$), 0.88 (6H, t, ^3J = 6.8 Hz, H_k); **^{13}C-NMR** (100 MHz, $CDCl_3$) δ 144.5, 119.4, 70.1, 69.4, 67.4, 50.2, 31.7, 30.2, 29.1, 24.0, 26.5, 22.6, 14.1; **MS** (ESI +ve) *m/z* 545.3039 ($[M + H]^+$, $C_{30}H_{45}{}^{56}FeN_6$, calc. 545.3050).

Neutral 1,1'-bis(iodotriazole) ferrocene receptor 3.21I



To a solution of receptor compound **3.21H** (59 mg, 0.108 mmol) in dry THF (7 mL) at -78 ^{o}C was added a 2.5 M solution of *n*-butyllithium in hexane (0.13 mL, 0.324 mmol) under N_2. After stirring the reaction at -78 ^{o}C for 30 minutes, a solution of iodine (82 mg, 0.324 mmol) in dry THF (1 mL) was added dropwise and the reaction was allowed to gradually warm up to ambient temperature and stirred for a further 30 minutes. After solvent removal *in vacuo*, chloroform (10 mL) was added and the organic phase was washed successively with saturated sodium thiosulfate (10 mL) and water (10 mL), then dried with brine (10 mL) and $MgSO_4$. Purification of the crude product by preparatory TLC (2 % methanol in dichloromethane) afforded receptor **3.21I** as an orange solid (77 mg, 90 %). **^{1}H-NMR** (400 MHz, $CDCl_3$) δ 5.08 (4H, m, H_a), 4.35 (4H, t, ^{3}J = 7.6 Hz, H_c), 4.30 (4H, m, H_b), 1.92 (4H, quint., ^{3}J = 7.2 Hz, H_d), 1.27-1.36 (20H, m, $H_{e\text{-}i}$), 0.89 (6H, t, ^{3}J = 7.0 Hz, H_k); **^{13}C-NMR** (100 MHz, $CDCl_3$) δ 148.0, 76.0, 74.5, 70.4, 68.0, 50.6, 31.7, 29.8, 29.1, 29.0, 26.5, 22.6, 14.1; **MS** (ESI +ve) *m/z* 797.0967 ($[M + H]^+$, $C_{30}H_{43}{}^{56}FeN_6{}^{127}I_2$, calc. 797.0982).

Dicationic 1,1'-bis(prototriazolium) ferrocene receptor 3.22H

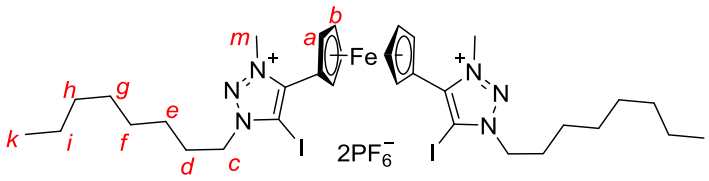


Note: Due to slight product instability in the presence of light, the reaction, purification and anion exchange were performed in the dark. The product was stored under N_2 in the freezer in the dark after synthesis.

Compound **3.21H** (40 mg, 0.073 mmol) was dissolved in dry dichloromethane (4 mL) and trimethyloxonium tetrafluoroborate (24 mg, 0.16 mmol) was added portionwise. The reaction was stirred under N_2 overnight before methanol (1 mL) was added. The solvent was removed

in vacuo to yield an orange solid which was purified by preparatory TLC (8 % methanol in dichloromethane). Anion exchange to the $2PF_6^-$ salt was then performed by washing a chlorofom solution of the product with 0.1 M NH_4PF_6 (10 x 20 mL), followed by water (2 x 10 mL). After drying the solution with $MgSO_4$, solvent removal then afforded the receptor **3.22H** as an orange solid (37 mg, 59 %). **^{1}H-NMR** (400 MHz, CD_3CN) δ 8.39 (2H, s, H_m), 4.92 (4H, m, H_a), 4.66 (2H, m, H_b), 4.53 (4H, t, ^3J = 7.6 Hz, H_c), 4.19 (6H, s, H_n), 2.00 (4H, quint., ^3J = 7.0 Hz, H_d), 1.31-1.39 (20H, m, H_{e-i}), 0.90 (6H, t, ^3J = 7 Hz, H_k); **^{13}C-NMR** (100 MHz, CD_3CN) δ 142.8, 128.2, 74.6, 71.2, 68.5, 54.4, 39.5, 32.0, 29.4, 29.3, 29.1, 26.2, 22.9, 14.0; **^{19}F-NMR** (376 MHz, CD_3CN) δ -72.8 (d, $^1J_{F-P}$ = 718 Hz); **^{31}P-NMR** (162 MHz, CD_3CN) δ -144.6 (sep., $^1J_{P-F}$ = 706 Hz); **MS** (ESI +ve) *m/z* 287.1713 ($[M]^{2+}$, $C_{32}H_{50}{}^{56}FeN_6$, calc. 287.1718).

Dicationic 1,1'-bis(iodotriazolium) ferrocene receptor 3.22I

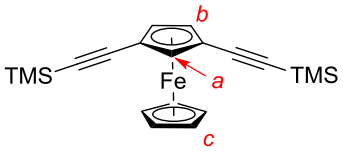


Note: Due to slight product instability in the presence of light, the reaction, purification and anion exchange were performed in the dark. The product was stored under N_2 in the freezer in the dark after synthesis.

Identical reaction procedure as that for receptor **3.22H**. Reagents: **3.21I** (40 mg, 0.050 mmol) and trimethyloxonium tetrafluoroborate (16 mg, 0.11 mmol) in dry dichloromethane (4 mL). Purification by preparatory TLC (8 % methanol in dichloromethane) followed by anion exchange by washing a chloroform solution of the product with 0.1 M NH_4PF_6 afforded the target dicationic receptor **3.22I** as an orange solid (28 mg, 50 %). **^{1}H-NMR** (400 MHz, d_6-acetone) δ 5.40 (4H, m, H_a), 4.97 (2H, m, H_b), 4.77 (4H, t, ^3J = 7.4 Hz, H_c), 4.19 (6H, s, H_m), 2.09 (4H, quint., ^3J = 7.2 Hz, H_d), 1.29-1.52 (20H, m, H_{e-i}), 0.88 (6H, t, ^3J = 6.8 Hz, H_k); **^{13}C-NMR** (100 MHz, d_6-acetone) δ 144.9, 141.3, 113.3, 87.3, 73.9, 71.2, 69.0, 54.9, 40.0, 31.6, 25.8, 22.4, 13.4; **^{19}F-NMR** (376 MHz, d_6-acetone) δ -72.8 (d, $^1J_{F-P}$ = 708 Hz); **^{31}P-NMR** (162

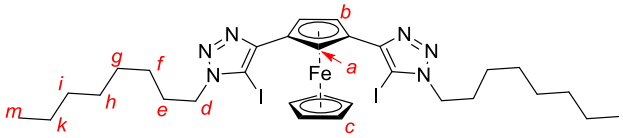
MHz, d_6-acetone) δ -144.4 (sep., $^1J_{P\text{-}F}$ = 708 Hz); **MS** (ESI +ve) *m/z* 287.1713 ($[M]^{2+}$, $C_{32}H_{50}{}^{56}FeN_6$, calc. 287.1718).

1,3-bis(trimethylsilylethynyl)-ferrocene 3.23



To a mixture of 1,3-diiodoferrocene[24] (240 mg, 0.55 mmol), copper(II) acetate hydrate (22 mg, 0.11 mmol) and bis(triphenylphosphine)palladium(II) dichloride (39 mg, 0.055 mmol) in a microwave vial was added *N*,*N*-diisopropylamine (2 mL) portionwise. The resulting suspension was degassed with N_2 for 5 minutes before ethynyltrimethylsilane (0.23 mL, 1.65 mmol) was added. After a microwave-assisted reaction at 110 ^oC for 1 hour, the resulting brown paste was mixed with hexane (20 mL) and the suspension was filtered through a plug of celite. The resulting red organic solution was washed successively with 1.0 M ammonium chloride (3 x 10 mL) and water (10 mL) before being dried with brine (10 mL) and $MgSO_4$. Purification by silica gel column chromatography (hexane) afforded the desired product as a red liquid (139 mg, 67 %). **^{1}H-NMR** (400 MHz, $CDCl_3$) δ 4.69 (1H, s, H_a), 4.44 (2H, s, H_b), 4.23 (5H, s, H_c), 0.22 (18H, s, SiCH_3); **^{13}C-NMR** (100 MHz, $CDCl_3$) δ 102.8, 91.1, 74.7, 72.1, 71.4, 65.5, 0.1; **MS** (ESI +ve) *m/z* 379.09940 ($[M + H]^+$, $C_{20}H_{27}{}^{56}Fe^{28}Si_2$, calc. 379.09952).

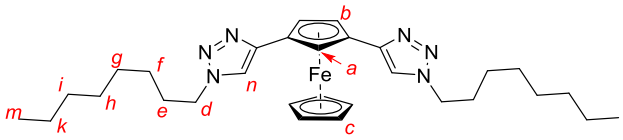
Neutral 1,3-bis(iodotriazole)-ferrocene receptor 3.24I



Tetrabutylammonium fluoride trihydrate (143 mg, 0.55 mmol) was added to a solution of compound **3.23** (69 mg, 0.18 mmol) in degassed THF (1 mL) and the reaction was stirred under N_2 for 30 minutes for TMS-deprotection. In a separate round bottom flask charged with degassed acetonitrile (1 mL), sodium iodide (229 mg, 1.53 mmol) and copper(II) perchlorate

hexahydrate (283 mg, 0.764 mmol) were added successively and stirred for 5 minutes to afford a brown suspension. Thereafter, TBTA (9.7 mg, 0.018 mmol), octyl azide (59 mg, 0.38 mmol) and triethylamine (50 µL, 0.36 mmol) were added, followed by the solution of TMS-deprotected alkyne portionwise to the reaction, which was left to stir for 16 hours under N_2 in the dark. The solvents were then removed *in vacuo* and the residue was re-suspended in chloroform (30 mL). The organic layer was washed with basic EDTA (2 x 10 mL) followed by water (8 x 10 mL) to completely remove any residual TBAF present. Purification by silica gel column chromatography (1 % methanol in dichloromethane *v/v*) afforded the product as an orange solid (113 mg, 78 %). **^{1}H-NMR** (400 MHz, $CDCl_3$) δ 5.94 (1H, m, H_a), 5.24 (2H, m, H_b), 4.43 (4H, t, ^3J = 7.2 Hz, H_d), 4.11 (5H, s, H_c), 1.97 (4H, quint., ^3J = 7.2 Hz, H_e), 1.30-1.40 (20H, m, $H_{f\text{-}k}$), 0.91 (6H, t, ^3J = 7.2 Hz, H_m); **^{13}C-NMR** (100 MHz, $CDCl_3$) δ 148.9, 75.8, 74.5, 71.0, 67.8, 65.6, 50.7, 31.7, 29.9, 29.1, 29.0, 26.4, 22.6, 14.1; **MS** (ESI +ve) *m/z* 797.09730 ($[M + H]^+$, $C_{30}H_{45}N_6{}^{56}Fe^{127}I_2$, calc. 797.09825).

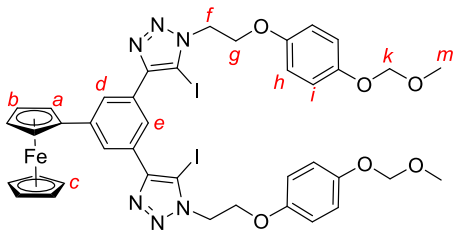
Neutral 1,3-bis(prototriazole)-ferrocene receptor 3.24H



Compound **3.23** (52 mg, 0.14 mmol) was dissolved in degassed THF (1 mL) before tetrabutylammonium fluoride trihydrate (90 mg, 0.34 mmol) was added. The red solution was stirred under N_2 for 30 minutes before degassed dichloromethane (1 mL), $[Cu(CH_3CN)_4]PF_6$ (20 mg, 0.055 mmol), TBTA (7.3 mg, 0.014 mmol), octyl azide (45 mg, 0.29 mmol) and DIPEA (0.070 mL, 0.41 mmol) were added portionwise. After an overnight reaction at room temperature, the reaction was then diluted with chloroform (20 mL), and the organic layer was washed with basic EDTA (2 x 10 mL) followed by water (8 x 10 mL) to completely remove any residual TBAF present. Purification by silica gel column chromatography (4 % methanol in dichloromethane) afforded the product as an orange solid (65 mg, 87 %). **^{1}H-NMR** (400 MHz, $CDCl_3$) δ 7.49 (2H, s, H_n), 5.27 (1H, m, H_a), 4.87 (2H, m, H_b), 4.36 (4H, t, ^3J = 7.2 Hz, H_d), 3.98

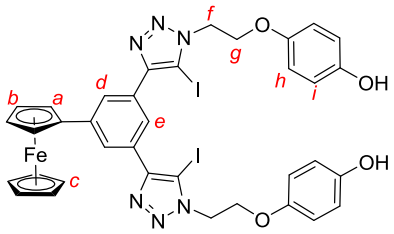
(5H, s, H_c), 1.93 (4H, quint., ^3J = 7.2 Hz, H_e), 1.27-1.36 (20H, m, $H_{f\text{-}k}$), 0.87 (6H, t, ^3J = 7.2 Hz, H_m); **^{13}C-NMR** (100 MHz, $CDCl_3$) δ 146.2, 118.8, 76.2, 71.1, 67.0, 65.0, 50.3, 31.7, 30.3, 29.1, 29.0, 26.5, 22.6, 14.1; **MS** (ESI +ve) *m/z* 545.30447 ($[M + H]^+$, $C_{30}H_{45}N_6{}^{56}Fe$, calc. 545.30496).

MOM-protected ferrocene-appended XB macrocycle precursor 3.25



MOM-protected azide **2.7** (113 mg, 0.508 mmol), $[Cu(CH_3CN)_4]PF_6$ (45 mg, 0.12 mmol), TBTA (12 mg, 0.024 mmol) and compound **3.10I** (136 mg, 0.242 mmol) were sequentially added to degassed THF (2 mL) under N_2. After stirring the reaction overnight at room temperature, the reaction was diluted with chloroform (30 mL) and washed successively with 10 % aqueous ammonia (2 x 15 mL), water (20 mL) and brine (20 mL) before drying with $MgSO_4$. Solvent removal followed by purification by silica gel column chromatography (2 % methanol in dichloromethane) afforded the product as a sticky orange paste (198 mg, 81 %). **^{1}H-NMR** (400 MHz, $CDCl_3$) δ 8.37 (1H, t, ^4J = 1.7 Hz, H_e), 8.12 (2H, d, ^4J = 1.7 Hz, H_d), 6.98 (4H, m, H_h), 6.85 (4H, m, H_i), 5.10 (4H, s, H_k), 4.88 (4H, t, ^3J = 5.7 Hz, H_f), 4.80 (2H, t, ^3J = 1.9 Hz, H_a), 4.47 (4H, t, ^3J = 5.7 Hz, H_g), 4.37 (2H, t, ^3J = 1.9 Hz, H_b), 4.12 (5H, s, H_c), 3.47 (6H, s, H_m); **^{13}C-NMR** (100 MHz, $CDCl_3$) δ 153.0, 151.9, 149.6, 140.4, 130.6, 125.4, 123.8, 117.6, 115.6, 95.2, 84.4, 77.9, 77.2, 69.7, 69.2, 66.7, 55.9, 49.9; **MS** (ESI +ve) *m/z* 1008.0259 ($[M + H]^+$, $C_{40}H_{38}N_6O_6{}^{56}Fe^{127}I_2$, calc. 1008.0286).

Ferrocene-appended bis-phenol XB macrocycle precursor 3.26

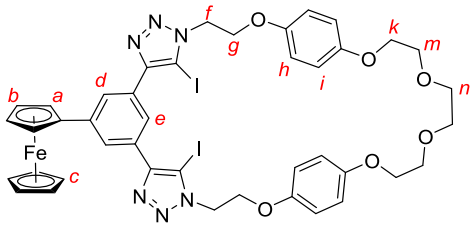


Method 1- MOM-deprotection of precursor ***3.25****:* Acetyl chloride (0.38 mL, 5.3 mmol) was added to methanol (2 mL) at 0 ^{o}C and stirred for 5 minutes, before being warmed to ambient temperature and stirred for a further 15 minutes. Compound **3.25** (180 mg, 0.158 mmol) was dissolved in dichloromethane (2 mL) and added portionwise to the vigorously-stirred acidic methanol solution and reacted for 2 hours. Removal of the solvent *in vacuo* yielded the target compound in good purity as an orange solid (145 mg, quantitative), which was used without further purification.

Method 2- CuAAC from ***3.10I****:* Azide **2.6** (90 mg, 0.50 mmol) and compound **3.10I** (135 mg, 0.240 mmol) were dissolved in degassed THF (3 mL), followed by the portionwise addition of $[Cu(CH_3CN)_4]PF_6$ (45 mg, 0.12 mmol) and TBTA (12 mg, 0.024 mmol). After stirring overnight, the crude mixture was partitioned between ethyl acetate (20 mL) and 1 M aqueous ammonium chloride (10 mL). The separated organic layer was washed with saturated Na_4EDTA solution (10 mL) and the combined aqueous layer was back-extracted with ethyl acetate (3 x 10 mL). The combined organics were dried with brine (20 mL) and $MgSO_4$, dried on a rotary, and silica gel column chromatography (5 % methanol in dichloromethane) afforded the product as an orange solid (171 mg, 78 %).

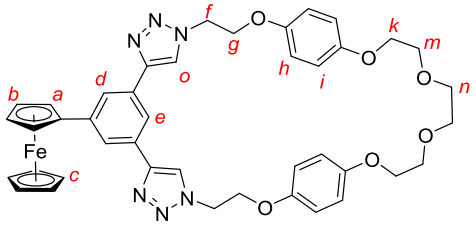
^{1}H-NMR (400 MHz, $CDCl_3$) δ 8.48 (1H, s, H_e), 8.22 (2H, s, H_d), 7.91 (br. s, OH), 6.83 (4H, d, ^{3}J = 8.8 Hz, H_h), 6.75 (4H, d, ^{3}J = 8.8 Hz, H_i), 4.93 (4H, t, ^{3}J = 5.2 Hz, H_f), 4.89 (2H, s, H_a), 4.52 (4H, t, ^{3}J = 5.4 Hz, H_g), 4.41 (2H, s, H_b), 4.13 (5H, s, H_c); **^{13}C-NMR** (100 MHz, $CDCl_3$) δ 152.8, 152.6, 149.8, 141.3, 132.4, 125.5, 124.5, 116.8, 116.7, 85.5, 80.1, 70.6, 70.2, 68.0, 67.6, 51.0; **MS** (ESI +ve) *m/z* 920.9841 ($[M + H]^+$, $C_{36}H_{31}N_6O_4{}^{56}Fe^{127}I_2$, calc. 920.9840).

Ferrocene-appended bis(iodotriazole) XB macrocycle 3.27I



To a solution of compound **3.26** (165 mg, 0.179 mmol) and triethylene glycol-bistosylate **2.3** (82 mg, 0.179 mmol) in dry degassed DMF (18 mL) was added cesium carbonate (292 mg, 0.895 mmol), and the reaction vigorously-stirred under N_2 at 70 ^oC overnight. Thereafter, azeotropic removal of DMF on a rotary with toluene was followed by partitioning of the crude mixture between water (20 mL) and chloroform (40 mL). The aqueous layer was then back-extracted with chloroform (3 x 20 mL) and the combined organics were dried with $MgSO_4$. Solvent removal and purification by preparatory TLC (1.5 % methanol in dichloromethane) afforded the product as an orange powder (57 mg, 31 %). **^{1}H-NMR** (400 MHz, $CDCl_3$) δ 8.15 (1H, s, H_e), 8.04 (2H, s, H_d), 6.79 (4H, d, ^3J = 9.2 Hz, H_h), 6.73 (4H, d, ^3J = 9.1 Hz, H_i), 4.88 (4H, t, ^3J = 4.7 Hz, H_f), 4.79 (2H, s, H_a), 4.44 (4H, t, ^3J = 4.7 Hz, H_g), 4.36 (2H, s, H_b), 4.12 (5H, s, H_c), 4.03 (4H, t, ^3J = 4.7 Hz, H_k), 3.78 (4H, t, ^3J = 4.7 Hz, H_m), 3.68 (4H, s, H_f); **^{13}C-NMR** (100 MHz, $CDCl_3$) δ 153.5, 152.2, 149.9, 140.5, 130.6, 125.6, 124.5, 115.7, 115.6, 84.4, 78.7, 70.8, 69.7, 69.6, 69.2, 68.2, 67.5, 66.8, 50.0; **MS** (ESI +ve) *m/z* 1035.0525 ($[M + H]^+$, $C_{42}H_{41}N_6O_6{}^{56}Fe^{127}I_2$, calc. 1035.0521).

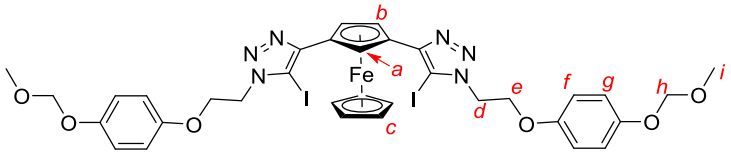
Ferrocene-appended bis(prototriazole) HB macrocycle 3.27H



Bis-azide **2.2** (150 mg, 0.32 mmol), bis-alkyne **3.10H** (98 mg, 0.32 mmol), $[Cu(CH_3CN)_4]PF_6$ (24 mg, 0.064 mmol) and TBTA (8.5 mg, 0.016 mmol) were dissolved in degassed dichloromethane (150 mL) before DIPEA (0.22 mL, 1.28 mmol) was added to the reaction. After stirring for 2 days under N_2 at room temperature, the solvent was removed on the rotary

till c.a. 20 mL remained, and the crude solution was washed successively with 1 M HCl (aq) (2 x 10 mL), basic EDTA (10 mL) and brine (20 mL) before being dried with $MgSO_4$. Solvent removal and purification using silica gel column chromatography (5 % methanol in dichloromethane) followed by preparatory TLC (2 % methanol in dichloromethane) yielded the product as an orange solid (78 mg, 31 %). **^{1}H-NMR** (400 MHz, $CDCl_3$) δ 8.15 (2H, s, H_d), 8.08 (2H, s, H_o), 7.66 (1H, s, H_e), 6.78-6.85 (8H, m, H_h + H_i), 4.81-4.84 (6H, m, H_a + H_f), 4.37 (2H, s, H_b), 4.34 (4H, t, ^3J = 4.6 Hz, H_g), 4.08 (5H, s, H_c), 4.05 (4H, t, ^3J = 4.9 Hz, H_k), 3.82 (4H, t, ^3J = 4.8 Hz, H_m), 3.71 (4H, s, H_f); **^{13}C-NMR** (100 MHz, $CDCl_3$) δ 153.5, 151.7, 147.4, 140.9, 130.8, 122.6, 120.8, 120.3, 115.6, 115.3, 84.0, 70.5, 69.4, 69.3, 68.9, 67.9, 67.1, 66.5, 49.8; **MS** (ESI +ve) *m/z* 805.2401 ($[M + Na]^+$, $C_{42}H_{42}N_6O_6{}^{56}Fe^{23}Na$, calc. 805.2408).

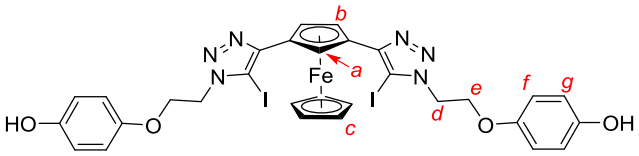
MOM-protected 1,3-bis(iodotriazole)-ferrocene macrocycle precursor 3.28



TMS-protected bis-alkyne **3.23** (50 mg, 0.13 mmol) was dissolved in degassed THF/ acetonitrile 1:1 (1 mL) and tetrabutylammonium fluoride trihydrate (104 mg, 0.396 mmol) was added portionwise and the resultant red-brown solution left to stir for 15 minutes at room temperature for TMS-deprotection. In a separate round-bottom flask containing the same solvent mixture (1 mL), sodium iodide (166 mg, 1.11 mmol) was added followed by copper(II) perchlorate hexahydrate (205 mg, 0.554 mmol) and vigorously stirred for 5 minutes. Thereafter, DBU (40 mg, 0.26 mmol), MOM-protected azide **2.7** (62 mg, 0.28 mmol) and TBTA (3.5 mg, 0.0066 mmol) were added successively. To this mixture was then added the deprotected alkyne solution portionwise and the reaction was stirred overnight in the dark under N_2. Thereafter, chloroform (20 mL) was added to dilute the reaction, which was washed successively with 10 % aqueous ammonia (20 mL), water (8 x 20 mL) and brine (20 mL). The viscous crude brown liquid obtained after solvent removal *in vacuo* was purified by silica gel column chromatography to give the target compound **3.28** as a sticky orange liquid (70 mg, 57

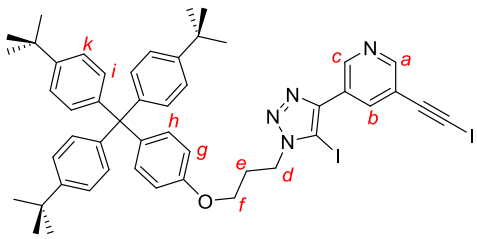
%). **^{1}H-NMR** (400 MHz, $CDCl_3$) δ 6.96 (4H, d, ^{3}J = 9.0 Hz, H_f), 6.82 (4H, d, ^{3}J = 9.0 Hz, H_g), 5.93 (1H, s, H_a), 5.22 (2H, d, ^{4}J = 1.2 Hz, H_b), 5.09 (4H, s, H_h), 4.81 (4H, t, ^{3}J = 5.7 Hz, H_d), 4.44 (4H, t, ^{3}J = 5.7 Hz, H_e), 4.09 (5H, s, H_c), 3.46 (6H, s, H_i); **^{13}C-NMR** (100 MHz, $CDCl_3$) δ 152.7, 151.6, 148.7, 128.2, 117.3, 115.2, 94.8, 75.3, 67.6, 66.5, 65.4, 58.5, 55.5, 49.3; **MS** (ESI +ve) *m/z* 933.0052 ($[M + H]^+$, $C_{34}H_{35}N_6O_6{}^{56}Fe^{127}I_2$, calc. 933.0057).

Bis-phenol 1,3-bis(iodotriazole)-ferrocene macrocycle precursor 3.29



Acetyl chloride (0.11 mL, 1.5 mmol) was added to methanol (1.5 mL) at 0 °C and stirred for 5 minutes, before being warmed to ambient temperature and stirred for a further 15 minutes. Compound **3.28** (70 mg, 0.075 mmol) was dissolved in dichloromethane (1.5 mL) and added portionwise to the acidic methanol solution and stirred for 2 hours. Removal of the solvent *in vacuo* yielded the target compound in good purity as an orange solid (63 mg, quantitative) in good purity, which was used without further purification. **^{1}H-NMR** (400 MHz, d_6-DMSO) δ 6.71 (4H, d, ^{3}J = 9.0 Hz, H_f), 6.64 (4H, d, ^{3}J = 9.0 Hz, H_g), 5.75 (1H, s, H_a), 5.12 (2H, s, H_b), 4.74 (4H, t, ^{3}J = 5.2 Hz, H_d), 4.35 (4H, t, ^{3}J = 5.2 Hz, H_e), 3.99 (5H, s, H_c).

Terminal Iodoalkyne Axle Precursor 3.31

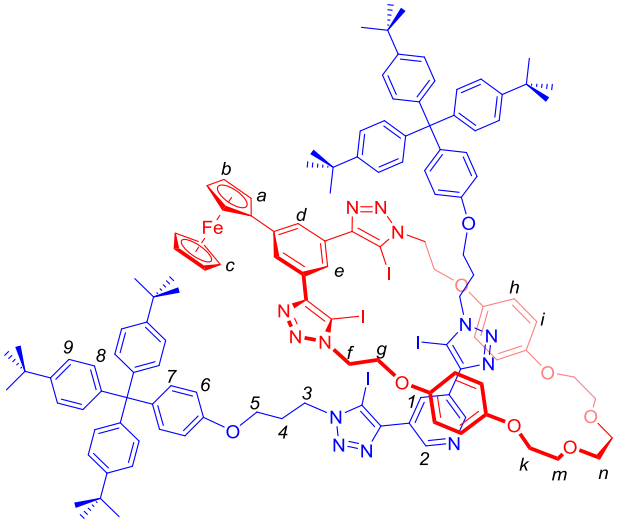


A modified procedure was adopted herein from that reported in the literature.[25]

Pyridine-3,5-bis(iodoalkyne) (150 mg, 0.396 mmol), TBTA (8.4 mg, 0.016 mmol) and copper(I) iodide (75 mg, 0.40 mmol) were suspended in degassed THF (4 mL). Separately, a solution of

stopper azide **2.10** (93 mg, 0.16 mmol) in degassed THF (2 mL) was taken up in a syringe and added slowly to the vigorously-stirred reaction over 3 hours, and the reaction was left to stir overnight under N_2. Thereafter, THF was removed on a rotary and chloroform (20 mL) was added to the reaction which was then washed with basic EDTA (2 x 20 mL), and the combined aqueous layer was back-extracted with chloroform (2 x 20 mL). The organics were dried with brine (20 mL) and $MgSO_4$ and the solvent removed to yield a brown solid. Silica gel column chromatography (gradient from 4 % to 7 % ethyl acetate in dichloromethane) afforded the target compound as a white solid (97 mg, 63 %). **^{1}H-NMR** (400 MHz, $CDCl_3$) δ 9.16 (1H, s, H_c), 8.70 (1H, s, H_a), 8.30 (1H, s, H_b), 7.24 (6H, d, ^3J = 8.4 Hz, H_i), 7.08-7.13 (8H, m, H_h + H_k), 6.78 (2H, d, ^3J = 8.8 Hz, H_g), 4.69 (2H, t, ^3J = 6.9 Hz, H_d), 4.06 (2H, t, ^3J = 5.6 Hz, H_f), 2.47 (2H, quint., ^3J = 6.2 Hz, H_e), 1.31 (27H, s, ^{t}Bu-*H*); **^{13}C-NMR** (100 MHz, $CDCl_3$) δ 156.1, 152.5, 148.3, 147.4, 146.3, 144.0, 140.1, 137.6, 132.3, 130.7, 126.0, 124.1, 120.3, 113.1, 90.4, 63.8, 63.0, 48.1, 34.3, 31.4, 29.6, 11.8; **MS** (ESI +ve) *m/z* 967.2297 ($[M + H]^+$, $C_{49}H_{53}N_4O^{127}I_2$, calc. 967.2303).

Neutral Ferrocene-appended All-XB Rotaxane 3.32I$_4$



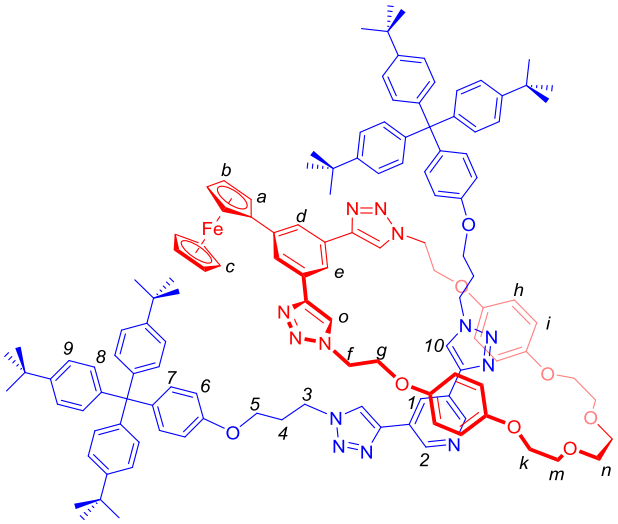
*Method 1 (Scheme 3.14, Chapter 3) using half-axle **3.31***: Macrocycle **3.27I** (22 mg, 0.021 mmol), half-axle **3.31** (82 mg, 0.084 mmol), stopper azide **2.10** (50 mg, 0.084 mmol) and $[Cu(CH_3CN)_4]PF_6$ (7.8 mg, 0.021 mmol) were mixed in a two-neck round-bottom flask and thoroughly degassed by three cycles of evacuation and refilling with N_2. Thoroughly-degassed

dry dichloromethane (2 mL) was then added and the resulting solution left to stir for three days, whereupon TLC analysis (eluent: 5 % methanol in dichloromethane) showed complete consumption of axle precursors. The reaction was then diluted with chloroform (20 mL) and washed with basic aqueous EDTA solution (2 x 10 mL) then dried with $MgSO_4$. Purification by preparatory TLC (2.5 % methanol in dichloromethane) yielded the target rotaxane as a light orange powder (18 mg, 33 %).

Method 2 (Scheme 3.14, Chapter 3) directly from pyridine-3,5-bis(iodoalkyne): Macrocycle **3.27I** (20 mg, 0.019 mmol), pyridine-3,5-bis(iodoalkyne) (29 mg, 0.077 mmol), stopper azide **2.10** (90 mg, 0.154 mmol) and $[Cu(CH_3CN)_4]PF_6$ (7.2 mg, 0.019 mmol) were mixed in a two-neck round-bottom flask and thoroughly degassed by three cycles of evacuation and refilling with N_2. Thoroughly-degassed dry dichloromethane (2 mL) was then added and the resulting solution left to stir till complete consumption of axle precursors was observed (7 days) by TLC analysis (eluent: 5 % methanol in dichloromethane). Aqueous work-up and purification was performed as described for Method 1 to yield the pure rotaxane (16 mg, 31 %).

^{1}H-NMR (500 MHz, $CDCl_3$) δ 9.20 (2H, s, H_2), 8.78 (1H, s, H_1), 8.27 (1H, t, ^4J = 1.5 Hz, H_e), 8.03 (2H, d, ^4J = 1.5 Hz, H_d), 7.22-7.24 (12H, m, H_8), 7.08-7.11 (16H, m, H_9 + H_7), 6.65 (4H, d, ^3J = 8.5 Hz, H_6), 6.44 (4H, d, ^3J = 8.9 Hz, H_h), 6.37 (4H, d, ^3J = 8.9 Hz, H_i), 4.82 (4H, t, ^3J = 4.7 Hz, H_f), 4.74 (2H, t, ^3J = 1.8 Hz, H_a), 4.32 (2H, t, ^3J = 1.8 Hz, H_b), 4.22 (4H, t, ^3J = 4.7 Hz, H_g), 4.18 (4H, t, ^3J = 6.0 Hz, H_3), 4.07 (5H, s, H_c), 3.91 (4H, t, ^3J = 4.3 Hz, H_5), 3.71-3.75 (8H, m, H_k + H_m), 3.67 (4H, s, H_n), 2.05 (4H, m, H_4), 1.31 (54H, stopper-^{t}Bu); **^{13}C-NMR** (125 MHz, $CDCl_3$) δ 156.2, 153.0, 151.7, 149.8, 148.3, 147.8, 146.4, 144.2, 144.0, 140.5, 139.8, 132.2, 131.8, 130.7, 126.2, 125.6, 124.8, 124.1, 115.0, 114.9, 113.1, 84.4, 70.9, 69.8, 69.7, 69.5, 69.2, 67.4, 66.8, 64.0, 63.1, 53.8, 50.1, 47.9, 34.3, 31.4, 29.3; **MS** (ESI +ve) *m/z* 2588.6719 ($[M + H]^+$, $C_{131}H_{142}N_{13}O_8{}^{127}I_4{}^{56}Fe$, calc. 2588.6627).

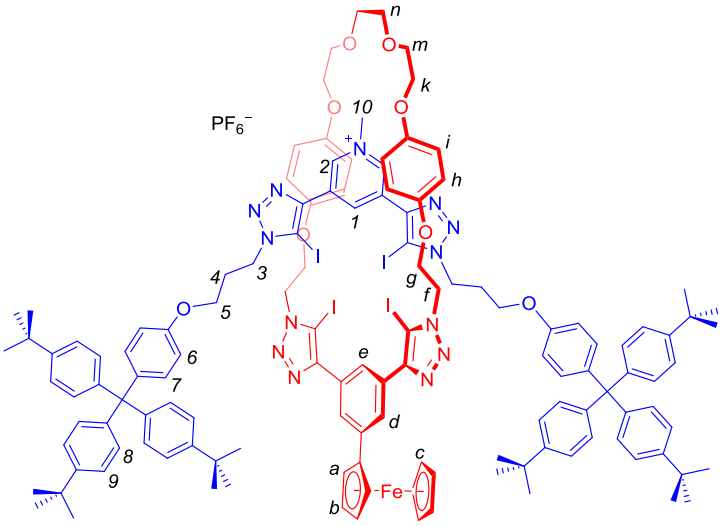
Neutral Ferrocene-appended All-HB Rotaxane 3.32H$_4$



Identical procedure followed as Method 2 for rotaxane **3.32I$_4$** under thoroughly-degassed conditions.

Reagents used: Macrocycle **3.27H** (25 mg, 0.032 mmol), 3,5-diethynylpyridine (16 mg, 0.13 mmol), stopper azide **2.10** (150 mg, 0.26 mmol), [Cu(CH$_3$CN)$_4$]PF$_6$ (12 mg, 0.032 mmol) in dichloromethane (3.2 mL). Complete consumption of axle precursors was found to occur after 2 days by TLC (10 % methanol in dichloromethane). Preparatory TLC (3 % methanol in dichloromethane) isolated that target rotaxane as an orange solid (4 mg, 6 %). **^{1}H-NMR** (500 MHz, CDCl$_3$) δ 8.81 (2H, d, ^4J = 1.9 Hz, H$_2$), 8.25 (2H, s, H$_o$), 8.23 (2H, d, ^4J = 1.4 Hz, H$_d$), 8.09 (1H, t, ^4J = 1.9 Hz, H$_1$), 7.92 (1H, s, H$_e$), 7.72 (2H, s, H$_{10}$), 7.21-7.24 (12H, m, H$_8$), 7.06-7.12 (16H, m, H$_9$ + H$_7$), 6.73 (4H, d, ^3J = 9.0 Hz, H$_6$), 6.35 (4H, d, ^3J = 9.0 Hz, H$_h$), 6.28 (4H, d, ^3J = 9.0 Hz, H$_i$), 4.28 (2H, t, ^3J = 1.8 Hz, H$_a$), 4.64 (4H, t, ^3J = 4.8 Hz, H$_f$), 4.37 (4H, t, ^3J = 7.2 Hz, H$_3$), 4.32 (2H, t, ^3J = 1.8 Hz, H$_b$), 4.19 (4H, t, ^3J = 4.9 Hz, H$_g$), 4.08 (5H, s, H$_c$), 3.89 (4H, t, ^3J = 5.6 Hz, H$_5$), 3.80-3.83 (4H, m, H$_k$), 3.71-3.72 (8H, m, H$_m$ + H$_n$), 2.27 (4H, quint., ^3J = 6.6 Hz, H$_4$), 1.30 (54H, stopper-^{t}Bu); **^{13}C-NMR** (125 MHz, CDCl$_3$) δ 156.0, 152.6, 151.0, 148.1, 147.3, 145.5, 143.8, 143.7, 140.9, 139.9, 132.1, 131.1, 130.4, 129.8, 129.0, 127.7, 126.3, 123.8, 122.6, 121.3, 120.5, 115.5, 114.4, 112.7, 84.1, 70.5, 69.5, 69.0, 67.2, 66.6, 66.5, 63.8, 62.8, 49.1, 47.0, 34.0, 31.1, 29.5; **MS** (ESI +ve) *m/z* 2085.0772 ([M + H]$^+$, $C_{131}H_{146}N_{13}O_8{}^{56}Fe$, calc. 2085.0761).

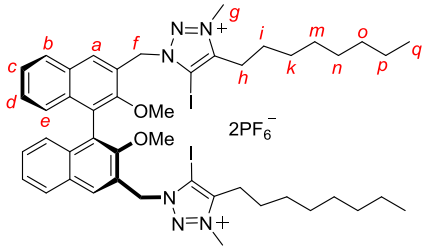
Cationic Ferrocene-appended All-XB Rotaxane 3.34I$_4$



To a solution of neutral rotaxane **3.32I$_4$** (20 mg, 7.7 μmol) in dry dichloromethane (0.5 mL) was added iodomethane (0.1 mL) and the reaction stirred overnight at room temperature. Removal of solvent *in vacuo* followed by purification by preparatory TLC (eluent: 4 % methanol in dichloromethane) afforded the product as an orange solid. Anion exchange was performed by dissolving the rotaxane in chloroform (20 mL) and repeated washing with 0.1 M NH_4PF_6 (aq.) (8 x 10 mL) followed by water (2 x 10 mL). The organic phase was dried with $MgSO_4$ (no brine!) and solvent removed to afford the PF_6^- salt of target rotaxane **3.34I$_4$** as a light orange solid (16 mg, 76 %). **^{1}H-NMR** (500 MHz, $CDCl_3$) δ 9.31 (2H, s, H_2), 8.76 (1H, s, H_1), 8.34 (1H, s, H_e), 8.06 (2H, s, H_d), 7.22 (12H, d, ^3J = 8.6 Hz, H_8), 7.11 (4H, d, ^3J = 8.9 Hz, H_7), 7.08 (12H, d, ^3J = 8.6 Hz, H_9), 6.78 (4H, d, ^3J = 8.7 Hz, H_6), 6.19 (4H, d, ^3J = 9.0 Hz, H_h), 6.07 (4H, d, ^3J = 9.0 Hz, H_i), 4.77-4.79 (6H, m, H_a + H_f), 4.70 (3H, s, H_{10}), 4.36 (4H, t, ^3J = 6.1 Hz, H_3), 4.31 (2H, s, H_b), 4.07-4.09 (9H, m, H_c + H_g), 3.93 (4H, t, ^3J = 5.6 Hz, H_5), 3.76-3.81 (12H, m, H_K + H_m + H_n), 2.27 (4H, quint., ^3J = 6.0 Hz, H_4), 1.30 (54H, stopper-^{t}Bu); **^{13}C-NMR** (125 MHz, $CDCl_3$) δ 156.3, 152.4, 151.7, 149.8, 148.3, 144.1, 141.9, 141.4, 141.0, 140.0, 133.7, 132.3, 130.9, 130.8, 130.7, 125.3, 124.1, 114.8, 114.2, 113.1, 84.1, 70.9, 70.2, 69.7, 69.4, 67.2, 66.8, 63.8, 63.1, 53.7, 50.1, 49.2, 48.1, 34.3, 31.4, 29.7; **^{19}F-NMR** (376 MHz, $CDCl_3$) δ -72.8 (d, $^1J_{F-P}$ = 720 Hz); **^{31}P-NMR** (162 MHz, $CDCl_3$) δ -144.4 (sep., $^1J_{P-F}$ = 720 Hz); **MS** (ESI +ve) *m/z* 2602.6733 ([M]$^+$, $C_{132}H_{144}N_{13}O_8{}^{127}I_4{}^{56}Fe$, calc. 2602.6784).

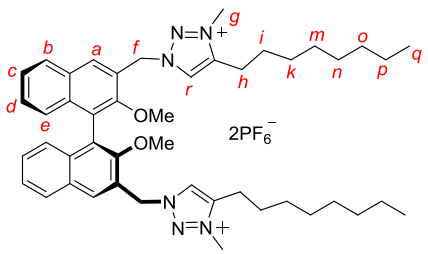
7.2.4 Synthesis of Novel Compounds from Chapter 4

3,3'-Disubstituted (*S*)-BINOL XB Dicationic Receptor 4.1I



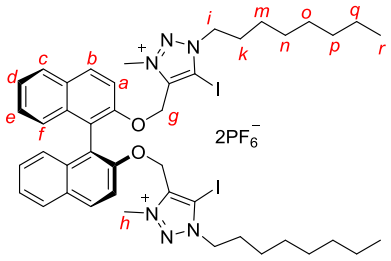
Neutral bis-iodotriazole precursor **4.5I** (25 mg, 0.026 mmol) was dissolved in dry dichloromethane (1 mL) and trimethyloxonium tetrafluoroborate (8.2 mg, 0.055 mmol) was added portionwise. The reaction was stirred overnight at room temperature before 1 drop of methanol was added and the solvent removed on a rotary. Purification by preparatory TLC (5 % methanol in dichloromethane) afforded the purified product, which was converted to its $2PF_6^-$ salt by passing a solution of the compound (0.5 % water in acetonitrile) down a PF_6^- -loaded Amberlite™ column five times. Removal of the solvent *in vacuo* afforded the product as a white solid (22 mg, 67 %). **^{1}H-NMR** (400 MHz, CD_3OD) δ 8.01 (2H, s, H_a), 7.98 (2H, d, ^3J = 6.8 Hz, H_b), 7.47 (2H, t, ^3J = 6.4 Hz, H_c), 7.35 (2H, t, ^3J = 6.4 Hz, H_d), 7.13 (2H, d, ^3J = 6.8 Hz, H_e), 6.05 (4H, m, H_f), 4.32 (6H, s, H_g), 3.27 (6H, s, OCH_3), 2.96 (4H, t, ^3J = 6.8 Hz, H_h), 1.70 (4H, m, H_i), 1.29-1.42 (20H, m, $H_{k\text{-}p}$), 0.88 (6H, t, ^3J = 6.4 Hz, H_q); **^{13}C-NMR** (100 MHz, CD_3OD) δ 153.9, 148.4, 134.7, 131.9, 130.2, 128.3, 127.5, 125.5, 125.2, 125.1, 123.4, 88.9, 60.0, 54.4, 37.4, 31.5, 28.8, 28.5, 28.4, 25.8, 23.6, 22.2, 13.0; **^{19}F-NMR** (376 MHz, CD_3OD) δ -74.6 (d, $^1J_{F\text{-}P}$ = 708 Hz); **^{31}P-NMR** (162 MHz, CD_3OD) δ -141.6 (sep., $^1J_{P\text{-}F}$ = 708 Hz); **MS** (ESI +ve) *m/z* 491.1423 ($[M]^{2+}$, $C_{46}H_{60}O_2N_6{}^{127}I_2$, calc. 491.1428); $[\alpha]_D^{25}$ -13.3 (c 0.31, acetonitrile).

3,3'-Disubstituted (*S*)-BINOL HB Dicationic Receptor 4.1H



Same procedure adopted as receptor **4.1I** as described. Reagents: **4.5H** (20 mg, 0.029 mmol) and trimethyloxonium tetrafluoroborate (9.3 mg, 0.063 mmol) in dry dichloromethane (1 mL). Purification by preparatory TLC (5 % methanol in dichloromethane) and anion exchange using a PF_6^- -loaded Amberlite™ column gave **4.1H** as a white solid (22 mg, 74 %). **^{1}H-NMR** (400 MHz, CD_3OD) δ 8.60 (2H, s, H_r), 8.23 (2H, s, H_a), 8.02 (2H, d, ^3J = 6.8 Hz, H_b), 7.48 (2H, t, ^3J = 6.4 Hz, H_c), 7.34 (2H, t, ^3J = 6.4 Hz, H_d), 7.11 (2H, d, ^3J = 6.8 Hz, H_e), 6.00 (4H, m, H_f), 4.21 (6H, s, H_g), 3.21 (6H, s, OCH_3), 2.86 (4H, t, ^3J = 6.8 Hz, H_h), 1.74 (4H, m, H_i), 1.28-1.40 (20H, m, $H_{k\text{-}p}$), 0.87 (6H, t, ^3J = 6.4 Hz, H_q); **^{13}C-NMR** (100 MHz, CD_3OD) δ 153.9, 148.4, 134.7, 131.9, 130.2, 128.3, 127.5, 125.5, 125.2, 125.1, 123.4, 88.9, 60.0, 54.4, 37.4, 31.5, 28.8, 28.5, 28.4, 25.8, 23.6, 22.2, 13.0; **^{19}F-NMR** (376 MHz, CD_3OD) δ -74.4 (d, $^1J_{F\text{-}P}$ = 708 Hz); **^{31}P-NMR** (162 MHz, CD_3OD) δ -141.7 (sep., $^1J_{P\text{-}F}$ = 708 Hz); **MS** (ESI +ve) *m/z* 477.1267 ($[M]^{2+}$, $C_{44}H_{56}O_2N_6{}^{127}I_2$, calc. 477.1272). $[\alpha]_D^{25}$ -3.0 (c 0.31, acetonitrile).

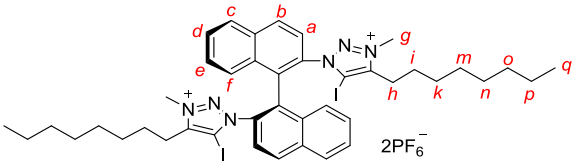
2,2'-Disubstituted (*S*)-BINOL Flexible Dicationic XB Receptor 4.2I



Same methylation procedure as that described for receptor **4.1I**. Reagents: neutral compound **4.6I** (52 mg, 0.056 mmol) and trimethyloxonium tetrafluoroborate (18 mg, 0.12 mmol) in dry dichloromethane (2 mL). Purification by preparatory TLC (5 % methanol in dichloromethane) and anion exchange with a PF_6^- -loaded Amberlite™ afforded the product as a pale yellow sticky solid (49 mg, 71 %). **^{1}H-NMR** (400 MHz, d_6-acetone) δ 8.27 (2H, d, ^3J = 9.1 Hz, H_a), 8.07 (2H, d, ^3J = 8.2 Hz, H_c), 8.02 (2H, d, ^3J = 9.0 Hz, H_b), 7.50 (2H, t, ^3J = 7.5 Hz, H_d), 7.29 (2H, t, ^3J = 7.5 Hz, H_e), 6.75 (2H, d, ^3J = 8.6 Hz, H_f), 5.56 (4H, m, H_g), 4.51 (4H, m, H_i), 3.73 (6H, s, H_h), 1.89 (4H, m, H_k),1.24-1.32 (20H, m, $H_{m\text{-}q}$), 0.85 (6H, t, ^3J = 6.8 Hz, H_r); **^{13}C-NMR** (100 MHz, d_6-acetone) 154.0, 144.3, 134.2, 131.8, 131.5, 129.6, 128.1, 126.1, 125.6, 122.4,

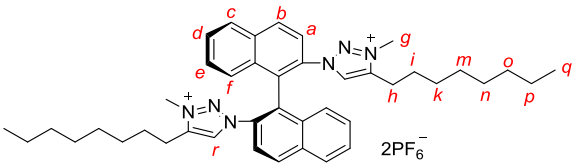
119.0, 91.3, 62.2, 55.7, 39.0, 32.5, 29.4, 26.6, 23.3, 14.4; **^{19}F-NMR** (376 MHz, d_6-acetone) δ -72.7 (d, $^{1}J_{F\text{-}P}$ = 707 Hz); **^{31}P-NMR** (162 MHz, d_6-acetone) δ -148.8 (sep., $^{1}J_{P\text{-}F}$ = 707 Hz); **MS** (ESI +ve) *m/z* 477.1267 ([M]$^{2+}$, $C_{44}H_{56}O_2N_6{}^{127}I_2$, calc. 477.1272); $[\alpha]_D^{25}$ +8.2 (c 0.10, acetone).

2,2'-Iodotriazolium (*S*)-BINOL Dicationic XB Receptor 4.3I



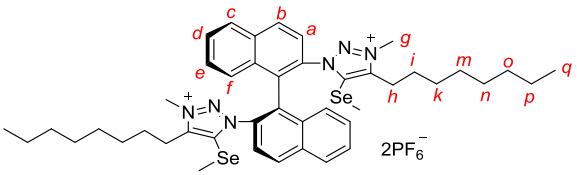
Methylation procedure as described for **4.1I**. Reagents: compound **4.7I** (62 mg, 0.072 mmol) with trimethyloxonium tetrafluoroborate (23 mg, 0.16 mmol) in dry dichloromethane (2 mL). Purification by preparatory TLC (4 % methanol in dichloromethane), and anion exchange performed by repeated washing a chloroform solution (30 mL) of the purified compound with 0.1 M NH_4PF_6 (aq.) (8 x 10 mL) followed by water (2 x 10 mL). Drying the organic phase with $MgSO_4$ and solvent removal *in vacuo* gave the target compound as a pale yellow solid (60 mg, 71 %). **^{1}H-NMR** (400 MHz, d_6-acetone) δ 8.54 (2H, d, ^{3}J = 8.9 Hz, H_a), 8.28 (2H, d, ^{3}J = 8.2 Hz, H_c), 8.04 (2H, d, ^{3}J = 8.9 Hz, H_b), 7.82 (2H, t, ^{3}J = 7.6 Hz, H_d), 7.65 (2H, t, ^{3}J = 7.6 Hz, H_e), 7.49 (2H, d, ^{3}J = 8.4 Hz, H_f), 4.05 (6H, s, H_g), 2.92 (4H, m, H_h), 1.49 (4H, m, H_i), 1.20-1.34 (20H, m, $H_{k\text{-}p}$), 0.89 (6H, t, ^{3}J = 7.2 Hz, H_q); **^{13}C-NMR** (100 MHz, d_6-acetone) δ 149.7, 135.2, 133.6, 132.8, 130.4, 130.0, 129.8, 129.7, 128.1, 124.9, 93.2, 39.2, 32.6, 29.8, 29.7, 27.8, 25.0, 23.4, 14.4; **^{19}F-NMR** (376 MHz, d_6-acetone) δ -72.7 (d, $^{1}J_{F\text{-}P}$ = 707 Hz); **^{31}P-NMR** (162 MHz, d_6-acetone) δ -144.4 (sep., $^{1}J_{P\text{-}F}$ = 707 Hz); **MS** (ESI +ve) *m/z* 447.1173 ([M]$^{2+}$, $C_{42}H_{52}N_6{}^{127}I_2$, calc. 447.1166); $[\alpha]_D^{25}$ +2.8 (c 0.10, acetone).

2,2'-Prototriazolium (*S*)-BINOL Dicationic HB Receptor 4.3H



Identical methylation procedure as that for **4.1I**. Reagents: **4.7H** (27 mg, 0.044 mmol) with trimethyloxonium tetrafluoroborate (14 mg, 0.097 mmol) in dry dichloromethane (2 mL). Purification by preparatory TLC (4 % methanol in dichloromethane) and anion exchange by washing with 0.1 M NH_4PF_6 (aq.) as described for receptor **4.3I** gave the product as a pale yellow solid (29 mg, 71 %). **^{1}H-NMR** (400 MHz, d_6-acetone) δ 8.65 (2H, s, H_r), 8.54 (2H, d, ^3J = 9.2 Hz, H_a), 8.29 (2H, d, ^3J = 8.2 Hz, H_c), 8.00 (2H, d, ^3J = 9.2 Hz, H_b), 7.81 (2H, t, ^3J = 7.6 Hz, H_d), 7.62 (2H, t, ^3J = 7.6 Hz, H_e), 7.42 (2H, d, ^3J = 8.6 Hz, H_f), 4.15 (6H, s, H_g), 2.81 (4H, m, H_h), 1.54 (4H, m, H_i), 1.19-1.31 (20H, m, H_{k-p}), 0.88 (6H, t, ^3J = 7.0 Hz, H_q); **^{13}C-NMR** (100 MHz, d_6-acetone) δ 146.3, 135.3, 133.6, 133.3, 133.2, 130.4, 130.2, 130.1, 130.0, 128.3, 127.4, 123.3, 38.4, 32.6, 29.8, 27.5, 23.5, 23.4, 14.4; **^{19}F-NMR** (376 MHz, d_6-acetone) δ -72.7 (d, $^1J_{F-P}$ = 707 Hz); **^{31}P-NMR** (162 MHz, d_6-acetone) δ -144.4 (sep., $^1J_{P-F}$ = 707 Hz); **MS** (ESI +ve) *m/z* 321.2199 ($[M]^{2+}$, $C_{42}H_{54}N_6$, calc. 321.2200); $[\alpha]_D^{25}$ -2.6 (c 0.10, acetone).

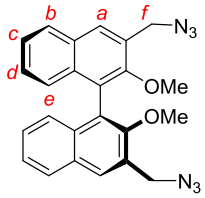
2,2'-Methylseleno-triazolium (*S*)-BINOL Dicationic ChB Receptor 4.3Se



Identical methylation procedure as that for **4.1I**. Reagents: **4.7Se** (45 mg, 0.056 mmol) with trimethyloxonium tetrafluoroborate (18 mg, 0.12 mmol) in dry dichloromethane (1.5 mL). Crude product was found to be very clean and hence no further purification was necessary. Anion exchange by washing with 0.1 M NH_4PF_6 (aq.) as described for receptor **4.3I** yielded **4.3Se** as a pale yellow solid (55 mg, 87 %). **^{1}H-NMR** (400 MHz, d_6-acetone) δ 8.49 (2H, d, ^3J = 8.8 Hz, H_a), 8.27 (2H, d, ^3J = 8.3 Hz, H_c), 7.95 (2H, d, ^3J = 8.8 Hz, H_b), 7.81 (2H, t, ^3J = 7.6 Hz, H_d), 7.63 (2H, t, ^3J = 7.6 Hz, H_e), 7.49 (2H, d, ^3J = 8.3 Hz, H_f), 4.08 (6H, s, H_g), 2.94 (4H, t, ^3J = 7.9

Hz, H_h), 2.52 (6H, s, SeCH_3), 1.48 (4H, m, H_i), 1.16-1.33 (20H, m, H_{k-p}), 0.89 (6H, t, ^3J = 7.0 Hz, H_q); **^{13}C-NMR** (100 MHz, d_6-acetone) δ 150.1, 135.4, 133.9, 132.8, 132.7, 132.0, 130.4, 130.2, 130.1, 129.9, 127.9, 124.9, 39.2, 32.8, 30.0, 29.9, 28.2, 24.6, 23.5, 14.6, 12.2; **^{19}F-NMR** (376 MHz, d_6-acetone) δ -72.7 (d, $^1J_{F\text{-}P}$ = 707 Hz); **^{31}P-NMR** (162 MHz, d_6-acetone) δ -144.4 (sep., $^1J_{P\text{-}F}$ = 707 Hz); **^{77}Se-NMR** (95 MHz, d_6-acetone) δ 105.0; **MS** (ESI +ve) *m/z* 415.1540 ([M]$^{2+}$, $C_{44}H_{58}N_6{}^{80}Se_2$, calc. 415.1521); $[\alpha]_D^{25}$ +4.4 (c 0.10, acetone).

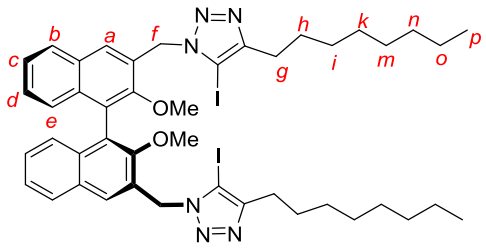
(*S*)-BINOL 3.3'-Disubstituted Bis-azide 4.4



(S)-BINOL 3,3'-bis-alcohol[26] (1.2 g, 3.2 mmol) was dissolved in dichloromethane (10 mL) and chilled to 0 ^oC. Triethylamine (1.78 mL, 12.8 mmol) was added dropwise with stirring, followed by methanesulfonyl chloride (0.62 mL, 8.0 mmol). After stirring the reaction overnight at room temperature, TLC analysis revealed complete consumption of the bis-alcohol starting material, and hence the reaction was quenched with 1 M HCl (30 mL) and stirred for a further 15 minutes. The aqueous and organic layers were separated, and the aqueous layer was extracted with ethyl acetate (4 x 30 mL). The combined organics were dried with brine and anhydrous $MgSO_4$, before the solvent was removed to afford the bis-mesylate intermediate as a yellow viscous oil which was used immediately without further purification. The product was taken up in DMSO (20 mL), and sodium azide (1.04 g, 16.0 mmol) was added slowly over 5 minutes, followed by 0.2 mL of water. After stirring overnight at room temperature under N_2, water (20 mL) and ethyl acetate (20 mL) were added to the reaction mixture and vigorously stirred till both organic and aqueous layers turned clear. Separation of both layers was followed by extraction of the aqueous layer with ethyl acetate (4 x 20 mL). The combined organic layer was washed with brine (3 x 20 mL) and dried with $MgSO_4$. Following solvent removal, purification by silica gel chromatography (25 % ethyl acetate in hexane) afforded **4.4**

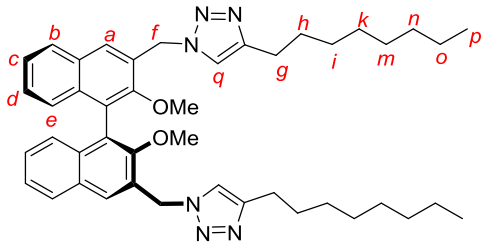
as a sticky white solid (1.02 g, 75 %). **^{1}H-NMR** (400 MHz, $CDCl_3$) δ 8.00 (2H, s, H_a), 7.93 (2H, d, ^{3}J = 6.8 Hz, H_b), 7.45 (2H, t, ^{3}J = 6.8 Hz, H_c), 7.30 (2H, t, ^{3}J = 6.8 Hz, H_d), 7.20 (2H, d, ^{3}J = 6.8 Hz, H_e), 4.68 (4H, m, H_f), 3.31 (6H, s, OCH_3); **^{13}C-NMR** (100 MHz, $CDCl_3$) δ 154.7, 134.4, 130.3, 130.0, 128.9, 128.2, 127.0, 125.7, 125.3, 124.2, 61.0, 50.9; **MS (ESI)** *m/z* calc. for $[M + Na]^+$ = 447.2, found 447.2.

Neutral 3,3'-Substituted XB Receptor Precursor 4.5l



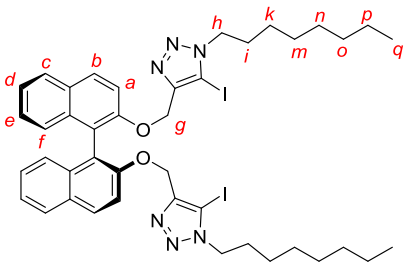
Sodium iodide (264 mg, 1.76 mmol) and copper(II) perchlorate hexahydrate (326 mg, 0.88 mmol) were mixed with acetonitrile/ THF 1:1 (2 mL), before DBU (66 µL, 0.44 mmol), TBTA (10 mg, 0.02 mmol), bis-azide **4.4** (85 mg, 0.20 mmol) and 1-decyne (79 µL, 0.44 mmol) were added sequentially. The reaction was stirred overnight in the dark under N_2, before it was diluted with chloroform (20 mL). The resulting suspension was washed with 10 % aqueous ammonia (2 x 10 mL), and the aqueous layer was back-extracted with chloroform (10 mL). The combined organics were then dried with brine and $MgSO_4$. Following solvent removal *in vacuo*, purification was achieved by silica gel chromatography (2 % methanol in dichloromethane) to afford **4.5l** as a viscous colourless oil (159 mg, 83 %). **^{1}H-NMR** (400 MHz, $CDCl_3$) δ 7.75 (2H, d, ^{3}J = 6.4 Hz, H_b), 7.40 (2H, t, ^{3}J = 6.4 Hz, H_c), 7.27 (4H, m, H_a + H_d), 7.17 (2H, ^{3}J = 6.8 Hz, H_e), 5.89 (4H, m, H_f), 3.30 (6H, s, OCH_3), 2.75 (4H, t, ^{3}J = 6.4 Hz, H_g), 1.76 (4H, m, H_h), 1.28-1.38 (20H, m, H_{i-o}), 0.89 (6H, t, ^{3}J = 5.4 Hz, H_p); **^{13}C-NMR** (100 MHz, $CDCl_3$) δ 153.8, 134.1, 130.3, 128.3, 128.2, 127.1, 125.6, 125.3, 123.8, 77.2, 60.9, 31.9, 29.3, 29.2, 29.1, 28.9, 26.2, 22.7, 14.1; **MS** (ESI +ve) *m/z* 953.2465 ($[M + H]^+$, $C_{44}H_{55}O_2N_6{}^{127}I_2$, calc. 953.2471).

Neutral 3,3'-Substituted HB Receptor Precursor 4.5H



Bis-azide **4.4** (60 mg, 0.14 mmol), 1-decyne (53 µL, 0.30 mmol), $[Cu(CH_3CN)_4]PF_6$ (16 mg, 0.042 mmol), TBTA (7.5 mg, 0.014 mmol) and DIPEA (74 µL, 0.42 mmol) were dissolved in dichloromethane (2 mL). The reaction was reacted for 16 h overnight before being diluted with chloroform (20 mL). The mixture was washed with 10 % aqueous ammonia (10 mL), followed by water (10 mL) and brine (10 mL). After drying with $MgSO_4$, the solvent was removed and purification by silica gel chromatography (3 % methanol in dichloromethane) afforded the product **4.5H** in good purity (64 mg, 65 %) as a viscous colourless oil. **^{1}H-NMR** (400 MHz, $CDCl_3$) δ 7.75 (2H, d, ^3J = 6.8 Hz, H_b), 7.65 (2H, s, H_q), 7.33 (4H, m, H_a + H_c), 7.20 (2H, t, ^3J = 6.8 Hz, H_d), 7.07 (2H, d, ^3J = 6.8 Hz, H_e), 5.64-5.77 (4H, m, H_f), 3.09 (6H, s, OCH_3), 2.66 (4H, t, ^3J = 6.4 Hz, H_g), 1.59 (4H, m, H_h), 1.17-1.28 (20H, m, H_{i-o}), 0.78 (6H, t, ^3J = 6.4 Hz, H_p); **^{13}C-NMR** (100 MHz, $CDCl_3$) δ 154.2, 148.8, 134.3, 130.3, 130.0, 128.4, 128.3, 127.3, 125.5, 125.5, 124.1, 121.1, 60.8, 49.9, 31.8, 29.5, 29.3, 29.2, 25.7, 22.6, 14.1; **MS** (ESI +ve) *m/z* 701.4530 ($[M + H]^+$, $C_{44}H_{57}O_2N_6$, calc. 701.4538).

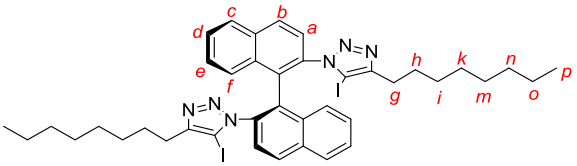
Neutral 2,2'-Substituted Flexible XB Receptor Precursor 4.6I



Sodium iodide (214 mg, 1.43 mmol) was mixed with THF/ acetonitrile 1:1 (4 mL) and copper(II) perchlorate hexahydrate (265 mg, 0.714 mmol) was added. The brown suspension was stirred

for 5 minutes before DBU (0.050 mL, 0.34 mmol), TBTA (9 mg, 0.017 mmol), octyl azide (67 mg, 0.43 mmol) and the (*S*)-BINOL bis-azide precursor (60 mg, 0.17 mmol), synthesised as reported,[27] were added sequentially. After an overnight reaction at room temperature, the reaction was partitioned between 10 % aqueous ammonia (20 mL) and chloroform (30 mL), and the organic layer separated. The aqueous layer was extracted with chloroform (3 x 20 mL) and the combined organics were washed successively with water (20 mL) and brine (20 mL) then dried with $MgSO_4$. Solvent removal then column chromatographic purification (2 % methanol in dichloromethane) isolated target **4.6l** as a very pale yellow sticky liquid. **^{1}H-NMR** (400 MHz, $CDCl_3$) δ 7.95 (2H, d, ^3J = 8.9 Hz, H_a), 7.84 (2H, d, ^3J = 8.1 Hz, H_c), 7.65 (2H, d, ^3J = 8.9 Hz, H_b), 7.30 (2H, t, ^3J = 7.6 Hz, H_d), 7.13 (2H, t, ^3J = 7.5 Hz, H_e), 6.98 (2H, d, ^3J = 8.4 Hz, H_f), 5.02-5.10 (4H, m, H_g), 4.04-4.17 (4H, m, H_h), 1.74 (4H, m, H_i),1.24-1.31 (20H, m, $H_{k\text{-}p}$), 0.85 (6H, t, ^3J = 6.8 Hz, H_q); **^{13}C-NMR** (100 MHz, $CDCl_3$) 154.1, 147.7, 134.7, 130.3, 129.7, 128.0, 126.4, 126.1, 124.2, 121.9, 117.6, 80.5, 64.2, 50.9, 32.0, 30.0, 29.3, 29.2, 26.6, 22.9, 14.4; **MS** (ESI +ve) *m/z* 925.2162 ($[M + H]^+$, $C_{42}H_{51}O_2N_6{}^{127}I_2$, calc. 925.2157).

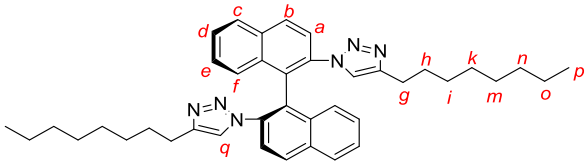
Neutral 2,2'-Iodotriazole XB Receptor Precursor 4.7l



Sodium iodide (150 mg, 1.00 mmol) and copper(II) perchlorate hexahydrate (185 mg, 0.500 mmol) were mixed in THF/ acetonitrile 1:1 (3 mL) before DBU (36 mg, 0.24 mmol), TBTA (3.2 mg, 0.0060 mmol), 1-decyne (0.045 mL, 0.25 mmol) and 2,2'-bis-azido-(S)-BINOL[28] (40 mg, 0.12 mmol) were added portionwise sequentially. Stirring the reaction overnight resulted in a yellow slurry which was diluted with chloroform (30 mL) and washed successively with basic EDTA (2 x 10 mL), water (10 mL), brine (10 mL). After drying the reaction with $MgSO_4$ and solvent removal *in vacuo*, column chromatography (1 % methanol in dichloromethane) afforded the target compound as a pale yellow sticky solid (100 mg, 97 %). **^{1}H-NMR** (400 MHz, $CDCl_3$) δ 8.00 (2H, d, ^3J = 8.8 Hz, H_a), 7.94 (2H, d, ^3J = 8.2 Hz, H_c), 7.52-7.56 (2H, m, H_b),

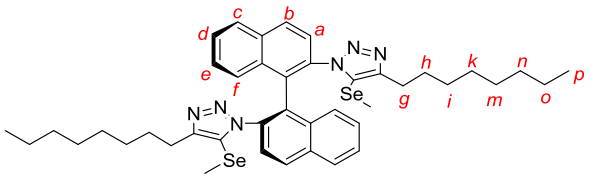
7.42 (2H, d, ^{3}J = 8.8 Hz, H_b), 7.36-7.39 (4H, m, H_e + H_f), 2.47-2.60 (4H, m, H_g), 1.54-1.61 (4H, m, H_h), 1.23-1.31 (20H, m, H_{i-o}), 0.88 (6H, t, ^{3}J = 6.9 Hz, H_p); **^{13}C-NMR** (100 MHz, $CDCl_3$) 151.3, 134.0, 132.7, 132.6, 130.1, 129.2, 128.0, 127.7, 127.0, 126.9, 124.0, 79.8, 31.5, 28.9, 28.8, 28.7, 28.2, 25.8, 22.3, 13.8; **MS** (ESI +ve) *m/z* 865.1945 ($[M + H]^+$, $C_{40}H_{47}N_6{}^{127}I_2$, calc. 865.1946).

Neutral 2,2'-Prototriazole HB Receptor Precursor 4.7H



2,2'-bis-azido-(*S*)-BINOL (40 mg, 0.12 mmol), $[Cu(CH_3CN)_4]PF_6$ (18 mg, 0.048 mmol), TBTA (3.2 mg, 0.0060 mmol), 1-decyne (0.045 mL, 0.25 mmol) and DIPEA (0.062 mL, 0.36 mmol) were dissolved in degassed dichloromethane (3 mL) and left to react under ambient conditions overnight. The reaction was then partitioned between chloroform (20 mL) and basic EDTA solution (10 mL). The organic layer was separated and washed with basic EDTA (10 mL), water (10 mL) and brine (10 mL) before being dried with $MgSO_4$ and dried *in vacuo*. Silica gel column chromatography (2 % methanol in dichloromethane) afforded the target compound as a viscous yellow liquid (59 mg, 81 %). **^{1}H-NMR** (400 MHz, $CDCl_3$) δ 8.07 (2H, d, ^{3}J = 8.3 Hz, H_a), 7.94 (2H, d, ^{3}J = 7.2 Hz, H_c), 7.73 (2H, d, ^{3}J = 8.3 Hz, H_b), 7.52 (2H, t, ^{3}J = 6.5 Hz, H_d), 7.36 (2H, t, ^{3}J = 6.5 Hz, H_e), 7.29 (2H, d, ^{3}J = 8.3 Hz, H_f), 7.23 (2H, s, H_q), 2.45 (4H, t, ^{3}J = 6.2 Hz, H_g), 1.18-1.33 (24H, m, H_{h-o}), 0.90 (6H, t, ^{3}J = 6.2 Hz, H_p); **^{13}C-NMR** (100 MHz, $CDCl_3$) δ 147.3, 134.7, 132.8, 131.9, 130.1, 128.0, 127.5, 127.3, 127.1, 125.8, 122.9, 121.9, 31.6, 28.9, 28.8, 28.7, 28.3, 24.8, 22.4, 13.8; **MS** (ESI +ve) *m/z* 613.4013 ($[M + H]^+$, $C_{40}H_{49}N_6$, calc. 613.4013).

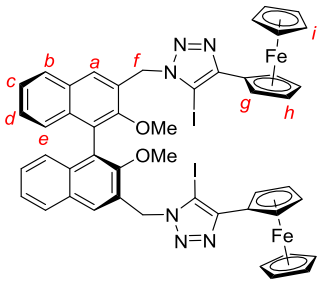
Neutral 2,2'-Methylseleno-triazole ChB Receptor Precursor 4.7Se



Warning: handle with care in fume cupboard due to malodourous nature of Se-containing volatiles formed in this reaction. All glassware in contact with the reaction was deodorized by soaking in bleach for at least 6 hours.

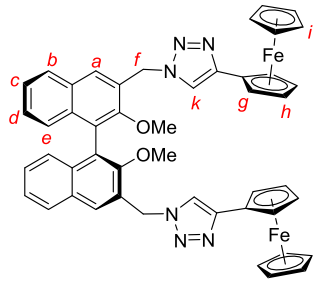
To a microwave vial containing powdered elemental selenium (71 mg, 0.90 mmol) was added a minimum amount of anhydrous THF to fully submerge the selenium. After sealing the vial under N_2, a 1.6 M solution of methyl lithium in hexane (0.56 mL, 0.90 mmol) was added with vigorous stirring at room temperature, whereupon a light brown slurry forms (sonicate if necessary to ensure homogeniety). The slurry was stirred for 30 minutes, before a solution of compound **4.7I** (65 mg, 0.075 mmol) in anhydrous THF (1.5 mL) was added portionwise to afford a dark brown solution, which was stirred at 100 ^{o}C in the dark for 2 days. Thereafter, the reaction was cooled to ambient temperature and iodomethane (0.1 mL) was added. The reaction was stirred vigorously for 30 minutes to form a light brown suspension before being poured into water (20 mL). The aqueous layer was extracted with chloroform (3 x 20 mL) and the combined organics were washed with brine (10 mL) and dried with $MgSO_4$. Solvent removal *in vacuo* and column chromatography (4 % methanol in dichloromethane) afforded the product as a pale yellow paste (45 mg, 75 %). **^{1}H-NMR** (400 MHz, $CDCl_3$) δ 7.95 (2H, d, ^{3}J = 8.9 Hz, H_a), 7.84 (2H, d, ^{3}J = 8.1 Hz, H_c), 7.65 (2H, d, ^{3}J = 8.9 Hz, H_b), 7.30 (2H, t, ^{3}J = 7.6 Hz, H_d), 7.13 (2H, t, ^{3}J = 7.5 Hz, H_e), 6.98 (2H, d, ^{3}J = 8.4 Hz, H_f), 5.02-5.10 (4H, m, H_g), 4.04-4.17 (4H, m, H_h), 1.74 (4H, m, H_i),1.24-1.31 (20H, m, H_{k-p}), 0.85 (6H, t, ^{3}J = 6.8 Hz, H_q); **^{13}C-NMR** (100 MHz, $CDCl_3$) δ 152.0, 134.1, 134.0, 132.9, 130.7, 129.1, 128.5, 127.9, 127.1, 126.9, 124.3, 122.2, 31.9, 29.3, 29.2, 29.1, 25.8, 22.7, 14.1, 9.9; **MS** (ESI +ve) *m/z* 801.2657 ($[M + H]^+$, $C_{42}H_{53}N_6{}^{80}Se_2$, calc. 801.2657).

Neutral Ferrocene XB (*S*)-BINOL Receptor Precursor 4.8I



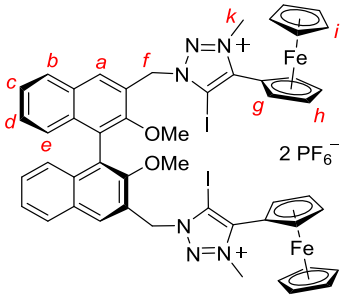
Sodium iodide (145 mg, 0.97 mmol) was mixed with THF/ acetonitrile 1:1 (2 mL) and copper(II) perchlorate hexahydrate (179 mg, 0.48 mmol) was added. The brown suspension was stirred for 5 minutes before DBU (36 µL, 0.24 mmol), TBTA (5.3 mg, 0.01 mmol), ethynylferrocene (50 mg, 0.24 mmol) and the (S)-BINOL bis-azide precursor **4.4** (46 mg, 0.11 mmol) were added sequentially. After an overnight reaction at room temperature, the reaction was partitioned between 10 % aqueous ammonia (20 mL) and chloroform (30 mL), and the organic layer separated. The aqueous layer was extracted with chloroform (3 x 20 mL) and the combined organics were washed successively with water (20 mL) and brine (20 mL) then dried with $MgSO_4$. Column chromatographic purification (1 % methanol in dichloromethane) isolated target **4.8I** as a sticky orange solid (113 mg, 95 %). **^{1}H-NMR** (400 MHz, d_6-acetone) δ 7.88 (2H, d, ^3J = 6.8 Hz, H_b), 7.40-7.44 (4H, m, H_a + H_c), 7.31 (4H, t, ^3J = 6.8 Hz, H_d), 7.17 (2H, ^3J = 6.8 Hz, H_e), 5.98 (4H, m, H_f), 5.10 (4H, m, H_g), 4.38 (4H, m, H_h), 4.14 (10H, s, H_i), 3.46 (6H, s, OCH_3); **^{13}C-NMR** (100 MHz, d_6-acetone) δ 154.1, 149.5, 134.0, 130.4, 129.5, 128.1, 128.1, 126.9, 125.5, 125.3, 124.1, 76.4, 75.6, 69.3, 68.6, 66.8, 60.3, 49.8; **MS** (ESI +ve) *m/z* 1118.9692 ($[M + Na]^+$, $C_{48}H_{38}O_2N_6{}^{56}Fe_2{}^{127}I_2Na$, calc. 1118.9737).

Neutral Ferrocene HB (*S*)-BINOL Receptor Precursor 4.8H



Bis-azide **4.4** (45 mg, 0.11 mmol), 1-decyne (47 mg, 0.22 mmol), $[Cu(CH_3CN)_4]PF_6$ (12 mg, 0.032 mmol), TBTA (5.6 mg, 0.011 mmol) and DIPEA (55 µL, 0.32 mmol) were dissolved in dichloromethane (2 mL). The reaction was reacted for 16 h overnight before being diluted with chloroform (20 mL). The mixture was washed with 10 % aqueous ammonia (10 mL), followed by water (10 mL) and brine (10 mL). After drying with $MgSO_4$, the solvent was removed and purification by silica gel chromatography (2 % methanol in dichloromethane) afforded the product **4.8H** (71 mg, 79 %) as a viscous colourless oil. **^{1}H-NMR** (400 MHz, d_6-DMSO) δ 8.24 (2H, s, H_k), 7.96 (2H, d, ^3J = 6.8 Hz, H_b), 7.87 (2H, s, H_a), 7.45 (4H, t, ^3J = 6.8 Hz, H_c), 7.32 (2H, ^3J = 6.8 Hz, H_d), 7.02 (2H, d, ^3J = 6.8 Hz, H_e), 5.84 (4H, m, H_f), 4.75 (4H, m, H_g), 4.30 (4H, m, H_h), 4.01 (10H, s, H_i), 3.20 (6H, s, OCH_3); **^{13}C-NMR** (100 MHz, d_6-DMSO) δ 154.5, 146.0, 134.1, 130.4, 130.3, 129.9, 128.7, 127.6, 125.9, 125.5, 124.4, 121.9, 76.4, 69.7, 68.8, 66.8, 60.8, 49.9 ; **MS** (ESI +ve) *m/z* 867.1770 ([M + Na]$^+$, $C_{48}H_{40}O_2N_6{}^{56}Fe_2Na$, calc. 867.1804)

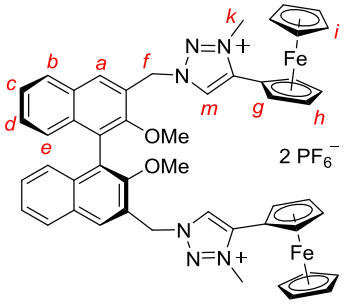
Dicationic Ferrocene XB (*S*)-BINOL Receptor 4.9I



Identical methylation procedure as that for **4.1I**, using **4.8I** (30 mg, 0.027 mmol) and trimethyloxonium tetrafluoroborate (8.4 mg, 0.057 mmol) in dry dichloromethane (1 mL). Purification was achieved by column chromatography (2 % methanol in dichloromethane) using activated Brockmann Grade 1 neutral alumina as the stationary phase. Following anion exchange using a PF_6^--loaded Amberlite™ column (solvent: 100 mL acetone with 0.5 mL water), **4.9I** was obtained as an orange-brown solid (29 mg, 64 %). **^{1}H-NMR** (400 MHz, CD_3CN) δ 7.99 (2H, d, ^3J = 6.8 Hz, H_b), 7.94 (2H, s, H_a), 7.51 (2H, t, ^3J = 6.8 Hz, H_c), 7.39 (2H, t, ^3J = 6.8 Hz, H_d), 7.15 (2H, d, ^3J = 6.8 Hz, H_e), 6.00 (4H, m, H_f), 5.02 (4H, m, H_g), 4.72 (4H, s, H_h), 4.36 (6H, s, H_k), 4.34 (10H, s, H_i), 3.34 (6H, s, OCH_3); **^{13}C-NMR** (100 MHz, CD_3CN) δ

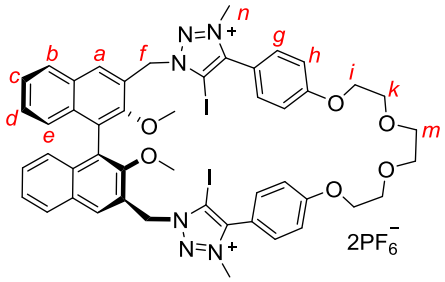
154.6, 147.7, 135.1, 131.4, 130.7, 128.5, 128.4, 126.5, 126.0, 125.9, 124.2, 87.1, 71.9, 70.9, 70.0, 67.0, 61.2, 55.2, 40.7; **^{19}F-NMR** (376 MHz, CD_3CN) δ -72.8 (d, $^1J_{F\text{-}P}$ = 708 Hz); **^{31}P-NMR** (162 MHz, CD_3CN) δ -144.6 (sep., $^1J_{P\text{-}F}$ = 708 Hz); **MS** (ESI +ve) *m/z* 563.0153 ($[M]^{2+}$, $C_{50}H_{44}O_2N_6{}^{127}I_2{}^{56}Fe_2$, calc. 563.0152); $[\alpha]_D^{25}$ -6.3 (c 0.32, CH_3CN).

Dicationic Ferrocene HB (*S*)-BINOL Receptor 4.9H



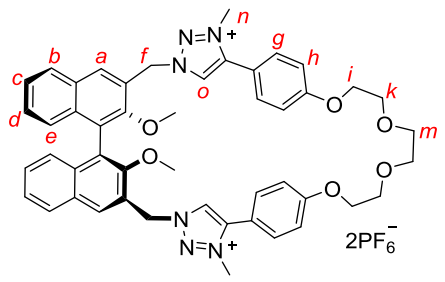
Identical methylation procedure as that for **4.1I**. Reagents: **4.8H** (30 mg, 0.036 mmol) and trimethyloxonium tetrafluoroborate (11 mg, 0.075 mmol) in dry dichloromethane (1 mL). Purification by preparatory TLC (7 % methanol in dichloromethane). Following anion exchange using a PF_6^--loaded Amberlite™ column (solvent: 100 mL acetone with 0.5 mL water), **4.9H** was obtained as an orange solid (31 mg, 75 %). **^{1}H-NMR** (400 MHz, d_6-acetone) δ 8.92 (2H, s, H_m), 8.33 (2H, s, H_a), 8.03 (2H, d, ^3J = 6.8 Hz, H_b), 7.50 (2H, t, ^3J = 6.4 Hz, H_c), 7.36 (2H, t, ^3J = 6.4 Hz, H_d), 7.16 (2H, d, ^3J = 6.4 Hz, H_e), 6.12 (4H, m, H_f), 4.93 (4H, m, H_g), 4.60 (4H, s, H_h), 4.42 (6H, s, H_k), 4.23 (10H, s, H_i), 3.31 (6H, s, OCH_3); **^{13}C-NMR** (100 MHz, d_6-acetone) δ 154.6, 144.3, 135.1, 132.7, 130.3, 128.7, 127.9, 127.3, 125.8, 125.6, 125.4, 123.7, 71.4, 70.2, 68.9, 65.9, 60.3, 54.0, 39.0; **^{19}F-NMR** (376 MHz, d_6-acetone) δ -72.3 (d, $^1J_{F\text{-}P}$ = 708 Hz); **^{31}P-NMR** (162 MHz, d_6-acetone) δ -144.4 (sep., $^1J_{P\text{-}F}$ = 708 Hz); **MS** (ESI +ve) *m/z* 437.1195 ($[M]^{2+}$, $C_{50}H_{46}{}^{56}Fe_2O_2N_6$, calc. 437.1185). $[\alpha]_D^{25}$ -7.6 (c 0.31, CH_3CN).

Dicationic Chiral XB Macrocycle 4.10I



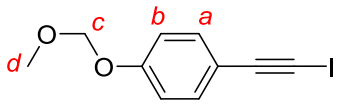
Identical methylation procedure as receptor **4.1I**. Reagents: neutral XB macrocycle **4.14I** (19.0 mg, 0.0185 mmol) and trimethyloxonium tetrafluoroborate (5.7 mg, 0.039 mmol) in dry dichloromethane (1 mL). Solvent removal in vacuo revealed very clean bis-methylation, with no purification necessary. Anion exchange to $2PF_6^-$ salt was performed by washing a chloroform solution of the dicationic macrocycle (30 mL) with 0.1 M aqueous NH_4PF_6 (8 x 10 mL), followed by water (2 x 10 mL). After drying the organic layer with $MgSO_4$, solvent removal in vacuo afforded the desired macrocycle product as a white solid (19 mg, 76 %). **^{1}H-NMR** (400 MHz, d_6-acetone) δ 8.43 (2H, s, H_a), 8.02 (2H, d, ^3J = 8.2 Hz, H_b), 7.47 (2H, t, ^3J = 8.2 Hz, H_c), 7.40 (4H, d, ^3J = 8.8 Hz, H_g), 7.35 (2H, t, ^3J = 8.2 Hz, H_d), 7.14 (2H, d, ^3J = 8.4 Hz, H_e), 7.02 (4H, d, ^3J = 8.8 Hz, H_h), 6.32 (2H, d, ^3J = 14.3 Hz, H_{f1}), 5.88 (2H, d, ^3J = 14.4 Hz, H_{f2}), 4.06 - 4.18 (10H, m, H_i + H_m), 3.79 (4H, t, ^3J = 4.6 Hz, H_j), 3.60 (4H, d, ^3J = 1.0 Hz, H_k), 3.02 (6H, s, OCH_3); **^{13}C-NMR** (100 MHz, d_6-acetone) δ 161.9, 155.2, 146.6, 135.1, 133.8, 131.8, 130.1, 128.8, 128.1, 125.8, 125.5, 125.4, 122.9, 115.7, 114.3, 70.8, 69.1, 68.1, 60.4, 56.2, 38.9; **^{19}F-NMR** (376 MHz, d_6-acetone) δ -72.6 (d, $^1J_{F\text{-}P}$ = 708 Hz); **^{31}P-NMR** (162 MHz, d_6-acetone) δ -144.3 (sep., $^1J_{P\text{-}F}$ = 708 Hz); **MS** (ESI +ve) *m/z* 528.07782 ($[M]^{2+}$, $C_{48}H_{46}O_6N_6{}^{127}I_2$, calc. 528.07786); $[\alpha]_D^{25}$ +68.0 (c 1.00, acetone).

Dicationic Chiral HB Macrocycle Analogue 4.10H



Identical methylation procedure as receptor **4.1I**. Reagents: neutral HB macrocycle 4.14H (15 mg, 0.019 mmol) and trimethyloxonium tetrafluoroborate (5.9 mg, 0.040 mmol) in dry dichloromethane (1 mL). Purification was performed by preparatory TLC (4 % methanol in dichloromethane). Anion exchange to the $2PF_6^-$ salt was performed in an identical manner as macrocycle **4.10I** above to give the target macrocycle as a white solid (19 mg, 91 %). **^{1}H-NMR** (400 MHz, $CDCl_3$) δ 8.51 (2H, s, triazole-*H*), 8.08 (2H, s, H_a), 7.91 (2H, d, ^3J = 8.2 Hz, H_b), 7.46 (2H, d, ^3J = 7.1 Hz, H_c), 7.31 - 7.40 (4H, m, H_d + H_e), 7.16 (4H, d, ^3J = 8.8 Hz, H_g), 6.88 (4H, d, ^3J = 8.8 Hz, H_h), 6.21 (2H, d, ^3J = 14.1 Hz, H_{f1}), 5.51 (2H, d, ^3J = 13.9 Hz, H_{f2}), 4.05 (6H, s, H_m), 3.68 - 3.91 (12H, m, H_i + H_j + H_k), 3.04 (6H, s, OC*H*$_3$); **^{13}C-NMR** (100 MHz, $CDCl_3$) δ 161.6, 155.2, 143.5, 135.1, 133.1, 130.3, 130.1, 128.8, 128.5, 128.0, 126.0, 125.5, 124.4, 123.7, 116.0, 113.3, 71.2, 69.4, 67.9, 61.2, 54.9, 38.3, 29.7; **^{19}F-NMR** (376 MHz, d_6- acetone) δ -72.6 (d., $^1J_{F\text{-}P}$ = 714 Hz); **^{31}P-NMR** (162 MHz, d_6- acetone) δ -144.4 (sep., $^1J_{P\text{-}F}$ = 714 Hz); **MS** (ESI +ve) *m/z* 402.18170 ($[M]^{2+}$, $C_{48}H_{48}O_6N_6$, calc. 402.18122); $[\alpha]_D^{25}$ -4.4 (c 1.00, acetone).

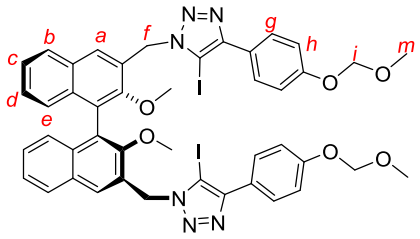
MOM-protected Aryl Iodo-alkyne 4.11I



MOM-protected 4-ethynyl phenol **4.11H** (180 mg, 1.11 mmol), synthesised as described,[29] was dissolved in dry THF (3 mL) and chilled to -78 ^{o}C. A 2.5 M solution of *n*-butyllithium in hexanes (0.67 mL, 1.67 mmol) was added dropwise to give a yellow solution which was stirred at -78 ^{o}C for 1 hour. Thereafter, a solution of iodine (282 mg, 1.11 mmol) in dry THF (1 mL) was added dropwise and the reaction was allowed to slowly warm up to ambient temperature and stirred for a further 2 hours. Diethyl ether (20 mL) was then added and the organic layer washed with saturated aqueous sodium thiosulfate (10 mL), then water (10 mL) and brine (10 mL). Solvent removal gave the product as a yellow solid (318 mg, 99 %) in excellent purity which was used without further purification. **^{1}H-NMR** (400 MHz, $CDCl_3$) δ 7.37 (2H, d, ^3J = 8.4 Hz, H_a), 6.97

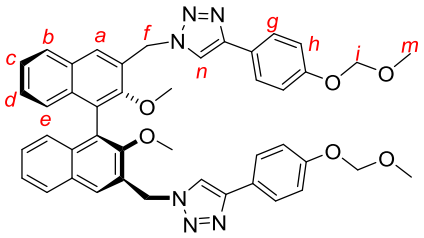
(2H, d, ^{3}J = 8.4 Hz, H_b), 5.18 (4H, s, H_c), 3.48 (6H, s, H_d); **^{13}C-NMR** (100 MHz, $CDCl_3$) δ 157.1, 134.1, 117.1, 116.3, 94.6, 94.1, 56.4, 4.4; **MS** (ESI/ EI/ FI +ve) *not observed*.

MOM-protected Chiral XB Macrocycle Precursor 4.12I



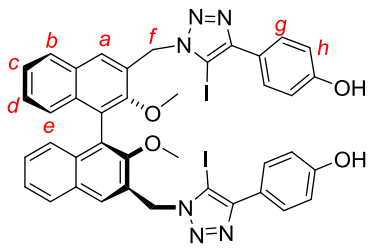
To a suspension of sodium iodide (566 mg, 3.78 mmol) in a THF/ acetonitrile 1.1 (4 mL) was added copper(II) perchlorate hexahydrate (700 mg, 1.89 mmol) and the resulting dark brown suspension was stirred for 5 minutes under N_2. Bis-azide **4.4** (100 mg, 0.236 mmol), TBTA (12.5 mg, 0.0236 mmol), DBU (0.14 mL, 0.94 mmol) and alkyne intermediate **4.11H** (153 mg, 0.944 mmol) were then added successively. The reaction was stirred in the dark for 24 hours at room temperature to result in full consumption of starting materials, and was then partitioned between 10 % aqueous ammonia solution (15 mL) and chloroform (30 mL). The separated organic layer was washed successively with 10 % aqueous ammonia solution (2 x 10 mL) followed by water (10 mL) and brine (20 mL), and then dried with $MgSO_4$. After removal of the solvent, purification by silica gel column chromatography (1 % methanol in dichloromethane) afforded the product as a pale yellow solid (224 mg, 95 %). **^{1}H-NMR** (400 MHz, $CDCl_3$) δ 7.88 - 7.94 (4H, m, H_g), 7.70 (2H, d, ^{3}J = 8.2 Hz, H_b), 7.30 - 7.35 (4H, m, H_a + H_c), 7.20 - 7.25 (2H, m, H_d), 7.07 - 7.14 (6H, m, H_e + H_h), 5.90 (4H, s, H_f), 5.17 (4H, s, H_i), 3.45 (6H, s, H_m), 3.27 (6H, s, OCH_3); **^{13}C-NMR** (100 MHz, $CDCl_3$) δ 157.6, 153.8, 150.0, 154.1, 130.3, 128.8. 128.4, 128.3, 127.2, 125.6, 125.4, 123.9, 123.8, 116.8, 94.4, 77.2, 76.4, 61.0, 56.1, 50.2; **MS** (ESI +ve) *m/z* 1001.10144 ($[M + H]^+$, $C_{44}H_{39}O_6N_6{}^{127}I_2$, calc. 1001.10150).

MOM-protected Chiral HB Macrocycle Precursor 4.12H



To a solution of bis-azide **4.4** (100 mg, 0.235 mmol) and aryl alkyne **4.11H** (80 mg, 0.493 mmol) in degassed dichloromethane (3 mL) were added $[Cu(CH_3CN)_4]PF_6$ (17.5 mg, 0.047 mmol) and DIPEA (0.12 mL, 0.705 mmol) successively. After stirring overnight under N_2 at room temperature, the reaction was diluted with chloroform (30 mL) and washed with an aqueous solution of basic EDTA (3 x 10 mL). The aqueous layer was back-extracted with chloroform (10 mL) and the combined organics were dried with brine (20 mL) and $MgSO_4$. Silica gel column chromatography (4 % methanol in dichloromethane) afforded the pure product as a pale yellow solid (168 mg, 95 %).**^{1}H-NMR** (400 MHz, $CDCl_3$) δ 7.81 - 7.89 (6H, m, H_a + H_b + H_n), 7.78 (4H, d, ^3J = 8.7 Hz, H_g), 7.44 (2H, t, ^3J = 7.5 Hz, H_c), 7.31 (2H, t, ^3J = 7.7 Hz, H_d), 7.19 (2H, d, ^3J = 8.5 Hz, H_e), 7.11 (4H, d, ^3J = 8.7 Hz, H_h), 5.93 (2H, d, ^3J = 12.1 Hz, H_{f1}), 5.83 (2H, d, ^3J = 12.1 Hz, H_{f2}), 5.22 (4H, s, H_i), 3.51 (6H, s, H_m), 3.21 (6H, s, OCH_3). **^{13}C-NMR** (100 MHz, $CDCl_3$) δ 157.3, 154.2, 147.9, 134.4, 130.3, 130.1, 128.4, 128.3, 127.4, 126.9, 125.6, 125.5, 124.5, 124.2, 119.3, 116.6, 94.4, 61.0, 56.1, 50.1; **MS** (ESI +ve) *m/z* 749.30811 ($[M + H]^+$, $C_{44}H_{41}O_6N_6$, calc. 749.30821).

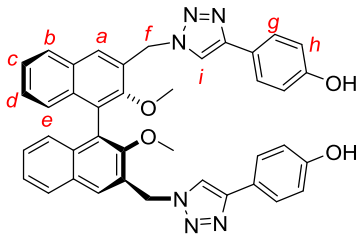
Bis-phenol Chiral XB Macrocycle Precursor 4.13I



To a 1:1 mixture of methanol and dichloromethane (10.0 mL) chilled to 0 °C was added acetyl chloride (0.81 mL, 11.4 mmol) dropwise, whereupon the reaction was warmed up to room temperature and stirred for 15 minutes. Compound **4.12I** (380 mg, 0.380 mmol) was then

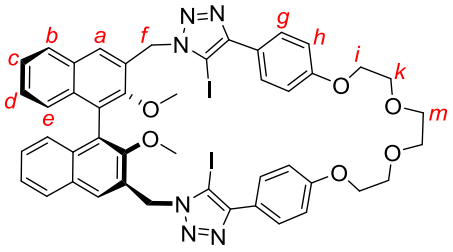
added portionwise and the reaction was stirred for 2 hours. Solvent removal *in vacuo* afforded the product as a beige solid (346 mg, quantitative) in good purity, and was used without further purification. **^{1}H-NMR** (400 MHz, CD_3OD) δ 7.89 (2H, d, ^3J = 8.2 Hz, H_b), 7.74 (4H, d, ^3J = 8.1 Hz, H_g), 7.68 (2H, s, H_a), 7.43 (2H, m, H_c), 7.31 (2H, m, H_d), 7.16 (2H, d, ^3J = 8.6 Hz, H_e), 6.94 (4H, d, ^3J = 8.1 Hz, H_h), 6.01 (4H, s, H_f), 3.32 (6H, br. s., OCH_3); **MS** (ESI +ve) *m/z* 935.03058 ($[M + Na]^+$, $C_{40}H_{30}O_4N_6{}^{127}I_2Na$, calc. 935.03101).

Bis-phenol Chiral HB Macrocycle Precursor 4.13H



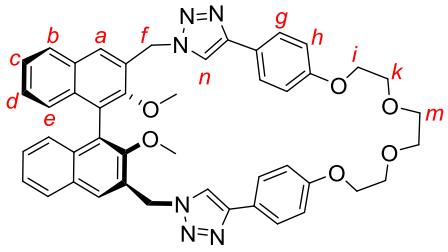
Identical procedure as compound **4.13I**. Reagents: **4.12H** (160 mg, 0.214 mmol), acetyl chloride (0.46 mL, 6.4 mmol) in methanol/dichloromethane 1:1 (5 mL) to obtain the product as a beige solid in good purity (140 mg, quantitative). Product was used in the next step without further purification. **^{1}H-NMR** (400 MHz, CD_3OD) δ 8.59 (2H, s, H_i), 8.17 (2H, s, H_a), 8.01 (2H, d, ^3J = 8.1 Hz, H_b), 7.64 (4H, d, ^3J = 8.7 Hz, H_g), 7.49 (2H, t, ^3J = 8.1 Hz, H_c), 7.35 (2H, t, ^3J = 8.1 Hz, H_d), 7.15 (2H, d, ^3J = 8.1 Hz, H_e), 6.91 (4H, d, ^3J = 8.7 Hz, H_h), 6.00 (4H, s, H_f), 3.21 (6H, s, OCH_3). **MS** (ESI +ve) *m/z* 661.25592 ($[M + H]^+$, $C_{40}H_{33}O_4N_6$, calc. 661.25578.

Neutral Chiral XB Macrocycle 4.14I



Macrocycle precursor **4.13I** (340 mg, 0.373 mmol), triethylene glycol-bis-tosylate **2.3** (171 mg, 0.373 mmol) and anhydrous cesium carbonate (608 mg, 1.87 mmol) were mixed together and suspended in dry degassed DMF (37 mL). The reaction was vigorously stirred under N_2 overnight at 70 ^{o}C and DMF was removed on the rotary by azeotroping with toluene. Chloroform (40 mL) was added to the residue and the suspension washed with water (2 x 20 mL). The aqueous layer was back-extracted with chloroform (2 x 10 mL) and the combined organics dried with brine (20 mL) and $MgSO_4$. Purification of the crude reaction mixture by silica gel column chromatography (30 % ethyl acetate in dichloromethane) afforded the target macrocycle as a white solid (107 mg, 28 %). **^{1}H-NMR** (400 MHz, $CDCl_3$) δ 8.10 (2H, s, H_a), 7.85 (2H, d, ^{3}J = 8.1 Hz, H_b), 7.54 - 7.60 (4H, m, H_g), 7.36 (2H, t, ^{3}J = 6.8 Hz, H_c), 7.22 (3H, t, ^{3}J = 6.8 Hz, H_d), 7.13 (2H, d, ^{3}J = 8.4 Hz, H_e), 6.80 - 6.87 (4H, m, H_h), 5.90 (2H, d, ^{3}J = 14.1 Hz, H_{f1}), 5.39 (2H, d, ^{3}J = 14.2 Hz, H_{f2}), 4.05 - 4.12 (4H, m, H_i), 3.79 - 3.85 (4H, m, H_k), 3.68 (4H, s, H_m), 2.77 (6H, s, OCH_3); **^{13}C-NMR** (100 MHz, $CDCl_3$) δ 159.1, 155.0, 149.5, 134.8, 132.2, 129.9, 129.1, 128.3, 127.7, 127.2, 125.5, 125.1, 123.3, 123.1, 114.7, 71.0, 69.7, 67.6, 60.2, 51.9; **MS** (ESI +ve) *m/z* 1049.09619 ($[M + Na]^+$, $C_{46}H_{40}O_6N_6{}^{127}I_2Na$, calc. 1049.09909).

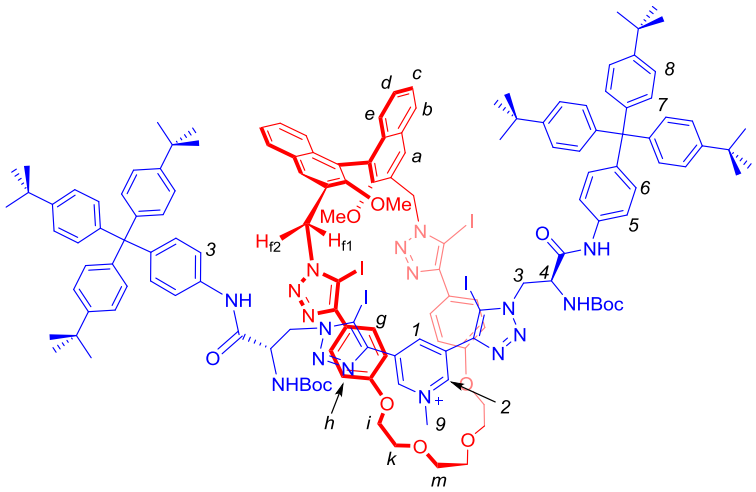
Neutral Chiral HB Macrocycle Analogue 4.14H



Identical procedure as macrocycle **4.14I**. Reagents: precursor compound **4.13H** (158 mg, 0.239 mmol), triethylene glycol-bis-tosylate **2.3** (110 mg, 0.239 mmol) and anhydrous cesium carbonate (389 mg, 1.20 mmol) in dry degassed DMF (24 mL). Purification by silica gel column chromatography (40 % ethyl acetate in dichloromethane), followed by preparatory TLC (2 % methanol in dichloromethane) afforded the target macrocycle as a white solid (47 mg, 25 %). **^{1}H-NMR** (400 MHz, $CDCl_3$) δ 8.12 (2H, s, H_a), 7.85 (2H, d, ^{3}J = 8.1 Hz, H_b), 7.75 (2H, s, H_n), 7.53 (4H, d, ^{3}J = 8.7 Hz, H_g), 7.37 (2H, t, ^{3}J = 7.6 Hz, H_c), 7.24 (2H, t, ^{3}J = 7.6 Hz, H_d),

7.14 (2H, d, ^{3}J = 8.4 Hz, H_e), 6.81 (4H, d, ^{3}J = 8.7 Hz, H_h), 5.59 - 5.72 (4H, m, H_f), 4.02 - 4.07 (4H, m, H_i), 3.76 - 3.81 (4H, m, H_k), 3.65 (4H, s, H_m), 2.90 (6H, s, OCH_3). **^{13}C-NMR** (100 MHz, $CDCl_3$) δ 158.9, 155.0, 147.6, 134.7, 132.3, 130.3, 128.4, 127.6, 127.5, 126.8, 125.6, 125.5, 124.0, 123.6, 119.6, 115.3, 71.0, 69.7, 67.8, 60.6, 51.1,; **MS** (ESI +ve) *m/z* 797.30560 ([M + H]$^+$, $C_{46}H_{42}O_6N_6Na$, calc. 797.30580.

Macrocycle- and Axle-chiral Monocationic XB [2]Rotaxane 4.15



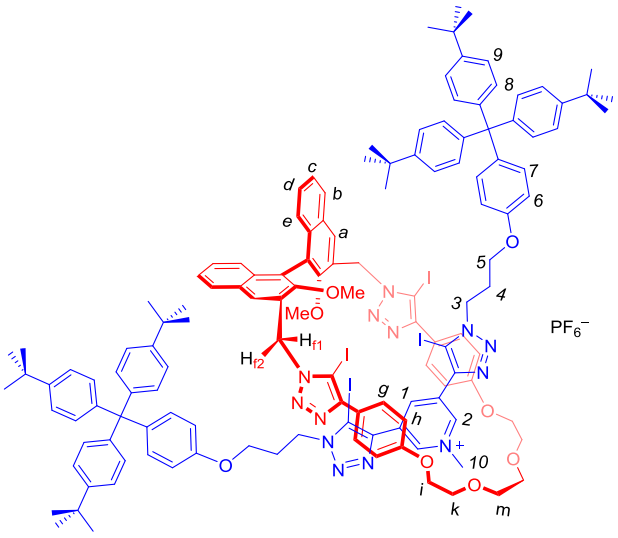
Neutral chiral macrocycle **4.14I** (18 mg, 0.018 mmol) and $[Cu(CH_3CN)_4]PF_6$ (6.7 mg, 0.018 mmol) were dissolved in dry thoroughly-degassed dichloromethane (1.8 mL) under N_2 and stirred for 5 minutes. Pyridine-3,5-bis(iodoalkyne) (27 mg, 0.072 mmol) and chiral stopper azide **4.20** (103 mg, 0.144 mmol) were then added portionwise successively under N_2 before the reaction was left to stir for 3 days under N_2 at room temperature. After complete consumption of starting materials was observed by TLC and ESI-MS, basic EDTA (10 mL) was added to the reaction mixture and vigorously stirred for 15 minutes. Following which, chloroform (20 mL) was added and the aqueous and organic layers were separated. The organic layer was washed with the same basic aqueous EDTA solution (10 mL), followed by water (20 mL) and dried with $MgSO_4$. Evaporation of the solvent on a rotary evaporator afforded the crude rotaxane as a brown solid. The desired rotaxane was isolated by preparatory TLC (2.5 % methanol in dichloromethane) to obtain the *neutral* rotaxane **4.21** as a

white powder (24 mg, 48 %). **MS** (ESI +ve) *m/z* 2837.84592 ($[M + H]^+$, $C_{145}H_{158}O_{12}N_{17}{}^{127}I_4$, calc. 2837.84827).

*Note: Due to the possibility of multiple coordination environments between the macrocycle and axle components in slow exchange, well-defined ^1H NMR spectra could not be obtained and assigned unambiguously for neutral rotaxane **4.21**.*

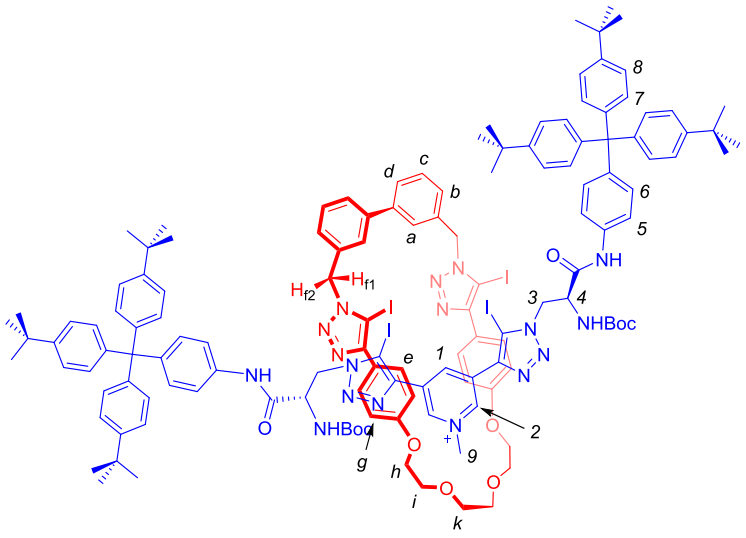
Subsequently, the purified neutral rotaxane **4.21** (17 mg, 6.0 μmol) was dissolved in dry dichloromethane (1 mL) and iodomethane (0.1 mL) was added portionwise. The reaction was stirred at room temperature for 2 days to afford the mono-methylated rotaxane as the major product. Further purification by preparatory TLC (4 % methanol in dichloromethane) afforded the pure mono-cationic rotaxane product. Anion exchange was performed by washing a chloroform solution of the purified rotaxane (20 mL) with 0.1 M NH_4PF_6 (aq.) (10 x 10 mL), followed by water (2 x 10 mL). Removal of solvent afforded rotaxane **4.15** as its PF_6^- salt as a white solid (14 mg, 78 %). **^{1}H-NMR** (500 MHz, d_6-acetone) δ 9.37 (2H, br. s., stopper-N*H*CO), 9.08 (2H, s, H_2), 8.53 (1H, s, H_1), 8.24 (2H, s, H_a), 7.76 (2H, d, ^3J = 7.2 Hz, H_b), 7.41 (4H, d, ^3J = 7.8 Hz, H_5), 7.28 (4H, d, ^3J = 8.5 Hz, H_g), 7.23 (2H, t, ^3J = 7.2 Hz, H_c), 7.15-7.19 (14H, m, H_7 + H_d), 6.98-7.01 (20H, m, H_6 + H_8 + H_e), 6.67 (2H, br. s., N*H*Boc), 6.14 (4H, d, ^3J = 8.5 Hz, H_h), 5.93 (2H, d, ^3J = 14.6 Hz, H_{f1}), 5.24 (2H, d, ^3J = 14.6 Hz, H_{f2}), 4.72-4.88 (6H, m, H_3 + H_4), 4.62 (3H, s, H_9), 3.95 (4H, m, H_i), 3.79-3.82 (8H, m, H_k + H_m), 3.23 (6H, s, BINOL-OC*H*$_3$), 1.29 (18H, s, Boc-^{t}Bu), 1.15 (54H, s, stopper-^{t}Bu); **^{13}C-NMR** (125 MHz, d_6-acetone) δ 167.3, 158.4, 155.1, 148.4, 146.7, 144.1, 143.1, 140.7, 136.3, 135.0, 133.8, 131.2, 130.5, 130.2, 128.4, 127.8, 127.3, 127.0,125.5, 124.3, 123.7, 122.4, 119.1, 119.0, 113.5, 79.6, 71.0, 69.8, 67.7, 63.3, 61.2, 54.6, 54.4, 52.1, 50.7, 48.8, 34.0, 34.0, 31.7, 30.8, 27.7; **^{19}F-NMR** (470 MHz, d_6-acetone) δ -72.7 (d, $^1J_{F\text{-}P}$ = 706 Hz); **^{31}P-NMR** (202 MHz, d_6-acetone) δ -144.3 (sep., $^1J_{P\text{-}F}$ = 706 Hz); **MS** (ESI +ve) *m/z* 2581.85874 ($[M]^+$, $C_{146}H_{160}O_{12}N_{17}{}^{127}I_4$, calc. 2581.85874); $[\alpha]_D^{25}$ -19.7 (c 1.00, acetone).

Macrocycle-chiral Monocationic XB [2]Rotaxane 4.16



Mono-methylation of neutral rotaxane **4.22** (15 mg, 5.8 µmol) was achieved as described previously by stirring the rotaxane with iodomethane (0.1 mL) in dry dichloromethane (1 mL) for 2 days at room temperature. Purification using TLC (3 % methanol in dichloromethane) and anion exchange by washing a chloroform solution (20 mL) of the purified rotaxane with 0.1 M NH_4PF_6 (as described for rotaxane **4.15**) gave the target rotaxane as a white solid (12 mg, 76 %). **^{1}H-NMR** (500 MHz, $CDCl_3$) δ 9.04 (2H, s, H_2), 8.78 (1H, s, H_1), 8.18 (2H, s, H_a), 7.92 (2H, d, ^{3}J = 8.3 Hz, H_b), 7.38 (2H, t, ^{3}J = 8.3 Hz, H_c), 7.30 (4H, d, ^{3}J = 8.8 Hz, H_g, 7.19 - 7.26 (14H, m, H_8 + H_d), 7.04 - 7.09 (18H, m, H_7 + H_9 + H_e), 6.68 (4H, d, ^{3}J = 8.8 Hz, H_6), 6.21 (4H, d, ^{3}J = 8.8 Hz, H_h), 5.87 (2H, d, ^{3}J = 14.0 Hz, H_{f1}), 5.11 (2H, d, ^{3}J = 14.0 Hz, H_{f2}), 4.64 (3H, s, H_{10}), 4.47 - 4.66 (4H, m, H_3), 3.84 - 4.04 (16H, m, H_5 + H_i + H_k + H_m), 3.30 (6H, s, BINOL-OCH_3), 2.43 (4H, m, H_4), 1.29 (54H, s, stopper-^{t}Bu); **^{13}C-NMR** (125 MHz, $CDCl_3$) δ 157.3, 155.3, 153.7, 147.4, 146.0, 143.0, 139.6, 139.0, 134.1, 132.7, 132.5, 131.3, 129.7, 128.9, 127.4, 126.6, 125.8, 125.7, 124.6, 123.0, 122.1, 120.8, 112.4, 112.0, 74.9, 70.1, 68.9, 66.5, 63.1, 62.0, 60.1, 51.2, 48.2, 47.3, 37.8, 33.3, 30.3, 28.7; **^{19}F-NMR** (376 MHz, $CDCl_3$) δ -72.8 (d, $^{1}J_{F-P}$ = 705 Hz); **^{31}P-NMR** (162 MHz, $CDCl_3$) δ -144.4 (sep., $^{1}J_{P-F}$ = 705 Hz); **MS** (ESI +ve) *m/z* 2595.73976 ($[M]^+$, $C_{136}H_{144}O_8N_{13}{}^{127}I_4$, calc. 2595.74676); $[\alpha]_D^{25}$ -4.2 (c 0.50, acetone).

Axle-chiral Monocationic XB [2]Rotaxane 4.17

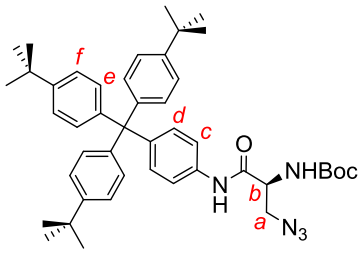


Active metal template synthesis of the neutral rotaxane precursor **4.28** was performed as described for **4.21** (see synthesis of **4.15**), where the achiral XB macrocycle **4.27** (25 mg, 0.029 mmol), $[Cu(CH_3CN)_4]PF_6$ (10.8 mg, 0.029 mmol), pyridine-3,5-bis(iodoalkyne) (44 mg, 0.12 mmol) and chiral axle azide precursor **4.20** (165 mg, 0.231 mmol) were reacted as a solution in dry degassed dichloromethane (2.9 mL) for 3 days under N_2 at room temperature. Following de-complexation of Cu(I) using basic EDTA, preparatory TLC (2.5 % methanol in dichloromethane) afforded neutral rotaxane **4.28** as a yellow solid (32 mg, 42 %). **MS** (ESI +ve) *m/z* 2677.78807 ($[M + H]^+$, $C_{135}H_{150}O_{10}N_{17}{}^{127}I_4$, calc. 2677.79584). Multiple conformations in slow exchange between the axle and macrocycle components of the rotaxane prevented ^1H NMR characterisation of **4.28**.

Following which, mono-methylation of neutral rotaxane **4.28** (30 mg, 0.011 mmol) was achieved with iodomethane (0.1 mL) in dry dichloromethane (1.0 mL) after 2 days at room temperature. Purification by preparatory TLC (4 % methanol in dichloromethane), followed by anion exchange using 0.1 M NH_4PF_6 (aq.) as previously described afforded mono-cationic rotaxane **4.17**, as its PF_6^- salt, as a yellow solid (20 mg, 63 %). **^{1}H-NMR** (500 MHz, d_6-acetone) δ 9.51 (2H, br.s., stopper-N*H*CO), 9.07 (2H, s, H_2), 8.20 (1H, s, H_1), 7.81 (2H, d, ^3J = 7.2 Hz, H_b), 7.74 (2H, s, H_a), 7.59-7.67 (8H, m, H_c + H_d + H_5), 7.24 (12H, d, ^3J = 8.6 Hz, H_7), 7.21 (4H, d, ^3J = 8.1 Hz, H_e), 7.15 (4H, d, ^3J = 8.4 Hz, H_6), 7.07 (12H, d, ^3J = 8.6 Hz, H_8), 6.82

(d, 2H, ^{3}J = 8.1 Hz, N*H*Boc), 6.27 (4H, d, ^{3}J = 8.1 Hz, H_g), 5.81 (2H, d, ^{3}J = 14.5 Hz, H_{f1}), 5.68 (2H, d, ^{3}J = 14.5 Hz, H_{f2}), 5.03 (2H, m, H_4), 4.83-4.95 (4H, m, H_3), 4.77 (3H, s, NCH_3), 3.99-4.08 (4H, m, H_h), 3.87-3.92 (8H, m, H_i + H_k), 1.51 (18H, s, Boc-^{t}Bu), 1.26 (54H, s, stopper-^{t}Bu); **^{13}C-NMR** (125 MHz, d_6-acetone) δ 167.2, 158.5, 155.3, 148.4, 147.9, 144.1, 144.0, 143.3, 141.7, 141.4, 140.5, 136.1, 135.9, 131.3, 130.5, 130.2, 129.8, 129.7, 128.4, 128.3, 127.1, 124.2, 122.3, 119.1, 113.3, 79.6, 76.5, 70.7, 69.6, 67.6, 63.3, 54.6, 54.5, 53.9, 51.3, 49.1, 34.0, 30.7, 27.8; **^{19}F-NMR** (470 MHz, d_6-acetone) δ -72.7 (d, $^{1}J_{F\text{-}P}$ = 706 Hz); **^{31}P-NMR** (202 MHz, d_6-acetone) δ -144.3 (sep., $^{1}J_{P\text{-}F}$ = 706 Hz); **MS** (ESI +ve) *m/z* 2691.80298 ($[M]^+$, $C_{136}H_{152}O_{10}N_{17}{}^{127}I_4$, calc. 2691.81149; $[\alpha]_D^{25}$ -19.0 (c 1.00, acetone).

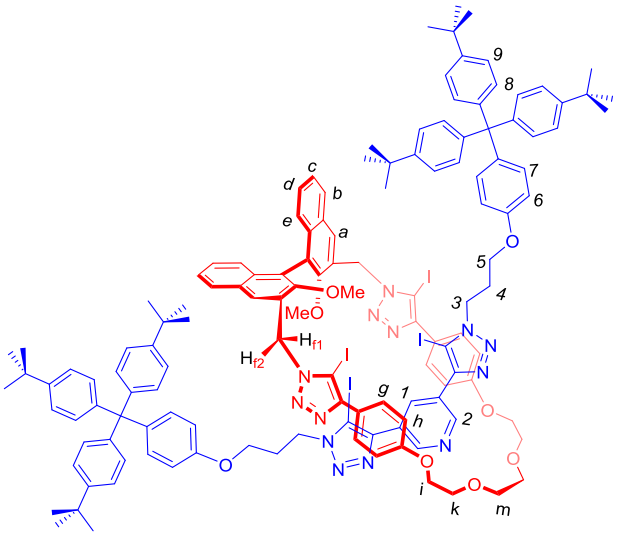
Chiral Stoppered Azide Axle Precursor 4.20



Azide **4.19**[30] (300 mg, 1.30 mmol) and stopper aniline[31] (761 mg, 1.43 mmol), hydroxybenzotriazole (HOBt) (264 mg, 1.95 mmol) and DMAP (32 mg, 0.261 mmol) were mixed together in dry THF (15 mL) and cooled to 0 ^{o}C before ethylcarbodiimide hydrochloride (EDC·HCl) (262 mg, 1.37 mmol) was added portionwise. After stirring at 0 ^{o}C for 10 minutes, the reaction was warmed up to room temperature and left to react for 2 days, whereupon the initially cloudy suspension turned into a clear. The solvent was then removed and taken up in chloroform (50 mL). The organic mixture was washed sequentially with water (2 x 20 mL), then dried with brine (20 mL) and $MgSO_4$. Purification of the crude mixture by column chromatography (dichloromethane) yielded the desired product as a pale yellow solid (679 mg, 73 %). **^{1}H-NMR** (400 MHz, $CDCl_3$) δ 8.02 - 8.14 (1H, br. S, amide-N*H*CO-), 7.31 (2H, d, ^{3}J = 8.7 Hz, H_c), 7.16 (6H, d, ^{3}J = 8.6 Hz, H_e), 7.10 (2H, d, ^{3}J = 8.8 Hz, H_d), 7.01 (6H, d, ^{3}J = 8.6 Hz, H_f), 4.26 - 4.35 (1H, m, H_b), 3.86 - 3.92 (1H, m, H_{a1}), 3.50 - 3.56 (1H, m, H_{a2}), 1.41 (9H, s, Boc-

^{t}Bu), 1.23 (27H, s, stopper-^{t}Bu); **^{13}C-NMR** (100 MHz, $CDCl_3$) δ 167.6, 155.8, 148.4, 144.1, 143.8, 134.7, 131.9, 130.7, 124.2, 118.9, 63.4, 51.8, 34.3, 31.4, 28.3; **MS** (ESI +ve) *m/z* 738.43536 ([M + Na]$^+$, $C_{45}H_{57}O_3N_5Na$, calc. 738.43536). $[\alpha]_D^{25}$ -6.3 (c 1.00, acetone).

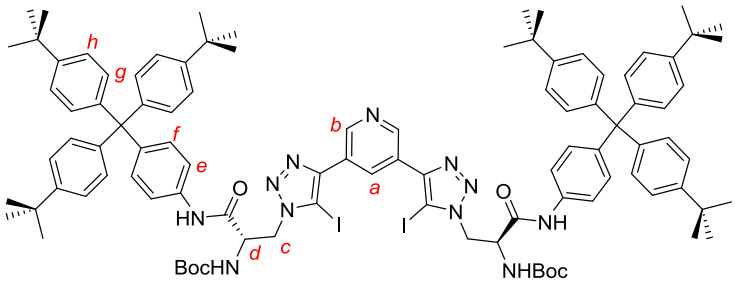
Neutral Chiral Rotaxane Precursor 4.22



Macrocycle **4.14I** (20 mg, 0.0195 mmol) was mixed with $[Cu(CH_3CN)_4]PF_6$ (7.3 mg, 0.0195 mmol) under N_2 and dissolved in thoroughly-degassed dichloromethane (2 mL). Pyridine-3,5-bis(iodoalkyne) (29.6 mg, 0.0780 mmol) and achiral propyl-spacered stopper azide **2.10** (92 mg, 0.156 mmol) were then added under N_2 and the reaction stirred for 3 days under N_2 at room temperature where complete consumption of axle precursors were seen from TLC analysis. The reaction was then quenched with basic EDTA (10 mL) before chloroform (20 mL) was added. The organic layer was separated and washed successively with basic EDTA (10 mL) and water (2 x 10 mL) and dried with $MgSO_4$. Purification by preparatory TLC (eluent: 2 % methanol in dichloromethane) afforded the neutral rotaxane **4.22** as a pale yellow solid (15 mg, 30 %). **^{1}H-NMR** (400 MHz, $CDCl_3$) δ 9.28 (2H, s, H_2), 8.91 (1H, s, H_1), 8.22 (2H, s, H_a), 7.94 (2H, d, ^{3}J = 8.2 Hz, H_b), 7.39- 7.44 (6H, m, H_c + H_g), 7.20-7.25 (14H, m, H_d + H_8), 7.05-7.12 (18H, m, H_9 + H_7 + H_e), 6.74 (4H, d, ^{3}J = 8.8 Hz, H_6), 6.52 (4H, d, ^{3}J = 8.8 Hz, H_h), 5.82 (2H, d, ^{3}J = 14.0 Hz, H_{f1}), 5.17(2H, d, ^{3}J = 14.0 Hz, H_{f2}), 4.19 (4H, m, H_3), 3.76 - 4.06 (16H, m, H_5 + H_i + H_k + H_m), 3.07 (6H, s, BINOL-OC*H*$_3$), 1.97 (4H, quint., ^{3}J = 6.0 Hz, H_4), 1.30 (54H, s,

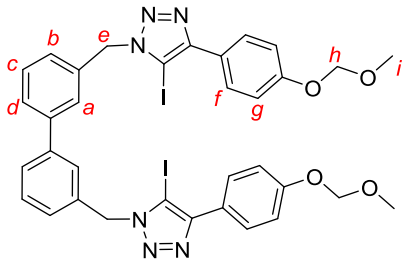
stopper-^{t}Bu); **^{13}C-NMR** (125 MHz, $CDCl_3$) δ 158.5, 156.4, 154.7, 148.3, 148.0, 147.9, 145.9, 144.1, 144.0, 139.9, 135.1, 134.0, 132.3, 130.7, 130.0, 128.4, 127.5, 127.2, 126.9, 125.9, 125.6, 125.4, 124.1, 122.9, 121.8, 114.4, 113.1, 79.0, 70.4, 69.4, 67.3, 64.4, 63.1, 60.7, 51.6, 48.0, 34.3, 31.4, 28.6; **MS** (ESI +ve) *m/z* 2581.73087 ([M + H]$^+$, $C_{135}H_{142}O_8N_{13}{}^{127}I_4$, calc. 2581.73087); $[\alpha]_D^{25}$ -17.4 (c 1.00, $CHCl_3$).

Neutral Free Chiral Axle 4.23



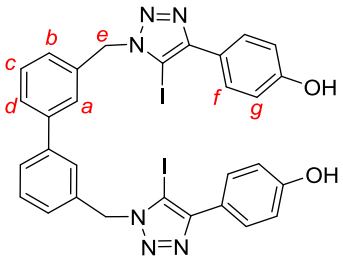
The neutral chiral axle were isolated as a side product from the active metal template synthesis of neutral chiral rotaxanes **4.21** and **4.28** (syntheses described as part of cationic rotaxanes **4.15** and **4.17** respectively) from the respective preparatory TLC plates as a white solid. **^{1}H-NMR** (400 MHz, d_6-acetone) δ 9.56 (2H, br. s., stopper-amide), 9.20 (2H, s, H_b), 8.90 (1H, s, H_a), 7.57 (4H, d, ^3J = 8.4 Hz, H_e), 7.31 (12H, d, ^3J = 8.6 Hz, H_g), 7.12-7.16 (16H, m, H_f + H_h), 6.53 (2H, d, ^3J = 8.6 Hz, N*H*Boc), 4.87-5.08 (6H, m, H_c + H_d), 1.33 (18H, s, *N*Boc-^{t}Bu-*H*), 1.30 (54H, s, stopper-^{t}Bu); **^{13}C-NMR** (100 MHz, d_6-acetone) δ 167.1, 155.1, 148.3, 147.4, 146.3, 144.1, 143.1, 136.3, 131.8, 130.5, 124.3, 118.9, 80.2, 79.3, 63.3, 54.7, 51.6, 33.9, 30.8, 27.6; **MS** (ESI +ve) *m/z* 1811.73324 ([M + H]$^+$, $C_{99}H_{118}O_6N_{11}{}^{127}I_2$, calc. 1811.73840).

MOM-protected Achiral XB Macrocycle Precursor 4.25



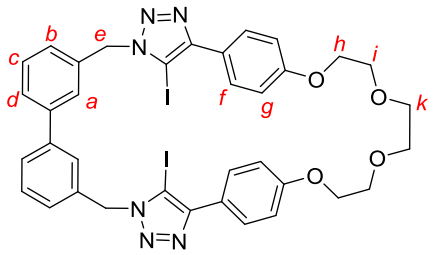
A mixture of achiral biphenyl bis-azide synthon **4.24** (75 mg, 0.284 mmol), prepared as reported,[32] and sodium iodide (510 mg, 3.40 mmol) were suspended in THF/ acetonitrile 1:1 (2.0 mL), and copper(II) perchlorate hexahydrate (630 mg, 1.70 mmol) was added portionwise to the reaction, whereupon a dark brown slurry was obtained. After stirring for 5 minutes, TBTA (7.5 mg, 0.014 mmol), DBU (0.13 mL, 0.851 mmol) and intermediate **4.11H** (138 mg, 0.851 mmol) were added successively. The reaction mixture was then left to stir in the dark under N_2 for 2 days, before being quenched by the addition of 10 % aqueous ammonia solution (10 mL) and chloroform (10 mL) and stirred for 15 minutes to obtain a biphasic mixture. The organic layer was separated from the aqueous layer and further diluted with chloroform (20 mL) before being washed with 10 % aqueous ammonia (2 x 10 mL) and water (10 mL). After drying the organic layer with brine and $MgSO_4$, the solvent was removed on a rotary evaporator to afford a light brown sticky paste. Purification via column chromatography (10 % ethyl acetate in dichloromethane) then afforded the product as a pale beige solid (121 mg, 51 %). **^{1}H-NMR** (400 MHz, $CDCl_3$) δ 7.88 (4H, d, ^3J = 8.4 Hz, H_f), 7.49 - 7.56 (4H, m, H_a + H_b), 7.44 (2H, t, ^3J = 7.5 Hz, H_c), 7.34 (2H, d, ^3J = 7.6 Hz, H_d), 7.13 (4H, d, ^3J = 8.4 Hz, H_g), 5.71 (4H, s, H_e), 5.23 (4H, s, H_h), 3.50 (6H, s, H_i); **^{13}C-NMR** (100 MHz, $CDCl_3$) δ 157.6, 141.1, 135.0, 129.5, 128.7, 127.3, 127.2, 126.8, 123.8, 116.2, 94.4, 56.1, 54.3, 31.6; **MS** (ESI +ve) *m/z* 841.04877 ($[M + H]^+$, $C_{34}H_{31}O_4N_6{}^{127}I_2$, calc. 841.04907).

Bis-phenol Achiral XB Macrocycle Precursor 4.26



Identical MOM-deprotection procedure as that for **4.13I**. Reagents: compound **4.25** (105 mg, 0.125 mmol) and acetyl chloride (0.27 mL, 3.8 mmol) in a 1:1 mixture of methanol and dichloromethane (5 mL). Solvent removal afforded the target compound as a light brown solid in excellent purity (94 mg, quantitative) which was used without further purification. **^{1}H-NMR** (400 MHz, CD_3OD) δ 7.70 (4H, d, ^{3}J = 7.4 Hz, H_f), 7.57 - 7.62 (4H, m, H_a + H_b), 7.48 (2H, t, ^{3}J = 7.7 Hz, H_c), 7.31 (2H, d, ^{3}J = 7.7 Hz, H_d), 6.90 (4H, d, ^{3}J = 7.4 Hz, H_g), 5.80 (4H, s, H_e); **MS** (ESI +ve) *m/z* 774.97809 ($[M + Na]^+$, $C_{30}H_{22}O_2N_6{}^{127}I_2Na$, calc. 774.97858).

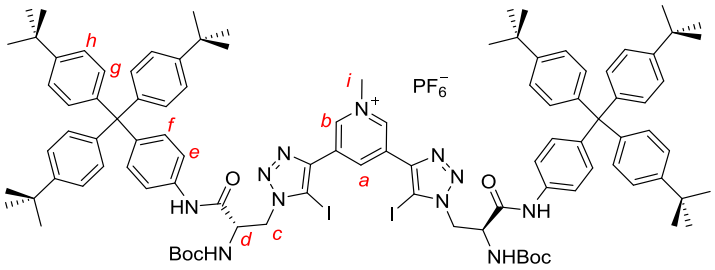
Neutral Achiral XB Macrocycle 4.27



Identical macrocycle ring-closing procedure as that described for **4.14I**. Reagents: precursor compound **4.26** (100 mg, 0.133 mmol), triethylene glycol-bis-tosylate **2.3** (61 mg, 0.133 mmol), cesium carbonate (217 mg, 0.665 mmol) in dry degassed DMF (13 mL). Purification by column chromatography (2 % methanol in dichloromethane) gave the target macrocycle as a white solid (34 mg, 30 %). **^{1}H-NMR** (400 MHz, $CDCl_3$) δ 7.80 (4H, d, ^{3}J = 8.7 Hz, H_f), 7.57 (2H, d, ^{3}J = 6.8 Hz, H_b), 7.43 - 7.49 (4H, m, H_c + H_d), 7.40 (2H, s, H_a), 6.95 (4H, d, ^{3}J = 8.7 Hz, H_g), 5.70 (4H, s, H_e), 4.18 (4H, t, ^{3}J = 4.9 Hz, H_h), 3.95 (4H, t, ^{3}J = 4.9 Hz, H_i), 3.80 (4H, s, H_k); **^{13}C-NMR** (100 MHz, $CDCl_3$) δ 159.2, 150.1, 140.6, 135.0, 129.5, 128.6, 127.3, 126.8, 126.7, 122.7,

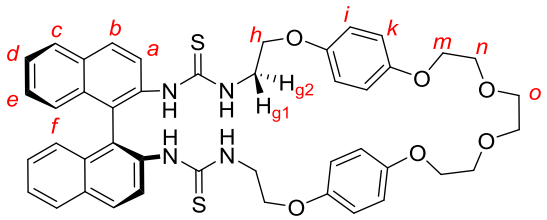
114.6, 76.2, 71.0, 69.6, 67.5, 54.2; **MS** (ESI +ve) *m/z* 867.06470 ($[M + H]^+$, $C_{36}H_{33}O_4N_6{}^{127}I_2$, calc. 867.06472).

Free Chiral XB Monocationic Axle 4.29



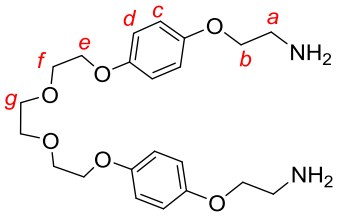
To a dichloromethane solution (1 mL) of the neutral chiral axle **4.23** (40 mg, 0.022 mmol) was added iodomethane (0.1 mL) and the reaction stirred under ambient conditions for 2 days. Thereafter, purification of the crude reaction mixture by preparatory TLC (4 % methanol in dichloromethane) afforded the product as a beige solid. Anion exchange was performed by washing a chloroform solution (30 mL) of the purified mono-cationic axle with 0.1 M NH_4PF_6 (aq.) (10 x 10 mL), followed by water (2 x 10 mL). Drying the organic phase with $MgSO_4$ and solvent removal *in vacuo* afforded the PF_6^- -salt of the axle as a very pale beige solid (35 mg, 80 %). **^{1}H-NMR** (400 MHz, d_6-acetone) δ 9.87 (1H, s, H_a), 9.61 (4H, br.s., H_b + stopper-amide), 7.54 (4H, d, ^3J = 8.2 Hz, H_e), 7.31 (12H, d, ^3J = 8.6 Hz, H_g), 7.12-7.16 (16H, m, H_f + H_h), 6.56 (2H, d, ^3J = 8.6 Hz, N*H*Boc), 5.11-5.16 (2H, m, H_{c1}), 5.01 (2H, m, H_d), 4.90-4.96 (2H, m, H_{c2}), 4.87 (3H, s, H_j), 1.33 (18H, s, Boc-^{t}Bu-*H*), 1.30 (54H, s, stopper-^{t}Bu); **^{13}C-NMR** (100 MHz, d_6-acetone) δ 166.9, 155.2, 148.4, 144.1, 143.2, 142.6, 142.0, 136.2, 131.1, 131.8, 131.2, 130.5, 124.3, 118.9, 83.4, 79.4, 63.3, 54.6, 51.9, 49.3, 34.0, 30.8, 27.7; **MS** (ESI +ve) *m/z* 1825.74980 ($[M]^+$, $C_{99}H_{118}O_6N_{11}{}^{127}I_2$, calc. 1825.75405); $[\alpha]_D^{25}$ -19.9 (c 1.00, acetone).

Chiral Thiourea Macrocycle 4.32



(*S*)-BINOL-2,2'-bis(isothiocyanate) **4.33**[33] (22 mg, 0.060 mmol) and bis-amine **4.34** (25 mg, 0.060 mmol) were mixed together and dissolved in dry dichloromethane (6 mL). After stirring under N_2 for two days, the solvent was removed *in vacuo* and column chromatography (15 % ethyl acetate in dichloromethane) afforded the target macrocycle as a white powder (15 mg, 32 %). **^{1}H-NMR** (400 MHz, $CDCl_3$) δ 7.90-7.95 (4H, m, H_a + H_c), 7.77 (2H, d, ^3J = 8.8 Hz, H_b), 7.48 (2H, t, ^3J = 7.3 Hz, H_d), 7.28 (2H, t, ^3J = 7.2 Hz, H_e), 7.08 (2H, d, ^3J = 8.4 Hz, H_f), 6.68-6.77 (8H, m, H_i + H_k), 4.01 (4H, t, ^3J = 4.7 Hz, H_m), 3.88 (4H, br. m, H_h), 3.78-3.83 (6H, m, H_{g1} + H_n), 3.68 (4H, s, H_o), 3.57-3.62 (2H, br. m, H_{g2}); **^{13}C-NMR** (100 MHz, $CDCl_3$) δ 181.5, 153.3, 152.6, 133.0, 132.0, 129.8, 128.5, 127.4, 126.4, 125.7, 124.9, 115.9, 115.7,70.8, 69.8, 68.3, 66.3, 44.1; **MS** (ESI +ve) *m/z* 789.2773 ($[M + H]^+$, $C_{44}H_{45}O_6N_4{}^{32}S_2$, calc. 789.2775).

Bis-amine Macrocycle Precursor 4.34

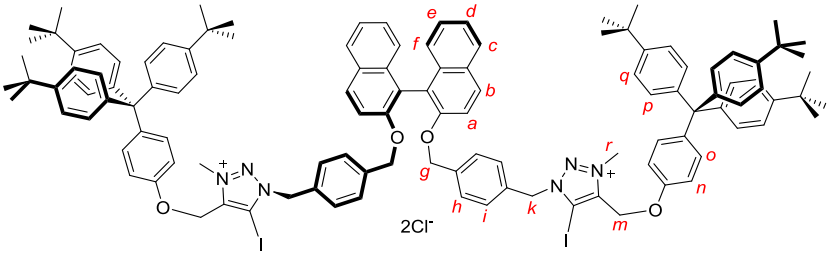


While the analogous compound containing a polyether chain with five oxygen atoms has been reported,[34] *this bis-amine macrocycle precursor, with a four oxygen polyether chain, is novel*.

Bis-azide compound **2.2** (400 mg, 0.847 mmol) was dissolved in methanol (15 mL) at elevated temperatures before 10% by weight Pd/C (70 mg) was added slowly and carefully to the solution. After hydrazine monohydrate (0.40 mL, 8.5 mmol) was added portionwise, the reaction was heated at reflux overnight and left to cool to ambient temperature. Filtration of the crude reaction mixture through a pad of celite, eluting the compound with dichloromethane and

solvent removal *in vacuo* afforded the target bis-amine **4.34** (351 mg, 99 %) in good purity which was used without further purification. **^{1}H-NMR** (400 MHz, $CDCl_3$) δ 6.84 (8H, m, H_c + H_d), 4.09 (4H, t, ^{3}J = 4.8 Hz, H_e), 3.94 (4H, t, ^{3}J = 5.2 Hz, H_b), 3.85 (4H, t, ^{3}J = 4.8 Hz, H_f), 3.75 (4H, s, H_g), 3.06 (4H, t, ^{3}J = 5.2 Hz, H_a), 2.02 (4H, br. s, NH_2); **^{13}C-NMR** (100 MHz, $CDCl_3$) δ 152.9, 152.8, 115.3, 115.1, 70.5, 70.4, 69.6, 67.8, 41.4; **MS** (ESI +ve) *m/z* 421.2332 ($[M + H]^+$, $C_{22}H_{33}O_6N_2$, calc. 421.2333).

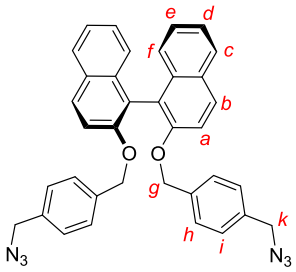
Chloride Salt of Dicationic Bis-iodotriazolium Ditopic Chiral Axle 4.35



To a vigorously-stirred suspension of silver triflate (50 mg, 0.19 mmol) in dry dichloromethane (1 mL) was added iodomethane (0.020 mL, 0.32 mmol) and left to react for 1 hour. The resulting yellow suspension was taken up in a 2 mL syringe and filtered through a syringe filter into a round bottom flask containing a solution of neutral precursor **4.37** (158 mg, 0.083 mmol) in anhydrous dichloromethane (2 mL). After stirring for 2 days at room temperature, TLC analysis showed complete bis-iodotriazole methylation and the volatiles were thus removed *in vacuo* to afford a yellow solid in excellent purity. Anion exchange was performed by dissolving the yellow solid in acetone (50 mL) containing 0.1 mL of water and the solution was passed through a Cl^--loaded Amberlite™ column 5 times to give a pale yellow filtrate. Solvent removal afforded **4.35** as a pale yellow solid (114 mg, 69 %). **^{1}H-NMR** (400 MHz, d_6-acetone) δ 8.02 (2H, d, ^{3}J = 8.9 Hz, H_a), 7.91 (2H, d, ^{3}J = 8.1 Hz, H_c), 7.59 (2H, d, ^{3}J = 9.1 Hz, H_b), 7.19-7.34 (20H, m, H_d + H_e + H_i + H_p); 7.04-7.15 (22H, m, H_f + H_h + H_o + H_q), 6.95 (4H, d, ^{3}J = 9.1 Hz, H_n), 5.89 (4H, s, H_m), 5.41 (4H, s, H_k), 5.14 (4H, s, H_g), 4.53 (6H, s, H_r), 1.26 (54H, s, stopper-^{t}Bu); **^{13}C-NMR** (100 MHz, d_6-acetone) δ 156.5, 155.2, 149.6, 145.3, 144.9, 142.7, 140.4, 135.3, 133.3, 132.1, 131.6, 130.8, 130.6, 129.9, 129.2, 128.6, 127.5, 126.3, 125.4, 124.9,

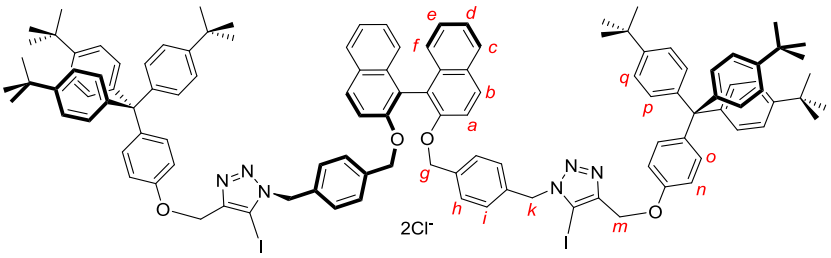
121.4, 116.8, 115.0, 92.0, 71.2, 70.0, 64.2, 55.7, 35.1, 32.3, 31.9; **MS** (ESI +ve) *m/z* 971.84 ($[M]^{2+}$, $C_{118}H_{124}O_4N_6{}^{127}I_2$, calc. 971.89).

(S)-BINOL Bis-azide Synthon 4.36



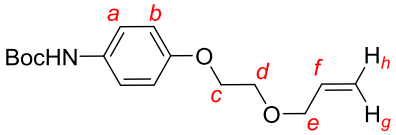
The (*S*)-BINOL bis-bromide precursor (260 mg, 0.399 mmol), synthesised as described,[35] was dissolved in DMSO (6.0 mL) under sonication and heating. After sodium azide (104 mg, 1.0 mmol) was added portionwise, the reaction was heated at 80 ^oC overnight under N_2, and the resulting mixture was then poured into water (30 mL) to afford a white suspension. Diethyl ether (20 mL) was added and stirred till all the white suspension dissolved, whereupon the aqueous and organic layers were separated. The aqueous layer was further extracted with diethyl ether (5 x 20 mL), and the combined organics were dried with brine and $MgSO_4$. The solvent was removed *in vacuo* to afford the product as a sticky white translucent solid (209 mg, 91 %) in good purity, and used directly without further purification. **^{1}H-NMR** (400 MHz, $CDCl_3$) δ 7.96 (2H, d, ^3J = 8.9 Hz, H_a), 7.90 (2H, d, ^3J = 8.2 Hz. H_c), 7.42 (2H, d, ^3J = 8.9 Hz, H_b), 7.36 (2H, m, H_d), 7.20 - 7.26 (4H, m, H_e + H_f), 7.03 (2H, d, ^3J = 8.1 Hz, H_h), 6.94 (4H, d, ^3J = 8.1 Hz, H_i), 5.05 (4H, s, H_g), 4.23 (4H, s, H_k); **^{13}C-NMR** (100 MHz, $CDCl_3$) δ 153.9, 137.7, 134.3, 134.1, 129.5, 129.4, 128.0, 127.9, 127.1, 126.4, 125.5, 123.8, 120.8, 115.9, 70.8, 54.5; **MS** (EI +ve) *m/z* 576.2272 ($[M]^+$, $C_{36}H_{28}O_2N_6$, calc. 576.2274).

Neutral Ditopic Bis-iodotriazole Chiral Axle 4.37



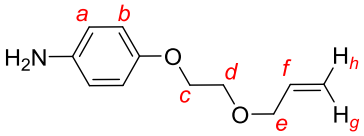
Sodium iodide (229 mg, 1.53 mmol) and copper(II) perchlorate hexahydrate (283 mg, 0.764 mmol) were stirred in THF/ acetonitrile 1:1 (4 mL) for 5 minutes. Bis-azide **4.36** (105 mg, 0.182 mmol), DBU (57 µL, 0.38 mmol), TBTA (9.7 mg, 0.018 mmol) and stopper alkyne **2.11H** (207 mg, 0.382 mmol) were then added sequentially, and the reaction left to stir at room temperature overnight. Thereafter, the reaction was partitioned between aqueous ammonia (20 mL) and chloroform (30 mL), and the separated organic layer was washed sequentially with basic EDTA (20 mL), water (20 mL) and dried with $MgSO_4$. After solvent removal, the crude reaction mixture was purified with a plug of silica (1 % methanol in dichloromethane) to afford the target compound as a pale yellow solid (315 mg, 91 %). **^{1}H-NMR** (400 MHz, $CDCl_3$) δ 7.82 (2H, d, ^{3}J = 8.9 Hz, H_a), 7.77 (2H, d, ^{3}J = 8.2 Hz, H_c), 7.26 (2H, d, ^{3}J = 8.9 Hz, H_b), 7.23 (2H, t, ^{3}J = 6.2 Hz, H_d), 7.14 (12H, d, ^{3}J = 8.5 Hz, H_p), 7.07-7.11 (4H, m, H_e + H_f); 6.98-7.03 (16H, m, H_q + H_i), 6.91 (4H, d, ^{3}J = 8.2 Hz, H_o), 6.77-6.80 (4H, m, H_h + H_n), 5.38 (4H, s, H_m), 4.96 (4H, s, H_k), 4.88 (4H, s, H_g), 1.21 (54H, s, stopper-^{t}Bu); **^{13}C-NMR** (100 MHz, $CDCl_3$) δ 155.9, 153.6, 148.0, 147.5, 143.7, 140.0, 137.7, 133.8, 132.7, 131.9, 130.4, 129.2, 129.1, 127.6, 127.5, 126.8, 126.1, 125.1, 123.7, 123.5, 120.5, 115.6, 113.2, 80.3, 70.4, 62.7, 61.4, 53.6, 33.9, 31.1; **MS** (ESI +ve) *m/z* 1913.7336 ($[M]^{2+}$, $C_{116}H_{119}O_4N_6{}^{127}I_2$, calc. 1913.7377).

4-Allylethoxy-*N*HBoc-aniline 4.38



To a solution of *N*Boc-protected 4-hydroxyaniline (200 mg, 0.96 mmol), synthesised as reported,[36] and allylethoxy tosylate (270 mg, 1.05 mmol) in acetone (5 mL) was added cesium carbonate (623 mg, 1.91 mmol) portionwise. The reaction was heated overnight under reflux, cooled down to room temperature and solvent removed *in vacuo*. The resulting brown solid was then partitioned between chloroform (30 mL) and water (20 mL). The organic layer was separated, washed with water (20 mL), brine (20 mL) and dried with $MgSO_4$. Purification using a silica plug (dichloromethane) afforded the product as sticky pale beige solid (270 mg, 96 %). **^{1}H-NMR** (400 MHz, $CDCl_3$) δ 7.24 (2H, m, H_a), 6.86 (2H, m, H_b), 6.34 (1H, br. s, N*H*Boc), 5.90-5.99 (1H, m, H_f), 5.29-5.34 (1H, m, H_g), 5.20-5.23 (1H, m, H_h), 4.08-4.12 (4H, H_c + H_e), 3.79 (2H, t, ^3J = 4.9 Hz, H_d), 1.51 (9H, s, Boc-^{t}Bu-*H*); **^{13}C-NMR** (100 MHz, $CDCl_3$) δ 155.2, 134.9, 131.9, 120.8, 117.7, 115.4, 72.7, 68.8, 68.1, 54.1, 29.6, 28.7; **MS** (ESI +ve) *m/z* 314.2 ([M + Na]$^+$, $C_{16}H_{21}NO_4Na$, calc. 314.1).

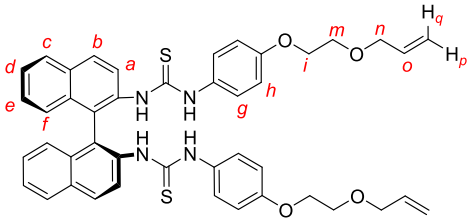
4-Allylethoxy-aniline 4.39



To a solution of compound **4.38** (270 mg, 0.92 mmol) in dichloromethane (1 mL) was added trifluoroacetic acid (0.42 mmol, 5.52 mmol) portionwise and the reaction stirred at room temperature overnight. Saturated aqueous sodium bicarbonate (10 mL) was then added dropwise to the reaction which was stirred till no further effervescence was observed. Following which, dichloromethane (20 mL) was added and the organic layer was separated. This layer was washed successively with saturated aqueous sodium bicarbonate (2 x 10 mL), water (10 mL) and brine (10 mL) before being dried with $MgSO_4$. Solvent was removed to give the product as a light brown oil (163 mg, 92 %) which was used without further purification. **^{1}H-**

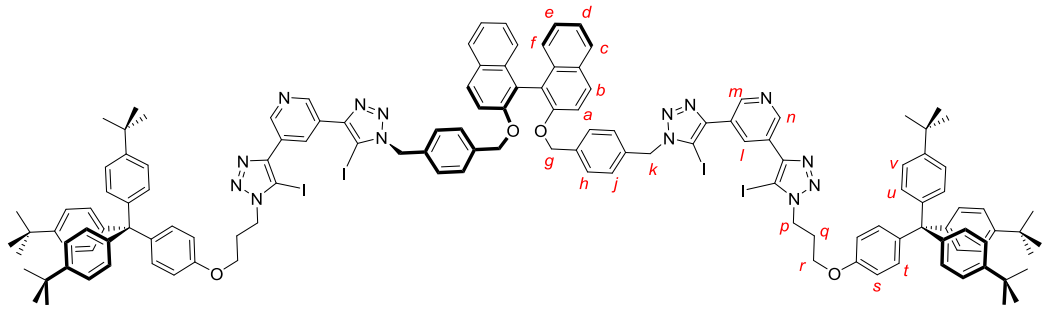
NMR (400 MHz, $CDCl_3$) δ 6.76-6.79 (2H, m, H_b), 6.62-6.65 (2H, m, H_a), 5.90-6.00 (1H, m, H_f), 5.28-5.34 (1H, m, H_g), 5.19-5.22 (1H, m, H_h), 4.06-4.10 (4H, H_c + H_e), 3.77 (2H, t, ^3J = 9.8 Hz, H_d); **MS** (ESI +ve) *m/z* 192.2 ($[M + H]^+$, $C_{11}H_{14}NO_2$, calc. 192.1).

2,2'-(S)-BINOL-Bis(thiourea) Bis-vinyl Macrocycle Precursor 4.40



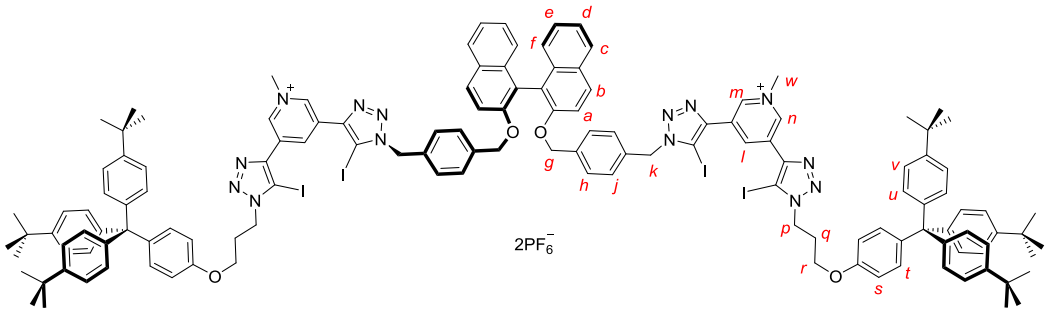
(*S*)-BINOL-2,2'-bis(isothiocyanate) **4.33** (60 mg, 0.163 mmol) and amine **4.39** (63 mg, 0.33 mmol) were dissolved in dichloromethane (2 mL) and left to react overnight. The solvent was removed *in vacuo* and column chromatography (15 % ethyl acetate in dichloromethane) yielded the target compound as a pale yellow solid (98 mg, 80 %). **^{1}H-NMR** (400 MHz, $CDCl_3$) δ 8.12 (2H, d, ^3J = 8.9 Hz, H_a), 7.97-8.01 (4H, m, H_b + H_c), 7.51 (2H, t, ^3J = 7.5 Hz, H_d), 7.37 (2H, s, thiourea-N*H*), 7.33 (2H, s, thiourea-N*H*), 7.27 (2H, t, ^3J = 7.5 Hz, H_e), 7.20 (2H, d, ^3J = 8.4 Hz, H_f), 6.46 (4H, d, ^3J = 8.8 Hz, H_g), 6.15 (4H, d, ^3J = 8.8 Hz, H_h), 5.93-6.02 (2H, m, H_o), 5.32-5.37 (2H, m, H_q), 5.23-5.26 (2H, m, H_p), 4.12 (4H, m, H_n), 4.04 (4H, t, ^3J = 4.8 Hz, H_i), 3.79 (4H, t, ^3J = 4.8 Hz, H_m); **^{13}C-NMR** (100 MHz, $CDCl_3$) δ 180.5, 158.1, 135.9, 134.5, 132.3, 128.2, 128.1, 127.8, 127.5, 127.3, 126.7, 126.3, 125.1, 117.4, 115.6, 72.4, 68.4, 67.6; **MS** (ESI +ve) *m/z* 753.27 ($[M + H]^+$, $C_{44}H_{41}N_4O_4{}^{32}S_2$, calc. 753.26).

Neutral Ditopic Pyridine-3,5-iodotriazole Chiral Axle Precursor 4.41



To a solution of bis-azide **4.36** (27 mg, 0.047 mmol) and stoppered pyridine iodoalkyne **3.31** (95 mg, 0.098 mmol) in dry degassed THF (2 mL) was added $[Cu(CH_3CN)_4]PF_6$ (3.5 mg, 0.0094 mmol) portionwise, and the reaction was stirred under N_2 at room temperature for 48 h. After TLC (5 % methanol in dichloromethane) confirming completion of reaction, basic EDTA (5 mL) was added to the reaction and stirred for 30 minutes. Following which, chloroform (20 mL) was added and the biphasic mixture stirred for 5 minutes before both layers were separated. The organic layer was washed again with the same basic EDTA solution (10 mL), and the aqueous layer was back-extracted with chloroform (3 x 10 mL). Drying the combined organics with $MgSO_4$ and column chromatography purification (5 % methanol in dichloromethane) isolated the neutral axle precursor **4.41** as a white powder (99 mg, 85 %). **^{1}H-NMR** (400 MHz, $CDCl_3$) δ 9.24 (4H, br. s, H_m + H_n), 8.86 (2H, s, H_l), 7.92 (2H, d, ^3J = 9.0 Hz, H_a), 7.86 (2H, d, ^3J = 8.0 Hz, H_c), 7.38 (2H, d, ^3J = 9.0 Hz, H_b), 7.33 (2H, t, ^3J = 7.2 Hz, H_d), 7.17-7.25 (16H, m, H_e + H_f + H_u), 7.08-7.12 (16H, m, H_t + H_v), 7.04 (4H, d, ^3J = 8.1 Hz, H_j), 6.93 (4H, d, ^3J = 8.2 Hz, H_h), 6.78 (4H, d, ^3J = 8.8 Hz, H_s), 5.58 (4H, m, H_k), 5.01 (4H, m, H_g), 4.68 (4H, t, ^3J = 7.0 Hz, H_p), 4.05 (4H, t, ^3J = 5.7 Hz, H_r), 2.46 (4H, quint., ^3J = 6.3 Hz, H_q), 1.30 (54H, s, stopper-^{t}Bu); **^{13}C-NMR** (100 MHz, $CDCl_3$) δ 156.5, 154.2, 148.6, 148.2, 148.1, 147.5, 147.2, 144.4, 140.4, 138.5, 134.4, 133.3, 133.1, 132.6, 131.0, 129.8, 129.7, 128.2, 128.1, 127.5, 126.7, 125.8, 124.4, 124.2, 121.0, 116.1, 113.4, 78.1, 77.5, 71.0, 64.3,63.4, 54.5, 48.5, 34.6, 31.7, 30.0; **MS** (ESI +ve) *m/z* 2509.68213 ($[M + H]^+$, $C_{134}H_{133}O_4N_{14}{}^{127}I_4$, calc. 2509.68075).

Dicationic Pyridinium-3,5-iodotriazole Chiral Axle 4.42 (PF_6^- salt)



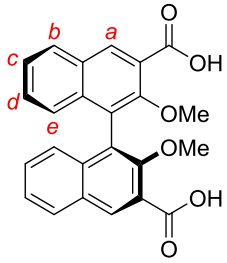
Neutral axle precursor **4.41** (40 mg, 0.016 mmol) was dissolved in dry dichloromethane (0.9 mL) and iodomethane (0.1 mL) was added. The reaction was stirred overnight at room temperature under N_2 to result in bis-methylation, forming a yellow suspension. After removal of the solvent *in vacuo*, the yellow solid was dissolved in chloroform (30 mL), and washed with 0.1 M NH_4PF_6 (aq.) (8 x 10 mL), followed by water (2 x 10 mL). Removal of the solvent *in vacuo* afforded the dicationic axle, as its $2PF_6^-$ salt, as a pale beige solid (29 mg, 70 %). **^{1}H-NMR** (400 MHz, d_6-DMSO) δ 9.52 (4H, br. s, H_m + H_n), 8.20 (2H, s, H_l), 8.02 (2H, d, ^3J = 9.2 Hz, H_a), 7.92 (2H, d, ^3J = 7.9 Hz, H_c), 7.59 (2H, d, ^3J = 8.9 Hz, H_b), 7.20-7.34 (18H, m, H_d + H_e + H_f + H_u), 6.95 - 7.06 (24H, m, H_j + H_k + H_t + H_v), 6.82 (4H, d, ^3J = 8.6 Hz, H_s), 5.70 (4H, br. s, H_k), 5.13 (4H, br.s, H_g), 4.68 (4H, t, ^3J = 7.2 Hz, H_p), 4.51 (6H, pyridinium-CH_3), 4.01 (4H, t, ^3J = 5.6 Hz, H_r), 2.33 (4H, quint., ^3J = 6.2 Hz, H_q), 1.24 (54H, s, stopper-^{t}Bu); **^{19}F-NMR** (376 MHz, d_6-DMSO) δ -70.2 (d, $^1J_{F-P}$ = 710 Hz); **^{31}P-NMR** (162 MHz, d_6-DMSO) δ -144.2 (sep., $^1J_{P-F}$ = 710 Hz); **MS** (ESI +ve) *m/z* 1269.35999 ($[M]^{2+}$, $C_{136}H_{138}O_4N_{14}{}^{127}I_4$, calc. 1269.35966); $[\alpha]_D^{25}$ -2.7 (c 0.10, acetone).

Dicationic Pyridinium-3,5-iodotriazole Chiral Axle 4.42 (Cl^- salt)

A solution of **4.42**, as its $2PF_6^-$ salt, in chloroform was vigorously stirred in the presence of brine (1:1 ratio by volume) for 1 hour. Thereafter, the aqueous and organic layer was separated, and the aqueous layer extracted with chloroform (5 x 20 mL) and dried with $MgSO_4$. Solvent removal afforded the product as a pale beige solid. **^{1}H-NMR** (500 MHz, d_6-DMSO) δ 9.56 (2H, s, H_l), 9.51 (4H, s, H_m + H_n), 8.02 (2H, d, ^3J = 9.2 Hz, H_a), 7.92 (2H, d, ^3J =

7.9 Hz, H_c), 7.59 (2H, d, ^3J = 8.9 Hz, H_b), 7.20-7.34 (18H, m, H_d + H_e + H_f + H_u), 6.96 - 7.05 (24H, m, H_j + H_k + H_t + H_v), 6.80 (4H, d, ^3J = 8.6 Hz, H_s), 5.68 (4H, br. s, H_k), 5.12 (4H, br.s, H_g), 4.67 (4H, t, ^3J = 7.2 Hz, H_p), 4.51 (6H, pyridinium-CH_3), 4.00 (4H, t, ^3J = 5.6 Hz, H_r), 2.32 (4H, quint., ^3J = 6.2 Hz, H_q), 1.23 (54H, s, stopper-^{t}Bu); **^{13}C-NMR** (126 MHz, d_6-DMSO) δ 156.0, 153.5, 147.7, 143.9, 143.2, 142.8, 142.3, 139.1, 137.5, 135.9, 133.9, 133.4, 131.4, 130.5, 130.4, 130.0, 129.3, 128.8, 128.0, 127.4, 127.1, 126.4, 125.5, 124.6, 124.3, 123.6, 121.3, 119.3, 79.2, 69.4, 65.5, 64.1, 62.5, 48.7, 48.0, 34.0, 31.1, 29.1.

(S)-BINOL 3,3'-Dicarboxylic Acid 4.43

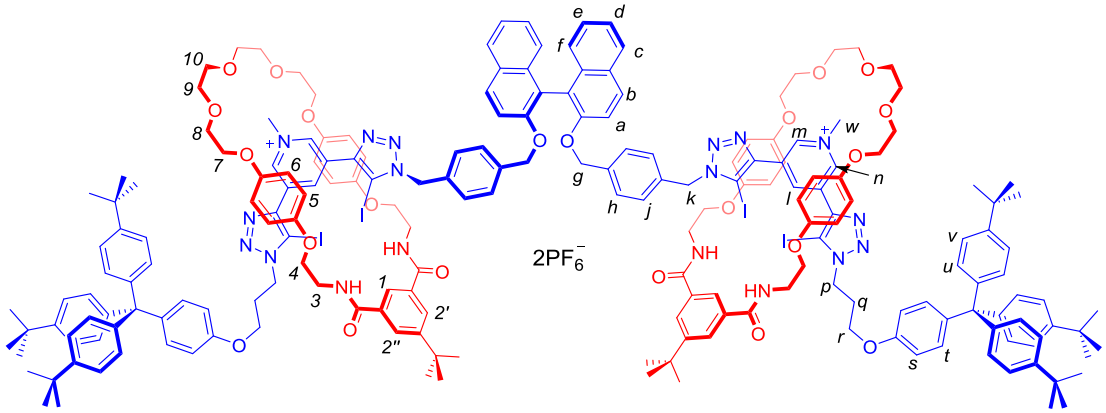


Although prior syntheses of this compound have been reported,[37] *a novel procedure was used in this thesis:*

To a solution of the (*S*)-BINOL bis-aldehyde precursor (220 mg, 0.594 mmol) in acetonitrile (2 mL) was added copper(I) chloride portionwise (29 mg, 0.30 mmol) followed by an aqueous solution (70 % by weight) of *tert*-butyl hydroperoxide (0.72 mL, 5.9 mmol). The reaction was stirred at room temperature for 3 days under N_2, and was then filtered through a plug of celite. After eluting the compound with ethyl acetate, the organic solution was concentrated on a rotary evaporator till c.a. 20 mL of solution was left. This organic solution was washed with 1 M aqueous sodium hydroxide (3 x 10 mL), and the combined aqueous layer was subsequently chilled in an ice bath to 0 ^{o}C and slowly acidified till pH c.a. 1 by slow addition of 10 % HCl (aq.). The resulting cloudy suspension was then extracted with ethyl acetate (4 x 15 mL) and the combined organics were washed with brine (20 mL) and dried with $MgSO_4$. Solvent removal *in vacuo* afforded the target compound as an orange solid (164 mg, 64 %). **^{1}H-NMR** (400 MHz, d_6-acetone) δ 8.64 (2H, s, H_a), 8.10 (2H, d, ^3J = 8.1 Hz, H_b), 7.49 (2H, t, ^3J = 7.4 Hz,

H_c), 7.39 (2H, t, ^3J = 7.4 Hz, H_d), 7.09 (2H, d, ^3J = 8.4 Hz, H_e), 3.49 (6H, s, OCH_3); **^{13}C-NMR** (100 MHz, d_6-acetone) δ 167.6, 155.6, 136.8, 134.5, 130.9, 130.4, 129.7, 127.1, 126.8, 126.5, 126.3, 62.5; **MS** (ESI +ve) *m/z* 425.0 ([M + Na]$^+$, $C_{24}H_{18}NaO_6$, calc. 425.1).

Chiral Dicationic [3]Rotaxane 4.44



To a vigorously-stirred suspension of tert-butyl isophthalic acid (6.1 mg, 0.028 mmol) in dry dichloromethane (0.5 mL) was added 1 drop of dry DMF, followed by oxalyl chloride (6.0 µL, 0.071 mmol). After stirring under N_2 for 2 hours, the solvent was removed from the resulting solution *in vacuo* to afford the bis-acid chloride as an off-white solid, which was used directly without further purification. In a separate vessel, the Cl^- salt of axle **4.42** (30 mg, 0.011 mmol) was dissolved in dry dichloromethane (5 mL) with sonication and dry trimethylamine (15 uL, 0.11 mmol) was added portionwise. The bis-amine macrocycle precursor (13 mg, 0.028 mmol) and the dried bis-acid chloride were dissolved separately in dry dichloromethane (1 mL each) and taken up in separate syringes. The contents of both syringes were then added portionwise to the stirred axle solution, and the reaction was left to stir overnight under N_2. Subsequently, chloroform (20 mL) was added to the reaction and the organic layer was washed with 0.1 M aqueous HCl (5 mL), followed by water (2 x 10 mL). After drying the organic layer with $MgSO_4$, solvent was removed *in vacuo*, and the target [3]rotaxane was isolated using preparatory TLC (4 % methanol in dichloromethane) as a yellow solid. The isolated rotaxane was dissolved in chloroform (30 mL), and washed successively with 0.1 M NH_4PF_6 (aq.) (8 x 10 mL), then water (2 x 10 mL). Drying of the resulting organic layer using $MgSO_4$, followed by solvent removal,

afforded the target rotaxane as a pale beige solid (11 mg, 37 %). **^{1}H-NMR** (500 MHz, $CDCl_3$/ CD_3OD 1:1 *v/v*) δ 9.45 (2H, s, H_m), 9.40 (2H, s, H_n), 8.83 (2H, s, H_l), 8.22 (2H, s, $H_{2''}$), 8.21 (2H, s, $H_{2'}$), 8.17 (2H, s, H_1), 7.65 (2H, d, ^{3}J = 9.0 Hz, H_a), 7.61 (2H, d, ^{3}J = 8.0 Hz, H_c), 7.30 (2H, d, ^{3}J = 8.9 Hz, H_b), 7.15-7.19 (14H, m, H_d + H_u), 7.10 (2H, t, ^{3}J = 7.8 Hz, H_e), 7.04 (4H, d, ^{3}J = 8.8 Hz, H_t), 6.97-7.01 (14H, m, H_f + H_v), 6.96 (4H, d, ^{3}J = 8.2 Hz, H_j), 6.92 (4H, d, ^{3}J = 8.2 Hz, H_h), 6.75 (4H, d, ^{3}J = 8.8 Hz, H_s), 6.01-6.04 (8H, m, H_5), 5.67-5.72 (8H, m, H_6), 5.27 (4H, br. s, H_k), 4.98 (4H, s, H_g), 4.56 (6H, s, H_w), 4.49 (4H, H_p, *obscured by H_2O peak*), 3.68-3.96 (34H, m, H_3 + H_4 + H_7 + H_8 + H_r), 3.51-3.53 (8H, m, H_9), 3.18-3.21 (8H, m, H_{10}), 2.31 (4H, m, H_q), 1.25 (54H, s, stopper-^{t}Bu); **^{13}C-NMR** (126 MHz, $CDCl_3$/ CD_3OD 1:1) δ 168.0, 157.0,154.4, 153.5, 153.1, 152.2, 149.0, 144.8, 143.3, 143.1, 140.8, 139.0, 134.6, 133.9, 133.7, 132.9, 131.3, 131.0, 130.9, 130.1, 130.0, 129.6, 128.8, 128.5, 128.1, 126.8, 125.9, 124.6, 124.3, 123.1, 121.1, 116.1, 115.5, 114.7, 114.6, 113.8, 71.7, 71.5, 71.0, 70.6, 68.2, 66.3, 64.8, 63.7, 54.5, 40.8, 35.6, 34.8, 32.5, 31.8, 31.6, 30.7, 30.2, 29.9; **^{19}F-NMR** (470 MHz, $CDCl_3$/ CD_3OD 1:1) δ -74.1 (d, $^{1}J_{F\text{-}P}$ = 710 Hz); **^{31}P-NMR** (202 MHz, $CDCl_3$/ CD_3OD 1:1) δ -144.5 (sep., $^{1}J_{P\text{-}F}$ = 710 Hz); ; **MS** (ESI +ve) *m/z* 1919.68054 ($[M]^{2+}$, $C_{208}H_{230}O_{22}N_{18}{}^{127}I_4$, calc. 1919.67999).

Tetrabutylammonium (TBA) salts of chiral anions and dicarboxylates

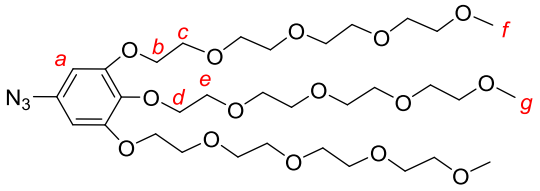
An analogous procedure as adopted as that reported by Dong et. al.[1]

To a chilled solution of the neutral acid (anion precursor) (1.0 eqv) in water/THF 10:1 *v/v* at 0 ^{o}C was added an appropriate stoichiometry of a methanolic solution of tetrabutylammonium (TBA) hydroxide (1.0 eqv for monobasic acids and 2.0 eqv for dibasic acids) over 5 minutes. The resulting reaction was allowed to warm up to ambient temperature and stirred for 3 hours. Following which, the reaction was extracted with dichloromethane (5 x 10 mL). The chiral TBA salt was obtained by removal of solvent *in vacuo* and leaving the salt to dry under high-vacuum for at least 3 days. The salts were stored in a vacuum dessicator with P_2O_5 dessicant at -20 ^{o}C.

7.2.5 Synthesis of Novel Compounds from Chapter 5

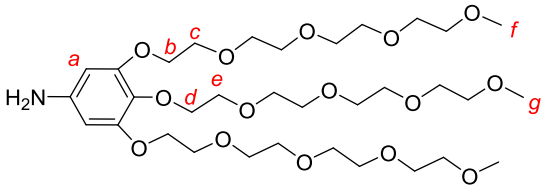
For all compounds in this section, TEG = $(CH_2CH_2O)_4CH_3$

5-azido-1,2,3-tris(tetraethylene glycol methyl ether)benzene 5.1



Aniline **5.3** (500 mg, 0.702 mmol) was dissolved in 25 % sulfuric acid (10 mL) and chilled to 0 ^oC in an ice bath. A saturated solution of sodium nitrite (97.0 mg, 1.40 mmol) was added dropwise and the reaction stirred at 0 ^oC for 1 hour. An aqueous solution of sodium azide (228 mg, 3.51 mmol) was then added carefully dropwise and the reaction was warmed up to ambient temperature and stirred for 4 hours. The dark red aqueous solution was then extracted with chloroform till the organic phase turned colourless. After drying with $MgSO_4$, solvent removal *in vacuo* gave the product as a red-brown liquid in excellent purity, and was used without further purification (492 mg, 95 %). **^{1}H-NMR** (400 MHz, $CDCl_3$) δ 6.26 (2H, s, H_a), 4.12 (4H, t, ^3J = 4.8 Hz, H_b), 4.08 (2H, t, ^3J = 5.1 Hz, H_d), 3.82 (4H, t, ^3J = 5.0 Hz, H_c), 3.76 (2H, t, ^3J = 5.2 Hz, H_e), 3.51-3.71 (36H, m, TEG alkyl-CH_2), 3.36 (s, 9H, H_f + H_g); **^{13}C-NMR** (100 MHz, $CDCl_3$) δ 153.5, 135.8, 135.4, 99.0, 72.6, 72.4, 71.9, 70.8, 70.6, 70.5, 70.3, 69.6, 69.0, 61.7, 59.0; **MS** (ESI +ve) *m/z* 760.3809 ($[M + Na]^+$, $C_{33}H_{59}N_3O_{15}Na$, calc. 760.3838).

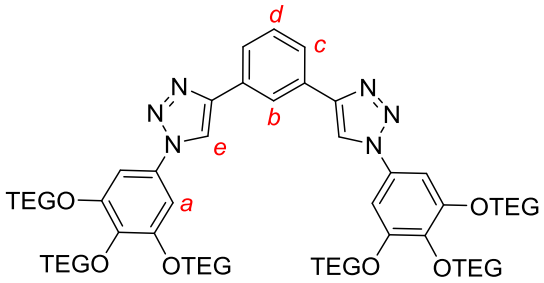
5-amino-1,2,3-tris(tetraethylene glycol methyl ether)benzene 5.3



The aryl bromide precursor **5.2** (245 mg, 0.319 mmol), synthesised as reported,[38] was dissolved in 28 % aqueous ammonia (6 mL) in a microwave vial before ethylene glycol (0.18 mL, 3.2 mmol) and copper(I) iodide (61 mg, 0.32 mmol) were added portionwise. The mixture was stirred to mix before being heated in a microwave reactor at 150 ^oC for 1 hour. Upon

cooling to ambient temperature, the brown aqueous mixture was diluted with water (10 mL) before extraction by chloroform (5 x 15 mL) till the organic layer was colourless. The combined organics were dried with $MgSO_4$ and solvent removed *in vacuo* to give the product as a brown liquid in good purity (221 mg, 98 %), which was used without further purification. **^{1}H-NMR** (400 MHz, $CDCl_3$) δ 5.97 (2H, s, H_a), 4.11 (4H, t, ^3J = 5.2 Hz, H_b), 4.04 (4H, t, ^3J = 5.2 Hz, H_d), 3.82 (4H, t, ^3J = 5.2 Hz, H_c), 3.76 (4H, t, ^3J = 5.2 Hz, H_e), 3.55-3.71 (36H, m, TEG alkyl-CH_2), 3.38 (9H, s, H_f + H_g); **^{13}C-NMR** (100 MHz, $CDCl_3$) δ 153.2, 142.9, 131.1, 95.6, 72.5, 72.4, 71.9, 70.8, 70.6, 70.5, 70.4, 70.3, 69.7, 68.7, 61.7, 59.0; **MS** (ESI +ve) *m/z* 712.4096 ($[M + H]^+$, $C_{33}H_{62}NO_{15}$, calc. 712.4114).

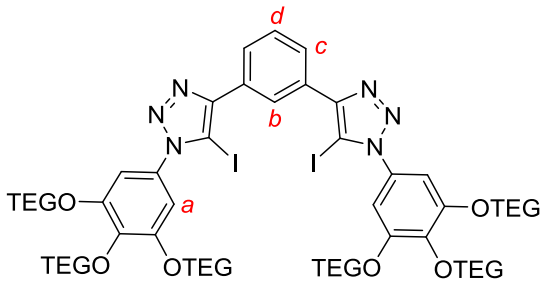
Neutral 1,3-bis(prototriazole)benzene receptor precursor 5.4H



Commercially-availale 1,3-diethynylbenzene (4.5 µL, 0.034 mmol) and aryl azide **5.1** (50 mg, 0.068 mmol) were dissolved in degassed dichloromethane (2 mL). To this mixture was added DIPEA (23 µL, 0.136 mmol), TBTA (9 mg, 0.017 mmol) and $[Cu(MeCN)_4]PF_6$ (6.3 mg, 0.017 mmol) and the reaction was stirred for 3 days at room temperature in a N_2 atmosphere. Subsequently, the reaction was washed with 10 % aqueous ammonia (2 x 5 mL), and the aqueous layer was back-extracted with chloroform (4 x 5 mL). The combined organics were dried with brine and $MgSO_4$ before the solvent was removed to yield a brown oil. Silica gel chromatography (6 % methanol in dichloromethane) gave the product as a sticky yellow liquid (41 mg, 76 %). **^{1}H-NMR** (400 MHz, $CDCl_3$) δ 8.46 (1H, s, H_b), 8.37 (2H, s, H_e), 7.93 (2H, d, ^3J = 7.6 Hz, H_c), 7.55 (1H, t, ^3J = 7.6 Hz, H_d), 7.10 (4H, s, H_a), 4.26 (8H, t, ^3J = 4.8 Hz, *meta*-TEG ArOCH_2), 4.20 (4H, t, ^3J = 4.8 Hz, *para*-TEG ArOCH_2), 3.86 (8H, t, ^3J = 4.8 Hz, *meta*-TEG Ar-OCH_2CH_2), 3.79 (4H, t, ^3J = 4.8 Hz, *para*-TEG Ar-OCH_2CH_2), 3.51-3.72 (72H, m, TEG alkyl-

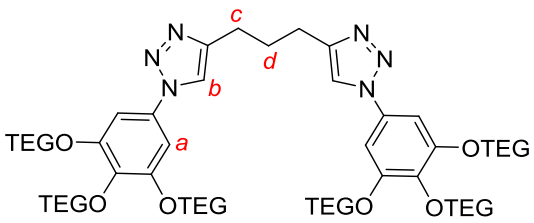
CH_2), 3.36 (6H, s, *para*-TEG-OCH_3), 3.33 (12H, s, *meta*-TEG-OCH_3); **^{13}C-NMR** (100 MHz, $CDCl_3$) δ 153.3, 147.8, 138.7, 132.5, 130.9, 129.5, 125.6, 123.0, 118.3, 100.7, 72.5, 71.8, 70.6, 70.5, 70.4, 70.3, 69.6, 69.3, 61.7, 58.9; **MS** (ESI +ve) *m/z* 1601.8441 ($[M + H]^+$, $C_{76}H_{125}N_6O_{30}$, calc. 1601.8435).

Neutral 1,3-bis(iodotriazole)benzene receptor precursor 5.4I



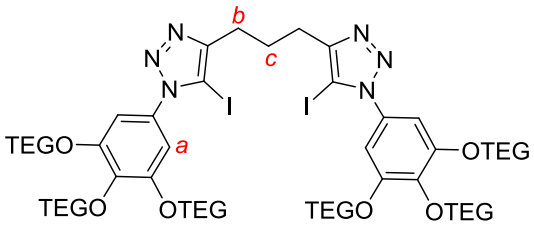
1,3-bis(iodoethynyl)benzene (25 mg, 0.068 mmol), prepared as described,[39] and aryl azide **5.1** (100 mg, 0.136 mmol) was dissolved in degassed THF (2 mL). TBTA (7.2 mg, 0.014 mmol) and $[Cu(MeCN)_4]PF_6$ (10 mg, 0.027 mmol) were added portionwise and the reaction stirred under N_2 for 2 days. Following which, the solvent was removed *in vacuo* and chloroform (10 mL) was added. After washing with 10 % aqueous ammonia (2 x 5 mL) and water (5 mL), the organic layer was dried with brine and $MgSO_4$. Purification by silica gel chromatography (5 % methanol in dichloromethane) gave the product as a bright yellow viscous liquid (112 mg, 89 %). **^{1}H-NMR** (400 MHz, CDCl) δ 8.68 (1H, s, H_b), 8.10 (2H, d, ^3J = 7.6 Hz, H_c), 7.65 (1H, t, ^3J = 7.6 Hz, H_d), 6.81 (4H, s, H_a), 4.21-4.27 (12H, m, TEG ArOCH_2), 3.84-3.90 (12H, m, TEG Ar-OCH_2CH_2), 3.54-3.75 (72H, m, TEG alkyl-CH_2), 3.38 (6H, s, *para*-TEG-OCH_3), 3.37 (12H, s, *meta*-TEG-OCH_3); **^{13}C-NMR** (100 MHz, $CDCl_3$) δ 152.8, 149.8, 139.8, 132.0, 130.5, 129.0, 128.0, 126.6, 106.5, 78.6, 72.6, 72.5, 71.9, 70.8, 70.6, 70.5, 70.4, 70.2, 69.6, 69.5, 69.3, 69.2, 61.7, 59.0; **MS** (ESI +ve) *m/z* 1853.6406 ($[M + H]^+$, $C_{76}H_{123}N_6O_{30}{}^{127}I_2$, calc. 1853.6368).

Neutral 1,3-bis(prototriazole)propyl receptor precursor 5.5H



Same procedure as **5.4H** above. Reagents and conditions: aryl azide **5.1** (100 mg, 0.136 mmol), commercially-available 1,6-heptadiyne (7.8 µL, 0.068 mmol), DIPEA (50 µL, 0.27 mmol), TBTA (18 mg, 0.034 mmol), $[Cu(CH_3CN)_4]PF_6$ (11 mg, 0.034 mmol) in dichloromethane (2 mL) at room temperature for 3 days. Silica gel column chromatography (6 % methanol in dichloromethane) gave **5.5H** as a pale yellow liquid (62 mg, 58 %). **^{1}H-NMR** (400 MHz, $CDCl_3$) δ 7.88 (2H, s, H_b), 7.00 (4H, s, H_a), 4.21 (8H, m, *meta*-TEG Ar-OCH_2), 4.17 (4H, t, ^3J = 4.8 Hz, *para*-TEG ArOCH_2), 3.86 (8H, m, *meta*-TEG Ar-OCH$_2$CH_2), 3.79 (4H, m, *para*-TEG Ar-OCH$_2$CH_2), 3.50-3.71 (72H, m, TEG alkyl-CH_2), 3.35 (6H, s, *para*-TEG-OCH_3), 3.34 (12H, s, *meta*-TEG-OCH_3), 2.89 (4H, m, H_c), 2.19 (2H, m, H_d); **^{13}C-NMR** (100 MHz, $CDCl_3$) δ 153.2, 147.8, 138.4, 132.6, 119.9, 100.6, 72.4, 71.8, 71.7, 70.7, 70.5, 70.4, 70.3, 69.6, 69.2, 58.9, 28.9, 24.8 (multiple peaks missing due to overlap); **MS** (ESI +ve) *m/z* 1567.8552 ($[M + H]^+$, $C_{73}H_{127}N_6O_{30}$, calc. 1567.8591).

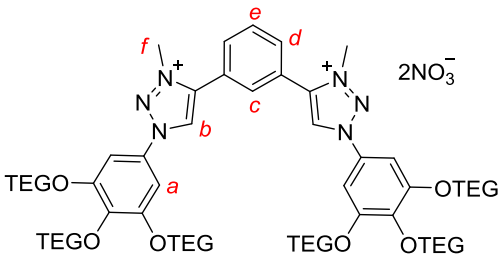
Neutral 1,3-bis(iodotriazole)propyl receptor precursor 5.5I



Same procedure as **5.4I** described above. Reagents and conditions: 1,7-diiodo-hepta-1,6-diyne[40] (23 mg, 0.068 mmol), aryl azide **5.1** (100 mg, 0.136 mmol), TBTA (7.2 mg, 0.014 mmol) and $[Cu(CH_3CN)_4]PF_6$ (8.6 mg, 0.027 mmol) in degassed THF (2 mL) for 3 days. Silica gel column chromatography (5 % methanol in dichloromethane) afforded the product as a yellow liquid (64 mg, 52 %). **^{1}H-NMR** (400 MHz, $CDCl_3$) δ 6.74 (4H, s, H_a), 4.22 (4H, t, ^3J = 4.8

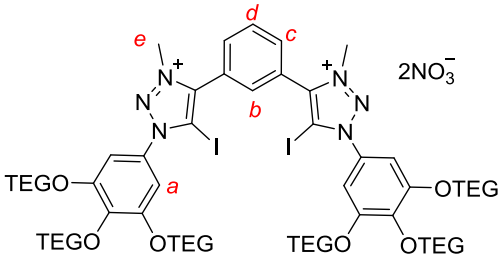
Hz, *para*-TEG ArOCH_2), 4.18 (8H, m, *meta*-TEG Ar-OCH_2), 3.87 (8H, m, *meta*-TEG Ar-OCH$_2$CH_2), 3.82 (4H, m, *para*-TEG Ar-OCH$_2$CH_2), 3.53-3.72 (72H, m, TEG alkyl-CH_2), 3.37 (6H, s, *para*-TEG-OCH_3), 3.36 (12H, s, *meta*-TEG-OCH_3), 2.89 (4H, m, H_c), 2.24 (2H, m, H_d); **^{13}C-NMR** (100 MHz, $CDCl_3$) δ 152.7, 151.5, 139.5, 132.1, 105.9, 72.5, 71.9, 70.8, 70.6, 70.5, 70.4, 69.5, 69.1, 59.0, 28.0, 25.8 (multiple peaks missing due to overlap); **MS** (ESI +ve) *m/z* 1819.6523 ([M + H]$^+$, $C_{73}H_{125}N_6O_{30}{}^{127}I_2$, calc. 1819.6524).

Dicationic 1,3-bis(prototriazolium)benzene receptor 5.6H



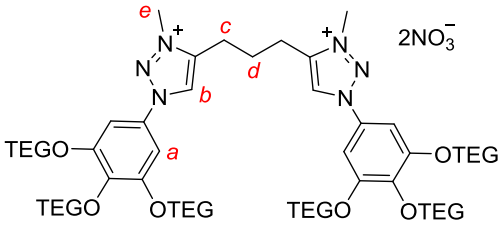
1,3-bis(prototriazole)benzene receptor precursor **5.4H** (40 mg, 0.025 mmol) was dissolved in dry dichloromethane (1 mL) and added to trimethyloxonium tetrafluoroborate (8.1 mg, 0.055 mmol). The reaction was stirred under N_2 for 2 days, before methanol (2 mL) was added to quench the reaction. The solvent was removed *in vacuo* before preparatory TLC (eluent: 7.5 % methanol in dichloromethane) afforded the purified product as a sticky pale yellow liquid. Anion exchange was performed by dissolving the purified product in methanol/ water 9:1 and passing it through a nitrate-loaded Amberlite™ anion exchange column thrice. The solvent was removed *in vacuo* to afford the $2NO_3^-$ salt of the compound as a sticky yellow solid (28 mg, 64 %). **^{1}H-NMR** (400 MHz, CD_3OD) δ 9.64 (2H, s, H_b), 8.25 (1H, s, H_c), 8.16 (2H, d, ^3J = 6.0 Hz, H_d), 8.02 (1H, t, ^3J = 6.0 Hz, H_e), 7.40 (4H, s, H_a), 4.54 (6H, s, H_f), 4.24-4.30 (12H, m, TEG Ar-OCH_2), 3.80-3.91 (12H, m, TEG Ar-OCH$_2$CH_2), 3.48-3.75 (72H, m, TEG alkyl-CH_2), 3.32 (6H, s, *para*-TEG-OCH_3), 3.30 (12H, s, *meta*-TEG-OCH_3); **^{13}C-NMR** (100 MHz, CD_3OD) δ 153.6. 142.5, 140.4, 132.4, 130.8, 130.4, 127.5, 124.1, 100.7, 72.5, 71.5, 70.3, 70.2, 70.1, 69.9, 69.3, 57.7, 54.5, 42.4, 38.6; **MS** (ESI +ve) *m/z* 815.4419 ([M]$^{2+}$, $C_{78}H_{130}N_6O_{30}$, calc. 815.4410).

Dicationic 1,3-bis(iodotriazolium)benzene receptor 5.6I



Identical methylation procedure as that for **5.6H**, using 1,3-bis(iodotriazole)benzene receptor precursor **5.4I** (50 mg, 0.027 mmol) and trimethyloxonium tetrafluoroborate (10 mg, 0.068 mmol) in dry dichloromethane (2 mL) for 3 days in the dark. Purification was achieved by alumina column chromatography (gradient from pure dichloromethane to 3 % methanol in dichloromethane), and anion exchange with a NO_3^--loaded Amberlite™ column furnished the product, as its $2NO_3^-$ salt, as a sticky white solid (43 mg, 79 %). **^{1}H-NMR** (400 MHz, CD_3OD) δ 8.17 (1H, s, H_b), 8.08 (3H, m, H_c + H_d), 7.17 (4H, s, H_a), 4.43 (6H, s, H_e), 4.23-4.30 (12H, m, TEG Ar-OC*H*$_2$), 3.78-3.89 (12H, m, TEG Ar-OCH$_2$C*H*$_2$), 3.48-3.71 (72H, m, TEG alkyl-C*H*$_2$), 3.32 (6H, s, *para*-TEG OC*H*$_3$), 3.30 (12H, s, *meta*-TEG-OC*H*$_3$); **^{13}C-NMR** (100 MHz, CD_3OD) δ 153.2, 145.6, 141.1, 133.7, 132.4, 131.0, 130.4, 124.7, 105.8, 93.8, 72.5, 71.6, 71.5, 70.5, 70.4, 70.3, 70.2, 69.9, 69.3, 69.2, 57.7, 38.8; **MS** (ESI +ve) *m/z* 941.3355 ($[M]^{2+}$, $C_{78}H_{128}N_6O_{30}{}^{127}I_2$, calc. 941.3377).

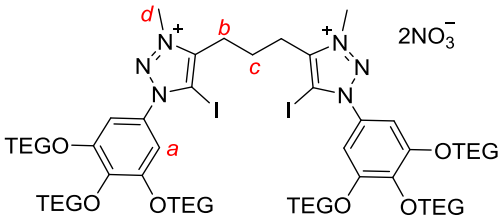
Dicationic 1,3-bis(prototriazolium)propyl receptor 5.7H



Identical methylation procedure as that for **5.6H**, using compound **5.5H** (30 mg, 0.019 mmol) and trimethyloxonium tetrafluoroborate (7.1 mg, 0.048 mmol) in dry dichloromethane (2 mL). Purification was performed using an alumina column (gradient from pure dichloromethane to 2 % methanol in dichloromethane), then anion exchange with a NO_3^--loaded Amberlite™ column

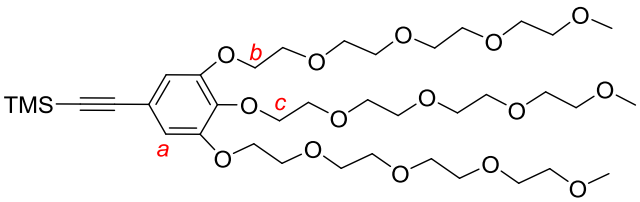
furnished the product, as its $2NO_3^-$ salt, as a sticky pale yellow solid (24 mg, 72 %). **^{1}H-NMR** (400 MHz, CD_3OD) δ 9.27 (2H, br. s, H_b), 7.32 (4H, s, H_a), 4.41 (6H, s, H_e), 4.27 (8H, m, *meta*-TEG Ar-OC*H*$_2$), 4.23 (4H, m, *para*-TEG ArOC*H*$_2$), 3.86 (8H, m, *meta*-TEG Ar-OCH$_2$C*H*$_2$), 3.82 (4H, m, *para*-TEG Ar-OCH$_2$C*H*$_2$), 3.49-3.73 (72H, m, TEG-alkyl-C*H*$_2$), 3.32 (18H, s, TEG-OC*H*$_3$), 3.19 (4H, t, ^3J = 7.6 Hz, H_c), 2.39 (2H, t, ^3J = 7.6 Hz, H_d); **^{13}C-NMR** (100 MHz, CD_3OD) δ 155.0, 146.0, 145.9, 141.6, 132.0, 127.7, 101.8, 74.0, 73.1, 71.9, 71.8, 71.7, 71.6, 71.5, 70.8, 70.7, 59.2, 38.7, 24.7, 23.8 (multiple peaks missing due to overlap); **MS** (ESI +ve) *m/z* 798.4469 ($[M]^{2+}$, $C_{75}H_{132}N_6O_{30}$, calc. 798.4488).

Dicationic 1,3-bis(iodotriazolium)benzene receptor 5.7I



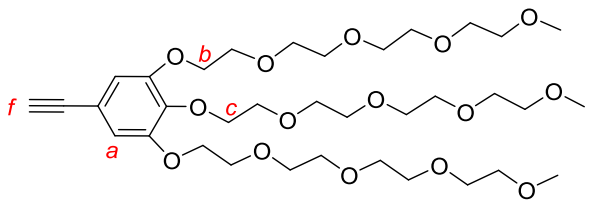
Identical methylation procedure as that for **5.6H**, using compound **5.5I** (26 mg, 0.014 mmol) and trimethyloxonium tetrafluoroborate (5.2 mg, 0.035 mmol) in dry dichloromethane (2 mL). The crude reaction product showed excellent purity and hence no further purification was necessary. Anion exchange with a NO_3^--loaded Amberlite™ column furnished the target receptor, as its $2NO_3^-$ salt, as a sticky pale yellow solid (26 mg, 93 %). **^{1}H-NMR** (400 MHz, CD_3OD) δ 7.16 (4H, s, H_a), 4.45 (6H, s, H_d), 4.24-4.28 (12H, m, TEG Ar-OC*H*$_2$), 3.86-3.88 (8H, m, *meta*-TEG Ar-OCH$_2$C*H*$_2$), 3.79-3.81 (4H, m, *para*-TEG Ar-OCH$_2$C*H*$_2$), 3.49-3.71 (72H, m, TEG-alkyl-C*H*$_2$), 3.24-3.32 (22H, s, H_b + TEG-OC*H*$_3$), 2.20 (2H, t, ^3J = 7.2 Hz, H_c); **^{13}C-NMR** (100 MHz, CD_3OD) δ 154.4, 148.3, 140.9, 132.6, 106.9, 93.0, 79.9, 73.0, 72.9, 71.6, 71.5, 71.4, 71.3, 71.2, 71.1, 70.4, 70.2, 59.2, 39.4, 25.9, 25.2; **MS** (ESI +ve) *m/z* 924.3427 ($[M]^{2+}$, $C_{75}H_{130}N_6O_{30}{}^{127}I_2$, calc. 924.3455).

TMS-protected tris(tetraethylene glycol methyl ether) aryl alkyne 5.8



Aryl bromide **5.2** (200 mg, 0.26 mmol), $Pd(PPh_3)_2Cl_2$ (18.2 mg, 0.026 mmol), copper(I) iodide (5.0 mg, 0.026 mmol) and dry triethylamine (0.36 ml, 2.6 mmol) were mixed together in degassed dry THF (1.0 ml), before ethynyltrimethylsilane (0.060 ml, 0.39 mmol) was added portionwise. The mixture was stirred and briefly purged with N_2 before reacting at 130 ^oC for 1.5 hours in the microwave reactor. After which, the solvent was removed, and the resulting brown solids re-dissolved in dichloromethane and the mixture filtered through celite. After collecting the filtrate and removing the solvent *in vacuo*, purification by silica gel chromatography (5 % methanol in dichloromethane) gave the product as a brown liquid (195 mg, 96 %). **^{1}H-NMR** (400 MHz, $CDCl_3$) δ 6.71 (2H, s, H_a), 4.14 (6H, m, H_b + H_c), 3.54-3.86 (42H, m, TEG alkyl-*H*), 3.38 (9H, s, OC*H*$_3$), 0.25 (9H, s, TMS-*H*); **^{13}C-NMR** (100 MHz, d_6-DMSO) δ 152.4, 139.5, 117.9, 111.6, 105.0, 93.1, 72.4, 72.0, 70.8, 70.7, 70.6, 70.5, 69.6, 68.8, 59.0, 0.0; **MS** (ESI +ve) *m/z* 793.4 ($[M + H]^+$, $C_{38}H_{69}O_{15}{}^{28}Si$, calc. 793.4).

Terminal tris(tetraethylene glycol methyl ether) aryl alkyne 5.9

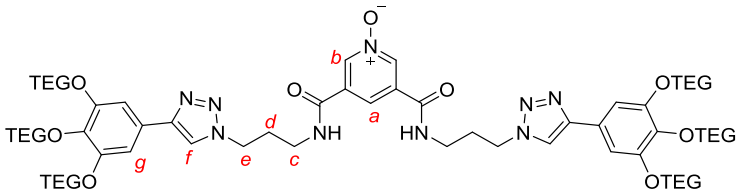


To a solution of the trimethylsilyl-protected alkyne **5.8** (48 mg, 0.061 mmol) in methanol (2 mL) was added anhydrous potassium carbonate (33.5 mg, 0.183 mmol) portionwise, and the reaction was stirred under N_2 at room temperature for 3 hours. Following which, the solvent was removed and water (3 mL) was added. The aqueous mixture was extracted with chloroform (5 x 10 mL), and the combined organics were dried with $MgSO_4$. Removal of solvent *in vacuo* gave the product as a brown liquid (39 mg, 88.6 %). **^{1}H-NMR** (400 MHz,

$CDCl_3$) δ 6.73 (2H, s, H_a), 4.13 (6H, m, H_b + H_c), 3.53-3.85 (42H, m, TEG alkyl-*H*), 3.37 (9H, s, OCH_3), 3.00 (1H, s, H_f); **^{13}C-NMR** (100 MHz, $CDCl_3$) δ 152.4, 139.8, 116.8, 111.8, 83.5, 76.2, 72.4, 71.9, 70.8, 70.7, 70.6, 70.5, 69.6, 69.1, 68.9, 59.0; **MS** (ESI +ve) *m/z* 721.3 ($[M + H]^+$, $C_{35}H_{61}O_{15}$, calc. 721.4).

Note: *When stored at room temperature, slow product decomposition was observed. When stored at -20 °C under N_2,* ***5.9*** *was stable for at least 3 months. TMS-protected precursor* ***5.8*** *was stable under ambient conditions indefinitely.*

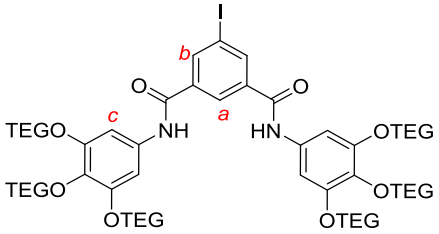
Preliminary pyridine *N*-oxide stopper 5.10



Bis-azide pyridine *N*-oxide **3.7** (22 mg, 0.063 mmol) was dissolved in THF (5 mL) with a minimum quantity of chloroform at elevated temperatures. Successively, the aryl alkyne **5.9** (91 mg, 0.126 mmol), DIPEA (0.11 mL, 0.63 mmol), TBTA (6.9 mmol, 0.013 mmol), ascorbic acid (33 mg, 0.19 mmol) and copper(I) iodide (4.8 mg, 0.025 mmol) were added portionwise, and the reaction mixture stirred under N_2 overnight. The solvent was removed *in vacuo* and residue re-suspended in chloroform (25 mL). The resulting brown suspension was washed with 2 % citric acid (3 mL), 10 % aqueous ammonia (2 x 5 mL) then brine (5 mL), then dried with $MgSO_4$. Removal of solvent under reduced pressure gave a brown liquid, which was purified by alumina column chromatography to give the product as a viscous yellow liquid (45 mg, 40 %). **^{1}H-NMR** (400 MHz, $CDCl_3$) δ 8.81 (2H, s, H_f), 8.56 (1H, s, H_a), 8.45 (2H, br. s, CON*H*), 8.16 (2H, s, H_b), 7.02 (4H, s, H_g), 4.55 (4H, t, ^3J = 5.0 Hz, H_e), 4.17 (8H, s, *meta*-TEG Ar-OCH_2), 4.16 (4H, s, *para*-TEG Ar-OCH_2), 3.76 (4H, t, ^3J = 4.8 Hz, H_c), 3.51-3.82 (84H, m, TEG alkyl-CH_2), 3.34 (6H, s, *para*-TEG OCH_3), 3.32 (12H, s, *meta*-TEG OCH_3), 2.32 (4H, quart. ^3J = 4.8 Hz, H_d); **^{13}C-NMR** (100 MHz, $CDCl_3$) δ 162.6, 152.7, 147.2, 140.4, 133.0,

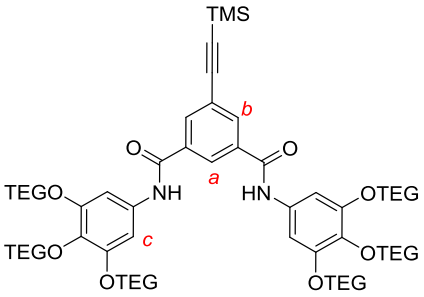
126.2, 121.0, 105.0, 72.3, 71.8, 70.6, 70.5, 70.4, 70.3, 69.6, 68.7, 59.0, 58.9, 48.2, 37.6, 31.8; **MS** (ESI +ve) *m/z* 1788.9392 ($[M + H]^+$, $C_{83}H_{138}N_9O_{33}$, calc. 1788.9391).

Bis-dendrimer isophthalamide aryl iodide 5.12



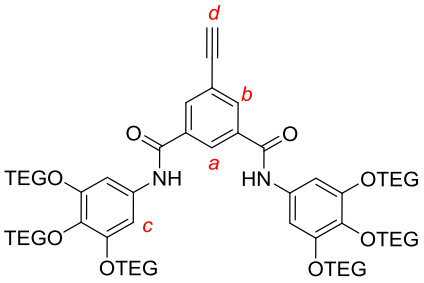
5-iodo-isophthalic acid (45 mg, 0.15 mmol), which was synthesised as described,[41] EDC•HCl (86 mg, 0.45 mmol), aniline **5.3** (220 mg, 0.31 mmol) and a catalytic quantity of DMAP were mixed in dry dichloromethane (4 mL). The reaction was stirred under a N_2 atmosphere at room temperature for 48 hours, before being diluted with dichloromethane (20 mL) and washed with 2 % citric acid (10 mL). The combined organics were dried with brine (10 mL) and $MgSO_4$, and the solvent was removed to give a brown oil. Purification by silica gel column chromatography (8 % methanol in dichloromethane) gave the product as a light brown oil (247 mg, 98 %). **^{1}H-NMR** (400 MHz, $CDCl_3$) δ 9.15 (2H, br. s, CON*H*), 8.65 (1H, s, H_a), 8.52 (2H, s, H_b), 7.14 (4H, s, H_c), 4.08-4.13 (12H, m, TEG Ar-OC*H*$_2$), 3.75-3.80 (12H, m, TEG Ar-OCH$_2$C*H*$_2$), 3.50-3.68 (72H, m, TEG alkyl-C*H*), 3.35 (6H, s, *para*-TEG OC*H*$_3$), 3.30 (12H, s, *meta*-TEG OC*H*$_3$); **^{13}C-NMR** (100 MHz, $CDCl_3$) δ 163.5, 152.4, 140.1, 136.7, 135.4, 134.2, 124.1, 101.2, 94.6, 72.6, 72.4, 71.9, 71.8, 70.6, 70.5, 70.4, 69.6, 68.9, 59.0, 58.9 ; **MS** (ESI +ve) *m/z* 862.3419 ($[M + 2Na]^{2+}$, $C_{74}H_{123}N_2O_{32}Na_2$, calc. 862.3444).

TMS-protected bis-dendrimer aryl alkyne stopper precursor 5.13



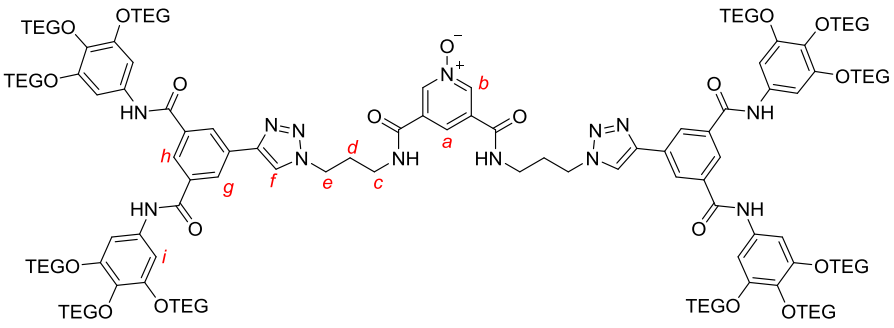
A solution of aryl iodide **5.12** (230 mg, 0.14 mmol) in dry degassed THF (1 mL) was added to a mixture of copper(I) iodide (11 mg, 0.056 mmol) and $Pd(PPh_3)_2Cl_2$ (20 mg, 0.028 mmol) in a microwave vial. To the rapidly stirred mixture was added dry triethylamine (0.20 mL, 1.4 mmol), then ethynyltrimethylsilane (0.040 mL, 0.28 mmol) and the mixture degassed for 1 minute. The reaction was then performed in a microwave reactor at 90 ^{o}C for 1 hour. After cooling to ambient temperature, dichloromethane (10 mL) was added and the crude mixture was filtered through celite, which was rinsed with dichloromethane (100 mL). Purification by silica gel chromatography (8 % methanol in dichloromethane) gave the product as a brown oil (191 mg, 85 %). **^{1}H-NMR** (400 MHz, $CDCl_3$) δ 9.48 (2H, br. s, CON*H*), 8.70 (1H, s, H_a), 8.24 (2H, s, H_b), 7.42 (4H, s, H_c), 4.22 (8H, m, *meta*-TEG Ar-OCH_2), 4.14 (4H, m, *para*-TEG Ar-OCH_2), 3.52-3.86 (84H, m, TEG alkyl-CH_2), 3.33 (6H, s, *para*-TEG OCH_3), 3.31 (12H, s, *meta*-TEG OCH_3), 0.25 (9H, s, TMS-*H*) ; **^{13}C-NMR** (100 MHz, $CDCl_3$) δ 164.7, 152.1, 135.3, 135.1, 124.9, 124.7, 103.7, 101.1, 96.4, 72.7, 72.4, 71.9, 71.8, 70.7, 70.6, 70.5, 70.4, 70.3, 69.6, 68.7, 59.2, 59.1, 0.0; **MS** (ESI +ve) *m/z* 847.4140 ($[M + 2Na]^{2+}$, $C_{79}H_{132}N_2O_{32}Na_2{}^{28}Si$, calc. 847.4139).

Terminal alkyne bis-dendrimer aryl alkyne stopper 5.14



To a solution of the TMS-protected alkyne **5.13** (190 mg, 0.136 mmol) in methanol (7 mL) was added anhydrous potassium carbonate (56.4 mg, 0.408 mmol) and the reaction stirred under nitrogen at room temperature for 4 hours. Water was then added to the resulting brown suspension, and the aqueous mixture extracted with chloroform till the organic layer was colourless. The solvent was removed *in vacuo* to give the product as a brown viscous liquid (153 mg, 85 %) in good purity and hence was used without further purification. **^{1}H-NMR** (400 MHz, CD_2Cl_2) δ 9.78 (2H, br. s, CON*H*), 8.87 (1H, s, H_a), 8.23 (2H, s, H_b), 7.33 (4H, s, H_c), 4.09-4.15 (12H, m, TEG Ar-OC*H*$_2$), 3.49-3.81 (84H, m, TEG alkyl-C*H*$_2$), 3.32 (1H, s, H_d), 3.30 (6H, s, *para*-TEG OC*H*$_3$), 3.29 (12H, s, *meta*-TEG OC*H*$_3$); **^{13}C-NMR** (100 MHz, CD_2Cl_2) δ 164.7, 152.8, 136.0, 135.5, 135.2, 126.2, 123.7, 101.0, 82.8, 79.3, 72.9, 72.4, 71.0, 70.9, 70.1, 69.1, 59.2, 59.1; **MS** (ESI +ve) *m/z* 1599.8024 ($[M + H]^+$, $C_{76}H_{124}N_2O_{32}Na$, calc. 1599.8024).

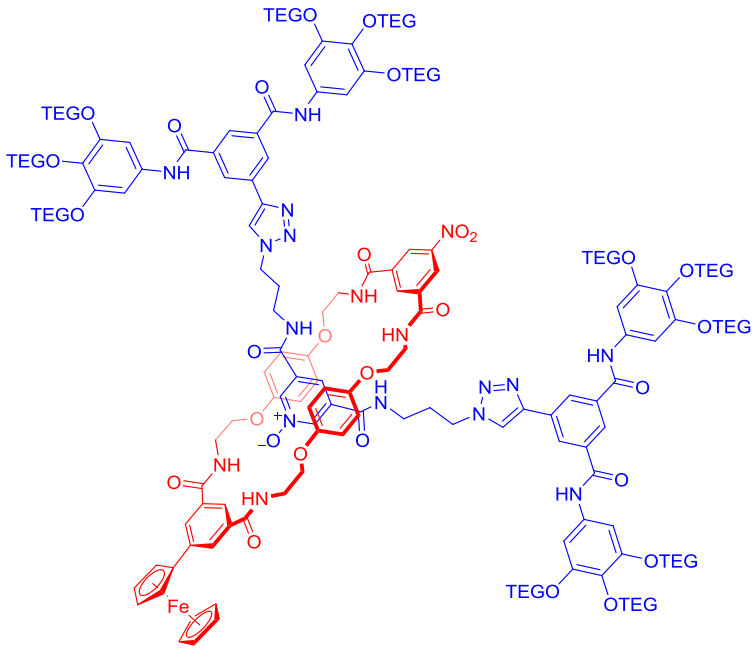
Water-soluble axle 5.15



Pyridine *N*-oxide bis-azide **3.7** (17 mg, 0.047 mmol) was dissolved in degassed THF (3 mL) with heating, and bis-alkyne **5.14** (150 mg, 0.095 mmol) was added. Successively, DIPEA (0.030 mL, 0.14 mmol), TBTA (2.5 mg, 0.0047 mmol), copper(I) iodide (2.0 mg, 0.0094 mmol)

and ascorbic acid (20.7 mg, 0.118 mmol) were added and the reaction stirred under N_2 for 24 hours at room temperature. To the reaction mixture was then added chloroform (20 mL), and the organic layer was washed with 2 % aqueous citric acid (10 mL), then brine (10 mL). The combined aqueous layer was back-extracted with chloroform (5 x 10 mL), and the combined organics were dried with $MgSO_4$. After solvent removal, the brown tarry liquid was purified using alumina column chromatography (1 % methanol in dichloromethane) to give the product as a viscous pale yellow liquid (84 mg, 51 %). **^{1}H-NMR** (400 MHz, CD_3OD) δ 8.57 (2H, s, H_b), 8.54 (2H, s, H_f), 8.44 (4H, s, H_g), 8.44 (2H, s, H_h), 8.20 (1H, s, H_a), 7.17 (8H, s, H_i), 4.57 (4H, t, ^3J = 5.0 Hz, H_e), 4.10 (24H, m, TEG Ar-OCH_2), 3.49-3.82 (172H, m, TEG alkyl-CH_2 + H_c), 3.33 (12H, s, *para*-TEG OCH_3), 3.31 (24H, s, *meta*-TEG OCH_3), 2.30 (4H, m, H_d); **^{13}C-NMR** (100 MHz, CD_3OD) δ 165.6, 162.5, 152.4, 145.7, 136.1, 134.5, 133.3, 131.2, 129.5, 126.9, 122.5, 100.1, 72.3, 71.5, 70.1, 70.0, 69.9, 69.4, 68.5, 57.7, 48.5, 37.6; **MS** (ESI +ve) *m/z* 1773.3766 ([M + 2Na]$^{2+}$, $C_{165}H_{265}N_{13}O_{67}Na_2$, calc. 1773.3757).

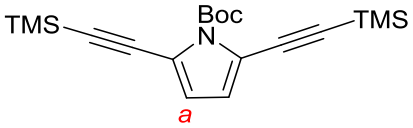
Water-soluble Type 1a dendrimer rotaxane 5.16



To a suspension of 5-nitro isophthalic acid (7.2 mg, 0.034 mmol) in dry dichloromethane (1 mL) containing a drop of DMF was added oxalyl chloride (9.0 µL, 0.10 mmol) and the reaction

was stirred for 2 hours to give a clear solution. After solvent removal *in vacuo*, the pale yellow bis-acid chloride was redissolved in dry dichloromethane (5 mL) and taken up in a syringe. In a separate round bottom flask containing activated 3 Å molecular sieves, axle **5.15** (80 mg, 0.023 mmol), trimethylamine (0.014 mL, 0.10 mmol) and bis-amine **3.5** (24 mg, 0.034 mmol) were dissolved in dry dichloromethane (10 mL) and stirred for 3 hours to remove any water present. Thereafter, the bis-acid chloride solution was added portionwise and the resulting clear orange reaction mixture was stirred under N_2 overnight. Following which, the organic layer was washed successively with 1 M citric acid (20 mL), saturated aqueous $NaHCO_3$ (20 mL), saturated aqueous silver nitrate (2 x 10 mL) and water (2 x 20 mL), before being dried with $MgSO_4$. The solvent was removed *in vacuo* to give an orange solid, which was purified using preparatory TLC (eluent: 7 % methanol in dichloromethane) to give the desired [2]rotaxane as an orange sticky solid (32 mg, 16 %). However, instability of the rotaxane to dethreading in solution negated any characterisation by NMR techniques. **MS** (ESI +ve) *m/z* 1482.41 ($[M + 3Na]^{3+}$, $C_{211}H_{308}{}^{56}FeN_{18}O_{77}Na_3$, calc. 1482.43).

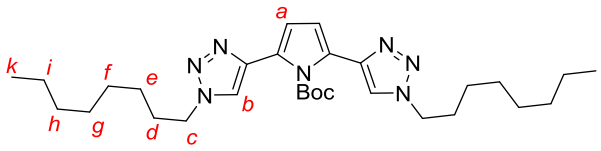
2,5-bis(TMS-ethynyl)-*N*Boc-pyrrole 5.17



2,5-dibromo-*N*Boc-pyrrole (200 mg, 0.62 mmol), prepared as reported,[42] was dissolved in thoroughly-degassed 1,4-dioxane (1.2 mL) in a microwave vial. To this solution was added $Pd(PPh_3)_2Cl_2$ (44 mg, 0.062 mmol), copper(I) iodide (12 mg, 0.062 mmol), anhydrous trimethylamine (0.60 mL, 4.3 mmol) and TMS-acetylene (0.26 mL, 1.86 mmol) sequentially and the mixture was sonicated for 2 minutes. The reaction was heated in the microwave reactor at 120 ^oC for 1 hour to give a dark brown suspension which was filtered through celite. After washing the celite with diethyl ether, the solvent was removed in vacuo and the brown crude mixture purified by silica gel column chromatography (1 % ethyl acetate in hexane) to give the product as a yellow oil (142 mg, 64 %). **^{1}H-NMR** (400 MHz, $CDCl_3$) δ 6.46 (2H, s, H_a), 1.64 (9H, s, Boc-^{t}Bu), 0.24 (18H, s, TMS-CH_3); **^{13}C-NMR** (100 MHz, CD_3OD) δ 147.6, 119.4,

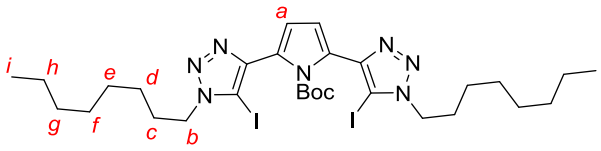
98.8, 95.6, 85.3, 26.8, -1.4, -1.5; **MS** (ESI +ve) *m/z* 382.1625 ($[M + Na]^+$, $C_{19}H_{29}NO_2Na^{28}Si_2$, calc. 382.1629).

Neutral *n*-octyl HB Receptor Precursor 5.18H



To a thoroughly-degassed solution of compound **5.17** (30 mg, 0.083 mmol) in THF (1 mL) was added tetrabutylammonium fluoride trihydrate (54 mg, 0.21 mmol) portionwise and the reaction stirred for 1 hour under N_2 to give a brown solution. Octyl azide (32 mg, 0.21 mmol), $[Cu(CH_3CN)_4]PF_6$ (10 mg, 0.033 mmol), TBTA (18 mg, 0.034 mmol) and DIPEA (0.060 mL, 0.033 mmol) were then added portionwise to the reaction which was then stirred for 2 days. Thereafter, the solvent was removed *in vacuo*, chloroform (20 mL) was added and the organic solution washed with 1 M NH_4Cl (aq.) (2 x 10 mL), water (5 x 10 mL) and dried with $MgSO_4$. Solvent removal gave a brown oil which was purified by silica gel column chromatography (30 % ethyl acetate in hexane) to yield the product as a yellow solid (20 mg, 45 %). **^{1}H-NMR** (400 MHz, $CDCl_3$) δ 7.77 (2H, s, H_b), 6.60 (2H, s, H_a), 4.39 (4H, t, ^3J = 7.2 Hz, H_c), 1.95 (4H, quint. ^3J = 7.1 Hz, H_d), 1.27-1.39 (29H, m, $H_{e\text{-}i}$ + *N*Boc-^{t}Bu), 0.88 (6H, t, ^3J = 6.8 Hz, H_k); **^{13}C-NMR** (100 MHz, CD_3OD) δ 149.4, 140.4, 126.1, 122.2, 113.8, 84.4, 50.4, 31.7, 30.3, 29.0, 28.9, 27.2, 26.5, 22.6, 14.0; **MS** (ESI +ve) *m/z* 526.3853 ($[M + H]^+$, $C_{29}H_{48}N_7O_2$, calc. 526.3864).

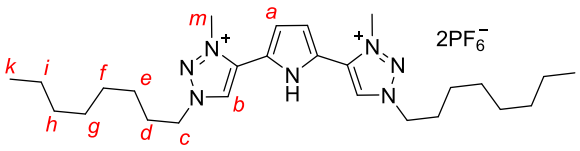
Neutral *n*-octyl XB Receptor Precursor 5.18I



Tetrabutylammonium fluoride trihydrate (66 mg, 0.25 mmol) was added to a solution of compound **5.17** (36 mg, 0.10 mmol) in THF/ acetonitrile 1:1 (1 mL) and the resulting purple-brown solution stirred for 45 minutes. In a separate round bottom flask charged with the same

solvent mixture (1 mL) was added sodium iodide (121 mg, 0.808 mmol), copper(II) perchlorate hexahydrate (150 mg, 0.404 mmol) and octyl azide (35 mg, 0.22 mmol) portionwise. After stirring for 5 minutes, DBU (0.028 mL, 0.19 mmol), TBTA (5.4 mg, 0.010 mmol) and the deprotected bis-alkyne solution were added, and the reaction stirred in the dark under N_2 for 24 hours. Thereafter, the solvent was removed *in vacuo* and the resulting brown tar was partitioned between chloroform (25 mL) and 10 % aqueous ammonia solution (10 mL). The aqueous layer was separated and back-extracted with chloroform (2 x 10 mL) and the combined organics were washed with water (10 mL), brine (10 mL) and dried with $MgSO_4$. Silica gel column chromatography (25 % ethyl acetate in hexane) afforded the product as a bright yellow liquid (50 mg, 63 %). **^{1}H-NMR** (400 MHz, $CDCl_3$) δ 6.47 (2H, s, H_a), 4.40 (4H, t, ^3J = 7.2 Hz, H_b), 1.95 (4H, quint. ^3J = 7.2 Hz, H_c), 1.28-1.41 (20H, m, $H_{d\text{-}h}$), 1.22 (9H, s, *N*Boc-^{t}Bu), 0.88 (6H, t, ^3J = 6.8 Hz, H_k); **^{13}C-NMR** (100 MHz, CD_3OD) δ 148.1, 145.9, 125.1, 115.3, 83.9, 81.2, 51.1, 31.7, 30.0, 29.1, 29.0, 27.3, 26.5,22.6, 14.1; **MS** (ESI +ve) *m/z* 778.1776 ([M + H]$^+$, $C_{29}H_{46}N_7O_2{}^{127}I_2$, calc. 778.1797).

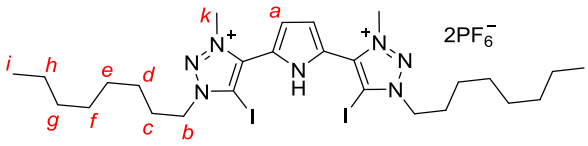
Dicationic *n*-octyl HB Receptor 5.19H



To a solution of the neutral receptor precursor **5.18H** (24 mg, 0.046 mmol) in dry dichloromethane (1.5 mL) was added trimethyloxonium tetrafluoroborate (20 mg, 0.14 mmol) abd the reaction was stirred overnight under N_2. ESI-MS analysis showed that double methylation and *in-situ* deprotection of the *N*Boc group had occurred, and the reaction was quenched with one drop of methanol and stirred for 15 minutes. After solvent removal *in vacuo*, the resulting brown solid was purified by preparatory TLC (9 % methanol in dichloromethane) to give the product as a yellow solid. Anion exchange was performed by washing a chloroform solution (30 mL) of the purified receptor with 0.1 M NH_4PF_6 (aq.) (8 x 10 mL) followed by water (2 x 10 mL). Drying the organic phase with $MgSO_4$ and solvent removal

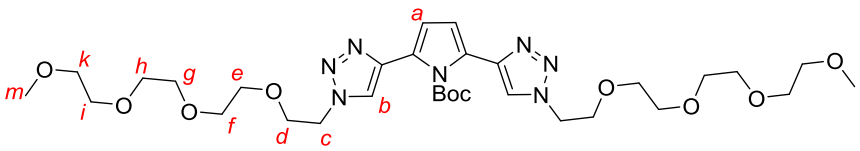
afforded **5.19H**, as its $2PF_6^-$ salt, as a yellow solid (18 mg, 53 %). **^{1}H-NMR** (400 MHz, CD_3OD) δ 8.77 (2H, s, H_b), 7.08 (2H, s, H_a), 4.67 (4H, t, ^3J = 7.3 Hz, H_c), 4.41 (6H, s, H_m), 2.08 (4H, quint. ^3J = 7.2 Hz, H_d), 1.29-1.43 (20H, m, $H_{e\text{-}i}$), 0.91 (6H, t, ^3J = 6.8 Hz, H_k); **^{13}C-NMR** (100 MHz, CD_3OD) δ 137.2, 128.5, 119.5, 116.2, 55.5, 39.8, 33.0, 30.4, 30.3, 30.1, 27.3, 23.8, 14.5; **^{19}F-NMR** (470 MHz, CD_3OD) δ -74.4 (d, $^1J_{F\text{-}P}$ = 706 Hz); **^{31}P-NMR** (162 MHz, CD_3OD) δ -144.7 (sep., $^1J_{P\text{-}F}$ = 706 Hz); **MS** (ESI +ve) *m/z* 227.6858 ($[M]^{2+}$, $C_{26}H_{45}N_7$, calc. 227.6863).

Dicationic *n*-octyl XB Receptor 5.19I



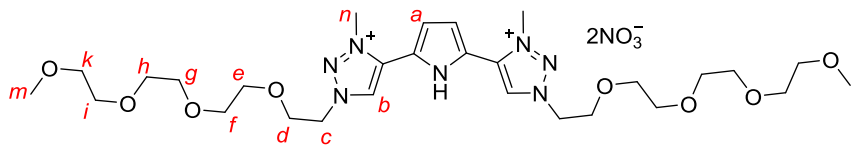
Identical procedure as that reported for **5.19H**, using precursor compound **5.18I** (49 mg, 0.063 mmol) and trimethyloxonium tetrafluoroborate (28 mg, 0.19 mmol) in dry dichloromethane (1.0 mL) for 2 days. Purification by preparatory TLC (10 % methanol in dichloromethane) and anion exchange by repeated washing with 0.1 M NH_4PF_6 (aq.) afforded the target compound as a yellow solid (23 mg, 42 %). **^{1}H-NMR** (400 MHz, CD_3OD) δ 7.05 (2H, s, H_a), 4.70 (4H, t, ^3J = 7.3 Hz, H_b), 4.36 (6H, s, H_k), 2.08 (4H, quint. ^3J = 7.2 Hz, H_c), 1.29-1.51 (20H, m, $H_{d\text{-}h}$), 0.92 (6H, t, ^3J = 6.8 Hz, H_i); **^{13}C-NMR** (100 MHz, CD_3OD) δ 140.5, 117.5, 116.1, 90.1, 54.8, 38.6, 31.7, 31.6, 29.4, 29.2, 28.8, 28.7, 25.8, 22.4, 13.1; **^{19}F-NMR** (470 MHz, CD_3OD) δ -74.4 (d, $^1J_{F\text{-}P}$ = 706 Hz); **^{31}P-NMR** (162 MHz, CD_3OD) δ -144.7 (sep., $^1J_{P\text{-}F}$ = 706 Hz); **MS** (ESI +ve) *m/z* 353.5824 ($[M]^{2+}$, $C_{26}H_{43}N_7{}^{127}I_2$, calc. 353.5829).

Neutral TEG HB Receptor Precursor 5.21H



Compound **5.17** (45 mg, 0.13 mmol) was dissolved in dry THF (1 mL) and cesium fluoride (57 mg, 0.38 mmol) was added and stirred at room temperature for 3 hours to give complete alkyne TMS-deprotection. To a separate round bottom flask containing a solution of TEG-azide **5.20**[43] (58 mg, 0.25 mmol) in degassed dichloromethane (1 mL) was added TBTA (20 mg, 0.038 mmol), $[Cu(CH_3CN)_4]PF_6$ (20 mg, 0.063 mmol) and DIPEA (0.087 mL, 0.50 mmol) sequentially, followed by the alkyne solution. After stirring for 3 days, solvent removal *in vacuo* and immediate purification by silica gel column chromatography (6 % methanol in dichloromethane) isolated the product as a viscous light brown oil (55 mg, 65 %). **^{1}H-NMR** (400 MHz, $CDCl_3$) δ 7.94 (2H, s, H_b), 6.56 (2H, s, H_a), 4.59 (4H, t, ^3J = 5.2 Hz, H_c), 3.91 (4H, t, ^3J = 5.1 Hz, H_d), 3.61-3.64 (20H, m, H_{e-i}), 3.53 (4H, m, H_k), 3.36 (6H, s, H_m), 1.29 (9H, s, *N*Boc-^{t}Bu); **^{13}C-NMR** (100 MHz, CD_3OD) δ 149.3, 140.7, 126.3, 123.4, 113.5, 84.2, 71.9, 70.6, 70.5, 70.4, 69.6, 59.0, 50.2, 27.2; **MS** (ESI +ve) *m/z* 682.3761 ($[M + H]^+$, $C_{31}H_{52}N_7O_{10}$, calc. 682.3770).

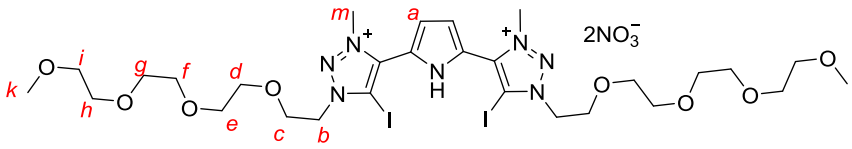
Dicationic TEG HB Receptor 5.22H



Identical methylation procedure as reported for **5.19H**. Reagents: **5.21H** (38 mg, 0.056 mmol) and trimethyloxonium tetrafluoroborate (25 mg, 0.17 mmol) in dry dichloromethane (3 mL) overnight. The resulting *N*Boc-deprotected product was purified by preparatory TLC (10 % methanol in dichloromethane), and anion exchange by dissolving the purified product in wet acetonitrile (0.1 mL water in 100 mL acetonitrile) and passing it though a NO_3^--loaded Amberlite™ column three times to give a sticky pale yellow solid (17 mg). **^{1}H-NMR** (500 MHz,

CD_3CN) δ 9.44 (2H, br. s, H_b), 6.96 (2H, s, H_a), 4.71 (4H, t, ^3J = 4.8 Hz, H_c), 4.43 (6H, s, H_n), 3.98 (4H, t, ^3J = 4.8 Hz, H_d), 3.63-3.66 (4H, m, H_e), 3.58-3.60 (4H, m, H_f), 3.52-3.54 (4H, m, H_g), 3.48-3.50 (8H, H_h + H_i), 3.41 (4H, m, H_k), 3.25 (6H, s, H_m); **^{13}C-NMR** (125 MHz, CD_3CN) δ 138.4, 128.2, 114.6, 72.6, 72.5, 71.4, 71.2, 71.1, 71.0, 70.9, 68.7, 58.9, 54.9, 40.8; **MS** (ESI +ve) *m/z* 305.6803 ($[M]^{2+}$, $C_{28}H_{49}N_7O_8$, calc. 305.6816).

Dicationic TEG XB Receptor 5.22I



Receptor **5.22H** (24 mg, 0.031 mmol) was dissolved in dry acetonitrile (1 mL) in a microwave vial before silver oxide (21 mg, 0.092 mmol) and activated 3 Å molecular sieves were added. The vial was sealed and the reaction heated at 75 °C overnight to give a beige suspension. After cooling the reaction to ambient temperature, it was filtered through celite which was flushed with acetonitrile (c.a. 20 mL), methanol (c.a. 30 mL) and acetone (c.a. 30 mL). Solvent removal *in vacuo* then yielded a yellow solid, which was re-suspended in dry acetonitrile (2 mL) and chilled in an ice bath to 0 °C in a N_2 atmosphere. A solution of iodine (17 mg, 0.068 mmol) in dry dichloromethane (2 mL) was then added dropwise, whereupon the reaction was stirred at 0 °C for 30 minutes before being warmed up to room temperature and stirred for a further 2 hours. Removal of solvent on a rotary evaporator and preparatory TLC purification (10 % methanol in dichloromethane) afforded the product as a yellow liquid. Anion exchange was performed by passing a solution of the purified product in wet acetonitrile (0.1 mL water in 100 mL acetonitrile) and passing it though a NO_3^--loaded Amberlite™ column three times to give a sticky yellow solid (3.3 mg, 10 %). **^{1}H-NMR** (500 MHz, CD_3CN) δ 6.95 (2H, s, H_a), 4.79 (4H, t, ^3J = 4.8 Hz, H_b), 4.31 (6H, s, H_m), 4.02 (4H, t, ^3J = 4.8 Hz, H_c), 3.43-3.63 (24H, m, $H_{d\text{-}i}$), 3.27 (6H, s, H_k); **^{13}C-NMR** (125 MHz, CD_3CN) δ 141.1, 129.2, 116.6, 114.9, 72.6, 71.4, 71.2, 71.1, 71.0, 70.9, 68.9, 59.6, 55.5, 40.3; **MS** (ESI +ve) *m/z* 431.5772 ($[M]^{2+}$, $C_{28}H_{47}N_7O_8{}^{127}I_2$, calc. 431.5782).

7.3 References

1 E. Zhou, J. Zhang and C. Dong, *ARKIVOC*, 2014, **v**, 351–364.
2 M. J. Hynes, *J. Chem. Soc. Dalton Trans.*, 1993, 311–312.
3 *SpecFit v. 2.02 ed.*, Spectrum Software Associates, Chapel Hill, NC, USA, 1997.
4 *www.supramolecular.org*.
5 A. Savitzky and M. J. E. Golay, *Anal. Chem.*, 1964, **36**, 1627–1639.
6 B. Kratochvil, E. Lorah and C. Garber, *Anal. Chem.*, 1969, **41**, 1793–1796.
7 B.-Y. Lee, S. R. Park, H. B. Jeon and K. S. Kim, *Tetrahedron Lett.*, 2006, **47**, 5105–5109.
8 A. Hassner and M. Stern, *Angew. Chem. Int. Ed. Engl.*, 1986, **25**, 478–479.
9 A. Hassner, M. Stern, H. E. Gottlieb and F. Frolow, *J. Org. Chem.*, 1990, **55**, 2304–2306.
10 A. Dalmia, R. F. Savinell and C. C. Liu, *J. Electrochem. Soc.*, 1996, **143**, 1827–1833.
11 M. Ogawa, M. Nagashima, H. Sogawa, S. Kuwata and T. Takata, *Org. Lett.*, 2015, **17**, 1664–1667.
12 T. R. Bell-Horwath, A. K. Vadukoot, F. S. Thowfeik, G. Li, M. Wunderlich, J. C. Mulloy and E. J. Merino, *Bioorg. Med. Chem. Lett.*, 2013, **23**, 2951–2954.
13 N. L. Kilah, M. D. Wise, C. J. Serpell, A. L. Thompson, N. G. White, K. E. Christensen and P. D. Beer, *J. Am. Chem. Soc.*, 2010, **132**, 11893–11895.
14 V. Aucagne, K. D. Hänni, D. A. Leigh, P. J. Lusby and D. B. Walker, *J. Am. Chem. Soc.*, 2006, **128**, 2186–2187.
15 B. Maji, K. Kumar, K. Muniyappa and S. Bhattacharya, *Org Biomol Chem*, 2015, **13**, 8335–8348.
16 S. W. Robinson, C. L. Mustoe, N. G. White, A. Brown, A. L. Thompson, P. Kennepohl and P. D. Beer, *J. Am. Chem. Soc.*, 2015, **137**, 499–507.
17 M. J. Langton, S. W. Robinson, I. Marques, V. Félix and P. D. Beer, *Nat Chem*, 2014, **6**, 1039–1043.
18 C. D. Campbell, R. L. Greenaway, O. T. Holton, H. A. Chapman and E. A. Anderson, *Chem Commun*, 2014, **50**, 5187–5189.
19 E. Ascic, R. G. Ohm, R. Petersen, M. R. Hansen, C. L. Hansen, D. Madsen, D. Tanner and T. E. Nielsen, *Chem. – Eur. J.*, 2014, **20**, 3297–3300.
20 N. H. Evans and P. D. Beer, *Org Biomol Chem*, 2011, **9**, 92–100.
21 J. M. Mercurio, F. Tyrrell, J. Cookson and P. D. Beer, *Chem Commun*, 2013, **49**, 10793–10795.
22 J. Isaad, *RSC Adv*, 2014, **4**, 49333–49341.
23 J. K. Pudelski and M. R. Callstrom, *Organometallics*, 1994, **13**, 3095–3109.
24 A. Zirakzadeh, A. Herlein, M. A. Groß, K. Mereiter, Y. Wang and W. Weissensteiner, *Organometallics*, 2015, **34**, 3820–3832.
25 S. W. Robinson and P. D. Beer, *Org Biomol Chem*, 2017, **15**, 153–159.
26 L. Yang, S. Qin, X. Su, F. Yang, J. You, C. Hu, R. Xie and J. Lan, *Org Biomol Chem*, 2010, **8**, 339–348.
27 T. J. Burchell, M. C. Jennings and R. J. Puddephatt, *Inorg Chim Acta*, 2006, **359**, 2812–2818.
28 Y. Takeda, M. Okazaki and S. Minakata, *Chem Commun*, 2014, **50**, 10291–10294.
29 K. Gebauer and A. Fürstner, *Angew. Chem. Int. Ed.*, 2014, **53**, 6393–6396.
30 R. Colombo, M. Mingozzi, L. Belvisi, D. Arosio, U. Piarulli, N. Carenini, P. Perego, N. Zaffaroni, M. De Cesare, V. Castiglioni, E. Scanziani and C. Gennari, *J. Med. Chem.*, 2012, **55**, 10460–10474.
31 C. J. Serpell, R. Chall, A. L. Thompson and P. D. Beer, *Dalton Trans.*, 2011, **40**, 12052–12055.
32 C. Joce, R. White, P. G. Stockley, S. Warriner, W. B. Turnbull and A. Nelson, *Bioorg. Med. Chem. Lett.*, 2012, **22**, 278–284.
33 C. Rampalakos and W. D. Wulff, *Adv. Synth. Catal.*, 2008, **350**, 1785–1790.
34 K.-Y. Ng, V. Felix, S. M. Santos, N. H. Rees and P. D. Beer, *Chem Commun*, 2008, 1281–1283.
35 M. Lamberto, I. Yildiz, S. Sortino and F. M. Raymo, *J Mater Chem*, 2010, **20**, 981–989.
36 L. Servinis, L. C. Henderson, L. M. Andrighetto, M. G. Huson, T. R. Gengenbach and B. L. Fox, *J Mater Chem A*, 2015, **3**, 3360–3371.
37 L.-J. Li, C.-C. Liu, M.-Z. Sun, Y. Qiao, Y.-Y. Huang and J.-L. Du, *Mol. Cryst. Liq. Cryst.*, 2014, **593**, 187–200.
38 J. Wu, J. Li, U. Kolb and K. Mullen, *Chem Commun*, 2006, 48–50.
39 F. Kniep, L. Rout, S. M. Walter, H. K. V. Bensch, S. H. Jungbauer, E. Herdtweck and S. M. Huber, *Chem Commun*, 2012, **48**, 9299–9301.
40 Y. Matano, M. Nakashima and H. Imahori, *Angew. Chem. Int. Ed.*, 2009, **48**, 4002–4005.
41 Z. Kokan and S. I. Kirin, *Eur. J. Org. Chem.*, 2013, **2013**, 8154–8161.
42 A. V. Predeus, V. Gopalsamuthiram, R. J. Staples and W. D. Wulff, *Angew. Chem.*, 2013, **125**, 945–949.
43 H. J. Kitto, E. Schwartz, M. Nijemeisland, M. Koepf, J. J. L. M. Cornelissen, A. E. Rowan and R. J. M. Nolte, *J Mater Chem*, 2008, **18**, 5615–5624.

Blank Page

Appendices

APPENDICES

Appendix A: Crystallographic Data

Macrocycle **2.9Se (2I$^-$ Adduct)**

Single crystal X-ray diffraction data for macrocycle **2.9Se** were collected using synchrotron radiation at Diamond Light Source (DLS), Beamline I19.[1] Using a Cryostream N_2 open-flow cooling device on the diffractometer,[2] the data were collected at 100(2) K. Cell parameters and intensity data (including inter-frame scaling) were processed using CrysAlis Pro (CrysAlis Pro, Agilent Technologies, 2010). Subsequently, the structure was solved using charge-flipping methods using SUPERFLIP,[3] and refined using full-matrix least-squares on F^2 within the CRYSTALS suite,[4,5] with help from Dr. Amber L. Thompson. All non-hydrogen atoms were refined with anisotropic displacement parameters. Hydrogen atoms were generally visible in the difference map and their positions and displacement parameters were refined using restraints prior to inclusion into the model using riding constraints.[6]

Crystals suitable for X-ray diffraction structural analysis were obtained for the iodide salt of macrocycle **2.9Se** by slow vapour diffusion of diethyl ether into a solution of the macrocycle in acetonitrile/ chloroform 1:1 (*v/v*). The crystals were small and weakly diffracting, which necessitated the use of synchrotron radiation. However despite this, the diffraction was weak and relatively low quality data were obtained. Nevertheless, the structure of the macrocycle the position of anion, as well as the acetonitrile solvent molecule could be determined unambiguously. Short contacts between the Se atoms iodide anions (Se···I$^-$ (2.987(6) Å) and (2.987(6) Å) respectively) indicated unambiguous ChB interactions, with distances shorter than the sum of the van der Waals' radii (ChB: 91 % and 97 % respectively), appearing to stabilize the macrocycle-iodide complex. Areas of diffuse electron density, which appear to result from disordered solvent molecules were present. While one molecule of acetonitrile was apparent from the difference map within the macrocycle structure, the remaining diffuse electron density could not be modelled sensibly. Therefore PLATON-SQUEEZE[7,8] was used to include this electron density in the refinement. Thermal motion of

the hydroquinone and polyether parts of **2.9Se**, as well as one of the iodide anions (I52), were evident, and it was possible to model the motion as positional disorder over two sites. Nevertheless, in some cases the ellipsoids for this part of the macrocycle were rather large due to the relatively low quality data obtained. As a result, restraints to bond lengths and angles, as well as thermal and vibrational ellipsoid parameters to the affected parts of the macrocycle were required to ensure a refinement which was chemically sensible. The majority of the hydrogen atoms were located from the difference map, but those attached to the $SeCH_3$ units were repositioned geometrically. The H atoms were initially refined with soft restraints on the bond lengths and angles to regularise their geometry and Uiso(H), after which the positions were refined with riding constraints.[6]

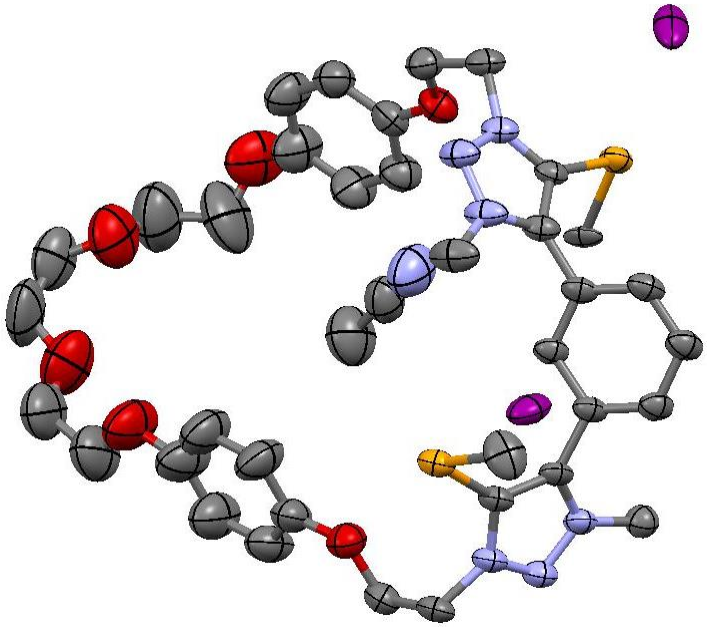


Figure A1. *X-ray crystal structure of the major component of dicationic macrocycle* ***2.9Se*** *as its iodide adduct. Thermal ellipsoids are displayed at the 50 % probability level and hydrogen atoms have been omitted.*

Table A1. Crystal structure data and refinement details for macrocycle **2.9Se** as its iodide salt.

Experimental details	
Chemical formula	$C_{36}H_{44}I_2N_6O_6Se_2 \cdot I_2$
M_r	1106.59
Crystal system, space group	Monoclinic, $P2_1/c$
Temperature/ K	100(2)
a, b, c/ Å	22.6944 (7), 21.4972 (5), 9.4414 (3)
β / ^{o}	99.847 (3)
Unit cell volume/ Å^3	4538.3 (2)
Z	4
μ/ mm^{-1}	3.04
Crystal size/ mm	0.03 x 0.02 x 0.01
No. of measured, independent and observed [$I > 2.0\sigma(I)$] reflections	93015, 22611, 6457
R_{int}	0.114
$(\sin \theta/\lambda)_{max}$ / Å^{-1}	0.861
Refinement	
$R[F^2 > 2\sigma(F^2)]$, $wR(F^2)$, S	0.068, 0.199, 0.99
No. of reflections	9208
No. of parameters	716
No. of restraints	1878
$\Delta\rho_{max}$, $\Delta\rho_{min}$ (e Å^{-3})	2.66, -1.34

Appendix B: Electrochemical Reversibility Studies

B1. Criteria for Electrochemical Reversibility

For a reversible electrochemical system displaying fast electron transfer kinetics, the following criteria needs to be met (terms defined in Figure B1.1):

- E_{pa} and E_{pc} independent of scan rate
- $I_{pa}/ I_{pc} = 1$
- $\Delta E = (E_{pa} - E_{pa}) = (59/n)$ mV, where n is the number of electrons transferred during the redox process. Therefore for a one electron-transfer process, the difference = 59 mV.
- I_{pa} and I_{pc} varies proportionally to the square root of the scan rate.

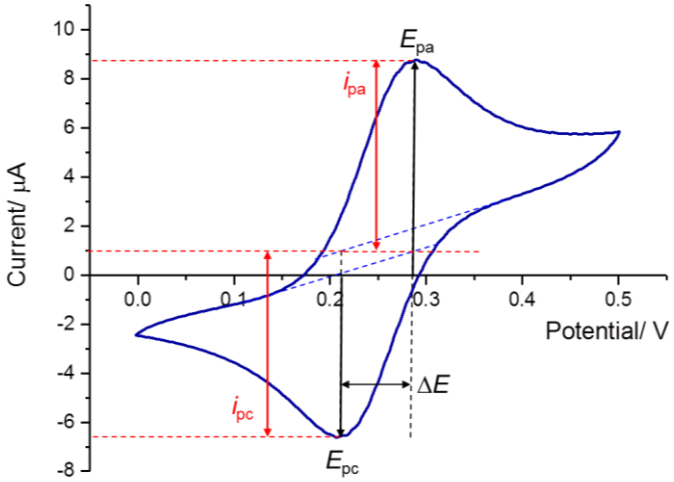


***Figure B1.1**. A labelled CV for definition of terms E_{pa}, E_{pc}, I_{pa}, I_{pc}.*

For all of the following receptors described herein, E_{pa} and E_{pc} were almost independent of scan rate at lower scan rates. With a few exceptions, I_{pa}/ I_{pc} are typically in the range of 0.90-1.10 and ΔE show notable variations from 60 to 110 mV. In all cases, I_{pa} and I_{pc} vary almost proportionally with the square root of the scan rate (Pearson's $R^2 > 0.94$). Thus, the redox-active receptors generally showed 'quasi-reversible' electrochemical behaviour, with no significant differences seen between HB or σ-hole donor hosts, or regardless of their structural complexity (i.e. acyclic, macrocyclic or interlocked hosts).

B2. Electrochemical Reversibility Studies on Redox-active Hosts

Macrocycle **3.6Bu**

Studies performed in 0.1 M $TBAPF_6$ in dichloromethane/ CH_3CN/ H_2O 1:1.

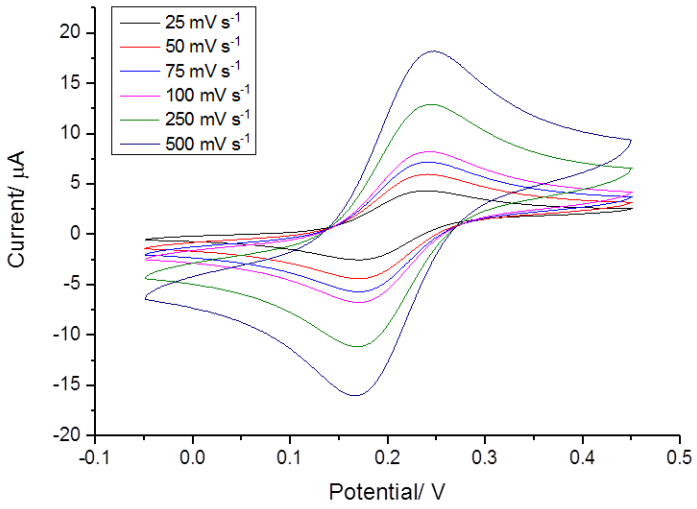


Figure B2.2. *CVs of macrocycle **3.6Bu** at different scan rates ([**3.6Bu**] = 0.5 mM, T = 293 K).*

Table B1. Values of E_{pc}, E_{pa}, I_{pa}, I_{pc}, ΔE and I_{pa}/ I_{pc} for macrocycle **3.6Bu** at different scan rates.

Scan rate/ mV s^{-1}	E_{pa}/V	E_{pc}/V	I_{pa}/ µA	I_{pc}/ µA	ΔE/ V	I_{pa}/ I_{pc}
25	0.233	0.174	2.900	2.910	0.059	0.997
50	0.232	0.174	4.600	4.550	0.058	1.011
75	0.239	0.176	6.880	6.720	0.063	1.024
100	0.238	0.180	7.380	7.580	0.058	0.974
250	0.238	0.178	11.730	11.590	0.060	1.012
500	0.240	0.175	16.500	15.900	0.065	1.038

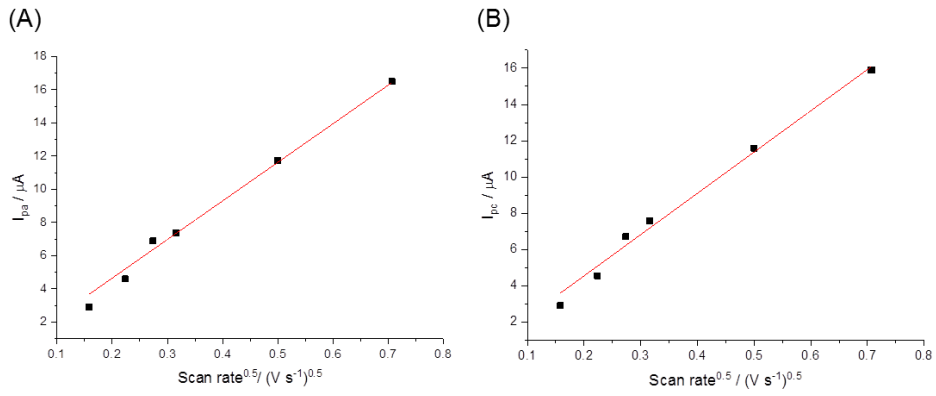


Figure B2.3. *Plots of (A) I_{pa} and (B) I_{pc} against (scan rate)$^{1/2}$ for macrocycle **3.6Bu**.*

Rotaxane **3.9Bu-H**

Studies performed in 0.1 M $TBAPF_6$ in dichloromethane/ CH_3CN/ H_2O 1:1.

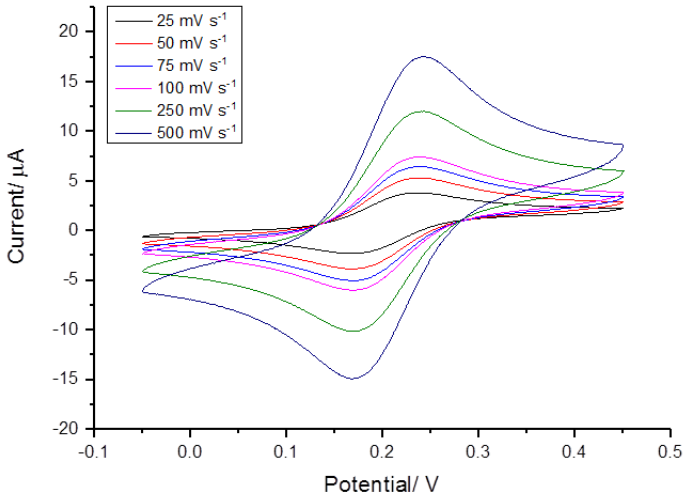


Figure B2.4. *CVs of [2]rotaxane **3.9Bu-H** at different scan rates ([**3.9Bu-H**] = 0.5 mM, T = 293 K).*

Table B2. Values of E_{pc}, E_{pa}, I_{pa}, I_{pc}, ΔE and I_{pa}/ I_{pc} for rotaxane **3.9Bu-H** at different scan rates.

Scan rate/ mV s^{-1}	E_{pa}/V	E_{pc}/V	I_{pa}/ µA	I_{pc}/ µA	ΔE/ V	I_{pa}/ I_{pc}
25	0.232	0.172	3.080	3.040	0.060	1.013
50	0.232	0.171	4.570	4.460	0.061	1.025
75	0.233	0.174	5.540	5.420	0.059	1.022
100	0.235	0.172	6.720	6.240	0.063	1.077
250	0.234	0.172	10.900	10.400	0.062	1.048
500	0.236	0.174	16.800	15.900	0.062	1.057

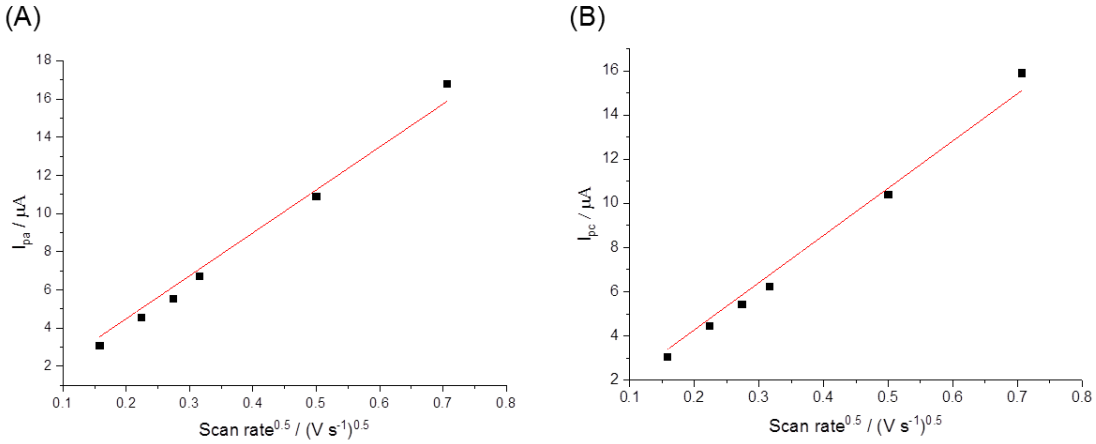


Figure B2.5. *Plots of (A) I_{pa} and (B) I_{pc} against (scan rate)$^{1/2}$ for [2]rotaxane **3.9Bu-H**.*

Rotaxane **3.9Fc-H**

Studies performed in 0.1 M $TBAPF_6$ in dichloromethane/ CH_3CN/ H_2O 1:1.

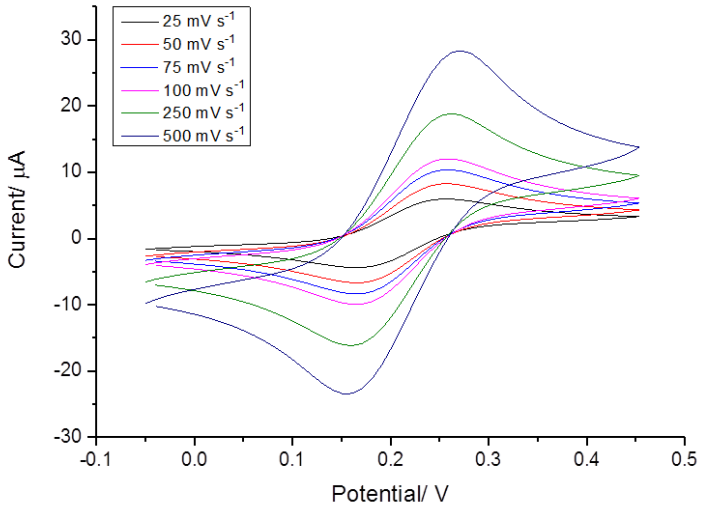


Figure B2.6. *CVs of [2]rotaxane **3.9Fc-H** at different scan rates([**3.9Fc-H**] = 0.5 mM, T = 293 K).*

Table B3. Values of E_{pc}, E_{pa}, I_{pa}, I_{pc}, ΔE and I_{pa}/I_{pc} for rotaxane **3.9Fc-H** at different scan rates.

Scan rate/ mV s^{-1}	E_{pa}/V	E_{pc}/V	I_{pa}/ µA	I_{pc}/ µA	ΔE/ V	I_{pa}/I_{pc}
25	0.252	0.172	4.569	4.635	0.080	0.986
50	0.252	0.172	6.589	6.643	0.080	0.992
75	0.252	0.172	8.258	8.309	0.080	0.994
100	0.252	0.172	9.671	9.712	0.080	0.996
250	0.262	0.161	15.140	15.270	0.101	0.991
500	0.272	0.161	22.440	21.750	0.111	1.032

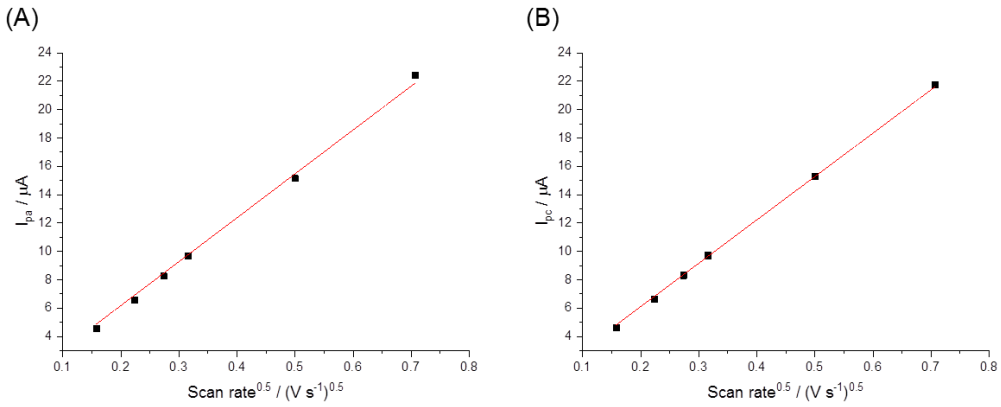


Figure B2.7. *Plots of (A) I_{pa} and (B) I_{pc} against (scan rate)$^{1/2}$ for [2]rotaxane **3.9Fc-H**.*

Rotaxane **3.9Py-H**

Studies performed in 0.1 M $TBAPF_6$ in dichloromethane/ CH_3CN/ H_2O 1:1.

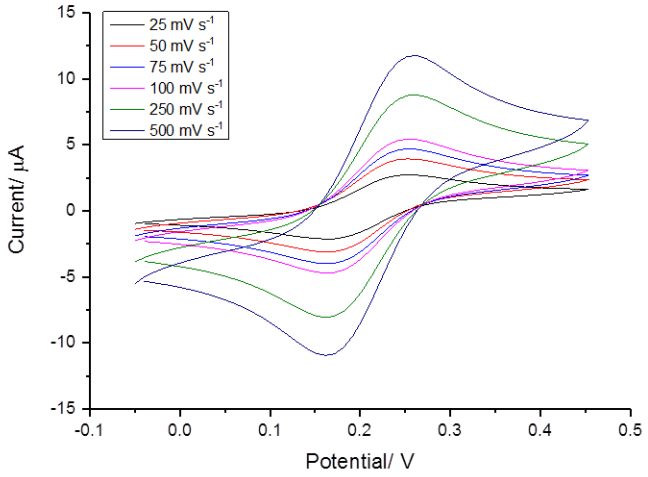


Figure B2.8. *CVs of [2]rotaxane **3.9Py-H** at different scan rates ([**3.9Py-H**] = 0.5 mM, T = 293 K).*

Table B4. Values of E_{pc}, E_{pa}, I_{pa}, I_{pc}, ΔE and I_{pa}/ I_{pc} for rotaxane **3.9Py-H** at different scan rates.

Scan rate/ mV s^{-1}	E_{pa}/V	E_{pc}/V	I_{pa}/ µA	I_{pc}/ µA	ΔE/ V	I_{pa}/ I_{pc}
25	0.252	0.172	2.042	2.078	0.080	0.983
50	0.252	0.172	2.954	2.971	0.080	0.994
75	0.252	0.172	3.645	3.654	0.080	0.998
100	0.252	0.172	4.257	4.263	0.080	0.999
250	0.252	0.172	6.840	7.183	0.080	0.952
500	0.252	0.172	9.272	9.759	0.080	0.950

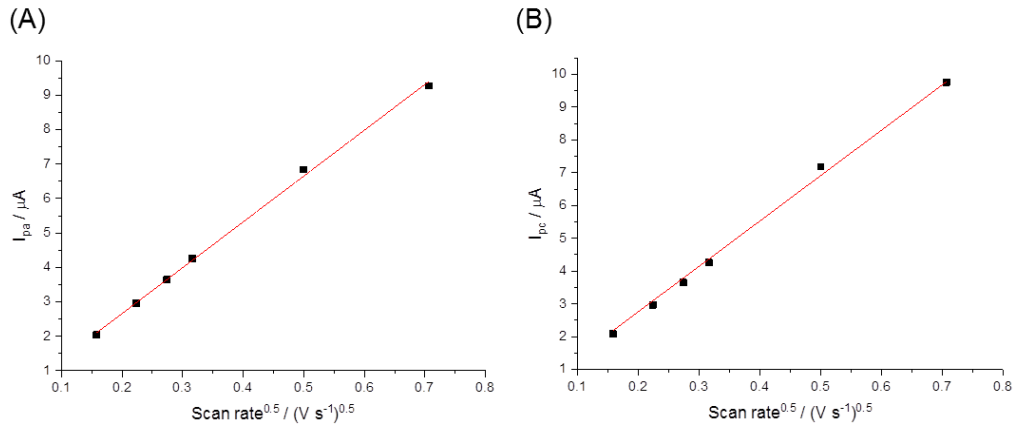


Figure B2.9. *Plots of (A) I_{pa} and (B) I_{pc} against (scan rate)$^{1/2}$ for [2]rotaxane **3.9Py-H**.*

Rotaxane **3.9NO$_2$-H**

Studies performed in 0.1 M $TBAPF_6$ in dichloromethane/ CH_3CN/ H_2O 1:1.

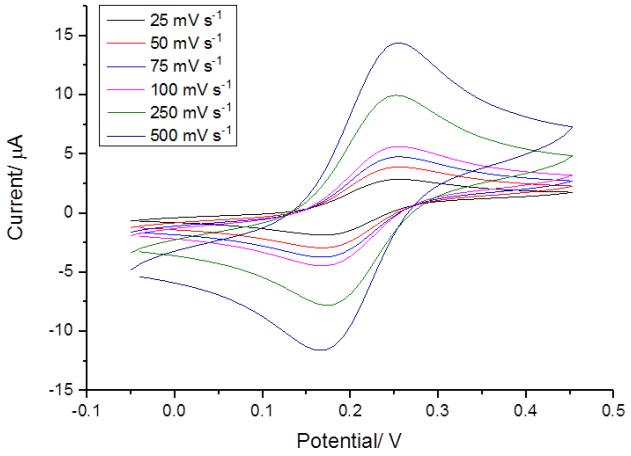


Figure B2.10. *CVs of [2]rotaxane* ***3.9NO$_2$-H*** *at different scan rates ([**3.9NO$_2$-H**] = 0.5 mM, T = 293 K).*

Table B5. Values of E_{pc}, E_{pa}, I_{pa}, I_{pc}, ΔE and I_{pa}/ I_{pc} for rotaxane **3.9NO$_2$-H** at different scan rates.

Scan rate/ mV s^{-1}	E_{pa}/V	E_{pc}/V	I_{pa}/ µA	I_{pc}/ µA	ΔE/ V	I_{pa}/ I_{pc}
25	0.252	0.182	2.018	2.024	0.070	0.997
50	0.252	0.182	2.904	2.950	0.070	0.984
75	0.252	0.182	3.603	3.648	0.070	0.988
100	0.252	0.182	4.270	4.320	0.070	0.988
250	0.252	0.182	7.890	7.413	0.070	1.064
500	0.252	0.172	11.210	10.480	0.080	1.070

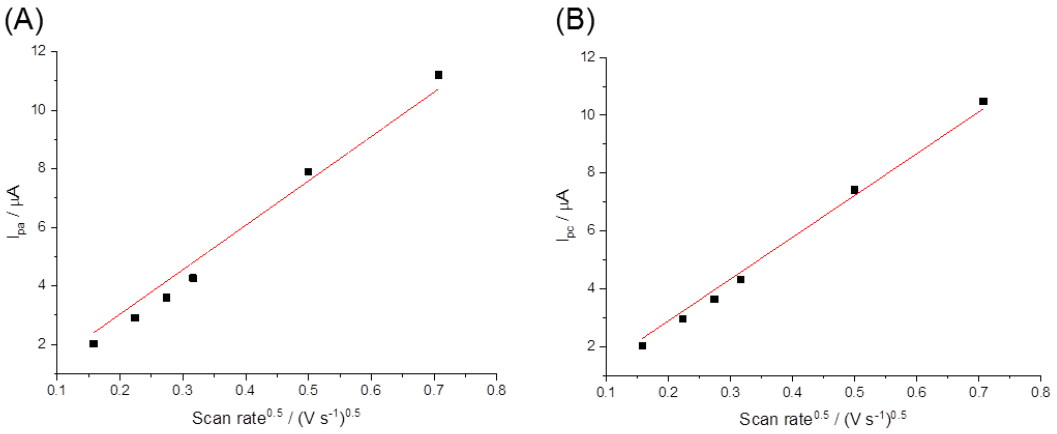


Figure B2.11. *Plots of (A) I_{pa} and (B) I_{pc} against (scan rate)$^{1/2}$ for [2]rotaxane* ***3.9NO$_2$-H****.*

Rotaxane **3.9Bu-I**

Studies performed in 0.1 M $TBAPF_6$ in dichloromethane/ CH_3CN/ H_2O 1:1.

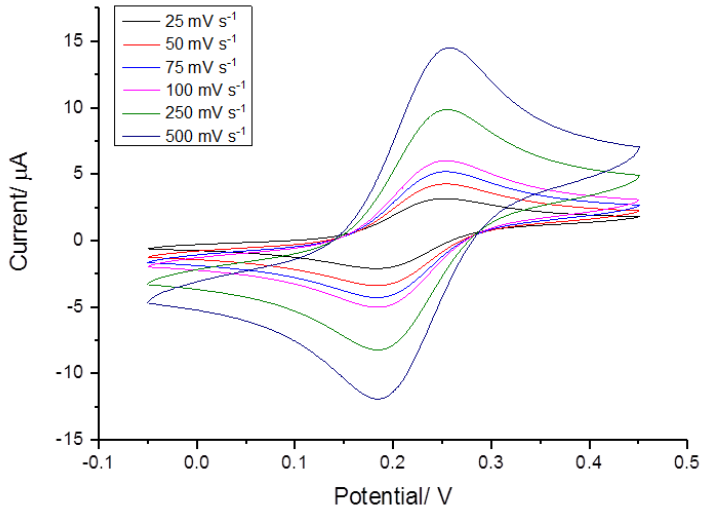


Figure B2.12. *CVs of [2]rotaxane **3.9Bu-I** at different scan rates ([**3.9Bu-I**] = 0.5 mM, T = 293 K).*

Table B6. Values of E_{pc}, E_{pa}, I_{pa}, I_{pc}, ΔE and I_{pa}/ I_{pc} for rotaxane **3.9Bu-I** at different scan rates.

Scan rate/ mV s^{-1}	E_{pa}/V	E_{pc}/V	I_{pa}/ µA	I_{pc}/ µA	ΔE/ V	I_{pa}/ I_{pc}
25	0.253	0.184	1.446	1.569	0.069	0.922
50	0.255	0.185	3.445	3.595	0.070	0.958
75	0.254	0.182	4.375	4.442	0.072	0.985
100	0.254	0.183	4.999	5.164	0.071	0.968
250	0.254	0.185	8.249	8.364	0.069	0.986
500	0.255	0.186	12.120	12.100	0.069	1.002

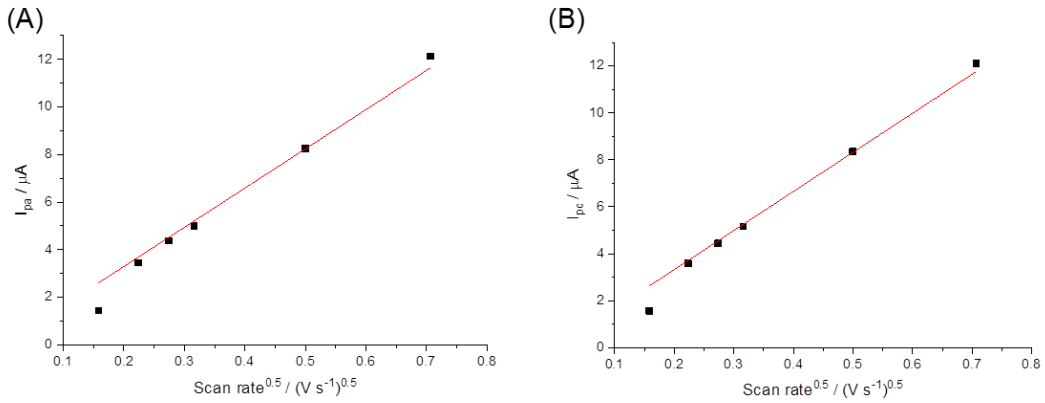


Figure B2.13. *Plots of (A) I_{pa} and (B) I_{pc} against (scan rate)$^{1/2}$ for [2]rotaxane **3.9Bu-I**.*

Receptor **3.19H**

Studies performed in 0.1 M $TBAPF_6$ in CH_3CN.

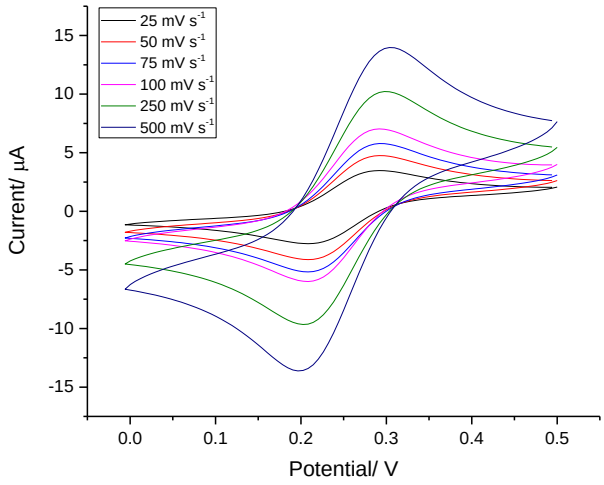


Figure B2.14. *CVs of receptor **3.19H** at different scan rates ([**3.19H**] = 0.5 mM, T = 293 K).*

Table B7. Values of E_{pc}, E_{pa}, I_{pa}, I_{pc}, ΔE and I_{pa}/I_{pc} for **3.19H** at different scan rates

Scan rate/ mV s^{-1}	E_{pa}/V	E_{pc}/V	I_{pa}/ µA	I_{pc}/ µA	ΔE_p / V	I_{pa} / I_{pc}
25	0.292	0.208	2.77	2.91	0.084	0.952
50	0.292	0.208	3.97	4.07	0.084	0.975
75	0.292	0.208	4.92	4.99	0.084	0.986
100	0.292	0.208	5.84	6.01	0.084	0.972
250	0.298	0.202	8.74	8.97	0.096	0.974
500	0.304	0.197	11.7	12.4	0.107	0.944

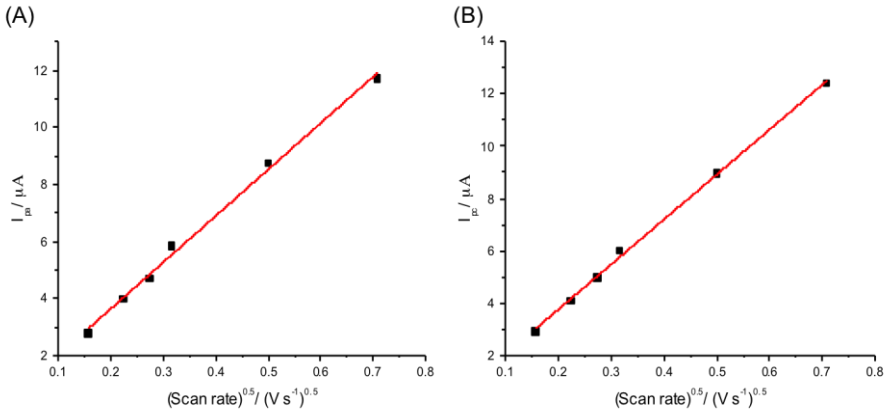


Figure B2.15*. Plots of (A) I_{pa} and (B) I_{pc} against (scan rate)$^{1/2}$ for receptor **3.19H**.*

Receptor **3.19l**

Studies performed in 0.1 M $TBAPF_6$ in CH_3CN.

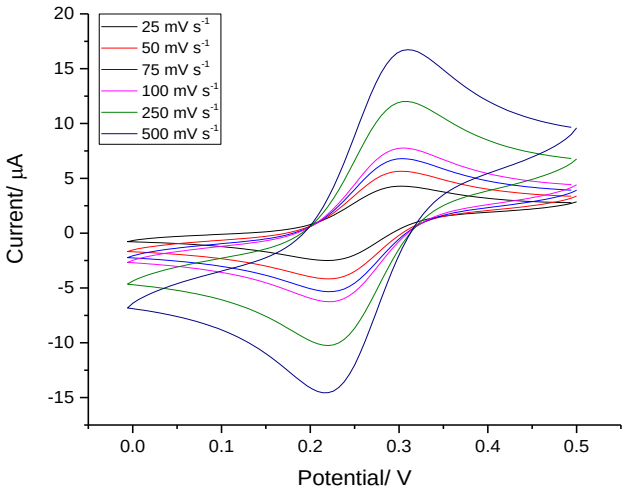


***Figure B2.16**. CVs of receptor **3.19l** at different scan rates ([**3.19l**] = 0.5 mM, T = 293 K).*

Table B8. Values of E_{pc}, E_{pa}, I_{pa}, I_{pc}, ΔE and I_{pa}/I_{pc} for **3.19l** at different scan rates

Scan rate/ mV s^{-1}	E_{pa}/V	E_{pc}/V	I_{pa}/ µA	I_{pc}/ µA	ΔE_p / V	I_{pa} / I_{pc}
25	0.304	0.220	2.96	3.17	0.084	0.932
50	0.304	0.220	4.30	4.52	0.084	0.952
75	0.304	0.220	5.26	5.62	0.084	0.936
100	0.304	0.220	6.16	6.44	0.084	0.956
250	0.310	0.220	9.61	10.3	0.090	0.937
500	0.310	0.214	13.6	14.2	0.096	0.960

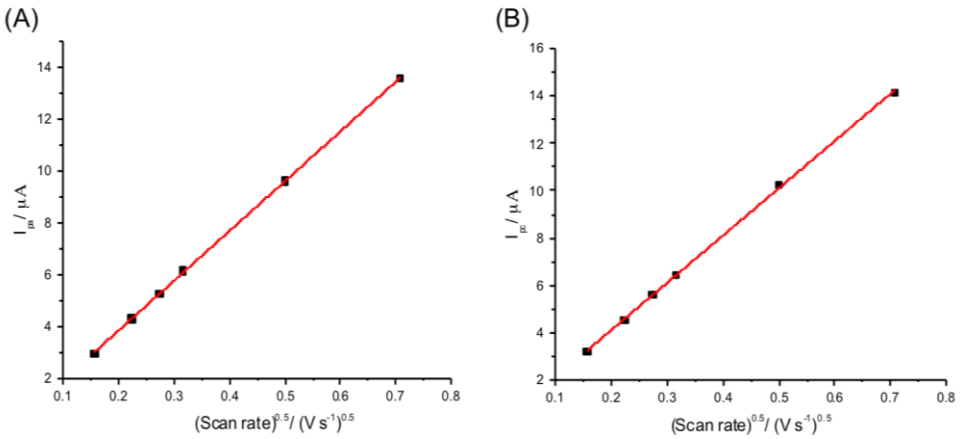


***Figure B2.17**. Plots of (A) I_{pa} and (B) I_{pc} against (scan rate)$^{1/2}$ for **3.19l**.*

Receptor **3.19Se**

Studies performed in 0.1 M $TBAPF_6$ in CH_3CN.

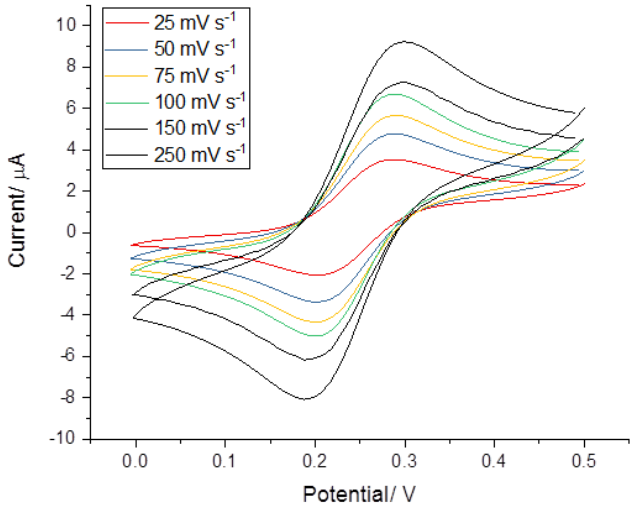


***Figure B2.18**. CVs of receptor **3.19Se** at different scan rates ([**3.19Se**] = 0.5 mM, T = 293 K).*

Table B9. Values of E_{pc}, E_{pa}, I_{pa}, I_{pc}, ΔE and I_{pa}/ I_{pc} for **3.19Se** at different scan rates

Scan rate/ mV s^{-1}	E_{pa}/V	E_{pc}/V	I_{pa}/ µA	I_{pc}/ µA	ΔE_p / V	I_{pa} / I_{pc}
25	0.286	0.202	2.348	2.220	0.084	1.06
50	0.292	0.202	3.356	3.176	0.090	1.06
75	0.292	0.202	4.000	4.214	0.090	0.949
100	0.292	0.197	4.777	4.963	0.095	0.963
150	0.289	0.198	5.478	5.663	0.091	0.967
250	0.299	0.198	7.015	6.841	0.101	1.03

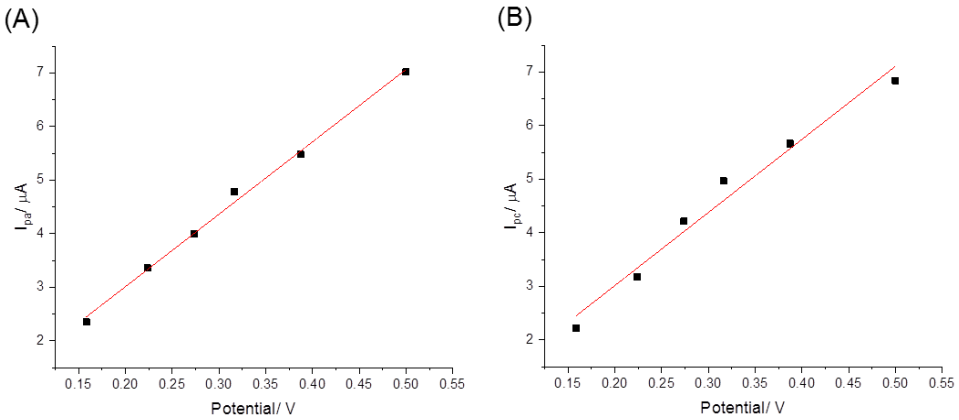


***Figure B2.19**. Plots of (A) I_{pa} and (B) I_{pc} against (scan rate)$^{1/2}$ for receptor **3.19Se**.*

Receptor **3.21H**

Studies performed in 0.1 M $TBAPF_6$ in CH_3CN.

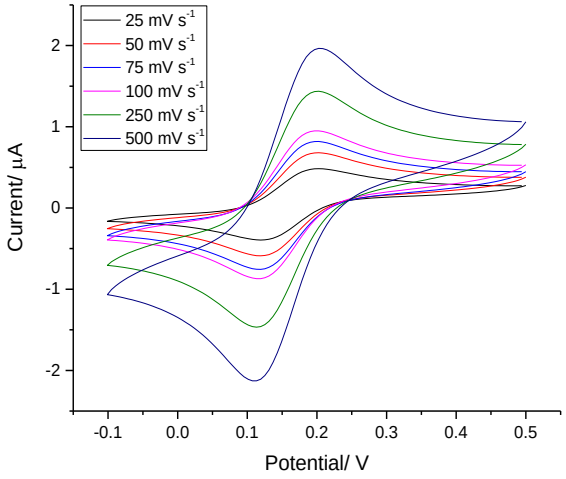


Figure B2.20. *CVs of receptor **3.21H** at different scan rates ([**3.21H**] = 0.5 mM, T = 293 K).*

Table B10. Values of E_{pc}, E_{pa}, I_{pa}, I_{pc}, ΔE and I_{pa}/ I_{pc} for **3.21H** at different scan rates

Scan rate/ mV s^{-1}	E_{pa}/V	E_{pc}/V	I_{pa}/ µA	I_{pc}/ µA	ΔE_p / V	I_{pa} / I_{pc}
25	0.202	0.119	3.99	3.11	0.083	1.28
50	0.202	0.119	5.32	5.09	0.083	1.05
75	0.202	0.119	6.67	6.23	0.083	1.07
100	0.202	0.113	7.76	7.46	0.089	1.04
250	0.202	0.113	12.0	11.8	0.089	1.02
500	0.202	0.113	16.9	16.2	0.089	1.04

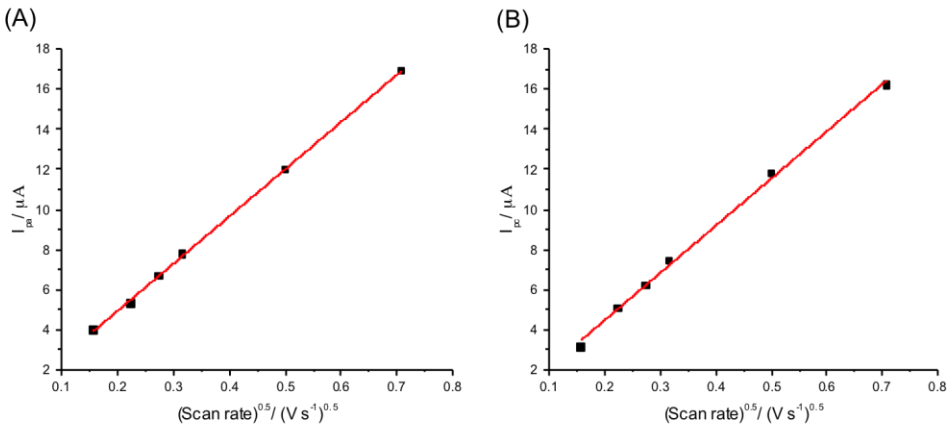


Figure B2.21. *Plots of (A) I_{pa} and (B) I_{pc} against (scan rate)$^{1/2}$ for receptor **3.21H**.*

Receptor **3.21l**

Studies performed in 0.1 M $TBAPF_6$ in CH_3CN.

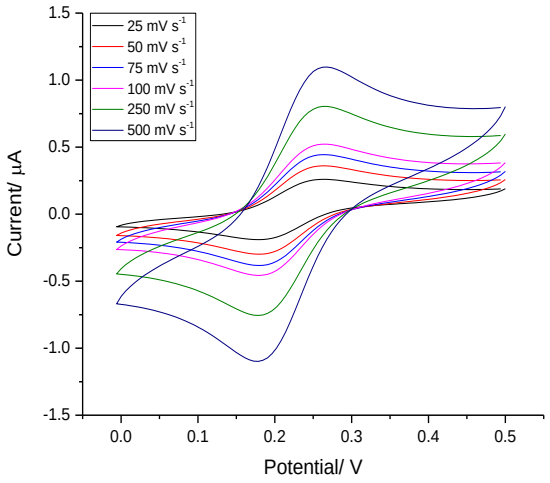


***Figure B2.22**. CVs of receptor **3.21l** at different scan rates ([**3.21l**] = 0.5 mM, T = 293 K).*

Table B11. Values of E_{pc}, E_{pa}, I_{pa}, I_{pc}, ΔE and I_{pa}/ I_{pc} for **3.21l** at different scan rates

Scan rate/ mV s^{-1}	E_{pa}/V	E_{pc}/V	I_{pa}/ µA	I_{pc}/ µA	ΔE_p / V	I_{pa} / I_{pc}
25	0.262	0.179	1.75	1.38	0.083	1.27
50	0.262	0.179	2.50	2.28	0.083	1.10
75	0.262	0.179	3.12	2.74	0.083	1.14
100	0.262	0.179	3.41	3.24	0.083	1.05
250	0.262	0.179	5.15	5.20	0.083	0.990
500	0.268	0.179	7.86	7.25	0.089	1.08

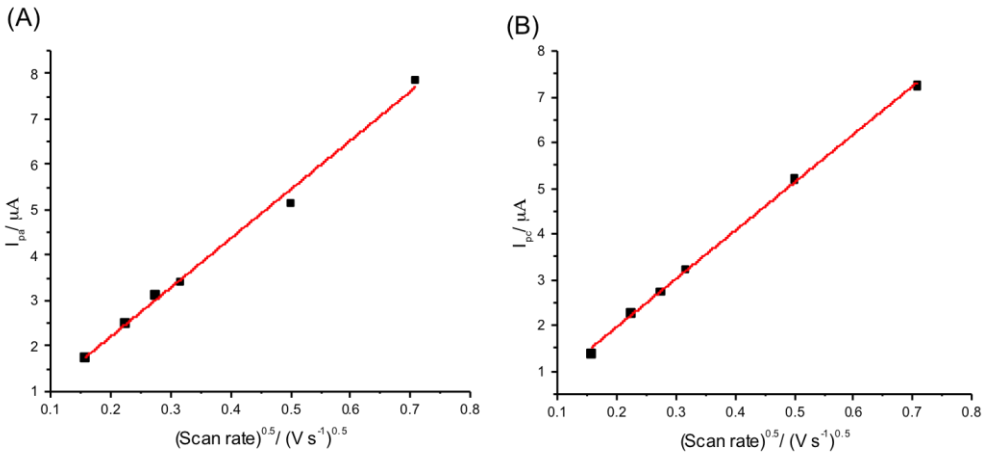


***Figure B2.23**. Plots of (A) I_{pa} and (B) I_{pc} against (scan rate)$^{1/2}$ for receptor **3.21l**.*

Receptor **3.24H**

Studies performed in 0.1 M $TBAPF_6$ in CH_3CN.

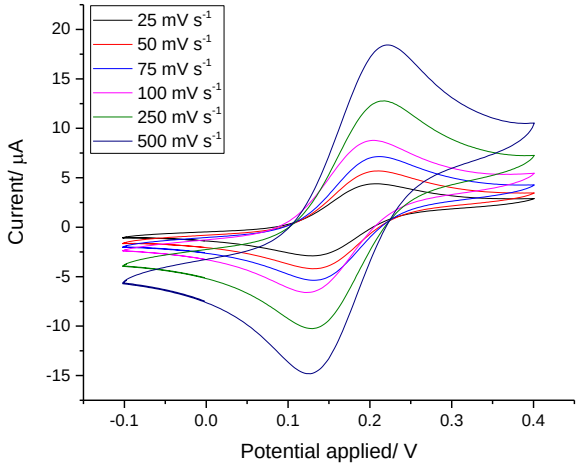


***Figure B2.24**. CVs of receptor **3.24H** at different scan rates ([**3.24H**] = 0.5 mM, T = 293 K).*

Table B12. Values of E_{pc}, E_{pa}, I_{pa}, I_{pc}, ΔE and I_{pa}/ I_{pc} for **3.24H** at different scan rates

Scan rate/ mV s^{-1}	E_{pa}/V	E_{pc}/V	I_{pa}/ µA	I_{pc}/ µA	ΔE_p / V	I_{pa} / I_{pc}
25	0.206	0.128	3.282	3.488	0.078	0.941
50	0.208	0.132	4.455	4.760	0.074	0.936
75	0.211	0.132	5.824	6.058	0.079	0.961
100	0.204	0.134	6.845	7.437	0.070	0.920
250	0.208	0.130	10.239	11.082	0.078	0.924
500	0.215	0.130	14.611	15.794	0.085	0.925

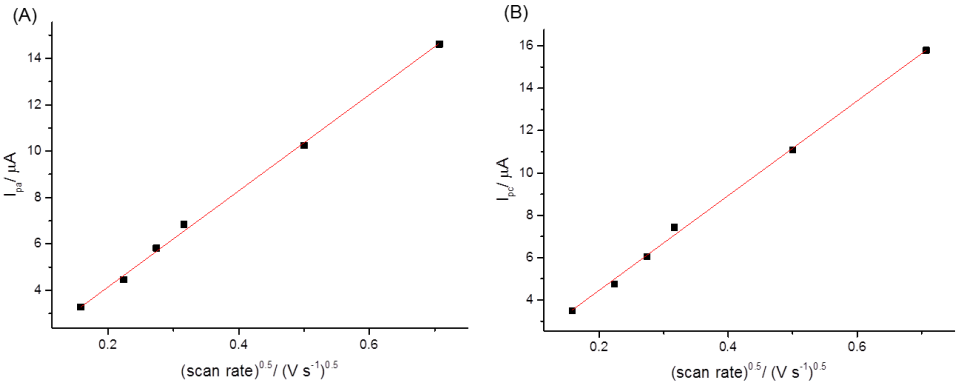


***Figure B2.25**. Plots of (A) I_{pa} and (B) I_{pc} against (scan rate)$^{1/2}$ for **3.24H**.*

Receptor **3.24l**

Studies performed in 0.1 M $TBAPF_6$ in CH_3CN.

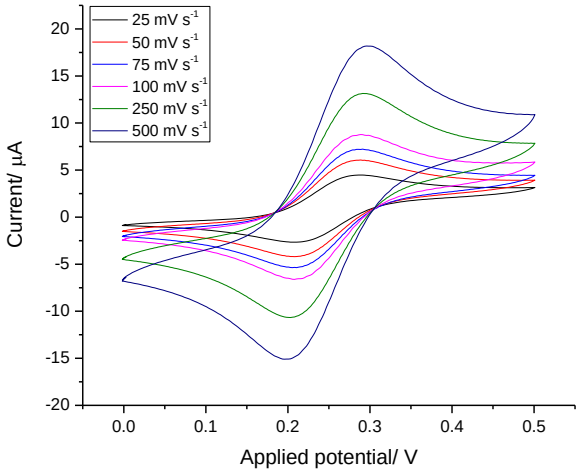


***Figure B2.26**. CVs of receptor **3.24l** at different scan rates ([**3.24l**] = 0.5 mM, T = 293 K).*

Table B13. Values of E_{pc}, E_{pa}, I_{pa}, I_{pc}, ΔE and I_{pa}/I_{pc} for **3.24l** at different scan rates

Scan rate/ mV s^{-1}	E_{pa}/V	E_{pc}/V	I_{pa}/ µA	I_{pc}/ µA	ΔE_p / V	I_{pa} / I_{pc}
25	0.279	0.213	3.563	3.562	0.066	1.000
50	0.279	0.211	4.983	5.023	0.068	0.992
75	0.281	0.211	6.087	6.097	0.070	0.998
100	0.281	0.208	6.858	6.953	0.073	0.986
250	0.286	0.208	10.973	11.064	0.078	0.992
500	0.288	0.203	15.296	15.459	0.085	0.989

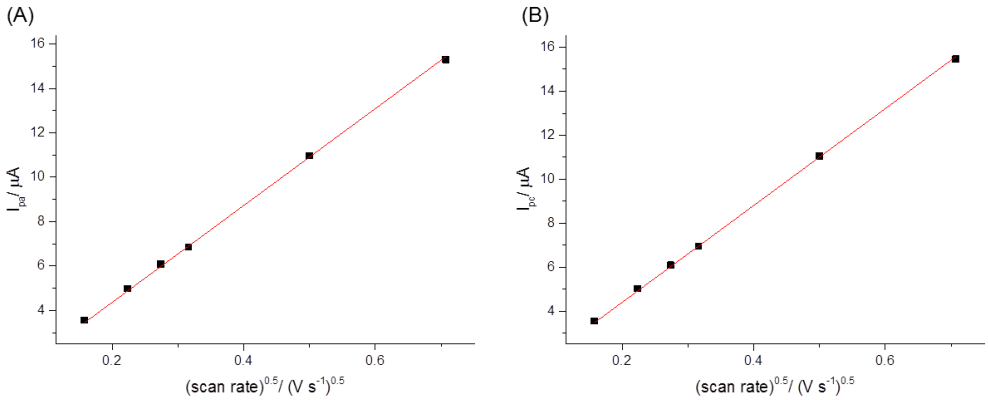


***Figure B2.27**. Plots of (A) I_{pa} and (B) I_{pc} against $(\text{scan rate})^{1/2}$ for **3.24l**.*

Macrocycle **3.27l**

Studies performed in 0.1 M $TBAPF_6$ in acetone/ CH_3CN 1:1.

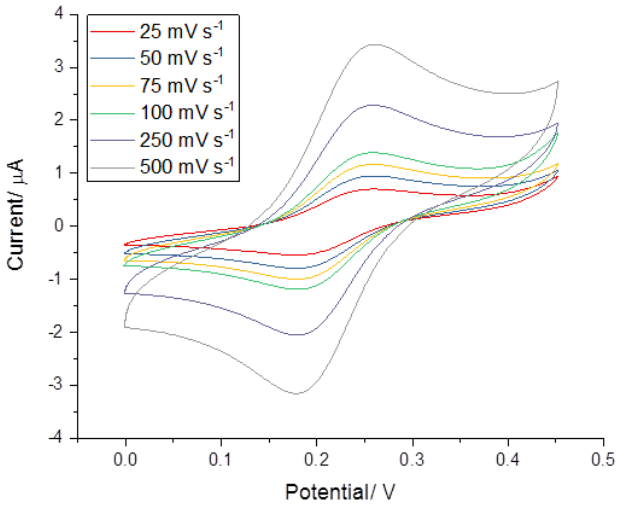


***Figure B2.28**. CVs of receptor **3.27l** at different scan rates ([**3.27l**] = 0.1 mM, T = 293 K).*

Table B14. Values of E_{pc}, E_{pa}, I_{pa}, I_{pc} ΔE_p and I_{pa}/ I_{pc} for **3.27l** recorded at different scan rates.

Scan rate/ mV s^{-1}	E_{pa}/V	E_{pc}/V	I_{pa}/ µA	I_{pc}/ µA	ΔE_p / V	I_{pa} / I_{pc}
25	0.247	0.186	0.416	0.514	0.061	0.809
50	0.245	0.187	0.611	0.707	0.058	0.864
75	0.247	0.186	0.775	0.860	0.061	0.901
100	0.247	0.189	0.865	1.120	0.058	0.772
250	0.247	0.189	1.584	1.742	0.058	0.909
500	0.249	0.187	2.382	2.576	0.062	0.925

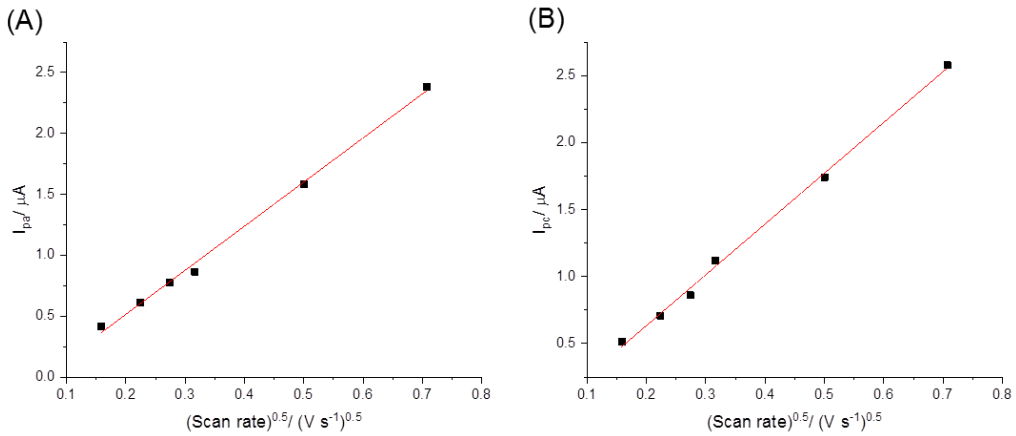


***Figure B2.29**. Plots of (A) I_{pa} and (B) I_{pc} against (scan rate)$^{1/2}$ for **3.27l**.*

Macrocycle **3.27H**

Studies performed in 0.1 M $TBAPF_6$ in acetone/ CH_3CN 1:1.

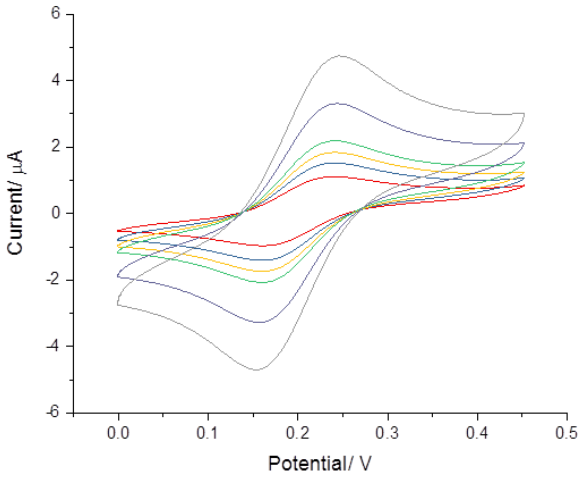


Figure B2.30. *CVs of receptor **3.27H** at different scan rates ([**3.27H**] = 0.1 mM, T = 293 K).*

Table B15. Values of E_{pc}, E_{pa}, I_{pa}, I_{pc} ΔE_p and I_{pa}/ I_{pc} for **3.27H** recorded at different scan rates.

Scan rate/ mV s^{-1}	E_{pa}/V	E_{pc}/V	I_{pa}/ µA	I_{pc}/ µA	ΔE_p / V	I_{pa} / I_{pc}
25	0.231	0.169	0.877	0.871	0.062	1.01
50	0.232	0.169	1.263	1.218	0.063	1.04
75	0.233	0.167	1.555	1.484	0.066	1.05
100	0.233	0.167	1.820	1.796	0.066	1.01
250	0.235	0.164	2.860	2.704	0.071	1.06
500	0.237	0.161	4.012	3.783	0.076	1.06

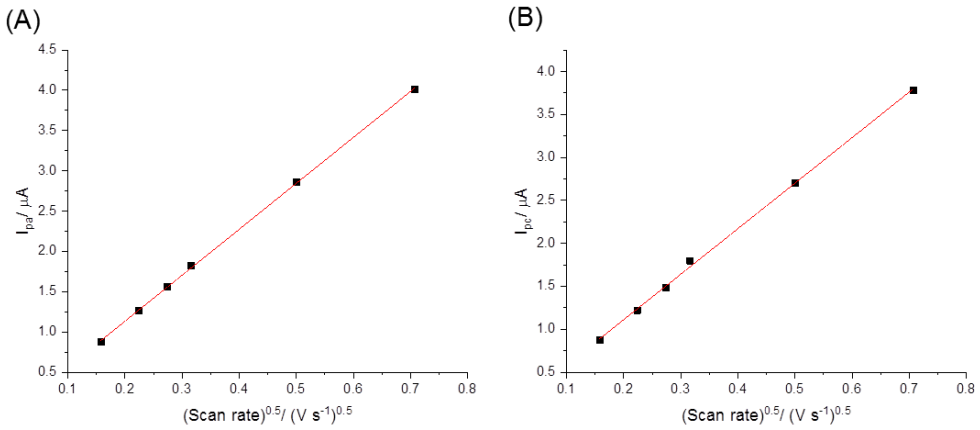


Figure B2.31. *Plots of (A) I_{pa} and (B) I_{pc} against (scan rate)$^{1/2}$ for **3.27H**.*

Rotaxane **3.34I$_4$** (dry solvent)

Studies performed in 0.1 M $TBAPF_6$ in acetone/ CH_3CN 1:1.

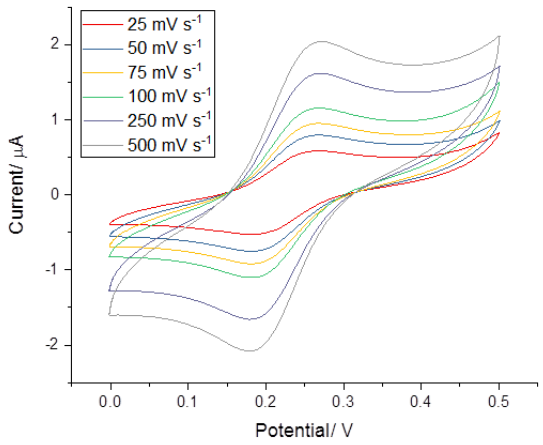


***Figure B2.32**. CVs of receptor **3.34I$_4$** at different scan rates ([**3.34I$_4$**] = 0.1 mM, T = 293 K).*

Table B16. Values of E_{pc}, E_{pa}, I_{pa}, I_{pc} ΔE_p and I_{pa}/ I_{pc} for **3.34I$_4$** recorded at different scan rates.

Scan rate/ mV s^{-1}	E_{pa}/V	E_{pc}/V	I_{pa}/ µA	I_{pc}/ µA	ΔE_p / V	I_{pa} / I_{pc}
25	0.252	0.193	0.359	0.410	0.059	0.876
50	0.254	0.193	0.516	0.560	0.061	0.921
75	0.254	0.193	0.629	0.677	0.061	0.929
100	0.254	0.193	0.751	0.804	0.061	0.934
250	0.257	0.191	1.121	1.155	0.066	0.971
500	0.256	0.191	1.396	1.432	0.065	0.975

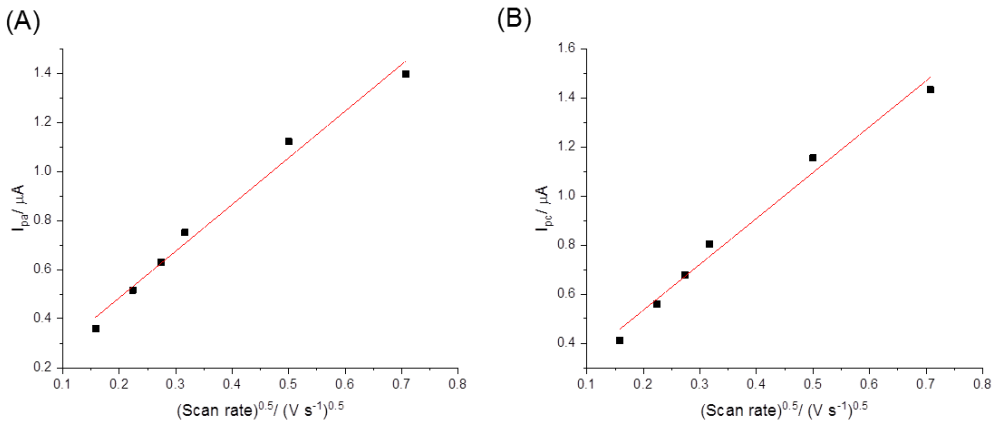


***Figure B2.33**. Plots of (A) I_{pa} and (B) I_{pc} against (scan rate)$^{1/2}$ for **3.34I$_4$**.*

Rotaxane **3.34I$_4$** (wet solvent)

Studies performed in 0.1 M $TBAPF_6$ in acetone/ CH_3CN/ H_2O 45:45:10.

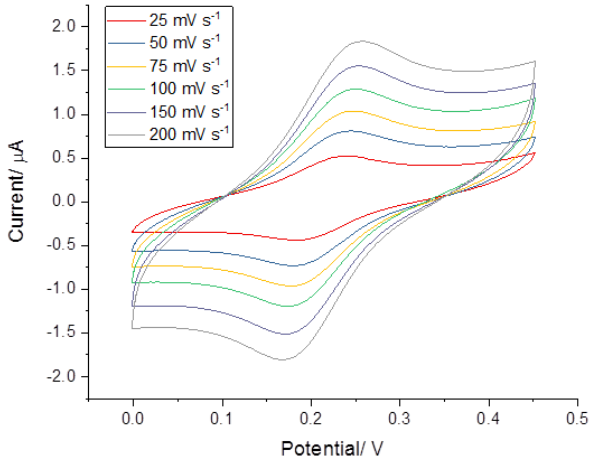


Figure B2.34. *CVs of receptor **3.34I$_4$** at different scan rates ([**3.34I$_4$**] = 0.1 mM, T = 293 K).*

Table B17. Values of E_{pc}, E_{pa}, I_{pa}, I_{pc} ΔE_p and I_{pa}/ I_{pc} for **3.34I$_4$** recorded at different scan rates.

Scan rate/ mV s^{-1}	E_{pa}/V	E_{pc}/V	I_{pa}/ µA	I_{pc}/ µA	ΔE_p / V	I_{pa} / I_{pc}
25	0.230	0.193	0.284	0.302	0.037	0.940
50	0.235	0.188	0.498	0.493	0.047	1.01
75	0.237	0.186	0.647	0.638	0.051	1.01
100	0.240	0.183	0.772	0.801	0.057	0.964
150	0.242	0.181	0.972	0.928	0.061	1.05
200	0.245	0.178	1.112	1.085	0.067	1.02

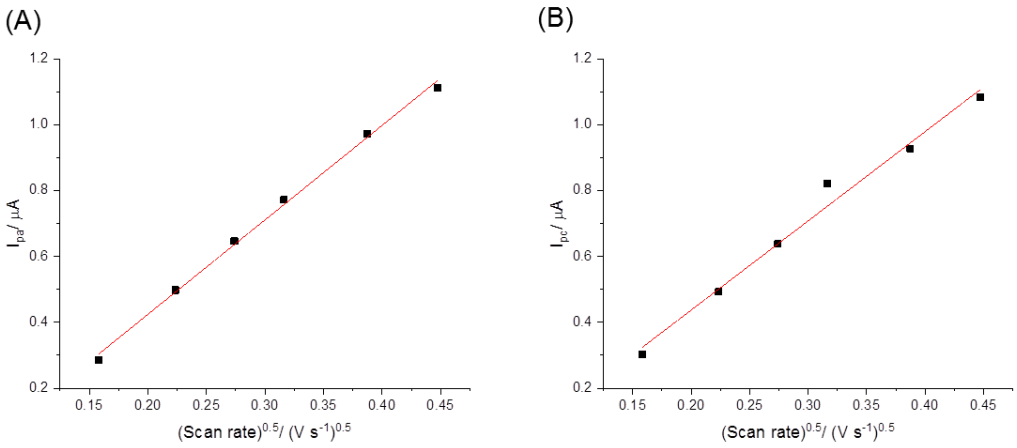


Figure B2.35. *Plots of (A) I_{pa} and (B) I_{pc} against (scan rate)$^{1/2}$ for **3.34I$_4$**.*

Chiral Receptor **4.9l**

Studies performed in 0.1 M $TBAPF_6$ in CH_3CN.

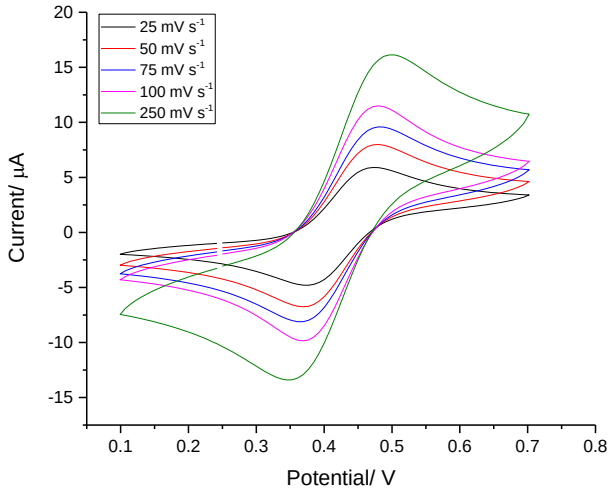


Figure B2.36. *CVs of receptor **4.9l** at different scan rates ([**4.9l**] = 0.5 mM, T = 293 K).*

Table B18. Values of E_{pc}, E_{pa}, I_{pa}, I_{pc}, ΔE and I_{pa}/ I_{pc} for **4.9l** at different scan rates

Scan rate/ mV s^{-1}	E_{pa}/V	E_{pc}/V	I_{pa}/ µA	I_{pc}/ µA	ΔE_p / V	I_{pa} / I_{pc}
25	0.480	0.369	4.73	5.03	0.111	0.94
50	0.480	0.369	6.34	6.79	0.111	0.93
75	0.480	0.369	7.46	7.96	0.111	0.94
100	0.480	0.369	9.14	9.79	0.111	0.93
250	0.496	0.345	11.52	12.25	0.151	0.94

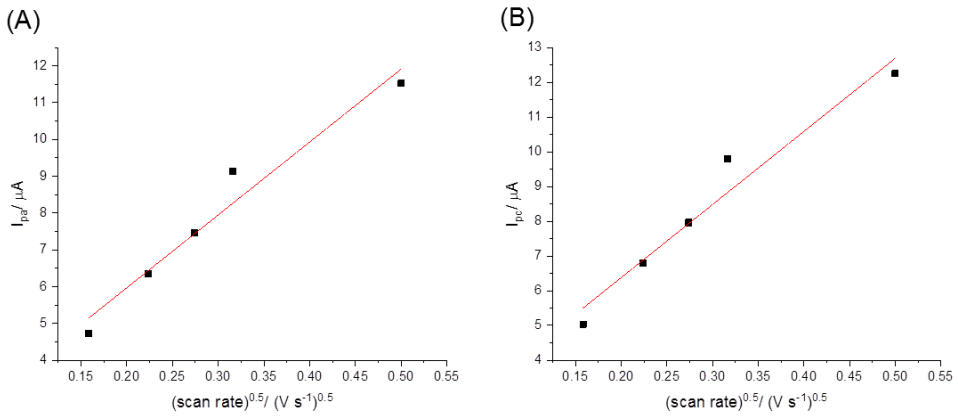


Figure B2.37. *Plots of (A) I_{pa} and (B) I_{pc} against $(\text{scan rate})^{1/2}$ for **4.9l**.*

Chiral Receptor **4.9H**

Studies performed in 0.1 M $TBAPF_6$ in CH_3CN.

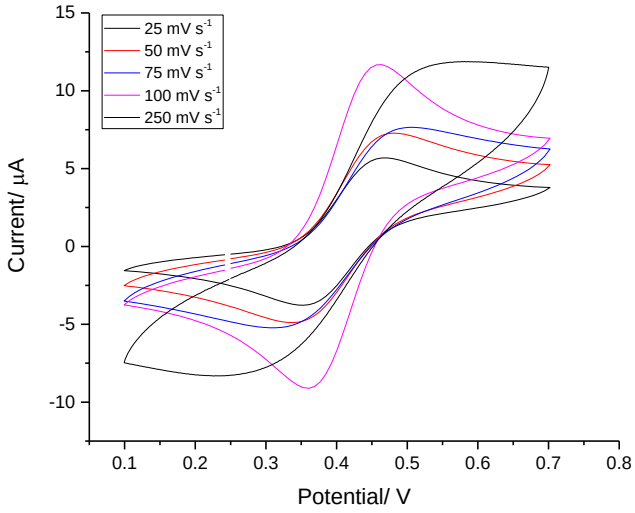


***Figure B2.38**. CVs of receptor **4.9H** at different scan rates ([**4.9H**] = 0.5 mM, T = 293 K).*

Table B19. Values of E_{pc}, E_{pa}, I_{pa}, I_{pc}, ΔE and I_{pa}/ I_{pc} for **4.9H** at different scan rates

Scan rate/ mV s^{-1}	E_{pa}/V	E_{pc}/V	I_{pa}/ µA	I_{pc}/ µA	ΔE_p / V	I_{pa} / I_{pc}
25	0.464	0.353	4.13	4.16	0.111	0.99
50	0.488	0.329	4.69	4.59	0.159	1.02
75	0.504	0.313	6.42	7.12	0.191	0.90
100	0.464	0.361	9.13	9.41	0.103	0.97
250	0.557	0.276	-[a)]	-[a)]	0.281	-[a)]

[a)] Not possible to accurately determine values of I_{pa} and I_{pc} from the CV obtained.

From the large fluctuations of ΔE_p and I_{pa}/ I_{pc} at different scan rates, and the poorly-defined CV obtained at a scan rate of 250 mV s^{-1}, receptor **4.9H** can be described as having poor electrochemical reversibility. Hence, it was not used for further sensing studies.

Appendix C: Computational Simulations

All computational modelling experiments were performed by Dr Igor Marques and Professor Vítor Felíx at the University of Aveiro, Portugal.

C1. Experiments for Chapter 2

Starting structures

The structure of the macrocyclic component of rotaxane **2.20Se$_2$H** was directly taken from the single crystal X-ray structure of macrocycle **2.9Se** reported in this work, while the structure of the axle was generated from the crystal structure of a rotaxane analogous deposited with the Cambridge Crystallographic Data Centre (CCDC)[9] under RefCode TACPUK.[10] The iodine atom of axle's triazolium core was just replaced by a hydrogen atom yielding the axle of **2.20Se$_2$H**. Subsequently, the ChB **2.20Se$_2$H** rotaxane was obtained by the assembly of these two components in an interlocked fashion with the C-H triazolium binding unit and the SeMe units of the macrocyclic cleft adopting an almost orthogonal relative disposition. The halide associations were further generated by the insertion of each anion into the **2.20Se$_2$H** binding cavity establishing two chalcogen bonds with the $SeCH_3$ groups and a C-H···O interaction with the C-H triazolium.

The force field parameterization of the chalcogen bonds was carried out using the model compound **2.9Se$_{methyl}$**, which was generated by capping the benzene-1,3-bis(triazolium) chalcogen binding motif of macrocycle **2.9Se** with two methyl groups.

Quantum calculations

All quantum calculations were carried out with the Gaussian09 software,[11] which included the optimization of the Cu(I) complexes of **2.1Se** and **2.1Te** in the acetone implicit solvent (Polarizable Continuum Model);[12] the optimization of the **2.9Se$_{methyl}$** halide associations in

gas-phase followed the analysis of their ChB interactions; and the derivatization of restrained electrostatic potential (RESP) charges for the macrocycle and axle of **2.20Se$_2$H**.

The **2.1Se** and **2.1Te** copper(I) complexes were optimized using the B3LYP functional and the 6-31+G** basis set for H, C, N and O and the aug-cc-pVDZ-PP basis set parameters for Cu, Se and Te heavy atoms, which were obtained from the EMSL database.[13,14]

All calculations involving **2.9Se$_{methyl}$** were performed with M06-2X functional and using the 6-311++G** basis set for the H, C and N atoms, and the aug-cc-pVDZ-PP basis set for the Se centers.

The distribution of the electrostatic potential, $V(\mathbf{r})$, mapped onto the molecular surface of **2.9Se$_{methyl}$** was computed through a single point on the previously optimized structures of **2.9Se$_{methyl}$**, free or chalcogen bond to halides, after removal of the anions. In this work, the $V(\mathbf{r})$ was evaluated on the 0.001 electrons Bohr^{-3} contour of $\rho(\mathbf{r})$. The electrostatic potential surface ranges, between the most negative and most positive values, were calculated using the *multiwfn* program.[15,16]

The Wiberg bond indices (WBI),[17] which consist in the sum of squares of off-diagonal density matrix elements between atoms, were ascertained from the DFT optimized structures of the halide associations of **2.9Se$_{methyl}$**. These calculations were carried out using the Natural Bond Orbital (*NBO*) Version 3.1 program,[18,19] within the Gaussian09 suite, with the M06-2X functional and the aug-cc-pVDZ-PP basis set for the Se centers and the 6-311++G** basis set for the H, C and N atoms.

Classical force field calculations

Molecular Mechanics (MM) calculations and Molecular Dynamics (MD) simulations were carried out with Amber 16.[20] The rotaxane components (axle and macrocycle) were described with parameters taken from the Generalized Amber Force Field (GAFF),[21,22] except those involving the selenium centers and RESP atomic charges.[23] Due to the inexistence of Se

parameters within the AMBER family of force fields, its bonding parameters were derived using *MCPB.py*[24] and *paramfit*[25] (*vide infra*), while its van der Waals parameters were taken from the Universal Force Field,[26] with the original radius (r_{vdw}) converted to the AMBER formalism as $r_{vdw} = r_{min}/2$, where r_{min} is 4.205 Å. The halides were described with a -1 discrete charge and van der Waals parameters developed for the TIP3P water model.[27] The water molecules were described with the TIP3P model,[28] while the all-atoms model of the acetone solvent molecules was described with OPLS-AA force field parameters and charges taken from ref. 29. The force field parameters and charges of the PF_6^- counter-ion were taken from ref. 30. The post-processing of trajectory files to obtain the structural data was performed with *cpptraj*.[31]

Determination of Se bonding parameters

Due to the inexistence of force field parameters within the AMBER family of force fields, specifically within GAFF, and to pursue the MM and MD studies of **2.20Se$_2$H**, it was necessary to develop Se bonding terms parameters for its macrocycle. This parameterization was carried out with the fragment depicted in Figure , together with its corresponding atom types.

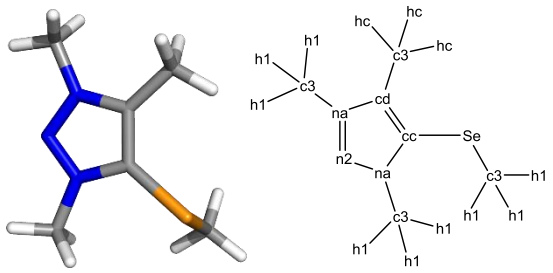


Figure C1.1. *1,3,4-trimethyl-5-(methylselanyl)-1H-1,2,3-triazolium fragment used in the parameterization of Se bonding terms along the employed GAFF atom types.*

This fragment was optimized at the B3LYP level, with the H, C and N atoms being described with the 6-311++G** basis set, while the Se atom was described with the aug-cc-pVDZ-PP basis set, obtained from the EMSL database.[13,14] From the quantum data of the

optimized structure, and using the Seminario method implemented in *MCPB.py*,[24] it was possible to generate the force field parameters for bond lengths and bond angles.

The *MCPB.py* utility does not generate dihedral angle terms. Most of the dihedral angle parameters involving selenium were obtained from GAFF replacing the *Se* atom type by the *ss* one. The dihedral angle terms centered at the *Se-cc* bond were obtained with *paramfit*.[25] The fragment of Figure was optimized at the MP2 level, with the H, C, and N atoms being described with the cc-pVDZ basis set, while the Se was still described with the aug-cc-pVDZ-PP basis set. After the structure optimization, a relaxed Potential Energy Surface scan was undertaken, with the dihedral angles *c3-Se-cc-na* and *c3-Se-cc-cd* being increased 1.8° for 199 times, resulting in a 360° scan around that bond. Subsequently, these dihedral force field parameters were obtained using the genetic algorithm of *paramfit* to fit MM energies to the quantum data.

The complete list of force field parameters incorporating the selenium center developed to be used in the classical force field calculations including the macrocycle **2.9Se** is summarized in Table C1.

Parameterization of the ChB interactions

The **2.9Se$_{methyl}$** halide associations were optimized using the M06-2X functional, using the aug-cc-pVDZ-PP basis set for Se, Br and I, and the aug-cc-pVDZ basis set for Cl, while the remaining centers were treated with the 6-311++G** basis set, as stated above. The optimized structures of **2.9Se$_{methyl}$** with halides, shown in Figures 8 and S7-2, allowed us to compute the Se···A distances (A = Cl^-, Br^-, I^-) and the C-Se···A angles (listed in **Error! Reference source not found.**), guiding the parameterization described below. Moreover, from these optimized structures, the distribution of the electrostatic potential was mapped onto the electron density surface of **2.9Se$_{methyl}$**. The relative positions of the most positive potential ($V_{S,max}$) with respect to each Se atom in the model compound halide association were

ascertained, as depicted in Figure 8 and S7-2 The Se···$V_{S,max}$ distances and the C-Se···$V_{S,max}$ angles are given in Table C2.

Table C1. Se force field parameters used in this work.

Mass	**Atomic weight (A_r)**			**Notes**
Se	78.96			Taken from ref. 32
Bond length	**K_r (kcal mol^{-1} Å^{-2})**	**r_{eq} (Å)**		**Notes**
Se-c3	132.7	1.9874		Determined with *MCPB.py*
Se-cc	169.6	1.9160		Determined with *MCPB.py*
Se-cd	169.6	1.9160		Determined with *MCPB.py*
Bond angle	**K_θ (kcal mol^{-1} rad^{-2})**	**θ_{eq} (°)**		**Notes**
Se-c3-h1	39.96	108.28		Determined with *MCPB.py*
Se-cc-cd	104.37	129.50		Determined with *MCPB.py*
Se-cd-cc	104.37	129.50		Determined with *MCPB.py*
Se-cc-na	107.78	125.57		Determined with *MCPB.py*
Se-cd-na	107.78	125.57		Determined with *MCPB.py*
cc-Se-c3	147.13	98.98		Determined with *MCPB.py*
cd-Se-c3	147.13	98.98		Determined with *MCPB.py*
Dihedral angles	**Scaling factor**	**$V_n/2$ (kcal mol^{-1})**	**γ (°)**	**periodicity *N***	**Notes**
Se-cc-na-c3	1	1.70000000	180.000	2.0	GAFF parameters for ss-cc-na-c3
Se-cd-na-c3	1	1.70000000	180.000	2.0	GAFF parameters for ss-cd-na-c3
Se-cc-na-n2	1	1.70000000	180.000	2.0	GAFF parameters for ss-cc-na-n2
Se-cd-na-n2	1	1.70000000	180.000	2.0	GAFF parameters for ss-cd-na-n2
Se-cc-cd-na	1	4.00000000	180.000	2.0	GAFF parameters for ss-cc-cd-na
Se-cd-cc-na	1	4.00000000	180.000	2.0	GAFF parameters for ss-cd-cc-na
Se-cc-cd-ca	1	4.00000000	180.000	2.0	GAFF parameters for ss-cc-cd-ca
Se-cd-cc-ca	1	4.00000000	180.000	2.0	GAFF parameters for ss-cd-cc-ca
cc-Se-c3-h1	1	0.33333333	0.000	3.0	GAFF parameters for cc-ss-c3-h1
cd-Se-c3-h1	1	0.33333333	0.000	3.0	GAFF parameters for cd-ss-c3-h1
c3-Se-cc-na	1	0.62620000	180.000	2.0	Determined with *paramfit*
c3-Se-cd-na	1	0.62620000	180.000	2.0	Determined with *paramfit*
c3-Se-cc-cd	1	0.08700000	180.000	-2.0	Determined with *paramfit*
c3-Se-cc-cd	1	1.30670000	180.000	3.0	Determined with *paramfit*
c3-Se-cd-cc	1	0.08700000	180.000	-2.0	Determined with *paramfit*
c3-Se-cd-cc	1	1.30670000	180.000	3.0	Determined with *paramfit*
Improper dihedral		**K_Φ (kcal mol^{-1})**	**Φ_0 (°)**	**periodicity *N***	**Notes**
Se-cc-cd-na		1.10000000	180.000	2.0	GAFF parameters for ss-cc-cd-na
Se-cd-cc-na		1.10000000	180.000	2.0	GAFF parameters for ss-cd-cc-na
Van der Waals		**r (Å)**	**ε (kcal mol^{-1})**		**Notes**
Se		2.1025	0.2910		Adapted from the UFF.[19]

Table C2. Internal coordinates of each $SeCH_3$ binging unit's $V_{S,max}$ in the optimized halide associations of **2.9Se$_{methyl}$**.

Halide	Se···$V_{S,max}$ (Å)	$C_{triazolium}$-Se···$V_{S,max}$ (°)	C_{methyl}-Se···$V_{S,max}$ (°)
Cl^-	2.071 ; 2.118	166.1 ; 160.0	73.3 ; 69.6
Br^-	2.068 ; 2.094	164.9 ; 161.2	72.7 ; 69.6
I^-	2.063 ; 2.087	163.3 ; 161.5	71.4 ; 70.0

Similarly to our previous classical MD investigations on anion recognition,[33–36] the ChB interactions were represented by the addition of a massless extra-point (EP) of charge to GAFF, following the methodology established by Ibrahim for halogen bonding interactions.[37] However, to more accurately reproduce the slightly bent $C_{triazolium}$-Se···A angles, the EP that will represent the σ-hole found in front of each C-Se activated bond cannot make a 180° $C_{triazolium}$-Se-EP angle. Therefore, having in mind the 98.98° angle parameterized with *MCPB.py* for $C_{triazolium}$-Se-C_{methyl} (*vide supra*), as well as the $C_{triazolium}$-Se···$\boldsymbol{V_{S,max}}$ and C_{methyl}-Se···$\boldsymbol{V_{S,max}}$ angle values listed in Table C2, a compromise was made and the $C_{triazolium}$-Se-EP and the C_{methyl}-Se-EP angles were set to 166 and 67°, respectively. This approach allowed reduction of the degrees of freedom in our parameterization effort, limiting it to the Se-EP distances.

Afterwards, several Se–EP distances were systematically tested in gas phase *via* MM energy minimizations of the halide associations of **2.20Se$_2$H**, using RESP charges estimated for each I–EP distance. In a previously B3LYP/6-31G* optimized structure of macrocycle **2.9Se**, an EP was positioned in front of each $C_{triazolium}$–Se bond at the fixed angles given above and at the desired Se–EP distances and then the corresponding atomic charges were obtained via two RESP fitting (*vide infra*) stages. The ranges of Se–EP distances tested for the three halide associations are gathered in Table toTable , together with the MM optimized Se···A distances and the atomic charges for Se and EP.

Table C3. Summary of MM optimized distances for **2.20Se$_2$H**·Cl$^-$ as function of the Se–EP distance, along with EP and Se RESP charges.

Distances (Å)		Charges *q(e)*	
Se-EP	Se···Cl$^-$	EP	Se
No EP	3.609 ; 3.648	--	0.074607
2.57	3.420 ; 3.406	0.039976	-0.000261
2.58	3.418 ; 3.401	0.039410	0.000851
2.59	3.415 ; 3.396	0.038846	0.001964
2.60	3.412 ; 3.390	0.038284	0.003079
2.61	3.408 ; 3.384	0.037722	0.004195
2.62	3.404 ; 3.377	0.037162	0.005312
2.63	3.400 ; 3.369	0.036603	0.006430
2.64	3.306 ; 3.456	0.036044	0.007550
2.65	3.306 ; 3.436	0.035487	0.008671
2.66	3.384 ; 3.335	0.034930	0.009793
2.67	3.294 ; 3.360	0.034374	0.010917
2.68	3.262 ; 3.292	0.033819	0.012041
2.69	Atomic clash	0.033265	0.013165

Table C4. Summary of MM optimized distances for **2.20Se$_2$H**·Br$^-$ as function of the Se–EP distance, along with EP and Se RESP charges.

Distances (Å)		Charges *q(e)*	
Se-EP	Se···Br$^-$	EP	Se
No EP	3.656 ; 4.031	--	0.074607
2.79	3.649 ; 3.643	0.027828	0.024263
2.80	3.649 ; 3.642	0.027308	0.025322
2.81	3.649 ; 3.641	0.026798	0.026359
2.82	3.649 ; 3.640	0.026299	0.027371
2.83	3.648 ; 3.638	0.025814	0.028350
2.84	3.648 ; 3.636	0.025346	0.029292
2.85	3.647 ; 3.634	0.024899	0.030188
2.86	3.646 ; 3.631	0.024474	0.031031
2.87	3.645 ; 3.627	0.024077	0.031813
2.88	3.643 ; 3.622	0.023711	0.032525
2.89	3.512 ; 3.749	0.023381	0.033160
2.90	3.501 ; 3.751	0.023089	0.033708
2.91	3.483 ; 3.753	0.022840	0.034165
2.92	3.436 ; 3.754	0.022634	0.034525
2.93	Atomic clash	0.022474	0.034785

Table C5. Summary of MM optimized distances for **2.20Se$_2$H**·I$^-$ as function of the Se–EP distance, along with EP and Se RESP charges.

Distances (Å)		Charges *q(e)*	
Se-EP	Se···I$^-$	EP	Se
No EP	4.003 ; 4.060	--	0.074607
3.05	3.922 ; 3.912	0.022963	0.032667
3.06	3.919 ; 3.905	0.023046	0.032417
3.07	3.915 ; 3.896	0.023114	0.032208
3.08	3.910 ; 3.887	0.023164	0.032048
3.09	3.906 ; 3.878	0.023194	0.031940
3.10	3.901 ; 3.867	0.023203	0.031891
3.11	3.749 ; 4.014	0.023189	0.031901
3.12	3.727 ; 4.013	0.023153	0.031973
3.13	3.680 ; 4.011	0.023093	0.032108
3.14	Atomic clash	0.023010	0.032305

Table through C5 show that several Se–EP distances can be applied on the gas phase optimizations by MM of the halide associations of **2.20Se$_2$H**. However, the successive use of the longer Se–EP distances (2.58 to 2.68 Å for **2.20Se$_2$H** ·Cl$^-$, 2.80 to 2.92 Å for **2.20Se$_2$H** ·Br$^-$, and 3.06 to 3.13 Å for **2.20Se$_2$H** ·I$^-$) in MD simulations of these associations, carried out in gas-phase at 300K for 5 ns, were shown to be instable, resulting in the definitive exclusion of these distance values. Therefore, these MD simulations were further extended to shorter Se–EP distances, and the 2.57, 2.79 and 3.05 Å distances were found as best Se-EP distances to carry out the MD simulations with **2.20Se$_2$H**·Cl$^-$, **2.20Se$_2$H**·Br$^-$, and **2.20Se$_2$H**·I$^-$, in this order. The average Se···A distances 3.455 ± 0.133 and 3.484 ± 0.131 Å were calculated for **11.Se**·Cl$^-$, while for other associations the following values were assessed: 3.701 ± 0.141 and 3.721 ± 0.148 Å for **2.20Se$_2$H** ·Br$^-$, and 3.948 ± 0.139 and 3.990 ± 0.144 Å for **2.20Se$_2$H**·I$^-$. Therefore, the 2.57, 2.79 and 3.05 Å Se–EP distances were definitively appointed for the subsequent MD simulations in the acetone/water solvent mixtures.

*Calculation of RESP charges of **2.20Se$_2$H** components*

The RESP charges of the macrocycle were derived considering one extra point of charge positioned at 2.57, 2.79 or 3.05 Å from each Se atom, with a $C_{triazolium}$-Se-EP angle of 166° and a C_{methyl}-Se-EP angle of 67°, as stated above. This was preceded by the initial optimization of the X-ray structure of **2.9Se** at B3LYP/6-31G*, followed by a single point calculation at the HF/6-31G* level, in agreement with the GAFF development. In both cases, the Se centers were treated with the aug-cc-pVDZ-PP basis set. The final charges were then derived considering the position of the two extra points. The RESP atomic charges in the absence of extra points were calculated using the same approach.

The RESP charges of the axle component of **2.20Se$_2$H** were obtained by optimization of the axle component (*vide supra*) at the B3LYP/6-31G* level of theory, followed by a single point calculation at the HF/6-31G* level.

General MD simulation methods

The starting geometries of the halide associations of **2.9Se** or **2.20Se$_2$H**, as well as the free macrocycle and rotaxane, were minimized in gas phase by MM until the convergence criterion of 0.0001 kcal mol^{-1} was achieved. Afterwards, the optimized structures were solvated in cubic boxes with different number of solvent molecules, in agreement with the solvent mixtures used in ^{1}H NMR experimental binding studies: for **2.9Se** – 1005 acetone molecules and 84 water molecules, in agreement with a 98:2 v/v acetone/water solvent mixture; for **2.20Se$_2$H** – 1802 acetone molecules and 1836 water molecules, in agreement with a 4:1 v/v acetone/water solvent mixture. A variable number of PF_6^- counter-ions was added to neutralize each system's net charge.

Each solvated system was equilibrated under periodic boundary conditions using the following multistage protocol. The system was relaxed by MM minimization of solvent molecules and by keeping the solutes fixed with a positional restraint of 500 kcal mol^{-1} Å^{-2}. The

restraint was then removed and the entire system was allowed to relax. Both minimization stages comprised an initial set of 10000 steepest descent algorithm steps, followed by 10000 steps of conjugated gradient algorithm. The equilibration stage proceeded with heating up the system to 300 K for 100 ps using a NVT ensemble and a weak positional restraint (10 kcal mol^{-1} $Å^{-2}$) on the solutes. Afterwards, each system's density was allowed to equilibrate in a NPT ensemble at 1 atmospheric pressure for 1 ns, at the same temperature, followed by a NPT data collection run of 10 ns for the systems with **2.9Se** or 50 ns for the systems with **2.20Se$_2$H**. The collection run's trajectory frames were saved every 1 ps. Three independent replicates were performed for each system. The CUDA version of the PMEMD executable was used for the simulation of all solvated systems.[38–40] The bond lengths involving all bonds to hydrogen atoms were constrained with the SHAKE algorithm allowing the usage of 2 fs time step.[41] The Particle Mesh Ewald (PME) method was used to treat the long range electrostatic interactions.[42] The non-bonded van der Waals interactions were truncated with a 10 Å cut-off.

C2. Experiments for Chapter 4

C2.1. Acyclic Chiral XB and HB Receptors

Starting structures for chiral substrates and receptors

Starting structures of receptors **4.1I** and **4.1H** and anionic substrates were generated through appropriated atomic manipulations of crystal structures deposited with the Cambridge Crystallographic Data Centre (CCDC).[9] The **4.1I** and **4.1H** with (*S*)-chirality on the BINOL fragment were constructed from the crystal structure with Refcode GEMZUU,[43] while the the *N*Boc-(*S*)-alanine, *N*Boc-(*S*)-leucine, *N*Boc-(*R*)-tryptophan and (*R*)-BINOL-phosphate substrates were obtained from the crystal structures with Refcodes NASQAZ,[44] FAYMEZ,[45] DIZNEG,[46] and SORREX,[47] respectively. The atomic coordinates of other enantiomers were obtained by inversion of the crystal structures of their counterparts with Mercury CSD 3.6.[48–51]

Quantum calculations

Overall, the quantum calculations carried out for this work were composed of geometry optimisations, distribution of electrostatic potential on the molecular surfaces **4.1I** and **4.1H**, derivatisation of restrained electrostatic potential (RESP) charges for **4.1I** and **4.1H** and the chiral substrates and natural bond orbital calculations (NBO), using the Gaussian09 software.[11]

Density functional theory (DFT) calculations were used to parameterise the XB interactions using model complexes. The RESP charges were obtained from single point calculations undertaken with Hartree-Fock (HF) method using previously optimised structures (as detailed below), the Gaussian IOp(6/33=2, 6/41=4, 6/42=6) and the 6-31G* basis set for all atoms, except for the iodine atoms, in agreement with the GAFF development.[21,22] In all calculations, the iodine atoms were described with the aug-cc-pVDZ-PP basis set, [52,53] obtained from the EMSL website.[13,14]

Classical force field calculations

All Molecular Mechanics (MM) and Molecular dynamics (MD) simulations were undertaken with Amber14.[54] The substrates and the tetrabutylammonium (TBA) counter-ion were described with default parameters taken from the Generalized Amber Force Field (GAFF)[21,22] and RESP charges,[23] while the hexafluorophosphate (PF_6^-) was described with parameters and charges taken from ref. 30. The receptors **4.1I** and **4.1H** were also described with default GAFF parameters, apart the triazolium moiety, which was parameterised using quantum mechanics structural data (*vide infra*). The solvent mixture was described with the TIP3P model for the water molecules, while the acetonitrile molecules were described with parameters and atomic charges taken from ref. 55. The structural data from MD simulations were obtained by post-processing of trajectory files with *cpptraj*.[31]

Parameterisation of XB interactions

The force field parameterisation of the XB interactions was preceded by DFT optimisations of model complexes with acetate (CH_3COO^-) or dihydrogen phosphate ($H_2PO_4^-$), as archetypes of the binding units for chiral substrates *N*Boc-protected amino acids and BINOL-PO_4, respectively. In these model complexes, the octyl chains of **4.1I** were replaced by ethyl groups (model $\mathbf{4.1I_{ethyl}}$). These optimisations were carried using the B3LYP functional, with the H, C, N, O and P atoms treated with the 6-31+G* basis set, while the iodine atoms were described with the aug-cc-pVDZ-PP basis set. The solvent effects were further taken into account (*see infra*) through the Polarizable Continuum Model (PCM), using the integral equation formalism variant (IEFPCM).[12] These optimised structures allowed us to ascertain the dimensions of XB interactions (I···O distances and C-I···O angles) in gas-phase or in continuum solvent medium of water or acetonitrile. Their values are gathered in Table C6 and were used as reference in the subsequent determination of the I-EP (iodine-extra point) optimal distance for XB interactions between each substrate and **4.1I**.

Table C6. I···O distances (Å) in DFT optimisations of $\mathbf{4.1I_{ethyl}}$ model complexes

Optimisation conditions	Model Complex	
	$\mathbf{4.1I_{ethyl}}\cdot CH_3COO^-$	$\mathbf{4.1I_{ethyl}}\cdot H_2PO_4^-$
Gas-phase	2.473 ; 2.495	2.505 ; 2.505
Water model continuum	2.593 ; 2.629	2.665 ; 2.665
Acetonitrile model continuum	2.599 ; 2.635	2.672 ; 2.672

In our previous works on halide and sulfate recognition by macrocyclic halo-imidazolium receptors[56,57] or rotaxane based halo-triazolium receptors,[34,35] the XB interactions were described with resort to an extra point (EP) of charge added to GAFF.[37] Furthermore, this EP has van der Waals parameter and mass set to zero, a C-I-EP angle of 180° with a 150 kcal mol^{-1} rad^{-2} angle bending force constant and an I-EP optimal distance determined for each substrate model, with a 600 kcal mol^{-1} $Å^{-2}$ bond stretching force constant. This methodology

was extended in this work to the enantioselective binding of chiral substrates mediated by XB bonds, as follows.

Different I-EP distances were systematically tested in gas-phase *via* MM energy minimisations of the model complexes between **4.1I** and CH_3COO^- or $H_2PO_4^-$ anions. To obtain atomic RESP charges adequate to XB interactions with the oxygen atoms of CH_3COO^- or $H_2PO_4^-$, the MM structure optimisations were preceded by the derivatisation of RESP charges at different I-EP distances. In a previously B3LYP/6-31G* optimised structure of **4.1I**, an extra point was positioned in front of each C-I bond at different I-EP distances and a C-I-EP angle of 180°. Subsequently, the electrostatic potential distribution of each structure, with two extra points at the same I-EP distances, was calculated followed by the RESP fitting (see below). Table C7 summarises the range of I-EP distances tested for two model complexes, as well as the I···O distances and the iodine and EP charges.

Table C8 shows that several I-EP distances can be applied in the MM geometry optimisation of **4.1I**·CH_3COO^- and **4.1I**·$H_2PO_4^-$. On the other hand, the use of the longer I-EP distances (2.00 to 2.03 Å) in 300 K, 5 ns long, gas phase MD simulations of **4.1I**·CH_3COO^- was shown to be instable, being ruled out. For the gas phase MD simulations of **4.1I**·$H_2PO_4^-$, the same problem was verified for the I-EP distances between 2.02 and 2.07 Å. These MD simulations were extended to the other I-EP distances, and the 1.99 and 2.01 Å distances were found as best I-EP distances found carry out the MD simulations with complexes **4.1I**·CH_3COO^- and **4.1I**·$H_2PO_4^-$, respectively. Given that these two I-EP distances only differed by 0.02 Å, the shortest I-EP distance was selected for the subsequent MM calculations on the complexes of **4.1I** with CH_3COO^- or $H_2PO_4^-$. With the I-EP distance of 1.99 Å, equivalent I···O distances were obtained in solution (a solvent mixture composed of 1426 acetonitrile molecules and 42 water molecules, as described in Section S6.7), as shown in Table C8.

Table C7. Summary of gas-phase MM optimised I···O distances (Å) for **4.1I**·CH_3COO^- and **4.1I**·$H_2PO_4^-$, as function of the I-EP distance (Å), listed along with EP and iodine RESP charges.

I-EP distance	EP charge	I charge	**4.1I**·CH_3COO^-	**4.1I**·$H_2PO_4^-$
No EP	---	0.271700	5.701 ; 5.109	5.101 ; 3.306
1.95	0.111177	-0.033441	2.826 ; 2.823	2.859 ; 2.859
1.96	0.109979	-0.031382	2.812 ; 2.806	2.853 ; 2.852
1.97	0.108795	-0.029335	2.804 ; 2.798	2.845 ; 2.845
1.98	0.107623	-0.027300	2.803 ; 2.798	2.839 ; 2.838
1.99	0.106464	-0.025276	2.790 ; 2.785	2.831 ; 2.830
2.00	0.105317	-0.023263	2.782 ; 2.779	2.822 ; 2.822
2.01	0.104182	-0.021261	2.770 ; 2.772	2.814 ; 2.814
2.02	0.103060	-0.019270	2.757 ; 2.750	2.804 ; 2.803
2.03	0.101950	-0.017289	2.746 ; 2.738	2.792 ; 2.791
2.04	0.100850	-0.015317	Atomic clash	2.780 ; 2.779
2.05	0.099763	-0.013356	Atomic clash	2.765 ; 2.765
2.06	0.098685	-0.011403	Atomic clash	2.745 ; 2.745
2.07	0.097621	-0.009461	Atomic clash	2.714 ; 2.714
2.08	0.096566	-0.007527	Atomic clash	Atomic clash

Table C8. Summary of solution MM optimised I···O distances (Å) for **4.1I**·CH_3COO^- and **4.1I**·$H_2PO_4^-$, for an I-EP distance of 1.99 Å.

Complex	**4.1I**·CH_3COO^-	**4.1I**·$H_2PO_4^-$
I···O distances (Å)	2.817 ; 2.852	2.857 ; 2.836

The I···O distances calculated for the structures of **4.1I**·CH_3COO^- and **4.1I**·$H_2PO_4^-$ optimised in solution by MM (Table C9) are only *ca.* 0.03 Å systematically longer than the distances obtained in the gas-phase MM optimisations (Table C8). On the other hand, the comparison presented in Table C7 between the I···O distances in model complexes of **4.1I$_{ethyl}$** shows that the inclusion of a solvent continuum of water or acetonitrile in DFT calculations leads to an increase of the I···O distances relatively to those computed in gas phase. Nevertheless, the I···O distances in both implicit solvent media compares fairly well with the I···O molecular mechanics distances in complexes of **4.1I** obtained in the solvent mixture (Table C9). Hence, the I-EP distance of 1.99 Å was definitively selected for the further conformational analyses and MD simulations in the acetonitrile/water solvent mixture (*vide infra*).

Calculation of RESP charges of receptors and substrates

The RESP charges of **4.1I** were derived in agreement with earlier parameterisation developed with **4.1I$_{ethyl}$** CH_3COO^- and $H_2PO_4^-$ complexes (previous section) considering one extra point of charge positioned in front of each iodine, at 1.99 Å distance and with a C-I-EP angle of 180°. This was preceded by initial optimisation of a single conformation of **4.1I** using B3LYP/6-31G*, followed by a single point calculation at the HF/6-31G* level, in agreement with the GAFF development aforementioned. The final charges were then derived considering the position of the two extra points. Concerning **4.1H**, its RESP atomic charges were straightforwardly obtained at the HF/6-31G* level after an initial optimisation of a single conformation at the same level of theory.

The (*S*)- and (*R*)-enantiomers of each anionic substrate were optimised with the B3LYP functional along with the 6-31+G* basis set, followed by electrostatic potential calculation through a single point carried out at the HF/6-31G* theory level. The electrostatic potentials of both enantiomers were concatenated and the final atomic charges of either chiral substrate (*S* or *R*) were computed through a multi-conformation RESP fitting based on the individual atomic charges of two enantiomers.

Triazolium ring force field parameterisation

The preliminary MM optimisations of **4.1I** or **4.1H**, with GAFF default parameters for the triazolium atom types (as assigned by *antechamber*[36] and depicted in red in Figure C1.2) resulted in bond lengths and angles that poorly reproduced the bond lengths and angles observed in the triazolium moieties of the DFT optimised structures. Therefore, all distances within the triazolium ring, along with the C-I or C-H bond, and all angles affected by those bonds were reparametrised using structural data from quantum mechanics optimised structures. Five crystal structures, containing a 5-iodo-1,2,3-triazolium moiety were obtained from CCDC: Refcodes DAMNOW,[58] DAMNUC,[58] TACPEU,[10] TACPIY,[10] and TACPOE.[10]

This series of molecules was extended with the addition of 5-iodo-1,3,4-trimethyl-*1H*-1,2,3-triazol-3-ium. All six structures were optimised at the B3LYP/6-31G* level. The bond lengths and angles obtained in the DFT optimised structures for the triazolium ring were averaged and used as equilibrium distances (r_{eq}) and equilibrium angles (θ_{eq}). Their values are listed in Table C9. The bond lengh and bond angles force constants (K_r and K_θ) were then calculated in agreement with the GAFF original paper.[21,22]

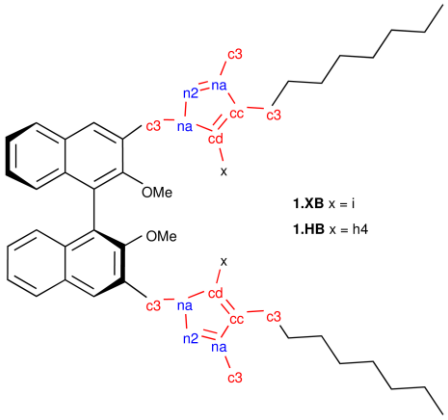


Figure C2.1. *GAFF atom types assigned for triazolium rings and carbon atoms attached of* ***4.1I*** *and* ***4.1H*** *by the antechamber utility.*

For receptor **4.1H**, the same parameters were used for the triazolium motifs, apart the bond lengths and angles involving the prominent C-H binding units, which were assigned as cd-h4 and described with default GAFF parameters. Only the bending angles between Cd-H4 and triazolium adjacent atom types (cc-cd-h4) and (na-cd-h4) angles were changed, as summarised in Table C10.

General MD simulation methods

The starting binding geometry of each diastereoisomeric complex was obtained positioning the anion with the pertinent oxygen atoms of the carboxylate (*N*Boc-amino acid derivatives) or unbound oxygen atoms (BINOL-PO_4) in the vicinity of the binding units of **4.1H** or **4.1I**. Afterwards, all complexes underwent a MD run of 10 ns in gas-phase at 350 K and

Table C9. Force field parameters for the two triazolium moieties of **4.1I**.

Force field parameter	**GAFF default parameters**		**Quantum mechanics derived parameters**	
Bond lengths	r_{eq} (Å)	K_r (kcal mol^{-1} Å^{-2})	r_{eq} (Å)	K_r (kcal mol^{-1} Å^{-2})
na-n2	1.3685	503.9	1.3198	592.991
na-cc	1.3710	438.8	1.3691	441.535
na-cd	1.3710	438.8	1.3691	441.535
cc-cd	1.3710	504.0	1.3926	469.956
cd-i	2.1530	223.2	2.0838	258.576
Bond angles	θ_{eq} (°)	K_θ (kcal mol^{-1} rad^{-2})	θ_{eq} (°)	K_θ (kcal mol^{-1} rad^{-2})
na-n2-na	107.00	73.47	105.117	76.857
cc-cd-na	109.42	72.91	106.040	73.521
cd-cc-na	109.42	72.91	103.730	74.335
cc-na-n2	122.96	66.83	113.136	70.938
cd-na-n2	122.96	66.83	111.977	71.304
c3-na-n2	120.05	65.48	118.383	66.900
c3-na-cc	125.09	62.56	129.044	61.632
c3-na-cd	125.09	62.56	129.044	61.632
na-cd-i	121.61	59.37	124.900	58.781
cc-cd-i	123.70	57.46	129.038	56.438
cd-cc-c3[a)]	119.45	64.81	131.841	61.310
na-cc-c3[a)]	122.78	65.50	124.029	65.200

[a)] These angles were obtained directly from the DFT optimised structure of 5-iodo-1,3,4-trimethyl-*1H*-1,2,3-triazol-3-ium.

Table C10. Additional force field parameters for the triazolium moiety of **4.1H**.

Force field parameter	**GAFF default parameters**		**Quantum mechanics derived parameters**	
Bond angles	θ_{eq} (°)	K_θ (kcal mol^{-1} rad^{-2})	θ_{eq} (°)	K_θ (kcal mol^{-1} rad^{-2})
na-cd-h4	119.66	50.22	124.900	49.212
cc-cd-h4	129.11	47.19	129.038	46.620

using a 1 fs time step length. 100000 structures were saved and further full energy minimised by means of MM until the convergence criterion of 0.0001 kcal mol^{-1} was achieved. In addition, the conformational analyses of the complexes of **4.1H** were undertaken with two 50 kcal mol^{-1} Å^{-2} C···O distance restraints, with C standing for each C-H binding unit carbon atom and O standing for the pertinent oxygen atom in the substrate) together with four 50 kcal mol^{-1} rad^{-2} angle restraints, two C-H···O and two H···O-A, where A stands for the carbon atom from carboxylate group in the *N*Boc-amino acid derivatives or for the phosphorus atom in BINOL-

PO_4). This second series of restraints was applied to maintain the two C-H···O intermolecular interactions with an approximately linear binding geometry.

The lowest energy structure for each anion complex, was then solvated in a cubic box with 1426 acetonitrile molecules and 42 water molecules in agreement with a 99:1 v/v concentration used in ^{1}H NMR binding studies. One TBA and two PF_6^- counter-ions were added to neutralise the system net charge. Each solvated system was equilibrated under periodic boundary conditions using the following multistage protocol. The system was relaxed by MM minimisation of solvent molecules and by keeping the substrate, receptor and the counter-ion(s) fixed with a positional restraint of 500 kcal mol^{-1} Å^{-2}. The restraint was then removed and the entire system was allowed to relax. Both minimisation stages comprised an initial set of 10000 steepest descent algorithm steps, followed by 10000 steps of conjugated gradient algorithm. The equilibration stage proceeded with heating up the system to 300 K for 100 ps using a NVT ensemble and a weak positional restraint (10 kcal mol^{-1} Å^{-2}) on the solutes. Afterwards, each system was allowed to equilibrate in a NPT ensemble at 300 K and 1 atm for 1 ns. Finally, NPT data collection runs were carried out for 100 ns (for systems with **4.1I**) or for 50 ns (for systems with **4.1H**), with the trajectory frames being saved every 1 ps. Three independent replicates were performed for systems with **4.1I**, while five independent replicates were carried out for systems with **4.1H**. The CUDA version of the PMEMD executable was used for the simulation of all solvated systems.[38–40] The bond lengths involving all bonds to hydrogen atoms were constrained with the SHAKE algorithm allowing the usage of 2 fs time step.[41] The Particle Mesh Ewald (PME) method was used to treat the long-range electrostatic interactions.[42] The non-bonded van der Waals interactions were truncated with a 10 Å cut-off.

The interactions between **4.1I** with the chiral oxoanions and surrounding solvent molecules were monitored throughout the simulation time of all MD runs and are plotted in Figures C2.2 to C2.5, together with the distance between the centre of mass defined by the two iodine atoms of **4.1I** and the centre of mass determined by the two pertinent oxygen atoms from the anionic substrate ($I_{COM,host}\cdots O_{COM,anion}$). Overall, **4.1I** maintains with the chiral

substrates two continuous halogen bonds, with exception of 8/24 MD runs (3 *N*Boc-(*S*)-alanine; 1 *N*Boc-(*R*)-leucine; 1 *N*Boc-(*S*)-tryptophan; 1 *N*Boc-(*R*)-tryptophan; and 2 (*S*)-BINOL-PO_4) where a C-I···O_{anion} XB interaction is sporadically interrupted (orange line in Figures C2.2 to C2.5). Concomitantly, a new HO–H···O_{anion} hydrogen bond emerges (blue line) together with a C-I···OH_2 halogen bonding interaction (purple line), leading to an increase of the $I_{COM,host}$···$O_{COM,anion}$ distance (red line). In contrast, the HO–H···I hydrogen bonds are undoubtedly in lesser number (green line) and seem to be interrupted when an XB interaction is formed with the water molecule. A movie showing the interactions between receptor **4.1I** and NBoc-tryptophan carboxylate is provided in the digital appendices.

DFT methods

The starting geometries of each diastereoisomeric complex of **4.1I** for geometry optimisations were the most frequent structures obtained from the cluster analysis of the 300 ns of MD trajectories, after striping the solvent molecules and counter-ions. As the complexes of **4.1H** were not stable throughout the MD simulations, the starting geometries of the diastereoisomers complexes of **4.1H** were generated from those of **4.1I** by replacement of the iodine triazolium substituents by hydrogen atoms. All complexes were optimised with the M06-2X functional along with the 6-31G* basis set.

The distribution of electrostatic potential, $V(r)$, on the molecular surfaces of **4.1I** and **4.1H** was computed at the M06-2X/6-31G* level from previously optimised structures of their complexes with *N*Boc-(*S*)-tryptophan substrate, after removal of chiral substrate of the corresponding complex. In this work, the $V(r)$ was evaluated on the 0.001 electrons $Bohr^{-3}$ contour of ρ(r), and is henceforth labelled $V_S(r)$. The electrostatic potential surface ranges, between the most negative and most positive values ($V_{S,min}$ and $V_{S,max}$, respectively), was ascertained using the *multiwfn* program.[15,16]

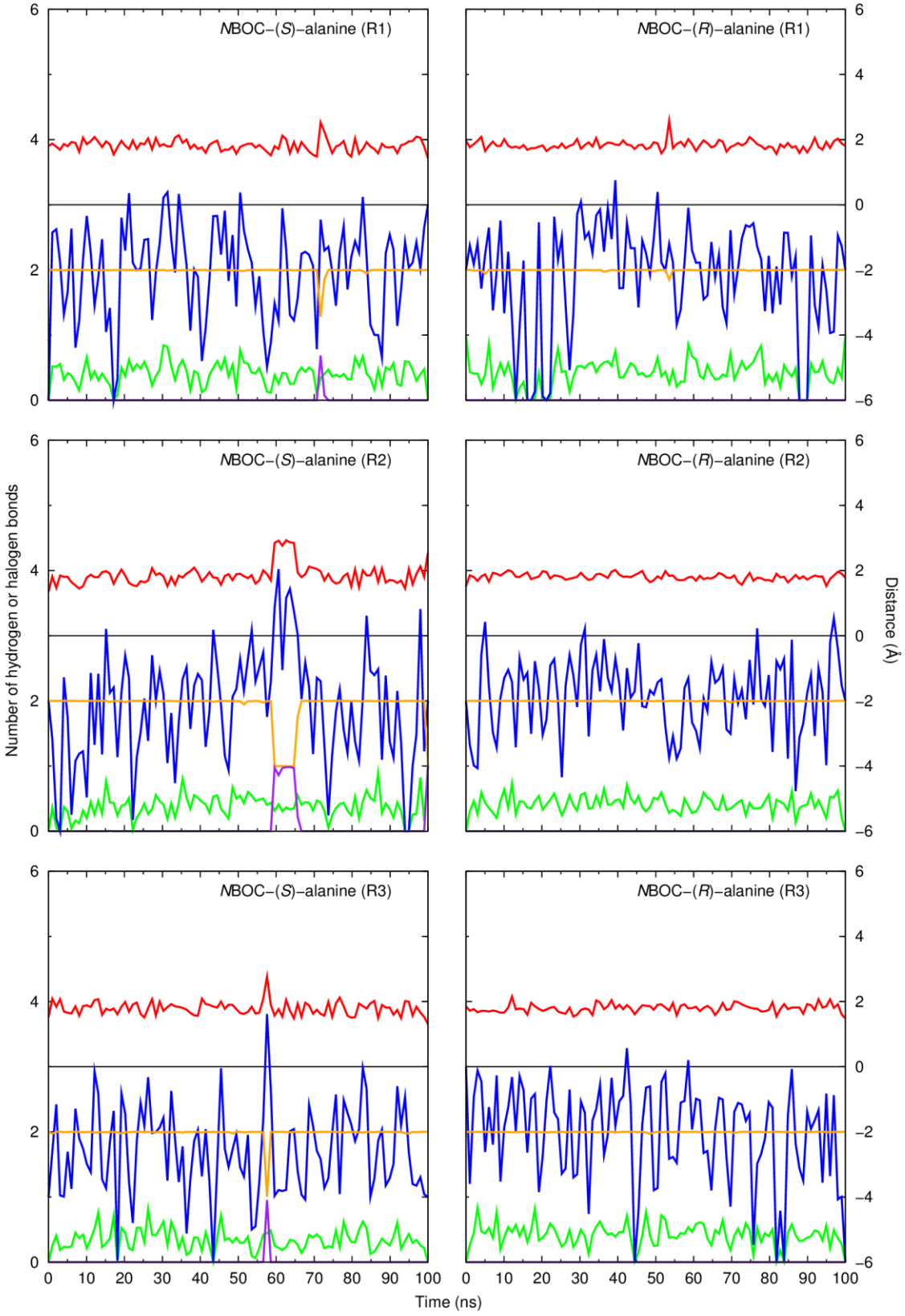


Figure C2.2. *Evolution of the $I_{COM,host}\cdots O_{COM,anion}$ distance (red line) throughout 100 ns of independent MD runs, together with the number of HB interactions, HO–H$\cdots O_{anion}$ (blue line) and HO–H$\cdots$I (green line), and the number of XB interactions, C-I$\cdots OH_2$ (purple line) and C-I$\cdots O_{anion}$ (orange line), for the diastereoisomeric complexes of* ***4.1I****.*

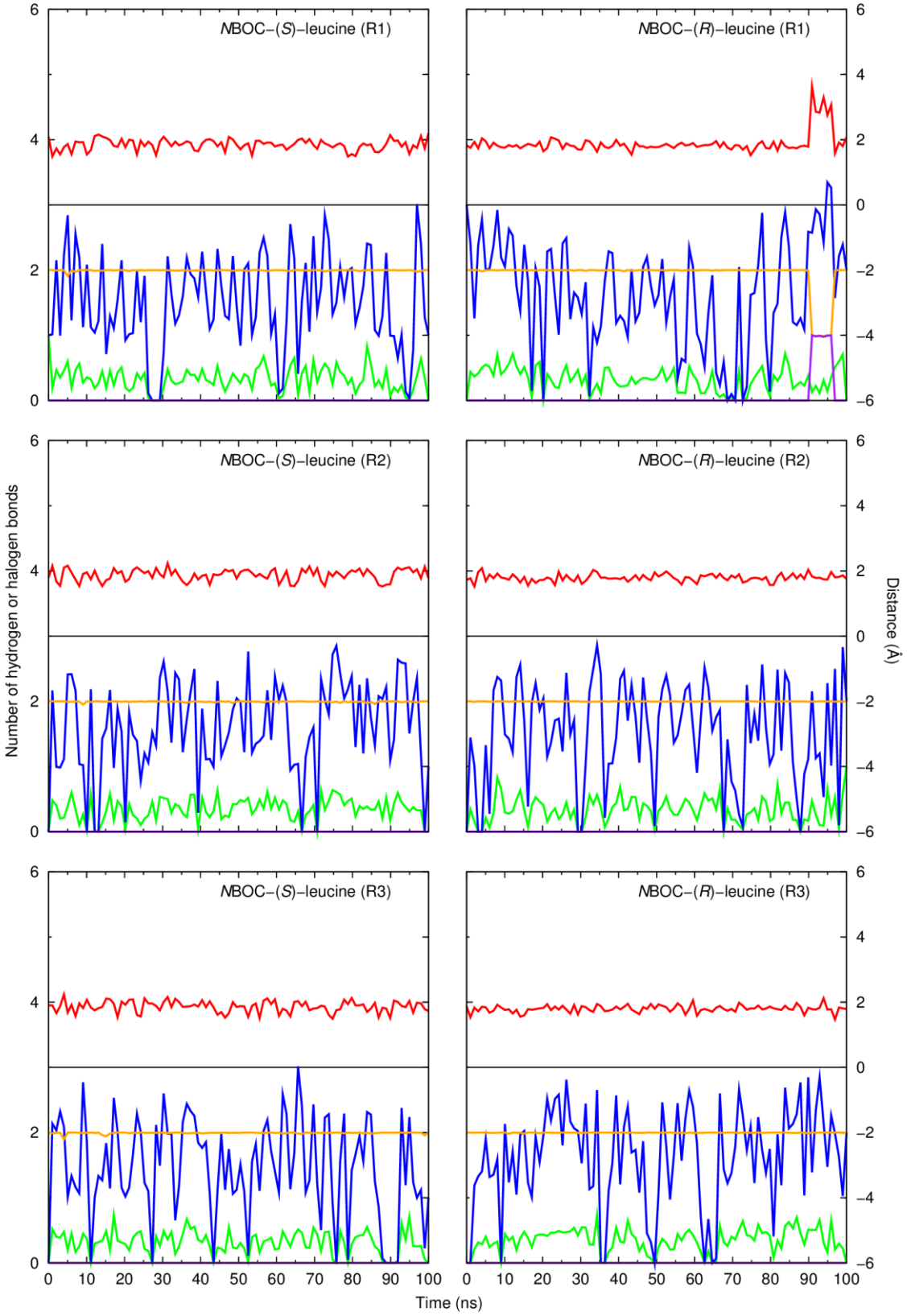


Figure C2.3. *Evolution of the $I_{COM,host}\cdots O_{COM,anion}$ distance (red line) throughout 100 ns of independent MD runs, together with the number of HB interactions, $HO–H\cdots O_{anion}$ (blue line) and HO–H···I (green line), and the number of XB interactions, $C\text{-}I\cdots OH_2$ (purple line) and $C\text{-}I\cdots O_{anion}$ (orange line), for the diastereoisomeric complexes of* ***4.1I****.*

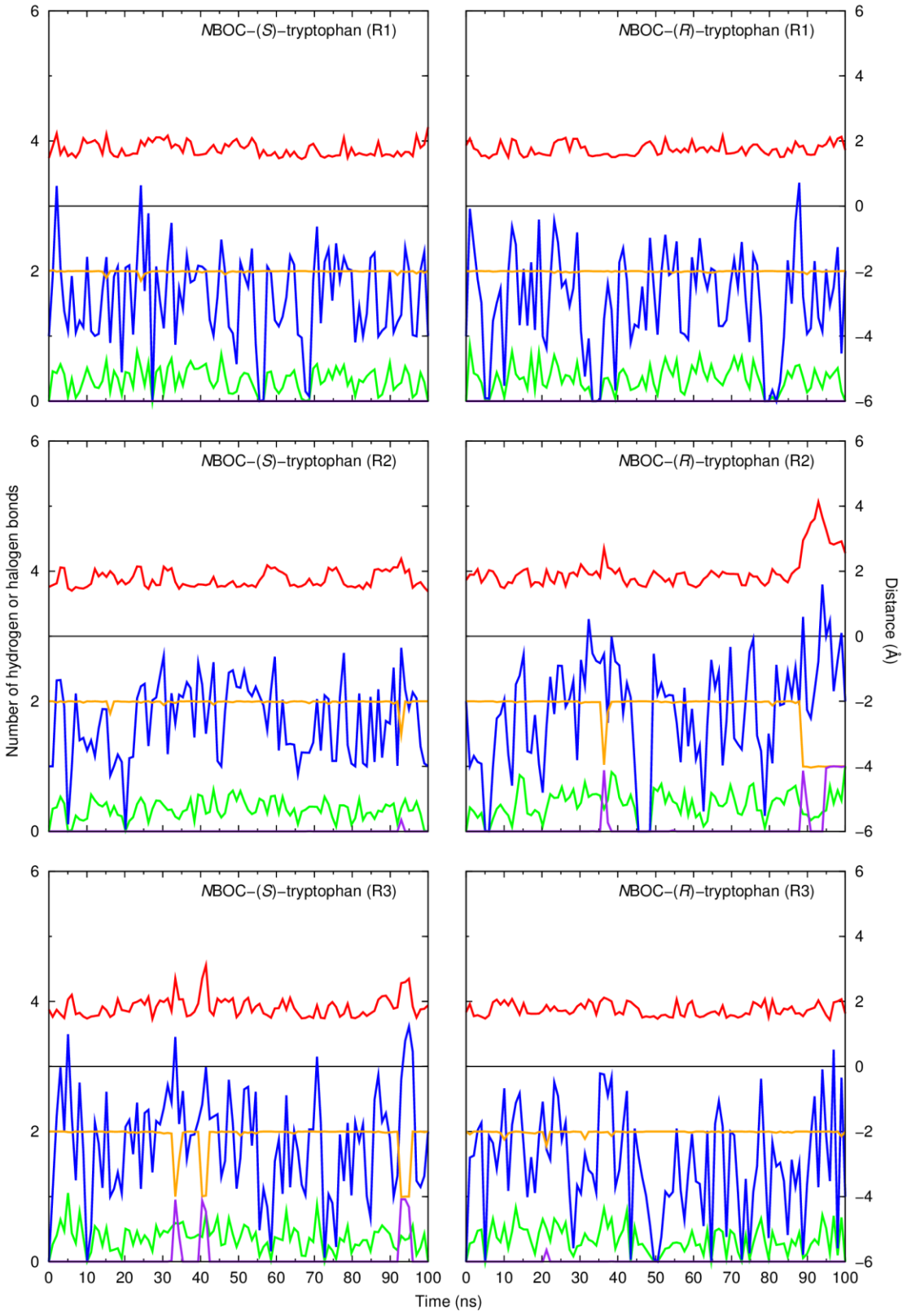


Figure C2.4. *Evolution of the $I_{COM,host}\cdots O_{COM,anion}$ distance (red line) throughout 100 ns of independent MD runs, together with the number of HB interactions, $HO–H\cdots O_{anion}$ (blue line) and $HO–H\cdots I$ (green line), and the number of XB interactions, $C\text{-}I\cdots OH_2$ (purple line) and $C\text{-}I\cdots O_{anion}$ (orange line), for the diastereoisomeric complexes of* ***4.1I****.*

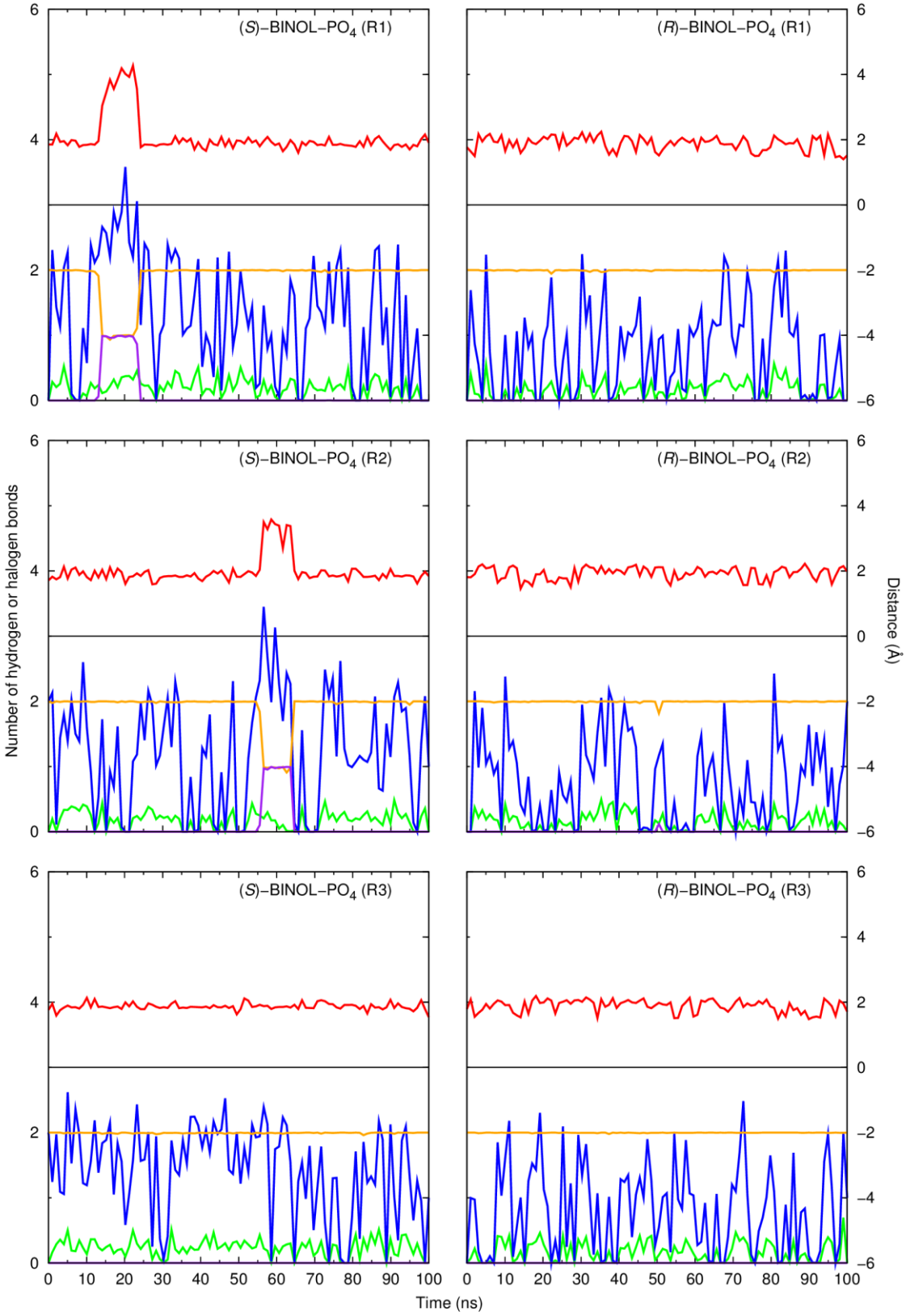


Figure C2.5. *Evolution of the $I_{COM,host}\cdots O_{COM,anion}$ distance (red line) throughout 100 ns of independent MD runs, together with the number of HB interactions, HO–H$\cdots O_{anion}$ (blue line) and HO–H$\cdots$I (green line), and the number of XB interactions, C-I$\cdots OH_2$ (purple line) and C-I$\cdots O_{anion}$ (orange line), for the diastereoisomeric complexes of* ***4.1I****.*

The Wiberg bond indices (WBI)[17] which consist in the sum of squares of off-diagonal density matrix elements between atoms. In this study, the WBI were ascertained from the DFT optimized structures of the diastereoisomeric complexes of **4.1I** or **4.1H**. These calculations were carried out using the Natural Bond Orbital (NBO) Version 3.1 program,[18,19] within the Gaussian09 suite, at the M06-2X/6-31G* level.

C2.2. Chiral XB Macrocycles and [2]Rotaxanes

Starting structures for chiral substrates and receptors

Starting structures of the macrocycles and axle components and anionic substrates were generated through adequate atomic manipulation of crystal structures deposited with the Cambridge Crystallographic Data Centre (CCDC).[9] Thus, the macrocycles **4.10I**, **4.10H**, and **4.14I** with (*S*)-helical chirality on the BINOL moiety were constructed from the crystal structure with Refcode VUTDIY,[59] while the chiral axle **4.29** was based on the following crystal structures: stoppers – Refcode LEVKII;[60] pyridinium-3,5-bis(iodotriazole) core – Refcode CUJTIM;[61] and (*S*)-chiral *N*Boc moieties – Refcode OFIJOD.[62] The achiral axle of rotaxane **4.16** was modified from **4.29**, while the achiral macrocycle of **4.17** was built from **4.14I**. The *N*Boc-(*S*)-proline and (*R*)-binol-phosphate substrates were obtained from the crystal structures with Refcodes AXCPRO,[63] and SORREX,[47] respectively. The atomic coordinates of (*S*)-binol-phosphate and *N*Boc-(*R*)-proline anions were obtained by inversion of atomic coordinates *N*Boc-(*S*)-proline and (*R*)-binol-phosphate, respectively.

For each **4.10H** and **4.10I** enantiomer association, two binding scenarios were built, with the anionic guest placed, as a rigid body, above the macrocyclic plane, with the oxygen atoms of the carboxylate group establishing putative hydrogen or halogen bonding interactions with the triazolium activated binding units. Thus, for the *N*Boc-(*S*)-proline, the chiral proton of this substrate points to either the BINOL aromatic region (S_A initial binding scenario) or to the ether macrocyclic loop (S_B), while for the *N*Boc-(*R*)-proline, it is the *N*Boc bulky group that

points towards the BINOL region (R_A)or to the ether loop (R_B). The rotaxane hosts were generated with the four C-I binding sites from the axle and macrocyclic components defining an orthogonal binding pocket. Moreover, given the large size of the axle components, their bulky stoppers were replaced by *tert*-butyl substituents affording the corresponding pseudo-rotaxanes **4.15**, **4.16** and **4.17**. Afterwards, each *N*Boc-proline enantiomer was positioned as a rigid body inside of the rotaxane's binding cavity, likewise for **4.10I** or **4.10H**. The *tert*-butyl capped axle **4.29** (**4.29$_{t\text{-butyl}}$**) was also complexed with each *N*Boc-(*S*/*R*)-proline enantiomer, but only in a single binding arrangement. The initial (*S*/*R*)-BINOP-PO_4^- complexes with pseudo-rotaxane **4.15** were built favouring the existence of π···π stacking interactions between the aromatic regions of the macrocycle and the enantiomers.

To obtain accurate binding scenarios for the molecular dynamics (MD) studies, all these starting models were optimised by DFT as described below and are presented in Figures C2.6 to C2.12.

Quantum calculations

The geometry optimisations of all anion complexes were carried out with TeraChem 1.9,[64–68] using the CAM-B3LYP functional and different basis sets, as follows. The oxygen atoms were treated with the 6-311++G** basis set, while the iodine atoms were described with the aug-cc-pVDZ-PP basis set. In the optimisations of the **4.10H**, **4.10I** and **4.29$_{t\text{-butyl}}$** anion complexes, the H, C and N centres were treated with the 6-31+G** basis set, while in the optimisations of the oxyanion complexes with pseudo-rotaxanes **4.15**, **4.16**, and **4.17** those elements were described with the 3-21G* basis set. Even taking advantage of GPU acceleration, these interlocked systems are still too large for a higher basis set. The phosphorus atoms of (*S*/*R*)-BINOL-PO_4^- anions complexed with pseudo-rotaxane **4.15**, were also described with 6-311++G**.

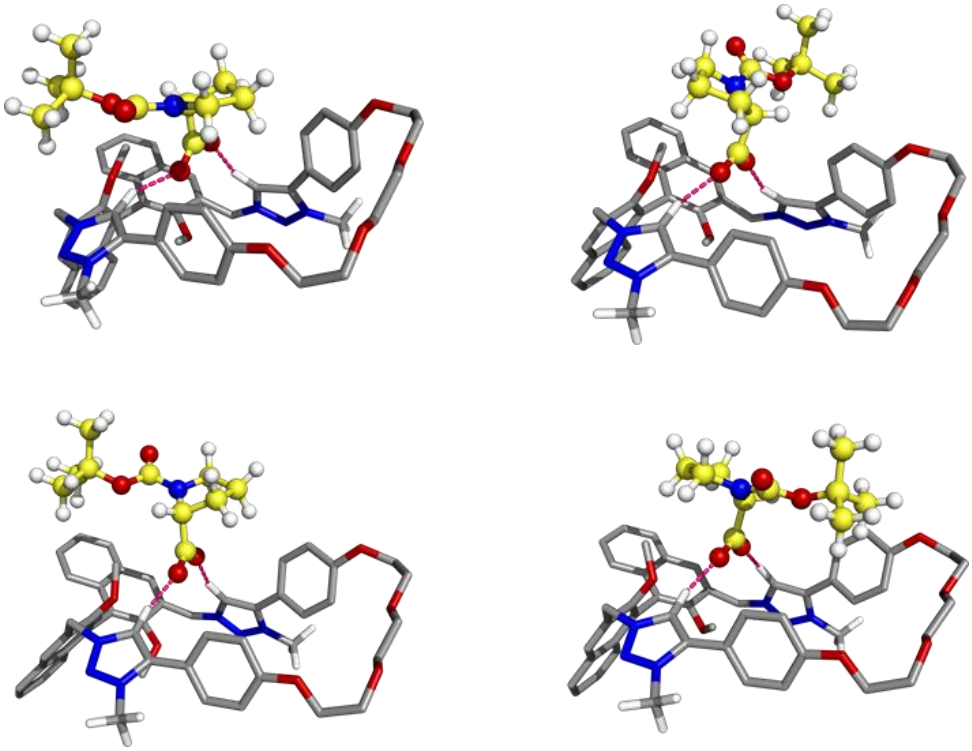


Figure C2.6. *DFT optimized structures of* ***4.10H*** *with the (S)- and (R)-NBoc-proline enantiomers, from initial binding scenarios S_A (top left), S_B (top right), R_A (bottom left) and R_B (bottom right). The HB interactions are shown as pink dashed lines.*

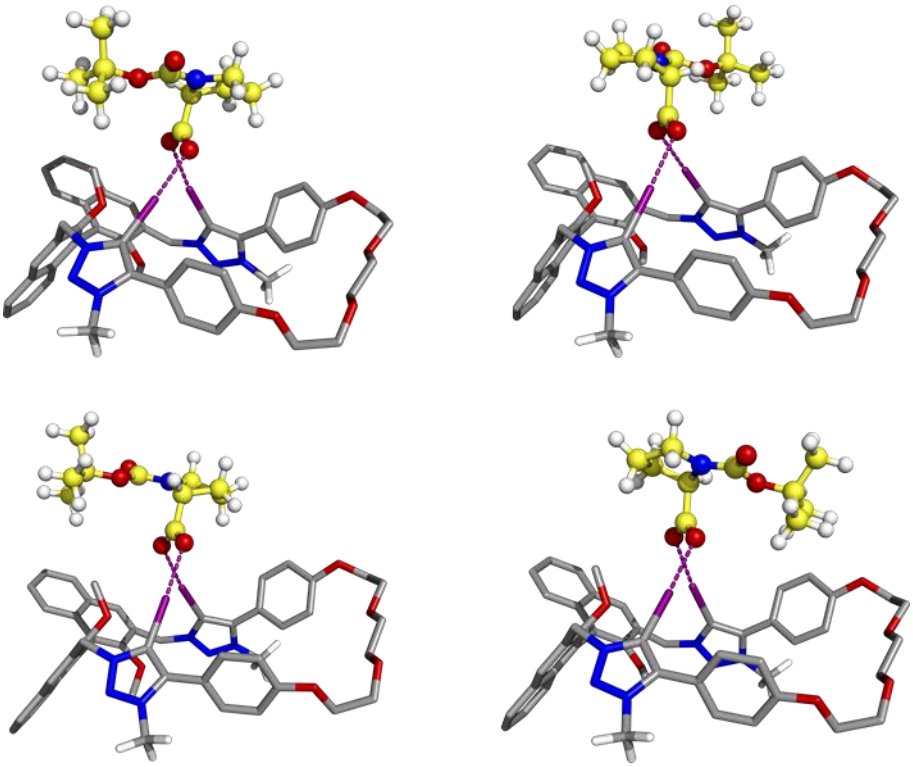


Figure C2.7. *DFT optimized structures of* ***4.10I*** *with the (S)- and (R)-NBoc-proline enantiomers, from initial binding scenarios S_A (top left), S_B (top right), R_A (bottom left) and R_B (bottom right). The XB interactions are shown as purple dashed lines.*

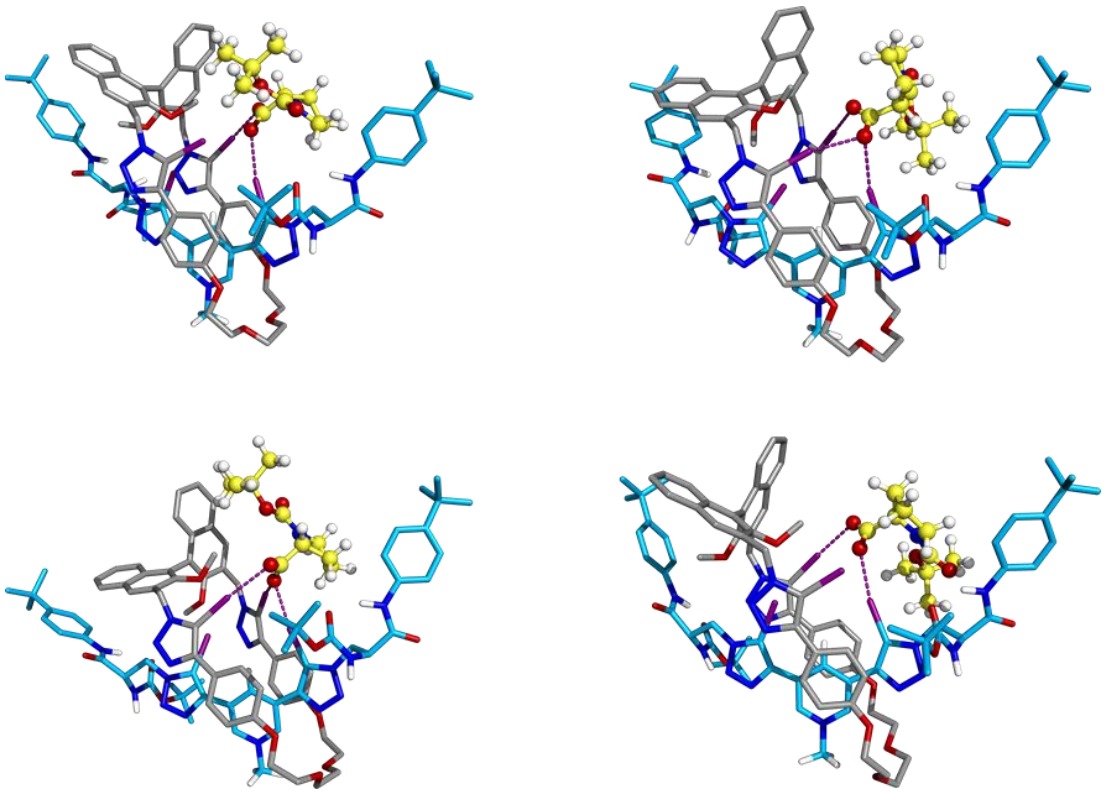


Figure C2.8. *DFT optimized structures of* ***4.15*** *with the (S)- and (R)-NBoc-proline enantiomers, from initial binding scenarios S_A (top left), S_B (top right), R_A (bottom left) and R_B (bottom right). The XB interactions are shown as purple dashed lines.*

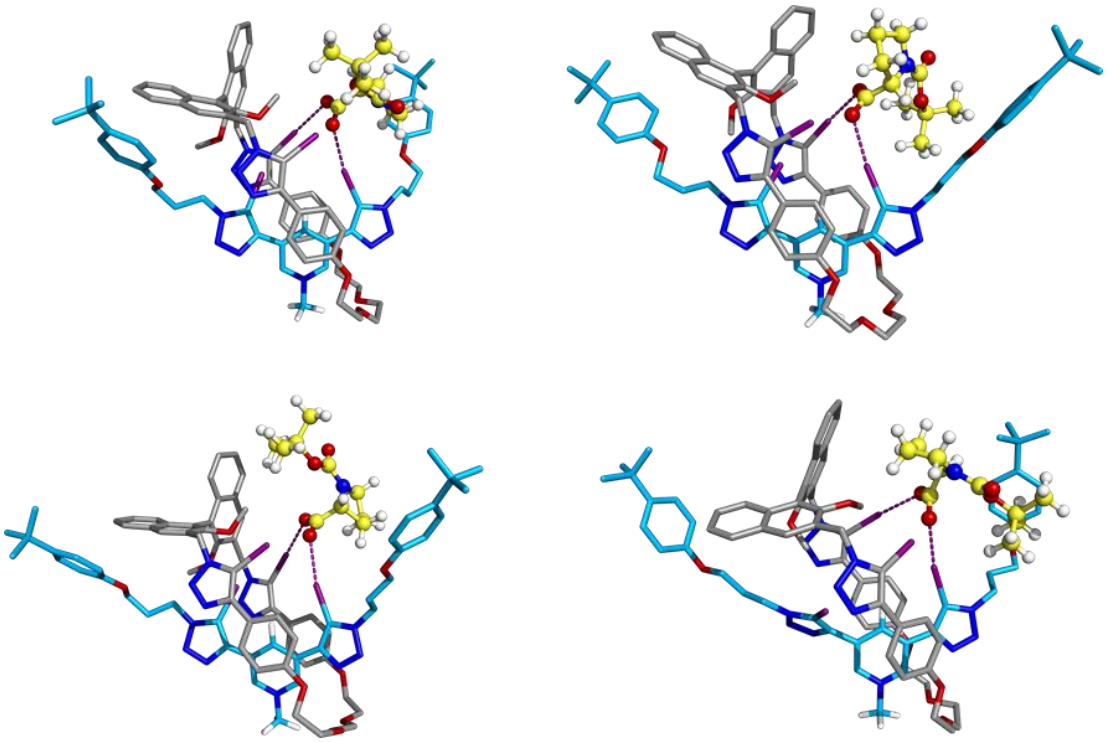


Figure C2.9. *DFT optimized structures of* ***4.16*** *with the (S)- and (R)-NBoc-proline enantiomers, from initial binding scenarios S_A (top left), S_B (top right), R_A (bottom left) and R_B (bottom right). The XB interactions are shown as purple dashed lines.*

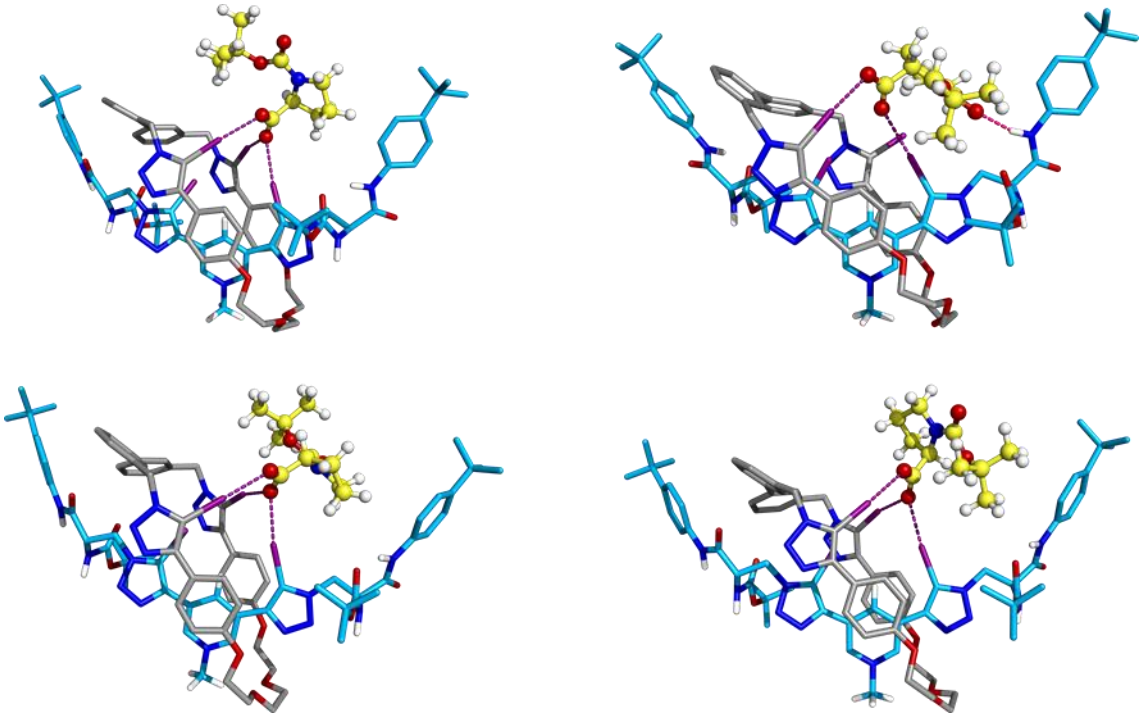


Figure C2.10. *DFT optimized structures of* ***4.17*** *with the (S)- and (R)-NBoc-proline enantiomers, from initial binding scenarios S_A (top left), S_B (top right), R_A (bottom left) and R_B (bottom right). The XB interactions are shown as purple dashed lines.*

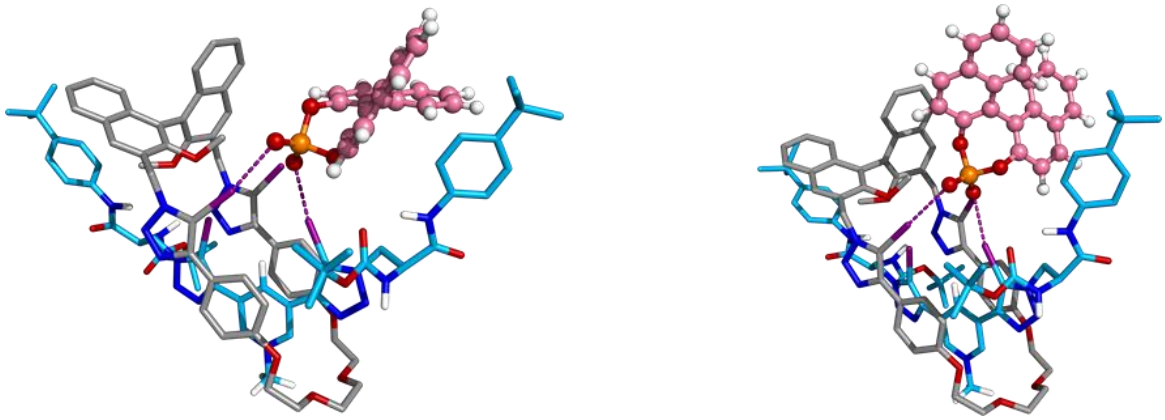


Figure C2.11. *DFT optimized structures of* ***4.15*** *with the (S)- and (R)-BINOL-PO_4^- enantiomers, on the left and right views, respectively. The XB interactions are shown as purple dashed lines.*

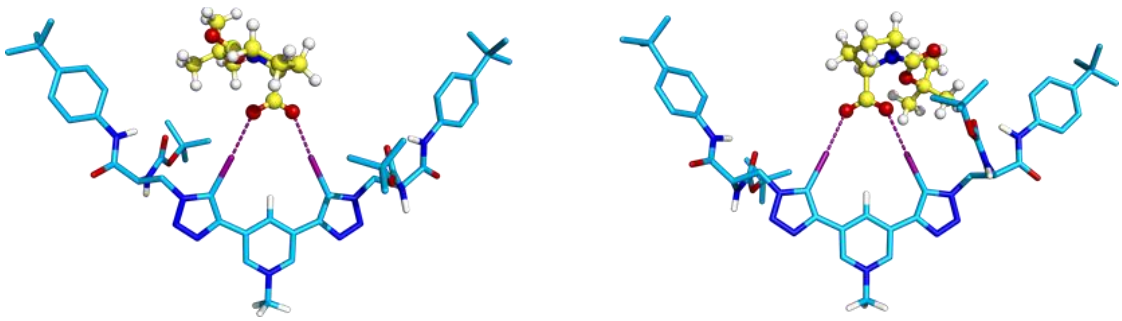


Figure C2.12. *DFT optimized structures of* ***4.29*** *with the (S)- and (R)-NBoc-proline enantiomers, on the left and right views, respectively. The XB interactions are shown as purple dashed lines.*

Classical force field calculations

All Molecular Mechanics (MM) and MD simulations were undertaken with Amber16 software suite.[20] The receptors and the oxyanions were described with default parameters taken from the Generalized Amber Force Field (GAFF)[21,22] and RESP charges,[23] while the hexafluorophosphate (PF_6^-) was described with parameters and charges taken from ref. 30. The solvent mixture was described with the TIP3P model for the water molecules,[28] while the acetone molecules were described with an all-atoms model, using standard RESP atomic charges, GAFF bonding parameters and vdW parameters taken from ref. 69. The structural data from MD simulations were obtained by post-processing of trajectory files with *cpptraj*.[31]

Parameterisation of XB interactions

The force field parameterisation of the XB interactions was based on the previous DFT optimisations of anion complexes of chiral receptors **4.10I** and **4.29**$_{t\text{-butyl}}$ with both enantiomers of *N*Boc-proline (*vide supra*). These optimised structures allowed us to ascertain the dimensions of XB interactions in gas-phase. Their values are gathered in Table C11 and were used as reference in the subsequent determination of the optimal I-EP (iodine-extra point) distance for XB interactions between each substrate and **4.10I** or **4.29**.

Table C11. I···O distances (Å) in DFT optimisations of **4.10I** and **4.29**$_{t\text{-butyl}}$ with the enantiomers of *N*Boc-proline.

Receptor	*N*Boc-(*S*)-proline	*N*Boc-(*R*)-proline
4.10I	2.475 ; 2.522	2.478 ; 2.522
4.29$_{t\text{-butyl}}$	2.509 ; 2.508	2.543 ; 2.508

In our previous works on halide anions and oxyanions recognition by macrocyclic halo-imidazolium receptors,[56,57] rotaxane based halo-triazolium receptors,[33–35] or (*S*)-BINOL based enantioselective receptors,[36] the XB interactions were described with resort to an extra point (EP) of charge added to GAFF.[37] Furthermore, this EP has van der Waals parameters and

mass set to zero, a C-I-EP angle of 180° with a 150 kcal·mol^{-1}·rad^{-2} angle bending force constant. In addition, an I-EP optimal distance determined for each receptor-substrate complex using a 600 kcal·mol^{-1}·Å^{-2} bond stretching force constant. This methodology was extended in this work to the enantioselective binding of chiral substrates mediated by XB bonds, as follows. Different I-EP distances were systematically tested in gas-phase *via* MM energy minimisations of the complexes between **4.10I** and **4.29** and both enantiomers of *N*Boc-proline. However, to obtain atomic RESP charges adequate to describe the XB interactions between carboxylate oxygen atoms of *N*Boc-proline, the MM structure optimisations were preceded by the derivatisation of RESP charges at different I-EP distances. In previously B3LYP/6–31G* optimised structures of **4.10I** and **4.29**, an extra point was positioned in front of each C-I bond at different I-EP distances and a C-I-EP angle of 180°. Subsequently, the electrostatic potential distribution of each structure, with two extra points at the same I-EP distance, was calculated followed by the RESP fitting (see next section). Tables C12 and C13 summarise the range of I-EP distances tested for two (*S*/*R*)-*N*Boc-proline complexes of **4.10I** and **4.29**, respectively, together with the computed I···O distances and the iodine and EP RESP charges.

Table C12. Summary of gas-phase MM optimised I···O distances (Å) for **4.10I**·*N*Boc-(*S*/*R*)-proline, as function of the I-EP distance (Å), listed along with EP and iodine RESP charges.

I-EP distance	EP charge	I charge	**4.10I**·*N*Boc-(*S*)-proline	**4.10I**·*N*Boc-(*R*)-proline
No EP	---	0.258286	3.218 ; 3.408	3.287 ; 3.413
1.98	0.094056	-0.036456	2.915 ; 2.958	2.891 ; 2.921
1.99	0.093020	-0.034561	2.896 ; 3.015	2.891 ; 2.904
2.00	0.091997	-0.032677	2.888 ; 3.024	2.888 ; 2.893
2.01	0.090984	-0.030803	2.893 ; 2.932	2.883 ; 2.890
2.02	0.089982	-0.028939	2.865 ; 3.120	2.872 ; 2.899
2.03	0.088991	-0.027086	2.875 ; 2.921	2.865 ; 2.872
2.04	0.088009	-0.025241	2.867 ; 2.912	2.856 ; 2.868
2.05	0.087039	-0.023406	2.858 ; 2.901	2.834 ; 2.910
2.06	0.086078	-0.021580	2.852 ; 2.878	2.837 ; 2.854
2.07	0.085127	-0.019763	2.837 ; 2.895	2.823 ; 2.848
2.08	0.084186	-0.017954	Atomic clash	Atomic clash

Table C13. Summary of gas-phase MM optimised I···O distances (Å) for **4.29**·*N*Boc-(*S*/*R*)-proline, as function of the I-EP distance (Å), listed along with EP and iodine RESP charges.

I-EP distance	EP charge	I charge	**4.29**·*N*Boc-(*S*)-proline	**4.29**·*N*Boc-(*R*)-proline
No EP	---	0.253568	3.257 ; 3.382	3.356 ; 3.354
1.98	0.112798	-0.097656	2.854 ; 2.854	2.817 ; 2.897
1.99	0.111548	-0.095281	2.843 ; 2.849	2.804 ; 2.905
2.00	0.110311	-0.092918	2.832 ; 2.842	2.797 ; 2.887
2.01	0.109088	-0.090568	2.816 ; 2.836	2.789 ; 2.862
2.02	0.107877	-0.088229	2.818 ; 2.822	2.776 ; 2.854
2.03	0.106680	-0.085902	2.798 ; 2.807	2.764 ; 2.838
2.04	0.105496	-0.083587	Atomic clash	Atomic clash

Tables C12 and C13 show that several I-EP distances can be applied in the MM geometry optimisations of the **4.10I** and **4.29** *N*Boc-proline complexes. On the other hand, the use of the longer 2.07 Å I-EP distance in 300 K, 5 ns long, gas phase MD simulations of **4.10I**·*N*Boc-(*S*/*R*)-proline was shown to be instable, being ruled out. For the gas phase MD simulations of **4.29**·*N*Boc-(*S*/*R*)-proline, the same problem was verified for the I-EP distances between 2.00 and 2.03 Å. These MD simulations were extended to the shorter I-EP distances, and the 2.06 and 1.99 Å distances were found as the best I-EP distances to carry out the MD simulations with complexes the *N*Boc-(*S*/*R*)-proline of **4.10I**·and **4.29**, respectively. Given that these two I-EP distances only differed by 0.07 Å, and that the previous parameterization effort with the (*S*)-BINOL based enantioselective receptors[36] also led to an 1.99 Å I-EP distance, this distance was also used to derivatise the RESP charges necessary to further describe the XB interactions of chiral macrocycle **4.14I**, the achiral axle of rotaxane **4.16**, as well as the achiral macrocycle of rotaxane **4.17** (see below).

Calculation of RESP charges for receptors and substrates

The RESP charges on free macrocycles, anion guests and axle components were calculated with Gaussian09 software.[11] For the XB molecular entities, the atomic charges were derived in agreement with the earlier parameterisation developed with **4.10I** and **4.29** complexed with *N*Boc-proline enantiomers (*vide supra*), considering one extra point of charge

positioned in front of each iodine, at 1.99 Å and with a C-I-EP angle of 180°. This was preceded by initial optimisation of a single conformation of each molecular entity at the B3LYP/6-31G* level of theory, followed by a single point calculation at the HF/6-31G* level, in agreement with the GAFF development (*vide supra*). Both in the optimization and in the single point, the iodine atoms were described with the aug-cc-pVDZ-PP basis set,[52,53] taken from the EMSL website.[13,14] The final charges were then derived considering the position of the two extra points, and the RESP charges of the extra points and of the iodine atoms are listed in Tables C12 (**4.10I**), C13 (**4.29**) and C14 (remaining molecules). Concerning **4.10H**, its RESP atomic charges were derived following the same procedure of optimization a single conformation at the B3LYP/6-31G* level, followed by a single point at the HF/6-31G* level. The *S* and *R* enantiomers of each anionic substrate were optimised with the B3LYP functional along with the 6-31+G** basis set, followed by electrostatic potential calculation through a single point carried out at the HF/6-31G* theory level. The electrostatic potentials of both enantiomers were concatenated and the final atomic charges of either chiral substrate (*S* or *R*) were computed through a multi-conformation RESP fitting based on the individual atomic charges of two enantiomers.

Table C14. EP and iodine RESP charges derivatized for an I-EP distance of 1.99 Å.

Molecular entity	EP charge	I charge
4.14I	0.086651	-0.194717
achiral axle (rotaxane **4.16**)	0.090185	-0.055582
achiral macrocycle (rotaxane **4.17**)	0.074991	-0.141503

General MD simulation methods

The binding scenarios for the anion-rotaxane systems, as well as for the (*S*/*R*)-*N*Boc-proline associations with **4.29** were generated from the corresponding DFT optimized capped counterparts by the addition of the bulky stoppers. In agreement with the 98:2 *v*/*v* concentration used in ^{1}H NMR binding studies, the optimized structures of the anion complexes of **4.10I** and **4.10H** (*vide supra*) were solvated in cubic boxes with 1337 acetone

molecules and 111 water molecules, while the optimized structures of the anion complexes of axle **4.29** and rotaxanes **4.15** and **4.17** were solvated in cubic boxes with 2877 acetone molecules and 239 water molecules. The anion complexes of rotaxane **4.16** were solvated in cubic boxes with 2906 acetone molecules and 120 water molecules, in agreement with the 99:1 *v*/*v* concentration used in ^{1}H NMR binding studies. One PF_6^- counter-ion was added to neutralise the **4.10I** and **4.10H** system's net charge.

Each solvated system was equilibrated under periodic boundary conditions using the following multistage protocol. The system was relaxed by MM minimisation of the solvent molecules and by keeping the substrate, receptor and the counter-ion (when appropriate) fixed with a positional restraint of 500 kcal mol^{-1} Å^{-2}. The restraint was then removed and the entire system was minimised. Both minimisation stages comprised an initial set of 10000 steepest descent algorithm steps, followed by 10000 steps of conjugated gradient algorithm. The equilibration stage proceeded with heating up the system to 300 K for 100 ps using a NVT ensemble and a weak positional restraint (10 kcal mol^{-1} Å^{-2}) on the solutes. Afterwards, each system was equilibrated in a NPT ensemble at 300 K and 1 atm for 1 ns. Finally, NPT data collection runs were carried out for 20 ns, with the trajectory frames being saved every 1 ps. Five independent replicates were performed for each system. The CUDA version of the PMEMD executable was used for the simulation of all solvated systems.[39,40] The bond lengths involving all bonds to hydrogen atoms were constrained with the SHAKE algorithm allowing the usage of 2 fs time step.[41] The Particle Mesh Ewald (PME) method was used to treat the long-range electrostatic interactions.[42] The non-bonded van der Waals interactions were truncated with a 10 Å cut-off.

Furthermore, two 50 kcal mol^{-1} Å^{-2} distance restraints between the **4.10H**'s triazolium C-H carbon atoms and the *N*Boc-(*S*/*R*)-proline's carboxylate carbon atom were employed during the NPT stages of MD simulation to sustain the anion complexes.

References

1 H. Nowell, S. A. Barnett, K. E. Christensen, S. J. Teat and D. R. Allan, *J. Synchrotron Radiat.*, 2012, **19**, 435–441.
2 J. Cosier and A. M. Glazer, *J. Appl. Crystallogr.*, 1986, **19**, 105–107.
3 L. Palatinus and G. Chapuis, *J. Appl. Crystallogr.*, 2007, **40**, 786–790.
4 P. W. Betteridge, J. R. Carruthers, R. I. Cooper, K. Prout and D. J. Watkin, *J. Appl. Crystallogr.*, 2003, **36**, 1487.
5 P. Parois, R. I. Cooper and A. L. Thompson, *Chem. Cent. J.*, 2015, **9**, 30.
6 R. I. Cooper, A. L. Thompson and D. J. Watkin, *J. Appl. Crystallogr.*, 2010, **43**, 1100–1107.
7 A. L. Spek, *J. Appl. Crystallogr.*, 2003, **36**, 7–13.
8 P. van der Sluis and A. L. Spek, *Acta Crystallogr. Sect. A*, 1990, **46**, 194–201.
9 C. R. Groom, I. J. Bruno, M. P. Lightfoot and S. C. Ward, *Acta Crystallogr. Sect. B*, 2016, **72**, 171–179.
10 N. L. Kilah, M. D. Wise, C. J. Serpell, A. L. Thompson, N. G. White, K. E. Christensen and P. D. Beer, *J. Am. Chem. Soc.*, 2010, **132**, 11893–11895.
11 M. J. Frisch, G. W. Trucks, H. B. Schlegel, G. E. Scuseria, M. A. Robb, J. R. Cheeseman, G. Scalmani, V. Barone, G. A. Petersson, H. Nakatsuji, X. Li, M. Caricato, A. V. Marenich, J. Bloino, B. G. Janesko, R. Gomperts, B. Mennucci, H. P. Hratchian, J. V. Ortiz, A. F. Izmaylov, J. L. Sonnenberg, Williams, F. Ding, F. Lipparini, F. Egidi, J. Goings, B. Peng, A. Petrone, T. Henderson, D. Ranasinghe, V. G. Zakrzewski, J. Gao, N. Rega, G. Zheng, W. Liang, M. Hada, M. Ehara, K. Toyota, R. Fukuda, J. Hasegawa, M. Ishida, T. Nakajima, Y. Honda, O. Kitao, H. Nakai, T. Vreven, K. Throssell, J. A. Montgomery Jr., J. E. Peralta, F. Ogliaro, M. J. Bearpark, J. J. Heyd, E. N. Brothers, K. N. Kudin, V. N. Staroverov, T. A. Keith, R. Kobayashi, J. Normand, K. Raghavachari, A. P. Rendell, J. C. Burant, S. S. Iyengar, J. Tomasi, M. Cossi, J. M. Millam, M. Klene, C. Adamo, R. Cammi, J. W. Ochterski, R. L. Martin, K. Morokuma, O. Farkas, J. B. Foresman and D. J. Fox, *Gaussian 09, revision A.01*, Gaussian Inc., Wallingford, CT, 2009.
12 S. Miertuš, E. Scrocco and J. Tomasi, *Chem. Phys.*, 1981, **55**, 117–129.
13 D. Feller, *J. Comput. Chem.*, 1996, **17**, 1571–1586.
14 K. L. Schuchardt, B. T. Didier, T. Elsethagen, L. Sun, V. Gurumoorthi, J. Chase, J. Li and T. L. Windus, *J. Chem. Inf. Model.*, 2007, **47**, 1045–1052.
15 T. Lu and F. Chen, *J. Mol. Graph. Model.*, 2012, **38**, 314–323.
16 T. Lu and F. Chen, *J. Comput. Chem.*, 2012, **33**, 580–592.
17 K. B. Wiberg, *Tetrahedron*, 1968, **24**, 1083–1096.
18 E. D. Glendening, A. E. Reed, J. E. Carpenter and F. Weinhold, *NBO Version 3.1*, .
19 A. E. Reed, L. A. Curtiss and F. Weinhold, *Chem. Rev.*, 1988, **88**, 899–926.
20 D. A. Case, R. M. Betz, W. Botello-Smith, D. S. Cerutti, T. E. Cheatham III, T. A. Darden, R. E. Duke, T. J. Giese, H. Gohlke, A. W. Goetz, N. Homeyer, S. Izadi, P. Janowski, J. Kaus, A. Kovalenko, T. S. Lee, S. LeGrand, P. Li, C. Lin, T. Luchko, R. Luo, B. Madej, D. Mermelstein, K. M. Merz, G. Monard, H. Nguyen, H. T. Nguyen, I. Omelyan, A. Onufriev, D. R. Roe, A. Roitberg, C. Sagui, C. L. Simmerling, J. Swails, R. C. Walker, J. Wang, R. M. Wolf, X. Wu, L. Xiao, D. M. York and P. A. Kollman, *AMBER 16*, University of California: San Francisco, 2016.
21 J. Wang, R. M. Wolf, J. W. Caldwell, P. A. Kollman and D. A. Case, *J. Comput. Chem.*, 2004, **25**, 1157–1174.
22 J. Wang, R. M. Wolf, J. W. Caldwell, P. A. Kollman and D. A. Case, *J. Comput. Chem.*, 2005, **26**, 114–114.
23 C. I. Bayly, P. Cieplak, W. Cornell and P. A. Kollman, *J. Phys. Chem.*, 1993, **97**, 10269–10280.
24 P. Li and K. M. Merz, *J. Chem. Inf. Model.*, 2016, **56**, 599–604.
25 R. M. Betz and R. C. Walker, *J. Comput. Chem.*, 2015, **36**, 79–87.
26 A. K. Rappe, C. J. Casewit, K. S. Colwell, W. A. Goddard and W. M. Skiff, *J. Am. Chem. Soc.*, 1992, **114**, 10024–10035.
27 P. Li, L. F. Song and K. M. Merz, *J. Chem. Theory Comput.*, 2015, **11**, 1645–1657.
28 W. L. Jorgensen, J. Chandrasekhar, J. D. Madura, R. W. Impey and M. L. Klein, *J. Chem. Phys.*, 1983, **79**, 926–935.
29 M. G. Martin and M. J. Biddy, *Fluid Prop. Simul. Chall. Spec. Issue Sect.*, 2005, **236**, 53–57.
30 Z. Liu, S. Huang and W. Wang, *J. Phys. Chem. B*, 2004, **108**, 12978–12989.
31 D. R. Roe and T. E. Cheatham, *J. Chem. Theory Comput.*, 2013, **9**, 3084–3095.
32 J. R. de Laeter, J. K. Bohlke, P. de Bievre, H. Hidaka, H. S. Peiser, K. J. R. Rosman and P. D. P. Taylor, *Pure Appl Chem*, 2003, **75**, 683–800.
33 T. A. Barendt, A. Docker, I. Marques, V. Félix and P. D. Beer, *Angew. Chem. Int. Ed.*, 2016, **55**, 11069–11076.
34 M. J. Langton, I. Marques, S. W. Robinson, V. Félix and P. D. Beer, *Chem. – Eur. J.*, 2016, **22**, 185–192.
35 M. J. Langton, S. W. Robinson, I. Marques, V. Félix and P. D. Beer, *Nat Chem*, 2014, **6**, 1039–1043.
36 J. Y. C. Lim, I. Marques, L. Ferreira, V. Felix and P. D. Beer, *Chem Commun*, 2016, **52**, 5527–5530.
37 M. A. A. Ibrahim, *J. Comput. Chem.*, 2011, **32**, 2564–2574.
38 A. W. Götz, M. J. Williamson, D. Xu, D. Poole, S. Le Grand and R. C. Walker, *J. Chem. Theory Comput.*, 2012, **8**, 1542–1555.
39 R. Salomon-Ferrer, A. W. Götz, D. Poole, S. Le Grand and R. C. Walker, *J. Chem. Theory Comput.*, 2013, **9**, 3878–3888.

40 S. Le Grand, A. W. Götz and R. C. Walker, *Comput. Phys. Commun.*, 2013, **184**, 374–380.
41 J.-P. Ryckaert, G. Ciccotti and H. J. . Berendsen, *J. Comput. Phys.*, 1977, **23**, 327–341.
42 T. Darden, D. York and L. Pedersen, *J. Chem. Phys.*, 1993, **98**, 10089–10092.
43 Y.-C. Qin, L. Liu, M. Sabat and L. Pu, *Tetrahedron*, 2006, **62**, 9335–9348.
44 L. Van Meervelt, K. De Wael and T. Zeegers-Huyskens, *J. Mol. Struct.*, 1995, **356**, 183–190.
45 P. Sahoo, R. Sankolli, H.-Y. Lee, S. R. Raghavan and P. Dastidar, *Chem. – Eur. J.*, 2012, **18**, 8057–8063.
46 G. Blaser, J. M. Sanderson, A. S. Batsanov and J. A. K. Howard, *Tetrahedron Lett.*, 2008, **49**, 2795–2798.
47 L. Fadini and A. Togni, *Tetrahedron Asymmetry*, 2008, **19**, 2555–2562.
48 R. Taylor and C. F. Macrae, *Acta Crystallogr. Sect. B*, 2001, **57**, 815–827.
49 I. J. Bruno, J. C. Cole, P. R. Edgington, M. Kessler, C. F. Macrae, P. McCabe, J. Pearson and R. Taylor, *Acta Crystallogr. Sect. B*, 2002, **58**, 389–397.
50 C. F. Macrae, P. R. Edgington, P. McCabe, E. Pidcock, G. P. Shields, R. Taylor, M. Towler and J. van de Streek, *J. Appl. Crystallogr.*, 2006, **39**, 453–457.
51 C. F. Macrae, I. J. Bruno, J. A. Chisholm, P. R. Edgington, P. McCabe, E. Pidcock, L. Rodriguez-Monge, R. Taylor, J. van de Streek and P. A. Wood, *J. Appl. Crystallogr.*, 2008, **41**, 466–470.
52 K. A. Peterson, D. Figgen, E. Goll, H. Stoll and M. Dolg, *J. Chem. Phys.*, 2003, **119**, 11113–11123.
53 K. A. Peterson, B. C. Shepler, D. Figgen and H. Stoll, *J. Phys. Chem. A*, 2006, **110**, 13877–13883.
54 D. A. Case, R. M. Betz, W. Botello-Smith, D. S. Cerutti, T. E. Cheatham III, T. A. Darden, R. E. Duke, T. J. Giese, H. Gohlke, A. W. Goetz, N. Homeyer, S. Izadi, P. Janowski, J. Kaus, A. Kovalenko, T. S. Lee, S. LeGrand, P. Li, C. Lin, T. Luchko, R. Luo, B. Madej, D. Mermelstein, K. M. Merz, G. Monard, H. Nguyen, H. T. Nguyen, I. Omelyan, A. Onufriev, D. R. Roe, A. Roitberg, C. Sagui, C. L. Simmerling, J. Swails, R. C. Walker, J. Wang, R. M. Wolf, X. Wu, L. Xiao, D. M. York and P. A. Kollman, *AMBER 14*, University of California: San Francisco, 2014.
55 X. Grabuleda, C. Jaime and P. A. Kollman, *J. Comput. Chem.*, 2000, **21**, 901–908.
56 F. Zapata, A. Caballero, N. G. White, T. D. W. Claridge, P. J. Costa, V. Félix and P. D. Beer, *J. Am. Chem. Soc.*, 2012, **134**, 11533–11541.
57 A. Caballero, F. Zapata, N. G. White, P. J. Costa, V. Félix and P. D. Beer, *Angew. Chem.*, 2012, **124**, 1912–1916.
58 N. L. Kilah, M. D. Wise and P. D. Beer, *Cryst. Growth Des.*, 2011, **11**, 4565–4571.
59 C. Coluccini, D. Dondi, M. Caricato, A. Taglietti, M. Boiocchi and D. Pasini, *Org Biomol Chem*, 2010, **8**, 1640–1649.
60 N. G. White and P. D. Beer, *Org Biomol Chem*, 2013, **11**, 1326–1333.
61 S. W. Robinson, C. L. Mustoe, N. G. White, A. Brown, A. L. Thompson, P. Kennepohl and P. D. Beer, *J. Am. Chem. Soc.*, 2015, **137**, 499–507.
62 T.-G. Liao, J. Ren, H.-F. Fan, M.-J. Xie and H.-J. Zhu, *Tetrahedron Asymmetry*, 2008, **19**, 808–815.
63 G. Kartha, T. Ashida and M. Kakudo, *Acta Crystallogr. Sect. B*, 1974, **30**, 1861–1866.
64 I. S. Ufimtsev and T. J. Martinez, *J. Chem. Theory Comput.*, 2009, **5**, 2619–2628.
65 A. V. Titov, I. S. Ufimtsev, N. Luehr and T. J. Martinez, *J. Chem. Theory Comput.*, 2013, **9**, 213–221.
66 C. Song, L.-P. Wang and T. J. Martínez, *J. Chem. Theory Comput.*, 2016, **12**, 92–106.
67 T. P. M. Goumans, C. R. A. Catlow, W. A. Brown, J. Kastner and P. Sherwood, *Phys Chem Chem Phys*, 2009, **11**, 5431–5436.
68 J. Kästner, J. M. Carr, T. W. Keal, W. Thiel, A. Wander and P. Sherwood, *J. Phys. Chem. A*, 2009, **113**, 11856–11865.
69 S. K. Burger and G. A. Cisneros, *J. Comput. Chem.*, 2013, **34**, 2313–2319.